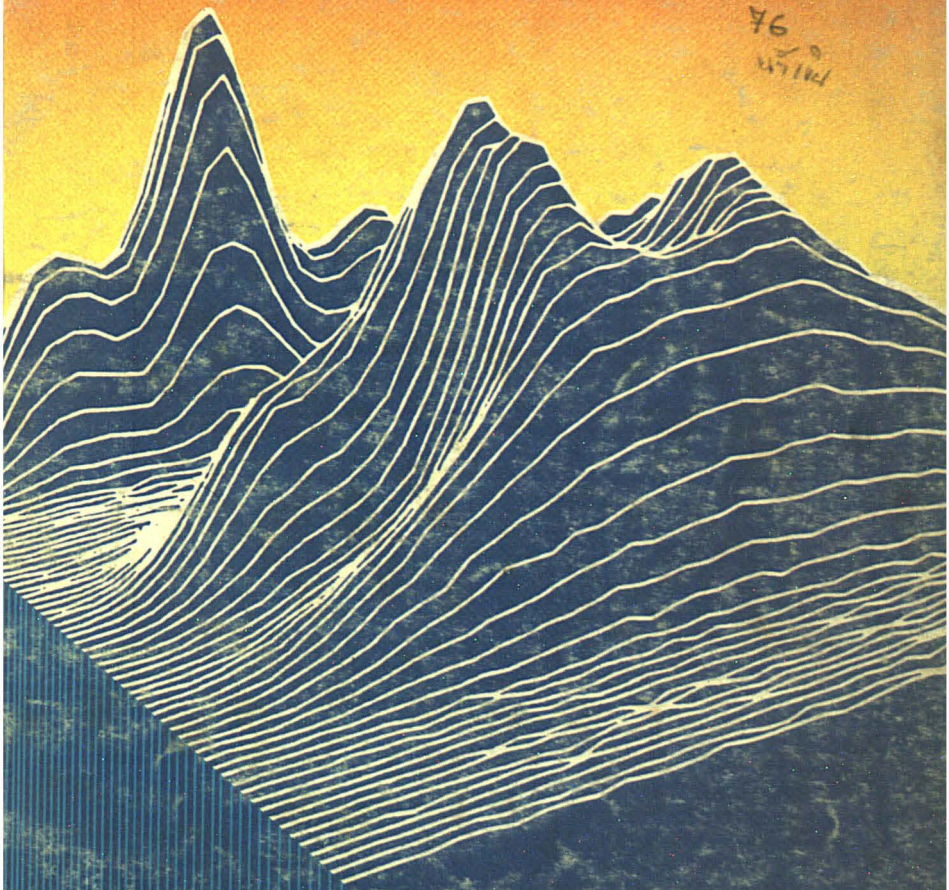
MARCH 1985

analytical chemistry



MULTIDIMENSIONAL LUMINESCENCE MEASUREMENTS 463A

BIOSYSTEMS UPDATE

Workshops on Peptide Synthesis

Applied Biosystems will conduct nine workshops on the latest methods in peptide synthesis. Cleavage, deprotection, characterization and purification techniques will also be surveyed. If you use or plan to use synthetic peptides, attending one of these workshops will be a unique opportunity to consult with scientists from the world leader in protein-peptide instrument-reagent systems.

Each workshop will include discussions of new approaches, instrumentation and software that make peptide synthesis more practical and affordable. In the past, synthesizing peptides required an in-depth understanding of the chemistry and tedious manipulations during the synthesis process. Today, peptides can be easily and routinely synthesized in any laboratory with unprecedented efficiency, speed and economy.

These workshops are free, but attendance is limited and advanced registration is required. To reserve a place, please telephone Heather Block at any of the U.S.A. telephone numbers listed below.

TOPICS TO BE REVIEWED WILL INCLUDE:

Organic Chemistry of Solid Phase Peptide Synthesis;
Polystyrene Support with PAM Linker;
Optimal Formation of Amino Acid Symmetric Anhydrides;
Automation of Pre-Activation Protocols;
Cleavage and Final Deprotection Strategies for the Resin-Bound Peptide;
Choosing the Most Suitable Tools and Methods for Characterization and Purification; and
Analytical and Preparative HPLC Methods

LOCATIONS and DATES	
Boston, Massachusetts	Monday, May 6, 1985
New York, New York	Wednesday, May 8, 1985
Philadelphia, Pennsylvania	Monday, May 13, 1985
Washington, D. C.	Wednesday, May 15, 1985
Raleigh-Durham, North Carolina	Friday, May 17, 1985
Houston, Texas	Tuesday, May 21, 1985
Chicago, Illinois	Friday, May 24, 1985
San Diego, California	Wednesday, May 29, 1985
San Francisco, California	Friday, May 31, 1985

Each workshop will be from 9:00 a.m. to 4:00 p.m.; the Applied Biosystems Model 430A Peptide Synthesizer will be available for demonstration. To ensure a place at one of these workshops, telephone your reservation to Heather Block as soon as possible.

Applied Biosystems

APPLIED BIOSYSTEMS, INC., 850 Lincoln Centre Drive, Foster City, CA 94404 • (800) 874-9868 • In California (800) 831-3582 Telex: 470052
IN EUROPE: APPLIED BIOSYSTEMS GMBH, Bergstrasse 104, D6102 Pfungstadt, West Germany • 06157-6036 Telex: 4191746

HPLC system selection made easy



Only from Gilson !!!

With Gilson, your chromatography won't be compromised with a system not specifically defined for your separation. All Gilson systems combine functional modularity with thoughtful definition to create products with a purpose. Every system represents our assurance that performance will meet your separation requirements.

Gilson Systems are of modular design. They use independent, computer-compatible modules which may be used alone, combined to make a system or recombined with new modules to create an upgraded chromatograph. All future components will be system-compatible so you can update, not outdate, your LC as application technology advances.

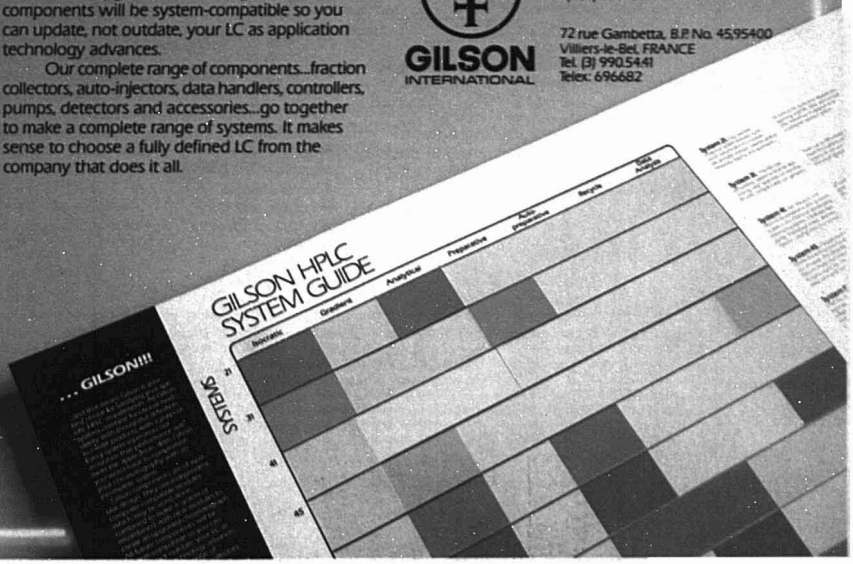
Our complete range of components...fraction collectors, auto-injectors, data handlers, controllers, pumps, detectors and accessories...go together to make a complete range of systems. It makes sense to choose a fully defined LC from the company that does it all.

To help you choose the right system for your separation goals, we have prepared a GILSON HPLC SYSTEM GUIDE. In a matter of minutes, you can find the system that's right for you instead of spending hours wading through piles of brochures. For your free copy of this easy-to-use Guide, circle the reader service number or contact us directly.

GILSON INTERNATIONAL

Box 27, 3000 W. Beltline
Middleton, WI 53562
(608) 836-1551

72 rue Gambetta, B.P. No. 45
95400 Villiers-le-Bel, FRANCE
Tel. (3) 990.54.41
Telec: 696682



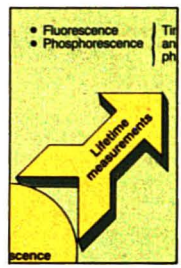
Circle 63 for literature. Circle 64 have your representative call us.

analytical chemistry®

MARCH 1985

COVER FEATURE





REPORT

The teaching of chemical instrumentation. Galen Ewing and Maarten van Swaay explore some of the questions and dilemmas facing those who teach instrumentation and those who establish undergraduate chemistry curricula

385 A

INSTRUMENTATION

Multidimensional luminescence spectroscopy, including excitation and emission measurements, time- and phase-resolved measurements, and polarization techniques, are discussed by Isiah Warner, Gabor Patonay, and Mark Thomas of Emory University

463 A

FOCUS

A glimpse into the future reveals more powerful NMRs, laboratory management software that runs on personal computers, and lab robots.

▶Investment analyst sees rosy industry prospects.

▶CHEMFETs are now available at production cost

398 A

Volume 57, No. 3
March 1985
ANCHAM
57(3) 365A–488A
577–784 (1985)
ISSN 0003 2700

Registered in U.S. Patent and Trademark Office; Copyright 1985 by the American Chemical Society

ANALYTICAL CHEMISTRY (ISSN 0003-2700) is published monthly except semimonthly in April and August by the American Chemical Society at 1155 16th St., N.W., Washington, D.C. 20036. Editorial offices are located at the same ACS address (202-872-4600; TDD 202-872-8733). Second-class postage paid at Washington, D.C., and additional mailing offices. Postmaster: Send address changes to Membership & Subscription Services, P.O. Box 3337, Columbus, Ohio 43210.

Claims for missing numbers will not be allowed if loss was due to failure of notice of change of address to be received in the time specified; if claim is dated (a) North America: more than 90 days beyond issue date, (b) all other foreign: more than one year beyond issue date, or if the reason given is "missing from files."

Copyright Permission: An individual may make a single reprographic copy of an article in this publication for personal use. Reprographic copying beyond that permitted by Section 107 or 108 of the U.S. Copyright Law is allowed, provided that the appropriate per-copy fee is paid through the Copyright Clearance Center, Inc., 21 Congress St., Salem, Mass. 01970. For reprint permission, write Copyright Administrator, B&J Division, ACS, 1155 16th St., N.W., Washington, D.C. 20036.

Registered names and trademarks, etc., used in this publication, even without specific indication thereof, are not to be considered unprotected by law.

Advertising Management: Centcom, Ltd., 25 Sylvan Road South, Westport, Conn. 06881 (203) 226-7131

Technical Contents/Briefs ..... 370 A
Meetings ..... 426 A
Short Courses ..... 426 A
For Your Information ..... 426 A
New Products ..... 434 A
Chemicals ..... 437 A
Software ..... 438 A
Manufacturers' Literature ..... 443 A
Advertising Index ..... 484 A
Author Index, Future Articles ..... inside back cover





NEWS

The ACS Spring National Meeting will be held April 28–May 3 in Miami Beach, Fla. The Analytical Division program will be highlighted by the presentation of five ACS awards

408 A

ANALYTICAL APPROACH

Gunpowders. Using the wrong type of powder can injure the shooter and result in lawsuits against the manufacturer. Peter Lott and Darwin Dahl describe their work to determine the powder involved in such cases

446 A

BOOKS

Critical reviews. Books on immunoassay, food analysis, and FT–NMR are reviewed by G. A. Hudson, J. F. Lawrence, and T. C. Farrar

455 A

EDITORIAL

The Center for Analytical Chemistry at NBS serves as the nation's reference laboratory for chemical composition measurements. With its broad base of expertise it can be considered our national analytical laboratory

577

1985 subscription rates include air delivery outside the U.S., Canada, and Mexico

	1 yr	2 yr
Members		
Domestic	20	34
Canada and Mexico	40	74
Europe	57	108
All Other Countries	80	154
Nonmembers		
Domestic	30	51
Canada and Mexico	50	91
Europe	99	179
All Other Countries	122	225

Three-year and other rates contact: Membership & Subscription Services, ACS, P.O. Box 3337, Columbus, Ohio 43210, (614) 421-3776.

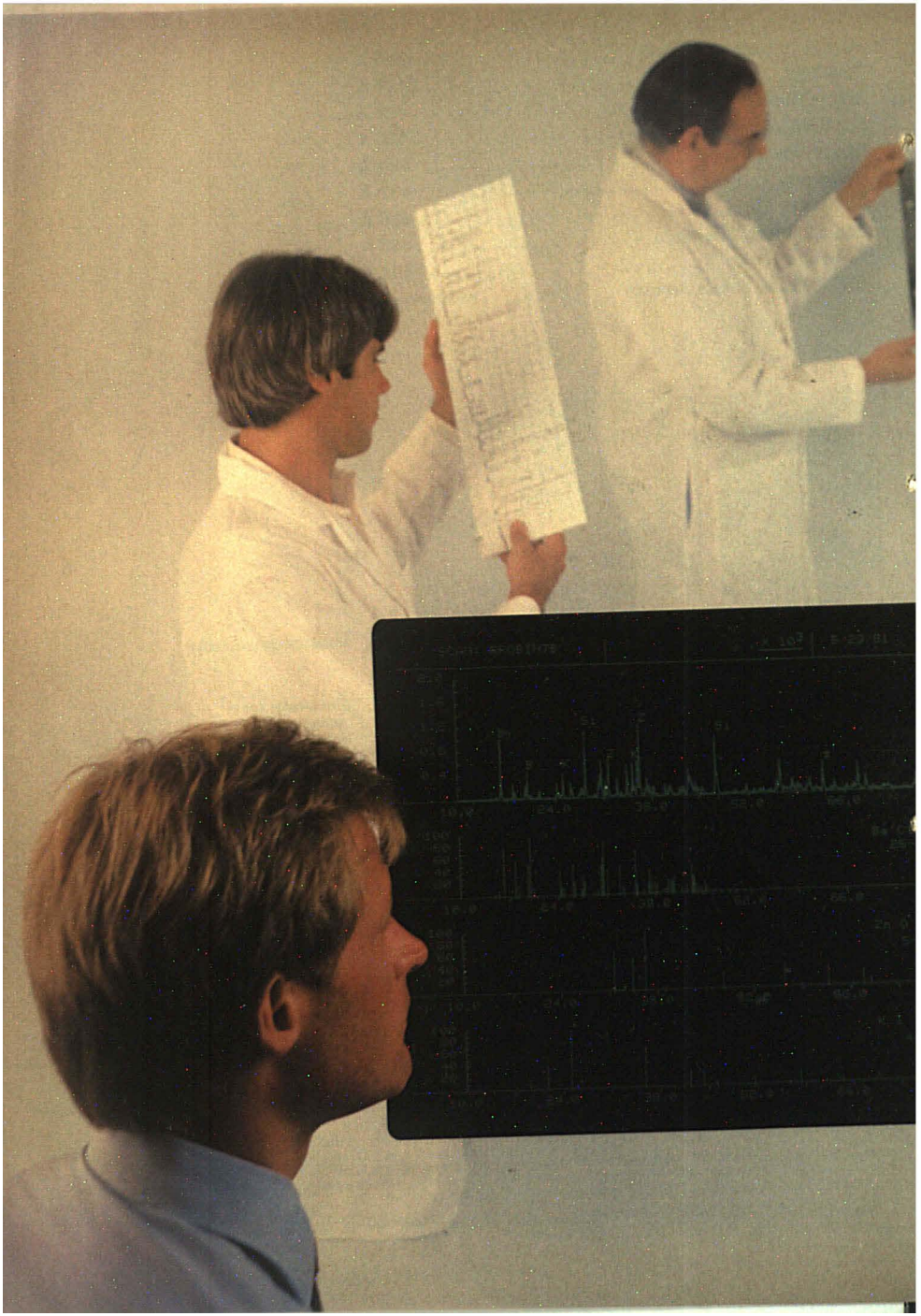
Subscription orders by phone may be charged to Visa, MasterCard, Barclay card, Access, or American Express. Call toll free at (800) 424-6747 from anywhere in the continental U.S.; from Washington, D.C., call 872-8065. Mail orders for new and renewal subscriptions should be sent with payment to the Treasurer's Office at the Washington address.

Subscription service inquiries and changes of address (include both old and new addresses with ZIP code and *recent mailing label*) should be directed to the ACS Columbus address noted above. Please allow six weeks for change of address to become effective.

ACS membership information: Ann Donahue, Washington address.

Single issues, current year, $7.50 except review issue and LabGuide, $8.50; **back issues and volumes and microform editions** available by single volume or back issue collection. For information or to order, call (800) 424-6747 or write the Sales Department at the Washington address.

Nonmember rates in Japan: Rates at left do not apply to nonmember subscribers in Japan, who must enter subscription orders with Maruzen Company Ltd., 3-10 Nihonbashi 2-chome, Chuo-ku, Tokyo 103, Japan. Tel: (03) 272-7211



Witness the evolution of advanced x-ray diffraction.

Stay ahead with Philips.

For nearly 80 years, innovations in x-ray diffraction by Philips have helped extend the value of this technology throughout the world. New configurations, the most advanced array of software and a wide range of accessories currently help solve an unparalleled range of analytical problems.

By combining extensive customer experience with the vast resources of our research laboratories, Philips has evolved analytical systems for the clear, consistent identification of crystallographic structures, compound constituents and physical properties. These ongoing advances have enabled Philips to provide you with analytical results often impossible with other techniques.

Philips x-ray diffractometer installations are attaining optimum system performance, high reliability and economy for both scientific and industrial applications. Our international network of sales, training and service personnel are readily available to help keep you and your work ahead of the field.

Make your analyses easier and more efficient. Call or write today for complete information.
Contact: Philips Analytical X-ray, Lelyweg 1,
7602 EA Almelo, The Netherlands. Tel. (31) 5490-18291.
(In U.S.A.) Philips Electronic Instruments, Inc.,
Analytical X-ray Group, 85 McKee Drive,
Mahwah, NJ 07430. Tel. (201) 529-3800.

CIRCLE 168 ON READER SERVICE CARD

PHILIPS

Scientific & Analytical Equipment

PHILIPS

Briefs

Microprocessor-Controlled ex Vivo Monitoring of Sodium and Potassium Concentrations in Undiluted Urine with Ion-Selective Electrodes 578

A single-drop flow-through measuring chamber allows stable readouts in undiluted urine and in the presence of sediments and gas bubbles. Comparison of values measured by this method and by flame photometry yields RSDs below 10%.

Stephan Dütsch, Hans-Beat Jenny, Konrad J. Schlatter, Philippe M. J. Pérrisset, Gunther Wolff, Jean Thomas Clerc, Ernö Pretsch, and Wilhelm Simon*, Department of Organic Chemistry, Swiss Federal Institute of Technology, CH-8092 Zürich, Switzerland *Anal. Chem., 57 (1985)*

Potentiometric Stripping Analysis: Theory, Experimental Verification, and Generation of Stripping Polarograms 581

Equations based on an assumed initial parabolic concentration gradient of the metal amalgam are derived for transient potential and transition time. Results are compared for conventional electrodes and fiber microelectrodes.

Abul Hussam and J. F. Coetzee*, Department of Chemistry, University of Pittsburgh, Pittsburgh, Pa. 15260 *Anal. Chem., 57 (1985)*

Pulse Polarography: Effects of Electrode Sphericity on the Current–Potential Curves in Normal Pulse Polarography, Reverse Pulse Polarography, and Differential Pulse Polarography 585

Equations that take into account the sphericity of the DME for reversible electrode processes are presented. Cases in which the reduction product dissolves in both the electrolyte solution and the electrode are considered.

Jesus Galvez, Laboratory of Physical Chemistry, Faculty of Science, Murcia 239169, Spain *Anal. Chem., 57 (1985)*

Electrocatalytic and Analytical Response of Cobalt Phthalocyanine Containing Carbon Paste Electrodes toward Sulfhydryl Compounds 591

Cysteine, *N*-acetylcysteine, and homocysteine are detected at 0.75 V vs. SCE with detection limits at the pmol level.

Mary Kim Halbert and Richard P. Baldwin*, Department of Chemistry, University of Louisville, Louisville, Ky. 40292 *Anal. Chem., 57 (1985)*

Infrared Spectrometric Studies of Cyanoalkyl Ligands Immobilized on Chromatographic Surfaces 596

Ligand–surface and ligand–solvent interactions are studied using cyanoalkyl ligands of various chain lengths chemically attached to silica.

B. R. Suffolk and R. K. Gilpin*, Department of Chemistry, Kent State University, Kent, Ohio 44242 *Anal. Chem., 57 (1985)*

Fluorescence Study of Ion Pair Interactions on Hydrocarbon Bonded Surfaces 602

The wavelength of maximum fluorescence of the ammonium salt of 8-aniline-1-naphthalenesulfonic acid (ANS) is a measure of the relative polarity of the hydrocarbon bonded surface.

Sally D. Dowling and W. Rudolf Seitz*, Department of Chemistry, University of New Hampshire, Durham, N.H. 03824 *Anal. Chem., 57 (1985)*

Characterization of a Chiral Tripeptide Stationary Phase for the Liquid Chromatographic Separation of Chiral Dipeptides 606

An intact tripeptide bonded to silica gel gives significantly different retention behavior for isomeric dipeptides than that reported for a tripeptide phase synthesized stepwise on the silica surface.

William A. Howard, Tau-Being Hsu, and L. B. Rogers*, Department of Chemistry, University of Georgia, Athens, Ga. 30602, and **David A. Nelson**, Department of Chemistry, University of Wyoming, Laramie, Wyo. 82071 *Anal. Chem., 57 (1985)*

Reversed-Phase Liquid Chromatography with Fourier Transform Infrared Spectrometric Detection Using a Flow Cell Interface 610

Postcolumn, segmented, flowing extraction of aqueous effluents is used. IR transparency that is significantly improved over the aqueous elution solvent system is observed.

Charles C. Johnson, John W. Hellgeth, and Larry T. Taylor*, Department of Chemistry, Virginia Polytechnic Institute and State University, Blacksburg, Va. 24061-0699 *Anal. Chem., 57 (1985)*

Fixed-Site Ion Exchanger for Liquid Chromatographic Determination of Multifunctional Carboxylic Acids 615

Simultaneous determination of metal ions and acids in chemical cleaning solutions at low μg/mL concentrations is shown. RSDs are 3–6%.

R. M. Cassidy* and S. Elchuk, General Chemistry Branch, Atomic Energy of Canada Limited, Research Company, Chalk River Nuclear Laboratories, Chalk River, Ontario, Canada K0J 1J0 *Anal. Chem., 57 (1985)*

Determination of Chloride, Bromide, and Iodide in Silver Halides by Ion Exchange and Ion Interaction Chromatography 621

Halide ratios are determined at the 0.005–100 mol% level in silver halides following reduction of Ag in basic aqueous hydrazine solution. Recoveries from synthetic standards average 98% for Cl, 94% for Br, and 92% for I with RSDs of better than 3%.

Frederick J. Gustafson* and Craig G. Markell, 3M, Central Research Laboratories, St. Paul, Minn. 55144, and **Sharon M. Simpson**, 3M, Photo Color Systems, St. Paul, Minn. 55144 *Anal. Chem., 57 (1985)*

* Corresponding author



(measurement capability) x 2

Dual-channel electrode inputs multiply the performance of the new EA™ pH/ISE meters from Orion.

One meter for all your pH and ISE work

Now you can combine pH and ISE testing on the same meter without disconnecting electrodes. These new meters calibrate and recall any two electrodes independently. And you can conveniently switch back and forth between the electrodes without recalibrating. A meter that works like two, for the price of one.

An investment with a future

EA identifies the new, top-of-the-line ORION pH/ISE meters as a unique, expandable design concept. These meters can be upgraded to assure that today's meters won't be obsolete tomorrow...they will expand to meet your growing needs.

Communication, not confusion

The EA 940 meter guides you through pH/ISE measurement and incremental techniques, including double known addition, an ORION exclusive. The EA 920 meter automatically advances, making calibration a simple, two-step operation. Both meters link up to recorder, printer or computer.

Dual electrode inputs, expandability, ease of use, and recorded test data are four of the many features of the new ORION meters.

Contact Orion for an EA 940 and EA 920 demonstration. Quality meters from Orion Research. Call 800-225-1480, or, in Massachusetts, call 617-864-5400.

ORION

Orion Research Incorporated
Laboratory Products Group
840 MEMORIAL DRIVE, CAMBRIDGE, MA 02139 U.S.A.
IN EUROPE: ORION RESEARCH AG
FÄHNLIBRUNNENSTRASSE 3, CH-8700 KÜSNACHT, SWITZERLAND
TELEPHONE 01-910-7858. TELEX 57829.

©1985 Orion Research Incorporated
ORION is a trademark registered in the U.S. Patent and Trademark Office

Circle 155 for a demonstration. Circle 156 for literature.

Briefs

Selective Determination of Trace Level Chromium(III) by Ion-Pair Reversed-Phase High-Performance Liquid Chromatography Based on Color Formation with 4-(2-Pyridylazo)resorcinol in the Presence of Triethanolamine 625

A detection limit of 0.5 ng/cm^3 Cr(III) is achieved in the presence of 100–200 ng/cm^3 of Al(III), V(V), Mn(II), Fe(II), Co(II), Ni(II), Cu(II), Zn(II), and Cd(II).

Hitoshi Hoshino* and Takao Yotsuyanagi, Department of Applied Chemistry, Tohoku University, Aoba, Aramaki, Sendai 980, Japan *Anal. Chem., 57 (1985)*

Separation Function for Measuring the Information in Complex Chromatograms 628

The separation function relates the information content of a chromatogram to the number of peaks and extent of resolution between adjacent peaks. The function is applied to both simulated and real separations.

D. R. Van Hare and L. B. Rogers*, Department of Chemistry, University of Georgia, Athens, Ga. 30602 *Anal. Chem., 57 (1985)*

Integrated, Multiple-Stage Chromatographic Method for the Separation and Identification of Polycyclic Aromatic Hydrocarbons in Complex Coal Liquids 633

Reduction in the chemical complexity of the neutral PAH fraction is achieved using fractional distillation, adsorption chromatography, and reverse-phase HPLC techniques. Identification of components in the subfractions is performed by capillary GC, GC/MS, and direct-probe MS.

Richard B. Lucke*, Douglas W. Later, Cherylyn W. Wright, Edward K. Chess, and Walter C. Weimer, Chemical Methods and Kinetics Section, Pacific Northwest Laboratory, Operated by Battelle Memorial Institute, Richland, Wash. 99352 *Anal. Chem., 57 (1985)*

Mathematical Modeling of Temperature Programmed Capillary Gas Chromatographic Retention Indexes for Polychlorinated Dibenzofurans 640

A simple 10-parameter mathematical model based on molecular structure can predict the retention indexes of 135 PCDFs with a SD of ± 7 index units.

Michael D. Hale, Fred D. Hileman*, Thomas Mazer, Traci L. Shell, Roy W. Noble, and Joseph J. Brooks, Monsanto Company, Dayton Laboratory, 1515 Nicholas Road, Dayton, Ohio 45418 *Anal. Chem., 57 (1985)*

Determination of Volatile Organics in Sediment at Nanogram-per-Gram Concentrations by Gas Chromatography 648

Volatile compounds are stripped from sediment samples onto a Porapak N cartridge and then eluted from the cartridge with methanol. Detection limits are ~ 7 ng/g for photoionization-active and 1 ng/g for electron-capturing analytes.

Thakor A. Amin and Rajinder Singh Narang*, Division of Environmental Sciences, Wadsworth Center for Laboratories and Research, New York State Department of Health, Albany, N.Y. 12201 *Anal. Chem., 57 (1985)*

Synthesis and Properties of High-Temperature Mesomorphic Polysiloxane Solvents: Biphenyl- and Terphenyl-Based Nematic Systems 651

Biphenyl- and terphenyl-based GC stationary phases exhibit broad nematic temperature ranges. The thermal stability and chromatographic efficiency of these phases are comparable to those of commonly used dimethyl- and methylphenylpolysiloxane solvents.

M. A. Apfel, H. Finkelmann, G. M. Janini, R. J. Laub*, B.-H. Lühmann, A. Price, W. L. Roberts, T. J. Shaw, and C. A. Smith, Department of Chemistry, San Diego State University, San Diego, Calif. 92182 *Anal. Chem., 57 (1985)*

Effect of Pulse Parameters on Analyses by Tandem-Cell Gas-Phase Coulometry 659

An unexpected dependence of GPC results on pulse frequency is observed. Several explanations for this behavior are considered.

S. W. Warden, R. J. Crawford, W. B. Knighton, and E. P. Grimsrud*, Department of Chemistry, Montana State University, Bozeman, Mont. 59717 *Anal. Chem., 57 (1985)*

Comparison of Hydrocarbon Composition in Complex Coal-Liquid Samples by Liquid Chromatography and Field-Ionization Mass Spectrometry 666

Hydrocarbon composition data from two nondistillable coal-liquid samples are compared graphically to illustrate major and minor differences between the samples.

Todd W. Allen and Robert J. Hurtubise*, Department of Chemistry, The University of Wyoming, Laramie, Wyo. 82071, and **Howard F. Silver,** Chemical Engineering Department, The University of Wyoming, Laramie, Wyo. 82071 *Anal. Chem., 57 (1985)*

Identification of Antioxidant and Ultraviolet Light Stabilizing Additives in Plastics by Liquid Chromatography/Mass Spectrometry 672

MS and UV absorbance detectors are operated in series with no significant loss of chromatographic resolution. Nanogram quantities of additives are detected by LC/MS with lower detection limits achieved by use of reconstructed ion chromatograms.

John D. Vargo* and Keith L. Olson, Analytical Chemistry Department, General Motors Research Laboratories, Warren, Mich. 48090-9055 *Anal. Chem., 57 (1985)*

Electrospray Interface for Liquid Chromatographs and Mass Spectrometers 675

Results with several nonvolatile solute species indicate that the system is not prone to fouling and is inherently stable. The ionization efficiency is relatively constant over a wide mass range.

Craig M. Whitehouse, Robert N. Dreyer, Masamichi Yamashita, and John B. Fenn*, Department of Chemical Engineering, Yale University, New Haven, Conn. 06520-2159 *Anal. Chem., 57 (1985)*

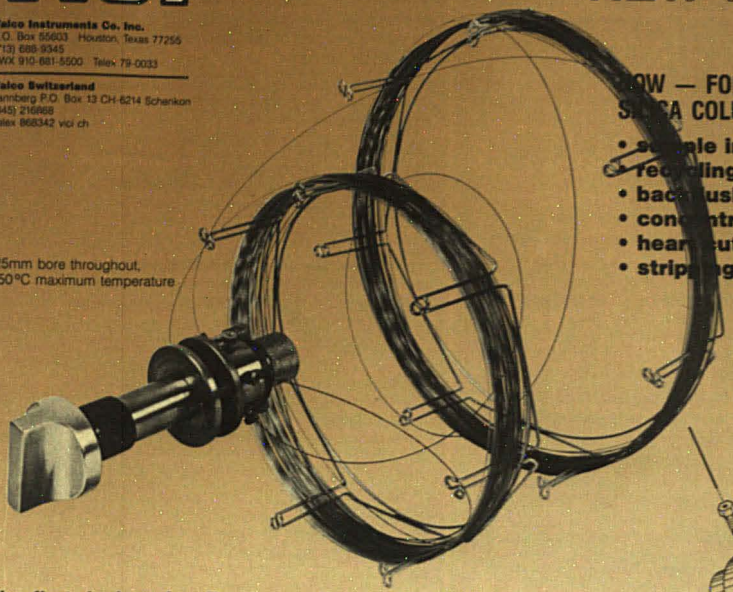
VICI

ANNOUNCING

NEW FOR GC

Valco Instruments Co. Inc.
P.O. Box 55603 Houston, Texas 77255
(713) 688-9345
TWX 910-881-5500 Telex 79-0033

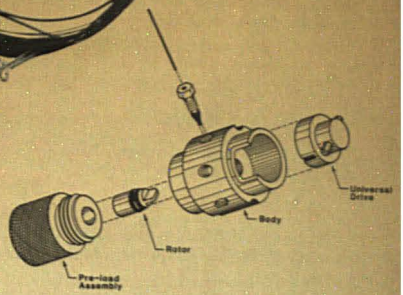
Valco Switzerland
Tannberg P.O. Box 13 CH-6214 Schenkon
(045) 216868
Telex 868342 vici ch



...OW — FOR FUSED ...ICA COLUMNS

- **...ple injection**
- **re...ling**
- **back...ushing**
- **con...ntration**
- **hear...utting**
- **strip...g**

.25mm bore throughout,
350°C maximum temperature

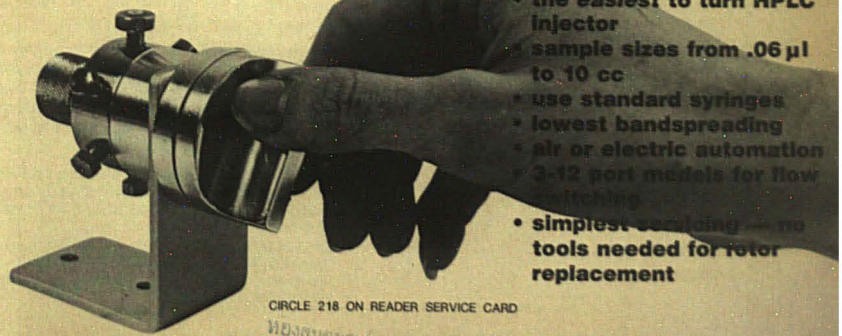


The first devices for direct sampling and switching of fused silica columns are now available from Valco and leading international dealers.

AND

NEW FOR HPLC

The most advanced "user friendly" HPLC sample injection and switching valves.



- **smallest internal volume of any HPLC valve**
- **the *easiest* to turn HPLC injector**
- **sample sizes from .06 µl to 10 cc**
- **use standard syringes**
- **lowest bandspreading**
- **air or electric automation**
- **3-12 port models for flow switching**
- **simplest servicing — no tools needed for rotor replacement**

CIRCLE 218 ON READER SERVICE CARD

Briefs

Comparison of Isopentane and Isobutane as Chemical Ionization Reagent Gases 680

Positive-ion CI spectra and sensitivities using isopentane as the reagent gas are very similar to those obtained using isobutane, although isopentane is more selective. Isopentane can be introduced as a CI reagent without a complex vacuum manifold.

Jeffrey M. McGuire and Burnaby Munson*, Department of Chemistry, University of Delaware, Newark, Del. 19716 *Anal. Chem., 57 (1985)*

Methane Enhanced Negative Ion Mass Spectra of Hexachlorocyclopentadiene Derivatives 684

Mass spectra of 24 bicyclic insecticides are presented. Interpretively useful spectral features are described, and the spectra are compared with previously reported data.

Elizabeth A. Stemmler and Ronald A. Hites*, School of Public and Environmental Affairs and Department of Chemistry, Indiana University, Bloomington, Ind. 47405 *Anal. Chem., 57 (1985)*

Combination of Chemical Reduction and Tandem Mass Spectrometry for the Characterization of Sulfur-Containing Fuel Constituents 692

The middle-distillate fraction of an SRC-II coal-derived liquid is characterized for thiophene derivatives using tandem MS with a calcium/mixed amines reduction system.

Karl V. Wood*, Engine/Fuels Laboratory, Chemistry Building, Purdue University, West Lafayette, Ind. 47907, and **R. Graham Cooks, James A. Laugal, and Robert A. Benkeser**, Department of Chemistry, Purdue University, West Lafayette, Ind. 47907 *Anal. Chem., 57 (1985)*

Identifying Alkylbenzene Isomers with Chemical Ionization–Proton Exchange Mass Spectrometry 694

The number of unsubstituted aromatic carbons in alkylbenzene isomers is determined, and positional isomers are identified. Alkylbenzenes in diesel exhaust are characterized.

Steven B. Hawthorne* and David J. Miller, University of North Dakota Energy Research Center, Box 8213, University Station, Grand Forks, N.D. 58202 *Anal. Chem., 57 (1985)*

Laser Mass Spectra of Simple Aliphatic and Aromatic Amino Acids 698

Quasi-molecular ions, $(M + H)^+$ and $(M - H)^-$, are produced in high yields. The major neutral fragment loss from $(M + H)^+$ corresponds to HCOOH with other acid losses related to the amino group position.

Cass D. Parker and David M. Hercules*, Department of Chemistry, University of Pittsburgh, Pittsburgh, Pa. 15260 *Anal. Chem., 57 (1985)*

Comparison of Canonical Variates Analysis with Target Rotation and Least-Squares Regression as Applied to Pyrolysis Mass Spectra of Simple Biochemical Mixtures 704

Canonical variates analysis is shown to be superior to target rotation or least-squares mixture analysis when replicate information is available.

Lloyd V. Vallis and Halliday J. MacFie*, Agricultural Research Council, Meat Research Institute, Langford, Bristol BS18 7DY, United Kingdom, and **Colin S. Gutteridge**, Cadbury Schweppes PLC, Group Research, Lord Zuckerman Research Centre, The University, Whiteknights, Reading, Berks, United Kingdom *Anal. Chem., 57 (1985)*

Carbon-13 Nuclear Magnetic Resonance Spectrometric and Gas Chromatography/Mass Spectrometric Characterization of Lipids in Corn Suspension Cells 710

Carbon-13 NMR shows >90% conversion of labeled oleate to linoleate after 24 h whereas GC/MS analysis suggests oleate/linoleate ratios can be used to characterize the neutral and polar lipids.

Dennis James Ashworth*, Douglas Owen Adams, Benjamin Yunwen Giang, Michael Tung-hai Cheng, and Rino Yul Lee, Western Research Center, Stauffer Chemical Company, 1200 South 47th Street, Richmond, Calif. 94804 *Anal. Chem., 57 (1985)*

Application of Auger Electron Spectrometry to Trace Analysis: Determination of Less Than 10 ppm Sulfur in Copper 716

Surface segregation kinetic measurements by AES combined with Ar ion sputtering are used to determine 4 ppm sulfur in copper with accuracy of ±10% and precision of ±0.5%.

Siegfried Hofmann* and Roland Frech, Max-Planck-Institut für Metallforschung, Institut für Werkstoffwissenschaften, Seestrasse 92, D-7000 Stuttgart 1, West Germany *Anal. Chem., 57 (1985)*

Two-Column Method for Preconcentration of Trace Metals in Natural Waters on Acrylate Resin 719

Trace metals in seawater and lakewater are concentrated on an XAD-7 resin column at pH 8 after interfering humic materials are removed.

Chi-Chung Wan, Solomon Chiang, and Alfio Corsini*, Department of Chemistry, McMaster University, Hamilton, Ontario, Canada L8S 4M1 *Anal. Chem., 57 (1985)*

Preconcentration of Cadmium from Highly Acidic Saline Solutions and Direct Determination of Bismuth, Cadmium, Mercury, Antimony, Tin, and Thallium in Highly Acidic Aqueous Solutions with Electrically Vaporized Thin Gold Film Atomic Emission Spectrometry 724

Batch separation and preconcentration with a micro-bed strong-base anion exchange resin allow determination of Cd(II) in complex acidic solutions at the 10-ppb level with 8% relative error.

Stephen W. Brewer, Chemistry Department, Eastern Michigan University, Ypsilanti, Mich. 48197, and **Richard D. Sacks***, Department of Chemistry, University of Michigan, Ann Arbor, Mich. 48109 *Anal. Chem., 57 (1985)*

PHARMACEUTICAL

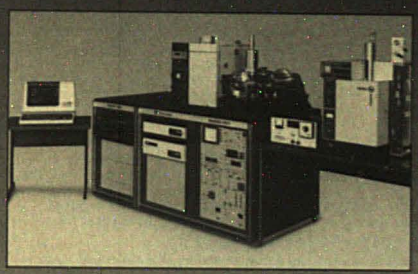
Thermospray

LC/MS

*Analyze Labile Samples
*Picogram Sensitivity.

The thermospray interface from Vestec* now makes it practical to do direct LC/MS analysis with picogram sensitivity. Compared to previous techniques it's so simple, you just add water!

Just Add Water



EPA

Automated

GC/MS/DS

*Meets All EPA Requirements
*Easy To Operate and Maintain

Load up the auto sampler, type in your sample info., and start the run. The system reports the results in EPA format. You can be assured of accurate, reliable results—everytime. For EPA water analysis . . . you only need to add the water!



Just Add Water

Extranuclear

Manufacturers of quality MS instrumentation for over 20 years.

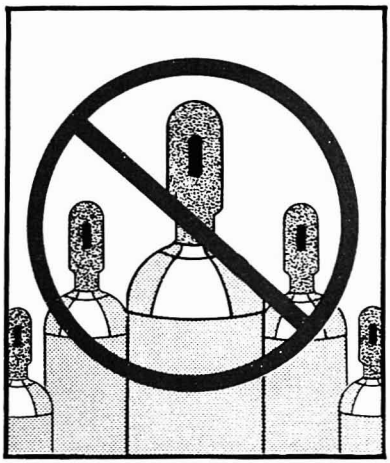
P.O. Box 11512 Pittsburgh, PA 15238
(412) 782-3884
Telex: 812-316 Extralab Pgh

* Vestec is a trademark of Vestec Corp.

Circle 51 for literature.

Circle 52 for sales representative to call you.

STOP
BUYING HYDROGEN
GENERATE YOUR OWN



The Packard® 7525 Hydrogen Generator produces 99.992% pure hydrogen using only deionized distilled water and a standard AC power source. A unique, patented solid polymer electrolyte based on General Electric's proven membrane electrolysis design uses no caustic soda, and eliminates gas stream contamination. The system provides 60 psig at a flow rate of 225 mL per minute — the perfect solution to the demands made for high purity hydrogen needed to feed your gas chromatograph.

Our electrolyte technology is providing safe and reliable operation in thousands of installations throughout the world.

Start producing your own hydrogen today. For a list of selected distributors, call or write: Packard Instrument Company, 2200 Warrenville Road, Downers Grove, IL 60515, U.S.A. Tel. (312) 969-6000. Packard Instrument B.V. P.O. Box 519, 2600 AM Delft, The Netherlands.

"Advancing science in over 50 countries around the world."

UNITED TECHNOLOGIES PACKARD

CIRCLE 171 ON READER SERVICE CARD

Briefs

Performance Studies under Flow Conditions of Silica-Immobilized 8-Quinolinol and Its Application as a Preconcentration Tool in Flow Injection/Atomic Absorption Determinations 729

Breakthrough capacity is evaluated under different flow, temperature, and geometric characteristics of the preconcentrating column. On-line preconcentration of Cu(II) in EPA water samples and tap water is reported.

Monte A. Marshall and Horacio A. Mottola*, Department of Chemistry, Oklahoma State University, Stillwater, Okla. 74078
Anal. Chem., 57 (1985)

Automated Iodometric Method for Determination of Trace Chlorate Ion Using Flow Injection Analysis 734

Two FIA methods for the determination of chlorate ion in drinking water are presented. The underlying chemical reactions and interactions of oxychlorine species are described.

Kevin G. Miller, Gilbert E. Pacey*, and Gilbert Gordon, Department of Chemistry, Miami University, Oxford, Ohio 45056
Anal. Chem., 57 (1985)

Determination of Nitrate by a Flow System with a Chemiluminescent NO_x Analyzer 737

Improved sensitivity is achieved for nitrate determination by reduction of nitrate to nitric oxide. The detection limit is 1 ng NO_3^-/mL for a 5-mL sample.

Kunio Yoshizumi* and Kazuyuki Aoki, Tokyo Metropolitan Research Institute for Environmental Protection, 2-7-1 Yuraku-cho, Chiyoda-ku, Tokyo 100, Japan, and **Toshikazu Matsuoka,** Department of Applied Science, Tokyo Denki University, 2-2 Kandanishiki-cho, Chiyoda-ku, Tokyo 101, Japan, and **Shukuji Asakura,** Department of Safety Engineering, Yokohama National University, 156 Tokiwadai, Hodogaya-ku, Yokohama 240, Japan
Anal. Chem., 57 (1985)

Estimation of Acidity in Rainfall by Electrical Conductivity 740

Measurement of electrical conductivity of rain samples before and after passage through an H^+ exchanger allows calculation of acidity and salinity.

Robert A. Stairs* and Jaleh Semmler, Department of Chemistry, Trent University, Peterborough, Ontario, Canada K9J 7B8
Anal. Chem., 57 (1985)

Hydration of Nitric Acid and Its Collection in the Atmosphere by Diffusion Denuders 743

Field and laboratory studies on the collection of nitric acid with tungstic acid and nylon denuders show that the species collected is $HNO_3 \cdot xH_2O$ (g). Collection efficiency of tungstic acid is affected by water vapor.

Delbert J. Eatough*, Vernon F. White, and Lee D. Hansen, Thermochemical Institute and Department of Chemistry, Brigham Young University, Provo, Utah 84602, and **Norman L. Eatough,** Department of Chemistry, California State Polytechnical University, San Luis Obispo, Calif. 93407, and **Elizabeth C. Ellis,** Southern California Edison, Rosemead, Calif. 91770
Anal. Chem., 57 (1985)

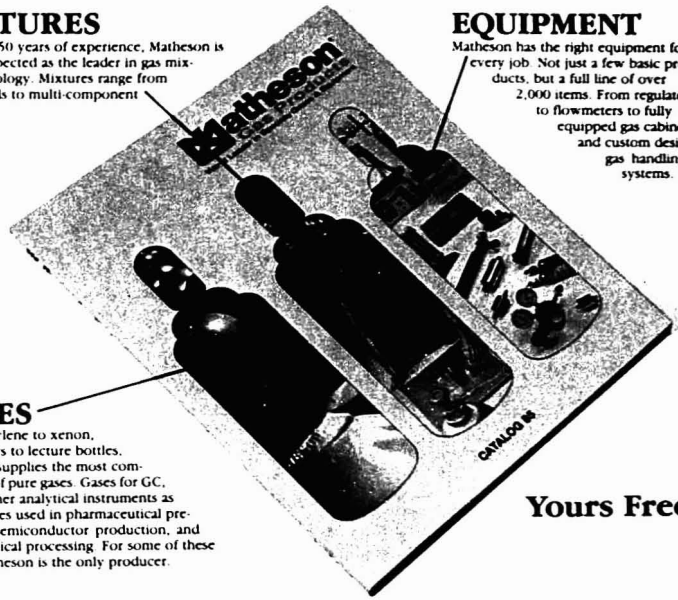
Three good reasons to follow the leader

MIXTURES

With over 50 years of experience, Matheson is widely respected as the leader in gas mixture technology. Mixtures range from basic blends to multi-component standards.

EQUIPMENT

Matheson has the right equipment for every job. Not just a few basic products, but a full line of over 2,000 items. From regulators to flowmeters to fully equipped gas cabinets and custom designed gas handling systems.



GASES

From acetylene to xenon, tube trailers to lecture bottles, Matheson supplies the most complete line of pure gases. Gases for GC, AA and other analytical instruments as well as gases used in pharmaceutical preparation, semiconductor production, and petrochemical processing. For some of these gases, Matheson is the only producer.

Yours Free!

Introducing Catalog 85 from Matheson, The World Leader in Speciality Gases and Equipment.

This Catalog introduces many new products. You'll find new purification devices like membrane filters and a 200 cfh hydrogen purifier, improved gas specifications like Chlorine, 99.99% and Boron trichloride 99.999%, electronic vacuum gauges, gas detectors, large capacity flowmeters and much more. This is the most complete specialty gas and equipment line to be featured in one catalog.

Virtually every significant advancement is specialty gas technology is a result of innovations developed by Matheson. Perhaps that's why our products flew with Apollo and climbed Mount Everest. They are used in virtually every university, to control petrochemical processes and as key ingredients in pharmaceutical and chemical processes. For over 50 years Matheson Specialty Gases and Equipment have supported research and development efforts worldwide.

To get your free copy of Catalog 85, call your nearest Matheson branch or circle the readers service card.

Matheson
Gas Products
World Leader in Specialty Gases & Equipment
30 Seaview Drive, Secaucus, NJ 07094

CIRCLE 138 ON READER SERVICE CARD



OMA III

The OMA III family is the culmination of over ten years experience in building and using optical multichannel analyzers.

The Model 1460 OMA III is our own 68000 based system processor designed specifically for extremely rapid parallel spectral data acquisition, analysis and presentation.

Our Model 1461 Detector Interface is designed to connect any of our solid state multichannel detectors to virtually any computer. The Model 1461 is easily programmed using high level mnemonic commands over RS232 or IEEE.



- Detectors include Diode Arrays and Vidicons.
- Soft-touch screen, IEEE, RS232, VME Expansion Capability.

EG&G
PRINCETON APPLIED RESEARCH
P.O. BOX 2565 • PRINCETON, NJ 08540, U.S.A. • 609/452 2111 • TELEX 843409

682

See us at the APS Show in Baltimore, MD March 26-28, Booth #'s 146 & 147

CIRCLE 47 ON READER SERVICE CARD

Briefs

Solution Studies of Systems with Polynuclear Complex Formation: Copper(II) and Cadmium(II) D-Gluconate Systems 749

Combined pH and pM measurements are used to study Cu^{2+} and Cd^{2+} systems. Dilution experiments indicate that dimeric species form in solutions containing an excess of the ligand.

Kjell Blomqvist and Ebbe R. Still*, Department of Chemistry, Åbo Akademi, SF-20500 Åbo 50, Finland *Anal. Chem., 57 (1985)*

High-Sensitivity Spectroelectrochemistry Based on Electrochemical Modulation of an Absorbing Analyte 752

A modulated potential is used to generate and remove the absorber, leading to a modulation diffraction intensity that is linearly related to concentration. The detection limit for trianisylamine in acetonitrile is 2×10^{-8} M.

Chwu-Ching Jan, Barry K. Lavine, and Richard L. McCreery*, Department of Chemistry, The Ohio State University, 140 West 18th Avenue, Columbus, Ohio 43210 *Anal. Chem., 57 (1985)*

Pulsed Infrared Laser Thermal Lens Spectrophotometry of Flowing Gas Samples 758

The TLS signal is found to be independent of the flow rate at all flow rates studied. The possibility of using this technique as a chromatographic detector for ultratrace amounts of analyte is also discussed.

Scott L. Nickolaisen and Stephen E. Bialkowski*, Department of Chemistry and Biochemistry, Utah State University, Logan, Utah 84322 *Anal. Chem., 57 (1985)*

Analysis of Polynuclear Aromatic Mixtures by Liquid Chromatography/Mass Spectrometry 763

Use of HPLC/MS for the determination of PAHs is discussed in terms of eluant composition and flow. Precision and accuracy are also evaluated.

Kenneth J. Krost, U.S. Environmental Protection Agency, Environmental Monitoring Systems Laboratory, Research Triangle Park, N.C. 27711 *Anal. Chem., 57 (1985)*

Correspondence

Ionization and Mass Analysis of Nonvolatile Compounds by Particle Bombardment Tandem-Quadrupole Fourier Transform Mass Spectrometry 765

Donald F. Hunt* and Jeffrey Shabanowitz, Department of Chemistry, University of Virginia, Charlottesville, Va. 22901, and **Robert T. McIver, Jr.* and Robert L. Hunter,** Department of Chemistry, University of California, Irvine, Calif. 92717, and **John E. P. Syka,** Finnigan-MAT Corp., 355 River Oaks Parkway, San Jose, Calif. 95134 *Anal. Chem., 57 (1985)*



- **Microprocessor controlled.**
- **Rapid . . . Results in 140 seconds.**
- **Compact . . . High power furnace plus determinator in a single bench-top instrument.**
- **Versatile . . . Accurate results regardless of the percentage of carbon contained in the sample.**

The always reliable WR-12 has been updated to include a high power furnace, microprocessor electronics, and a built-in printer. Whether you analyze catalysts or marine sediment, metal carbides or irons and steels, the new WR-112 determines the carbon content within ±0.5% of carbon present.

Microprocessor control means easy one-step operation and automatic calculation. Simply raise the sample into position in the furnace to start the analysis. Weight compensation and calibration factors are applied to results automatically. Self Diagnostics assure the operator that systems are within assigned parameters at all times and alert him if changes occur.

A convenient interface for a LECO® analytical balance is provided. This allows weight resolution to four decimal places, with automatic tare if desired.

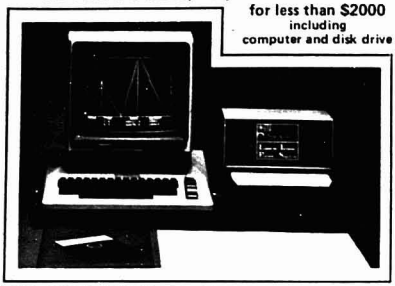
To learn more about this new LECO® instrument, call or write today!

LECO®

LECO CORPORATION
3000 Lakeview Avenue
St. Joseph, MI 49085-2396
(616) 983-5531
Cable: LECO
Telex: 72 9411

CIRCLE 125 ON READER SERVICE CARD

LABORATORY INTERFACE PERIPHERAL SUBSYSTEM
AUTOMATE SPECs, GCs, GEL SCANNERs
for less than $2000
including
computer and disk drive



CHROMATOGRAPHY SOFTWARE — Auto or manual peak detection and integration. Store and retrieve scan on floppy.

16 BIT ADCs — Four independent channels of 16 bit ADCs giving 1 part in 65000 resolution throughout ADC span. (Other mfgrs. use 12 bit ADCs resolving to only 1 part in 4096.) Differential inputs with dedicated integrator for each channel for optimum noise rejection. Full-scale sensitivities of 10 mv to 10 volts available.

DIGITAL I/O — 24 lines of digital input/output included.

DAC CHANNELS — Optional analog output with full-scale voltages of 1 to 15 volts for controlling devices or data output.

HIGH RESOLUTION — VERSATILE COMPLETE — 4 channels of ADC with digital I/O and chromatography software for only $1185.

205 Weaver Street / Carrboro, N.C. 27510
(919) 929-5001 for more information

SPECTROFUGE
CORPORATION OF NORTH CAROLINA, INC.

CIRCLE 196 ON READER SERVICE CARD

NEWS from the
KRATOS HPLC APPLICATION LAB

Ask for any of these FREE HPLC Lab Reports:

UROPORPHYRINS Circle No. 112	GLYPHOSATE Circle No. 113
AMINO GLYCOSIDES (GENTAMYCIN) Circle No. 114	PEPTIDES Circle No. 115

Ask for details on this or other pioneering HPLC Applications from Kratos
Call or Write:

KRATOS ANALYTICAL
a division of SPECTROS
170 Williams Drive • Ramsey, N.J. 07446
Telephone: 201/934-9000 • Telex: 6853505

Briefs

Hollow Fiber Postcolumn Reactor for Liquid Chromatography 768
James C. Davis* and Dennis P. Peterson, Dow Chemical USA, Midland, Mich. 48640 *Anal. Chem., 57 (1985)*

Adding Forward Searching Capabilities to a Reverse Search Algorithm for Unknown Mass Spectra 771
Douglas B. Stauffer and Fred W. McLafferty*, Chemistry Department, Cornell University, Ithaca, N.Y. 14853, and **Robert D. Ellis and David W. Peterson,** Scientific Instrument Division, Hewlett-Packard, 1501 California Avenue, Palo Alto, Calif. 94304 *Anal. Chem., 57 (1985)*

Trace Element Determination in Flames by Laser Enhanced Ionization Spectrometry 773
Ove Axner, Ingvar Lindgren, Ingemar Magnusson, and Halina Rubinsztein-Dunlop*, Department of Physics, Chalmers University of Technology/University of Gothenburg, S-412 96 Göteborg, Sweden *Anal. Chem., 57 (1985)*

Differentiation of Cationic from Neutral Transition-Metal Complexes Using Wires as Field Desorption Emitters 776
Steve E. Unger, The Squibb Institute for Medical Research, P.O. Box 4000, Princeton, N.J. 08540 *Anal. Chem., 57 (1985)*

Aids for Analytical Chemists

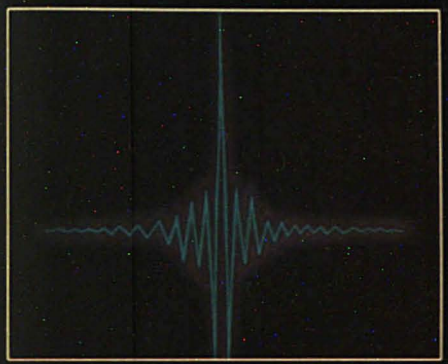
Modified Interface for Pyrolysis Gas Chromatography with Capillary Columns 778
Robert S. Whiton and Stephen L. Morgan*, Department of Chemistry, University of South Carolina, Columbia, S.C. 29208 *Anal. Chem., 57 (1985)*

Anion Contamination of Environmental Water Samples Introduced by Filter Media 780
P. C. Jay, Environmental Research Branch, Atomic Energy of Canada Limited, Chalk River Nuclear Laboratories, Chalk River, Ontario, Canada K0J 1J0 *Anal. Chem., 57 (1985)*

Corrosion Resistant Coating for Laboratory Equipment 782
Larry P. Morgenthaler* and Armand F. Lange, Jr., Quality Assurance Laboratory, University of Nevada at Las Vegas, 4505 Maryland Parkway, Las Vegas, Nev. 89154 *Anal. Chem., 57 (1985)*

Two-Phase Titration of Poly(oxyethylene) Nonionic Surfactants with Tetrakis(4-fluorophenyl)borate 783
Masahiro Tsubouchi*, Nakamichi Yamasaki, and Kazumichi Yanagisawa, Laboratory of Chemistry, Kochi Medical School, Nankoku, Kochi 781-51, Japan *Anal. Chem., 57 (1985)*

BOMEM



Interferogram of a crystal taken through a 12 micron pinhole, no beam condensing, 300-400 nm.

elegant FTIR

the DA3.10 – THE BEST ALTERNATIVE
From the FAR IR to the UV, the DA3.10 gives you the power of FT techniques for your analyses.

AQUEOUS SAMPLES long a problem for IR, are now routine when you use commercial accessories in the DA3.10.

MICROSAMPLES as small as 10 microns can be analysed without delicate beam condensers.

POWDERS are easily analysed by reflectance, pellets, or other techniques.

POLYMERS and other samples requiring time resolved and/or temperature controlled studies are swiftly examined with the DA3.10's Vacuum or purge modes.



Powerful Library Search Routines for fast identification



Bomem Inc., 625, Marais, Vanier, Québec G1M 2Y2 (418) 683-1707 Telex: 051-3438

INTRODUCING GALAXY™ BALANCES. EASY TO USE. EASIER TO READ. AND AS PRECISE AS YOU ARE.

Sleek, slim and sophisticated. The new GALAXY™ electronic analytical and toploading balances. The first laboratory balances created with *your* needs in mind.

Fast and dependable, our new GALAXY™ balances offer the weighing precision you need. And, we've incorporated every major feature you'll ever need — or want — into all models.

GALAXY™ balances represent precision from a new perspective. At a price you can afford. From the American manufacturer who sells more laboratory balances than any other. Ohaus.

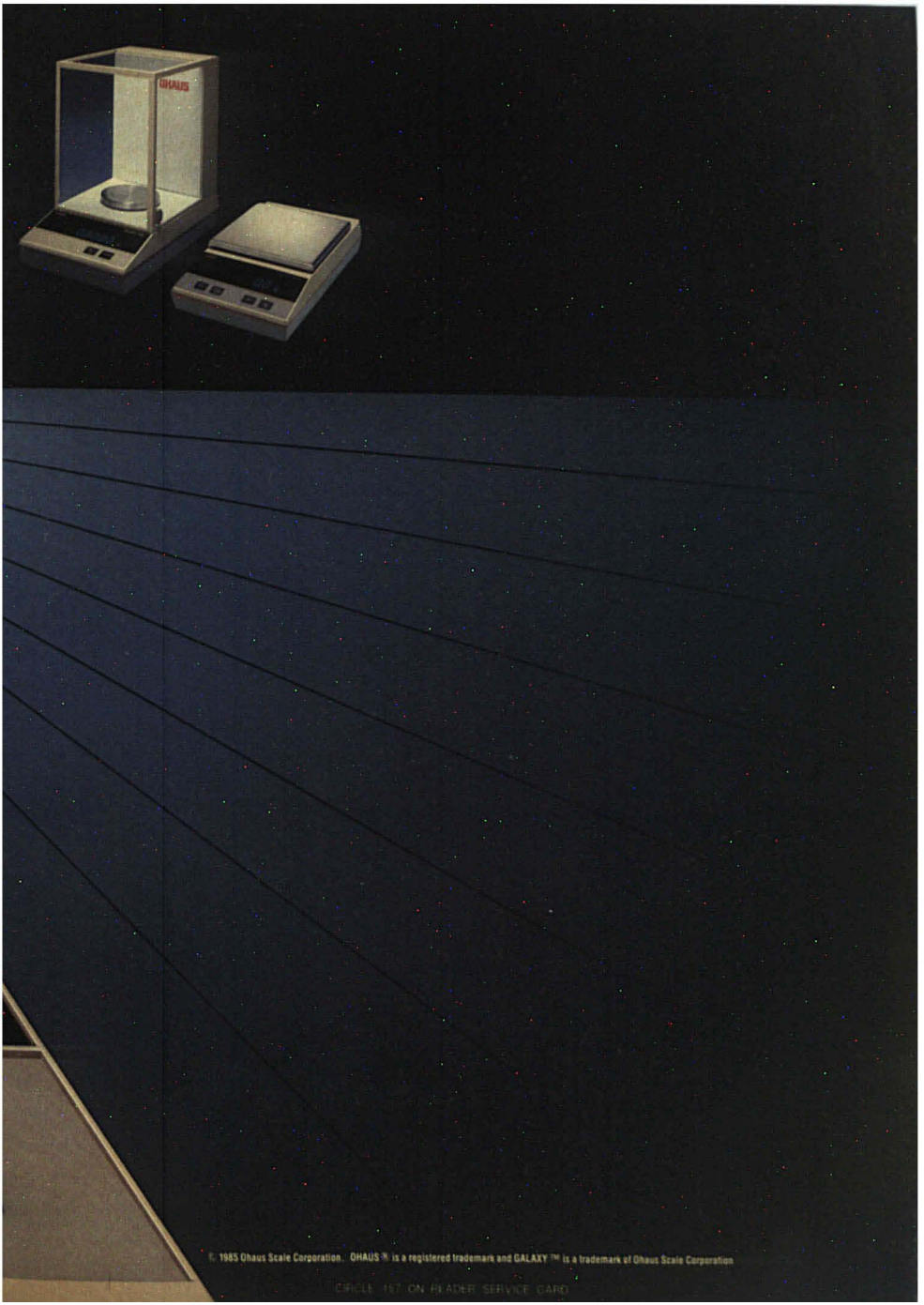
Call 800-672-7722 today for a demonstration. And discover laboratory balances as precise as you are!

Ohaus Scale Corporation, 29 Hanover Road, Florham Park, New Jersey 07932

OHAUS

THE NEW POWERHOUSE IN ELECTRONIC BALANCES.



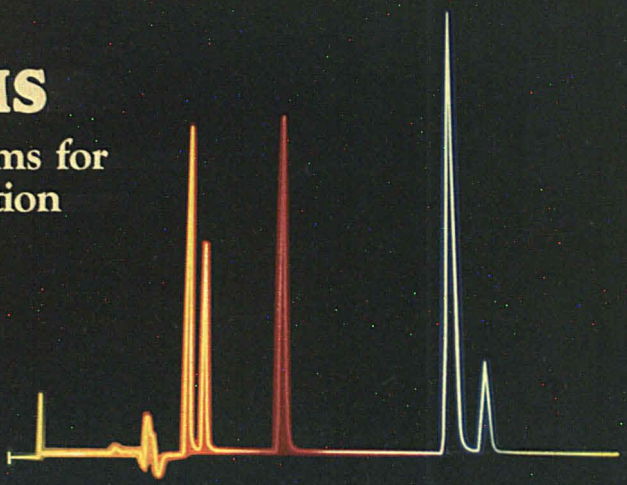


© 1985 Ohaus Scale Corporation. OHAUS ® is a registered trademark and GALAXY ™ is a trademark of Ohaus Scale Corporation

CIRCLE 157 ON READER SERVICE CARD

HPLC SYSTEMS

Flexible systems for every application



BIORESEARCH - Amino Acids • Proteins • Peptides

FOOD/AGRICULTURE - Pesticides • Herbicides • Carbohydrates Vitamins

CLINICAL - Therapeutic Drug Monitoring • Catecholamines Forensics

INDUSTRIAL - Polymers • Organic Synthesis • Process Chemistry Chemical Formulations

ENVIRONMENTAL - Wastewater Treatment • Trace Analysis

For more information call LDC/Milton Roy



LDC/Milton Roy

U.S. HEADQUARTERS, P.O. Box 10235, Riviera Beach, FL 33404 Toll-free: 800-327-6182, In Florida: (305) 844-5241 Telex: 441098
UNITED KINGDOM, LDC UK, Milton Roy House, 52 High Street, Stone, Staffordshire ST15 8AR England Telephone: (0) 785-81-3542 Telex: 36623
FRANCE, LDC S.A., 15 rue Guyton de Morveau, Paris 75013, France Telephone: 588-2800 Telex: 205331
WEST GERMANY, Milton Roy (Deutschland) GMBH Jahnstrasse 22-24 6467 Hasselroth 2, West Germany Telephone: (0) 6055-3366 (2031) Telex: 4184357
JAPAN, Milton Roy K.K., Takanawa Dai-Ichi Building 21-41, Takanawa 2-Chome, Minato-Ku, Tokyo 108, Japan Telephone: (03) 473-3181 Telex: 242-4296

CIRCLE 126 ON READER SERVICE CARD

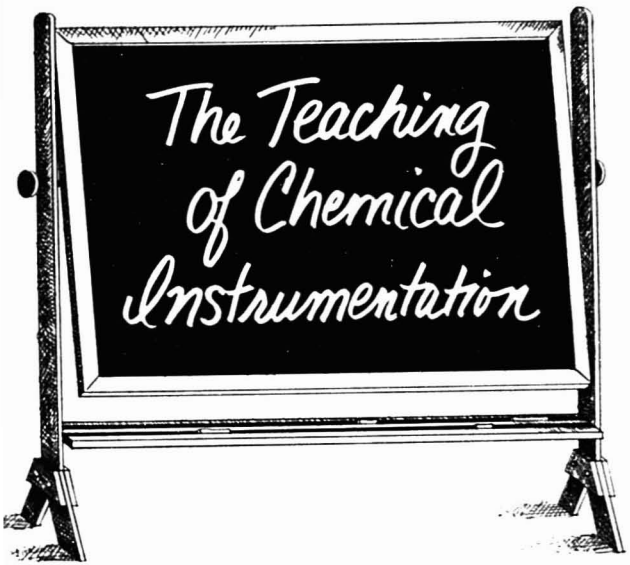
Report

Galen W. Ewing *

Benedict Visiting Distinguished Professor
Carleton College
Northfield, Minn.

Maarten van Swaay

Professor of Computer Science
Kansas State University
Manhattan, Kan.



The subject of instrumentation is of such importance in modern chemistry that teaching about it on both the undergraduate and graduate levels is essential to all disciplines in which chemistry plays a part. This REPORT explores some of the questions and dilemmas facing those who teach the subject and those who establish undergraduate curricula in chemistry.

Separate courses in instrumental analysis, as they were developed soon after World War II, generally paid scant attention to the basic chemistry of analytical procedures. Often only a few commercial instruments, such as pH meters and photoelectric photometers, were available for student use, and much time was spent on the design of home-built apparatus. Other types of instruments, such as spectrographs and polarographs, could be treated only as library research projects. There seemed to be no way to integrate this material with classical analysis.

Over the years, as more and more instruments were developed, it became less realistic to maintain artificial barriers between "instrumental" and "noninstrumental" analysis. Nevertheless, this dichotomy has been perpetuated in many institutions for reasons of expediency.

One factor with far-reaching ramifications has been the extensive treatment of certain instrumental techniques in college courses that are not labeled as "analytical." This trend originated long ago with the study of spectroscopic methods in connection with the elucidation of atomic and molecular structure, as presented in the physical chemistry course. It has been accentuated by the reliance of organic chemists on data from absorption spectroscopy, NMR, and mass spectrometry. Thus it has become convenient for curriculum planners to assume that all the necessary information about these important techniques is adequately covered in other courses.

At first glance, this would seem to be an efficient and satisfactory arrangement, wherein each technique is taught by those most interested in its application. The danger is, however, that students will be led to take for granted the internal operation of instruments, without adequate appreciation of their limitations. Additionally, the instructor in organic chemistry may have neither the time nor the interest in the theory of instrumentation to enter into a detailed examination of alternative instrument designs. It seems clear to us that instrumental analysis should always be taught by an analytical chemist.

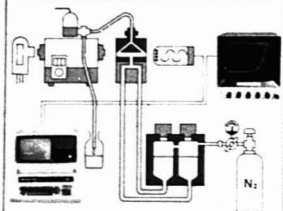
In some institutions an attempt has been made to integrate instrumental and classical analytical techniques into a single course, typically under a title such as "Quantitative Chemistry." The presentation can then be problem oriented, making use of any appropriate techniques, whether classical or instrumental. This has the great advantage of more closely duplicating real-life situations that an analytical chemist is likely to encounter, in which he or she must select as well as implement the method to be used to solve a problem most effectively. However, this may result in a course that is too long to fit readily into the curriculum.

Hence in many schools two separate courses persist. The instrumental segment invariably comes later in the student's program than the conventional "quant" course, thus taking advantage of greater preparation in physics and physical chemistry. This course may or may not be required of chemistry majors and is seldom taken by biology or premedical students.

* Present address: P.O. Box 2573, Las Vegas, N.M. 87701

0003-2700/85/0357-385A$01.50/0
© 1985 American Chemical Society

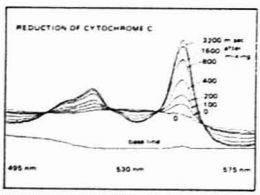
UNION GIKEN
First choice for
STOPPED FLOW
reaction analysis



Union Giken apparatus achieves a dead time as short as ½ millisecond for measurement of fast reactions. Gas pressure is directly applied to the surface of the reactants in each reservoir, mixing and flow being controlled from the end of the system by a high-response stop valve. The RA-401 STOPPED FLOW SPECTROMETER is the ideal match for fast reactions.



The RA-451 DATA PROCESSOR generates a simulated reaction curve from the measured results and automatically calculates the rate constant.



The RA-415 RAPID SCAN ATTACHMENT monitors the change in absorption spectrum during the reaction.

Other attachments are available for T-jump, P-jump, fluorescence and flash photolysis.

Contact the sole export agent for more details:—

ATAGO BUSSAN CO., LTD.
7-23, 5-chome Shimbashi, Minato-ku,
Tokyo 105, Japan
Telex: 28421 Cable: TAGOA TOKYO
Phone: (03) 432-8741

CIRCLE 1 ON READER SERVICE CARD

The instrumental analysis course

Let us assume, then, that the instrumental aspects of analytical chemistry will be taught in a separate course. What should be included and what omitted?

The necessary compromise between breadth and depth presents a knotty problem. Should we be satisfied with a relatively superficial treatment of many types of instrumentation, or would it be preferable to select a few areas and explore them more fully? One possibility that may be attractive to the professor is to treat in considerable detail one or two subjects with which he or she feels most at home. The hope then is that the general method of approach developed here can readily be adapted to other disciplines. This may, however, give the student a distorted view of the relative importance of various techniques.

No matter what approach is adopted, there must be a decision as to the degree of mathematical and physical detail to be introduced. Should all equations be rigorously derived, or should those of lesser pertinence be taken on faith, with references given to more complete coverage in the literature?

For example, Fick's laws of diffusion as applied to polarography can easily be used without theoretical background, but a rigorous derivation of the Ilkovic equation is essential. Few chemistry teachers would attempt to explain in detail the algorithm for the fast Fourier transform or the detailed theory of the Michelson interferometer as necessary background for a discussion of FT-IR.

The real question is where to draw the line, and this is a decision that must be left to the professor. He or she will, no doubt, take into account the available textbooks, and there is quite a variety from which to choose. The professor may prefer a text that includes in an encyclopedic manner a great deal of factual and theoretical material, including the derivation of all significant mathematical relations from first principles. Such a text can hardly be covered in toto in a one- or even two-semester course, so that the instructor must specify which chapters or portions of chapters will be included. On the other hand, it is possible to choose a text that presents the framework on which the instructor can hang as much or as little detail as seems desirable, often amplifying the textual material in his or her own field of expertise.

The treatment of each type of instrument should stress the flow of information from the chemical domain, via a transducer and suitable electronics and data processing, to a final report in a form that is directly meaningful to the ultimate user. The limitations of each instrument should be presented in a format that permits easy intercomparisons of parameters such as signal-to-noise ratio, sensitivity, achievable limits of detection, and speed of measurement.



Instruments for teaching laboratories are likely to be old models, donated to the school by local industries that see a chance to combine academic goodwill with a sizable tax writeoff.

The laboratory

Curriculum planners must decide whether or not to include laboratory sessions specifically tied to instrumentation. Some top-rated institutions do not, relying on a generalized "Advanced Lab" course to include sufficient experience with instruments. If a separate laboratory for instrumental analysis is decided on, a question arises regarding the desirable degree of involvement of the student in the design of instruments as contrasted with their use only.

If only commercial instruments are used, experiments must be specifically designed to acquaint the student with



DELTARANGE. MORE ACCURACY AT THE POINT YOU NEED IT.

Accurate weighing is essential for today's scientific and industrial laboratories.

That's the reason Mettler makes DeltaRange® balances, both analyticals and top-loaders. They allow you to do work, on one Mettler, that usually requires two balances.

For example, the most exacting formulations can be made quickly and precisely on a Mettler DeltaRange balance. The DeltaRange feature increases the readability of our PE360 ten times, moves it from 10 mg to 1 mg, with just a touch of the control bar. And this moveable 60 g fine range goes throughout the balance's entire weighing range, 0-360 g.

As a result, formula weighing can be done quickly. Productivity in your lab goes up. And, at the same time you can be sure the weighing activities are being performed accurately.

Today's Mettler balances have been designed and manufactured to give you what you need in today's laboratories. And, because of the technological advances we've made, your cost of moving to a Mettler is down. You can own a Mettler DeltaRange balance for as little as $1395.

Write to us for information. Mettler Instrument Corporation, Box 71, Hightstown, NJ 08520. Phone (609) 448-3000.

Mettler

CIRCLE 140 ON READER SERVICE CARD

We're giving away our entire product line.



It's all in our free Special Gases & Equipment Catalog. It lists and describes pure, mixed and electronic gases from Argon to Zenon. Plus all the regulators, flowmeters, instrumentation, fittings, cylinders and other gas handling equipment you'll ever need. To get your free copy of everything we sell, just fill out the information below and mail.

Name _____
Title _____
Company _____
Address _____
City _____ State _____
Zip _____ Phone _____

AIRCO

Airco Special Gases, 575 Mountain Avenue
Murray Hill, New Jersey 07974

CIRCLE 5 ON READER SERVICE CARD



A good curriculum should provide students with enough understanding of electronics, mechanics, optics, and computer science to allow them to cooperate effectively with experts in those fields.

the many available modes of operation. A difficulty often encountered with this latter approach is the unavailability of state-of-the-art instruments in purely educational laboratories. In many institutions expensive items are necessarily purchased on research grants and can be used only by participants in the designated research programs. Instruments for teaching laboratories are likely to be old models, donated to the school by local industries that see a chance to combine academic goodwill with a sizable tax writeoff. In this respect some small undergraduate colleges may be better off than their large university neighbors; there is a closeness between students and research projects in the smaller institutions that makes modern instruments available to all if they are present anywhere in the department. Lacking such instruments, the instructor should consider the use of computer simulation—programming a computer to produce data that appear to have come from an analytical instrument.

On the other hand, a modular approach can be adopted. The student is asked to synthesize working instruments from available parts, such as light sources, monochromators, and detectors, together with a large selection of electronic building blocks and measuring gear.

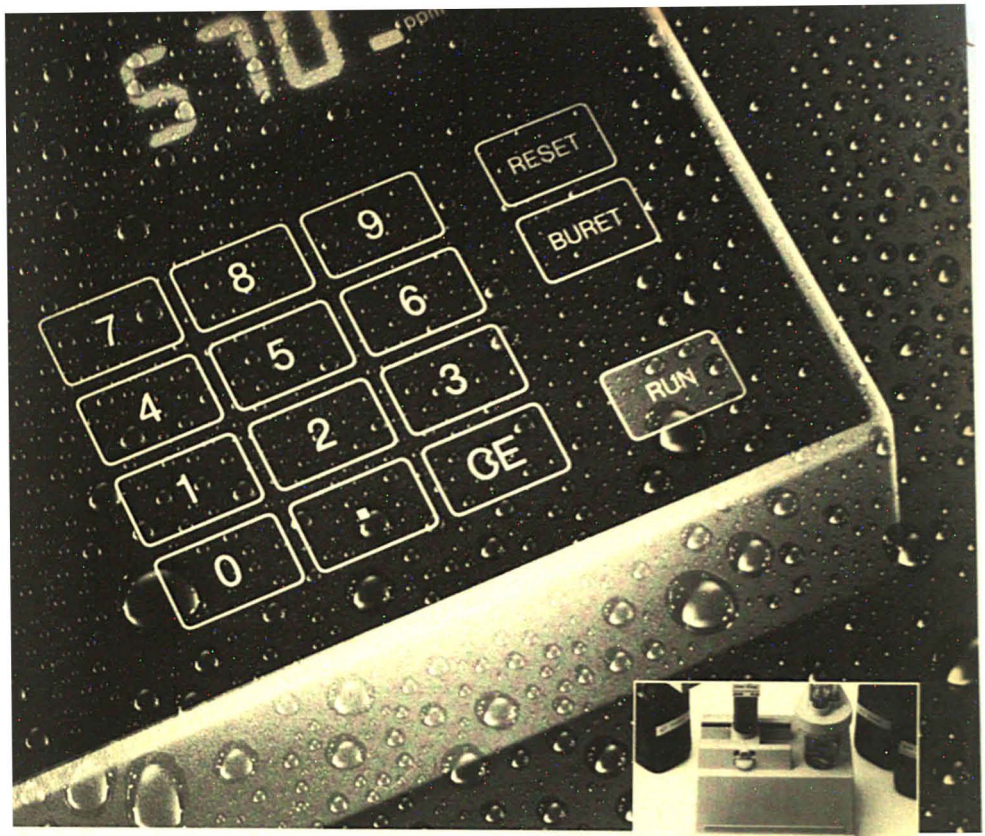
It is obviously impossible to train a student to be a competent mechanic, an up-to-date electronics wizard, an expert in optics, and a polished computer programmer, as well as a good chemist. The ideal is a noble one, but the practice must be more realistic. A good instrumentation curriculum should provide students with enough understanding of the fields of electronics, mechanics, optics, and computer science to allow them to cooperate effectively with experts in those fields.

It is unlikely that a computer scientist will spend the time to learn the details of, for example, NMR, or that an electrical engineer will be familiar with the nonlinear behavior of the impedance of an electrode surface. In contrast, the chemist is invariably confronted with equipment that relies heavily on state-of-the-art electronics, mechanics, and optics. It is therefore incumbent upon chemists to learn enough of the technical fields that they can at least make their wishes known and be able to evaluate with reasonable confidence the tools constructed by their technical friends—to be sure that such tools will fill the requirements of their chemical problems.

Electronics

Over the past 10 years electronics has progressed to the point where the transfer functions of standard and easily used building blocks can be represented by simple mathematical expressions with an accuracy that meets or exceeds that of most of the sensors found in the laboratory. A good grasp of mathematics will then go a long way toward the implementation of many useful pieces of equipment. Similarly, standard digital function blocks allow the construction of impressive pieces of dedicated logic with only modest understanding of the circuitry inside the individual units.

The convenience of standard electronic building blocks has allowed chemistry students to achieve a useful degree of proficiency in their use in a very short time. This apparent success, however, comes at the expense of instilling a false sense of competency. A semester of electronics dealing with potentiostats, integrators, temperature controllers, and digital timers is by no means comparable to a curriculum in electrical engineering. The goal of the electronics exposure thus must





New. The Mettler DL18 automatic Karl Fischer Titrator.

For $3,950 complete...

Accurate Karl Fischer titrations over the full range.

Now, just one microprocessor-controlled instrument gives you water content detection from 1ppm to 100%. The Mettler DL18 Karl Fischer Titrator covers practically all applications previously handled by systems for trace and higher water content analysis.

Fast, easy, accurate.
Karl Fischer titration procedures are routine tasks performed daily in all types of laboratories, from food and chemicals to plastics and petroleum. Obtaining precise information about water content in samples can be a chore. The DL18 turns this into an easily accomplished task, at the push of a button. Automatic results in mg, percent, or ppm of water are quickly and reliably determined. Very simple and extremely accurate.

A complete, clean system.
You don't need expensive accessories when you purchase the DL18. Everything you need is included, even an automatic device for changing the titrant and incidental items, such as titration beakers and drying media.

A complete line.
The DL18 joins the DL40RC all-purpose and DL20 dedicated titrators to provide the most complete and cost-effective solutions to titration problems today. For details call or write Mettler Instrument Corporation, Box 71, Hightstown, NJ 08520. (609) 448-3000.

LIMITED SPECIAL OFFER

14 day **Free** trial evaluation. We know you will be satisfied. If not, simply return it. Ask for details.

Mettler

CIRCLE 141 ON READER SERVICE CARD

THE
STANDARD
OF
HIGH PURITY
HPLC
SOLVENTS
from
American Burdick & Jackson

Specially purified to meet the exacting requirements of HPLC, gas chromatography, fluorescence and spectrophotometric analysis.

Acetone
Acetonitrile UV
Benzene
n-Butyl Alcohol
2-Butanol
n-Butyl Acetate
n-Butyl Chloride
Carbon Tetrachloride
Chlorobenzene
Chloroform
Cyclohexane
Cyclopentane
Decahydronaphthalene
ortho-Dichlorobenzene
Dimethyl Acetamide
Dimethyl Formamide
Dimethyl Sulfoxide
Dioxane
2-Ethoxyethanol
Ethyl Acetate
Ethyl Ether
Ethylene Dichloride
Glyme
Heptane
Hexane UV
Isobutyl Alcohol
Isopropyl Alcohol
Methanol
2-Methoxyethanol
2-Methoxyethyl Acetate
Methyl t-Butyl Ether
Methylene Chloride
Methyl Ethyl Ketone
Methyl Isoamyl Ketone
N-Methylpyrrolidone
Pentane
n-Propyl Alcohol
Propylene Carbonate
Pyridine
Tetrahydrofuran UV
Toluene
1,2,4-Trichlorobenzene
Trichloroethylene
1,1,2-Trichlorotrifluoroethane
2,2,4-Trimethylpentane
Water
ortho-Xylene

For complete information, contact American Burdick & Jackson, 1953 S. Harvey St., Muskegon, MI 49442. Phone: 616 726 3171.

American Burdick & Jackson
Subsidiary of American Hospital Supply Corporation

CIRCLE 3 ON READER SERVICE CARD

be twofold: The student should be convinced that much useful equipment can be created with a very modest amount of circuit design but must also recognize that such results are possible only because the performance of the building blocks available usually far exceeds a student's needs. The design of equipment that approaches the limit of electronic performance will always require competence far beyond what can be offered in a chemistry curriculum.

Computer use

The place of computers in the chemistry environment has changed just as spectacularly as that of electronics, but with entirely different consequences. In contrast with most other equipment, computers can accumulate a mass of recorded data for future digestion. Consequently, computer applications tend to be used not only by the designer and programmer, but also by his or her teammates and successors. This dictates rigid discipline in areas such as program structure and style, data representation, and documentation.

Only a few years ago, the primary use of computers in the chemistry laboratory was for data acquisition. Operating systems would support only a limited set of operations, including storage of data on tape or disks. Inspection and processing of data were almost invariably done in a separate step (off-line) to avoid real-time complications. Consequently the data acquisition could be kept very simple, and any processing of data was effectively shielded from the laboratory environment. The demands on programming skill were correspondingly modest, and most students could create programs that satisfied the needs of their own research or course work. Quite often, however, such programs could only be called disposable: They might be useful to the designer, but they could not be maintained and would invariably contain quirks that precluded their use by others.



The cost of computers has gone down, their performance has improved, and the ambitions of the chemists using them have grown.

Recently, however, the cost of computers has gone down, their performance has improved, and the ambitions of the chemists using them have grown correspondingly. Chemists are no longer satisfied with mere data logging; they wish to control their experiments on the basis of the current data stream. In addition, the convenience of data collection has resulted in rapid accumulation of large files of data that can be managed only with the help of computer search tools and other data-handling techniques. These higher ambitions are directly reflected in program complexity, which in turn requires expanded program investment.

As a result of these developments, chemists now realize that proper programming style and documentation habits are no longer mere buzzwords used by computer scientists, but are becoming a necessary discipline for the chemist who uses a computer. Here again, teachers of instrumentation in chemistry must strike a balance. They can introduce enough material in one semester to allow students to create small programs that will meet their immediate needs, but they cannot hope to train programmers or computer scientists in that time. Unless students are warned explicitly, their success in making a computer obey them may give them an inflated sense of their ability. It is only too easy to find lab drawers full of disks and tapes with undecipherable data that were collected without regard for program discipline.

There can be no doubt that exposure to computers has a place in the chemistry curriculum. It is also true that those aspects that are specific to the laboratory environment (analog-to-digital conversion, experiment synchronization, data representation as x–y plots, and so on) cannot readily be treated in service courses offered by computer science or engineering departments. The limited amount of time available for computers in the chemistry curriculum must be reserved for information that students cannot obtain elsewhere. These might include discussions about interfaces to instruments available in the department and exposure to application software packages that have been developed for such use.

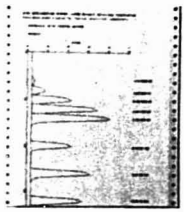
The task of instilling good habits of program style and documentation is

No Other Software Can Turn Your Personal Computer Into A Powerful, Integrated Lab Workstation.

Appligration II, Universal Lab Workstation Software integrates data acquisition, instrument control, data reduction, results reporting, and data communications functions for many instrumental chemistry and experimental tasks. It can be general-purpose, allowing you to design your own analytical procedures by menu or custom program. It can be specific, transforming your computer into a powerful workstation with accessory Appli-Pac software.



Powerful Video Stripchart™ Graphics



Publication Quality Printouts

Appli-Pacs customize the Starter Set for many common applications like GC, LC, HPLC with gradient control, IR, UV/VIS, thermal analysis, continuous-flow analysis, and more. All Appli-Pacs are written in easy to use Chemsoft BASIC. They are made to be modified.

Appligration II works with the best off-the-shelf data acquisition and control products like Cyborg ISAAC, Keithley DAS, and others.

At An Affordable Price Like This.

The Appligration II Starter Set converts your Apple computer into a universal lab workstation that will rival the best. Anywhere. More features. More flexibility. More integrity. More value. The Starter Set is $1995, Appli-Pacs are $495.

For More Information Contact:

Dynamic Solutions Corporation
61 S. Lake Avenue, Suite 305
Pasadena, California 91101
(818) 577-2643, Telex 887571



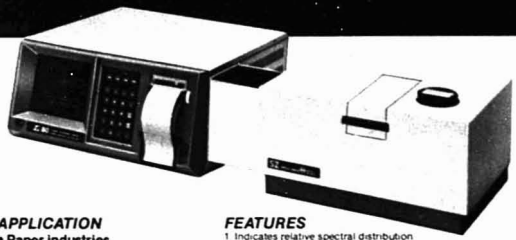
CIRCLE 43 ON READER SERVICE CARD

SZ-Σ80

FOR SCIENTIFIC COLOR CONTROL

SPECTRO COLORI METER

Computerized Color Measuring & Difference Calculating Meter



APPLICATION

- **Paper industries**
- **Metal**
- **Consumer electric appliances**
- **Paint or ink**
- **Food manufacturer**
- **Fishing**
- **Cosmetics**
- **Drug**
- **Dyeing and clothing**
- **Automobile and motorcycle**
- **Dental college or hospital**

FEATURES

1 Indicates relative spectral distribution
2 Color measurement using 3 light sources, A, C, and D65 in 2-degree
3 Allows measurement in 10-degree field under D65
4 Metamerism analyzing capability
5 Standard white plate calibrated according to DIN5033
6 SZ-Σ80 inspected with tinted glass filter (umber, orange, green, and blue, each inspected by Japan Color Research Institute) according to method recommended by Japan Color Science Association of Japan
7 Accuracy: Stability tolerance — Less than 0.2% at full scale of standard white plate (24 hours). Drift — ±0.02 at 0
8 CRT displays relative spectral distribution, color difference analysis chart, and various UCS chromaticity diagrams
9 Amount and orientation of color difference can be verified at a glance. Color names are displayed on the coordinates

We also supply electronic parts

SUN TSUSHO CO., LTD.

6-9, Higashi-kanda 2-chome, Chiyoda-ku, Tokyo 101 Japan TEL: 03-864-8761, TLX: J25638 ZIPANGU, FAX: 03-864-8766

CIRCLE 193 ON READER SERVICE CARD

Our MICRO/IR System runs transmittance or reflectance spectra on samples as small as 10 microns.

Integrated into the powerful Qualimatic FT-IR spectrometer, our MICRO/IR System features a microscope with a horizontal stage up to 6" × 6", a turret of objectives (4x, 32x) for easy sample location and uncompromised performance, Cassagrainian optics, and an integral, permanently aligned 0.25 mm MCT detector.

Send today for our MICRO/IR System Brochure to BIO-RAD, Digilab Division, 237 Putnam Avenue, Cambridge, MA 02139. Or call (800) 225-1248.

BIO-RAD ***Digilab Division***



DIGILAB MICRO FT-IR

...because you never know when you'll need high performance.

CIRCLE 18 ON READER SERVICE CARD

best left to those who have made that their business, namely, the computer scientists. Although many good programmers can be found among chemists, it is unrealistic to expect that such persons will spend their time teaching programming. Such an activity would divert their talents from their primary task, that of teaching and doing research in chemistry. It can be very beneficial, however, to maintain a link between chemistry and computer science in the form of a faculty or staff member who can serve as an interface between the two disciplines. It is important that this be a permanent position: The usefulness of such a person depends crucially on the development of long-term associations both with the needs of the chemistry department and with developments in computer science.

Acknowledgment

The authors wish to acknowledge with thanks suggestions for this article from Professors Edward H. Piepmeier and Frank A. Settle, Jr.



Galen Ewing (right) received his formal schooling at the College of William and Mary and the University of Chicago. His industrial experience includes work at the Sterling-Winthrop Research Institute and at Central Scientific Company. His chief interest, however, has been in education. He has taught at Blackburn and Union Colleges and at New Mexico Highlands and Seton Hall Universities. Now retired, he continues writing textbooks in analytical instrumentation and electronics.

Maarten van Swaay received his education in the Netherlands and at Princeton University. In 1963, he joined the faculty of Kansas State University as an analytical chemist. Over the years, he became progressively more interested in instrumentation and then in computer applications. For the past three years, he has been a full-time member of the Department of Computer Science at Kansas State, still maintaining ties with his former colleagues in chemistry.

VG MANAGER™

The only software manager your lab needs for GC/LC.

The VG MANAGER is a comprehensive package of modular software and hardware, written in Pascal high-level language, that interfaces directly with a wide variety of GCs and LCs to your VAX, PDP11 or PRO380 series computer systems.

Tailored to your needs, the VG MANAGER easily and efficiently organizes your lab, handles data flow of up to 32 channels per system, provides simultaneous multiuser and multitasking operation, and allows the data systems to be networked to each other using Ethernet/DECNet.

As well as foolproof sample identification, easier work scheduling, and automatic data storage, the VG MANAGER offers data processing of shoulder and rider peaks, automatic baseline forcing facilities, user-definable reports and plots, and expand and rescale of chromatograms instantaneously by cursor position on the CRT, among numerous other capabilities.

The most flexible and versatile system available for GC/HPLC, the VG MANAGER can interface and control Thermal Analysis, GPC and Autoanalysis — and the range is expanding constantly.

For more information on the only software manager your lab needs, call VG Instruments (203) 322-4546.



VG INSTRUMENTS

VG Instruments, Inc.
300 Broad Street
Stamford, CT 06901
(203) 322-4546

Mass Spectrometers
Gas Analysis MS
Isotope Ratio MS
LC-MS • MBE • ICP-MS
Ion Beam Lithography

VAX, PDP11, and DECNet are registered trademarks of Digital Equipment Corporation.

CIRCLE 222 ON READER SERVICE CARD


USA
NASA
Challenger
400 ml
PYREX®
USA
No. 1000
ml ©
±5%
50
100
150
200
250

FROM THE BENCHTOP TO THE HEAVENS

70 YEARS OF VISION FROM CORNING

Every view man has ever had from a U.S. ship in space has been through a Corning window. Every manned shuttle has reentered the earth's atmosphere wrapped in a Corning heat-resistant shield. You will soon see the elaborate space telescope launched with a Corning lens inside.

Our special perspective from space sheds light on our total perspective in scientific research and discovery. Our focus in the lab is on quality, innovative products. It's a vision that's evolved for 70 years, ever since we originated the low-expansion borosilicate Pyrex® beaker in 1915.

Our eye on detail and performance led us to develop Accu-Red™ markings to enhance readings and precision.

We put the first hexagonal bases on cylinders for stability. We created chemically strengthened Corex® glass pipets and centrifuge tubes.

Our foresight led us to develop durable Pyroceram® hotplate tops. The all-glass still. Corning pH meters that have evolved to our latest, innovative delta design. And rapid, accurate X-EL® electrodes.

We are directly involved in the explosion in biotechnology, supplying a continuing array of quality tissue culture flasks, dishes, filters, plates, bottles, and other products for cell biology. And the list goes on.

The future offers a wondrous opportunity for discovery. We want you to know that Corning is with you all the way.

WIN YOUR PLACE IN SPACE Let Corning take your work off the benchtop. We'll put your experiment in space. Enter the Corning Shuttle Space Sweepstakes and win 5.0 cubic feet of cargo area to fill with any experiments you devise. Corning will pay your freight on a future space shuttle flight. We'll even donate any Corning labware you need aboard the shuttle.

SWEEPSTAKES INFORMATION AND FREE SHUTTLE BEAKER



Rush me the sweepstakes official entry blank and free commemorative shuttle beaker. Send me more information on Corning's 70 year specials celebration. Mail coupon on letterhead with name, title and address to Corning Glass Works, Science Products, P.O. Box 1150, Elmira, New York 14902-9944. Offer ends November 29, 1985.

AC-03-85-VS

The Most Trusted Tools Of Science

CORNING

CIRCLE 33 ON READER SERVICE CARD

We're Kno

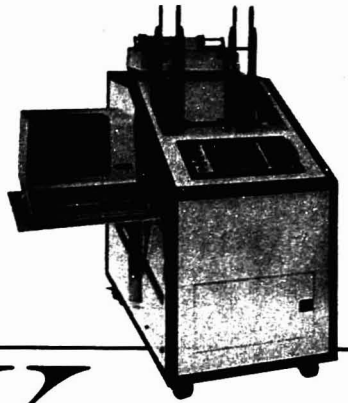
The Compa

and the people we help!

AerojetNuclearUnionCarbideRockwellInte
rnationalMineralandChemicalCorporationStateofFl
oridaFermilabCommonwealthEdisonGeneralElectricEG&Gld
ahoMcCoy&McCoyAberdeenProvingGroundsStateofMarylandArme
dForcesRadiologicalResearchInstituteNationalBureauofStandardsMaineYank
eeAtomicPowerNorthernStatePowerDukePowerCarolinaPowerNebraskaPublicPo
werOmahaPublicPowerPublicServiceGas&ElectricSandiaNationalLabsReynoldsEle
ctric&EngineeringCompanyArmyMedLabWestValleyNuclearBattelleOhioDepartme
ntofHealthClevelandElectricGPUNuclearNuclearUtilitiesServicesCorporationDuque
snePowerPennsylvaniaStateUniversityWestinghouseSouthCarolinaElectric&GasM
ason&HangerTexasUtilitiesBabcock&WilcoxWashingtonPublicPowerTennesseeVal
eyAuthorityArizonaPublicServicePacificGas&ElectricLawrenceLivermoreLaboratori
esUnitedStatesNuclearRegulatoryCommissionCaliforniaEdisonColoradoStateUniver
sityBCResearchNewBrunswickPowerAtomicEnergyCommissionofCanadaOntarioHy
droGeorgiaPowerIowaElectricExxonNuclearArgonneNationalLabsAlliedChemicalNu
clearMetalsBostonEdisonWalterReedArmyMedicalCenterConsumersPowerDowCh

That's why Tennelec is the largest supplier of low

MANUAL AND AUTOMATIC SAMPLE CHANGERS / ACCOMMODATING 1" TO 5" DIAMETER SAMPLE



wn By ny We Keep

emical DetroitEdisonMinnesotaDepartmentofHealthCombustionEngineering
UnionElectricMississippiPowerStateofNorthCarolinaCarolinaPowerandLightBell
TelephoneLaboratoriesPrincetonUniversityStateofNewJerseySandiaLosAlamosNational
LaboratoryLongIslandLightingRensselearPolytechnicBrookhavenNatioalLaboratory
NASADepartmentofEnergyOregonStateUniversityRadiationManagementCorporation
CarolinaMetalsNavalSupplyCenterChem-NuclearStateofSouthDakotaDavidson
SpecialtyTennesseeNuclearSpecialtiesOakRidgeAssociatedUniversitiesAlphaNuclear
TexasInstrumentsTexasUtilitiesAramcoHoustonLightingandPowerCompanyBechtel
UniversityofVirginiaPhillipMorrisVirginiaCommonwealthGSIStateofWisconsinCore
LabsLawrenceBerkeleyLaboratoryCityofSanDiegoSanFranciscoWaterDepartment
DenverWaterDepartmentCoorsPorcelainEnvironmentalSciencesPembrokeLaboratories
PolkCountyHealthDepartmentGeorigaInstituteofTechnologyMartinMariettaGovernment
ofKoreaHoneywellStateofMississippiOlkonCorporationMonsantoOregonState
UniversityPennsylvaniaPower&LightRadianCorporationEastTexasStateUniversityEcology
AuditsGettyOilWashingtonStateUniversityPetrotomicsCompanyUnitedStates
EnvironmentalProtectionAgencyToledoEdisonQuadrexCorporationVermontYankee

background Alpha/Beta/Gamma Counting Systems

S / GAS FLOW PROPORTIONAL AND PHOSWICH DETECTORS / TABLE TOP AND MOBILE CABINETS

TENNELEC, INC.

601 Turnpike, Oak Ridge, Tennessee 37830 USA Telephone 615-483-8405/TWX 810-572-1018
Muenchner Strasse 50, D 8025 Unterhaching West Germany Telephone 089/611-5060/TLX 5215959 FRIE D

CIRCLE 202 ON READER SERVICE CARD

A Glimpse into the Future

Instrument executives hint at future plans

At the Financial Conference for the Analytical Instruments Industry, sponsored by the Scientific Apparatus Makers Association (SAMA) and held this past December in Boston, major instrument company executives provided attendees with a rare glimpse at some of their plans for the future. These plans include a personal computer-based laboratory management system, new robotics systems for sample preparation, and more powerful magnetic resonance products.

Michael Moore, vice-president and general manager of Perkin-Elmer's instrument group, sees more laboratory computerization and automation. One major Perkin-Elmer effort in this area involves continuing software development work on the company's laboratory information management system (LIMS), which, said Moore, is currently offered as a minicomputer-based product in the $50,000–$400,000 range. Moore estimated that the market for the minicomputer-based LIMS consists of approximately 4000 scientific laboratories worldwide, which translates to a total of about $600 million in sales revenues.

But, according to Moore, minicomputers are no longer required to implement a LIMS; microcomputers such as the International Business Machines (IBM) Personal Computer AT or the Perkin-Elmer 7000 series of computers are now sufficiently powerful to meet the needs of many smaller labs. "Such a microcomputer-based LIMS will be developed and introduced in the near future," he said. It does not take a reckless leap of the imagination to surmise that Perkin-Elmer is probably itself involved in such an effort. "We estimate," said Moore, "that the micro- or PC-based



LIMS will add approximately 12,000 labs or $500 million to this market."

Computerization has also spurred automation, and Moore predicts that as the decade ends, the effect of automation will begin to be as profound as the computer's has been thus far. Analytical instrument automation originally involved dedicated accessories, such as autosamplers, that facilitated instrument operation, but the industry is now on the threshold of automation's second phase: robotization.

"Within the next five years," said Moore, "robots will be produced to perform a variety of tasks in the lab, primarily in the area of sample preparation and delivery." Indeed, at last month's Pittsburgh Conference, Perkin-Elmer introduced its first lab robot.

"Some of the sample preparation will not be preset, but will actually be determined in real time by the instruments themselves," Moore continued. "If the sample concentration is too high for the instrument to work properly, the robot will be told to add more diluent. We refer to this as soft automation, in contrast to the hard automation of earlier years." The software to make such a system work is very difficult to develop, Moore admitted, but the result will be very worthwhile—the transformation of the analytical laboratory "into a highly productive, flexible, auto-analysis center."

Allen J. Lauer, president of Varian Associates instrument group, addressed himself primarily to the nuclear magnetic resonance (NMR) business, which he described as "Varian's fastest growing product line. Orders were up something like 27% last year, and in the U.S. we were up significantly above that. We expect to see strong continued growth in NMR through 1985 and, actually, through the end of the decade."

Lauer explained that the field strengths of the superconducting magnets used in state-of-the-art NMR instruments have been rising. Today, 11.7-tesla magnets are available, and research efforts are presently attempting to provide 14-tesla magnets. "Higher magnetic fields are important," said Lauer, "because they allow the scientist to look at larger, more complex molecules by dispersing overlapping peaks. This is very important in the biomedical area, where the molecules are very large and complex."

An important Varian effort in the biomedical field involves the company's agreement, announced this past November, to cooperate with Technicare Corporation (a Johnson & Johnson company) on in vivo NMR research. In his SAMA presentation, Lauer said that this project will result in the development of a small-animal NMR imager and spectrometer that will be offered "within about a year."

S.A.B.

0003-2700/85/0357-398A$01.50/0
© 1985 American Chemical Society

ITD
ION TRAP DETECTOR

The Power of Mass Spectrometry in a Routine GC Detector... Finnigan MAT Makes It a Reality



Easy to Use

The Finnigan MAT Ion Trap Detector™ is a simple, elegant implementation of an advanced technology. Operation of the ITD™ is straightforward. Maintenance is minimal. Set-up, data collection and processing are handled with an IBM Personal Computer XT.™ The software "coaches" you through every step of your capillary-column GC analysis.

Yet the power of mass spectrometry is there...

Universal and Specific

The ITD lets you streamline your laboratory procedures by handling the job of several conventional GC detectors. Use the universal detection mode on the ITD to record the chromatogram and complete mass spectra. The specific detection mode gives you added sensitivity and selectivity for your most demanding samples. You monitor only selected masses characteristic of the analytes of interest.

Positive Identification

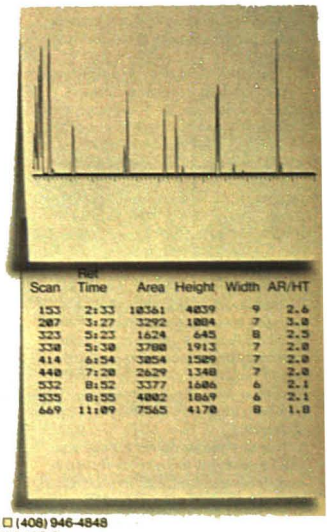
The ITD adds a new dimension to capillary-column gas chromatography: the analytical sample is separated by mass as well as retention time. For positive identification, you supplement retention time data with mass spectra. This identification is further facilitated by the extensive library search capabilities of the system.

Interference-Free Quantitation

With characteristic masses you can quantitate the analyte of interest even when complete separation is not achieved on the column. Errors due to coeluting peaks are eliminated. Sample throughput is increased as cleanup requirements are reduced. And, you can use isotopically-labelled analogs as quantitative standards, an option not available with conventional GC detectors.

See for Yourself

See the Finnigan MAT Ion Trap Detector in action at one of the seminars and exhibits near you. Circle **65** for a product brochure and a schedule of the presentations. Circle **66** if you wish to discuss your application with a Finnigan MAT representative.



Scan	Ret Time	Area	Height	Width	AR/HT
153	2:33	10361	4839	9	2.6
287	3:27	3292	1084	7	3.8
323	5:23	1624	645	8	2.5
338	5:38	3788	1913	7	2.8
414	6:54	3854	1529	7	2.8
448	7:28	2629	1348	7	2.8
532	8:52	3377	1686	6	2.1
535	8:55	4882	1869	6	2.1
669	11:09	7565	4178	8	1.8

355 River Oaks Parkway, San Jose, CA 95134, USA □ (408) 946-4848
Postfach 14 40 62, D-2800 Bremen 14, FRG □ (0421) 54 93-0
Paradise, Hemel Hempstead, Herts HP2 4TG, UK □ (0442) 4 04 91

Finnigan MAT

Rosy Prospects for the Analytical Instrument Industry

Under President Ronald Reagan, U.S. government policy is currently favoring moderate economic growth, a return to free markets whenever possible, and low inflation. These factors augur well for most industries in the U.S. and, hence, for the analytical instrument industry as well, according to Stan Feldman, vice-president of Data Resources Inc., who spoke at the SAMA Financial Conference for the Analytical Instruments Industry (see previous story).

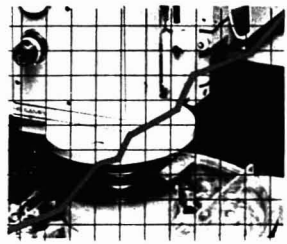
"The notion has been that the large [U.S. federal budget] deficit will either create hyperinflation or that it will limit economic growth. Neither will happen," said Feldman, in part because a significant amount of the deficit is being "financed" by a healthy, strong dollar.

With a low inflation rate in place, the U.S. government has been able to move toward a less restrictive monetary policy. This, in turn, is stimulating moderate economic growth, partly due to the lower interest rates (and consequent increased investment spending) that result when there is more money floating around in the economy.

The analytical instrument industry benefits when capital equipment spending is high. As it happens, capital equipment investment spending as a percentage of gross national product (GNP)—with all amounts corrected for inflation—has been increasing significantly since about 1979, said Feldman. "I wouldn't call it a capital boom," he said, "but historically, relative to the 1970s, the percent of GNP allocated to equipment investment has been increasing." There are several reasons for this, including the increased cost competitiveness of world markets, which induces companies to increase their investment in equipment—including modern, computerized analytical instrumentation—that can help improve efficiency and productivity.

Another major driver for the analytical instrument industry is research and development (R&D) spending. In the private sector of the economy, said Feldman, R&D spending as a percentage of before-tax corporate profits has more than doubled since 1978.

This trend is corroborated in Battelle Memorial Institute's 1985 R&D forecast (released in January 1985), which concludes that real (inflation-



corrected) industrial support of R&D has increased at an average annual rate of 5.4% during the past decade and that it will account for about 51% of total R&D funding in 1985. The remainder of the funding is supplied by the federal government (about 45%), academic institutions (2%), and nonprofit organizations (1%). Until 1979 the federal government supported more R&D than did industry; thus, the trend toward increasing industrial support appears to be continuing.

The Battelle study predicts that the military share of federal R&D spending will rise from about 62% in 1984 to over 66% in 1985. "The share of the total output going to the military has increased dramatically," said Feldman at the SAMA meeting. "That's another driver for the analytical instrument industry. By 1986, the military will purchase about half of the output of engineering and scientific instruments."

Another factor behind Feldman's rosy forecast involves the effect of recent government regulations on hospitals and, hence, on clinical chemistry instrumentation. "The hospitals will soon be under a ceiling as to how much Medicare money goes to patient medical services," Feldman explained. "Instead of hospitals just submitting bills and the government paying them, now there will be limits. The hospitals are thus under cost constraints, and there is a move on to become more productive, which means they will lay off people. How do you become more efficient? You substitute capital equipment for people. So we will be selling equipment for the hospital service industry that will allow it to be more efficient and more productive."

Speaking again of the analytical instrument industry as a whole, Feldman concluded that "the overall economy is going to help this industry, and the performance of the economy is likely to be much less variable between now and 1990 than ever before. Most markets that use analytical instruments are growing fast and have good prospects."

S.A.B.

CHEMFETs Available at Production Cost

Chemically sensitive field effect transistors, or CHEMFETs, will soon be available at production cost to academic and industrial chemists for research purposes.

According to Jiri Janata, chairman of the University of Utah's Department of Bioengineering, the solid-state chemical sensors will be manufactured at the Hedco Microelectronics Laboratory, a $10-million facility in the university's Department of Electrical Engineering, and distributed to scientists in hopes of stimulating interest in novel uses for the devices.

"We know of no other places that supply these devices," Janata notes. "The Hedco lab has the capacity and expertise to do so. We cannot recommend that the CHEMFETs be used for human experiments, but the devices should enable people to build a research base on which eventual human use will follow."

A CHEMFET consists of a conventional insulated-gate field effect transistor whose metallic gate contact has been replaced by a chemically sensitive coating and a reference electrode.

CHEMFETs can be used in a wide variety of ways, as reported recently in ANALYTICAL CHEMISTRY (*1*). Numerous cations and anions in solution can be sensed by coating the gate region with an ion-sensitive membrane. These ion-sensitive CHEMFETs (or ISFETs) have been used to detect H^+, K^+, Ca^{2+}, Cl^-, I^-, and CN^- with near Nernstian response.

A very sensitive hydrogen gas sen-



Sam™ - Laboratory Information Management System

A sophisticated management tool for the laboratory that is available for the popular IBM PC series of microcomputers

Radian Corporation's Sample and Analysis Management (Sam) System is a software system for controlling and handling information from all laboratories. Sam provides a dynamic, easy-to-use method for tracking, scheduling, reporting, and statistically analyzing results.

Multiterminal options available through local area networking

For more information contact:

RADIAN CORPORATION
8501 Mo-Pac Blvd.
P.O. Box 9948
Austin, Texas 78766
(512)454-4797

A company of The Hartford Steam Boiler Inspection and Insurance Company

CIRCLE 181 ON READER SERVICE CARD

sor is obtained if the gate is coated with a thin film of palladium—a detection limit of less than 1 ppm of H_2 is possible. Detection of other gases, such as H_2S, NH_3, and CO, has also been reported.

The small size and low output impedance of the CHEMFET make it ideal for in vivo monitoring and analysis of small sample volumes. Janata and his co-workers at the University of Utah are developing devices that will detect accumulations of trace heavy metals, such as lead and cadmium, in the body. According to Janata, the electrochemical approach to analyzing trace heavy metals is more sensitive and accurate than the currently used optical techniques. The simplicity of the CHEMFET would also allow it to be used in physicians' offices rather than in remote laboratories.

Janata and his group are also investigating enzymatic coatings for the sensors. ENFETs (enzymatic field effect transistors) could be used to monitor enzymatic reactions. The small size of the CHEMFET is particularly important if expensive enzymes are to be used in the device.

"There are some 1500 different enzymes that could be used," explains Janata. "So it's a matter of putting an enzyme on a transistor that is sensitive to a particular species for which that enzyme is the catalyst." Many industrial processes, especially those in biotechnology, require careful monitoring of reactions, and the probes would be suitable for these.

The small size of the CHEMFET enables multiple sensors to be placed on the probe tips, allowing simultaneous monitoring of many different compounds. Such multisensors would be especially useful to biomedical researchers, but Janata points out that they may also find applications in such diverse fields as agriculture, mineral resource exploitation, and effluent monitoring.

The main technological problem that has prevented wide-scale use of CHEMFETs is the difficulty of properly encapsulating the device (*1*). Microsensors are routinely exposed to media that are incompatible with the CHEMFET's solid-state electronic circuitry. Instability can result if even a trace of moisture or ionic contaminant penetrates the encapsulation coating of a CHEMFET.

According to Janata, "The bulk of the problems that remain are in the area of materials science, not in solid-state electronics or chemistry." He hopes to find a partner in industry interested in refining the encapsulation and packaging techniques that protect the sensor and its electronic components from inherently hostile environments.

The University of Utah lab will build the basic chips, up to and including the solid-state electronics, but researchers who purchase the sensors will have to coat the probe with the desired chemically selective membrane and encapsulate it themselves. Cost feasibility of the project is based on providing 50,000 chips per year—the cost of the probes will depend somewhat on the number of requests received.

For further information, contact Jiri Janata, Dept. of Bioengineering, University of Utah, Salt Lake City, Utah 84112, 801-581-3837.

Reference

(1) Wohltjen, H. *Anal. Chem.* **1984**, *56*, 87–103 A.

M.D.W.

NEW... on a cage

Now our FS-capillary columns have their own place...

...coiled on to a cage*

This means some real advantages, which not only make life easier, but also offer more efficiency through

- more convenient handling
- far less breakages
- higher thermal mass
- better temperature distribution

Stock products

3 different inner diameters (0.25, 0.32 and 0.53 mm)

6 different CB-phases each with 3 standard film thicknesses (other film

Column: cat.No.: 723318
25 m FS-OV1701-CB-0.25

1. Benzene
2. Toluene
3. Ethylbenzenene
4. p-Xylene
5. o-Xylene
7. o-Cresol
8. 2,6-Xylenol
9. p-Cresol
10. 2,4-Xylenol
11. 2,4,6-Trimethyl-

Columns for special separation problems such as haloforms, pesticides, PCB's, PAH's etc...

Re-coating service with various phases at competitive prices.

Comprehensive programme of accessories including test and standard mixtures.

A free GC brochure covering our complete range of capillary columns is available on request.

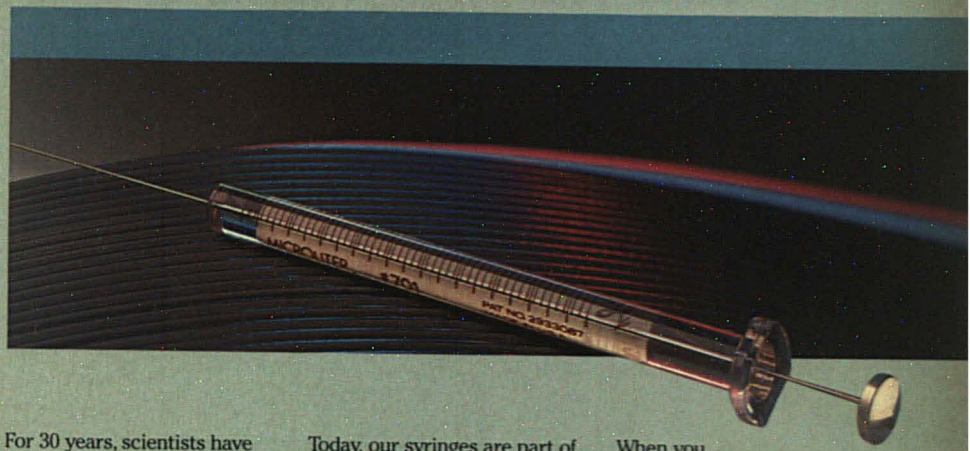
Macherey-Nagel · P.O.Box 307 · D-5160 Düren · W. Germany · ☎ 02421-61071 · Tx 833893 mana d

MACHEREY-NAGEL · DÜREN

MN

CIRCLE 144 ON READER SERVICE CARD

Here's where accuracy and precision begin.



For 30 years, scientists have depended on the Hamilton Microliter® Syringe for accurate transfer and injection of precise volumes of liquids and gases.

There are good reasons why. Commitment to quality. Attention to detail. And constant improvement of our manufacturing and quality control procedures. We always keep your analytical needs in mind. For example, our 10 μl syringes carry a stringent bore tolerance of 50 millionths of an inch which ensures accuracy to within 0.52%.

Today, our syringes are part of a comprehensive line of high quality products that includes liquid diluter/dispensers, miniature valves and fittings, chromatography columns and accessories, and advanced sample handling and analysis systems.

As our product line grows, we continue to place the same premium of quality on everything we manufacture—from the precision Microliter® Syringes to the most sophisticated liquid handling instruments.

See Us at FASEB, Booth #'s 1703-1707.

CIRCLE 96 ON READER SERVICE CARD

When you demand accurate analytical results, begin with Hamilton.

For your copy of our latest catalog, call (800) 648-5950. Or write to the Hamilton Company, P.O. Box 10030, Reno, Nevada 89520.

HAMILTON

The measure of excellence.

HIRE TECHNOLOGY

PUT ELECTROCHEMISTRY TO WORK!

BAS introduced the first commercial liquid chromatography/electrochemistry instrument in 1974. LCEC has become the fastest growing electrochemical technique. Thousands of our systems are in routine use for environmental, pharmaceutical, biomedical, industrial, and forensic applications. Nitro compounds, phenols, aromatic amines, thiols, and many heterocycles are ideal candidates for trace determination by LCEC. Detection limits of well below 1 picomole can now be achieved in a few minutes using apparatus of very modest cost.

The latest addition to our family is the BAS 100 ELECTROCHEMICAL ANALYZER. This interactive microprocessor based instrument is capable of performing over 25 electroanalytical techniques including cyclic voltammetry, chronocoulometry, differential pulse voltammetry, phase selective AC voltammetry, electrocapillary measurements, and virtually all forms of polarography. The BAS 100 is the first commercial instrument capable of square wave voltammetry, a powerful new technique for both analytical and fundamental studies. The first "smart" iR compensation approach is included, as are various statistical and background subtraction routines. Experimental parameters and data are available on a video screen and publishable figures are rapidly plotted.

The BAS 100 was designed by and for chemists. It's ready to go to work for you.

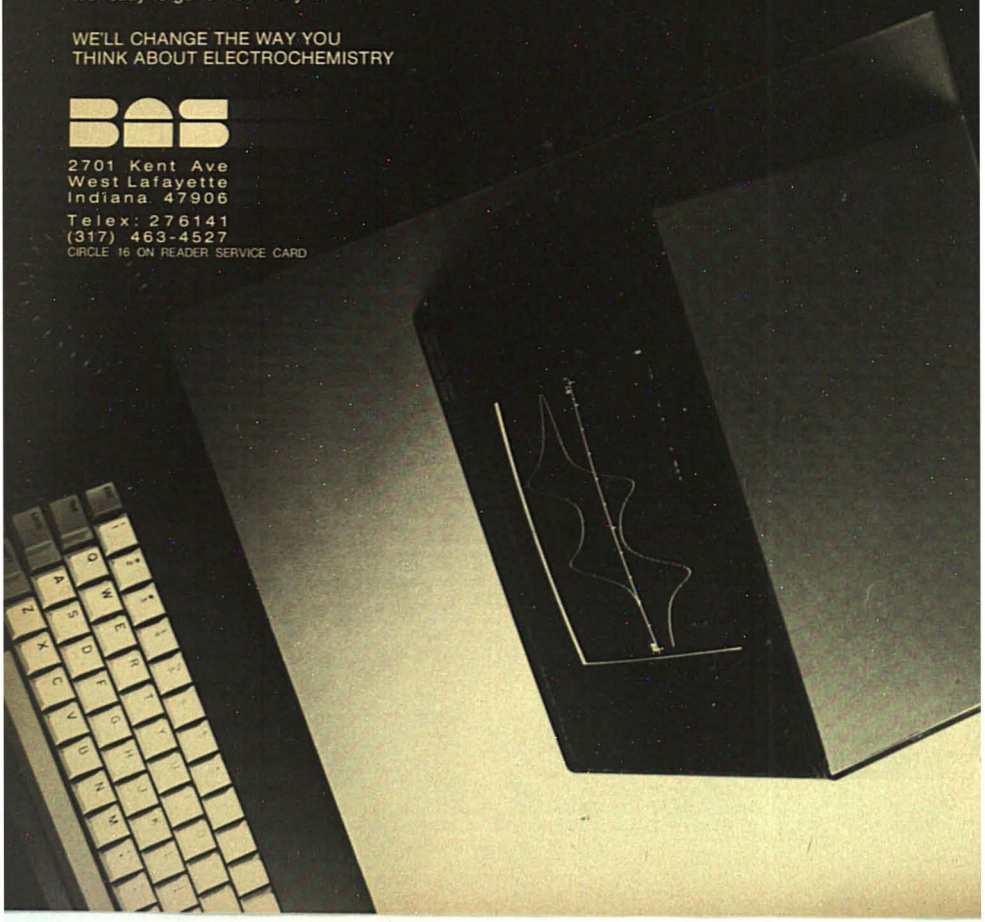
WE'LL CHANGE THE WAY YOU
THINK ABOUT ELECTROCHEMISTRY

BAS

2701 Kent Ave
West Lafayette
Indiana 47906

Telex: 276141
(317) 463-4527

CIRCLE 16 ON READER SERVICE CARD





Is your silicone supplier a jack of too many trades?

Nowadays you simply cannot be everything to everybody. That's why Dow Corning specializes in one thing—silicones.

We're the only global company that has built a business exclusively around the development and marketing of silicones and related specialty materials. So you can be more confident of getting the technically-advanced silicones you need. You choose from the world's largest selection of problem-solving silicones. The kind that help you build differentiation into your products, and help you grow.

You get even more with our silicones. You get the added value of our technical service, backed by the largest research and development investment in the industry. And we have worldwide capabilities, including basic manufacturing operations on three continents. So we're ready to respond wherever—and whenever—you need us.

Quite simply, we offer you the silicones, the technical service and the marketing support you need. So why work with a jack of too many trades when you can work with a master of the one you need?

Dow Corning Corporation, Dept. F4021, Midland, MI 48640.

Source One for Silicones.

DOW CORNING

DOW CORNING

CIRCLE 41 ON READER SERVICE CARD

Linking Value to Performance.

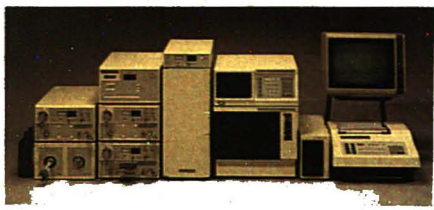
Perfect Quality LC.



Gradient

◀ ***Gradient LC System G-II***

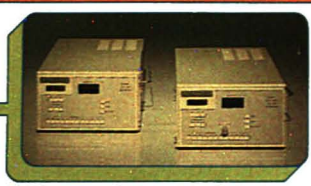
- *Complete automation of binary gradient LC*
- *Complete data station*



Universal

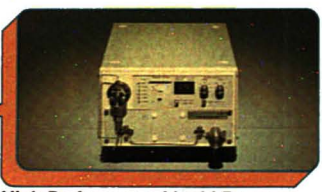
◀ ***Universal LC System U-I***

- *Complete automation of ternary gradient LC as well as low and high pressure valve control*
- *Complete data station*



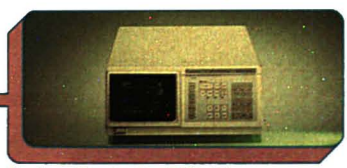
UV Spectrophotometric Detector SPD-6A,
UV-VIS Spectrophotometric Detector SPD-6AV

- *SPD-6A has wavelength range of 195-350nm and SPD-6AV of 195-700nm*
- *Extended range of sensitivity (0.001-2.56 AUFS)*
- *Auto zero function is standard*



High Performance Liquid Pump LC-6A

- *Capable of stable flow rate between 0.01-9.9ml/min*
- *Upgradability to ternary gradient elution*



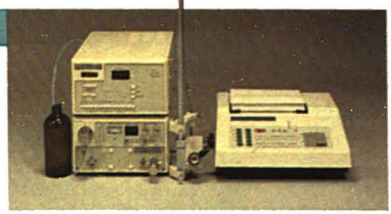
System Controller SCL-6A

- *Complete control of LC module as well as external devices*
- *Menu driven control of parameters*

Low-pressure Stream Valve FCV-3AL
High-pressure Stream Valve FCV-2AH
Sample Injector
Injector Holder
Preheater

Introducing Shimadzu's full spectrum of modular HPLC Systems.

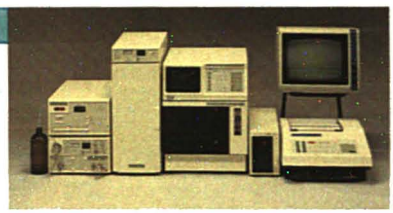
Simple



Simple LC System S-I ►

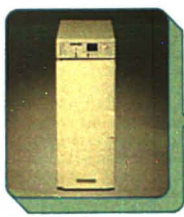
- *Simple and low cost yet high performance*

Automated



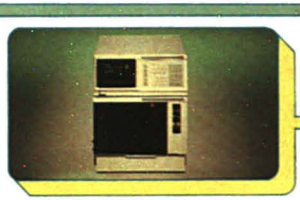
Automated LC System A-II ►

- *Complete automation of isocratic LC*
- *Complete data station*



Column Oven CTO-6A

- *Temperature control up to 99°C*
- *Precision: ±0.1°C*



Auto Injector SIL-6A

- *Complete random accessibility*
- *Capability of 100 samples*
- *Reproduceable injection between 1μl–500μl*

SPD-M1A
UV-VIS Spectrophotometric Detector for HPLC
- *Three-dimensional spectro-chromatogram*

RF-530
Fluorescence HPLC Monitor



Data Processor C-R3A

- *Large capacity for chromatogram memory (176 KByte)*
- *BASIC programmability*

For full value HPLC systems, ask for the Shimadzu LC-6A. From simple to complex LC, the new high-performance Shimadzu LC-6A Liquid Chromatograph System can meet any requirement perfectly. The modular design provides an easy and cost-efficient way to upgrade any system. But this isn't all you get with Shimadzu. You get competitive specifications at the lowest cost. Proven reliability, a one-year warranty at no extra cost. And applications support. Important reasons to consult Shimadzu today about the full value LC-6A.

For further information, please contact:

Shimadzu Scientific Instruments, Inc.
7102 Riverwood Drive, Columbia, MD 21046, U.S.A.
Phone: (301) 997-1227

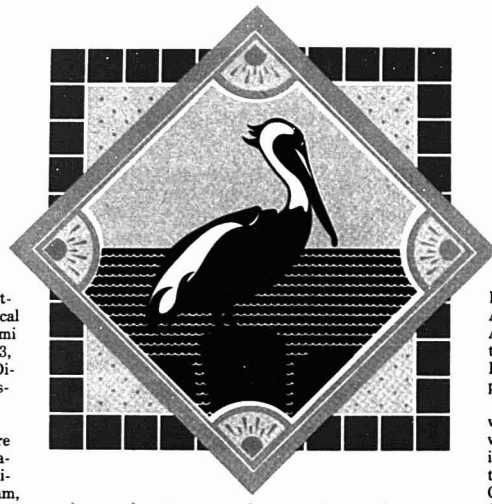
Shimadzu (Europa) GmbH
Acker Strasse 111, 4000 Düsseldorf, F.R. Germany
Phone: (0211) 666371
Telex: 08586839

Shimadzu Corporation, International Marketing Div.
Shinjuku-Mitsui Building, 1-1, Nishishinjuku 2-chome, Shinjuku-ku, Tokyo 160, Japan
Phone: Tokyo 03-346-5641
Telex: 0232-3291 SHMDT J.

SHIMADZU

CIRCLE 189 ON READER SERVICE CARD

News



189th ACS National Meeting
April 28–May 3, 1985

The 189th National Meeting of the American Chemical Society will be held in Miami Beach, Fla., April 28–May 3, 1985. At the meeting, the Division of Analytical Chemistry will sponsor or jointly sponsor technical sessions and symposia at which more than 200 technical presentations are scheduled. In addition to the technical program, the meeting will feature an address by Nobel Laureate Glenn T. Seaborg; a National Employment Clearinghouse; meetings of the ACS council and board of directors; ACS short courses; and a series of social events, including the ACS awards dinner (Monday, April 29), an ACS mixer (Tuesday, April 30), the Analytical Division dinner (Tuesday, April 30), and tours and plant trips throughout the Miami area.

On-site registration facilities will be located in the Convention Center, south lobby; the Fontainebleau Hilton, Grand Gallery; and the Omni International, International Promenade. Registration hours will be Sunday, April 28, 3:00 P.M. to 8:00 P.M.; Monday, April 29 through Thursday, May 2, 8:00 A.M. to 4:00 P.M.; and Friday, May 3, 8:00 A.M. to 10:00 A.M. An exposition of chemicals, instruments, services, and literature will run for three days in conjunction with the meeting. The exposition will be housed in the South Hall of the Convention Center.

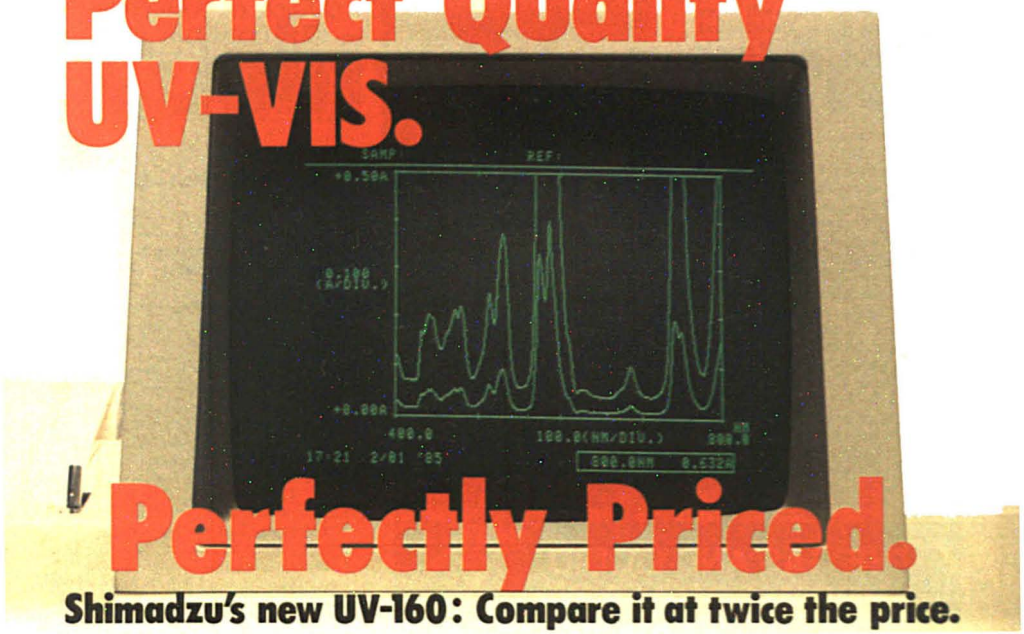
The following Analytical Division symposia and general sessions are scheduled: coupling of liquid chromatography and mass spectrometry; analytical methods in forensic chemistry; the analytical–biotechnology interface; ACS Chromatography Award symposium; ACS Analytical Chemistry Award symposium; X-ray diffraction and crystallographic bases; mass spectrometry of middle molecules—Garvan Medal symposium; countercurrent chromatography; impact of mass spectrometry on science—Frank H. Field and Joe L. Franklin Award for Outstanding Achievement in Mass Spectrometry symposium; ACS Pure Chemistry Award symposium; and general papers.

The Analytical Division will cosponsor a symposium with the Computer Secretariat and the Physical Chemistry, Chemical Information, Computers in Chemistry, and Chemical Education Divisions entitled "Use of Computers in Chemistry: Computer Secretariat Inaugural." All technical sessions sponsored or jointly sponsored by the Analytical Division will be held in the Convention Center.

The Analytical Division program will be highlighted by the presentation of five awards. The ACS Award in Chromatography will be presented to Leslie Ettre. Ettre's award address on Tuesday, April 30, is entitled "Open-Tubular (Capillary) Columns—Evolution, Present Status, and Future." The ACS Award in Analytical Chemistry will be presented to James Fritz, who will speak on "The Role of Separations in Analytical Chemistry" on Wednesday, May 1. Catherine Fenselau, recipient of the Garvan Medal, will deliver a talk on Wednesday, May 1, on "Middle Molecule Mass Spectrometry: Applications to Biomolecules." On Thursday, May 2, the Frank H. Field and Joe L. Franklin

Linking Value to Performance.

Perfect Quality UV-VIS.



Perfectly Priced.

Shimadzu's new UV-160: Compare it at twice the price.

With one design, one price and no costly options, Shimadzu's UV-160 UV-VIS Recording Spectrophotometer has everything you need for rapid and accurate spectrophotometry — including flexible data processing functions, CRT and printer output. The double beam design means freedom from baseline drift. Five different multi-component analysis methods mean high-precision quantitation. And the error-free scanning speed of 2400nm/min means you can scan the full range, 1100 to 200nm and display the spectrum, in roughly 25 seconds.



Competitive features include stored and realtime spectrum manipulation. Find out more about the full value spectrophotometer.

For further information, please contact:

Shimadzu Scientific Instruments, Inc.
7102 Riverwood Drive, Columbia, MD 21046, U.S.A.
Phone: (301) 997-1227

Shimadzu (Europa) GmbH
Acker Strasse 111, 4000 Düsseldorf, F.R. Germany
Phone: (0211) 666371 Telex: 08586839

Shimadzu Corporation, International Marketing Div.
Shinjuku-Mitsui Building, 1-1, Nishishinjuku 2-chome,
Shinjuku-ku, Tokyo 160, Japan
Phone: Tokyo 03-346-5641
Telex: 0232-3291 SHMDT J.

SHIMADZU

CIRCLE 190 ON READER SERVICE CARD

Award for Outstanding Achievement in Mass Spectrometry will be presented to A.O.C. Nier. Nier's award address will be entitled "Mass Spectrometry in Perspective." The ACS Award in Pure Chemistry will be presented to Ben Freiser, who will speak on "Reactions of Metal Ions and Their Clusters in the Gas Phase Using Laser Ionization–Fourier Transform Mass Spectrometry" on Thursday, May 2.

The Analytical Division dinner will be held Tuesday, April 30, at the Roney Pub, 2301 Collins Ave. The social hour begins at 6:00 P.M. with dinner following at 7:00 P.M. Cost is $20 per person. See the March 18 issue of *Chemical & Engineering News* for ticket ordering information.

The ACS Department of Educational Activities will offer a series of short courses at the Miami meeting. For further information, see p. 426 A of this issue or contact the Department of Educational Activities, American Chemical Society, 1155 16th St., N.W., Washington, D.C. 20036, 202-872-4508.

Preregistration forms and additional detailed information about the meeting are available in the Feb. 18 and March 18 issues of *C&EN*. The latter issue contains the complete final program for the meeting. The program that follows includes all sessions sponsored or jointly sponsored by the ACS Division of Analytical Chemistry.



Jai alai is a popular sport in Miami

PROGRAM

DIVISION OF ANALYTICAL CHEMISTRY

D.D. Bly, Chairman
L.N. Klatt, Secretary

Monday Morning

SECTION A

Symposium on the Coupling of Liquid Chromatography and Mass Spectrometry

G. Guiochon, *Presiding*

9:00 Mechanisms of Ion Formation in Thermospray and Other "Matrix Assisted" Desorption Techniques. **R.J. Cotter** and C. Fenselau

9:35 Role of Transport and Intrinsic Efficiency in Sampling Ions from Solution. **K.D. Cook**

10:10 Thermospray LC/MS on a Magnetic-Sector Instrument: Theory and Application. **J.R. Chapman** and J.A.E. Pratt

11:00 Thermospray LC/MS: A Practical Solution to a Difficult Problem. **M.L. Vestal**

11:35 Liquid Chromatography–Mass Spectrometry Coupling for the Analysis of Both Polar and Nonpolar Compounds by Thermospray. **P.C. Goodley**

SECTION B

Analytical Chemistry of Nitrated Polycyclic Aromatic Hydrocarbons

C.M. White, *Presiding*

9:00 Analysis of Nitrated Polycyclic Aromatic Hydrocarbons by Gas Chromatography. **C.M. White**

9:25 Chromatographic Detectors Used for the Determination of Nitrated Polycyclic Aromatic Hydrocarbons. **B.A. Tomkins**

9:50 Comparative Analysis of Nitro-PAHs by Capillary Gas and Supercritical Fluid Chromatography Methods. **B.W. Wright,** E.K. Chess, H.T. Kalinoski, R.D. Smith, and C.W. Wright



CIRCLE 42 ON READER SERVICE CARD

Linking Value to Performance.

Perfect Quality Integration.

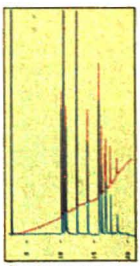


Integrated Quality.

Affordable GC/LC data processing for reliable peak identification even for demanding capillary GC work. Put the C-R3A to work with any GC or LC or better yet, with a modular Shimadzu system, and marvel at its processing power at less than one third the cost of most chromatography data systems.

Reprocess and re-plot the raw data of multiple chromatograms in minutes as many times and with as many different parameters as you like—from one injection only. No other integrator lets you establish the best processing conditions for each task so easily, so fast and so accurately.

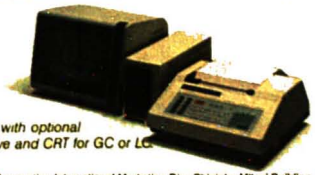
Get 176 Kbyte memory, a host of options and a one-year warranty. If 6 hours of multiple chromatogram storage is not enough, get up to hundreds of hours with a floppy disk option. User-programming in BASIC is standard, and our unmatched 1-year warranty gets back to the basics of what "integrated quality" is all about.



Baseline compensation for better quantitation.

Ask for the facts and discover the Shimadzu secret of guaranteed integrated quality. Circle the Reader Service No. for a full info-package or a demo in *your* lab. And discover the best kept secret in chromatography data processing today.

Shimadzu Scientific Instruments, Inc.,
Columbia, MD 21046, (301) 997-1227



C-R3A with optional diskdrive and CRT for GC or LC

SHIMADZU

Shimadzu Corporation International Marketing Div.: Shinjuku-Mitsui Building, 1-1, Nishishinjuku 2-chome, Shinjuku-ku, Tokyo 160, Japan. Tel: Tokyo 03-346-5641 Telex: 0232-3291 SHIMDT J
Shimadzu (Europa) GmbH: Acker Strasse 111, 4000 Düsseldorf, F.R. Germany. Tel: (0211) 666371 Telex: 08588539

Circle 191 for information. Circle 192 for a demonstration.



Garden Center and Conservatory houses plant life indigenous to Florida

10:15 Development of a Routine Technique for Analysis of Nitro-PAHs in Diesel Particulate Extract. **K.T. Menzies,** C.M. Wong, L.H. Magni, and M.A. Randel

10:55 Determination of 1-Nitropyrene and Selected Other N-PAHs in Diesel Particulate Extracts Using Liquid Chromatography with Reductive Electrochemical Detection. **W.A. MacCrehan** and W.E. May

11:15 Chromatographic Analysis of Nitrated Polycyclic Aromatic Hydrocarbons Employing Chemiluminescent Detection. **A. Robbat, Jr.,** P.J. Doherty, and N. Corso

11:35 Identification and Quantification of OH-NO_2-PAHs and NO_2-PAHs in an Ambient Air Particulate Extract by NCI HRGC/MS. **M.G. Nishioka,** S. V. Lucas, and J. Lewtas

11:55 Identification of *x*-Nitro-4,5-Methylenephenanthrene in the Atmosphere. **T. Nielsen**

SECTION C

Symposium on Analytical Methods in Forensic Chemistry

M.H. Ho, *Presiding*

8:30 Introductory Remarks

8:40 Potential and Limitations of Forensic Analysis of Physiological Materials. **B.W. Grunbaum**

9:20 How to Approach Systematic Toxicological Analysis. **R.A. de Zeeuw,** J.P. Franke

9:50 On Some Trends in Generation and Interpretation of Toxicological Data. **R. Ludewig**

10:20 Evaluation of Method Precision for Forensic Toxicology Samples—The State of the Art. **J. Balkon** and B. Donnelly

10:40 Analytical Toxicology Samples—Considerations and Problems in Handling. **A. Stavrou**

11:00 GLP and Its Implications for an Analytical Laboratory. **A. Stavrou**

11:20 Electrochemistry: A New Analytical Tool in Forensic Science. **R.C. Briner**

11:50 Forensic Applications of Flow Injection Analysis. **M.H. Ho**

SECTION D

General—Electrochemical Studies and Molecular Spectroscopy

L.A. Bottomley, *Presiding*

9:00 Spectroelectrochemistry of the Oxo and Nitrido Bridged Dimers of Iron Phthalocyanine. **L.A. Bottomley,** J.N. Gorce, and C. Ercolani

9:15 Oxidative Spectroelectrochemistry of Chalcocarbonyl Iron Porphyrins. **J.N. Gorce** and L.A. Bottomley

9:30 Theoretical Conductivity Studies of Ag/Ag_2S Ion-Selective Electrodes. **V.Y. Young**

9:45 Cyclic Voltammetry with Cyclic Iminium Ions: Implications for Charge Transfer in Biological Systems. **M.D. Ryan,** S. Brandange, P. Kovacic, and J.R. Ames

10:00 Differential Pulse Voltammetric Studies of the Complexation of Rhodium Carboxylates with Ligands Containing Phosphorus and Sulfur Donor Atoms. **B.L. Thorpe** and L.A. Bottomley

10:15 Electrochemistry of Rhenium Tricarbonyl and Technetium Tricarbonyl Porphyrins. **G.E. Steiger,** L.A. Bottomley, and R.J. Clark

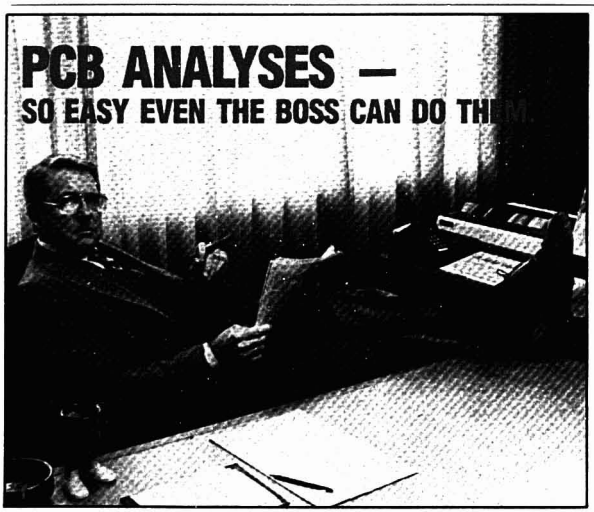
10:45 Electrochemistry of Oxo-Rhenium Schiff Base Complexes. **P.E. Wojciechowski** and L.A. Bottomley

11:00 Flow Injection Analysis of Iron(III) and Aluminum with Indirect Electrochemical Detection. **D.S. Owens** and P.E. Sturrock

11:15 Performance Optimization in Tunable Atomic Line Molecular Spectroscopy. **R.E. Berkley,** D.R. Scott, and R.L. Hedgecoke

11:30 Novel Spectrometer Design for AES. **G.M. Levy,** A. Quaglia, R.E. Lazure, and R.L. Lyke

11:45 Chemiluminescent Determination of Chlorine and Chlorine Dioxide Using Gas Diffusion Flow Injection. **D.A. Hollowell,** G.E. Pacey, and G. Gordon



THE PCBA-102: FAST, SIMPLE, DIRECT

FOR MORE INFORMATION ABOUT THE PCBA-102 CALL OR WRITE:

S-CUBED/Maxwell
P.O. Box 1620 • La Jolla, CA 92038
(619) 453-0060

CIRCLE 199 ON READER SERVICE CARD

SIEMENS

The Choice You Can Believe In

The SRS 300 X-ray Spectrometer System



With the SRS 300 spectrometer, Siemens has developed a system that answers the needs of today's analytical chemist. Its success in the user's laboratory has proven that this is a spectrometer system that you can believe in for reliability, user convenience, and analytical performance for not only today but the future.

The unique automation system of the SRS 300 puts you, the operator, in complete control — allowing you the advantage of end window x-ray optics for better sensitivity and low Z analysis, sample handling capabilities, trouble-free control of crystals, filters, collimator masks, and sample changers among numerous other high-performance features of the SRS 300.

Our new software system, SPECTRA 300, makes total analysis possible by giving you full control of the spectrometer, data collection — both quantitative and qualitative — data refinement and data processing.

When you choose the SRS 300, you can be confident in its long-term performance and reliability — Siemens is a company that you can believe in. For more information, write or call: Siemens AG, Analytical Systems E 689, D 7500 Karlsruhe 21, P.O. Box 21 1262, Federal Republic of Germany, Tel: (0721) 595-2425, Telex: 7826851. Siemens-Allis, Inc., Analytical Systems, One Computer Drive, P.O. Box 5477, Cherry Hill, NJ 08034, (609) 424-9210.

Siemens...The company you can believe in.

CIRCLE 197 ON READER SERVICE CARD

12:00 Analytical Capabilities of Chromogenic Anion-Selective Crown Ethers. **G.E. Pacey,** K. Sasaki, and Y. Fujii

Monday Afternoon

SECTION A

Symposium on the Coupling of Liquid Chromatography and Mass Spectrometry

R.J. Cotter, *Presiding*

1:30 MAGIC–LC/MS: Instrumental Developments and Applications to Environmental Samples. P. Winkler, L. Abbey, and **R.F. Browner**

2:05 LC/MS Studies Using Moving-Belt and Thermospray Interfaces. **D.E. Games,** I.G. Beattie, A.J. Berry, M.L. Kimber, A.V. Moncur, E.D. Ramsey, K.A. Rouse, and P.W. Skett

2:40 LC/MS Analysis of an Antioxidant Mixture: Comparison of Results Obtained Using a Thermospray Interface and a Moving-Belt Interface. **W.H. McFadden,** S.A. Lammert, and J. Wellby

3:30 Recent Applications of Tandem Mass Spectrometry to Liquid Chromatography/Mass Spectrometry. **J.D. Henion,** T.R.Cowey, and J. Crowther

4:05 Liquid Ionization Mass Spectrometry for Liquid Chromatography. **M. Tsuchiya,** K. Sasagawa, and K. Otsuka

SECTION B

Analytical Chemistry of Nitrated Polycyclic Aromatic Hydrocarbons

C.M. White, *Presiding*

2:00 Analysis of Nitrated Polycyclic Aromatic Hydrocarbons (Nitro-PAHs) by Mass Spectrometry. **D. Schuetzle and T.E. Jensen**

2:25 Synthesis of Nitrated Polycyclic Aromatic Hydrocarbons. **P.H. Ruehle** and W.P. Duncan

2:50 Analytical Standards and Methods for the Analysis of Nitrated Polycyclic Aromatic Hydrocarbons. **W.E. May,** W.F. Kline, L.R. Hilpert, and W.A. MacCrehan



3:15 Formation of Nitroarenes from the Reaction of Polycyclic Aromatic Hydrocarbons with Gaseous Dinitrogen Pentoxide. **B. Zielinska,** J.N. Pitts, Jr., J.A. Sweetman, A.M. Winer, and R. Atkinson

4:00 Nitrated Polycyclic Aromatic Hydrocarbons in Particulate Matter. **T.L. Gibson**

4:25 Considerations of Particulate Sampling Associated with Mutagenicity Studies on Airborne Particles. **T.S. Chan** and J. Siak

4:50 Detection of Nitro-Polynuclear Aromatic Compounds by Surface-Enhanced Raman Spectroscopy. **T. Vo-Dinh**

SECTION C

Symposium on Analytical Methods in Forensic Chemistry

D.D. Fetterolf, *Presiding*

1:30 Introductory Remarks

1:35 Chiroptical Spectroscopy in Drug Analysis. **N. Purdie,** S.M. Han

2:05 Three-Dimensional Fluorescence Spectroscopy of Commercial Products of Forensic Significance. **J.A. Siegel**

2:25 FTIR Spectroscopy Coupled with Microscopy—A New Tool for the Forensic Scientist. **S. Palenik**

2:45 Use of NMR Analysis in the BKA Forensic Science Laboratory. **G. Vordermaier**

3:15 Specimen Preparation and Analysis for Trace Metals by Flame and Flameless Atomic Absorption Spectrophotometry. **N.W. Alcock**

3:35 MS/MS: Tandem Mass Spectrometry for Forensic Chemistry and Toxicology. **R.A. Yost**

3:55 Rapid Drug Screening by Tandem Mass Spectrometry (MS/MS). **D.D. Fetterolf**

4:15 Detection of Underivatized Drug Metabolites Using Fast Atom Bombardment–Mass Spectrometry. **B.W. Elledge** and B.A. Charpentier

4:35 Analysis of Doxylamine and Related Compounds under Chemical Ionization Mass Spectrometric Conditions. **C.L. Holder,** W.A. Korfmacher, A.B. Gosnell, and W. Slikker, Jr.

SECTION D

General—Gas Chromatography

P.N. Keliher, *Presiding*

2:00 Errors in the GC Analysis of D/L-Amino Ratios Induced by Diastereomeric Derivatization. **I. Payan,** R. Cadilla, G.H. Fisher, and E.H. Man

2:15 Serum Bile Acid Analysis Using Capillary Gas–Liquid Chromatography. **A.K. Batta,** G. Salen, and S. Shefer

2:30 Determination of Surface Polarity by Heterogeneous Gas–Solid Chromatography. **S.P. Boudreau** and W.T. Cooper

2:45 Detailed Analysis of Gasoline Range Hydrocarbons by Multidimensional Gas Chromatography with Postcolumn Reaction. **P.M. Bergquist** and F.P. DiSanzo

3:00 Separation and GC/MS Analysis of Petroleum-Derived Fuels. **G.W. Mushrush,** J.V. Cooney, and R.N. Hazlett

3:30 Two-Oven Gas Chromatography Applied to Flavors and Fragrances. M. Motto, N. Secord, **J.Q. Walker,** and S.M. Sonchik

3:45 Methods Development for Analysis of Organomercury Species in Complex Mixtures. **D.K. Sklarew,** K.B. Olsen, and J.C. Evans

4:00 Gas Chromatographic Characterization of Organolithium Modified Kel-F 6300 Particles as a Column Packing. **L.G. Beaver** and N.D. Danielson

UV/VIS PERFORMANCE:

The plot quickens!



Packed into the compact cabinetry of the Beckman DU-7 are a range of features that have established the standards for performance in spectrophotometry.

Our unique Stable Beam optics, together with a response time of just 0.05 second, allows the DU-7 to scan at a phenomenal 1200nm/min. — with no tracking error.

But you don't have to sacrifice sensitivity for speed. The DU-7's signal-to-noise ratio is far superior to any other comparable UV/spectrophotometer. Baseline flatness is ± 0.001A for precise readings. And the system has the ability to compensate for highly absorbing blanks up to approximately 2.0A.

Once scanning data are stored in the DU-7's memory, they can be recalled and manipulated at will to achieve the most accurate data analysis possible. And for long-term data storage, you can interface the DU-7 with *popular PC's*.

In industrial applications, you get fast, fully *automated answers* without compromising data quality. The DU-7 allows unattended analysis of over 100 samples with automatic printout of data — including results for quantitative analysis and wavelength scans.

Analysis capabilities include linear and non-linear *standard curves* with statistical analysis of standard curves and storage of calibration data.

Multicomponent analysis is available for mixtures of up to five components. And you can calibrate with standards that are themselves mixtures.

Start plotting to acquire a DU-7 today by contacting your Beckman representative or Beckman Instruments, Inc., P.O. Box C-19600, Irvine, CA 92713.

SEE OUR NEW PC SOFTWARE AT FASEB.

CIRCLE 21 ON READER SERVICE CARD

BECKMAN

4:15 Quantitation of the Complete Butyltin Sequence in Environmental Media Employing a New Butyltin Reference Material. **C.L. Matthias,** W.R. Blair, G.J. Olson, J.M. Bellama, and F.E. Brinckman

Tuesday Morning

SECTION A

Symposium on the Coupling of Liquid Chromatography and Mass Spectrometry

D.E. Games, *Presiding*

9:00 On-Line Precolumn Trace Enrichment and Postcolumn Extraction in HPLC with Mass Spectrometric Detection. **U.A.Th. Brinkman,** R.W. Frei, and F.A. Maris

9:35 Rapid and High-Resolution Methods for Capillary SFC–MS: An Alternative to LC/MS. **R.D. Smith,** H.T. Kalinoski, E.K. Chess, B.W. Wright, and H.R. Udseth

10:10 Postcolumn Chemical Derivatization in HPLC/MS Using a Moving-Belt Interface. **P. Vouros,** A. Sahil, C.P. Tsai, and B.L. Karger

11:00 Monodisperse Aerosol Generation Interface for Combining Liquid Chromatography with Mass Spectrometry (MAGIC): General Applications. **R.C. Willoughby** and R.F. Browner

11:35 DLI–LC/MS Experiments with Nucleosides. **E.L. Esmans,** Y. Luyten, and F.C. Alderweireldt

SECTION B

Symposium on Analytical Methods in Forensic Chemistry

R.A. Yost, *Presiding*

8:45 Introductory Remarks

8:50 Gas Chromatography/Mass Spectrometry in Arson Analysis. **R.M. Smith**

9:10 Forensic Analysis of Drugs and Technical Products by GC and MS. **M. Gloger**

9:30 GC/Selected Ion MS Monitoring of Isotope Ratio in ^{13}C-Labeled Methamphetamine. **R.L. Furner,** I.A. Low, E.G. Piotrowski, and R.H. Liu

9:50 HPLC and GC/MS Methods for the Quantitation of Common Antidepressants in Overdose Suicide Cases. **N. Narasimhachari,** S. Bogema, J.C. Valentour, and R.C. Dorey

10:10 Monitoring of Endogenous Formation and Metabolic Activation of Nitrosamines by N-15-Stable-Isotope Tracer Technique. **H. Frank** and H. Remmer

10:40 Applications of GC/FT–IR in the Forensic Sciences. **R.D. Blackledge**

11:00 Potential of Phosphorescent Detection in the High-Performance Liquid Chromatography of Drugs. **P.E. Nelson** and L.V. Murray

11:20 Potentials of HPLC with a Multichannel Diode Array Spectrophotometric Detector in Systematic Toxicological Analysis. **R.A. de Zeeuw,** J-P. Franke, and M. Bogusz

11:40 Forensic Analysis of Explosives by LC/MS. **J. Yinon** and D.G. Hwang

SECTION C

Symposium on the Analytical–Biotechnology Interface

J.L. Glajch, *Presiding*

8:30 Capabilities and Applications of Modern Methods for Protein/Peptide Primary Structure Analysis. **M.W. Hunkapiller**

9:10 Microanalytical Methods in the Purification and Structural Analysis of Protein. **J.J. L'Italien**

9:50 New Strategies in Biomolecular Mass Spectrometry. **H.R. Morris**

10:40 Solid-State NMR of Biological Systems. **S.J. Opella**

11:20 Microbial Enzymes in Clinical Diagnosis. **T. Atkinson,** M.D. Scawen, C.P. Price, and P.M. Hammond

SECTION D

Symposium on the Use of Computers in Chemistry: Computer Secretariat Inaugural

Cosponsored with Computer Secretariat and Divisions of Chemical Education, Chemical Information, Computers in Chemistry, and Physical Chemistry

R. J. Marcus, *Presiding*

9:00 Introductory Remarks

9:10 The Electronic Laboratory. **R.E. Dessy**

9:50 Computer-Assisted Studies of Molecular Structure–Biological Activity Relationships. **P.C. Jurs**

10:40 Computers in Theoretical Chemistry. **B. Alder**

11:20 Computer-Assisted Design in Organic Synthesis. **W.T. Wipke**

Tuesday Afternoon

SECTION A

Symposium on the Coupling of Liquid Chromatography and Mass Spectrometry

P. Vouros, *Presiding*

1:30 Measurement of Metabolic Kinetics by Thermospray LC/MS and Stable Isotopic Tracers. N.V. Esteban, D.L. Liberato, and **A.L. Yergey**

2:05 Analysis of Heterocycles by Combined LC/MS. **C.G. Edmonds,** J.A. McCloskey, H. Kasai, and S. Nishimura

2:40 Determination of Aldehydes and Ketones by Derivatization and Liquid Chromatography–Mass Spectrometry. **K.L. Olson** and S.J. Swarin

3:30 Application of Thermospray HPLC/MS to the Analysis of Dyes. **R.D. Voyksner** and J.T. Bursay

4:05 Application of LC/MS in the Analysis of Explosives and Their Metabolites. **J. Yinon** and H.-G. Hwang

SECTION B

Symposium on Analytical Methods in Forensic Chemistry

R.C. Briner, *Presiding*

1:30 Introductory Remarks

1:35 Trace Analysis of Drugs in Illicit Preparations and Biological Fluids Using HPLC–Photolysis–Electrochemical Detection (HPLC–hv–EC). **C.M. Selavka,** I.S. Krull, R.J. Nelson, and I. Lurie

1:55 Postcolumn Techniques to Improve the Selectivity and Sensitivity of High-Performance Liquid Chromatography in Forensic Applications. **P.E. Nelson** and S.L. Nolan

2:15 Photochemical Postcolumn Derivatization to Increase Specificity and Sensitivity of Drug Determinations in Samples of Biological Origin. **M. Uihlein**

2:35 Utilization of Ion Chromatography in Forensic Science. **T.L. Rudolph** and E.C. Bender

2:55 Application of Gel Permeation Chromatography to Forensic Science. B.R. Baer, **T.L. Rudolph,** E.C. Bender, and P. Sanderson



"...Outstanding quantitative depth profiling..."

"...Unsurpassable trace analysis..."

"...The INA 3 is a real alternative..."

The first commercial realization of Secondary Neutral Mass Spectrometry, the INA 3 profiled its analytical capabilities at the 1985 Pittsburgh Conference, receiving rave reviews from show attendees.

No wonder. The INA 3 couples ppm sensitivity with fast quantitative analysis. So it readily characterizes the distribution of elements in a multilayer sample.

The sample is sputtered by low-energy ions extracted from a low-pressure plasma. This minimizes atomic mixing and thus ensures unparalleled depth resolution. The sputtered neutrals are ionized in the plasma and subsequently analyzed by the INA 3's quadrupole mass spectrometer. Use it to detect all elements and their isotopes from hydrogen up with comparable sensitivities.

LEYBOLD-HERAEUS

Leybold-Heraeus Vacuum Products, Inc.
5700 Mellon Road, Export, PA 15632
(412) 327-5700 Ext. 528
In Canada (416) 746-0050

CIRCLE 128 ON READER SERVICE CARD

3:25 Applications of the HPLC Retention Index Scale in the Identification of Narcotic Analgesics and in the Identification of Drug Metabolites. **J.K. Baker**
3:45 Analysis, Isolation, and Identification of Phencyclidene Cosynthetics. **L.A. Jones**
4:05 Dopamine and Artifacts in Brain Indicating Cause and Manner of Death. **B. Kaempe,** P. Geertinger, J.L. Pedersen, and K. Helweg-Larsen
4:25 Modified Lipids Arising from Intoxication with Tetrachloromethane. **H. Frank,** B. Link, H. Durk, and D. Thiel

SECTION C

Symposium on ACS Award in Chromatography

A. Zlatkis, *Presiding*

2:00 Investigation of Operating Parameters in High-Performance Displacement Chromatography. **Cs. Horvath,** J. Frenz, and P. van der Schrieck
2:30 Column Selection in Gas Chromatography: Evolutionary Complications. **W. Jennings**
3:00 Smectic Biphenylcarboxylate Ester Liquid-Crystalline Polysiloxane Stationary Phases for Capillary Gas Chromatography. **M.L. Lee,** M. Nishioka, K.E. Markides, B.J. Tarbet, C. Schregenberger, and J.S. Bradshaw
3:50 Recent Developments in Microcolumn Liquid Chromatography. **M. Novotny**
4:20 Open-Tubular (Capillary) Columns—Evolution, Present Status, and Future. **L.S. Ettre**
5:00 Open Meeting of Chromatography and Separations Chemistry Subdivision

SECTION D

General and Mass Spectrometry

N.D. Jespersen, *Presiding*

2:00 Elucidation of Oxygen–Silica Catalytic Reaction Mechanisms at High Temperatures Using Stable-Isotope Mass Spectrometry. **C.E. Batten,** B.T. Upchurch, G.M. Wood, R.T. Swann, R.F. Hoyt, and G.J. Allen
2:15 MS/MS Study of a Chlorine Migration. **G.W. Sovocool,** J.M. Ballard, and J.R. Donnelly
2:30 HPLC–EC and GC/MS Methods in Spin Trapping. **E.G. Janzen,** H.J. Stronks, J.R. Weber, and D.L. Haire
2:45 Application of SIMCA Pattern Recognition to Mass Spectra. **M.G. Koehler** and W.J. Dunn III
3:00 Direct Exposure Mass Spectral Analysis of Prostaglandin H_2. **A.B. Schilling,** D.L. Venton, E.R. Hall, I.M. Zulak, and M.L. Puttemans

SECTION E

Symposium on the Use of Computers in Chemistry: Computer Secretariat Inaugural

Cosponsored with Computer Secretariat and Divisions of Chemical Education, Chemical Information, Computers in Chemistry, and Physical Chemistry

R.J. Marcus, *Presiding*

2:00 Molecular Graphics: Computer-Assisted Insight and Reasoning in Three Dimensions. **R. Langridge**
2:40 Mainframes Here, Minis There, Micros Everywhere: Computers in the Chemistry Curriculum. **J.W. Moore,** E.A. Moore
3:20 Computer-Aided Instruction of the Future. **W.M. Butler**
4:00 The Path of Computerized Chemical Information. **A.K. Valicenti,** R.E. Buntrock
4:40 Computer Hardware and Software in Chemical Information Processing. **J.E. Rush**

Wednesday Morning

SECTION A

Symposium on Analytical Methods in Forensic Chemistry

D.J. Berry, *Presiding*

8:30 Introductory Remarks
8:35 Approaches to Drug Sample Differentiation. **R.H. Liu**
9:05 Comparative Analyses. C.C. Clark and **A. Romano, Jr**
9:25 Methods for the Determination of Anticonvulsant Drugs and Their Metabolites in Biological Samples Following Self-Poisoning. **D.J. Berry**
9:45 Separation of Tedral-Type Drugs by High-Performance Liquid Chromatography. **D. Trivedi**
10:15 Trace Evidence Detection of Amphetamine and Some Other Illicit Drugs. **A.H. Lawrence**
10:35 Radioimmunological Screening and the Identification and Quantitation by HPLC of Barbiturates in Postmortem Blood. **E.M. Koves** and W.C. Sun
10:55 Semiautomated Extraction and Spotting System for TLC Analysis of Drugs in Physiological Fluids. **J.A. Vinson,** J.J. Urash, and D.J. Lopatofsky
11:15 Single-Shot Multidrug Analysis, aka Getting Maximum Output from Minimum Sample Input. **H.K. Garber**
11:35 Spectrophotometric Determination of Sulfa Drugs with Osmium–Tetraoxide. **A. Srivastava** and P.C. Yadav

SECTION B

Retention Mechanisms in Liquid Chromatography

B.A. Bidlingmeyer, *Presiding*

9:00 Retention Mechanism Investigation on Ion Pair Reversed-Phase Chromatography. **S. Ahuja**
9:30 Recent Advances in UV Visualization. **C.T. Santasania,** F.V. Warren, and B.A. Bidlingmeyer
10:00 A Fluorescence Study of Ion Pair Interactions on Hydrocarbon Bonded Surfaces. **S.D. Dowling** and W.R. Seitz
11:00 Buffer Adsorption Effects in Reversed-Phase High-Performance Liquid Chromatography. **S.N. Deming** and J.H. Nickel
11:30 Chromatographic Capabilities of Micellar Mobile Phases. **J.G. Dorsey**

SECTION C

Symposium on ACS Award in Analytical Chemistry

D.C. Kennedy, *Presiding*

9:00 ACS Award in Analytical Chemistry Address: The Role of Separations in Analytical Chemistry. **J.S. Fritz**
10:00 Effects of Reaction Conditions on Porous Chelating Polymers Designed for the Decontamination of Nuclear Waste. **J. Kaczvinsky,** J.S. Fritz, and D.D. Walker
10:20 Chromatographic Strategies for the Separation of Analyte Ions. **D.J. Pietrzyk,** G.L. Schmitt, P.G. Rigas, T.A. Walker, and S.H. Edelmuth

Ion analyses in 20 seconds. Let us show you the way.

Flow Injection Analysis is the fastest and most effective method for routine analyses of ions in water, soil, fertilizers and beverages, for example analyses of NO_2^-, NO_3^-, PO_4^{3-}, NH_4^+, SO_2 and CO_2.

We have led the development of this method and it has resulted in the highly advanced system we have named FIAstar® System.

FIAstar provides for analyses at a very high speed, with production of results within 20 seconds. The consumption of both sample and reagents is extremely low and the rapid start-up/shut-down enable changes of method to be carried out very quickly. In addition FIAstar calculates the results immediately and shows them on a display and a printer/plotter.

Flow Injection Analysis is already well established in a number of fields, which have been the subject of hundreds of publications. Its growth and expansion into new fields is continual, thanks to intensive development of methodology in our application laboratories and in the hands of users all over the world.

Why not allow us to teach you about Flow Injection Analysis? We are world leaders in our fields and we hold seminars at frequent intervals as well as workshops in numbers of cities.

We will be happy to send you more information about the analytical technique of the future, Flow Injection Analysis.



tecator

WE MAKE ROUTINE ANALYSIS SIMPLE.

CIRCLE 201 ON READER SERVICE CARD

Tecator AB. Box 70, S-26301 Höganäs, Sweden. Telephone + 46 42 42330. Telex 72695.
UK: Tecator Ltd, Bristol. Telephone (0454) 417798. USA: Tecator Inc. Herndon, Virginia. Telephone (703) 435 3300.
GERMANY: Tecator GmbH, Rodgau. Telephone (06106) 13072-73. FRANCE: Tecator S.A., Paris. Telephone (1) 260 24 24.

10:50 Recent Developments in Qualitative Gas Chromatography. **R.J. Phillips**
11:10 Fluorescence Activation of Substituted Benzoic Acids. **G.H. Schenk**
11:30 Iodine-129 Analysis in Radioactive Waste. **J.P. Ryan** and W.C. Winn
11:50 Use of Macroreticular Nonionic Resins in Analytical Chemistry and Toxicology. **J.A. Vinson**
12:10 Analysis of 2,3,7,8-Tetrachlorodibenzo-*p*-dioxin in High-Organic Matrices by High-Resolution Gas Chromatography, Low-Resolution Mass Spectrometry. **D.C. Kennedy,** C.H. Byington, M.C. Winter, and P.L. Woods

Wednesday Afternoon

SECTION A

Symposium on X-ray Diffraction and Crystallographic Data Bases: Practices, Problems, Potential

R.L. Harlow, *Presiding*

1:30 Hardware and Software for Analytical Single-Crystal Structure Determination. **R.A. Sparks**
2:00 Two-Dimensional X-ray Detector System for Small-Molecule/Protein Crystallography. **R. Burns**
2:30 Caveat Crystallographer. **R.E. Marsh**
3:00 Use of the NBS Crystal Data File as an Analytical Tool. **A.D. Mighell**
3:30 Crystal Structures from Powder Data. **A. Clearfield** and P.R. Rudolf
4:00 Chemical Applications of Crystal Structures. **P. Murray-Rust**

SECTION B

Symposium on Analytical Methods in Forensic Chemistry

R.H. Liu, *Presiding*

1:30 Introductory Remarks
1:35 Developments in the Detection of Firearms Discharge Residues. **C.R. Midkiff, Jr.**
1:55 Computer Applications in Gunshot Residue Analysis. **J.W. Kilty**
2:15 Multisample Analysis of Bullet Lead Specimens by Neutron Activation. **J.W. Kilty**
2:35 Characterization and Identification of Water-Soluble Explosives. **T.J. Hopen** and J.H. Kilbourn
2:55 Development of Analytical Methods for the Forensic Comparison of Petroleum Products. **D.D. Fetterolf,** D. Thomsen, and B. Baer
3:25 Characterization and Differentiation of Petroleum Jelly in Rape and Child Abuse Cases. **W.A. Morris**
3:45 Presumptive Color Test for Urine Stains. **H.K. Garber**
4:05 Field and Laboratory Screening Test For Methaqualone. J.F. Fischer and **W.A. Morris**
4:25 Sequential Analysis of Latent Fingerprints. **H.C. Lee** and R.E. Gaensslen
4:45 Chemical Tests Employed in Certification of Breath Analyzer Ampules. **H.K. Garber**

SECTION C

Retention Mechanisms in Liquid Chromatography

B. A. Bidlingmeyer, *Presiding*

2:00 Quantitative-Solute Stationary-Phase Interaction. **R. Hartwick** and R.R. Kaliszan
2:30 New Approaches for Investigating Chromatographic Mechanisms. **R.K. Gilpin**
3:00 Solvatochromic Solvent Polarity Measurements and Retention in Reversed-Phase Chromatography. **B.P. Johnson** and J.G. Dorsey
3:45 Discussion of Selectivity and Variability in LC Columns. **S. Ahuja,** Moderator

SECTION D

Symposium on Mass Spectrometry of Middle Molecules; Garvan Medal

R.J. Cotter, *Presiding*

2:00 Introductory Remarks
2:05 Middle-Molecule Mass Spectrometry: Applications to Biomolecules. **C. Fenselau,** K. Hyver, and R. Cotter
2:40 Mass Spectrometry and Biological Chemistry: An Emerging Molecular Symbiosis. **A.L. Burlingame**
3:15 Mass Spectral Approaches to Structural Determination of Large, Biologically Active Molecules. **C.E. Costello**
4:00 Solution of Biomedical Peptide and Carbohydrate Structural Problems by Mass Spectrometry. **I. Jardine**
4:35 High-Field Mass Spectrometry of Glycoconjugates and Polysaccharides. **A. Dell**

Thursday Morning

SECTION A

Symposium on Countercurrent Chromatography

N.B. Mandava, *Presiding*

9:00 Introductory Remarks
9:05 Historical Development of Countercurrent Chromatography. **Y. Ito**
9:35 Theoretical Aspects and Recent Applications of Countercurrent Chromatography. **W.D. Conway**
10:05 Droplet Countercurrent Chromatography in Natural-Products Isolation. **K. Hostettmann**
10:55 Isolation of Bioactive Natural Products by Rotation Locular Countercurrent Chromatography. **I. Kubo**
11:30 Application of Centrifugal Countercurrent Chromatography in the Natural-Product Field. **R.C. Bruening,** F. Derguini, R.K. Okuda, and K. Nakanishi

SECTION B

Symposium on the Impact of Mass Spectrometry on Science; Frank H. Field and Joe L. Franklin Award for Outstanding Achievement in Mass Spectrometry

F.W. McLafferty, *Presiding*

8:45 Introductory Remarks
8:55 Mass Spectrometry in Chemistry. **F.H. Field**
9:30 Extraterrestrial Mass Spectrometry. **K. Biemann**
10:05 Mass Spectrometry in Nuclear Science and Industry. **J.A. Carter,** R.L. Walker, D.H. Smith, and W.H. Christie
10:55 Isotopically Ordered World—Mass Spectrometry in Geochemistry. **J.M. Hayes**
11:30 Mass Spectrometry in Perspective. **A.O.C. Nier**

Not only does the Series 6000 system deliver the best in innovative software for chromatography data handling, it's evolutionary as well. Enhanced and updated on an ongoing basis, this software protects your system from obsolescence.

Evolutionary software maintains your investment over time. It ensures a path for system development by giving you access to the most advanced software, hardware and peripherals as they become available.

Teamed with the HP 1000A Series computer, our powerful software forms a true multi-tasking, multi-user system.

This system adeptly supports your laboratory's data acquisition, calculation, reporting and archiving needs.

Powerful interactive graphics offer unparalleled flexibility. And



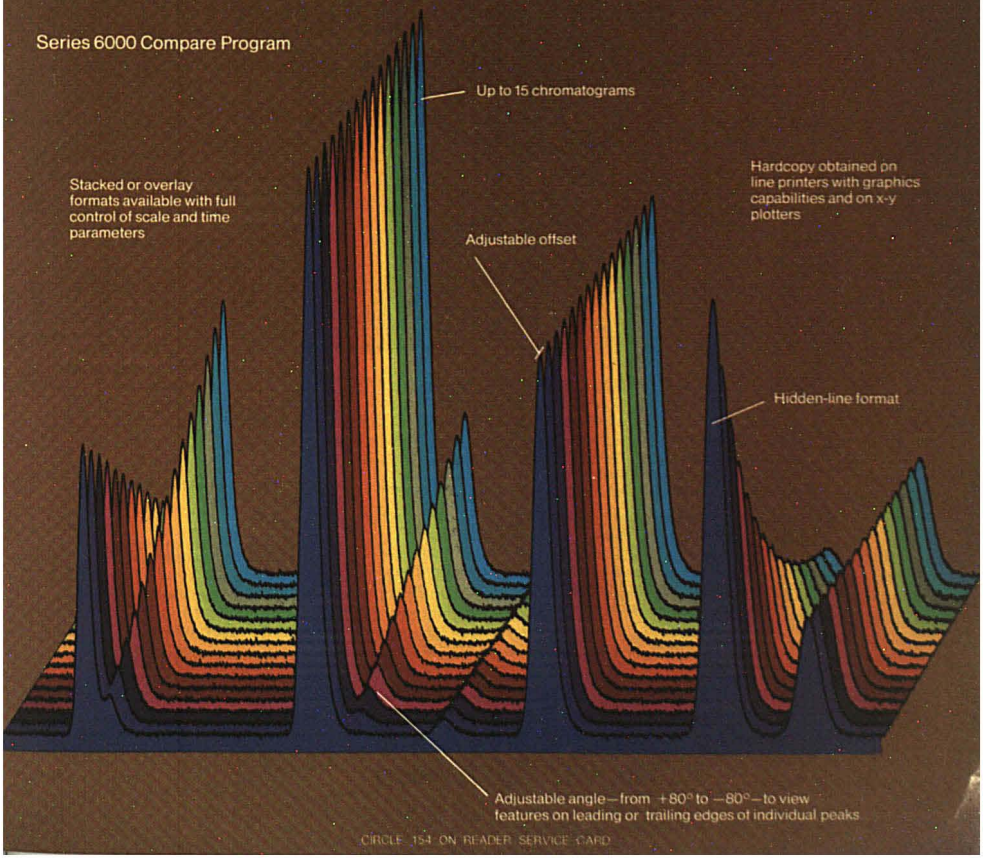
when it comes to networking, the Series 6000 can transfer files between HP 1000A Series, DEC VAX and HP desktop computers.

And to address your lab management needs, a new companion software package, the LMS 7000, handles data base and sample management.

Please call or write for more information. 10061 Bubb Road, Cupertino, California 95014, (408) 725-1107. East Coast: 205 Robin Road, Paramus, New Jersey 07652, (201) 967-8980.

nelson ANALYTICAL

Beyond COMPARE. Our evolving software for the multi-user laboratory environment.



CIRCLE 154 ON READER SERVICE CARD

SECTION C

Symposium on Analytical Methods in Forensic Chemistry

F.P. Smith, *Presiding*

8:45 Introductory Remarks
8:50 Theory and Use of Radiative Energy Attenuation for the Quantitation of Analytes in Forensic Samples. **D.A. Yost**
9:10 Quantitation of Ethanol in Forensic Samples by Radiative Energy Attenuation. **P.L. Cary**
9:30 Simultaneous Electrophoretic Determination of Phosphoglucomutase Subtypes, Adenosine Deaminase, Erythrocyte Acid Phosphatase, and Adenylate Kinase Enzyme Phenotypes. **T.L. Wolson** and W.C. Stuver
9:50 Ultrathin Polyacrylamide Isoelectric Focusing of Phosphoglucomutase (PGM_1) Allozymes: Further Modifications. B. Budowle and **R.S. Murch**
10:20 Applications of Radioimmunoassay in Forensic Science. **F.P. Smith**
10:40 Latex Particle Agglutination Techniques in Immunoassay. **J.E. Craine**
11:00 Use of Enzymes as Reagents in Forensic Chemistry. **C.P. Price**

SECTION D

General—Liquid Chromatography

J.G. Nikelly, *Presiding*

9:00 Reversed-Phase Liquid Chromatography Using a Chromophore in the Mobile Phase. P.K. Gupta and **J.G. Nikelly**
9:20 Deconvolution of Overlapping Chromatograms Using Constrained Nonlinear Optimization. **R.A. Vaidya** and R.D. Hester
9:40 Effect of the Silica Support of Bonded Reversed-Phase Columns on Chromatography of Some Antibiotic Compounds. **W.A. Moats**
10:00 Analysis of Anticonvulsants in Serum by Internal-Surface Reversed-Phase HPLC. **T.C. Pinkerton,** H.I. Hagestam, and T.D. Miller
10:40 Chemical Derivatization Approach to Sensitive Analysis of Quaternary Ammonium Compounds. **S.L. Abidi**
11:00 Determination of the Decomposition Products of BHT in Aqueous Systems. **S.L. Varner** and C.V. Breder
11:20 Analytical Procedure for Measuring Levels of Organic Additives in Compounded, Uncured EPDM Rubber. **M.E. Quinn**
11:40 HPLC Determination of Lincomycin and Spectinomycin Using a Single Analytical System. **S.M. Ledden,** T.A. Zwier, and P.B. Bowman

Thursday Afternoon

SECTION A

Symposium on Countercurrent Chromatography

W.D. Conway, *Presiding*

2:00 Introductory Remarks
2:05 Application of Countercurrent Chromatography to Agrochemicals. **N.B. Mandava**
2:35 Countercurrent Chromatography in Drug Discovery and Development. **D.G. Martin**

This catalog offers over 125 gases and 250 equipment items.



Get one. FREE.

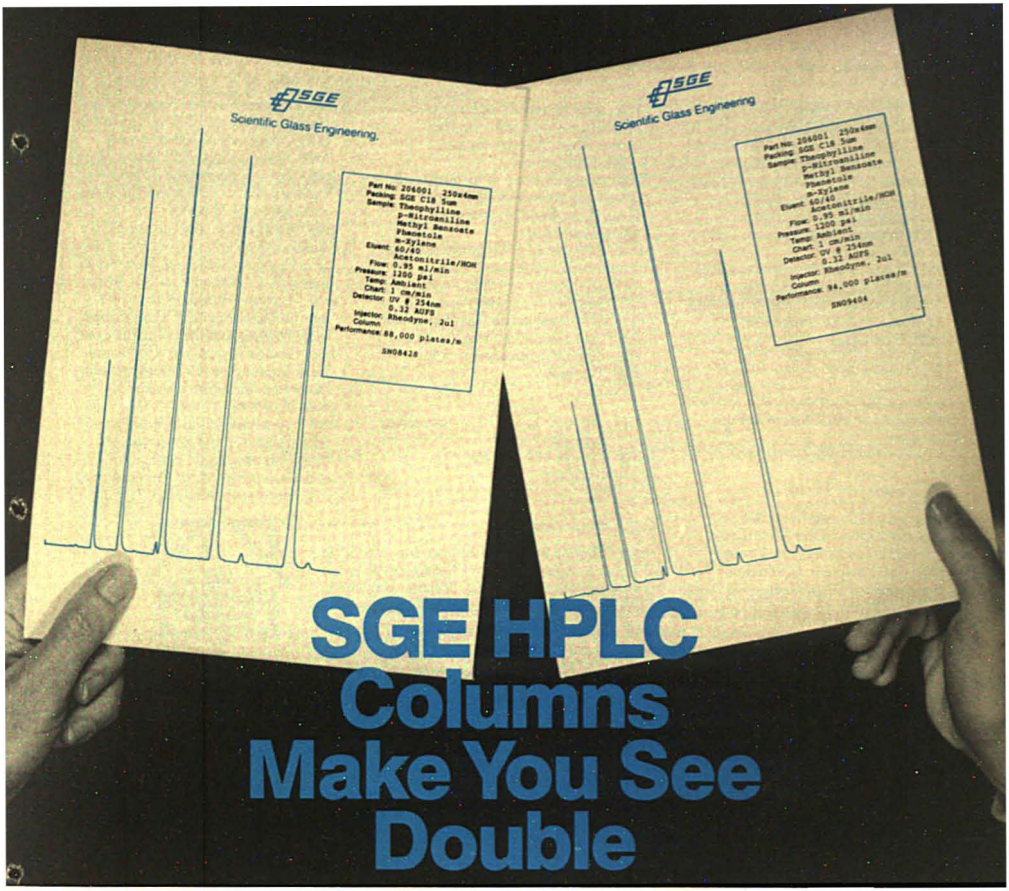
The new MG catalog #484 is a comprehensive guide to hundreds of specialty gases and gas handling equipment items—all at very reasonable prices. It lists research grade gases, instrument carrier gases, calibration mixtures, EPA protocol standards and it includes a new section on specialty gases for electronics, semiconductors, plasma etching and lasers.

We give you a choice of hardware including brass or high purity stainless steel regulators, a variety of specialty valves, filters, purifiers and electronic mass flowmeters and controllers. And you'll find everything you need to know about safe handling of gases and selection of the proper equipment. Write for your copy today.

MG Industries, P.O. Box 945, Valley Forge, PA 19482.

MG Industries™
Scientific Gas Division

CIRCLE 146 ON READER SERVICE CARD



SGE HPLC Columns Make You See Double

...thanks to Glass Lined Tubing (GLT)

CLEAN—nothing to contaminate the packing material

SMOOTH—for consistently high column efficiency

UNIFORM—for reproducible retention times

INERT—nothing to contaminate the packing or detector, or affect the sample

The Proof is in the Chromatography

SGE endeavors to produce the highest quality HPLC columns in the industry.

We start out with precision tubing; our own glass-lined-stainless-steel tubing (GLT) with an inner surface as "smooth as glass." Silica particles that are closely controlled in porosity, surface area and particle size are then packed at high pressures. These are two of the most important factors that control reproducibility and high performance. Plate counts for our 4mm I.D. C_{18} columns exceed 80,000 plates/meter. Each column is individually tested and shipped with the test chromatogram.

SGE SCIENTIFIC GLASS ENGINEERING

7 Argent Place, Ringwood, Victoria, 3134. Australia. Tel: (03) 874 6333

Potters Lane, Kiln Farm, Milton Keynes MK11 3LA, Great Britain, Tel: (0908) 56 8844

2007 Kramer Lane, Suite 100, Austin, Texas 78758. U.S.A. Tel: (512) 837 7190

Fichtenweg 15, D-6108 Weiterstadt 1, West Germany Tel: (06150) 40662

10 Rue Henri Janin F94190 Villeneuve St Georges France Tel 1/382 29 43

CIRCLE 198 ON READER SERVICE CARD

3:05 Countercurrent Chromatography of Synthetic Peptides on the Ito Coil Planet Centrifuges. **M. Knight**
3:55 Organelle Fractionation in Aqueous Two-Phase Polymer Systems Using Countercurrent Chromatography. I.A. Sutherland, **D. Haywood-Waddington,** and T.J. Peters
4:25 Countercurrent Chromatography of Biological Membranes in Phase Transfer Systems Consisting of Water-Soluble Polymers. **S.D. Flanagan**

SECTION B

Symposium on ACS Award in Pure Chemistry

W.D. Reents, Jr., *Presiding*

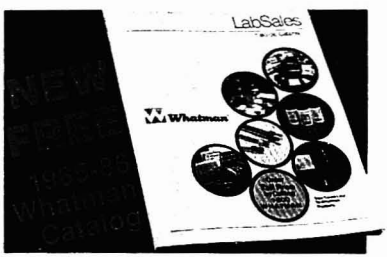
2:00 Introductory Remarks
2:05 Solution-Phase Metal Ion-Molecule Chemistry. **H. Freiser**
2:35 Ion Cyclotron Resonance Spectroscopy: Two Decades of Development and Application. **J.L. Beauchamp**
3:05 Fundamentals of Fourier Transform Ion Cyclotron Resonance Mass Spectroscopy. **M.B. Comisarow**
3:45 Identification of Impurities in Electronic Gases Using Fourier Transform Mass Spectrometry. **W.D. Reents, Jr.**
4:15 Chemistry of Organotransition Metal Ions in the Gas Phase. **D.B. Jacobson** and B.S. Freiser
4:45 Reactions of Metal Ions and Their Clusters in the Gas Phase Using Laser Ionization–Fourier Transform Mass Spectrometry. **B.S. Freiser**

SECTION C

General—Gas and Liquid Chromatography

D.E. Jones, *Presiding*

2:00 Eluent Pressure Detector for Aqueous Size Exclusion Chromatography of High-Molecular-Weight Water-Soluble Polymers. R.D. Hester and **C.E. Lundy**
2:20 Application of a Swept-Potential Electrochemical Detector to the HPLC Analysis of Nitrosamines. **M.B. Thomas** and P.E. Sturrock
2:40 New Concepts for Enhancing the Flexibility of Micromeritics Autoinjectors. **H. Joshua**
3:00 Calibration Method for PCB Analysis by Capillary GC with Electron Capture Detection. **R.E. Wagner,** J.C. Carnahan, and R.J. May
3:40 Internal Standard for Capillary GC Analysis of PCB Mixtures. R.E. Wagner and **J.C. Carnahan**
4:00 Redox Chemiluminescence: A New Approach to Chromatography Detection. R.E. Sievers and **S.A. Nyarady**
4:20 Investigation into Relation of GLC Behavior and Structure of Simple Heterocyclic Compounds and Derivatives. **S.M. Farroha,** A.E. Habboush, and M.B. Hemza



This full-color, easy-to-use catalog describes thousands of products for handling your HPLC, TLC, AIEC, membrane filtration, and instrumentation needs ...with new products and much, much more.

To Order your free catalog:

Call Toll-Free
1-800-WHATMAN
In Oregon, Alaska
or Hawaii dial
(503) 648-0762

Or write to
Whatman LabSales
P.O. Box 1359
Hillsboro, OR 97123

Whatman
A Part of Whatman International

CIRCLE 34 ON READER SERVICE CARD

Attention: **Chemical Scientists**

Do you want to . . .

- Keep up to date?
- Increase professional contacts?
- Receive substantial discounts on publications?
- Present your latest research?
- Receive assistance in financial planning?
- Attend chemical expositions?
- Find a new position?
- Continue your chemical education?

If you can say "yes" to even one of these the **ACS** should be *your* Society!

Write or call today for information about these and many other benefits.

Membership Development Office
American Chemical Society
1155 16th St., N.W.
Washington, D.C. 20036
202-872-4437

15-DAY FREE EXAM—BOOKS FROM WILEY-INTERSCIENCE

MODERN PRACTICE OF GAS CHROMATOGRAPHY, 2nd Edition

Robert L. Grob

This handy reference treats the theory, instrumentation, and applications of chromatography. Completely up to date, it includes new chapters on applications to the petroleum field, high resolution gas chromatography, and more.
approx. 732 pp. (1-87157-5) **May 1985** $65.00

RECEPTOR MODELING IN ENVIRONMENTAL CHEMISTRY

Philip K. Hopke

Systematically presents the analytical and mathematical methods that have been developed and used to characterize airborne particulate matter and indentify its sources.
approx. 352 pp. (1-89106-1) **April 1985** $75.00

A GUIDE TO THE HPLC LITERATURE

Volume 1: 1966-1979
Volume 2: 1980-1981
Volume 3: 1982

Henri Colin, Ante M. Krstulovic, Jean-Louis Excoffier & Georges Guiochon

Vol. 1: approx. 960 pp. (1-87993-2) **1984** $125.00
Vol. 2: approx. 928 pp. (1-87992-4) **March 1985** $125.00
Vol. 3: approx. 536 pp. (1-80687-0) **March 1985** $100.00
3 Vol. Set (1-82056-3) **March 1985** $300.00

BLACK CARBON IN THE ENVIRONMENT

Edward D. Goldberg

A concise introduction to the properties of black carbons produced, by coal, wood, and vegetable combustion. Examines the behavior and effects of natural and anthropogenic black carbons on our physical and biological environments.
150 pp. (1-81979-4) **April 1985** In Press

COAL LIQUIFICATION PRODUCTS NMR Spectroscopic Characterization and Production Processes, Vol. 1

Edited by H.D. Schultz

The contributors to this volume cover the lab experimentation and applications of coal liquifaction and chart the latest developments in liquifaction fuel development.
415 pp. (1-89232-7) **1983** $69.95

ANALYTICAL SOLUTION CALORIMETRY

Edited by J. Keith Grime

A comprehensive guide to the application of calorimetry in analytical chemistry and the determination of thermodynamic parameters.
approx. 400 pp. (1-86942-2) **April 1985** $60.00

BASIC BIOCHEMICAL METHODS

Renee R. Alexander, Joan M. Griffiths & Maria L. Wilkinson

The only biochemistry manual to explain and illustrate methods developed within the past six years, including Bradford protein-dye binding and recombinant DNA methodology.
approx. 256 pp. (1-88027-2) **1985** $24.95 (paper)

INSTRUMENTATION FOR ENVIRONMENTAL MONITORING Volume 2: Water, 2nd Edition

Lawrence Berkeley Laboratory

Updated to reflect recent developments, this book presents all available data on environmental monitoring instruments in one comprehensive source.
approx. 1,200 pp (1-88567-3) **May 1985** In Press

AUGER ELECTRON SPECTROSCOPY

Michael Thompson, M.D. Baker, Alec Christie & J.R. Tyson

The first comprehensive treatment of AES, covering all aspects from theoretical calculations to practical surface analysis.
384 pp. (1-04377-X) **1985** $75.00

TECHNIQUES AND APPLICATIONS OF THIN LAYER CHROMATOGRAPHY

Edited by Joseph C. Touchstone & Joseph Sherma

Comprehensive, current information on the application of thin layer chromatography (TLC) as presented at the December 1982 Third Biennial Symposium.
400 pp. (1-88017-5) **February 1985** $70.00

INORGANIC CHROMATOGRAPHIC ANALYSIS

Edited by John C. MacDonald

An introductory monograph summarizing inorganic chromatographic analysis. As the first book in the field, it treats the principles and applications of the analysis in its various forms including ion chromatography.
approx. 450 pp. (1-86263-0) **March 1985** $65.00

SPOT TEST ANALYSIS Environmental, Forensic and Geochemical Applications

Ervin Jungreis

Presents the fastest, least expensive ways to perform detailed, accurate spot and screening tests for a variety of applications in the clinical, forensic, geochemical, soil, food and water, and occupational safety fields.
315 pp. (1-86524-9) **1985** $60.00

MOLECULAR LUMINESCENCE SPECTROSCOPY Part 1: Methods and Applications

Edited by Stephen G. Schulman

The most up-to-date, encyclopedic coverage available of methods of luminescence analysis, including flourescence, phosphorescence, and chemiluminescence.
approx. 830 pp. (1-86848-5) **April 1985** $85.00

MASS SPECTROMETRY OF HETEROCYCLIC COMPOUNDS, 2nd Edition

Q. N. Porter

Covering the important mass spectrometry literature since 1981, this volume contains six new chapters and nearly twice as much material as the previous edition, including discussions of chemic ionization, field ionization and desorption, and negative ions.
approx. 1,000 pp. (1-09901-5) **April 1985** $250.00

ANALOG AND DIGITAL ELECTRONICS FOR SCIENTISTS, 3rd Edition

Basil H. Vassos & Galen W. Ewing

Third edition of the standard reference on practical electronics for laboratory scientists. Contains improved coverage of microprocessors and microcomputers, as well as interfacing components. Expanded treatment of equivalent circuits, Kirschoff's laws, Nyquist and Bod diagrams, and more. New chapter on Boolean algebra and Karvaugh maps.
approx. 450 pp. (1-81138-6) **May 1985** * In Press

KIRK-OTHMER CONCISE ENCYCLOPEDIA OF CHEMICAL TECHNOLOGY

1,300 pp. (1-86977-5) **January 1985** $99.95
(Special Introductory Price. After June 30, 1985—$129.95)
Available through your bookstore or phone for 15-day free examination

TO ORDER FOR 15-DAY FREE EXAM,

CALL TOLL FREE
1 800 526-5368

In New Jersey, call collect (201) 342-6707 Order code #5-1724

WILEY-INTERSCIENCE
a division of John Wiley & Sons, Inc.
605 Third Avenue, New York, N.Y. 10158
In Canada: 22 Worcester Road, Rexdale, Ontario M9W 1L1
Prices subject to change and higher in Canada 092-5-1724

CIRCLE 234 ON READER SERVICE CARD

SACP Starter Grant Program Announced

The Society for Analytical Chemists of Pittsburgh (SACP) will award $5000 grants to two recently appointed assistant professors of analytical chemistry. The grants are meant to encourage research and to promote the development of graduate students in the field.

The competition is open to any assistant professor who has accepted a college or university appointment since Dec. 31, 1981. Application forms are available from J. D. Sember, Calgon Corporation, P.O. Box 1346, Pittsburgh, Pa. 15230, 412-777-8555. Completed applications are due by April 15; winners will be announced in May.

Meetings

The following meetings are newly listed in ANALYTICAL CHEMISTRY. *Other 1985 meetings are listed in the January and February issues.*

■ **Applications and Techniques of Modern Spectrochemistry.** May 13–14. Albuquerque, N.M. *Contact: L. J. Radziemski, New Mexico State University, Las Cruces, N.M. 88003-0004*

■ **7th Symposium on Applied Surface Analysis.** May 15–17. College Park, Md. *Contact: J. S. Murday, Naval Research Lab, Washington, D.C. 20375*

■ **Annual Meeting of the American Association of Bioanalysts.** May 20–25. Orlando, Fla. *Contact: American Association of Bioanalysts, Suite 918, 818 Olive St., St. Louis, Mo.*

■ **Annual Meeting of the Council for Optical Radiation Measurements.** May 29–30. Gaithersburg, Md. *Contact: Norbert Johnson, 3M Center, Bldg. 582-1-15, St. Paul, Minn. 55144*

■ **International Symposium on Nuclear Analytical Chemistry.** June 5–7. Halifax, Canada. *Contact: R. E. Jervis, Chemical Engineering & Applied Chemistry, 200 College St., Toronto M5S 1A4, Ontario, Canada*

■ **7th International Conference on Laser Spectroscopy.** June 24–28. Kaanapali, Maui, Hawaii. *Contact: T. W. Hansch, SEICOLS '85, Department of Physics, Stanford University, Stanford, Calif. 94305*

■ **International Meeting on NMR Spectroscopy.** July 8–12. Cambridge, England. *Contact: John Gibson, Royal Society of Chemistry, Burlington House, London W1V 0BN, England*

■ **40th Annual Calorimetry Conference.** Aug. 25–30. Asilomar, Calif. *Contact: Stephen Mraw, Exxon, Rt. 22 East, Clinton Township, Annandale, N.J. 08801*

■ **28th ORNL Conference on Analytical Chemistry in Energy Technology.** Oct. 1–3. Knoxville, Tenn. *Contact: W. S. Lyon, Analytical Division, Oak Ridge National Laboratory, P.O. Box X, Oak Ridge, Tenn. 37830*

■ **2nd Symposium on Handling of Environmental and Biological Samples in Chromatography.** Oct. 24–25. Freiburg, F.R.G. *Contact: M. Frei-Hausler, Postfach 46, CH-4123 Allschwil 2, Switzerland*

Short Courses

ACS courses. These new courses will be listed only once. For information on other ACS courses, see back issues and contact Department of Educational Activities, American Chemical Society, 1155 16th St., N.W., Washington, D.C. 20036, 202-872-4508.

The following courses are being offered in conjunction with the 189th ACS National Meeting in Miami Beach, Fla., April 28–May 3, 1985.

Statistics for Experimental Design. April 26–28. Stanley Deming, Stephen Morgan. $615, ACS members; $695, nonmembers

Liquid Chromatography—Mass Spectrometry. April 27–28. Jack Henion, Dai Games. $485, ACS members; $535, nonmembers

Quality Assurance of Chemical Measurements. April 27–28. John K. Taylor. $485, ACS members; $535, nonmembers

Effective Management of Chemical Analysis Laboratories. April 27–28. John H. Taylor, Mary McKown. $485, ACS members; $535, nonmembers

Capillary Gas Chromatography: Techniques and Problem Solving. April 28–29. Milos Novotny, Stuart Cram. $485, ACS members; $535, nonmembers

Introduction to HPLC with Biological Applications. April 29–30. David Freeman, Frederic Rabel, M. Patricia Strickler. $485, ACS members; $535, nonmembers

For Your Information

Pragma Bio-Tech, Inc. has added an analytical laboratory to its clinical pharmacology research facility. The lab will enable Pragma's staff to generate drug level data on-site with state-of-the-art instrumentation and a computer data management system. Chromatographic and immunoassay methodologies are being established as the major analytical techniques. Contact Pragma Bio-Tech, Inc., 225 Belleville Ave., Bloomfield, N.J. 07003 for further information.

The National Bureau of Standards has made the first major revision of procedures for the **National Voluntary Laboratory Accreditation Program** (NVLAP) since it was established eight years ago. Among the major revisions are a simplified method for requesting a new accreditation program, updated NVLAP criteria for compatibility with new national and international standards criteria, and reciprocal recognition of NVLAP-accredited labs by foreign accreditation systems. For a copy of the new procedures contact: Associate Manager Laboratory Accreditation, A531 Administration Building, National Bureau of Standards, Gaithersburg, Md. 20899, 301-921-3431.

Hewlett-Packard's Analytical Products Group has consolidated all of its supplies product lines into the **Analytical Supplies Operation** (ASO). Chartered to provide columns and other supplies to the analytical instrumentation market, ASO is headquartered at H-P's division in Avondale, Pa. The major activities of the new operation are the development, manufacture, and marketing of GC and LC columns. Supplies will continue to be available through the field sales force or by calling the Corporate Parts Center's toll-free number, 800-227-9770.

IT Corporation has announced the acquisition of **Stoner Laboratories** of Santa Clara, Calif., making it the sixth in IT's network of environmental analytical facilities. Stoner Labs has specialized in pesticide analysis for over 25 years. This acquisition will allow IT to offer a full range of analytical services to northern California. The new site is located at 397 Mathew St., Santa Clara, Calif. 95050, 408-727-4277.

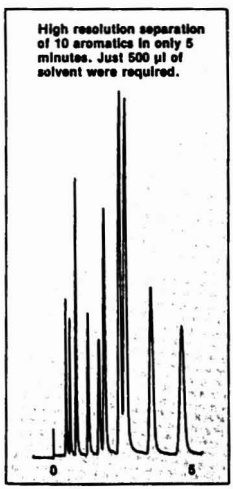
ISCO'S NEW MICROBORE LC GIVES YOU BETTER RESOLUTION AND PICOGRAM DETECTION.

With 1 mm columns and flow rates below 100 µl/min, micro LC dramatically increases analytical performance, saves expensive solvents, and lets you use smaller samples. But most of the micro LC systems available throw away much of the advantage. All but ISCO use a detector cell that wastes resolution and sensitivity with a 0.5 to 3 µl volume and short pathlength, and most systems lose even more because they utilize an ordinary HPLC reciprocating pump and have external fittings and tubing.

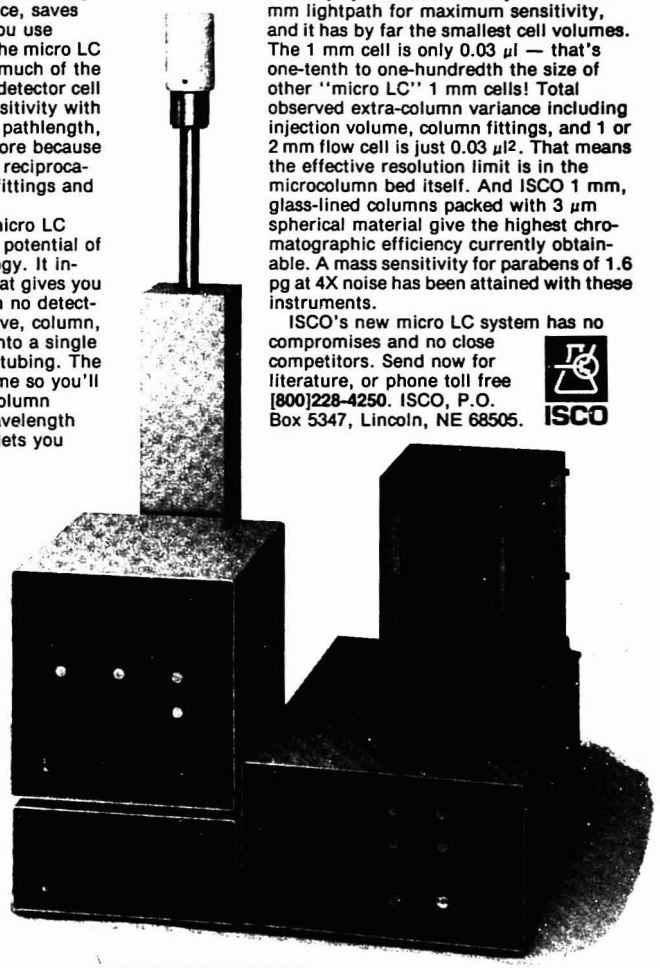
ISCO's second generation micro LC system lets you realize the full potential of current microbore LC technology. It includes a 50 ml syringe pump that gives you absolutely pulse-free flow with no detectable pump noise. Injection valve, column, and cell all connect together into a single assembly with no intervening tubing. The detector has a 0.05 sec rise time so you'll see the peaks exactly as the column resolved them. Continuous wavelength selection from 190 to 750 nm lets you always work under the best conditions. It's the only system that offers you a full 10 mm lightpath for maximum sensitivity, and it has by far the smallest cell volumes. The 1 mm cell is only 0.03 µl — that's one-tenth to one-hundredth the size of other "micro LC" 1 mm cells! Total observed extra-column variance including injection volume, column fittings, and 1 or 2 mm flow cell is just 0.03 μl^2. That means the effective resolution limit is in the microcolumn bed itself. And ISCO 1 mm, glass-lined columns packed with 3 µm spherical material give the highest chromatographic efficiency currently obtainable. A mass sensitivity for parabens of 1.6 pg at 4X noise has been attained with these instruments.

ISCO's new micro LC system has no compromises and no close competitors. Send now for literature, or phone toll free [800]228-4250. ISCO, P.O. Box 5347, Lincoln, NE 68505.

ISCO



High resolution separation of 10 aromatics in only 5 minutes. Just 500 µl of solvent were required.

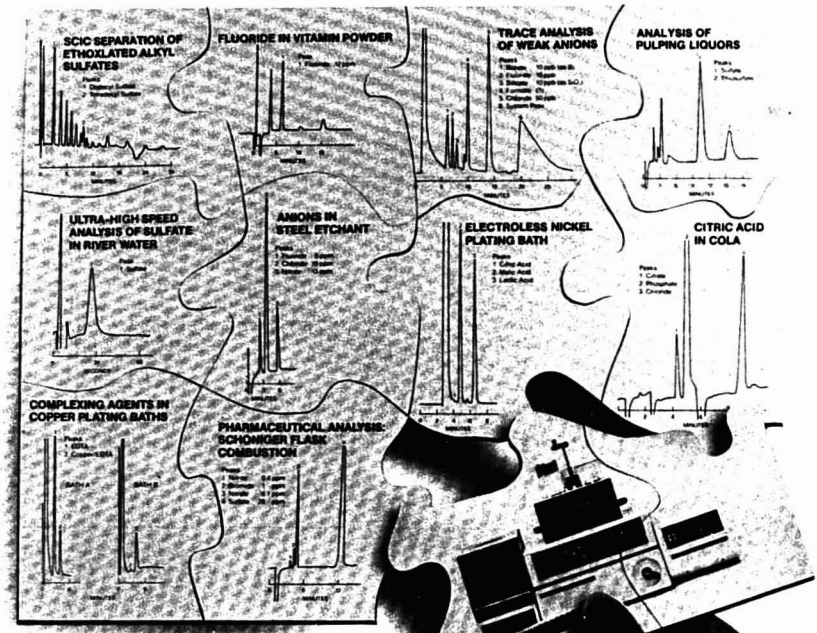


CIRCLE 105 ON READER SERVICE CARD

Solving the Ion Analysis Puzzle.

Here are just 10 of the many hundred solutions from

WESCAN



Bringing it all together:

We can help you analyze for virtually any ionic species: ☐ Anions ☐ Cations ☐ Organic Acids ☐ Surfactants ☐ Metals. With sensitivity down to the parts-per-billion level, and analysis times measured in seconds. Want to find out how WE can help YOU save time, effort, money in ion analysis? Just contact the Wescan Applications Group.

WESCAN

WESCAN INSTRUMENTS, INC.

3018 Scott Blvd., Santa Clara, CA 95054, (408) 727-3519, TELEX 171627 ATTN: WESCAN

CIRCLE 235 ON READER SERVICE CARD

Chemistry and Crime

From Sherlock Holmes to Today's Courtroom



Samuel M. Gerber, *Editor*

An illuminating view of forensic science in fact and fiction. Underlines the relationship between detective fiction and the development of modern forensics. Begins with examples of chemistry at work in the novels of crime fiction writers such as Arthur Conan Doyle and Dorothy L. Sayers. Recounts how the sleuthing techniques in detective fiction laid the foundation for the sophisticated analytical methods of modern forensic science. Relates case histories in which modern forensics played a keynote role.

CONTENTS

Medical School Influences on the Fiction of Arthur Conan Doyle • Strong Poison: Chemistry in the Works of Dorothy L. Sayers • A Study in Scarlet: Blood Identification in 1875 • Forensic Science: Winds of Change • Chemistry and the Challenge of Crime • The Elemental Comparison of Bullet-Lead Evidence Specimens • Bloodstain Analysis: Case Histories • Bloodstain Analysis: Serological and Electrophoretic Techniques • Forensic Data in the Judicial Process

Based on a symposium sponsored by the Division of History of Chemistry of the American Chemical Society

135 pages (1983) Clothbound
LC 83-11907 ISBN 0-8412-0784-4
US & Canada **$19.95** Export **$23.95**

135 pages (1983) Paper
LC 83-11907 ISBN 0-8412-0785-2
US & Canada **$14.95** Export **$17.95**

Order from:
American Chemical Society
Distribution Office Dept. 54
1155 Sixteenth St., N.W.
Washington, DC 20036
or CALL TOLL FREE 800-424-6747
and use your VISA or MasterCard.

MARCH 1985 — **VALID THROUGH JULY 1985**

ADVERTISED PRODUCTS:

7	8	9	10	11	12	13	14	15	16	17
18	19	20	21	22	23	24	25	26	27	28
29	30	31	32	33	34	35	36	37	38	39
40	41	42	43	44	45	46	47	48	49	50
51	52	53	54	55	56	57	58	59	60	61
62	63	64	65	66	67	68	69	70	71	72
73	74	75	76	77	78	79	80	81	82	83
84	85	86	87	88	89	90	91	92	93	94
95	96	97	98	99	100	101	102	103	104	105
106	107	108	109	110	111	112	113	114	115	116
117	118	119	120	121	122	123	124	125	126	127
128	129	130	131	132	133	134	135	136	137	138
139	140	141	142	143	144	145	146	147	148	149
150	151	152	153	154	155	156	157	158	159	160
161	162	163	164	165	166	167	168	169	170	171
172	173	174	175	176	177	178	179	180	181	182
183	184	185	186	187	188	189	190	191	192	193
194	195	196	197	198	199	200	201	202	203	204
205	206	207	208	209	210	211	212	213	214	215
216	217	218	219	220	221	222	223	224	225	226
227	228	229	230	231	232	233	234	235	236	237
238	239	240	241	242	243	244	245	246	247	248
249	250	251	252	253	254	255	256	257	258	259
260	261	262	263	264	265	266	267	268	269	270
271	272	273	274	275	276	277	278	279	280	281
282	283	284	285	286	287	288	289	290	291	292
293	294	295	296	297	298	299	300	301	302	303
304	305	306	307	308	309	310	311	312	313	314

NEW PRODUCTS:

401	402	403	404	405	406	407	408	409	410	411
412	413	414	415	416	417	418	419	420	421	422
423	424	425	426	427	428	429	430	431	432	433
434	435	436	437	438	439	440	441	442	443	444
445	446	447	448	449	450	451	452	453	454	455
456	457	458	459	460	461	462	463	464	465	466
467	468	469	470	471	472	473	474	475	476	477
478	479	480	481	482	483	484	485	486	487	488
489	490	491	492	493	494	495				

TO VALIDATE THIS CARD, PLEASE CHECK ONE ENTRY FOR EACH CATEGORY BELOW:

Intensity of product need:
- ☐ 1. Have salesman call
- ☐ 2. Need within 6 mos.
- ☐ 3 Future project

Primary field of work:
- ☐ A. Energy
- ☐ B. Environmental
- ☐ C. Medical/Clinical
- ☐ D. Drug/Toiletries
- ☐ E. Forensic/Narcotic
- ☐ F. Biotechnology
- ☐ G. Metals
- ☐ H. Pulp Paper/Wood
- ☐ I. Soaps Cleaners
- ☐ J. Paint Coating Ink
- ☐ K. Electrical Electronic
- ☐ L. Instrument Dev./Des
- ☐ M. Plastic Polymer/Rub
- ☐ N. Agricultural Food
- ☐ O. Inorganic Chemicals
- ☐ P. Organic Chemicals

Primary area of employment.

INDUSTRIAL
- ☐ A. Research/Development
- ☐ B. Quality/Process Control

MEDICAL/HOSPITAL
- ☐ C. Research/Development
- ☐ D. Clinical/Diagnostic

GOVERNMENT
- ☐ E. Research/Development
- ☐ F. Regulate/Investigate

COLLEGE/UNIVERSITY
- ☐ G. Research/Development
- ☐ H. Teaching

INDEPENDENT/CONSULTING
- ☐ I. Research/Development
- ☐ J. Analysis/Testing

CIRCLE 314 FOR SUBSCRIPTION FORM TO ANALYTICAL CHEMISTRY

NAME _____

TITLE _____

FIRM _____

STREET _____

CITY _____

STATE _____ ZIP _____

PHONE (___) _____

NEED MORE INFORMATION?

CIRCLE a key number. . .

SEND IN the postage paid reply card. . .

AND GET free data on any product advertised in this issue. . .

NO POSTAGE NECESSARY IF MAILED IN THE UNITED STATES

BUSINESS REPLY CARD

FIRST CLASS Permit #27346 Philadelphia, Pa

POSTAGE WILL BE PAID BY ADDRESSEE

analytical chemistry

P.O. BOX #7826
PHILADELPHIA, PA 19101

NO POSTAGE NECESSARY IF MAILED IN THE UNITED STATES

BUSINESS REPLY CARD

FIRST CLASS Permit #27346 Philadelphia, Pa

POSTAGE WILL BE PAID BY ADDRESSEE

analytical chemistry

P.O. BOX #7826
PHILADELPHIA, PA 19101

NEED MORE INFORMATION?

CIRCLE a key number. . .

SEND IN the postage paid reply card. . .

AND GET free data on any product advertised in this issue. . .

MARCH 1985

VALID THROUGH JULY 1985

ADVERTISED PRODUCTS:										
7	8	9	10	11	12	13	14	15	16	17
18	19	20	21	22	23	24	25	26	27	28
29	30	31	32	33	34	35	36	37	38	39
40	41	42	43	44	45	46	47	48	49	50
51	52	53	54	55	56	57	58	59	60	61
62	63	64	65	66	67	68	69	70	71	72
73	74	75	76	77	78	79	80	81	82	83
84	85	86	87	88	89	90	91	92	93	94
95	96	97	98	99	100	101	102	103	104	105
106	107	108	109	110	111	112	113	114	115	116
117	118	119	120	121	122	123	124	125	126	127
128	129	130	131	132	133	134	135	136	137	138
139	140	141	142	143	144	145	146	147	148	149
150	151	152	153	154	155	156	157	158	159	160
161	162	163	164	165	166	167	168	169	170	171
172	173	174	175	176	177	178	179	180	181	182
183	184	185	186	187	188	189	190	191	192	193
194	195	196	197	198	199	200	201	202	203	204
205	206	207	208	209	210	211	212	213	214	215
216	217	218	219	220	221	222	223	224	225	226
227	228	229	230	231	232	233	234	235	236	237
238	239	240	241	242	243	244	245	246	247	248
249	250	251	252	253	254	255	256	257	258	259
260	261	262	263	264	265	266	267	268	269	270
271	272	273	274	275	276	277	278	279	280	281
282	283	284	285	286	287	288	289	290	291	292
293	294	295	296	297	298	299	300	301	302	303
304	305	306	307	308	309	310	311	312	313	314

NEW PRODUCTS:				401	402	403	404	405	406	407
408	409	410	411	412	413	414	415	416	417	418
419	420	421	422	423	424	425	426	427	428	429
430	431	432	433	434	435	436	437	438	439	440
441	442	443	444	445	446	447	448	449	450	451
452	453	454	455	456	457	458	459	460	461	462
463	464	465	466	467	468	469	470	471	472	473
474	475	476	477	478	479	480	481	482	483	484
485	486	487	488	489	490	491	492	493	494	495

TO VALIDATE THIS CARD, PLEASE CHECK ONE ENTRY FOR EACH CATEGORY BELOW:

Intensity of product need:
- ☐ 1. Have salesman call
- ☐ 2. Need within 6 mos.
- ☐ 3. Future project

Primary field of work:
- ☐ A. Energy
- ☐ B. Environmental
- ☐ C. Medical/Clinical
- ☐ D. Drug/Toiletries
- ☐ E. Forensic/Narcotic
- ☐ F. Biotechnology
- ☐ G. Metals
- ☐ H. Pulp, Paper/Wood
- ☐ I. Soaps/Cleaners
- ☐ J. Paint/Coating/Ink
- ☐ K. Electrical/Electronic
- ☐ L. Instrument Dev./Des
- ☐ M. Plastic/Polymer/Rub
- ☐ N. Agricultural/Food
- ☐ O. Inorganic Chemicals
- ☐ P. Organic Chemicals

Primary area of employment.

INDUSTRIAL
- ☐ A. Research/Development
- ☐ B. Quality/Process Control

MEDICAL/HOSPITAL
- ☐ C. Research/Development
- ☐ D. Clinical/Diagnostic

GOVERNMENT
- ☐ E. Research/Development
- ☐ F. Regulate/Investigate

COLLEGE/UNIVERSITY
- ☐ G. Research/Development
- ☐ H. Teaching

INDEPENDENT/CONSULTING
- ☐ I. Research/Development
- ☐ J. Analysis/Testing

CIRCLE 314 FOR SUBSCRIPTION FORM TO ANALYTICAL CHEMISTRY

NAME: _____

TITLE: _____

FIRM: _____

STREET: _____

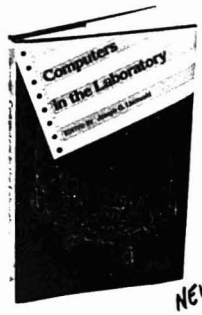
CITY: _____

STATE: _____ ZIP _____

PHONE: (___) _____

Computers in the Laboratory

Current Practice and Future Trends



NEW!

Joseph G. Liscouski, *Editor*
Digital Equipment Corporation

Spotlights the computer revolution with descriptions of state-of-the-art automation for the lab. Explores what is being done today and projects areas where the revolution is headed. Evaluates the use of robots for routine sample preparation and discusses the use of graphic displays to make information easier to understand. Looks at analyzing information in data bases, modeling from experimental data, and surviving the flood of data from modern chemical instrumentation. Shows how to effectively extract useful information from volumes of data. Conveys the breadth of computer usage in chemistry and the gains to be made with their use.

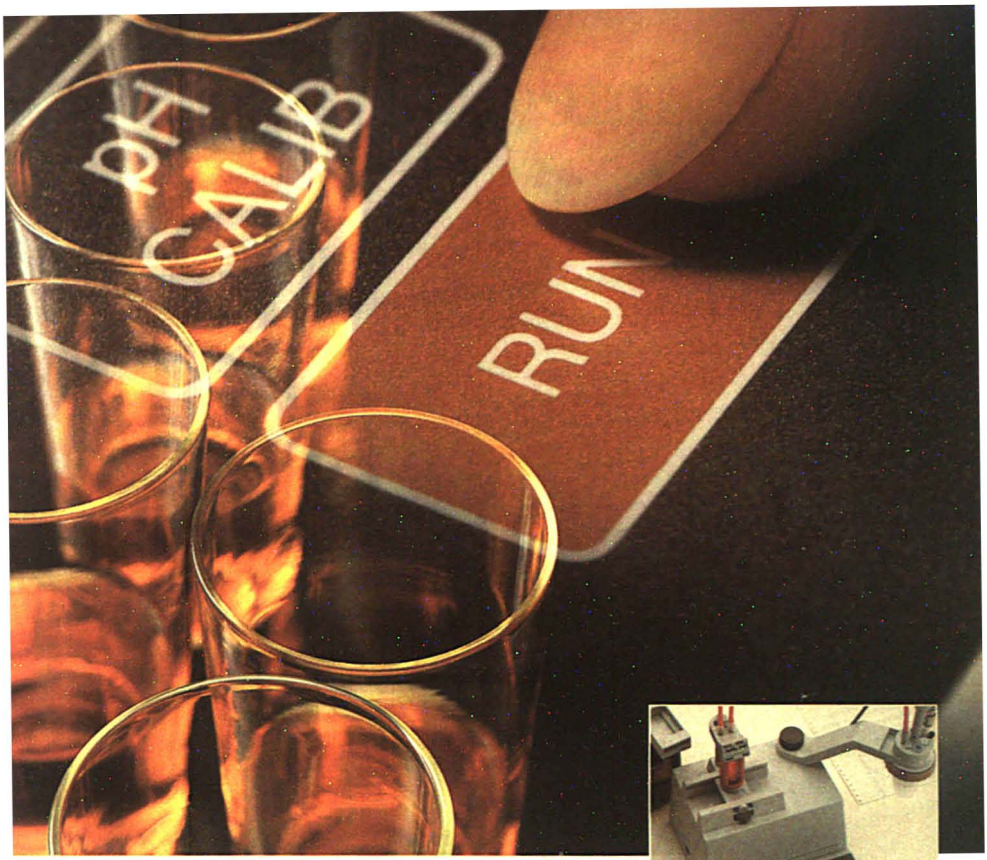
CONTENTS

Robots and Robotics in the Lab • General Lab Data Management and Specific Lab Needs • Applying Database Management in the Analytical Chemistry Lab • Planning an Approach to Lab Automation • Network and Communications • Introduction to Graphics • Chemists and Computers in the Corps of Engineers • Computer Generation of Structure–Effect Relationships from Text Data Bases • Coping with the Information Explosion Provided by Modern Chemical Instrumentaion • The Universe is Stochastic and Nonlinear

Based on a symposium sponsored by the Division of Computers in Chemistry of the American Chemical Society

ACS Symposium Series No. 265
128 pages (1984) Clothbound
LC 84-18518 ISBN 0-8412-0867-0
US & Canada **$34.95** Export **$41.95**

Order from:
American Chemical Society
Distribution Office Dept. 14
1155 Sixteenth St., N.W.
Washington, DC 20036
or CALL TOLL FREE 800-424-6747
and use your VISA, MasterCard
or American Express credit card.





The new Mettler DL20 CompactTitrator. $4,950 complete

No more manual and recording titrations...

Mettler's new DL20 titrator gets down to specifics

Designed for efficient routine analysis, the DL20 permits exact repetition of specific titrations with speed, accuracy and reliability—even after a change in operating personnel.

Practical

From simple acid/base to more difficult TAN/TBN in oil determinations, the DL20 CompactTitrator performs according to your specified titration method at the touch of a button. Quick sample change, rapid rinsing of the titration head, easy push-button operation and short titration time assure high productivity.

Mettler's rugged DL20 is extremely compact. It can be set up anywhere—in research or quality control labs—even out in the production area.

Precise and economical

Mettler burettes can dispense even the smallest increments precisely. Reproducible results are achieved with very small sample quantities and reagents can be used sparingly. With a price of $4,950, the DL20 is a good investment.

For more information on the new DL20 CompactTitrator, the DL40RC all-purpose and DL18 Karl Fischer titrators, contact Mettler today. Mettler Instrumen Corporation, Box 71, Hightstown, NJ 08520. Phone (609) 448-3000.

Limited Introductory TRADE-IN OFFER

Mettler gives you up to $500 off of the DL20 for:

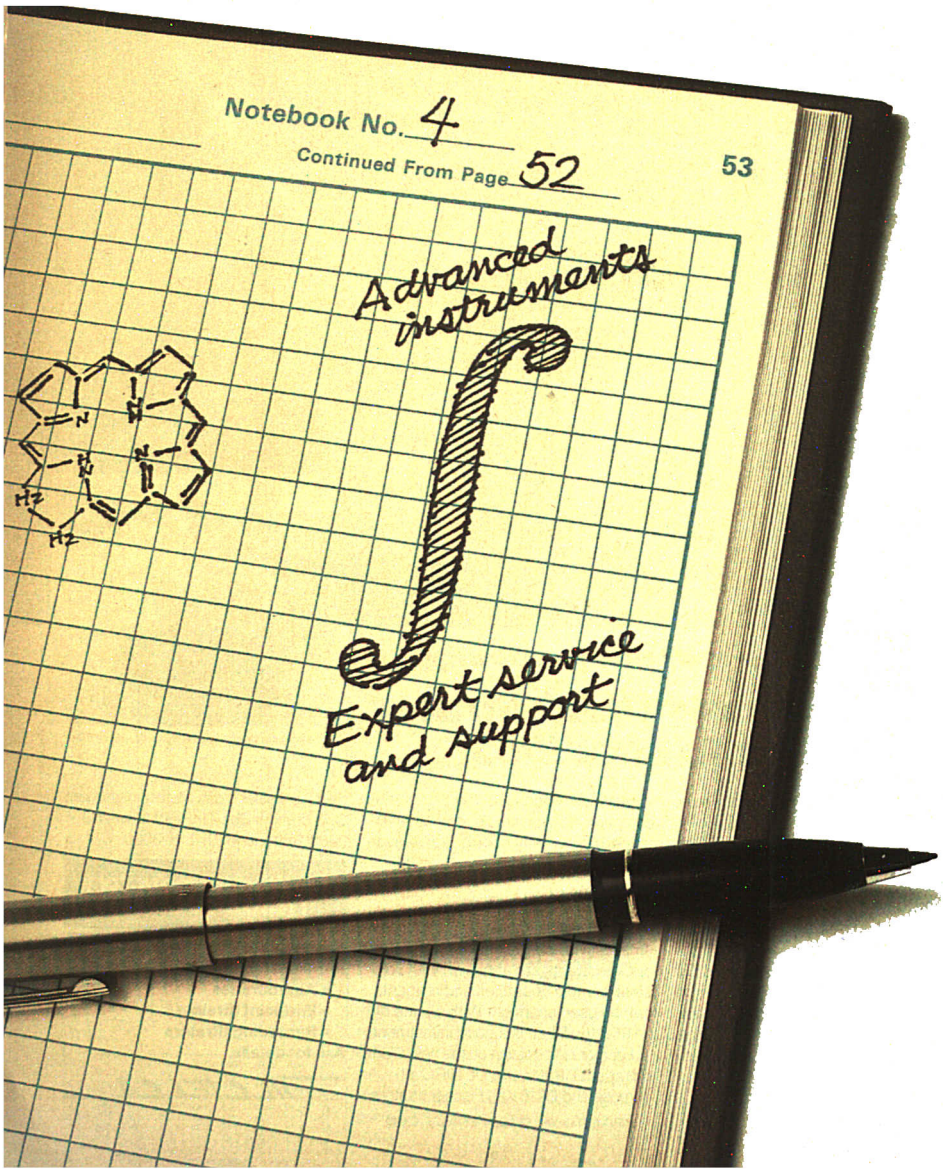
- **Autoburettes**
- **Endpoint titrators**
- **Recording titrators**

Ask for details.

Mettler

CIRCLE 143 ON READER SERVICE CARD

Integrated solutions



from IBM Instruments.

Our formula for solving analytical laboratory problems is a simple one.

We carefully study your current and future application requirements. Then, we work with you to develop a solution that addresses your analytical laboratory needs—in the most efficient, cost-effective manner possible.

We call this an integrated solution. Because it brings together all the necessary components that allow you to characterize, purify or quantify more productively than ever before. A solution that integrates the latest advances in instrument technology with the high levels of service and support associated with IBM.

Family of products. We offer you a full family of spectrometers (NMR, EPR and FTIR), spectrophotometers (UV/Vis) and chromatographs (LC and GC). Plus powerful, real-time computers designed specifically for the laboratory.

But our quality products are only part of the formula. We also have expert applications scientists, customer service engineers and marketing representatives.

Expertise and research. When you sit down with us to discuss your analytical problems, you will be talking with someone who speaks your language. Who knows your application. Its chemistry. Its technology. And its critical requirements. Who can back you up with support centers, laboratories, methods analysis, equipment recommendations, documentation, training and service. Who can support you with expertise that is second to none.

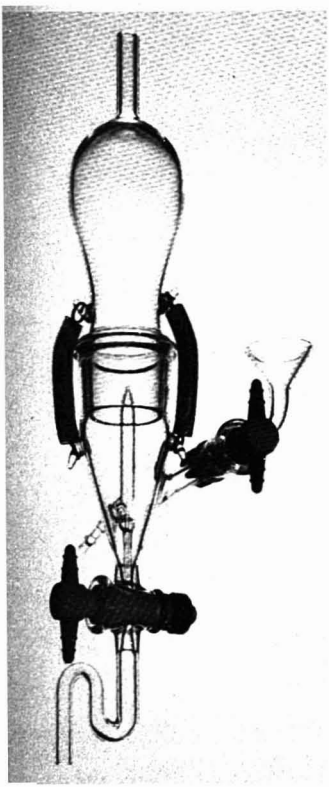
And who knows how to work with you to develop the best solution for your application problem... an integrated solution.

Call or write us today. If you would like to find out how our formula for integrated solutions can work in your laboratory, call us at 1-800-243-7054 (in Connecticut, 1-800-952-1073), or write IBM Instruments, Inc., Orchard Park, P.O. Box 332, Danbury, CT 06810.

IBM Instruments Inc.

CIRCLE 106 ON READER SERVICE CARD

New Products



Nebulizer reflux system RS-xx-Cy meets the growing demand for small-sample ICP applications by recirculating aerosol coalescing in the spray chamber. It also yields a prolonged standing signal, which is important to sequential ICP spectrometry and to plasma diagnostics that require long-term sample transport consistency. J E Minehard Associates Inc. **401**

LC detector

Model 2195 pH/ion monitor has a working range of 4 to 40 °C and is designed for use in series with a UV detector. Direct on-line monitoring of pH or conductivity, or simultaneous monitoring of both parameters is possible. It can also be used to determine the precise elution conditions for a sample component and to determine when column reequilibration is complete after ion exchange separations. LKB **406**

ICP data acquisition

VFS data acquisition system, a hardware–software system, allows transient signal measurement and specialized data processing and reporting for use with Baird's simultaneous ICP spectrometers. It provides for ultratrace determination of contaminants in microliter volumes of gases and can measure up to 60 elements at up to six integrations per second. Baird **407**

HPLC detector

Model 490 is a programmable multiwavelength UV–VIS detector that provides seven programmable modes of operation on up to four output channels. Peak to peak noise is typically 5×10^{-5} absorbance units (with flowing solvent), allowing accurate quantitation even of trace elements. The wavelength range is from 190 to 600 nm with attenuation settings from 0.001 to 3.0 AUFS. Waters Chromatography Division **408**

Sample evaporation and concentration

Model 600 AutoVap automatically evaporates and concentrates, solvent exchanges, and transfers samples to GC/HPLC autoloader vials for analysis. Reproducibility during the evaporation process is achieved by controlling the pressure to ±2 torr and the temperature to ±0.1 °C. Analytical Bio-Chemistry Laboratories, Inc. **409**



Model 267 portable ion chromatography system incorporates a pumping system, injection valve, column–cell compartment with active temperature control, and conductivity detector in a 40-lb package. Only ac power is required for operation; no compressed air is necessary. Standard column kits are available for determination of anions, cations, metals, surfactants, and organic acids in a variety of matrices. Wescan Instruments **402**

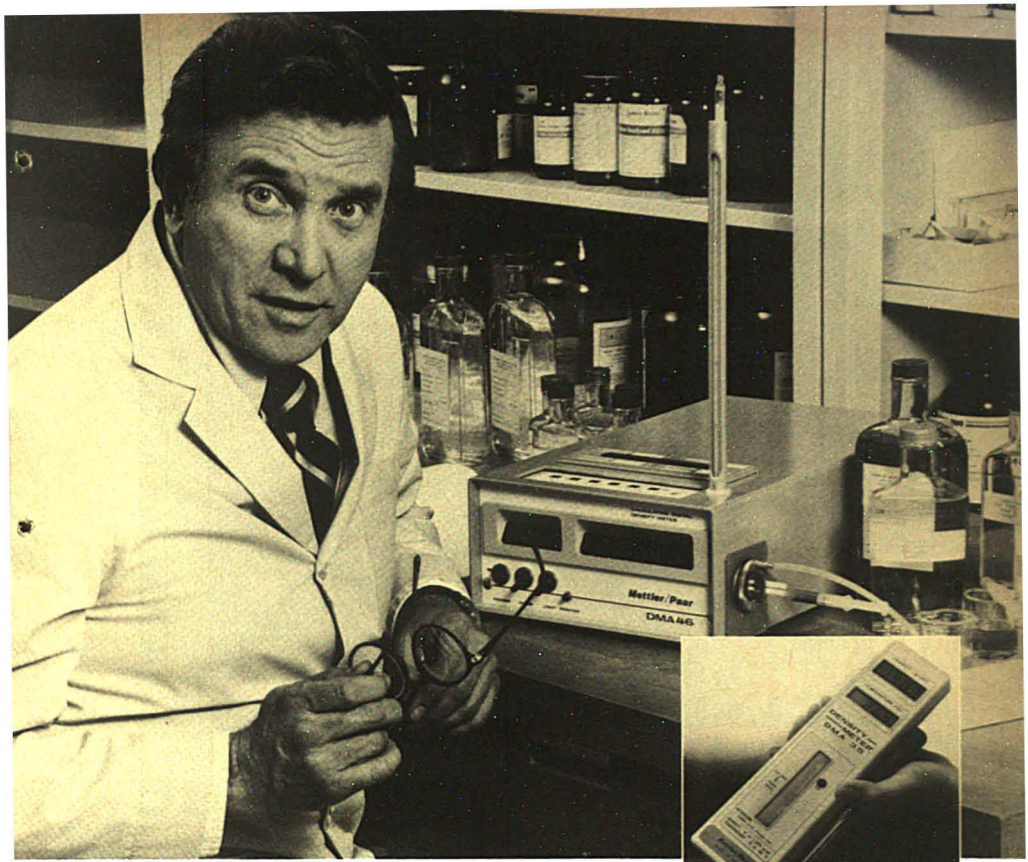
IC

Series 8000 ion chromatographic analyzer is specifically designed for on-line operation in plant environments. It features complete control over sampling of up to 18 streams and data handling including permanent storage to disk. Alarms for user-specified maximum concentration limits and programmable control of external devices are included. Dionex **410**

Stream splitter

AN-580 electronic digital stream splitter allows selection of split percentages from 1% to 99% at 1% intervals and cycle times of 1.5, 3, 7.5, and 15 s. Applications include postcolumn reactions, preparative LC, fraction collection, and multidetector stream splitting. Anspec **416**

For more information on listed items, circle the appropriate numbers on one of our Readers' Service Cards





The Mettler/Paar DMA35 is the only totally portable, hand-held density meter.

Accurate fluid density measurement without hydrometers and pycnometers.

Mettler/Paar Digital Density Meters
All the cumbersome procedures you're accustomed to, all the time spent and money lost on measuring density, specific gravity or concentration, can now be things of the past.

With Mettler/Paar digital density meters, you can obtain accurate results—quickly, easily, and reliably. No hydrometer breakage, time-consuming pycnometer measurements or weighing procedures to be concerned with. Think how much more effectively you can tighten manufacturing procedures, lower production costs and improve product quality.

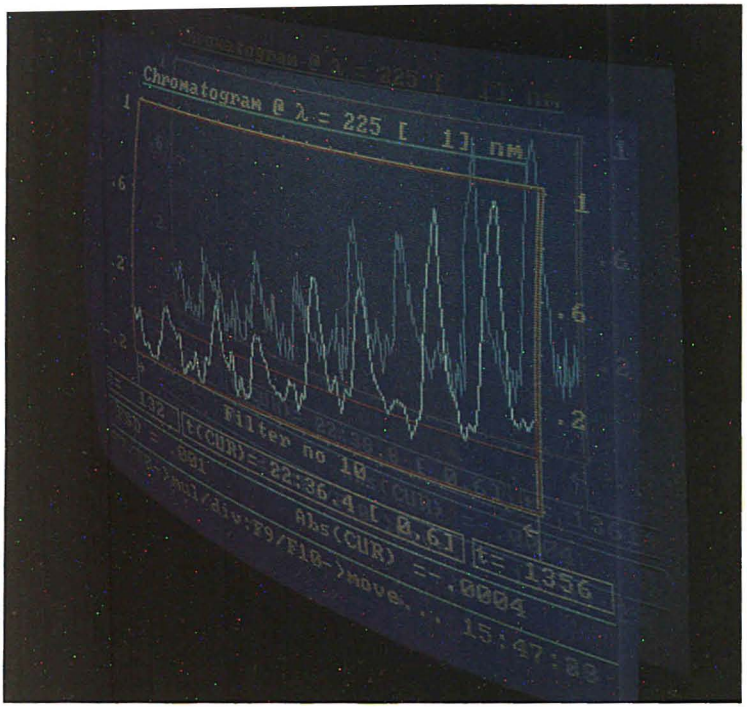
Unlimited application
Mettler/Paar density meters are used everywhere. Whether for research, quality or process control—in petrochemical, electronics, food and beverage, general chemical, and pharmaceutical industries. There are several models to choose from to fit your specific requirements.

For example, in the lab, the DMA46 offers 4-place precision and simple operation. It has a built-in thermostat and microprocessor to calculate and display density, specific gravity, concentration and other density related values. And for work outside the lab, take the portable DMA35 anywhere you need on-the-spot determinations. For in-line measurement and control, choose from a variety of DPR process and control systems.

Meeting your needs
Models are available with precision from 10^{-3}g/cm^3 to 10^{-6}g/cm^3 and are well-suited for many ASTM, AOAC and brewing industry methods. Results can be obtained in percent alcohol, Brix or API values. Prices range from about $1,000 for portable meters to $4,000 and up for lab and process systems. For more information, contact Mettler today. Instruments are also available for titration, thermal analysis and reaction calorimetry. Mettler Instrument Corporation, Box 71, Hightstown, NJ 08520. Or call: (609) 448-3000.

Mettler

CIRCLE 142 ON READER SERVICE CARD



New detector software separates noise from peaks!

New Wavescan™ software adds extra power to LKB's computer-based diode array detection system. Wavescan makes it easy. Gets rid of the guesswork. Automatically lets you access isograms, chromatograms and spectra. Now you'll discover, reveal and analyse every single peak—wherever it's hidden!

With real time display and raw data storage, LKB's Rapid Spectral Detector lets you manipulate original data to instantly give you the complete picture—without reruns!

And Wavescan lets you compare outputs, minimize noise, guard against peak distortion and still get the clearest peaks possible—you just can't miss them!

Want spectral overlay, normalized spectra or peak integration? They're all yours at the touch of a button. Getting peak purity control and positive component identification is now rapid, reliable and surprisingly simple—every time!

So if your HPLC can't tell the difference between noise and peaks, just take a look at Wavescan and Rapid Spectral. They'll give you the breakthrough your research needs.

Get in touch with LKB—today!



LKB
BROMMA

Head office: LKB-Produkter AB, Box 305, S-161 26 Bromma, Sweden. Tel. 08-98 00 40, telex 10492
Main US sales office: LKB Instruments, Inc. 9319 Gaither Road, Gaithersburg, Maryland 20877. Tel. 301-963-3200, telex 909870 (dom.), 64634 (intern.)
UK sales office: LKB Instruments Ltd., 232 Addington Road, S. Croydon, Surrey CR2 8YD, England. Tel. 01-657 88 22, telex 264414
Other sales offices in: Antwerp, Athens (for Middle East), Bangkok, Copenhagen, Lucerne, Madras, Moscow, Munich, Paris, Rome, Tokyo, Turku, Vienna, Zoetermeer

CIRCLE 127 ON READER SERVICE CARD



FIAstar, a fully automated, microprocessor-controlled FIA analysis system, consists of an analyzer, spectrophotometer detector system, printer, and sampler. Up to 300 analyses per hour can be performed with response times as low as 5 s. Applications include analysis of water, soil, fertilizers, and beverages. Tecator, Inc. **403**

SEM

Stereoscan S90B SEM has a magnification range from 10X to 300,000X with a continuous zoom facility and a precision multispecimen stage for specimens up to 100 X 100 mm. Additional features include quick pump-down, compact column with guaranteed resolution of 70 Å, and a linear measurement capability. Cambridge Instruments **411**

Surface wettability

WET-TEK is a dynamic contact angle balance that can determine the wetting properties and surface dynamics of virtually any surface. Industrial applications include quality control for fibers, paints, and coatings; surface analysis applications include detection of surface oxidation, contamination, and surfactant leaching. Biomaterials International, Inc. **412**

LC/MS

LC/MS25RFA includes a fully laminated, constant-focus, 60° dual-resolution inhomogeneous magnet with a mass range of 4000 amu that scans up to five full scans across 1-s-wide GC peaks. Other features are a new turbomolecular binary LC pump system, thermospray interface, and a microprocessor-based LC data system. Kratos Analytical **413**

ICP sample introduction

Conductive-solids nebulizer sample introduction system, for use with ARL ICP systems, allows analyses of metals and other conductive solid samples without dissolution of the sample. When used with a vacuum ICP spectrometer, it can determine C, P, S, and B as well as other elements whose optimum spectral lines occur below 200 nm. Applied Research Laboratories **414**

Preparative HPLC

St/Lab 800A system is designed for milligram to multigram separations and to use smaller particle packing media for increased separation efficiency. Features include a solvent delivery system, fluid control panel, stainless steel column, and pumps that deliver a maximum flow of 800 mL/min at 1800 psi for either isocratic or binary gradient solvent applications. Separations Technology **415**

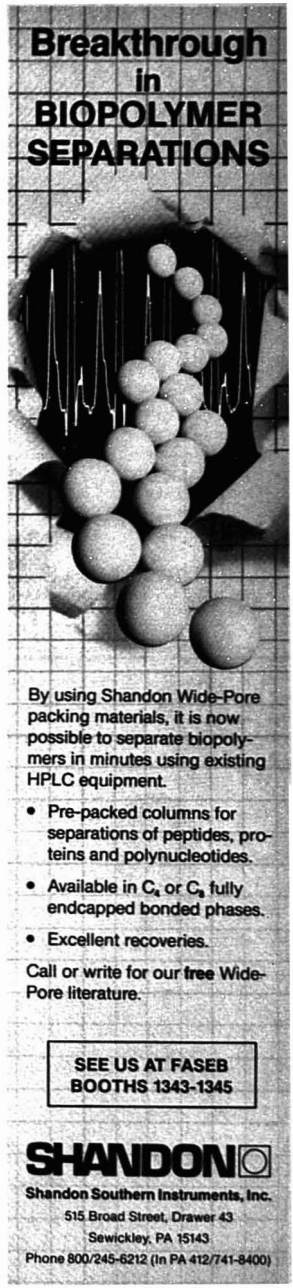
Chemicals

HPLC phosphate buffer kit

Kit allows convenient preparation of interference-free mobile phases and contains purified KH_2PO_4 and Baker Analyzed HPLC water. Prepared solutions offer lower UV absorbance and freedom from extraneous chromatographic peaks compared to previously available buffers. J. T. Baker **418**

Polystyrene latex particles

Sub-micrometer-size particles have a mean diameter of 0.8 μm and are available plain, coated with functional sur-



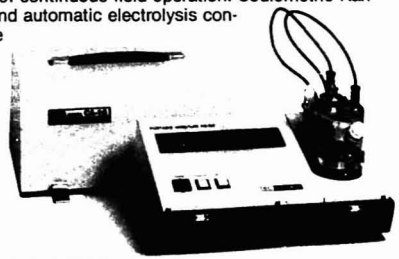
CIRCLE 195 ON READER SERVICE CARD

HIGH ACCURACY MEASUREMENT—ANYWHERE.

MCI's New CA-10 Portable Moisture Meter.

Wherever you have to take a measurement, the handy CA-10 Portable Moisture Meter makes it easy. This advanced AC/DC unit features a rechargeable battery pack, with battery alarm, that enables 10 hours of continuous field operation. Coulometric Karl Fischer titration and automatic electrolysis control assure reliable high precision and speed.

Contact MCI today for more information on the efficient new CA-10 Portable Moisture Meter.



MITSUBISHI CHEMICAL INDUSTRIES LIMITED

Instruments Dept., Mitsubishi Bldg., 5-2, Marunouchi 2-chome, Chiyoda-ku, Tokyo 100, Japan
Telex: J24901 Cable Address: MBISHICHEMICAL TOKYO Tel: (03) 455-4220

CIRCLE 139 ON READER SERVICE CARD



Chemists and cooks get better reactions with **Experiment with a Chemist** aprons.

For soup or synthesis, this practical, versatile apron is a winner. Sturdy and handsome heavyweight 100% cotton fabric makes it as useful at the barbecue pit as at the bunsen burner! "Experiment with a Chemist" design in navy and red on natural background, one size fits all. $12.50 each (write for quantity discounts).

Phone (202) 872-4588 for credit card orders.

American Chemical Society
P.O. Box 57136
West End Station
Washington, D.C. 20037

Please send me _____ "Experiment with a Chemist" aprons @ $12.50 each.
Please add $1.90 postage and handling charge per order. In Calif. please add 6% State Tax. Foreign shipment surcharge is $0.75 per apron to Canada; other countries, $1.75 per apron.

☐ Check enclosed ☐ Charge my: ☐ VISA ☐ Mastercard
☐ ACCESS ☐ Barclay Card

Account No. _____
Interbank Code (MasterCard Only) _____
Exp. Date _____ Signature _____
Name _____
Address _____
City/State/Zip _____

E710

New Products

face groups (carboxyl, hydroxyl, amino, and avidin), and tagged with different fluorophors. Applications include particle concentration fluorescence immunoassay, solid phase for RIA or EIA, nephelometry, and turbidity standards.
Pandex **419**

Endotoxin removal

Detoxi-Gel is an affinity chromatography support designed to remove endotoxins from aqueous and physiological solutions. It uses a special ligand covalently bound to an agarose matrix and has a high capacity for endotoxins.
Pierce Chemical Co. **420**

SRM

SRM 1618, vanadium and nickel in residual fuel oil, is intended for use as an analytical standard for the accurate determination of high V and Ni in fuel oils or materials of similar matrices. It consists of 100 mL of a No. 6 residual fuel oil with nominal concentrations of V and Ni of 423 μg/g and 75 μg/g, respectively.
NBS **421**

Prostaglandin E_2 kit

^{125}I-RIA kit for measurement of prostaglandin E_2 in biological samples is a sequential overnight assay that allows readings below 2.0 pg/tube using a simple second-antibody procedure. The assay requires 100 μL of sample, and the kit contains 100 tubes with standard, tracer, antisera, buffer, second antibody, and instructions.
Seragen, Inc. **422**

Software

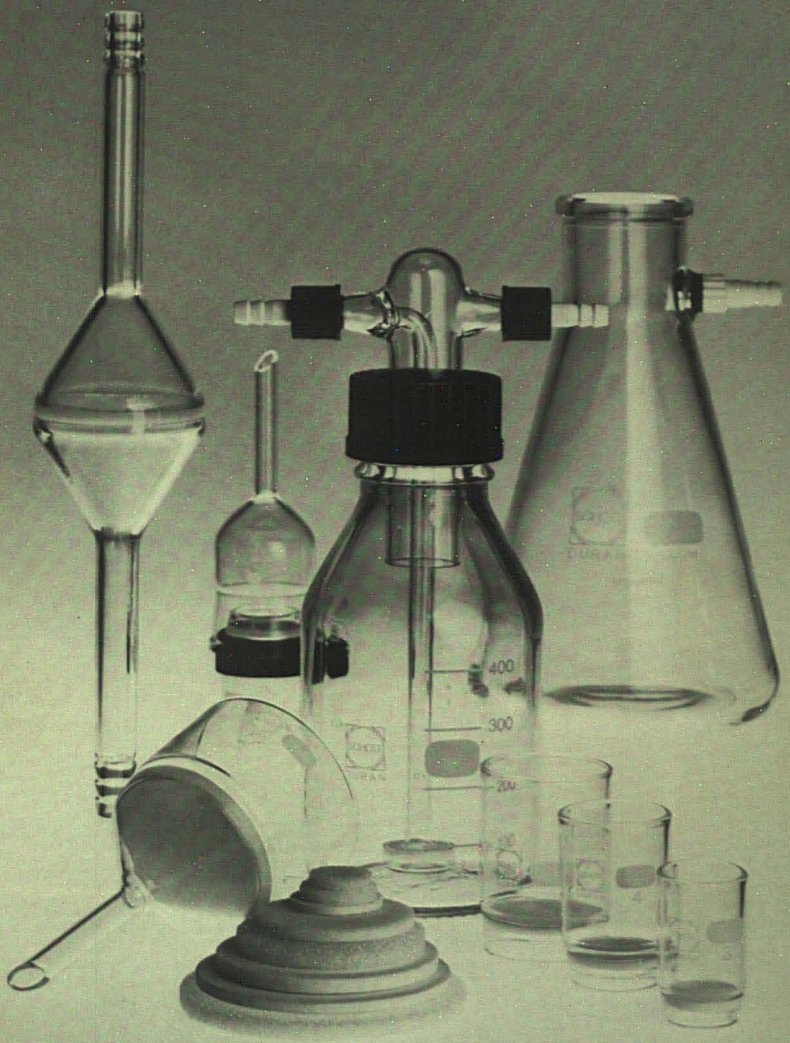
X-ray fluorescence

XRF4 and Corset, designed for IBM PC, Apple I, and CP/M computers, provide data reduction models and fundamental parameters, respectively. XRF4 calculates 6 elements for 50 analyses, and Corset manages up to 10 elements. Disk file management routines and sample data files are included.
Research Corporation **424**

Signal processing

DT/ILS-PC 1, compatible with IBM PC computers, is an interactive digital signal-processing package that includes on-line help or prompting. It supports continuous data acquisition to disk at up to 27,500 samples per second. Data analysis features include file management, waveform display and editing, and spectral analysis. Data Translation **425**

DURAN® is your yardstick for quality laboratory glassware.



SCHOTT

DURAN® laboratory glassware is available through leading laboratory suppliers.

SCHOTT GLASWERKE, Laboratory Glassware Product Group
D-6500 Mainz (West Germany)
Hattenbergstr. 10, Tel. (06131) 661, Telex 4187 9230 smd

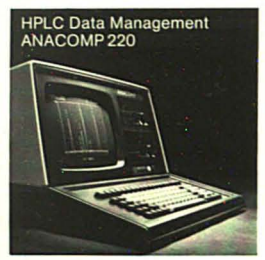
Circle Reader Service Card No. 187

SCHOTT GROUP

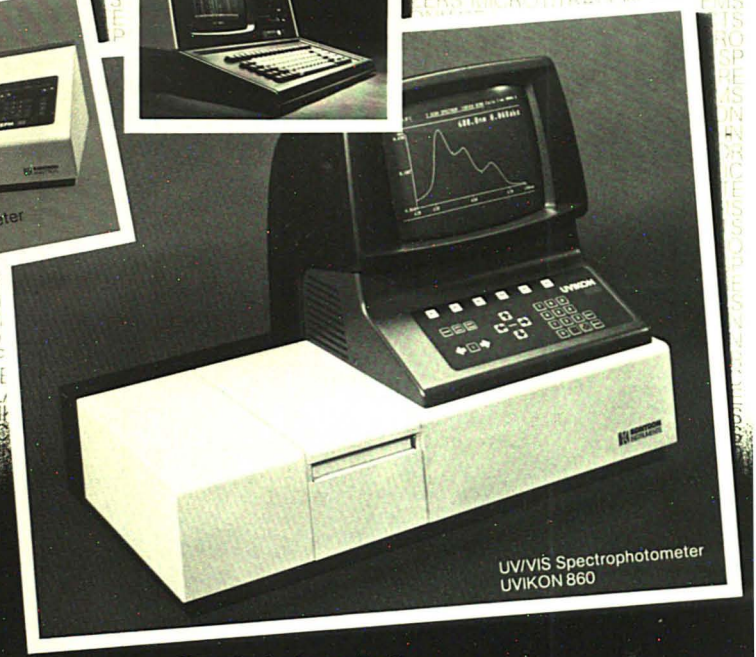
KONTRON INSTRUMENTS

your partner in science and health

UV/VIS SPECTROPHOTOMETRY







Your partner in science and health

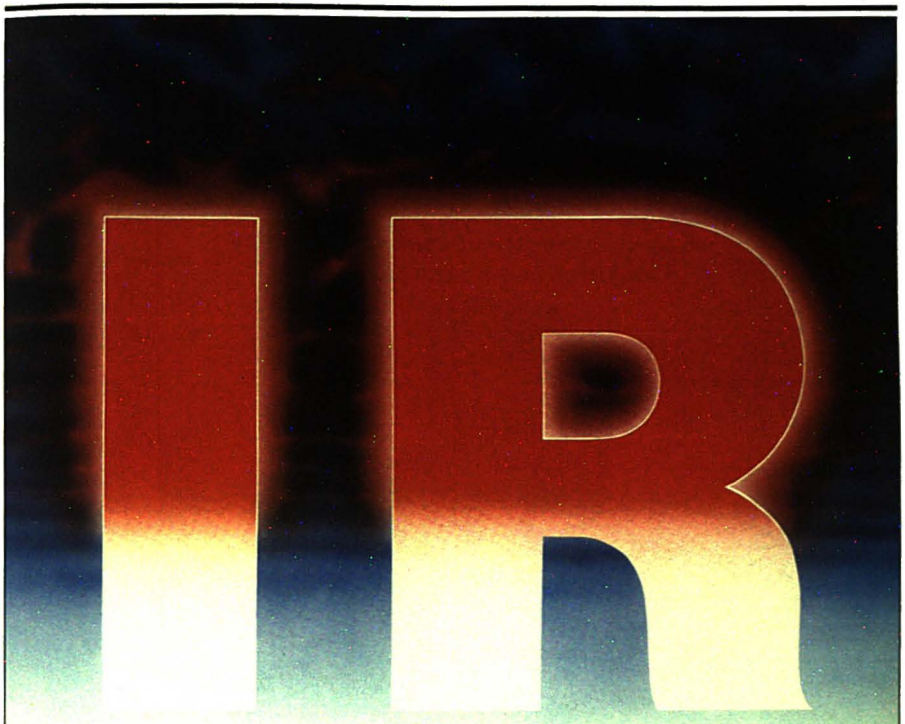
KONTRON INSTRUMENTS

For further information please contact your local KONTRON Company

Austria (Vienna)	(0222) 670631	Japan (Tokyo)	(03) 2634801
France (Montigny le Br.)	(3) 0438152	Scandinavia (Stockholm)	(08) 7567330
Germany (Munich)	(08165) 771	Spain (Madrid)	(01) 7291155
Great Britain (St. Albans)	(0727) 66222	Switzerland (Zurich)	(01) 4354111
Italy (Milan)	(02) 50721	USA (Everett/Mass.)	(617) 3896400

International Marketing Services, KONTRON AG, Bernerstrasse Süd 169, 8048 Zurich/Switzerland
Telephone (01) 435 4111, Telex 822 191

CIRCLE 117 ON READER SERVICE CARD



Do you only know the half of it?

Two names stand out for infrared spectrophotometry world-wide.

Philips Analytical presents a viable and highly competitive challenge to the obvious contender with a superior range of spectrophotometers, data systems and Library Search software.

If you are buying IR you've got to look at both alternatives.

Circle reader inquiry no. 80 for the other half of the story.

Pye Unicam Ltd
York Street Cambridge
Great Britain CB1 2PX
Tel (0223) 358866 Telex 817331

IR05

PHILIPS

Scientific & Analytical Equipment

PHILIPS

CIRCLE 80 ON READER SERVICE CARD

Practical methods to enhance efficiency and versatility of NMR

Fourier Transform NMR Spectroscopy

an audiocassette course produced by The American Chemical Society

- **Shows how to run and analyze previously unobtainable spectra**
- **Features a wide range of applications in chemical and biological systems**
- **Explains how Pulse FT NMR speeds process of running spectra**

Probably the single most important and far-reaching advance in NMR techniques in the last fifteen years has been the development and widespread adoption of Fourier Transform methods.

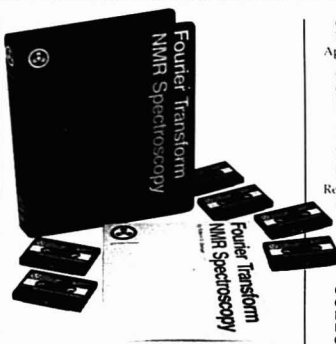
This course examines those methods, the rationale for their use, and some of the ways they are being used to solve chemical and biochemical problems. The concentration is on techniques with the approach to theory largely descriptive rather than highly mathematical. The course emphasizes, in a practical manner, optimum ways to use the Fourier Transform methods it covers.

INSTRUCTOR

Dr. Edwin D. Becker, Associate Director of Research Services, National Institutes of Health, is author or coauthor of approximately 75 research papers and 2 books. He has received the Coblentz Memorial Prize in Chemical Spectroscopy.

UNIT

Six audiotape cassettes (4.3 hours playing time) and a 90-page manual, $245.00, U.S. price. Additional manuals for group use: $13.50 each, U.S. price. *(Catalog no. 71CE)*



COURSE OUTLINE

The Physical Basis of NMR
- Introduction: Scope of the Course
- The Rotating Frame
- Nuclear Relaxation
- Means of Exciting NMR Spectra
- Characteristics of the Free Induction Decay
- Fourier Transformation: Time and Frequency Domains

Pulse-Fourier Transform NMR
- The Pulse Spectrometer
- Pulse Power and the 90° Pulse Width
- Phase Sensitive Detection
- Determination of the Spectral Width
- Acquisition Time: Resolution and Signal-Noise
- Exponential Filtering
- Zero Filling
- Phase Corrections
- Other Software Features
- Decoupling

Applications of Pulse-FT NMR
- Typical Time-saving in Data Acquisition
- Study of Rapid Reactions
- Coherent Time-averaging
- Instrumental Factors Affecting Signal Noise
- ^{1}H NMR: Examples and Current Status
- ^{13}C NMR
- ^{15}N NMR
- Study of Other Nuclei
- Biological Samples
- Measurement of Relaxation Times

Relaxation — Mechanisms and Applications
- Molecular Motions and Fluctuating Fields
- Nuclear Relaxation Mechanisms
- Some Applications of Relaxation Data
- Applications to Exchange and Diffusion Measurements
- High Resolution NMR in Solids
- Magnetic Dipolar Interactions
- Chemical Shift Anisotropy
- Quadrupole Interactions
- Line-narrowing Pulse Cycles
- Dipolar Decoupling
- Cross Polarization
- Magic Angle Spinning
- Multiple Quantum Coherence

More General Fourier Transform Methods
- Rapid Scan Correlation Technique
- Stochastic Excitation
- Synthesized Excitation
- Methods of Overcoming Incoming Interference by Solvents
- Two-dimensional Fourier Transform Methods
- NMR Imaging Methods
- Other Branches of Spectroscopy

NO-RISK GUARANTEE

Order *Fourier Transform NMR Spectroscopy* at no risk. If you are not completely satisfied, simply return it to us within 10 days for a full refund or cancellation of invoice.

CALL TOLL FREE 1-800-424-6747, WRITE OR USE COUPON TO SPEED YOUR ORDER.



FREE! Precision-Engineered Headset with every purchase of an ACS Audio Course

Listen to audiocassettes in complete privacy wherever you are! This handsome headset has comfortable, foam-filled ear cushions; adjustable ear pieces for good fit; long-life cord; sturdy construction.

(Because of customs restrictions, this offer applies only to purchases within the U.S.)

American Chemical Society, Education Division
1155 Sixteenth Street, NW, Washington, DC 20036

Please send _____ cop(ies) of *Fourier Transform NMR Spectroscopy* at $245.00 each. (Export price: $305.00.)
Also please send _____ additional manuals at $13.50. (Export price: $17.00.)

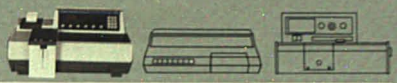
☐ Free Headset with each complete unit (Does not apply to purchasers outside the U.S.)

SUB-TOTAL _____
California purchasers add 6% sales tax _____
56313 2600 E710 TOTAL _____

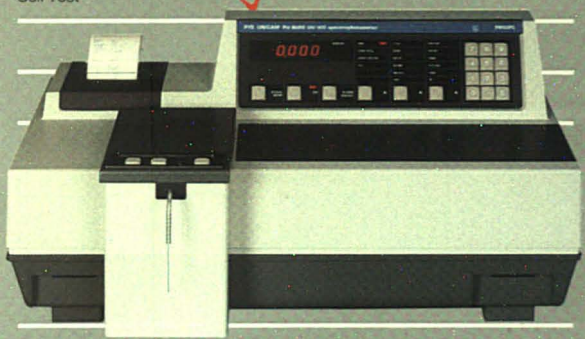
☐ Payment Enclosed ☐ Purchase Order Enclosed
☐ Charge my ☐ VISA ☐ MasterCard ☐ Access ☐ Barclaycard ☐ American Express

Complete Account No. _____ Expiration Date _____
Name of Cardholder _____
Signature _____ Interbank Code _____ (MasterCard Only)
Name _____ Phone No. _____
Organization _____
Address _____
City, State, Zip _____

Nothing compares with the PU 8600



10 Stored Methods	✓		
True Digital Keypad	✓		
Peak Seek	✓		
Integral Printer	Option		
Self Test	✓		



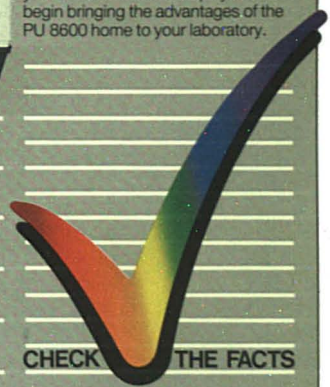
Integral Kinetics	Option		
Delay, Repeat & Timer Functions	✓		
Autozero	✓	✓	
Autocell	Option	Option	Option
Signal Averaging	✓		
Autoconcentration	✓	✓	
New Low Prices	✓		

Impressed? You should be. We've compared the PU 8600 Series with its nearest rivals and allowed the facts to speak for themselves.

Yet despite the PU 8600 Series' evident superiority, there's little or no premium to pay. Indeed, these remarkable instruments offer features that are uncommon at twice the price!

And only from Philips do you get a promise of sparkling performance that endures, thanks to a master holographic grating, silica-coated optics and robust construction that's an inherent part of the PU 8600 pedigree.

The Series consists of four main models – standard or kinetics configuration with VIS or UV/VIS options. Each is available in a range of extremely compact analytical systems to suit practically every application, workload and budget. The choice is yours. Use the reader inquiry service to begin bringing the advantages of the PU 8600 home to your laboratory.



Pye Unicam Ltd
York Street Cambridge
Great Britain CB1 2PX
Tel (0223) 358866 Telex 817331

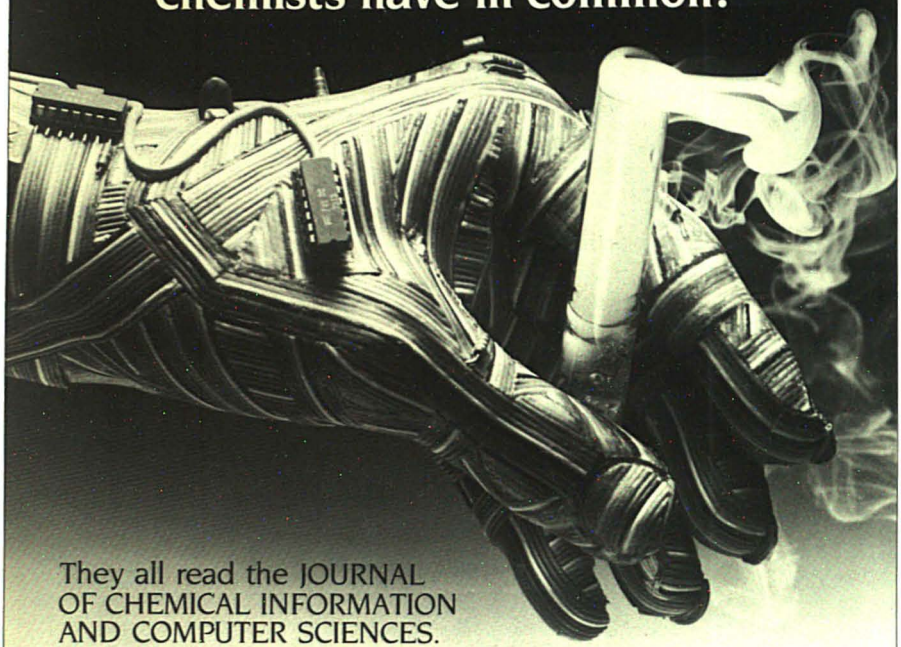
UV 08

PHILIPS Analytical Equipment

CIRCLE 79 ON READER SERVICE CARD

PHILIPS

What do chemical information specialists, computer scientists, and chemists have in common?



They all read the JOURNAL OF CHEMICAL INFORMATION AND COMPUTER SCIENCES.

—published by the American Chemical Society and edited by Thomas L. Isenhour—

Each quarterly issue of the JOURNAL OF CHEMICAL INFORMATION AND COMPUTER SCIENCES is packed with exciting, new, peer-reviewed research articles on computerized applications in chemistry.

And now, new feature articles written by James Avery and John Marshall keep you up-to-date on microcomputer hardware and software developments.

Join the thousands of chemists, computer scientists, and chemical information specialists who are making the JOURNAL OF CHEMICAL INFORMATION AND COMPUTER SCIENCES the fastest growing journal in its field.

Order your subscription today. Call toll free **800-424-6747.** Or write American Chemical Society, 1155 Sixteenth Street, NW, Washington, DC 20036.

1985 Subscription Rates (U.S.)
ACS Members $17
Nonmembers $90

American Chemical Society chemical publishers since 1879

UPDATE

New dual role GC



PU 4550 is a dual role gas chromatograph from Philips Analytical which offers operational flexibility, research grade performance and the power and accuracy of microprocessor technology.

It has been designed to meet the need for high resolution stand alone capillary chromatography and is also capable of functioning as a separation station in a complex data system.

Reader inquiry no. 70

GC29

IR background

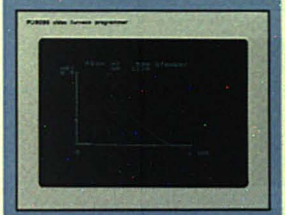


The versatile background correction system employed by the Pye Unicam PU 9510/20 programmable IR series aids the spectroscopist in two important ways. It removes virtually any uneven background caused by sampling accessories and in some instances can perform spectral subtractions without the use of a dedicated data system.

Reader inquiry no. 71

IR26

Informed AA



No other AA video system keeps you quite so well informed as the PU 9095 Data Graphics System from Philips Analytical. As well as monitoring your analysis, it offers over 150 pages of information including a full flame and furnace cookbook, calibration graphs and transient peaks.

Reader inquiry no. 72

AA25

New LC pump



Pye Unicam's new PU 4015 liquid chromatography pump incorporates two flow rate ranges which can be push-button selected for Microbore, FAST and conventional LC.

Its dual piston design ensures smooth, precise solvent delivery, a new low volume check valve design and flow-through pressure transducer minimising hold-up in the solvent delivery system.

Reader inquiry no. 73

LC28

For more information . . .

Use the reader inquiry service to obtain further details of the products which interest you.

PU 4550 gas chromatograph	**70**
IR spectrophotometry	**71**
AA spectrophotometry	**72**
PU 4015 LC pump	**73**
Other LC products	**74**
Other gas chromatographs	**75**
UV/VIS spectrophotometry	**76**
pH, ion selective, conductivity	**77**

Pye Unicam Ltd
York Street Cambridge
Great Britain CB1 2PX
Tel (0223) 358866 Telex 817331

PHILIPS Analytical Equipment

PHILIPS

An Invitation to Submit Manuscripts to

Langmuir

The ACS Journal of Surfaces and Colloids

Arthur Adamson, Editor
Arthur Hubbard, Associate Editor



This new journal published by the American Chemical Society will fill the void existing in current literature available today— *Langmuir's broad coverage will bring together authoritative papers from all aspects of this major field of chemistry!*

Scope

Langmuir will include fundamental and applied papers covering ultra-high vacuum surface chemistry and spectroscopy, heterogeneous catalysis, all aspects of interface chemistry involving fluids, and disperse systems.

Specifically, Langmuir will publish peer-reviewed research in

- **'Wet' Surface Chemistry**

  surface tension • spread monolayers • wetting and contact angle • adsorption from solution • nucleation and fundamental aspects of flotation, detergency, emulsions, foams, lubrication, etc.

- **'UHV' Surface Chemistry**

  solid surfaces in ultra-high vacuum including surface structure, composition and spectroscopy • and fundamental papers in heterogeneous catalysis

- **Disperse Systems**

  colloidal suspensions including aerosols • microemulsions • biological and polymeric colloids and membrane systems

- **Electrochemistry**

  related to interfacial structure and processes

Bimonthly issues of Langmuir will feature experimental and theoretical original papers, letters to the editor, and book reviews, as well as some selected symposium collections. Papers having applied aspects will be included.

The editors of the journal welcome research papers in all areas of surface and colloid chemistry, and will guide the journal to become a unifying influence on research in this field.

Langmuir will not have page charges.

Editorial Advisory Board

N.R. Armstrong, *University of Arizona*
G.T. Barnes, *University of Queensland, AUSTRALIA*
P. Biloen, *University of Pittsburgh*
K.S. Birdi, *Technical University of Denmark, DENMARK*
A.M. Bond, *Deakin University, AUSTRALIA*
B.V. Derjaguin, *Academy of Science of USSR, USSR*
D.D. Eley, *University of Nottingham, ENGLAND*
G. Ertl, *Technical University of Munich, WEST GERMANY*
J. Fendler, *Clarkson College of Technology*
T. Fort, Jr., *California Polytechnic State University*
G. Gaines, Jr., *General Electric Corporate R&D*
W.A. Goddard, III, *California Institute of Technology*
R.S. Hansen, *Iowa State University*
J. Lyklema, *Agricultural University, THE NETHERLANDS*
R.J. Madix, *Stanford University*
J.A. Mann, Jr., *Case Western Reserve University*
P. Mukerjee, *University of Wisconsin*
K.J. Mysels, *Research Consulting*
A.W. Neumann, *University of Toronto, CANADA*
R. Ottewill, *University of Bristol, ENGLAND*
G.D. Parfitt, *Carnegie-Mellon University*
H. Reiss, *University of California at Los Angeles*
H.A. Resing, *Naval Research Laboratory*
T. Rhodin, *Cornell University*
S. Ross, *Rensselaer Polytechnic University*
J. Rouquerol, *Centre de Thermodynamique et de Microcalorimetrie du CNRS, FRANCE*
R.L. Rowell, *University of Massachusetts*
R. Rye, *Sandia National Laboratory*
H. Seki, *IBM*
K. Shinoda, *Yokohama National University, JAPAN*
G.A. Somorjai, *University of California at Berkeley*
W.A. Steele, *Pennsylvania State University*

General Information for Authors

Manuscript instructions are available in "Handbook for Authors of Papers in American Chemical Society Publications" (1978).

Manuscripts should be submitted to either:

Dr. Arthur Adamson, Editor
Department of Chemistry
University of Southern California
Los Angeles, CA 90089

Dr. Arthur T. Hubbard, Associate Editor
Department of Chemistry
University of California at Santa Barbara
Santa Barbara, CA 93106

Subscription Information

Langmuir
Published Bimonthly

American Chemical Society
1155 Sixteenth St., N.W.
Washington, D.C. 20036

One Volume Issued Per Year
Volume 1 Number 1 January–February 1985
ISSN: 0743-7463

1985 Subscription Rates

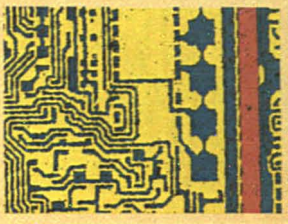
	U.S.	Foreign-Air Delivery Included
ACS Members	$ 49	$ 58
Nonmembers*	$299	$308

To subscribe, call Toll Free 800-424-6747

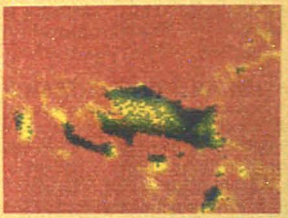
Now, improve microanalysis 6 ways. EDAX 9100-LX.



EDAX® answers your microanalytical needs with proven Application **Software** in EDS, EELS, diffraction, WEDAX, stage control and particle detection; and with Software that provides precise beam control in SEM and STEM. **EDscan™ X-ray and Electron Imaging** for spatially related chemical analyses in full color. And **Standardless Quantitative Analysis** with automatic peak identification. World renowned **ECON® Series Detectors** for light element analysis down to boron.



Color-coded digitized BSE image.



Composite x-ray image showing areas of B K = yellow, FeL = red, and SiK = blue.



User-definable **Dynamic Function Keys** for one-keystroke ease of operation. And the **Dynastatic Display** for smooth automatic vertical scaling change and easy-to-read spectral display.

System 9100-LX. The proven answer to your microanalytical needs.

Ask about it. Contact EDAX at (312) 634-0600.

ECON is a registered trademark and EDscan is a trademark of EDAX International, Inc.

EDAX INTERNATIONAL, INC., P.O. Box 135, Prairie View, IL 60069

EDAX®

FIRST NAME IN MICROANALYSIS

CIRCLE 50 ON READER SERVICE CARD

New From The World of EM SCIENCE

EM AQUASTAR™

TITRATORS & REAGENTS



AQUASTAR™ COULOMETRIC TITRATORS are the most advanced automatic instruments for detecting trace quantities of moisture.

AQUASTAR's unique preprogrammed microprocessor controls all titration, detection, and data manipulations necessary to perform accurate, precise, rapid moisture determinations.

AQUASTAR C1000 Features:

- **DATA REDUCTION**
  Calculates Mean, Standard Deviation, Coefficient of Variation for up to 20 Samples
- **BUILT IN PRINTER**
  Provides Hard Copy of Data in μg, %, PPM, plus Graphical Titration Display.
- **VERSATILITY**
  Handles Solids, Liquids or Gas samples
- **ACCURATE**
  Within ± 1 μg at 10 μg H_2O level
- **EASY OPERATION**
  Total Microprocessor Control
- **FAST, EFFICIENT**
  Titrates 1 mg H_2O in 50 sec.
- **EASY MAINTENANCE** Quick Draining Titration Cell, Easy Membrane Replacement
- **BALANCE/COMPUTER INTERFACE** Reduces Operator Time
- **"NO LEMON" WARRANTY** Assured Reliability

AQUASTAR™ VOLUMETRIC TITRATORS are the most sophisticated automatic instruments for detecting moisture ranging from low to high levels.

Exclusive microprocessor control coupled with standard twin burette system allows easy reagent standardization, direct and back titrations.

AQUASTAR V3000 Features:

- **DATA REDUCTION**
  Calculates Mean, Standard Deviation, Coefficient of Variation for up to 20 Samples.
- **EASY OPERATION**
  Microprocessor Allows 1 Button Standardization
- **FAST, EFFICIENT**
  Accurate Results Within Minutes
- **ACCURATE/PRECISE**
  Within 0.15% with ± 0.01 ml Reproducibility
- **VERSATILITY**
  Handles Solids, Liquids or Gas samples
- **BUILT IN PRINTER**
  Provides Hard Copy of Data in mg, %, PPM Plus Graphical Titration Display
- **BALANCE/COMPUTER INTERFACE**
  Reduces Operator Time
- **"NO LEMON" WARRANTY**
  Assured Reliability



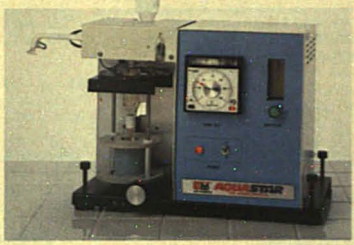
Innovative Moisture Determination Systems

AQUASTAR™ SOLID EVAPORATOR provides fast, easy moisture measurement of hard to dissolve solid/powder samples.

AQUASTAR Solid Evaporator Features:

- **IMPROVED RESULTS**
  Eliminates Interferences of Ambient Humidity
- **SAVES TIME/MONEY**
  Replaces Loss on Drying Procedures
- **EASY OPERATION**
  Permits Direct Moisture Measurement





AQUASTAR™ OIL EVAPORATOR allows efficient measurement of moisture in oils which normally interfere with KF reactions.

AQUASTAR Oil Evaporator Features:

- **SAVES TIME**
  Results Within Minutes
- **EASE OF OPERATION**
  Eliminates Sample Preparation
- **SAVES MONEY**
  Reduces operator Time and reagent Usage

AQUASTAR PYRIDINE FREE REAGENTS are direct replacements of traditional pyridine containing volumetric and coulometric KF reagent.

AQUASTAR Reagents provide stable end points, rapid titrations and prolonged stability without the unpleasant pyridine odor!

Additionally, EM SCIENCE offers a complete line of specially prepared anhydrous solvents, standards and desiccants for all KF applications.



Use the attached coupon, call or write today for further information.

EM SCIENCE
A Division of EM Industries, Inc.
111 Woodcrest Rd.
Cherry Hill, NJ 08034-0395
(609) 354-9200
(800) 922-1084
Associate of E. Merck, Darmstadt, Germany

Yes, I'm interested in AQUASTAR™ Systems!

Please ☐ Send Instrument Literature ☐ Send Reagent Literature ☐ Have Representative Call

Need ☐ Immediate ☐ 3-6 Months

Name _____

( ) Phone _____

Firm _____

Address _____

City _____ State _____ Zip _____

CIRCLE 48 ON READER SERVICE CARD

Distributed Nationally by: CMS Curtin Matheson Scientific, Inc.

VWR Scientific division of Unrivar

See us at the Federation Meeting—Booths 2125, 2127, 2129.

Nalgene® Labware

A world of choices for whatever work you do



Nalgene Bottles and Carboys

Choose from more than 40 styles and 19 sizes . . . from seven materials according to your needs, including polypropylene for autoclavability, polycarbonate for transparency, Teflon FEP for exceptional chemical resistance, high-density polyethylene for extra durability. Nalgene "Clear-boys" are clear, autoclavable and highly impact-resistant; they're ideal for cold rooms, even subfreezing temperatures. All Nalgene bottles are metric and tougher and lighter than glass.

CIRCLE 147 ON READER SERVICE CARD



Nalgene Centrifuge Ware

Whatever your centrifuge application, we've got a tube or bottle for you. Seven configurations, eight sizes from 3.5 to 1000 mL and nine plastics, many of them autoclavable—including strong, clear polycarbonate and chemical-resistant Teflon FEP. Manufactured to fit all major manufacturers' rotors, including Beckman, Sorvall and IEC.

CIRCLE 148 ON READER SERVICE CARD



Nalgene Polyurethane Tubing

A high-purity lab tubing that will stand up to very demanding applications. Clear and flexible. Contains no plasticizers and low levels of extractables, so it's ideal for high-purity work. Won't collapse under full vacuum. Available in 8 sizes, all continuously printed with I.D. and wall thickness as well as footmarks for easy measuring.

CIRCLE 149 ON READER SERVICE CARD



Nalgene Fluoropolymer Labware

The ultimate material for critical applications! Teflon FEP resists virtually any chemical and withstands temperatures from −270°C to +205°C. This durable, flexible, transparent material is also very low in trace organic and inorganic content. You can sterilize it by any chemical or thermal method. Choose from Nalgene FEP bottles, wash bottles, centrifuge ware, flasks, beakers and sep funnels.

CIRCLE 150 ON READER SERVICE CARD



Nalgene Filter Holders

Available with receiver or with funnel. For many membrane filtration applications using pressure or vacuum. Can be used with any 47-mm membrane. These reusable holders include two membrane support plates, one for efficient analytical filtration, the other for quick flow-through sterilization filtration. Polysulfone construction for clarity, repeated autoclavability. Cost less than comparable plastic, glass or stainless steel holders. Capacity: 250 mL.

CIRCLE 151 ON READER SERVICE CARD



Nalgene Syringe Filters with Nylon or Teflon PTFE membranes

The ideal choice for filtering aggressive solvents used in gas chromatography, high-pressure liquid chromatography and chemical etching. Fit standard or Luer-lok syringes. Both membrane materials available in 0.20- and 0.45-micron pore sizes. Available presterilized and individually bagged, or bulk-packed (non-sterile).

CIRCLE 152 ON READER SERVICE CARD

1985 Nalgene Labware Catalog New, illustrated 104-page catalog contains comprehensive specifications and descriptions for over 350 Nalgene plastic labware products. Plus—chemical resistance and physical properties data, and guidelines for the use and care of plastic labware.

CIRCLE 153 ON READER SERVICE CARD

For information or literature, contact Nalgene Labware Department, Nalge Company, Box 365, Rochester, N.Y. 14602. Phone (716) 586-8800.

Order these and all Nalgene Labware products from your authorized Nalgene Labware Dealer.

SYBRON

Nalge

Manufacturers' Literature

"Silicon Compounds: Register & Review." Literature provides physical and chemical properties of approximately 1000 silicon compounds and polymers, including structural formulas, copolymerization parameters, and application and thermodynamic data. Stationary-phase materials for GC, LC, and TLC are described. 240 pp. Petrarch Systems, Inc. **426**

FIAtron Analytica. Vol. 3, No. 1 features an up-to-date bibliography (emphasizing 1980–84) of pre- and post-column derivatization reactions in HPLC. References are indexed by area of chemical analysis and, in most cases, by species or derivatizing agent. 4 pp. Fiatron Laboratory Systems **427**

Porosimeter. Brochure describes the 200 Series automatic mercury pressure porosimeter, which automatically determines pore size, volume, and pore size distribution from 0.0037 to 7.5 μm. Pore shape information is obtained with a fully programmable hysteresis cycle. Applications include ceramics, plastics, foods, and pharmaceuticals. 8 pp. Carlo Erba Strumentazione **428**

Air-sampling standards. Guide to NIOSH and OSHA air-sampling standards lists more than 550 chemical and particulate hazards alphabetically. It also includes established sampling and analysis procedures, as well as recommended collection equipment. SKC Inc. **429**

Laboratory mills. Comparison chart provides specifications for mills and mixers and permits selection of the correct mill for a particular sample preparation. Specifications include typical sample volumes, range of sample sizes that can be accommodated, available vial materials, and timer characteristics. Spex Industries **430**

FPLC BioCommunique. Vol. 1, No. 1 features articles on preparative columns of MonoBeads, multisample automated chromatography, and a biomedical applications reference list. The newsletter is dedicated to fast protein, peptide, polynucleotide LC and to FPLC, an HPLC system with specific design features for separation of biomolecules. 6 pp. Pharmacia Fine Chemicals **431**

Balances. Catalog lists specifications and features of the AE and PE series of electronic balances and scales, two electronic microbalances, and five Mettler Pacs, which are designed to dedicate balances to specific weighing tasks or to transfer data to computers and printers. 20 pp. Mettler **432**

Data acquisition and control. Literature describes ISAAC hardware and software products for use in process monitoring and control, product and materials testing, and chemical research and analysis. Systems are compatible with IBM PC and Apple II personal computers. 13 pp. Cyborg **433**

Controlled-temperature baths. Bulletin provides descriptions of Grant controlled-temperature laboratory equipment, including stirred and unstirred thermostatic baths, circulators, block thermostats, control units, CO_2 incubators, shaking baths, recorders, and probes. 6 pp. Science/Electronics, Inc. **434**

Volatile halocarbons. Technical note GC-72 describes use of the EPA standardized liquid/liquid extraction technique for the determination of many environmentally important halocarbons in groundwater by capillary column GC. Chromatograms and tables showing analysis results are included. 6 pp. Varian **435**

Catalogs

Chromatography supplies. Catalog 23 includes GC, HPLC, custom, and capillary columns; septa; custom glassware; industrial hygiene supplies; highly concentrated priority pollutant standard; and more than 30 pages of applications. Supelco **436**

Biochemical and organic compounds. 1985 catalog lists more than 17,000 biochemicals and organic compounds, as well as tissue culture reagents, standards and controls, chromatography supplies, research kits and reagents, diagnostic kits and reagents, and technical inserts. 1279 pp. Sigma Chemical Co. **437**

Chemicals. More than 1000 research organic chemicals and intermediates, including liquid crystals, are listed together with compound classes and empirical formulas. 88 pp. Frinton Laboratories **438**

Lab instruments. New products include the Model VI still, a manometric gage, a micrometer manometer, and two tilting McLeod gages. Reprinted technical papers, vacuum control and pressure gages, viscometers, and a Warburg microметric gasometer are also featured. 64 pp. Gilmont Instruments **439**

Lab supplies. Eppendorf, Oxford, and Finn pipettors; radiation and biohazard safety supplies; colorimeters; microprocessor-based pH meters; conductivity meters; electrodes; and spectrophotometer cells--cuvettes are described. 108 pp. Markson Science **440**

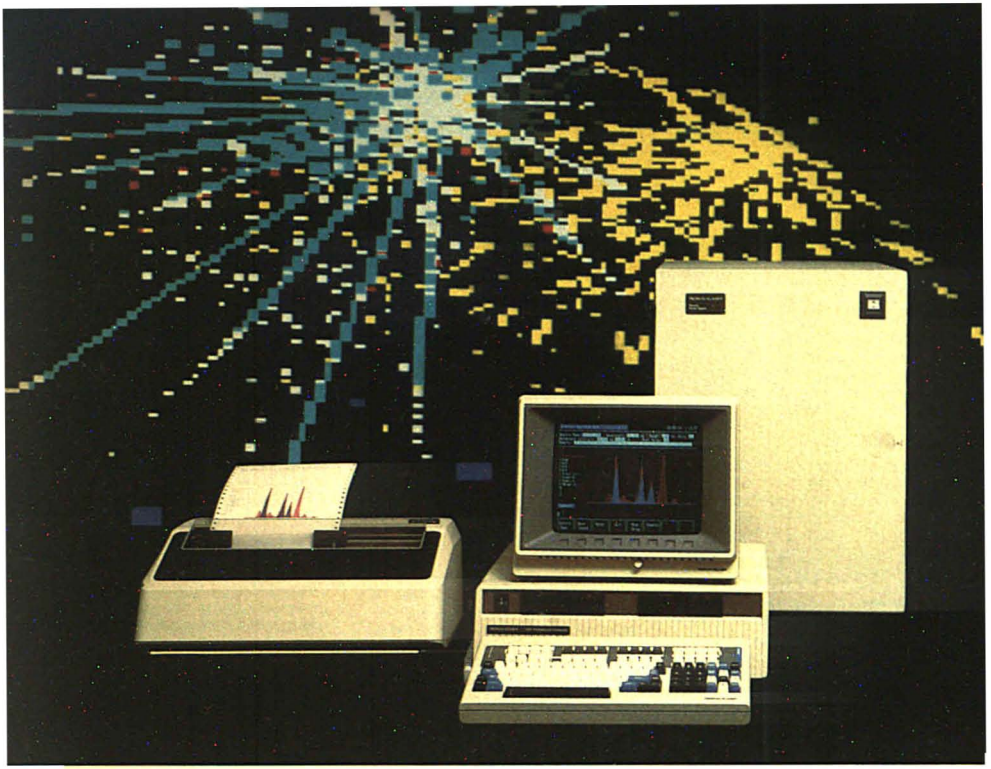
Safety equipment. 1985 catalog contains information about protective clothing and equipment, biosafety, laboratory and radiation safety, spill control, emergency response, and ventilation systems. 200 pp. Lab Safety Supply **441**

Laboratory products. 1985–86 catalog is divided into sections covering instrumentation, pH measurement, HPLC, advanced ion exchange cellulose, TLC, and membrane filtration. 65 pp. Whatman LabSales Inc. **442**

Liquid handling. Products presented include positive- and air-displacement pipettors, fixed-volume pipettors, repeating pipets and syringes, bottle-top dispensers, and pipet aids. VWR **443**

Filtration. Filter media, holders, and devices for laboratory process or monitoring applications are listed. Products include membrane filters of cellulose esters and regenerated esters; borosilicate and quartz microfiber filters; and ultrafilters available in three polymers and six molecular-weight cutoffs. Micro Filtration Systems **444**

For more information on listed items, circle the appropriate numbers on one of our Readers' Service Cards

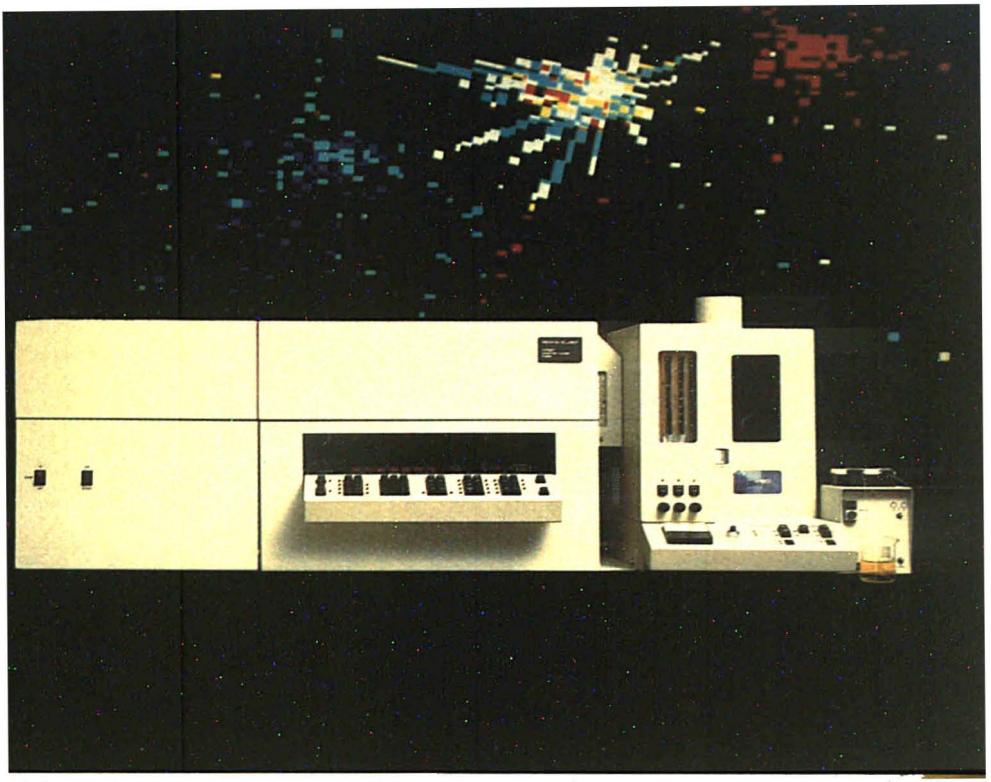


Celebrating the newest element in a sophisticated line. ICP/6500 from Perkin-Elmer.

Our new sequential ICP emission spectrometer. It incorporates all the sophistication of its highly regarded forerunner, the ICP/6000. With additional elegant refinements.

A superior torch and power supply.

High performance is inherent in the new torch assembly and power supply. Designed and manufactured by Perkin-Elmer, both units are highly reliable. The new power supply is quite compact, for convenient placement in your lab.



The most powerful ICP software available.

Perkin-Elmer's top of the line ICP software leads the field in ease, speed and flexibility. You can determine more than 20 elements/minute and analyze samples at any wavelength without prior wavelength calibration. The page-oriented display for modes of operation lets you perform analyses easily. For sequential multi-element analysis, methods can be built which contain up to 108 wavelengths. Data as generated can be stored automatically for reporting under a customized laboratory heading report. From on-line listings of over 50,000 analytical wavelengths to instructional and diagnostic utilities, this ICP software gives you unparalleled efficiency and productivity.

Select the model you want from superb hardware.

The ICP/6500 utilizes the powerful 16-bit PE 7300 Professional Computer in one of two configurations. For sophisticated applications, the PE 7300 includes a 15 megabyte hard disk, two floppy diskette drives, and brilliant color graphics and alpha-numerics. Or, you may select the monochrome display module with two floppy diskette drives. The PE 7300 is an EVERYWARE™ computer. Its industry standard hardware and operating system provide efficient software transportability and connectivity with other devices. And its capabilities can be further extended by interfacing it to a Laboratory Information Management System (LIMS).

Best of all.

This improved reliability and performance is provided at no increase in price. With its standard low UV capability; rugged cross flow nebulizer; corrosion resistant demountable torch; and high performance optics, the ICP/6500 is the ideal choice for your ICP needs.

For complete information, contact your local Perkin-Elmer representative. For literature, call 1-800-762-4000.

Perkin-Elmer Corp., Main Ave. (MS-12), Norwalk, CT 06856 U.S.A. Tel. (203) 762-1000. Telex 965-954.
Bodenseewerk Perkin-Elmer & Co., GmbH, Postfach 1120, 7770 Ueberlingen, Federal Republic of Germany. Tel. (07551) 811.
Perkin-Elmer Ltd., Post Office Lane, Beaconsfield, Bucks HP9 1QA, England. Tel. Beaconsfield (049 46) 6161.

EVERYWARE is a trademark of The Perkin-Elmer Corp.

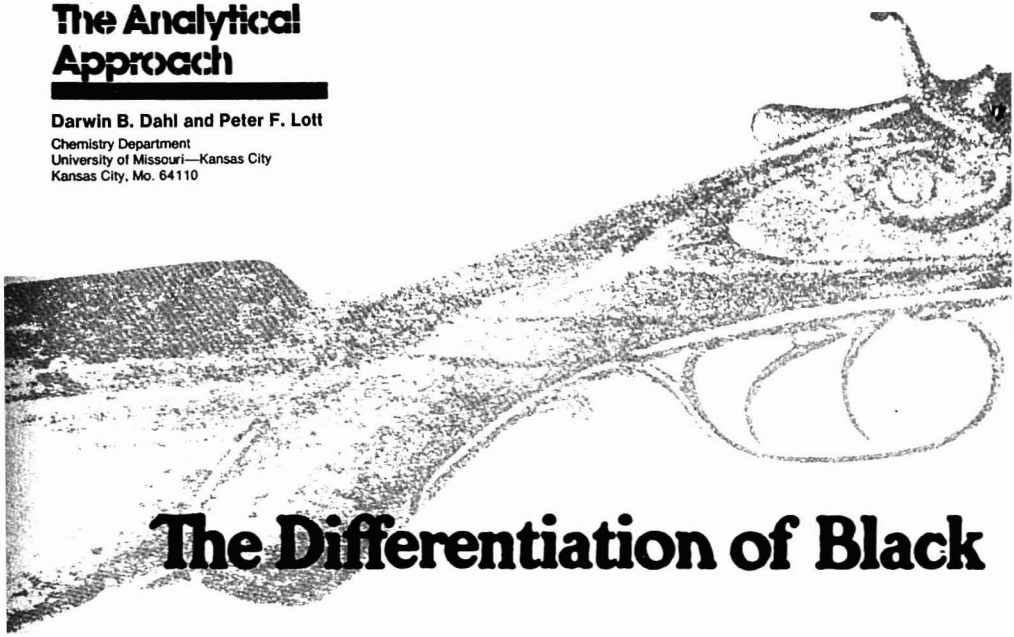
PERKIN-ELMER

The science and computer company.
Where solutions come first.

CIRCLE 170 ON READER SERVICE CARD

The Analytical Approach

Darwin B. Dahl and Peter F. Lott
Chemistry Department
University of Missouri—Kansas City
Kansas City, Mo. 64110



The Differentiation of Black

"HERE'S THE PROBLEM. We are being sued for millions because this black-powder gun blew up. We are certain smokeless powder was used, but how can we show it? Our situation is made worse by the fact that we did not test-fire the gun before it left the plant. You know, of course, that the U.S. has no proof laws. I know, I know, don't tell me—we should have proof-fired the gun. The crucial point in the litigation is whether or not smokeless powder was used."

With the present renewed interest in pioneer activities, such lawsuits are not rare occurrences, and injuries to the shooter can be very severe. Before the problem can be solved, we need information about the chemical content, appearance, and characteristics of black powder and smokeless powder. To the chemist, black powder is that mixture containing 75% potassium nitrate, 12.5% charcoal, and 12.5% sulfur. To the uninitiated it might simply be any gunpowder that looks black and that perhaps can be purchased relatively cheaply at a garage sale. Consequently, entirely through circumstances of chance and ignorance, it is quite possible that this recreational device, designed to use only black powder, could be loaded with smokeless powder, which develops excessive pressure upon firing and blows up the gun. Or the hobbyist may intentionally use a "duplex" load, a mixture of black and smokeless powder, either to improve the ballistic characteristics or to reduce the amount of fouling left in the gun. Or, one might think that any gun of modern manufacture would be safe with smokeless powder and that the type of gunpowder used, as long as it looked black, was irrelevant.

The outcome of such errors can be long remembered, quite expensive, and devastating both to the injured party and the manufacturer of the firearm if litigation ensues.

Thus, the analytical problem is how to check both the remains in the powder flask and the residue left in the gun for either smokeless powder, black powder, or a mixture that might consist of black powder and smokeless powder. Immediately we recognize that there is not going to be much residue and that, if at all possible, the testing should be performed by two independent methods so as to produce unquestioned results. Ideally, the initial screening should also be quickly performed using a simple method with minimum equipment.

One of the first questions to be considered is whether black powder varies considerably from manufacturer to manufacturer. Since it is composed of crystalline constituents, it should give an X-ray diffraction pattern. Furthermore, X-ray diffraction can be applied to the analysis of small amounts of material, and the diffraction pattern for a substance provides an unquestioned identification. Consequently X-ray diffraction patterns were recorded for several black powders as well as for a recently developed black-powder-type propellant made for use in black-powder guns, Pyrodex. The superimposed diffraction patterns for current as well as several older black powders are shown in Figure 1. Mili-

0003-2700/85/0357-446A$01.50/0
© 1985 American Chemical Society



and Smokeless Gunpowders

tary black-powder cartridges, which can be relatively easily obtained from cartridge collectors, were taken apart; some of the black powder was finely ground to obtain the diffraction patterns. Surprisingly, very little change was seen in the patterns for black powders currently made compared with those made more than 100 years ago. Nor did it seem to make much difference where the ammunition was manufactured, and neither did age seem to change black powder. Obviously, an analysis for trace components would show differences, but overall the composition of the black powders, except for Pyrodex, is equivalent. Black-powder formulations that use sodium nitrate or ammonium nitrate instead of potassium nitrate do exist, and some contain no sulfur. These compositions are seldom used in firearm ballistic formulations because such mixtures are more difficult to ignite. Of interest are the compositions of several older gunpowders, shown in Table I.

In contrast, smokeless powder, a nitrocellulose, does not give a diffraction pattern. To the trained eye, smokeless powder has a different appearance than black powder. It also has a distinctly different hardness. Figure 2



Nineteenth-century hammer-type Parker shotgun after smokeless powder was fired in the gun

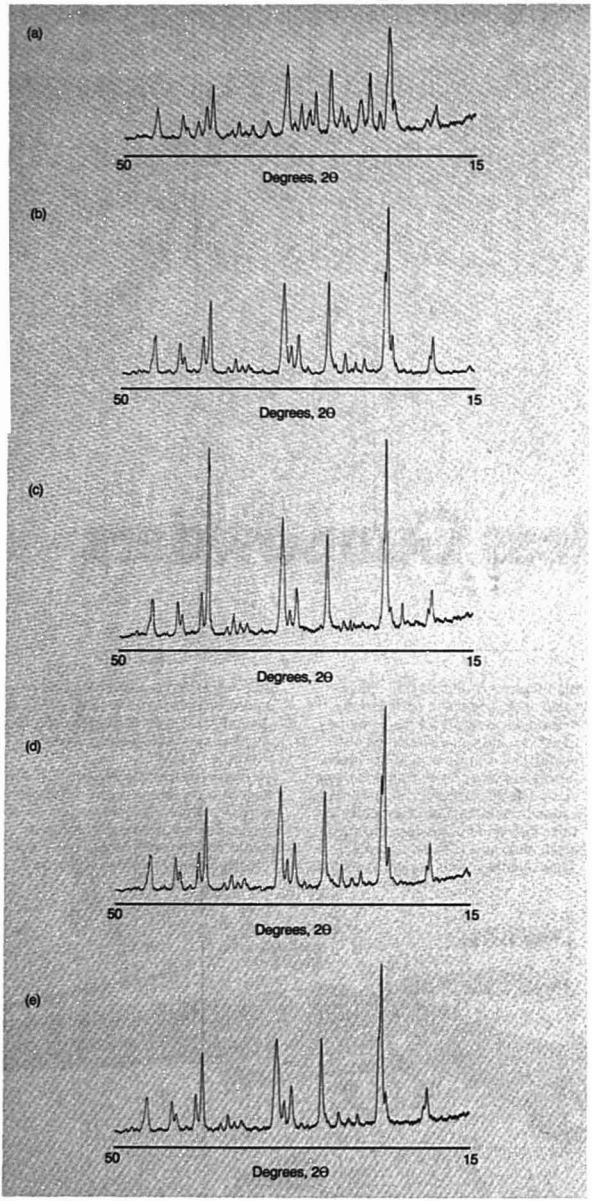


Figure 1. X-ray diffraction patterns (instrument response vs. 2θ value) for modern black powders and black powders from antique rifle cartridges

(a) Pyrodex powder, U.S. manufacture, 1984, (b) Goez black powder, U.S. manufacture, 1983, (c) 10.75 × 58 Russian Berdan cartridge, 1884, (d) 11 × 59R French Gras cartridge, 1874, (e) 0.56–56 U.S. Spencer cartridge, 1862

shows a 3× magnification of several smokeless gunpowders and black powder. Thus by simple visual examination it may be possible to distinguish black powder from smokeless powder and to separate the individual components physically for further tests; black powder has the appearance of miniature lumps of coal.

One flake of smokeless powder gives enough material for several chemical tests, and visual examination could also serve as one identification. Were we to check for the presence of smokeless powder, our initial aim would be to detect nitrocellulose or the distinctive additives in smokeless powder. Finding nitrocellulose might be questioned, as a number of consumer products, for example, certain fingernail polishes as well as wood finishes, may contain nitrocellulose. Consequently, one would also determine the stabilizers in gunpowder, the most common of which is diphenylamine, which is present at the 1–2% level.

Nitrocellulose powders are a colloided nitrocellulose. If they are double-based powders, nitroglycerin has been added. In its manufacture the finished smokeless powder is often glazed with graphite, which gives it a black appearance. Graphite glazing is performed to stabilize the moisture content of the powder and lessen the absorption of moisture, as well as to make the powder electrically conductive so as to minimize dangers in blending from static electricity. This black appearance can be a major cause of a person assuming that any gunpowder that is black is black powder.

Spot tests

Where might you find a flake of smokeless powder? In the powder flask, the container used to dispense the desired amount of gunpowder. Take the flask apart; carefully examine any crevice where a particle might be caught as well as any threaded parts, as flakes might be trapped between the threads. If a flake of smokeless powder is recovered, it can be dissolved in acetone or methylene chloride, and its infrared (IR) spectrum can be run. Or, colorimetric spot tests can be used. Surprisingly, black powder is virtually insoluble in acetone. In contrast, smokeless powder is quite soluble. Thus treatment of the material with anhydrous acetone provides an excellent separation. We were first made aware of this procedure through a private communication from John A. Reffner of American Cyanamid Research Laboratories. The acetone extract can now be tested for the presence of nitrocellulose by its reaction with certain chromogenic reagents such as chromotropic acid or, interestingly, diphenylamine. A few drops



You Can Cut Separation Time In Half... And Still Get Excellent Resolution.

Whatman RAC II—Second Generation Rapid Analysis Chromatography. The 4.6 mm x 10 cm long column prepacked with proven 5 μm Partisil media offers guaranteed performance that is simply faster and more efficient.

In fact, compared to the standard 25 cm long column used in most applications, RAC II gives you equal resolution with no change in flow rate or mobile phase composition...with one-half the solvent usage...twice the sample throughput...in one-half the time. That's productivity.

And, you may choose from six different phases to handle virtually all LC separation needs, including ODS-3, C_8, Silica, and the *new* PAC, SAX and SCX.

RAC II special geometry eliminates unswept corners to maximize peak symmetry and resolution. Whatman compression screw end fittings provide for uniform sample distribution to improve effectiveness and lower asymmetry values.

Get speed, get resolution, get RAC II. Call a Whatman technical representative now to discuss your applications. Toll-free 800-922-0361. (In N.J. 201-773-5800.)

RAC is a trademark of Whatman, Inc.

Whatman

See Us at FASEB, Booths #2009-2017.

CIRCLE 233 ON READER SERVICE CARD

PACKARD GAS CHROMATOGRAPHS

meet all your requirements for routine and research gas chromatography



Model 438A
Packard's most flexible compact GC, with our renowned Analytical Module for rapid and easy change of analytical configuration.

Model 437A
Our most cost-effective GC. Ideal for routine packed and capillary applications, it features an LCD display and is a real workhorse.

Model 436
A dedicated capillary system and our latest GC. It has outstanding oven specifications.

Model 439
The ultimate research GC, with modular design for unsurpassed flexibility. Featuring a CRT display and user-friendly programming, it also functions as a Network control station.

GC Network
Up to 12 satellites or conventional GCs can be programmed and supervised from a Model 439 GC or the stand-alone Network Manager. The Network offers substantial cost and operational benefits, including unmatched system security, and is ideally suited for routine plant process control environments where reliability is of paramount importance.

And of course, all Packard GCs are backed by expert service support and a full range of high quality accessories.

Ask for our brochures!

UNITED TECHNOLOGIES PACKARD

PACKARD INSTRUMENT COMPANY, INC.
2200 Warrenville Rd./Downers Grove, IL 60515/U.S.A.

PACKARD INSTRUMENT INTERNATIONAL S.A.
Renggerstrasse 3/CH-8038 Zurich/Switzerland

PACKARD INSTRUMENT B.V.
P.O. Box 519/2600 AM Delft/The Netherlands

CIRCLE 167 ON READER SERVICE CARD

Table I. Percentage composition of black gunpowders [a]

Type	Potassium nitrate	Charcoal	Sulfur
8th century, Marcus Graecus	66.66	22.22	11.11
8th century, Marcus Graecus	69.22	23.07	7.69
c. 1252, Roger Bacon	37.50	31.25	31.25
1350, Arderne (laboratory recipe)	66.6	22.2	11.1
1560, Whitehorne	50.0	33.3	16.6
1560, Bruxelles studies	75.0	15.62	9.38
1635, British government contract	75.0	12.5	12.5
1781, Bishop Watson	75.0	15.0	10.0

[a] Davis, Tenny L. "The Chemistry of Powder and Explosives, Vol. I"; John Wiley and Sons: New York, N.Y., 1941; p. 39.

of the acetone extract are transferred to a spot plate, and the solvent is carefully evaporated using a gentle stream of air. The residue is reconstituted with five drops of concentrated H_2SO_4. Three drops of a 100-ppm solution of diphenylamine in concentrated H_2SO_4 are added to a separate compartment of the spot plate, and then one drop of the reconstituted gunpowder solution is added. A positive test for nitrocellulose is a change from clear to blue. If the sample has a large amount of diphenylamine in it already the addition of the sulfuric acid suffices for the color change. A positive test is certainly indicative of the presence of smokeless powder, although not conclusive in itself. Further quick verification can be made by adding a few drops of this acetone extract to a microscope slide and allowing it to evaporate. A white spot appears; if it is nitrocellulose it often gives a lacelike pattern when examined under a microscope at 100-fold magnification, as shown in Figure 3.

A quick spot test for black powder can be made by adding a few drops of the 100-ppm diphenylamine solution to the residue left from the initial acetone extraction. Formation of a blue color indicates the presence of black powder. Extracting black powder with acetone and then testing this acetone extract with the diphenylamine reagent invariably showed no color reaction with the diphenylamine reagent. Accordingly, three independent tests can be done quickly: visual examination of the material, microscopic examination, and color tests in a spot plate. A test for sulfur, an ingredient in black powder and not in nitrocellulose powders, can also be performed by transferring some of the residue to a test tube and adding a small amount of benzoin. A piece of lead acetate paper is fixed over the mouth of the tube, and the test tube is inserted into a glycerin bath (a beaker filled with glycerin) heated to 130 °C. The temperature is raised to 150 °C. Formation of a black precipitate of lead sulfide on the paper is a positive test for sulfur and indicative of black powder.

Testing the gun

Although finding flakes of smokeless powder in the powder flask would be quite fortunate, it still does not give proof that the smokeless powder was fired in a gun. Thus, tests need to be performed on the gun itself. The same spot tests can be used. Depending on the situation, portions of the debris in the gun can be scraped out, then treated with acetone as in the previously described procedure. Or parts of the gun can be immersed in an acetone solution in a beaker, which is placed in an ultrasonic cleaner. The acetone solution is partially evaporated, and the color tests and microscopic examination for nitrocellulose previously described are performed. The residue from the acetone extraction is treated with water and tested for the presence of potassium nitrate using the diphenylamine test previously described. Or the residue may be collected and an X-ray diffraction pattern can be taken. The advantage of this approach is that the X-ray diffraction pattern is definitive, nondestructive, and leaves the sample available for further testing.

The major interest, obviously, is in the detection of smokeless powder. If the tests so far are inconclusive, chances are that the amounts present are very small, and instrumental methods must be used. Conventional

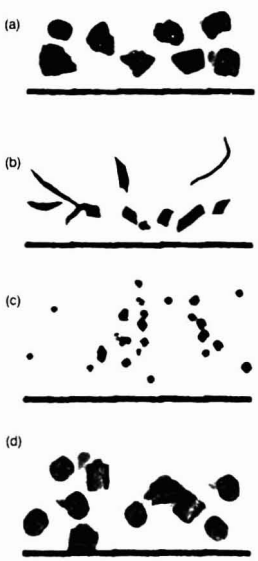


Figure 2. Macrophotograph (3X) of black powder and certain smokeless powders

(a) Black powder, (b) Alcan AL-7 smokeless powder, (c) Hodgdon H110 spherical smokeless powder, (d) Du Pont No. 4759 extruded smokeless powder

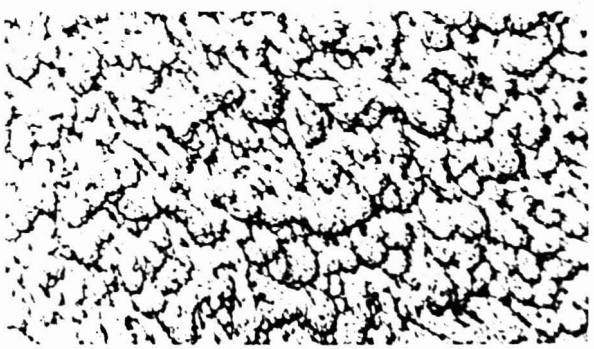


Figure 3. Photomicrograph (100X) of nitrocellulose

BEING BIG
DIDN'T SAVE THE
DINOSAUR EITHER



THE PACKED COLUMN
ALTERNATIVE

MEGABORE

- Easy to Install
- Cost Effective
- One Configuration
- Fits All G.C.s
- Highly Reproducible
- Highly Inert
- Preconditioned & Tested
- Bonded Phases

FREE! 32-PAGE BROCHURE WITH
APPLICATIONS AND INFORMATION

J&W SCIENTIFIC, INC.

3871 SECURITY PARK DRIVE, RANCHO CORDOVA, CA 95670
(916) 351-0387

CIRCLE 110 ON READER SERVICE CARD

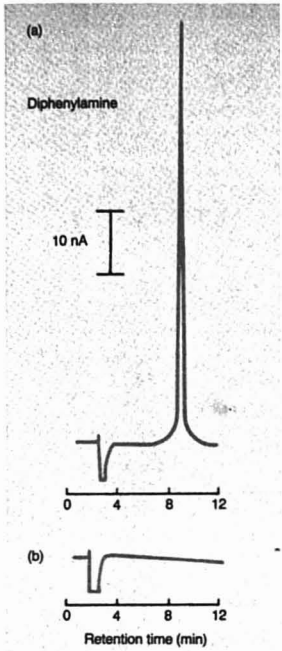
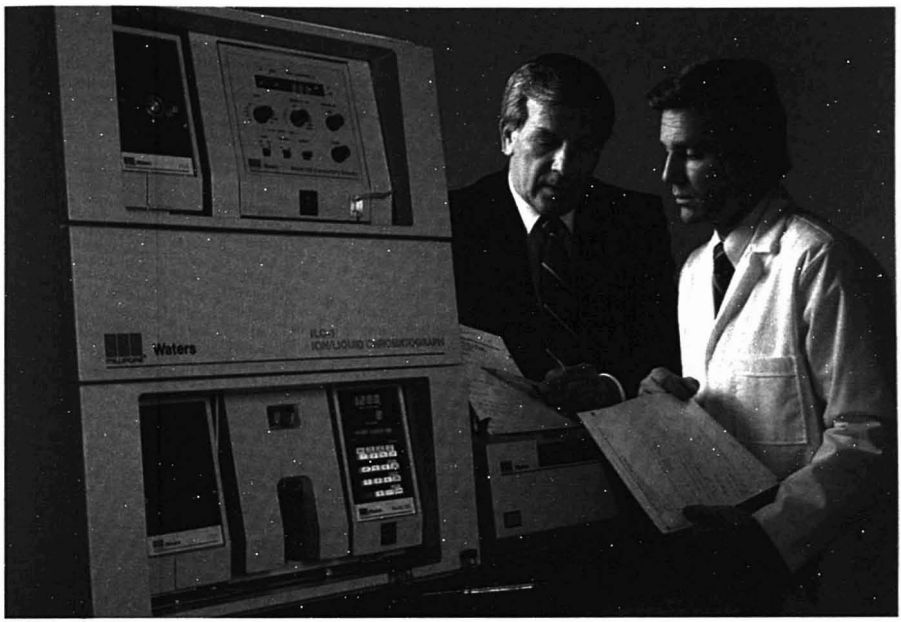


Figure 4. Chromatogram of (a) smokeless powder and (b) black powder

IR or NMR measurements would probably not be a worthwhile effort because the concentrations are too small. Mass spectrometry may work; the appearance of a peak for diphenylamine would be conclusive proof. Using gas chromatography to detect traces of powder residue can be difficult. Furthermore, because of the number of peaks that may be obtained, a positive identification based only on a gas chromatographic pattern could be questioned.

High-performance liquid chromatography could offer a reasonable possibility. The optical detectors, such as the UV detector, probably will not show sufficient sensitivity and may be bothered by the presence of interferences in the sample matrix, such as fragments of the finish from the gun stock. An electrochemical detector, however, can provide additional selectivity and sensitivity. The separation can be obtained quite quickly and easily; picogram amounts of diphenylamine can be determined. One disadvantage is that the method will not pick up the "centralites," substituted phenyl ureas added in some smokeless gunpowders as stabilizing agents.

Buy a Waters™ Ion Chromatograph, and get more than just an instrument.



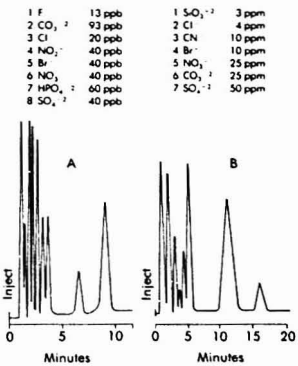
© 1984 Millipore Corporation

In-depth applications development...responsive customer support and service...20 years of chromatography expertise. The same qualities that established our world leadership in HPLC are a part of every Waters ILC Series Ion/Liquid Chromatograph.

The result of our commitment is advanced Ion Chromatography capabilities. Now you can change selectivity without switching columns–just by changing eluents. Routinely quantitate ions at sub-ppb levels. Analyze a wider range of ions without added system complexity (no expensive post-column chemistries required).

Our worldwide support network includes a dedicated group of ion chromatographers and over 300 technical, sales and field service personnel. Together, they have provided answers for a broad spectrum of application problems.

To learn more about how Waters Ion Chromatography expertise can go to work for you, please call the Ion Chromatography Hotline at (617) 478-2000, ext. 2500. In Canada, call 1-800-268-4881. Or write to the Ion Chromatography Group, Millipore Corporation, Waters Chromatography Division, 34 Maple Street, Milford, MA 01757.



Eight anions determined at low ppb levels (A); by simply changing eluents on the same column, you can also determine *silicate* and *cyanide* (B).

MILLIPORE
Waters Chromatography Division

CIRCLE 231 ON READER SERVICE CARD

They are used much less commonly than diphenylamine. We are currently working to extend the detection approach to the centralites.

With electrochemical detectors, one would gain additional selectivity and sensitivity over optical detectors. In using a conventional electrochemical detector, a hydrodynamic voltammogram needs to be constructed first to obtain proper operating conditions for the detector. The normal procedure is to set the voltage on the detector to a fixed value, inject the sample, and when the peak appears for the desired constituent, measure the peak height, finish the separation, and inject the next samples with the detector set at successively higher voltages. This is quite time-consuming. One simple solution to the problem is to prepare a stock solution of diphenylamine in the same eluting solvent as is used for the chromatographic separation. Pour this solution into a buret and connect the plastic tubing that enters into the flow cell to the buret tip. Control the buret to deliver a slow, continuous flow of solvent with the stopcock. Preferably, the flow should be the same as that which might be used in the separation, for example, 1 mL per minute. Change the voltage, measure the recorder deflection, and repeat. Because it is a polarographic procedure, it is really rather similar to obtaining a polarogram with a manual polarograph. Because an oxidative mode of detection is used, we selected acetone as the major component in the mobile phase rather than methanol—which was used by other investigators—due to acetone's greater stability toward oxidation. This makes it easier to determine diphenylamine and increases the sensitivity of the method. A typical chromatogram for smokeless powder, showing the diphenylamine peak, is presented in Figure 4. The peak was verified as diphenylamine by the collection of a sample and by running its mass spectrum. Furthermore, linear calibration curves can be obtained by varying the concentration of diphenylamine, so that a quantitative determination of the amount of diphenylamine can be obtained.

Thus in many cases simple visual observation, chemical tests, and instrumental methods can be used to obtain irrefutable evidence as to whether or not smokeless powder was used in a black powder gun. In addition there is one other simple examination that may provide additional information. Look at the injured party. The powder burns of black powder differ from those of smokeless powder. A black-powder discharge throws out very small particles of carbon that tattoo the skin. The carbon is embedded in the skin and may take years to go away. The burns are quite visible for about 6 years and may possibly still be seen 10 or more years later. Embedded particles of smokeless powder are more gray than black and will disappear much more quickly, possibly within a year. The information obtained by observation of the powder burns may not be conclusive, but could certainly aid in confirmation.

Acknowledgment

We thank John C. Cayton and Stephen C. Warlen of the Kansas City Regional Criminalistics Laboratory, Kansas City, Mo., for their assistance in providing ruptured firearms and photographs. This work was presented at the Benedetti-Pichler Symposium of the American Microchemical Society, held at the Eastern Analytical Conference, New York City, November 1984. The detailed procedure for obtaining hydrodynamic voltammetry plots is scheduled to appear in the April issue of the *Microchemical Journal*.

Hazards in the Chemical Laboratory
3rd Edition



Published by the Royal Society of Chemistry, London

L. Bretherick, *Editor, BP Research Centre, Sunbury*

This easy-to-use plastic-covered handbook belongs in every chemical laboratory. Its convenient dictionary form lists alphabetically 480 explosive, corrosive, and/or toxic substances, giving information on the toxic effects of these substances as well as hazardous reactions, first aid, flash points, and disposal methods. Rounding out the book are special chapters on safety planning and management, fire protection, reactive chemical hazards, chemical hazards and toxicology, health care and first aid, and precautions against radiations. No laboratory should be without this comprehensive edition.

CONTENTS

Introduction • Health and Safety at Work Act 1974 • Safety Planning and Management • Fire Protection • Reactive Chemical Hazards • Chemical Hazards and Toxicology • Health Care and First Aid • Hazardous Chemicals • Precautions Against Radiations

586 pages (1981) Plastic
ISBN 0-85186-419-8
US & Canada **$35.00** (International customers should contact the RSC directly)

Order from:
American Chemical Society
Distribution Office Dept. 35
1155 Sixteenth St., N.W.
Washington, DC 20036
or CALL TOLL FREE 800-424-6747
and use your VISA or MasterCard

NMR Spectroscopy: New Methods and Applications



ACS Symposium Series No. 191

George C. Levy, *Editor, Syracuse University*

Based on a symposium jointly sponsored by the Divisions of Analytical, Organic, and Physical Chemistry of the ACS.

This 17-chapter volume outlines some of the more recent NMR applications. The development of methodology to obtain high resolution NMR represents one of the promising new areas of research. At the same time, the FT technique makes high resolution experiments much easier to be performed at high pressure. The ^{13}C NMR experiments of rhodium carbonyl clusters presented in this text are an illustrative example of the application of this technique to homogeneous catalytic processes. The nature of solid fossil fuels is probed with high resolution FT NMR using cross-polarization and magic angle spinning techniques. Two-dimensional FT NMR and the new information this technique can provide also are discussed.

CONTENTS

Ultra High-Field NMR • NMR Spectroscopy at 600 MHz • Two-dimensional Fourier Spectroscopy • Quadrupolar Metallic Nuclei • Deuterium NMR Spectroscopy • Metabolism of ^{13}C Labeled Substrates • Chemical Bond Labeling and Double-Cross Polarization NMR • NMR Spectroscopy at High Pressure • ^{13}C Cross Polarization Magic Angle Spinning NMR • NMR of Linear and Cyclic Peptides • ^{31}P NMR Studies • ^{13}C NMR Studies of DNA Dynamics • Photo-Chemically Induced Nuclear Polarization of Biological Molecules • ^{13}C NMR Characterization of Solid Fossil Fuels • Polyester Thermoplastic Elastomers • ^{23}Na NMR Studies

388 pages (1982) Clothbound
LC 82-11458 ISBN 0-8412-0723-2
US & Canada **$54.95** Export **$65.95**

Order from:
Distribution Office — 2
American Chemical Society
1155 Sixteenth St., N.W.
Washington, D.C. 20036
or CALL TOLL FREE 800-424-6747
and use your credit card.

1985 Beckman/Altex Column Catalog—circle #20 for a free copy ⟶

A Survey of Immunoassay Techniques

Practical Immunoassay: The State of the Art. Wilfrid Butt, Ed. ix + 318 pp. Marcel Dekker, 270 Madison Ave., New York, N.Y. 10016. 1984. $55

Reviewed by Gail Hudson, Foundation for Blood Research, P.O. Box 190, Scarborough, Maine 04074

This survey of immunoassay techniques is for those who already have a basic knowledge of immunochemistry but want more information on specific topics. The book's 10 chapters, which deal with various aspects of immunoassay, are written by those active in the field. Most contain a brief description of theory, a summary of published work, and several references to more detailed descriptions of the topic. Emphasis is on providing the practical information necessary for designing an immunoassay, not necessarily by giving exact experimental details, but rather by pointing out factors that must be considered in assay design. For example, sample blanks and polymer enhancement are emphasized in the chapter on nephelometry, and the selection of enzymes is discussed under enzyme immunoassay.

Several chapters contain additional outstanding features. The chapter on nephelometry contains detailed descriptions of available instrumentation, including advantages and disadvantages. The chapter on pulsed-light, time-resolved fluoroimmunoassay contains an out-of-place, yet excellent discussion on the differences between the factors that affect sensitivity of sandwich-type and competitive assays. The chapter on free hormones in blood emphasizes the distributional role of serum-binding proteins in the measurement of free hormone. The chapter on monoclonal antibodies provides practical instructions for making monoclonal antibodies, based on the author's own experience. An excellent chapter on data analysis and quality control assumes a basic knowledge of statistical terms and concentrates on applications to ligand-binder assays.

Other chapters cover chemiluminescence, labeled antibody immunoassays, and iodination.

This book provides a wealth of useful information. Most chapters contain excellent summaries of their topics, especially those on nephelometry, pulsed fluoroimmunoassay, free hormones in blood, and data analysis. However, several important techniques have been omitted. They are gel techniques, particle-based assays, competitive radioimmunoassay, and traditional fluoroimmunoassay (without time resolving). The volume also lacks a section that compares the sensitivity, ease of operation, cost, etc., of the various types of immunoassays and discusses the situations where each is usually used. For the most part, the depth of presentation is appropriate, with the exception of the chapters on enzyme immunoassay and labeled antibody immunoassays, which give complete cookbook directions from the author's own publications. Overall, I found the book excellent and definitely recommend it for graduate students and practicing immunochemists.

Food Analysis: Principles and Techniques. Vol. 1. D. W. Gruenwedel, J. R. Whitaker, Eds. xi + 338 pp. Marcel Dekker, 270 Madison Ave., New York, N.Y. 10016. 1984. $59.75

Reviewed by James Lawrence, Food Directorate, Health Protection Branch, Tunney's Pasture, Ottawa, Ontario K1A 0L2, Canada

This is the first volume of a planned eight-volume series devoted to meeting "the need for an up-to-date detailed treatment of the methods of modern food analysis." Its subject is methods of physical characterization of foods. As the editors state, "The treatise is not a handbook of methods of analysis . . . ," and "is not intended as a primary textbook," but is "intended for use by graduate students and all scientists involved in the analysis of biological materials." This reviewer agrees with the first two statements but exactly how or for what purpose graduate students or scientists will use the volume (and the series) is unclear. What the volume *does* provide are essentially individual overviews in the area of physical characterization of foods. Most of the seven chapters include an introduction, a brief history, principles of the techniques, and some applications. The book suffers, however, from unevenness in the choice of subject matter. Only four of the seven chapters are directly related to physical characterization of foods. The chapters on statistical evaluation and computers are of a more general nature, whereas the chapter on automated techniques discusses only chemical analysis and would have been better suited to a later volume of this series.

The first chapter, on statistical evaluation, is directed toward experimental design and treatment of data. It is sufficiently general to be applicable to data generated for purposes other than physical characterization of foods. The chapters on sensory techniques and color measurement are well prepared and make for interesting and informative reading. They discuss the necessity of testing foods for attractiveness in terms of color, taste, texture, etc., since the consumer's perception of food is of prime importance to the food industry. Chapters 4 and 5 deal with rheological and mechanical properties of foods and discuss the importance of this area to food production and processing and to the design of processing equipment. Unfortunately these two chapters contain a significant degree of unnecessary duplication. Most of the references quoted in Chapter 5, for example, have already been cited in the previous chapter. These two chapters could have been made more complementary with closer editorial scrutiny. Chapter 6 discusses applications of continuous-flow systems to automated food analysis and includes, exclusively, the latest developments in Technicon automated analyzers with examples of the determination of food constituents, additives, contaminants, and enzymes. No discussion of flow injection or other automated techniques is presented. The final chapter is on

← 1985 Beckman/Altex Column Catalog—circle #20 for a free copy.

Swagelok®
TUBE FITTINGS
...a tradition of Excellence



Unique Swaging Action

• Provides a seal between ferrule and body at a point different from where the heavy work is performed • Supports tube ahead of seal to resist vibration • Does not create torque or leave residual strain on tubing • Does not significantly reduce flow area.

Patented

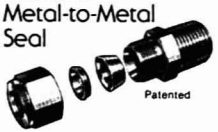


Inspection Gage Assures Sufficient Pull-Up



• Useful for both the installer and inspector • If the gage will not fully enter the gap between the nut and body shoulder, fitting pull-up is sufficient • If the gage enters the gap, you'll know pull-up is incomplete.

Effective Metal-to-Metal Seal



Patented

• Interaction of precision parts — body, front ferrule, back ferrule and nut — produces a leak-free seal with simple 1-1/4 turn pull-up • Works on thick or thin wall tubing • Seals repeatedly under make-and-break conditions • Seals consistently over a wide range of pressures, temperatures and temperature cycling.

Only SWAGELOK Tube Fittings offer gageability of straight fittings, and forged shaped elbows and tees in stainless steel and steel. Gages are available for 1/8" through 1" sizes. Torque-free swaging action, effective sealing and gageability are just three of the many elements of excellence for which SWAGELOK Tube Fittings are known and respected...a tradition of Excellence.

Swagelok® TUBE FITTINGS

CRAWFORD FITTING COMPANY
29500 Solon Road, Solon, Ohio 44139
Crawford Fittings (Canada), Ltd., Ontario
© 1981 MARKAD SERVICE CO. / all rights reserved C-36f

CIRCLE 32 ON READER SERVICE CARD

Books

laboratory computers and provides the reader with discussions on computer terminology, advances in hardware and software, and how to best use computers in the laboratory.

In spite of the shortcomings mentioned above, this book is very readable, well illustrated, and the subjects are all treated to a uniform depth. Although several chapters do not strictly deal with physical characterization of foods they certainly do fall within the scope of the series.

Fourier Transform N.M.R. Spectroscopy. 2nd ed. Derek Shaw. xi + 344 pp. Elsevier Science Publishing Co., 52 Vanderbilt Ave., New York, N.Y. 10017. 1984. $75

Reviewed by Thomas Farrar, Department of Chemistry, University of Wisconsin, 1101 University Ave., Madison, Wis. 53706

For the most part, the second edition of this book is very like the first and has the same strengths and weaknesses. A number of new sections are added to accommodate some of the more important recent developments, such as two-dimensional Fourier transform NMR and NMR imaging.

The Introduction and Chapter 2, "Principles of Magnetic Resonance," are very interesting and well done. Chapter 3, "The Mathematics of Fourier NMR," is a reasonably complete, clear, and accurate presentation of the principles on which FT-NMR is based. The basic pulsed NMR experiments are covered in Chapters 4 ("Excitation Techniques in NMR") and 5 ("Pulsed NMR"). In Chapter 5 we find the first material not present in the first edition. The presentation of multipulse and composite pulse techniques to the NMR observation channel is well done, and a few examples are given. For some reason the author makes no mention of the rather substantial advances that have taken place in decoupling experiments as a result of sophisticated multipulse experiments in the decoupling channel (for example, MLEV and WALTZ).

Chapter 6 on instrumentation is rather weak and misses what in my view is one of the central points about the modern NMR spectrometer—the computer is the heart and mind of the spectrometer. It plays a central, vital role in every aspect of all NMR experiments. It controls the pulse timing and rf phase of the pulses in observe, lock, and decouple channels; it controls all aspects of the various rf receivers; and, of course, it is fully responsible for the large and complex



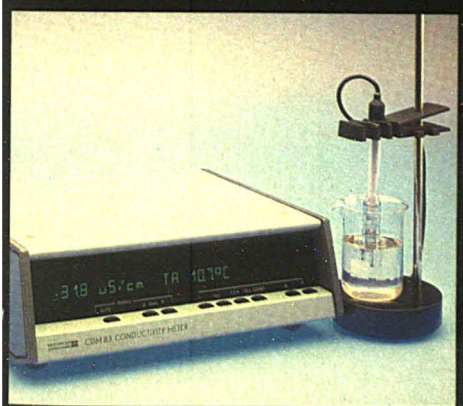
The case of the disused dial

»A thick ground fog spread over the streets of the city. The dial lay among the leaves scattered by a gentle breeze...«

On Radiometer's new CDM83 Conductivity Meter with microprocessor controls, dials are out. We've developed the CDM83 to save you time and errors.

The CDM83 has auto-ranging and auto-frequency-shifting combined with a 20-character alphanumerical display offering full operator prompting. The CDM83 gives you the accurate facts day in and day out.

So hire your nearest Radiometer technical detectives to find out how the CDM83 can bail you out. You need the whole story to wrap up the case.



RADIOMETER COPENHAGEN

Analytical Instruments Division

Radiometer A/S, Emdrupvej 72, DK-2400 Copenhagen NV, Denmark

CIRCLE 180 ON READER SERVICE CARD

task of data reduction. In the most modern spectrometers it controls all of the magnetic field gradient coils and the sample spinning.

Shaw has omitted, correctly I think, the chapter entitled "The NMR Spectrum," which appeared in the first edition. I think he should also have omitted Chapters 7 and 8 on "Experimental Techniques" and "Multiple Resonance." These chapters add little to the book, are too short to be really useful, and the material is covered much better in other recent books. Chapters 9 ("Relaxation") and 10 ("Multidimensional NMR and Imaging") include a number of recent advances in NMR and are quite worthwhile. It's a pity that Shaw did not spend more time on NMR imaging.

Overall, this is a good book that complements rather nicely a number of others on the market. The chapter on the mathematics of FT-NMR is especially well done. By far the biggest problem with the book is the new low point it sets in editing. There is hardly a page in the book that does not contain an error in punctuation, grammar, syntax, or spelling. Often a combination of these errors comes together and the sentences are unintelligible. Even a casual reading by a graduate student could have caught and corrected most of these sloppy and inexcusable errors.

Books Received

Treatise on Analytical Chemistry. Vol. 4, Pt. 1. 2nd ed. Philip Elving, Ed. xxxix + 675 pp. John Wiley & Sons, 605 Third Ave., New York, N.Y. 10016. 1984. $75

Automated Stream Analysis. Vol. 2. Dan Manka, Ed. xiv + 205 pp. Academic Press, Orlando, Fla. 32887. 1984. $59

Drug Dynamics for Analytical, Clinical, and Biological Chemists. B. J. Gudzinowicz, B. T. Younkin, M. J. Gudzinowicz. vii + 176 pp. Marcel Dekker, 270 Madison Ave., New York, N.Y. 10016. 1984. $39.75

Food Analysis. Principles and Techniques. Vol. 2. D. W. Gruenwedel, J. R. Whitaker, Eds. xvi + 591 pp. Marcel Dekker, 270 Madison Ave., New York, N.Y. 10016. 1984. $107.50

Affinity Chromatography. Herbert Schott. x + 234 pp. Marcel Dekker, 270 Madison Ave., New York, N.Y. 10016. 1984. $49.50

Analytical Profiles of Drug Substances. Vol. 13. Klaus Florey, Ed. lx + 771 pp. Academic Press, 111 Fifth Ave., New York, N.Y. 10003. 1984. $56.50

Microwave Molecular Spectra. 3rd ed. Walter Gordy, Robert Cook. xiv + 929 pp. John Wiley & Sons, 605 Third Ave., New York, N.Y. 10016. 1984. $175

A Guide to the HPLC Literature. Vol. 1: 1966–1979. Henri Colin et al. xi + 947 pp. John Wiley & Sons, 605 Third Ave., New York, N.Y. 10016. 1984. $125

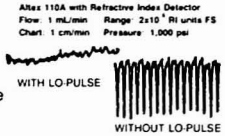
Vibrational Spectroscopy at High External Pressures. John Ferraro. xiv + 645 pp. Academic Press, 111 Fifth Ave., New York, N.Y. 10003. 1984. $59

HPLC in Nucleic Acid Research. Phyllis Brown, Ed. 424 pp. Marcel Dekker, 270 Madison Ave., New York, N.Y. 10016. 1984. $59.75

Water Analysis. Vol. 3. Roger Minear, Lawrence Keith, Eds. xii + 456 pp. Academic Press, 111 Fifth Ave., New York, N.Y. 10003. 1984. $69

Do You Want To Upgrade Your HPLC System?

With the SSI LO-Pulse pulse damper, you can enhance the performance of any single-piston reciprocating pump. It's simple design smoothes the pulsed flow of the mobile phase and results in reduced noise in flow-sensitive detectors. This gives you better detection limits and more reliable chromatography.





LO-PULSE



GUARDIAN

The SSI Guardian enables you to add to your low-cost pump features available only in more expensive systems. The Guardian includes the LO-Pulse pulse damper described above plus a pressure readout. Adjustable upper and lower pressure limits protect your HPLC system by shutting off the pump if either limit is exceeded. A prime/purge valve simplifies pump priming, line purging and the release of system pressure. An easily accessible in-line filter protects expensive columns from particulate matter.

Want to know more? Call us at (814) 234-7311, or write to:

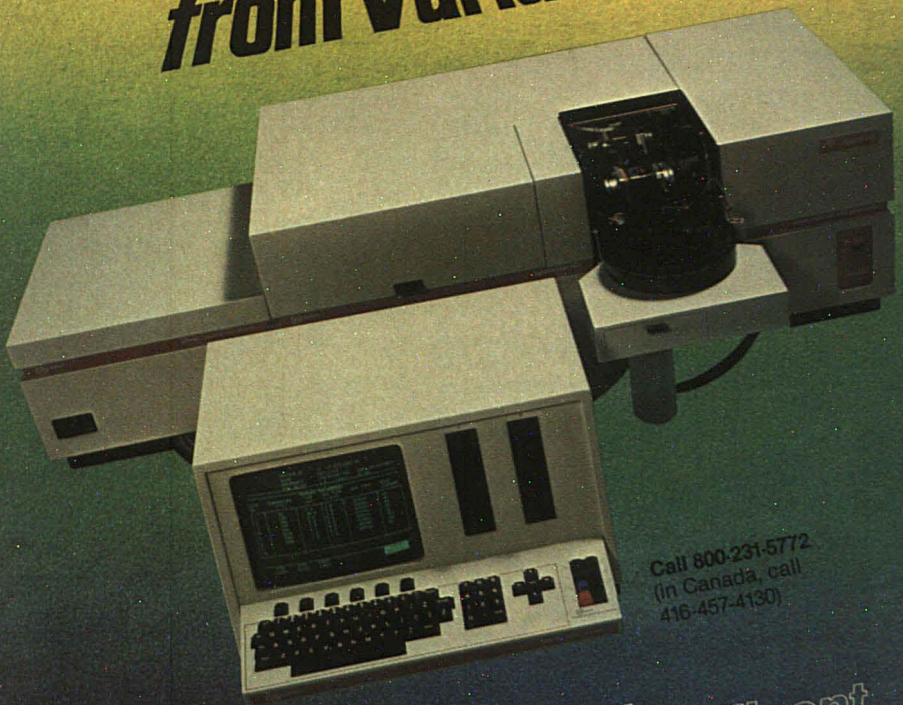
SSI **Scientific Systems, Inc.**
1120 West College Avenue
State College, Pa 16801

CIRCLE 186 ON READER SERVICE CARD

NEW!

Atomic absorption with central control.

SpectrAA Series from Varian!



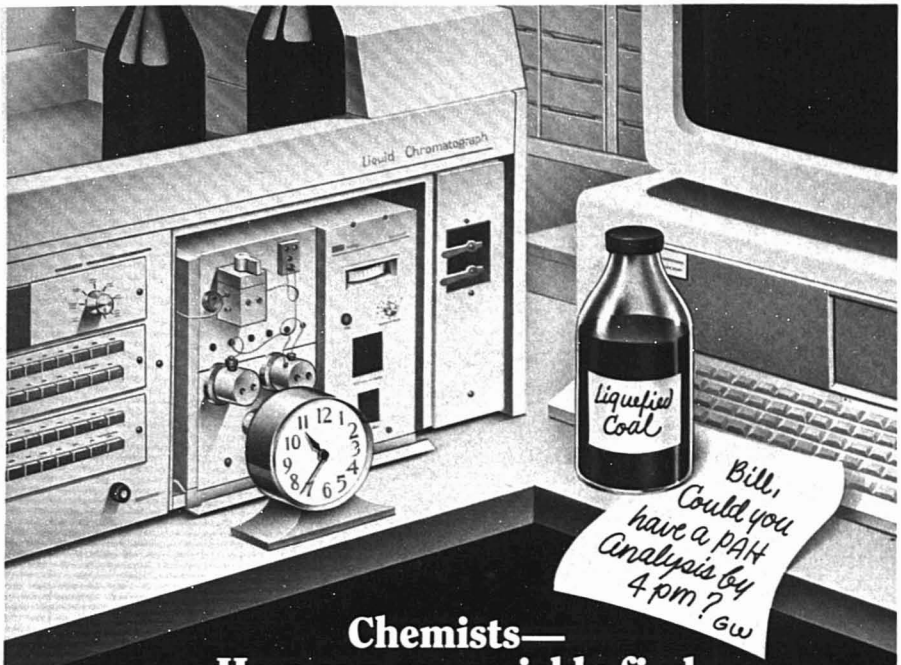
Call 800-231-5772
(in Canada, call
416-457-4130)

MORE
variantelligent
INSTRUMENTS

varian

• **Varian Instrument Group,** 220 Humboldt Court, Sunnyvale, CA 94089 • **In Canada:** 332 Guelph Street, Georgetown, Ontario L7G 4B5 • **In Europe:** Steinhauser-strasse, CH-6300 Zug, Switzerland

CIRCLE 220 ON READER SERVICE CARD



Chemists— How can you quickly find an analytical procedure to solve this problem?

Search ACS JOURNALS ONLINE.

ACS JOURNALS ONLINE is a high-efficiency chemical information search system that can save you hours of searching through chemical journals for an analytical procedure.

You can use it right in your laboratory. Just turn on your computer or terminal.

In minutes you'll be reading about the analytical procedure you need.

> In this case, it's a high-performance liquid chromatography procedure for determining polycyclic aromatic hydrocarbons in liquid coal.

And with the touch of a key, you can even zero in on specific paragraphs that contain the data you need.

Find out how you can make this high-efficiency chemical information search system work for you. Call an American Chemical Society sales representative today at 800-424-6747. The call is free.

Or write, Sales Office, American Chemical Society, 1155 Sixteenth Street, N.W., Washington, D.C. 20036.

ACS JOURNALS ONLINE contains: Accounts of Chemical Research, Analytical Chemistry, Biochemistry, Chemical Reviews, Environmental Science & Technology, Industrial & Engineering Chemistry—Fundamentals—Process Design & Development—Product Research & Development, Inorganic Chemistry, Journal of Agricultural and Food Chemistry, Journal of Chemical and Engineering Data, Journal of the American Chemical Society, Journal of Chemical Information and Computer Sciences, Journal of Medicinal Chemistry, The Journal of Organic Chemistry, The Journal of Physical Chemistry, Langmuir, Macromolecules, and Organometallics.

The Computer-Powered Full-Text Search System From The American Chemical Society

ACS JOURNALS ONLINE

1155 Sixteenth Street, N.W., Washington, D.C. 20036



Solids NMR? Varian's got the Magic Angle!

Now, Varian CP/MAS solves your materials science problems faster.



Here's how:

- ☐ You change samples without changing the probe . . . loading is faster and easier.
- ☐ Our double air-bearing rotor design provides stabilized spinning at over 5000 Hz, with no need to adjust the magic angle on each sample.
- ☐ You can use the multi-nuclear capability to observe nuclei from silicon to aluminium.
- ☐ Variable temperature option lets you study molecular dynamics and species that are normally unstable at room temperature.
- ☐ Powerful pulse programming capability allows routine use of sideband suppression techniques on complex materials.

Varian Instrument Group, 220 Humboldt Court, Sunnyvale, CA 94089
- **In Canada:** 332 Guelph Street, Georgetown, Ontario L7G 4B5
- **In Europe:** Steinhauserstrasse, CH-6300 Zug, Switzerland

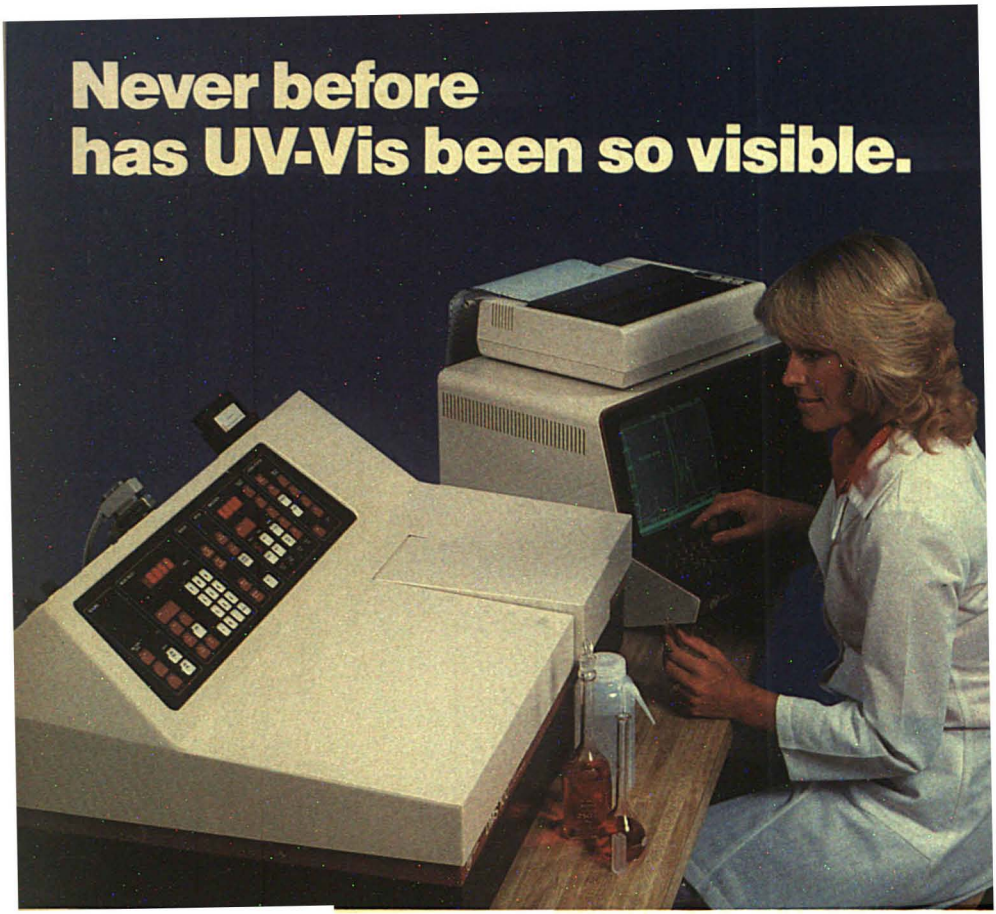
For immediate assistance, call
800-231-5772
In Canada, call 416-457-4130.
In Europe, call Zug, Switzerland, at (042) 23 25 75;
Darmstadt, Germany, at (06151) 7030.

CIRCLE 221 ON READER SERVICE CARD

varian

MORE
varian*telligent*
INSTRUMENTS

Never before has UV-Vis been so visible.



With the new DMS 100 UV-Vis Spectrophotometer and DS 15 Data Station, you are unquestionably in command. You can look at your results in a variety of ways, store spectral information and methods on floppy discs, and use an array of software programs, such as wavelength scanning, single- and multicomponent analysis, kinetics assays, color measurement, and gel scan integration.

But even without the Data Station, the DMS 100 is a strikingly intelligent spectrophotometer. It works fast and visibly, lets you watch your spectrum unfold in real time on a video monitor. Simultaneously, the spectrum is stored in memory—to be recalled anytime you snap your fingers.

You can

- replot the spectrum in a variety of photometric modes
- overlay separate plots, like absorbance and second-derivative scans
- zoom in on a portion of the spectrum and expand over the full video screen
- change the ordinate scale and replot
- safeguard your method storage with an optional memory-protect module
- get a permanent record with a digital printer/plotter

The DMS 100/DS 15 System offers you the most visible UV-Visible you could wish for.

Call 800-231-5772 (in Canada, call 416-457-4130)

• **Varian Instrument Group,** 220 Humboldt Court, Sunnyvale, CA 94089 • **In Canada:** 332 Guelph Street, Georgetown, Ontario L7G 4B5 • **In Europe:** Steinhauser-strasse, CH-6300 Zug, Switzerland

See us at the FASEB in Anaheim, CA, April 21-26

varian

MORE

varian*telligent*

INSTRUMENTS

CIRCLE 219 ON READER SERVICE CARD

Isiah M. Warner
Gabor Patonay
Mark P. Thomas
Department of Chemistry
Emory University
Atlanta, Ga. 30322

MULTIDIMENSIONAL LUMINESCENCE MEASUREMENTS

Analytical measurement techniques that use more than one parameter for a single measurement can be termed *multiparameter techniques*. Thus, the measurement of luminescence is inherently a multiparameter technique because even the simplest such measurements involve the exploitation of more than one parameter.

For example, the measurement of the luminescence (phosphorescence or fluorescence) from a sample involves the simultaneous use of an absorption wavelength and a luminescence wavelength since a molecule must absorb energy at wavelength λ_{ex} and be promoted to an excited state before luminescing at wavelength λ_{em}. The measured luminescence intensity, I_L, can then be represented as a function of λ_{ex} and λ_{em}

$$I_L = f(\lambda_{ex},\lambda_{em}) \qquad (1)$$

Selective measurement of individual luminophores in simple (*1*, *2*) or even complex mixtures (*3*, *4*) can be achieved by varying these two parameters; a number of examples were detailed as early as 1969 in a review article by Sawicki (*4*).

Another parameter often used in luminescence measurement is the lifetime of the luminophore. The luminescence decay after initial excitation will generally follow first-order kinetics. The time for the decay to reach $1/e$ of its initial value is a characteristic parameter of the molecule. Thus, the use of this parameter in combination with Equation 1 provides increased selectivity. A number of representative examples in which the decay time of luminescing species is used to achieve additional selectivity can be cited (*5*–*7*).

In recent years, novel advances in instrumentation (*8*) and data reduction strategies (*9*) have encouraged the simultaneous exploitation of multiple parameters to achieve selective measurements. Consequently, the selectivity of luminescence measurements can be enhanced through both instrumental and mathematical approaches.

Figure 1 is a diagrammatic representation of several luminescence parameters that can be used for selective luminescence measurements. Clearly, many parameters of luminescence can be simultaneously exploited to achieve

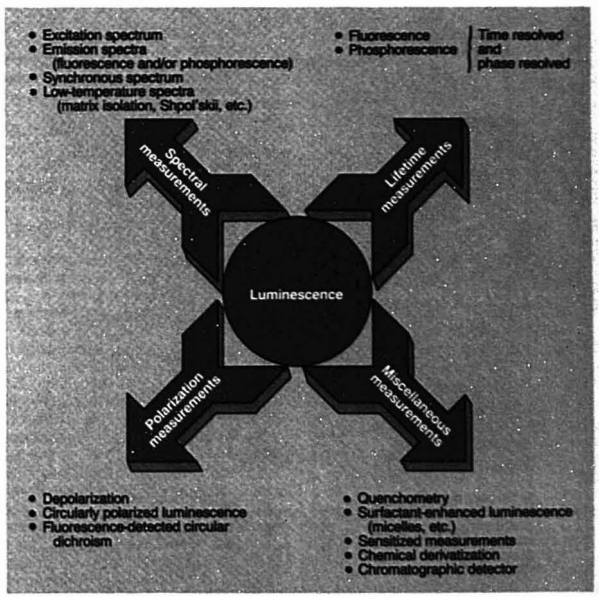


Figure 1. Examples of luminescence parameters that can be exploited to achieve selective measurement

0003-2700/85/0357-463A$01.50/0
© 1985 American Chemical Society



CIRCLE 2 ON READER SERVICE CARD

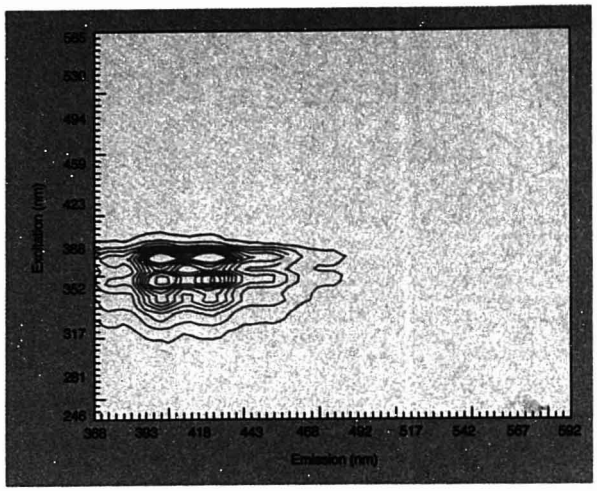


Figure 2. Contour plot of an emission–excitation matrix of 8.3×10^{-5} M anthracene in cyclohexane
Data were acquired in 0.6 s on a video fluorometer (*29*) in a 64 × 64 format

a high degree of selective measurement and, ultimately, specific measurement. One obvious approach to additional selectivity is to obtain I_L in terms of three parameters

$$I_L = f(\lambda_{ex}, \lambda_{em}, P) \qquad (2)$$

where P is an arbitrary parameter selected from among the many listed in Figure 1. Furthermore, more than three variables could be used in Equation 2 to increase the selectivity of the measurement.

A number of other parameters could also be included (*10*) in Figure 1, particularly under the miscellaneous category. However, we have necessarily limited our diagram to include widely used parameters and those that are increasingly being used for selective measurement. It should also be noted that some of the parameters listed in the miscellaneous category are really not characteristic parameters of the molecule in the excited state. However, these characteristic properties of the molecule can be combined with excited-state information to increase selectivity.

This article discusses multidimensional luminescence measurement (MLM) and its applications in analytical chemistry. The MLM approach involves the simultaneous use of two or more parameters of luminescence for selective measurement. We term this approach multidimensional rather than multiparametric since, in this article, we will primarily emphasize data acquisition, display, and processing in a multidimensional format. There are a number of advantages for reduction of data using a multidimensional format (*9*). An example of such an approach was presented in a recent A-page article by McGown and Bright (*11*) in which phase-resolved fluorescence intensity is derived as a function of synchronously scanned wavelengths and of detector phase angle.

Our discussion in this article will be divided into the four major classifications of spectral measurements, lifetime measurements, polarization measurements, and miscellaneous approaches, as depicted in Figure 1. The utility of MLM will be demonstrated using one or two examples in each classification.

Spectral measurements

Theory. The discussion provided here is necessarily brief; either of two useful monographs (*12, 13*) can be consulted for detailed discussions on the general theory of luminescence. Luminescence measurements have had widespread applications in the analytical studies of large, unsaturated, highly conjugated, organic molecules such as polynuclear aromatic compounds (PNAs). Organic molecules generally have an even number of electrons. Therefore, the absorption and fluorescence transitions occur between singlet states.

Phosphorescence generally involves an intersystem crossing to a triplet

Ten years of research stand behind these LC injectors.

And Rheodyne's not done yet.

You can expect Rheodyne always to be designing and testing new LC sample injectors. Doing just that, we've acquired a lot of valuable knowledge that we can pass on to you. Both in the form of better-designed sample injectors—and in the form of expert advice on the most effective way to use them.

Our aim has always been to make injectors more versatile and easier to use, while maximizing the precision and resolution of your liquid chromatograph. Rheodyne's Model 7125, pictured in the foreground below, is an excellent example of this philosophy. It injects sample either from a loop that's completely filled (to maximize precision) or from a loop that's partially filled using a syringe (to save time). The 7125 offers unexcelled versatility, ease of use, and reliability.

Expert advice on how to use sample injectors is available to you in Rheodyne's Technical Note No. 5. It tells how to achieve high precision while avoiding sample wastage and cross contamination. Ask your Rheodyne dealer for free copies of all our Technical Notes and our catalog.

Or contact Rheodyne, Inc., P.O. Box 996, Cotati, California 94928, U.S.A. Phone (707) 664-9050.



RHEODYNE

THE LC CONNECTION COMPANY

CIRCLE 179 ON READER SERVICE CARD

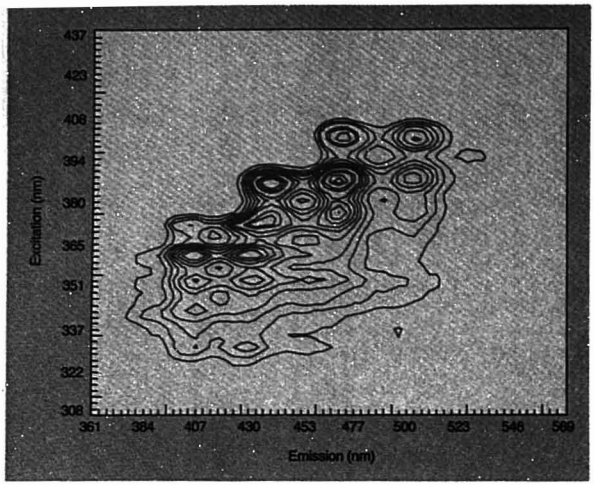


Figure 3. The contour plot of an EEM of an approximately equifluorescent six-component mixture of the PNAs benzo[*k*]fluoranthrene, 2,3-benzanthracene, fluoranthrene, perylene, 2-ethylanthracene, and pyrene in cyclohexane
Data were acquired in 0.6 s on a video fluorometer (*29*) in a 64 × 64 format

state with subsequent radiative decay to the ground singlet state. Since this transition is quantum mechanically forbidden (long-lived), and therefore more subject to nonradiative decay processes in fluid solutions, phosphorescence is usually observed under cryogenic conditions. Some recent studies have provided useful approaches to room-temperature phosphorescence measurements (*14*).

Two useful properties of most luminescing molecules provide the selectivity of Equation 1 described earlier. The first property is that for most pure luminophores, the observed emission spectrum is independent of the excitation wavelength. The second property is that the excitation spectrum is independent of the monitored emission wavelength. Thus, variations in the emission profile with variations in the excitation wavelength suggest that more than one luminescing component is present in a sample. A similar conclusion could be drawn from variations in the excitation spectrum with monitored emission wavelengths.

Many early analytical investigators of luminescence measurements varied the excitation and monitored luminescence wavelengths to achieve selectivity (*2*, *4*). However, for complex molecules with broad-band absorption and emission spectra, the selectivity of this approach decreases rapidly as the number of components increases. Optimum selectivity is likely to occur with narrow-band excitation and with an emission resolution better than the bandwidth of the monitored components. In addition, the number of excitation and/or emission wavelengths used should equal or exceed the number of emitting components (*15*).

Figure 2, which illustrates the preceding point, is a contour plot of a typical one-component fluorescence–excitation matrix. Note that, within the defined contour levels, this pure compound adheres to the two properties of excitation and emission previously discussed. A more complex, six-component mixture is shown in Figure 3. It is visually obvious that this is a multicomponent system because the emission profile changes several times with variations in the excitation wavelength. A similar conclusion can be drawn about variations in the excitation spectra with emission wavelength. In fact, the number of changes noted in the emission or excitation profile is an indication of the minimum number of luminescing species (rank) contributing to the matrix.

Instrumentation. The utility of obtaining luminescence spectra as a function of multiple excitation and multiple emission wavelengths encouraged some researchers to digitize and generate such information by manual manipulation of data from luminescence spectrometers (*16*). Such studies demonstrated the need for an automated luminescence spectrometer. An early automated luminescence spectrometer was developed and described by Wampler and DeSa in 1971 (*17*). The data were digitized and could be output in a suitable form for postprocessing. An automated instrument was also described by O'Haver et al. in 1973 (*18*). However, this instrument acquired data in analog form for plotting on an x–y recorder. Consequently, the data were not in a suitable form for postprocessing. In the same year, Holland et al. (*19*) described a completely automated system capable of simultaneous absorption and fluorescence measurements. This system was interfaced to a dedicated digital computer for data processing.

Perhaps the most completely automated luminescence spectrometer was described by Haugen et al. in 1975 (*20*). This spectrometer was interfaced to a general-purpose computer and operated in a time-share mode. Six modes of operation were possible for data acquisition, and the data could be stored on magnetic tape for further processing. Commercially available instrumentation capable of similar operations has been reported.

Despite the high degree of automation in the instrumentation described in the preceding paragraph, the acqui-

Table I. Chronology of developments in luminescence spectrometers

Instrument (year noted in literature) (*a*)	No. of λ_{ex} by No. of λ_{em}	Acquisition time (*b*)	Reference
Turner fluorometer (1964)	100 × 100	Several hours	21
Microfluorometer (1974)	100 × 500	3.2 s	22
Computerized fluorometer (1975)	200 × 134	Hours	20
Video fluorometer (1975)	256 × 256	17 ms	23
Commercial fluorometer (1979)	200 × 200	1.5 h	27

(*a*) These are selected examples from the literature. Other examples were published around the same time.
(*b*) Most of these times are estimates from the information presented in the referenced articles. In general, these times do not include digitization, storage, and processing time.

INORGANIC ELEMENTAL ANALYSIS

Simultaneous, Non-Destructive, Wide Dynamic Range

EDXRF

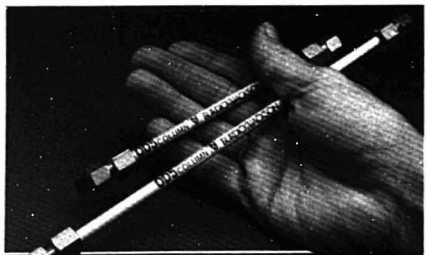


- **Sample Form**
  Solid, Powder or Liquid
- **Dynamic Range**
  PPM to 100%
- **Ease of Use**
  Fully Automated, Single Pushbutton Analysis of up to Ten Samples
- **Analysis Time**
  All Elements Simultaneously, in Minutes

Tracor Xray

TEL. 415/967-0350

CIRCLE 200 ON READER SERVICE CARD



GUARANTEED!

C18 HPLC COLUMN PROVIDES EFFICIENT SEPARATIONS.

American Burdick and Jackson's model OD5 LC Column delivers guaranteed quality and performance for Reverse Phase Liquid Chromatography. Developed to meet B&J internal quality control requirements, it features:

- Fully endcapped monomeric C18 bonded phase 5 μM spherical silica
- Fingertight endfittings included
- Rigorous quality control testing
- Choice of two column sizes for specific applications.

For a free technical bulletin complete with typical applications—contact American Burdick & Jackson, 1953 South Harvey Street, Muskegon, MI USA 49442. Phone: 616 726-3171

American Burdick & Jackson Subsidiary of American Hospital Supply Corporation

©1985 American Hospital Supply Corporation

CIRCLE 4 ON READER SERVICE CARD

ULTRA PURE ACIDS

- Double sub-boiling distilled in Quartz.
- Produced under CLASS 100 clean room conditions.
- Certificate of Analysis.
- The world's highest purity acids available commercially.
- Ultra cleaned TEFLON acid containers are returnable. Low cost refills.

Seastar

SEASTAR CHEMICALS
(A Division of Seastar Instruments)
MANUFACTURERS OF ULTRA PURE ACIDS

2045 MILLS ROAD,
SIDNEY, B.C., CANADA V8L 3S1
(604) 656-0891 • TELEX 049-7526

CIRCLE 188 ON READER SERVICE CARD

sition of luminescence data as a function of multiple excitation and multiple emission wavelengths was a time-consuming process. Table I provides a chronology of the improvements in the data acquisition time of luminescence data. Note that a significant decrease in data acquisition time was not realized until around 1974, and in 1975 when a video fluorometer was developed at the Univ. of Washington (*23*).

The video fluorometer's decrease in data acquisition time was due to a novel concept of polychromatic illumination coupled with the rapid two-dimensional data acquisition capabilities of an intensified vidicon detector (*24*). As is often the case with such developments, some trade-offs had to be made. In this case, the video fluorometer is less sensitive than conventional luminescence instrumentation. However, the sensitivity of the instrumentation could be increased by using the integrating capabilities of the vidicon detector with a concomitant sacrifice in rapid data acquisition. A video fluorometer similar to the one developed at the University of Washington has also been described (*25, 26*). The incorporation of shutters and cryogenic equipment for low-temperature operation has also allowed this instrumentation to be used for phosphorescence studies (*28, 29*).

Lifetime measurements

Theory. As mentioned earlier, the luminescence lifetime is another parameter that can be used for multiparametric evaluation of the luminescence information. This can be an especially important property of the luminescing molecules if there is a significant overlap in the excitation and emission bands. In such cases, the lifetime of the luminophore may be a distinguishing factor.

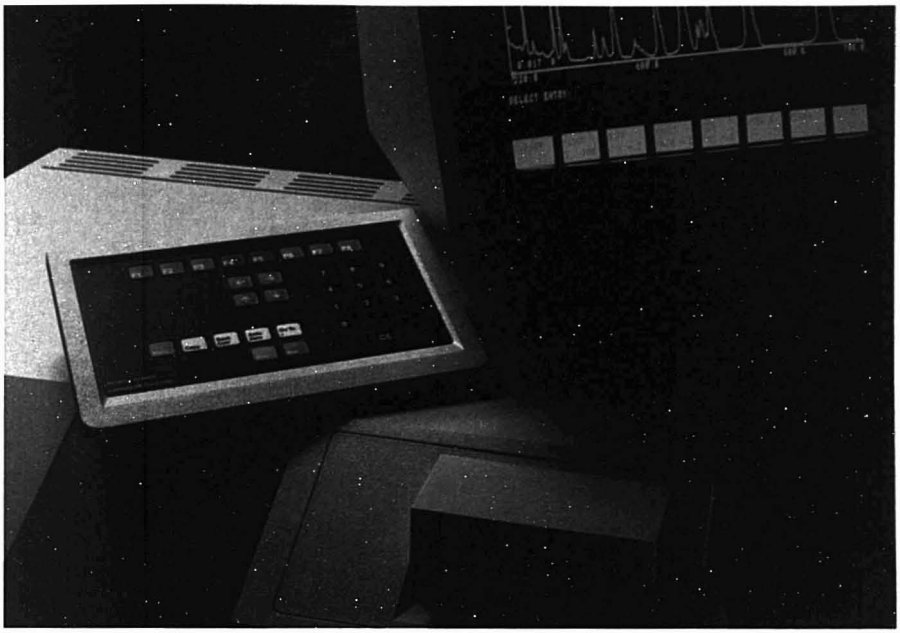
The luminescence lifetime is the time required for the luminescence intensity to decay to $1/e$ of its initial value (*12*). Hence, the luminescence intensity can be obtained as a function of monitored wavelength of emission and the observation time after termination of the excitation pulse, t_i,

$$I_L = f(\lambda_{em}, t_i) \qquad (3)$$

A complete mathematical description of the luminescence intensity would require an equation in the form of Equation 2

$$I_L = f(\lambda_{ex}, \lambda_{em}, t_i) \qquad (4)$$

Practical considerations determine the approach to acquiring data in the form of Equations 3 and 4. For instance, two parameters can be fixed and the third one varied (*30*). Obviously, the specific instrumentation will determine the necessary acquisi-



Lambda 4B

Introducing the Lambda 4 Series!

One of Perkin-Elmer's three new UV/Vis Spectrophotometers is ideal for your application and budget.

Lambda 4A – the lowest-cost version, uses an advanced LCD display and high speed printer/plotter.

Lambda 4B – for the mid-price range, where graphics is standard on a large, integrated, high resolution monitor.

Lambda 4C – the most powerful version, uses the Perkin-Elmer Series 7000 Professional Computer, a 16/32 bit microcomputer, as the controller.

Application specific

But Lambda 4 is more than three versions of a new, high performance spectrophotometer. Each version allows you to select software designed for your application. Because the software is specific to an application, it includes only methods and parameters which are of interest to you.

More than ten applications including basic scanning, spectral data processing, kinetics, automatic sampling, cell programming and advanced quantitative analysis are available now. And more application specific software will be introduced soon.

Optical performance

Perkin-Elmer's commitment to optical excellence continues in Lambda 4 by incorporating double-beam optics for superior photometric range and better long term stability. Resolution to 0.25 nm allows separation of close bands and better photometric accuracy. Stray light to 0.0005% ensures accurate readings at high absorbance.

Find out more!

For more information, call (800) 323-7155, (in Illinois, call (312) 887-0770), or contact one of the offices below.

Perkin-Elmer Corp., Analytical Instruments Main Avenue, (MS-12), Norwalk, CT 06856 U.S.A. Tel (203) 762-1000. Telex 965-954

Bodenseewerk Perkin-Elmer & Co., GmbH, Postfach 1120, 7770 Ueberlingen, Federal Republic of Germany. Telex: (07551) 811

Perkin-Elmer Ltd., Post Office Lane, Beaconsfield, Bucks, HP9 1QA, England. Tel. Beaconsfield (049 46) 6161

PERKIN-ELMER

The science and computer company.
Where solutions come first.

CIRCLE 169 ON READER SERVICE CARD

ENCORE



The new AFS-2000: Unprecedented performance by a solo, unattended instrument.

When you need detection limits beyond the limitations of AA, the new Baird Plasma/AFS-2000™ has them. For most elements, it's ten times more sensitive than its predecessor (and ten times more than flame AA), because of our exclusive new UDX sample delivery system.

Three ppb Pb at S/N = 2, e.g.! One ppb Au. Or 0.02 ppb Hg with our hydride/cold vapor mercury system. New performance limits, too, for P, S, As, Se and dozens more.

Our "encore", the second-generation AFS-2000, benefits from three years refinement and experience since our introduction of the first commercially available atomic fluorescence spectrometer in 1981.

All basic features have been enhanced: Determination of one to twelve elements per minute, and 1000 determinations per hour. No background correction required. No baseline drift. Large linear dynamic range (1×10^5). Virtually no spectral interferences. In short, the simplicity and specificity of atomic absorption and the multielement and linearity advantages of optical emission spectroscopy in one high-performance analytical instrument.

We can easily stage a performance for you! For complete details, write or call Baird Corporation.

BAIRD

125 Middlesex Turnpike, Bedford, Massachusetts 01730. Telephone (617) 276-6363.

CIRCLE 19 ON READER SERVICE CARD.

The Spectroscopy People

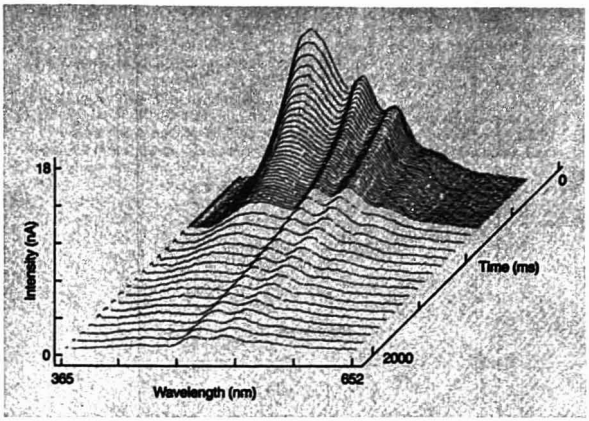


Figure 4. Typical time-resolved ETM of 2-naphthoic acid and *p*-amino-benzoic acid
Reprinted from Reference 31

tion time and data format. Since several methods of determining the luminescence lifetime can be used, it is useful at this point to discuss briefly the theory of the two commonly used techniques (*12*). These methods are based on the use of two types of instrumentation: time resolved and phase resolved.

In the time-resolved method, the sample is excited with a short-duration pulse of light, and the time-dependent decay of the luminescence intensity can be used to calculate the lifetime. In the phase-resolved method, the sample is excited with sinusoidally modulated light. The phase shift and demodulation of the emission, relative to the incident light, are parameters that can be used for calculation of the lifetime. Both methods require some calculations to obtain the luminescence lifetime of the luminophore. This is especially true for the second method if the sample contains more than one luminophore.

In general, the excitation of a luminophore with an infinitely short pulse of light (δ function) provides the best approach to explaining the luminescence decay. The luminescence intensity as a function of time after the excitation pulse is assumed to be an exponential decay curve since the luminescence decay process usually obeys first-rate kinetics

$$\frac{I_L(t)}{I_L(0)} = e^{-kt} \qquad (5)$$

where $I_L(t)$ and $I_L(0)$ are the intensities of the luminescence at time t and time 0, respectively. The parameter k is the first-order rate constant for the decay process.

Equation 5 indicates that a time–luminescence decay curve can be obtained if an ideal delta pulse excitation is used. Unfortunately, any practical instrument is nonideal and can provide only an excitation pulse of finite duration. In addition, the associated electronics will have a response function of finite width. Consequently, the use of a nonideal lifetime instrument will produce data that are a convolution of several response characteristics. A mathematical process is therefore needed to deconvolute the time decay curve.

With an appropriate modulation frequency for the excitation beam, the luminescence will also have an associated modulation depending on the time delay. This property is used in phase-resolved luminescence measurements. The phase-resolved method uses a continuous sinusoidally modulated excitation beam. If the modulation frequency (f) and degree of modulation of the excitation source are known, a simple derivation (*12*) of the phase difference, ϕ, between the excitation source and the fluorescence gives the lifetime, τ, as

$$\tau = \frac{1}{2\pi f}(\tan \phi) \qquad (6)$$

Similarly, the observation of the demodulation (M) is also suitable for calculation of the lifetime since

$$\tau = \frac{1}{2\pi f}\sqrt{\frac{1}{M^2} - 1} \qquad (7)$$

Equations 6 and 7 are valid if the emission of the luminophore is spectrally homogeneous. If the system is more complex, the calculation of the lifetimes is more complicated.

CHEMTECH
inspires the innovator
Why do so many innovators in all chemical fields turn to CHEMTECH each month?
. . . One of the best condensed technical news sources I get . . . Outstanding melding of social, political, and scientific literature . . . The fresh glibness and tongue-in-cheek style are unique and welcomed . . . I am impressed with the quality, scope and personal touch of the articles . . . I almost dread it when each issue arrives because I know I will take the time, whether I have it to spare or not, to read it from cover to cover.
Join your satisfied colleagues and subscribe to the innovator's magazine . . .
CHEMTECH
Call now to order:
800-424-6747

It should be apparent that each lifetime method has certain advantages and disadvantages. The selection of the proper method will depend on several variables including the nature of samples, deviation of decay from ideality, and lifetime range desired (*12*). For this discussion, namely, use in multidimensional luminescence measurements, the format of the data must first be examined.

Several choices in multiparametric representation of the luminescence data are available depending on the complexity of the data set. If one desires a two-dimensional format, the data can be acquired using either the emission spectra or the excitation spectra as a function of luminescence decay time while fixing the other parameter. In both cases, a two-dimensional data matrix is formed (*30*, *31*). The intensity data can be represented as an ($m \times n$) matrix where m is the number of wavelengths observed in each excitation or emission spectrum and n is the number of time intervals at which spectra are obtained. The time difference between the two excitation or emission measurements greatly depends on the lifetime of the luminophore in the mixture. Typically, this value may range from ~0.1 ns (fluorescence) to the order of ms or s (phosphorescence).

Obviously, the multidimensional representation can also be extended according to Equation 4. Here, the intensity data are represented as an ($m \times n \times o$) matrix where m is the number of excitation wavelengths, n is the number of emission wavelengths, and o is the number of time intervals at which spectra are obtained. The advantages of this approach are clear since it is very unlikely that two components will have the same lifetime as well as the same excitation and emission spectra.

Instrumentation. Because of the short lifetime of most fluorophores, phosphorescence lifetime techniques were developed much earlier than fluorescence lifetime techniques. A pulse source phosphorescence lifetime technique was described in 1974 (*32*). A complete two-dimensional time-resolved technique, according to Equation 3, was reported as early as 1975 (*33*). The method was fairly tedious and complicated due to mechanical control of the emission monochromator. However, this instrument was able to acquire data in an emission–time matrix (ETM) format.

A more sophisticated time-resolved phosphorescence spectrometer was developed by Goeringer and Pardue in 1979 (*31*). A silicon intensified target (SIT) vidicon was used to collect the data in the ETM format (Figure 4). However, this instrumentation did not exploit the excitation information because the sample was irradiated with undispersed light. A complete time-resolved technique was reported in 1982 (*29*). Since this instrumentation incorporates a polychromator to disperse the excitation source, a complete phosphorescence–excitation–time matrix (PETM) is obtained. Although the representation of such data in a four-dimensional format is difficult because of the number of variables (Figure 5), it should be clear that this format provides the greatest information. The development of comparable fluorescence instrumentation would require much more sophisticated techniques because of the much shorter time intervals (nanoseconds).

Although a great deal of work has been done in that field (*34*), the unavailability of complete multidimensional fast-scanning instrumentation similar to that reported by Ho and Warner (*29*) is understandable because of the lack of superfast (response time in the order of ns) SIT vidicons. However, there are several methods available that are able to obtain the data in a fluorescence–excitation–time matrix (FETM) (*33*, *35*). It is interesting to note that the ultrafast, picosecond spectroscopic techniques belong to the general field of multiparametric measurement. Although these methods have been used for studies of ultrafast physical and chemical processes, the use of streak cameras (*36*) should also be applicable to ultrafast multidimensional fluorescence measurements.

The phase-resolved approach differs significantly in implementation. Because the data are not easily represented in an ETM or FETM format, a different approach to multidimensional luminescence measurement is necessary. A good example of this is the use of synchronously scanned wavelengths as a function of phase angle (*11*).

Polarization measurements

Theory. When a luminophore is excited with linearly polarized light, those molecules with their absorption dipoles aligned with the electric vector

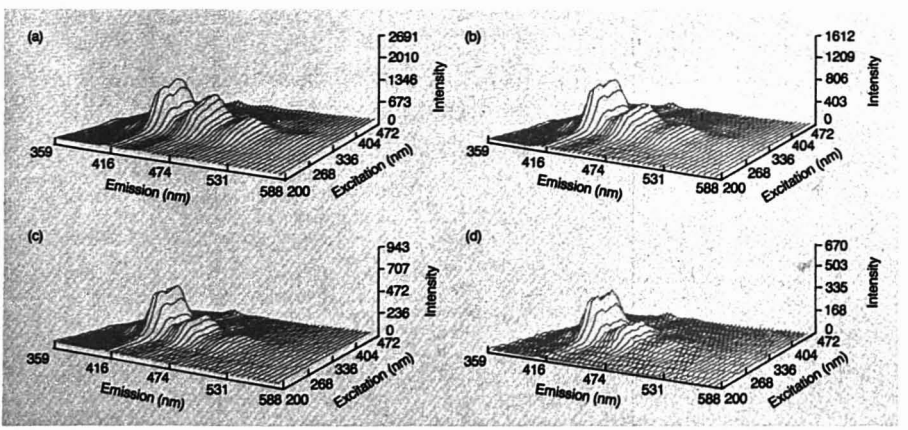
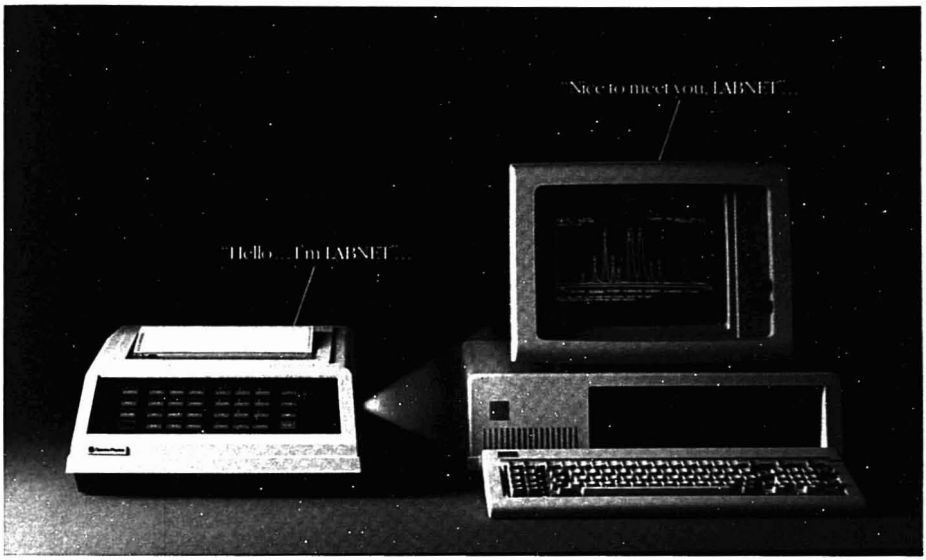


Figure 5. Time-resolved PETM of a binary mixture of phenanthrene and triphenylene. (a) t = 0 s; (b) t = 5.5 s; (c) t = 12.5 s; (d) t = 17.5 s

Reprinted from Reference 29

WE'RE NOW MAKING CONNECTIONS WITH THE BEST PEOPLE AROUND.



ANNOUNCING LABNET-XT MULTI-CHANNEL DATA SYSTEM

High performance for small and medium-sized chromatography labs.

Until now, if you wanted big lab capabilities – direct control of your LCs and GCs from a keyboard; rapid graphic manipulation and mass storage of chromatographic data; sophisticated business software for improved efficiency – you also needed a big lab's data system.

Here's good news.

Spectra-Physics' LABNET XT Multi-Channel Data System provides all the big lab capabilities in an eminently compact and affordable package.

LABNET + IBM® XT = chromatography computer, interactive terminal, and business tool.

With just an IBM Personal Computer XT, LABNET interface kit, and Spectra-Physics' SP4200 or SP4270 Computing Integrators, your lab can become a smart lab. Use the integrators you have now to achieve concurrent data collection, review, and editing. Reprocess your chromatograms on the IBM XT's screen while storing the raw data intact. Take advantage of the wealth of software for the IBM PC.

Start with what you have.

Spectra-Physics modular approach to data systems gives you neither too much nor too little. To find out how LABNET XT can smarten up your lab, call Spectra-Physics today and ask for the brochure. In California: (408) 946-9682, Texas: (713) 688-9886, New Jersey: (201) 981-0390. Elsewhere: (800) 253-8324. Spectra-Physics, 3333 North First Street, San Jose, California 95134. In Europe contact Spectra-Physics, GmbH, Siemensstrasse 20, D-6100 Darmstadt-Kranichstein, Fed. Rep. Germany.



CIRCLE 194 ON READER SERVICE CARD

Spectra-Physics

THE PERFORMANCE LEADER IN AUTOMATED CHROMATOGRAPHY

Start Your Own Analytical Chemistry Reference Library



The ANALYTICAL CHEMISTRY Library Case . . . a handsome and convenient way to keep your ANALYTICAL CHEMISTRY issues protected and easy to reach.

Each specially-designed library case holds up to seven issues—one-half year's subscription of ANALYTICAL CHEMISTRY. Designed to keep your ANALYTICAL CHEMISTRY issues at your fingertips, the ANALYTICAL CHEMISTRY Library Case is perfect for home, office, or library.

The Library Case is available in two styles: the slipcase or the binder. Both styles are covered in attractive navy leatherette with embossed gold lettering and both are reasonably priced. You pay only $6.95 for the slipcase and $8.50 for the binder.

Order your ANALYTICAL CHEMISTRY Library Case today! Your satisfaction is unconditionally guaranteed or your money will be immediately refunded. Simply fill in the coupon below and mail in with your payment.

Please send me:

____ ANALYTICAL CHEMISTRY Library Slipcase(s) at $6.95 each

____ ANALYTICAL CHEMISTRY Library Binder(s) at $8.50 each

I am enclosing a check or money order for $_____.* (Make payable to Jesse Jones Industries. Add $2.50 per case for orders outside the U.S.)

Name _____

Address _____

_____

City/State/Zip _____

*Payment must accompany all orders and must be made in U.S. currency only. Orders from outside the U.S. add $2.50 per case. Mail to: Jesse Jones Industries, P.O. Box 5120 ANALY-C, Philadelphia, PA 19141

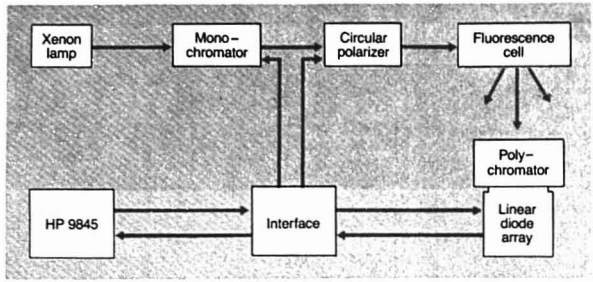


Figure 6. Block diagram of fluorescence-detected circular dichroism spectrometer

of the polarized light have the highest probability of excitation. The rules of photoselection dictate that the luminescence resulting from this absorption is also polarized. Because these molecules remain in the excited state for a finite time before they luminesce and because they are free to rotate during this time, some depolarization will occur.

The amount of depolarization due to rotational diffusion is dependent on the size and shape of the molecule as well as solvent viscosity and is often used in biochemistry to investigate many important processes such as ligand binding, denaturation, and aggregation (*12*). In some cases energy transfer is a major contributor to depolarization, and luminescence polarization experiments can yield information on the excited states of the luminescing molecule (*12*).

In luminescence polarization measurements, spectra are obtained by scanning wavelengths selected by an excitation monochromator and measuring the luminescence intensity parallel ($\parallel$) and perpendicular ($\perp$) to the polarization of the exciting light. The degree of polarization is then given by

$$P = \frac{I_\parallel - I_\perp}{I_\parallel + I_\perp} \qquad (8)$$

where $I_\parallel$ and $I_\perp$ are, respectively, the intensities of the components of the emission parallel and perpendicular to the polarization plane of the excitation beam.

In much of the luminescence literature, polarization data are reported in terms of anisotropy, which eases the theoretical derivation of model systems. The anisotropy is related to the polarization and is defined as

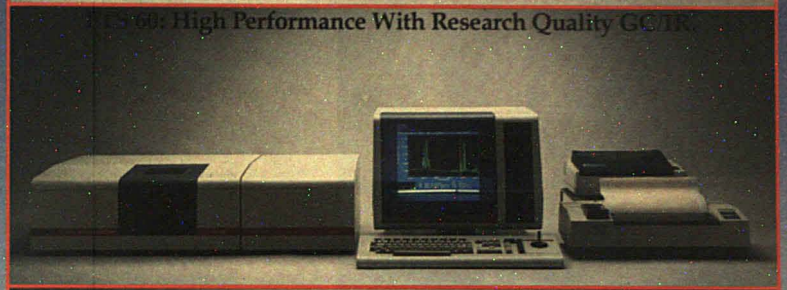
$$r = \frac{I_\parallel - I_\perp}{I_\parallel + 2I_\perp} \qquad (9)$$

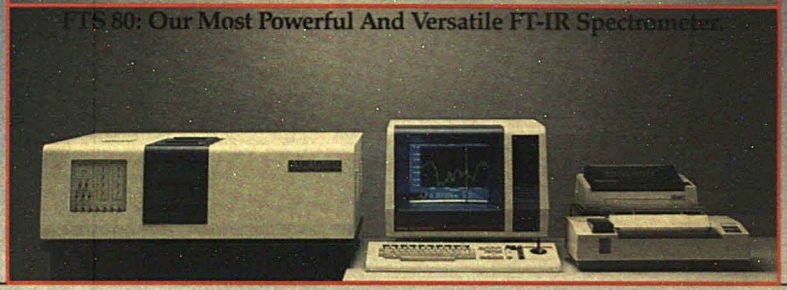
Circularly polarized light can also be used for molecular excitation. When light is passed through a doubly refracting crystal that has been oriented so that the light traverses the crystal in a direction perpendicular to the optical axis, the ordinary and extraordinary rays are not separated but travel at different speeds. When the rays exit the crystal, they are out of phase, and the resulting beam of light is said to be elliptically polarized. The *ellipticity* is then given by the angle, θ, whose tangent is equal to the ratio of the minor axis to the major axis of the optical ellipse. If the crystal is of a thickness such that the rays exit with a phase difference of $\pi/2$ for a given frequency, the light is circularly polarized (*37*). In circular polarization, the electric vector does not oscillate in one plane but actually is constant in magnitude and describes a circular motion about the axis of propagation either clockwise (righthanded) or counterclockwise (lefthanded).

In 1895, A. M. Cotton (*38*) discovered that chiral molecules differentially absorb left and right circularly polarized light. This discovery laid the foundation for the field of circular dichroism (CD). Experimentally, the CD spectrum of a sample is obtained by measuring the difference in the intensities of transmitted left and right circularly polarized light. Today, CD is an accepted technique for the study of chiral molecules and has been used most often in determining structural interactions between biomolecules (*39*).

A new technique has been developed within the past 10 years that uses the Cotton effect to analyze chiral fluorescent molecules. Fluorescence detected circular dichroism (FDCD) is related to the classical CD method much as the fluorescence excitation spectrum is related to the absorption spectrum. Turner and Tinoco (*40*) first presented the concepts and preliminary experimental results of FDCD in 1974. This method is based on the assumption that the experimentally corrected excitation spectrum of a luminophore has the same profile as its absorption spectrum. This assumption is generally valid in







DIGILAB FT-IR: RESEARCH GRADE PERFORMANCE IN THREE NEW CONFIGURATIONS

When you buy one of the three new FTS spectrometers shown above, you are buying a spectrometer that is discriminating enough to resolve even minor spectral components, sensitive enough to detect trace concentrations and fast enough for GC/IR and kinetics.

Research grade performance, applications experience, customer support, value…when you buy a Digilab FTS spectrometer, you are getting one of the industry's finest instruments.

For literature, send the coupon today to Bio-Rad, Digilab Division, 237 Putnam Avenue, Cambridge, MA 02139. Or call TOLL FREE (800) 225-1248.

Name Title:

Affiliation:

Street & No.:

City & State: Zip: Telephone: ( )

Applications:

Please send me a brochure on the (check one): FTS 50: FTS 60: FTS 80:

BIO-RAD Digilab Division

CIRCLE 17 ON READER SERVICE CARD

ENVIRONMENTAL SCIENCE & TECHNOLOGY

ES&T



The premiere research publication in the environmental field.

Environmental science continues to be one of the fastest growing fields. And ES&T has grown right along with it!

ES&T continues to give you the practical, hard facts you need on this science . . . covering research, techniques, feasibility, products and services.

Essential reading for environmental scientists both in the business and academic world . . . ES&T has increased its emphasis on peer-reviewed research dealing with water, air, and waste chemistry in addition to adding critical reviews of important environmental science issues—all relevant to understanding the management of our natural environment.

Also included are discussions on environmental analyses, governmental regulations, current environmental lab activities, and much more!

For rate information, and to subscribe, call toll free:

(800) 424-6747

the absence of effects such as energy transfer.

In FDCD, the differential absorption of left and right circularly polarized light is detected by the relative intensity differences of the fluorescence light. Thus, the FDCD spectrum is related to the CD spectrum since the intensity of fluorescence is proportional to the intensity of absorbed light at low absorbance. The major advantages gained by FDCD are greater sensitivity and selectivity. Selectivity is gained because not every chromophore in a chiral mixture will fluoresce. This technique allows the potential of isolating a single chiral fluorophore in a mixture of chiral chromophores for determination of the structure at that particular location.

A theoretical discussion of the FDCD technique has already been published (*41*). Early publications cited some problems in the theoretical and experimental techniques (*42–44*), but these were later resolved (*45*). The first application of FDCD demonstrated the validity of the technique and showed the method's usefulness as a bioanalytical tool (*46*).

Instrumentation. Conventional spectrometers can be used to measure luminescence polarization by adding linear polarizers in the excitation and emission beams of light. Several commercial instruments are available with polarization attachments. Polarization spectra must be corrected to account for a wavelength-dependent polarization response inherent in the detection system (monochromator, optics, detector). There are several methods to calculate the instrumental correction constant, the G factor. Techniques for determining the G factor and further details on the theory of luminescence polarization and depolarization are given elsewhere (*12*).

Many early experiments in the field of FDCD were done on conventional CD instruments that were modified by placing a photomultiplier tube at a right angle to the excitation beam. Recently a new multidimensional instrument has been described that acquires ellipticity as a function of multiple excitation and emission wavelengths through the use of an intensified diode array combined with a polychromatic dispersion system (*47*). A block diagram of this instrument is given in Figure 6. The instrument acquires complete fluorescence spectra at an excitation wavelength by illuminating the sample with left circularly polarized light and then with right circularly polarized light. The FDCD in terms of ellipticity spectra is acquired as a difference in these two measurements. The data are temporarily stored in the memory of a microprocessor-based interface that also controls the excita-

Ten Reasons X-Ray Microanalysis Systems from Tracor Northern are superior to all others



REASON NO. 2 MORE ADVANCED APPLICATIONS THAN ANY OTHER MANUFACTURER

No competitive system can even begin to compare to x-ray microanalysis systems by Tracor Northern. In fact, when comparing advanced application such as those listed below, Tracor Northern outperforms every manufacturer by a wide margin. We even outperform the promises of our competition.

☑ **System Automation**
- WDS Automation
- Stage Automation

☑ **X-ray Quantitative Analysis**
- ZAF Matrix Correction
- Bence-Albee Matrix Correction
- Phi Rho Z Matrix Correction
- BIO-Q Biological Quantification
- Analytical Electron Microscopy Quantification

☑ **Electron Energy Loss Spectroscopy (ELS)**

☑ **Electron Diffraction Pattern Analysis (EDPA)**
- Computer aided pattern acquisition
- Display and plotting of acquired and theoretical patterns including oriented pairs of diffraction patterns
- Plotting of stereographic projections

☑ **Digital Beam Control (DBC)**
- Quantitative Line Profiles
- Real-time Particle Analysis and Chemical Characterization
- Stored Image Particle Analysis and Chemical Characterization
- Linewidth Measurement
- Image Storage and Retrieval
  - from SEM
  - from Microprobe
  - from STEM
  - from Video Camera
- Image Processing
  - Image Mathematics
  - Arithmetic Operations
  - Boolean Operations
  - Logical Operations
- Two Dimensional Point Filters
  - Smoothing
  - Difference
- Transforms
  - Log
  - Gamma
  - Histogram Equalized
- Pan and Zoom Image Display
- True Grey Scale Display
- Scanned Transmission Image Collection and Processing

Performance, not promises . . . the main reason Tracor Northern is the world leader in x-ray microanalysis, with more advanced systems installed than all our competitors combined.

Tracor Northern

World Leader in X-ray Microanalysis Systems

TRACOR NORTHERN 2551 WEST BELTLINE HIGHWAY MIDDLETON, WISCONSIN 53562-2697 (608) 831-6511

CIRCLE 203 ON READER SERVICE CARD

AN10000
X-RAY MICROANALYSIS SYSTEM

AN10000 is the result of a carefully planned development program from a company renowned for its innovative approach to systems engineering. Computer technology never before available in a standard system brings to the analyst a powerful yet user friendly system.



* Advanced technology computer hardware.
* Winchester disk as standard.
* High resolution colour display.
* Comprehensive software with user programmability.
* Superior range of Si(Li) spectrometers.
* Convenient packaging.

THE X-RAY ANALYSER YOU'VE ALWAYS PROMISED YOURSELF

CIRCLE 129 ON READER SERVICE CARD

LINK SYSTEMS

LINK SYSTEMS LIMITED,
HALIFAX ROAD,
HIGH WYCOMBE,
BUCKS HP12 3SE,
ENGLAND.
TEL: 0494 442255
TELEX: 837542 LINK HWG

LINK SYSTEMS (FRANCE),
LE MAZIERE,
RUE DES MAZIERES,
91033 EVRY CEDEX.
TEL: (6) 078-10-20.
TELEX: 691 884 F

LINK ANALYTICAL
PO BOX 50810,
3290 WEST BAYSHORE ROAD,
PALO ALTO,
CALIFORNIA 94303, USA.
TEL: (415) 856 2726
TELEX: 334420 MCI PLA

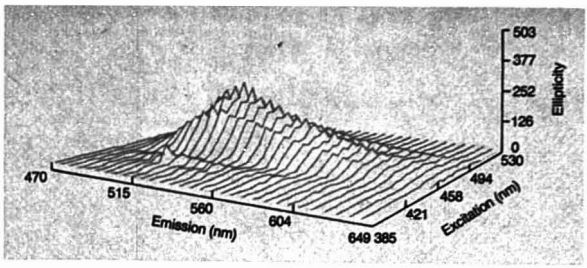


Figure 7. Spectrum of cyclodextrin-induced chirality in acridine orange acquired on FDCD instrument in 32 × 32 format

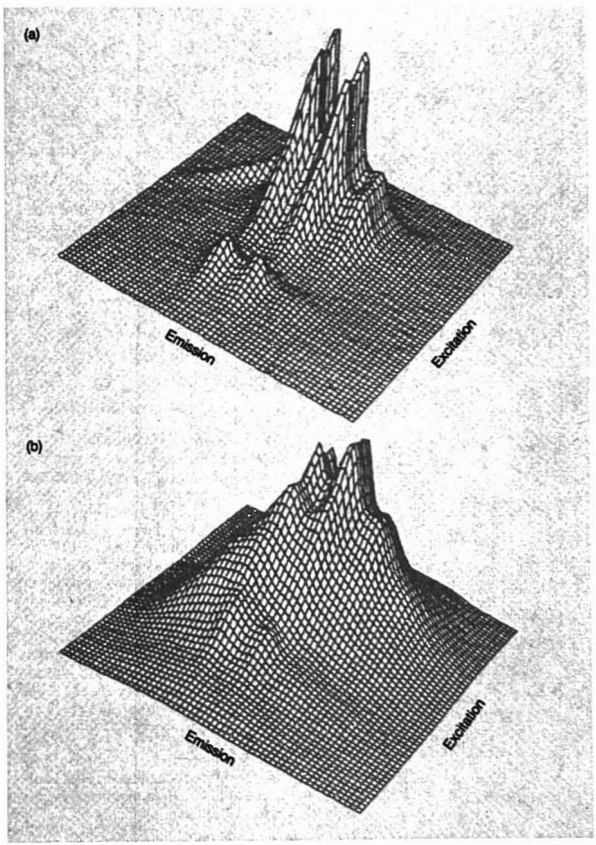


Figure 8. Three-dimensional projection of EEMs acquired at retention time of benzo[*a*]pyrene (BaP) from (a) BaP standard chromatogram and (b) shale oil chromatogram

Reprinted from Reference 55

tion monochromator, polarizers, and detection interfaces, allowing for total instrumental control. Several FDCD spectra may be obtained as the excitation monochromator is scanned through a series of wavelengths.

This new instrument allows acquisition of fluorescence data in the form of a matrix of ellipticity as a function of multiple absorption and emission wavelengths. Figure 7 is an example of such data. It is evident that a number of possibilities exist for more rapid analysis of multicomponent chiral fluorophores. This technique should minimize the necessity of time-consuming preseparation procedures for complex mixtures of optically active luminophores. This is particularly important since preseparation often introduces changes in the chemistry of the system under investigation.

Miscellaneous measurement

Theory. Note in Figure 1 that we listed five possible parameters that could be used to increase selectivity in this category. This list is obviously abbreviated since other parameters such as luminescence induced by chemical reactions (chemiluminescence) could also be included (*48*). The important point to recognize is that although these parameters are often not properties of the luminescence measurement, they are properties of the molecule that can be coupled with the luminescence measurement.

For example, fluorescence has long been recognized as a selective chromatographic detector for high-performance liquid chromatography (HPLC) (*49*). Thus, the selectivity of the fluorescence measurement coupled with the great resolving power of modern HPLC techniques provides an immensely selective measuring technique (*50*). Other examples in this category use selective fluorescence quenching (*51*), micelle enhanced luminescence (*14*, *52*, *53*), and chemical derivatization (*54*) to increase the selectivity of the measurement.

Instrumentation. The basic luminescence instrumentation described in the previous sections is also applicable here. Certain modifications such as miniaturization of the sample cell may be required for specific applications such as HPLC detection (*49*). Many of these requirements are adequately covered in the monographs (*12*, *13*) or references previously listed (*52*, *53*) and will not be discussed here.

One example of multidimensional HPLC detection involves the use of a video fluorometer as a detector for HPLC (*55*). In this example, a video fluorometer is interfaced to a high-performance liquid chromatograph using a laminar flow cell to minimize dead volume and scattered light. The

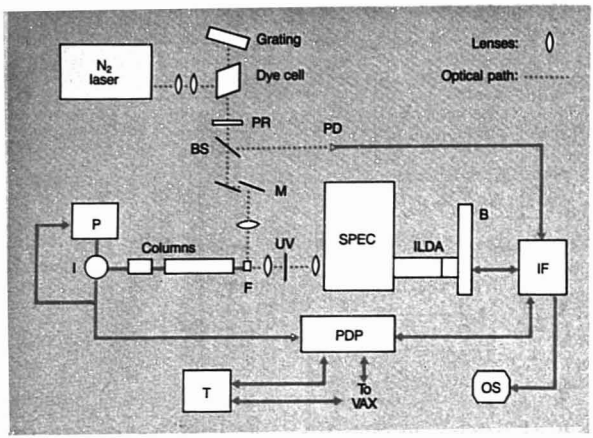


Figure 9. The laser video fluorometer HPLC system

PR, partial reflector in the dye laser cavity; BS, beam splitter; PD, photodiode; M, beam steering mirrors; P, HPLC solvent programmer, dual-solvent pumps, and solvent mixer; I, HPLC injector; F, HPLC fluorescence flow cell; UV, ultraviolet cutoff filter; SPEC, spectrograph; ILDA, microchannel-plate-intensified, cooled, linear photodiode array; B, Reticon diode array evaluation board; IF, computer interface; T, CRT terminal; PDP, Digital Equip. Corp. PDP-1104 minicomputer; OS, oscilloscope

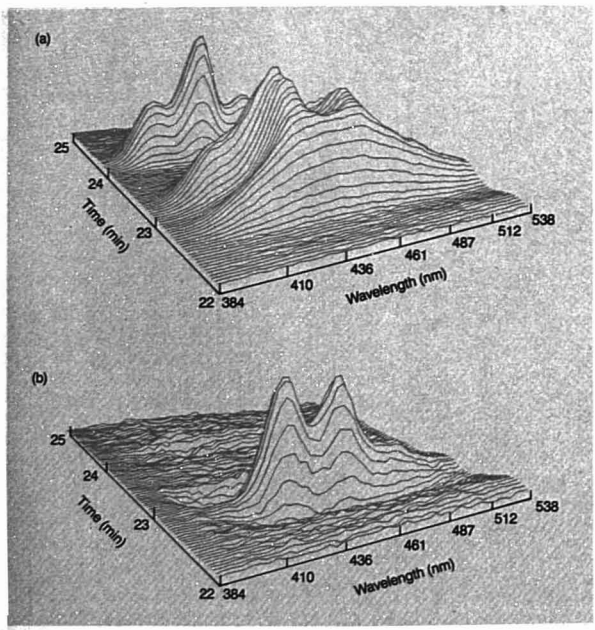


Figure 10. Partial fluorescence chromatogram of an extract of soil that was found to be contaminated with PNAs

(a) A segment of the chromatogram in which benzo[*b*]fluoranthene, benzo[*k*]fluoranthene, and benzo[*a*]-pyrene (BaP) are known to elute. BaP is the compound with the longest retention time. (b) The same segment as in (a), but after subtraction of the appropriate amount of the known standard matrices

characteristic polychromatic illumination method of the video fluorometer was used to acquire real-time fluorescence–excitation matrices as a function of chromatographic retention time.

Figure 8 provides an example of data from this study. In this example, the top EEM was acquired at the retention time of benzo[*a*]pyrene (BaP) using a BaP standard mixture whereas the bottom EEM was acquired at the same retention time for a shale oil sample. Another video fluorometer has been used with a conventional flow cell (*56*) to characterize the fluorescent components from a sample of burned crude oil.

Another excellent example of multidimensional instrumentation in this category is a second-generation laser video fluorometer–HPLC system recently developed by Skoropinski et al. (*57*) at the University of Washington. This instrument features a tunable dye laser as excitation source and a microchannel plate intensified diode array detector for fluorescence characterization of the HPLC eluate (Figure 9). The dye laser grating is mounted on a galvanometer scanner, permitting the laser to be tuned to a specific wavelength on the millisecond time scale. The computer-controlled system can obtain and store up to 10 fluorescence spectra per second as a chromatographic peak elutes.

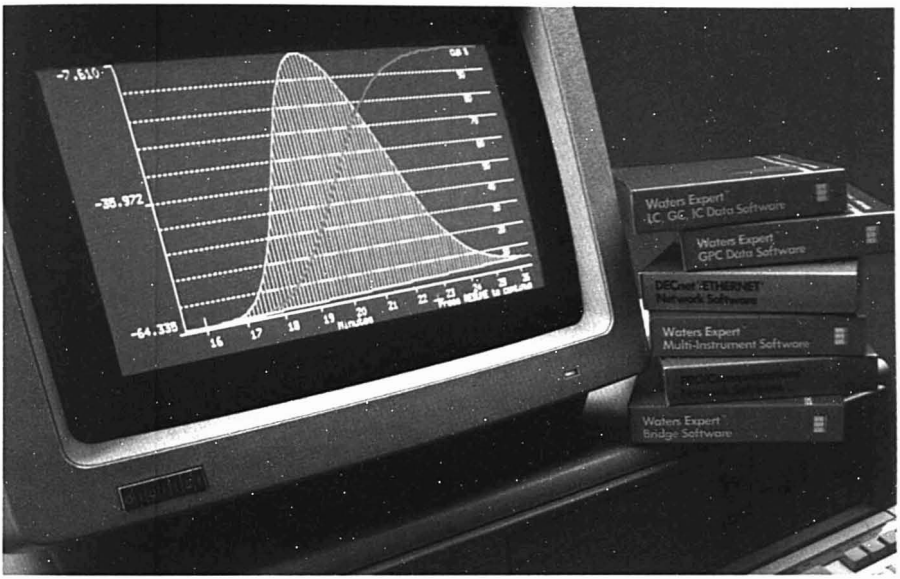
A portion of a two-dimensional chromatogram of a soil extract obtained with the laser video fluorometer HPLC system described in the preceding paragraph is shown in Figure 10a. These data were analyzed using standard chromatograms of the compounds benzo[*b*]fluoranthene, benzo[*k*]fluoranthene, and benzo[*a*]pyrene, known to elute in this region. These chromatograms were fit to the observed matrix by least squares. The residual matrix, however, shown in Figure 10b, clearly revealed the presence of a "hidden" fourth component. Comparison with the spectra of other PNAs of comparable composition led to the identification and quantitation of the compound as 2 ng of perylene.

A final example in this category is the coupling of fluorescence lifetime with fluorescence detection in HPLC (*58*). In this example, data are presented in a three-dimensional display of fluorescence intensity vs. chromatographic retention time and luminescence decay time. The utility of this approach was demonstrated using structurally similar PNAs.

Conclusion

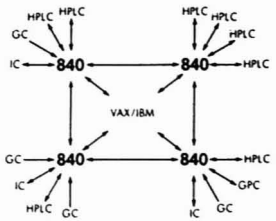
The discussion provided here demonstrates the tremendous selectivity of luminescence measurements. The selectivity is even applicable to struc-

The data/control station that thinks like a chromatographer, now thinks like a lab manager, too. The Waters™ 840.



Now get expanded capability for HPLC, GPC, IC and GC data reduction. The Waters 840 has set a new standard for ease and sophistication in HPLC data management and system control – as the only data/control station that works the way a chromatographer thinks. Now you get even more capability with new Waters Expert™ chromatography software for GPC, GC, ion chromatography, post-run statistical analysis, and more.

Plus, new multi-instrument software allows data acquisition from up to 4 different systems and 16 detectors simultaneously.



The Waters 840 gives you virtually unlimited communications capabilities, including ETHERNET® compatibility for high speed data transfer. No matter what your current data management requirements are, the Waters 840 can meet them – and expand as your needs grow.

No other data/control station gives you so much multi-tasking capability. Acquire and store months of raw data, and reprocess it in seconds. At the same time you can also watch your separations as they run, or use the screen to set up new methods, or perform other computer tasks such as word processing.

See the new power of the Waters 840. Call now: (617) 478-2000, or write Millipore, Waters Chromatography Division, 34 Maple St., Milford, MA 01757.

MILLIPORE
Waters Chromatography Division

ETHERNET is a registered trademark of Xerox Corporation. VAX, DECnet and PRO/Communications are registered trademarks of Digital Equipment Corporation.
Waters and Waters Expert are trademarks of Millipore Corporation. © 1984 Millipore Corporation

CIRCLE 230 ON READER SERVICE CARD

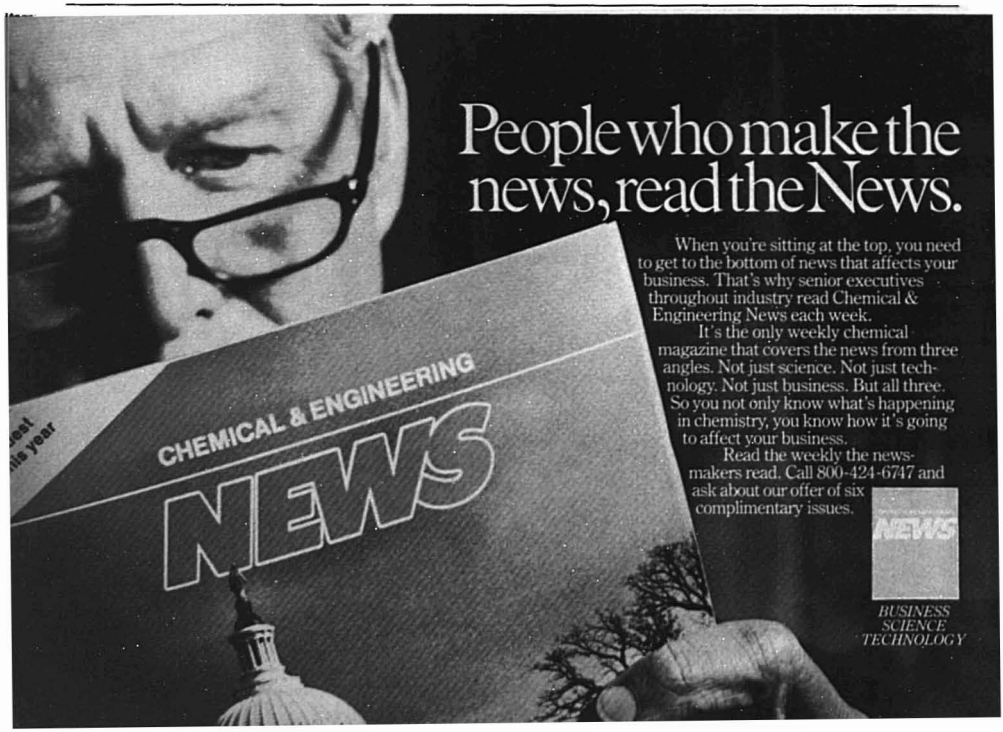
turally similar compounds. This is in direct contrast to the usual notion that absorption and luminescence measurements are spectrally too broad banded to be useful for analytical measurement of similar compounds. It is apparent from the above discussion that a combination of multidimensional luminescence measurement techniques provides the greatest selectivity.

It should be noted that no single instrument has ever been developed for measurement of all of the various luminescence parameters that we have discussed. It is doubtful that such an instrument will ever be developed. However, one can easily conceive of a complete fluorescence laboratory with an array of luminescence instrumentation capable of measuring many of the parameters provided in Figure 1. Thus, the desired selectivity can be achieved through the use of a combination of luminescence instrumentation. The cost of such instrumentation will likely decrease while instrumental sophistication will increase due to improvements in electronics, detectors, optics, and computers for data acquisition and control.

Finally, we have primarily emphasized the theory and instrumentation of MLM techniques. The development of such techniques necessarily requires the development of novel computer algorithms for reduction and interpretation of such large data sets. This parallel development has provided novel algorithms for the quantitative and qualitative analysis of these data (*9*, *30*, *59–61*).

References

(1) Farooq, R.; Kirkbright, G. F. *Analyst* **1976**, *101*, 566–73.
(2) Richardson, J. H.; Ando, M. E. *Anal. Chem.* **1977**, *49*, 955–59.
(3) Sawicki, E.; Hauser, T. R.; Stanley, T. W. *Int. J. Air Pollut.* **1960**, *2*, 253–72.
(4) Sawicki, E. *Talanta* **1969**, *16*, 1231–66.
(5) Richardson, J. H.; Larson, K. M.; Haugen, G. R.; Johnson, D. C.; Clarkson, J. E. *Anal. Chim. Acta* **1980**, *1161*, 407–11.
(6) Alfano, A. J.; Fong, E. K.; Lytle, F. E. *Rev. Sci. Instrum.* **1983**, *54*, 967–72.
(7) Hieftje, G. M. *Clin. Chem.* **1983**, *29*, 1659–64.
(8) Berndt, K.; Durr, H.; Palme, D. *Opt. Commun.* **1983**, *47*, 321–23.
(9) Warner, I. M. "The Analysis of Matrix Formatted Multicomponent Data," in "Contemporary Topics in Analytical and Clinical Chemistry, Vol. 4"; Hercules, D. M.; Hieftje, G. M.; Snyder, L. R.; Evenson, M. A., Eds.; Plenum Press: New York, N.Y., 1982.
(10) Wehry, E. L. *Anal. Chem.* **1984**, *56*, 156–73 R.
(11) McGown, L. B.; Bright, F. V. *Anal. Chem.* **1984**, *56*, 1400–1416 A.
(12) Lakowicz, J. R. "Principles of Fluorescence Spectroscopy"; Plenum Press: New York, N.Y., 1983.
(13) Birks, J. B. "Photophysics of Aromatic Molecules"; Wiley-Interscience: New York, N.Y., 1970.
(14) Miller, J. N. *Trends Anal. Chem.* **1981**, *1*, 31–34.
(15) Warner, I. M.; Callis, J. B.; Christian, G. D.; Davidson, E. R. *Anal. Chem.* **1977**, *49*, 564–73.
(16) Ginell, R.; Feuchtbaum, R. J. *J. Appl. Bacteriol.* **1972**, *35*, 29–36.
(17) Wampler, J. E.; DeSa, R. J. *Appl. Spectrosc.* **1971**, *25*, 623–27.
(18) O'Haver, T. C.; Green, G. L.; Keppler, B. R. *Chem. Instrum.* **1973**, *4*, 197–201.
(19) Holland, J. F.; Teets, R. E.; Timnick, A. *Anal. Chem.* **1973**, *45*, 145–53.
(20) Haugen, G. R.; Raby, B. A.; Ridgon, L. P. *Chem. Instrum.* **1975**, *6*, 205–25.
(21) Turner, G. K. *Science* **1964**, *146*, 183–89.
(22) Kohen, E.; Thorell, B.; Kohen, C.; Solomon, J. M. "Microfluorometric Monitoring of Dehydrogenase Systems in the Intact Cell," in "Techniques of Biochemical and Biophysical Morphology, Vol. 12"; Click, D.; Rosenbaum, R. M., Eds.; Wiley-Interscience: New York, N.Y., 1975; pp. 157–95.
(23) Warner, I. M.; Callis, J. B.; Davidson, E. R.; Gauteman, M.; Christian, G. D. *Anal. Lett.* **1975**, *8*, 665–81.
(24) Johnson, D. W.; Gladden, J. A.; Callis, J. B.; Christian, G. D. *Rev. Sci. Instrum.* **1979**, *50*, 118–26.
(25) Fogarty, M. P.; Warner, I. M. *Appl. Spectrosc.* **1980**, *34*, 438–45.
(26) Warner, I. M.; Fogarty, M. P.; Shelly, D. C. *Anal. Chim. Acta* **1979**, *109*, 361–72.
(27) Gaugh, T. *Science* **1979**, *203*, 1330–31.
(28) Ho, C.-N.; Warner, I. M. *Trends Anal. Chem.* **1982**, *1*, 159–63.
(29) Ho, C.-N.; Warner, I. M. *Anal. Chem.*



1982, *54*, 2486–91.
(30) Knorr, F. J.; Harris, T. M. *Anal. Chem.* **1981**, *53*, 272–76.
(31) Goeringer, D. E.; Pardue, H. L. *Anal. Chem.* **1979**, *51*, 1054–60.
(32) Hapbaugh, K. F.; O'Donnell, C. M.; Wineforder, J. D. *Anal. Chem.* **1974**, *46*, 1206–9.
(33) Wilson, R. M.; Miller, T. L. *Anal. Chem.* **1975**, *47*, 256–61.
(34) Ghiggino, K. P.; Roberts, A. J.; Phillips, D. *J. Phys. E.* **1980**, *5*, 446–50.
(35) Haar, H. P.; Mauser, M. *Rev. Sci. Instrum.* **1978**, *49*, 631–33.
(36) Rentzepis, P. M. *Science* **1978**, *202*, 174–82.
(37) Sears, F. W.; Zemansky, M. W.; Young, H. D. "University Physics"; Addison-Wesley: Reading, Mass., 1977.
(38) Cotton, A. M. *Am. Chim. Physique* **1896**, *8*, 347.
(39) Kreuger, W. C.; Pschigoda, L. M.; Reusser, F. J. *J. Antibot.* **1973**, *26*, 424–28.
(40) Turner, D. H.; Tinoco, I., Jr. *J. Am. Chem. Soc.* **1974**, *96*, 4340–42.
(41) Tinoco, I., Jr.; Turner, D. H. *J. Am. Chem. Soc.* **1976**, *98*, 6453–66.
(42) White, T. G.; Pao, Y. H.; Tang, M. M. *J. Am. Chem. Soc.* **1975**, *97*, 4751–53.
(43) Ehrenberg, B.; Steinberg, I. Z. *J. Am. Chem. Soc.* **1976**, *98*, 1293–95.
(44) Tinoco, I., Jr.; Ehrenberg, B.; Steinberg, I. Z. *J. Chem. Phys.* **1977**, *66*, 916–20.
(45) Lobenstein, E. W.; Turner, D. H. *J. Am. Chem. Soc.* **1979**, *101*, 2205–7.
(46) Turner, D. H.; Tinoco, I., Jr.; Maestre, M. F. *Biochemistry* **1975**, *14*, 3794–99.
(47) Thomas, M.; Patonay, G.; Simpson, O.; Warner, I. M., 187th National Meeting of the American Chemical Society, St. Louis, Mo., April 8–13, 1984; Abstract No. 25.
(48) Seitz, W. R.; Neary, M. P. *Anal. Chem.* **1974**, *46*, 188–202 A.
(49) Shelly, D. C.; Warner, I. M. In "Fluorescence Detectors in High Performance Liquid Chromatography Detectors," T. M. Vickrey, Ed.; Marcel Dekker: New York, N.Y., 1983; pp. 87–123.
(50) Guthrie, E. J.; Jorgenson, J. W. *Anal. Chem.* **1984**, *56*, 483–86.
(51) Sawicki, E.; Stanley, T. W.; Johnson, H. *Mikrochim. Acta* **1965**, *1*, 178–92.
(52) Cline-Love, L. J.; Habarta, J. G.; Dorsey, John G. *Anal. Chem.* **1984**, *56*, 1132–48 A.
(53) Hinze, W. L.; Riehl, T. E.; Singh, H. N.; Baba, Y. *Anal. Chem.* **1984**, *56*, 2180–91.
(54) Seiler, N.; Demisch, L. In "Handbook of Derivatives for Chromatography"; Blau, K.; King, G., Eds.; Heyden: Philadelphia, Pa., 1978; pp. 346–90.
(55) Hershberger, L. W.; Callis, J. B.; Christian, G. D. *Anal. Chem.* **1981**, *53*, 971–75.
(56) Shelly, D. C.; Fogarty, M. P.; Warner, I. M. *J. High Resolut. Chromatogr. Chromatogr. Commun.* **1981**, *4*, 616–26.
(57) Skoropinski, D. B.; Callis, J. B.; Danielson, J. D. S.; Christian, G. D., private communication, January 1985.
(58) Imasaka, T.; Ishibashi, K.; Ishibashi, N. *Anal. Chim. Acta* **1982**, *142*, 1–12.
(59) Appellof, C. J.; Davidson, E. R. *Anal. Chem.* **1981**, *53*, 2053–56.
(60) Ho, C.-N.; Christian, G. D.; Davidson, E. R. *Anal. Chem.* **1980**, *52*, 1071–79.
(61) Moran, M. G.; Kowalski, B. R. *Anal. Chem.* **1979**, *51*, 776–89 A.

Some of the studies discussed in this manuscript were supported in part by grants from the National Science Foundation and the Office of Naval Research. Isiah M. Warner is also grateful for partial support from a Presidential Young Investigator Award during the preparation of this manuscript. The authors gratefully acknowledge the technical assistance of Thomas M. Rossi, Sharon L. Neal, and Cleophas Boudreau.



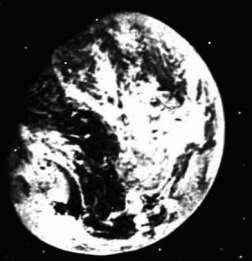
Isiah M. Warner (left) received his BS degree from Southern University in Baton Rouge in 1968 and his PhD from the University of Washington in 1977. He worked as a research chemist at Battelle Northwest in Richland, Wash., from 1968 to 1973. His current research interests include molecular absorption and luminescence spectroscopy, development of novel analytical instrumentation, and the reduction and interpretation of multicomponent chemical data.

Gabor Patonay (center) received his MS and PhD degrees from the Technical University of Budapest, Hungary, in 1973 and 1979, respectively. He is currently research associate professor at Emory University, performing research in collaboration with I. M. Warner. His research interests include molecular absorption and luminescence spectroscopy, electronics, development of novel analytical instrumentation, and applications of computers in analytical chemistry.

Mark P. Thomas (right) received his BS degree from Davidson College in North Carolina in 1982. He is a graduate student completing work for a PhD degree under the direction of I. M. Warner. His research involves the development and application of rapid-scanning fluorescence-detected circular dichroism in analytical chemistry.

ENVIRONMENTAL SCIENCE & TECHNOLOGY

ES&T



The premiere research publication in the environmental field.

Environmental science continues to be one of the fastest growing fields. And ES&T has grown right along with it!

ES&T continues to give you the practical, hard facts you need on this science . . . covering research, techniques, feasibility, products and services.

Essential reading for environmental scientists both in the business and academic world . . . ES&T has increased its emphasis on peer-reviewed research dealing with water, air, and waste chemistry in addition to adding critical reviews of important environmental science issues—all relevant to understanding the management of our natural environment.

Also included are discussions on environmental analyses, governmental regulations, current environmental lab activities, and much more!

For rate information, and to subscribe, call toll free:

(800) 424-6747

LABORATORY SERVICE CENTER

Allyl Thiourea • Benzamide • Caffeic Acid • iso-Caproic Acid
2,3-Dibromopropanol • Dimedone • 3,5-Dinitrobenzoic Acid • Dulcitol
Ethyl Pyruvate • Hydroxylamide HCl & Sulfate • INT • Levulinic Acid
Levulose • Malonic Acid • Methylacetamide • Methyl-tert-Butyl Ether
β-Naphthyl Acetate • p-Nitrobenzaldehyde • Orcinol • Phenolphthalein
Phenylurea • Propyl Caprylate • Pyridine-4-Aldehyde • Pyrogallol
Salicin • Sodium-4-Hydroxy Butyrate • Sodium Succinate • Suberic Acid
Triphenylmethylphosphonium Bromide • Triphenylphosphine • Veratrole

Write for our Products List of over 3000 chemicals

Tel: 516-273-0900 • TOLL FREE: 800-645-5566 TWX: 510-227-6230

EASTERN CHEMICAL
A Division of UNITED-GUARDIAN, INC.
P. O. Box 2500
DEPT AC
SMITHTOWN, N. Y. 11787

LIQUID CHROMATOGRAPHY SPECIALISTS
POLYMER PROBLEMS?
WE OFFER • Complete Polymer Deformulation
• Good vs Bad Comparison
• Gel Permeation Chromatography MWD Mn Mw Mz
• Additive Package Analysis
All work done is treated as strictly confidential. For more information please write or call us at
617·376·8883
JORDI ASSOCIATES INC
397 Village Street
Millis, Massachusetts 02054

COMPREHENSIVE ENVIRONMENTAL SERVICES.
EA ENVIRONMENTAL SCIENCE AND ENGINEERING

Laboratory Service Center (Equipment, Materials, Services, Instruments for Leasing). Maximum space — 4 inches per advertisement. Column width, 2-3/16″; two-column width, 4-9/16″. Artwork accepted. No combination of directory rates with ROP advertising. Rates based on number of inches used within 12 months from first date of first insertion. Per inch: 1″ — $125; 12″ — $123; 24″ — $120; 36″ — $115; 48″ — $112.

CALL OR WRITE JANE GATENBY

ANALYTICAL CHEMISTRY
25 Sylvan Road South
P.O. Box 231
Westport, Ct. 06881
203-226-7131

USE LABORATORY SERVICE CENTER

INDEX TO ADVERTISERS IN THIS ISSUE

CIRCLE INQUIRY NO.	ADVERTISERS	PAGE NO.
5	*Airco Industrial Gases Hammond Farrell	388A
2	*Alltech Associates SMS Marketing Services	464A
3–4	*American Burdick & Jackson Nordstrom/Cox Marketing	390A, 468A
xxx	Applied Biosystems Lincoln Associates	IFC
1	*Atago Bussan Company, Ltd. Echo Japan Corp.	386A
19	Baird Corporation	470A
21	Beckman Instruments Cochrane, Chase, Livingston & Co.	415
20	Beckman Instruments Lapointe, Schott & Smith Inc.	454B1–454B34
16	Bioanalytical Systems Inc. Kissinger Advertising Assoc.	404A
17–18	Bio-Rad Digilab Division	392A, 475A
15	Bomen, Inc.	381A
33	Corning Glass Works/Science Products Winterkorn Lillis Inc.	394A–395A
32	*Crawford Fitting Company Falls Advertising	456A
41	Dow Corning Corp. Marsteller, Inc.	405A
43	Dynamic Solutions Corp.	391A
42	Dynatech Precision Sampling D. Allen & Assoc.	410A
50	Edax International STG Marketing	439A
47	EG&G/PARC The Message Center	378A
48	EM Science G&C Advertising & Marketing Inc.	440A–441A
51–52	Extranuclear Laboratories Communications Ink, Inc.	375A
65–66	Finnigan MAT Corp.	399A
63–64	*Gilson Medical Electronics Lapointe, Schott & Smith, Inc.	365A
96	*Hamilton Company	403A
106	*IBM Instruments, Inc. Marquardt & Roche	432A–433A
105	*ISCO Farneaux Associates	427A
110	*J&W Scientific, Inc.	452A
117	**Kontron Ltd. Promotion-Kontron AG	438C
112–115	*Kratos Studio 21 Advertising	380A
126	LDC/Milton Roy HRS Communications	384A
125	*Leco Corporation	379A
128	Leybold Heraeus Vacuum Products Inc.	417A
129	Link Systems USA Inc.	478A

INDEX TO ADVERTISERS IN THIS ISSUE

CIRCLE INQUIRY NO.	ADVERTISERS	PAGE NO.
127	LKB/Produkter AB Marketing Service	436A
144	Macherey-Nagel Wergeagentur Beier	402A
138	*Matheson Gas Products Kenyon Hoag Associates	377A
137	*Mattson Instruments Lucarelli Ltd.	OBC
140-143	*Mettler Instrument Corp. McKinney Inc.	387A, 389A, 431A, 435A
146	MG Industries Techmarketing, Inc.	422A
139	*Mitsubishi Chemical Industries Global Advertising	438A
147-153	Naige Company Hutchins Y&R	442A
154	*Nelson Analytical Moran, Lanig & Duncan	421A
157	*Ohaus Scale Corp. Barbetta Miller Inc.	382A-383A
155-156	Orion Research Inc. OBC Advertising	371A
167, 171	Packard Instrument	376A, 450A
170	*Perkin-Elmer Corp. AC&R Advertising Inc.	444A-445A
169	Perkin-Elmer/Oakbrook Instrument Div.	469A
168	Philips Analytical X-Ray STG Marketing	368A-369A
70-77, 79-80	**Pye Unicam Ltd. Connors Publicity Ltd.	438D, 438F, 438H
181	Radian Corp.	401A
180	Radiometer A/S	457A
179	*Rheodyne, Inc. Bonfield Associates	465A
199	S-CUBED/Maxwell	412A
187	**Schott/Mainz Werbeagentur Frenz	438B
198	Scientific Glass Engineering Arden Advertising Agency	423A
186	Scientific Systems	458A
188	Seastar Instruments	468A
195	Shandon Southern Instruments Inc. Downing Industrial Advertising	437A
189-192	*Shimadzu Scientific Instruments General Advertising	406A-407A 409A, 411A
197	Siemens AG Barbeau-Hutchings Advertising	413A
194	*Spectra-Physics	473A
196	Spectrofuge Corporation	380A
193	Sun Tsusho Company, Ltd. General Advertising	392A
201	Tecator, Inc.	419A
202	Tennelec, Inc. Sun Graphics, Inc.	396A-397A
203	*Tracor Northern	477A
200	*Tracor X-Ray	467A
218	*Valco Instruments Technical Advertising Assoc.	373A
219-221	*Varian Moran, Lanig & Duncan	459A, 461A, 462A
222	VG Instruments Barbeau-Hutchings Advertising	393A
230-231	Waters Associates Mintz & Hoke, Inc.	453A, 481A
235	*Wescan Instruments Webb & Associates	428A
233	*Whatman, Inc. Communique	449A
34	Whatman LabSales	424A
234	John Wiley & Sons Gaynor Media Corp.	425A

* See ad in ACS Laboratory Guide
** Company so marked had advertisement in Foreign Regional edition only.

Advertising Management for the American Chemical Society Publications

CENTCOM, LTD

President
Thomas N. J. Koerwer

Executive Vice President **James A. Byrne** *Senior Vice President* **Benjamin W. Jones**

Alfred L. Gregory, *Vice President*
Clay S. Holden, *Vice President*
Robert L. Voepel, *Vice President*
Joseph P. Stenza, *Production Director*

25 Sylvan Rd. South
P.O. Box 231
Westport, Connecticut 06881
(Area Code 203) 226-7131
Telex No. 643310

ADVERTISING SALES MANAGER
James A. Byrne, VP

ADVERTISING PRODUCTION MANAGER
Jane F. Gatenby

SALES REPRESENTATIVES

Philadelphia . . . Dean A. Baldwin, Patricia O'Donnell, CENTCOM, LTD., GSB Building, Suite 425, 1 Belmont Avenue, Bala Cynwyd, Pa. 19004. Telephone: 215-667-9666

New York . . . Dean A. Baldwin, Edward M. Black, John Raftery, CENTCOM, LTD., 60 East 42nd St., 212-972-9660, New York, N.Y. 10165

Westport, CT . . . Edward M. Black, CENTCOM, LTD., 25 Sylvan Rd. South, P.O. Box 231, Westport, Ct. 06881. Telephone: 203-226-7131, Telex 643310

Cleveland . . . Bruce E. Poorman, CENTCOM, LTD., 325 Front St., Suite 2, Berea, Ohio 44017, 216-234-1333

Chicago . . . Michael J. Pak, CENTCOM, LTD., 540 Frontage Rd., Northfield, Ill. 60093, 312-441-6383

Houston . . . Dean A. Baldwin, CENTCOM, LTD., 215-667-9666

San Francisco, CA . . . Paul M. Butts, CENTCOM, LTD., Suite 1070, 2672 Bayshore Frontage Road, Mountainview, CA 94043. Telephone: 415-969-4604

Los Angeles . . . Clay S. Holden, CENTCOM, LTD., Newton Pacific Center, 3142 Pacific Coast Highway, Suite 200, Torrance, CA 90505, 213-325-1903

Boston, MA . . . Edward M. Black, CENTCOM, LTD. Telephone: 203-226-7131

Atlanta, GA . . . Edward M. Black, CENTCOM, LTD. Telephone: 203-226-7131

Denver . . . Paul M. Butts, CENTCOM, LTD., 415-969-4604

United Kingdom

Reading, England . . . Malcolm Thiele, Technomedia Ltd., Wood Cottage, Shurlock Row, Reading RG10 0QE. Berkshire, England. Telephone: 0734-343302

Lancashire, England . . . Technomedia Ltd., c/o Meconomics Ltd., Meconomics House, 31 Old Street, Ashton Under Lyne, Lancashire, England. Telephone: 061-308-3025

Continental Europe . . . Andre Jamar, International Communications, Inc., Rue Mallar 1, 4800 Verviers, Belgium. Telephone: (087) 22-53-85, Telex #49263

Tokyo, Japan . . . Shuji Tanaka, International Media Representatives Ltd., 2-29 Toranomon, 1-Chome Minato-ku Tokyo 105 Japan. Telephone: 502-0656, Telex #22633

RECRUITERS ... EDUCATORS ... CHEMISTS ...

NOW AVAILABLE FROM ACS

THE DIRECTORY OF CHEMISTRY CO-OP



The indispensable guide to cooperative education programs in the U.S. and Canada.

If you are interested in co-op programs as participant, sponsor, or advisor, take advantage of this unique, authoritative reference! Get practical, accurate information on 265 chemistry, chemical engineering, and chemistry-related cooperative education programs in the U.S. and Canada.

In-depth coverage includes contact names and addresses, program size, typical work schedules, academic requirements, geographical and program indices, and a great deal more.

As a reference, this timely resource is essential for:

- Schools interested in starting co-op
- Employers seeking sources of co-op students
- High school students and advisors wishing to locate co-op schools
- Co-op professionals requiring a convenient source of information

SAVE 25%!

This informative, 280-page paperbound volume is available for just $15.00 a copy (After April 1, 1985, the price will be $20.00) Order now to take advantage of these special introductory savings.

PHONE TOLL FREE!

Call 1-800-424-6747 (credit card orders only) to order your copy at this special price or mail coupon today!

Please send _____ copies of the *ACS Directory of Chemistry Co-op* @ $15.00 per copy to:

Name _____

Address _____

_____

Check the method of payment: ☐ Check or money order enclosed ☐ Credit card: ☐ Visa ☐ MasterCard ☐ Barclay ☐ Access ☐ American Express

Cardholder Name _____

Card No. _____

Exp. Date _____ Interbank No. _____
(MasterCard and Access only)

Signature _____

Amount Enclosed $ _____ .
Make checks payable to **ACS Co-op Directory.**
Orders must be prepaid. California residents, add 6% sales tax.

Return to: **Office of Cooperative Education**
American Chemical Society
1155 Sixteenth St., N.W.
Washington, DC 20036

56309/2171/E721

You'll read it

LANGMUIR—*New in 1985!*

Arthur Adamson, Editor; University of Southern California

Bimonthly journal covering all areas of fundamental surface and colloid science... wet surface chemistry, 'uhv' surface chemistry, disperse systems, electrochemistry.

	U.S.	Canada	Europe	All Other Countries
Member	$ 49	$ 58	$ 58	$ 58
Nonmember	$299	$308	$308	$308

ANALYTICAL CHEMISTRY

George H. Morrison, Editor; Cornell University

This monthly journal is the world's foremost publication in the vital field of measurement science.

	U.S.	Canada	Europe	All Other Countries
Member	$ 20	$ 40	$ 57	$ 80
Nonmember	$ 30	$ 50	$ 99	$122

ACCOUNTS OF CHEMICAL RESEARCH

Joseph F. Bunnett, Editor; University of California, Santa Cruz

Monthly publication offering short, critical reviews written by scientists active in the research described.

	U.S.	Canada	Europe	All Other Countries
Member	$ 22	$ 26	$ 28	$ 31
Nonmember	$ 96	$102	$102	$105

CHEMTECH

Benjamin J. Luberoff, Editor; ACS

Stimulating, personal monthly helping chemists and engineers arrive at innovative solutions to real problems.

	U.S.	Canada	Europe	All Other Countries
Member	$ 27	$ 33	$ 37	$ 44
Nonmember				
Personal	$ 38	$ 44	$ 48	$ 55
Institutional	$199	$205	$209	$216

ENVIRONMENTAL SCIENCE & TECHNOLOGY

Russell F. Christman, Editor; Univ. of North Carolina, Chapel Hill

Monthly for scientists engaged in study and maintenance of environment through the application of chemical principles.

	U.S.	Canada	Europe	All Other Countries
Member	$ 26	$ 34	$ 40	$ 49
Nonmember				
Personal	$ 35	$ 43	$ 49	$ 58
Institutional	$149	$157	$163	$172

JOURNAL OF THE AMERICAN CHEMICAL SOCIETY

Allen J. Bard, Editor; University of Texas

Most quoted biweekly journal of the widest possible interest to research workers and students in all areas of chemistry.

	U.S.	Canada	Europe	All Other Countries
Member	$ 61	$ 96	$129	$161
Nonmember	$299	$334	$367	$399

SI in American Chemical Society Publications.

From chemical news today to peer-reviewed research in print for the first time... ACS publishes worldwide developments in chemistry for you.

CALL TOLL FREE 800-424-6747

*Air Service Delivery included in all rates listed for Europe and All Other Countries.

AMERICAN CHEMICAL SOCIETY, 1155 16th St., N.W., Washington, D.C. 20036 1985
CALL TOLL FREE 800-424-6747

Please enter a one-year subscription for the following publications:

	PRICE		PRICE
1.		2.	
3.		4.	

Name _____ Position _____

Company _____ Address ☐ Home ☐ Business _____

City _____ State _____ Zip _____

☐ Payment enclosed _____ (Payable to American Chemical Society) ☐ Bill me ☐ Bill company

Charge my ☐ MasterCard ☐ VISA Account No. _____ Interbank No. _____ (MasterCard only)

Expire Date _____ Signature _____

Nature of Your Employer's Business: ☐ Manufacturing ☐ Government ☐ University

☐ Other (Please indicate) _____

☐ I am ☐ I am not an ACS member.

☐ Please send me information on how to become an ACS member.

Member rates are for personal use only.

Journal subscriptions start January 1985 and expire December 1985. Member subscriptions to Analytical Chemistry, Environmental Science & Technology, and CHEMTECH will start the month the order is placed and expire one year later unless subscriber requests a January start date.

Foreign payment must be made in U.S. currency by international money order, UNESCO coupons, U.S. bank draft, or through your subscription agency. For rates in Japan, contact Maruzen Co., Ltd.

3147R

BIOCHEMISTRY

Hans Neurath, Editor; University of Washington

Offers results of original research in all recognized or developing areas of biochemistry. Biweekly.

	U.S.	Canada	Europe	All Other Countries
Member	$ 59	$ 92	$117	$149
Nonmember	$303	$336	$361	$393

CHEMICAL & ENGINEERING NEWS

Michael Heylin, Editor; ACS

Chemical newsweekly and the official publication of the ACS that all members receive as part of their dues.

	U.S.	Canada	Europe	All Other Countries
Nonmember	$ 37	$ 61	$ 88	$116

(Via surface mail outside U.S. and Canada, $61)

CHEMICAL REVIEWS

Josef Michl, Editor; University of Utah

Reviews of research of chemistry that eliminate the need to scan scores of articles concerning particular fields. Bimonthly.

	U.S.	Canada	Europe	All Other Countries
Member	$ 19	$ 24	$ 28	$ 33
Nonmember	$ 76	$ 81	$ 85	$ 90

I&EC FUNDAMENTALS

Robert L. Pigford, Editor; University of Delaware

Publishes, quarterly, original scientific papers dealing with the very frontiers of chemical engineering understanding.

	U.S.	Canada	Europe	All Other Countries
Member	$ 15	$ 19	$ 27	$ 28
Nonmember	$ 67	$ 71	$ 79	$ 80

I&EC PROCESS DESIGN AND DEVELOPMENT

Hugh M. Hulburt, Editor; Northwestern University

Quarterly contains original papers and occasionally critical reviews, that present theoretical and experimental results relating to the development of processes and process equipment.

	U.S.	Canada	Europe	All Other Countries
Member	$ 15	$ 19	$ 30	$ 32
Nonmember	$ 76	$ 80	$ 91	$ 93

I&EC PRODUCT R&D

Jerome A. Seiner, Editor; PPG Industries

Publishes original research on broadly varied product related topics in an interdisciplinary manner. Quarterly.

	U.S.	Canada	Europe	All Other Countries
Member	$ 15	$ 19	$ 30	$ 32
Nonmember	$ 76	$ 80	$ 91	$ 93

INORGANIC CHEMISTRY

M. Frederick Hawthorne, Editor; University of California, Los Angeles

Biweekly journal publishes fundamental studies, experimental and theoretical, in all phases of inorganic chemistry.

	U.S.	Canada	Europe	All Other Countries
Member	$ 70	$101	$105	$146
Nonmember	$373	$404	$408	$449

JOURNAL OF AGRICULTURAL AND FOOD CHEMISTRY

Irvin E. Liener, Editor; University of Minnesota

Bimonthly reporting of original research into the chemical aspects of agriculture and food.

	U.S.	Canada	Europe	All Other Countries
Member	$ 22	$ 29	$ 36	$ 45
Nonmember	$116	$123	$130	$139

JOURNAL OF CHEMICAL AND ENGINEERING DATA

Bruno J. Zwolinski, Editor; Texas A & M University

This quarterly journal is primarily concerned with the presentation of data of lasting value.

	U.S.	Canada	Europe	All Other Countries
Member	$ 27	$ 31	$ 32	$ 35
Nonmember	$148	$152	$153	$156

JOURNAL OF CHEMICAL INFORMATION AND COMPUTER SCIENCES

T. L. Isenhour, Editor; Utah State University

Quarterly reporting on new R&D, concepts, systems, and programs in all areas of information and computers relevant to chemistry and chemical technology.

	U.S.	Canada	Europe	All Other Countries
Member	$ 17	$ 21	$ 21	$ 24
Nonmember	$ 90	$ 94	$ 94	$ 97

JOURNAL OF MEDICINAL CHEMISTRY

Phillip S. Portoghese, Editor; University of Minnesota

Monthly journal concerned with the relationship of chemistry to biological activity, including rapid communication of major advances in drug design and development.

	U.S.	Canada	Europe	All Other Countries
Member	$ 33	$ 43	$ 52	$ 64
Nonmember	$172	$182	$191	$203

THE JOURNAL OF ORGANIC CHEMISTRY

Frederick D. Greene, Editor; Massachusetts Institute of Technology

Biweekly offering critical accounts of original work and interpretative reviews of existing data that present new viewpoints.

	U.S.	Canada	Europe	All Other Countries
Member	$ 45	$ 71	$ 95	$110
Nonmember	$233	$259	$283	$298

THE JOURNAL OF PHYSICAL CHEMISTRY

Mostafa A. El-Sayed, Editor; University of California, Los Angeles

Biweekly journal of experimental and theoretical research on fundamental aspects of physical chemistry and chemical physics.

	U.S.	Canada	Europe	All Other Countries
Member	$ 56	$ 86	$108	$145
Nonmember	$333	$363	$385	$422

JOURNAL OF PHYSICAL AND CHEMICAL REFERENCE DATA

David R. Lide, Jr., Editor; National Bureau of Standards

Quarterly published with Amer. Inst. of Physics and N.B.S. presenting critically evaluated data on physical and chemical properties.

	U.S.	Canada	Europe	All Other Countries
Member (ACS, AIP, affiliated societies, personal)	$ 50	$ 60	$ 75	$ 85
Nonmember	$200	$210	$225	$235

MACROMOLECULES

Field H. Winslow, Editor; Bell Telephone Laboratories

Monthly original material on all fundamental aspects of polymer chemistry.

	U.S.	Canada	Europe	All Other Countries
Member	$ 44	$ 57	$ 68	$ 82
Nonmember	$254	$267	$278	$292

ORGANOMETALLICS

Dietmar Seyferth, Editor

Massachusetts Institute of Technology

Monthly journal with an interdisciplinary approach to organometallic chemistry: synthesis; structure and bonding; reactivity and mechanism; applications in organic, inorganic, polymer, and solid state chemistry, and materials science.

	U.S.	Canada	Europe	All Other Countries
Member	$ 40	$ 54	$ 60	$ 73
Nonmember	$229	$243	$249	$262

ACS SINGLE ARTICLE ANNOUNCEMENT

Semi-monthly current awareness service reproduces contents pages of all ACS primary journals, so you may order articles of your choice using a form provided.

	U.S.	Canada	Europe	All Other Countries
Member	$ 50	$ 60	$ 70	$ 70
Nonmember	$100	$110	$120	$120

***Air Service Delivery included in all rates listed for Europe and All Other Countries.**

NO POSTAGE NECESSARY IF MAILED IN THE UNITED STATES

BUSINESS REPLY CARD

FIRST CLASS PERMIT NO. 10094 WASHINGTON, D.C.

POSTAGE WILL BE PAID BY ADDRESSEE

AMERICAN CHEMICAL SOCIETY
Attn: Periodicals Marketing Dept.
1155 Sixteenth Street, N.W.
Washington, D.C. 20036

For over six decades



...the leader in the field.

☐ **YES,** send me my own personal copy of **Analytical Chemistry.**

Published monthly One Year	U.S.	Mexico & Canada	Europe	All Other Countries
ACS Members*	☐ $20	☐ $40	☐ $57	☐ $ 80
Nonmembers*	☐ $30	☐ $50	☐ $99	☐ $122

☐ Payment Enclosed (Payable to American Chemical Society)
☐ Bill Me ☐ Bill Company Charge my: ☐ VISA ☐ MasterCard

Card No. _____

Exp. Date _____ Interbank # _____ (Mastercard Only)

Signature _____

Name _____

Title _____ Employer _____

Address _____

City, State, Zip _____

Employer's Business: ☐ Manufacturing, type _____

☐ Academic ☐ Government ☐ Other _____

*Subscriptions at these rates are for personal use only.
All foreign subscriptions are now fulfilled by air delivery. Foreign payment must be made in U.S. currency by international money order, UNESCO coupons, U.S. bank draft, or order through your subscription agency. For nonmember subscription rates in Japan, contact Maruzen Co., Ltd.
Please allow 45 days for your first copy to be mailed.
Redeem until December 31, 1985. 1985

560 **MAIL THIS POSTAGE-PAID CARD TODAY!** 3144P

For over six decades



...the leader in the field.

☐ **YES,** send me my own personal copy of **Analytical Chemistry.**

Published monthly One Year	U.S.	Mexico & Canada	Europe	All Other Countries
ACS Members*	☐ $20	☐ $40	☐ $57	☐ $ 80
Nonmembers*	☐ $30	☐ $50	☐ $99	☐ $122

☐ Payment Enclosed (Payable to American Chemical Society)
☐ Bill Me ☐ Bill Company Charge my: ☐ VISA ☐ MasterCard

Card No. _____

Exp. Date _____ Interbank # _____ (Mastercard Only)

Signature _____

Name _____

Title _____ Employer _____

Address _____

City, State, Zip _____

Employer's Business: ☐ Manufacturing, type _____

☐ Academic ☐ Government ☐ Other _____

*Subscriptions at these rates are for personal use only.
All foreign subscriptions are now fulfilled by air delivery. Foreign payment must be made in U.S. currency by international money order, UNESCO coupons, U.S. bank draft, or order through your subscription agency. For nonmember subscription rates in Japan, contact Maruzen Co., Ltd.
Please allow 45 days for your first copy to be mailed.
Redeem until December 31, 1985. 1985

560 **MAIL THIS POSTAGE-PAID CARD TODAY!** 3144P



(800) 424-6747 (U.S. only)



NO POSTAGE NECESSARY IF MAILED IN THE UNITED STATES

BUSINESS REPLY CARD

FIRST CLASS PERMIT NO 10094 WASHINGTON D C

POSTAGE WILL BE PAID BY ADDRESSEE

American Chemical Society
Periodicals Marketing Dept.
1155 Sixteenth Street, N.W.
Washington, D.C. 20036



(800) 424-6747 (U.S. only)



NO POSTAGE NECESSARY IF MAILED IN THE UNITED STATES

BUSINESS REPLY CARD

FIRST CLASS PERMIT NO 10094 WASHINGTON D C

POSTAGE WILL BE PAID BY ADDRESSEE

American Chemical Society
Periodicals Marketing Dept.
1155 Sixteenth Street, N.W.
Washington, D.C. 20036

analytical chemistry

EDITOR: **GEORGE H. MORRISON**

EDITORIAL HEADQUARTERS
1155 Sixteenth St., N.W.
Washington, D.C. 20036
Phone: 202-872-4570 Teletype: 710-8220 151

Executive Editor: Josephine M. Petruzzi
Associate Editors: Stuart A. Borman, Marcia S. Vogel
Assistant Editors: Rani A. George, Louise Voress, Mary D. Warner
Production Manager: Leroy L. Corcoran
Art Director: Alan Kahan
Designer: Sharon Harris Wolfgang
Production Editor: Gail M. Mortenson
Circulation: Cynthia G. Smith
Editorial Assistant, LabGuide: Joanne Mullican

Journals Dept., Columbus, Ohio
Associate Head: Marianne Brogan
Associate Editor: Rodney L. Temos

Advisory Board: Shier S. Berman, Brian S. Bidlingmeyer, Henry N. Blount, Gary D. Christian, Dennis H. Evans, Jack W. Frazer, Gary M. Hieftje, William R. Heineman, Harry S. Hertz, Roland F. Hirsch, Atsushi Mizuike, Melvin W. Redmond, Jr., Herbert L. Retcofsky, Martin A. Rudat, Wilhelm Simon, Charles L. Wilkins. *Ex Officio:* Donald D. Bly

Instrumentation Advisory Panel: Richard S. Danchik, Thomas C. Farrar, Larry R. Faulkner, John F. Holland, F. James Holler, Peter N. Keliher, Curt Reimann, D. Warren Vidrine, Andrew T. Zander

Contributing Editor, A/C Interface: Raymond E. Dessy

The Analytical Approach Advisory Panel: Edward C. Dunlop, Robert A. Hofstader, Wilbur D. Shults

Published by the
AMERICAN CHEMICAL SOCIETY
1155 16th Street, N.W.
Washington, D.C. 20036

Books and Journals Division
Director: D. H. Michael Bowen
Journals: Charles R. Bertsch
Production: Elmer Pusey, Jr.
Research and Development: Lorrin R. Garson

Manuscript requirements are published in the January 1985 issue, page 395. Manuscripts for publication (4 copies) should be submitted to ANALYTICAL CHEMISTRY at the ACS Washington address.

The American Chemical Society and its editors assume no responsibility for the statements and opinions advanced by contributors. Views expressed in the editorials are those of the editors and do not necessarily represent the official position of the American Chemical Society.

Our National Analytical Laboratory

The National Bureau of Standards (NBS) occupies a special place in the lives of American analytical chemists. Although we immediately associate the bureau with its role as the provider of standard reference materials (SRMs) for the calibration of analytical instruments and the validation of new methods, the bureau plays a much larger role in servicing American science and industry in the field of measurement standards.

Founded in 1901, NBS has had a long and distinguished career in advancing the science of measurement in all areas. Originally located on 56 acres of land on Connecticut Avenue in Washington, D.C., it now resides on an impressive modern campus in Gaithersburg, Md.

With regard to analytical chemistry, William F. Hillebrand served as its first chief chemist from 1908 to 1925. A graduate of Cornell, he is particularly known for his methods for the analysis of silicate and carbonate rocks. Another giant in the field was G.E.F. Lundell, a Cornell graduate and faculty member, who served the NBS from 1917 to 1948 and was the acknowledged dean of applied analysis in the United States. Other pioneers in analytical chemistry at the bureau included E. Wichers and J. I. Hoffman.

Today the Center for Analytical Chemistry at the bureau has a staff of 154 (49% hold the PhD degree) under the leadership of Dr. Harry Hertz and performs a variety of important functions. Its mission is to serve as the nation's reference laboratory for chemical composition measurements. Among its objectives and services are the improvement of accuracy of chemical measurements, the development of measurement methods, the certification of SRMs, and the provision of information and advice. The center consists of three divisions: inorganic analytical research, organic analytical research, and gas and particulate science. Most of the modern analytical techniques are used at the center, and a broad base of expertise exists, so it can be thought of as our national analytical laboratory.

Analytical chemists are invited to visit the laboratories in Gaithersburg when they are in the Washington area. It is a worthwhile experience, and I thoroughly enjoyed my most recent visit there a few months ago. It should also be noted that the National Research Council provides competitive postdoctoral research fellowships for young chemists to work at NBS. This is an excellent opportunity for them to explore new areas of analytical research in a productive environment.

G. H. Morrison

Microprocessor-Controlled ex Vivo Monitoring of Sodium and Potassium Concentrations in Undiluted Urine with Ion-Selective Electrodes

Stephan Dütsch, Hans-Beat Jenny, Konrad J. Schlatter, Philippe M. J. Périsset, Gunther Wolff,[1] Jean Thomas Clerc,[2] Ernö Pretsch, and Wilhelm Simon*

Department of Organic Chemistry, Swiss Federal Institute of Technology, CH-8092 Zürich, Switzerland

A microprocessor-controlled system performing automatic ex vivo measurements of Na^+ and K^+ in urine using ion-selective liquid membrane electrodes was realized. A single drop flow-through measuring chamber allows for stable readouts even in undiluted urine samples and in the presence of sediments and gas bubbles. Ion concentrations are calculated by using an automatic calibration system and an iterative procedure for the evaluation of activity coefficients. Over a concentration range of 50–250 mmol L^{-1} (Na^+) and 5–120 mmol L^{-1} (K^+) the relative standard deviations between values measured with this system and by flame photometry were below 10%.

For routine measurements of sodium and potassium in clinical chemistry, flame photometry is successively replaced by ion-selective electrode techniques (*1*). Although there exist a series of instruments using ion-selective electrodes for Na^+ and K^+ determinations in urine (*2–9*), measurements in undiluted urine exhibited until recently a high bias (*10, 11*). With adequate membrane technology, this interference by lipophilic ions may be circumvented (*12*). This opens up the possibility for continuous ex vivo measurements of sodium and potassium in undiluted urine of catheterized patients. Efforts in this direction have recently been described (*13, 14*). There however still remain problems due to sediments, air bubbles, and extreme variation of ionic strength of the sample. Here we report on an automatic system resolving these sampling, calibration, and evaluation problems.

EXPERIMENTAL SECTION

Scheme of Instrument. A scheme of the instrument developed is given in Figure 1. Urine samples were taken by means of a peristaltic pump from a siphon, which was part of the bladder catheter assembly. This siphon separated the patient from the monitor to prevent any contamination. The sample then passed through a urine flow meter consisting of a drop counting, L1, and a drop volume calibrating device, L2 and L3 in Figure 1. The latter is necessary since the drop volume of undiluted urine can vary in a wide range. It consisted of a glass tube (o.d. 7 mm, i.d. 5 mm, length 12 cm) installed vertically at the outlet of the drop counter. At its lower end, the tube was equipped with an electromagnetically driven pinch valve (V8 in Figure 1; Angar Pinch Valve 373-12-5 E, Angar Scientific, Cedar Knolls, NJ) which allowed damming up the sample in the tube. Near the lower and the upper ends of the tube two optical levels detectors (L2 and L3 in Figure 1) were installed. Each of them consisted of a light emitting diode and of a phototransistor (TIL31 and TIL81, Texas Instruments, Dallas, TX) which were mounted at an angle ~120° to each other. In this arrangement the receiver detected the light reflected at the inner side of the glasswall of the empty tube. When the tube was filled with any aqueous solution, no optical total reflection occurred and therefore no signal was detected by the receiver. While the pinch valve V8 was held closed, the urine sample was transferred to the measuring chamber by means of a processor controlled peristaltic pump (P1 in Figure 1, capacity 11.7 mL/min). Excess sample flowed to the urine collector by opening the pinch valve V8. A pinch valve of the same type was applied after the measuring chamber (V7) which let urine samples pass to the urine collector and rinsing or calibrating solutions pass to the waste.

Ion-Selective Electrode Cell System. The silicone rubber membrane (*15*) of the K^+-selective minielectrode (*12*) consisted of 85.3 wt % Silopren K1000, 12.5 wt % cross-linking agent KA-1 (both obtained from Bayer AG, Leverkusen, GFR), and 2.2 wt % valinomycin (Fluka AG, Buchs, Switzerland). Electrode preparation and selectivity data are given in ref 12.

The membrane of the Na^+-selective minielectrode (*16*) was made of 66.0 wt % bis(1-butylphenyl) adipate (BBPA, Fluka AG, Buchs, Switzerland), 33.0 wt % PVC (S704, high molecular, Lonza AG, Visp, Switzerland), and 1.0 wt % sodium ionophore ETH 227 (1,1,1-tris[1′-(2′-oxa-4′-oxo-5′-aza-5′-methyl)dodecanyl]propane (*17*), Fluka AG, Buchs, Switzerland). Electrode preparation is given in ref 16. A slight improvement of the selectivity vs. K^+ in respect to reported values (*16*) was achieved through the choice of the plasticizer BBPA ($\log K^{Pot}_{NaK} = -1.94$).

A saturated calomel reference electrode Philips R44/2 (Joint removed, N. V. Phillips' Gloeilampenfabrieken, Eindhoven, The Netherlands) was used. Its liquid junction was formed by a zirconium oxide diaphragm at the end of a glass capillary (o.d. 1.1 mm, i.d. 1.0 mm, length 30 mm) filled with a 3 M NH_4Cl solution as bridge electrolyte. This glass capillary was fixed on the reference electrode body with a PVC gasket.

A platinum wire of 0.5 mm diameter served as a low impedance common electrode. The potential measurements were carried out in a differential mode (*18, 19*).

The four electrodes were arranged in the measuring chamber in such a way that it was possible to build up a hanging sample drop contacting all the electrodes but without touching the cell walls (see Figures 2 and 3). This setup allows samples containing gas bubbles as well as sediments to pass the sensitive area around the electrode tips without causing any troubles. Furthermore only small sample volumes of 50–70 μL are needed in spite of the relatively large dimension of the sensing electrodes of about 3 mm diameter. This dimension is necessary because of the high impedance (~10^9 Ω) of the silicone rubber electrode. In order to increase signal stability, the outside of the cell was covered with an aluminum sheet which was electrically grounded. The stray capacitance was reduced by connecting the shield to the output of the impedance converter. The common electrode was also grounded so that no static potential could build up in the sample drop.

The impedance converters (AD515KH, Analog Devices, Norwood, MA) are mounted directly on the electrodes. To each channel (two measuring and one reference electrode) its own bessel filter of fourth order is added (3 dB, frequency 16 Hz). The dominant part of the low frequency noise is synchronous to the line (50 Hz). It could be eliminated by taking the mean value of an even number of readings triggered by the two half waves of the line. With these precautions the drift and the noise of the measuring system were minimized so that a standard deviation of ±30 μV ($N = 15$) was measured over a time period of 5 h.

[1] Present address: Klinische Physiologie der Klinik für Herz- und Thoraxchirurgie, Kantonsspital Basel, 4031 Basel, Switzerland.
[2] Present address: Pharmazeutisches Institut, Universität Bern, Baltzerstrasse 5, 3012 Bern, Switzerland.

0003-2700/85/0357-0578$01.50/0 © 1985 American Chemical Society

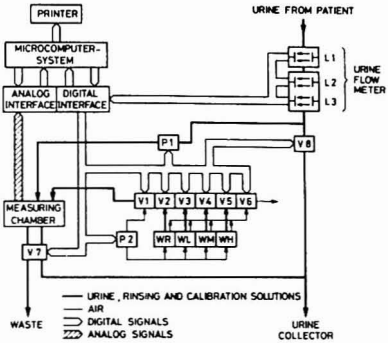


Figure 1. Scheme of the instrument: V1–V6, magnetic valves; V7, V8, pinch valves; L1, drop counter; L2, L3, optical level detectors; P1, peristaltic pump; P2, air pump; WR, rinsing solution; WL, WM, WH, calibration solutions.

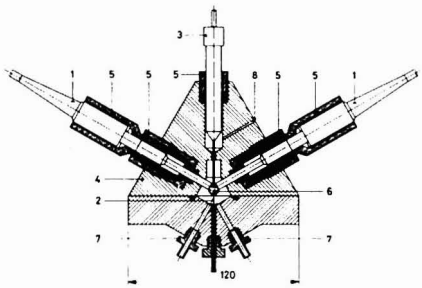


Figure 2. Cross section of the measuring chamber (front view): 1, impedance converters with minielectrodes; 2, common electrode (platinum wire); 3, reference electrode; 4, polypropylene body, the top and bottom part are screwed; 5, screwthreads for fixing the electrodes; 6, sample drop; 7, joints for outlet drains; 8, bore for pressure equalization.

For analog to digital conversion a 16-bit ADC (MN6280, Micro Network Corp., Worcester, MA) working by the method of successive approximation with a conversion time of less than 100 μs is used. The full scale is ±500 mV which corresponds to a resolution of 15.3 μV.

The electrodes were cleaned and recalibrated automatically with a 0.1 M H_3PO_4 rinsing solution (WR, Figure 1) and three calibrating solutions I to III containing NaCl and KCl within the physiological range of urine. The concentrations of NaCl and KCl were as follows: (given in units of mmol/L): I (WL) 60 and 40; II (WM) 100 and 66.7; III (WH) 180 and 120, respectively. All the solutions were transferred to the measuring cell by a slight overpressure produced by an aquarium air pump while they were selected by electromagnetic valves (LF AA 1200618H; The Lee Co., Westbrook, CT) controlled by the microprocessor.

Microcomputer System. The microcomputer system is based on an iSBC 80/20-4 (Intel Corp., Santa Clara, CA) single board. The 8080A microprocessor and the following components of this board are essential: 4K static RAM for storing program parameters and the measured results between two plot outputs; sockets for EPROM 2716; the software written in assembly level resides on 2 EPROMS (2732A-4), using about 7.5 kbytes; two parallel interface adapters 8255 for connecting the analog (multiplexer and ADC) and the digital (valves and pumps) interface; one serial interface adapter 8251 for driving the printer; one interrupt controller 8259 for generating the jump vectors of the five possible

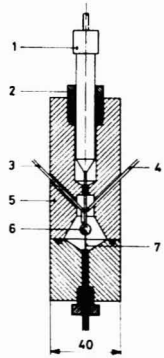


Figure 3. Cross section of the measuring chamber (side view): 1, reference electrode; 2, screwthreads for fixing the reference electrode; 3, inlet for rinsing and calibration solutions and air; 4, inlet for urine; 5, polypropylene body; 6, sample drop; 7, common electrode.

interrupts and for resolving their priority: (1) interrupt switch, (2) line trigger (100 Hz real time clock), (3) drop counter, (4) raising tube level detectors, (5) serial interface interrupt. Furthermore an AMC 95/6011 (Advanced Micro Computers, Santa Clara, CA) arithmetic processor board is added to perform 16- and 32-bit fixed point and 32-bit floating point arithmetic.

Although not necessary in routine operation there is a primitive way of changing program parameters by four BCD switches which are read when the interrupt switch on the front panel of the system has been pressed. Output in listed and plotted form is to a printer, Swiss-Print Matrix, Wenger Datentechnik, Basel, Switzerland.

Flame Photometry. Flame photometric determinations were performed at the Medico-Chemical Central Laboratory of the University Hospital Zürich by using a IL-343 flame photometer (Instrumentation Laboratory Inc., Lexington, MA). The urine samples were mixed with a 1 M LiCl, 1 M Li_2SO_4 solution and with double distilled water in the ratio of 1:1:200. The photometer was operated with a propane/air flame and calibrated with a solution of NaCl and KCl (120 mmol/L each).

RESULTS AND DISCUSSION

Operation of the System. After program start up no further operator interaction is required. A measuring cycle is started by closing the valve V8 (Figure 1) at the lower end of the raising tube. When the urine reaches the upper level detector (L2), a concentration determination is initialized and the actual drop volume is calculated. For a concentration determination the urine is transferred by the peristaltic pump P1 from the lower end of the tube into the measuring chamber. A new cycle is then started by opening the valve V8 and closing it again when the tube is empty.

Urine flow is measured by a drop counter (see Experimental Section). This measurement allows an estimate of the time, when a sample in the measuring cell has left the kidney. For this purpose each time 1 mL of urine has passed the drop counter, the data in the shift register representing the volume between the kidney and the measuring chamber are shifted by one position and the actual value of time is entered at the beginning of the register.

The synchronization of the measurement with the line frequency was performed with a line trigger interrupt. A/D conversion is started immediately after entry to this interrupt routine. Then the clock was updated and on exit the value from the ADC is stored if required. Every hour the system performed a rinsing and a three point calibration of the electrodes. The stability of each potential and the quality of the linear regression applied to the calibration points of each

Table I. Influence of the Iterative Evaluation of Concentrations on the Linear Correlation between the Results of Potentiometric and Flame Photometric Measurements of Sodium in Urine

coefficients[a]	values not corrected for ionic strength[b]	values corrected for ionic strength[c]
A	−6.01 ± 2.79 mM	−0.35 ± 2.25 mM
B	1.05 ± 0.02	1.00 ± 0.001
s	4.1 mM	3.3 mM

[a] $Y = A\ (\pm s_A) + B\ (\pm s_B) \cdot X$: Y, ion selective electrode measurements; X, flame photometric measurements, range 26–265 mM, mean 165 mM; s, residual standard deviation; number of samples, 21. [b] Calibration based on concentration values. [c] Calbration based on activity values.

electrode were checked before the values were accepted.

Evaluation of the Concentrations. Since the ionic strength of urine samples can vary over a range of more than 1 order of magnitude, no reliable direct determination of the concentration is possible. The measured values of activities were therefore converted into concentrations by an iterative procedure. Starting with assumed single ion activity coefficients of $\gamma_i = 0.7$, a first estimate of Na^+ and K^+ concentrations was calculated. Assuming that only Na^+, K^+, and Cl^- are present, the ionic strength I was then evaluated. With this ionic strength value the next estimate of the activity coefficients was computed by the Debye–Hückel formalism (*20–22*)

$$\log \gamma_{\pm} = -\frac{0.5108 I^{1/2}}{1 + 0.328 A_i I^{1/2}} + B_i I \qquad (1)$$

$\gamma_{\pm}$ is the mean ion activity coefficient. Since monovalent ions dominate in urine, we assume that $\gamma_i = \gamma_{\pm}$. A_i and B_i are 4.35 and 0.026 for NaCl and 3.90 and 0.004 for KCl, respectively. This allowed a next estimation of the ionic strength. After three cycles of this iteration procedure the calculated γ_i values were stable within 1%. This procedure improves the linear correlation between the results of potentiometric and flame photometric measurements of sodium significantly (see Table I).

Application to Open Heart Surgery. The system described has been repeatedly used in intensive care units and during open heart surgery. A fully automatic run obtained during an operation for valve replacement at extracorporeal circulation is represented in Figure 4 together with values (dots) determined by flame photometry. Artifacts may be due to the rather large dead space volume between the localization of glomerular filtration of urine and sensor assembly. This dead space volume consists of the intrarenal volume of the tubular system and the pyelon, of the ureters, emptying the peristaltic contraction, of a very small residual volume of the drained urine bladder and of the constant volume of the urine catheter itself including the draining and measuring system outside the patient. Total dead space volume of both kidneys estimated after intravenous injection of a rapidly filtered indicator sums up to 30–40 mL in the healthy adult. The contribution of the catheter amounts to about 90%.

Flame photometric reference values were taken from the samples in the raising tube after performing the potentiometric measurements. Although the samples for both measurements were not strictly identical, the agreement with a relative standard deviation of about 7% is compatible with the values given in Table I which, after conversion to the relative scale, are about 2%. This compares well with the corresponding value of 1.8% obtained earlier with a different cell assembly (*23*).

In about 20 runs up to 24 h of a development and test phase of the monitor, no deterioration of the sensor performance

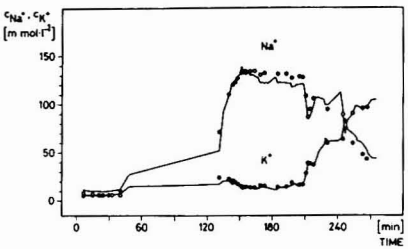


Figure 4. Automatic on-line determination of Na^+ and K^+ concentrations in urine during open heart surgery. The symbols ○ and ● mark flame photometric determinations.

was observed, if the rinsing procedure described above was strictly applied. In all systems applying liquid membrane electrodes, the inherent problem of possible interferences of lipophilic ionic species must however be kept in mind (*10, 11*).

ACKNOWLEDGMENT

We thank R. Asper for performing flame photometric measurements in the Medico-chemical Central Laboratory of the University Hospital Zürich.

Registry No. Na, 7440-23-5; K, 7440-09-7.

LITERATURE CITED

(1) Schindler, J. G.; Schindler, M. M. "Bioelektrochemische Membran-Elektroden"; de Gruyter: Berlin, New York, 1983.
(2) Epstein, E. E. *Clin. Chem. (Winston-Salem, N.C.)* **1981**, *27*, 1111.
(3) Chan, D. W.; White, J. *Clin. Chem. (Winston-Salem, N.C.)* **1981**, *27*, 1111.
(4) Blumenfeld, T. A.; Griffith, B. *Clin. Chem. (Winston-Salem, N.C.)* **1980**, *26*, 1883.
(5) Keller, M.; Niederer, R.; Richter, W. *Biomed. Tech.* **1980**, *25*, 42.
(6) Pelleg, A.; Levy, G. B. *Clin. Chem. (Winston-Salem, N.C.)* **1975**, *21*, 1572.
(7) Koch, D. D.; Parrish, D.; Ladenson, J. H. *Clin. Chem. (Winston-Salem, N.C.)* **1981**, *27*, 1110.
(8) Ladenson, J. H. *Clin. Chem. (Winston-Salem, N.C.)* **1979**, *25*, 757.
(9) Lambert, W. J.; Byrnes, R. J. *Clin. Chem. (Winston-Salem, N.C.)* **1981**, *27*, 1110.
(10) Koch, D. D.; Ladenson, J. H. *Anal. Chem.* **1983**, *55*, 1807.
(11) Koch, D. D.; Parrish, D.; Ladenson, J. H. *Clin. Chem. (Winston-Salem, N.C.)* **1983**, *29*, 1090.
(12) Jenney, H.-B.; Riess, C.; Ammann, D.; Magyar, B.; Asper, R.; Simon, W. *Mikrochim. Acta* **1980**, *II*, 309.
(13) Nikkiso, Co., Ltd. Jpn. Kokai Tokkyo Koho, Japan Patent No. 58 155 353; 16.9.1983.
(14) Toshiba Corp., Jpn. Kokai Tokkyo Koho, Japan Patent No. 81 155 850; 2.12.1981.
(15) Lindner, E.; Wuhrmann, P.; Simon, W.; Pungor, E. Proceedings of the 2nd Symposium on Ion-Selective Electrodes, Matrafüred, Hungary, Oct 18–21, 1976; "Ion-Selective Electrodes"; Pungor, E., Buzas, I., Eds.; Akadémial Klado: Budapest, 1977; p 159.
(16) Jenny, H.-B.; Ammann, D.; Dörig, R.; Magyar, B.; Asper, R.; Simon, W. *Mikrochim. Acta* **1980**, *II*, 125.
(17) Güggi, M.; Oehme, M.; Pretsch, E.; Simon, W. *Helv. Chim. Acta* **1976**, *59*, 2417.
(18) Brand, M. J. D.; Rechnitz, G. A. *Anal. Chem.* **1970**, *42*, 616.
(19) Osswald, H. F.; Asper, R.; Dimal, W.; Simon, W. *Clin. Chem. (Winston-Salem, N.C.)* **1979**, *25*, 39.
(20) Robinson, R. A.; Stokes, R. M. "Electrolyte Solutions"; Butterworth: London, 1968.
(21) Bates, R. G.; Alfenaar, M. In "Ion-Selective Electrodes"; Durst, R. A. Ed.; National Bureau of Standards: Washington, DC, 1969; Special Publication 314.
(22) Meier, P. C. *Anal. Chim. Acta* **1982**, *136*, 363.
(23) Anker, P.; Jenny, H.-B.; Wuthier, U.; Asper, R.; Ammann, D.; Simon, W. *Clin. Chem. (Winston-Salem, N.C.)* **1983**, *29*, 1508.

RECEIVED for review October 1, 1984. Accepted November 26, 1984. This work was partly supported by the Eidgenössische Stiftung zur Förderung der Schweizerischen Volkswirtschaft durch wissenschaftliche Forschung and by the Schweizerischer Nationalfonds zur Förderung der wissenschaftlichen Forschung.

Potentiometric Stripping Analysis: Theory, Experimental Verification, and Generation of Stripping Polarograms

Abul Hussam and J. F. Coetzee*

Department of Chemistry, University of Pittsburgh, Pittsburgh, Pennsylvania 15260

The theory for potentiometric stripping analysis is presented. Equations based on an assumed initial parabolic concentration gradient of the metal amalgam are derived for the transient potential as a function of time and for the transition time. Results are compared for conventional electrodes and for fiber microelectrodes. In addition, the theoretical basis for the generation of stripping (pseudo-) polarograms by potentiometric stripping analysis is also presented. Experimental verification of some of the theoretical relationships is provided.

Potentiometric stripping analysis (PSA) is a useful and relatively new trace analytical tool (*1*). It differs from the much better known voltammetric stripping analysis (VSA) in that the preconcentrated analyte is stripped chemically, rather than electrochemically. The two techniques are compared in Table I. Both oxidative (*1*) and reductive (*2*) PSA, corresponding to anodic and cathodic VSA, have been developed. We have recently extended PSA to the determination of the alkali metal ions in aqueous samples by addition of appropriate cosolvents (*3*).

Although PSA already has been widely exploited for analytical purposes, its underlying theory has not been sufficiently examined. We have recently (*3*) reported equations for the transition time and the transient potential in PSA; these were based on an assumed time-independent concentration gradient of the metal ion during stripping. At approximately the same time, Chau et al. (*4*) presented a theoretical treatment based on an assumed initial linear concentration gradient of the metal in the mercury electrode and of a time-dependent concentration gradient of the metal ion during stripping. They further assumed that the diffusion layer thickness of the metal ion remains unchanged during stripping. Experimental proof was provided for the case of deposition in a stirred solution and stripping in a quiet solution, conditions similar to those used in VSA. In this paper, we consider an initial parabolic concentration gradient of the metal in mercury, which is a more realistic model, and stripping in a stirred solution, which is the usual condition for PSA. Relationships derived for macroelectrodes and for microelectrodes (fibers) are compared. We also consider the effect of the deposition potential on the stripping time and of its application in the generation of stripping (or pseudo-) polarograms. Finally, advantages and limitations of PSA in the speciation of metal ions are compared with those of VSA.

THEORY

Concentration gradients during the two steps (1 and 2.2) outlined in Table I are shown schematically in Figure 1. Since two uncoupled diffusion processes are involved, two variables (x and y) are used.

Step 1. Potentiostatic Deposition. The general expression for the current resulting from the potentiostatic deposition of the metal as a function of deposition time, t_d, is

$$i(t_d) = nFAk[C_{M^{n+}}(y = 0,t_d)\exp(-\alpha\theta) - C_R(x = l,t_d)\exp[(1 - \alpha)\theta]] \quad (1)$$

Table I. Comparison of Potentiometric Stripping Analysis with Voltammetric Stripping Analysis

1. Deposition (Preconcentration) Step
   $M^{n+} + ne + xHg \rightarrow M(Hg)_x$
   electrode: thin film of mercury on glassy carbon substrate
2. Stripping Step
   2.1 voltammetric stripping
   $M(Hg)_x - ne \rightarrow M^{n+} + xHg$
   monitor i or $\Delta i = f(E)$
   2.2 potentiometric stripping
   $M(Hg)_x + (n/2)Hg^{2+} \rightarrow M^{n+} + (x + n/2)Hg$
   monitor $E = f(t)$

where k is the formal rate constant for the deposition reaction at a potential E_d, $C_{M^{n+}}(y = 0,t_d)$ and $C_R(x = l,t_d)$ are the surface concentrations of the metal ion and the reduced metal, A is the area of the electrode, α is the transfer coefficient, $\theta = (nF/RT)(E_d - E°)$, and all other terms have their usual meaning. For a stirred solution and assuming that the concentration of M^{n+} does not change appreciably during the deposition time, eq 2 applies

$$C_{M^{n+}}(y = 0,t_d) = C°_{M^{n+}} - \frac{i(t_d)}{nFA}\left(\frac{\delta}{D}\right)_{M^{n+}} \quad (2)$$

where D is the diffusion coefficient, δ is the diffusion layer thickness, and $C°_{M^{n+}}$ is the bulk concentration of the metal ion. De Vries and Van Dalen (*5*, *6*) have shown that the reduced metal concentration profile $C_R(x,t_d)$ in the mercury film is best approximated by

$$C_R(x,t_d) = C°_R + kx^2 \quad (3)$$

where

$$C°_R = \frac{i(t_d)t_d}{nFAl} - \frac{i(t_d)l}{6nFAD_R} \quad (4)$$

and

$$k = \frac{i(t_d)}{2nFAD_Rl} \quad (5)$$

Here, D_R is the diffusion coefficient of the metal in the mercury phase and l is the thickness of the mercury film. Equation 3 will become more and more accurate at increasing t_d and decreasing l, and should apply to typical PSA experiments. The surface concentration of the amalgam, $C_R(x = l,t_d)$, can then be calculated from eq 3

$$C_R(x = l,t_d) = \frac{i(t_d)}{nFA}\left(\frac{t_d}{l} + \frac{l}{3D_R}\right) \quad (6)$$

By use of eq 1, 2, and 6, the potentiostatic deposition current can be expressed by the relation

$$i(t_d) = \frac{nFAC°_{M^{n+}}}{\left(\frac{\delta}{D}\right)_{M^{n+}} + \frac{\exp(\alpha\theta)}{k} + \left(\frac{t_d}{l} + \frac{l}{3D_R}\right)\exp(\theta)} \quad (7)$$

Therefore, at any deposition potential, $C°_R$ and k can be calculated by using eq 4, 5, and 7.

0003-2700/85/0357-0581$01.50/0 © 1985 American Chemical Society

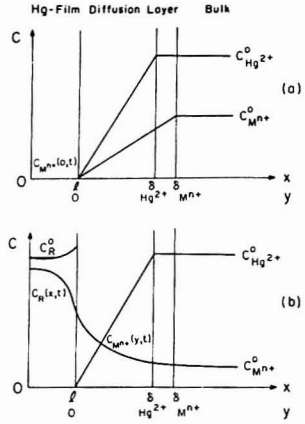


Figure 1. Assumed concentration profiles during (a) potentiostatic deposition and (b) potentiometric stripping.

Step 2.2. Stripping of the Deposited Metal by an Oxidizing Agent. To calculate the change of C_R as a function of the transient time, t, Fick's second law for the linear diffusion of R in the mercury film under proper initial and boundary conditions must be solved

$$0 < x < l: \quad \frac{\partial C_R}{\partial t} = D_R \frac{\partial^2 C_R}{\partial x^2} \tag{8}$$

At $t = 0$, the potentiostatic control is removed and the potential of the mercury electrode is monitored as a function of time. The initial and boundary conditions are given in eq 9–12, where $J_{Hg^{2+}}$ represents the flux of the stripping agent, mercury(II) ion.

$$t = 0,\ 0 < x < l: \quad C_R = C^{\circ}_R + kx^2 \tag{9}$$

$$t > 0: \quad J_{Hg^{2+}} = \left(\frac{D}{\delta}\right)_{Hg^{2+}} C^{\circ}_{Hg^{2+}} \tag{10}$$

$$t > 0,\ x = l: \quad D_R\left(\frac{\partial C_R}{\partial x}\right) = -J_{Hg^{2+}}\left(\frac{2}{n}\right) \tag{11}$$

$$t > 0,\ x = 0: \quad D_R\left(\frac{\partial C_R}{\partial x}\right) = 0 \tag{12}$$

The initial condition (eq 9) states that C_R is a parabolic function of x. Unlike in VSA, in PSA the stripping process begins immediately after the deposition step; therefore, a parabolic gradient is a realistic one. The boundary condition in eq 10 is valid only for a stirred solution; $J_{Hg^{2+}}$ during stripping in a stationary solution is a time-dependent function related by the Cottrell equation $J_{Hg^{2+}}(\text{stationary}) = D^{1/2}_{Hg^{2+}} C^{\circ}_{Hg^{2+}}/(\pi t)^{1/2}$, making eq 8 more difficult to solve. Solving eq 8 for $C_R(x = l,t)$ by conventional Laplace transformation, eq 13 is obtained.

$$C_R(l,t) = C^{\circ}_R + kl^2 + 2kD_R t - \left(2kl + \frac{2J_{Hg^{2+}}}{nD_R}\right)(2)\left(\frac{D_R t}{\pi}\right)^{1/2}\left[\sum_{j=0}^{\infty}\left\{\exp\left(-\frac{j^2 l^2}{D_R t}\right) + \exp\left(-\frac{l^2(j+1)^2}{D_R t}\right)\right\} - l\left(\frac{\pi}{D_R t}\right)^{1/2}\sum_{j=1}^{\infty} j\ \text{erfc}\ \frac{jl}{(D_R t)^{1/2}}\right] \tag{13}$$

Equation 13 can be generalized for any oxidant (ox) by simply replacing $J_{Hg^{2+}}$ in eq 10 by J_{ox}. For values of $l/(D_R t)^{1/2}$ much less than unity, the term in brackets in eq 13 reduces to $(\pi D_R t)^{1/2}/2l$. Equation 13 then can be simplified to

$$C_R(l,t) = C^{\circ}_R + kl^2 - \frac{2J_{Hg^{2+}} t}{nl} \tag{14}$$

When t is equal to the transition time, τ', $C_R(l,\tau') = 0$, so that

$$\tau' = (C^{\circ}_R + kl^2)\frac{nl}{2J_{Hg^{2+}}} \tag{15}$$

Inserting eq 4, 5, 7, and 10 for C°_R, k, $i(t_d)$, and $J_{Hg^{2+}}$, respectively, into eq 15, eq 16 is obtained

$$\tau' = \left(\frac{n}{2}\right)\frac{C^{\circ}_{M^{n+}}}{C^{\circ}_{Hg^{2+}}}\left(\frac{\delta}{D}\right)_{Hg^{2+}} \times \frac{t_d + l^2/3D_R}{\left(\frac{\delta}{D}\right)_{M^{n+}} + \frac{\exp(\alpha\theta)}{k} + \left(\frac{t_d}{l} + \frac{l}{3D_R}\right)\exp(\theta)} \tag{16}$$

This is the general equation for the transition time obtained when the metal ion is deposited at a potential E_d for any time t_d and then stripped with a constant oxidant flux, both steps being carried out in a stirred solution. Equation 16 is related to the equations for "stripping polarograms" ("pseudopolarograms") given by Zirino (7) and Brown (8). Stripping polarograms generated by linear sweep or staircase voltammetry have been successfully applied to the study of metal ion speciation in very dilute solutions such as natural water. Equation 16 predicts that the same purpose can be accomplished by PSA.

For a reversible deposition reaction and when $E_d << E^{\circ}$, $\exp(\alpha\theta)/k$ and $(t_d/l + l/3D_R)\exp(\theta)$ can be neglected in comparison to $(\delta/D)_{M^{n+}}$. Also, for a sufficiently thin mercury film and long deposition time, it can be assumed that $t_d >> l^2/3D_R$. Equation 16 then takes the simple form

$$\tau = \frac{n}{2}\frac{C^{\circ}_{M^{n+}}}{C^{\circ}_{Hg^{2+}}}\frac{D_{M^{n+}}}{D_{Hg^{2+}}} t_d \tag{17}$$

This is the theoretical basis for quantitative applications of PSA. It shows that under the assumed conditions, all reduced metal is removed from the thin mercury film at the transition time, so that successive stripping transitions should be free of any cumulative effect of preceding oxidations, a distinct advantage over the bulk mercury electrode. Transition times directly proportional to concentration of analyte have also been observed in chronopotentiometry in a thin-layer cell (9), chronopotentiometry with $i \propto t^{1/2}$ (10) and chronopotentiometric stripping analysis at a thin-film mercury electrode (11).

Calculation of $C_{M^{n+}}(y,t)$. To find the concentration of M^{n+} in the diffusion layer of the solution phase during the stripping process, the diffusion equation

$$\frac{\partial C_{M^{n+}}(y,t)}{\partial t} = D_{M^{n+}}\frac{\partial^2 C_{M^{n+}}(y,t)}{\partial y^2} \tag{18}$$

must be solved with the following initial and boundary conditions:

$$t = 0,\ 0 < y < \delta: \quad C_{M^{n+}}(y,0) = C^{\circ}_{M^{n+}}(y/\delta) \tag{19}$$

$$t > 0,\ y = 0: \quad D_{M^{n+}}\left(\frac{\partial C_{M^{n+}}}{\partial y}\right) = -2J_{Hg^{2+}}/n \tag{20}$$

$$t > 0,\ y = \delta: \quad C_{M^{n+}}(\delta,t) = C^{\circ}_{M^{n+}} \tag{21}$$

The solution of eq 18 at $y = 0$ is

$$C_{M^{n+}}(0,t) = \frac{4C^\circ_{Hg^{2+}}}{n}\frac{(Dt)^{1/2}}{\delta}\left[\pi^{1/2} + 2\sum_{j=1}^{\infty}(-1)^j i \operatorname{erfc}\frac{j\delta}{(Dt)^{1/2}}\right] \quad (22)$$

When $\delta/(Dt)^{1/2} >> 3$, the term in the summation part of eq 22 becomes less than 0.0001, meaning that it can be neglected when $t > 10$ ms (for $\delta = 10^{-3}$ cm and $D = 10^{-5}$ cm^2 s^{-1}). With this approximation, eq 23 is obtained.

$$C_{M^{n+}}(0,t) = \frac{4}{n}C^\circ_{Hg^{2+}}\left(\frac{Dt}{\delta^2\pi}\right)^{1/2} \quad (23)$$

If it is assumed that a steady state concentration of M^{n+} is reached after a short time, then $C_{M^{n+}}(0,t)$ can be derived from Fick's first law.

$$C_{M^{n+}}(0,t) = \left(\frac{D}{\delta}\right)_{Hg^{2+}}\left(\frac{\delta}{D}\right)_{M^{n+}}\left(\frac{2}{n}\right)C^\circ_{Hg^{2+}} + C^\circ_{M^{n+}} \quad (24)$$

For an electrode whose radius is greater than the diffusion layer thickness, δ, eq 23 describes $C_{M^{n+}}(0,t)$, while for a planar microelectrode (radius ~ 5 μm), or at a high stirring rate, a constant concentration gradient of M^{n+} will be established within a few milliseconds after stripping begins; eq 24 then describes $C_{M^{n+}}(0,t)$ adequately. This time-independent concentration gradient is a unique property of microelectrodes for which simpler mathematical expressions therefore can be used. The applications of microelectrodes in PSA will be described elsewhere (*12*).

Shape of the Transient Potential–Time Curve. The Nernst equation during the stripping process can be written in the form

$$E_t = E^\circ - \frac{RT}{nF}\ln\frac{C_R(l,t)}{C_{M^{n+}}(0,t)} \quad (25)$$

Substituting eq 14 and 23 into eq 25, and assuming that $E_d << E^\circ$, $t_d >> l^2/3D_R$ and $D_{M^{n+}} = D_{Hg^{2+}}$, eq 26 is obtained

$$E_t = E^\circ - \frac{RT}{nF}\ln\left\{n\left(\frac{\pi D\tau}{2l^2}\right)^{1/2}\right\} - \frac{RT}{nF}\ln\left\{\frac{(1-\phi)}{\phi^{1/2}}\right\} \quad (26)$$

where $\phi = t/\tau$. At $t = \tau/2$, eq 27 applies

$$E_{\tau/2} = E^\circ - \frac{RT}{nF}\ln\left\{\frac{n}{2}\left(\frac{\pi D\tau}{l^2}\right)^{1/2}\right\} \quad (27)$$

For a planar microelectrode (graphite or noble metal fiber), the transient potential E_t can be obtained from eq 14, 24, and 25, assuming that $C^\circ_{Hg^{2+}} >> C^\circ_{M^{n+}}$.

$$E_t = E^\circ - \frac{RT}{nF}\ln\left(\frac{D\tau}{\delta l}\right) - \frac{RT}{nF}\ln(1-\phi) \quad (28)$$

Therefore, for a microelectrode, the initial drop in the transient potential will occur faster than that for a macroelectrode. The analogous expression for the transient potential in chronopotentiometric stripping at a thin mercury film is given by eq 29

$$E_t = E^\circ - \frac{RT}{nF}\ln\left\{\frac{1}{2}\left(\frac{\pi D\tau}{l^2}\right)^{1/2}\right\} - \frac{RT}{nF}\ln\left\{\frac{(1-\phi)}{\phi^{1/2}}\right\} \quad (29)$$

which differs from eq 26 only in the second term (the potentiometric part) and which is the same in the time-dependent part. This shows that whether oxidation of the deposited amalgam is carried out by a constant oxidant flux or by a constant current in a stirred solution, the shape of the transient potential–time curve will be the same.

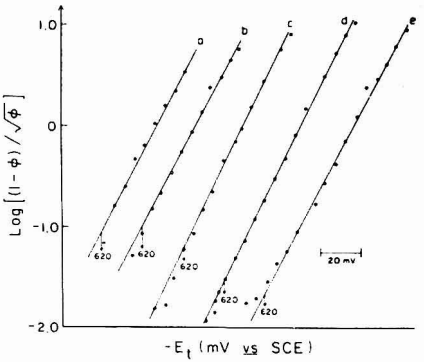


Figure 2. Plot of eq 26 for deaerated aqueous solution containing 2 × 10^{-5} M $Cd(ClO_4)_2$ + 5 × 10^{-4} M $HgCl_2$ + 1 × 10^{-1} M $NaClO_4$, adjusted to pH 2.1 with $HClO_4$; $E_d = -1.0$ V vs. SCE. Lines a through e apply to deposition times of 60, 120, 240, 480 and 960 s, respectively, and are offset by 20 mV for clarity.

Table II. Potentiometric Stripping Analysis of Cadmium: Theoretical vs. Experimental Correlation[a]

run no	t_d, s	τ, s	$-E_{\tau/2}{}^c$ (mV vs. SCE)	$-E_{\tau/2}{}^b$ (mV vs. SCE)	slope,[c] mV
1	60	1.41	637.5	641.0	26.0
2	120	3.20	641.5	644.0	28.0
3	240	6.60	646.0	648.0	26.0
4	480	13.50	652.0	654.0	26.0
5	960	26.80	660.0	660.0	28.5

[a] From the experimental response at $t = \tau/2$. [b] From the plot of log $[(1-\phi)/\phi^{1/2}]$ vs. $-E_t$ at $\phi = 1/2$. [c] Slope of the plot of footnote *b*. [d] Conditions: 2 × 10^{-5} M $Cd(ClO_4)_2$ + 5 × 10^{-4} M $HgCl_2$ + 1 × 10^{-1} M $NaClO_4$, pH 2.1 by adding $HClO_4$, deaerated; $E_d = -1.0$ V vs. SCE.

EXPERIMENTAL SECTION

Experiments were carried out as described before (*3*), except that data were collected with an Aminco DASAR system, using sampling times of 20, 50, or 100 ms, depending on the transition time, and using a time constant of 50 ms. Potentials were measured against the Ag^+ (acetonitrile)/Ag reference electrode (*3*) when dimethyl sulfoxide was the solvent, and against the saturated calomel electrode (SCE) when water was the solvent; the potential of the Ag^+/Ag electrode is +0.30 V vs. SCE.

RESULTS AND DISCUSSION

Transient Potential–Time Relationship. Figure 2 provides experimental proof of eq 26 for five different deposition times for cadmium in water. In Table II, further proof is provided by comparing $E_{\tau/2}$ values derived from such plots to values read directly from the original E_t vs. t responses; agreement is reasonable. The data also show that the transition time is less sensitive to the nature of the mercury film than transient potentials are.

Figure 3 provides a test of eq 27. The slope of the plot is 30.5 mV, in reasonable agreement with the theoretical value of 29.6 mV. From the intercept at $\tau = 1$, E° can be calculated from eq 27 if D and l are known. Equation 26 also predicts a dependence of transient potentials on the dimensionless parameter $D\tau/l^2$; this dependence is illustrated in Figure 4.

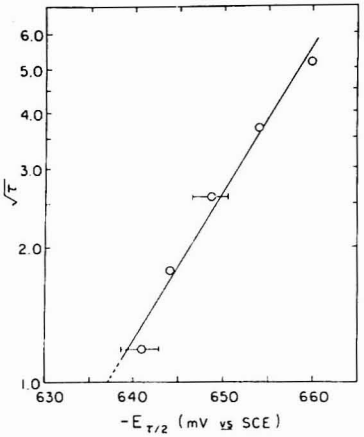


Figure 3. Plot of eq 27 for the same system as in Figure 2 and Table II. Error bars represent estimated experimental uncertainty of ±2 mV.

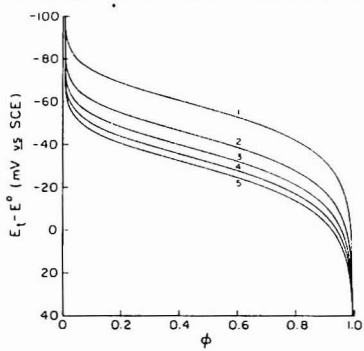


Figure 4. Theoretical dependence of transient potential–time curves on values of $D\tau/l^2$ (eq 26). Curves 1 through 5 apply to values of 2380, 595, 264, 148, and 95, respectively.

Generation of Stripping Polarograms. Equation 16 can be rewritten for the special case of a reversible deposition reaction at a thin-film electrode in the following form:

$$E_d = E^\circ + \frac{RT}{nF} \ln (\delta l/Dt_d) + \frac{RT}{nF} \ln \{(\tau - \tau')/\tau'\} \qquad (30)$$

In Figure 5, curves a and b are plots of the normalized response, τ'/τ, vs. the deposition potential for cadmium in water and sodium in dimethyl sulfoxide. Such plots are "stripping polarograms". It should be possible to use such plots to study the speciation of metal ions at concentrations too low to permit the direct use of voltammetry, in the same way as analogous plots based on voltammetric stripping have been used (*8*). For such purposes, PSA has the advantage over VSA that the stripping polarograms can be generated more quickly. Plots c and d (reciprocal slopes = 29 ± 2 and 62 ± 2 mV) show that eq 30 applies. It is noteworthy that no significant corrosion of sodium amalgam occurred in dimethyl sulfoxide during the duration of the experiments.

Maximum Surface Concentration of the Metal Ion and Formation of Interfering Precipitates on the Electrode Surface. A potential complication in PSA is that the concentration of the stripped metal ion at the electrode surface may become sufficiently high to induce precipitation of compounds of the metal ion on the electrode surface, thereby interfering with the stripping process. This is a complication, not only in PSA but in all stripping techniques, and it has been treated in detail by Buffle (*13*). The maximum value of $C_{M^{n+}}$ in eq 23 is given when $t \to \tau$, so that

$$(C_{M^{n+}})_{max} = (4/n)C^\circ_{Hg^{2+}}(D\tau/\delta^2\pi)^{1/2} \qquad (31)$$

By use of the same numbers as Buffle (t_d = 300 s, $C^\circ_{M^{2+}} = 1 \times 10^{-8}$ M, $C^\circ_{Hg^{2+}} = 5 \times 10^{-6}$ M, $D = 1 \times 10^{-5}$ cm^2 s^{-1}, and $\delta = 3 \times 10^{-3}$ cm), eq 17 and 31 predict a $(C_{M^{2+}})_{max}$ value of 4.6×10^{-6} M, which is 9 times larger than the value calculated by Buffle. The discrepancy is caused by Buffle's assumption of a time-independent concentration gradient of M^{2+} during the stripping process, which is not strictly valid for stripping at a macroelectrode. From eq 31, the maximum concentration of an anion, A^{m-}, that may be present without causing precipitation of M_mA_n can be calculated if the solubility product of M_mA_n is known. Equations 17 and 31 also show that such precipitation problems can be minimized by using lower concentrations of the stripping agent and by decreasing the diffusion layer thickness by increasing the stirring rate (or by using a microelectrode). Examples of complications caused by precipitation on the electrode surface in the stripping analysis of natural water samples have been discussed by Buffle. Another example is the precipitation of (highly insoluble) alkali and alkaline-earth metal hydroxides in aprotic solvents caused by reaction of residual water with the highly reactive amalgams (*3*).

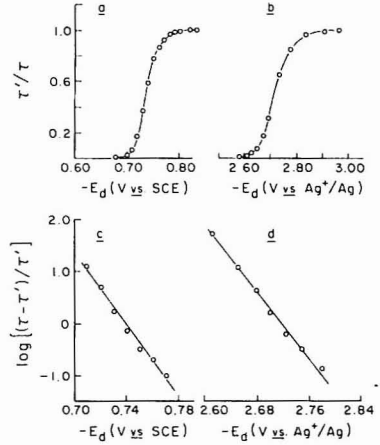


Figure 5. Stripping polarograms generated by potentiometric stripping analysis: (a) Cd in water, with 1×10^{-5} M $Cd(NO_3)_2$ + 1×10^{-4} M $HgCl_2$ + 1×10^{-1} M KCl, and t_d = 120 s; (b) Na in dimethyl sulfoxide, with 4×10^{-4} M NaCl + 1×10^{-3} M $HgCl_2$ + 1×10^{-1} M Et_4NClO_4, and t_d = 60 s; (c) plot of eq 30 for data of curve a; (d) plot of eq 30 for data of curve b.

Other Considerations. Operationally, potentiometric stripping analysis differs from chronopotentiometric stripping analysis (CPSA) only in that stripping is carried out with a constant stripping agent flux in PSA but with a constant current in CPSA. Like CPSA (and VSA), PSA is not free from perturbations caused by double layer charging (*14*), although this problem is less important at microelectrodes. However,

PSA is free from errors caused by iR drop and by the presence of oxidizable impurities in solution.

In conclusion, the theory presented in this paper applies to stripping in a stirred solution. For the case of stripping in a stationary solution, when the flux of the stripping agent is a function of time, it may still be possible to solve the diffusion equations (*15*). It also would be interesting to study the kinetics of metal ion complexation during stripping into solutions containing ligands; the advantages of using flow cells for such purposes have been pointed out by Jagner et al. (*16*). The theory for such processes can be worked out by including the proper kinetic terms in the diffusion equations. Finally the use of microelectrodes (graphite or noble metal fibers) offers special advantages for PSA, as shown by eq 28 and also by other considerations; we shall report elsewhere (*12*) experimental proof that these expectations can be realized.

ACKNOWLEDGMENT

We thank S. G. Weber of this department for valuable discussions.

LITERATURE CITED

(1) Jagner, D.; Aren, K. *Anal. Chim. Acta* **1978**, *100*, 375.
(2) Christensen, J. K.; Kryger, L.; Mortensen, J.; Rasmussen, J. *Anal. Chim. Acta* **1980**, *121*, 71.
(3) Coetzee, J. F.; Hussam, A.; Petrick, T. R. *Anal. Chem.* **1983**, *55*, 120.
(4) Chau, T. C.; Li, D. Y.; Wu, Y. L. *Talanta* **1982**, *29*, 1083.
(5) De Vries, W. T.; Van Dalen, E. *J. Electroanal. Chem.* **1964**, *8*, 366.
(6) De Vries, W. T.; Van Dalen, E. *J. Electroanal. Chem.* **1967**, *14*, 315.
(7) Zirino, A.; Kounaves, S. P. *Anal. Chem.* **1977**, *49*, 56.
(8) Brown, S. D.; Kowalski, B. R. *Anal. Chem.* **1979**, *51*, 2133.
(9) Christensen, C. R.; Anson, F. C. *Anal. Chem.* **1963**, *35*, 205.
(10) Hurwitz, H.; Gierst, L. *J. Electroanal. Chem.* **1961**, *2*, 128.
(11) Perone, S. P.; Brumfield, A. *J. Electroanal. Chem.* **1967**, *13*, 124.
(12) Coetzee, J. F.; Hussam, A., unpublished results, University of Pittsburgh, 1984.
(13) Buffle, J. *J. Electroanal. Chem.* **1981**, *125*, 273.
(14) Mortensen, J.; Britz, D. *Anal. Chim. Acta* **1981**, *131*, 159.
(15) Hussam, A. Ph.D. Thesis, University of Pittsburgh, 1982.
(16) Anderson, L.; Jagner, D.; Josefson, M. *Anal. Chem.* **1982**, *54*, 1371.

RECEIVED for review August 2, 1984. Accepted November 16, 1984. This work was supported by the National Science Foundation under Grant No. CHE-8106778.

Pulse Polarography: Effects of Electrode Sphericity on the Current–Potential Curves in Normal Pulse Polarography, Reverse Pulse Polarography, and Differential Pulse Polarography

Jesus Galvez

Laboratory of Physical Chemistry, Faculty of Science, Murcia 239169, Spain

Equations which take into account the sphericity of the DME for reversible electrode processes in normal pulse polarography (NPP), reverse pulse polarography (RPP), and differential pulse polarography (DPP) have been derived in a rigorous way. We have considered the cases where the reduction product dissolves both in the electrolyte solution and in the electrode. In DPP the effect exerted by the sphericity of the electrode is much more marked for systems involving amalgam formation than for reductions to a solution-soluble product. In RPP this influence is very significant for both types of processes, although it acts in an opposite way for amalgam-forming systems than for those systems where the reduced form is soluble in the solution. Finally, in NPP the current–potential curves show only a small dependence on whether there is amalgam formation or not.

Pulse polarography (NPP, RPP, DPP) has become one of the most powerful electroanalytic techniques both for chemical analysis and for the study of electrode processes (*1–13*). Regarding the theory of the current–potential curves several approaches have been developed, although in all of them, the expanding plane electrode model (EP) was normally adopted for the DME. Only Los and co-workers (*14*, *15*) and more recently Galvez and co-workers (*16–22*) have also considered the more rigorous expanding sphere electrode model (ES), but just for some types of limiting currents in NPP. The aim of the present paper is, therefore, to extend the theory of the current–potential curves in pulse polarography with the following assumptions

(a) The treatment adopted is based in obtaining the solution of the system of differential equations which describe the boundary value problem for the ES model separately for both pulses. Under these conditions the solution to the first system of equations becomes the initial condition for the second one (*10*, *11*, *23*).

(b) In order to obtain these solutions we have applied the dimensionless parameter method previously described (*16*).

Table I. Notation and Definitions

r	distance from the center of the electrode
r_0	electrode radius at time t
$A(t)$	time-dependent electrode area
m	rate of flow of mercury
$\mathcal{J}$	$(3m/4\pi d)^{1/3}$
Γ	Euler gamma function
ξ_i	$(12D_i/7\mathcal{J}^2)^{1/2}t^{1/6}$
γ	$(D_A/D_B)^{1/2}$
K_i	$\exp(nF(E_i - E°)/RT)$
Ω_i	$(1 \pm K_i)/(1 + \gamma K_i)$
Θ	$7p_{1/7}/11$ (=0.7868)
τ	$t'/(t_1 + t')$
$f(\tau)$	$1 + \tau/3 + 7\tau^2/54 + 4\tau^3/81 + \ldots$
$g(\tau)$	$1 - 5\tau^2/48 \ldots$
M	$1 + 7p_0(\gamma \pm 1)\xi_A/(11\gamma(1 + \gamma K_1))$
Z	$1/(1 + \gamma K_2) - 1/(1 + \gamma K_1)$
	other definitions are conventional

0003-2700/85/0357-0585$01.50/0 © 1985 American Chemical Society

This allows then solving the problem through concentration profiles for any value of r and t so that the use of linearized profiles (*23*) can be avoided.

(c) The case where the reduction product dissolves in the electrode will also be considered because this situation has not been reported in the literature to our knowledge.

(d) The equations obtained will be applied to the different modes of pulse polarography mentioned above, e.g., NPP, RPP, and DPP, so that the influence exerted by the sphericity of the electrode on the current–potential curves will be discussed.

THEORY

Notation and definitions are given in Table I. If we consider the reversible charge transfer reaction

$$A + ne^- \rightleftarrows B$$

and the product B is soluble in the electrolyte solution (amalgamation reaction will be discussed later), the expanding sphere boundary value problem is given by

$$\hat{D}_A C_A = \hat{D}_B C_B = 0 \tag{1}$$

$$\left.\begin{matrix} t = 0,\ r \geq r_0 \\ t > 0,\ r \to \infty \end{matrix}\right\} C_A = C_A^*,\ C_B = 0 \tag{2}$$

$t > 0,\ r = r_0$:

$$C_A(r_0,t) = C_B(r_0,t)\ \exp\left[\frac{nF}{RT}(E - E^\circ)\right] \tag{3}$$

$$\frac{i(t)}{nFA(t)} = D_A\left(\frac{\partial C_A}{\partial r}\right)_{r=r_0} = -D_B\left(\frac{\partial C_B}{\partial r}\right)_{r=r_0} \tag{4}$$

where $\hat{D}_i$ is the operator (*24*)

$$\hat{D}_i = \frac{\partial}{\partial t} - D_i\left(\frac{\partial^2}{\partial r^2} + \frac{2}{r}\frac{\partial}{\partial r}\right) + \frac{\mathscr{F}^3}{3r^2}\frac{\partial}{\partial r} \tag{5}$$

In the following we shall suppose that the potential is set on a constant value E_1 from $t = 0$ (beginning of the drop growth) to $t = t_1$, and at $t = t_1$ it is stepped up from E_1 to the other constant value E_2. Under these conditions the solution of eq 1–4 during the period $0 < t < t_1$ can be readily obtained (*25*) and so, if we only consider the first-order spherical correction we find

$$C_A(s_A,\xi_A) = \rho_0(s_A) + \xi_A\rho_1(s_A)$$
$$C_B(s_B,\xi_B) = \phi_0(s_B) + \xi_B\phi_1(s_B) \tag{6}$$

where

$$s_i = \left(\frac{7}{12D_i t}\right)^{1/2}(r - r_0)$$
$$\xi_i = \left(\frac{12D_i}{7\mathscr{F}^2}\right)^{1/2} t^{1/6} \tag{7}$$

$$\rho_0(s_A) = a_0\Psi_0(s_A) + C_A^*\ \mathrm{erf}\ (s_A)$$
$$\rho_1(s_A) = \frac{7C_A^* p_0}{11(1+\gamma K_1)}\left[\left(1 - \frac{3}{7}s_A^2\right)e^{-s_A^2} - \Omega_1\Psi_{1/7}(s_A)\right]$$
$$a_0 = \frac{\gamma K_1}{1+\gamma K_1}\,C_A^* \tag{8}$$
$$\gamma = (D_A/D_B)^{1/2} \tag{9}$$
$$K_1 = \exp\left[\frac{nF}{RT}(E_1 - E^\circ)\right] \tag{10}$$
$$\Omega_1 = \frac{1+K_1}{1+\gamma K_1} \tag{11}$$
$$p_j = \frac{2\Gamma(1 + j/2)}{\Gamma((1+j)/2)} \tag{12}$$
$$\phi_0(s_B) = b_0\Psi_0(s_B)$$
$$\phi_1(s_B) = -\frac{7C_A^* p_0\gamma}{11(1+\gamma K_1)}\left[\left(1 - \frac{3}{7}s_B^2\right)e^{-s_B^2} - \gamma\Omega_1\Psi_{1/7}(s_B)\right]$$
$$b_0 = \frac{\gamma C_A^*}{1+\gamma K_1} \tag{13}$$

and being the Ψ's the functions defined by Koutecký (*25*). In addition, from eq 4, 6, and 8 the current, $i_1(t)$, is given by

$$i_1(t) = nFA(t)\left(\frac{7D_A}{3\pi t}\right)^{1/2}\frac{C_A^*}{1+\gamma K_1}(1 + \Theta\Omega_1\xi_A) \tag{14}$$

with

$$\Theta = \frac{7}{11}p_{1/7}\ (=0.7868) \tag{15}$$

For $t > t_1$ we may write $t = t_1 + t'$ and so, eq 1 remains valid if in eq 5 we substitute t by t'. In turn, the boundary value problem is given now by

$$t' = 0 \qquad C_A(r,t) = C_A(s_A,\xi_A)$$
$$C_B(r,t) = C_B(s_B,\xi_B) \tag{16}$$

$t' > 0,\ r = r_0$

$$C_A(r_0,t) = K_2 C_B(r_0,t) \tag{17}$$

$$\frac{i_2(t)}{nFA(t)} = D_A\left(\frac{\partial C_A}{\partial r}\right)_{r=r_0} = -D_B\left(\frac{\partial C_B}{\partial r}\right)_{r=r_0} \tag{18}$$

with

$$K_2 = \exp\left[\frac{nF}{RT}(E_2 - E^\circ)\right] \tag{19}$$

In addition, it is held

$$\lim_{E_2 \to E_1} C_i(r,t) = C_i(s_i,\xi_i) \tag{20}$$

i = A or B

where C_i values in eq 16 and 20 are defined by eq 6.

The solution of eq 1 (with t' instead of t) and eq 16–18 can be obtained proceeding as follows:

With the variables

$$s_i' = \frac{r - r_0}{2(D_i t')^{1/2}}$$
$$\epsilon_i = \frac{2(D_i t')^{1/2}}{r_0}$$
$$\tau = \frac{t'}{t_1 + t'} \tag{21}$$

eq 1 become

$$\frac{\partial^2 C_i}{\partial s_i'^2} + 2s_i'\frac{\partial C_i}{\partial s_i'} - 2\epsilon_i\frac{\partial C_i}{\partial \epsilon_i} - 4\tau\frac{\partial C_i}{\partial \tau} = -\Phi(s_i',\epsilon_i,\tau)\frac{\partial C_i}{\partial s_i'} - \frac{4\tau}{3}\left(\epsilon_i\frac{\partial C_i}{\partial \epsilon_i} + 3\tau\frac{\partial C_i}{\partial \tau}\right) \tag{22}$$

where

$$\Phi(s_i',\epsilon_i,\tau) = \frac{2\epsilon_i}{1 + s_i'\epsilon_i} + \frac{4\tau}{3\epsilon_i}\left[1 - \frac{1}{(1 + s_i'\epsilon_i)^2}\right] \tag{23}$$

By expanding C_A and C_B as

$$C_A = \sum_{i,j} \sigma_{i,j}(s'_A)\epsilon_A{}^i\tau^j$$

$$C_B = \sum_{i,j} \delta_{i,j}(s'_B)\epsilon_B{}^i\tau^j \quad (24)$$

and inserting these expressions in eq 22 we obtain for $\sigma_{i,j}(s'_A)$ and $\delta_{i,j}(s'_B)$ the following system of recurrent differential equations:

$$\sigma''_{i,j} + 2s'_A\sigma'_{i,j} - 2(i+2j)\sigma_{i,j} = -\left\{\sum_{k+l+1=i} c_k\sigma'_{l,j}(s_A') + \sum_{r+p=i} d_r\sigma'_{p,j-1}(s'_A) + \frac{4}{3}(i+3j-3)\sigma_{i,j-1}(s'_A)\right\} \quad (25)$$

$$\delta''_{i,j} + 2s'_B\delta'_{i,j} - 2(i+2j)\delta_{i,j} = -\left\{\sum_{k+l+1=i} c_k\delta'_{l,j}(s'_B) + \sum_{r+p=i} d_r\delta'_{p,j-1}(s'_B) + \frac{4}{3}(i+3j-3)\delta_{i,j-1}(s'_B)\right\} \quad (26)$$

where

$$c_k = 2(-1)^k(s'_i)^k;\ c_k = 0 \text{ for } i = 0$$

$$d_r = 4(-1)^r(r+2)(s'_i)^{r+1}/3;\ d_r = 0 \text{ for } j = 0 \quad (27)$$

In turn, the boundary conditions (16)–(18) now are

$$s'_i \to \infty:\ \sigma_{0,0} = C_A(s_A,\xi_A);\delta_{0,0} = C_B(s_B,\xi_B)$$

$$\sigma_{i,j} = \delta_{i,j} = 0 \text{ unless } i = j = 0 \quad (28)$$

$$s'_i = 0:\ \gamma^i\sigma_{i,j}(0) = K_2\delta_{i,j}(0) \quad (29)$$

$$\gamma^{i+1}\sigma'_{i,j}(0) = -\delta'_{i,j}(0) \quad (30)$$

while condition (20) becomes

$$\lim_{E_2\to E_1} \begin{cases} \sigma_{0,0}(s'_A) = C_A(s_A,\xi_A);\ \delta_{0,0}(s'_B) = C_B(s_B,\xi_B) \\ \sigma_{i,j}(s'_A) = \delta_{i,j}(s'_B) = 0 \text{ unless } i = j = 0 \end{cases} \quad (31)$$

Note that the functions $\sigma_{0,j}(s'_A)$ and $\delta_{0,j}(s'_B)$ are the solutions for the expansing plane electrode model and that they must be known before deriving the solution for the ES model. Thus, we have:

Expanding Plane Electrode. If $i = 0$ eq 25 and 26 become

$$\sigma''_{0,j} + 2s'_A\sigma'_{0,j} - 4j\sigma_{0,j} = -(8/3)s'_A\sigma'_{0,j-1} - 4(j-1)\sigma_{0,j-1}$$

$$\delta''_{0,j} + 2s'_B\delta'_{0,j} - 4j\delta_{0,j} = -(8/3)s'_B\delta'_{0,j-1} - 4(j-1)\delta_{0,j-1} \quad (32)$$

These functions can be obtained by combining eq 32 and 28–31 and following the same derivational pattern previously described (*16*). Thus, we find

$$\sigma_{0,0}(s'_A) = C_A(s_A,\xi_A) - MZC_A{}^*\Psi_0(s'_A)$$

$$\delta_{0,0}(s'_B) = C_B(s_B,\xi_B) + MZC_A{}^*\Psi_0(s'_B) \quad (33)$$

where

$$M = 1 + \frac{7p_0(\gamma-1)\xi_A}{11\gamma(1+\gamma K_1)} \quad (34)$$

$$Z = \frac{1}{1+\gamma K_2} - \frac{1}{1+\gamma K_1} \quad (35)$$

In turn, the first functions for $j > 0$ are given in the Appendix.

Expanding Sphere Electrode. If we consider only the first-order spherical correction, the set of equations (25 and 26) must be solved for $i = 1$. In the Appendix we show the procedure to follow in order to obtain the corresponding functions $\sigma_{1,j}(s'_A)$ and $\delta_{1,j}(s'_B)$. Finally, combining eq 18, 21, and 24 and taking into account the expressions for $\sigma_{i,j}(s'_A)$ defined by eq 33 and A1–A4, the following expression for the current is obtained:

$$i_2(t) = i_1(t) + nFA(t)\left(\frac{D_A}{\pi t'}\right)^{1/2} C^*_A MZ\left\{f(\tau) + \left(\frac{7\pi\tau}{12}\right)^{1/2}\Omega_2\xi_A g(\tau)\right\} \quad (36)$$

where

$$f(\tau) = 1 + \frac{1}{3}\tau + \frac{7}{54}\tau^2 + \frac{4}{81}\tau^3 + \ldots$$

$$g(\tau) = 1 - \frac{5}{48}\tau^2 \ldots \quad (37)$$

$$\Omega_2 = \frac{1+K_2}{1+\gamma K_2} \quad (38)$$

As expected, if $E_2 \to E_1$, $Z \to 0$ (see eq 35) and $i_2(t) = i_1(t)$. In addition, the corresponding expression for the current in the expanding plane electrode model is readily obtained by making $\xi_A = 0$ in eq 36

$$i_2(t) = i_1(t) + nFA(t)\left(\frac{D_A}{\pi t'}\right)^{1/2} C^*_A Zf(\tau) \quad (39)$$

Note that in this case the values of the current computed with eq 39 do not depend on whether there is amalgam formation or not.

Amalgam Formation. In this case we must rewrite the boundary value problem as follows: eq 2 is now

$$t = 0,\ r > 0: \qquad C_A = C^*_A,\ C_B = 0$$

$$t > 0,\ r \to \infty: \qquad C_A = C^*_A,\ r \to -\infty,\ C_B = 0$$

the minus sign in eq 4 and 18 is changed to plus.

The procedure of derivation to follow by using these new conditions differs slightly from that adopted previously (see Appendix) although, we find that the expression for the current is also given by eq 36 if in this equation Ω_i and M are defined as

$$\Omega_i = \frac{1 \pm K_i}{1+\gamma K_i} \qquad (i = 1, 2)$$

$$M = 1 + \frac{7p_0(\gamma \mp 1)\xi_A}{11(1+\gamma K_1)} \quad (40)$$

where the upper sign relates to a solution-soluble product and the lower sign to the amalgamation reaction (this rule will be maintained for the next sections).

RESULTS AND DISCUSSION

From eq 36 and 40 we may easily obtain the expressions for the different modes of pulse polarography by introducing the experimental conditions corresponding to the mode employed. Thus, we have the following.

Normal Pulse Polarography. In NPP, the initial potential E_1 is maintained at an initial value at which no current flows. The scan of the potential E_2 is then made to the cathodic direction. Hence, $K_1 \to \infty$ and introducing this condition in eq 36 and 40 we obtain

$$i_{NPP} = nFA(t)\left(\frac{D_A}{\pi t'}\right)^{1/2} C^*_A \frac{1}{1+\gamma K_2}\left\{f(\tau) + \left(\frac{7\pi\tau}{12}\right)^{1/2}\Omega_2\xi_A g(\tau)\right\} \quad (41)$$

In turn, the limiting current can be obtained by inserting the condition $E_2 \to -\infty$ (i.e., $K_2 \to 0$) in eq 41

$$i_{lim} = nFA(t)\left(\frac{D_A}{\pi t'}\right)^{1/2} C^*_A\left\{f(\tau) + \left(\frac{7\pi\tau}{12}\right)^{1/2}\xi_A g(\tau)\right\} \quad (42)$$

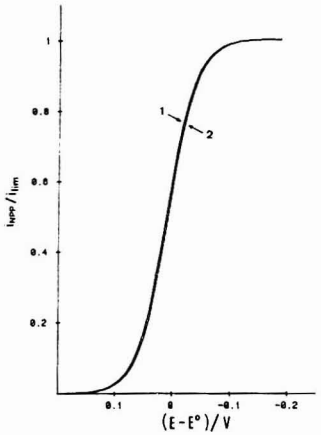


Figure 1. NPP current–potential curves computed from eq 41 and 42 for $\gamma = 0.7$, $\xi_A = 0.15$, $t = 1$ s, and $\tau = 0.05$: (1) without amalgam formation; (2) reduction product dissolved in the electrode.

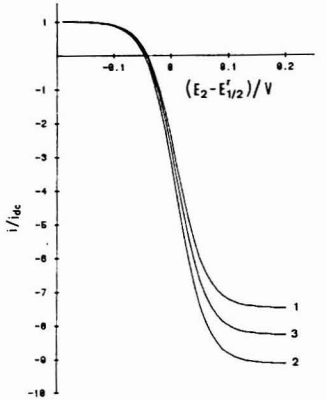


Figure 2. RPP current–potential curves computed from eq 46 for $\tau = 0.005$: (1) without amalgam formation, $\xi_A = 0.15$, $\gamma = 1.1$; (2) amalgam formation, $\xi_A = 0.15$, $\gamma = 0.8$; (3) EP model, $\xi_A = 0$.

This particular boundary value problem has been previously solved by Galvez and Serna (*16*) and their solution is identical with eq 42.

In any case, it is interesting to show that both in NPP and in dc polarography (*26*), the limiting current does not depend on whether the process involves amalgam formation or not. An example of this is shown in Figure 1. The characteristics of the current potential curves are similar to those previously described in dc polarography (*26*) and for this reason further discussion is not given here.

Reverse Pulse Polarography. In RPP (*6*), or scan-reversal pulse polarography (*4*), the initial potential E_1 is set on the cathodic diffusion current plateau and the potential E_2 is scanned anodically. This is a powerful technique to characterize electrode processes (*6*, *27*), although the expression for the current has only been derived for the EP model (*1*, *6*). However, this model is not sufficient to explain the behavior of the current potential curves obtained experimentally and so, Osteryoung and Kirowa-Eisner reported (*6*): "it appears to be the case that amalgam-forming systems and systems for which both the oxidized and reduced forms are soluble in the solution behave differently" (see also Figure 3 in ref 6). However, we show in this section that this different behavior can be explained taking into account the ES model. Thus, inserting the condition $E_1 \to -\infty$ (i.e., $K_1 \to 0$) in eq 36 and 40 we obtain

$$i_2(t) = i_{dc} - nFA(t) \times \left(\frac{D_A}{\pi t'}\right)^{1/2} C_A^* M \frac{\gamma K_2}{1+\gamma K_2}\left(f(\tau) + \left(\frac{7\pi\tau}{12}\right)^{1/2} \Omega_2 \xi_A g(\tau)\right) \quad (43)$$

where

$$i_{dc} = nFA(t)\left(\frac{7D_A}{3\pi t}\right)^{1/2} C_A^*(1+\Theta\xi_A) \quad (44)$$

$$M = 1 + \frac{0.718(\gamma \mp 1)\xi_A}{\gamma} \quad (45)$$

with $7p_0/11 = 0.718$. From eq 43 and 44 the relationship $i_2(t)/i_{dc}$ is given by

$$\frac{i_2(t)}{i_{dc}} = 1 - \left(\frac{3}{7\tau}\right)^{1/2} \frac{M}{1+\Theta\xi_A} \frac{\gamma K_2}{1+\gamma K_2}\left(f(\tau) + \left(\frac{7\pi\tau}{12}\right)^{1/2} \Omega_2 \xi_A g(\tau)\right) \quad (46)$$

The anodic limiting current, i_{RP}, is obtained by introducing the condition $K_2 \to \infty$ in eq 46

$$-\frac{i_{RP}}{i_{dc}} = \left(\frac{3}{7\tau}\right)^{1/2} \frac{M}{1+\Theta\xi_A}\left(f(\tau) \pm \left(\frac{7\pi\tau}{12}\right)^{1/2} \frac{\xi_A}{\gamma} g(\tau)\right) - 1 \quad (47)$$

Note that the corresponding expression for the EP model is only a particular case of eq 47 and so, for $\xi_A = 0$ we have

$$-\frac{i_{RP}}{i_{dc}} = \left(\frac{3}{7\tau}\right)^{1/2} f(\tau) - 1 \quad (48)$$

This equation is equivalent to that previously derived for Oldham and Parry (*1*) for this electrode model, and it is readily shown that the values of $-i_{RP}/i_{dc}$ computed from both equations differ about 1% or less even for $t' \lesssim 0.2t$. Equations 46 and 47 predict that the behavior of the processes involving amalgam-formation must be different from those where the product dissolves in the electrolyte solution. This is shown in Figure 2 where we have plotted current potential curves for $\gamma = 0.8$ (amalgam formation), $\gamma = 1.1$ (without amalgamation reaction), $\xi_A = 0.15$, and $\tau = 0.005$. For comparison we have also included the corresponding curve for $\xi_A = 0$. This different behavior is also shown in Figure 3 in which we have plotted $-i_{RP}/i_{dc}$ vs. $F(\tau)$ (being $F(\tau)$ the right-hand side of eq 48 for several values of τ. These plots are practically linear and from eq 47 and 48 we find that their slope, a, is given by

$$a \approx \frac{\gamma + 0.718(\gamma \mp 1)\xi_A}{\gamma(1+0.787\xi_A)} \quad (49)$$

Accordingly, if there is amalgam formation we have $a > 1$ (unless $\gamma > 10.4$), while for processes where the product is

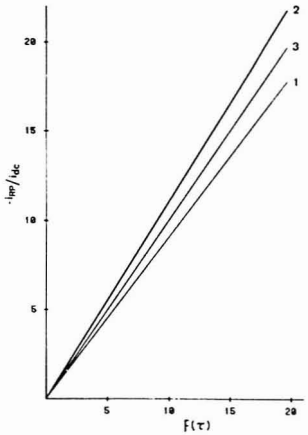


Figure 3. RPP dependence of $-i_{RP}/i_{dc}$ (eq 47) on $F(\tau)$. Other conditions are given in Figure 2.

Table II. Deviations of the Values of $-i_{RP}/i_{dc}$ as a Function of ξ_A and γ[a]

ξ_A	γ	% (I)	% (II)
0.10	0.7	11.3	−8.1
	1.0	7.9	−5.7
	1.4	5.7	−4.0
0.15	0.7	17.2	−11.4
	1.0	11.8	−8.0
	1.4	8.5	−5.6
0.20	0.7	23.3	−14.2
	1.0	15.7	−10.1
	1.4	11.2	−7.1

[a] Deviations between the values of $-i_{RP}/i_{dc}$ obtained with the EP and ES models (eq 51): (I) reduction product dissolves in the electrolyte solution; (II) amalgam-forming systems.

soluble in the solution a must be <1. Note that this behavior is in agreement with the data reported in Figure 3 of ref 6. In addition, if we take into account that the intercept, b, of these plots is small ($b \simeq 0$), it follows that for $\tau << 1$ an excellent approximation to eq 47 is

$$-\frac{i_{RP}}{i_{dc}} = a\left(\left(\frac{3}{7\tau}\right)^{1/2} f(\tau) - 1\right) \qquad (50)$$

Hence, if the values of $-i_{RP}/i_{dc}$ are computed by adopting the EP model, deviations between eq 48 and 50 are given by

$$\% \approx \frac{(0.069\gamma \pm 0.718)\xi_A}{\gamma + 0.718(\gamma \mp 1)\xi_A} \times 100 \qquad (51)$$

and they increase as ξ_A becomes greater. An example of this is given in Table II. In short, values of $-i_{RP}/i_{dc}$ computed from the ES model are greater or smaller than those obtained with the EP model for processes involving amalgamation reaction or not.

Differential Pulse Polarography. In differential pulse polarography (DPP), both the potentials E_1 and E_2 are scanned simultaneously toward the cathodic direction with their difference, $E_1 - E_2 = \Delta E$, being kept constant. In addition, the current in this mode, i_{dpp}, is normally measured

Table III. Deviations of the Peak Current Values as a Function of ξ_A and γ[a]

ξ_A	γ	% (I)	% (II)
0.10	0.7	2.5	7.6
	1.0	3.3	6.8
	1.4	3.8	6.3
0.15	0.7	3.2	10.5
	1.0	4.3	9.5
	1.4	5.1	8.8
0.20	0.7	3.9	13.3
	1.0	5.4	12.0
	1.4	6.4	11.1

[a] Deviations between the values of the peak current obtained with the EP and ES models (eq 55): $\Delta E = 10$ mV, $n = 2$, $\tau = 0.03$; (I) reduction product dissolves in the electrolyte solution; (II) amalgam-forming systems.

as a difference between i_2 at $t = t_1 + t'$ and i_1 at $t = t_1$. Hence, combining eq 36 and 14 we find

$$\frac{i_{dpp}}{i_{d,p}} = \frac{\tau^{1/2}}{1 + \gamma K_1}(1 - \tau^{*1/6} + \Theta\Omega_1\xi_A(1 - \tau^{*1/2})) + \left(\frac{3}{7}\right)^{1/2} MZ\left(f(\tau) + \left(\frac{7\pi\tau}{12}\right)^{1/2}\Omega_2\xi_A g(\tau)\right) \qquad (52)$$

where

$$\tau^* = 1 - \tau$$

$$i_{d,p} = nFA(t)\left(\frac{7D_A}{3\pi t'}\right)^{1/2} C_A^* \qquad (53)$$

and Ω_i ($i = 1, 2$) computed with the condition $E_2 = E_1 - \Delta E$. For $\xi_A = 0$ eq 52 becomes

$$\frac{i_{dpp}}{i_{d,p}} = \frac{\tau^{1/2}}{1 + \gamma K_1}(1 - \tau^{*1/6}) + \left(\frac{3}{7}\right)^{1/2} Zf(\tau) \qquad (54)$$

which is the expression for the current in the EP model. In turn, if $\tau << 1$, it followed that $f(\tau) \simeq 1$ and eq 54 becomes identical with the other equations previously derived in the literature (*2, 3, 5*). The maximum current, $i_{p\text{-}dpp}$, is obtained for $(E_1)_p \simeq E^r_{1/2} + \Delta E/2$ (see below) and from eq 52 and 54 we find that deviations for the peak current values when the curvature of the electrode is not taken into account are given by

$$\% \simeq \frac{\gamma(1 + X)f_1(\tau) + G\xi_A}{\gamma(1 + X)f(\tau) + G\xi_A} \times 100 \qquad (55)$$

where

$$f_1(\tau) = f(\tau) - 1$$

$$G = 0.718(\gamma \mp 1)f(\tau) + 1.354\tau^{1/2}g(\tau)(\gamma X \pm 1) \qquad (56)$$

$$X = \exp\left[\frac{nF\Delta E}{2RT}\right]$$

In Table III we have computed from eq 55 these deviations for $t' = 0.03$ s, $t = 1$ s, $\Delta E = 10$ mV, $n = 2$, and different values of ξ_A and γ. Note that deviations are greater for amalgam-forming systems than for processes where the reduced form is soluble in the solution. In addition, in Figure 4 we have computed from eq 52 the differential pulse polarogram for 1 mM solution of Tl(I) with $\Delta E = 10$ mV, $t = 3$ s, $\tau = 0.03$, $m = 0.5$ mg·s^{-1} while the values of D_A (1.74×10^{-5} cm^2 s^{-1}) and γ (=1.33) have been taken from the literature (*28*). In this figure we have also included for comparison the corresponding curve computed from eq 54 (with $f(\tau) = 1$). Note that if the sphericity is not considered, the deviations obtained are quite

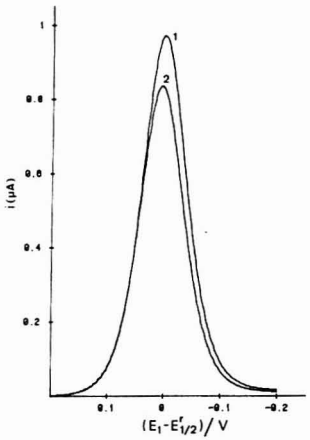


Figure 4. DPP differential pulse polarogram of 1 mM Tl(I), ΔE = 10 mV, t = 3 s, τ = 0.03, m = 0.5 mg-s^{-1}: (1) computed from eq 52; (2) computed from eq 54.

Table IV. Dependence of $(E_1)_p - E'_{1/2}$ on ΔE, ξ_A, and γ^a

ΔE/mV	ξ_A	γ = 0.7 D/mV	γ = 1.0 D/mV	γ = 1.4 D/mV
5	0.00	2	2	2
	0.05	0	0	1
	0.10	−1	−1	0
	0.15	−3	−2	−1
	0.20	−4	−3	−2
10	0.00	5	5	5
	0.05	3	3	3.5
	0.10	1.5	2	2.5
	0.15	0	1	1
	0.20	−1	0	0.5
20	0.00	10	10	10
	0.05	8	8.5	9
	0.10	7	7	°
	0.15	5	6	7
	0.20	4	5	6

[a] Values of D $(=(E_1)_p - E'_{1/2})$ for a system involving amalgam formation: n = 1, τ = 0.05.

significant principally for the $i_{p\text{-}dpp}$ values.

Finally, another interesting effect exerted by the sphericity of the electrode is the shift found in the values of E_1 at which $i_{p\text{-}dpp}$ is obtained. Thus, if $\xi_A = 0$ it is known (3) that the values of $i_{p\text{-}dpp}$ are found at $(E_1)_p = E'_{1/2} + \Delta E/2$. However, in Table IV we have computed from eq 52 the $(E_1)_p$ values for an amalgam-forming system with n = 1, τ = 0.05, and different values of γ, ξ_A, and ΔE. Note that there is a shift of $(E_1)_p$ toward negative values which depends on ξ_A, γ, and ΔE. Conversely, for a system where the reduced form is soluble in the solution, this effect is very small. Hence, it follows that the equation $(E_1)_p = E'_{1/2} + \Delta E/2$ is applied to systems where there is no amalgamation reaction, while in those cases where the reduced form is soluble in the electrode, that rule can only be considered as an approximation.

APPENDIX

In eq 32 the $\sigma_{0,j}(s_A')$ and $\delta_{0,j}(s_B')$ functions are obtained by using the dimensionless parameter method previously described (16). Thus, for j = 1, 2 we have

$$\sigma_{0,1}(s_A') = (1/3)p_0MZC_A^*s_A'e^{-s_A'^2}$$

$$\delta_{0,1}(s'_B) = -(1/3)\gamma p_0MZC_A^*s'_Be^{-s'^2_B} \quad \text{(A1)}$$

$$\sigma_{0,2}(s'_A) = (7/54)p_0MZC_A^*(s'_A - (6/7)s'^3_A)e^{-s'^2_A}$$

$$\delta_{0,2}(s'_B) = -(7/54)p_0\gamma MZC^*_A(s'_B - (6/7)s'^3_B)e^{-s'^2_B} \quad \text{(A2)}$$

Once $\sigma_{0,j}(s'_A)$ and $\delta_{0,j}(s'_B)$ are known the $\sigma_{1,j}(s'_A)$ and $\delta_{1,j}(s'_B)$ functions are obtained by introducing eq 33, A1, and A2 in eq 25 and 26 and proceeding as described in ref 16. Thus, for j = 0 and 1 we find

$$\sigma_{1,0}(s'_A) = (1/2)p_0MZC^*_A(e^{-s'^2_A} - \eta\Psi_1(s'_A))$$

$$\delta_{1,0}(s'_B) = -(1/2)\gamma p_0MZC^*_A(e^{-s'^2_B} - \gamma\eta\Psi_1(s'_B)) \quad \text{(A3)}$$

$$\sigma_{1,1}(s'_A) = (1/6)p_0MZC^*_A((\eta - 4s'^2_A)e^{-s'^2_A} - 3\eta\Psi_1(s'_A) + 2\eta\Psi_3(s'_A))$$

$$\delta_{1,1}(s'_B) = -(1/6)\gamma p_0MZC^*_A((\gamma\eta - 4s'^2_B)e^{-s'^2_B} - 3\gamma\eta\Psi_1(s'_B) + 2\gamma\eta\Psi_3(s'_B)) \quad \text{(A4)}$$

where

$$\eta = \frac{1 + K_2}{1 + \gamma K_2}$$

For processes involving amalgam formation the Λ's functions must be defined as

$$\Psi_\alpha^+ = K_\alpha + p_\alpha L_\alpha \quad \text{(A5)}$$

where K_α, p_α, and L_α have been already defined in ref 14 and 25.

The properties of these new functions can be obtained proceeding as described in ref 14 and 29 and so, we have

$$\Psi_\alpha^+(0) = 1 \quad \text{(A6)}$$

$$\Psi_\alpha^+(-\infty) = 0 \quad \text{(A7)}$$

$$\Psi'^+_\alpha(s) = p_\alpha\Psi^+_{\alpha-1}(s) \quad \text{(A8)}$$

$$\Psi'^+_\alpha(0) = p_\alpha \quad \text{(A9)}$$

$$s\Psi_\alpha^+(s) = p_\alpha(\Psi^+_{\alpha+1}(s) - \Psi^+_{\alpha-1}(s))/2 \quad \text{(A10)}$$

Equations A5–A10 must be used to solve the corresponding boundary value problem by following a procedure similar to that adopted when the product dissolves in the electrolyte solution.

Registry No. Hg, 7439-97-6.

LITERATURE CITED

(1) Oldham, Keith B. *Anal. Chem.* **1970**, *42*, 229.
(2) Christie, J. H.; Osteryoung, R. A. *J. Electroanal. Chem.* **1974**, *49*, 301.
(3) Birke, R. L. *Anal. Chem.* **1978**, *50*, 1489.
(4) Ružić, I. *J. Electroanal. Chem.* **1977**, *75*, 25.
(5) Heijne, G. J. M.; van de Linden, W. E. *Anal. Chim. Acta* **1978**, *99*, 183.
(6) Osteryoung, J.; Klrowa-Eisner, E. *Anal. Chem.* **1980**, *52*, 62.
(7) Aoki, K.; Osteryoung, J.; Osteryoung, R. A. *J. Electroanal. Chem.* **1980**, *110*, 1.
(8) Aoki, K.; Osteryoung, J. *J. Electroanal. Chem.* **1980**, *110*, 19.
(9) Matsuda, H. *Bull. Chem. Soc. Jpn.* **1980**, *53*, 3439.
(10) Birke, R. L.; Kim, M.-H.; Strassfeld, M. *Anal. Chem.* **1981**, *53*, 852.
(11) Lovrić, M.; Osteryoung, J. *Electrochim. Acta* **1982**, *27*, 963.
(12) Kim, M.-H.; Birke, R. L. *Anal. Chem.* **1983**, *55*, 522.
(13) Kim, M.-H.; Birke, R. L. *Anal. Chem.* **1983**, *55*, 1735.
(14) Brinkman, A. A. A. M.; Los, J. M. *J. Electroanal. Chem.* **1964**, *7*, 171.
(15) Brinkman, A. A. A. M.; Los, J. M. *J. Electroanal. Chem.* **1967**, *14*, 269, 285.
(16) Galvez, J.; Serna, A. *J. Electroanal. Chem.* **1976**, *69*, 133, 145, 157.
(17) Galvez, J.; Serna, A.; Fuente, T. *J. Electroanal. Chem.* **1979**, *96*, 1.
(18) Galvez, J.; Molina, A. *J. Electroanal. Chem.* **1980**, *107*, 87.
(19) Galvez, J.; Serna, C.; Molina, A.; Serna, A. *J. Electroanal. Chem.* **1980**, *115*, 1.
(20) Galvez, J.; Molina, A. *J. Electroanal. Chem.* **1980**, *115*, 15.

(21) Galvez, J.; Molina, A.; Serna, C. J. Electroanal. Chem. 1981, 121, 85.
(22) Galvez, J.; Molina, A.; Serna, C. J. Electroanal. Chem. 1981, 124, 201.
(23) Ferrier, R. D.; Schroeder, R. R. J. Electroanal. Chem. 1973, 45, 343.
(24) Heyrovsky, J.; Kuta, J. "Principles of Polarography"; Academic Press: New York, 1966; p 542.
(25) Kouteckỳ, J. Czech. J. Phys. 1953, 2, 50.
(26) Heyrovsky, J.; Kuta, J. "Principles of Polarography"; Academic Press: New York, 1966; p 137.
(27) Saito, A.; Himeno, S. J. Electroanal. Chem. 1979, 101, 257.
(28) Heyrovsky, J.; Kuta, J. "Principles of Polarography"; Academic Press: New York, 1966; pp 106-107.
(29) Galvez, J. Doctoral Dissertation, Universidad de Murcia, 1973.

RECEIVED for review July 18, 1984. Accepted November 5, 1984. We thank the Comision Asesora de Investigación Científica y Técnica for supporting this study.

Electrocatalytic and Analytical Response of Cobalt Phthalocyanine Containing Carbon Paste Electrodes toward Sulfhydryl Compounds

Mary Kim Halbert and Richard P. Baldwin*

Department of Chemistry, University of Louisville, Louisville, Kentucky 40292

Chemically modified electrodes, constructed by incorporating cobalt phthalocyanine (CoPC) into the graphite powder/Nujol oil matrix used to fabricate conventional carbon paste electrodes, were shown to catalyze the electrooxidation of sulfhydryl-containing compounds including cysteine, homocysteine, *N*-acetylcysteine, and glutathione. The sulfhydryl oxidation occurred at 0.75–0.85 V vs. Ag/AgCl, the same potential observed for the CoPC oxidation both in solution and after addition to the carbon paste. When used as the sensing electrodes in amperometric detection following liquid chromatography, the CoPC electrodes permitted detection of the compounds at similar values of applied potential. Detection limits of 2.7 pmol were obtained for cysteine, *N*-acetylcysteine, and homocysteine; and electrode response was linear up to 270 pmol injected. Different carbon paste surfaces renewed in the standard manner yielded chromatographic peak currents with a reproducibility of 7%.

In recent years, electrodes possessing specific chemical functionalities intentionally linked to their surface have been demonstrated to possess distinct advantages over conventional electrode substrates in numerous application areas including electrosynthesis, electrocatalysis, and photoelectrochemistry (*1*, *2*). In principle, such chemically modified electrodes (CMEs) should also be able to provide enhanced performance in the area of electroanalysis as well. However, to date, instances involving the utilization of CMEs for such purposes have not been extensively documented despite the potential advantages which might be expected to accrue.

One of the important properties of CMEs which has been the object of considerable study has been their ability to catalyze the oxidation or reduction of solute species which exhibit high overvoltages at unmodified surfaces and consequently are not ideally suited to quantitative determination via conventional electrochemical approaches. Since the major effect of such CME electrocatalysis consists of the lowering of the potential required for the electrolysis of the catalyzed redox system, these electrodes should possess direct application in a variety of analytical situations. In particular, their use should greatly improve the capabilities of electrochemical detection techniques in liquid chromatography (LCEC) where sensitivity and selectivity are directly dependent on the magnitude of the electrode potential required to produce the desired electrode reaction (*3*). In previous work in our laboratory, CMEs formed both by electrochemical pretreatment of glassy carbon (*4*, *5*) and by the addition of cobalt phthalocyanines to ordinary carbon paste (*6*) have been shown to enhance significantly the LCEC determination of hydrazine compounds—a family of compounds which can generally be oxidized only at relatively high, positive potentials greater than +1 V vs. Ag/AgCl. However, when either of the abovementioned CMEs was employed, the potential required for the oxidation was reduced by 0.5 to 1 V; and detection limits obtained were some 2 to 3 orders of magnitude below those attainable at unmodified electrodes even at considerably higher values of applied potential.

In view of the well-known catalytic activity of metallophthalocyanines toward a wide variety of redox systems (*7*), we have continued to investigate the use of phthalocyanine-containing carbon paste CMEs as analytical sensors in voltammetry and LCEC. In particular, we have considered the application of cobalt phthalocyanine (CoPC) electrodes for the electrocatalytic determination of sulfhydryl compounds. At most conventional electrodes, sulfhydryls exhibit irreversible oxidations requiring extreme positive potentials. Consequently, electrochemical detection of these species is usually performed at mercury or mercury amalgam electrodes at which the mercury sulfide species formed can be oxidized at comparatively modest values of applied potential (*8–10*). In this work, we report on an alternate approach for the detection of sulfhydryls at lowered potentials at CoPC-CMEs. The response of these electrodes toward a variety of sulfur-containing species and their utility for the LCEC detection of cysteine and several related compounds are described.

EXPERIMENTAL SECTION

Reagents. Cobalt phthalocyanine was obtained from Eastman Kodak Co. Cobalt phthalocyaninetetrasulfonate was prepared and purified according to the procedure of Weber and Busch (*11*). Because the monosodium salt of 4-sulfophthalic acid required for the procedure could not be obtained commercially, it was prepared in our laboratory according to ref 12. With the exception of Captopril (provided by E. R. Squibb and Son, Inc.), all thiol compounds used in this work were obtained from Sigma Chemical Co. The sodium salt of 1-octanesulfonic acid, used as an ion-pairing agent, was also obtained from Sigma. All reagents were

0003-2700/85/0357-0591$01.50/0 © 1985 American Chemical Society

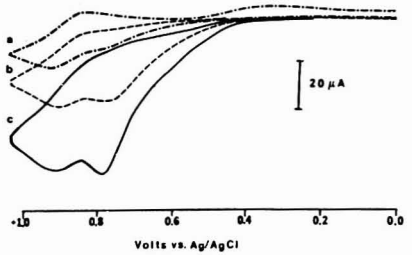


Figure 1. Cyclic voltammograms of 1.0×10^{-3} M cobalt phthalocyaninetetrasulfonate at unmodified carbon paste electrodes: (a) in 0.05 M H_2SO_4; (b) same as (a) but with 1.0 mM cysteine added; (c) same as (a) but with 2.0 mM cysteine added. Scan rate was 100 mV/s.

used as received without further purification.

Working Electrodes. Carbon paste for unmodified electrodes was made by thoroughly hand mixing 5 g of graphite powder (Fisher Scientific Co.) with 3 mL of Nujol oil (McCarthy Scientific Co., Fullerton, CA) in a mortar and pestle. Modified carbon pastes were prepared similarly except that the appropriate weight of CoPC was first mixed with the graphite powder. The Nujol oil was then added and ground with the graphite mixture for 30 min. The concentration of the phthalocyanine in the CME was described on a percent basis as the weight of the CoPC added to the 5 g of graphite powder.

Apparatus. Cyclic voltammetry was performed with a Bioanalytical Systems (W. Lafayette, IN) Model CV-1B potentiostat. A carbon paste working electrode (with or without CoPC), a saturated Ag/AgCl reference electrode, and a platinum wire counterelectrode were used for all experiments. Flow injection analysis and liquid chromatography were performed with a Perkin-Elmer Series 10 pump, a Rheodyne (Berkeley, CA) Model 7125 injector with a 20-μL loop, and an IBM Model EC/230 amperometric detector. Chromatography was performed with an IBM 15-cm octadecylsilane column.

RESULTS AND DISCUSSION

Solution-Phase Catalysis. Among the compounds whose redox reactions have been shown to be catalyzed by metallophthalocyanines are cysteine and several other sulfhydryl-containing species (*13–18*). In view of the importance of these compounds in a number of biological, pharmaceutical, and environmental areas, we chose to investigate the application of CoPC-CMEs for their determination. We began by examining the electrocatalysis of cysteine by solution-phase CoPC. In order to obtain a phthalocyanine possessing sufficient solubility in aqueous solution to be of use, the tetrasulfonate derivative of CoPC was synthesized as described in the Experimental Section. All subsequently described solution-phase studies were conducted with this CoPC derivative.

Previous voltammetric studies of the tetrasulfonate derivative of CoPC at platinum electrodes have reported the occurrence of two anodic processes for the compound (*12*, *19*). The first, at lower potentials, was assigned to the Co(II)–Co(III) oxidation while the higher potential process consisted of a degradative ring oxidation. A cyclic voltammogram (CV) obtained in our laboratory at a conventional carbon paste electrode for an aqueous solution of the same compound is shown for comparison in Figure 1 (curve a). Under the conditions employed, two anodic waves were observed. Because the CV remained virtually unchanged on subsequent scans, neither of the oxidations apparently corresponded to the CoPC-degrading process. Thus, the reversible, higher potential wave at +0.93 V vs. Ag/AgCl presumably involved the Co(II) oxidation. Since the oxidation at +0.77 V continued to be observed even after removal of the electrode from the phthalocyanine solution, thorough rinsing of the surface, and reimmersion into a blank solution containing no CoPC, it most likely corresponded to the same redox process for adsorbed CoPC. In addition, several small cathodic waves were observed at less positive potentials on the reverse scan; although always comparatively small in amplitude, the specific occurrence of these reductions was a complicated function of the potential scan rate, the solution pH, and the past history of the electrode surface.

When cysteine was added to the tetrasulfonated CoPC solution, the CVs shown in curves b and c of Figure 1 were obtained. The principal changes which resulted consisted of a marked increase in the current level associated with the CoPC oxidation waves and a complete absence of reduction current on the reverse scan. On subsequent cycles, the anodic currents between +0.7 V and +1.0 decreased in magnitude as the cysteine concentration became depleted near the electrode surface; and the voltammogram gradually started to resemble that seen above for the CoPC compound in the absence of cysteine. The initial increase in current was proportional to the concentration of cysteine added. In the absence of the phthalocyanine compound, no current for the direct electrooxidation of cysteine was observed in the potential range examined.

The observations described above are essentially those which would be expected for a two-step electrocatalytic process initiated by the electrochemical oxidation of the cobalt(II) phthalocyanine compound to a Co(III) species and completed by the chemical oxidation of the cysteine in a redox reaction which also serves to regenerate the Co(II) form of the phthalocyanine. Previous studies (*13–18*) of cysteine oxidation by CoPC compounds have indicated that, depending on solution pH, both the +2 and +3 states are capable of carrying out the sulfhydryl oxidation. However, under the acidic conditions employed in this work and necessary for the optimum chromatographic retention and separation of these zwitterionic species, the strongest and most consistently observed cysteine oxidation occurred in the potential region assigned to Co(III) formation. When neutral or basic solutions were employed, increases in anodic current were also noted at lower potentials. This could be indicative of cysteine oxidation by Co^{II} PC species in solution of higher pH. But it appeared in general that the higher oxidation state of the phthalocyanine, once produced electrochemically, was a much more effective electrocatalyst under the conditions employed.

CME Electrocatalysis. In several previous studies, a variety of metallophthalocyanines have been attached both to graphite and to metal oxide surfaces by silane formation (*19*), vapor deposition (*20*), and direct adsorption (*21*). In our laboratory, we have recently shown that stable phthalocyanine CMEs can also be constructed simply by addition of the desired compound to the graphite powder/Nujol oil matrix used to fabricate conventional carbon paste electrodes (*6*). Because of their ease of construction and the capability for rapid, quantitatively reproducible surface renewal, the latter approach involving chemically modified carbon paste was chosen for use here.

The CVs obtained for a CoPC-containing carbon paste CME immersed both in 0.05 M H_2SO_4 blank solution and in the same solution doped with 1×10^{-3} M cysteine are shown in Figure 2. The CoPC-CME employed here and subsequently in this work represented a phthalocyanine doping level of 2% by weight; CMEs containing higher modifier concentrations were not found to yield significantly higher current levels and thus were not investigated further. By itself, the CoPC-CME exhibited only a single anodic wave when cycled in blank over positive potentials not exceeding +1.0 V vs. Ag/AgCl. This wave occurred at +.077 V vs. SCE and closely

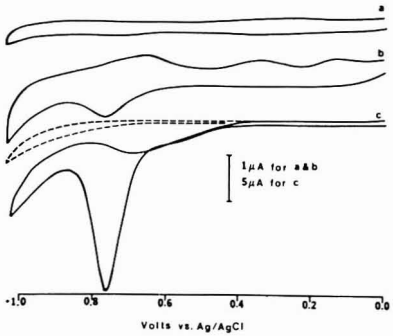


Figure 2. Cyclic voltammograms of (a) unmodified carbon paste electrode, (b) 2.0% CoPC carbon paste electrode, and (c) 1.0 mM cysteine at 2.0% CoPC carbon paste electrode. Dashed line (– – –) shows the voltammogram obtained for 1.0 mM cysteine at an unmodified electrode. Electrolyte was 0.05 M H_2SO_4; scan rate was 100 mV/s.

matched the adsorption wave observed for a CoPC solution in Figure 1. Several relatively small reductions were seen on the reverse scan, their relative intensity dependent on the potential scan rate employed and the positive potential limit of the scan.

As with the solution-phase CoPC tetrasulfonate system, the introduction of a sulfhydryl compound such as cysteine to this CME/solution system resulted in a marked increase in current at the Co(II)–Co(III) oxidation wave, greatly exceeding that observed either for the CoPC-CME in the absence of the sulfhydryl or for a plain carbon paste electrode exposed to the same sulfhydryl concentration. As before, the catalytic currents observed were proportional to the cysteine concentration; and no cathodic currents were seen on the reverse scan. Further, the currents due to the sulfhydryl oxidation were diffusion controlled, exhibiting a linear dependence on the square root of the scan rate for the scan rates as high as 600 mV/s. These observations are roughly the same as those of Zagal et al. (*21*) who reported a catalytic oxidation of cysteine via cobalt phthalocyaninetetrasulfonate adsorbed onto pyrolytic graphite.

Analogous CV results were obtained at 2.0% CoPC electrodes for a series of sulfhydryl species including 2-mercaptoethanol, 3-mercaptopropionic acid, the antitumor drug 6-mercaptopurine, the antihypertensive agent Captopril, penacillamine, homocysteine, *N*-acetylcysteine, and the cysteine-containing tripeptide glutathione. This is illustrated in Figure 3 for the last three compounds. Note that, unlike the voltammograms shown previously, these were run in pH 2.4 phosphate buffer. Because our eventual objective entailed the use of these CME systems in LCEC detection, it was appropriate to examine the electrocatalytic processes under less acidic solution conditions more directly compatible with liquid chromatographic instrumentation. In general, the affect of increasing the solution pH was a modest shift of the catalytic waves to lower potentials. For all the above compounds similar but not identical increases in anodic current were observed at the CME in the potential region of the CoPC oxidation. As with cysteine, the catalytic waves were irreversible with no cathodic current seen on the reverse scan. Further, although the anodic peak currents showed a linear dependence on the square root of the potential scan rate, the oxidation waves failed to exhibit the usual broad tailing characteristic of simple diffusion-limited processes; and the

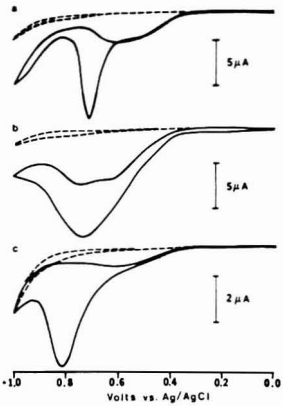


Figure 3. Cyclic voltammograms of (a) *N*-acetylcysteine, (b) homocysteine, and (c) glutathione at unmodified carbon paste (– – –) and 2.0% CoPC carbon paste (—) electrodes. All concentrations are 1.0 mM. Electrolyte was 0.05 M phosphate buffer (pH 2.43); scan rate was 30 mV/s.

reverse scans sometimes became irregular in shape, showing unexpected anodic dips in current as the potential was cycled back in the cathodic direction. The reason for this nonideal behavior is not yet known and requires continued investigation. However, ongoing work in our laboratory involving the phthalocyanine-mediated oxidation of several organic compounds in addition to sulfhydryls indicates that such CV behavior is a generally observed phenomenon for CoPC electrocatalysis. A possible explanation for the adsorption-like CV behavior is that one step of the oxidation process consists of the slow or irreversible chelation of the thiol group to the phthalocyanine metal center. Some evidence for the involvement of such a complexation step in the homogeneous electrocatalytic process has been demonstrated in previous electrochemical and spectroscopic investigations (*13–18*).

Other sulfur-containing compounds examined included cystine, methionine, and malathion. Of these, only cysteine showed enhanced anodic current at the CoPC-CMEs. For this compound, no oxidation was seen for the initial scan in the positive direction. However, when the potential was first scanned sufficiently far in the negative direction to reduce cysteine (presumably to the sulfhydryl form), subsequent scans to positive potentials exhibited current–voltage behavior similar to that observed for cysteine itself.

LCEC. Despite some uncertainty concerning the catalysis mechanism, it was apparent that the response enhancement produced by the use of CoPC-containing CMEs should make their usage attractive in a number of analytical applications. One area where their use could be of particular advantage is as the sensing electrode for the detection and determination of sulfhydryl compounds following LCEC. For such applications, it is necessary that the analyte of interest be oxidized or reduced at a relatively low potential. The lower the potential required, the better is the sensitivity and selectivity that is expected to result (*3*).

Hydrodynamic voltammograms (HDVs) obtained for cysteine, homocysteine, and *N*-acetylcysteine via flow injection are shown in Figure 4. They were obtained by recording the response of the CoPC-CME placed in the conventional thin-layer cell configuration ordinarily employed in LCEC but with a short length of narrow stainless steel tubing inserted in place of the column between the injector and detector. The HDVs

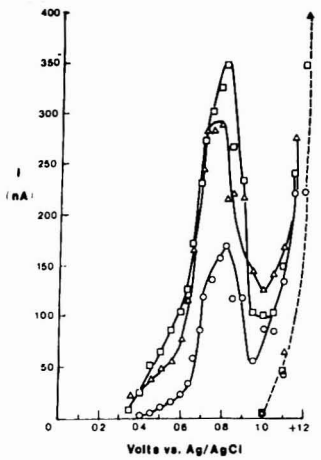


Figure 4. Hydrodynamic voltammograms of cysteine (○), homocysteine (□), and *N*-acetylcysteine (▲) at a 2.0% CoPC electrode. Mobile phase was 5% CH_3OH/95% 0.05 M phosphate buffer (pH 2.43) with 1.0 mM octanesulfonate. Flow rate was 1.0 mL/min.

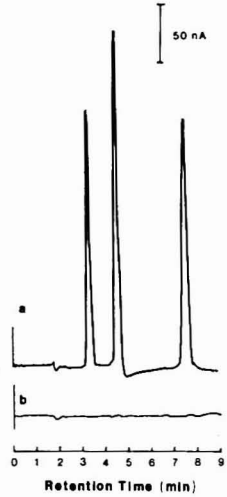


Figure 5. Chromatogram of cysteine, *N*-acetylcysteine, and homocysteine at (a) 2.0% CoPC carbon paste electrode and (b) unmodified carbon paste electrode. Concentrations were 1.0×10^{-5} M; E = +0.75 V vs. Ag/AgCl; same mobile phase and flow rate as in Figure 4.

possessed virtually the same shape for all three compounds; as in their CVs, only a single region of electrochemical activity was observed: an anodic wave which reached a maximum at approximately +0.8 V vs. Ag/AgCl and rapidly decreased at higher potentials. Also provided for comparison are the HDVs obtained at unmodified carbon paste which, as in CV, showed no response at potentials lower than +1.0 The mobile phase employed in these flow injection experiments and in the LCEC experiments described below consisted of 5% CH_3OH/95% 0.05 M phosphate buffer (pH 2.4) containing 10^{-3} M sodium octanesulfonate.

As was observed earlier for the CVs of the sulfhydryl compounds at the CoPC-CMEs, the shapes of the HDVs obtained for the same analytes also were not consistent with that ordinarily observed for a simple diffusion-limited oxidation. Rather, the decreases in chromatographic peak currents that occurred at higher potentials were indicative of the occurrence of a potential-dependent electrode deactivation process which, as will be discussed below, severely limited the high potential operation of the electrode as an LCEC detector. In fact, operation at potentials greater than +0.85 V vs. Ag/AgCl for even a few chromatograms resulted in a marked decrease in the low potential electrode response compared to that observed for a fresh electrode surface. Furthermore, after HDVs were obtained in the usual manner by starting at low potentials and then proceeding to more positive values, subsequent attempts to reproduce the HDVs by changing the applied potential in the reverse direction yielded i–E profiles of the same shape but much reduced in magnitude.

On the basis of the HDVs, it was apparent that the optimum potential for LCEC detection of these thiols at CoPC CMEs should fall between +0.70 and +0.80 V vs. Ag/AgCl. Accordingly, the chromatogram shown in Figure 5 was subsequently generated with an octadecylsilane column and a detector potential of +0.75 V. As expected, well-formed anodic peaks were obtained at this potential only when the CoPC electrode was employed and not for unmodified carbon paste or glassy carbon electrodes. Under these conditions, calibration curves for each of the sulfhydryl compounds were linear for injected amounts of analyte from 270 to 2.7 pmol. In all cases, the latter amount yielded a S/N of approximately 2 and thus represented the detection limit for all three species. The linearity was evaluated by least-squares analysis of data taken for seven concentrations over this range. The compounds yielded correlation coefficients ranging from 0.997 to 0.999; the slopes of the calibration curves varied from 1.88 nA/pmol for homocysteine to 1.50 nA/pmol for *N*-acetylcysteine.

One of the principal advantages of carbon paste electrodes over solid electrodes is their capacity for easy and relatively reproducible generation of new surfaces. Likewise, one of the primary strengths of chemically modified carbon paste electrodes compared to CMEs formed by the usual methods involving adsorption, covalent attachment, or polymer coating onto solid substrates lies in their similar capacity for rapid generation of quantitatively reproducible modified surfaces (6). Accordingly, evaluations were made of the reproducibility of repeated injections of the identical sulfhydryl solutions when the carbon paste CME surface was replaced between each injection. Typical peak currents obtained in this manner for the injection of 1.0×10^{-4} M cysteine solution yielded a relative standard deviation of 6.98% for nine successive trials. This level of reproducibility is not appreciably less than that expected for the repeated renewal of ordinary carbon paste surfaces (22).

Finally, the stability of the CME response in LCEC was evaluated by placing the CoPC-containing electrode in the flowing mobile phase stream and following its current response toward the sulfhydryl compounds over an extended length of time. Typical results obtained for repeated injections of 1.0×10^{-4} M homocysteine are shown in Figure 6. Similar stability was observed for cysteine and *N*-acetylcysteine as well. When the electrode was maintained at +0.75 V vs. SCE (curve a), peak heights decreased by 1–2%/h; as a result, CMEs ordinarily retained 85–90% of their original activity following 8 h of continuous exposure to the methanol/H_2O

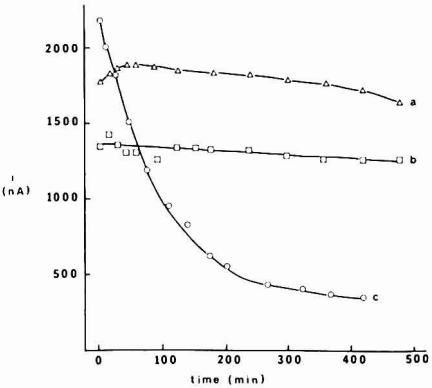


Figure 6. Electrode response for 1.0×10^{-4} M homocysteine vs. time immersed in flow injection system: (a) $E = +0.75$ V vs. Ag/AgCl; (b) $E = +0.65$ V; (c) $E = +0.85$ V. Same conditions as in Figure 4.

stream. As seen in curve c, operation at higher potentials resulted in a much more dramtic decrease in electrode response that was sufficiently rapid that, after 7 h (or more than 100 injections), measured currents were reduced to only 16% of those initially observed at the fresh electrode surface. However, operation at +0.65 V (curve b) caused practically no electrode deactivation even after a full day of continuous operation. Most likely, most of the instability at the more positive LCEC potentials was related to the nondiffusion phenomena observed at similar potentials in both CVs and HDVs. In addition, it is possible that some of the decrease in electrode response was due to the gradual leaching of CoPC from the CME surface. In fact, some decreases in response have been observed previously even for conventional carbon paste electrodes in LCEC upon long-term exposure to a binary mobile phase containing a small fraction of organic components such as methanol or acetonitrile. In any case, however, the CoPC/carbon paste surface could be rapidly and reproducibly renewed if desired. Further, after surface regeneration, a period of only 5–10 min was required for the electrode to reach the optimum level at +0.75 V vs. Ag/AgCl, the potential required for this determination.

It is clear that, as for hydrazine, phthalocyanine-containing CMEs possess considerable potential for use in the voltammetric and LCEC determination of sulfhydryl compounds. All –SH compounds examined in our laboratory have shown enhanced response with CoPC CMEs exceeding that obtained with conventional carbon paste and glassy carbon electrodes and approaching that for Hg/Au amalgam electrodes. Extension of this work to include applications involving the practical determination of specific sulfhydryl compounds is continuing. In addition, it is apparent that electrocatalytic CMEs, whether constructed by the addition of the modifying species to carbon paste or by the other electrode modification methods, offer the possiblity of extending voltammetric and LCEC techniques to include several classes of compounds otherwise poorly suited to electroanalysis.

ACKNOWLEDGMENT

The authors wish to thank E. R. Squibb & Sons, Inc., for their generous donation of the Captopril sample used in this work.

Registry No. CoPC, 3317-67-7; carbon, 7440-44-0; cysteine, 52-90-4; homocysteine, 6027-13-0; *N*-acetylcysteine, 616-91-1; glutathione, 70-18-8.

LITERATURE CITED

(1) Snell, K. D.; Keenan, A. G. *J. Chem. Soc., Chem. Soc. Rev.* **1979**, *8*, 259–282.
(2) Murray, R. W. *Acc. Chem. Res.* **1980**, *13*, 135–141.
(3) Kissinger, P. T. *Anal. Chem.* **1977**, *49*, 447A–456A.
(4) Ravichandran, K.; Baldwin, R. P. *Anal. Chem.* **1983**, *55*, 1782–1786.
(5) Ravichandran, K.; Baldwin, R. P. *J. Liq. Chromatogr.*, in press.
(6) Korfhage, K. M.; Ravichandran, K.; Baldwin, R. P. *Anal. Chem.* **1984**, *56*, 1514–1517.
(7) Moser, F. H.; Thomas, A. L. "The Phthalocyanines"; CRC Press: Boca Raton, FL, 1983; Vol. 1.
(8) Rabenstein, D. L.; Saetre, R. *Anal. Chem.* **1977**, *49*, 1036–1039.
(9) Saetre, R.; Rabenstein, D. L. *Anal. Chem.* **1978**, *50*, 276–280.
(10) Allison, L. A.; Shoup, R. E. *Anal. Chem.* **1983**, *55*, 8–12.
(11) Weber, J. H.; Busch, D. H. *Inorg. Chem.* **1965**, *4*, 469–471.
(12) Rollman, L. D.; Iwamoto, R. T. *J. Am. Chem. Soc.* **1968**, *90*, 1455–1463.
(13) Kundo, N. N.; Keier, N. P.; Glazneva, G. V.; Mamaeva, E. K. *Kinetika Kataliz* **1967**, *8*, 1325–1330.
(14) Kundo, N. N.; Keier, N. P. *Russ. J. Phys. Chem.* **1968**, *42*, 707–711.
(15) Kundo, N. N.; Keier, N. P. *Kinetika Kataliz* **1970**, *11*, 91–99.
(16) Dolansky, J.; Wagnerova, D. M.; Verprek-Siska, J. *Collect. Czech. Chem. Commun.* **1976**, *41*, 2326–2332.
(17) Skorobogaty, A.; Smith, T. D. *J. Mol. Catal.* **1982**, *16*, 131–147.
(18) Brouner, W. M.; Piet, P.; German, A. L. *Polym. Bull.* **1982**, *8*, 245–251.
(19) Shepard, V. R.; Armstrong, N. R. *J. Phys. Chem.* **1979**, *83*, 1268–1276.
(20) Green, J. M.; Faulkner, L. R. *J. Am. Chem. Soc.* **1983**, *105*, 2950–2955.
(21) Zagal, J.; Fierro, C.; Rozas, R. *J. Electroanal. Chem.* **1981**, *119*, 403–408.
(22) Adams, R. N. "Electrochemistry at Solid Electrodes"; Marcel Dekker: New York, 1969; p 283.

RECEIVED for review August 3, 1984. Accepted December 5, 1984. This work was supported by the Graduate School of the University of Louisville. It was presented in part at the 187th National Meeting of the American Chemical Society.

Infrared Spectrometric Studies of Cyanoalkyl Ligands Immobilized on Chromatographic Surfaces

B. R. Suffolk and R. K. Gilpin*

Department of Chemistry, Kent State University, Kent, Ohio 44242

Long and intermediate chains of cyanoalkyl ligands were attached to porous silica-base material by using monoreactive chemistry, and short cyanoalkyl chains were attached by using mono-, di-, and trireactive chemistry. Subsequently, the microchemical structures of these materials were studied with Fourier transform infrared (FT-IR) techniques. In a nonpolar liquid (i.e., hexane) infrared spectra for the nitrile band were extremely broad and asymmetrical. Deconvolution of these bands produced a doublet which suggested the presence of at least two different types of attached ligands. These bands support the idea of a certain population of nitrile groups which hydrogen bond with free surface silanol groups and a population of nitrile groups which sterically cannot hydrogen bond. This is possible by assuming a nonuniform distribution of groups. Groups bonded within a rich area or cluster would be restricted from surface interaction by surrounding groups or neighboring groups, whereas groups at the edges of such a cluster or groups bonded in sparcely populated areas could hydrogen bond. In a polar solvent (i.e., 1-butanol) the groups were displaced from the surface and showed ligand–solvent interaction.

The utilization of chemically bonded stationary phases for high-performance liquid chromatography has offered great rewards in terms of selectivity and stability over the earlier physically coated packings (*1*). These stationary phases generally are prepared by immobilizing various organosilane molecules to porous silica-base materials. The most popular chemically bonded phases are those with hydrocarbon ligands (either octyl or octadecyl), which are used typically in the reversed-phase mode. Probably next in popularity are the more polar chemically altered surfaces formed by attaching either an amino or a cyano group via a short hydrocarbon spacer arm. These latter materials are used in both the reversed-phase as well as the normal-phase mode.

Over the course of their development, the physical nature of chemically modified surfaces has been a subject of both interest and controversy (*1*). Although the chemistry to prepare useful materials has progressed to a rather mature state, a detailed understanding of the stereochemistry of the system is emerging only now (2). During the synthesis of bonded phases, the actual degree of modification is dependent upon a number of factors including backbone chemistry, surface area and porosity of the sorbent, and reagent structure (i.e., size and shape). On a macro basis synthetic procedures are usually such that statistically about one-quarter to one-half of the available silanol groups are involved in the reactions. On an actual microchemical basis the extent and uniformity of coverage may be much more complicated. This has been demonstrated recently by several techniques (*3–6*).

Historically, most descriptions of the surface were based solely on chromatographic results (*7*). More recently, chromatographic surfaces have been probed with a variety of methods. Although initial experiments were concerned with the degree and type of surface reactivity, the information currently being derived is providing new insights about surface–ligand structure and interaction, bonded layer solvation, and segmental and total chain mobility. Specific examples of these include: 1. investigations of surface homogeneity by examing the fluorescence behavior of chemically attached pyrene probes (*3*), 2. nuclear magnetic resonance studies of the preferential solvation and motional dynamics of immobilized ligands (*7–10*), and 3. the elucidation of conformational features for silica immobilized dimethyl-*n*-alkyl (*11*) and acetoacetamide (*12*) ligands using FT-IR.

By use of monochlorosilanes or monoalkoxysilanes, chemical bonded phases can be prepared which are reproducible and efficient (*6, 13*). This is because the bonding chemistry is relatively simple, involving the replacement of the surface silanol proton with the silane ligand. However, since di- or trichloro and di- or trialkoxysilanes have multireactive sites, they are inherently more difficult to control and hence they are less defined and reproducible (*6, 14*). For steric reasons it is more likely that the di- or trichloro and di- or trialkoxysilanes react to form cross-linked attached layers rather than multiattached centers (*6*). Formerly most commercial bonded phases were prepared with either bifunctional or trifunctional silanes, but because of the advantages of reproducibility, they are now generally manufactured with monofunctional silanes (*9, 15*).

In the current study long and intermediate cyanoalkyl chains were attached to silica surfaces by using monoreactive chemistry, and short cyanoalkyl chains were attached by using monoreactive, direactive, and trireactive chemistry. Subsequently the microchemical structures of these materials were studied by FT-IR techniques. Infrared spectrometry was chosen here as a tool to investigate chemically bonded stationary phases, since solvent environments can be made to simulate liquid chromatographic experiments. For the cyanoalkyl phases infrared spectrometry is especially suited, since the C≡N stretch band is isolated from interference bands arising from the siloxane structure and surface silanol/water. Two major points were of interest: 1. the type and uniformity in distribution of the ligand population and 2. the degrees of ligand–surface and ligand–solvent interactions.

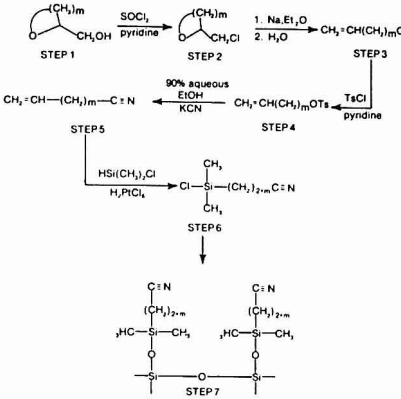
EXPERIMENTAL SECTION

Materials. Tetrahydro-2-furancarbinol was purchased from Pfaltz and Bauer, Inc. Tetrahydropyran-2-methanol (98%), 10-undecen-1-ol (99%), and acrylonitrile (99+%) were purchased from Aldrich Chemical Co., Inc. Dimethylchlorosilane, (2-cyanoethyl)methyldichlorosilane, (2-cyanoethyl)trichlorosilane, (3-cyanopropyl)dimethylchlorosilane, and (3-cyanopropyl)trichlorosilane were obtained from Petrarch Systems, Inc. Alkylnitrile groups were bonded onto Li Chrosorb Si 60 silica (mean particle size 10 μm and surface area 550 m^2/g) from E Merck. HPLC grade hexane and 1-butanol were obtained from MCB Manufacturing Chemists, Inc., and spectrograde chloroform (0.75% ethanol preservative) was obtained from Fisher Scientific Co.

Synthesis of the Noncommercially Available. (Cyanoalkyl)dimethylchlorosilanes. Tetrahydrofuran-2-methyl chloride and tetrahydropyran-2-methyl chloride were synthesized

0003-2700/85/0357-0596$01.50/0 © 1985 American Chemical Society

Scheme I



from tetrahydro-2-furancarbinol and tetrahydropyran-2-methanol, respectively, as described by Kirner (*16*). From the tetrahydrofuran-2-methyl chloride and the tetrahydropyran-2-methyl chloride, 4-penten-1-ol and 5-hexen-1-ol were prepared by an initial reaction with sodium and subsequent hydrolysis according to the procedure of Baubert, Linstead, and Rydon (*17*). Tosylates were synthesized from the alcohols, as described by Gangoda and Gilpin (*18*). Tosylates were converted to nitriles using a method similar to Wilt, Massie, and Dabek (*19*). To carry out the final coupling step in the synthesis of the monochlorosilanes, 50 drops of 0.1 M hydrogen hexachloroplatinate in 2-propanol was added to a 1:1.15 ratio of an alkenylnitrile to dimethylchlorosilane mixture. The contents were heated in a 50-mL stainless steel tube at 100 °C for 2 days. Purification of the product was obtained by vacuum distillation. Structures of the synthesized silanes were verified by ^1H and ^{13}C NMR.

Preparation of the Alkylnitrile Bonded Phases. A 1.5-g portion of silica was slurried with water, and the excess water was decanted away. The silica was dried at 110 °C for 2 h and then conditioned with water-saturated toluene overnight to establish the degree of surface hydration. The silica was refluxed with 55 mL of a 10% reaction mixture of the (cyanoalkyl)dimethylchlorosilane, (cyanoalkyl)methyldichlorosilane, or (cyanoalkyl)trichlorosilane monomer in water-saturated toluene. While conditioning the silica surfaces and also during the reaction, dried nitrogen was bubbled through the bottom of the reaction vessel to provide mild agitation of the reaction mixture and to expel HCl generated by the silane reaction. Subsequently, the chemically modified silica was exhaustively washed with four 50-mL portions of dry toluene, two 50-mL portions of water-saturated toluene, and two 50-mL portions of ether, dried overnight in a 110 °C oven, and then stored in a desiccator.

The stabilized (3-cyanopropyl)trimethylsilane was synthesized from methylmagnesium iodide and (3-cyanopropyl)trichlorosilane in sodium-dried ether.

Spectrometry. Fourier transform infrared spectra were scanned with a Nicolet 7199 FT-IR spectrometer equipped with a MCT detector and operated to give 1 cm^{-1} resolution. The cyanoalkylsilanized silica was placed between two KCl windows of a Connecticut Instrument Corp. demountable liquid cell equipped with a 0.1- or 0.2-mm spacer. After the demountable cell was assembled, the appropriate liquid medium was added through the two liquid ports via a dropper. Ratios of 250 sample scans vs. 100 nitrogen-atmosphere background scans were taken. The absorbances of the C≡N band maxima varied from 0.42 to 0.99. No base line corrections or subtractions were employed.

In a 0.1074-mm Perkin-Elmer liquid cell, a 1:20 dilution of (3-cyanopropyl)trimethylsilane in hexane or 1-butanol was scanned. The measured absorbance readings of the C≡N band maxima in hexane and 1-butanol were 0.14 and 0.21, respectively.

Scheme II

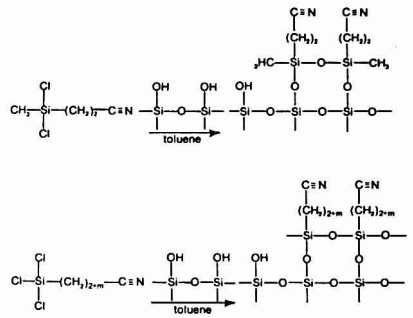


Table I. Surface Coverage for the Chemically Bonded Alkylnitriles

		surface coverage[b]	
n[a]	bonding chemistry	% bound carbon	normalized carbon
2	monochloro	5.8	1.2
3	monochloro	6.6	1.1
5	monochloro	8.6	1.1
6	monochloro	9.2	1.0
11	monochloro	9.9	0.7
2	dichloro	8.0	2.0
2	trichloro	6.3	2.1
3	trichloro	7.9	2.0

[a] Length of the alkyl spacer arm (i.e., $>SiO\text{-}\overset{|}{Si}\text{-}(CH_2)_nC{\equiv}N$). [b] Manufacturer listed surface area of 550 m^2/g.

A FORTRAN computer program was written to access the file on the hard disk where each spectrum was stored and then to select the band maxima and to compute the asymmetry ratio, a/b, of the C≡N stretch bands. For bonded phases in chloroform and hexane, base lines between 2295 and 2162 cm^{-1} were used. For bonded phases in 1-butanol, base lines between 2299 and 2210 cm^{-1} were used. Fourier self-deconvolution (*20*) was performed with the Nicolet IRDCON.FTN program (*21*).

RESULTS AND DISCUSSION

The reaction scheme which was used to synthesize the (cyanoalkyl)silanized silicas from (cyanoalkyl)dimethylchlorosilanes involved the steps shown in (Scheme I). When $m = 3$ or 4, $m = 9$, $m = 0$, or $m = 1$, the syntheses began at steps 1,3,5, or 6, respectively. Likewise, the reaction schemes utilized in the preparation of (cyanoalkyl)silanized silicas from the (cyanoalkyl)dichloromethylsilane and the (cyanoalkyl)-trichlorosilanes ($m = 0$ or 1) are shown in (Scheme II).

Surface coverages for the various cyanoalkyl bonded phases prepared in the current study are shown in Table I. Results are listed in terms of both weight percent and normalized values. For the bonded phases synthesized from either mono-, di-, or trichlorosilanes, the normalized carbon was found by dividing the percent bound carbon by $n + 3$, $n + 2$, and $n + 1$, respectively. In this relationship n is equal to the number of carbons (i.e., the length of the spacer arm) the cyano group is removed the silane atom. Except for the longer cyanoundecyl chain, the normalized carbon values were nearly the same for all monochloro modified materials. In the cases of the di- and the trichloromodified materials, coverage was about twice that obtained with the (cyanoalkyl)monochlorosilanes.

(3-, 5-, 6-, and 11-Cyanoalkyl)silanized Silicas. The infrared spectra of the C≡N stretch region for each of the

Table II. Band Maxima and Asymmetry for the C≡N Stretch Band of Various Immobilized Cyanoalkyl Ligands in 1-Butanol, Chloroform and Hexane

		a/b[b]			ν_{max}, cm^{-1}			
n[a]	bonding chemistry	1-butanol	chloroform	hexane	1-butanol	chloroform	hexane	hexane[c]
3	monochloro	1.3	2.5	3.1	2251.4	2248.5	2248.0	2256.9, 2247.1
5	monochloro	1.6	1.8	2.9	2250.0	2249.0	2248.5	2258.0, 2247.8
6	monochloro	1.8	2.0	2.7	2248.5	2247.6	2248.0	2257.8, 2246.8
11	monochloro	1.6	1.8	1.9	2249.5	2248.5	2251.9	2258.9, 2248.8
3	trichloro	1.5	1.8	2.0	2250.4	2249.5	2250.0	2257.4, 2248.1
2	monochloro	1.6	2.4	3.0	2228.8	2226.3	2226.3	2234.5, 2226.1
2	dichloro	1.5	1.6	1.9	2251.9	2251.9	2250.9	2259.7, 2250.1
2	trichloro	1.1	1.2	1.0	2255.8	2256.2	2257.7	2258.4, 2253.1

[a] See Table I. [b] Band asymmetry. [c] Deconvoluted doublet.

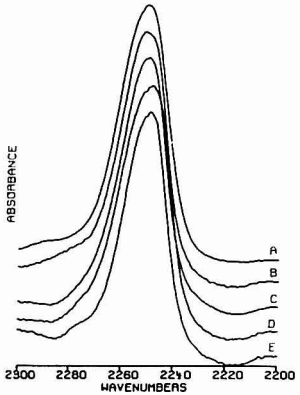


Figure 1. FT-IR spectra of C≡N stretch bands for various immobilized cyanoalkyl ligands. Surfaces prepared from (A) (3-cyanopropyl)trichlorosilane, (B) (3-cyanopropyl)dimethylchlorosilane, (C) (5-cyanopentyl)dimethylchlorosilane, (D) (6-cyanohexyl)dimethylchlorosilane, and (E) (11-cyanoundecyl)dimethylchlorosilane. Liquid medium was 1-butanol.

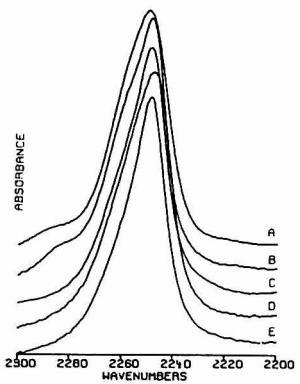


Figure 2. C≡N stretch bands of the same (cyanoalkyl)silanized silicas (A–E) shown in Figure 1. Liquid medium was chloroform.

cyanoalkyl bonded phases using 1-butanol, chloroform, or hexane as liquid media are shown in Figures 1, 2, and 3, respectively. Corresponding band asymmetry ratios, a/b, were

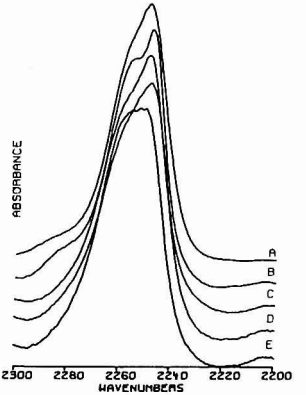


Figure 3. C≡N stretch bands of the same (cyanoalkyl)silanized silicas (A–E) shown in Figure 1. Liquid medium was hexane.

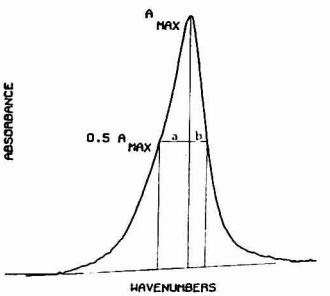


Figure 4. Asymmetry ratio a/b of each C≡N stretch band, measured by dividing the distance a by the distance b.

calculated as illustrated in Figure 4 and are summarized in Table II. Generally for a given solvent, changes in length of the alkyl spacer arm did not affect band contour significantly. However, comparing results among solvent types, the asymmetry increased in the order of decreasing polarity of the media in contact with the surface (i.e., 1-butanol < chlorofrom < hexane).

In hexane (Figure 3), the bands for the immobilized groups were extremely asymmetrical and distorted to the point that shoulders were noted. The Fourier self-deconvolution of these,

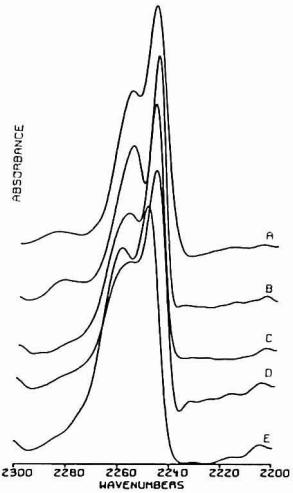


Figure 5. Fourier self-deconvolution of the C≡N stretch bands shown in Figure 3.

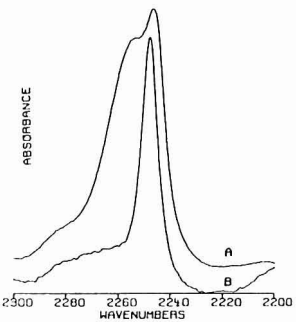


Figure 6. FT-IR spectra of (A) (3-cyanopropyl)silanized silica and (B) (3-cyanopropyl)trimethylsilane (i.e., stabilized analogue) in hexane.

which are shown in Figure 5, demonstrate that the asymmetrical bands obtained in hexane were actually unresolved doublets. The observed frequencies of each of the resulting deconvoluted peaks are consistent with the work of Rochester et al., which is discussed below.

Infrared spectra of the nitrile region obtained in hexane and 1-butanol, respectively, for the (3-cyanopropyl)dimethyl immobilized ligand and for the corresponding stabilized monomer, (3-cyanopropyl)trimethylsilane, are shown in Figure 6 and 7. Due to the inherent problems of reactivity with the chlorosilane monomers, (3-cyanopropyl)trimethylsilane was used as the unbound control compound. These latter spectra illustrate the presence of two types of band distortion, asymmetry and broadening. Referring to Figure 6, changes in band contour in an apolar solvent (i.e., hexane) easily can be seen by comparing the control compound in the absence of silica to the similar immobilized ligand. In contrast to the extremely asymmetric C≡N stretch band of the chemically immobilized form (a/b = 3.1), the C≡N stretch band of the nonimmobilized, free form was very sharp and nearly symmetric (a/b = 0.9). In 1-butanol (Figure 7) the asymmetrical distortions in the nitrile band for both the free (a/b = 1.0) and immobilized (a/b = 1.3) forms were not present. However, the C≡N stretch bands were much broader in 1-butanol (Figure 7) than the free form in hexane (Figure 6).

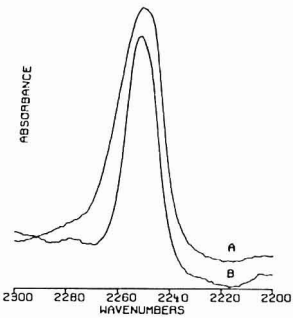


Figure 7. FT-IR spectra of (A) (3-cyanopropyl)silanized silica and (B) (3-cyanopropyl)trimethylsilane (i.e., stabilized analogue) in 1-butanol.

Bellamy (*22*) has stated that band broadening and asymmetry have been found in both OH and NH hydrogen-bonded systems. Likewise, the above changes in C≡N band symmetry are consistent with the idea of hydrogen bonding. In the present investigation the observed changes in band shape between free and immobilized nitrile groups acquired in an apolar vs. polar solvent are indicative of two types of hydrogen bonding: 1. ligand–surface and 2. ligand-solvent. The extremely asymmetric C≡N stretch for the modified materials in contact with hexane results from hydrogen bonding between a portion of the chemical immobilized groups and free surface silanol groups and will be considered in greater detail below. In 1-butanol, both the free silane and the chemically modified silica exhibited broad bands indicative of hydrogen bonding with the solvent. In the absence of hydrogen bonding (i.e., stabilized control silane in hexane) the C≡N stretch band was sharp and symmetric.

The idea of specific ligand surface interactions has been suggested for another system. Leyden et al. (*12*) have suggested that hydrogen bonds are probably formed with unreacted surface silanols in their investigations of immobilized acetoacetamide, which was synthesized by reacting diketene with either (3-aminopropyl)trimethoxysilane or (*N*-(2-aminoethyl)-3-aminopropyl)trimethoxysilane bound to silica. Leyden et al. suggested that since the silica surface was polar, it could function as a donor in hydrogen bonding with the bound amide groups.

The current data are also consistent with nitrile adsorption studies. Rochester et al. have investigated changes in the infrared spectra for the adsorption of propionitrile on silica (*23*, *24*). Self-supporting disks of Aerosil silica were placed between two silica windows of an infrared cell, and the assembly was evacuated at 873 K. Subsequently, various binary solutions of propionitrile in heptane were introduced into the cell. As the concentration of propionitrile was increased, the intensities of the 3705 cm^{-1} free Si–OH stretch band decreased linearly as a broad 3395 cm^{-1} band and a band at 2260 cm^{-1} increased. The authors rationlized these spectroscopic changes in terms of the formation of hydrogen bonds between the surface silanol groups and the cyano groups of adsorbed propionitrile molecules. The broad band at 3395 cm^{-1} was attributed to hydrogen-bonded Si–OH groups, and the band at 2260 cm^{-1} was attributed to hydrogen-bonded C≡N groups.

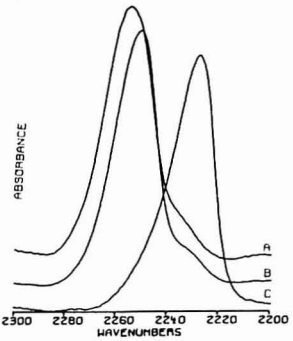


Figure 8. FT-IR spectra of C≡N stretch bands for (2-cyanoethyl)-silanized silicas prepared using different backbone chemistry. Surface was prepared from (A) (2-cyanoethyl)trichlorosilane, (B) (2-cyanoethyl)methyldichlorosilane, and (C) (2-cyanoethyl)dimethylchlorosilane. Liquid medium was 1-butanol.

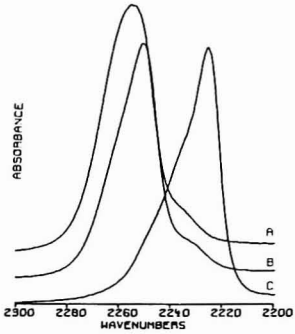


Figure 9. C≡N stretch bands of the same (2-cyanoethyl)silanized silicas shown in Figure 8. Liquid medium was chloroform.

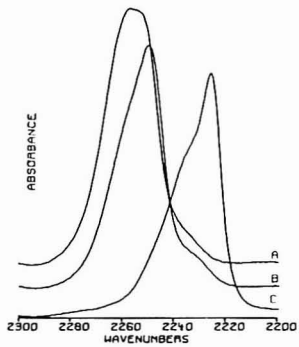


Figure 10. C≡N stretch bands of the same (2-cyanoethyl)silanized silicas shown in Figure 8. Liquid medium was hexane.

Spectroscopic results for the adsorption of propionitrile on silica immersed in 2,2,4-trimethylpentane or toluene were similar, except that the maxima of the silanol groups perturbed by toluene was at 3595 cm^{-1} instead of 3395 cm^{-1}. In the absence of silica, infrared symmetric C≡N stretch bands occurred at 2249 cm^{-1} for propionitrile in heptane and 2248 cm^{-1} for propionitrile in 2,2,4-trimethylpentane or toluene. The 2260 cm^{-1} band arising from hydrogen-bonded propionitrile adsorbed on silica appeared at the same frequency for all three liquid media.

The frequencies of the band maxima, ν_{max}, for the spectra shown in Figure 1–3 are summarized in Table II. Within a given solvent ν_{max} was nearly independent of spacer arm length for the 3-, 5-, 6-, and 11-cyanoalkyl immobilized ligands. In both 1-butanol and chloroform the current ν_{max} values are similar to those reported by Rochester et al. for propionitrile in heptane, 2,2,4-trimethylpentane, or toluene in the absence of silica. As such, these data suggest the absence of significant ligand–surface interaction via hydrogen bonding when the immobilized groups are solvated by polar liquids like 1-butanol or chloroform.

Values of ν_{max} for the deconvoluted spectra obtained in hexane (Figure 5) are also listed in Table II. The lower frequency values of the deconvoluted doublets are similar in frequency to the band maxima for the modified silica in contact with eiher 1-butanol or chloroform and also are similar in frequency to the non-hydrogen-bonded C≡N stretch bands obtained by Rochester et al. Therefore it seems reasonable to suggest that the bands at the lower ν were the result of a certain percentage of cyano groups which did not hydrogen bond with the surface. However, since the bands at the higher ν correspond closely in frequency with the hydrogen-bonded form of propionitrile reported by Rochester et al., it seems reasonable also to suggest the existence of hydrogen bonding between the attached cyano groups and unreacted silanol groups on the silica surface.

West and Baney (25) have shown that for hydrogen bonding systems, silanols are more associated than carbinols at any given concentration, but the differences are not large. We also found that hydrogen bonding between immobilized nitrile groups and the silanols resulted in larger band shifts than did the nitrile–carbinol hydrogen-bonding interaction. In hexane, the lower frequency non-hydrogen-bonded bands and the higher frequency hydrogen-bonded bands (Figure 5) were separated by 8 to 11 cm^{-1}. With the exception of the 11-cyanoundecyl surface, for a given spacer arm in 1-butanol the values of ν_{max} were shifted 0.5 to 3 cm^{-1} higher in frequency than when there was no ligand–solvent hydrogen bonding.

(2-Cyanoethyl)silanized Silicas. The infrared spectra of the C≡N stretch region for the (2-cyanoethyl)silanized silicas in 1-butanol, chloroform, and hexane are shown in Figures 8, 9, and 10, respectively. The asymmetry and band broadening arguments presented above for the longer cyanoalkyl immobilized ligands also hold for the 2-cyanoethyl groups attached via either mono- or dichloro chemistry (Table II). For these backbone chemistries the asymmetry of the nitrile bands increased in the order of decreasing polarity of the liquid medium (i.e., 1-butanol < chloroform < hexane). In the case of the immobilized 2-cyanoethyl ligands synthesized from trichlorosilane, broadened symmetrical C≡N stretch bands were observed regardless of solvent type. Each of the spectra of the (2-cyanoethyl)silanized silicas in hexane yielded two bands after undergoing Fourier self-deconvolution (Figure 11). These results also are consistent with the above data obtained from the longer immobilized groups.

In comparison to the (3-, 5-, 6-, and 11-cyanoalkyl)silanized silicas and the (2-cyanoethyl)silanized silica synthesized from (2-cyanoethyl)methyldichlorosilane, ν_{max} values for the 2-cyanoethyl surface synthesized from the corresponding monochlorosilane and trichlorosilane were about 22 cm^{-1} lower and about 7 cm^{-1} higher, respectively. These shifts are reasonable based on changes in the electronic environment

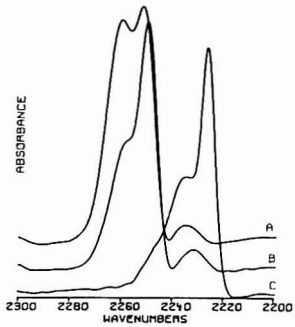


Figure 11. Fourier self-deconvolution of the C≡N stretch bands shown in Figure 10.

surrounding the β-carbon. For (2-cyanoethyl)silanized silica, made with the mono-, di-, and trichlorosilanes, two methyl groups and one oxygen atom, one methyl group and two oxygen atoms, and three oxygen atoms, respectively, were attached to the silicon atom. Kitson and Griffith (*26*) have shown previously that band shifts take place when substitutions are made in the β-position of alkylnitriles. They observed that when electronegative groups were substituted on β-carbon atoms, shifts to slightly higher frequencies occurred.

CONCLUSION

The above data thus support the idea that in hexane a certain population of immobilized groups can hydrogen bond with surface silanols and a certain population of attached groups sterically cannot hydrogen bond. For this to occur the ligands which do not hydrogen bond with the surface must be sterically restricted. Such restriction is most likely possible through formation of a nonuniform distribution of immobilized surface groups. During the synthesis process areas which are organically rich and organic areas which are sparsely populated form. Groups bonded within rich areas or clusters sterically cannot hydrogen bond with free silanols because of other surrounding cyanoalkyl chains. In sparsely populated organic areas or at the edges of clusters, cyano groups can hydrogen bond.

Based on luminescence studies of (3-(3-pyrenyl)propyl)-dimethylchlorosilane chemically bonded to microparticulate silica, Lochmüller et al. (*3*) also have proposed that surface immobilized ligands do not bond evenly. Rather the synthesis process results in an inhomogeneous distribution with high density regions and molecular aggravation or "clustering". Likewise, clustering has been suggested by Gilpin et al. to explain solvent entrapment in a chemically bonded decyl HPLC stationary phase (*6*).

LITERATURE CITED

(1) Gilpin, R. K. *Am. Lab. (Fairfield, Conn.)* **1982** (March), 103–108.
(2) Gilpin, R. K. *J. Chromatogr. Sci.* **1984**, *22*, 371–377.
(3) Lochmüller, C. H.; Colborn, A. S.; Hunnicutt, M. L.; Harris, J. M. *Anal. Chem.* **1983**, *55*, 1344–1348.
(4) Lochmüller, C. H.; Wilder, D. R. *J. Chromatogr. Sci.* **1979**, *17*, 574–579.
(5) Marshall, D. B.; Stutler, K. A.; Lochmüller, C. H. *J. Chromatogr. Sci.* **1984**, *22*, 217–220.
(6) Gilpin, R. K.; Gangoda, M. E.; Krishen, A. E. *J. Chromatogr. Sci.* (**1982**), *20*, 345–348.
(7) Gilpin, R. K.; Gangoda, M. E. *J. Chromatogr. Sci.* **1983**, *21*, 352–361.
(8) Sindorf, D. W.; Maciel, G. E. *J. Am. Chem. Soc.* **1983**, *105*, 1848–1851.
(9) Gilpin, R. K.; Gangoda, M. E. *Anal. Chem.* **1984**, *56*, 1470–1473.
(10) Slotfeldt-Ellingsen, D.; Resing, H. A. *J. Phys. Chem.* **1980**, *84*, 2204–2209.
(11) Sander, L. C.; Callis, J. B.; Field, L. R. *Anal. Chem.* **1983**, *55*, 1068–1075.
(12) Leyden, D. E.; Kendall, D. S.; Burggraf, L. W.; Pern, F. J.; De Bello, M. *Anal. Chem.* **1982**, *54*, 101–105.
(13) Berendsen, G. E.; Pikaart, K. A.; De Galan, L. *J. Liq. Chromatogr.* **1980**, *3*, 1437–1464.
(14) Berendsen, G. E.; De Galan, L. *J. Liq. Chromatogr.* **1978**, *1*, 561–586.
(15) Grushka, E.; Kikta, E. J., Jr. *Anal. Chem.* **1977**, *49*, 1004A–1014A.
(16) Kirner, W. R. *J. Am. Chem. Soc.* **1930**, *52*, 3251–3256.
(17) Gaubert, P.; Linstead, R. P.; Rydon, H. N. *J. Chem. Soc.* **1937**, 1971–1979.
(18) Gangoda, M. E.; Gilpin, R. K. *J. Labelled Compd. Radiopharma.* **1982**, *19*, 1051–1055.
(19) Wilt, J. W.; Massie, S. N.; Dabek, R. B. *J. Org. Chem.* **1970**, *35*, 2803–2805.
(20) Kauppinen, J. K.; Moffatt, D. J.; Mantsch, H. H.; Cameron, D. G. *Appl. Spectrosc.* **1981**, *35*, 271–276.
(21) Compton, D. A. C. *Spectral Lines* **1983**, *5*, 4–7. Reprinted as Nicolet FT-IR Application Note 8311.
(22) Bellamy, L. J. "The Infrared Spectra of Complex Molecules", 2nd ed.; Chapman and Hall: New York, 1980; p 241.
(23) Rochester, C. H. Trebilco, D. A. *Chem. Ind.* **1978**, 127–128.
(24) Rochester, C. H.; Yong, G. H. *J. Chem. Soc., Faraday, Trans. 1* **1980**, *76*, 1466–1475.
(25) West, R.; Baney, R. H. *J. Am. Chem. Soc.* **1959**, *81*, 6145–6148.
(26) Kitson, R. E.; Griffith, N. E. *Anal. Chem.* **1952**, *24*, 334–337.

RECEIVED for review September 28, 1984. Accepted December 3, 1984.

Fluorescence Study of Ion Pair Interactions on Hydrocarbon Bonded Surfaces

Sally D. Dowling and W. Rudolf Seitz*

Department of Chemistry, University of New Hampshire, Durham, New Hampshire 03824

The ammonium salt of 8-aniline-1-naphthalenesulfonic acid (ANS) was used to probe ion pair interactions with hydrocarbon bonded surfaces used in reversed-phase liquid chromatography. The wavelength of maximum ANS fluorescence emission serves as a measure of the relative polarity of ANS environment. Variables investigated were cation structure (tetramethylammonium, tetrabutylammonium, and myristyl) and concentration, bonded phase structure (methyl, octyl, octadecyl, and phenyl), and solvent (methanol and water). In most systems reducing the concentration of lipophilic cation causes increased lipophilic interaction between ANS and the surface. This is attributed to reduced surface charge density at lower cation concentrations. High concentrations of tetrabutylammonium ion cause a rearrangement of the octadecyl surface in water. Methanol tends to exclude ANS from the alkyl bonded phases causing it to experience a predominantly solvent environment. $\pi-\pi$ interactions enhance the interaction of ANS with the phenyl phase.

Organic ions can be separated by reversed-phase liquid chromatography (LC) if a lipophilic counterion is added to the mobile phase. This technique is known as reversed-phase ion pair chromatography.

The mechanism of reversed-phase ion pair LC has been a subject of considerable interest. Three models have been proposed. According to the "ion pair" model, the liophilic counterions pair with the ions being separated in the mobile phase. The ion pair then partitions onto the nonpolar stationary phase. A completely different mechanism is postulated by the "dynamic ion exchange" model. The lipophilic counterion ion is thought to adsorb on the nonpolar stationary phase causing it to act as an ion exchanger. Both of these models represent extreme views and are not successful in rationalizing all the observed chromatographic behavior.

The "ion-interaction" model proposes a third more complex view of ion pair separations (*1*). It allows for both electrostatic and lipophilic interactions between the ions and the nonpolar stationary phase. In addition it takes into account the electrical double layer which forms on the surface of the stationary phase. Recent reviews summarize the proposed mechanism for reversed-phase ion pair separations and cite experimental evidence which supports the ion-interaction model (*2*, *3*).

The mechanism of ion pair separations is further complicated by rearrangements of the alkyl bonded stationary phases commonly used for reversed phase LC (*4–6*). In water C_{18} bonded phases assume a "folded" configuration in which the alkyl chains preferentially associate with each other rather than the aqueous phase. However, in less polar solvents the alkyl chains are solvated and adopt a "bristle" configuration in which the alkyl chains extend out into solvent. The lipophilic counterions used for ion pair separations may influence the structure of the surface in addition to interacting with the ions being separated.

We have used the fluorescence of the ammonium salt of 8-anilinonaphthalenesulfonic acid (ANS) to study the environment of ions under conditions used in reversed-phase ion pair LC. ANS is ideally suited to this application. Because is is an anion, it is typical of ions separated by ion pair LC. It does not fluoresce in water. In other solvents its wavelength of maximum emission varies as a function of solvent polarity (*7*, *8*). By measuring the wavelength of maximum emission, we can estimate the relative polarity of ANS environment as a function of variables of chromatographic interest. The variables that we have studied include the amount and structure of added lipophilic cation and the structure of the alkyl bonded surface. Fluorescence has previously been successful in probing the behavior of alkyl bonded phases but not under ion pairing conditions (*9*, *10*).

Table I. Reversed-Phase Surface Coverage

phase	% C	μmol/mg
RP2	6.59	1.85
RP8	12.23	1.04
RP18	10.38	0.43
DP	3.80	0.10

EXPERIMENTAL SECTION

Reagents. All chemicals were ACS reagent grade or better and used without further purification. The lipophilic cations used were: tetrabutylammonium phosphate (TBA), 0.5 M in water, pH 7.4 (Rainin, Woburn, MA); tetramethylammonium hydroxide (TMA), 2.2 M in methanol (Aldrich); trimethylmyrisylammonium bromide (MYR), powder (Aldrich). Stock solutions of the ammonium salt of 8-anilinonaphthalene-1-sulfonic acid (Aldrich) were prepared in water and methanol. These solutions were stored in the dark to prevent photodecomposition. Methanol was HPLC grade (Fisher). Water was doubly deionized and glass distilled.

Reversed-phase supports were commercially prepared as monomeric materials. Methyl- (RP2), octyl- (RP8), and octadecyl- (RP18) silane phases were bonded to 10-μm LiChrosorb (Brownlee Labs, Santa Clara, CA). The diphenyl (DP) phase was Supelco 5-μm LC-3DP. Carbon loading was determined on a Perkin-Elmer carbon–hydrogen–nitrogen (CH&N) analyzer (Table I).

Apparatus. All spectra were obtained on a Perkin-Elmer MPF-44E spectrofluormeter with slits set at 2 nm using 378-nm excitation. Spectra are not corrected for variations in detection sensitivity with wavelength.

Procedures. Fifteen milligram samples of reversed-phase material were treated with cations in 200-μL methanol/water solutions in 1-dram vials. The resultant slurry was mixed thoroughly and gently dried in a vacuum oven at 30–45 °C for up to 2 h. Once dry, the preconditioned phase was packed into glass melting point capillary tubes. A small plug of silanized glass wool (Supelco) was used to contain the support in the tube. The capillary was then inserted in 100 μL of an ANS solution which was drawn into the tube by capillary action. This process was complete in 4–8 h for methanol solutions and 16–72 h for aqueous ANS solutions. Cation and ANS amounts are indicated on the data tables.

Since ANS fluoresces weakly in methanol, care was taken to ensure that the observed signal was only from surface-bound ANS. ANS concentrations were well below those needed to completely cover the surface. Direct visual examination indicated intense emission from particles and no visible emission from voids in the column. In systems showing wavelength shifts, there was no evidence of spectral broadening or development of shoulder peaks that would accompany a background due to nonsurface bound ANS in methanol.

Solution spectra were obtained for 10 μM ANS and 1–1.3 mM cation (maxima, Table II) in a 1-cm quartz cell. Surface spectra were measured directly in the packed capillary tubes. The tubes

0003-2700/85/0357-0602$01.50/0 © 1985 American Chemical Society

Table II. Reference Emission Maxima

a. 10 μM ANS + 1 mM Cation in Solution

cation	λ_{max}, nm H_2O	MeOH
TMA	492	484
TBA	502	491
MYR	480	482
ammonium		475

b. ANS + Untreated Surfaces

surface	λ_{max}, nm H_2O	MeOH
RP18	474	478
RP8	474	476
RP2	470	476
DP	474	474

Table III. Wavelengths of Maximum Emission for Tetramethylammonium Ion (TMA) Treated Surfaces

surface bonded phase	100 μmol TMA 100 nmol ANS –	10 μmol TMA 100 nmol ANS λ_{max}, nm	1 μmol TMA 2.5 nmol ANS –
		a. H_2O	
RP18	474	461 (459, 463, 466[a])	450
RP8	480	465 (462, 467, 467[a])	
RP2	472	468	446
DP	474	474	458
		b. Methanol	
RP18	484	476 (474, 479, 479[a])	469
RP8	486	474 (474, 474, 474[a])	468
RP2	483	470	467
DP	482	483	456

[a] Data measured using 12.5 nmol ANS.

were reproducibly positioned in the excitation beam by guiding them through a hole drilled in a cuvette cover supported by the fluorescence cuvette. Replicates of some surfaces were prepared to determine the reproducibility of the preparation technique.

RESULTS

Wavelengths of maximum fluorescence emission for all systems studied are presented in Tables II–V. Pure solvent and blank surface data appear in Table II. Data for various surfaces with TMA, TBA, and MYR are presented in Tables III–V, respectively. For systems where replicate surfaces were prepared, individual determinations are presented in parentheses separated by commas.

In all systems the amount of lipophilic cation was much greater than the amount of ANS. Levels were chosen to correspond to those typically used in reversed-phase ion pair LC. To determine whether the level of ANS might be a variable, surfaces treated with 10 μmol of cation were tested at two different ANS levels, 12.5 nmol and 100 nmol. With one intriguing exception the level of ANS did not significantly influence the observed wavelength of maximum emission.

The observed shifts in emission wavelengths were not accompanied by spectral broadening. Thus there is no evidence to indicate that ion pairs may be interacting with unreacted silanol groups on the silica in addition to interacting with the alkyl bonded surface.

DISCUSSION

Interpretation. The photophysics of ANS derivatives are well understood (*8*). Shifts in wavelengths of maximum emission can be correlated with solvent polarity parameters. However, because of the uncertainties associated with the behavior of ANS at an interface, quantitative interpretation of our data has not been attempted. Instead wavelength shifts are interpreted qualitatively in terms of relative polarity of the ANS environment. The shorter the wavelength of maximum emission, the more strongly the ANS is interacting with the nonpolar stationary phase. As a reference point, ANS emission maxima are in the range from 440 to 455 nm in aliphatic and aromatic hydrocarbon solvents (*7*), while emission maxima in aliphatic alcohols vary from 490 nm in methanol to 477 nm in 1-butanol (*11*).

Reference Emission Maxima. Table IIa lists the wavelengths of maximum emission in pure solvent. The fact that emission is observed in water when lipophilic ions are present indicates that ion pair formation is occurring. However, the concentrations of lipophilic cation are higher than those in the surface experiments. At the highest concentration used in the surface experiments, only the myristyl cation showed measurable fluorescence with ANS in water. Thus the limiting case of ion pairing in solution prior to association with the nonpolar surface is not important in this study.

The emission maxima listed for water in Table IIa represent the situation where ANS is interacting primarily with water. Thus they serve as a reference point for comparing the emission maxima that are observed on the hydrocarbon bonded surfaces. There is some lipophilic interaction between the cation and ANS as evidenced by the fact that emission is observed at all. The system with the myristyl cation has the shortest wavelength emission maximum which is consistent with the fact that the long alkyl chain on MYR can interact more effectively with ANS than the shorter chains of TBA and TMA. In methanol the lipophilic cation actually causes

Table IV. Wavelengths of Maximum Emission for Tetrabutylammonium (TBA) Treated Surfaces

surface bonded phase	100 μmol TBA 100 nmol ANS –	10 μmol TBA 100 nmol ANS λ_{max}, nm	1 μmol TBA 2.5 nmol ANS –
		a. H_2O	
RP18	444 (440, 448)	454 (457, 452, 468[a])	450
RP8	470	467 (465, 468, 469, 469[a])	457
RP2	466	474	462
DP	467	475	452
		b. Methanol	
RP18	477	474 (474, 474, 474[a])	468
RP8	478	474 (468[a])	472
RP2	482	475	469
DP	478	474	466

[a] Data measuring using 12.5 nmol ANS.

Table V. Wavelengths of Maximum Emission for Myristyltrimethylammonium (MYR) Treated Surfaces

surface bonded phase	100 μmol MYR 100 nmol ANS –	10 μmol MYR 100 nmol ANS γ_{max}, nm	1 μmol MYR 2.5 nmol ANS –
		a. H_2O	
RP18	469 (468, 470)	466 (465, 466, 469, 462[a])	467
RP8	468 (467, 469)	467 (463, 467, 467, 467[a])	
RP2	472 (468, 475)	467 (465, 468)	467
DP	475	475	467
		b. Methanol	
RP18	479	473 (472, 474, 472[a])	470
RP8	479	475 (473, 476, 476[a])	467
RP2	478	479	469
DP	478	472 (469, 476)	458

[a] Data measuring using 12.5 nmol ANS.

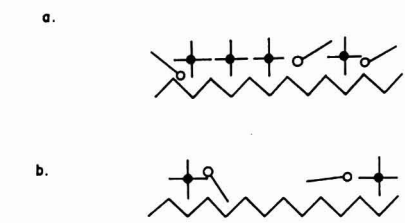


Figure 1. Schematic representation of effect of cation concentration on ANS environment. "A" represents case of high cation concentration which causes a high surface charge density thereby excluding ANS from lipophilic interaction with the hydrocarbon surface. "B" represents low cation concentration. In this case surface charges are further apart allowing greater lipophilic interaction with the surface. The representation is based on Bidlingmeyer (*2*, *3*). ⁓ represents an alkyl chain; ● represents a positive charge; O represents a negative charge; and — represents the aromatic part of ANS.

emission to shift to longer wavelength.

Table IIb lists emission maxima for the various surfaces in the absence of added lipophilic cation In water there is only a small shift relative to the maxima in the absence of surface. This shift plus the fact that there is observable fluorescence at all implies that there is a weak interaction between ANS and the surface but the ANS remains in a predominantly polar environment.

In methanol there is no shift at all caused by the presence of the alkyl bonded surface. The observation that there is a greater wavelength shift in water is consistent with the stronger solvophobic forces in water.

TMA in Water. The data listed in Table IIIa show that for all four surfaces, maximum emission shifts to considerably shorter wavelengths as the level of TMA is reduced. The implications of this observation are depicted in Figure 1. At high levels the TMA associates with the surface causing it to have a high charge density. The charge excludes ANS forcing it to remain in a predominantly solvent environment. As the level of TMA decreased, the charge density decreases and there is more opportunity for lipophilic interactions between ANS and the hydrocarbon surface. At the lowest level of the TMA there are very strong lipophilic interactions as evidenced by the fact that the emission maxima correspond to those observed in hydrocarbon solvents.

The DP phase shows a smaller effect than the alkyl bonded phases. This may reflect the fact that is has the lowest carbon content, rather than implying a different type of interaction.

TMA in Methanol. In methanol at the highest TMA level the emission maxima are the same as those observed in the absence of surface. As in water, reduced TMA levels are accompanied by shifts to shorter wavelengths implying greater lipophilic interaction. However, the shifts are not as large as those obtained in water reflecting the weaker solvophobic forces in methanol.

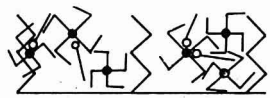


Figure 2. Schematic representation of the effect of TBA on the RP18 surface. The interactions between the alkyl groups of the ion and the hydrocarbon surface chain cause the surface to change from a "folded" to a "bristle" configuration allowing ANS to penetrate the surface and experience a predominantly hydrocarbon environment.

The alkyl bonded phases all behave similarly. However the DP phase shows a large shift at the lowest TMA level. In fact for the DP phase the emission maximum is at a slightly shorter wavelength in methanol than in water. This observation implies that ANS associates directly with the DP phase while with the alkyl bonded phases ANS has to compete with methanol for access to the hydrocarbon surface. $\pi-\pi$ interactions and steric considerations favor the association of the aromatic fluorescent probe with the aromatic surface.

TBA in Water. The TBA system behaves quite differently from TMA (Table IV). The most dramatic result is the extremely short wavelength emission maximum observed for the RP18 phase at the highest TBA level. The implications of this are represented in Figure 2. The TBA must interact with the RP18 phase in such a way as to cause the alkyl chains to unfold. This in turn allows the ANS to partition in between the alkyl chains where it experiences an environment which is essentially completely hydrocarbon. The alkyl chains may actually fold over the ion pairs completely isolating them from the solvent. The effect is also observed for the intermediate level of TBA although not to the same extent. The higher TBA level is apparently more effective at causing the alkyl chains to unfold. At the lowest TBA level it is not certain whether an unfolding is occurring or whether it is acting the same as the lowest level of TMA.

At the intermediate level of TBA on RP18, the emission wavelength for 12.5 nmol ANS is significantly longer than the wavelength for 100 nmol of ANS. This suggests that the anion may play a role in causing the alkyl chains to unfold, since the shorter wavelengths are observed for the higher ANS level. This interesting observation was not followed up, however.

The RP8 and RP2 show less of an effect since shorter alkyl chains have less freedom to rearrange. Nonetheless there is still some effect as evidenced by the fact that at the highest cation loadings the wavelengths are shorter for TBA than for

TMA. Since this effect is observed with RP2 which cannot rearrange at all, it suggests that shifts for TBA relative to TMA reflect the fact that the surface charge density does not get as high when the cation with the longer alkyl chain is used.

The observation that the maximum emission wavelength is quite short for the DP phase at the lowest TBA loading implies that there is a direct interaction between ANS and the aromatic surface as was also observed for the TMA–methanol system.

TBA in Methanol. In methanol the alkyl chains are already solvated and a TBA-induced surface rearrangement is not possible. The emission maxima shift to slightly lower values as the cation level decreases. This is consistent with the idea that lower surface charge densities allow more opportunity for lipophilic interactions. Nevertheless in all cases the emission maxima occur at relatively long wavelengths implying that ANS is experiencing a predominantly methanol environment. ANS is not competing effecively with methanol for access to the hydrocarbon bonded surface. All four surfaces show essentially the same behavior.

MYR in Water. The emission maxima for all systems are very similar for MYR (Table V). The wavelength implies that lipophilic interactions are relatively weak. There is only a small shift to shorter wavelength at lower levels of MYR. MYR does not induce a surface rearrangement. Instead it coats the surface of the phase. The charge density on the surface is high enough to limit the extent of lipophilic interactions between ANS and the surface. The charge density on the surface seems to be similar for all MYR levels. At the highest MYR levels the alkyl chain occupies part of the surface which remains nonpolar and capable of interaction with ANS. Thus emission maxima are at shorter wavelength for the highest MYR level than for the highest TMA level. However, the long alkyl chain of MYR acts to cause efficient association of MYR with the hydrocarbon surface even at the lowest MYR level. Thus the charge density effect remains significant even at this level.

MYR in Methanol. ANS remains in a predominantly methanol environment in all systems. The only exception is the DP phase at the lowest loadings where as in other cases there is direct association with ANS.

CONCLUSION

The fluorescence probe technique has provided direct evidence for surface charge density effects and surface rearrangments which affect the extent of lipophilic interactions between an organic solute ion and a hydrocarbon bonded surface. The results help to show that the ion pair and dynamic ion exchange models are oversimplifications and to confirm that the more complex ion interaction approach is required to adequately explain the mechanisms of reversed-phase ion pair liquid chromatography.

ACKNOWLEDGMENT

The spectrofluorometer was loaned to us by the United States Geological Survey.

Registry No. ANS-NH_3, 28836-03-5; Me_4N^+, 51-92-3; Bu_4N^+, 10549-76-5; trimethylmyristylammonium, 10182-92-0; methanol, 67-56-1.

LITERATURE CITED

(1) Bidlingmeyer, B. A.; Deming, S. N.; Price, W. P., Jr.; Sachok, B.; Petrusek, M. *J. Chromatogr.* **1979**, *186*, 419.
(2) Bidlingmeyer, B. A. *J. Chromatogr. Sci.* **1980**, *18*, 525.
(3) Bidlingmeyer, B. A. *LC, Liq. Chromatogr. HPLC Mag.* **1983**, *1*, 344.
(4) Scott, R. P. W.; Simpson, C. R. *J. Chromatogr.* **1980**, *197*, 11.
(5) Gilpin, R. K.; Gangoda, M. E. *J. Chromatogr. Sci.* **1983**, *21*, 352.
(6) Gilpin, R. K. *Am. Lab. (Fairfield, Conn.)* **1982**, *14* (3), 104.
(7) Kosower, E. M.; Kanety, H. *J. Am. Chem. Soc.* **1978**, *100*, 4179.
(8) Kosower, E. M. *Acc. Chem. Res.* **1982**, *15*, 259.
(9) Bogar, R. G.; Thomas, J. C.; Callis, J. B. *Anal. Chem.* **1984**, *56*, 1080.
(10) Lochmüller, C. H.; Colburn, A. S.; Hunnicutt, M. L.; Harris, J. M. *Anal. Chem.* **1983**, *55*, 1344.
(11) Ware, W. R.; Chakrabarti, S. K. *J. Chem. Phys.* **1971**, *55*, 5495.

RECEIVED for review August 30, 1984. Accepted November 26, 1984. This work was supported by National Science Foundation Grant CHE80-25568.

Characterization of a Chiral Tripeptide Stationary Phase for the Liquid Chromatographic Separation of Chiral Dipeptides

William A. Howard,[1] Tau-Being Hsu, and L. B. Rogers*

Department of Chemistry, University of Georgia, Athens, Georgia 30602

David A. Nelson

Department of Chemistry, University of Wyoming, Laramie, Wyoming 82071

A tripeptide-bonded stationary phase was synthesized by bonding the tripeptide, L-Val-L-Ala-L-Pro, to a reactive silane bonded to silica gel. The retention behavior of several isomeric dipeptides was examined as a function of pH and buffer composition. Although retention behaviors were similar to those reported for the nominally same tripeptide phase prepared in another way, the data indicated that the phases were significantly different. In addition, for the new phase at pH 7.4, a buffer effect was found in which retentions decreased on going from a phosphate–citrate–chloride (McIlvaine) to phosphate buffer alone, to citrate alone, and to pyrophosphate. However, with respect to selectivity, the McIlvaine and pyrophosphate buffers were superior to citrate and, in turn, phosphate.

The present study follows up the very interesting work by Grushka and co-workers (*1–3*) in which a chiral tripeptide was synthesized on the surface of silica and then used to fractionate chiral dipeptides. There is no doubt that chirality was contributing to the observed retentions. For the most part, diastereomers were not examined, but crossovers in retentions of diastereoisomers with pH were noted in their work. Fong and Grushka prepared their tripeptides on the surface by a stepwise manner analogous to a Merrifield synthesis in which a solid phase is used as the support. Even if individual steps produced nearly a 95% yield, a substantial fraction of the surface should be derivatized with mono- and dipeptide groups. Hence, although their work demonstrated the feasibility of using a bonded tripeptide phase, the mixed nature of the derivatized surface introduced some ambiguity into the interpretations of results obtained using their packing.

The present study was designed to circumvent the problems of multiple derivatives by synthesizing the intact tripeptide before attaching it to the surface. Admittedly, the surface would not be homogeneous; silanols, especially, would be present in abundance. However, although silanols would contribute to the retention of a dipeptide solute, they would make no chiral contribution. Assuming that significant racemization can be avoided, conclusions about the contribution of chirality, including any templates and conformational effects, should be sound.

The first goal, therefore, was to prepare a phase having the same tripeptide but prepared by attaching the intact tripeptide. Then, the phase was to be tested by using some of the same dipeptides (pairs of sequence isomers) used by Fong and Grushka so as to compare on a relative basis their retentions in terms of the capacity ratio, k, and especially their changes with pH. It was also of interest to observe the effects on the ratios of the k values (α values), both before and after the derivatized packing had partially decomposed (with use). While it is possible that decomposition might have increased, rather than decreased, the k and α values as dilution has been shown to do (*4*), it seemed unlikely to be important for the relatively small extent of decomposition that was anticipated.

Finally, it was of interest to explore in a preliminary way the effects of different anions in several buffers, each at the same pH. Because an effect has been reported for phosphate (*5*), it was used alone in one buffer as was citrate. In addition, a McIlvaine buffer, which contains both citrate and phosphate (plus chloride to attain the desired ionic strength), was also examined. Finally, a pyrophosphate buffer was included so as to see if it behaved much the same as phosphate.

EXPERIMENTAL SECTION

Chemicals and Reagents. LiChrospher Si 100, silica having a 10-μm particle diameter, was used for preparation of the bonded phase (Alltech Associates, Norcross, GA). The 1-(dimethylchlorosilyl)-2-(4-chloro-3-methylphenyl)ethane silane reagent used to bond the peptide to silica was obtained from Petrarch Systems (Bristol, PA).

All chemicals were J. T. Baker (Phillipsburg, NJ) reagent grade, HPLC grade, or better unless otherwise stated. The following reagents were obtained for synthesizing the tripeptide L-valine-L-alanine-L-proline (L-Val-L-Ala-L-Pro) using isobutylchloroformate. The amino acid derivatives used in this synthesis were *tert*-butoxycarbonyl-L-valine (BOC-L-Val) from U.S. Biochemicals Corp. (Cleveland, OH) and the methyl ester hydrochlorides of alanine and proline from Chemalog (South Plainfield, NJ). The reagents used for coupling the amino acids were isobutylchloroformate and *N*-methylmorpholine, both from Aldrich Chemical Co. (Milwaukee, WI) as were the triethylamine and tetrahydrofuran (THF). The THF was distilled over potassium prior to use.

The workup of the coupling reactions employed house doubly distilled deionized water plus ethyl acetate, anhydrous magnesium sulfate, sodium chloride, and hydrochloric acid, along with sodium hydroxide from Fisher Scientific Co. (Norcross, GA). The methyl ester of the peptide was hydrolyzed and worked up with sodium hydroxide, methanol, diethyl ether, citric acid monohydrate, sodium chloride, and chloroform.

Solvents used for bonding the silane reagent to silica and then the peptide to the silane-derivatized silica were toluene and acetonitrile. The toluene was either distilled or dried over calcium chloride before being stored over sodium. Proton Sponge, a catalyst from Aldrich (Milwaukee, WI), was used to accelerate the bonding reactions. Formic acid (88%) was used to remove the BOC protecting group. Chloroform, THF, and DME were used in the syntheses of the tripeptide. The DME was dried over sodium or molecular sieve 5A prior to use. Isooctane, cyclohexanol, carbon tetrachloride, and 2-propanol were used to pack the column. Methylene chloride and methanol were used to wash the column after packing.

Dipeptide standards were used to evaluate the peptide bonded phase columns. These included L-valine-L-phenylalanine (L-Val-L-Phe), L-phenylalanine-L-valine (L-Phe-L-Val), L-alanine-L-phenylalanine (L-Ala-L-Phe), and L-phenylalanine-L-alanine (L-Phe-L-Ala), all from Sigma Chemical. The peptides were prepared as 1 mg/mL solutions in distilled water and stored in the refrigerator overnight.

[1] Present address: Burroughs Wellcome Co., P.O. Box 1887, Greenville, NC 27834.

0003-2700/85/0357-0606$01.50/0 © 1985 American Chemical Society

Doubly distilled deionized water was used for preparing the buffers used as mobile phases. The buffer reagents included anhydrous monosodium phosphate and tetrasodium pyrophosphate decahydrate (both from Sigma), anhydrous dibasic sodium phosphate, dibasic sodium phosphate dodecahydrate, tribasic sodium citrate dihydrate, and citric acid monohydrate. The citrate, phosphate, and pyrophosphate buffers were prepared as 0.10 M solutions and adjusted to the appropriate pH using 0.1 M solutions of sodium hydroxide and hydrochloric acid. The McIlvaine buffer was prepared according to Elving et al. (6). The mobile phases were filtered through 0.50 μm cellulose acetate and nitrate (HAWP) Millipore filters (Bedford, MA) before being degassed with helium prior to use.

Apparatus. The chromatographic system consisted of an isocratic Spectraphysics Model SP8770 pump (San Jose, CA), a Rheodyne Model 7125 injection valve (Cotati, CA), a Kratos Model 770 liquid chromatographic detector (Ramsey, NJ) set a 254 nm and 0.04 AUFS, unless specified otherwise, and a Linear Model 585 (Reno, NV) chart recorder.

The columns were packed with a SC Hydraulics Model 10-600-50 pump (Los Angeles, CA) and a homemade slurry bomb.

Procedures. *Derivatization Reactions.* The peptide L-Val-L-Ala-L-Pro was synthesized by using the procedures of Vaughan and Osato (7) and Galobardes (8). A typical peptide synthesis proceeded as follows. *N*-Methylmorpholine (11 mmol) dissolved in THF (10 mL) was added to a 0 °C solution of BOC-L-Val (10 mmol) in THF (20 mL). Isobutylchloroformate (11 mmol) in THF (10 mL) was added and the reaction stirred for 30 min. A well-stirred suspension of L-Ala-OMeHCl (11 mmol) and *N*-methylmorpholine (11 mmol) in THF was added to the reaction mixture and stirred for 12 h. The reaction mixture was filtered and the THF removed in vacuo. The crude product was dissolved in ethyl acetate:water (80 mL to 80 mL) and washed successively with 80 mL each of water, 1% aqueous citric acid, water, 10% aqueous sodium bicarbonate, and water. The solvent was removed in vacuo to yield the product BOC-L-Val-L-Ala-OMe.

The protected dipeptide, BOC-L-Val-L-Ala-OMe, was hydrolyzed to yield a free carboxylic acid for coupling. A solution of the dipeptide methyl ester (10 mmol) in methanol (50 mL) containing sodium hydroxide (28 mmol) was stirred for 3 h at room temperature. After dilution with water (40 mL) and extraction twice with 40 mL of ethyl acetate, the organic layer was discarded. The aqueous layer was cooled, acidified to pH 2 with citric acid, and saturated with ammonium chloride before being extracted 3 times with 50 mL of chloroform. The chloroform extracts were combined, washed with water, and concentrated in vacuo to yield the free dipeptide acid, BOC-L-Val-L-Ala-COOH.

The dipeptide acid, BOC-L-Val-L-Ala-COOH, was coupled with L-Pro-OMeHCl using the coupling procedure described previously. The product, BOC-L-Val-L-Ala-L-Pro-OMeHCl, was hydrolyzed to the free acid, BOC-L-Val-Ala-L-Pro-COOH. The average overall yield of the tripeptide (five runs) was 78%. The mixed-anhydride methods used for this synthesis were reported to give no racemization (7). One indication of the stereochemical homogeneity of the product was a single peak on HPLC analysis using two different C-18 columns and a variety of mobile phases.

The silane-derivatized silica for bonding the tripeptide to the silica surface was prepared by suspending silica gel in boiling toluene (100 mL) and adding the silane reagent 1-(dimethylchlorosilyl)-2-(4-chloro-3-methylphenyl)ethane (17 mmol). The reaction was allowed to proceed for 24 h before the product was collected and washed successively with 100 mL of each of the following solvents: toluene, methanol, methanol:water (1:1), water, methanol, and ether. The derivatized silica was dried at 110 °C in vacuo. Elemental analysis of this silica yielded 10.2% carbon, 1.55% hydrogen, and 2.35% chlorine (Atlantic Microlab, Inc., Atlanta, GA). This is equivalent to a ligand density of 3.1 μmol/m^2, assuming a surface area of 300 m^2/g for LiChrosphere Si-100. Calculations of surface coverage were made by using the formulas of Berendsen and de Galan (9, 10).

The tripeptide was bonded to the derivatized silica by suspending the derivatized silica (2.0 g) in acetonitrile (100 mL) and adding the free tripeptide BOC-L-Val-L-Ala-L-Pro (13 mmol) and Proton Sponge (3.5 g) as a catalyst. After 2 days, the tripeptide bonded phase was collected and washed successively with 100 mL each of acetonitrile, methanol, and water, before being dried at 110 °C in vacuo for 12 h. The BOC group was removed with formic acid. Elemental analysis of the peptide bonded phase yielded 11.5% carbon, 1.80% hydrogen, and 0.82% nitrogen (Atlantic Microlab, Inc., Atlanta, GA). This corresponds to a 30% conversion of the original chlorine to tripeptide, based on nitrogen analysis. This percent conversion is similar to that achieved by Grushka (1, 3) for other tripeptide phases.

All of the reactions were monitored by reversed-phase liquid chromatography where appropriate. A Spectraphysics octadecyl column (C18), eluted by 30:70 acetonitrile:water adjusted to pH 2 with phosphoric acid, was employed to fractionate the reaction mixtures. An increase in the concentration of a product or decrease in reactant was used to follow the reaction's progress. Also, proton and carbon-13 nuclear magnetic resonance (NMR) spectrometry were used to confirm the structure of the peptide intermediates.

Chromatographic Procedures. The tripeptide bonded phase was packed into 316 stainless steel (SS) tubing 25.0 cm × 0.32 cm i.d. × 0.635 cm o.d. (Alltech Associates). The columns were terminated with 0.635 cm ($^1/_4$ in.) to 0.159 cm ($^1/_{16}$ in.) zero dead volume Swagelok reducing unions (Georgia Valve and Fitting, Atlanta, GA) having 2-μm stainless frits (Alltech). All tubing and reducing unions were washed successively with THF, methanol, water, 3 N nitric acid, water, methanol, and acetone before being dried with nitrogen.

The columns were packed using the viscosity technique (11). A 10% slurry (w:v) of the bonded phase in cyclohexanol:2-propanol (3:1, v:v) was placed in the slurry packer and displaced into the column with isooctane at a pressure of 650 bar. Carbon tetrachloride, placed in the column prior to packing, prevented the slurry from settling into the column. Methylene chloride and methanol (100 mL each) were used to wash the column prior to evaluation.

The mobile phase flow rate was 0.33 mL/min for all studies. The column was equilbrated with the appropriate mobile phase for 3 h prior to a chromatographic run. A precolumn, 5 cm × 0.46 cm i.d. × 0.635 cm o.d. packed with Corasil (Water Associates, Milford, MA) was placed between the pump and the injection valve in order to saturate the mobile phase with silicic acid. This helped to minimize degradation of the tripeptide bonded phase column at high pH. In addition, columns were usually flushed with methanol before being stored overnight, but for shorter times, the column was flushed only with distilled-deionized water.

The time (volume) for a nonretained substance, used in calculating the capacity factor, k, was determined by injecting water into the eluent. Because peaks for the solutes were quite symmetrical, the retention times (volumes) were taken at the peak maximum. Values for k from replicate runs usually agreed within 1%.

RESULTS AND DISCUSSION

Retentions of Amino Acids. The amino acid components of the dipeptide solutes were examined using a 0.1 M phosphate buffer at pH 7.4 so as to estimate the relative contribution of each L-amino acid to the overall retentions of the dipeptides. The k values for alanine, valine, and phenylalanine were 0.086, 0.117, and 0.290. These show that the amino acids eluted in the order of increasing hydrophobicity, an order consistent with that reported by Fong and Grushka (3), for the phenylthiohydantoin (PTH) derivatives. The quantitative relationships developed by Rekker (12) and cited by Horvath (13) for the hydrophobic contributions of the amino acid side chains also agree very well for the elution order and are useful for making predictions. Therefore, a reversed-phase mechanism contributes in a major way to the overall retention of the dipeptides on a tripeptide bonded stationary phase.

Effect of pH. A series of dipeptide solutes were examined in order to characterize their retention behaviors on the tripeptide bonded stationary phase. Again, the peptides eluted in the order of increasing hydrophobicity. Figure 1 shows that the k values increased as the pH of the eluent increased with the greatest retention near pH 7—and were still rising. The k value for L-Phe-L-Val increased faster with pH than those of the other dipeptides.

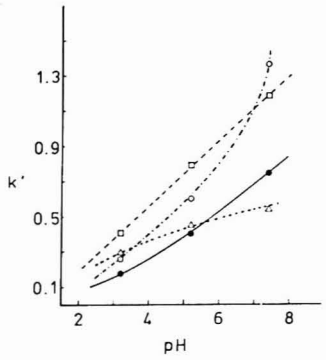


Figure 1. Effect of pH on k values of dipeptides in McIlvaine buffers of ionic strength, I = 0.5 M: △, L-Ala-L-Phe; ●, L-Phe-L-Ala, □, L-Val-L-Phe, ○, L-Phe-L-Val.

The elution order and the increase of k values as a function of pH agree very well with the data reported by Fong and Grushka (*3*). Both the magnitudes and trends of the k values are consistent for the two studies as seen in Figure 2. The main difference occurred at about pH 7.4 where the dipeptide solutes and the tripeptide bonded stationary phase were most sensitive to small changes in proton concentration.

The selectivity, α, changed steadily as a function of pH as seen in Figure 3. The selectivity values have been defined as follows:

$$\alpha_1 = \frac{k_{\text{L-Val-L-Phe}}}{k_{\text{L-Phe-L-Val}}} \quad (1)$$

$$\alpha_2 = \frac{k_{\text{L-Ala-L-Phe}}}{k_{\text{L-Phe-L-Ala}}} \quad (2)$$

$$\alpha_3 = \frac{k_{\text{L-Phe-L-Ala}}}{k_{\text{L-Phe-L-Val}}} \quad (3)$$

$$\alpha_4 = \frac{k_{\text{L-Ala-L-Phe}}}{k_{\text{L-Val-L-Phe}}} \quad (4)$$

A selectivity ratio near unity represents the most difficult separation whereas any increase or decrease in the absolute difference from unity indicates an easier separation. Note that α_1 and α_2 involve dipeptide pairs of sequence isomers while α_3 and α_4 measure the separations between the two sets of dipeptides in which valine and alanine (combined with phenylalanine) can be compared. The separation as defined by α_1 and α_2 would be the most difficult between pH 6 and 7 where α is close to unity. For pH >4 the α_1 was greater than α_2 while α_3 was greater than α_4. Below pH 4, the selectivities were reversed.

The α values for the isomeric pair L-Val-L-Phe and L-Phe-L-Val are compared in Figure 4 with those from Fong and Grushka's study under identical conditions. The selectivities found in the present study change in ways very similar to theirs.

Effect of Buffer Composition. The effect of buffer compositions at pH 7.4 was examined to evaluate the contribution of the buffer to the retention mechanism. For the dipeptide solutes the lines between the data points in Figure 5 have no significance and were added only to ease visual interpretation. All buffers were at 0.1 M except for the McIlvaine at I = 0.5 M. The retention was greatest for the McIlvaine buffer and may be an ionic strength effect because

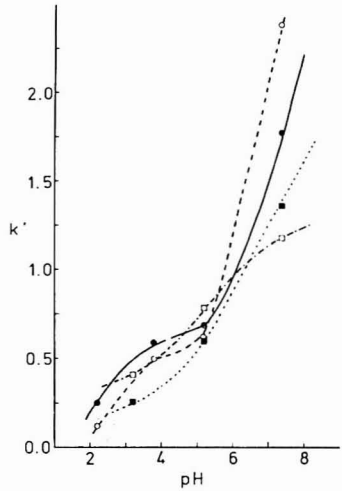


Figure 2. Effect of pH on k values of dipeptides in McIlvaine buffer, I = 0.5 M, comparison of Fong and Grushka vs. the present study: (ref 3) ●, L-Val-L-Phe; ○, L-Phe-L-Val; (present study) □, L-Val-L-Phe; ■, L-Phe-L-Val.

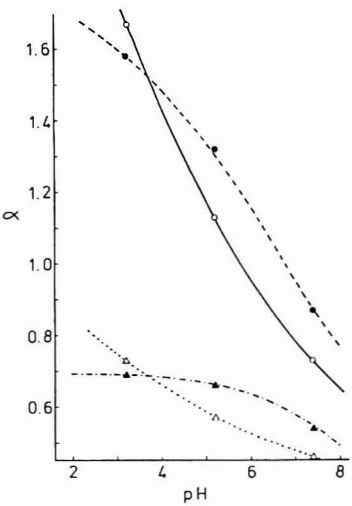


Figure 3. Effect of pH on the α values in a McIlvaine buffer, I = 0.5 M: ●, $k_{\text{L-Val-L-Phe}}/k_{\text{L-Phe-L-Val}}$; ○, $k_{\text{L-Ala-L-Phe}}/k_{\text{L-Phe-L-Ala}}$; ▲, $k_{\text{L-Phe-L-Ala}}/k_{\text{L-Phe-L-Val}}$; △, $k_{\text{L-Ala-L-Phe}}/k_{\text{L-Val-L-Phe}}$.

the retentions were greater in it (a mixture of phosphate and citrate) than in either of its components alone. The pyrophosphate buffer gave the smallest retentions. Hence, one can change significantly the absolute retentions of dipeptides on a tripeptide stationary phase by changing the buffer composition. These differences in retention were probably due to differing abilities of the buffer species to interact with the

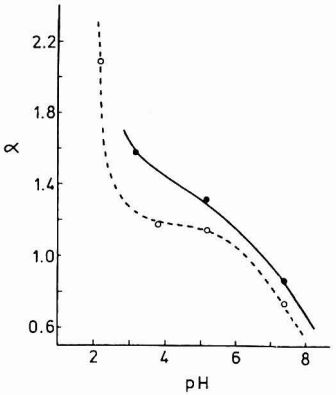


Figure 4. Effect of pH on the α values for the dipeptide pair L-Phe-L-Val and L-Val-L-Phe in a McIlvaine buffer, I = 0.5 M: O, ref 3; ●, present study.

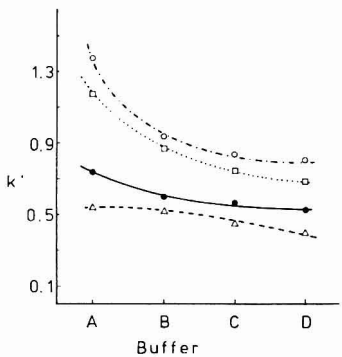


Figure 5. Effect of buffer composition at pH 7.4 on k values: △, L-Ala-L-Phe; ●, L-Phe-L-Ala; □, L-Val-L-Phe; O, L-Phe-L-Val. Mobile phases were (A) McIlvaine, (B) phosphate, (C) citrate, and (D) pyrophosphate.

dipeptide solute and/or with the tripeptide stationary phase.

The effect of the buffer composition on $1/\alpha$ values can be seen in Figure 6. The McIlvaine and pyrophosphate buffers gave the best selectivities while phosphate gave the worst. It is interesting that the pyrophosphate buffer exhibited the least retention but gave good selectivity. This served to emphasize the independence of retention and selectivity.

Long-Term Stability. The long-term stability of the tripeptide bonded phase columns as a function of time in contact with aqueous solutions was a prime concern since a pH >7.5 can solubilize silica gel. Therefore, some experiments were repeated under identical conditions after about 2 months of continuous use to see if there were any changes in the k or α values.

Results of the amino acids retentions are shown in Table I. The retentions decreased by more than 50% for alanine and about 20% for valine, while phenylalanine remained unchanged. This suggests that the silanol interaction was smallest for alanine. The k values for the dipeptides changed in a manner consistent with the behavior of the amino acids they contained. The alanine-containing dipeptides changed more than the valine-containing ones. The α values also changed, but correspondingly less due to the presence of phenylalanine in each dipeptide.

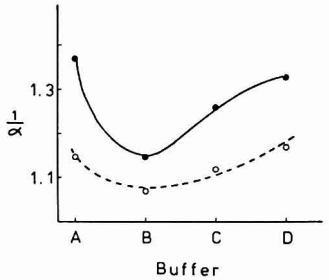


Figure 6. Effect of buffer composition at pH 7.4 on the $1/\alpha$ values for sequence isomeric pairs with phenylalanine: valine (●) and alanine (O) pairs; Mobile Phases were (A) McIlvaine, (B) phosphate, (C) citrate, and (D) pyrophosphate. ●, $k_{\text{L-Val-L-Phe}}/k_{\text{L-Phe-L-Val}}$; $k_{\text{L-Val-L-Phe}}/k_{\text{L-Phe-L-Val}}$; O, $k_{\text{L-Ala-L-Phe}}/k_{\text{L-Phe-L-Ala}}$.

Table I. Retentions of Amino Acids in 0.1 M Phosphate Buffer, pH 7.4

	k	
amino acid	1st expt	2nd expt
Ala	0.086	0.036
Val	0.117	0.093
Phe	0.290	0.296

Table II. Retentions of Dipeptides in 0.1 M Phosphate Buffer, pH 7.4

	1st expt		2nd expt	
dipeptide	k	α	k	α
L-Ala-L-Phe	0.52		0.35	
		0.86		0.80
L-Phe-L-Ala	0.61		0.44	
L-Val-L-Phe	0.94		0.64	
		0.94		0.90
L-Phe-L-Val	1.00		0.70	

CONCLUSIONS

This study demonstrated the feasibility of bonding an intact tripeptide, L-Val-L-Ala-L-Pro, to silica gel for separating dipeptide isomers. When the retentions of the dipeptides (Table II) and the selectivities of the separations using this phase were examined as a function of pH, the trends were very similar to those reported by Fong and Grushka (*3*), and the dipeptides that contain valine have the greatest k values at higher pH. However, retentions of dipeptides reported by Fong and Grushka (*3*) at high pH were significantly greater than those in the present study in spite of having approximately the same carbon percentages (12.3% (*3*) and 11.5%) in the two studies. Greater retention suggests that there was more valine on their surface because its hydrophobicity is greater than that of alanine or proline. Therefore, their surface is quite probably not the pure tripeptide, but a mixture of valine, valine-alanine, and valine-alanine-proline. The α values for dipeptides as a function of pH reported in Figure 3 show that, at low pH, protonation of the N-terminal aliphatic amino acid appears to increase the selectivity for the isomeric pair more than protonation of the N-terminal phenylalanine. Going to higher pH values decreased the α values. In fact, below an α value of 1.00, ionization resulted in greater se-

lectivity for L-Phe-L-Val and L-Val-L-Phe; at least its effect was greater for aliphatic than for aromatic amino acids. A greater effect was also found for the ionization of valine relative to alanine.

The retentions of the dipeptides and the selectivities of the separations were also examined as a function of buffer composition. Pietrzyk and co-workers (*14–16*) discussed as a function of pH the different mechanisms for retention by more conventional (nonchiral) packings. In the present study, there appears to be an additional factor influencing the separations as evidenced by the following. The McIlvaine buffer, which contains both phosphate and citrate, gave greater retention and selectivity than a buffer of either of its components. This difference may be the result of a difference in ionic strength. The greater ionic strength may have resulted in greater dehydration of ions which may, in turn, have increased the selectivity of the separation, as cited by Niederwieser (*17*). However, Krummen and Frei (*18*) have also shown the opposite trend to be possible, depending upon the range of the ionic strength involved.

The pyrophosphate buffer gave the smallest retention. However, it gave almost as good a selectivity as the McIlvaine buffer, even though its retention values were smaller. Hence, one wonders if ion pairing or a conformational change was the source of the differences. As a result, the use of pyrophosphate as an eluent is being explored. In the future, it will be of interest to immobilize different tripeptides so as to examine in more detail the effects of chirality on the k and α values for selected isomeric dipeptides. It will also be interesting to examine the effects of having Zn (*19, 20*) or cupric ion (*21*) in acidic buffers, such as those of ammonium acetate, so as to take advantage of ligand exchange behavior.

ACKNOWLEDGMENT

We thank Mercedes Galobardes for her preliminary work. We also thank Spectrophysics for the loan of a SP8770 pump.

Registry No. Ala, 56-41-7; Val, 72-18-4; Phe, 63-91-2; L-Ala-L-Phe, 3061-90-3; L-Phe-L-Ala, 3918-87-4; L-Val-L-Phe, 3918-92-1; L-Phe-L-Val, 3918-90-9.

LITERATURE CITED

(1) Kikta, E. J., Jr.; Grushka, E. *J. Chromatogr.* **1977**, *135*, 367.
(2) Fong, G. W.-K.; Grushka, E. *J. Chromatogr.* **1977**, *142*, 299.
(3) Fong, G. W.-K.; Grushka, E. *Anal. Chem.* **1978**, *50*, 1154.
(4) Felbush, B.; Cohen, M. J.; Karger, B. L. *J. Chromatogr.* **1983**, *282*, 3.
(5) Hancock, W. S.; Bishop, C. A.; Prestidge, R. L.; Harding, D. R. K.; Hearn, M. R. W. *J. Chromatogr.* **1978**, *153*, 399.
(6) Elving, P. J.; Markowitz, J. M.; Rosenthal, I. *Anal. Chem.* **1956**, *28*, 1179.
(7) Vaughan, J. R., Jr.; Osato, R. L. *J. Am. Chem. Soc.* **1952**, *74*, 676.
(8) Galobardes, M., The University of Georgia, unpublished results, 1982.
(9) Berendsen, G. E.; deGalan, L. *J. Liq. Chromatogr.* **1978**, *1*, 561.
(10) Berendsen, G. E.; Pikaart, K. A.; deGalan, L. *J. Liq. Chromatogr.* **1980**, *3*, 1437.
(11) Siemon, C. C. *J. Liq. Chromatogr.* **1983**, *6*, 765.
(12) Rekker, R. F. "The Hydrophobic Fragmental Constant"; Elsevier: New York, 1977; p 301.
(13) Molnar, I.; Horvath, C. *J. Chromatogr.* **1977**, *142*, 623.
(14) Kroeff, E. P; Pietrzyk, D. J. *Anal. Chem.* **1978**, *50*, 1353.
(15) Kroeff, E. P.; Pietrzyk, D. J. *Anal. Chem.* **1978**, *50*, 502.
(16) Pietrzyk, D. J.; Smith, R. L.; Cahill, W. R., Jr. *J. Liq. Chromatogr.* **1983**, *6*, 1645.
(17) Niederwieser, A. In "Chromatography"; Heftmann, E., Ed.; Van Nostrand-Reinhold: New York, 1975; p 417.
(18) Krummen, K.; Frei, R. W. *J. Chromatogr.* **1977**, *132*, 27.
(19) Cooke, N. H. C.; Viavattene, R. L9; Eksteen, R.; Wong, W. S.; Davies, G.; Karger, B. L. *J. Chromatogr.* **1978**, *149*, 391.
(20) Karger, B. L.; Wong, W. S.; Viavattene, R. L.; Lepage, J. N.; Davies, G. *J. Chromatogr.* **1978**, *167*, 253.
(21) Roumeliotis, P.; Unger, K. K.; Kurganov, A. A.; Davankow, V. A. *J. Chromatogr.* **1983**, *255*, 51.

RECEIVED for review February 6, 1984. Resubmitted September 27, 1984. Accepted November 16, 1984. We acknowledge partial support of this work by the National Science Foundation, Grant No. CHE78-13269. W.A.H. also thanks the Eastman Kodak Co. for a fellowship and the University of Georgia, Department of Chemistry, for an H. L. Richmond Scholarship.

Reversed-Phase Liquid Chromatography with Fourier Transform Infrared Spectrometric Detection Using a Flow Cell Interface

Charles C. Johnson,[1] John W. Hellgeth, and Larry T. Taylor*

Department of Chemistry, Virginia Polytechnic Institute and State University, Blacksburg, Virginia 24061-0699

The results from preliminary investigations into the use of segmented, flowing extraction of aqueous effluents from a reversed-phase HPLC system for flow cell FTIR detection are presented. The use of a hydrophobic membrane phase separator facilitated the operation of the RP-HPLC/FTIR instrument. By incorporating this technique with chloroform as the extraction solvent, one observes significantly improved infrared transparency over the aqueous, elution solvent system. Further improvements were observed with carbon tetrachloride, not only in the infrared transparency of the solvent system but also in the wider range of compounds that were extracted from the methanol/water elution solvent system. Infrared spectra obtained match standard reference spectra peak-for-peak.

[1]Current address: The Procter and Gamble Co., 6210 Center Hill Rd., Cincinnati, OH 45224.

Recently we have reported several developments involving the Fourier transform infrared (FTIR) spectrometer as a detector for normal-phase high-performance liquid chromatography (NP-HPLC) employing a flow cell interface (*1–5*). These developments described the use of semipreparative, analytical, and microbore scales of NP-HPLC applied to the identification of nonpolar and polar components in various coal-derived products. Earlier work had shown moderate sensitivity for this technique, but a greater problem at the time was the infrared absorbance by the mobile phase (*6*). The use of chlorinated and deuterated solvents in our work has afforded ample mobile phase transparency for flow cell HPLC-FTIR. Furthermore, various methodological and flow cell improvements have now yielded detection limits below 40 ng of injected material (*5*).

Aqueous-based, reversed-phase systems are reportedly used in well over 60% of all HPLC separations. Unfortunately the intense infrared bands of water and methanol, and to a lesser

0003-2700/85/0357-0610$01.50/0 © 1985 American Chemical Society

degree tetrahydrofuran and acetonitrile, necessitate very short optical path lengths if adequate infrared transparency is to be observed over a relatively wide range of IR frequencies in flow cell RP-HPLC/FTIR experiments (*6*, *7*). This consequent lack of sensitivity has severely limited the utility of reversed-phase systems with infrared detection using flow cells. Several on-line strategies which have been used include resorting to nonaqueous reversed-phase separations (*8*) and monitoring only C—H and C=O absorption regions with a very short path length flow cell (*9*). Even the off-line HPLC/DRIFT (Diffuse Reflectance Infrared Fourier Transform Spectrometry) method has been unsuitable to date for RP-HPLC/FTIR because of the inability of the KCl used for eluent deposit to tolerate even small amounts of water (*10*, *11*).

Several newer approaches to RP-HPLC/FTIR are currently being pursued which involve removal of water from the HPLC effluent. One approach incorporates the postcolumn, acid-catalyzed reaction of 2,2-dimethoxypropane with water in the mobile phase to form acetone and methanol (*12*). The reacted RP-HPLC effluent is then deposited onto KCl substrate for DRIFT detection. The acetone and methanol have sufficient volatility that this approach has had reasonable success. It is not yet clear what classes of compounds can be conveniently used with 2,2-dimethoxypropane without sample derivatization occurring. The information content of the 3100–3700-cm^{-1} region employing this method is also unknown.

A less intrusive but slightly more complicated approach to RP-HPLC/FTIR incorporating both DRIFT detection and segmented, flowing extraction has been reported (*13*, *14*). Briefly, the components in the effluent from the RP-HPLC separation are extracted in a segmented stream into methylene chloride. The two phases are separated by density using a tee in which the similar solvent segments recombine and flow out either of the opposing coaxial ends. The organic stream is then deposited onto the KCl substrate according to the usual DRIFT procedure. More recent results using this technique with methylene chloride extraction have been described (*15*). The method, however, suffers from several problems. The number of critical instrumental components (i.e., the FTIR system, the HPLC system, the flowing extraction system, plus the DRIFT interface) has become excessively large. The integrity of the KCl substrate for diffuse reflectance measurements is affected by residual water. Methylene chloride, being slightly soluble in water as well as miscible with methanol, carries a considerable amount of dissolved water with methanol onto the KCl substrate. This inherent drawback may limit the applicability and/or sensitivity of RP-HPLC/FTIR using this approach.

We have chosen to approach the RP-HPLC/FTIR problem by using a flow cell interface. In this paper, we will discuss preliminary results from experiments which employed (i) flowing extraction with two different solvents of the RP-HPLC effluent, (ii) subsequent separation of the immiscible solvents with a hydrophobic membrane, and (iii) FTIR detection with a flow cell interface. We believe that this approach is a less intrusive but a more pragmatic method for the RP-HPLC/FTIR experiment.

EXPERIMENTAL SECTION

A schematic diagram of the entire instrument is shown in Figure 1. the individual components are described below.

HPLC System. An IBM Instruments Model LC/9533 ternary gradient liquid chromatograph (Danbury, CT), equipped with a Rheodyne Model 7125 injector (Cotati, CA) and an IBM Instruments Model LC/9522 fixed wavelength (254 nm) UV detector, was used. The fixed injection loop size was 20 μL, although several injections were made with partial loop filling. The HPLC column, an IBM 4.6 mm i.d. × 25 cm 5-μm octadecyl bonded silica (C18), was employed in all experiments. Model compound

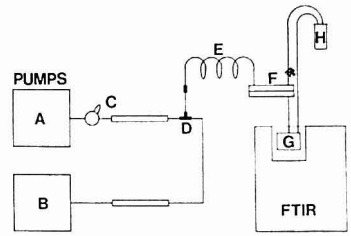


Figure 1. Schematic diagram of RP-HPLC/FTIR instrument: (A) pump delivering methanol/water solution; (B) pump delivering extraction solvent; (C) HPLC Injector and C18 column; (D) segmenting tee; (E) extraction coil; (F) membrane phase separator; (G) zero dead volume flow cell interface; (H) waste.

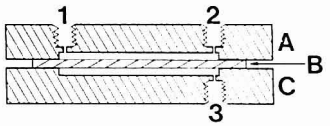


Figure 2. Cross-sectional view of membrane separator: (A and C) upper and lower stainless steel membrane holders; (B) 0.2-μm Gore-Tex membrane; (1) segmented stream inlet; (2) aqueous waste outlet; (3) organic-phase outlet.

mixtures were eluted with 65% HPLC grade methanol (Fisher, Fairlawn, NJ) and 35% water (distilled and deionized in-house) at a flow rate of 0.8 mL/min for all experiments. A Waters Associates Model R401 refractive index detector (Millford, MA) was used for some auxiliary experiments.

Extraction System. A second IBM Instruments Model LC/9533 ternary gradient liquid chromatograph delivered the extraction solvent to the mobile phase at a flow rate of 1.0 mL/min for all experiments. An IBM 4.6 mm i.d. × 25 cm 5-μm silica column provided back pressure to the pump in order that reliable solvent delivery could be achieved. Extraction solvents were ethanol-free chloroform and carbon tetrachloride (Burdick and Jackson, Muskegon, MI). To create a segmented stream, the extraction solvent and RP-HPLC effluent streams were combined in a standard Swagelok SS-100-3 tee union. These streams were connected to the opposing coaxial ports of the tee. A 1 mm i.d. × 10 cm stainless steel tube was attached to the side arm to permit proper formation of the exiting segmented extraction stream. A 0.5 mm i.d. × 1 m length of PTFE tubing, connected to the side-arm tube, provided a residence time for extraction prior to phase separation.

The membrane separator (*16*), shown in Figure 2, was machined from 316 stainless steel. The connections were made to accommodate standard flanged PTFE connectors. The volume on either side of the membrane was calculated to be 16 μL. The membrane material was an expanded PTFE with 0.2-μm pores (Gore-Tex, W. L. Gore, Elkton, MD). The Gore-Tex membrane, when compressed, provided a seal between the polished faces of the membrane holder. By regulation of the differential pressure across the membrane with a tubing clamp on the segmented stream outlet, the amount of organic solvent that is squeezed through the Gore-Tex membrane can be controlled to the exclusion of the water/methanol phase. A 45 cm length of 0.3 mm i.d. PTFE tubing was used to connect the outlet of the separator to the FTIR interface.

FTIR System. A Nicolet 6000C FTIR (Madison, WI) equipped with a narrow-band (5000-700 cm^{-1}) Model 7010A mercury–cadmium–telluride (MCT-A) detector was used for these experiments. Time-resolved, 4 cm^{-1} resolution spectra were collected with the standard Nicolet software package. In all cases, four interferograms were coadded and stored as a single file, thus giving time resolution between each collected file of ca. 3 s. The zero dead volume (ZDV) flow cell interface used for this study

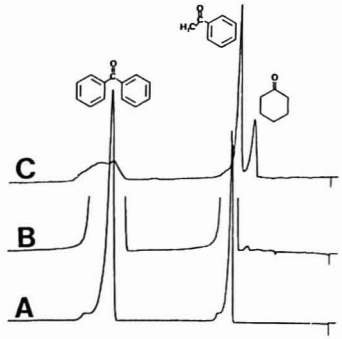


Figure 3. Ketone separation on C18: (A) UV254, 0.500 AUFS, 5-μL injection of 10% v/v solution; (B) UV254, 0.050 AUFS, 20-μL injection of 10% v/v solution; (C) RI 4× attenuation, 5-μL injection of stock solution.

has been previously reported (*5*). The ZDV cell crystal used was drilled from CaF_2 and had an effective path length of ca. 0.5 mm. A Barnes Model 600 4× beam condenser (Spectra-Tech, Inc., Stamford, CT) was used to reduce the infrared beam focal diameter to ca. 0.75 mm, thereby providing an effective cell volume of 0.33 μL.

Sample Mixtures. A ketone model mixture was prepared by mixing 1.0 g of each of the following: cyclohexanone (Eastman Organic Chemicals, Rochester, NY), acetophenone and benzophenone (both Fisher Certified, Fairlawn, NJ). This mixture was diluted to 0.5% v/v in the mobile phase (65% methanol/35% water) to provide a stock solution. Another concentrated column test mixture was prepared as follows: 0.16 g of phenol (J. T. Baker USP grade, Phillipsburg, NJ), 0.16 g of acetophenone, 0.16 g of nitrobenzene, and 0.16 g of methyl benzoate (all Fisher Certified, Fairlawn, NJ), and 0.16 g of toluene (Fisher HPLC grade, Fairlawn, NJ) were dissolved in 1.0 g of methanol (Fisher HPLC grade, Fairlawn, NJ). This mixture was filtered through a 0.45-μm Swinny filter prior to injection.

RESULTS AND DISCUSSION

The objective of this study was to demonstrate the feasibility of using the FTIR as a detector for reversed-phase HPLC with a flow cell interface. With the use of the postcolumn flowing extraction method in the interface, two questions need to be addressed before realization of the objective is achieved. Is the resulting extract sufficiently transparent in the mid-infrared to yield spectra of the eluents? And, does the partitioning between the HPLC solvent system and the organic extraction solvent favor the organic phase for a wide variety of compounds? This discussion concerns the interpretation of our results with respect to these two questions.

Methanol and water both exhibit maximum transparency at approximately 1800 cm^{-1} (*6*). Even at this maximum, the mid-infrared throughput is extremely low for pure methanol or water. It has been suggested that the longest, practical path length for an infrared flow cell directly coupled to a reversed-phase HPLC column is approximately 25 μm. At such a low path length, the infrared sensitivity is too low for the FTIR to be practically used as an HPLC detector. It was hoped in this study that the extraction system, which incorporates the membrane phase separator, would greatly reduce the concentration of the water and methanol in the effluent without significantly reducing the analyte concentration.

A separation of a mixture containing three ketones was chosen for the first extraction experiment because of the intense carbonyl stretching vibration that is observed near

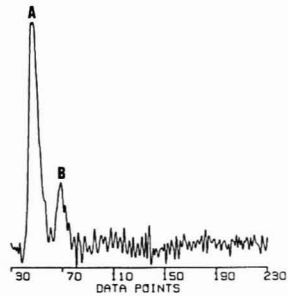


Figure 4. Gram–Schmidt reconstructed chromatogram from FTIR detection of ketone separation with chloroform extraction, 5 μL of stock solution injected: (A) cyclohexanone; (B) acetophenone, benzophenone not detected.

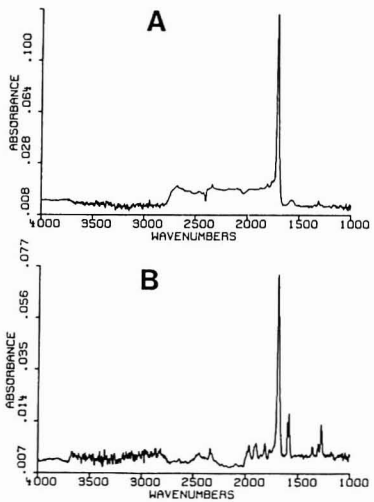


Figure 5. Infrared spectra obtained from ketone separation with chloroform extraction: (A) cyclohexanone; (B) acetophenone.

the frequency of maximum IR throughput in methanol and water. Initial separations without flowing extraction are shown in Figure 3. With UV detection at 254 nm, which is perhaps the most widely used RP-HPLC detector, only benzophenone and acetophenone are detected (Figure 3A) with good sensitivity. If the column loading and attenuation are increased, cyclohexanone is detected as a very weak peak by the UV 254-nm detector (Figure 3B). A further increase in column loading allows the use of a refractive index detector. In this case, only cyclohexanone and acetophenone are detected (Figure 3C) with reasonable sensitivity while benzophenone gave a fairly weak response. In fact, the impurity eluting just after benzophenone shows an equal RI response close to that of benzophenone.

The first solvent extraction attempted was with chloroform since this solvent has relatively good infrared transparency. A Gram–Schmidt reconstructed chromatogram of the separation (i.e., flowing extraction and phase separation) with FTIR detection is shown in Figure 4. Only the first two peaks

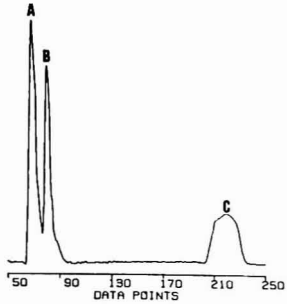


Figure 6. Gram-Schmidt reconstructed chromatogram from FTIR detection of ketone separation with carbon tetrachloride extraction: (A) cyclohexanone; (B) acetophenone; (C) benzophenone.

are detected, and the spectra obtained (Figure 5) are relatively poor. Enough analyte has been extracted to give a good response for the carbonyl stretch, but the concentration of water and methanol in the chloroform is great enough that the regions on either side of the carbonyl are virtually opaque to the infrared. The observed carbonyl stretching absorbances, however, are indicative of each of the two compounds. Failure to observed the third component is probably due to the fact that benzophenone is not extracted into the chloroform to a detectable degree under these conditions.

It should be noted that the ZDV cell which is used in these experiments, because of its multi path length, circular cross section, does not show solvent bands in the resulting spectra. Although a zero absorbance base line is observed across strong solvent bands, the solution remains opaque to the infrared in these regions. Consequently, sample spectra are obscured in those regions where strong infrared absorbance due to the solvent are expected. This phenomenon has been previously discussed (*5*).

Closer inspection of the acetophenone spectrum (Figure 5B) reveals that several bands other than the carbonyl stretch are weakly observed. For example, the substitution overtone bands between 2000 and 1750 cm^{-1} appear to be slightly exaggerated relative to the C=O stretch. This suggests that the intensity of the observed carbonyl stretch is somewhat attenuated because of the reduced throughput at this particular wavenumber that results from the presence of methanol and water that have dissolved in the chloroform. In any event, the weakly observed bands are not particularly useful for comparison to library spectra because of the intensity distortions that have resulted.

The results from the chloroform extraction experiments while discouraging nevertheless encouraged further investigation into the development of flow cell RP-HPLC/FTIR. The major problem with the use of chloroform as the extraction solvent appeared to be relatively excessive solubility for the water/methanol mobile phase. Carbon tetrachloride was next investigated as an extraction solvent. Not only does carbon tetrachloride have very good window regions in the mid-infrared but this nonpolar solvent dissolves a wide variety of compounds as well. Also, the solubility of water in carbon tetrachloride is much less than that in chloroform.

An experiment involving a separation of the same three ketones gave greatly improved results when carbon tetrachloride was used as the extraction solvent. The Gram-Schmidt reconstructed chromatogram is shown in Figure 6. Comparison to the reconstructed chromatogram obtained with chloroform as the extraction solvent reveals that not only are all three ketones detected but also the signal-to-noise ratio

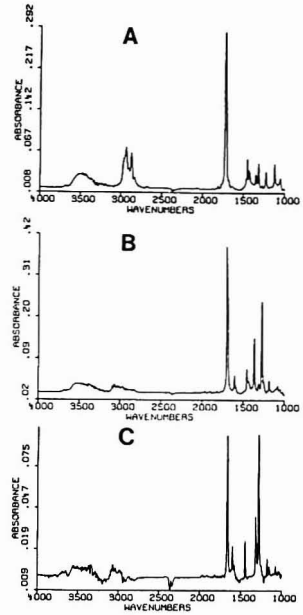


Figure 7. Infrared spectra obtained from ketone separation with carbon tetrachloride extraction: (A) cyclohexanone; (B) acetophenone; (C) benzophenone.

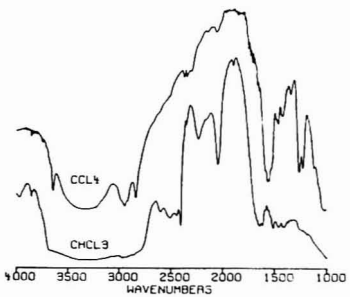


Figure 8. Single-beam spectra of solvent background in RP-HPLC/FTIR using carbon tetrachloride and chloroform as extraction solvents. The arbitrary *y*-axis is normalized for each spectrum to the same scale; the CCl_4 spectrum is offset in the *y* direction.

is much better using carbon tetrachloride. The corresponding file spectra are shown in Figure 7. These spectra also have extremely good signal-to-noise ratios. Furthermore, these spectra match standard, reference spectra peak for peak, thus allowing conclusive identification. The weak broad absorbance around 3500 cm^{-1} is no doubt traces of unextracted H_2O–C-H_3OH. The C–H stretching region however exhibits absorbance characteristic of the compound in question.

Inspection of the single-beam spectra (Figure 8) of the background using chloroform and carbon tetrachloride as extraction solvents reveals that carbon tetrachloride extraction

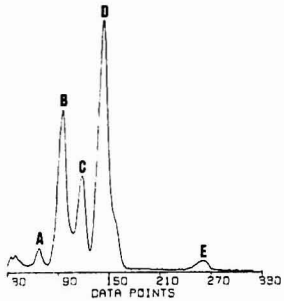


Figure 9. Gram–Schmidt reconstructed chromatogram from FTIR detection of test mixture separation with carbon tetrachloride extraction, 5 μL of stock solution injected (ca. 300 μg of each component): (A) phenol; (B) acetophenone; (C) nitrobenzene; (D) methyl benzoate; (E) toluene.

has indeed afforded greater IR transparency. The methanol bands, which are quite apparent in the chloroform extraction spectrum, are virtually absent in the carbon tetrachloride extraction spectrum. In addition, the intense, characteristic water absorbances at each end of the mid-infrared spectrum are observed to a much lesser degree when using carbon tetrachloride. Although the absolute amount of water and methanol extracted into the carbon tetrachloride is unknown, the infrared transparency of the solution is more than adequate. This clearly explains the increased quality of file IR spectra using carbon tetrachloride.

The final concern of this preliminary study is whether or not carbon tetrachloride extracts a wide variety of compounds. A five-component column test solution in methanol was injected on the RP-HPLC/FTIR system using carbon tetrachloride as the extraction solvent. The resulting Gram–Schmidt reconstructed chromatogram is shown in Figure 9. The five components (i.e., phenol, acetophenone, nitrobenzene, methylbenzoate, toluene), which represent a wide range of polarities, are distinctly detected as well as the solvent front. The corresponding file spectra are shown in Figure 10. Again, excellent signal-to-noise ratio is observed in the spectra. Comparison to standard, reference spectra conclusively identifies each of the five components.

In summary, we have demonstrated for the first time a practical method for flow cell detection of reversed-phase HPLC eluents using the Fourier transform infrared spectrometer. No attempt has been made as yet to optimize the

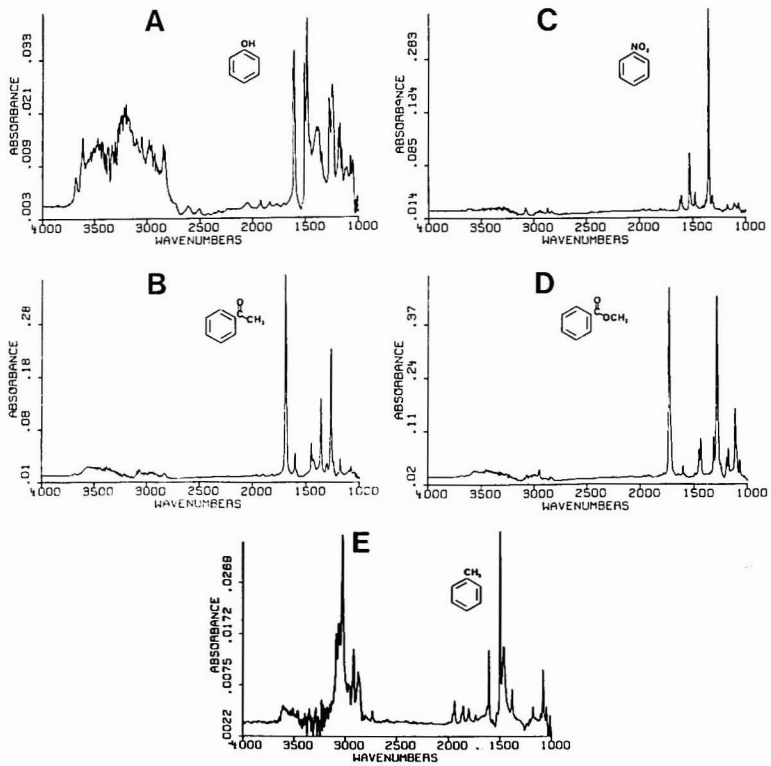


Figure 10. Infrared spectra obtained from test mixture separation with carbon tetrachloride extraction: (A) phenol; (B) acetophenone; (C) nitrobenzene; (D) methyl benzoate; (E) toluene.

extractor/separator portion of this apparatus. In spite of this, readily identifiable, high signal-to-noise, on-line spectra are obtained with less than 300 μg of injected sample. Carbon tetrachloride has been demonstrated to possess all of the necessary characteristics in order for it to be employed as an infrared-transparent, flowing-extraction solvent. Thorough investigation of this RP-HPLC/FTIR method is currently under way.

ACKNOWLEDGMENT

The authors wish to thank the following people for their assistance: Robert A. Sanders of Procter and Gamble for discussions at the inception of this RP-HPLC/FTIR approach; Gil Pacey of Miami University for encouraging discussions on flow injection analysis and for supplying a sample of the Gore-Tex membrane; Harry C. Dorn of VPI & SU for the loan of one of the IBM LC pumps; and Don Sting of Spectra-Tech, Inc., for use of the Barnes Model 600 beam condenser.

LITERATURE CITED

(1) Johnson, C. C.; Taylor, L. T. *Anal. Chem.* **1983**, *55*, 436-441.
(2) Brown, R. S.; Taylor, L. T. *Anal. Chem.* **1983**, *55*, 1492-1497.
(3) Amatels, P. G.; Taylor, L. T. *Anal. Chem.* **1984**, *56*, 966-971.
(4) Brown, R. S.; Amatels, P. G.; Taylor, L. T. *Chromatographia* **1984**, *18*, 396-400.
(5) Johnson, C. C.; Taylor, L. T. *Anal. Chem.* **1984**, *56*, 2642-2647.
(6) Vidrine, D. W. In "Fourier Infrared Spectroscopy"; Ferraro, J. R., Basile, L. J., Eds.; Academic Press: New York, 1979; Vol. 2, pp 129-164.
(7) Jinno, K.; Fujimoto, C. *Chromatographia* **1983**, *17*, 259-262.
(8) Parris, N. A. *J. Chromatogr. Sci.* **1979**, *17*, 541-545.
(9) Jinno, K.; Fujimoto, C.; Uematsu, G. *Am. Lab.* (*Fairfield, Conn.*) **1983**, 39-45.
(10) Kuehl, D. T.; Griffiths, P. R. *J. Chromatogr. Sci.* **1979**, *17*, 471-476.
(11) Kuehl, D. T.; Griffiths, P. R. *Anal. Chem.* **1980**, *52*, 1394-1399.
(12) Kalasinsky, K. S.; McDonald, J. T., Jr.; Kalasinsky, V. F. *FT-IR Spectral Lines* **1983**, *5*, 14-15.
(13) Duff, P. J.; Conroy, C. M.; Griffiths, P. R.; Karger, B. L.; Vouros, P.; Kirby, D. P. *Proc. Soc. Photo-Opt. Instrum. Eng.* **1981**, *289*, 53-56.
(14) Karlberg, B.; Thelander, S. *Anal. Chim. Acta* **1978**, *98*, 1-7.
(15) Conroy, C. M.; Griffiths, P. R.; Duff, P. J.; Azarraga, L. V. *Anal. Chem.* **1984**, *56*, 2636-2642.
(16) Nord, L.; Karlberg, B. *Anal. Chim. Acta* **1980**, *118*, 285-292.

RECEIVED for review October 1, 1984. Accepted December 13, 1984. The IBM LC/9533 chromatograph was a donation to VPI & SU from IBM Instruments, Inc., through their University Gifts program. The financial support of the Department of Energy through Grant No. DE-FG22-84PC70799 and the Commonwealth of Virginia is appreciated.

Fixed-Site Ion Exchanger for Liquid Chromatographic Determination of Multifunctional Carboxylic Acids

R. M. Cassidy* and S. Elchuk

General Chemistry Branch, Atomic Energy of Canada Limited, Research Company, Chalk River Nuclear Laboratories, Chalk River, Ontario, Canada K0J 1J0

Reversed phases coated with a "permanently" sorbed ion exchanger and indirect UV detection have been investigated for the determination of simple and multifunctional carboxylic acids in chemical cleaning solutions. The advantages of being able to vary both the ion-exchange capacity and the hydrophobic interactions on these types of ion exchangers for the optimization of resolution and detection are illustrated, and the selection of optimum separation conditions is discussed. Dissolved iron interferes with the analysis due to photochemical, redox, and kinetic effects but good recoveries can be obtained after reduction of the iron with hydroxylamine and complexation with 1,2-diaminocyclohexanetetraacetic acid. Detection limits (3× base line noise) for oxalate, citrate, ethylenediaminetetraacetate, and hydroxyethylenediaminetriacetate are 0.6–20 μg·mL^{-1} for a 20-μL sample, and relative standard deviations are 3 to 5% in the 75–350 μg·mL^{-1} range. Analysis results for reactor decontamination solutions containing up to 250 μg·mL^{-1} of iron agree with results obtained by other techniques, and it is shown that this technique should also be useful for determination of metal ions in the samples. A determination of the above reagents in the presence of Fe(II) and Ni(II) takes 7 to 12 min after a 5 to 10 min reduction step. Cr(III) forms nonlabile complexes with ethylenediaminetetraacetic acid, and its presence will cause low results for this acid.

Multifunctional carboxylic acids are used in formulations for boiler treatment, chemical cleaning of process systems, and decontamination of nuclear reactor components. Our main interest in the determination of these reagents has been related to their use for reactor decontamination. Previously we developed a gas chromatographic procedure (*1*) based on the separation of methylated esters of the acids (*2*). However, this method requires a derivatization step, which makes the method relatively slow and susceptible to errors, and the use of gas cylinders can make this method cumbersome for in-field analysis. High-performance liquid chromatography (HPLC) has a number of potential advantages for these analyses, but the techniques reported thus far (*3–8*) are suitable for only a limited number of acids. Most of the methods (*4–8*) are based on the separation of metal chelates of the acids and are only applicable to acids forming stable chelates. These techniques also limit the choice of eluent pH and buffers, due to possible precipitation of metal ion added to form the chelates. We had previously examined ion pairing and metal chelate (Fe and Cu) HPLC separations for the determination of these acids but had only limited success. Our recent studies with reversed-phase columns that are "permanently" coated with large hydrophobic quaternary amines (*9*) to give a charged surface that can be used for ion exchange, have shown that such columns can offer distinct advantages over either dynamic ion pairing or bonded-phase ion-exchange separations. This paper reports the results of studies of these columns with both direct and indirect UV detection for the determination of multifunctional carboxylic acids. The main acids of concern in this study were oxalic, citric, hydroxyethylethylenediaminetriacetic (HEDTA), and ethylenediaminetetraacetic (EDTA) acids. Decontamination solutions can also contain large concentrations of iron (up to 250 μg·

0003-2700/85/0357-0615$01.50/0 © 1985 American Chemical Society

Table I. Eluents Used for Indirect Detection

compound	source[a]	wavelength maxima, nm	molar absorptivity, L·mol^{-1}·cm^{-1}	molar absorptivity at 254 nm, L·mol^{-1}·cm^{-1}
4-hydroxyphthalic acid	A	280	1300	5800
		245	7100	
benzenesulfinic acid (Na salt)	B	260	1200	960
1,2,4,5-benzenetetracarboxylic acid	C	295	2000	7500
		245	9000	
1,2,3-benzenetricarboxylic acid	C	280	750	1200
1,2,4-benzenetricarboxylic acid	C	285	1600	6300
		240	9500	
1,3,5-benzenetricarboxylic acid	C	280	1000	2500
benzoic acid	D	265	560	660
phthalic acid (mono K$^+$ salt)	E	280	1400	1300
salicylic acid	E	295	3600	300
		230	7200	
m-sulfobenzoic acid (mono Na$^+$ salt)	F	273	1100	900
o-sulfobenzoic acid (mono NH_4 salt)	F	265	1300	880
5-sulfosalicylic acid	G	295	3000	440

[a] A Alfa Products; B, Eastman Kodak; C, Aldrich Chemical Co., D, ICN Pharmaceuticals; E, Fisher Scientific; F, Pfaltz & Bauer Inc.; G, J. T. Baker Chemical Co.

mL^{-1}) as well as smaller concentrations of some other metal ions (chromium and nickel in particular), and the effects of these metal ions on the analyses have also been examined.

EXPERIMENTAL SECTION

Apparatus. The chromatographic system consisted of M6000A Waters pumps, a Beckman 332 pumping system, a Rheodyne sampling valve, a Schoefell SF 770 variable wavelength detector, and a Spectra Physics 4270 computing integrator. The columns used were as follows: 10 μm PRP-1, 4.1 × 150 mm (Hamilton Co.); 5 μm Supelcosil LC-18, 4.6 × 150 mm (Supelco Inc.); and 3 μm Supelcosil LC-18, 4.6 × 75 mm.

Reagents. The organic anions used both for elution and as chromophores for indirect detection of the multifunctional organic acids are listed in Table I; these reagents were used as received from the supplier (Table I). The tetrabutylammonium hydroxide (TBAOH) was purified by placing a 40% (w/v) aqueous solution in a freezer at −20 °C until ~80% of the volume was precipitated, and the precipitated TBAOH was washed with water at 0 °C and then analyzed by titration with 1 mol·L^{-1} HCl. The 1,2-diaminocyclohexanetetraacetic acid (DCTA) was purified by precipiatation of the DCTA from a basic solution by slow addition of HCl to give a final pH of 2. All other reagents were prepared from HPLC-grade solvents and water purified by triple distillation or double distilled water purified in a Milli-Q (Millipore) system.

Column Coating. The column coating procedure given here is for a 3 μm C_{18} reversed phase, the column recommended for this analysis. Coating procedures for the other columns are similar, and have been discussed elsewhere (*9*).

A precolumn and analytical column were connected in series and washed with 1.4 L of 5 × 10^{-4} mol·L^{-1} cetylpyridinium chloride in 23% (v/v) acetonitrile–water; the precolumn was a guard column that contained PRP-1 or C_{18} bonded phase, depending on which type of analytical column was used. The eluent was changed to that used for the analytical separation (contained 1 to 7% (v/v) acetonitrile and one of the acids in Table I; typical eluents are given in Tables II and III) and the column was equilibrated with ~150 mL of this eluent. The precolumn was placed upstream of the injector to ensure that cetylpyridinium was not eluted from the analytical column, and samples of EDTA were injected until a constant peak height was obtained.

Standard Preparation. To simulate decontamination solutions, iron powder was added to a helium degassed solution containing EDTA, oxalic acid and citric acid, and stirred and heated under helium in an opaque container at 50 °C until the iron powder was dissolved (~30 min). This solution was then stored in a sealed volumetric in the dark. A typical standard contained 300, 400, 300, and 160 μg·mL oxalate, EDTA, citrate and Fe^{2+}, respectively. Some standards were also made directly from the free acids with $NaFe^{III}EDTA$ (Alfa Products) or $FeCl_3$ used as the source of iron. Reagent-grade chemicals were used for preparation of the standards.

Sample Analysis. When possible, sample bottles were opaque and the sample was protected from exposure to light. One milliliter of 3000 μg·mL^{-1} DCTA, which had been adjusted to pH 4 with tris(hydroxymethyl)aminomethane (THAM), 15 μL of 100 μg·mL^{-1} NH_2OH·HCl, and 0.5 mL of the sample were added to

Table II. Detection Limits

eluent	wavelength, nm	detection limit[a] μg·mL^{-1} Ox	CIT	EDTA	μg injected Ox	CIT	EDTA
sulfosalicylate[b]	295	0.8	4	3	0.02	0.08	0.06
phthalate[c]	254	2	9	5	0.04	0.2	0.1
1,2,4-benzenetricarboxylate[c]	257	0.6	5	3	0.01	0.1	0.06
1,3,5-benzenetricarboxylate[c]	254	2.1	20	5	0.04	0.4	0.1

[a] Three times peak-to-peak base line noise. [b] PRP-1 column. [c] 5 μm C_{18} column.

Table III. Values of *k'* for Different Eluent Systems

anion	eluent[a] and *k'* values A	B	C	D	E	F
diglycolate						3.6
tartronic						4.0
ketomalonic						4.3
gluconic		1.9				
HEDTA	2.0	21		2.8	1.9	
maleic						6.9
oxalate	3.5	30	3.0	3.9	2.0	4.4
FeEDTA		15			1	
EDTA	14		9.3	16.8	7.5	6.3
citrate	23		12	22	8.8	9.1
DCTA			27	37	15.4	11.5

[a] A, 1.0 × 10^{-3} mol·L^{-1} 1,3,5-tricarboxylic acid, pH 7.3, 80 mg coating on PRP-1; B, 3.0 × 10^{-3} mol·L^{-1} benzoic acid, pH 7.3, 80 mg coating on PRP-1; C, 5.0 × 10^{-4} mol·L^{-1} 1,2,4-tricarboxylic acid, pH 7.3, 23 mg coating on PRP-1; D, 1.5 × 10^{-3} mol·L^{-1} phthalic acid, pH 7.3, 23 mg coating on PRP-1; E, 5 × 10^{-4} mol·L^{-1} sulfosalicylate, pH 7.3, 23 mg coating on PRP-1; F, 5 × 10^{-4} mol·L^{-1} sulfosalicylate, pH 5.6, 80 mg coating on PRP-1. All eluents except F contained ~1 × 10^{-3} mol·L^{-1} THAM buffer.

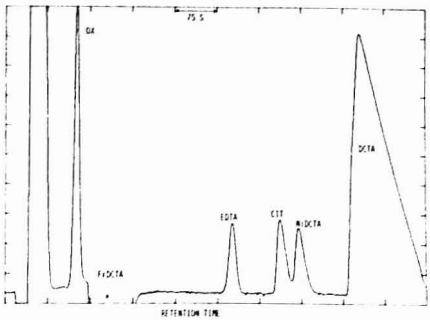


Figure 1. Separation of oxalate, citrate, and EDTA anions in presence of iron and nickel. Experimental conditions: 4 × 75 mm, 3 μm C_{18} column coated with 5×10^{-4} mol·L^{-1} cetylpyridinium chloride in 23% (v/v) acetonitrile; eluent, 1.5×10^{-3} mol·L^{-1} phthalate, 1.8×10^{-3} mol·L^{-1} THAM buffer, 7% (v/v) acetonitrile, and flow rate of 2 mL·min^{-1}; sample, 20 μL of solution containing 100, 117, 67, 33, and 100 μg·mL^{-1} of oxalate (OX), EDTA, citrate (CIT), Ni(II), and Fe(III), respectively; detection at 254 nm.

a 4-mL scintillation vial equipped with a Teflon-lined cap. The vial was capped and heated for 5–10 min at 100 °C in a water bath that was covered with aluminum foil. The sample was cooled for a few seconds under a stream of water, and ~60 μL of 1 mol·L^{-1} NaOH was added to give a pH of 7.3–8.0. An aliquot (normally 20 μL) was then injected into the chromatograph; chromatographic conditions recommended for most samples are those given in Figure 1. Quantitation was done by comparison of peak areas with those for standards reacted similarly.

RESULTS AND DISCUSSION

Detection. Because of the variation in the physical and chemical properties of the different acids used for chemical cleaning, it is difficult to find one property that can be used to monitor the elution of all the reagents, particularly at low microgram per milliliter concentrations. The methods examined in this work were detection in the low UV range (215 nm), and indirect (vacancy) detection.

Many of the acids studied absorbed light in the low UV region, but there were wide variations in molar absorbtivities. Detector sensitivity was especially poor for citrate (~400 μg·mL^{-1} for 3 × base line noise) and sensitivity improvements obtained at lower wavelengths could not be used due to the presence of large background absorption from small concentrations of iron–phosphate complexes, which were formed by the reaction of the phosphate buffer in the eluent with the steel surface of the HPLC system. The effect of pH (3 to 10) on retention was examined, and phosphate was the only buffer found to be reasonably compatible with detection at 215 nm. Gradient elution was required to ensure removal of the iron phosphate which otherwise sorbed onto the column and ruined column performance. The presence of iron in the samples was a further complication due to precipitation of iron phosphate and the formation of iron complexes with the acids. Consequently this system was not studied further and, unless specified otherwise, the remainder of the discussions in this paper are limited to indirect detection systems.

For indirect UV detection the absorbance of an eluent component (visualization reagent) is monitored, and the changes in its concentration as a sample component is eluted can be related to the concentration of the sample component in the eluate (*9–11*). A particularly attractive feature of indirect detection for ion-exchange separations is that, in principle, it can be used for the detection of all anions without wide variations in sensitivity. The basic principles of the detection mechanism (exchange of visualization–reagent anion for sorbed sample anion) are simple, but for successful application the interrelationships between eluent strength, eluent–anion charge, eluent concentration, background absorbance, and pH effects must be considered; with "permanently" sorbed exchange sites the effective ion-exchange capacity of the column can be varied to help optimize these interrelationships. In this study a number of visualization reagents were tested, and these are listed in Table I. All of these compounds can be used as eluents for indirect detection, but benzoic, benzenesulfinic, and salicylic were too weak (long retention times) and 1,2,4,5-benzenetetracarboxylic acid was too strong (short retention times) for separation of the multifunctional carboxylic acids studied here; benzoic acid was useful for separation of weakly retained carboxylic acids.

The sensitivity of indirect detection depended on the charge on the eluent and sample anions (this determined the number of molecules of eluent anion exchanged for one sample anion), the molar absorptivity of the eluent anion, and the concentration of other anions in the eluent. The detection limits given in Table II (3 times peak-to-peak base line noise) illustrate the dependence of sensitivity on eluent charge and molar absorptivity (Table I). Anionic buffers (such as phosphates) or other anions in the eluent reduced sensitivity due to competition with the indirect-detection reagent for free ion-exchange sites when sample anions were eluted. Consequently a cationic buffer, THAM, was used, as it had no appreciable effect on sensitivity. THAM was added to the acid form of the visualization reagent and thus was present as a salt of the visualization reagent.

Column Systems. Both bonded-silica (C_{18}) and styrene–divinylbenzene (PRP-1) reversed phases were used in these studies. The PRP-1 phase could be used at higher pH values, but the UV absorbance of OH^- limited the usefulness of this feature. The C_{18} phases were more efficient, due to their smaller particle size, and the best performance was obtained with the 3 μm C_{18} phase. Dynamic ion-exchange (ion pairing) separations were investigated on these columns with tetrabutylammonium salts, but this approach was unsuccessful due to the reasons discussed in "Detection". Some of the eluent systems used for indirect detection with "permanently" coated columns are given in Table III. Figure 1 shows a separation that is typical of the different systems studied, and essentially the same system was used in field tests during reactor decontamination. Both PRP-1 and C_{18} "permanently" coated columns were used for periods of 3–5 months, and only small changes in column efficiency and retention times were noted. The "permanently" coated exchangers were superior to dynamic ion exchangers (ion-pair chromatography) for indirect detection because the presence of the dynamic modifier in the mobile phase can complicate detector response. The columns did not appear to be susceptible to poisoning, but if a problem was encountered the ion exchanger was stripped (*9*) and then recoated. The ability to vary the ion-exchange capacity of the columns was found to be important for adjustment of retention times as the background absorbance in indirect detection places limitations on the changes that can be made in eluent strength for any one eluent system. A number of the parameters affecting column selectivity were examined, and these are discussed below.

All of the eluents listed in Table I influenced column selectivity, due to ion exchange effects arising from changes in charge and concentration, and due to hydrophobic interactions on the reversed phase; the latter are discussed in more detail below. Table III lists capacity factors, k', for some of the eluents used. For some of these eluents the effect of pH on selectivity was studied over the range of 2.7–9.3. All of the eluents listed in Table III became stronger eluents with in-

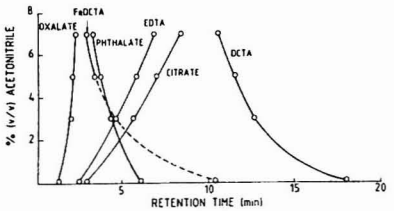


Figure 2. Effect of acetonitrile on retention time. Experimental conditions similar to those given in Figure 1.

Table IV. Effect of Column Capacity on Retention Time[a]

anion	retention time, min		k' values relative to oxalate	
	20 mg[b]	80 mg[b]	20 mg[b]	80 mg[b]
oxalate	1.9	2.6	1	1
FeDCTA	3.3	2.0	7.1	0.4
EDTA	5.3	8.9	12.3	4.1
citrate	6.0	10.9	14.2	5.0
DCTA	9.8	15.0	24	7.0

[a] Eluent, 5×10^{-4} mol·L^{-1} sulfosalicylate, 1.5×10^{-3} mol·L^{-1} THAM at pH 7.3; flow rate, 2.0 mL·min^{-1}. [b] Weight of cetylpyridinium chloride sorbed onto PRP-1 column.

creasing pH values, but the charge on some of the sample anions, such as EDTA and DCTA, increased with pH faster than that for the eluent anions. Consequently high pH values could not be used due to the long retention times for these acids. Some changes in selectivity with pH were observed, and this was a factor in the differences in retention time obtained between E and F in Table III. Eluents with pH values below 5 were not useful as most of the sample acids were close to fully protonated at this pH; thus sorption was weak and similar for most of the acids, which made their separation difficult. For most of the compounds studied the optimum pH range was ~7 to 8; pH 7.3 was chosen as a compromise between column stability and the buffering capacity of THAM.

Hydrophobic interactions also influenced retention and the magnitude of this effect depended on pH, ion exchange capacity of the column, and solvent composition. Figure 2 shows that modification of the hydrophobic effects with acetonitrile could cause significant differences in relative retention. The retention of the more hydrophobic and lower-charged anions decreased with increased addition of acetonitrile to the eluent while the opposite effect was observed with the more polar anions. The hydrophobic effect is an attractive feature of these "permanently" coated reversed phases as it is another parameter that can be used to optimize separations; however, if more than ~10% (v/v) acetonitrile is used the "permanently" sorbed ion exchanger may be slowly eluted.

The ion-exchange capacity of the "permanently" coated columns can be changed quickly, and this can be also used to optimize selectivity. This is illustrated by the retention times given in Table IV for a PRP-1 column with two different exchange capacitites. The retention time for $Fe^{III}DCTA^-$ decreased unexpectedly with an increase in ion-exchange capacity. This decrease is likely related to the hydrophobic effects discussed above; the increased surface coverage of cetylpyridinium ions would reduce the hydrophobic surface area on PRP-1 and this would decrease retention for those ions where hydrophobic effects are important for sorption.

Metal Ion Interferences. The presence of dissolved metal ions, particularly iron, is a common feature of chemical cleaning procedures. For acids that function as multidentate chelating agents, well-defined metal–chelate peaks were often observed, and this was investigated as a basis for their determination. However, the addition of excess metal ion to the sample or to the eluent was required, and some of the excess metal ion usually sorbed onto the column (or precipitated onto the column) and caused badly skewed peaks for some of the acids which formed less stable metal chelates. This sorption of metal ions was particularly evident when salicylate eluents were used, and although it was much less important for phthalate eluents, the latter eluents also gave unsatisfactory results for the separation of a number of acids as metal chelates. Thus a different approach was examined, consisting of the addition of excess DCTA to the sample to complex all of the free metal ions, and subsequent analysis of the free acids. The effectiveness of this approach was first examined for iron, because it was the predominant metal ion in the sample, and was present in concentrations up to ~250 μg·mL^{-1}. Aside from forming complexes with the acids, dissolved iron introduced analytical errors due to redox, photochemical, and kinetic effects.

Ferric complexes of multifunctional carboxylic acids can be photoreduced (*1*, *12–16*) to produce Fe(II) and ligand oxidation products. This reaction caused low results when samples were not protected from light. $Fe^{III}EDTA^-$ can also undergo a thermally activated reduction accompanied by oxidation of EDTA (*17*) but this should not occur with the experimental condition used for sample analysis (see Experimental Section). When dissolved oxygen was present, Fe(II) was rapidly oxidized to Fe(III), and thus a cyclic oxidation–reduction occurred if light was present also. This cyclic reaction eventually destroyed the acids, and Fe(III) precipitated due to a rise in pH. Consequently it is imperative that all samples be protected from light.

Dissolved oxygen caused additional problems when it was present during the preparation of standards containing iron by the direct reaction between the acids and iron powder. Under these conditions 90% to 100% losses were observed for EDTA, and a peak for a decomposition product was observed. Good recoveries were obtained when standards were prepared under helium, but dissolution of the iron powder was much slower, which suggests that Fe(III) or dissolved oxygen may affect the mechanism of interaction between these acids and iron surfaces. Standards prepared under helium were only faintly colored, and rapidly changed to green-yellow when exposed to air.

The exchange of iron among the ligands was rapid only for Fe(II). For Fe(III), however, especially for multidentate ligands such as EDTA, exchange is slow (half-life = 16 h at pH 2), and the half-life increases with pH (*12*). Consequently liberation of the free acids by the preferential complexation of Fe(III) by DCTA was slow, and low recoveries were obtained. The effects of this slow exchange are illustrated by the data in Table V. Total elimination of oxygen was difficult, and even with a He purge low recoveries (70–90%) were obtained (sample 1). If the sample was allowed to stand prior to addition of DCTA (sample 2) larger losses were obtained due to oxidation of Fe(II) from oxygen that diffused through the polyethylene container. Good recoveries were obtained if DCTA was added during dissolution of the standards (sample 3), but this cannot be used for the analysis of samples. However, reduction of the Fe(III) by hydroxylamine hydrochloride (sample 4) promoted rapid exchange of the iron and good recoveries were obtained (sample 4).

Investigation of this reduction procedure showed that less than 50% of the iron was complexed by DCTA after 1.5 h when reduction was done at ambient, but rapid (5–10 min) reduction and complexation by DCTA were achieved if the

Table V. Recovery of Acids in Presence of Dissolved Iron[a]

	% sample recovery			
anion	1 He purge (new)	2 He purge (4-days old)	3 He purge (DCTA added)	4 NH_2OH·HCl reduction
oxalate	106 (33)[b]	109 (33)	104 (60)	106 (100)
EDTA	86 (44)	32 (44)	102 (80)	102 (116)
citrate	110 (33)	103 (33)	101 (60)	101 (67)
Fe concn ($\mu g \cdot mL^{-1}$)	(22)	(22)	(30)	(33)

[a] Experimental conditions: All samples were made 1000 $\mu g \cdot mL^{-1}$ in DCTA prior to analysis; samples 1–3 were prepared by dissolution of Fe powder by the acids under He; DCTA was added to 3 prior to dissolution of Fe; the Fe in sample 4 was added as $NaFe^{III}$ EDTA prior to reduction. All recoveries were calculated from response factors obained in the absence of Fe. [b] Numbers in parentheses are starting concentrations in $\mu g \cdot mL^{-1}$.

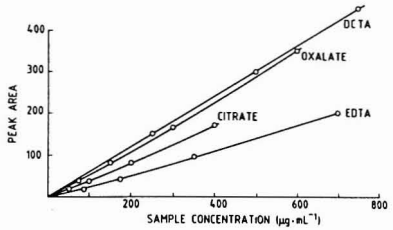


Figure 3. Calibration curves for separation on a coated 3 μm column. Experimental conditions similar to those given in Figure 1.

samples were heated in a 100 °C water bath. The pH also affected this reaction and lower pH values (2 to 4) gave better recoveries. Small losses (5–7%) were sometimes observed if the samples were heated for 1 h or more, or when they were allowed to stand for 1 day; for these samples small peaks for decomposition products were also observed. During these studies it was found that cap liners of the sample vials could cause significant loses of some acids when the samples were heated to 100 °C; this effect was eliminated by the use of Teflon-lined caps, and 100% recoveries were obtained for the acids tested (HEDTA, oxalate, EDTA, citrate, and DCTA).

The effect of Ni(II) and Cr(III) was also studied briefly. Ni(II) formed a stable complex with EDTA (this is probably true for the other multidentate ligands) but was quantitatively exchanged to DCTA after 10 min at 100 °C; recoveries for 350 $\mu g \cdot mL^{-1}$ EDTA were 97% and 98% in the presence of 50 and 100 $\mu g \cdot mL^{-1}$ Ni(II), respectively. Cr(III) slowly (few minutes) formed a nonlabile complex with EDTA and no exchange with DCTA was observed even after reaction at 100 °C for 30 min. As the Cr^{III}EDTA was eluted at the solvent front, EDTA bound by Cr(III) could not be determined; this may be possible if weaker eluents are used.

Analytical Performance. Figure 3 shows calibration curves obtained for separations on a 3 μm C_{18} column. The curves were slightly nonlinear, and this was especially evident for EDTA at low concentrations, which was attributed to interactions of EDTA with metal surfaces or metal ion impurities. At the start of each day low results (~10%) were observed for EDTA, and two to three injections were required to condition the system. Peak areas were used for quantitation, because indirect detection is an inherently nonlinear system, and peak heights, which are more sensitive to peak shape, usually gave calibration plots that had much smaller linear ranges. Reproducibilities (1σ) for the analysis procedure

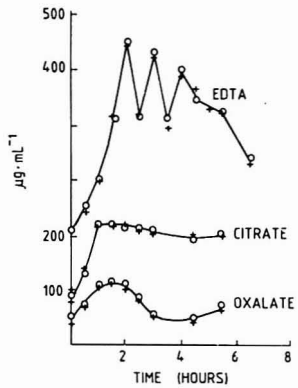


Figure 4. Comparison of analytical results obtained during reactor decontamination: HPLC data indicated by O, data from other techniques indicated by +. Experimental conditions: HPLC results obtained with 10 μm C_{18} column under conditions similar to those for Figure 1; results for EDTA obtained by GC procedure (*1*); ion chromatographic separation for oxalate and citrate done by standard ion-exclusion procedure of Dionex Corp.

were determined several times, and were always in the range of 3 to 5% for HEDTA, oxalate, citrate, EDTA, and DCTA in the concentration range of 75 to 350 $\mu g \cdot mL^{-1}$; these data were obtained under conditions similar to those given for Figure 1. A complete separation (Figure 1) took ~11 min (5–7 min at faster flow rates) and with a 5–10 min reaction with hydroxylamine and DCTA, total turn-around time was 15 to 21 min for any one sample. Any anion that is sorbed strongly onto anion exchangers is a potential interferent; of the common inorganic anions tested (F^-, Cl^-, NO_3, NO_2, Br^-, and SO_4^{2-}) only SO_4^{2-} showed appreciable sorption and gave a positive interference for oxalate (10 $\mu g \cdot mL^{-1}$ of SO_4^{2-} gave a peak corresponding to ~10 $\mu g \cdot mL^{-1}$ of oxalate). The pH of the injected sample affected peak shape for some of the acids and the size of the system peak; the magnitude of these effects depended on the eluent. Sample pH, which was studied over the pH range of 2.7–9.3, was unimportant for the sulfosalicylate eluent but was important for the phthalate eluent. For this latter eluent sample pH should be 7.3–8.0, especially for EDTA determinations; this pH adjustment is not difficult as the sample is buffered by THAM, and the same volume of base is usually sufficient for pH adjustment of all samples obtained during a decontamination.

Figure 4 shows a summary of some of the results of obtained during tests of these techniques during reactor decontaminations; the data generated by the power-plant staff (Figure 4) were obtained by gas chromatography for EDTA (nitrogen selective detector) and by ion chromatography (Dionex) for citrate and oxalate. These results show that good agreement was obtained; the iron concentrations in these samples varied from 20 to 250 $\mu g \cdot mL^{-1}$.

This chromatographic system can also be used to determine metal ions simultaneously with the acids; such analyses are used to monitor corrosion. For iron, which will usually be the major metal ion present, this determination can be direct (measurement of the negative $Fe^{III}DCTA^-$ peak) or indirect (measurement of change in peak area for DCTA). For some of the chromatographic systems tested, inadequate resolution prevented direct measurement and the indirect measurement was used. Table VI shows a comparison of the indirect HPLC and atomic absorption (AA) results for a number of samples

Table VI. Comparison of Indirect HPLC and Atomic Absorption Results for Iron in Chemical Cleaning Solutions[a]

Fe concn found, $\mu g \cdot mL^{-1}$		
HPLC	AA	ratio (HPLC/AA)
197	178	1.107
205	197	1.041
171	185	0.924
194	190	1.021
215	191	1.126
203	202	1.005
192	180	1.067
212	196	1.082
192	180	1.067
248	220	1.127
180	170	1.059
248	230	1.078

[a] Average of ratios = 1.059. Standard deviation = 0.057.

obtained during different decontamination tests. These data show that there was a reasonable agreement between the two techniques, but a "t test" showed that the average of the ratios was significantly different from 1.0 at the 99% confidence level. The presence of a significant positive bias for the HPLC results is supported by the fact that although HPLC calibration curves for iron were linear, they gave a positive intercept at the "Y" axis. A possible source of this positive bias may be the reaction of DCTA with metal surfaces or with other metal ion impurities in the HPLC system. Direct measurement of the $Fe^{III}DCTA^-$ peak was preferable, especially for small iron concentrations, and linear calibration curves, which went through the origin, were obtained; detection limits were 0.4 $\mu g \cdot mL^{-1}$. Adjustment of the hydrophobic interactions via acetonitrile content of the mobile phase was useful for resolving $Fe^{III}DCTA^-$ from the acids of interest.

The $Ni^{II}DCTA^{2-}$ chelate gave a well-defined peak (Figure 1), and thus it should also be possible to determine the concentration of this metal ion; however, this was not investigated. It should also be possible to use the acetonitrile composition to adjust the relative retention time of this $Ni^{II}DCTA^{2-}$ chelate.

CONCLUSIONS

Ion exchangers formed by the sorption of hydrophobic cations onto reversed phases can offer significant advantages over bonded phase exchangers for the separation and determination of multifunction carboxylic acids that are used for chemical cleaning of industrial components such as heat-transport systems of nuclear-power reactors. The ability to optimize ion-exchange capacity and hydrophobic effects permits the development of separations that may be difficult on other types of ion exhcangers. This system has been proven to give reliable analysis under actual decontamination conditions and should be capable of replacing the two to three instruments used for such analyses in the past.

Registry No. EDTA, 60-00-4; HEDTA, 150-39-0; citric acid, 77-92-9; oxalic acid, 144-62-7; iron, 7439-89-6.

LITERATURE CITED

(1) Cassidy, R. M.; Harpur, R.; Elchuk, S. *J. Chromatogr.* **1980**, *190*, 188–192.
(2) Rudling, L. *Water Res.* **1971**, *5*, 831–837.
(3) Chen, S. G.; Cheng, K. L.; Vogt, C. R. *Microchim. Acta* **1983**, 473–481.
(4) Perfetti, G. A.; Warner, C. R. *J. Assoc. Anal. Chem.* **1979**, *62*, 1092–1095.
(5) Parkes, D. G.; Caruso, M. G.; Spradling, J. E., III *Anal. Chem.* **1981**, *53*, 2154–2156.
(6) Chinnick, C. C. T. *Analyst (London)* **1981**, *106*, 1203–1207.
(7) Harmsen, J.; Van Den Toorn, A. *J. Chromatogr.* **1982**, *249*, 379–384.
(8) Venezky, D. L.; Rudzinski, W. E. *Anal. Chem.* **1984**, *56*, 315–317.
(9) Cassidy, R. M.; Elchuk, S. *J. Chromatogr. Sci.* **1983**, *21*, 454–459.
(10) Small, H.; Miller, T. E., Jr. *Anal. Chem.* **1982**, *54*, 462–469.
(11) Hackzell, L.; Schill, G. *Chromatographia* **1982**, *15*, 437–444.
(12) Jones, S. S.; Long, F. A. *J. Phys. Chem.* **1952**, *56*, 5–33.
(13) Hill-Gottingham, D. G. *Nature (London)* **1955**, *175* 347–348.
(14) Hall, L. H.; Lambert, J. L. *J. Am. Chem. Soc.* **1968**, *90*, 2036–2039.
(15) Trott, T.; Hemwood, R. W.; Lanford, C. H. *Environ. Sci. Technol.* **1972**, *6*, 367–368.
(16) Natarajan, P.; Endicott, J. F. *J. Phys. Chem.* **1973**, *77*, 2049–2054.
(17) Motekaitis, R. J.; Martell, A. E.; Hayes, D. *Can. J. Chem.* **1980**, *58*, 1999–2005.

RECEIVED for review September 20, 1984. Accepted November 27, 1984.

Determination of Chloride, Bromide, and Iodide in Silver Halides by Ion Exchange and Ion Interaction Chromatography

Frederick J. Gustafson* and Craig G. Markell

3M, Central Research Laboratories, St. Paul, Minnesota 55144

Sharon M. Simpson

3M, Photo Color Systems, St. Paul, Minnesota 55144

An ion chromatographic method is described by which halide ratios in silver halide matrices can be determined over the range of 0.01 to 100 mol %. Halides are recovered from silver halides dissolved in a cyanide-free system by reduction of silver in basic aqueous hydrazine solution. Preparative cation exchange subsequently eliminates hydrazine and hydroxide from the sample which is analyzed by ion exchange chromatography for chloride and bromide and by ion interaction chromatography for iodide. Chromatographic conditions have been established for halide elution in less than 10 min with complete separation of the individual halides at all concentration (mol %) ratios and complete separation from anions of insoluble silver salts. Recoveries for mixed halide standards were 98% for chloride, 94% for bromide, and 92% for iodide with a reproducibility better than 3% relative standard deviation.

The primary light sensitive properties of a photographic emulsion are determined by the molar ratios of silver chloride, silver bromide, and silver iodide in the emulsion (*1*). A number of procedures have been developed in response to the need for an analytical method to determine silver halide ratios. Przybylowicz et al. (*2*), Gerard et al. (*1*), and Russel (*3*) have reviewed these techniques which include potentiometric titration with silver nitrate, automatic coulometric titration, polarography, X-ray spectrometry, neutron activation analysis, and activation analysis using a ^{252}Cf neutron multiplier.

Difficulties inherent in the polarographic and potentiometric methods include inadequate differentiation between responses of one halide ion from another particularly when one halide is present at a low mole percent value. The neutron activation analysis method developed by Gerard et al. (*1*) is fast and accurate for the determination of halides over a wide mole percent range. The limitations of neutron activation stem from the relative thermal neutron absorption cross sections of silver and the halides. Because silver has a cross section 10 times greater than any of the halides, the sample cannot be accurately analyzed without first complexing the silver with aqueous cyanide. The chloride detection limit is greater than the bromide and iodide detection limits because the chloride cross section is 5 times less than the cross sections for the other two halides.

This paper describes a cyanide-free procedure for dissolving silver halides by reduction of silver ion in basic aqueous hydrazine solution. Hydrazine was initially described by Andresen (*4*, *5*) as a weak photographic developing agent in strongly alkaline solution. Reduction of silver in silver halides by hydrazine is thermodynamically favorable according to the standard potentials of the reactions. Previous two-step halide isolation procedures have used cyanide (*6*) or ammonia (*7*) to form silver complexes followed by zinc reduction of silver. In the one-step method to be described, the only anions present in the system are hydroxide and the halides. Hydroxide and hydrazine are subsequently eliminated by passage of the sample through a hydrogen-form cation exchange resin column.

Ion chromatography is capable of determining sub-part-per-million levels of halides in the presence of other anions. In the analysis of real silver halide samples, the chromatography must be capable of separating the halides from essentially all anions of insoluble silver salts. These constraints made it necessary to utilize ion exchange chromatography (IEC) for the determination of chloride and bromide and ion interaction chromatography (IIC) for the determination of iodide.

The original IEC method of Small et al. (*8*) cannot be used for determining all three halides in a single injection due to severe tailing of iodide on the polymeric resin column. The postsuppression gradient elution method of Sunden et al. (*9*) is characterized by poor iodide peak shape and an iodide elution time of greater than 20 min. Other single injection procedures on polymeric anion exchange columns include the column-switching dual detector method of Wang et al. (*10*) and the aromatic eluant method in the Wescan Instrument (Santa Clara, CA) applications literature. Both techniques compromise resolution of chloride and bromide for the ability to elute iodide with minimal tailing. Silica based anion exchange columns do not cause iodide to tail. Silica slowly dissolves in aqueous mobile phases causing a decrease in ion exchange capacity and analyte retention times. IEC on polymeric anion exchange columns is useful for the separation of chloride and bromide from virtually all other anions.

The determination of chloride, bromide, and iodide by IIC has been demonstrated by Iskandarani and Pietrzyk (*11*) using a mobile phase containing tetrapentylammonium salts as the ion interaction agent. The column was packed with macroreticular styrenedivinylbenzene resin. Due to the long equilibration time of the tetrapentylammonium ion with the column, tetrabutylammonium salts were employed in this study. Carbonate was used as the eluant counterion because of its compatibility with eluant suppression and conductivity detection (*12*). Carbonate also controls the selectivity of the analysis. All of the tested divalent anions eluted before iodide, and iodide was cleanly separated from monovalent anions such as formate, chloride, bromide, thiocyanate, nitrate, cyanide, and perchlorate. Because of this selectivity, IIC was the method of choice for determining iodide.

EXPERIMENTAL SECTION

Apparatus. Liquid chromatography was performed on a Dionex Model 2120i LC (Dionex, Inc., Sunnyvale, CA) and an IBM Model 9533 LC (IBM Instruments, Inc., Danbury, CT) equipped with a Wescan Model 213A conductivity detector (Wescan Instruments, Santa Clara, CA) and a Perkin-Elmer Model LC-75 ultraviolet absorption detector (Perkin-Elmer Corp., Norwalk, CT). Data were recorded and integrated on an H-P

0003-2700/85/0357-0621$01.50/0 © 1985 American Chemical Society

Table I. Conditions for Ion Exchange and Ion Interaction Chromatography

	ion exchange for Cl^- and Br^-	ion interaction for I^-
analytical column	4 × 250 mm Dionex AS4	4 × 250 mm Dionex NS1
guard column	4 × 50 mm Dionex AG4	4 × 50 mm Dionex NG1
suppressor column	Dionex AFS fiber suppressor	10 × 100 mm Dionex packed anion suppressor
eluant	7×10^{-4} M $NaHCO_3$	10^{-3} M tetrabutylammonium hydroxide
	5.6×10^{-4} M Na_2CO_3	15% (v/v) acetonitrile, 3×10^{-3} M Na_2CO_3
flow rate	2.0 mL/min	1–1.5 mL/min
injection volume	15–50 μL	15–50 μL
detector sensitivity	1 μS full scale (Wescan detector)	1 μS full scale (Wescan detector)

Model 3390 integrator (Hewlett-Packard Co., Avondale, PA), or an IBM Model 9000 computer (IBM Instruments, Inc., Danbury, CT). Ion chromatography columns were purchased from Dionex and are described in Table I.

Reagents. Water used in this study was purified with a Millipore RO-4 reverse osmosis unit followed by Milli-Q mixed bed ion exchange and organic removal cartridges (Millipore Corp., Bedford, MA). Tetrabutylammonium hydroxide (0.4 M from Eastman Kodak Co., Rochester, NY) was purified by passage through a strong base cation exchanger, Amberlite IRA-400 (Mallinkrodt Chemical Works, St. Louis, MO). This resin had been previously converted to the hydroxide form with aqueous NaOH. Amberlite IR-120 H C.P. (Mallinkrodt) was used in sample preparation. This hydrogen form strong acid resin was extensively prerinsed in the filter section of a solvent filtration flask to remove residual chloride. Halide free aqueous hydrazine solutions were prepared from anhydrous hydrazine (99%, MCB Manufacturing Chemists, Norwood, OH). Due to its toxicity, concentrated hydrazine was handled in a hood. Silver halide (99% purity) standards were obtained from Aldrich Chemical Co. (Milwaukee, WI). UV grade acetonitrile was obtained from Burdick and Jackson Laboratories (Muskegon, MI). All other inorganic salts used in this study were analytical reagent grade and used without further purification.

Sample Preparation. Up to 30 mg of silver halide was weighed into a glass vial with a polyethylene-lined cap. Five milliliters of 6% (w/v) aqueous hydrazine and 1 mL of 0.25 M NaOH were pipetted into the vial. The vial was capped and placed in a heating block for 24 h at 60–70 °C. Reduction of silver was apparent by the appearance of metallic silver. The sample was cooled and filtered through a 0.45 μm pore size Nylon 66 membrane filter (Rainin Instrument Co., Inc., Woburn, MA) placed on the end of a plastic syringe. To analyze major constituents of the sample, a 1-mL aliquot was diluted to 100 mL and analyzed without removing base and hydrazine. Repeated injections of 0.06% hydrazine did result in some deterioration of the performance of the anion exchange column evidenced by peak broadening.

In order to determine halides at trace levels, hydrazine must be removed from the samples. Four milliliters of the sample was passed through a 10-mL column of a hydrogen form strong acid cation exchange resin and collected in a 25-mL volumetric flask. The resin converts sodium hydroxide and hydrazine into water. A few drops of 0.25 M NaOH were added to the volumetric flask before collecting the sample to retard acid-catalyzed air oxidation of iodide. Rinsings of the resin column with small portions of deionized water were added to the volumetric flask until 25 mL was collected.

RESULTS AND DISCUSSION

Reduction of Silver. Halides can be liberated from silver halides by reduction (*3*), complexation (*7*), or ligand exchange

Table II. Recovery of Halides from Silver Halides

$[N_2H_4]$ (v/v %)	[NaOH], M	T, °C	% halide recovered Cl^-	Br^-	I^-
5.0	0.04	70	98 ± 3.0[a]	94.5 ± 2.4[a]	92.0 ± 2.1[a]
0.5	0.04	70	97 ± 4.5[b]	88 ± 3.2[b]	96 ± 7.0[b]
5.0	0.01	22	[c]	90 ± 1.0[b]	8.5 ± 8.0[b]
0.5	0.01	22	97 ± 1.5[b]	98 ± 1.9[b]	6.5 ± 2.8[b]

[a] Average recovery of five separate samples with relative standard deviation given. [b] Average recovery of two separate samples with average deviation given. [c] Chloride was not present in this sample.

with anions such as sulfide (*13*). In this study, silver ion was reduced by hydrazine according to the following reaction (*14*)

$$4AgX + 4OH^- + N_2H_4(aq) \rightarrow 4Ag(s) + 4X^- + 4H_2O + N_2(g)$$

Hydrazine reduction is thermodynamically favorable for all three silver halides and does not introduce anionic interferences into the sample. Recoveries of halides in mixed silver halide standards (10 mg of AgCl, 10 mg of AgBr, and 10 mg of AgI) were greater than 90% as shown in Table II. The low solubility product of silver iodide ($K_{sp} = 8 \times 10^{-17}$) results in low iodide recoveries at room temperature. The rate of silver reduction was greater at 70 °C, and the average iodide recovery increased to 92%. The relative standard deviation of the halide recoveries for five mixed halide standards was less than 3% for each halide ion.

When the samples were stirred during the silver reduction, halide recoveries were low. Samples were turbid after 24 h at 70 °C. Filtration through 0.45 μm pore size nylon filters did not always eliminate the turbidity. Turbid solutions were probably due to silver halide particles dispersed in the sample. The cause of the turbidity was not investigated.

Chromatography. Since an unknown silver halide sample can contain halides at various ratios as well as other anionic impurities, the chromatographic methods used in this study were developed to separate chloride, bromide, and iodide without interferences from other anions. IEC was used to determine chloride and bromide. The eluant composition in Table I was chosen to allow a chloride peak from a 30 mg sample of silver chloride to decay to base line before a small bromide peak eluted (Figure 1A). Trace chloride can be determined in a similar fashion in 30 mg of silver bromide (Figure 1B). Trace level quantitation of one halide was not affected by injections of up to 50 μg of another halide.

Under conditions suitable for separating chloride and bromide, iodide eluted with severe tailing ($k' = 40$). High concentrations of iodide did not directly interfere with the chloride and bromide separation or quantitation. The chromatographic behavior of other possible interfering anions was also investigated. Capacity factors for these anions are presented in Table III. All of these anions were completely resolved from chloride and bromide. Figure 1C shows the separation of iodate, chloride, bromide, sulfite, and phosphate.

The IIC mode was used to separate and determine iodide in this study because IIC can separate iodide from all of the anions listed in Table III. This was not the case with the anion exchange columns evaluated for iodide determination. For example, sulfate and iodide were incompletely resolved by the Dionex AS5 column under standard eluant conditions. IIC is also advantageous in that capacity factors and selectivities of anions can be independently controlled by changing mobile phase conditions. Pietrzyk and co-workers (*11*, *15*, *16*) have published a series of papers on the IIC of anions on resin columns using mobile phases consisting of tetraalkylammonium (R_4N^+) ions, water, acetonitrile, and inorganic

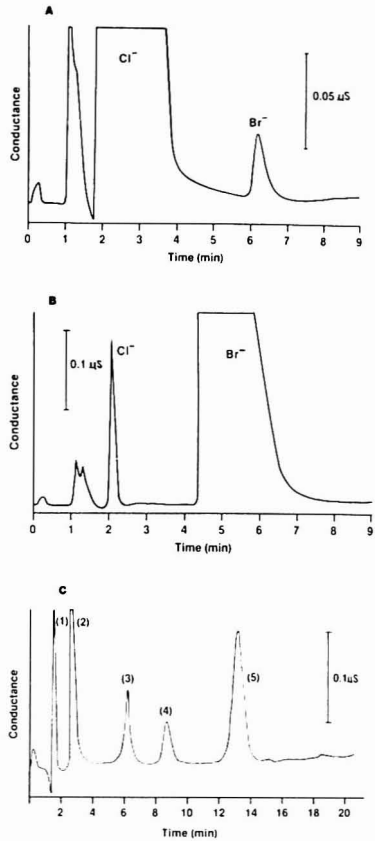


Figure 1. Ion exchange chromatography conditions as in Table I: (a) separation of 50 μg of chloride and 100 ng of bromide; (b) separation of 100 ng of chloride and 50 μg of bromide; (c) separation of (1) iodate, (2) chloride, (3) bromide, (4) phosphate, and (5) sulfite. Approximately 100 ng of each anion injected.

anions. In an expression derived from equilibria and mass balance equations, the capacity factor of a monovalent anion was shown to be directly proportional to the R_4N^+ concentration in the mobile phase and inversely proportional to the concentrations of the monovalent eluant anion and the analyte ion (*16*).

In this study, the R_4N^+ ion was tetrabutylammonium at a concentration of 10^{-3} M in the mobile phase. Tetrabutylammonium ion was chosen over tetrapentylammonium because the latter compound required an hour of equilibration time with the column. Retention of anions was controlled by the acetonitrile concentration in the mobile phase as shown in Figure 2. Capacity factors for all anions decreased with increasing acetonitrile concentration primarily due to desorption of tetrabutylammonium from the column. Selectivity was controlled by the mobile phase carbonate concentration as shown in Figure 3. Divalent anions were forced to elute before some monovalent anions by increasing the carbonate concentration. Under the chromatographic conditions described in Table I, no divalent anion was found to elute after iodide (Table III). Iodide was separated from bromide even when 50 μg of bromide was injected as shown in Figure 4.

Table III. Capacity Factors of Anions

ion	K' (IEC)[a]	K' (IIC)[a]
formate	0.1	<0.1
iodate	0.1	<0.1
chloride	1.0	0.3
bromide	4.2	0.5
iodide	40	1.3
phosphate	6.4	0.75
sulfite	10	0.75
sulfate	33	0.75
oxalate	>40	0.57
nitrate	5.1	0.6
chromate	>20	0.85
thiosulfate	>20	0.89
thiocyanate	>20	2.3
perchlorate	>20	>10
carbonate	13	0.5
cyanide	<1	<1
sulfide	<1	<1

[a] Conditions of analysis as in Table I. Column void volumes were measured by using strong eluants to elute an essentially unretained anion (formate) in both the IEC and IIC modes.

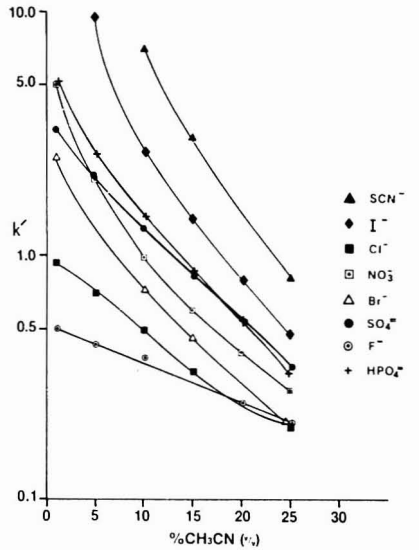


Figure 2. Retention of anions in IIC as a function of acetonitrile concentration. Mobile phase is 10^{-3} M tetrabutylammonium hydroxide, 3×10^{-3} M Na_2CO_3, and acetonitrile as indicated. Other conditions are given in Table I.

Quantitative Analysis. Although IIC is not affected by samples containing hydrazine, a large negative base line excursion is observed in IEC when hydrazine at a concentration above 0.06% (w/v) was injected onto the column. This base line excursion interferes with the determination of chloride and also broadens the chloride peak. Samples should not be injected onto the column unless diluted 100-fold or passed through a hydrogen form cation exchanger to eliminate hydroxide and hydrazine. A sample in which hydrazine is absent

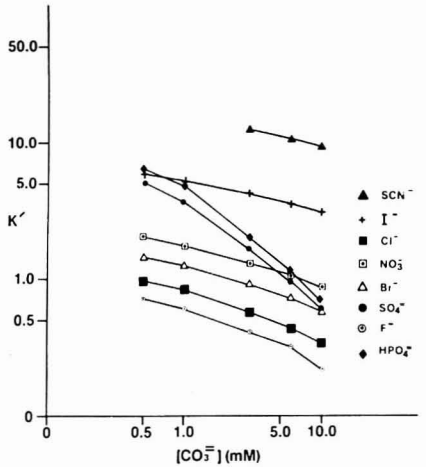


Figure 3. Retention of anions in IIC as a function of mobile phase carbonate concentration. The mobile phase is 10^{-3} M tetrabutylammonium hydroxide, 7.5% (v/v) acetonitrile, and sodium carbonate concentration as noted. Other conditions are given in Table I.

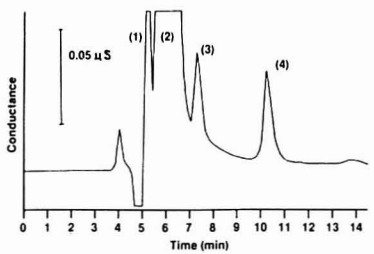


Figure 4. Ion interaction chromatography conditions as in Table I: separation of (1) 100 ng of chloride, (2) 50 μg of bromide, (3) unknown impurity anion, and (4) 100 ng of iodide.

will not decolorize a dilute potassium permanganate solution.

The detection limits for chloride and bromide (IEC) and iodide (IIC) using conductometric detection were determined to be 0.4 ng, 1 ng, and 2.4 ng injected, respectively, at a signal-to-noise ratio of 4. The detection limit for iodide using the ultraviolet absorption detector at 200 nm was in the range of 1–10 ng injected. Quantitation of halides was shown to be independent of the concentrations of other halides present in the samples. In IIC, the predicted reduction in capacity factor with increased levels of iodide injected (*16*) was studied. When up to 5 μg of iodide was injected, the iodide capacity factor decreased by less than 7%. Calibration curves for chloride, bromide, and iodide were found to be linear over 3 orders of magnitude. The detection limits for the determination of trace halides in silver halides are presented in Table IV for analysis by ion chromatography and neutron activation. Detection limits for ion chromatography are based on the reduction of a 30-mg sample, a final sample volume following ion exchange of 25 mL, and an injection volume of 50 μL. Chloride and bromide can be determined at lower mole percent levels by ion chromatography than by neutron activation analysis (*1*).

Table IV. Mole Percent Detection Limits for Halides in Silver Halides

	IEC and IIC			neutron activation analysis[a]		
salt	Cl	Br	I	Cl	Br	I
AgCl	–	0.008	0.010	–	0.1	0.01
AgBr	0.005	–	0.015	0.4	–	0.01
AgI	0.005	0.013	–	0.4	0.1	–

[a] From ref 1.

The reproducibility of the method is demonstrated in Table II in which halide recoveries on five separate mixed halide synthetic standards were measured. The relative standard deviation of the recovery for each individual halide ion was less than 3%. When five separate samples of 0.027 mol % silver iodide in silver bromide were analyzed, the recovery of iodide was 93.2% (±2% RSD) and for bromide it was 90.5% (±3.2% RSD). The experimentally determined mole percent of iodide to bromide was 0.027 (±3% RSD).

With the ability to dissolve insoluble silver salts and to separate many different anions, ion chromatography should have wide applicability in the photographic industry for the determination of trace impurities in silver nitrate solutions, soluble halide salts, and silver halides. Other applications of ion chromatography can be envisioned for the analysis of developer solutions, anionic and cationic dyes, surfactants and antistatic agents, hardeners, and other ionic film additives.

Registry No. Cl^-, 16887-00-6; Br^-, 24959-67-9; I^-, 20461-54-5; AgCl, 7783-90-6; AgBr, 7785-23-1; AgI, 7783-96-2.

LITERATURE CITED

(1) Gerard, J. T.; Swanson, C. C.; Ver Weire, L. J.; Pietruszewski, J. L. J. *Radioanal. Chem.* **1979**, *54*, 59–68.
(2) Przybylowicz, E. P.; Smith, G. W.; Suddueth, J. E.; Nargolwalla, S. S. *Anal. Chem.* **1969**, *41*, 819–823.
(3) Russel, G. "Chemical Analysis in Photography"; The Focal Press: London, 1965; pp 184–187.
(4) Andresen, M. *Photogr. Mitt.* **1891**, *28*, 286.
(5) Andresen, M. *Photogr. Mitt.* **1892**, *28*, 296.
(6) Clark, W. J. *Chem. Soc.* **1926**, 749.
(7) Siemer, D. *Anal. Chem.* **1980**, *52*, 1874–1877.
(8) Small, H.; Stevens, T. S.; Bauman, W. C. *Anal. Chem.* **1974**, *47*, 1801–1809.
(9) Sunden, T.; Cedergren, A.; Siemer, D. D. *Anal. Chem.* **1984**, *56*, 1085–1089.
(10) Wang, C.; Bunday, S. D.; Tarter, J. G. *Anal. Chem.* **1983**, *55*, 1617–1619.
(11) Iskandarani, Z.; Pietrzyk, D. J. *Anal. Chem.* **1982**, *54*, 2427–2431.
(12) Pohl, C. U.S. Patent No. 4 265 634, May 5, 1981.
(13) Baldock, T. W. U.S. Patent No. 1 358 163, June 26, 1974.
(14) James, T. H., Ed. "The Theory of the Photographic Process", 4th ed., Macmillan: New York, 1977; p 297.
(15) Rotsch, T. D.; Pietrzyk, D. J. *Anal. Chem.* **1980**, *52*, 1323–1327.
(16) Iskandarani, Z.; Pietrzyk, D. J. *Anal. Chem.* **1982**, *54*, 1065–1071.

RECEIVED for review September 10, 1984. Accepted November 19, 1984. This paper was presented in part at the Minnesota Chromatography Forum Spring Symposium, April 1984.

Selective Determination of Trace Level Chromium(III) by Ion-Pair Reversed-Phase High-Performance Liquid Chromatography Based on Color Formation with 4-(2-Pyridylazo)resorcinol in the Presence of Triethanolamine

Hitoshi Hoshino* and Takao Yotsuyanagi

Department of Applied Chemistry, Tohoku University, Aoba, Aramaki, Sendai 980, Japan

The color reaction of chromium(II) ion with 4-(2-pyridylazo)resorcinol is quantitatively accomplished within 30 min in boiling triethanolamine buffer solution at pH 8.5–8.9 to produce the red chelate having the molar absorption coefficient of 6.21×10^4 dm^3 mol^{-1} cm^{-1} at 525 nm. On the basis of this finding, a rapid and highly selective ion-pair reversed-phase partition liquid chromatography/photometric detection system has been developed for the determination of trace chromium at the ng cm^{-3} level. A detection limit of chromium is down to 0.5 ng cm^{-3} at 0.005 absorbance unit full-scale range (525 nm), being free from the interferences by 100–200 ng cm^{-3} each of common cations such as Al(III), V(V), Mn(II), Fe(III), Co(II), Ni(II), Cu(II), Zn(II), and Cd(II) ions.

Trace determination of chromium(III) ion is now increasingly important in biological, clinical, and evironmental analyses. The photometric method for trace chromium seems to be limited actually to the well-known 1,5-diphenylcarbohydrazide method (*1*, *2*), in which chromium(III) ion is converted to the hexavalent form before the color development. Several workers have reported the color reaction of highly sensitive reagent, 4-(2-pyridylazo)resorcinol (PAR, H_2L) with chromium(III) ion and have suggested the analytical potentially (*3–5*). However, the methods have suffered from the lengthy and incomplete color development even under heating conditions. Certain auxiliary ligands which accelerate the color formation, thus, have been desired. We have now found that the formation of a Cr(III)–PAR chelate is greatly enhanced by triethanolamine (TEA) in slightly alkaline solution (pH 8.5–8.9, boiling for 30 min) to produce an anionic chelate which has the larger molar absorption coefficient (ϵ) value, 6.21×10^4 dm^3 mol^{-1} cm^{-1} at 525 nm than any chelate reported previously (*4*, *5*). This ϵ value is also 1.3 times larger than that of the 1,5-diphenylcarbohydrazide complex ($\epsilon = 4.17 \times 10^4$) reported by Allen (*6*).

Nonetheless, the major problems which arose in application of the PAR method to chromium assay of biological or environmental materials were the provision of sufficient sensitivity and selectivity to detect the ng cm^{-3} concentration in various matrix compositions.

We developed successfully an ion-pair reversed-phase high-performance liquid chromatography (IPHPLC) system for Fe(III)–, Co(III)–, and Ni(II)–PAR chelates (*7*, *8*), which is an alternative approach to conventional photometry for solving the sensitivity and the selectivity problems. The highly inert Cr(III)–PAR chelate is separated effectively by IPHPLC using a bolaform electrolyte (diquaternary ammonium salt) as an ion-pairing reagent in the mobile phase. Hence, the combination of Cr(III)–PAR chelate (enhanced by TEA) and the IPHPLC separation will provide sufficient selectivity and sensitivity for the chromium determination within an acceptable analysis time.

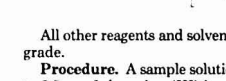
Some reports have appeared about the practical use of the HPLC method in chromium determination (*9–14*); however, they seem to be unsatisfactory in some respects, i.e., incomplete peak resolution, low sensitivity, or requirement of a more sophisticated detection system. The method proposed in this work is applicable to a sample containing chromium in the ng cm^{-3} range and 100–200 ng cm^{-3} each of Fe(III), Co(II), Ni(II), Mn(II), Cu(II), V(V), Zn(II), Cd(II), and Al(III) ions as the matrices.

EXPERIMENTAL SECTION

Apparatus. A Horiba M-5 pH meter and a Hitachi Model 124 double-beam recording spectrophotometer were used. The HPLC setup used consisted of a TWINCLE pump unit, a UVIDEC 100-III spectrophotometric detector with an 8 μL flow cell of 1 cm light path length, and a VL 611 loop injector (100 mm^3) from Japan Spectroscopic Co., Ltd. (Hachioji, Tokyo, Japan). The detector settings of 0.01 and 0.005 absorbance unit full-scale (aufs) were used for 10 mV recorder output. A column used was a Hiber column packed with LiChrosorb RP-18 (ODS type 10 μm, 4 mm bore × 250 mm in length) from Cica-Merck (Tokyo Japan).

Reagents. A standard chromium(III) solution (0.01 mol dm^{-3}) was prepared from guaranteed reagent grade $KCr(SO_4)_2 \cdot 12H_2O$, and was standardized by back titration with standard EDTA and zinc chloride solutions. Other metal ion solutions were prepared from the chlorides of nitrates and were standardized by accepted EDTA titrations. A triethanolamine solution (2.5 mol dm^{-3}) was prepared from "for masking grade" TEA obtained from Dojindo Laboratories) (Kumamoto, Japan), and pH of the solution was adjusted to 8.7 with hydrochloric acid. A solution of PAR, 2.5×10^{-3} mol dm^{-3} was prepared and standardized as reported previously (*15*). A bolaform electrolyte, *N,N,N,N',N',N'*-hexamethyl-1,4-butanediammonium dibromide ($BoBr_2$) was synthesized from trimethylamine and 1,4-dibromobutane by refluxing in ethanol for 1.5 h (*16*).

$BoBr_2$:



All other reagents and solvents used were of guaranteed reagent grade.

Procedure. A sample solution (40 cm^3 or less) containing 0.020 to 2.5 μg of chromium(III) ion is pipetted into a 100-cm^3 beaker to which 2 cm^3 each of PAR and TEA solutions are added. The mixture is boiled down cautiously to 30 cm^3 for 30 min. After cooling, the solution is transferred into a 50-cm^3 volumetric flask and diluted to the mark. An aliquot of the solution (ca. 1 cm^3) is injected into the HPLC system through a 100-mm^3 loop. The Cr(III)–PAR chelate eluted is detected at 525 nm. As the mobile phase, an aqueous methanol (40 wt %) solution containing 9.8×10^{-3} mol kg^{-1} $BoBr_2$, 2×10^{-3} mol kg^{-1} Tris-HCl buffer (pH 7.5) and 10^{-4} mol kg^{-1} disodium EDTA was used in a flow rate of 1.0 cm^3 min^{-1}.

0003-2700/85/0357-0625$01.50/0 © 1985 American Chemical Society

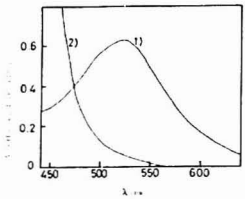


Figure 1. Absorption spectra of Cr(III)–PAR chelate and PAR at pH 8.7: (1) Cr(III)–PAR, corrected for the spectrum of excess PAR, (2) PAR; $C_{Cr} = 1.03 \times 10^{-5}$ mol dm^{-3}, $C_L = 1.0 \times 10^{-4}$ mol dm^{-3}, boiling for 30 min in 0.054 mol dm^{-3} TEA solution.

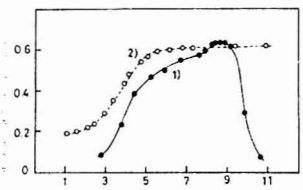


Figure 2. Absorbance–pH curves of the Cr(III)–PAR system: (1) Cr(III)–PAR–TEA system, absorbances corrected for those of excess PAR at 525 nm, $C_{Cr} = 1.02 \times 10^{-6}$ mol dm^{-3}, $C_L = 1.06 \times 10^{-4}$ mol dm^{-3}, $C_{TEA} = 0.05$ mol dm^{-3}, after 2 h of boiling; (2) prepared Cr(III)–PAR chelate used, at 525 nm, $C_{Cr} = 9.94 \times 10^{-6}$ mol dm^{-3}.

RESULTS AND DISCUSSION

Absorption Spectra and Effect of pH. Absorption spectra of Cr(III)–PAR chelate ($\lambda_{max} = 525$ nm) and PAR in slightly alkaline solution are shown in Figure 1. The absorption–pH curve after the Cr(III)–PAR–TEA system was boiled for 2 h is shown in Figure 2 (curve 1). The maximal absorbance was obtained in the pH range 8.5–8.9. The formation of Cr(III)–PAR chelate was strongly facilitated in slightly alkaline solution as compared with that in the acetate buffer solution system (*4*). This indicates that the hydrolysis of Cr(III) ion is favorably avoided by the formation of Cr(III)–TEA complex. Once the color was developed, the absorbance was constant over the pH range 6–11 (Figure 2, curve 2). In this case, the decrease in the absorbance below pH 6 is due to the protonation equilibria represented as (*17*)

$$[Cr(HL)_2]^+ \xrightleftharpoons{pK_{a1} = 3.22} [Cr(HL)L] \xrightleftharpoons{pK_{a2} = 4.35} [CrL_2]$$

The highly inert Cr(III)–PAR chelate is not decomposed even at pH 2 at room temperature. The predominant species under the condition with the TEA buffer solution is the anionic one. The mobile phase pH should also be adjusted at 7 to 8.

Molar Ratio Plots and the ϵ Value. The molar ratio plots for the Cr(III)–PAR chelate are given in Figure 3. In the concentrations of TEA, 0.05, 0.10, and 0.25 mol dm^{-3}, the chelate was quantitatively formed when at least 4-fold molar excess of PAR (4×10^{-5} mol dm^{-3}) against Cr(III) ion was added. The plots clearly show that the composition of the chelate is Cr:PAR = 1:2. The ϵ value of the chelate is calculated from the plots to be 6.21×10^4 dm^3 mol^{-1} cm^{-1} which is similar to that of the Fe(III)–PAR chelate, 6.11×10^4 at 495 nm (*8*).

Rates of Color Development. Boiling time–absorbance curves for the Cr(III)–Par–TEA system at various pH and TEA concentrations are shown in Figure 4. Ten cubic centimeter aliquots of the reaction mixture on boiling in a three-necked flask fitted with a dimroth condenser were pipetted at prescribed time intervals and were added to 10 cm^3 of ice-cooled water. The absorbance values in Figure 4 are, thus, one-half of those for the reaction mixture. Consequently, when more than 0.04 mol dm^{-3} of TEA is added at pH above 7.5, the constant absorbance is reached within 30 min. On the basis of the results given in Figures 2, 3, and 4, boiling for 30 min with 1.0×10^{-4} mol dm^{-3} of PAR and 0.10 mol dm^{-3} of TEA at pH 8.7 is recommended for the color development. Reasonably, this is also the case for Cr(III) ion at ultratrace concentration as pseudo-first-order conditions with respect to Cr(III) ion may hold, i.e., the relatively high concentrations of PAR and TEA being used.

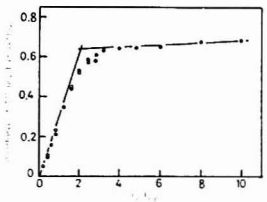


Figure 3. Molar ratio plots for Cr(III)–PAR chelate at pH 8.7 in the presence of TEA after 2 h of boiling: $C_{Cr} = 1.02 \times 10^{-6}$ mol dm^{-3}; full circles, $C_{TEA} = 0.05$ mol dm^{-3}; open circles, $C_{TEA} = 0.1$ mol dm^{-3}.

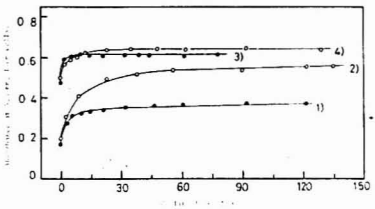


Figure 4. Boiling time–absorbance curves for Cr(III)–PAR–TEA system. $C_{Cr} = 2.03 \times 10^{-5}$ mol dm^{-3}; $C_L = 2.12 \times 10^{-4}$ mol dm^{-3}; (1) $C_{TEA} = 0.01$ mol dm^{-3}, pH 8.22; (2) $C_{TEA} = 0.04$ mol dm^{-3}, pH 5.88; (3) $C_{TEA} = 0.1$ mol dm^{-3}, pH 9.25; (4) $C_{TEA} = 0.04$ mol dm^{-3}, pH 7.99. Absorbance values on the ordinate are half those of the reaction mixture.

Carbonate, nitrite, sulfite, and tartrate ions as well as urea have been known as an accelerator in the formation of Cr(III)–EDTA chelate (*18*, *19*) but in the PAR system they failed to work, since the final absorbances were quite small under any pH conditions. Yamamoto and Takano (*5*) examined an acceleration effect of hydrogen peroxide on the Cr(III)–PAR chelate formation in acetate buffer solution at pH 5.3. However, they reported the somewhat smaller ϵ value, 5.10×10^4 at 530 nm, as compared with that obtained in this work, 5.86×10^4 (from the data in Figure 2, curve 2 at pH 5.3).

TEA is an excellent auxiliary ligand for acceleration of the aqueous complexation of Cr(III) ion with PAR. The Cr(III)–TEA complex intermediate may undergo the replacement reaction with PAR much faster than aquo or hydroxo Cr(III) species do. A further role of TEA is to prevent hydrolytic olation of Cr(III) ion, thus providing quantitative formation of the PAR chelate in slightly alkaline solution.

Chromatography and Interference Studies. Typical chromatograms are shown in Figure 5. The IPHPLC separation of PAR chelates of Fe(III), Co(III), and Ni(II) ions (*7*) and Pd(II) and Pt(II) ions (*20*) on an ODS column have been developed using tetrabutylammonium bromide (TBABr) as an ion-pairing reagent in aqueous methanol or aqueous tetrahydrofuran mobile phase. Under the conditions similar to those in ref *7* and *20*, however, the satisfactory resolution of Cr(III)–PAR chelate from the corresponding chelates of Fe(III)

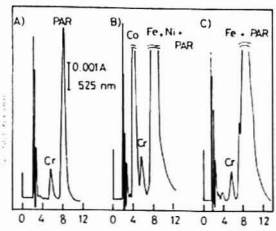


Figure 5. IPHPLC separation of Cr(III)–PAR chelate: sample, C_{Cr} = 1.23 × 10^{-7} mol dm^{-3}, C_L = 1.0 × 10^{-4} mol dm^{-3}, C_{TEA} = 0.1 mol dm^{-3}; foreign metal ions (A) none, (B) the same as sample no. 3 in Table I, (C) the same as sample no. 5 in Table I; column, Hiber column (LiChrosorb RP-18); mobile phase, 40.0 wt % aqueous methanol containing 9.8 × 10^{-3} mol kg^{-1} $BoBr_2$, 2 × 10^{-3} mol kg^{-1} Tris–HCl, and 10^{-4} mol kg^{-1} EDTA; flow rate, 1 cm^3 min^{-1}.

and Co(III) could not be obtained. By the use of a bolaform electrolyte, $BoBr_2$, peak resolution was successfully achieved as shown in Figure 5. The bolaform cation affects the resolution differently than TBA^+ ion. TEA gave no effects on the separation of the PAR chelates under the conditions. The Co(III)–PAR chelate is eluted faster than the Cr(III) chelate, while the Fe(III) and Ni(II) chelates have an almost similar retention time to PAR (HL^-) as shown in Figure 5B. The peaks of cobalt and chromium seem to badly overlap in chromatogram B, but they are well base-line resolved when the cobalt concentration is below 10^{-6} mol dm^{-3}. Under such the conditions, cobalt can be determined simultaneously with chromium.

Actually, there are no interferences by the metal ions at their molar concentrations comparable to that of Cr(III) ion. The main potential interferences are caused by iron, cobalt, and nickel ions in large amount, since they produce the very stable and inert PAR chelates whose peaks appear in the chromatogram. These can be circumvented by adding PAR in sufficient excess and by judicious adjustment of the mobile phase conditions. Under the conditions, Co(II) and Ni(II) ions were tolerated up to the weight ratios against 6.4 ng cm^{-3} Cr(III) ion of Co/Cr = 30 and Ni/Cr = 50, respectively. Ferric ion, which is most likely to be encountered in a real system, did not interfere individually at 1.22 × 10^{-5} mol dm^{-3} (680 ng cm^{-3}, Fe/Cr = 106) as shown in chromatogram C in Figure 5. Phosphate ion, added as KH_2PO_4, at 4 × 10^{-3} mol dm^{-3} had no influence on both the color development and the IPHPLC.

Calibration Curve and Reproducibility. The peak height calibration at 0.005 and 0.01 aufs is linear over the concentraton range of Cr(III) ion, (0.10–6.0) × 10^{-7} mol dm^{-3} (0.5–30 ng cm^{-3}), which is represented by the following equation:

$$\text{recorder response in absorbance unit} = 9.84 \times 10^{-3}\ \text{Cr}\ (\mu\text{mol dm}^{-3}) - 1.80 \times 10^{-5}$$

The lower limit of detection is at a concentration which gives a signal twice the peak-to-peak base-line noise. The absolute on-column detection limit is down to 1.0 pmol of chromium. The sensitivity of the method is very high, comparable with flameless atomic absorption spectrophotometry (*21*), gas chromatography with electron capture detection (*22*, *23*), neutron activation analysis (*24*), and a chemiluminescence method (*25*). As the blank (or contamination) value was approximately equal to the detection limit, extra care should always be taken to prevent contamination from laboratory dust, vessels, reagents, solvents, and solutions. The reproducibility of the method is shown in Table I, where an acceptable precision [relattive standard deviation 1.90% (n = 9)] is obtained for 6.4 ng cm^{-3} chromium in the presence of various metal ions. One HPLC run takes as little as 15 min or less and the overall analysis time for one sample with four calibration standards does not exceed 2 h.

Table I. Reproducibility of the Chromium Determination

sample no.	concns of foreign metal ions (10^{-6} mol dm^{-3})	run no.	peak height,[a,b] cm
1	none	1	3.00
		2	3.10
		3	2.95
2	Fe 1.77, Co 1.74, Ni 1.56, Cu 1.60, Mn 1.59, V 1.60, Al 1.60, Zn 1.58, Cd 1.92, Mg 3.2, Ca 3.2, Sr 3.2, Ba 3.2	4	3.00
		5	2.90
3	Fe 3.54, Co 3.48, Ni 3.12, Cu 3.20, Mn 3.18, V 3.20, Al 3.20, Zn 3.16, Cd 3.84, Mg 6.4, Ca 6.4, Sr 6.4, Ba 6.4	6	2.95
		7	2.95
4	Fe 5.11	8	3.00
5	Fe 12.2	9	2.95
			2.98 ± 0.04 av 1.90% RSD

[a] 0.01 aufs at 525 nm, 0.001 absorbance/2.5 cm. [b] Chromium added 1.23 × 10^{-7} mol dm^{-3} (6.40 ng cm^{-3}).

PAR is one of the most sensitive reagents for the photometric determination of chromium. The analytical sensitivity can be further increased by use of a highly sensitive photometric detector (0.005 aufs range is readily available). In addition, interference problems can be eliminated to a great extent by coupling with the IPHPLC separation system. The HPLC technique is now universally available in most chemical and clinical laboratories. An on-line preconcentration method for the Cr(III)–PAR chelate in a manner similar to that described by Haring and Ballschmiter (*26*) seems highly promising for the determination of chromium in the picogram per cubic centimeter range. Since the use of TEA in the Cr(III)–PAR system as an accelerator has yielded a sufficient reduction in analysis time, the IPHPLC method, inherently sensitive and selective, has proved to be compatible with the practical applicability on a routine basis.

In addition, when iron, cobalt, and nickel ions are to be determined in the presence of chromium ion in the same sample, the color development for those ions with PAR can be made at room temperature, followed by IPHPLC separation under the conditions reported previously (*7*, *8*). The detection limits of those metal ions are also at the sub-nanogram-per-cubic-centimeter level.

Registry No. PAR, 1141-59-9; TEA, 102-71-6; Cr, 7440-47-3.

LITERATURE CITED

(1) Sandell, E. B. "Colorimetric Determination of Traces of Metals 3rd. Ed"; Interscience: New York, 1959; p 392.
(2) Bryson, W. G.; Goodall, C. M. *Anal. Chim. Acta* **1981**, *124*, 391.
(3) Tataev, O. A.; Abdulaev, R. R. *Zh. Anal. Khim.* **1970**, *25*, 930.
(4) Yotsuyanagi, T.; Takeda, Y.; Yamashita, R.; Aomura, K. *Anal. Chim. Acta* **1973**, *67*, 297.
(5) Yamamoto, K.; Takano, Y. *Bunseki Kagaku* **1978**, *27*, 460.
(6) Allen, T. L. *Anal. Chem.* **1958**, *30*, 447.
(7) Hoshino, H.; Yotsuyanagi, T.; Aomura, K. *Bunseki Kagaku* **1978**, *27*, 315.
(8) Hoshino, H.; Yotsuyanagi, T. *Talanta* **1984**, *31*, 525.
(9) Willet, J. D.; Knight, M. M. *J. Chromatogr.* **1982**, *237*, 99.
(10) Krull, I. S.; Bushee, D.; Savage, R. N.; Schleicher, R. G.; Smith, S. B., Jr. *Anal. Lett.* **1982**, *15* (A–3), 267.
(11) Larochelle, J. H.; Johnson, D. C. *Anal. Chem.* **1978**, *50*, 240.
(12) Wenclawiak, B. *Fresenius' Z. Anal. Chem.* **1982**, *310*, 144.
(13) Tande, T.; Petersen, J. E.; Torgrimsen, T. *Chromatographia* **1980**, *13*, 607.
(14) Bond, A. M.; Wallace, G. G. *Anal. Chem.* **1982**, *54*, 1706.
(15) Hoshino, H.; Yotsuyanagi, T.; Aomura, K. *Anal. Chim. Acta* **1976**, *83*, 317.

(16) Menger, F. M.; Wrenn, S. J. Phys. Chem. 1974, 78, 1387.
(17) Hoshino, H., Tohoku University, unpublished results, 1982.
(18) Phatak, G. M.; Bhat, T. R.; Shankar, J. J. Inorg. Nucl. Chem. 1970, 32, 1305.
(19) Ohashi, K.; Suzuki, S.; Kubo, K.; Yamamoto, K. Bunseki Kagaku 1976, 25, 693.
(20) Watanabe, E.; Nakashima, H.; Ebina, T.; Hoshino, H.; Yotsuyanagi, T. Bunseki Kagaku 1983, 32, 469.
(21) Surles, T.; Tuschal, J. R., Jr.; Collins, T. T. Environ. Sci. Technol. 1975, 9, 1073.
(22) Gosink, T. A. Anal. Chem. 1975, 47, 165.
(23) Lovett, R. J.; Lee, G. F. Environ. Sci. Technol. 1976, 10, 67.
(24) Salbu, B.; Steinnes, E.; Pappas, A. C. Anal. Chem. 1975, 47, 1011.
(25) Hoyt, S. D.; Ingle, J. D., Jr. Anal. Chim. Acta 1976, 87, 163.
(26) Haring, N.; Balischmiter, K. Talanta 1980, 27, 873.

RECEIVED for review May 25, 1984. Accepted November 15, 1984.

Separation Function for Measuring the Information in Complex Chromatograms

D. R. Van Hare[1] and L. B. Rogers*

Department of Chemistry, University of Georgia, Athens, Georgia 30602

The separation function for use in the optimization of complex separations relates the information content of a chromatogram to the number and the extent of resolution between adjacent peaks. Each fully resolved peak is arbitrarily assigned 2.0 bits of information while partially resolved peaks are assigned 1 to 2 bits depending upon the depth of the valley between them. Pairs that give no valley but are detectable using a second-derivative method are assigned 0.5 bit. No a priori information is needed so the separation function may be easily incorporated into existing optimization schemes.

Recently, the optimization of chromatographic separations has moved away from conventional methods in which a chromatographer uses experience and intuition to judge the quality of a complex separation. Systematic methods are now being used which provide a more objective optimization of separations and are amenable to computer control. Laub and Purnell (*1*) searched for conditions that gave the highest minimum α value (ratio of capacity factors) for all pairs of adjacent peaks. Later Glajch et al. (*2*) used resolution in a similar manner. Morgan and Deming (*3*) suggested the use of a peak separation factor (*4*) as a quality measure in their simplex optimization procedure. Later Watson and Carr (*5*) added a weighting factor for the time of analysis as well as a consideration of the actual peak separation compared to the desired peak separation.

Wegscheider et al. (*6*) developed a response function that operates differently than those mentioned above, i.e., as a product rather than a summation, and it takes into account the noise level of the chromatogram. In addition, there have also been peak-counting algorithms. Spencer and Rogers (*7*) proposed a separation number using a procedure that obtained information from badly overlapped peaks, even before a valley appeared. Later, Berridge (*8*) introduced a response function in which the resolution of each pair of adjacent peaks was summed up to a maximum value of 2.0. In addition, the number of peaks was weighted as were the analysis times for the first and last peaks in the chromatogram.

A new response function has been developed to overcome some of the limitations of the previous functions. For example, those that utilize the natural logarithm of a fraction will approach zero at the optimum. However, one cannot determine whether a large number of peaks has been fairly well separated or a few have been poorly separated. In addition, peak crossing causes problems since the function is zero for totally overlapped pairs of peaks, causing false optima. The function of Wegscheider et al. (*6*), even though it operates as a product of the individual peak separations rather than the sum of natural logarithms, suffers from the same problems. Furthermore, for all of the above functions, the number of components being separated should be known in order to ensure proper operation of the function. Berridge's response function (*8*) does keep track of the number of peaks detected during each separation. One drawback of his function is the need for calculating the resolution of each adjacent pair of components. In practice, unsymmetrical and severly overlapped peaks may present problems. In contrast, the separation number of Spencer and Rogers (*7*) is essentially a peak-counting algorithm that can provide information about overlapped peaks and does not require the calculation of resolution. However, the information for an isolated peak depended upon its shape and retention time. Furthermore, the function lacked general applicability because it was limited to isothermal or isocratic separations.

In the present study, a new response function has been tested which incorporates some aspects of the others. It operates as a peak-counting function that assigns a value between 0.5 and 2.0 for each component that is detected. It is applicable to the optimization of all chromatographic methods and requires no a priori information. Furthermore, it can easily be expanded to include additional weighting terms similar to those of Watson and Carr (*5*) and Berridge (*8*). Both simulated and real chromatograms have been examined in this study.

EXPERIMENTAL SECTION

Chemicals. All of the chemicals were reagent grade or better and were used without further purification. Ethanol (U.S. Industrial Chemicals Co., New York) was used as the solvent for the gas chromatographic test mixture. This mixture was composed of 2,3,3-trimethylbutane, 2-pentanol, 2-methylheptane, cycloheptane, *n*-octane (Aldrich Chemical Co., Inc., Milwaukee, WI), tetrahydrofuran, *m*-xylene (J. T. Baker Chemical Co., Phillipsburg, NJ), 2-pentanone, *o*-xylene (Eastman Kodak, Rochester, NY), and cyclohexane (Fisher Scientific Co., Norcross, GA).

The compressed gases used to operate the gas chromatograph were all obtained from the same source (Selox, Inc., Gainesville, GA). They were first passed through a gas purifier (Alltech Associates, Norcross, GA) which contained Drierite and molecular

[1] Present address: Savannah River Laboratory, E. I. du Pont de Nemours and Co., Inc., Aiken, SC 29801.

0003-2700/85/0357-0628$01.50/0 © 1985 American Chemical Society

sieve 5A. Nitrogen was the carrier gas while hydrogen and compressed air were used with the flame ionization detector.

Apparatus. A Hewlett-Packard 5880A Level 4 gas chromatograph was used to generate the chromatograms. This instrument was configured with a split/splitless capillary inlet system and a flame ionization detector. A Hewlett-Packard 0.2 mm × 12.5 m fused silica capillary column coated with cross-linked dimethylsilicone was used to effect the separations. Injections were made with a Hamilton 701-N 10-μL syringe.

The digital output from the 5880A was converted to an analog signal by using the Hewlett-Packard analog output board option. A 0–10 V range was selected on the output board and the analog signal was then passed through an operational amplifier circuit. The purpose of this circuit was to create a bipolar analog signal, −5.12 V to +5.12 V, for input to the analog-to-digital converter (A/D).

A MINC laboratory computer (Digital Equipment Corp., Maynard, MA) was used for acquisition and storage of the gas chromatographic data. The MINC contained a full complement of I/O accessories including a MNCAD module which provided 16 channels of A/D input and a MNCKW programmable real-time clock which was used for initiating A/D conversions. An RT-11 foreground/background operating system was used to run the data acquisition programs which were written in Fortran IV. In addition, extensive use was made of the REAL-11/MNC library subroutines supplied with the MINC. The data were stored on 8-in., double density, floppy disks.

A PDP 11/23 computer (Digital Equipment Corp.) running an RSX-11M operating system was used for the analysis of the chromatographic data and for chromatographic simulations.

Procedures. *Simulations.* Peaks for the simulated chromatograms were generated from either the equation for a normalized Gaussian

$$Y = \frac{N}{\sigma(2\pi)^{1/2}} \exp\left[-\left(\frac{X_i - \bar{X}}{2\sigma^2}\right)\right] \quad (1)$$

or that for an exponentially modified Gaussian (*10*)

$$Y = \frac{N}{\tau\sigma(2\pi)^{1/2}} \int_0^\infty \exp\left(-\left[\frac{(X_i - \bar{X} + \tau - t')^2}{2\sigma^2}\right]\right) \exp\left[\frac{-t'}{\tau}\right] dt' \quad (2)$$

where Y is the response, N the scale factor, σ the standard deviation, X_i the sample time, $\bar{X}$ the peak mean, τ the time constant of the exponential decay, and t' the dummy variable of integration. Gaussian peaks were used for the simulations involving comparisons between the SEP functions and the others. Exponentially modified Gaussian peaks were used to examine the contribution of peak tailing.

Several inputs were necessary for the generation of a simulated chromatogram. The number of theoretical plates, P_t, in a hypothetical column was needed to determine the standard deviation of the peaks from the equation

$$\sigma = \bar{X}P_t^{1/2} \quad (3)$$

The sampling rate or the time between data points as well as the threshold value were also specified. The threshold refers to a response value below which no information was generated. For tailing peaks, a skewing factor (τ/σ) was entered from which the τ value could be determined. Finally, the number of peaks to be generated in the chromatogram was entered. For each peak, the peak mean, $\bar{X}$, and the peak-height scaling factor, N, were input. Unless otherwise stated, standard values for the input parameters were a 5000-plate column, sampling rate of 0.1 time units, scale factor of 1.0, threshold value of 0.0001, and peak mean for a single peak of 30.0 time units.

Calculations of Response Functions. Resolution, R, was defined as

$$R = \frac{\Delta T}{2(\sigma_1 + \sigma_2)} \quad (4)$$

where ΔT is the time between two peak means and σ_1 and σ_2 are the standard deviations of the two peaks. The chromatographic response function, CRF, as specified by Morgan and Deming (*3*), was calculated from

$$\mathrm{CRF} = \sum_{i=1}^{n} \ln (f_i/g_i) \quad (5)$$

where n is the number of adjacent peak pairs, f_i is the distance from a line connecting the peak maxima to the valley between the peaks, and g_i is the distance from the connecting line to the base line. The CRF was derived from Kaiser's peak separation, f_i/g_i (*4*), which is equal to 1.0 for completely resolved peaks.

The separation number, SN, is a measure of the total information in a chromatogram, i.e., it is simply the sum of information from all of the data points (*7*). That is

$$\mathrm{SN} = -\sum \log_2 Q \quad (6)$$

where Q is defined below. This information is calculated from the difference between a predicted value and the actual value for a datum. Predictions are based upon knowledge of the preceding data values and the near Gaussian nature of chromatographic peaks. The expected or predicted value is compared to the actual value using the equation

$$Q = X/(2X - Y) \quad (7)$$

where Q is the error in prediction, X is the larger of the predicted and actual value, and Y is the smaller of the two values. Since Q will take values between 1/2 and 1, the negative logarithm (base 2) of Q will range between 0 and 1. Thus, depending upon the size of the error in prediction, any one datum may contain between 0 and 1 bit of information.

Two forms of the separation function, SEP, were used in the comparison studies. They were

$$\mathrm{SEP_p} = N_p + \sum_{i=1}^{n} P_i + 0.5N_s \quad (8)$$

$$\mathrm{SEP_v} = N_p + \sum_{i=1}^{n} (1 - V_i) + 0.5N_s \quad (9)$$

where N_p is the number of peaks detected in the chromatogram, P_i is Kaiser's peak separation as defined previously, N_s is the number of shoulders as determined by a second-derivative method, and V_i is the valley-to-peak ratio (*10*). The valley-to-peak ratio is simply the height above base line of the valley between two peaks divided by the height of the smaller peak. This ratio becomes zero when the two peaks are fully resolved.

In the present study, a second-derivative operation was performed on the data and the number of minima was determined. The number of peak shoulders in the chromatogram corresponded to the number of minima minus the number of peaks detected. Each peak shoulder was arbitrarily assigned a value of 0.5 bit of information. This corresponds well with its relative importance to the overall separation since a barely resolved peak contains just over 1.0 bit of information.

In the first comparison, a group of six peaks was simulated starting at 30 time units and having one time unit between each peak mean. The time between peak means was incremented by 0.5 time unit each cycle to determine its effect on the SN, resolution, CRF, and both of the separation functions.

In the second comparison, optimization of a four-component mixture was simulated in the manner of Debets et al. (*10*). The retention times of the components were changed linearly as a function of the hypothetical solvent composition. The retention times ranged from 20 time units to 29 time units and a 2000-plate hypothetical column was used to obtain chromatograms that closely resembled those obtained by Debets et al. The simulation was performed over 41 different solvent compositions and the effects on the response functions were determined.

Real Analyses. Typical GC operating conditions were as follows: injection port temperature, 250 °C; detector manifold temperature, 275 °C; nitrogen carrier gas flow rate, 2.0 mL/min at 70 °C; nitrogen makeup gas flow rate, 30 mL/min; and split ratio, 75:1. The flame ionization detector was set up in accordance with the manufacturer's specifications. The analyses were run isothermally with the oven temperature ranging from 40 °C to 100 °C in increments of 10 °C.

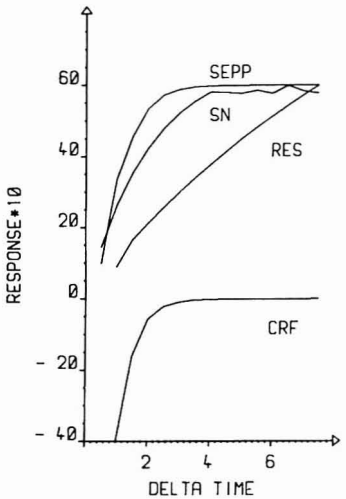


Figure 1. Separation function (SEPP), separation number (SN), total resolution (RES), and chromatographic response function (CRF) vs. the time between peak means for a six-peak separation.

A test mixture was prepared containing 2% (v/v) of each of the following compounds in 100% ethanol: 2,3,3-trimethylbutane, 2-pentanol, 2-pentanone, cyclohexane, cycloheptane, 2-methylheptane, *n*-octane, *o*-xylene, *m*-xylene, and tetrahydrofuran. The sample size used was 0.5–1.0 μL.

The analog output from the gas chromatograph was updated at a rate of 8 Hz. Sampling of this analog signal by the MINC A/D occurred at a rate of 80 Hz so that 10 successive values were averaged, thus minimizing fluctuations in the analog signal. The averaged data values were stored in 480 point arrays with each array corresponding to 1 min of output from the gas chromatograph. The first 100 points of data after injection were used to determine the base line and threshold values. This corresponded to a peak-free region of the chromatogram before the solvent peak was eluted. The threshold was taken as 10 times the standard deviation of the first 100 points and the base line used was equal to the mean value over this region.

The response functions were calculated from both raw and smoothed data. The data were smoothed twice in succession using either a five-point or a nine-point cubic quadratic smooth. Peak shoulders were determined by a second-derivative method in which the presence of peaks and peak shoulders was related to the magnitude of the negative peaks from the second derivative of the data. Both five-point and nine-point second-derivative operations (*11*) were examined as a function of the signal-to-noise ratio of the second-derivative peaks.

RESULTS

Simulation Studies. A comparison between the resolution, CRF, SN, and the separation functions, SEP_p and SEP_v, is shown in Figure 1 for six overlapped peaks. Delta time, plotted on the *X* axis, refers to the time between each of the peak means. The resolution increased linearly as the time between the peak means increased, even after the peaks were completely resolved. The CRF started at a large negative number and became zero at base-line resolution. This occurred at a delta time of 4 units. The SN increased more gradually than the CRF but reached a maximum value at the same delta time. SEP_p and SEP_v gave identical values for this simulation so only SEP_p was plotted. The shape of the separation function closely followed that of the CRF while

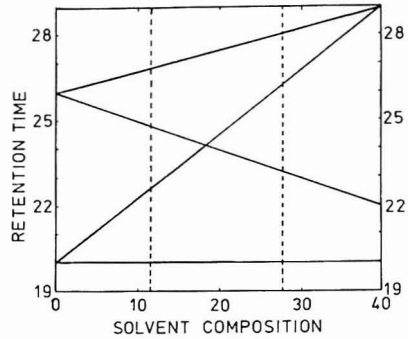


Figure 2. Retention time vs. solvent composition used for modeling the optimization of a four-peak separation.

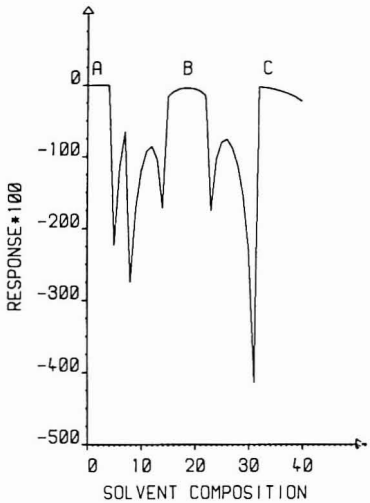


Figure 3. CRF vs. solvent composition for the four-peak separation. A, B, and C correspond to the solvent compositions that give optimal values for the CRF.

being shifted to positive values. The maximum value for SEP_p was also reached at 4 delta time units. The results from this simulation showed that, while resolution was not suited to multiple peak separations, the other response functions were. They all reached a maximum value at a base-line separation corresponding to a delta time of 4. In addition, SN approached its maximum response more gradually than either CRF or SEP_p, both of which used Kaiser's peak separation as a determining factor. This explains the similarity in the shapes of the curves for these two functions.

The effects of solvent composition on retention times (Figure 2) and their effects on the CRF, SEP_p, and SEP_v are shown in Figures 3 and 4 for a four-peak separation. Figure 3 shows the behavior of the CRF which found three optimum areas corresponding to regions A, B, and C. However, the chromatogram for region A has only two peaks while B and C have only three. This confirms what Debets et al. (*10*) found for the CRF when no a priori information was given about

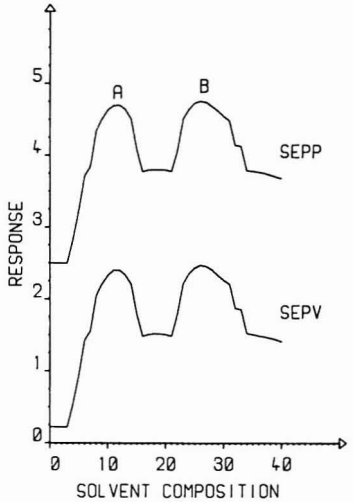


Figure 4. SEP_p and SEP_v vs. solvent composition for the four-peak separation. A and B correspond to the solvent compositions that give optimal values for the separation functions.

the number of components present. This is because the CRF cannot distinguish between a single peak and two highly overlapped peaks.

SEP_p and SEP_v gave identical results for the optimization simulations as shown in Figure 4. Two optimum regions were found and correspond to the solvent compositions represented by the two dotted lines in Figure 2. The behavior of the separation functions compared favorably with that found by Debets et al. (*10*) for the CRF and other response functions when information concerning the number of components in the mixture was provided. The separation functions, however, needed none of that information since the number of peaks detected at any solvent composition was included in the calculation of the functions. Although Figure 4 shows no significant difference between SEP_p and SEP_v, other simulations showed SEP_v to be less affected by large differences in peak height. Hence, SEP_v is the preferred function.

Real Analyses. The effect of different second-derivative operations was examined as a function of the signal-to-noise ratio, SNR. The results are shown in Table I for the *o*-xylene peak run at 40 °C. The *o*-xylene peak was chosen because it was the most strongly retained and, thus, the most broadened of the peaks in the test mixture. Since the magnitude of the negative peak from the second derivative was inversely proportional to the peak width, a worst-case example was used. The noise level used for the SNR was equal to three times the standard deviation of the base line after derivitization. For both types of smoothing, the nine-point second derivative gave much better SNR values than the five-point second derivative. In addition, the nine-point smooth gave better SNR values than the corresponding five-point smooth. However a five-point smooth was found to produce less peak distortion; it was used with the nine-point second derivative to determine the separation number of real chromatograms.

The response functions were next calculated for the separation of the ten-component test mixture at various GC oven temperatures. Figure 5 shows a plot of the SN, CRF, and SEP_v as a function of oven temperature. Essentially base-line

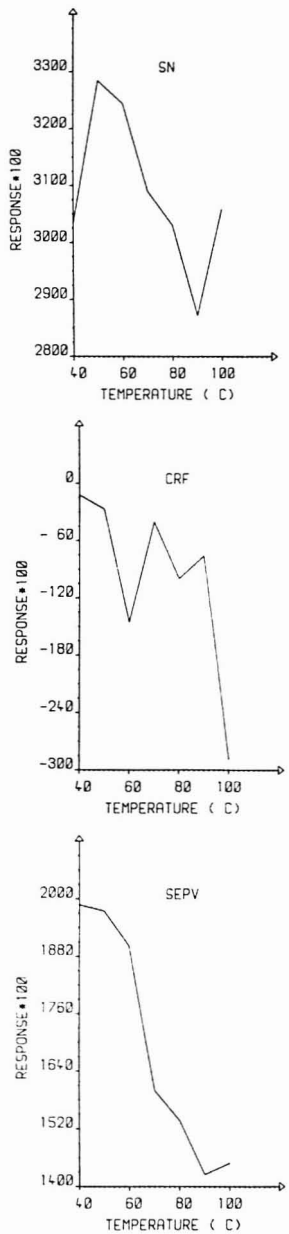


Figure 5. SN, CRF, and SEP_v vs. GC oven temperature for the separation of the ten-component test mixture.

Table I. Effect of Smoothing Real Data on the Signal-to-Noise Ratio of Second Derivative Minima

no. of pts in smooth	no. of pts in derivative	*S/N*
5	5	3.6
5	9	9.7
9	5	10.6
9	9	14.5

resolution of all components occurred at an oven temperature of 40 °C. This corresponded to a SN of 30.3. At 50 °C, the peaks for cyclohexane and 2-pentanol started to overlap, yet the SN rose to 32.8. From 50 °C to 90 °C, the SN decreased to a value of 28.7 before increasing at 100 °C to 30.6. Since the SN is supposed to be an absolute measure of the quality of a separation (7), these results indicated that the best separation occurred at oven temperatures in the 50 °C to 60 °C region rather than at 40 °C. Further examination of the SN data showed that the retention time of a peak played an important part in determining the SN, especially if the peak was non-Gaussian. Peaks at short retention times gave more information than peaks at long retention times. This caused the SN algorithm to shift the optimum separation to shorter analysis times. Thus, at 50 °C, the partial overlap of two peaks was more than offset by the 32% reduction in analysis time. At 60 °C, however, the additional peak overlap had a greater effect than a 28% reduction in analysis time and the SN decreased slightly from 32.8 to 32.4. As the oven temperature was raised from 60 °C to 90 °C, the overlapping peaks caused the SN to decrease to 28.7. However, a 100 °C the SN again increased to a value of 30.6. This increase was due to a slight decrease (14%) in analysis time coupled with partial resolution of the cycloheptane–*n*-octane peak pair which appeared as a single peak at 90 °C.

Next the CRF was examined as a function of oven temperature. As expected, the highest value for the CRF occurred at 40 °C where the peaks were nearly base-line resolved. The CRF, however, showed erratic behavior by increasing to relatively high values at 70 °C and 90 °C. These increases occurred at points where partially resolved peaks became totally overlapped and is a well recognized trait of the CRF (7).

Finally, since all of the peaks in the chromatograms were about the same height, SEP_p and SEP_v were identical and thus only SEP_v was plotted. The largest value for SEP_v was attained at 40 °C with relatively large values also at 50 °C and 60 °C. Over this region, all ten peaks were still separated to some extent. At 70 °C, there was a large decrease in the value of SEP_v from 19.02 to 16.01. This occurred due to the total overlap of two pairs of peaks such that eight peaks and one peak shoulder were detected. SEP_v decreased further to 14.25 at 90 °C where seven peaks and one peak shoulder were detected. Finally, at 100 °C there was a slight increase in SEP_v to 14.49 due to the partial resolution of an overlapped peak pair. As in the case of the SN, the partial resolution of the cycloheptane–*n*-octane peak pair more than offset the poorer resolution of the other peaks.

DISCUSSION

This study has shown once again that the CRF alone does not provide an accurate indication of the quality of a separation especially when peak crossing occurs (*10*). Either the number of peaks to be expected must be known or the number of peaks present in the chromatogram must be tracked. Otherwise, optimal values for the response may occur when some peaks are strongly overlapped. SEP_v does not suffer from that problem. In addition, SEP_v enjoys one advantage of SN, i.e., it provides an indication of badly overlapped peaks well before a valley forms between them. Hence, it overcomes one limitation of the overall function reported by Berridge (*8*). The importance of analysis time and weighting of peaks can easily be added to the SEP_v algorithm so as to incorporate those factors as done either by Watson and Carr (*5*) or by Berridge (*8*). Furthermore, other refinements could be added such as weighting small regions of a chromatogram in order to maximize the importance of a few peaks of interest.

ACKNOWLEDGMENT

We are indebted to Hewlett-Packard for the gift of the gas chromatograph to the Department of Chemistry. D.V.H. thanks the Division of Analytical Chemistry of the American Chemical Society for a Summer Fellowship.

LITERATURE CITED

(1) Laub, R. J.; Purnell, J. H. *J. Chromatogr.* **1975**, *112*, 71.
(2) Glajch, J. L.; Kirkland, J. J.; Squire, K. M.; Minor, J. M. *J. Chromatogr.* **1980**, *199*, 57.
(3) Morgan, S. L.; Deming, S. N. *J. Chromatogr.* **1975**, *112*, 267.
(4) Kaiser, R. "Gas Phase Chromatography"; Butterworths: London, 1963; Vol. 1, p 39.
(5) Watson, M. W.; Carr, P. W. *Anal. Chem.* **1979**, *51*, 1835.
(6) Wegscheider, W.; Lankmayr, E. P.; Budna, K. W. *Chromatographia* **1982**, *15*, 498.
(7) Spencer, W. A.; Rogers, L. B. *Anal. Chem.* **1980**, *52*, 950.
(8) Berridge, J. C. *J. Chromatogr.* **1982**, *244*, 1.
(9) Pauls, R. E.; Rogers, L. B. *Sep. Sci.* **1977**, *12*, 395.
(10) Debets, H. J. G.; Bajema, B. L.; Doornbos, D. A. *Anal. Chim. Acta* **1983**, *151*, 131.
(11) Savitzky, A.; Golay, M. J. *Anal. Chem.* **1964**, *36*, 1627.

RECEIVED for review February 23, 1984. Resubmitted October 29, 1984. Accepted December 5, 1984. This work was partially supported by the Department of Basic Energy Sciences, Department of Energy under Grant No. DE-AS09-76ER00854.

Integrated, Multiple-Stage Chromatographic Method for the Separation and Identification of Polycyclic Aromatic Hydrocarbons in Complex Coal Liquids

Richard B. Lucke,* Douglas W. Later, Cherylyn W. Wright, Edward K. Chess, and Walter C. Weimer

Chemical Methods and Kinetics Section, Pacific Northwest Laboratory, Operated by Battelle Memorial Institute, Richland, Washington 99352

A multiple-stage methodology is described for the separation and identification of neutral polycyclic aromatic hydrocarbons (PAH) in complex coal liquids. Fractional distillation followed by adsorption chromatography on neutral alumina with subsequent reverse-phase high-performance liquid chromatography were used for the isolation of neutral PAH subfractions. Capillary column gas chromatography, gas chromatography–mass spectrometry, and direct-probe mass spectrometry were used for the identification of sample components. This method results in chemically less complex subfractions which enable more detailed characterization of both trace level and major neutral PAH components. The applicability of this multiple-stage separation method is demonstrated with a solvent refined coal (SRC) II material.

In recent years, synfuels have become of increased interest because of their potential as an alternate energy source. The need to identify potentially toxic and carcinogenic compounds which may be present in alternate fuel materials has resulted in an increased effort to obtain detailed information about their chemical composition as it relates to biological response observed in laboratory test systems. However, synfuels, such as coal-derived liquids, are extremely complex, and the relationships between chemical composition and biological response are not always straightforward. The molecular weight distribution, degree of alkylation and hydrogenation, chemical functionality, and heteroatom content of coal liquids are all variables that contribute to the increased complexity of these materials. This complexity has led to the development of a wide variety of analytical methods aimed at achieving improved separations for chemical and biological characterization of synfuels.

Coal liquid fractionation procedures have included fractional distillation (*1–4*), size-exclusion chromatography (*5–9*), solvent extraction (*10–15*), adsorption chromatography with alumina and/or silica (*16–20*), normal-phase high-performance liquid chromatography (HPLC) (*21–24*), and reverse-phase HPLC (*25–28*). Analytical methods using combinations of these separation techniques are often required for complete chemical characterization and biological testing of these highly complex mixtures. For example, multidimensional coupled-column HPLC techniques that produce discrete fractions have been used to analyze polycyclic aromatic hydrocarbons (PAH) in coal liquids (*28, 29*). However, coupled-column HPLC requires modified instrumentation and is impractical for the preparative-scale fractionation of material that is often required for biological testing.

In this laboratory, a four-step analytical methodology for the separation, identification, and quantitation of neutral PAH and their alkylated analogues in coal liquids has been developed and applied (Figure 1). In general, the neutral PAH are the most abundant compound class in coal-derived synfuels and have been shown to be primarily responsible for the tumorigenic activity of these materials (*30, 31*). The integrated multiple-stage chromatographic method described in this paper employs fractional distillation followed by adsorption chromatography on neutral alumina, with subsequent reverse-phase HPLC. The combination of these separation techniques produces fractions which are chemically much less complex than the starting crude material and which are well defined in terms of chemical class and subclass. Furthermore, correlation of biological response to chemical constituency is facilitated. Capillary column GC, GC/MS, and direct-probe MS are used for the identification and quantitation of individual PAH components in each fraction.

EXPERIMENTAL SECTION

Materials. This analytical approach was demonstrated using a solvent refined coal II (SRC II) material from the Fort Lewis, WA, pilot plant. Fractional distillation of the full boiling range material (stage one of the separation methodology) was performed by Gulf Research and Development Co. (*32*). A distillate cut with a boiling point range of 800–850 °F was used in this investigation.

Alumina Adsorption Column Chromatography. The adsorption method used for separating the neutral PAH fraction from coal liquids has been described by Later et al. (*16*). Briefly, 150–200 mg of the 800–850 °F distillate cut was adsorbed on 3 g of neutral aluminum oxide and packed on top of 6 g of neutral aluminum oxide (Brockman activity I, 80–200 mesh, Fisher No. A 950, Pittsburgh, PA). The alumina was stored in an oven at 160 °C prior to use in the adsorption column chromatographic step. This oven temperature produced an alumina with ~1.5% water content (by weight). The details of this alumina standardization technique are available elsewhere (*33*). Sequential elution with hexane, benzene, and chloroform with 1% ethanol and methanol (spectral grade, Burdick & Jackson, Muskegon, MI) was done to obtain four fractions: aliphatic hydrocarbons (AH), neutral polycyclic aromatic hydrocarbons (PAH), nitrogen-containing polycyclic aromatics compounds (N-PAC), and hydroxy PAH (HPAH), respectively (see Figure 1). The PAH fraction was dried under nitrogen for gravimetric analysis and redissolved in methylene chloride (spectral grade, Burdick & Jackson) for further separation by HPLC.

Reverse-Phase High-Performance Liquid Chromatography. The PAH fraction was further separated and analyzed by using a Spectra Physics 8100 liquid chromatograph equipped with a Spectra Physics 8110 autosampler and a Waters Assoc. 440 UV absorbance detector fixed at a wavelength of 254 nm. A Spectra Physics 4100 computing integrator was used for data readout. Samples (subfractions) were collected with a modified Hewlett-Packard 79825 fraction collector.

A Supelcosil RP8-DB, 5 μm, 25 cm × 10 mm i.d. reverse-phase column was used for the HPLC separation. The mobile-phase profile consisted of 69% methanol (spectral grade, Burdick & Jackson) in water (doubly distilled, deionized, Milli Q grade) for 40 min followed by a 20-min linear gradient to 79% methanol and a 10-min linear gradient to 100% methanol which was then held for 10 min. Finally, a 12-min period was used to return and equilibrate to initial conditions for repetitive injections. The column temperature was held at 50 °C, with an eluent flow rate of 6 mL/min. The injection volume was 50 μL. Twenty repetitive

0003-2700/85/0357-0633$01.50/0 © 1985 American Chemical Society

Table I. Weight Percent of Fractions from a Full Boiling Range SRC II Coal Liquid Obtained from the Different Fractionation Stages

fraction	wt % of full bp SRC II material	wt % of 800–850 °F distillate cut	rel wt % distribution of PAH in HPLC subfraction
800–850 °F SRC II distillate cut	3.5		
PAH fraction of 800–850 °F SRC II distillate cut	1.7	49	
HPLC subfraction 1	0.04	1.2	2.5
HPLC subfraction 2	0.11	3.0	6.1
HPLC subfraction 3	0.06	1.6	3.3
HPLC subfraction 4	0.10	2.9	6.0
HPLC subfraction 5	0.28	7.9	16.1
HPLC subfraction 6	0.34	9.8	20.1
HPLC subfraction 7	0.21	6.0	12.2
HPLC subfraction 8	0.32	9.2	18.7
HPLC subfraction total	1.46	41.6	85.0

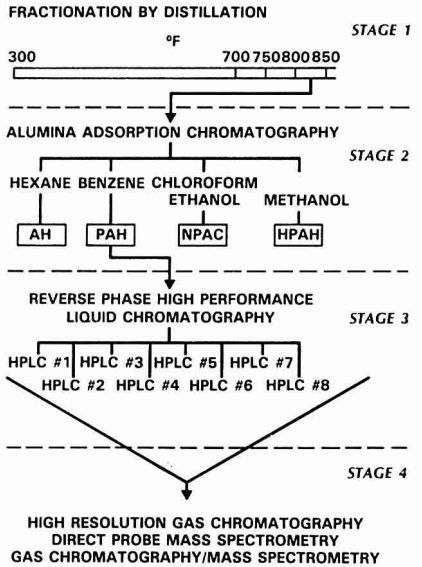


Figure 1. Integrated multiple-stage chromatographic scheme for complex coal liquids: aliphatic hydrocarbons (AH), neutral polycyclic aromatic hydrocarbons (PAH), nitrogen-containing polycyclic aromatic compounds (N-PAC), and hydroxy-PAH (HPAH).

automated injections (at 4 mg/injection) were required to obtain adequate sample material in the eight selected subfractions for chemical characterization by GC, GC/MS, and MS. Sample workup of the HPLC subfractions was accomplished by reducing the methanol/water effluent volume under reduced pressure on a rotary evaporator to near dryness. The samples were then blown to dryness under nitrogen at 50 °C for gravimetric analysis.

Gas Chromatography. The PAH fraction and each of the HPLC subfractions were analyzed using an Hewlett-Packard (HP) 5880A gas chromatograph equipped with a flame ionization detector (FID) held at 300 °C and a 25 m × 0.25 mm i.d. DB-5 fused silica column (0.25-μm film thickness, J & W Scientific, Rancho Cordova, CA). Helium was used as a carrier gas at a linear velocity of 50 cm/s. Samples were injected by the splitless vaporization technique with the injector temperature set at 285 °C. The temperature of the GC oven was linearly programmed from 50 to 100 °C at 10 °C/min and then 100 to 300 °C at 3 °C/min during the analyses of the SRC II 800-850 neutral PAH fraction. For the GC analyses of the HPLC subfractions, the oven temperature profile was 50–300 °C at 3 °C/min.

Quantitation was based on the average response factors of standard compounds chromatographed at eight concentrations ranging over 2 orders of magnitude as previously described (*34*, *35*). All standard compounds used were either purchased from Aldrich Chemical Co. (Milwaukee, WI) or obtained from private sources. In all cases the purity of the standard reference compounds was >98% as determined by GC. Additionally, the National Bureau of Standards SRM 1647 (priority pollutant PAH) was analyzed as an internal check of the response factors of solutions made in this laboratory. When standard compounds were not available, the response factors for compounds of similar retention time and chemical class were used.

The PAH fraction of the 800–850 °F distillate cut was analyzed by an external calibration method only, while the HPLC subfractions were analyzed by an external calibration method using 2-chloroanthracene as an internal standard at a final concentration of 50 μg/mL. All quantitation was based on dilutions of the dried fractions from a single separation at three different concentration levels. The PAH fraction was analyzed at concentrations of 10, 5, and 2.5 mg/mL. The HPLC subfractions were analyzed at 8, 4, and 2 mg/mL. Components in these complex mixtures were identified by absolute retention time, GC/MS, and retention index system (*36*). Values are reported as the average of the three determinations with appropriate standard deviations of the means.

MS And GC/MS. Identification of constituents in each HPLC subfraction was achieved using mass spectrometry (MS). Initially, the HPLC subfractions were analyzed by probe inlet MS to determine the major PAH components present and to establish the mass range of each fraction. These analyses were performed at low resolution (1:2000) on a VG Micromass ZAB-1F double-focusing mass spectrometer operated at 6000-V accelerating potential at a scan rate of 3 s/decade from 50 to 400 amu. The source temperature was held at 250 °C during the analyses with a source trap current of 200 μA for 70-eV analyses and 50 μA for 10-eV analyses. Data were acquired, stored, and processed on a PDP8A-based VG 2035 data system. HPLC subfractions 1–4 were analyzed by electron impact mass spectrometry using 70-eV ionizing energy. Due to the increased amount of fragmentation observed for the higher alkylated PAH analogues (greater than C_1) which eluted predominantly in subfractions 5–8, these HPLC isolates were analyzed at both 70 eV and at a lower ionizing energy, nominally 10 eV, to reduce the degree of fragmentation observed in the respective spectra and to allow molecular weight determinations of highly alkylated PAH species (alkylated analogues greater than C_3) in the HPLC subfractions.

A HP 5982A GC/MS system interfaced to a HP 5934A data system was used to obtain the mass spectra of the specific PAH compounds in each of the HPLC subfractions. The gas chromatograph was equipped with a 15 m × 0.25 mm i.d. DB-5 (J & W Scientific) fused silica capillary column; the oven temperature was programmed from 50 to 280 °C at 8 °C/min. Both on-column and vaporization injection techniques were used. The mass spectrometer was operated in the electron impact mode at 70-eV

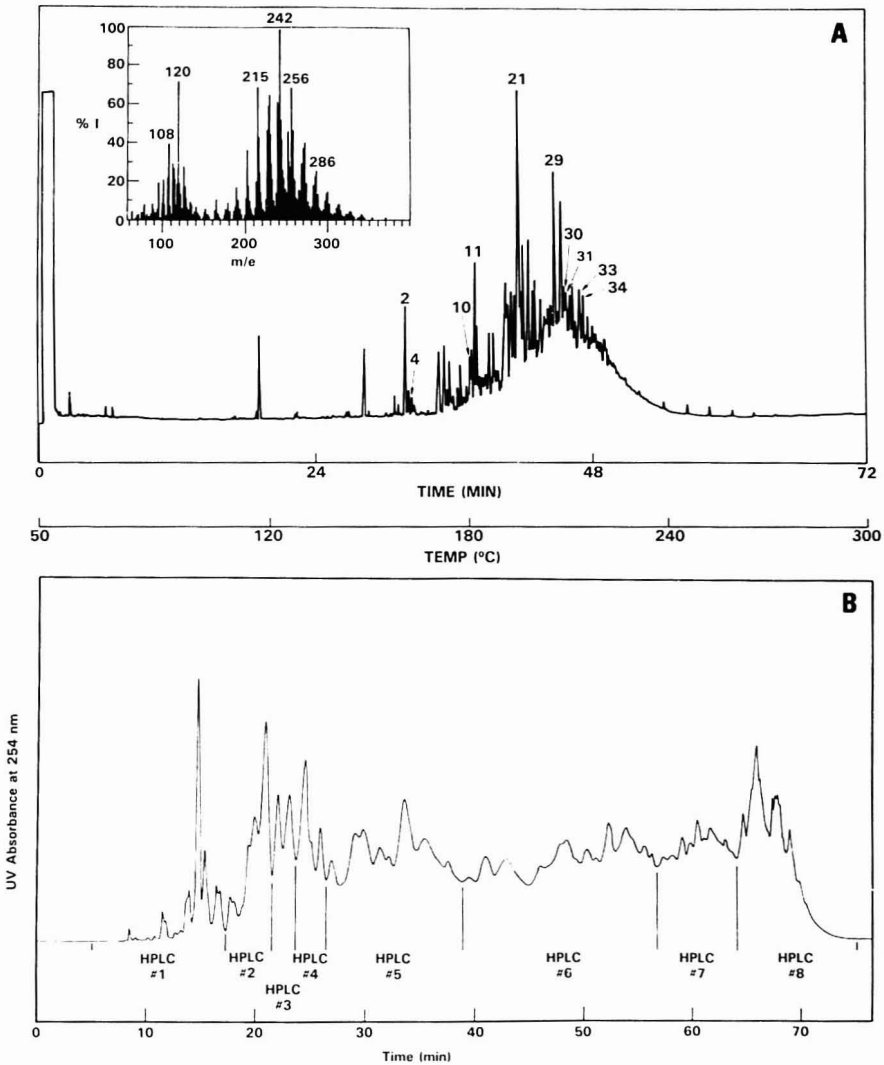


Figure 2. (A) Capillary column gas chromatogram with 70-eV direct-probe mass spectrum inset of the neutral PAH fraction from the SRC II 800–850 °F distillate cut. (B) High-performance liquid chromatogram (semipreparative scale) with subfraction designations.

ionizing energy with a 15-mA emission current. Spectra were acquired at a scan rate of 150 amu/s over a mass range of 50–350 amu. Mass spectrometric identifications from the GC/MS data were made by comparison of spectra from either available standard compounds or published spectra from the EPA/NIH Library of Mass Spectra.

RESULTS AND DISCUSSION

Fractional distillation (stage one of Figure 1) provided gross fractionation of components in coal-derived process materials according to boiling point, which correlates roughly to molecular weight. Previous studies have demonstrated that high-boiling distillate fractions are generally responsible for the majority of the biological activity of coal liquids (*1–4*). The chemical class separation of polycyclic aromatic compounds (PAC) by alumina adsorption column chromatography (stage two of Figure 1) has been reported for several coal-derived materials (*16, 33, 37*). Collection of a discrete PAH fraction from the SRC II 800–850 °F distillate cut was achieved by

Table II. Identification and Quantitation of Selected Components in the HPLC Subfractions of the PAH Fraction of SRC II 800–850 °F Boiling Point Cut

peak no.[a]	molecular wt	compound[b]	quantitation (parts per thousand)[c] HPLC 1	HPLC 2	HPLC 3	HPLC 4	HPLC 5	HPLC 6	HPLC 7	HPLC 8	neutral PAH fraction: HPLC subfractions[h]	neutral PAH fraction: alumina fraction
1	216	benzo[*a*]fluorene,[d] methylpyrene	8.45 ± 0.14	*f*								
2	216	benzo[*b*]fluorene,[d] 4- or 2-methylpyrene	17.3 ± 0.4	2.87 ± 0.28	0.30[g]	1.73 ± 0.08					0.97 ± 0.02	5.74 ± 0.20
3	218	benzo[*b*]naphthofuran isomer, C_1-phenylnaphthalene		6.20 ± 1.18	0.13[g]							
4	216	1-methylpyrene[d]	1.05 ± 0.04	3.25 ± 0.53		0.43 ± 0.09					0.35 ± 0.04	1.31 ± 0.18
5	230	C_1-benzofluorenes, C_2-pyrenes		48.2 ± 4.0[e]	45.8 ± 8.7[e]	36.0 ± 1.6[e]						
6	232	C_1-benzo[*b*]naphthofurans				32.1 ± 2.2[e]						
7	234	benzo[*b*]naphtho[2,1-*d*]thiophene[d]	30.6 ± 2.9	5.61 ± 0.83								
8	234	benzo[*b*]naphtho[1,2-*d*]thiophene	4.23 ± 0.46[e]									
9	234	benzo[*b*]naphtho[2,3-*d*]thiophene	17.0 ± 2.5[e]									
10	228	benz[*a*]anthracene[d]	81.6 ± 12.7	5.28 ± 0.27	0.98 ± 0.02	1.04 ± 0.03					3.29 ± 0.37	3.00 ± 0.28
11	228	chrysene,[d] triphenylene	245 ± 50.9	3.84 ± 0.95	5.03 ± 0.32	1.64 ± 0.05					8.86 ± 1.47	7.32 ± 0.60
12	244	C_2-benzofluorenes, C_3-pyrenes					33.3 ± 6.1[e]					
13	228	benz[*b*]anthracene[d]		13.7 ± 0.2								
14	248	C_1-benzo[*b*]naphthothiophenes				32.4 ± 2.6[e]						
15	242	C_1-benzanthracenes, C_1-triphenylenes		158 ± 2[e]	128 ± 30[e]	13.4 ± 1.5[e]						
16	258	C_3-benzofluorene, C_4-pyrene						21.4 ± 1.6				
17	258	C_3-benzofluorene, C_4-pyrene						11.5 ± 2.0				
18	242	3-methylchrysene[d]	3.40 ± 0.68	60.9 ± 1.2	29.4 ± 8.4							
19	242	2-methylchrysene,[d] 12- or 4-methylbenz[*a*]anthracene		0.93 ± 0.10	13.3 ± 8.6							
20	242	5-methylchrysene	3.17 ± 0.36	6.62 ± 1.08								
21	242	6- or 4-methylchrysene[d]			47.3 ± 8.7	380 ± 47	14.3 ± 7.4				36.31 ± 3.64	35.20 ± 5.00
22	242	1-methylchrysene,[d] 7-methylbenz[*a*]anthracene	2.67 ± 0.99	23.7 ± 1.2								
23	254	binaphthyls, phenylphenanthrenes/anthracenes			177 ± 37[e]	28.0 ± 4.6[e]						
24	256	C_2-benzathracenes, C_2-chrysenes					128 ± 21[e]	6.02 ± 1.01[e]				
25	272	C_4-benzofluorene, C_3-pyrene							8.76 ± 2.35			
26	272	C_4-benzofluorene, C_3-pyrene							26.6 ± 1.6			

27	256	C_2-benzanthracene, C_2-chrysene				54.7 ± 4.3				
28	268	C_1-binaphthyls, C_1-phenylphenanthrenes/anthracenes				25.7 ± 1.0[e]				
29	252	benzo[*j* or *b*]fluoranthene[d]	5.14 ± 1.85	91.1 ± 11.5	18.2 ± 2.8	17.7 ± 1.9			9.97 ± 0.85	9.59 ± 2.60
30	252	benzo[*k*]fluoranthene[d]	1.02 ± 0.16	14.8 ± 3.7	1.97 ± 0.45				1.35 ± 0.26	3.97 ± 0.50
31	256, 268	7,12-dimethylbenz[*a*]anthracene,[d] C_1-binaphthyl[f]					10.0 ± 3.3		2.20 ± 0.63	4.53 ± 1.32
32	286	C_1-benzofluorene, C_4-pyrene							6.10 ± 1.00	
33	252	benzo[*e*]pyrene[d]	3.53 ± 1.32	46.0 ± 7.7	0.85 ± 0.22				3.96 ± 0.55	6.14 ± 0.72
34	252	benzo[*a*]pyrene[d]	3.41 ± 1.29	12.0 ± 2.0	9.87 ± 2.33				1.55 ± 0.18	3.53 ± 0.39
35	252	perylene[d]	0.90[g]	2.71 ± 0.46						
36	300	C_4-benzofluorene, C_1-pyrene							4.14 ± 0.85	
37	278	dibenzophenanthrenes/anthracenes				10.5 ± 4.0[e]				

[a] Refers to peaks in Figures 2A and 3. [b] Tentatively identified by retention time and GC/MS. [c] Based on three determinations using response factors of standards when noted and response factors of standards with similar retention times when standards were not available. [d] Identified and quantified with standard compounds. [e] Quantitative estimation based on the addition of major peaks with the same *m/z* from GC/MS. [f] Blank: below 100 ppm. [g] One determination. [h] Values corrected for HPLC recovery and reported as parts per thousand in neutral PAH fraction. [i] Other C_2-benzanthracene/chrysenes might also coelute.

alumina adsorption chromatography and used for HPLC subfractionation.

The PAH fraction of the 800–850 °F coal liquid distillate cut obtained from the adsorption chromatographic step required an additional separation by reverse-phase HPLC for two reasons. First, the PAH fraction of this 50 °F distillate cut was still extremely complex, even after chemical class fractination. This is demonstrated by the complexity of the GC trace and mass spectrum in Figure 2A. Inspection of the gas chromatogram revealed the presence of many closely eluting components and lack of base-line resolution. In addition, the mass spectrum indicated that components of a wide mass range were present. Clearly, further separation was required to facilitate chemical analysis and to allow adequate separation of minor constituents that may be important in determining biological response. Second, certain PAH fractions isolated from coal liquids with constituents that have more than three aromatic rings have been shown to be potential carcinogens and mutagens (*30*, *31*, *38*); however, relatively little is known about the synergistic and/or antagonistic effects of complex mixtures on the biological expression of individual PAH. Hence, separation of the neutral PAH fraction into well-characterized subfractions would permit investigation of such effects. Biological testing of the subfractions using the microbial mutagenicity and initiation/promotion mouse skin tumorigenicity assays could provide valuable insights for understanding the matrix effects of complex, coal-derived mixtures on carcinogenesis and mutagenesis.

Reverse-phase HPLC was chosen for further separation of the PAH fraction (stage three of Figure 1) because of its ability to resolve the nonpolar PAH and to separate the parent and alkylated PAH (*25*, *29*, *39*). Initially, 14 HPLC subfractions were arbitrarily designated and collected for GC/MS analysis to determine the proper selection of HPLC cut points for preparation of subfractions of this material for biological testing. Subsequently, eight subfractions (shown in Figure 2B) were selected so that the parent and alkylated PAH components of interest would generally be grouped in separate subfractions. The selection process for designating the HPLC subfraction cut points was based solely on results from GC and GC/MS analyses; preselected standard reference compounds were not used to define subfraction parameters. The eight HPLC subfractions chosen provided an optimum number of fractions in terms of effort required for chemical analysis and information obtained from correlated chemical/biological investigations.

The relative and normalized weight contributions of each HPLC subfraction as determined by gravimetric measurements are shown in Table I. It is apparent that the subfractions are greatly simplified compared to the full boiling point range material. For example, when normalized, HPLC subfraction 1 constituted only 0.04% of the full boiling range crude material from which the distillate cuts were obtained. Almost 80% of the overall weight of the initial PAH fraction was isolated in HPLC cuts 5–8. The average recovery for 10 replicate runs in the alumina adsorption step was 95% (by weight) of the initial quantity of crude distillate cut introduced onto the column; 85% average total recovery was achieved for the HPLC fractions in 20 replications.

Figure 3 shows the capillary gas chromatograms and the direct-probe mass spectra insets for three of the HPLC subfractions; Table II lists the identification and quantitation of the specific components in each of the eight HPLC subfractions. Comparison of the GC traces of the HPLC subfractions with that of the initial PAH fraction in Figure 2A reveals that the complexity of the HPLC cuts is indeed greatly reduced. HPLC subfractions 1 and 2 showed base-line GC resolution

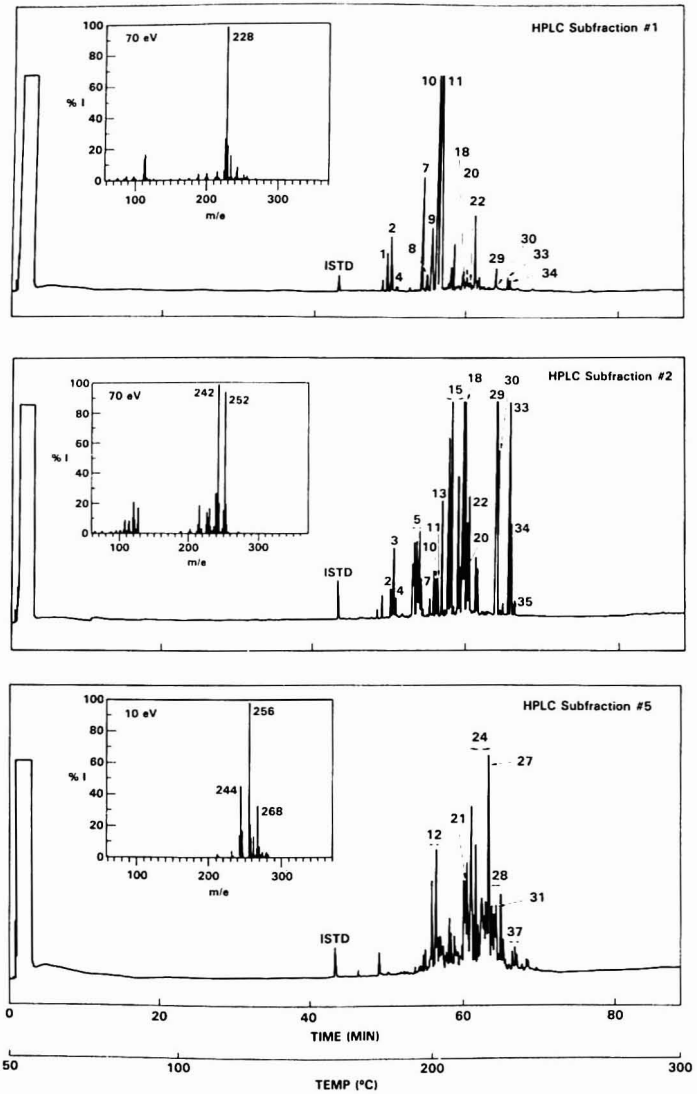


Figure 3. Capillary column gas chromatograms with mass spectrum insets of selected HPLC subfractions from the SRC II 800–850 °F neutral PAH fraction. (See Table II for peak identifications.)

for most components while GC analyses of HPLC subfractions 5–8 showed increased complexity and decreased resolution due to the high degree of alkylation and the increased number of possible isomers (Figure 3). Nonalkylated PAH were the major components in subfractions 1–3 while the alkylated PAH are the major components in the remaining five subfractions. The six isomers of methylchrysene were major components in the neutral PAH fraction and were detected in HPLC subfractions 1–5.

Minor components that were not identified in the PAH fraction were separated and could readily be identified in the HPLC subfractions. For example, the sulfur-containing PAH which often require oxidation, further separation, and reduction before identification (*40*) or sulfur specific detection

are now directly identified without undergoing these procedures. The benzonaphthothiophenes were well resolved in HPLC subfraction 1, and the methylbenzonaphthothiophenes were identified in HPLC subfraction 4.

Since only selected components were identified and quantified, the sum total of the concentrations of components in Table II does not account for the total weight found in the HPLC subfractions. When comparing the quantitative composition of the PAH fraction before and after HPLC separation (last two columns in Table II), quantitative agreement was observed in some cases, although discrepancies in concentration are noticeable. The differences can be partly explained by errors in integration due to differences in the base-line definition of unresolved components in the more complex neutral PAH fraction vs. the less complex HPLC subfractions. Furthermore, the combined HPLC subfraction component concentrations were only corrected by using the 85% recovery obtained from gravimetric analysis of the HPLC subfractions and not from the recovery of individual compounds spiked into the complex mixture. It is also possible that coeluting components were present in the GC analysis of the neutral PAH fraction prior to HPLC separation.

This separation method is of interest from the biological testing standpoint for two reasons. First, it isolates discrete chemical fractions in which the parent PAH are separated from their alkylated species. Also, it isolates many of the putative carcinogens such as benzo[*a*]pyrene, 5-methylchrysene, and 7,12-dimethylbenz[*a*]anthracene. The biological responses of the individual HPLC subfractions compared to that of the unfractionated neutral PAH fraction may give valuable information in understanding the effect of the complex sample matrix on the biological expression of PAH components in a coal-derived process material.

The integrated multiple-stage chromatographic methodology presented and discussed in this paper has been applied to the separation and analyses of a wide variety of coal liquefaction process materials including SRC II 800–850 °F and 850 °F plus distillate cuts, 650–700, 700–750, and >800 °F distillate cuts from the EDS process, and an integrated two-stage liquefaction (ITSL) 850 °F plus distillate cut. Results from the detailed chemical analyses of the SRC II 800–850 °F distillate were presented in this paper. Results of the biological testing of the HPLC subfractions will appear in a subsequent paper. To date, this multiple-stage separation scheme has only been applied for analysis of the PAH fraction but could easily be extended for analysis of the AH, N-PAC, and HPAC fractions from the alumina column chromatographic separation.

Registry No. 1-Methylpyrene, 2381-21-7; methylbenzo[*b*]naphthofuran, 93755-97-6; benzo[*b*]naphtho[2,1-*d*]thiophene, 239-35-0; benzo[*b*]naphtho[1,2-*d*]thiophene, 205-43-6; benzo[*b*]naphtho[2,3-*d*]thiophene, 243-46-9; benz[*a*]anthracene, 56-55-3; benz[*b*]anthracene, 92-24-0; methylbenzo[*b*]naphthothiophene, 67526-85-6; 3-methylchrysene, 3351-31-3; 5-methylchrysene, 3697-24-3; methylchrysene, 41637-90-5; benzofluoranthene, 56832-73-6; benzo[*k*]fluoranthene, 207-08-9; benzo[*e*]pyrene, 192-97-2; benzo[*a*]pyrene, 50-32-8; perylene, 198-55-0; benzo[*e*]-pyrene, 192-97-2; benzo[*a*]pyrene, 50-32-8; perylene, 198-55-0.

LITERATURE CITED

(1) Wilson, B. W.; Willey, C.; Later, D. W.; Lee, M. L. *Fuel* **1982**, *61*, 473–477.
(2) Wilson, B. W.; Pelroy, R. A.; Mahlum, D. D. In "Chemical Characterization and Genotoxic Potential Related to Boiling Point for Fractionally Distilled SRC-I Coal Liquids"; NTIS: Springfield, VA, 1982; PNL-4277.
(3) Later, D. W.; Wright, C. W.; Wilson, B. W. *Prepr. Pap.—Am. Chem. Soc., Div. Fuel Chem.* **1983**, *28*, 273–284.
(4) Pelroy, R. A.; Wilson, B. W. In "Fractional Distillation as a Strategy for Reducing the Genotoxic Potential of SRC II Coal Liquids"; NTIS: Springfield, VA, 1981; PNL-3787.
(5) Streuli, C. A. *J. Chromatogr.* **1971**, *56*, 225–229.
(6) Jones, A. R.; Geurin, M. R.; Clark, B. R. *Anal. Chem.* **1977**, *49*, 1766–1771.
(7) Rao, T. K.; Allen, B. E.; Ramey, D. W.; Epler, J. L.; Rubin, I. B.; Guerin, R. M.; Clark, B. R. *Mutat. Res.* **1981**, *85*, 29–39.
(8) Ho, C.-h.; Ma, C. Y.; Clark, B. R.; Guerin, M. R.; Rao, T. K.; Epler, J. L. *Environ. Res.* **1980**, *22*, 412–422.
(9) Toste, A. P.; Sklarew, D. S.; Pelroy, R. A. *J. Chromatogr.* **1982**, *249*, 267–282.
(10) Mima, M. J.; Schultz, H.; McKinstry, W. E. In. "Analytical Methods for Coal and Coal Products"; Karr, C, Ed.; Academic Press: New york, 1978; Vol. 1, Chapter 19, p 557.
(11) Burke, F. P.; Winschel, R. A.; Wooton, D. L. *Fuel* **1979**, *58*, 539–541.
(12) Schwager, I.; Yen, T. F. *Fuel* **1978**, *57*, 100–104.
(13) Steffgen, F. W.; Schroeder, K. T.; Bockrath, B. C. *Anal. Chem.* **1979**, *51*, 1164–1167.
(14) Boduszynski, M. M.; Hurtubise, R. J.; Silver, H. F. *Anal. Chem.* **1982**, *54*, 372–375.
(15) Schweighardt, F. K.; Thames, B. M. *Anal. Chem.* **1978**, *50*, 372–375.
(16) Later, D. W.; Lee, M. L.; Bartle, K. D.; Kong, R. C.; Vassilaros, D. L. *Anal. Chem.* **1981**, *53*, 1612–1620.
(17) Callen, R. B.; Simpson, C. A.; Bendoraitis, J. G.; Votz, S. E. *Ind. Eng. Chem. Prod. Res. Dev.* **1976**, *15*, 222–233.
(18) Boduszynski, R. J.; Hurtubise, R. J.; Silver, H. F. *Anal. Chem.* **1982**, *54*, 375–381.
(19) Leary, J. A.; Lafluer, A. L.; Longwell, J. P.; Peters, W. A.; Kruzel, E. L.; Biemann, K. In "Polynuclear Aromatic Hydrocarbons: Formation, Metabolism, and Measurement"; Cook, M., Dennis, A. J., Eds.; Battelle Press: Columbus, OH, 1983; pp 799–808.
(20) Farcasiu, M. *Fuel* **1977**, *56*, 9–14.
(21) Toste, A. P.; Sklarew, D. S.; Pelroy, R. A. In "Advance Techniques in Synthetic Fuels Analysis"; Wright, C. W., Weimer, W. C., Felix, D. W., Eds.; NTIS: Springfield, VA, 1983; Chapter 5, pp 74–94.
(22) Wise, S. A.; Chesler, S. N.; Hertz, H. S.; Hilpert, L. R.; May, W. E. *Anal. Chem.* **1977**, *49*, 2306–2310.
(23) Hertz, H. S.; Brown, J. M.; Chesler, S. N.; Guenther, F. R.; Hilpert, L. R.; May, W. E.; Parris, R. M.; Wise, S. A. *Anal. Chem.* **1980**, *52*, 1650–1657.
(24) Tomkins, B. A.; Griest, W. H.; Caton, J. E.; Reagan, R. R. In "Polynuclear Aromatic Hydrocarbons: Physical and Biological Chemistry"; Cooke, M., Dennis, A. J., Fisher, G. L., Eds.; Battelle Press: Columbus, OH, 1982; pp 813–824.
(25) Burke, F. P.; Winschel, R. A.; Pochapsky, T. C. *Prepr. Pap.–Am. Chem. Soc., Div. Fuel Chem.* **1981**, *60*, 562–572.
(26) Dark, W. A.; McFadden, W. H. *J. Chromatogr. Sci.* **1978**, *16*, 269–229.
(27) Chmielowiec, J. *Anal. Chem.* **1983**, *55*, 2367–2374.
(28) Ogan, K.; Katz, E. *Anal. Chem.* **1982**, *54*, 169–173.
(29) Sonnefeld, W. J.; Zoller, W. H.; May, W. E.; Wise, S. A. *Anal. Chem.* **1982**, *54*, 723–727.
(30) Mahlum, D. D. *J. Appl. Toxicol.* **1983**, *3*, 1, 31–33.
(31) Later, D. W.; Pelroy, R. A.; Mahlum, D. D.; Wright, C. W.; Lee, M. L.; Weimer, W. C.; Wilson, B. W. In "Polynuclear Aromatic Hydrocarbons: Seventh International Symposium on Formation, Metabolism, and Measurement"; Cooke, M. W., Dennis, A. J., Eds.; Battelle Press: Columbus, OH, 1982; pp 771–783.
(32) Gary, J. A. "Solvent Refined Coal (SRC) Process: Selected Physical, Chemical and Thermodynamic Properties of Narrow Boiling Range Coal Liquids for the SRC II Process"; NTIS: Springfield, VA, 1981.
(33) Later, D. W.; Lee, M. L. In "Advanced Techniques for Synthetic Fuels Analysis"; Wright, C. W., Weimer, W. C., Felix, W. D., Eds.; NTIS: Springfield, VA, 1983; Chapter 4, pp 44–73.
(34) Wilson, B. W.; Pelroy, R. A.; Mahlum, D. D.; Frazier, M. E.; Later, D. W.; Wright, C. W. *Fuel* **1984**, *63*, 48–55.
(35) Wright, C. W. *HRC CC, J. High Resolut. Chromatogr. Chromatogr. Commun.* **1984**, *7*, 83–88.
(36) Vassilaros, D. L.; Kong, R. C.; Later, D. W.; Lee, M. L. *J. Chromatogr.* **1982**, *252*, 1–20.
(37) Later, D. W.; Lee, M. L.; Wilson, B. W. *Anal. Chem.* **1982**, *54*, 117–123.
(38) Mahlum, D. D.; Wright, C. W.; Chess, E. K.; Wilson, B. W. *Cancer Res.* **1984**, *44*, 5176–5181.
(39) May, W. E.; Wise, S. A. *Anal. Chem.* **1984**, *56*, 225–232.
(40) Willey, C.; Iwao, M.; Castle, R. N.; Lee, M. L. *Anal. Chem.* **1981**, *53*, 400–407.

RECEIVED for review July 2, 1984. Accepted October 10, 1984. This work was supported by the Department of Energy under Contract DE-AC06-76RLO.

Mathematical Modeling of Temperature Programmed Capillary Gas Chromatographic Retention Indexes for Polychlorinated Dibenzofurans

Michael D. Hale, Fred D. Hileman,* Thomas Mazer,[1] Traci L. Shell, Roy W. Noble, and Joseph J. Brooks

Monsanto Company, Dayton Laboratory, 1515 Nicholas Road, Dayton, Ohio 45418

A model is developed describing the relationship between retention characteristics on a gas chromatographic column and molecular structure of the chlorinated dibenzofurans. Model variables account for (1) number and position of chlorines present, (2) relations between chlorines on each aromatic ring, and (3) interactions between the two rings. The model has proven to be useful for validation and prediction, and evidence suggests that the general principles may be applied to structurally similar compounds.

A number of techniques have been used for the analysis of polychlorinated dibenzofurans (PCDFs) (*1–4*), but gas chromatography remains the primary separation technique used for their analysis. Gas chromatographic retention parameters are typically used to qualitatively identify which PCDF congeners are present in the sample being analyzed. Mazer et al. recently reported on the preparation of the 38 tetrachlorodibenzofurans (TCDFs) and the determination of their retention characteristics on two different chromatographic phases (*5*). On review of those results, the retention data showed definite patterns which could be interpreted from a molecular structure viewpoint (*6*). This kind of approach in chromatographic data interpretation has gained widespread use (*7–9*), and it is believed that a mathematical model that describes the pattern in these retention data would be of great analytical value. First, it could be used to examine the retention data for consistency. This is important because of the difficulties associated with preparing and then positively identifying any particular PCDF. Second, it could predict retention characteristics of PCDFs which had not yet been synthesized. With this method, it would be possible to greatly narrow the window of observation to search for and identify a given PCDF.

The work described here involves the development of a model describing the relationship between the molecular structure of a PCDF and its retention index on a nonpolar capillary gas chromatography column. The descriptive structural parameters are, for the most part, directly related to conventional organic structural relationships, such as ortho, meta, and para orientation of chlorine atoms about an aromatic ring. Using the technique described here, one can predict the retention index for any given PCDF having only a knowledge of its chlorine substitution pattern.

EXPERIMENTAL SECTION

Congener Synthesis. Of the 135 different PCDFs, 110 were prepared by using the techniques described previously (*5, 6*) or obtained from commercial or government sources. Briefly, the synthesis involved the careful oxidative thermal degradation of specific polychlorinated biphenyl congeners to form PCDFs via the mechanisms proposed by Buser (*10*). Additional PCDFs were formed by either chlorination of a selected PCDF congener using antimony pentachloride or by dechlorination of a selected PCDF congener using ultraviolet light. The various PCDFs formed in these reactions were continually cross correlated with each other to ensure that the proper identification had been made.

Data Collection. A Hewlett-Packard 5985B GC/MS system with a 30 m J & W DB-5 fused silica capillary column operated in the splitless injection mode was used to analyze the various PCDF congeners. The column was temperature programmed from 175 °C with an initial hold of 1 min to 300 °C at a rate of 6 °C/min. Helium was used as a carrier gas at 7 psi head pressure and the column was directly coupled to the ion source of the mass spectrometer.

The mass spectrometer was operated in the selected ion monitoring mode following ions characteristic of monochlorothrough octachlorodibenzofuran. In addition, a mixture of normal hydrocarbons, including octadecane (n-$C_{18}H_{38}$) through tetratricontane (n-$C_{34}H_{70}$), was obtained from Supelco and coinjected with each sample. Normal hydrocarbons lower than octadecane were readily observed as trace impurities in the dodecane used as the splitless injection solvent. The mass spectrometer also monitored an ion characteristic of these normal hydrocarbons. Thus, a scale was built into every GC/MS analysis allowing a hydrocarbon number (retention index) to be assigned to a PCDF as shown in Figure 1.

In some situations, the identification of a specific PCDF congener on the DB-5 column was ambiguous, requiring independent confirmation. These cases were most often resolved by analyzing the PCDFs in question on a highly polar SP-2330 fused silica capillary column also obtained from Supelco. Though providing better discriminating power in most cases, this type of column had difficulty in eluting the entire range of congeners being studied without going to extended isothermal temperature holds at the column's upper temperature limit.

The temperature programmed retention index system was chosen for this work (*11*). This retention index (RI) is calculated by using the following equation:

$$\mathrm{RI} = 100\,\frac{T_r(\mathrm{PCDF}) - T_r(\mathrm{C}_z)}{T_r(\mathrm{C}_{z+1}) - T_r(\mathrm{C}_z)} + 100Z$$

where T_r(PCDF) is the retention time of the PCDF in question and $T_r(C_z)$ and $T_r(C_{z+1})$ are the retention times of the normal hydrocarbons bracketing the PCDF with carbon numbers z and z plus one. The temperature program used with the DB-5 column was chosen so that the monochloro- through octachlorodibenzofurans would elute without experiencing excessively long retention times. In addition, the linear temperature program that was employed had the hydrocarbons eluting linearly in the retention range for all PCDFs.

Data Analysis. Regression analysis was the primary method for examining the retention data. PROC GLM and PROC NLIN of the Statistical Analysis System (SAS) were used to perform the required analyses (*12*).

RESULTS AND DISCUSSION

First Steps. In order to describe the retention index of a chlorinated dibenzofuran molecule as a function of structure, it is helpful to consider that dibenzofurans are symmetrical about a plane dividing the molecule into two parts. Those two parts are the two aromatic rings (arbitrarily labeled as ring 1 and ring 2), with the plane dividing the molecule through the biphenyl and ether linkages. If each half of the

[1] Present address: Brehm Laboratory, Wright State University, Dayton, OH 45435.

0003-2700/85/0357-0640$01.50/0 © 1985 American Chemical Society

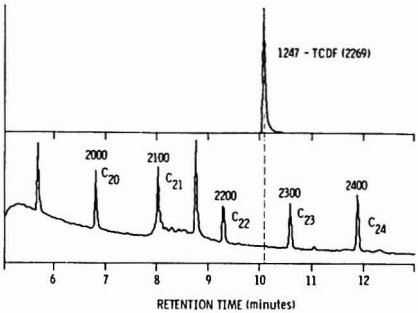


Figure 1. Determination of the retention index for 1247-TCDF.

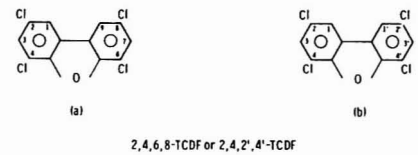


Figure 2. Comparison of the conventional numbering scheme (a) and the numbering scheme used in this work (b) for chlorinated dibenzofurans.

molecule (each aromatic ring) contributes to the retention index in an additive manner, then a very simple mathematical model

retention index =
ring 1 effect + ring 2 effect + random variation (Model 1)

can be used to describe the retention index as a function of structure. This approach has been used before in an independent work, where a similar model was used to describe the retention behavior of chlorinated biphenyls (*13*). The random variation term includes instrument, sampling, and all of the other variabilities involved in making a measurement and will hereafter be referred to simply as "variation".

The numbering scheme normally used for PCDFs with one ring numbered 1–4 and the other ring as 6–9 obscures the similarity of the two aromatic rings as shown in Figure 2a. Thus, throughout this work the positions numbered 1,2,3,4 were retained and positions 6 through 9 were renumbered using 1′,2′,3′,4′. With this notation, 2468-TCDF becomes 242′4′-TCDF as shown in Figure 2b. Every congener has a unique representation using this convention, in which the numbers are listed in ascending order, with nonprimed numbers before primed numbers. This notation makes it easy to identify the inter- and intra-ring relationships used in the mathematical model described here and emphasizes the similarity of the two rings.

The TCDFs provide a good starting place for testing this simple model since their complete retention characteristics have already been established (*5*). Additionally, they yield retention indexes which cover the middle of the range of the retention indexes for the PCDFs. More importantly, the TCDFs have representative examples of all possible substitution patterns for an individual ring. That is, every possible substitution pattern for an aromatic ring in a PCDF can be found in one (or more) of the TCDFs.

The first step in the search for patterns linking retention behavior with structural characteristics was the construction of Table I, which organizes the 2:2 substituted TCDFs (those

Table I. Observed Retention Indexes for the 2:2 Substituted TCDFs

ring 2 substitution pattern	ring 1 substitution pattern					
	12	13	14	23	24	34
12	2406	2341	2364	2322	2281	2329
13	2341	2273	2296	2263	2226	2272
14	2364	2296	2314	2290	2242	2288
23	2322	2263	2290	2338	2298	2354
24	2281	2226	2242	2298	2254	2304
34	2329	2272	2288	2354	2304	2362
grand mean	2302					

Table II. First Residuals for the Decomposition of the Retention Indexes for the 2:2 Substituted TCDFs

ring 2 substitution pattern	ring 1 substitution pattern						
	12	13	14	23	24	34	row mean
12	104	39	62	20	−21	27	38
13	39	−29	−6	−39	−76	−30	−24
14	62	−6	12	−12	−60	−14	−3
23	20	−39	−12	−36	−4	52	8
24	−21	−76	−60	−4	−48	2	−35
34	27	−30	−14	52	2	60	16
column mean	38	−24	−3	8	−35	16	

isomers which have two chlorine substitutions on each of the aromatic rings). The table was structured so that the retention index for a given 2:2 substituted TCDF isomer could be found at the intersection of the column and row which have the appropriate substitution patterns for ring 1 and ring 2, respectively. Note that this organization makes the table symmetrical about the principal diagonal, simplifying the calculations and aiding in the identification of patterns.

First, a grand mean was computed for Table I. This value, 2302, was then subtracted from each entry in Table I, leaving residuals as shown in Table II. This operation corresponds to fitting a model

retention index =
constant (grand mean) + variation (residual)

Row and column averages were computed for those residuals and are listed in the right-hand column and bottom row of Table II. (Note: column i mean = row i mean, by construction.)

Substitution patterns with comparable row mean values are grouped together in Figure 3, revealing a definite pattern. The substitutions with the greatest average negative residuals from the grand mean (13-substitution and 24-substitution) contain neither vicinal chlorines nor hydrogens (Figure 3a). Likewise, substitutions with the greatest average positive residuals have both vicinal chlorines and hydrogens (Figure 3c). Finally, substitutions with average residuals near zero have only vicinal chlorines or vicinal hydrogens (Figure 3b). One interpretation of these data is that vicinal-like atoms increase the retention of a TCDF.

To refine the model, a methodology was employed (*14*) in which new residuals were calculated for each entry in Table I by adding the appropriate row and column mean from Table II to the grand mean and subtracting this from the observed values in Table I. Table III shows the results of these calculations. This procedure has now actually yielded an implementation of model 1. The row (or column) mean for a particular substitution pattern provides an estimate of the retention effect for that pattern.

retention index =
constant (grand mean) + ring 1 effect (column mean)
+ ring 2 effect (row mean) + variation (residual)

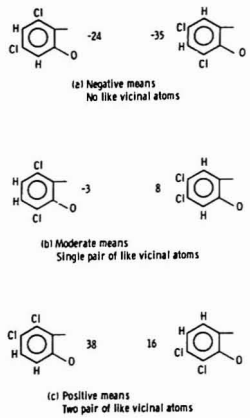


Figure 3. Comparison of the row (column) means from Table II for the various chlorine and hydrogen substitution patterns.

Table III. Decomposition of Retention Indexes for the 2:2 Substituted TCDFs[a]

ring 2 substitution pattern	ring 1 substitution pattern					
	12	13	14	23	24	34
12	28	25	27	−27	−24	−27
13	25	19	21	−23	−17	−22
14	27	21	18	−17	−22	−27
23	−27	−23	−17	20	23	28
24	−24	−17	−22	23	22	21
34	−27	−22	−27	28	21	28

[a] Note: Rows and columns do not add to zero because of rounding. During actual calculations, carry decimal places instead of rounding to whole numbers.

A serious deficiency in the simple additive model 1 can be observed in Table III by the obvious pattern of 3 × 3 blocks of residuals of the same sign. The pattern results from arranging the table so that the first three columns and first three rows all have a chlorine atom in the 1 position, while the other rows and columns do not. This positive–negative pattern indicates an interaction between the two rings involving the 1 and 1′ positions, a feature not explained by the simple additive model 1. Thus, model 1 does not provide an adequate description of the data because it assumes that the two halves of the PCDF behave independently with no provision for interaction between the two rings. Perhaps even more striking is that the residuals in Table III are all of approximately the same magnitude. This implies that model 1 would be significantly improved by including one additional factor to describe this inter-ring interaction. This simple refinement yields a better model

retention index = constant + ring 1 effect + ring 2 effect + ring interaction effect + variation (Model 2)

At this stage of the analysis, it was clear that there were at least two explanations for the interaction phenomenon. If both the 1 and 1′ positions were chlorinated, then steric crowding could distort the molecule from planarity, giving an increased retention index as shown by the positive residuals in the upper left quadrant of Table III. This type of steric crowding has been suggested in other compounds containing the five-member ring structure (*15*). Another possibility is that when only one of the 1 or 1′ positions is chlorine substituted, a hydrogen bonding effect between the hydrogen and the chlorine atoms (*16*) occupying those positions decreases chromatographic retention shown as the negative residuals in upper right and lower left quadrants of Table III. Either of these two possibilities would cause the same pattern of residuals that is observed in Table III. An independent method is needed to determine which type of interaction is actually occurring, because the type of mathematical model developed here cannot distinguish between those two cases. (In statistical parlance, the models are said to be linearly equivalent.) The question of which possibility is "correct" will not be addressed and both interactions will be illustrated by the working models presented here.

Model Development. The methods developed in the previous section serve as good diagnostic tools. In fact, a spreadsheet program on a microcomputer may be used to good advantage, implementing this tabular approach in a "hands on" interactive environment. Further model development requires more powerful methods, however, and is better done using regression techniques.

The regression analog of the tabular approach is implemented by using dummy variables to represent the possible substitution patterns. Each variable takes the values 0, 1, and 2, depending on whether that pattern does not occur, occurs once, or occurs twice, respectively, for the given PCDF. *By creating variables this way, the regression coefficient for a variable is used as an estimate of the effect for the corresponding chlorination pattern.* The notation Ax is used to denote the dummy variable for the pattern x. As an example for 122′4′-TCDF, the variable A12 = 1, the variable A24 = 1, and all of the other variables = 0.

To implement model 2, a variable representing the ring-interaction must also be included. The variable HBOND is created to model the latter possibility of inter-ring hydrogen bonding. This variable is −1 when only one chlorine has been substituted in either the 1 or 1′ position, and +1 otherwise. For the above case of 122′4′-TCDF, HBOND equals −1. The values 1 and −1 were chosen for simple agreement with Table III so that the average size of the residual would yield the coefficient for HBOND. The values 1 and 0 work as well, doubling the size of the coefficient but are not intuitive from the table. Later in this description, one of the other possible explanations for interaction will be illustrated in a more refined model using the variable STERIC, which is 0, unless both the 1 and 1′ positions are chlorine substituted, in which case STERIC is 1.

Table IV shows regression coefficients for the various substitution patterns for all PCDFs using model 2. The size of the HBOND coefficient, −23 when present, 23 when absent, is quite notable and accounts for a good deal of the fine detail in the model. Without this term, the model degrades dramatically, showing little discriminating power among congeners with the same number of chlorine substitutions. A second ring-interaction variable, FOURFOUR, having a much smaller effect, i.e., smaller coefficient, has been introduced in Table IV. The need for this ring interaction variable only became apparent after all of the gross effects were identified and the residuals carefully examined. The variable FOURFOUR is 1 when both 4 positions are chlorine substituted, and 0 otherwise. The variable FOURFOUR was constructed to correspond to the effect of the two chlorines blocking the interaction of the ether linkage oxygen with the chromatographic liquid phase. The decrease in this interaction then results in decreased retention (i.e., negative coefficient as shown in Table IV) of the PCDFs with this substitution pattern.

Table IV. Regression Coefficients for Model 2

dummy variable	substitution pattern	coefficient	av[a]
constant (intercept)	none	1540	
A1	1	206	
A2	2	189	
A3	3	182	193
A4	4	195	
A12	12	419	
A13	13	357	
A14	14	384	
A23	23	387	383
A24	24	350	
A34	34	401	
A123	123	602	
A124	124	565	
A134	134	561	572
A234	234	591	
A1234	1234	799	799
HBOND[b]		±23	
FOURFOUR[b]		−9	

[a] See text. [b] See text for an explanation of HBOND and FOURFOUR.

To use the coefficients in Table IV, one identifies the pattern on each of the rings, selects the corresponding estimates of effect from the table, and adds those values together. To predict a retention index for 122′4′-TCDF, one would begin by taking the constant term (1540), add the coefficient calculated for the pattern 12 (419), add the coefficient calculated for the pattern 24 (350), and finally include the appropriate interaction terms. In this case, the HBOND coefficient (−23) is included and the FOURFOUR coefficient (−9) is excluded since only one 4-chlorine is present. The calculated value of 2286 compares well with the observed value of 2281.

The agreement between observed and fitted indexes, the R^2 value of 0.999, and the standard deviation of 6.3 all indicate that this model works quite well to describe the retention indexes of all analyzed PCDFs. Several of the congeners had been prepared via alternate routes so that several replicate values were used for the regression analysis. Thus, for model 2 there were 246 data values for 110 different congeners. No simple mathematical model will account for the variation observed between replicates and certainly would not be useful for prediction if it could. Although a "lack-of-fit" test indicates significant model inadequacy, many of the repeated values were not true replicates, causing the estimate of "pure error" to be much too small. The standard deviation of 6.3 is anticipated given the broad range of values present in this set of data. The initial data set covered retention indexes from approximately 1880 to 3140. A 95% confidence interval for a single future reading is approximately 25 units wide, so that the window of observation for a new PCDF can be considerably narrowed using model 2 and the values in Table IV.

This model has proven useful in validating the structural assignments given to a PCDF. One 3:1 substituted TCDF did not fit the model and an error in structure assignment was detected and reported (*17*). This approach provided yet another check on the structural assignment given to a specific PCDF in addition to the cross correlations mentioned in the section on congener synthesis.

Improving the Model. Although model 2 works well, it lacks the simplicity and unifying theme of a parsimonious description. A model with few simple descriptors, which could be identified with structural characteristics of the molecule, is highly desirable. To accomplish this, the coefficients in Table IV were carefully examined for patterns which might allow the further consolidation of parameters. One of the real advantages of the approach in the preceding section is that it effectively provided for the reduction of information from 110 congeners to a much smaller set of numbers, clearly associated with different chlorine substitution patterns.

Table V. Determination of Primary Intra-ring Interactions

substitution pattern	A1 (206)	A2 (189)	A3 (182)	A4 (195)	Σ	model 2	Δ	av Δ
			Meta					
A13	X		X		388	357	−31	−32
A24		X		X	384	350	−34	
			Ortho					
A12	X	X			395	419	+24	
A23		X	X		371	387	+16	+21
A34			X	X	377	401	+24	
			Para					
A14	X			X	401	384	−17	−17

First, a simplification of the data in Table IV was obtained by calculating an average coefficient value for each degree of chlorine substitution. For example, the average for the four monochloro substitution pattern coefficients is 193, while the average value for the dichloro coefficients is 383, approximately two times that of the monochloro coefficients. This pattern is consistent through the trichloro and tetrachloro averages, with values of 572 and 799 being approximately three times and four times that of the monochloro coefficients, respectively. Thus, each chlorine substitution adds an increment of approximately 190 retention index units to the constant value. This increment may be used to reduce the number of structural parameters under consideration for a model. The magnitude of this increment is consistent with comparable values reported by Haken et al. (*18*) in their evaluation of the increase in retention indexes with increasing number of chlorines present in chlorobenzenes on a comparable chromatographic phase. The consistency in these data indicates that this model may also be used to describe the retention behavior of compounds similar in nature to the chlorinated dibenzofurans.

Second, the values in Table IV were much simpler to deal with than the raw data in identifying interactions of chlorines on the same aromatic ring. Much of the "noise" in the data was stripped away by the initial data analysis so that underlying relationships, that were otherwise obscured, were made more apparent. The analysis process began by comparing various combinations of the structural effect estimates. For example, one might compare the coefficient for A13 (357) with the sum of the Al (206) and A3 (182) coefficients. This sum, 388, is 31 retention units greater than the coefficient for A13 (357). Likewise, when the coefficient for A2 (189) is added to the coefficient for A4 (195), their sum of 384 is 34 units greater than the coefficient for A24 (350). A tabulation of all the various combinations of two chlorines is given in Table V showing the summed results (Σ) vs. the directly calculated regression coefficients from model 2. A delta value is also provided which serves as a measure of decreased or increased retention of a particular substitution pattern as compared to the sum of its components.

Table V is organized so that the patterns with similar delta values are grouped together. In the first two cases a meta relationship is introduced, while in the next three cases the chlorines are placed in an ortho relationship. The final case represents the only way to introduce two chlorines in a para relationship. The delta values provide a quantitative restatement of the ordering expressed in Figure 3 in which ortho chlorine substitution (vicinal chlorines) increased retention of the PCDFs relative to meta chlorine substitution (nonvicinal chlorines). Again these same relationships may be observed in the data shown by Haken et al. (*18*). In that work, the

Table VI. Determination of the Effect of Intervening Chlorines on Intra-ring Interactions

substitution pattern	A1 (206)	A2 (189)	A3 (182)	A4 (195)	A12 (419)	A13 (357)	A14 (384)	A23 (387)	A24 (350)	A34 (401)	Σ	ortho (21)	meta (−32)	para (−17)	corrected Σ	model 2	Δ	av Δ
								"Closed"										
A123	X							X			593	X	X		582	602	−20	
A123		X				X					546	XX			588	602	−14	
A123			X		X						601	X	X		590	602	−12	−16
A234		X								X	590	X	X		579	591	−12	
A234			X						X		532	XX			574	591	−17	
A234				X				X			582	X	X		571	591	−20	
								"Open"										
A124	X								X		556	X		X	560	565	−5	
A124		X					X				573	X	X		562	565	−3	
A124				X	X						614		X	X	565	565	0	
A134	X									X	607		X	X	558	561	−3	−4
A134			X				X				566	X	X		555	561	−6	
A134				X		X					552	X		X	556	561	−5	

m-dichlorobenzene eluted prior to the *o*-dichlorobenzene. Also, the 1,3,5-trichlorobenzene was the first trichlorobenzene to elute and 1,2,3-trichlorobenzene was the last. The consistency in these data again indicates that the models developed in this work can be applied to similar systems.

Following these ideas, a new model was developed which had simple parameters to account for (1) the number and position of the chlorines present, (2) the structural relationships between the chlorines on each ring (intra-ring effects), and (3) the interactions between the rings (inter-ring effects). The hypothesis was evaluated by regressing the coefficient values from Table IV on dummy variables ONE, TWO, THREE, and FOUR (position variables) followed by ORTHO, META, and PARA (intra-ring variables). The variable ONE takes the values 0, 1, and 2, by simply counting the number of chlorine substitutions in the 1 and 1′ positions. TWO, THREE, and FOUR are defined similarly for the other positions. The intra-ring variables ORTHO, META, and PARA were originally defined to count the number of ortho, meta, and para relationships, respectively. While the regression worked fairly well, it was clear that there were intra-ring factors at work that were not accounted for by the simple ORTHO, META, and PARA effects observed here. This is illustrated in Table VI, which is in the same format as Table V except that now an attempt is made to calculate the trichloro substitution coefficients using combinations of the monochloro and dichloro substitution coefficients from Model 2. In Table VI, the intra-ring coefficients determined in Table V are included as modifiers to the summed value (Σ) resulting from the relationships that are introduced. As an example, if A123 is formed by adding A1 plus A23, an ortho relationship (1 to 2) and a meta relationship (1 to 3) are introduced. The coefficients for these intra-ring parameters are used to correct the summed (Σ) value in Table VI. No consideration is given to the ortho relationship present in A23 since this is already included implicitly in the original coefficient for A23; i.e., the regression coefficient for A23 estimates a net effect for the 23 substitution pattern.

The trichloro substitutions in Table VI fall into two groups. The groups defined as "closed" groups consist of substitution patterns with two pairs of vicinal chlorines (123 and 234) while the "open" groups contain patterns with one pair of vicinal chlorines separated from a lone chlorine by a hydrogen (124 and 134). The delta values for "closed" group substitutions are all comparable with an average value of −16. What is postulated as occurring is that the strength of the meta effect is reduced by an intervening chlorine. For example, in making the META modification for the case of A1 plus A23, this meta effect is mediated by the intervening 2-position chlorine and the correction should be cut in half (i.e., from −32 to −16). A similar situation occurs for A13 plus A2 except that the META effect inherent in the A13 coefficient is reduced, again by the insertion of the intervening 2-position chlorine. Similarly, "open" group substitution patterns have similar delta values and can be considered as having para-substituted chlorines which have been mediated by an intervening chlorine.

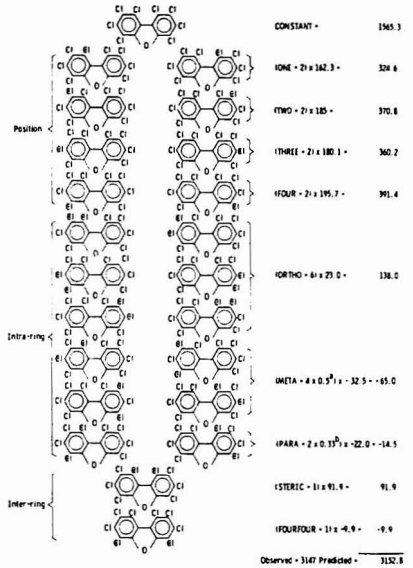
Chart I

position variables	ONE:	chlorines in the 1 position
	TWO:	chlorines in the 2 position
	THREE:	chlorines in the 3 position
	FOUR:	chlorines in the 4 position
intra-ring variables	ORTHO:	ortho relationships
	META:	meta relationships
	PARA:	para relationships
inter-ring variables	STERIC:	steric hindrance
	FOURFOUR:	ether linkage blocking

Pursuing this idea, the regression mentioned in the previous paragraph was applied again, but this time the META and PARA variables were adjusted if intervening chlorines were present, to account for the disruption of the usual META and PARA relationships. The dummy variable META now takes the value 0 when there are no meta relationships present, 1 when there is one meta relationship, and 0.5 when there is a meta relationship with an intervening chlorine present. (Note: A1234 is considered to have two meta relationships, each with an intervening chlorine, so that META = 1 for A1234.) In a similar fashion, the dummy variable PARA was redefined to be zero when no para relationships exists, 1 when one para relationship exists, 2/3 when there is one intervening chlorine, and 1/3 when there are two intervening chlorines. Finally, the variable ORTHO remains a count of the number of ortho relationships present, which cannot be modified by intervening chlorines. On identification of these intraring effects by examination of the regression coefficients of model 2, it was possible to postulate the following model to describe the relationships between molecular structure and retention index present in the original data

$$\text{retention index} = \text{constant} + \text{position effect} + \text{intra-ring effect} + \text{inter-ring effect} + \text{variation} \quad \text{(Model 3)}$$

To fit model 3, the original PCDF retention indexes were regressed against the variables shown in Chart I. The resulting coefficients in Table VII gave a good regression fit using these new variables. The variables are grouped to correspond to the three objectives stated previously. The position effect variables (ONE, TWO, THREE, FOUR) which take on the



[a]META is multiplied by 0.5 since there is one intervening chlorine
[b]PARA is multiplied by 0.33 since there are two intervening chlorines

Figure 4. Prediction of the retention index for octachlorodibenzofuran using model 3.

Table VII. Regression Coefficients for Model 3

dummy variable	coefficient
constant	1565.3
ONE	162.3
TWO	185.4
THREE	180.1
FOUR	195.7
ORTHO	23.0
META	−32.5
PARA	−22.0
STERIC	91.9
FOURFOUR	−9.9

values 0, 1, and 2, account for both the number of chlorines present in the congener, as well as the positional effects. Recalling the differences in coefficients for A1, A2, A3, and A4 as shown in Table IV, the model suffers greatly if these positional differences are ignored. The intra-ring variables account for the relationships between chlorines on a given ring. The inter-ring variables represent the interactions between the rings as described during the development of model 2.

Illustration of Model 3. To use the coefficients in Table VII, one identifies the appropriate chlorinated positions, intra-ring parameters, and inter-ring parameters, adding the corresponding coefficients to the constant value. As an example, consider again 122'4'-TCDF. Take the constant term of 1565.3 and add to it 162.3 (one 1 position) plus 370.8 (two 2 positions) plus 195.7 (one 4 position) plus 23 (the ortho relationship for 12) minus 32.5 (the meta relationship for 2'4') to obtain 2285 which again compares well with the observed value of 2281.

To further illustrate the intra-ring and inter-ring parameters in Table VII, consider the extreme case of predicting the retention index of octachlorodibenzofuran (OCDF). The calculation of this index using Table VII is illustrated in Figure 4. The portions of the molecule involved in a particular calculation have been designated by a dot. In this example, all the parameters in Table VII are used and provision has been made for intervening chlorines in the calculation of the META and PARA variables.

The position and intra-ring variables used in model 3 are familiar to structural organic chemistry. The inter-ring variables are considerably less familiar, especially the variable STERIC, and its counterpart HBOND used in Model 2. Figure 5 is presented so that the nature of these inter-ring variables and their relationship to each other may be more clearly understood. A special regression analysis was performed on a second set of dummy variables to better delineate the effects of the dummy position variables already introduced (i.e., ONE, TWO, THREE, and FOUR). Each of the position variables was decomposed into three variables, corresponding to 0, 1, and 2 chlorine substitutions for that position. Figure 5 plots the coefficients for these dummy variables for ONE against 0, 1, and 2. Similar plots for TWO and THREE, not included here, reveal that the three points nearly fall on a straight line. For ONE, however, there is a severe nonlinearity. The same is true for FOUR, but to a lesser extent. The

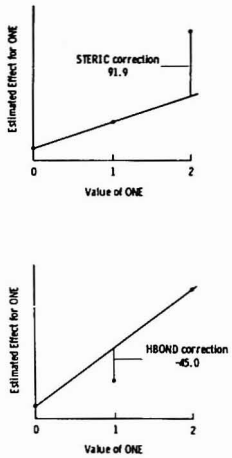


Figure 5. Comparative interpretation of the STERIC and HBOND interactions.

Table VIII. Analysis of Variance for Model 3[a]

source	DF	sum of squares	mean square	F value	prob <F	R^2
model	9	22 168 843	2 463 204.8	53 572.8	0.0001	0.9995
residual	262	12 046	46.0			
corrected total	271	22 180 890				

[a]Standard deviation of regression = 6.78. Press statistic = 13 004.

Table IX. Comparison of the Predicted vs. the Measured Retention Indexes for Polychlorinated Dibenzofurans on a DB-5 Column

conventional nomenclature	substitution pattern ring 1	substitution pattern ring 2	retention index predicted	retention index measd	residual	conventional nomenclature	substitution pattern ring 1	substitution pattern ring 2	retention index predicted	retention index measd	residual
1-	none	1	1728	1739	11	1234-	none	1234	2318	2310	−8
3-	none	3	1745	1749	4	1236-	4	123	2318	2307	−11
2-	none	2	1751	1749	−2	2349-	1	234	2318	2308	−10
4-	none	4	1761	1760	−1	1469-	14	14	2319	2314	−5
13-	none	13	1875	1884	9	1278-	23	12	2324	2322	−2
14-	none	14	1901	1913	12	1349-	1	134	2333	2325	−8
17-	1	3	1908	1910	2	1267-	34	12	2335	2329	−6
18-	1	2	1913	1925	12	2347-	3	234	2336	2337	1
24-	none	24	1914	1912	−2	1279-	13	12	2338	2341	3
16-	1	4	1923			1249-	1	124	2339	2335	−4
37-	3	3	1925	1930	5	2348-	2	234	2342	2340	−2
27-	2	3	1931	1930	−1	2346-	4	234	2342	2339	−3
12-	none	12	1936	1934	−2	2378-	23	23	2342	2338	−4
28-	2	2	1936	1935	−1	2367-	23	34	2353	2354	1
36-	3	4	1941	1944	3	3467-	34	34	2353	2362	9
26-	2	4	1946	1946	0	1269-	14	12	2364	2364	0
46-	4	4	1947	1953	6	1239-	1	123	2377	2369	−8
23-	none	23	1954	1939	−15	1289-	12	12	2398	2406	8
34-	none	34	1964	1959	−5	13468-	24	134	2418		
19-	1	1	1982	1975	−7	12468-	24	124	2423		
137-	3	13	2055	2057	2	23479-	13	234	2466	2467	1
138-	2	13	2060	2070	10	13478-	23	134	2468	2469	1
136-	4	13	2071	2072	1	13467-	34	134	2468	2469	1
249-	1	24	2076	2082	6	12368-	24	123	2471		
134-	none	134	2079	2088	9	12478-	23	124	2473		
147-	3	14	2081	2086	5	12467-	34	124	2473	2465	−8
124-	none	124	2084	2085	1	13479-	13	134	2481	2473	−8
148-	2	14	2087	2100	13	23469-	14	234	2482	2476	−6
146-	4	14	2087	2094	7	12479-	13	124	2486	2479	−7
247-	3	24	2094	2099	5	23468-	24	234	2495	2495	0
248-	2	24	2099	2097	−2	13469-	14	134	2497		
246-	4	24	2100	2101	1	12347-	3	1234	2498	2495	−3
239-	1	23	2116	2111*	−5	12469-	14	124	2502	2497	−5
127-	3	12	2116	2109	−7	12348-	2	1234	2503	2508	5
128-	2	12	2121	2129	8	12346-	4	1234	2504	2496	−8
123-	none	123	2123	2113	−10	12378-	23	123	2511	2507	−4
349-	1	34	2126	2125*	−1	12367-	34	123	2522	2540	18
139-	1	13	2129	2124	−5	12379-	13	123	2524		
126-	4	12	2132	2125	−7	23489-	12	234	2527	2521	−6
237-	3	23	2134	2134	0	13489-	12	134	2542		
238-	2	23	2139	2132	−7	23478-	23	234	2545	2551	6
347-	3	34	2144	2150	6	23467-	34	234	2545	2555	10
348-	2	34	2149	2151	2	12489-	12	124	2547	2559	12
236-	4	23	2149	2141	−8	12369-	14	123	2551	2546*	−5
346-	4	34	2150	2152	2	12349	1	1234	2572		
149-	1	14	2155	2151	−4	12389-	12	123	2585	2593*	8
234-	none	234	2156	2148	−8	123468-	24	1234	2656	2650	−6
129-	1	12	2190			134678-	134	234	2660		
1368-	24	13	2224	2227	3	124678-	124	234	2665		
1468-	24	14	2240	2242	2	134679-	134	134	2675		
2468-	24	24	2252	2254	2	124679-	124	134	2680		
1347-	3	134	2259	2257	−2	124689-	124	124	2685	2686	1
1378-	23	13	2264	2263	−1	123478-	23	1234	2706	2708	2
1247-	3	124	2264	2264	0	123467-	34	1234	2707	2706	−1
1348-	2	134	2264	2276	12	123678-	123	234	2714		
1346-	4	134	2265	2262	−3	123479-	13	1234	2719	2720	1
1248-	2	124	2270	2274	4	123679-	123	134	2728		
1246-	4	124	2270	2264	−6	123689-	123	124	2734		
1367-	34	13	2274	2272	−2	123469-	14	1234	2736		
1379-	13	13	2277	2273	−4	234678-	234	234	2737	2748	11
1268-	24	12	2284	2281	−3	123789-	123	123	2772		
1478-	23	14	2290	2290	0	123489-	12	1234	2780		
1467-	34	14	2290	2288	−2	1234678-	234	1234	2899	2898	−1
2368-	24	23	2302	2297	−5	1234679-	134	1234	2914	2913	−1
2467-	24	34	2303	2305	2	1234689-	124	1234	2919	2922	3
1369-	13	14	2303	2296	−7	1234789-	123	1234	2967	2986	19
1237-	3	123	2303	2294	−9	12346789-	1234	1234	3152	3147	−5
1238-	2	123	2308	2307	−1						

STERIC variable (or HBOND) merely corrects for this nonlinearity in ONE. That is, the effect of having both 1 positions chlorinated is not twice that of having a single 1 position chlorinated. FOURFOUR performs the same correction for the position variable FOUR. Figure 5a shows a straight line plotted through the leftmost point and the center point. The

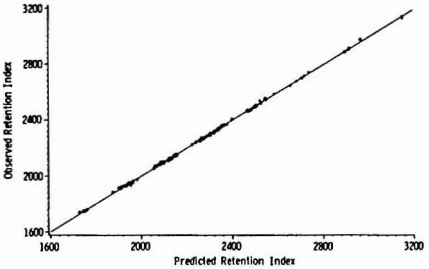


Figure 6. Observed vs. the predicted retention indexes for PCDFs using model 3.

deviation of the rightmost point above the line shows the effect called STERIC (notice its magnitude and sign are the coefficient for STERIC). Figure 5b is similar, connecting the outermost points, with the deviation of the center point from the line representing HBOND. Perhaps the "true" line lies somewhere between these two cases, but as stated before this analysis of the retention data cannot make the distinction. An alternative approach, eliminating both HBOND and STERIC, involves redefining ONE to be a nonlinear variable, but offers no improvement over the present model.

Advantages of Approach. The approach taken here, the organization and reduction of data, proved useful in identifying retention behavior related to common structural features. The structure in the raw data was considerably obscured by the presence of the two interactions between the rings, represented by STERIC and FOURFOUR. It was only after the interactions were discerned and accounted for that the common behavior of ortho-, meta-, and para-substituted congeners became apparent. Those interactions are of great significance for this model, in that the model would lose much of its predictive power without them.

Another benefit of this "bottom up" approach, decomposing each congener into its constituent parts, is that it revealed a common behavior whenever more than two chlorines were present on one ring. That is, the meta and para effects were not nearly as prominent when there were intervening chlorines present. Pursuing this observation, a nonlinear regression was performed to obtain least-squares estimates. The value obtained for a meta relationship with an intervening chlorine was 0.5 that of a meta relationship with no intervening chlorine. For the para relationship, the values obtained were 0.70 and 0.31 for one and two intervening chlorines, respectively. Further investigation showed that 2/3 and 1/3 work virtually as well and hence were adopted because they are simpler and more intuitive.

Statistical Examination of Model 3. The regression using these variables was found to work quite well with fewer parameters (10 vs. 18) than model 2. Table VIII gives the analysis of variance table. The standard error for model 3 increased slightly over that of model 2, but the PRESS statistic is very satisfactory. The PRESS statistic (predicted error sum of squares) is one of the most reliable measures of model adequacy when properly applied. This statistic is the sum of squared residuals, when each residual is calculated by deleting the present observation from the regression, i.e., so that the present observation has no influence on the regression. This is particularly appropriate when there are many unique (nonreplicated) points in the independent variable space. Outlying points that are replicated or near one another (in the independent variable space) can mask each other, reducing the value of the PRESS statistic as a check on model adequacy, so that caution must be applied. A first step to alleviate this problem involved removing replicate values by using a mean index for each congener. The PRESS statistic was found to still be quite satisfactory, indicating that any of the indexes can be well predicted from the other indexes.

That model 3 works well is evident from Figure 6, where observed values are plotted against predicted or fitted values. Table IX is a list of observed and predicted values for all of the congeners. In those cases where the PCDF was not available, only the value predicted by model 3 is given, leaving the measured value blank. Congeners that have been synthesized and have had retention indexes calculated since this model was developed are denoted in the table with an asterisk. As is evident from the table, these "new" values have agreed well with the model predictions. As long as there are blanks in the table there is the possibility that these data have been misinterpreted. However, in view of the excellent agreement to date, this possibility is considered unlikely.

Further Work. Other researchers trying to obtain these values should remember that the parameters given in Tables IV and VII were developed on one column using one temperature program. A column with different characteristics or using a different program could be expected to yield different coefficients. To make full use of this as a tool, several different congeners should have retention indexes measured on the column of interest so that regression can be used to yield the best values of the parameter for that particular column–program combination.

An interesting related question, as yet unanswered, is the following: What minimum set of congeners is needed in order to develop the coefficients for models such as the ones presented here? This is of great interest since it is reasonable to expect that these methods will prove useful in studying structurally similar compounds, such as the chlorinated dibenzo-*p*-dioxins (*6*), chlorinated biphenylenes, and chlorinated naphthalenes. Preliminary research has shown that the TCDFs alone provided excellent coefficients for ORTHO, META, and PARA as well as for STERIC and FOURFOUR. However, each of these isomers has four chlorines, so that an important piece of information is missing. That is, what is the effect of adding an additional chlorine? Some congeners having fewer or greater than four chlorines are needed in order to assess the gross effect of an additional chlorine. As previously noted, as one goes from mono- to di- to trichloro, etc., the retention index increases by approximately 190, with the inter-ring and intra-ring parameters in the model giving the refinement necessary to make a good prediction (i.e., the actual congener can vary widely from this 190 value). The tetrachloro data alone do not provide the necessary information to arrive at this good predictive ability. Resolving this issue is an important task that is the subject of current study. An intuitive rule of thumb would dictate that every possible substitution pattern for an individual ring should be represented at least twice in the initial data set.

LITERATURE CITED

(1) Rappe, C. In "Halogenated Biphenyls, Terphenyls, Naphthalenes, Dibenzo-p-dioxins, and Related Products"; Kimbrough, R. D., Ed.; Elsevier/North Holland Biomedical Press: New York, 1980; pp 48–68.
(2) Buser, H. R.; Rappe, C.; Gara, A. *Chemosphere* **1978**, *5*, 439–449.
(3) Rappe, C.; Buser, H. R.; Stalling, D. L.; Smith, L. M.; Dougherty, R. C. *Nature (London)* **1981**, *292*, 524–526.
(4) Korfmacher, W. A.; Mitchum, R. K.; Hileman, F. D.; Mazer, T. *Chemosphere* **1983**, *12*, 1243–1249.
(5) Mazer, T.; Hileman, F. D.; Nobel, R. W.; Brooks, J. J. *Anal. Chem.* **1983**, *55*, 104–110.
(6) Mazer, T.; Hileman, F. D.; Hale, M. D.; Noble, R. W.; Brooks, J. J. In "Chlorinated Dioxins and Dibenzofurans in the Total Environment"; Choudhary, G., Keith, L. H., Rappe, C., Eds.; Butterworth: Boston, MA, 1983; pp 23–58.
(7) Whalen-Pedersen, E. K.; Jurs, P. C. *Anal. Chem.* **1981**, *53*, 2184–2187.
(8) Buydens, L.; Massart, D. L.; Geerlings, P. *Anal. Chem.* **1983**, *55*, 738–744.

(9) Buydens, L.; Massart, D. L. Anal. Chem. 1981, 53, 1990-1993.
(10) Buser, H. R.; Rappe, C. Chemosphere 1979, 3, 157-174.
(11) Van Den Dool, H.; Kratz, P. D. J. Chromatogr. 1963, 11, 463-471.
(12) "SAS User's Guide: Statistics, 1982 Edition"; SAS Institute Inc.: Cary, NC, 1982.
(13) Albro, P. W.; Haseman, J. K.; Clemmer, T. A.; Corbett, B. J. J. Chromatogr. 1977, 136, 147-153.
(14) Mosteller, F.; Tukey, J. "Data Analysis and Regression"; Addison-Wesley: New York, 1977.
(15) Banerjee, A. Acta Crystallogr., Sect. B 1973, B29, 2070-2074.
(16) McKinney, J. D.; Albero, P. W.; Cox, R. H.; Hass, J. R.; Walters, D. B. In "The Pesticide Chemist and Modern Toxicology"; Bandal, S. K., Marco, G. J., Golbert, L., Leng, M. L., Eds.; American Chemical Society: Washington, DC, 1981; ACS Symposium Series No. 160, pp 439-460.
(17) Mazer, T.; Hileman, F. D.; Noble, R. W.; Brooks, J. J. Anal. Chem. 1983, 55, 1648.
(18) Haken, J. K.; Korhonen, I. O. O. J. Chromatogr. 1983, 265, 323-327.

RECEIVED for review July 27, 1984. Resubmitted December 7, 1984. Accepted December 7, 1984.

Determination of Volatile Organics in Sediment at Nanogram-per-Gram Concentrations by Gas Chromatography

Thakor A. Amin and Rajinder Singh Narang*

Division of Environmental Sciences, Wadsworth Center for Laboratories and Research, New York State Department of Health, Albany, New York 12201

Volatile compounds were stripped from sediment samples and absorbed on cartridges filled with Porapak N. The compounds were eluted from the cartridges with methanol. The eluate was assayed for various organic compounds by gas chromatography with electron-capture and photoionization detection. A detection limit of 7 ng/g for each photoionization-active and 1 ng/g for electron-capturing compound was achieved. Time study experiments showed that, while untreated samples should be analyzed within 7 days after collection, samples stored in methanol could be held for up to 90 days without significant loss of the volatile compounds.

Volatile organics in sediment can be analyzed by two general approaches: (i) diluting the sample with water and carrying out the purge-and-trap procedure (*1*) used for water analysis or (ii) extracting organics from the sediment by vacuum into a trap cooled with liquid nitrogen, adding interference-free water, and carrying out a normal trap-and-purge procedure (*2*). Invariably sediments, and especially those containing clays, contain significant amounts of humus and other materials that, when purged after dilution with water, tend to foam and make stripping very difficult. Vacuum stripping involves special hardware and multiple steps and is slow to carry out. We describe a method in which closed-loop stripping is combined with steam distillation of the volatile organics onto an absorbent (Porapak N) in a single step. The volatile compounds are eluted from the absorbent with methanol. The eluate is analyzed by gas chromatography with electron-capture (EC) or photoionization (PI) detectors.

EXPERIMENTAL SECTION

Equipment and Materials. The following equipment is required: test tubes, 1.8 × 15 cm, with serum-bottle-type tops; small serum bottles, 5–10 mL; assorted Swagelok fittings; Pyrex tubes, 6 mm × 25 cm; a Metalbellows pump (M-41); Sharon MA); a block heater; Hycar septums, 18 mm, with aluminum caps and crimper; and four pieces of stainless-steel tubing, one 0.16 × 45 cm, one 0.16 × 15 cm with one end sharpened into a needle (needle A), one 0.16 × 45 cm with both ends sharpened (needle B), and one 0.16 × 60 cm with one end sharpened (needle C).

Interference-free methanol and Porapak N (80–100 mesh) cartridges were prepared as previously described (*3*, *4*).

Assembly of Apparatus. The purging apparatus is assembled as shown in Figure 1. Whenever necessary Swagelok fittings are used to make connections. One end of the absorbent tube is attached to the outlet of the pump, while the other is attached to the blunt end of needle A. The needle end of A is pushed through the septum of the small vial so that the end is near the bottom of the septum. One end of needle B is pierced through the septum of the small vial so that the end touches the bottom of the vial. The other end of B is pushed through the septum of the sample tube so that the end is about 2 cm below the septum. The needle end of needle C is pierced through the septum of the sample tube so that the end is as near the sample as possible. The blunt end of C is attached to the inlet of the pump.

Table I. Analytes

chloroform	bromoform
1,1,1-trichloroethane	1,1,2,2-tetrachloroethane
trichloroethylene	benzene
carbon tetrachloride	toluene
bromodichloromethane	chlorobenzene
1,1,2-trichloroethane	*o,p*-xylene
tetrachloroethylene	*o,p*-chlorotoluene
1,2-dibromoethane	fluorobenzene[a]

[a] Used as an internal standard.

Standards. Standard solutions of each analyte (Table I) were prepared in interference-free methanol at 1000 μg/mL. Appropriate mixed standards and dilutions were then made as required.

Spiking of Sediments. *Injection (Method SS-1).* Dry sediment (clay, 5 g) was placed in a serum tube, which was then sealed with an aluminum cap lined with a Hycar septum. The tube was inverted, and 10–20 μL of methanol containing the appropriate volumes of analytes was injected into the body of the clay. The tube was shaken manually for 10 min.

Addition to Spiked *Water (Method SS-2).* Cold interference-free water (1.5 mL) was poured into a serum tube and spiked with 10–20 μL of methanol containing the appropriate volumes of analytes. Clay (5 g) was added, and the tube was sealed immediately with an aluminum cap lined with a Hycar septum.

Purging and Elution. *Without Additional Water (Method PE-1).* The sample was spiked with 1 μg of fluorobenzene, and the tube was placed in the heating block and kept at 120 °C. The pump was started, and after 30 min of purging the pump was stopped. The sampling cartridge was removed and placed on a stand so that the packed end was near the 1-mL mark of a 5-mL graduated tube. It was then eluted with methanol, and the volume of the eluate was recorded.

With Additional Water (Method PE-2). The sample was placed in the test tube and sealed with an aluminum cap lined with a Hycar septum for processing in the apparatus shown in Figure 1. Interference-free water (8–10 mL) was injected through the septum via a 10-mL glass syringe equipped with a fine needle. The tube was tapped a few times to make a slurry. It was then spiked with 1 μg of fluorobenzene. The pump was started, and

0003-2700/85/0357-0648$01.50/0 © 1985 American Chemical Society

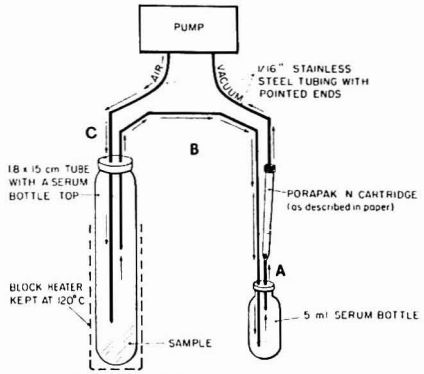


Figure 1. Assembled stripping apparatus.

the purging was carried out for 30 min at room temperature. The cartridge was eluted as in Method PE-1.

Time Study. *Using Aqueous Spiking Solution (Method TS-1).* Sediment (clay, 5 g) was spiked by Method SS-2 with selected analytes from Table I at 0.2 μg/g. The sample tubes were then frozen at −5 °C till ready for analysis. Method PE-1 was used for purging.

Using Excessive Methanolic Spiking Solution (Method TS-2). Sediment (clay, 5 g) was spiked by Method SS-1 with selected analytes from Table I at 0.2 μg/g in 1 mL of methanol. The spiked samples were frozen at −5 °C till ready for analysis. Method PE-2 was used for purging.

Transfer of Samples. *Large-Volume Transfer (Method TR-1).* Chilled clay (25 g) was added to 7.5 mL of water spiked with 1 μg/mL of various analytes and kept over ice. After the clay was mixed for 15–30 s with a spatula, 6.5-g aliquots were weighed out immediately in sampling tubes and sealed with aluminum caps lined with Hycar septums. These were purged by Method PE-1.

Individual-Aliquot Transfer (Method TR-2). Aliquots of sediment (clay, 5 g) were spiked by Method SS-2, quantitatively transferred into other sample tubes, and purged by Method PE-1.

Gas Chromatography. A PI detector equipped with a 10.2-eV lamp and electrometer (Method P-101, HNU Systems) was mounted on a Hewlett-Packard 5840 gas chromatograph. The signal from the electrometer was fed into the build-in data System of the chromatograph for recording and integrating the chromatographic peaks.

The PI active compounds were separated on a 2.7 m × 2 mm column packed with Supelcoport (100–120 mesh) coated with 4% OV-11 and 6% SP2100. The oven temperature was held at 40 °C for 5 min and then programmed to 70 °C at a rate of 3 °C/min. Other general conditions of analysis were as follows: N_2 carrier gas, 30 mL/min; detector, 255 °C; injection port, 190 °C.

The electron-capturing compounds were separated on a 3.6 m × 2 mm column packed with AWDMCS Chromosorb W (100–120 mesh) coated with 15% SF-96 and 6% OV-225. The oven temperature was either (i) held at 60 °C for 10 min, programmed to 80 °C at a rate of 3 °C/min and held at the final temperature for 10 min or (ii) held constant at 65–70 °C. Other conditions of analysis were as follows: detector, 300 °C, injection port, 190 °C, carrier gas (Ar/Me 95:5) flow, 27 mL/min.

Both PI-active and electron-capturing compounds were also separated using a fused silica (60 m × 0.25 mm) DB-5 capillary column with 1 μm coating (purchased from J & W Scientific, Rancho Cardova, CA). A splitless mode of injection was used. He was used as the carrier gas with a linear velocity of 60 cm/s. Other conditions of analysis were as follows: for PI-active compounds, injector 200 °C, detector 220 °C, makeup gas He (8 mL/min); oven temperature programmed from 50 to 170 °C at rate of 4 °C/min with a hold of 15 min at initial temperature and 14 min at final temperature; for electron-capturing compounds, injector 200 °C, detector 300 °C, makeup gas Ar/Me (95:5; 45 mL/min), oven temperature programmed from 50 to 260 °C at a rate of 8 °C/min with a hold of 4 min at initial temperature and 10 min at final temperature.

Table II. Recoveries (%) after Various Methods of Spiking and Purging[a]

compound	methods (spiking/purging) SS-1/PE-1	SS-1/PE-2	SS-2/PE-1
chloroform	81 ± 4	96 ± 4	78 ± 2
1,1,1-trichloroethane	84 ± 6	101 ± 3	70 ± 3
carbon tetrachloride	80 ± 12	102 ± 3	70 ± 1
trichloroethylene	83 ± 4	84 ± 6	70 ± 1
bromodichloromethane	86 ± 7	87 ± 5	78 ± 1
1,1,2-trichloroethane	77 ± 3	91 ± 4	84 ± 2
tetrachloroethylene	91 ± 2	88 ± 4	69 ± 1
dibromochloromethane	84 ± 12	83 ± 7	79 ± 1
bromoform	71 ± 2	73 ± 5	79 ± 1
1,2-dibromoethane	73 ± 3	81 ± 6	ND[c]
1,1,2,2-tetrachloroethane	60 ± 5	82 ± 6	ND[c]
fluorobenzene[b]	111 ± 7	96 ± 5	85 ± 1

[a] Recovery values are mean ± standard deviation. [b] Internal standard. [c] ND Not done.

RESULTS AND DISCUSSION

Spiking and Purging. The sediment can be spiked either by placing it in a closed container and then injecting the required amount of various analytes in methanol (Method SS-1) or by adding it to water spiked with the required analytes (Method SS-2). The sediment can then be purged without (Method PE-1) or with (Method PE-2) additional water. The recoveries of various analytes after various combinations of these methods showed no significant differences (Table II). Practical limitations, however, make some methods better than others.

To achieve a good spike it is important that the sediment be coated uniformly with the various analytes. When the spiking is done with a few microliters of methanol or any other solvent, this uniform distribution is difficult to achieve. Water, on the other hand, is invariably present in significant amounts in any sediment sample. A more uniform spike can be achieved by using enough aqueous solution of various analytes to wet the whole sediment. We observed that 1.5 mL of water was required to wet completely 5 g of sediment (clay), and this method of spiking was used for all of the following studies.

Organics can be purged with or without addition of water. When water is added for purging, it is possible to strip the organics at room temperature. Such purging, however, usually causes samples to foam: this is difficult to control, and the emulsions formed are carried through the system, invariably plugging it. In contrast, when a small amount of water (1.5 mL) has been used for spiking or when the sample is analyzed as received, purging must then be carried out at a higher temperature (120 °C—but no emulsions are formed; there is no need to prepare interference-free water; and at the end of the run the exact weight of the dry sediment can be calculated. This method was used in the following studies.

To determine the effect of storage of sediment samples on the recovery of volatile compounds, clay samples (5 g) were spiked with each analyte at 0.2 μg/g by Method PE-2. These were stored at −5 °C and analyzed over a span of 1–60 days. The results (Table III) show that samples can be stored up to 7 days without significant loss of any volatile. Between 14 and 60 days of storage, losses up to 50% occur. However, when samples were stored with small amounts of methanol (1 mL), losses were negligible over a period of 90 days (Table IV).

Transfer of samples between containers entailed a considerable loss of volatile compounds regardless of whether the sample was aliquoted from a large sample or was merely

Table III. Time Study of Recovery (%) after Spiking by Method SS-2 and Purging by PE-1[a]

compound	% recovery									
	day 1	day 2	day 3	day 4	day 7	day 14	day 28	day 35	day 50	day 60
chloroform	78 ± 2	75 ± 10	69 ± 5	77 ± 4	75 ± 3	49 ± 5	25 ± 3	49 ± 3	46 ± 14	40 ± 4
1,1,1-trichloroethane	70 ± 3	70 ± 11	67 ± 6	71 ± 1	75 ± 4	42 ± 15	42 ± 3	37 ± 9	46 ± 21	36 ± 5
carbon tetrachloride	70 ± 1	66 ± 12	62 ± 11	68 ± 2	71 ± 4	46 ± 7	46 ± 2	46 ± 5	44 ± 13	40 ± 7
trichloroethylene	70 ± 1	67 ± 6	63 ± 4	63 ± 3	68 ± 1	41 ± 7	35 ± 3	38 ± 4	37 ± 12	31 ± 4
bromodichloromethane	78 ± 1	78 ± 3	72 ± 4	74 ± 6	72 ± 2	48 ± 8	43 ± 2	47 ± 5	43 ± 11	40 ± 4
1,1,2-trichloroethane	84 ± 2	85 ± 3	77 ± 4	81 ± 4	77 ± 2	52 ± 9	65 ± 14	56 ± 2	46 ± 6	43 ± 16
tetrachloroethylene	69 ± 1	69 ± 3	71 ± 16	63 ± 3	65 ± 5	42 ± 7	39 ± 1	42 ± 3	38 ± 8	37 ± 11
dibromochloromethane	79 ± 1	86 ± 1	71 ± 3	74 ± 5	72 ± 1	47 ± 9	47 ± 1	48 ± 4	43 ± 8	34 ± 8
bromoform	79 ± 1	79 ± 3	72 ± 2	70 ± 2	65 ± 2	45 ± 5	42 ± 3	46 ± 3	39 ± 6	41 ± 5
benzene	72 ± 5	73 ± 8	71 ± 4	74 ± 3	71 ± 6	49 ± 8	40 ± 4	46 ± 5	41 ± 13	28 ± 2
toluene	75 ± 1	76 ± 3	69 ± 5	66 ± 3	68 ± 4	45 ± 7	37 ± 1	41 ± 5	37 ± 6	33 ± 5
chlorobenzene	68 ± 3	70 ± 2	64 ± 2	64 ± 5	63 ± 2	42 ± 8	34 ± 2	38 ± 4	31 ± 7	29 ± 4
p-xylene	70 ± 1	72 ± 2	65 ± 2	64 ± 4	66 ± 2	42 ± 8	33 ± 2	38 ± 3	32 ± 6	33 ± 9
o-xylene	68 ± 2	72 ± 2	66 ± 3	65 ± 4	64 ± 2	41 ± 8	34 ± 3	37 ± 3	32 ± 6	32 ± 7
o-chlorotoluene	65 ± 1	70 ± 4	63 ± 2	63 ± 4	61 ± 2	40 ± 6	32 ± 4	42 ± 4	34 ± 9	29 ± 4
p-chlorotoluene	69 ± 3	72 ± 4	66 ± 1	67 ± 6	62 ± 1	44 ± 10	36 ± 3	44 ± 4	37 ± 11	32 ± 2
fluorobenzene[b]	85 ± 1	92 ± 4	87 ± 3	87 ± 4	89 ± 4	85 ± 4	80 ± 1	86 ± 2	90 ± 4	80 ± 8

[a] Recovery values are mean ± standard deviation. (n = 3). [b] Internal standard.

Table IV. Time Study % Recovery of Various Organics from Spiked Clay[a]

compound	% recovery				
	day 1	day 7	day 14	day 30	day 90
carbon tetrachloride	94 ± 4	76 ± 8	83 ± 6	103 ± 8	93 ± 7
1,2-dibromoethane	87 ± 6	76 ± 6	75 ± 5	84 ± 3	71 ± 2
1,1,2,2-tetrachloroethane	78 ± 8	77 ± 10	76 ± 3	72 ± 5	81 ± 6
benzene	99 ± 2	86 ± 10	88 ± 9	96 ± 14	84 ± 7
toluene	95 ± 9	95 ± 8	96 ± 6	111 ± 7	86 ± 7
chlorobenzene	76 ± 6	75 ± 8	86 ± 1	86 ± 3	72 ± 6
p-xylene	70 ± 5	79 ± 7	85 ± 1	88 ± 3	70 ± 6
o-xylene	74 ± 5	69 ± 6	82 ± 10	78 ± 2	59 ± 7
o-chlorotoluene	57 ± 8	58 ± 3	61 ± 8	62 ± 5	40 ± 2
p-chlorotoluene	57 ± 2	66 ± 2	61 ± 8	59 ± 7	28 ± 1
fluorobenzene	88 ± 9	80 ± 11	86 ± 4	86 ± 7	95 ± 3

[a] All analysis were done in triplicate. Method "PE-2" of purging was used.

Table V. Losses on Transfer by Two Methods[a]

compound	method	
	TR-1	TR-2
benzene	11 ± 1	37 ± 4
toluene	13 ± 2	36 ± 3
chlorobenzene	18 ± 3	34 ± 5
o-xylene	20 ± 2	31 ± 5
p-xylene	21 ± 6	37 ± 5
o-chlorotoluene	22 ± 2	35 ± 7
p-chlorotoluene	24 ± 3	35 ± 7
chloroform	13 ± 2	33 ± 6
1,1,1-trichloroethane	8 ± 1	22 ± 5
carbon tetrachloride	7 ± 1	14 ± 4
trichloroethylene	15 ± 1	34 ± 6
bromodichloromethane	17 ± 3	36 ± 2
1,1,2-trichloroethane	30 ± 4	45 ± 3
tetrachloroethylene	20 ± 2	29 ± 4
1,2-dibromoethane	29 ± 3	45 ± 5
1,1,2,2-tetrachloroethane	36 ± 5	42 ± 6
bromoform	33 ± 4	53 ± 5
fluorobenzene	80 ± 4	88 ± 6

[a] Recovery values are mean ± standard deviation (n = 3).

Table VI. Recovery[a] (%) in Spiked Clay[b]

compound	recovery, %	recovery,[c] %
chloroform	98 ± 3	114 ± 7
1,1,1-trichloroethane	86 ± 3	107 ± 12
carbon tetrachloride	73 ± 4	89 ± 12
trichloroethylene	102 ± 4	94 ± 17
bromodichloromethane	94 ± 6	90 ± 60
1,1,2-trichloroethane	97 ± 7	ND
tetrachloroethylene	87 ± 5	136 ± 25
dibromochloromethane	92 ± 6	74 ± 25
bromoform	80 ± 1	69 ± 4
benzene	122 ± 4	ND[d]
toluene	102 ± 4	ND
chlorobenzene	84 ± 1	ND
p-xylene	77 ± 2	ND
o-xylene	79 ± 1	ND
o-chlorotoluene	83 ± 3	ND
p-chlorotoluene	80 ± 3	ND
1,1,2,2-tetrachloroethane	87 ± 0	52 ± 8
fluorobenzene	90 ± 6	83 ± 8

[a] Recovery values are mean ± standard deviation. [b] 15 g of clay spiked with 0.1 μg of each analyte in 4.5 mL of water using method SS-2 of spiking and PE-1 of purging. [c] Spiking and purging were done as above but with 0.015 μg of each analyte. [d] ND = not detected.

transferred from one container to another (Table V).

We have shown that volatiles in sediments can be analyzed by closed-loop stripping with Porapak N as adsorbent. This method does not require any special equipment and is easy to carry out. By use of the criteria of signal to noise ratio of 5:1 for a 15-g sample, a detection limit of 7 ng/g for PI-active and 1 ng/g for most electron-capturing compounds can be achieved (Table VI). To achieve analytical accuracy the methanol eluate can be subjected to multiple analyses on various columns or detectors. To keep handling of the samples to a minimum, the same container should be used for sampling and purging. If a sample must be stored for an extended time,

methanol should be added to keep the loss of volatiles to a minimum.

Registry No. Chloroform, 67-66-3; 1,1,1-trichloroethane, 71-55-6; trichloroethylene, 79-01-6; carbon tetrachloride, 56-23-5; bromodichloromethane, 75-27-4; 1,1,2-trichloroethane, 79-00-5; tetrachloroethylene, 127-18-4; 1,2-dibromoethane, 106-93-4; bromoform, 75-25-2; 1,1,2,2-tetrachloroethane, 79-34-5; benzene, 71-43-2; toluene, 108-88-3; chlorobenzene, 108-90-7; *p*-xylene, 106-42-3; *o*-xylene, 95-47-6; *p*-chlorotoluene, 106-43-4; *o*-chlorotoluene, 95-49-8.

LITERATURE CITED

(1) May, W. F.; Chester, S. N.; Crain, S. P.; Gump, B. H.; Hertz, H. S.; Enagonio, D. P.; Dyszel, S. M. *J. Chromatogr. Sci.* **1975**, *13*, 535-540.
(2) Hiat, M. H. *Anal. Chem.* **1981**, *53*, 1541-1543.
(3) Van Tassel, S.; Amalfatino, N.; Narang, R. S. *Anal. Chem.* **1981**, *53*, 2130-2135.
(4) Bush, B.; Narang, R. S. *Anal. Chem.* **1980**, *52*, 2076-2079.

RECEIVED for review July 16, 1984. Accepted November 9, 1984.

Synthesis and Properties of High-Temperature Mesomorphic Polysiloxane Solvents: Biphenyl- and Terphenyl-Based Nematic Systems

M. A. Apfel, H. Finkelmann,[1] G. M. Janini,[2] R. J. Laub,* B.-H. Lühmann,[1] A. Price, W. L. Roberts, T. J. Shaw, and C. A. Smith

Department of Chemistry, San Diego State University, San Diego, California 92182

The synthesis and characterization of a variety of mesomorphic (liquid-crystalline) side-chain polysiloxane (MEPSIL) solvents, said to be useful as gas chromatographic stationary phases, are described and discussed. The synthetic scheme is based upon the hydrosilation reaction that occurs when 4-(allyloxy)benzoyl esters are contacted with poly(methylsiloxane) in the presence of a dicyclopentadienylplatinum(II) catalyst, while product characterization is carried out by IR, NMR, GC, DSC, elemental analysis, and direct-observation hot-stage light-polarized microscopy. Selectivity of the MEPSIL phases is shown to differ very substantially from those exhibited by all other common GC solvents. The MEPSIL found overall to be the best suited as a GC stationary liquid exhibits a melting point of 139 °C (k → n) and a nematic/isotropic (n → i) transition temperature of 319 °C, while the practical operating limits of the material span 150 to in excess of 300 °C.

The development and optimization of chromatographic techniques for maximal resolution in minimal time of analysis, coupled with maximum sample throughput, continue to represent a substantial problem when dealing with analytes comprised of structurally related isomers. Among the most notably difficult of these are polycyclic aromatic hydrocarbons (PAH) which are, at the very least, ubiquitous environmental pollutants produced by the incomplete combustion of organic matter. Moreover, some of the most efficient carcinogens known at present are members of, or products derived directly from, this class of compounds. In addition, the carcinogenic and mutagenic properties of these materials are frequently found to be isomer specific. Major efforts have therefore been directed in chromatography at the separation of these species (*1*).

Reverse-phase packings and selective detection in column-liquid (*2*) and supercritical fluid (*3*) chromatographic techniques have been utilized for the separation of PAH isomers in a number of cases; however, the present state of technology in each of these methods precludes the high column efficiency necessary for analysis of complex mixtures comprised of large numbers of components.

In gas-liquid chromatography (GLC), studies of the separation of PAH have been concerned mainly with the fabrication of open-tubular columns of ever-higher efficiency with "slightly polar" phases such as SE-52 and SE-54. And, while some degree of success has certainly attended these efforts (*4, 5*), it is nonetheless fair to say that the resolution of isomers such as anthracene/phenanthrene, benz[*a*]anthracene/triphenylene/chrysene, and benzo[*a*]pyrene/benzo[*e*]pyrene/perylene/benzofluorenes is not entirely satisfactory, particularly when quantitation of these materials is attempted at parts-per-billion levels in natural or industrial matrices.

In contrast, it has been recognized for some time that liquid-crystalline (mesomorphic) stationary phases (the nematic state in particular) provide enhanced GLC separations of many isomeric species, including PAH, that are difficult or impossible to resolve by other traditional chromatographic techniques (*1, 6-13*). Unlike most other common GLC solvents that provide separations based upon solute vapor pressure and/or differential solubility arising from specific energetic interactions, nematic stationary phases yield separations based upon differences in solute molecular shape or, in the instance of cholesteric phases, solute chirality. Simply put, rodlike mesomorphs exist in the bulk-liquid state in well-ordered domains such that the more rodlike the solute isomer, the more readily it is accommodated into the nematic matrix and, hence, the longer it is retained. Thus, mesomorphic solvents provide selectivity on an entirely different basis from all other GLC stationary phases.

However, the liquid-crystal phases reported to date suffer from column bleed as a result of volatility at high temperatures, poor column efficiency as a result of slow kinetics of mass transfer, and restricted useful nematic ranges. Even so, Laub and his co-workers (*14-18*) have argued that a suitable member representative of this class of materials must be

[1] Present address: Institut für Physikalische Chemie der Technischen Universität Clausthal, D-3392 Clausthal-Zellerfeld, West Germany.
[2] Present address: Department of Chemistry, University of Kuwait, Kuwait, Kuwait.

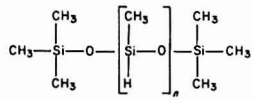
0003-2700/85/0357-0651$01.50/0 © 1985 American Chemical Society

defined in order, if nothing else, to identify a standard set of stationary phases (i.e., no more than a half dozen or so solvents) with which all GLC separations can be achieved (*19–26*). Accordingly, and in attempts at overcoming the limitations of mesomorphic materials, Laub, Roberts, and Smith (*18*) blended *N,N'*-bis(*p*-butoxybenzylidene)-α,α'-bi-*p*-toluidine (BBBT; nematic) stationary phase with SE-52. This resulted in much improved column efficiency but, in spite of the reduction of column bleed in approximate accord with Raoult's law, there remained the inconvenience of fabrication of blended-phase systems; nor could the useful temperature range of the liquid–crystalline phase be expanded.

As a result, the synthesis of nematic siloxane polymers exhibiting high column efficiency as well as low bleed, yet providing high selectivity over a wide temperature span, was undertaken by us several years ago, the preliminary results of which we have reported elsewhere (*17, 27*). The compounds synthesized initially comprised a series of grafted polymers in which the liquid–crystalline side chains resembled the teeth of a comb, attached with flexible spacers, running the length of the polymer backbone. However, in independent evaluations carried out by others on materials synthesized in this laboratory (*28*), the earlier versions of these species, since christened by us MEPSIL (mesomorphic polysiloxanes), were found to suffer from the drawbacks of comparatively meager column efficiency and poor thermal stability arising from incomplete substitution of all available hydrogen on the starting poly(methylsiloxane), as well as polymer cross linking. Moreover, the batch-to-batch reproducibility of the synthetic procedures, as well as yields, was poor. We therefore undertook to clarify, then simplify, the synthesis scheme, and then to synthesize and characterize fully a variety of MEPSIL products. We report in this work the results for biphenyl- and terphenyl-based nematic systems. In addition, and for the first time, we provide in detail descriptions of each synthetic step, including equivocal aspects that we have come across during the course of our studies, in order to encourage continued investigations of these materials by others (*29*).

EXPERIMENTAL SECTION

Materials. Poly(methylsiloxane) of the general formula



was obtained from Silar, Petrarch, or Wacker Chemie (Munich, West Germany). All other chemicals and reagents were from Aldrich Chemical Co.

Apparatus and Equipment. Differential scanning calorimetry (DSC) was performed with a Perkin-Elmer Model DSC-2. Light microscopy was carried out with a Leitz (West Germany) microscope equipped with a cross-polarized light source and fitted with a Reichert (Austria) hot stage. Viscosities were measured with an Ostwald tube at 25 °C (*30*) utilizing water as a reference. Systems were thermostated with a Neslabs RTE-8 water bath. Gel permeation chromatography (GPC) was conducted with a TSK-3000 column (Varian) and THF solvent, with a Varian Model 5000 liquid chromatograph and Varian Variable UV-Vis detector set at 220 nm. The gas chromatograph used throughout was a Carlo Erba 4160. Chromatograms were obtained on a 1-mV full-scale Linear strip chart recorder at the highest electrometer setting of the GC. Pyrex glass-capillary columns (15 m × 0.25 mm i.d.) were drawn with a Shimadzu GDM-1 glass-drawing machine. Mass spectral data were acquired with an AEI MS-9 mass spectrometer. Infrared spectrometry was performed with a Perkin-Elmer Model 337, while nuclear magnetic resonance spectrometry was carried out with a Varian Model HA-100. The rotating-disk thin-layer chromatograph was an Hitachi CLC-5 equipped with a 5-cm spacer ring. Elemental analyses were performed by Galbraith Laboratories. The centrifuge was a Du Pont Sorval Model RC-5B refrigerated superspeed.

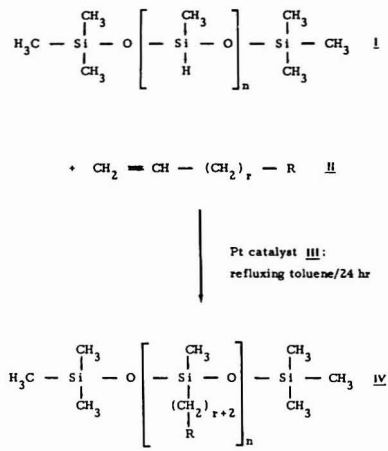


Figure 1. Reaction scheme for synthesis of MEPSIL solvents.

GC Column Fabrication and Utilization. Drawn tubes were leached with 20% HCl overnight and subsequently flushed with 0.75 M HCl and then water. They were dried at 250 °C, followed by silylation with hexamethyldisilazane as described by us previously (*14, 31*). After being rinsed with methanol and dried with nitrogen, a typical column was filled with a solution of 1.6 mg cm^{-3} MEPSIL polymer in chloroform, calculated so as to produce a film thickness of ca. 0.1 μm. One end was then sealed and the other end attached to a vacuum pump, and the entire column placed in a water bath at 35 °C in order to hasten the evaporation of volatile solvent. Columns were conditioned at 300 °C with hydrogen (the carrier gas in all instances) until a stable base line was obtained at the maximum sensitivity of the instrument. The mobile phase was split at a ratio of 50:1 in order to maintain an average linear velocity of 40 cm s^{-1} as measured from the retention time of methane.

Synthetic Procedures. The general reaction scheme is shown in Figure 1. Poly(methylsiloxane) (I) is contacted (refluxing toluene solvent; 24 h) with monomer II containing a vinyl group whereupon, in the presence of a platinum catalyst III, hydrosilation takes place yielding the desired mesomorphic polysiloxane (MEPSIL) IV.

Preparation and Properties of Reactant Polymer I. Poly(methylsiloxane) materials vended commercially are polydisperse, and it was found to be beneficial from the standpoint of product reproducibility to remove low- to intermediate molecular weight homologues. This was carried out just prior to use of the polymer in grafting reactions by isothermal dissolution of the starting material twice from benzene by the addition of methanol at 20 °C (*32*). Thus, 20 cm^3 polymer was taken up in 80 cm^3 benzene and placed in a 250-cm^3 separatory funnel to which had been attached a glass water jacket. Methanol (140 cm^3) was then added gradually with mechanical stirring with a glass rod. The solution was allowed to stand for 2 h, whereupon two phases separated. The lower layer (ca. 80% v/v of the starting polymer) was then drawn off and the procedure was repeated with it with 80 cm^3 benzene and 100 cm^3 methanol. The recovered polymer was then placed in a vacuum line at 10^{-3} torr for 12 h in order to remove any residual dissolved methanol. The product was stored under nitrogen; recoveries amounted routinely to 40% v/v, i.e., 8 cm^3 of polymer. The appearance of gas bubbles upon the addition of methanol indicated that the solution temperature was too high: methanol reacts with siloxane hydrogen at elevated temperatures to produce molecular hydrogen (given off as a gas) and poly(methoxymethylsiloxane).

The densities of the starting polymers (Silar, I.A.1; Petrarch, I.B.1; Wacker, I.C.1) were all ca. 0.98–1.02 g cm^{-3} at 25 °C. The averages of three repetitive determinations of viscosities at 25 °C were as follows: I.A.1, (value not quoted by the manufacturer), 28.8 mm^2 s^{-1} found; I.B.1, 15–30 mm^2 s^{-1} stated by the manufacturer, 26.4 mm^2 s^{-1} found; I.C.1, 30 mm^2 s^{-1} stated, 31.9 mm^2 s^{-1} found. The stated molecular weights were 3500 for I.A.1 (n = 58 in Figure 1) and 2270 for I.C.1 (n = 38), although the viscosities belie these values. No molecular weight information was provided for I.B.1 although, considering the viscosity data, it must presumably be less than ca. 2500 (n = 40). The high molecular weight fraction of the Silar polymer, I.A.2, was used throughout in what follows.

Synthesis of 4-(Allyloxy)benzoyl Chloride. The spacer group linking the polymer backbone with the mesomorphic side-chain unit comprised throughout this work 4-(allyloxy)benzoic acid ester, the acid chloride precursor to which was synthesized in two stages. First, 4-(allyloxy)benzoic acid was prepared as follows: into a 1-L three-neck round-bottom flask equipped with a reflux condenser, an addition funnel, a heating bath, and a magnetic stirrer was placed 90 g (0.65 mol) of 4-hydroxybenzoic acid; to this was added 400 cm^3 of methanol at 25 °C, which produced a brown solution. To this solution was added dropwise 105 g (1.9 mol) of potassium hydroxide in 125 cm^3 of distilled water. The reaction was heated to reflux and 90 g (0.74 mol) of allyl bromide was then added over a 1-h period. The reaction mixture was allowed to reflux for 8 h at which point 250 cm^3 of methanol was removed by single-stage distillation. The remainder of the reaction mixture was cooled to 25 °C and added to 1 dm^3 of distilled water. The aqueous solution was extracted three times with 200 cm^3 of diethyl ether to remove organic impurities and the ether layer was discarded. The remaining aqueous phase was heated to 40 °C in a fume hood and neutralized with 300 cm^3 of 20% aqueous HCl, which caused the product to precipitate. The crude acid was recovered by suction filtration and purified by recrystallizing twice from ethanol, yielding 107 g (60%), mp 165 °C.

4-(Allyloxy)benzoyl chloride was then prepared as follows: to a 100-cm^3 round-bottom flask equipped with a reflux condenser, a drying tube, a magnetic stirrer, and a heating bath was added 50 g (0.28 mol) of 4-(allyloxy)benzoic acid prepared as above, 50 cm^3 (0.42 mol) of thionyl chloride, and 10 drops of dimethylformamide. The reaction mixture was protected from moisture and allowed to stir overnight at room temperature. It was then heated to 60 °C for 2 h to ensure complete reaction. The excess thionyl chloride was removed in vacuo and the crude product was vacuum distilled at 100 °C/1 torr yielding 50 g (90%) as a pale yellow liquid which was stored in a tightly sealed glass bottle.

Synthesis of [4-(Allyloxy)benzoyl]-4-methoxyphenyl Monomer II.A. Into a 250-cm^3 three-neck round-bottom flask equipped with a reflux condenser, a drying tube, a dropping funnel, and a magnetic stirrer was placed 14 g (0.11 mol) of 4-methoxyphenol, 150 cm^3 of dry THF, and 16 cm^3 of pyridine. The mixture was protected from moisture with nitrogen. Over a 2-h period, 22 g (0.11 mol) of 4-(allyloxy)benzoyl chloride in 20 cm^3 of dry pyridine was added through the dropping funnel. The mixture was stirred at room temperature for 4 h after the addition was completed. It was then heated to 60 °C for 2 h; after cooling, the reaction mixture was added to 200 cm^3 of distilled water and then neutralized with 20% aqueous hydrochloric acid. The solution was then extracted three times with diethyl ether, the organic phase being saved. The ether was removed by rotary evaporation and the crude product, II.A, was recrystallized twice from ethanol yielding 20 g (64%), mp 87–88.5 °C.

Synthesis of 4-[[4-(Allyloxy)benzoyl]oxy]-4'-methoxybiphenyl Monomer II.B. To 400 cm^3 of 10% aqueous sodium hydroxide cooled to 0 °C in an ice bath was added 75 g (0.40 mol) of 4,4'-dihydroxybiphenyl with vigorous stirring. Fifty grams (0.40 mol) of dimethyl sulfate was then added under a nitrogen atmosphere to the reaction mixture over a period of 1 h, again with vigorous stirring. After the addition was complete, the resultant precipitate was removed by filtration with a sintered glass filter and redissolved in 400 cm^3 of 10% aqueous sodium hydroxide. The solution was heated briefly to boiling and allowed to cool, followed by filtration. The solid mass was placed in 2 dm^3 of water, heated to boiling, and this time filtered while hot. The filtrate was then heated to 70 °C, and 20% aqueous hydrochloric acid was added until the solution became acidic. The product thereupon precipitated as white crystals, which were recrystallized twice from ethanol yielding 24 g (30%) of 4-hydroxy-4'-methoxybiphenyl.

Next, into a 250-cm^3 three-neck round-bottom flask equipped with a dropping funnel, a reflux condenser, and a magnetic stirrer was placed under a nitrogen blanket 12 g (0.06 mol) of 4-hydroxy-4'-methoxybiphenyl, prepared as above, dissolved in 100 cm^3 of dry pyridine. To this solution was added 12 g (0.06 mol) of 4-(allyloxy)benzoyl chloride dissolved in 20 cm^3 of pyridine over a 1-h period with stirring. The mixture was stirred for an additional 3 h at room temperature, and then heated to 60 °C for 2 h. It was cooled again to room temperature, and then added to 400 cm^3 of distilled water, following which the mixture was acidified with 20% aqueous hydrochloric acid. The resultant precipitate was removed by suction filtration and washed with 400 cm^3 of saturated aqueous sodium bicarbonate, and then with 400 cm^3 of distilled water. The crude solid, II.B, was recrystallized twice from acetone yielding 15 g (70%), mp 147–148.5 °C.

Synthesis of 4-[[4-(Allyloxy)benzoyl]oxy]-4'-methoxy-p-terphenyl Monomer II.C. Into a 2-dm^3 three-neck round-bottom flask equipped with an addition funnel, a reflux condenser, and a mechanical stirrer was placed 11 g (0.45 mol) of magnesium turnings and 8 cm^3 of p-bromoanisole dissolved in 200 cm^3 dry tetrahydrofuran (THF). A small crystal of iodine was introduced and the reaction mixture, under nitrogen, was heated to reflux with a water bath. After the reaction had begun, 48 cm^3 of p-bromoanisole dissolved in 900 cm^3 of THF was added over a 1-h period with stirring. To the product mixture, i.e., p-anisylmagnesium bromide, still under nitrogen, was added 25 g (0.22 mol) of 1,4-cyclohexadienone dissolved in 220 cm^3 of THF over a 35-min period. Vigorous stirring was continued for an additional hour. The resultant solution was then poured into 1 dm^3 of 10% aqueous ammonium chloride. The organic phase was recovered in a separatory funnel, washed with water, and dried over sodium sulfate. The solvent was removed by rotary evaporation, yielding 57 g of an oil. This was redissolved in 1.30 dm^3 of toluene containing 3.6 g of p-toluenesulfonic acid. The reaction mixture was refluxed for 6 h, water produced during the reaction being removed with a Dean–Stark trap. The solution was then cooled in ice water, and the solid precipitate, 4,4'-dimethoxy-p-terphenyl, was removed by filtration yielding 10 g (15%), mp 270–275 °C.

Next, in a 1-dm^3 three-neck round-bottom flask equipped with a reflux condenser, a pressure-equalizing addition funnel, a magnetic stirrer, and an oil bath was placed the above-described 10 g (0.034 mol) of 4,4'-dimethoxy-p-terphenyl in 600 cm^3 of dry benzene, the mixture then being taken to reflux. To this solution was added 11 cm^3 of 1 M boron tribromide in benzene over a 2-h period. The mixture was refluxed an additional 2 h and then cooled to room temperature. Subsequently, it was added to 400 cm^3 of water, the organic phase was removed, and the aqueous phase extracted with two 500-cm^3 portions of warm toluene. All of the organic phases were combined and reduced to dryness by rotary evaporation. The crude product, 4-hydroxy-4'-methoxy-p-terphenyl, was purified by rotating-disk thin-layer chromatography (*33*, *34*) with silica stationary phase and dichloromethane mobile phase; the yield was 0.3 g (3%).

Finally, into a 25-cm^3 round-bottom flask equipped with a reflux condenser, a magnetic stirrer, and an oil bath was placed the above-described 0.3 g (0.0011 mol) of 4-hydroxy-4'-methoxy-p-terphenyl and 0.5 g (0.0025 mol) of 4-(allyloxy)benzoyl chloride in 15 cm^3 of dry pyridine. The mixture was refluxed for 24 h; after cooling to room temperature, it was added to 30 cm^3 of distilled water and acidified with 20% aqueous hydrochloric acid. The precipitate was filtered off and washed with 50 cm^3 of saturated aqueous sodium bicarbonate, and then 75 cm^3 of distilled water. The crude product, II.C, was purified by rotating-disk thin-layer chromatography, yielding 0.2 g (41%).

Synthesis of [4-(Allyloxy)benzoyl]biphenyl Monomer II.D. Into a 250-cm^3 round-bottom flask equipped with a reflux condenser and a magnetic stirrer was placed 4.85 g (0.029 mol) of 4-phenylphenol dissolved in 50 cm^3 of dry pyridine under nitrogen. To this solution was added 5.7 g (0.029 mol) of 4-(allyloxy)benzoyl chloride with stirring. The mixture was stirred for 3 h at room temperature and then heated to 60 °C for an additional 2 h. After the reaction mixture had cooled, it was added to 200 cm^3 of water, and then acidified with 20% aqueous hydrochloric acid. The

resultant precipitate was removed by suction filtration and washed with 200 cm^3 of distilled water. The crude product, II.D, was recrystallized from 1:1 v/v acetone:ethanol yielding 7 g (75%), mp 138–140 °C.

Synthesis of [4-(Allyloxy)benzoyl]-p-terphenyl Monomer II.E. To a vigorously stirred suspension of 50 g (0.22 mol) of *p*-terphenyl in 250 cm^3 of refluxing glacial acetic acid was added a solution of 35 cm^3 red fuming nitric acid and 55 cm^3 of acetic acid over a 4-h period. The mixture was then cooled in an ice bath, whereupon the solid yellow precipitate, 4-nitro-*p*-terphenyl, was removed by filtration with a sintered glass funnel. The crude product was recrystallized from nitromethane yielding 50 g (85%), mp 209–213 °C.

Next, into a 2-dm^3 three-neck round-bottom flask equipped with a mechanical stirrer, a reflux condenser, a dropping funnel, and an oil bath was placed 20 g (0.07 mol) of 4-nitro-*p*-terphenyl, prepared as described above, and 1 dm^3 of 95% ethanol. After warming to 50 °C, 0.1 g of a catalyst consisting of 10% palladium on charcoal was added and stirring was commenced. Ten cubic centimeters of hydrazine hydrate was then added from the dropping funnel over a period of 30 min. After the addition was complete, another 0.1 g of catalyst was added and the mixture then refluxed for 4 h. The hot solution was filtered through Celite to remove the catalyst and the filtrate taken to dryness with a rotary evaporator. The crude product, 4-amino-*p*-terphenyl, was purified by rotating-disk thin-layer chromatography. The yield was 17 g (85%), mp 200–202 °C.

4-Hydroxy-*p*-terphenyl was then prepared as follows: in a 1-dm^3 three-neck round-bottom flask fitted with a mechanical stirrer, a dropping funnel, and a thermometer was placed 8.9 g (0.036 mol) of 4-amino-*p*-terphenyl in 250 cm^3 of glacial acetic acid. The mixture was heated to 70 °C with stirring. Next, 32 cm^3 of concentrated sulfuric acid was added dropwise as the mixture was cooled to 0 °C in an ice–salt bath. A solution of 3.4 g of sodium nitrite in 15 cm^3 of water was then added over a 20-min period. Stirring was continued for 15 min, following which 250 cm^3 of ice water containing 4 g of urea was added in small portions. The mixture was filtered by suction while being maintained at 5 °C. Separately in a 2-dm^3 one-neck round-bottom flask was placed 500 cm^3 of water and 120 cm^3 of concentrated sulfuric acid. The mixture was heated to reflux, to which was added the cold diazonium solution over a 20-min period, refluxing then being continued for an additional 30 min. The mixture was then cooled and the crude product, 4-hydroxy-*p*-terphenyl, was purified by sublimation at 170 °C/0.2 torr yielding 0.5 g (5%), mp 273–276 °C.

Finally, into a 50-cm^3 round-bottom flask equipped with a reflux condenser, a magnetic stirrer, and an oil bath was placed 0.43 g (0.0017 mol) of 4-hydroxy-*p*-terphenyl and 0.5 g (0.0025 mol) of 4-(allyloxy)benzoyl chloride dissolved in 20 cm^3 of dry pyridine. The mixture was refluxed for 24 h. After cooling to room temperature, the reaction mixture was added to 50 cm^3 of distilled water, and then acidified with 20% aqueous hydrochloric acid. The precipiate was filtered and washed with 100 cm^3 saturated aqueous sodium bicarbonate, followed by 100 cm^3 of distilled water. The crude product, II.E, was recrystallized from toluene yielding 0.5 g (72%).

Synthesis of Dicyclopentadienylplatinum(II) Chloride Catalyst III. The catalyst used for all grafting reactions was dicyclopentadienylplatinum(II) chloride, III. We found that the synthesis of this material described by Stille and Fox (*35*) did not proceed as described and that what yields were obtained were poor; we therefore developed a synthetic route to the catalyst that was based upon those reported by Kharasch and Ashford (*36*) and Drew and Doyle (*37*). Thus, 2.76 g of hydrated chloroplatinic acid was dissolved in 6 cm^3 of glacial acetic acid in a 25-cm^3 flask. The solution was diluted with 10 cm^3 of water and then heated to 70 °C. Two cubic centimeters of dicyclopentadiene was then added to the reaction vessel, and the mixture was stirred vigorously for 24 h at this temperature. The crude product was collected by filtration, decolorized with charcoal, and finally recrystallized twice from tetrahydrofuran, yielding 1.2 g (71%), mp 218 °C. The structure wsa verified by NMR and by MS.

Synthesis of MEPSIL Polymers IV.A–E. Into a 250-cm^3 round-bottom flask modified with a stopcock and an injection port was placed 2.3×10^{-3} mol of 4-allyloxybenzoyl ester II (e.g., 1.0 g of II.B) dissolved in 100 cm^3 of dry and freshly distilled toluene. Into this was pipetted 0.15 g (4.29×10^{-5} mol; 60.1 g $equiv^{-1}$) of starting polymer I.A.2, i.e., a 10% excess of monomer over a mole ratio of 1:1 based upon siloxane hydrogen. The flask was then equipped with a reflux condenser and the contents were protected from moisture and air with a stream of nitrogen. The reaction mixture was heated to boiling, and 100 μg of catalyst per gram of product, III, was then injected with a syringe as a solution (1 mg cm^{-3}) in dichloromethane. The mixture was refluxed under nitrogen atmosphere at 110 °C for 24 h. The solution was then cooled and the product precipitated by the addition of an excess of methanol. Following this, the product was collected by centrifugation at 15 000 rpm for 20 min. The supernatant was discarded and the polymer taken up in toluene, following which it was reprecipitated with methanol and collected once more by centrifugation. The wet gellike material was partially dried under a stream of nitrogen, drying being taken to completion in a vacuum oven at 110 °C for 24 h.

Replicate elemental analyses were performed on MEPSIL IV.B. Anal. Calcd. for $Si_{60}C_{1398}H_{1410}O_{291}$: Si, 6.86; C, 68.39; H, 5.79; O, 18.96 w/w. Found: Si, 6.96; C, 67.48; H, 5.81; and O, 19.47 w/w.

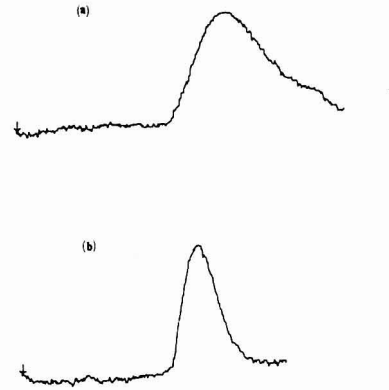


Figure 2. Gel permeation chromatograms (a) of reactant-polymer I.A.1 as received and (b) after fractional dissolution twice from benzene: column, TSK 3000H; detection at 220 nm; 0.05 absorbance units full scale; flow rate, 1.0 cm^3 min^{-1} of tetrahydrofuran mobile phase.

RESULTS AND DISCUSSION

Reactant–Polymer Preparation. Figure 2 illustrates the effects of the clean-up procedure on the molecular weight distribution of the reactant polymer I. The trace shown in (a) is the gel permeation chromatogram of starting material as received from Silar (I.A.1), while that in (b) (I.A.2) shows the GPC obtained after fractional dissolution. The polydispersity has clearly been reduced substantially. The material in (b), the higher molecular weight fraction of the starting polymer, was utilized in all subsequent reactions except as noted.

Extent of Completion of Reaction. The extent of completion of hydrosilation had previously been assessed by us by grating IR, where the Si–H absorption band at 2180 cm^{-1} was monitored. We have since found this method to be insensitive above ca. 75% completion and so utilized throughout this work the proton NMR band seen for Si–*H*. Typical NMR spectra of unreacted polymer I.A.2 (a), monomer II.B (b), and fully reacted polysiloxane polymer IV.B (c) are given as examples in Figure 3. The band-broadening seen in (c) is characteristic generally of the NMR spectra of side-chain polymers.

Transition Temperatures of Homomonomer MEPSIL Solvents. Table I lists the transition temperatures of mo-

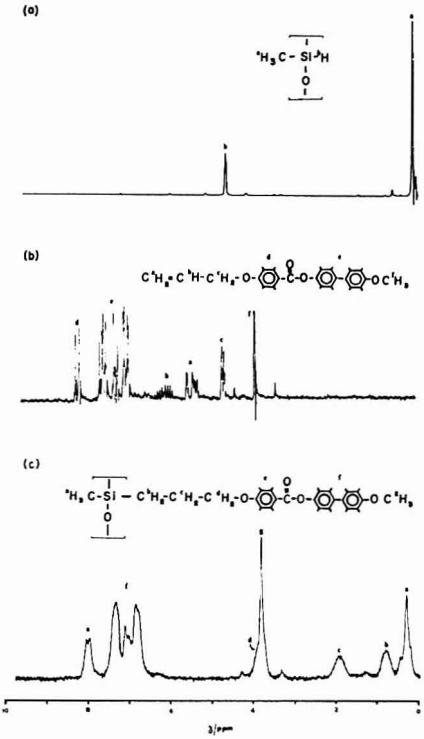


Figure 3. Proton NMR spectra (a) of unreacted starting poly(methylsiloxane) I.A.2, (b) (4-allyoxybenzoyl)-4′-methoxybiphenyl starting monomer II.B, and (c) fully reacted MEPSIL IV.B.

nomers II.A–E as well as those of the resultant MEPSIL polymers IV.A–E. These data demonstrate that attachment of the low molecular weight mesomorphs utilized in this work to a polymeric backbone via a flexible spacer does not result in destruction of the liquid-crystalline nature of the monomers but does alter their transition temperatures, although the extent to which this occurs is at present difficult to predict in advance. For example, mesomorphic monomers may give polymers that do not exhibit liquid crystallinity, while the converse is also true, that is, nonmesomorphic monomers in some instances yield mesomorphic polymers (cf. MEPSIL IV.A).

Dependence of Transition Temperatures on Reactant–Polymer Molecular Weight. We observed during the course of these studies that utilization of reactant polymers of different average molecular weights with the same mesomorphic monomer produced MEPSIL's with different melting points but with identical mesomorphic–isotropic transition temperatures. Thus, MEPSIL's IV.B (reactant-polymer I.A.2, $n = 58$ in Figure 1) and IV.F (reactant-polymer I.C.1, $n = 38$) gave melting points of 139 and 91 °C, respectively, but near-identical nematic–isotropic transitions of 319 and 317 °C. The former data are a consequence of the dependence of the melting point on precise close packing of the molecules in the solid state, where polymers with different molecular weights pack differently. On the other hand, the only ordering

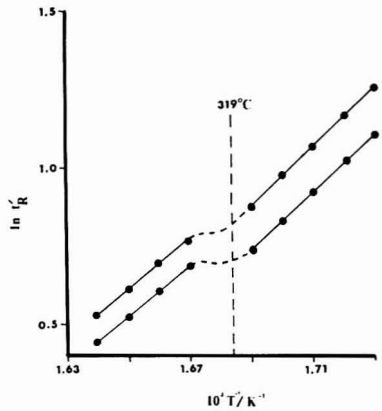
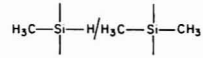


Figure 4. Plots of log t_R' against reciprocal absolute temperature for benzo[*a*]pyrene (upper curve) and benzo[*e*]pyrene solutes with MEPSIL IV.B stationary phase. Polymer transition temperature is indicated by the vertical dashed line at 319 °C.

that occurs in the liquid-crystalline state is an averaged parallel orientation of the long axis of the mesomorphic side chains, which are free to cluster regardless of the length of the backbone to which they are attached. Thus, mesomorphic–isotropic transition temperatures hardly appear to be affected by the reactant–polymer molecular weight.

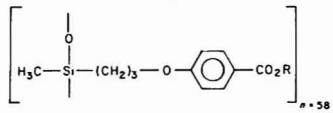
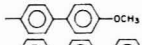
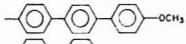
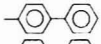
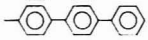
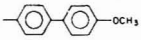
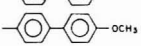
Transition Temperatures of Comonomer MEPSIL Solvents. Mesomorphic transition temperatures of MEPSIL's can be altered by the attachment of additional nonmesomorphic segments to the polymer backbone, analogous to our previous finding that dilution of low molar-mass liquid crystals substantially lowers their transition temperatures (*17*). We provide illustration of this in Table I, where MEPSIL IV.G was synthesized with a Petrarch reactant-polymer comprised of



units (i.e., methylsiloxane + dimethylsiloxane) in the number ratio 10/17. This MEPSIL gave a nematic/isotropic transition temperature of 169 °C, fully 150° lower than the corresponding MEPSIL IV.B. In addition, a smectic phase was observed for the former which extended from the melting point, 88 °C, to 115 °C, whereas the melting point of MEPSIL IV.B was 139 °C. Thus, although the melting points of MEPSIL's can be lowered by attachment of methyl groups to the polymer backbone, the upper (nematic/isotropic) transition temperatures are thereby reduced also. Even so, we believe at the present time that with the proper choice of backbone length, mesomorphic group, spacer, and percent nonmesomorphic side chains, MEPSIL's with melting points of close to room temperature as well as nematic/isotropic ranges of in excess of 300 °C may in fact be realized.

Comparison of Transition Temperatures of MEPSIL Solvents in Bulk-Liquid and Thin-Film States. We show in Figure 4 plots of log (adjusted retention time, t_R') against reciprocal absolute temperature observed for benzo[*a*]pyrene (upper curve) and benzo[*e*]pyrene with MEPSIL IV.B. The abscissa encompasses the transition of the polymer from the nematic state to the isotropic (DSC: 319 °C; vertical line in Figure 4), which is clearly visible as a discontinuity in each set of retention data. The transition temperature of meso-

Table I. Transition Temperatures[a] of Parent 4-(Allyloxy)benzoyl Ester Monomers II.A–II.E and Resultant MEPSIL Polymers IV.A–IV.G

monomer R group	R =	polymer designation	transition temp/°C monomer	transition temp/°C polymer
				
II.A		IV.A	k 88 i	g 15 n 61 i
II.B		IV.B	k 147 n 249 i	k 139 n 319 i
II.C		IV.C	k > 350	k 200 n 360 (dec) i
II.D		IV.D	k 139 i	k 95 n 125 i
II.E		IV.E	k > 350	k 200 n 360 (dec) i
II.B		IV.F[b]	k 147 n 249 i	k 91 n 317 i
II.B		IV.G[c]	k 147 n 249 i	k 87 s 124 n 170 i

[a] DSC, GLC, microscopy: g, glassy; k, crystalline; s, smectic; n, nematic; i, isotropic. [b] $n = 38$. [c] Methylsiloxane/dimethylsiloxane number ratio of 10/17.

morph IV.B in the thin-film state (i.e., GLC) hence appears to be identical with that observed for the bulk liquid (DSC), as was true also for all other MEPSIL solvents studied here. However, this may not be the case generally. Depending on the nature of the substrate upon which the liquid crystal is coated, there is the possibility that, in fact, the transition temperature might well be altered substantially. For example, separation of the two test solutes is clearly preserved (albeit diminished) with the isotropic form of MEPSIL IV.B at well in excess of 320 °C whereas, even with stationary phases that give rise to strongly energetic solute/solvent interactions (e.g., Lewis acids), the separation of benzo[a]pyrene from benzo[e]pyrene is notoriously difficult at these temperatures. Thus, there appears to exist some residual ordering of the MEPSIL solvent in the thin-film state.

Of compelling interest in this regard is the alignment of liquid crystals within what are said to be "boundary layers" existing at liquid/solid interfaces: such "boundaries" extend over several thousand angstroms in some cases, and transitions within such layers (whether first or second order is not clear at present) differ measurably from those observed for the bulk liquid (*38–42*). The matter is currently under further study, and we intend reporting shortly our work on separations carried out with MEPSIL phases in the isotropic as functions of the film thickness as well as column-wall surfaces derivatized with silylating reagents comprising a variety of chemical types.

Practical Operating Temperature Limits of MEPSIL Solvents. We found that plots of log (adjusted retention) of all test solutes with MEPSIL IV.B increased monotonously with reciprocal absolute temperature from 300 to 100 °C, which indicates that there is no change in the physical state of the mesomorphic melt on cooling to this limit. That is, MEPSIL phases can be supercooled substantially below their nominal melting points. However, by way of contrast, we show in Figure 5 plots exemplifying the relative separations (α values; here, $\alpha = k'_{\text{anthracene}}/k'_{\text{phenanthrene}}$) and resolution ($R_s$) as functions of temperature that are typical of those that we observed throughout this work. While the separation factor continues to increase as the temperature is decreased, the

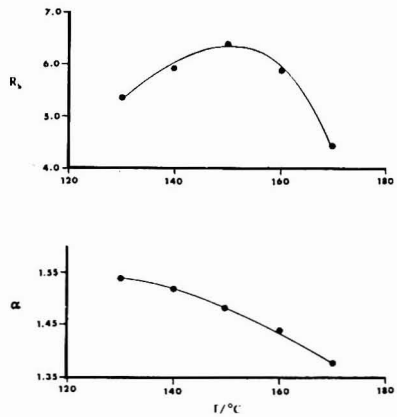


Figure 5. Plots of α values and resolution R_s against temperature for anthracene and phenanthrene solutes with MEPSIL IV.B.

resolution, which takes account of peak widths as well as peak positions, shows a maximum at ca. 150 °C. That is, there was a substantial decrease in column efficiency (increased peak broadening) near the nominal melting point. We therefore consider 150 °C to be the lower practical operating limit of MEPSIL IV.B.

The upper practical operating limits of MEPSIL phases are governed primarily by two considerations, namely, the mesomorphic–isotropic transition temperatures (beyond which, generally, the selectivity of the phases is substantially reduced) and the thermal stability of the materials. As illustrated in Figure 4, MEPSIL IV.B is in fact selective to well in excess of 320 °C; however, the thermal stability of similar compounds synthesized by us previously precluded continuous operation at much above 300 °C. Therefore, in order to test the stability

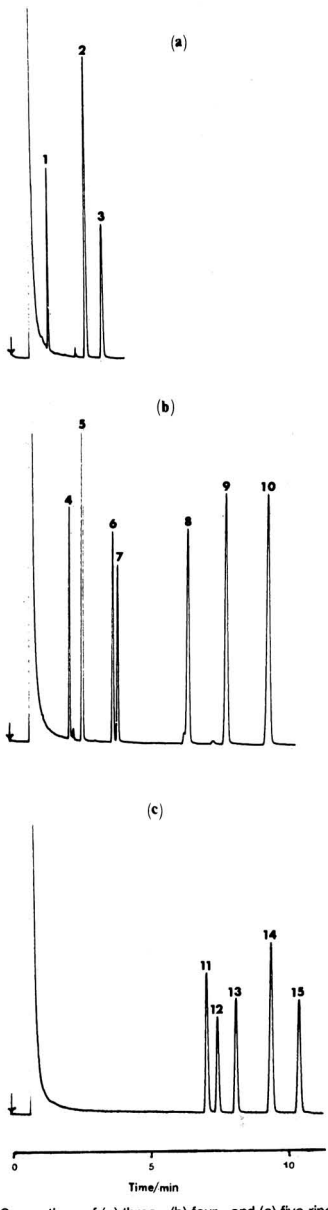


Figure 6. Separations of (a) three-, (b) four-, and (c) five-ring PAH with MEPSIL IV.B. Solutes: fluorene (1); phenanthrene (2); anthracene (3); fluoranthene (4); pyrene (5); 1,2-benzofluorene (6); 2,3-benzofluorene (7); triphenylene (8); benz[*a*]anthracene (9); chrysene (10); benzo[*b*]fluoranthene (11); benzo[*k*]fluoranthene (12); benzo[*e*]pyrene (13); perylene (14); and benzo[*a*]pyrene (15). Column temperatures: (a), 180; (b), 235; (c), 275 °C isothermal.

of materials synthesized in this work, the number of theoretical plates for benzo[*a*]pyrene and the resolution of benzo[*a*]pyrene/benzo[*e*]pyrene with several MEPSIL's were determined as functions both of temperature and time. For MEPSIL IV.B, both N and R_s were found to be constant to within 5% over 1 week of continuous operation at 280 °C.

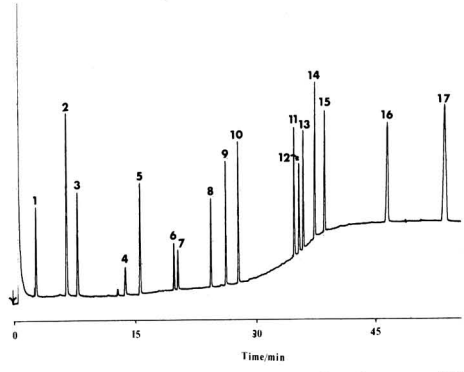


Figure 7. Programmed-temperature separation of common PAH. Solutes numbered as in Figure 6. Additional solutes: 1,2,3,4-dibenzanthracene (16); benzo[*ghi*]perylene (17). Column temperature: 140 °C/3 min; 140–280 °C at 4 °C min^{-1}.

Moreover, only gradual deterioration was observed when columns containing this phase were operated continuously at or above 300 °C. Thus, MEPSIL IV.B can be used at least for brief periods (as in temperature programming) at upward of as much as 300 °C without seriously affecting column performance. The practical operating temperature limits of the phase therefore encompass virtually the entire mesomorphic range exhibited by the material. This was observed to be the case generally for all MEPSIL solvents synthesized in this work.

Column Efficiency of MEPSIL Solvents. MEPSIL phases were found in this work to provide satisfactory column efficiency (see chromatograms presented below), which we ascribe mainly to the unique flexibility of the polysiloxane backbone and its concomitant low surface tension. Thus, glass-capillary columns containing MEPSIL IV.B yielded about 2450 plates/m, N/m (chrysene solute; 230 °C), which compares favorably with about 3000 N/m we have observed elsewhere (*14*, *31*) for columns of identical dimensions that contain SE-30 and SE-52. [In contrast, we have found, e.g., that BBBT (monomeric liquid crystal) yields on average only 880 N/m (*14*).]

Practical Application of MEPSIL Solvents. To illustrate the practical utility of the mesomorphic polysiloxane solvents synthesized in this work, we present as examples the separation of three-, four-, and five-ring PAH with MEPSIL IV.B in Figure 6. Figure 7 then provides the programmed-temperature separation of a synthetic mixture of 17 of the three-to-five-ring PAH encountered most frequently inter alia in environmental samples.

We note in passing that the elution order of the five-ring PAH with conventional polymeric liquid phases is benzo[*e*]pyrene, followed by benzo[*a*]pyrene, and perylene (*1*, *15*, *17*). In contrast, the elution pattern of these solutes with mesomorphic polysiloxanes is consistent with the degree of their rodlike geometry, the more rodlike being retained longer. Thus, benzo[*e*]pyrene elutes first (and well before the rest) with MEPSIL IV.B, followed by perylene, and then benzo[*a*]pyrene.

Selection of a Representative MEPSIL Solvent as a Standard GLC Phase. As mentioned at the outset, it was our intention to synthesize a mesomorphic polysiloxane that would provide satisfactory column efficiency, as well as selectivity on a basis entirely different from conventional phases, in our efforts at defining a set of standard GLC solvents. To date, we have selected and characterized a standard "boiling-point" phase (either OV-1 or SE-30, whose physico-

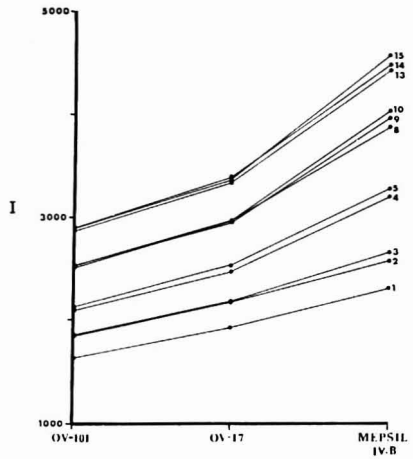


Figure 8. Plots of retention indices for PAH numbered as in Figures 6 and 7 with OV-101 and OV-17 (*43*) and MEPSIL IV.B stationary phases. Lines were drawn between points without regard for intermediate compositions. Data for the lower five compounds correspond to 230 °C, remaining at 270 °C.

chemical and chromatographic properties are virtually equivalent), as well as a solvent of some aromatic content, OV-7 (*22–26*). On the basis of the results of this work, we tentatively select MEPSIL IV.B as representative of nematic polysiloxanes, since it provides the broadest nematic range, highest column efficiency, and greatest thermal stability of the MEPSIL's synthesized by us thus far. Accordingly, we illustrate graphically in Figure 8 the variation of retention indices (hence separations) of selected PAH on passing from the conventional ("nonpolar") phase OV-101, through ("polar") OV-17, to (mesomorphic) MEPSIL IV.B solvent. On the basis of these data, we anticipate that the selectivity afforded by the nematic polysiloxane will differ equally as substantially from those exhibited by OV-1 (separations based on solute volatility) and OV-7 (London interactions), the first two of our set of standard phases. The matter is currently under further study, the results of which we hope soon to report.

Generality of the Synthetic Scheme. Finally, we note that the synthetic procedure outlined in Figure 1 is completely general and should therefore prove useful in the fabrication of polysiloxanes comprised of side chains with other specific functional groups, e.g., chiral centers, Lewis acid sites, and so forth. The only requirement of monomer starting material is that an hydroxyl group be present for attachment, via esterification, to the 4-(allyloxy)benzoyl spacer. However, even this may not be necessary since intermediates can be linked directly to the polymer backbone through hydrosilation if the monomer itself possesses active hydrogen, as is the case, for example, with Schiff bases (*6–9, 44*). In addition, we of course recognize the potential for attachment of liquid-crystal monomers to silica packings utilized commonly in liquid chromatography, for which we are currently developing appropriate derivatizing agents.

LITERATURE CITED

(1) Laub, R. J.; Roberts, W. L. In "Polynuclear Aromatic Hydrocarbons: Analysis, Chemistry, and Biology"; Bjorseth, A., Dennis, A. J., Eds.; Battelle Press: Columbus, OH, 1980; pp 25–58.
(2) May, W. E.; Wise, S. A. *Anal. Chem.* **1984**, *56*, 225–232.
(3) Randall, L. G. *ACS Symp. Ser.* **1984**, *No. 250*, 135–169.
(4) Bjorseth, A., Ed. "Handbook of Polycyclic Aromatic Hydrocarbons"; Marcel Dekker: New York, 1983.
(5) Lee, M. L.; Novotny, M.; Bartle, K. D. "Analytical Chemistry of Polycyclic Aromatic Compounds"; Academic Press: New York, 1981.
(6) Janini, G. M. *Adv. Chromatogr.* **1979**, *17*, 231–277.
(7) Zielinski, Jr., W. L.; Janini, G. M.; Muschik, G. M.; Sato, R. I.; Miller, M. M.; Young, R. M.; Jerina, D. M.; Thakker, D.; Yagi, H.; Levin, W. Paper presented at the Pittsburgh Conference, Cleveland, OH, 1978, paper no. 210.
(8) Zielinski, Jr., W. L.; Jonston, K.; Muschik, G. M. *Anal. Chem.* **1976**, *48*, 907–910.
(9) Janini, G. M.; Muschik, G. M.; Manning, W.; Zielinski, W. L., Jr. *J. Chromatogr.* **1980**, *193*, 444–450.
(10) Analabs Applications Notes, Analabs, North Haven, CT, 1976.
(11) Wasik, S.; Chesler, S. *J. Chromatogr.* **1976**, *122*, 451–458.
(12) Hall, M; Mallen, D. N. B. *J. Chromatogr.* **1976**, *118*, 268–269.
(13) Pailer, M.; Hlozek, V. *J. Chromatogr.* **1976**, *128*, 163–165.
(14) Laub, R. J.; Roberts, W. L.; Smith, C. A. *HRC CC, J. High Resolut. Chromatogr. Chromatogr. Commun.* **1983**, *3*, 355–356.
(15) Laub, R. J.; Roberts, W. L.; Smith, C. A. In "Polynuclear Aromatic Hydrocarbons: Chemical Analysis and Biological Fate"; Cooke, M., Dennis, A. J., Eds.; Battelle Press: Columbus, OH, 1981; pp 287–295.
(16) Laub, R. J. In "Chromatography, Equilibria, and Kinetics: Proceedings of the Faraday Society Symposium (No. 15)"; Young, D. A., Ed.; Royal Society of Chemistry: London, 1981; pp 179–180.
(17) Finkelmann, H.; Laub, R. J.; Roberts, W. L.; Smith, C. A. In "Polynuclear Aromatic Hydrocarbons: Physical and Biological Chemistry", Cooke, M. W., Dennis, A. J., Fisher, G. L., Battelle Press: Columbus, OH, 1982; pp 275–285.
(18) Laub, R. J. In "Physical Methods in Modern Chemical Analysis"; Kuwana, T., Ed.; Academic Press: New York, 1983; Vol. 3, Chapter 4.
(19) Laub, R. J. *Anal. Chem.* **1980**, *52*, 1219–1221.
(20) Chien, C.-F.; Kopečni, M. M.; Laub, R. J. *Anal. Chem.* **1980**, *52*, 1402–1407.
(21) Chien, C.-F.; Kopečni, M. M.; Laub, R. J. *Anal. Chem.* **1980**, *52*, 1407–1411.
(22) Chien, C.-F.; Kopečni, M. M.; Laub, R. J. *HRC CC, J. High Resolut. Chromatogr. Chromatogr. Commun.* **1981**, *4*, 539.
(23) Chien, C.-F.; Furio, D. L.; Kopečni, M. M.; Laub, R. J. *HRC CC, J. High Resolut. Chromatogr. Chromatogr. Commun.* **1983**, *6*, 577–580.
(24) Chien, C.-F.; Furio, D. L.; Kopečni, M. M.; Laub, R. J. *HRC CC, J. High Resolut. Chromatogr. Chromatogr. Commun.* **1983**, *6*, 669–679.
(25) Chien, C.-F.; Kopečni, M. M.; Laub, R. J. *J. Chromatogr. Sci.* **1984**, *22*, 1–6.
(26) Ashworth, A. J.; Chien, C-F.; Furio, D. L.; Hooker, D. M.; Kopečni, M. M.; Laub, R. J.; Price, G. J. *Macromolecules* **1984**, *17*, 1090–1094.
(27) Finkelmann, H.; Laub, R. J.; Roberts, C. A.; Smith, C. A. Paper presented at the Sixth International Symposium on Polynuclear Aromatic Hydrocarbons, Columbus, OH, 1981.
(28) Kong, R. C.; Lee, M. L.; Tominaga, Y.; Pratap, R.; Iwao, M.; Castle, R. N. *Anal. Chem.* **1982**, *54*, 1802–1806.
(29) Allen, R. C.; Yilgor, I.; Wu, D.; Wilkes, G. L.; McGrath, J. E. *Polym. Prepr., Am. Chem. Soc., Div. Polym. Chem.* **1983**, *24*, 257.
(30) Findlay, A. "Practical Physical Chemistry"; Kitchener, J. A., 8th Rev. Ed.; Longmans: London, 1965; Chapter 5.
(31) Lambert, B. J.; Laub, R. J.; Roberts, W. L.; Smith, C. A. *ACS Symp. Ser.* **1984**, *No. 250*, 49–58.
(32) Koltera, A. In "Polymer Fractionation"; Cantow, M. J. W., Ed.; Academic Press: New York, 1967; pp 44–65.
(33) Laub, R. J.; Zink, D. L. *Am. Lab. Fairfield Conn.* **1981**, *13* (1), 55–58.
(34) Laub, R. J.; Zink, D. L. In "Recent Developments in Separations Science"; Calo, J. M., Li, N. L., Eds.; CRC Press: Boca Raton FL, 1985; Vol. IX, Chapter 11.
(35) Stille, J. K.; Fox, D. B. *J. Am. Chem. Soc.* **1970**, *92*, 1274–1278.
(36) Kharasch, M. S.; Ashford, T. A. *J. Am. Chem. Soc.* **1936**, *58*, 1733–1738.
(37) Drew, D.; Doyle, J. R. In "Inorganic Synthesis"; Cotton, F. A., Ed.; McGraw-Hill: New York, 1971; Vol. XIII, pp 47–50.
(38) Castellano, J. A. *Liq. Cryst. Ordered Fluids* **1984**, *4*, 763–780.
(39) Sheng, P. *Liq. Cryst. Ordered Fluids* **1984**, *4*, 889–899.
(40) Barbero, G.; Bartolino, R.; Meuti, M. *J. Phys. Lett.* **1984**, *45*, 449–458.
(41) Rayss, J.; Waksmundzki, A. *J. Chromatogr.* **1984**, *292*, 207–216.
(42) Blinov, L. M.; Davydova, N. N.; Sonin, A. A.; Yudin, S. G. *Kristallografiya* **1984**, *29*, 537–541.
(43) Grimmer, G.; Bohnke, H. *J. Assoc. Off. Anal. Chem.* **1975**, *58*, 725–733.
(44) Janini, G. M.; Laub, R. J.; Shaw, T. J. Paper presented at LabCon West Meeting, Long Beach, CA, May 1984.

RECEIVED for review October 18, 1984. Accepted December 3, 1984. Support provided for this work by the Alcoa Foundation, the Department of Energy Office of Basic Energy Sciences (monomers II.A-E and MEPSIL's IV.A-E), and the National Science Foundation (MEPSIL's IV.F and G) is gratefully acknowledged.

Effect of Pulse Parameters on Analyses by Tandem-Cell Gas-Phase Coulometry

S. W. Warden, R. J. Crawford, W. B. Knighton, and E. P. Grimsrud*

Department of Chemistry, Montana State University, Bozeman, Montana 59717

The analyses of several halogenated methanes by gas-phase coulometry (GPC) and two identical tandem electron capture detectors (ECD) are reported. A dependence of the GPC results on pulse frequency is observed which is not accommodated by present theory of the method. The effects of other variations of the pulsing parameters are also reported. Several potential explanations for these unexpected results are considered. An initially favored candidate, that due to the collection of anions at the anode, is not supported here by experiments designed to test it. It is concluded that the method of GPC, as it presently exists, probably is not yet one which offers an independent means for high-accuracy determinations. Because of the unexplained dependence of the GPC result on pulse frequency, calibration of the GPC response against reliable reference standards is presently necessary if accuracies of a few percent or better are sought.

The concept of gas-phase coulometry (GPC) by the electron capture detector (ECD) for gas chromatography (GC) was first described by Lovelock, Maggs, and Adlard (*1*) in 1971. This article caused considerable interest in the field of trace organic analysis because, in theory, this method offered a convenient means for the quantitative analysis of certain substances at concentration levels where accurate calibration standards are difficult to prepare. Several other studies of GPC have also been reported (2–7) in which various aspects of the method have been addressed. Nevertheless, the technique of GPC for GC detection has not yet matured to the point where it enjoys general acceptance and usage as a quantitative tool. This is probably because the chemical and physical complexities of the gaseous reaction medium within an ECD are difficult to characterize in complete detail and, therefore, it has been reasonable to doubt that accurate coulometric determinations could be readily derived from such a device. On the other hand a great deal of insight into the physical and chemical dynamics of the pulsed ECD has been obtained in recent years and it is now possible to characterize several critical aspects of the pulsed ECD in greater detail than was possible at the conception of GPC. In this article experiments concerning the GPC analysis of several halogenated methanes are reported and assessed relative to a model for GPC, also developed here, which encompassess all of the presently known factors of the pulsed ECD which are thought to have a direct bearing on GPC.

In relating this new information and how it fits into existing theory, it is useful to first consider a broad view of GPC. As with any *chemical method* (GPC is basically a chemical method based on the reaction of gaseous thermalized electrons with the analyte), the following criteria must be satisfied:

(1) The EC reaction must be stoichiometrically distinct.

(2) The reaction must proceed to either completion or to a known fraction of completion.

(3) Uncompensated side reactions of the analyte must not occur.

(4) Uncompensated side reactions of the reagent (electrons) must not occur.

(5) The transducer used to observe the EC reaction must accurately measure the loss of the reagent.

A consideration of existing literature reveals no compelling reason to date why the above criteria should not be met for at least certain compounds. Support for this statement is provided below by brief summarys of each criterion listed above.

Criterion 1. With the possible exception of the iodo compounds, the halogenated methanes appear to react with thermalized electrons with a one-to-one stoichiometry. This conclusion was drawn in a study of the negative ions observed by atmospheric pressure ionization mass spectrometry (APIMS) when $CBrCl_3$ was passed through the source (*6*). The results indicated that the neutral products CCl_3 and $CBrCl_2$, of this EC reaction, do not undergo additional electron capture during their residence time within the cell. Also, it has been shown that the neutral products formed by the recombination of Cl^- and Br^- with positive ions do not undergo further electron attachment (*8*). The positive ion recombination product of I^-, however, probably does undergo electron capture, at least at low detector temperatures (*8*).

Criterion 2. Very strong electron attaching molecules have second-order EC rate constants of approximately 2×10^{-7} cm^3 s^{-1} (*9*). In the typical ^{63}Ni-ECD, the electron population is about 10^8 if the pulsing frequency is only moderately fast (*10*). Thus, the pseudo-first-order constant for electron attachment is about 20 s^{-1} and the lifetime of the analyte against attachment is about 0.05 s. This lifetime is very short relative to the residence time of the molecule as it passes through the detector (for example, with a flow rate of 60 mL min^{-1} and a cell volume of 1 cm^3, the residence time is 1 s). Therefore, the EC reactions of strongly responding compounds should proceed to a reasonably large fraction of completion in the typical ECD. Furthermore, with use of tandem ECD cells (*3*), the fraction of reaction completion is also measured so that a correction for the unreacted portion of the analyte is provided.

Criterion 3. Side reactions of the analyte might include degradation on cell surfaces, reactions with positive ions, or reactions with reactive species such as free radicals. Reactions on surfaces can be minimized by use of lower detector temperatures. Reactions with positive ions should not be competitive with fast electron capture since they occur with maximum rate constants of about 1×10^{-9} cm^3 s^{-1} (*11*). If desired, however, positive ion chemistry can be quenched by doping the carrier gas with strong gas-phase bases such as trimethyl- or triethylamine (*12*, *13*). These dopants form unusually stable and unreactive positive ions and do not attach electrons. Concerning the remaining possible side reaction of the analyte, reaction with reactive neutral species such as free radicals, relatively little is known. In general, these processes should also be much slower than fast electron capture reactions as long as the concentration of reactive radicals is not considerably greater than that of electrons.

Criterion 4. Electrons can undergo several loss processes other than reaction with analyte. These include reaction with carrier gas impurities, recombination with positive ions, neutralization on cell walls, and, of course, collection at the

0003-2700/85/0357-0659$01.50/0 © 1985 American Chemical Society

anode during a pulse. As will be related in Theory below, it is thought that all of these processes, except neutralization on cell walls, can be measured and accounted for in the GPC result. Furthermore, as long as a reasonably fast pulsing frequency is used (*10*), neutralization on the cell walls will be completely prevented. This is because a positive ion space charge then is continuously maintained within the ionized gas. This self-generated electric field "holds" electrons within the gas and presents their transport to the walls during the periods between pulses.

Criterion 5. Recent insight into the effect of positive ions on the current measured with an ECD has shown that a correction for their presence is generally necessary (*14–16*), but that a magnitude for this correction can be readily determined (*16*). With use of this correction factor an accurate electrometer is expected to provide a measure of electron population in the cell and the integrated GC peak area should provide a measure of the loss of electrons during the elution of the analyte.

A simple model of the GPC experiment can be envisioned which incorporates all of the factors discussed above concerning the individual criteria of GPC. This model will be developed in Theory and then will be tested in Results and Discussion. The experiments have been performed with two almost perfectly matched tandem ECD's. The effects of pulsing parameters on the GPC results will be of particular interest because the theory of GPC claims to be able to predict and accommodate the effects of these. The compounds to be studied here are ones which have previously been suggested to be amenable to analysis by GPC.

THEORY

In the pulsed ECD the instantaneous electron population increases rapidly following electron removal by a pulse. Electrons will not be well-mixed throughout the cell but will be contained by a positive ion space charge within a specific region of the plasma (*15*). The location and size of this region will depend on cell design and on the frequency of applied pulses. For the GPC model an expression for *average* population rather than instantaneous population of electrons is desired. The rate of change in average population can be written as follows:

$$d\bar{N}_e/dt = S - \bar{I}_e - \alpha FC_0 - Rn_+\bar{N}_e - Bn_b\bar{N}_e \quad (1)$$

where $\bar{N}_e$ is the average electron population over several pulse cycles, S is the electron–positive ion production rate by ^{63}Ni, $\bar{I}_e$ is the time-averaged loss rate of electrons to the electrometer, α is the fraction of solute molecules reacted as they pass through the detector, F is the carrier gas flow rate, C_0 is the concentration of solute in the carrier gas as it first enters the detector, R is the electron–positive ion recombination rate, n_+ is the positive ion density, and B is the electron attachment constant for carrier gas impurities of concentration n_b. Other means of electron loss such as ventilation through the cell and diffusion to the walls have been shown to be of negligible importance (*10, 17*). Loss of electrons by migration through contact potentials may be important, but only with pulsing periods of 2 ms or greater for these cells (*10*). It is reasonable to assume that $\bar{N}_e$ will be maintained at some steady-state value over the time span of several pulse cycles, so that eq 1 can be set equal to zero.

It is important to point out that the EC reaction efficiency term, α, will be constant for a given compound at a given set of detector conditions only if the concentration of the analyte is kept very small. If sample sizes which are too large are used, the average electron population will be reduced by the EC reaction and then, of course, α will also be reduced. For this reason, our treatment will assume that sample sizes are always very small so the decrease in measured current caused by the analyte is always very small relative to the standing current ($\Delta I \ll I$). Over this range, α can be assumed to be a constant value.

The average electron current, $\bar{I}_e$, is related to the instantaneous electron population existing at the last moment of each pulse period, N_e^T, by the relationship, $\bar{I}_e = N_e^T \times f$, where f is the frequency of pulsing. Also, N_e^T and $\bar{N}_e$ can be related to each other by $\bar{N}_e = \phi N_e^T$ where ϕ is a constant value at a given frequency and has a magnitude between 0.50 and 1.00. The precise magnitude of ϕ can be calculated for the pulse frequency chosen from an equation to be derived later in this section. (For the experimental conditions to be most frequently used here, the value of ϕ will be close to 0.5.) Equation 1 then becomes

$$S = \bar{I}_e + \alpha FC_0 + \frac{(Rn_+ + Bn_b)\phi\,\bar{I}_e}{f} \quad (2)$$

Solving for the electron current and setting $Rn_+ + Bn_b = L$ (the total extra-analyte electron loss constant)

$$\bar{I}_e = \frac{S - \alpha FC_0}{1 + \phi LT} \quad (3)$$

where $T = 1/f$ is the pulse period. The reduction in $\bar{I}_e$ due to the presence of sample, $\Delta\bar{I}_e$, is given by

$$\Delta\bar{I}_e = \frac{\alpha FC_0}{1 + \phi LT} \quad (4)$$

Now $\bar{I}_e$ is not necessarily equal to the current measured by the electrometer. The measured current, I, is a composite of the electron contribution to measured current and a positive ion contribution. This positive ion effect on current has been studied and characterized in several previous studies (*7, 14–16*). The electron current can be determined from measured current by the relationship $\bar{I}_e = I/(1 - \delta)$, where δ is the fraction of positive ions which migrate to the anode (*15*). The magnitude of δ is characteristic of a given cell design and, for ^{63}Ni cells, is independent of the frequency of pulsing. Thus, the following equation can be written:

$$\Delta I = \frac{\alpha FC_0(1 - \delta)}{1 + \phi LT} \quad (5)$$

where ΔI is the measured current response to the analyte. The integrated or peak area response is then

$$Q_1 = \frac{\alpha A(1 - \delta)}{1 + \phi LT} \quad (6)$$

where Q_1 is the peak area (in units of either electrons or coulombs) measured by a single detector and A is the total number of analyte molecules which eluded from the column ($A = \int (FC_0)\,dt$). The final expression for the single cell result is then given by

$$A = \frac{Q_1(1 + \phi LT)}{\alpha(1 - \delta)} \quad (7)$$

This expression is useful only if α can be assumed to be unity (100% EC efficiency) or if the efficiency of the EC reaction in the single cell is known. If tandem cells are used and if they are identical so that the response of each to the analyte is identical, then $\alpha = 1 - Q_2/Q_1$ where Q_2 is the peak area of the second cell. Thus, the result, A, is obtained from the tandem cell analysis by

$$A = \left(\frac{Q_1}{1 - Q_2/Q_1}\right)\left(\frac{1 + \phi LT}{1 - \delta}\right) = A'W \quad (8)$$

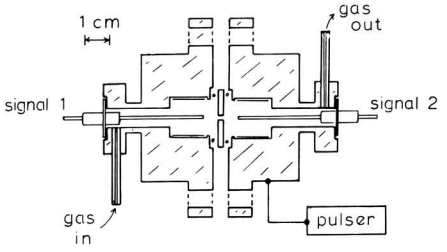


Figure 1. Tandem ECD cells used for GPC determinations.

where A' is the apparent GPC result obtained directly from the two peak area measurements and W is the correction factor for the combined effects of the positive ions on the measured responses and for the extra analyte electron loss processes. Equation 8 should apply at all pulse frequencies because the accompanying changes in EC efficiency should be corrected for by the measured ratio, Q_2/Q_1.

Determination of δ, L, and ϕ. In order to use eq 8, the three parameters δ, L, and ϕ, must first be determined. The correction for positive ion contribution to the measured current, δ, is obtained by measuring the positive standing current obtained when the polarity of the applied pulses is reversed (*14–16*). The fraction of positive ions which migrate to the central pin, δ, is then given by $I_r/(I_n + I_r)$ where I_n and I_r are the standing currents measured with normal and reverse polarity pulsing, respectively. For a ^{63}Ni cylindrical cell, the magnitude of δ has been shown to be the same at all pulse frequencies (*16*).

The magnitude of the extra-analyte electron loss processes, L, is obtained by measuring the standing current as a function of pulse period (*10*) and fitting the resulting data to the following equation:

$$N_e^T = \frac{IT}{1-\delta} = \frac{S}{L}(1 - e^{-LT}) \qquad (9)$$

The shape of the N_e^T vs. T curve is determined by the term, $1 - \exp(-LT)$, so that the magnitude of S does not have to be determined.

The value for ϕ at each pulse frequency is determined from

$$\phi = \frac{\bar{N}_e}{N_e^T} = \frac{\frac{1}{T}\int_0^T N_e^t \, dt}{N_e^T} = \frac{1}{1 - e^{-LT}} - \frac{1}{LT} \qquad (10)$$

where N_e^t is the instantaneous electron population existing between adjacent pulses. In this derivation, expressions for N_e^t and N_e^T are obtained from eq 9.

Propagation of Errors. Equation 11 expresses the ratio of uncertainties (standard deviation) of the GPC result, σ_A, and the uncertainties of the peak area measurements, $\sigma_Q = \sigma_{Q_1} = \sigma_{Q_2}$.

$$\frac{\sigma_A}{\sigma_Q} = W\left(\frac{2(1 - 2Q_2/Q_1 + 2Q_2^2/Q_1^2}{(1 - Q_2/Q_1)^4}\right)^{1/2} \qquad (11)$$

This equation has been obtained by the usual propagation of errors treatment (*18*) of eq 8 where Q_1 and Q_2 are assumed to be the variables of greatest uncertainty. From eq 11, it is seen that with use of the tandem cells, the uncertainty of the GPC result increases continuously as Q_2/Q_1 approaches unity (or as the EC efficiency is reduced). For examples: for $Q_2/Q_1 = 0.05$, $\sigma_A/\sigma_Q = 1.5$; for $Q_2/Q_1 = 0.25$, $\sigma_A/\sigma_Q = 2.0$; for $Q_2/Q_1 = 0.50$; $\sigma_A/\sigma_Q = 4.0$; for $Q_2/Q_1 = 0.75$, $\sigma_A/\sigma_Q = 18$, and for $Q_2/Q_1 = 0.90$, $\sigma_A/\sigma_Q = 128$ (assuming the correction factor, W, is close to unity).

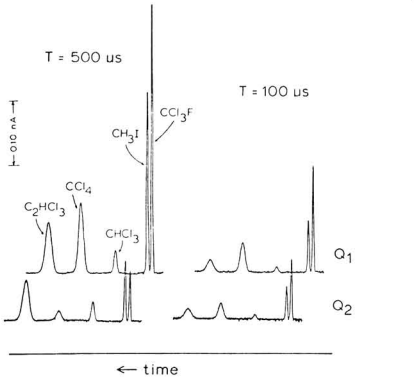


Figure 2. Typical chromatograms obtained with tandem ECD cells with use of two different pulse frequencies.

EXPERIMENTAL SECTION

The tandem ECD cells used in this study are shown in Figure 1. They were fabricated from stainless steel and are of concentric coaxial design where the cylindrical walls are formed by two, matched ^{63}Ni-on-platinum foils (New England Nuclear). Each foil has an activity of 15 mCi. The two cells were generally attached together as shown in Figure 1 where a $^1/_{16}$-in. hole in a $^1/_8$-in. disk allowed the passage of carrier gas from one cell to the next. The internal diameter and length of each cylindrical cell are 1.4 cm. Pulses of negative polarity are applied to the entire cell block which is electrically isolated from earth ground. The two ECD signals are obtained by connecting two matched electrometers to the two $^1/_{16}$-in. stainless rods which serve as the anodes of the cells. The electronic package, which included one fixed-frequency pulser and two electrometers, was home built according to previously described circuit designs (*19*). The ECD currents are obtained by operational amplifiers (RCA CA3140S) with 10^9-Ω precision (±1%) feedback resistors. The detectors are housed in an oven which was maintained at 100 °C.

The gas chromatograph (Gow-Mac, Model 750) was generally operated at room temperature. The column was a 10 ft by $^1/_8$ in. stainless tube packed with 10% SF-96 on Chromosorb W. Gaseous samples are introduced to the GC with a 2.0-mL gas sampling loop (Carle 8030). The carrier gas was 10% methane in argon (Matheson) and was first passed through water-removing ($CaSO_4$ and 13X molecular sieve) and oxygen-remaining (Altech Oxytrap) traps.

Samples were prepared by the successive dilution into nitrogen of the pure halocarbon using airtight glass vessels. The final dilution is into a 22-L carboy which is pressurized to 200 torr above atmospheric pressure. From this reservoir numerous aliquots of the prepared sample could be transferred to the GC sampling loop by a 100-mL glass syringe. The reproducibility of this method of sample introduction is excellent (better than ±1%) because the fixed volume of the sampling loop determines the amount of gaseous sample delivered to the GC. No claim as to the absolute accuracy of the prepared standards is made here.

Typical tandem cell chromatograms obtained with the above system are shown in Figure 2. The two analyses shown are of the same sample but where two different frequencies of pulsing have been used. Peak areas are obtained from the recorder traces by use of a planimeter. In order to determine if the two ECD's and the two electrometers are, in fact, identical, analyses such as shown in Figure 2 were repeated after reversing the direction of gas flow through the tandem cells. Also, the electrometer connections to the two anodes where reversed. Neither of these changes caused measurably different chromatograms. That is, the two electrometers and two detectors behaved identically.

RESULTS

In order to test the use of eq 8 for tandem cell GPC analyses it is first necessary to determine the magnitudes of the parameters δ, L, and ϕ, as described in the theoretical section.

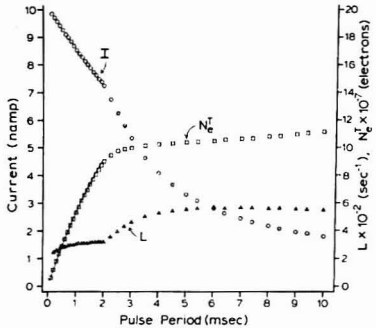


Figure 3. Measured standing current, I, and calculated values of electron population, N_e^T, and extra-analyte loss constant, L, as a function of pulse period.

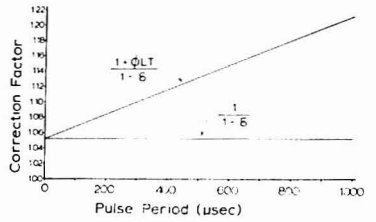


Figure 4. Complete and partial GPC correction factors, W, at all pulse periods for $\delta = 0.05$, $\phi = 0.50$, and $L = 300\ s^{-1}$.

For the cells used here, the determination of δ has been previously described in ref 16. For our cells of truncated cylindrical design $\delta = 0.05$ for all pulse periods used in this study. That is, only 5% of the excess positive ions migrate to the central anode during the periods between pulses.

Standing current measurements as a function of pulse frequency were used to determine the magnitude of L by the procedure described in Theory. The standing current measurements and the subsequent calculations of N_e^T and L at each pulse period are shown in Figure 3. For this experiment, pulse periods out to 10 ms were used. The magnitude of L appears to be constant at about $L = 300\ s^{-1}$ for the periods of interest, up to $T = 1$ ms. (The cause of the discontinuity of L observed at about $T = 2$ ms has been discussed previously (*10*).) The value of ϕ at each pulse frequency is then determined from eq 10 where $L = 300\ s^{-1}$ is used. In this manner, it is found that $\phi = 0.50$ provides a reasonably accurate estimate of ϕ for all pulse periods up to 1 ms. For example, at $T = 100\ \mu s$, $\phi = 0.502$, and for $T = 1000\ \mu s$, $\phi = 0.525$. Equation 8 for our GPC result then becomes

$$A = \left(\frac{Q_1}{1 - Q_2/Q_1}\right)\left(\frac{1 + 150T}{0.95}\right) \qquad (12)$$

where T is in units of seconds.

The composite term in eq 12 which contains the corrections for δ, L, and ϕ is plotted in Figure 4 against pulse period. It is seen that term is moderately dependent on pulse period, where at $T = 100\ \mu s$, this term equals 1.07, at $T = 500\ \mu s$, 1.13, and at $T = 1000$ s, 1.21.

With the tandem cells a prepared standard containing CCl_4 and $CFCl_3$ was analyzed repeatedly while the frequency of pulsing was varied from $T = 20\ \mu s$ to $T = 1000\ \mu s$. In each

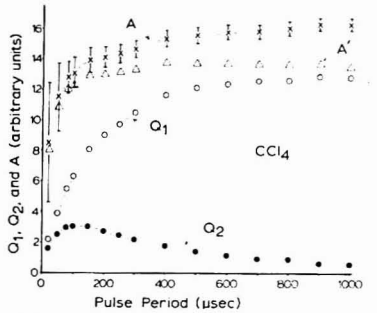


Figure 5. Tandem cell analyses of CCl_4 sample as a function of pulse period used. Q_1 and Q_2 are the peak areas of the first and second detectors. A and A' values are the net GPC results with and without use of the correction factor, W.

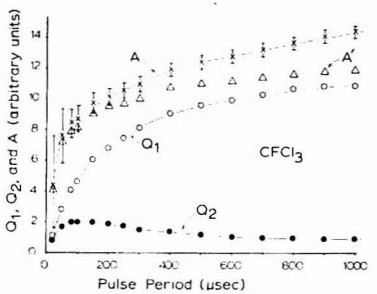


Figure 6. Tandem cell analyses of $CFCl_3$ sample as a function of pulse period used.

analysis the magnitude of Q_1 and Q_2 was measured and then the GPC determinations for total molecules, A, was calculated according to eq 12. Numerous experiments of this type consistently produced results such as are shown in Figures 5 and 6, for CCl_4 and $CFCl_3$, respectively. In Figures 5 and 6 the measured value of Q_1 decreases strongly as the frequency of pulsing is made faster. This is expected since the electron population and reaction efficiency should decrease continuously with faster pulsing. The theory described above, however, predicted that the overall GPC result, A, with tandem measurements of Q_1 and Q_2 should not decrease with variations in pulse frequency. The data, however, indicate that for CCl_4 and especially for $CFCl_3$, the magnitude of A decreases significantly with use of faster pulse frequencies. The variation in A with pulse period is greater than the uncertainty of the measurements indicated by the error bars with each value of A. The estimated uncertainties, which were determined by eq 11 become quite large as the ratio of Q_2 to Q_1 approaches unity. However, numerous repeated experiments of this type invariably show this trend of decreasing A with decreasing pulse period. These data suggest that the theory used to determine A from Q_1 and Q_2 is either flawed or is incomplete and lacks at least one significant factor which is necessary to explain the significant variations of the GPC result with pulse frequency observed here. Also shown in Figures 5 and 6 are the calculated A' values for each analysis where the correction factor in eq 8 was not used. It is seen that for $T > 200\ \mu s$, the A' values show less variation with T than did the A values. For $T < 200\ \mu s$, however, the A' values

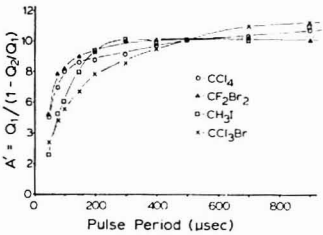


Figure 7. Tandem cell GPC analyses of CCl_4, CF_2Br_2, CH_3I, and CCl_3Br samples as a function of pulse period used. Results are normalized with respect to A' values measured with T = 500 μs.

also decrease rapidly with faster pulsing.

It is appropriate at this point to consider the absolute accuracy of the determinations shown in Figures 5 and 6. In these experiments prepared samples of high reproducibility but of unspecified accuracy have been used. We have intentionally claimed no specific level of accuracy of our standards here because, even with great care in preparation, systematic errors in the preparation of parts-per-trillion level standards are commonplace. Therefore, we prefer not to ask the reader to "trust" the accuracy of our standards and will, instead, use background air as a "standard" with respect to its $CFCl_3$ and CCl_4 concentrations. Because of the stratospheric-ozone question (*20*), the halocarbon content of the earth's atmosphere has been studied extensively in the last 10 years. In particular, extended measurements of $CFCl_3$ in the troposphere indicate that its concentration in 1980 was 168 parts per trillion by volume (pptr) and was increasing annually at a rate of 5.7% (*21*). In 1981 the concentration of CCl_4 was 118 and was increasing 1.8% annually (*22*). From these data, therefore, it is estimated that the present (summer, 1984) concentrations of $CFCl_3$ and CCl_4 in background air of the northern hemisphere is about 210 and 120 pptr (*21*), respectively, and is uniform throughout that air mass. We have measured numerous samples of air obtained from local relatively pristine rural areas and have found that our GPC analyses with the tandem cells indicate A' values for $CFCl_3$ and CCl_4 of 188 ± 10 and 130 ± 20 pptr, respectively, if a pulse period of T = 400 μs is used. After either of the two correction factors shown in Figure 4 are applied, these results are increased by either 5% or 10% and are then in good agreement with the expected composition of the background air samples. It is encouraging, indeed, that the GPC results appear to be relatively accurate when a pulse period of 400 μs is used. However, if the results with T = 400 μs are accurate, then in Figures 5 and 6 it appears that the GPC results obtained with T < 300 μs are too low and those with T > 600 μs appear to be somewhat high, especially where the complete correction factor for extra-analyte electron loss is applied. With the use of long pulse periods, the error for $CFCl_3$ appears to be greater than that for CCl_4, which is relatively minor. In an effort to determine the cause(s) of the dependence of the GPC results described above on the frequency of pulsing, several additional studies of various chemicals and pulsing parameters were made.

The two compounds considered in Figures 5 and 6 are ones which produce Cl^- after electron attachment. In Figure 7 the GPC results for CF_2Br_2, CCl_3Br, and CH_3I along with CCl_4 are shown where the uncorrected A' values for each have been used. Also, these determinations of A' have been normalized with respect to each other by equating the results obtained within each set at T = 500 μs. It is seen that for CCl_3Br and CH_2I, which produce predominately Br^- and I^- upon electron

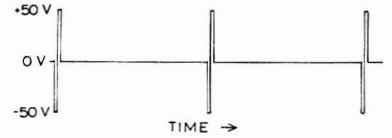


Figure 8. Bipolar pulsed wave form applied to cell walls.

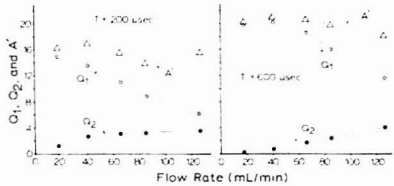


Figure 9. Effect of flow rate on GPC analyses using two different pulse frequencies.

attachment, the degree of response dependence on pulse period is even greater than with CCl_4. It is interesting to note, however, that CF_2Br_2, which also produces Br^-, behaves much like CCl_4 in the tandem cells. This experiment suggest that the cause of the response dependence on pulse frequency may be at least partially related to chemical factors of the analyte.

In other experiments, the voltage of pulses was varied from −50 down to −20 V (where the standing current first began to show a detectable decrease with a further decrease in voltage). Over this range of pulse voltage, no dependence of response on pulse voltage was observed at all pulse frequencies. Also, the width of the pulse was varied from 0.5 to 5 μs. No effect of pulse width was observed with slow to moderate pulse frequencies. With fast pulsing (T < 100 μs) some dependence of response on pulse width was observed, but this was attributed to the fact that the width-to-period ratio is then becoming too large as to allow interpretation of results within the context of the pulsed mode.

A bipolar pulse wave form was also tested. This wave form, shown in Figure 8, contains a positive-going pulse of amplitude and duration equal to the usual negative-going pulse which precedes it. The use of this pulsed wave form rather than the usual negative-going pulser had no measurable affect on the standing currents or on the responses at all pulse frequencies.

Another variable which, in theory, should alter the Q_2 to Q_1 ratio, but not the net GPC result is that of flow rate. In Figure 9 the Q_1, Q_2, and A' measurements of a CCl_4 sample are shown where the flow rate was increased form 18 to 127 mL/min. As expected, the ratio of Q_2 to Q_1 increases with an increased flow rate and a decreased residence time of the analyte in each cell. This experiment was done with T = 200 μs and with T = 600 μs. While a slight decrease of A' with faster flow rate may be inferred from these experiments, it is seen that this dependence is weaker than that caused by the pulse period change from 200 to 600 μs.

DISCUSSION

The results related above indicate that a uniform GPC result is not obtained at all pulse periods. Therefore, the GPC method is not at this point in complete harmony with its theory. In order to improve the method, it appears necessary to explain the basis of the pulse frequency dependence and either eliminate that dependence or determine the precise experimental conditions over which accurate measurements can be expected. In this section some discussion concerning the possible causes of the frequency dependence will be provided by considering the five criteria listed in the intro-

duction and trying to identify potential sources of error within each of these.

The first criterion, that the reaction be stoichiometrically distinct (one-to-one in the cases considered here), has the support of seemingly definitive APIMS measurements (*16*), at least for the cases where CCl_3 or $CBrCl_2$ are formed as products of the electron capture reactions. Furthermore, if further electron attachment to EC products such as CCl_3 did occur, the GPC results would have tended to be only higher than but not lower than the expected result. As was noted in Figures 5–7, low results were frequently observed. For the case of CH_3I, electron capture by the product (probably HI) of positive ion–I^- recombination is thought to occur to some extent (*18*). This may contribute to a frequency dependence of the CH_3I response but, again, cannot be invoked to account for the low results obtained for CH_3I with fast pulsing. In summary, there appears to be no compelling reason which suggests that failure of criterion 1 is the cause of error.

Criterion 2 insists that the fraction of analyte reacted be accurately known. The ECDs used here were identical with respect to construction details and also were shown in separate experiments to respond identically to various molecules. The results obtained were independent of the direction of flow through the cell. With the small sample concentrations used here, the response of each cell should have been proportional to concentration. All of the above considerations suggest that the measured ratio of Q_2/Q_1 should have provided an accurate measurement of the electron capture efficiency of each cell. Furthermore, if the molar response of the second cell was in error and was greater than that of the first cell due to the presence of EC products produced in the first and carried to the second, then a GPC result greater than the expected value should have been measured at all pulse frequencies. Thus, this potential explanation of error also does not fit the measurements where low results were obtained.

In considering criterion 3, uncompensated side reactions of the analyte, various means of analyte destruction where envisioned. The analyte could possibly be degraded on the hot surfaces of the cell. However, no significant differences in the GPC analyses of CF_2Br_2 and $CFCl_3$ at detector temperatures of 100 and 150 °C were observed. A small portion of the analyte could conceivably be lost by reaction with positive ions. However, when the carrier gas was doped with 100 ppm NH_3, no detectable change in the GPC result is observed. If positive ion–molecule reactions were a significant cause of error, this error would have been reduced with NH_3 addition because of the less reactive set of positive ions then present (*12*). Analyte molecules could conceivably be lost by reactions with reactive species such as free radicals. Relatively little is known of the free radicals within the ECD and this possibility cannot be ruled out. It is difficult at present to envision, however, how such reactions might have caused the frequency dependencies of responses observed here.

Criterion 4, side reactions of the electrons, was accounted for here by determining of the extra-analyte loss constant, L, and then incorporating it into the total GPC result as expressed by eq 8. Error in the magnitude of L could cause a frequency-dependent error in the GPC result. However, as shown in Figure 4 and eq 12, the contribution of this term does not appear to be sufficiently large as to explain the sharp decreases in the GPC result observed here with fast pulsing. Error in L may contribute to total analysis error when relatively long pulse periods are used. In fact, the results shown in Figures 5 and 6 suggest that our choice of $L = 300\ s^{-1}$ appears to overcompensate for nonanalyte electron losses. A value of $L = 0$ (no correction for extra-analyte electron losses used) appeared to produce a GPC result which was less variant with T. It is possible that the method of measuring L used here and throughout the ECD literature is not appropriate for $T < 1$ ms where the curvature of N_e^T vs. T curve in Figure 3 is weak and provides an L value in this region of greater uncertainty.

Within the context of criterion 5, error caused by the transducer, several possible causes of error in the GPC result can be envisioned. One of these has been particularly closely examination here. That is, if the ions within the ECD are moved sufficiently by the application of the electron collecting pulses, a continuous loss of signal with faster pulsing might be expected. This would occur if some of the negative ions formed by the EC reaction were collected at the central anode during the application of negative-going pulses to the wall. If this were to occur, no indication of the EC reaction of the molecule which produced that negative ion would be recorded by the electrometer. Simon and Wells (*23*) have recently suggested that this process is an important cause of nonlinearity with their constant-current ECD. This source of error would be expected to increase continuously with the use of faster pulse frequencies. Therefore, our data shown in Figures 5–7 would be neatly accommodated by this potential explanation, and it is tempting to endorse it. Upon further consideration, however, several factors indicate that the migration of negative ions to the anode is probably not the cause of the reduced GPC responses observed here with faster pulsing. First, in a previous study (*16*) of the positive ions within an ECD/APIMS, it was shown that positive ions within an ECD are not moved significantly by the pulsed field, itself. It seems, therefore, that negative ions also would not be moved by the pulse. Also, the GPC results described here were not affected by the magnitude of the pulse voltage. If error is caused by the migration of negative ions in the applied pulsed field, a larger pulsed field should have caused an increased error. Also, the bipolar pulsed wave form shown in Figure 8 was used specifically to examine this potential explanation. The idea behind its use was that if the ion cloud is being perturbed by the pulsed field, it will be repaired by the second half of this pulse which has opposite polarity. Electron collection should be complete after the first half and, therefore, be unaffected by use of the bipolar pulse. Since these experiments indicated that the same standing currents and responses are obtained with use of the bipolar and normal, single polarity pulses, we again conclude that the ion cloud is not being perturbed by the single polarity pulses. Finally, the Figure 7 it was shown that the greatest error with fast pulsing occurs with the molecules which produce the most massive negative ions, $CBrCl_3$ and CH_3I. If negative ions were being moved significantly by migration in the pulsed field, the greatest error would have been observed with the molecules, $CFCl_3$ and CCl_4, which produce the more mobile, Cl^- ion. In summary, motion of the ion cloud by the applied pulses does not appear to be the cause of the response variations.

Another possibility is that electronic factors associated with the electrometer circuit cause a frequency dependent error in the current measurement. We have checked the current measurements of our electrometers at all pulse frequencies against those obtained with commercial electrometers of high specified accuracy. Both home-built electrometers were in agreement to within ±1% of the commercial electrometers. Also, if the problem was simply related to electronics, the chemical effects on responses shown in Figure 7 would still be left unexplained.

One final possibility which might best fit into this discussion of criterion 5 has been considered. According to the space–charge model of the ECD (*15*), electrons exist only in a specific region of the ECD volume. This region is determined by a positive ion space–charge potential which contains the electrons within the ionized gas. The size of the electron-con-

taining region is frequency dependent and made continuously smaller by more rapid pulsing (*15*). It seems possible that in this region of space, the population of analyte molecules is significantly lessened by the EC reaction so that the detector then trends to be no longer "well-mixed" with respect to analyte concentration as the theory assumes. This effect, if operative, would explain a weakened GPC response with faster pulsing. While this idea has considerable merit, it does not by itself explain the chemical dependence on response as shown in Figure 7. Our measurements (as shown in Figure 2, for example) indicated that the EC reactions of CCl_4 and $CFCl_3$ are faster than that of CH_3I and would be expected, therefore, to be more sensitive rather than less sensitive to this problem.

CONCLUSION

We have shown here that the method of GPC by tandem, identical cells provides a quantitative determination of $CFCl_3$ and CCl_4 which appears to be at least approximately accurate over a specific range of pulse frequencies. We have also shown, however, that with the tandem-cell GPC method, a dependence of the GPC result on pulse frequency is observed which presently can neither be eliminated or convincingly explained by present theory. Also, it appears that the correction used here for extra-analyte electron losses, overcompensates for this effect. Therefore, in order to use GPC for quantitative analysis at this time, it appears that the method should be "calibrated" against known standards in order to determine the pulsing parameters which appear to provide the most accurate analyses for each compound. Of course, this approach does not constitute a truely independent coulometric method of analysis but rather one which still depends on the accuracy of prepared standards. If the method of GPC is to become a truly self-calibrated tool capable of accuracies to within a few percent or better, a greater understanding than presently exists of its underlying principles is required. We have provided here some speculation concerning the possible cause(s) of error in GPC. It seems quite possible that more than one uncontrolled parameter is operative in causing the results reported here for, at least some of the compounds studied. We have specifically explored an initially favored explanation, that movement of the ion cloud by the pulse has caused the effects observed. This possibility was not supported by experiments specifically designed to test it. Other possible causes of error have been suggested but have not yet been tested by definitive experiments. Recently, Aue and Siu (*24*) described several unusual response dependencies on pulsing parameters which, like the measurements reported here, could not be accommodated by the existing literature of the ECD. Perhaps their measurements and ours share a common basis. The overall conclusion of this study is that greater knowledge of the transducer–plasma–analyte interface of the pulsed ECD is required if its more quantitatively exacting application, that of GPC, is to become a completely independent means for making quantitative measurements which are accurate to within a few percent.

Registry No. C_2HCl_3, 79-01-6; CCl_4, 56-23-5; $CHCl_3$, 67-66-3; CH_3I, 74-88-4; CCl_3F, 75-69-4; CF_2Br_2, 75-61-6; CCl_3Br, 75-62-7.

LITERATURE CITED

(1) Lovelock, J. E.; Maggs, R. J.; Adlard, E. R. *Anal. Chem.* **1971**, *43*, 1962.
(2) Lovelock, J. E. *J. Chromatogr.* **1974**, *99*, 3.
(3) Lillian, D.; Singh, H. B. *Anal. Chem.* **1974**, *46*, 1060.
(4) Lovelock, J. E.; Watson, A. J. *J. Chromatogr.* **1978**, *158*, 123.
(5) Lee, J. D.; Hirsch, R. G. *Atmos. Environ.* **1979**, *13*, 1305.
(6) Grimsrud, E. P.; Kim, S. H. *Anal. Chem.* **1979**, *51*, 537.
(7) Grimsrud, E. P.; Warden, S. W. *Anal. Chem.* **1980**, *52*, 1842.
(8) Grimsrud, E. P.; and Knighton, W. B. *Anal. Chem.* **1982**, *54*, 565.
(9) Christophorou, L. G. *Chem. Rev.* **1976**, *76*, 409.
(10) Knighton, W. B.; Grimsrud, E. P. *J. Chromatogr.* **1984**, *288*, 237.
(11) Harrison, A. G. "Chemical Ionization Mass Spectrometry"; CRC Press: Boca Raton, FL, 1983; p 12.
(12) Grimsrud, E. P. *Anal. Chem.* **1984**, *56*, 1797.
(13) Grimsrud, E. P. *J. Chromatogr.* **1984**, *312*, 49.
(14) Grimsrud, E. P.; Kim, S. H.; Gobby, P. L. *Anal. Chem.* **1979**, *51*, 223.
(15) Gobby, P. L.; Grimsrud, E. P.; Warden, S. W. *Anal. Chem.* **1980**, *52*, 473.
(16) Connolly, M. J.; Knighton, W. B.; Grimsrud, E. P. *J. Chromatogr.* **1983**, *265*, 145.
(17) Siegel, M. W.; McKeown, M. C. *J. Chromatogr.* **1976**, *122*, 397.
(18) Peters, D. G.; Hayes, J. M., Hieftje, G. M. "Chemical Separations and Measurements"; W. B. Saunders: Philadelphia, PA, 1974; p 19.
(19) Knighton, W. B.; Grimsrud, E. P. *Anal. Chem.* **1982**, *54*, 1812.
(20) Molina, J. J.; Rowland, F. S. *Nature (London)* **1974**, *249*, 810.
(21) Cunnold, D. M.; Prinn, R. G.; Rasmussen, R. A.; Simmonds, P. G.; Alyea, F. N.; Cardelino, C. A.; Craward, A. J.; Fraser, P. J.; Rosen, R. D. *J. Geophys. Res.* **1983**, *88*, 8379.
(22) Simmonds, P. G.; Alyea, F. N.; Carlelino, C. A.; Crawford, A. J.; Cunnold, D. M.; Lane, B. C.; Lovelock, J. E.; Prinn, R. G.; Rasmussen, R. A. *J. Geophys. Res.* **1983**, *88*, 8427.
(23) Simon, R. K.; Wells, G. J. Proceedings of the 20th International Symposium on Advances in Chromatography, New York City, April 16–18, 1984, paper 31.
(24) Aue, W. A.; Siu, K. W. M. *J. Chromatogr.* **1982**, *239*, 127.

RECEIVED for review September 25, 1984. Accepted December 6, 1984. This work is supported by the National Science Foundation under Grant No. CHE-8119857.

CORRECTION

Comparison of Hydrocarbon Composition in Complex Coal-Liquid Samples by Liquid Chromatography and Field-Ionization Mass Spectrometry

Todd W. Allen, Robert J. Hurtubise, and Howard F. Silver (*Anal. Chem.* 1985, *57*, 666–671).

The weight percent of the double bond fractions for the Wyodak coal liquid data in Table I was taken from Boduszynski et al. (*Anal. Chem.* 1983, *55*, 225). In addition, mol % data from the Wyodak sample was taken from the previous reference and Boduszynski et al. (*Anal. Chem.* 1983, *55*, 232). These data were converted to wt % data for the Wyodak sample in Figures 1, 2, 3, and 4 and Table III.

We inadvertently gave the impression, for instance, in our conclusions, that the HPLC–FIMS method discussed in the paper was developed by the present authors while the original combination of HPLC–FIMS for the characterization of hydrocarbons in coal liquids was first introduced by Boduszynski et al. (*Anal. Chem.* 1983, *55*, 225 and 232).

Work by Boduszynski et al. (*Fuel* 1984, *63*, 93 (ref 24)) is mistakenly referred in the text to St. John et al. "Organic Chemistry of Coal"; Larson, J. W., Ed.; American Chemical Society: Washington, DC, 1978; ACS Symp. Ser. No. 71, Chapter 17 (ref 23).

Comparison of Hydrocarbon Composition in Complex Coal-Liquid Samples by Liquid Chromatography and Field-Ionization Mass Spectrometry

Todd W. Allen and Robert J. Hurtubise*

Department of Chemistry, The University of Wyoming, Laramie, Wyoming 82071

Howard F. Silver

Chemical Engineering Department, The University of Wyoming, Laramie, Wyoming 82071

Low-pressure liquid chromatography, high-performance liquid chromatography, and field-ionization mass spectrometry were used to obtain compositional data on the hydrocarbons in two nondistillable coal-liquid samples. Two approaches for analysis of the field-ionization mass spectral data are presented. Detailed compositional information could be obtained by one approach, while with another approach, a general comparison of a large amount of mass spectral data could be made on the basis of weight percent and Z series. The methods developed can generally be applied for the analysis of complex hydrocarbon samples, and they allow for relatively easy comparison of hydrocarbon composition between samples.

Considerable work has been done on the separation and characterization of coal liquids and related samples (*1–22*). Many of the methods developed give general information on the composition of these complex samples. This information is useful; however, there is a need for more compositional details in many situations such as in process control work, in environmental studies, and in understanding the chemistry of coal liquefaction.

Recently, we described methods for the determination of hydrocarbon compositions in high-boiling and nondistillable coal liquids by liquid chromatography and field ionization mass spectrometry (FIMS) (*8, 9*). The general approach involved a combination of low-pressure liquid chromatography, high-performance liquid chromatography (HPLC), and FIMS. In this work, the previous methods were used to compare hydrocarbons from subbituminous and bituminous nondistillable coal-liquid samples. In addition, the data are reported on a weight percent basis rather than a mole percent basis as done previously, and the hydrocarbon data are compared by a pseudo-three-dimensional computer graphing method. Although coal-liquid samples were used in this work, the general approach reported for hydrocarbon analysis should be applicable to a variety of different samples.

EXPERIMENTAL SECTION

Material Studied. The two coal-liquid samples studied were produced by direct liquefaction in an SRC-I process. The Wyodak sample, produced from a subbituminous coal from the Canyon Anderson seams in the Amax Coal Co., Belle AyrMine in Wyoming, was supplied by Catalytic, Inc., from the Southern Company Services, Inc., SRC pilot plant located at Wilsonville, AL. This sample had an ash content of 0.52 wt. % ash and represented nondistillable material boiling above 427 °C.

The second sample was produced from a bituminous Kentucky 9/14 coal. It had an ash content of 0.09 wt % ash and represented nondistillable material boiling above 524 °C. The sample was supplied by the Pittsburgh and Midway Coal Mining Co. SRC pilot plant near Tacoma, WA. Both samples were used as received.

Apparatus and Chemicals. The liquid chromatograph consisted of a Waters Associates Model 6000A pump, a Model U6K injector, a Model ALC 201 differential refractometer, and a Model 440 UV absorbance detector in series, a strip chart recorder, and a Bascom Turner Model 8120 computerized recorder. A 10-μm particle size semipreparative μBondapak NH_2 column (Waters Associates) with *n*-heptane (MCB Omnisolve) at 0.8 mL/min was used in the separation. MCB Omnisolve grade *n*-heptane was filtered through a Millipore type F-H 0.45-μm filter and degassed by helium sparging.

Sample Separation. Hydrocarbon fractions were isolated from "oils" (hexane solubles) of the Wyodak and Kentucky samples using previously described procedures (*5, 6*). The weight percents of the hydrocarbon fractions were determined by first removing most of the solvent with a rotary evaporator. Then the concentrate was transferred to preweighed vials, dried carefully with a stream of nitrogen gas, and weighed. The hydrocarbon fractions were then separated into various fractions based on the number of double bonds in the structure, using an HPLC procedure which was discussed earlier (*8, 9*). The determination of weight percent of these fractions was similar to that for "oils" except the volumes of solvent encountered did not require the use of a rotary evaporator. Only the hydrocarbons isolated from "oils" were further separated by HPLC because of the small amounts of hydrocarbons found in "asphaltenes" (toluene soluble, hexane insoluble).

Field-Ionization Mass Spectrometry. Field-ionization mass spectra of the HPLC fractions were obtained by SRI International in Menlo Park, CA. The field ionization mass spectrometer used in this study was designed and built at SRI International. It was interfaced to and controlled by a PDP 11/10 Computer System. An activated metal foil was used for field ionization, and mass analysis was performed with a 10-in. radius, 60° magnetic sector mass analyzer. The mass spectrometer was operated at a nominal resolving power of 800 (20% valley). The ion detector uses ion-counting electronics, and the data were collected in a multichannel analyzer with 4096 channels. Details of the mass spectrometer were described earlier (*23*).

Typically, about 40–80 μg of the sample was introduced with a direct insertion probe. The sample was initially cooled to −78 °C, and the spectrometer was set to repeatedly scan the desired mass range, usually 100 to 800 amu, at a speed of 56 ms/amu. The sample was then slowly heated, and the mass spectra of the evolving materials were acquired. Care was taken so as not to overload any of the channels of the multichannel analyzer. If the signal became too intense, the sample was cooled. Cumulative data for every eight scans were stored as a spectrum in the computer, and the acquisition continued till there was no more evolution of the sample at the maximum temperature, generally set at 450 °C. Depending upon the sample, the distillation lasted anywhere from 40 min to 2 h. The various spectra acquired over the entire mass range were mass analyzed with a calibration curve obtained with known compounds under the same mass spectrometer operating conditions. The mass-analyzed spectra were added together, and conversion from ion counts to corrected intensity was automatically performed by the computer using the following equation:

$$I_i = \frac{20(\text{ion counts})_i}{M_i} \qquad (1)$$

where $(\text{ion counts})_i$ is the number of ion counts in the ith peak

0003-2700/85/0357-0666$01.50/0 © 1985 American Chemical Society

Table I. Weight Percent of Double Bond Fractions in Kentucky and Wyodak Coal Liquid Samples

hydrocarbon fraction	wt % in total sample[a]	
	Kentucky[b]	Wyodak[c]
saturates	0.16	0.49
3 double bonds	0.21	0.14
5 double bonds	0.57	0.63
6 double bonds	0.51	0.28
7 double bonds	1.50	1.40
8 double bonds	1.34	1.40
9 double bonds	0.98	0.98
10 and 11 double bonds	0.98	2.10
≥12 double bonds	1.65	2.18
recovery	7.90	9.60

[a] Average of duplicate runs. [b] Total hydrocarbons isolated from "oils" is 7.9%. [c] Total hydrocarbons isolated from "oils" is 10.4%.

and M_i is the mass of the ith peak. These intensities were automatically normalized to 10 000 for each spectrum according to

$$RI_i = \frac{10000 I_i}{\sum_i I_i} \tag{2}$$

where I_i is from eq 1 and $\sum_i I_i$ is the sum of all I_i. The values which result from eq 2 are provided by SRI International for each analysis.

An HP-87 computer with an HP Model 82901M flexible disk drive and an HP Model 82905B printer were used to evaluate the data in this work. Computer programs were devised which allow for correction of peak intensities for natural abundance of carbon-13, for subsequent conversion to weight percent of the total sample, and for plotting of the weight percent data.

Elemental Analysis. Elemental analysis of the total hydrocarbons found in the Wyodak sample was performed in duplicate by Huffman Laboratories, Inc., in Wheatridge, CO.

RESULTS AND DISCUSSION

Separation of Hydrocarbons from Nondistillable Coal-Liquid Samples. The separation procedures developed previously were shown to effectively separate hydrocarbons in high boiling and nondistillable coal-liquid samples from other compound class fractions (*5*, *6*, *24*).

The results in Table I show that hydrocarbons isolated from "oils" (hexane solubles) account for 7.9 wt % of the Kentucky coal-liquid sample and 10.4 wt % of the Wyodak coal-liquid sample. Hydrocarbons isolated from "asphaltenes" (toluene soluble, hexane insoluble) were ≤0.5 wt % and were not considered further. Some analytical data on hydrocarbons and other compound class fractions from the two samples have been reported (*23*). The averages of duplicate elemental analyses for hydrocarbons in the Wyodak sample were 91.6 wt % carbon, 7.1 wt % hydrogen, 0.1 wt % nitrogen, 1.4 wt % oxygen, and 0.1 wt % sulfur. Composition of hydrocarbons in the Kentucky sample is expected to be similar, although elemental analysis is needed to confirm this.

Separation of Hydrocarbons by HPLC. Hydrocarbons isolated from "oils" of the two coal-liquid samples were further separated by HPLC. The HPLC approach was described previously, and was shown to be effective in separating hydrocarbon mixtures according to the number of aromatic double bonds present in a given hydrocarbon structure (*8*, *9*). Little or no effect of alkyl substitution was observed. Nine fractions were obtained by the HPLC method. These were a saturates fraction and double bond aromatic fractions containing 3, 5, 6, 7, 8, 9, 10 and 11, and ≥12 double bonds.

Results of the HPLC separation are presented in Table I. The data show that although the Kentucky sample contains less hydrocarbons than the Wyodak sample (7.9 wt % and 10.4 wt %, respectively), the Kentucky sample contains more of the 3 double bond, 6 double bond, and 7 double bond type hydrocarbons. Amounts of the 9 double bond fractions are equal, and the Wyodak sample contains more of all the other fractions, especially the 10–11 double bond fraction and the ≥12 double bond fraction.

Table II. Percent Volatility and Number Average Molecular Weight of Double-Bond Hydrocarbon Fractions

fraction	% volatility[a]		no. av mol wt[a]	
	Kentucky	Wyodak	Kentucky	Wyodak
saturates	100	92	395.7	339.0
3 double bonds	100	100	476.5	396.3
5 double bonds	99	99	316.3	307.9
6 double bonds	97	100	333.8	285.7
7 double bonds	94	100	277.3	319.4
8 double bonds	100	100	298.6	285.1
9 double bonds	90	100	348.8	329.4
10 and 11 double bonds	100	99	382.1	351.6
≥12 double bonds	95	100	446.4	417.7

[a] Data reported by SRI International.

The separation into double bond fractions is essential for the subsequent analysis by FIMS, because it prevents overlap of components with the same mass but different molecular structure. The implications of this have been discussed in more detail (*8*, *9*, *25*).

Field-Ionization Mass Spectrometry. Field ionization mass spectrometry is unique in its ability to produce unfragmented molecular ions and their isotopic signals (*26*) and is ideally suited to the analysis of components in coal derived liquids (*15*, *21–23*, *27–30*). FIMS combined with HPLC provides detailed information on the composition of coal-liquid samples which previously was unavailable.

The hydrocarbon double bond fractions, isolated from Kentucky and Wyodak samples, exhibited high volatility under the conditions of the FIMS analysis as shown in Table II. Number average molecular weights (MW_n) were provided with the analysis for each fraction, and were calculated by using

$$MW_n = \frac{\sum_i (M_i I_i)}{\sum_i I_i} \tag{3}$$

where I_i is the intensity of the ith component according to eq 1 and M_i is the mass of the ith component. Values for MW_n are given in Table II for each fraction. In general, the Kentucky fractions yielded higher values for MW_n than the Wyodak fractions, indicating greater amounts of material at higher masses.

After correction of individual intensity values in the FI mass spectrum for natural abundance of ^{13}C, it was possible to convert the individual relative intensity values in each double bond fraction to weight percent in the coal-liquid sample. The weight percent values can be calculated by using eq 4, a form of which was recently reported by Yoshida et al. (*22*)

$$wt\%_i = wt\%_{total} \frac{M_i I_i}{\sum_i (M_i I_i)} \tag{4}$$

where $wt\%_i$ is the weight percent of the ith component, $wt\%_{total}$ is the weight percent of the double bond fraction in the coal-liquid sample, and M_i and I_i are as before. However, eq 4 is awkward to use in that the term $\sum_i (M_i I_i)$ is tedious to calculate. After combining eq 2, 3, and 4 and introducing a term to account for percent volatility of the fraction, we obtained eq 5. This equation is easily used to find weight percent of any component in the total coal-liquid sample

$$wt\%_i = wt\%_{total} F \frac{M_i\, RI_i}{10000 MW_n} \tag{5}$$

where $wt\%_i$, $wt\%_{total}$, and M_i are as before, RI_i is the relative

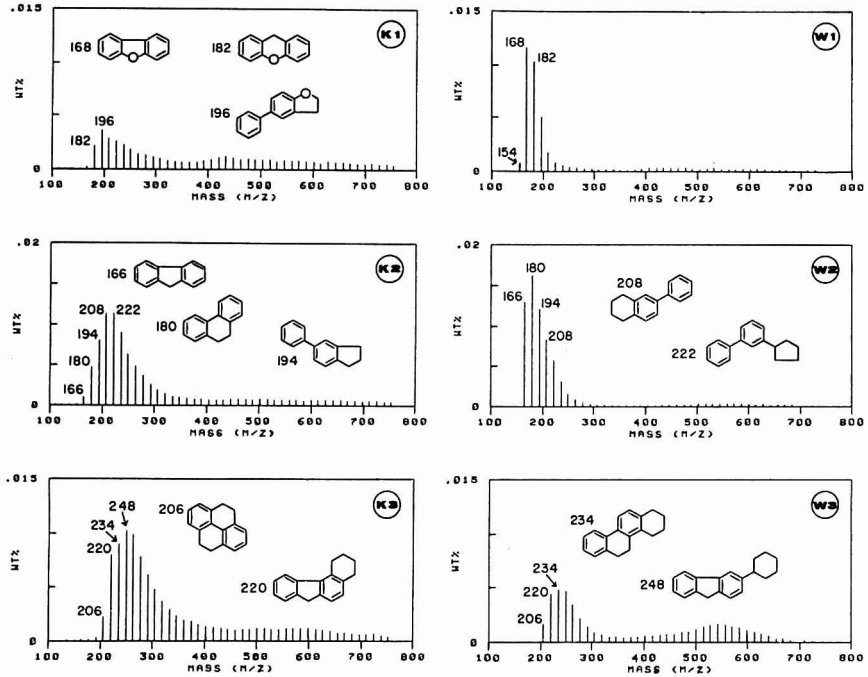


Figure 1. Selected *Z* series in the FI mass spectra of the 6 double bond hydrocarbon fraction isolated from Kentucky (K) and Wyodak (W) coal-liquid samples: (1) C_nH_{2n-14}; (2) C_nH_{2n-16}; (3) C_nH_{2n-18}.

(normalized) intensity of the *i*th component in the spectrum (corrected for ^{13}C abundance), MW_n is the number average molecular weight of the double bond fraction, and *F* is fractional volatility of the double bond fraction. It should be noted that eq 4 and 5 represent the limiting case, where mole sensitivities for field ionization of compounds in each fraction are assumed to be equal (*31*). For fractions composed of related compound types, this assumption has been shown to result in acceptable quantitative distributions in the field ionization analysis (*21*, *31*). Considering the high selectivity of sample separation obtained for the material in this study, which produces hydrocarbon fractions, the assumption is applicable in our work.

In correcting peak intensities for the presence of ^{13}C, the molecular formula and intensity at each even mass, along with the natural percentage of the ^{13}C isotope, were used to calculate expected isotope intensities at only the next higher, adjacent odd mass. Results of the calculation generally reduced the intensities at odd masses to negligible levels, indicating very low levels of nitrogen-containing species. This is consistent with the low nitrogen content (0.1 wt %) found in the total hydrocarbon fraction by elemental analysis.

Weight Percent of *Z* Series in Double Bond Fractions. Total weight percent values of the various homologous *Z* series present in each double bond hydrocarbon fraction from the Kentucky and Wyodak samples are presented in Table III, where the *Z* numbers refer to the formula C_nH_{2n+Z}. In general, for each double bond fraction, decreasing *Z* number corresponds to increasing hydroaromatic character. The more detailed information in Table III reveals that some conclusions made from data in Table I can be misleading, illustrating the importance of FIMS analysis. For example, although the Kentucky sample was shown in Table I to contain more 7 double bond hydrocarbons than the Wyodak sample, the Wyodak sample actually contains more of the −22, −24, −26, and −28 *Z* series in this fraction (Table III). Similarly, the Wyodak sample contains more 5 double bond and 8 double bond hydrocarbons overall (Table I), but the Kentucky sample contains more of some of the *Z* series in both fractions (Table III). The 9 double bond fraction, which overall represents equal amounts in the two samples (Table I), contains differing amounts of the various *Z* series (Table III).

Detailed Comparison of Field-Ionization Mass Spectra. By use of methods developed previously by us and an adaptation of a program which aids in structural assignments, it was possible to carry out a detailed comparison of the hydrocarbon composition in two or more coal-liquid samples (*8*, *9*, *25*, *32*). Figure 1, for example, illustrates the −14, −16, and −18 *Z* series from the 6 double bond hydrocarbon fractions of both coal-liquid samples. The C_nH_{2n-14} hydrocarbon series can be composed of biphenyl (*m*/*z* 154) and its alkyl-substituted homologues. However, biphenyl is a very weak band for the Wyodak sample or a nonexistent band for the Kentucky sample in Figure 1. Because no other parent (i.e., unsubstituted) 6 double bond hydrocarbons can appear in this series, and because of the large intensities at *m*/*z* 168, 182, and 196 compared to the intensity at *m*/*z* 154 (biphenyl), various furan types ($C_nH_{2n-16}O$) which also contain 6 double bonds are assumed to be prevalent in the C_nH_{2n-14} series. Generally, furans were found to behave as hydrocarbons under

Table III. Weight Percent of Various *Z* Series in Hydrocarbon Fractions from Kentucky (K) and Wyodak (W) Coal-Liquid Samples

	saturates		3 d.b.[a]		5 d.b.		6 d.b.		7 d.b.		8 d.b.		9 d.b.		10–11 d.b.		12+ d.b.	
Z	K	W	K	W	K	W	K	W	K	W	K	W	K	W	K	W	K	W
+2	0.027	0.047																
0	0.023	0.043																
−2	0.016	0.039																
−4	0.013	0.042																
−6	0.018	0.051	0.022	0.015														
−8	0.019	0.067	0.032	0.027														
−10	0.011	0.057	0.029	0.023														
−12			0.031	0.018	0.045	0.087	0.039	0.015										
−14			0.030	0.015	0.14	0.19	0.045	0.039										
−16			0.020	0.009	0.15	0.13	0.087	0.069	0.051	0.050								
−18			0.014	0.008	0.087	0.073	0.098	0.048	0.29	0.12								
−20					0.052	0.046	0.087	0.043	0.38	0.33	0.089	0.089						
−22					0.034	0.031	0.067	0.032	0.29	0.38	0.40	0.51	0.069	0.058				
−24					0.024	0.022	0.050	0.019	0.17	0.21	0.32	0.31	0.13	0.20				
−26									0.11	0.12	0.22	0.21	0.16	0.21	0.084	0.15		
−28									0.065	0.070	0.12	0.12	0.17	0.18	0.15	0.37		
−30											0.077	0.073	0.14	0.14	0.18	0.38		
−32											0.068	0.059	0.098	0.092	0.18	0.41	0.19	0.26
−34													0.073	0.059	0.15	0.31	0.22	0.31
−36															0.11	0.24	0.23	0.32
−38															0.084	0.16	0.22	0.34
−40																	0.20	0.30
−42																	0.20	0.28
−44																	0.18	0.24

[a] d.b. = double bond.

conditions of the separation (*6*, *8*, *9*). Although elemental analysis of the total hydrocarbon fraction indicated the presence of some oxygen-containing species, high resolution mass spectrometry and/or elemental analysis of this fraction and other fractions would be necessary to confirm the presence of furans. Notice in Table III that this series ($Z = -14$ from 6 double bonds) accounts for nearly the same amounts in both the Kentucky and Wyodak samples (0.045 wt % and 0.039 wt %, respectively), suggesting that this Z series is similar in the two samples. However, the Kentucky sample is distinctly different from the Wyodak sample as seen in Figure 1. The Wyodak sample contains a large peak at m/z 168 (dibenzofuran) which is absent in the Kentucky sample. Also, more material in the Kentucky sample is distributed in the higher mass range (300–750).

The C_nH_{2n-16} series in the 6 double bond fraction is composed of fluorene, dihydrophenanthrene/anthracene, phenylindan, phenyltetralin, and their alkyl-substituted homologues. The Kentucky sample contains more of this series overall (Table III). Figure 1 reveals that the Kentucky sample actually contains greater amounts of components at m/z 208, 222, and all higher masses in this series, while the Wyodak sample contains greater amounts of components at m/z 166, 180, and 194.

The C_nH_{2n-18} series in the 6 double bond fraction contains compounds such as tetrahydropyrene, tetrahydrobenzofluorene, hexahydrobenzophenanthrene/anthracene, cyclohexylfluorene, and their alkyl-substituted homologues as indicated in Figure 1. Again the Kentucky sample contains much more of this series (Table III), but the Wyodak sample has slightly more material in the mass range 500–600.

It is emphasized that such detailed analysis of each double bond fraction and its Z series is important, but the data generated are extensive and can obscure the overall compositional picture. For example, while Figure 1 shows some dramatic differences between the selected Z series, these Z series are relatively minor components of the hydrocarbons as a whole (Table I and Table III).

General Comparison of Hydrocarbon Composition. Because of the large amount of data from the FIMS experiment, it becomes very difficult to compare the overall hydrocarbon composition of two or more samples. In this work, a pseudo-three-dimensional computer graphing method was developed for the rapid comparison of all the data from the double bond hydrocarbon fractions. Figures 2–4 show the comparison of the FIMS data. All Z series present in all the double bond fractions are given for comparison. Many of the significant compositional differences between the two samples can be easily seen.

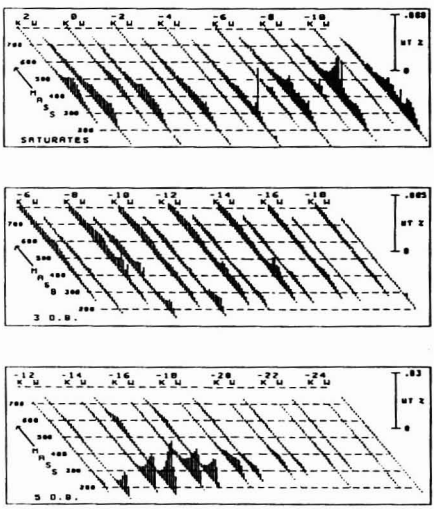


Figure 2. Comparison of mass Z series in saturates, 3 double bond (D.B.), and 5 double bond hydrocarbons isolated from Kentucky (K) and Wyodak (W) coal-liquid samples.

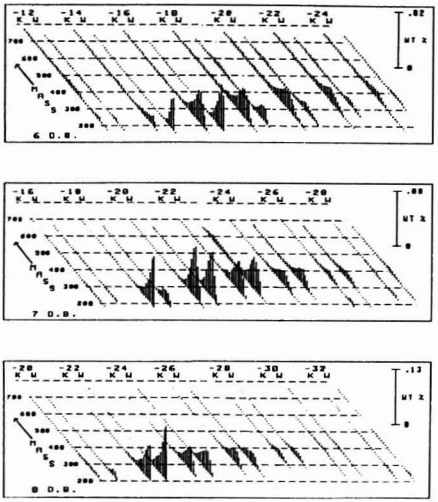


Figure 3. Comparison of mass Z series in 6 double bond (D.B.), 7 double bond, and 8 double bond hydrocarbons isolated from Kentucky (K) and Wyodak (W) coal-liquid samples.

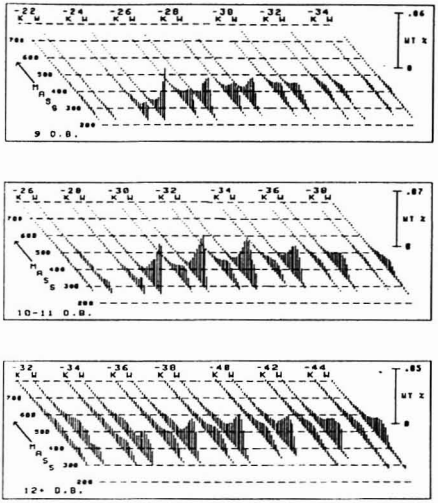


Figure 4. Comparison of mass Z series in 9 double bond (D.B.), 10 and 11 double bond, and ≥12 double bond hydrocarbons isolated from Kentucky (K) and Wyodak (W) coal-liquid samples.

Saturates in the Kentucky and Wyodak samples are present at 0.16 wt % and 0.49 wt %, respectively (Table I), and the Wyodak sample dominates in every Z series (Table III). Figure 2 shows that in the C_nH_{2n+2}, C_nH_{2n}, and C_nH_{2n-2} series the maxima are shifted to higher masses in the Kentucky sample. A prominent peak for a tricyclic terpane in the C_nH_{2n-4} series from the Wyodak sample is absent in the Kentucky sample. The Wyodak sample contains some lower molecular weight material in all Z series which is absent in the Kentucky sample.

Hydrocarbons containing 3 double bonds are present at 0.21 wt % and 0.14 wt % in the Kentucky and Wyodak samples, respectively, and the Kentucky sample has more material in every Z series (Table III). Figure 2 shows that the Kentucky sample generally has much more material at higher masses, which is reflected in the higher average molecular weight for the Kentucky 3 double bond fraction (Table II). In the C_nH_{2n-8} and C_nH_{2n-10} series, the Wyodak sample contains some low molecular weight material (below 220) which is absent in the Kentucky sample (Figure 2).

Hydrocarbons containing 5 double bonds are present at 0.57 wt % and 0.63 wt % in the Kentucky and Wyodak samples, respectively. Although Table III shows that the Wyodak sample does contain more material in some Z series (i.e. C_nH_{2n-12} and C_nH_{2n-14}), the Kentucky sample has more material in the other five series, which are more hydroaromatic in nature. Furthermore, Figure 2 reveals that the Wyodak sample has more material in the higher mass range compared to the Kentucky sample. Interestingly, the C_nH_{2n-12} and C_nH_{2n-14} series in Figure 2 for the 5 double bond fractions show prominent peaks at the beginning of the Wyodak series that are missing in the Kentucky series.

Hydrocarbons containing 6 double bonds are present at 0.51 wt % and 0.28 wt % in the Kentucky and Wyodak samples, respectively (Table I). The Kentucky sample dominates in every Z series (Table III). Significant differences for three of the 6 double bond series, C_nH_{2n-14}, C_nH_{2n-16}, and C_nH_{2n-18}, revealed in Figure 3, were discussed in detail earlier (Figure 1).

Hydrocarbons containing 7 double bonds are present at 1.50 wt % and 1.40 wt % in the Kentucky and Wyodak samples, respectively (Table I). However, Table III shows that the Wyodak sample contains more of the C_nH_{2n-22}, C_nH_{2n-24}, C_nH_{2n-26}, and C_nH_{2n-28} series while the Kentucky sample contains more of the C_nH_{2n-18} and C_nH_{2n-20} series. Differences in distribution are easily seen in Figure 3. The initial peak in the C_nH_{2n-18} series, representing phenanthrene and/or anthracene, is prominent in the Kentucky sample but is diminished in the Wyodak sample. This is true also of the next three peaks in the series, which represent the C_1 to C_3 alkyl substituted homologues.

Hydrocarbons containing 8 double bonds are present at 1.34 wt % and 1.40 wt % in the Kentucky and Wyodak samples, respectively (Table I). The C_nH_{2n-22} series (pyrenes, fluoranthenes, benzofluorenes, etc.) is dominated by the Wyodak sample, while the Kentucky sample has somewhat more material in the C_nH_{2n-24}, C_nH_{2n-26}, C_nH_{2n-30}, and C_nH_{2n-32} series (Table III). Figure 3 shows that the distribution of material in most Z series from the 8 double bond fractions is similar for the two samples.

Hydrocarbons containing 9 double bonds, present at 0.98 wt % in both samples (Table I), were discussed earlier and were seen to contain differing amounts of the various Z series (Table III). This is seen more clearly in Figure 4, which also shows slight differences in distribution in the Z series. The most apparent difference is in the C_nH_{2n-24} series, where the initial peaks (representing chrysene and/or tetracene and their alkyl-substituted homologues) are prominent in the Wyodak sample and diminished in the Kentucky sample.

Hydrocarbons containing 10 and 11 double bonds are present at 0.98 wt % and 2.10 wt % in the Kentucky and Wyodak samples, respectively (Table I). The Wyodak sample contains much more of every Z series (Table III). Differences in distribution of material within each Z series are revealed in Figure 4, where the maxima in the Kentucky Z series profiles are generally at higher masses than the Wyodak

maxima. Also, initial peaks that are prominent in the Wyodak series are generally diminished in the Kentucky series.

Hydrocarbons containing 12 and greater double bonds are present at 1.65 wt % and 2.18 wt % in the Kentucky and Wyodak samples, respectively (Table I), and the Wyodak sample dominates all Z series (Table III). However, Figure 4 reveals interesting differences within the Z series, many of which have a distinct bimodal profile. This strongly indicates the presence of two homologous Z series in each profile, for example, C_nH_{2n-32} and C_nH_{2n-46} or C_nH_{2n-34} and C_nH_{2n-48}. In these series, the maxima of the Kentucky profiles are again at higher masses. Initial peaks in the C_nH_{2n-34}, C_nH_{2n-36}, C_nH_{2n-38}, and C_nH_{2n-40} series which are prominent in the Wyodak sample are diminished in the Kentucky sample. A major difference occurs in the C_nH_{2n-42} series where the Wyodak series begins abruptly at mass 378 and has its maximum at mass 392, while the Kentucky series shows a smooth distribution with a maximum at mass 462.

In Table III and Figures 1–4, some relatively low molecular weight material appears. This indicates that there is not a sharp distinction between distillable and nondistillable coal-liquid samples. Because of the complex nature of coal liquids, it may be difficult to establish true equilibrium in the simple distillation step used to obtain a distillable sample and a nondistillable sample. In addition, it is possible that some of the distillable material becomes physically entrapped in the complex nondistillable portion.

The methods discussed in this paper allow for detailed comparison of complex hydrocarbon samples (Figure 1) and general comparison of a large body of hydrocarbon data (Figures 2–4). It was empirically estimated from the FIMS data that the smallest detectable amount of a hydrocarbon was approximately 1.1×10^{-3} wt %. In addition, the methods developed are such that they should be generally applicable to a variety of complex hydrocarbon samples.

ACKNOWLEDGMENT

The authors thank Stuart E. Scheppele for his helpful comments on this manuscript and Ripudaman Malhotra for providing information on the experimental and instrumental conditions for the field-ionization mass spectrometer.

LITERATURE CITED

(1) Schiller, J. E. *Anal. Chem.* **1977**, *49*, 2292.
(2) Farcasiu, M. *Fuel* **1977**, *56*, 9.
(3) Schabron, J. F.; Hurtubise, R. J.; Silver, H. F. *Anal. Chem.* **1977**, *49*, 2253.
(4) Hurtubise, R. J.; Allen, T. W.; Schabron, J. F.; Silver, H. F. *Fuel* **1981**, *60*, 385.
(5) Boduszynski, M. M.; Hurtubise, R. J.; Silver, H. F. *Anal. Chem.* **1982**, *54*, 372.
(6) Boduszynski, M. M.; Hurtubise, R. J.; Silver, H. F. *Anal. Chem.* **1982**, *54*, 375.
(7) Felice, L. J. *Anal. Chem.* **1982**, *54*, 869.
(8) Boduszynski, M. M.; Hurtubise, R. J.; Allen, T. W.; Silver, H. F. *Anal. Chem.* **1983**, *55*, 225.
(9) Boduszynski, M. M.; Hurtubise, R. J.; Allen, T. W.; Silver, H. F. *Anal. Chem.* **1983**, *55*, *232*.
(10) Burke, F. P.; Winschel, R. A.; Pochapsky, T. C. *Fuel* **1981**, *60*, 562.
(11) Later, D. W.; Lee, M. L.; Bartle, K. D.; Kong, R. C.; Vassilaros, D. L. *Anal. Chem.* **1981**, *53*, 1612.
(12) Romanowski, T.; Funcke, W.; Grossman, I.; Konig, J.; Balfanz, E. *Anal. Chem.* **1983**, *55*, 1030.
(13) Matsunaga, A. *Anal. Chem.* **1983**, *55*, 1375.
(14) White, C. M.; Li, N. C. *Anal. Chem.* **1982**, *54*, 1570.
(15) Yoshida, T.; Maekawa, Y.; Higuchi, T.; Kubota, E.; Itagaki, Y.; Yokoyama, S. *Bull. Chem. Soc. Jpn.* **1981**, *54*, 1171.
(16) Holstein, W.; Severin, D. *Chromatographia* **1982**, *15*, 231.
(17) Swansiger, J. T.; Best, H. T.; Danner, D. A.; Youngless, T. L. *Anal. Chem.* **1982**, *54*, 2576.
(18) Wozniak, T. J.; Hites, R. A. *Anal. Chem.* **1983**, *55*, 1791.
(19) Brown, R. S.; Taylor, L. T. *Anal. Chem.* **1983**, *55*, 723.
(20) Chmielowiec, J. *Anal. Chem.* **1983**, *55*, 2367.
(21) Scheppele, S. E.; Grizzle, P. L.; Greenwood, G. J.; Marriott, T. D.; Perreira, N. B. *Anal. Chem.* **1976**, *48*, 2105.
(22) Yoshida, T.; Maekawa, Y.; Shimada, T. *Anal. Chem.* **1982**, *54*, 967.
(23) St. John, G. A.; Buttrill, S. E.; Anbar, M. "Organic Chemistry of Coal"; Larson, J. W., Ed.; American Chemical Society: Washington, DC, 1978; ACS Symp. Ser. No. 71, Chapter 17.
(24) Boduszynski, M. M.; Hurtubise, R. J.; Silver, H. F. *Fuel* **1984**, *63*, 93.
(25) Boduszynski, M. M.; Hurtubise, R. J.; Allen, T. W.; Silver, H. F. *Fuel*, in press.
(26) Beckey, H. D. "Field Ionization Mass Spectrometry"; Pergamon Press: Oxford, 1971.
(27) Scheppele, S. E.; Greenwood, G. J.; Benson, P. A. *Anal. Chem.* **1977**, *49*, 1847.
(28) Buttrill, S. E. *Org. Coat. Plast. Chem.* **1980**, *43*, 330.
(29) U.S. Department of Energy, Bartlesville Energy Technology Center, Quarterly Technical Progress Report, DOE/BETC/QPR-81/3 Section C, 1981.
(30) Buttrill, S. E. Final Technical Report, SRI Project PYU8903, 1981.
(31) Scheppele, S. E.; Benson, P. A.; Greenwood, G. J.; Grindstaff, Q. G.; Aczel, T.; Beier, B. F. In "Chemistry of Asphaltenes"; Bunger, J. W., Li, N. C., Eds.; American Chemical Society: Washington, DC, 1981; Adv. Chem. Ser. No. 195, Chapter 5.
(32) Holdsworth, D. K. *J. Chem. Educ.* **1980**, *57*, 99.

RECEIVED for review July 30, 1984. Accepted November 26, 1984. Financial support for the project was provided by the U.S. Department of Energy, Contract No. DE-AC22-79ET14874 and DE-AC22-83PC60015. Partial support was also provided by Electric Power Research Institute, Contract No. RP2147-3.

Identification of Antioxidant and Ultraviolet Light Stabilizing Additives in Plastics by Liquid Chromatography/Mass Spectrometry

John D. Vargo* and Keith L. Olson

Analytical Chemistry Department, General Motors Research Laboratories, Warren, Michigan 48090-9055

The information obtained by absorbance detection when coupled with liquid chromatography is usually not specific enough to allow the qualitative identification of compounds present in complex samples with any degree of certainty. With the use of mass spectrometric detection (LC/MS), characteristic mass spectral data can be obtained which greatly aid in elucidating the identity of unknown compounds. In this paper, mass spectrometric detection is used in series with absorbance detection to identify or characterize antioxidants and UV light stabilizing additives in plastic materials which were separated by liquid chromatography. The two detectors were operated in series without any significant loss of chromatographic resolution. Nanogram quantities of additives could be detected by LC/MS. Lower detection limits were achieved by reconstructing mass chromatograms for selected ions. These studies demonstrate the feasibility of using LC/MS to characterize additives in plastic materials.

Chemical additives are frequently used to enhance the useful lifetime of polymeric materials. Antioxidants and ultraviolet (UV) light stabilizers are added to minimize potential polymer degradation by oxidative (*1-3*) or photochemical processes (*3, 4*). Identification and quantitation of these compounds are necessary for polymer degradation studies and for quality-assurance tests.

Due to the low concentration of additives in the polymer matrix (typically less than 1%), a sensitive method of analysis must be employed. The high molecular weight and polarity of many antioxidants and UV light stabilizers often precludes the use of gas chromatography. High-performance liquid chromatography has been used to effectively separate these compounds (*2, 5-9*). Identification of compounds present in real samples is based on comparison of the peaks' retention times or capacity factors (k') with those of known standards. Identification by this method not only is tedious and time-consuming but also requires one to have all of the suspected compounds on hand so that tentative identifications can be made. Even so, erroneous identifications can often be made due to the relatively poor separating ability of HPLC (compared to capillary gas chromatography) and the chemical similarity of many compounds.

The combination of liquid chromatography with mass spectrometric detection (LC/MS) can circumvent many of these problems. Many compounds, such as distearyl thiodipropionate (DSTDP), which do not absorb ultraviolet light at standard UV detection wavelengths (254 nm and 280 nm) will not be detected with a conventional UV absorbance detector. The mass spectrometer is a more universal detector. The information yielded by LC/MS greatly aids in elucidating the structure of unknown compounds.

In our laboratory, ultraviolet absorbance and mass spectrometric detection were used in series to provide unique qualitative and quantitative information on plastic additives separated by liquid chromatography. Additional peak broadening introduced by this detection arrangement was minimal. The system was used to characterize the additives present in several polymeric samples.

EXPERIMENTAL SECTION

Standards and Extracts. Antioxidant standards were obtained from Chem Service, Inc., West Chester, PA. The ultraviolet stabilizers, Cyasorb UV 5411 and UV 531, were purchased from American Cyanamid Co., Wayne, NJ. Trade names and chemical names for the additives are listed in Table I. Standard stock solutions were made up in acetonitrile with enough tetrahydrofuran (THF) added to dissolve the compounds.

Plastic samples were cut into small shavings with a drill bit prior to extraction. Approximately 1 g of the plastic shavings was extracted overnight with 5 mL of acetonitrile. The extraction was performed at ambient temperature in a sealed amber vial with constant stirring. The additives of interest were sufficiently soluble in the acetonitrile extracting solvent due to the small amounts of analyte present. The extract solutions were filtered prior to analysis. Future experiments will evaluate the efficiency of various solvents for the extraction of additives in plastic materials.

Liquid Chromatography. Liquid chromatographic separations were achieved with a dual pump-gradient system (Model 6000A pumps, Model 680 LC gradient controller, Waters Associates, Milford, MA). Ultraviolet absorbance detection was accomplished with a Kratos Model 773 variable wavelength detector equipped with a 0.5-μL flow cell (Kratos Analytical Instruments, Westwood, NJ). All absorbance detection was done at 280 nm. Chemical separations were achieved on a $^1/_8$ in. o.d. × 2.1 mm i.d. × 25 cm long column packed with 5-μm diameter ODS particles (Alltech Associates, Inc., Deerfield, IL). Sample injections were made with a Valco injection valve (Valco, Houston, TX) equipped with a 10-μL loop. A precolumn filter was used to remove particulate material from the injection sample (Upchurch Scientific, Oak Harbor, WA).

The gradient elution scheme shown in Table II was used for the LC separations. The acetonitrile used was HPLC grade. THF was freshly distilled in the laboratory. The gradient controller was set for a flow rate of 0.2 mL/min. At this flow rate, it takes approximately 10 min for the mobile phase in the solvent mixing chamber to reach the column inlet. Therefore, injections were not made until the gradient controller was 7.0 min into the gradient elution program. This reduced the amount of computer time and disk space required to record an LC/MS chromatogram.

Mass Spectrometry. Mass spectrometric detection was achieved with a Finnigan-MAT Model 4615 quadrupole mass spectrometer which was equipped with a moving belt LC/MS interface (Finnigan-MAT, San Jose, CA). Methane chemical ionization (CI) was used for most of the experiments. The ion source was pressurized to 0.3 torr with methane reagent gas, which was ionized with 70-eV electrons. Typically, solutes were desorbed from the polyimide LC/MS interface belt at 230 °C. The ion source temperature was 120 °C. Chemical ionization spectra from m/z 200 to 1200 were recorded repetitively at 3 s/scan. Electron ionization spectra were recorded from m/z 50 to 800 at 3 s/scan.

The LC/MS moving belt interface was modified so that the column effluent was deposited on the belt in a fine spray. The design of the nebulizer was similar to the one described by Karger et al. (*10*). With this system, the LC/MS interface was capable of efficient operation with the mobile phases used at flow rates up to 0.2 mL/min. There was no significant loss of resolution

0003-2700/85/0357-0672$01.50/0 © 1985 American Chemical Society

Table I. Trade Names, Chemical Names, and Mass Spectral Data for Antioxidant and UV-Stabilizer Additives

trade name	chemical name	characteristic ions in methane chemical ionization mass spectrum: most intense ion, m/z	predominant molecular ion species[d]: m/z	predominant molecular ion species[d]: rel int[e]
BHT[a]	2,6-di-*tert*-butyl-4-methylphenol	220	220	100
Santowhite Powder	4,4'-butylidenebis(3-methyl-6-*tert*-butylphenol)	219	383[b]	18
Topanol CA	1,1,3-tris(2-methyl-4-hydroxy-5-*tert*-butylphenyl)butane	381	544	71
UV 5411	2-(2-hydroxy-5-octylphenyl)benzotriazole	324	324[b]	100
UV 531	2-hydroxy-4-(*n*-octyloxy)benzophenone	327	327[b]	100
Irganox 1010	pentaerythritol tetra-3-(3,5-di-*tert*-butyl-4-hydroxyphenyl)propionate	221	1176	nd[c]
Ionox 330	1,3,5-trimethyl-2,4,6-tris(3,5-di-*tert*-butyl-4-hydroxybenzyl)benzene	219	774	4
Irganox 1076	octadecyl 3-(3,5-di-*tert*-butyl-4-hydroxyphenyl)propionate	475	530	37
DSTDP	distearyl thiodipropionate	325	683[b]	9

[a] Many other trade names. [b] Protonated molecular ion. [c] Intensity relative to the most intense ion in the spectrum. [d] Molecular ions and protonated molecular ions were observed in the mass spectra. [e] nd, not detected.

Table II. Gradient Elution Scheme

time, min	% solvent A[a]	% solvent B[b]
0	100	0
10	60	40
20	0	100
30	0	100
32	100	0

[a] Solvent A, 75% acetonitrile and 25% water. [b] Solvent B = 50% THF and 50% acetonitrile.

Table III. Comparison of LC Column Efficiencies Determined by Absorbance Detection and LC/MS[a]

test compd	column efficiency (N): abs, detection	column efficiency (N): LC/MS
phenol	6900	7000
o-cresol	7900	7400
3,5-dimethylphenol	7700	7100

[a] Isocratic elution with 50% CH_3CN/H_2O.

or efficiency in going from the absorbance detector to the mass spectrometer when the two detectors were used in series. When the absorbance detector and mass spectrometer were operated in series, a 20-cm length of 0.01 in. i.d. stainless steel tubing was used to connect the absorbance detector outlet to the LC/MS interface.

RESULTS AND DISCUSSION

Evaluation of the LC/MS Interface. Extracolumn broadening of the chromatographic peaks was found to be minimal for mass spectrometric detection with our system. In a preliminary experiment, the observed column efficiency (N) for a mixture of three phenolic compounds was compared for absorbance detection and mass spectrometric detection (Table III). The observed values of N are very similar for both detection systems. These data indicate that the LC/MS connective tubing, interface, and mass spectrometer itself do not contribute significant peak broadening when the system is optimized.

LC/MS of Antioxidants and UV Light Stabilizers. A complex mixture of nine commonly used antioxidants and UV light stabilizers (Table I) was used to develop a general gradient elution scheme and to optimize the LC/MS parameters. The separation of these compounds with near base line resolution is presented in Figure 1. Detection was achieved with the absorbance and mass spectrometric detectors in series. The resolution between adjacent chromatographic peaks (i.e., peaks 4 and 5) was not significantly affected by our dual

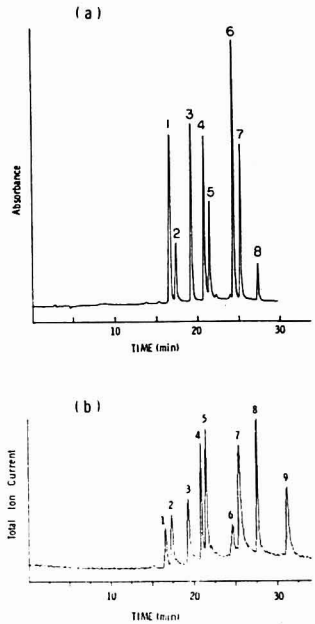


Figure 1. Absorbance chromatogram at 280 nm (a) and total ion current chromatogram (b) of antioxidants and ultraviolet light stabilizers: (1) BHT, 3.1 μg; (2) Santowhite, 0.9 μg; (3) Topanol CA, 2.7 μg; (4) UV 531, 0.66 μg; (5) UV 5411, 0.68 μg; (6) Irganox 1010, 4.5 μg; (7) Ionox 330, 2.4 μg; (8) Irganox 1076, 1.2 μg; (9) DSTDP, 1.7 μg. DSTDP was not detected with absorbance detector at 280 nm.

detection arrangement. Compounds which may not sufficiently absorb light at the monitored absorbance wavelength can often be detected by the mass spectrometer, as was the case for DSTDP (peak 9).

Limits of Detection. The limits of detection ($S/N = 3$) were experimentally determined with a three-component mixture consisting of Santowhite, UV 5411, and Ionox 330. The compounds were detected by both absorbance and mass spectrometric detection. Mass spectrometric detection limits

Table IV. Limits of Detection

	detection limit, ng		
	Santowhite	UV 5411	Ionox 330
abs at 280 nm	3	2	5
total ion current	80	60	150
selected ion current $S/N = 3$	4[a]	2[b]	30[c]

[a] $m/z = 219$. [b] $m/z = 324$. [c] $m/z = 219$.

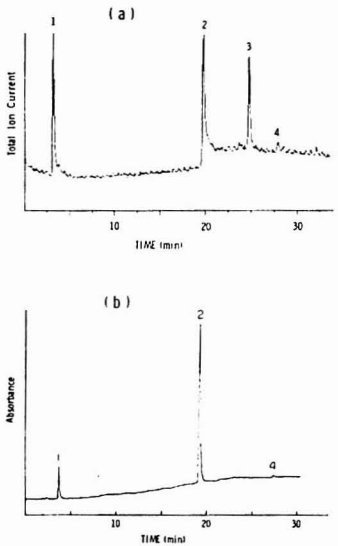


Figure 2. Total ion current chromatogram (a) and absorbance chromatogram at 280 nm (b) of extract from polypropylene beads: (1) unidentified mixture, (2) Topanol CA, (3) octadecanol, (4) Irganox 1076.

were determined from total ion current chromatograms (m/z 200 to 1200) and from reconstructed mass chromatograms of selected ions. Molecular ions or protonated molecular ions and characteristic fragment ions were selected for the reconstructed mass chromatograms (Table I). The limits of detection for the discussed modes are presented in Table IV. Reconstructed mass chromatograms significantly improved the mass spectrometric detection limits because of the relatively intense total ion current background associated with LC/MS. Presumably, even lower detection limits could be obtained with selected ion monitoring.

Characterization of Additives in Plastics. The leachable additives in the extracts from two plastic samples were separated and characterized by liquid chromatography with both absorbance and mass spectrometric detection in series. Some of the additives were identified and quantitated by standard addition with absorbance detection.

Figure 2 shows the chromatogram obtained by both detectors for the separation of additives in the extract from polypropylene beads. Topanol CA and a small amount of Irganox 1076 were present. Octadecanol was also determined to be present in the extract by mass spectrometric detection. By standard addition and absorbance detection, the concentration of Topanol CA in the original sample was determined to be 0.95 mg/g.

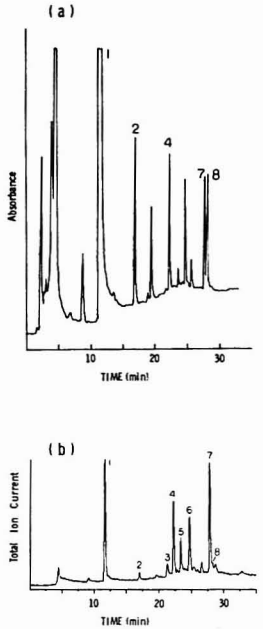


Figure 3. Absorbance chromatogram at 280 nm (a) and total ion current chromatogram (b) of an extract from a molded polypropylene part: (1) unidentified, mol wt 240; (2) BHT; (3) palmitic acid; (4) dioctyl phthalate plasticizer; (5) stearic acid; (6) octadecanol; (7) unidentified, mol wt 390; (8) Irganox 1076.

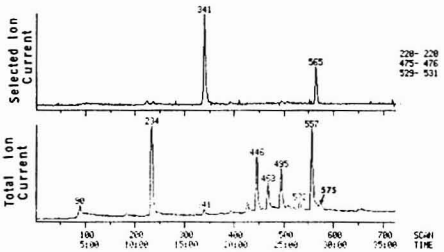


Figure 4. Identification of antioxidants in the extract from a molded polypropylene part by plotting selected ion current profiles. The numbers above peaks correspond to the computer scan number (3 s/scan). Scan number 341 is BHT while scan number 565 corresponds to Irganox 1076.

The additives in an automotive component molded from polypropylene were separated and identified (Figure 3). BHT and Irganox 1076 were identified in the extract. By standard addition and absorbance detection, the amounts of BHT and Irganox 1076 in the original sample were determined to be 0.25 mg/g and 0.072 mg/g, respectively. In addition, several other additives were identified. Identification of these additional additives was simplified by the availability of both electron ionization and chemical ionization mass spectra. Unidentified compounds, which presumably have large molar absorptivities at 280 nm, were detected by the absorbance

detector but not by the mass spectrometer. Those compounds account for the four unidentified peaks appearing between 15 and 30 min in the absorbance chromatogram (Figure 3).

The utility of reconstructed mass chromatograms is evident in Figure 4. BHT and Irganox 1076 are easily detected in the reconstructed mass chromatogram, but in the total ion current chromatogram, Irganox 1076 is obscured by the peak at scan 557.

LITERATURE CITED

(1) Wheeler, D. A. *Talanta* **1968**, *15*, 1315.
(2) Wims, A. M.; Swarin, S. J. *J. Appl. Polym. Sci.* **1975**, *19*, 1243.
(3) Rodriguez, F. "Principles of Polymer Systems", 2nd ed.; McGraw-Hill: New York, 1982; pp 277–302.
(4) "Cyasorb UV 531 Light Absorber"; Technical Bulletin D-42, American Cyanimid Co.: Wayne, NJ, 1982.
(5) Lichtenthaler, R. G.; Ranfelt, F. *J. Chromatogr.* **1978**, *149*, 553.
(6) Schabron, J. F.; Fenska, L. E. *Anal. Chem.* **1980**, *52*, 1411.
(7) Pasteur, G. A. *Anal. Chem.* **1977**, *49*, 363.
(8) Peristein, P. *Anal. Chim. Acta* **1983**, *149*, 21.
(9) Hanley, M. A.; Dark, W. A. *J. Chromatogr. Sci.* **1980**, *18*, 655.
(10) Hayes, M. J.; Lankmayer, E. P.; Vouros, P.; Karger, B. L.; McGuire, J. M. *Anal. Chem.* **1983**, *55*, 1745.

RECEIVED for review October 18, 1984. Accepted December 7, 1984.

Electrospray Interface for Liquid Chromatographs and Mass Spectrometers

Craig M. Whitehouse, Robert N. Dreyer,[1] Masamichi Yamashita,[2] and John B. Fenn*

Department of Chemical Engineering, Yale University, New Haven, Connecticut 06520-2159

Electrospraying LC effluent into a dry bath gas creates a dispersion of charged droplets which rapidly evaporate. As the droplets grow smaller the increase in surface charge density and the decrease in radius of curvature result in electric fields strong enough to desorb solute ions. Part of the resulting dispersion of ions in bath gas passes through a small orifice or channel into an evacuated region to form a supersonic free jet. The core of this jet passes through a conical skimmer orifice and transports the ions to the inlet of a mass analyzer. The reported results suggest that from the standpoints of flexibility, convenience, sensitivity, cleanliness, and ease of maintenance, this ESPI source may comprise an effective and practical LC–MS interface.

The successful union of gas chromatography with mass spectrometry spawned a revolution in chemical analysis. An important impediment to the marriage was a basic incompatibility between vital features of each partner's mode of operation. The lifeblood of a gas chromatograph is the flow of carrier gas in which the species of analytical concern are usually present in only trace amounts. To the mass spectrometer, which is happy only under high vacuum, the prospective flood of carrier gas diluent was anathema. Clearly needed to overcome this impediment was a means of removing and discarding a large fraction of the carrier gas before the stream to be analyzed entered the mass spectrometer. One of the early and most successful devices for accomplishing this removal was the so-called jet separator first described by Ryhage and still widely used in one form or another (*1*). This device derived from the research of E. W. Becker and his colleagues who were exploring the use of supersonic free jets expanding into vacuum for molecular beam sources as had been proposed by Kantrowitz and Grey (2). Surprisingly large species separation effects were observed when the free jet gas comprised a mixture of heavy and light molecules (*3*, *4*). Originally attributed to pressure diffusion during the expansion, this separation was subsequently shown to stem from preferential inertial penetration of heavier species into the stagnation zone behind the bow shock wave on the sampling probe immersed in the supersonic flow (*5*, *6*).

More recently the rapid and highly successful development of high-performance liquid chromatography (HPLC) has reached the stage where its practitioners have for some time also been contemplating the advantages of mass spectrometric detection. As was the case in GC–MS there is an impediment to the union of LC with MS that is similar but even more formidable. To be successful an LC–MS interface must not only divert a large fraction of the mobile phase from the mass spectrometer inlet but it must also make possible the transformation of nonvolatile and fragile species from solutes in a liquid to ions in a vacuum ready for mass analysis. To accomplish the latter step has been an exceedingly refractory problem to which until recently there have been no really satisfactory solutions even when the sample is static and there are no harsh constraints on the time available for preparation.

In the last few years there has emerged a new breed of ion sources that to a much greater extent than their predecessors seem at once to be effective, easy to use, and compatible with both partners of the LC–MS union. Similar in some sense to the field ionization (FI) and field desorption (FD) sources introduced by Beckey and his collaborators, the newcomers apparently share a common mechanism: field ion desorption from liquids (FIDL) (*7*). Their membership includes the electrohydrodynamic (EHD) source of Evans and co-workers, the atmospheric pressure ion evaporation (APIE) source of Iribarne and Thomson, and the Thermospray (TS) source of Vestal and his colleagues (*8–18*). Along with other techniques for the ionization of nonvolatile molecules, these FIDL sources have recently been reviewed by Vestal (*19*).

In this paper we report some experience and results with another variation on the FIDL theme, an electrospray ion (ESPI) source that has its roots in some experiments performed 15 years ago by Malcolm Dole and his collaborators. They attempted to produce beams of charged macromolecules by electrospraying a solution of polystyrene molecules into a bath gas to form a dispersion of macroions that was ex-

[1] Present address: Department of Pharmacology, Yale University.
[2] Present address: Institute of Space and Astronautical Science, Tokyo 153, Japan.

0003-2700/85/0357-0675$01.50/0 © 1985 American Chemical Society

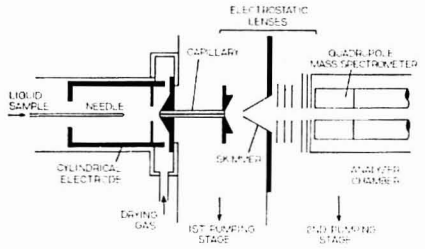


Figure 1. Schematic diagram of the apparatus for mass spectrometry with an electrospray ion source.

panded through an orifice as a supersonic free jet into vacuum (*20–22*). Those authors believed that as the droplets evaporated, the increasing coulomb repulsive forces came to exceed the surface tension so that the droplet underwent fission. Successive fissions ultimately gave rise to droplets containing a single solute molecule that retained the droplet charge as the remaining solvent evaporated. In the case of smaller solute ions with which we have been working, it appears that the high field formed at the surface of an evaporating charged droplet desorbs solute ions into the bath gas in much the same way as in APIE and TS (*23*).

ESPI is operationally different from TS and APIE in the way it produces charged droplets. The latter two techniques disperse liquid into droplets by hydrodynamic forces. Statistical fluctuations in the distribution of solute anions and cations result in a net positive or negative charge on each droplet. In TS the sample liquid is passed through a small bore tube whose walls are hot enough to vaporize most of the solvent. The consequent expansion accelerates the flow and atomizes the remaining liquid so that a dispersion of approximately equal numbers of positively and negatively charged droplets in solvent vapor issues from the tube as a supersonic jet into the first stage of the vacuum system. In APIE the liquid sample is nebulized by a jet of air in the vicinity of a polarizing electrode at high voltage. The resulting field not only determines the sign of the droplet charge but also greatly enhances its magnitude. Whereas TS and APIE produce charging by atomization, ESPI produces atomization by charging. The sample liquid is injected into the bath gas through a metal hypodermic tube at a potential of several kilovolts relative to the surrounding chamber walls. Charge is thus deposited on the surface of the emerging liquid and produces coulomb repulsion forces sufficient to overcome surface tension so that the liquid is dispersed in a fine spray. In all three techniques evaporation of solvent from the droplets increases the surface charge density and decreases the radius of surface curvature. The resulting increase in electric field strength finally reaches levels high enough to desorb ions into the ambient gas. Also common to APIE, TS, and ESPI is the use of a supersonic free jet to transport the ions from relatively high pressure in the desorption region into the vacuum of the mass spectrometer chamber. In sum, it would appear that history has once again succumbed to repetition, if not bigamy. The same supersonic free jet that aided the marriage of MS and GC now promises to abet the union of MS with LC!

EXPERIMENTAL SECTION

Figure 1 shows the essential features of our most recent version of an ESPI source. Sample solution at flow rates typically between 5 and 20 μL/min enter the electrospray chamber through a stainless steel hypodermic needle. Representative values of applied voltage are in parentheses after each of the following components: needle (ground), cylindrical electrode (−3500), metalized inlet and exit ends of the glass capillary that passes ion-bearing gas into the first stage of the vacuum system (−4500 and +40, respectively), the skimmer aperture between the first and second vacuum stages (−20), the ion lens in front of the quadrupole (−100). To produce negative ions, voltages of similar magnitude but opposite sign are applied. We have not yet operated this new apparatus in the negative ion mode but in an earlier apparatus we obtained equivalent results with both polarities (*24*).

A first glance the indicated potential differences of 4540 V between the inlet and exit ends of the glass capillary may seem startling. We have found that with carrier gas at a pressure of about 1 atm, the ion mobility is so low that the flow can lift the ions out of the potential well at the capillary inlet. Consequently, only a few elements inside the apparatus need be at high voltage. All the external parts are at ground potential and pose no hazard to an operator. Indeed, we have been able to "pump" ions through a potential difference of at least 15 kV. Thus we can readily provide the ion energies necessary for injection into a magnetic sector analyzer. This possibility is not so readily realized with some of the other sources. The capillary, with a bore of 0.2 × 60 mm, for given inlet conditions passes just about the same flux of both gas and ions as the thin plate orifice, 0.1 mm in diameter, that it replaced.

The high field at the needle tip charges the surface of the emerging liquid which, as mentioned above, becomes dispersed by coulomb forces into a fine spray of charged droplets. Driven by the electric field the droplets migrate to the inlet of the glass capillary through a countercurrent stream of bath gas (nitrogen) at a pressure that is slightly above 1 atm, typically 1000 torr, a temperature that we have varied from 50 °C to 80 °C or more, and a flow rate typically in the range of 150 cm^3/s. The performance of the source is not at all sensitive to these variables. The droplets rapidly evaporate and the solvent vapor along with any other uncharged material is swept away by the flow of bath gas. Desorbed ions arriving in the vicinity of the capillary inlet are entrained in dry bath gas and transported into the first vacuum chamber where they emerge in the supersonic jet of carrier gas leaving the capillary. Pressure in this first vacuum chamber is maintained at 5×10^{-4} or less by an oil diffusion pump with an effective speed of about 1000 L/s. A portion of the free jet flow passes through the 2-mm aperture of the skimmer into a second vacuum chamber containing a quadrupole mass spectrometer (VG Micromass 1212) whose output is monitored by a UV chart recorder. Pressure in the quadrupole chamber is maintained at about 10^{-6} torr.

When the field at the needle tip exceeds a critical value determined by temperature, pressure, and composition of bath gas, configuration of electrodes, and solution composition, electrical breakdown occurs and results in a sustained corona discharge. Typically, this discharge starts at voltages between 4 and 6 kV. Under these "high voltage" conditions the spectra are markedly different and are characterized by substantial attenuation of the parent solute peaks along with the appearance of other peaks corresponding to species found in discharges as a result of ion molecule reactions. All of the spectra shown in this report were obtained at voltages below the breakdown value. Thus, essentially all of the peaks correspond to solute ions present in the original solution, sometimes in aggregation with one or more un-ionized solvent or solute molecules. We have not yet studied them in detail, but it seems quite likely that the differences between spectra obtained at high and low voltage will contain information useful in identifying the structure of the unfragmented parent ions.

RESULTS AND DISCUSSION

The ESPI results in our previous papers (*23, 24*) were obtained with an apparatus in which the upper limit for the mass range of the quadrupole analyzer was between 300 and 400 daltons. They showed that for a wide variety of species, the primary peaks in both positive and negative modes comprised solute ions in aggregation with one or more nonionic solvent or solute molecules. In the new apparatus described in the previous section the quadrupole analyzer can resolve masses up to 1500 daltons. Thus, one principal objective of the present study was to determine whether ESPI would work

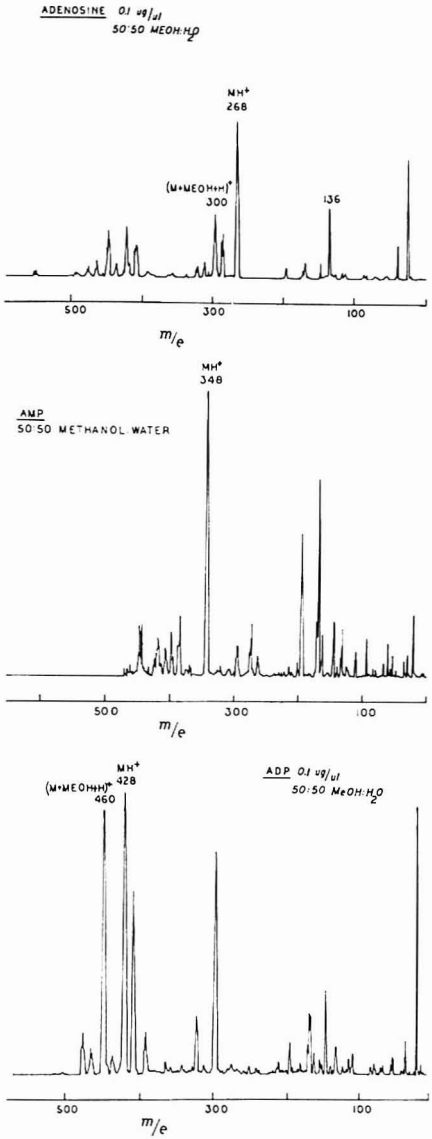


Figure 2. Electrospray mass spectra for adenosine (a), adenosine monosphate (b), and adenosine diphosphate (c). All were present at concentrations of 0.1 μg/μL in 50–50 methanol–water. The liquid flow rate was 6 μL/min. The full mass scan took 5 min.

as effectively in the higher mass range that our new apparatus can probe. However, for a first test of the new system we tried some of the same species we had used in the earlier studies.

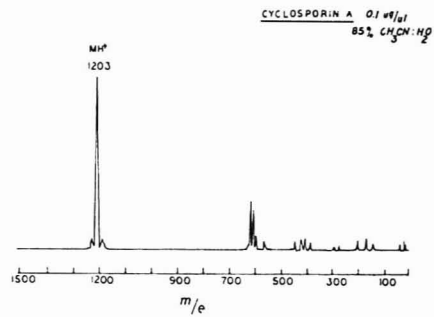


Figure 3. Electrospray mass spectrum for 0.1 μg/μL of cyclosporin A in an 85–15 acetonitrile–water solution. Liquid flow rate was 6 μL/min. The mass scan took 5 min.

Figure 2a shows the spectrum obtained with a solution of adenosine in a 50–50 methanol–water solvent at a concentration 0.1 μg/mL. The liquid flow rate was 6 μL/min during the 5 min it took to obtain this spectrum. The principal peak is at a mass of 268 daltons and corresponds to a protonated adenosine molecule. Also labeled is the peak at 300 daltons which we think corresponds to the same species solvated with one molecule of methanol. The fairly pronounced peak labeled 136 could be due to a doubly charged parent ion peak but is more likely due to a combination of the mass 133 and 134 fragments into which adenosine can readily split. We emphasize that all of the peak assignments in this report must be regarded as tentative. The quadrupole is still not working well, so that with these relatively dilute sample solutions the actual masses may be up to three units in error in the low mass range and ten or more at the high masses. We believe that all of the other peaks correspond to small cations, e.g., Na^+ or H^+, with one or more molecules of solvation, as was the case in the very similar spectrum obtained in the old system. Figure 2b,c shows spectra obtained respectively for the mono- and diphopsphates of adenosine. The peak corresponding to the protonated parent molecule is identified in each case. It is interesting that a strong peak corresponding to the parent together with one methanol molecule of solvation appears in the AD case but not the AMP case. We have not tried to make definite assignments for the other peaks because of the uncertainty in mass mentioned above. However, the similarity between these results and those obtained in the original system, where we were able to make assignments with more confidence, persuade us that no appreciable fragmentation of the parent species occurs.

Figure 3 shows the spectrum obtained with a solution comprising 0.1 μg/μL of the peptide cyclosporin A, an antilymphocytic agent, in an 85–15 acetonitrile–water solution. The primary peak is the singly protonated parent molecule. The width of the peak at the base clearly reveals the inadequate resolution of our quadrupole, so we make no attempt to interpret the small shoulders on either side of the peak base. The smallest peak of the triplet near mass 600 is probably due to a doubly protonated parent molecule. Our confidence in this assignment stems from experiments with high concentrations at which the improved resolution make it quite clear that the apparent mass difference in isotopic peaks is half that to be expected for singly charged ions. The two slightly larger peaks seem likely to stem from the presence respectively of one and two water molecules of solvation. Relative to the singly charged ion the higher polarity of the doubly charged ion may enhance its affinity for water enough

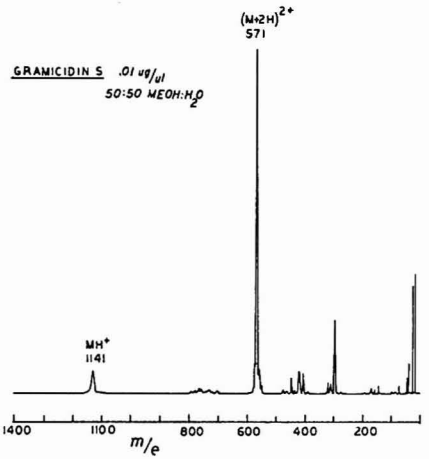


Figure 4. Electrospray mass spectrum for 0.01 $\mu g/\mu L$ gramicidin S in 50–50 methanol–water. Note that the predominant peak is the doubly charged ion. Flow rate was 6 $\mu L/min$. Mass scan took 5 min.

to compensate for the relatively hydrophobic exterior of the parent molecule.

Figure 4 shows the spectrum obtained with the antibiotic gramicidin S at a concentration of 0.01 $\mu g/\mu L$ in 50–50 methanol–water. It is interesting that the predominant peak is due to the doubly charged ion, identified from isotopic mass intervals when experiments were carried out with higher concentrations of analyte as mentioned above. In this case, the presence of double charge does not give rise to the solvation that seemed to occur with cyclosporin A. It is appropriate to remark on sensitivity. The spectrum shown in Figure 4 required 5 min for the complete mass scan because at higher scan rates the mass markers do not appear in the chart output of the recorder that is our only present means of collecting data. The sample liquid flow rate was 6 $\mu L/min$ so that 0.3 μg of analyte passed through the system during the scan. We estimate that the fraction of the total scan devoted to the primary peak was roughly 15/1500 or 0.01. Thus, the amount of analyte in the peak is about 3 ng. when we use an oscilloscope to monitor the output signal, we can carry out a complet scan in 1 s and obtain relative peak heights exactly the same as those for the slow scan. We conclude that we would thus need only $^1/_{300}$ of 3 ng or 10 pg of analyte to obtain a peak equivalent to that in Figure 4. The apparent signal/noise in the recorder spectrum is at least 200 and probably more. If we assume that S/N or 2 represents detectability, we conclude that we can detect as little as 100 fg of this material. This argument assumes that S/N is not significantly greater in the fast scan, a not unreasonable assumption for the dc mode in which we operate. Just because the peak that we discern contains only 100 fg of analyte does not mean that we can detect this amount of material in any arbitrary sample introduced at random into the ion source. Detectability in any unconstrained sense will always have a marked dependence on scan rate, resolution, concentration, and injection time. These factors will all be different from laboratory to laboratory and experiment to experiment. A perhaps more meaningful basis upon which to compare instrument senstivities, especially in the case when sample is introduced continuously, albeit for short periods, rather than in batches, is the minimum steady state flow rate of analyte

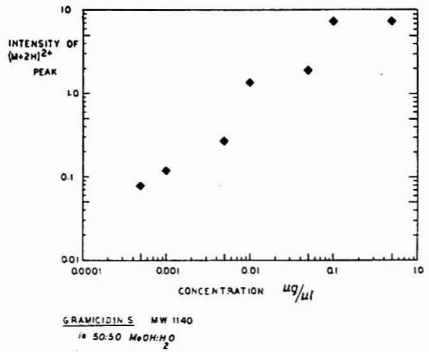


Figure 5. Dependence of mass spectrometer signal on analyte concentration for the case of gramicidin S in methanol–water solution.

that will give rise to a discernible mass peak. On this basis the experiments that led to Figure 5 provide a useful perspective. For the lowest concentration of gramicidin S, 5×10^{-4} $\mu g/mL$, we could obtain a discernible peak with S/N of order 2 at a flow rate of 1.0 $\mu L/min$ with a single mass scan at a rate of 20 amu/s. In other words we were detecting an analyte flow rate of 8 pg, or roughly 7 fmol, per second. If enough sample is available to permit multiple scans and signal averaging, the minimum detectable flow rate could be substantially less. These numbers are not ultimate in any sense. We are still on the steep part of the learning curve for this technique and have every reason to expect substantial improvements in sensitivity.

We have obtained entirely similar results with the peptides bleomycin and "Substance P" that have molecular weights respectively of about 1375 and 1348. The actual predominant peak with the sample of commercial bleomycin that we used (Blenoxane) was the complex with copper having a mass 1440. For both of these substances, as well as for gramicidin S, the doubly charged ion peaks predominate. This propensity toward multiple charging is provocative. If we can determine when, why, and how it occurs, we may be able to promote it and thus to extend substantially the effective mass range, not only of the ESPI source but of available mass analyzers as well.

It is important for quantitative analysis that the mass spectrometer signal have a near linear dependence upon the concentration of analyte. In Figure 5 is an example that shows such a near-linear dependence over 4 orders of magnitude in the concentration of gramicidin S in methanol–water. Moreover, the data for gramicidin S in Figure 6 demonstrate that the signal does not depend strongly on the liquid flow rate. These features of ESPI behavior are reassuring because they mean that peak heights (areas) obtained with LC effluents will not be distorted by an ESPI interface.

Of course, the key concern in this forum is how well that the ESPI source will stabilize the LC–MS union. Before definitive conclusions can be reached, we must actually couple a chromatograph with a mass spectrometer by means of an ESPI source. Thanks to Whatman, Ltd., we have in fact obtained a microbore column with a 1 mm i.d. and a length of 250 mm and, except for appropriate injection valves, are ready to make the acid test. Indeed, in some preliminary experiments, we have injected a sample of cyclosporin A into the column and passed the effluent into the source. We obtained a spectrum essentially identical with the one shown in Figure 3. Unfortunately, the injected sample was 20 μL,

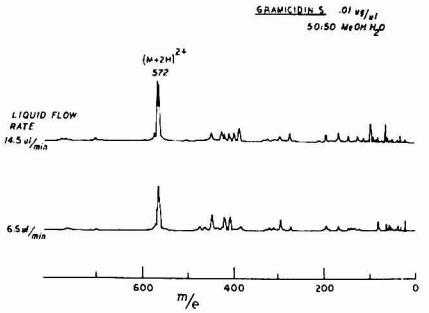


Figure 6. Independence of mass spectrometer signal on sample flow rate for the case of gramicidin S in methanol–water solution.

so large that we overloaded the column with the result that the "elution" time or peak width was 52 min for 2 μg of analyte! With an oscillating mass scan of 8 daltons centered at mass 1203, we were able to determine the shape of the leading and trailing edges of the peak. They were very abrupt and sharp, indicating minimal tailing. Thus, the ESPI source has virtually no dead volume.

It is clear that until we have acquired more experience with an actual LC–ESPI–MS combination we will be in no position to make any meaningful judgement on the extent to which ESPI can be considered a solution to the interface problem. However, our experience to date seems to provide grounds for optimism. We close with some observations on practical operational features of ESPI that seem pertinent.

1. The system is not prone to fouling. The countercurrent flow of bath gas sweeps away all the solvent vapor and other uncharged material. In effect, only ions are carried into the vacuum system by the free jet of bath gas. We have run pretty steadily for periods as long as a month without any decrease in performance. Even then, there was no appreciable fouling in the vacuum system. The major problem was a slight accumulation of salt deposit at the end of the hypodermic injection tube and on the side walls of the electrospray chamber. Both of these elements are in the high pressure section of the system and thus readily accessible for cleaning.

2. Thus far we have found no evidence to suggest that sensitivity depends upon the molecular weight of the analyte beyond what one would expect for decreases in quadrupole transmission and multiplier response for ions of increasing mass. In other words, the ionization efficiency seems to be relatively constant over the mass range. Of course, we have as yet tried relatively few materials, but our confidence in this conclusion is increasing.

3. The system seems inherently stable. Small fluctuations in liquid flow rate do not cause ripples in the signal output. Modest changes in temperature and flow rate of bath gas do not markedly affect the signal. Consequently, these variables do not need to be controlled all that carefully. The variable of most immediate and direct influence on performance is the voltage applied to the liquid injection needle so that a reasonably well stabilized power supply is needed. Optimal voltage, bath gas flow rate, and temperature settings are identical for all compounds run thus far. Consequently, adjustments need not be made to optimize sensitivity from one compound to the next.

4. The ability to use viscous drag forces during bath gas flow through the capillary to "pump" ions to any voltage that would be required for injection into a mass magnetic sector mass analyzer is very important. It means that all the advantages of such instruments in the analysis of very heavy ions will be accessible to LC/MS analysis.

In sum, though our experience is thus far limited, results with ESPI along with those obtained by Vestal with TS and by Iribarne and Thomson with APIE give more reasons for hope than despair in the quest for a practical LC–MS interface.

ACKNOWLEDGMENT

We gratefully acknowledge the interest, support, and encouragement of VG Analytics who provided the quadrupole mass spectrometer and other reenforcement. We also record our gratitude for the cooperation and support that our colleagues at Yale have so generously provided. In particular, the yeoman efforts of Chin-Kai Meng and Ted Grabowski have been invaluable.

LITERATURE CITED

(1) Ryhage, R. *Anal. Chem.* **1964**, *51*, 359.
(2) Kantrowitz, A.; Grey, J. *Rev. Sci. Instrum.* **1951**, *22*, 328.
(3) Becker, E. W.; Bier, K.; Burghoff, H. *Z. Naturforsch., Teil A* **1955**, *10*, 565.
(4) Becker, E. W.; Bier, K.; Ehrfeld, W.; Schubert, K.; Schutte, R.; Seidel, D. In "Nuclear Energy Maturity"; Zaleski, P., Ed.; Pergamon: Oxford, 1975; p. 172.
(5) Reis, V. H.; Fenn, J. B. *J. Chem. Phys.* **1963**, *39*, 3240.
(6) Sherman, F. S. *Phys. Fluids* **1965**, *8*, 773.
(7) Beckey, H. D. "Principles of Field Ionization and Field Desorption Mass Spectrometry"; Pergamon: New York, 1977.
(8) Stimpson, B. P.; Simons, D. S.; Evans, C. A., Jr. *J. Phys. Chem.* **1978**, *82*, 660.
(9) Evans, C. A. Jr.; Hendricks, C. D. *Rev. Sci. Instrum.* **1972**, *43*, 1527.
(10) Simons, D. S.; Colby, B. N.; Evans, C. A., Jr. *Int. J. Mass Spectrom. Ion. Phys.* **1974**, *15*, 291.
(11) Stimpson, B. P.; Evans, C. A., Jr. *Biomed. Mass Spectrom.* **1978**, *5*, 52.
(12) Iribarne, J. B.; Thomson, B. A. *J. Chem. Phys.* **1976**, *64*, 2287.
(13) Thomson, B. A.; Iribarne, J. B. *J. Chem. Phys.* **1979**, *71*, 4451.
(14) Iribarne, J. B.; Dziedzic, P. J.; Thomson, B. A. *Int. J. Mass Spectrom. Ion. Phys.* **1983**, *50*, 331.
(15) Blakley, C. R.; Carmody, J. J.; Vestal, M. L. *J. Am. Chem. Soc.* **1980**, *102*, 5931.
(16) Blakley, C. R.; Carmody, J. J.; Vestal, M. L. *Clin. Chem. (Winston-Salem, N.C.)* **1980**, *26*, 1467.
(17) Blakley, C. R.; Carmody, J. J.; Vestal, M. L. *Anal. Chem.* **1980**, *52*, 1636.
(18) Blakley, C. R.; Vestal, M. L. *Anal. Chem.* **1983**, *55*, 750.
(19) Vestal, M. L. *Mass Spectrom. Rev.* **1983**, *2*, 447.
(20) Dole, M.; Mack, L. L.; Hines, R. L.; Mobley, R. C.; Ferguson, L. D.; Alice, M. B. *J. Chem. Phys.* **1968**, *49*, 2240.
(21) Mack, L. L.; Kralik, P.; Rheude, A.; Dole, M. *J. Chem. Phys.* **1970**, *52*, 4977.
(22) Dole, M.; Cox, H. L., Jr.; Gieniec, J. *Adv. Chem. Ser.* **1973**, *No. 125*, 73.
(23) Yamashita, M.; Fenn, J. B. *J. Phys. Chem.* **1984**, *88*, 4451.
(24) Yamashita, M.; Fenn, J. B. *J. Phys. Chem.* **1984**, *88*, 4671.

RECEIVED for review October 8, 1984. Accepted December 6, 1984. This research has been sponsored in part by the National Science Foundation (Grant ENG-7910843), the U.S. Department of Energy (Grant ET-78-G-01-3246), and the National Cancer Institute (Grant C288-52/04). C.M.W. acknowledges with appreciation a fellowship award from the Exxon Corp. M.Y. acknowledges support from the Institute of Space and Aeronautical Sciences that made his participation possible.

Comparison of Isopentane and Isobutane as Chemical Ionization Reagent Gases

Jeffrey M. McGuire[1] and Burnaby Munson*

Department of Chemistry, University of Delaware, Newark, Delaware 19716

The CI spectra obtained with i-C_5H_{12} as the reagent gas are frequently very simple and provide abundant $(M + H)^+$ ions for compounds more basic than i-C_5H_{10}. The i-C_5H_{12} spectra are similar to i-C_4H_{10} CI spectra but may contain somewhat fewer fragment ions and frequently more molecular ions, M^+, from charge exchange by the relatively abundant i-$C_5H_{10}^+$ ion. In addition, i-C_5H_{12} may be somewhat more selective than i-C_4H_{10}. The two reagents can probably be used interchangeably. One advantage of using i-C_5H_{12} is the ease by which the vapor may be introduced without a complex vacuum manifold.

Perhaps the most commonly used reagent gas in chemical ionization mass spectrometry (CIMS) is the first reagent gas used, CH_4 (*1*). Methane has the advantage that the two reagent ions, CH_5^+ and $C_2H_5^+$, react with virtually every organic compound with similar rate constants (*2*) since CH_4 and C_2H_4 are weaker bases than practically all other organic compounds. The spectra obtained with CH_4 as the reagent gas generally contain structurally useful fragment ions and frequently contain $(M + H)^+$ and/or $(M - H)^+$ ions for the determination of molecular weights. In analytical problems for which fragmentation is not necessary, weaker acids are used. One of the most common reagent gases for simplified spectra is isobutane (*3, 4*). The *tert*-butyl ion is a much weaker acid than CH_5^+ or $C_2H_5^+$ and i-C_4H_{10} CI spectra show less fragmentation than CH_4 CI spectra. However, $(M + H)^+$ ions are not always observed in isobutane CI spectra (*3*), and the absence of these ions may result from X^- transfer to give $(M - X)^+$ and t-C_4H_9X rather than from dissociative proton transfer (*5*). In earlier work on thermally labile compounds with in-beam CI, surface CI, direct exposure (or any of the other names suggested for the technique), we routinely used i-C_5H_{12} as the reagent gas (*6*). We wish to report a comparison of i-C_5H_{12} and i-C_4H_{10} as general CI reagents.

EXPERIMENTAL SECTION

The experiments were performed with a Du Pont 21-110B mass spectrometer, modified for high-pressure operation. The data were acquired with a Data General Nova 1200 computer (*6-8*). The source was a collinear design in which the electrons enter and the ions leave the source along the same axis (*7*). The electron energy was nominally 630 eV and the ion exit plate was maintained at a potential of -2 V with respect to the source block. Some samples were introduced from a glass probe at temperatures of 35-170 °C, depending on the volatilities of the compounds. Other samples were introduced with a gas chromatograph through an interface which has been described previously (*7*). The source temperatures were 100-150 °C for these experiments. The i-C_4H_{10} (99.5%, Matheson) was introduced through a conventional glass gas-handling manifold with a low-pressure gas regulator (Matheson) to maintain a constant pressure. The i-C_5H_{12} (95+%, Fisher) was introduced from a small bulb of degassed liquid. A constant source pressure of i-C_5H_{12} was easily maintained if this bulb was immersed in a beaker of water to maintain a constant temperature of the liquid i-C_5H_{12}. The samples which were analyzed were obtained from several commercial sources and were of the highest purity available. The pesticides were NBS standards.

RESULTS AND DISCUSSION

The ion/molecule reactions in i-C_5H_{12} have been reported previously to give m/z 71$^+$, t-$C_5H_{11}^+$, as the major product (*9*). Figure 1 shows plots of relative abundances of the major ions in i-C_4H_{10} and i-C_5H_{12} as functions of pressure. The dominant product ions for these two compounds at high pressures are the alkyl ions, $C_4H_9^+$ in i-C_4H_{10}, and $C_5H_{11}^+$ in i-C_5H_{12}. Alkene ions, $C_4H_8^+$ in i-C_4H_{10} and $C_5H_{10}^+$ in i-C_5H_{12}, are also present as reagent ions at high pressures. The extent of conversion of C_2 and C_3 ions to $C_5H_{10}^+$ and $C_5H_{11}^+$ with i-C_5H_{12} is greater than the extent of conversion of C_2 and C_3 ions to $C_4H_8^+$ and $C_4H_9^+$ with i-C_4H_{10} at comparable pressures. Similar pressure plots will be observed in other high pressure sources, but the relative abundances of the ions at a given pressure will depend on the source geometry (ion path length) and the field strength within the source (repeller or ion exit plate voltage). The relative abundances of the ionic species can be used to check the pressure of the reagent gas on a day-to-day basis after such a plot has been obtained with a given mass spectrometer. A kinetic method for estimating source pressures from the ion/molecule reactions in i-C_4H_{10} and other reagent gases has been reported (*10*).

Plots of total ion current vs. pressure pass through a sharp maximum slightly below 0.1 torr for both i-C_4H_{10} and i-C_5H_{12}. Figure 2 shows plots of sample ion current, as $(M + H)^+$ ions for a constant amount of decanophenone, $C_6H_5COC_9H_{19}$, for each of these two gases. The maxima in the plots of sample ion current vs. pressure occur at pressures that are slightly higher than the pressures for the maxima in the plots for total ion current vs. pressure. Pressure plots such as these will be observed for these gases with all mass spectrometer sources. The decreases in ion current at higher pressures result from the loss of ions by scattering outside the source and from a decreased penetration of the electrons into the source. Similar plots which show maxima in sample ion current vs. pressure are observed with all CI reagent gases. The pressures of the maxima in sample ion current are inversely related to the molecular weights of the reagent gases. That is, one can achieve a good sensitivity in CI operation at a significantly higher pressure of CH_4 or NH_3 than of i-C_4H_{10} or i-C_5H_{12}.

These experiments were performed with $C_6H_5COC_9H_{19}$ introduced with the glass probe using the same values of source and probe temperatures, electron current, and electron multiplier voltage for all pressures of i-C_4H_{10} and i-C_5H_{12}. Comparisons between reagent gases of sample ion currents at the same reagent gas pressure indicate a slightly lower sensitivity for i-C_5H_{12} than for i-C_4H_{10}. However, there are comparable sensitivities for the two reagent gases at all pressures and the pressures for the maximum sensitivities are approximately the same.

Maximum sensitivity occurs at pressures of about 0.1 torr for both gases. However, at 0.1 torr, the ratio, $C_4H_9^+/C_3H_7^+$, is about 1.7 for i-C_4H_{10} and the $C_5H_{11}^+/C_3H_7^+$ ratio for i-C_5H_{12}

[1] Present address: Hercules, Inc., Research Center, Wilmington, DE 19894.

0003-2700/85/0357-0680$01.50/0 © 1985 American Chemical Society

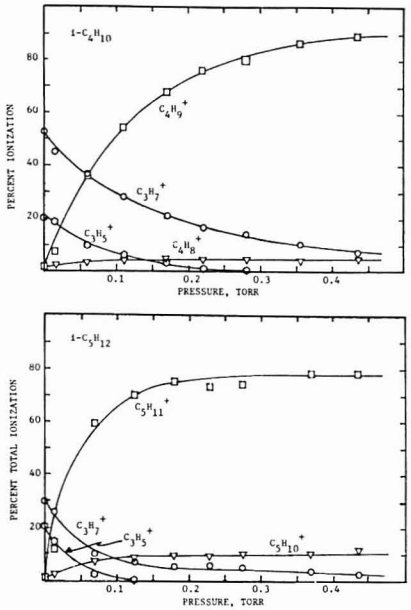


Figure 1. Pressure variation of relative abundances of major ions in isobutane (top) and isopentane (bottom).

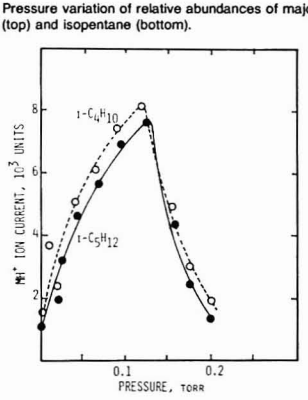


Figure 2. Pressure variation of sample ion current for MH^+ ions from decanophenone with isobutane and isopentane.

is about 8. There are few data for direct comparison, but such data indicate that $C_3H_7^+$ reacts more rapidly than $t\text{-}C_4H_9^+$ and that $t\text{-}C_4H_9^+$ reacts more rapidly than $t\text{-}C_5H_{11}^+$ for exothermic reactions (*11*). In addition, $s\text{-}C_3H_7^+$ reacts rapidly with many compounds with which $t\text{-}C_4H_9^+$ and $t\text{-}C_5H_{11}^+$ do not react because the reactions of $t\text{-}C_4H_9^+$ and $t\text{-}C_5H_{11}^+$ with the compounds are endothermic and reactions of $s\text{-}C_3H_7^+$ with the same compounds are exothermic. At 150 °C a reaction with an activation energy of 3 kcal/mol will occur at only 3% of the rate for the reaction without an activation energy.

One may expect very similar reactivities for $t\text{-}C_4H_9^+$ and $t\text{-}C_5H_{11}^+$ as CI reagent ions from thermochemical considerations. Both ions are weak Bronsted acids for proton transfer reactions

$$C_xH_{2x+1}^+ + B \rightarrow BH^+ + C_xH_{2x} \quad (1)$$

The heats of these proton transfer reactions are calculated from the proton affinities (or basicities) of the neutral molecules

$$\Delta H_1 = PA(C_xH_{2x}) - PA(B) \quad (2)$$

The proton affinity is defined as

$$PA(X) = \Delta H_f(X,g) + \Delta H_f(H^+,g) - \Delta H_f(XH^+,g) \quad (3)$$

The *tert*-butyl ion is a slightly stronger Bronsted acid than the *tert*-pentyl ion, since $PA(i\text{-}C_4H_8) = 195.9$ kcal/mol and $PA(i\text{-}C_5H_{10}) = 196.4$ kcal/mol (*12*); that is, $i\text{-}C_4H_8$ is a slightly weaker base than $i\text{-}C_5H_{10}$. For comparison, $PA(C_3H_6) = 179.5$ kcal/mol (*12*); consequently, $s\text{-}C_3H_7^+$ is a much stronger Bronsted acid than $t\text{-}C_4H_9^+$ or $t\text{-}C_5H_{11}^+$.

Both are relatively weak Lewis acids for hydride transfer reactions

$$C_xH_{2x+1}^+ + AH \rightarrow C_xH_{2x+2} + A^+ \quad (4)$$

The heats of these hydride transfer reactions can be calculated from the hydride affinities (or the acid strengths) of the ions

$$\Delta H(4) = H^-A(A^+) - H^-A(C_xH_{2x+1}^+) \quad (5)$$

The hydride affinity of the ion is defined as

$$H^-A(A^+) = \Delta H_f(A^+,g) + \Delta H_f(H^-,g) - \Delta H_f(AH,g) \quad (6)$$

The *tert*-butyl ion is a slightly stronger Lewis acid than the *tert*-pentyl ion: $H^-A(t\text{-}C_4H_9^+) - H^-A(t\text{-}C_5H_{11}^+) = 3.2$ kcal/mol (*13–15*). One would expect similar small differences in Lewis acid strengths of these two ions for the abstraction of Cl^- or OH^- groups. The hydride affinity of $s\text{-}C_3H_7^+$ is about 16 kcal/mol greater than the hydride affinity of $t\text{-}C_4H_9^+$; consequently, $s\text{-}C_3H_7^+$ is a significantly stronger Lewis acid than $t\text{-}C_4H_9^+$ or $t\text{-}C_5H_{11}^+$.

CI spectra obtained with $i\text{-}C_4H_{10}$ at low pressures (~0.1 torr) include significant contributions to sample ionization from reactions of $s\text{-}C_3H_7^+$ as well as from the expected reactions of $t\text{-}C_4H_9^+$. CI spectra obtained with $i\text{-}C_5H_{12}$ at comparable pressures will contain much smaller contributions from reactions of $s\text{-}C_3H_7^+$ and will result primarily from reactions of $t\text{-}C_5H_{11}^+$. The present set of experiments was designed primarily to study the reactions of $t\text{-}C_4H_9^+$ and $t\text{-}C_5H_{11}^+$; consequently, the experiments were performed at reagent gas pressures greater than 0.25 torr.

In general, the $i\text{-}C_4H_{10}$ and $i\text{-}C_5H_{12}$ CI spectra are very similar. Simple ketones and amines give $(M + H)^+$ ions as the only significant species. For aliphatic alcohols, the dominant ions are $(M - OH)^+$ with small amounts of $(M - H)^+$. For simple esters, the dominant species are the $(M + H)^+$ ions. Low sensitivities are noted with branched hydrocarbons to give $(M - H)^+$ ions with little fragmentation; $i\text{-}C_5H_{12}$ discriminates against aliphatic hydrocarbons more strongly than $i\text{-}C_4H_{10}$. For some substituted aromatic compounds, the $i\text{-}C_5H_{12}$ spectra contain significantly more $M^{+\cdot}$ ions than the $i\text{-}C_4H_{10}$ spectra, presumably from charge exchange reactions of $C_5H_{10}^+$.

Spectra of several pesticides with these two reagent gases (Table II) were very simple and very similar. For ronnel (see Table I for structures), both spectra contain $(M + H)^+$ ions as the base peak and only two minor fragment ions whose abundances are the same for the two reagent gases: $(M + H - CH_3OH)^+$, 1%, and 111^+, 3%, of the base peak. For dimethoate, $(M + H)^+$ is the base peak and the only fragment ion is 125^+, probably $(CH_3O)_2PS^+$, 14% of the base peak with both reagent gases. The spectra of CIPC are shown in Table

Table I. Structures of Pesticides and Steroids

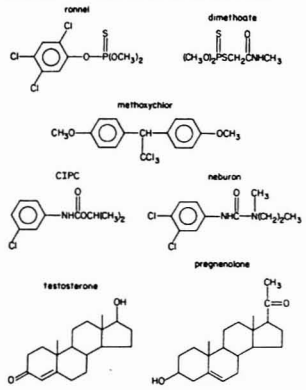


Table II. Comparison of i-C_4H_{10} and i-C_5H_{12} CI Spectra of Pesticides

ion	% base peak[a] i-C_4H_{10}	% base peak[a] i-C_5H_{12}
CIPC		
$(M + H)^+$	100	100
$M^{+\cdot}$	1.7 ± 0.7	20 ± 2
$(M + H - C_3H_6)^+$	54 ± 5	79 ± 5
$ClC_6H_4NH_3^+$	2.2 ± 0.5	≤0.5
Methoxychlor		
$(M + H)^+$	61 ± 10	7 ± 3
$M^{+\cdot}$	5 ± 2	≤0.5
$(M - Cl)^+$	86 ± 14	8 ± 1
$(M - CCl_3)^+$	4 ± 2	5 ± 1
$(M - C_6H_4OCH_3)^+$	100	100

[a] Average value ± standard deviation of 10 measurements for each compound. All Cl isotopes are included. $P(i\text{-}C_4H_{10}) \simeq P(i\text{-}C_5H_{12})$ = 0.3 torr; t(source) = 135 °C.

II. Again, both reagents give $(M + H)^+$ as the base peak and the dominant fragment ion is the loss of C_3H_6 from $(M + H)^+$, 55% of the base peak for i-C_4H_{10} and 80% for i-C_5H_{12}. Significantly more molecular ions are present in the i-C_5H_{12} CI spectrum than in the i-C_4H_{10} spectrum, presumably because of the greater abundance of $C_5H_{10}^+$ from i-C_5H_{12} than $C_4H_8^+$ from i-C_4H_{10}. Also perhaps some of the $M^{+\cdot}$ ions of CIPC formed by the higher energy charge exchange reaction with $C_4H_8^+$ have decomposed. If we assume that $C_4H_8^+$ is the isobutene ion, IP(i-C_4H_8) = 9.2 eV (*16*), and that $C_5H_{10}^+$ is the lower energy isopentene ion, IP($CH_3CH{=}C(CH_3)_2$) = 8.7 eV (*16*), then the presence of an abundant $M^{+\cdot}$ ion in the i-C_5H_{12} CI spectrum of CIPC indicates that CIPC has an ionization energy less than 8.7 eV. The spectra of neburon contain two major ions, $(M + H)^+$ and 88^+: there is a difference in the ratio of the two major peaks, $88^+/(M + H)^+$ = 0.8 for i-C_4H_{10} and 1.2 for i-C_5H_{12}. The ion at $m/z = 88^+$ is perhaps $CH_3(C_4H_9)NH_2^+$ formed in a cyclic rearrangement decomposition of $(M + H)^+$.

The spectra of methoxychlor are listed in Table II. The CH_4 CI spectrum of methoxychlor is also relatively simple: $(M + H)^+$, 39%; $(M - Cl)^+$, 100%; $(M - CCl_3)^+$, 5%; and $(M - C_6H_4OCH_3)^+$, 93%. The expectation was, of course, that decreasing the acid strength of the reagent ions would decrease the extent of fragmentation and increase the abundance of $(M + H)^+$ ions. This expectation was achieved to some extent by changing from CH_4 to i-C_4H_{10}: $(M + H)^+$ = 39% of base peak or 17% of sample ionization with methane and 61% of base peak or 24% of sample ionization with i-C_4H_{10}. The weaker Bronsted acid, t-$C_5H_{11}^+$, gives only small amounts of $(M + H)^+$ ions, 7% of base peak or 6% of sample ionization. Perhaps, then, the proton affinity of methoxychlor is less than that of isopentene. If this is the case (and no data are available on the proton affinity of methoxychlor), then additional reactions must be postulated to explain the base peak in the spectrum, $(M - C_6H_4OCH_3)^+$. Indeed, it is surprising that this ion, $(M - C_6H_4OCH_3)^+$, is the most abundant ion in the i-C_4H_{10} CI spectrum of methoxychlor. A reaction which is possible, although it cannot be established from these data, is the attack by t-$C_4H_9^+$ or t-$C_5H_{11}^+$ on the aromatic ring to alkylate the species, followed by the loss of an alkylated anisole so that the $(M - C_6H_4OCH_3)^+$ ion could be represented as $(M + R - RC_6H_4OCH_3)^+$. This type of reaction is an extenstion of the X^- transfer reaction observed with t-$C_4H_9^+$ and alkyl halides or alcohols (and indicated by the $(M - Cl)^+$ ions in the spectra of methoxychlor in Table II). Since the i-C_4H_{10} CI spectrum of methoxychlor contains 5% M^+ and the i-C_5H_{12} spectrum contains very little M^+, ≤0.5%, we suggest that the ionization potential of methoxychlor (which has not yet been reported) lies in the range, 8.7 < IP < 9.2 eV.

Table III. Comparison of i-C_4H_{10} and i-C_5H_{12} CI Spectra of Steroids

ion	% base peak[a] i-C_4H_{10}	% base peak[a] i-C_5H_{12}
Testosterone		
$(M + 57)^+$	3.6 ± 0.4	≤0.5
$(M + 57 - 18)^+$	2.9 ± 0.9	≤0.5
$(M + H)^+$	100	100
M^+	≤0.5	2.5 ± 0.9
$(M - H)^+$	2.2 ± 0.4	5 ± 2
$(M - OH)^+$	3 ± 1	12 ± 3
$(M - OH - H_2O)^+$	2.5 ± 0.4	6 ± 2
$(M - H - 2H_2O)^+$	4.1 ± 0.7	4.1 ± 0.4
Pregnenolone		
$(M + 57 - 18)^+$	3.4 ± 0.4	≤0.5
$(M + H)^+$	100	100
$M^{+\cdot}$	3.6 ± 0.2	23 ± 2
$(M - H)^+$	3.5 ± 0.4	≤0.1
$(M - OH)^+$	90 ± 3	97 ± 4

[a] Average ± standard deviation of 10 measurements. $P(i\text{-}C_4H_{10}) \simeq P(i\text{-}C_5H_{12})$ = 0.3–0.4 torr; t(source) = 130 °C.

For a series of steroids the CI spectra with i-C_4H_{10} and with i-C_5H_{12} are also simple and similar. Table III shows a comparison of spectra for two steroidal keto-alcohols. The differences in the spectra are small, probably real, and difficult to interpret. These differences in spectra are perhaps less than the differences in spectra from one instrument to another. Similar small differences were observed for several other steroids. In general, there was a greater abundance of $M^{+\cdot}$ ions in i-C_5H_{12} than in i-C_4H_{10} CI spectra. Although $(M + C_4H_9)$ + and $(M + C_4H_9 - H_2O)^+$ ions were observed in the i-C_4H_{10} CI spectra of some of the steroids, the analogous ions, $(M + C_5H_{11})^+$ and $(M + C_5H_{11} - H_2O)^+$, were not observed with i-C_5H_{12}. These dehydrated adduct ions are somewhat confusing since $(M + 57 - H_2O)^+$ and $(M - OH)^+$ ions may be considered as indicating an impurity of molecular weight, M − 18. The absence of $(M + C_5H_{11})^+$ and $(M + C_5H_{11} - H_2O)^+$ ions may be an advantage for steroid analysis.

The i-C_4H_{10} and i-C_5H_{12} CI spectra of a series of amino acids were very simple, mostly $(M + H)^+$ with small amounts of (M

Table IV. Relative Sensitivities with i-C_4H_{10} and i-C_5H_{12}[a]

	i-C_4H_{10}	i-C_5H_{12}
2-methylheptane, $(M - H)^+$	0.29	0.08
1-chlorohexane, $(M - Cl)^+$	0.41	0.13
3-ethyl-3-pentanol, $(M - OH)^+$	0.44	0.27
cyclohexanone, $(M + H)^+$	1.00	0.85
butyl butyrate, $(M + H)^+$	0.30	0.22
tripropylamine, $(M + H)^+$	0.37	0.31

[a] Average of three determinations, relative errors ±15%; cyclohexanone = 1; t = 110 °C; 0.33 torr i-C_4H_{10} + 0.62 torr He; 0.36 torr i-C_5H_{12} + 0.62 torr He.

$+ H - CO_2H_2)^+$. Much less decomposition is observed in these spectra than is observed with CH_4 as the CI reagent gas (*17*). The i-C_4H_{10} CI spectrum of isoleucine is similar to that reported previously for leucine (*18*). The major decomposition ion for these amino acids was $(M + H - CO_2H_2)^+$ and somewhat less of this ion was produced with i-C_5H_{12} than with i-C_4H_{10}: 1% vs. 6% for threonine; 3% vs. 6% for isoleucine; 3% vs. 5% for methionine. Adduct ions, $(M + C_4H_9)^+$ and $(M + C_5H_{11})^+$, were observed for most of these amino acids, as well as small amounts of the dehydrated adduct ions, $(M + C_4H_9 - H_2O)^+$ and $(M + C_5H_{11} - H_2O)^+$.

Relative sensitivities, Table IV, , were determined for several compounds with these two reagent gases by measuring the total areas of characteristic sample ions as known amounts of the compounds were separated by the gas chromatograph and passed into the source of the mass spectrometer. Comparisons of relative sensitivities for different compounds with the same reagent gas are reliable because the experimental parameters can be maintained constant during the chromatographic experiment and the relative values are not strongly dependent on the experimental conditions (*3*, *7*). Comparisons of sensitivities between CI reagent gases with the same compound depend strongly on the experimental conditions and may not constitute a comparison between the maximum sensitivities of each reagent gas.

Sensitivities with i-C_5H_{12} are slightly lower than sensitivities with i-C_4H_{10} under comparable conditions of temperature and pressure for polar compounds for which exothermic proton transfer reactions are likely for both t-$C_4H_9^+$ and t-$C_5H_{11}^+$: cyclohexanone, butyl butyrate, and tripropylamine, Table IV. The differences are relatively small. Significant differences in sensitivities are noted for other compounds. Hydroxide transfer from the tertiary alcohol and hydride transfer from 2-methylheptane are slightly exothermic reactions with t-$C_4H_9^+$ and the reactions are a few kcal/mol less exothermic with t-$C_5H_{11}^+$. The lower sensitivity of i-C_5H_{12} than of i-C_4H_{10} with hydrocarbons may be an advantage in the selective detection of polar compounds in hydrocarbon mixtures by reactant ion monitoring in GC/CI MS (*19*). The Cl^- abstraction reaction from n-$C_6H_{13}Cl$ is endothermic for both t-$C_4H_9^+$ and t-$C_5H_{11}^+$ and the $C_6H_{13}^+$ ion may result from reactions of other ions from the reagent gases.

Precise mass measurements can be made with both i-C_4H_{10} and i-C_5H_{12} as CI reagent gases. Our experience is that the standard fluorinated mixtures, PFK and PFTBA, are not satisfactory because of the low sensitivities for these compounds. For compounds with molecular weights of 200–400, it was possible to find an amine, a ketone, or an ester of approximately the correct molecular weight for accurate mass determination by peak matching.

The CI spectra obtained with i-C_5H_{12} are generally very simple and provide abundant $(M + H)^+$ ions with little fragmentation for compounds more basic than i-C_5H_{10}. The spectra are quite similar to those obtained with i-CH_{4}. The sensitivities of the two reagent gases are nearly the same for basic compounds. The two reagent gases, i-C_4H_{10} and i-C_5H_{12}, can probably be used interchangeably, although i-C_5H_{12} may be somewhat more selective than i-C_4H_{10}. One advantage of the use of i-C_5H_{12} is the ease with which the vapor may be introduced from the liquid without an extensive vacuum manifold.

Registry No. CICP, 101-21-3; i-C_5H_{12}, 78-78-4; i-C_4H_{10}, 75-28-5; methoxychlor, 72-43-5; testosterone, 58-22-0; pregnenolone, 145-13-1; 2-methylheptane, 592-27-8; 1-chlorohexane, 544-10-5; 3-ethyl-3-pentanol, 597-49-9; cyclohexanone, 108-94-1; butyl butyrate, 109-21-7; tripropylamine, 102-69-2; decanophenone, 6048-82-4; threonine, 72-19-5; isoleucine, 73-32-5; methionine, 63-68-3.

LITERATURE CITED

(1) Munson, M. S. B.; Field, F. H. *J. Am. Chem. Soc.* **1966**, *88*, 2621–2630.
(2) Polley, C. W., Jr.; Munson, B. *Anal. Chem.* **1981**, *53*, 308–312.
(3) Field, F. H. *J. Am. Chem. Soc.* **1969**, *91*, 2827–2839.
(4) Milne, G. W. A.; Fales, H. M.; Axenrod, T. *Anal. Chem.* **1971**, *43*, 1815–1820.
(5) Jelus, B. L.; Murray, R. K., Jr.; Munson, B. *J. Am. Chem. Soc.* **1975**, *97*, 2362–2365.
(6) Hansen, G.; Munson, B. *Anal. Chem.* **1978**, *50*, 1130–1134.
(7) Hatch, F. W.; Munson, B. *J. Phys. Chem.* **1978**, *82*, 2362–2369.
(8) Polley, C. W., Jr. Ph.D. Thesis, University of Delaware, 1980.
(9) Long, J.; Munson, B. *J. Am. Chem. Soc.* **1972**, *94*, 3339–3342.
(10) Hancock, R. A.; Walder, R.; Weigel, H. *Org. Mass Spectrom.* **1979**, *14*, 507–511.
(11) Sieck, L. W.; Lias, S. G. *J. Phys. Chem. Ref. Data* **1976**, *5*, 1123–1146.
(12) Lias, S. G.; Liebman, J. F.; Levin, R. D. *J. Phys. Chem. Ref. Data*, in press.
(13) Solomon, J. J.; Field, F. H. *J. Am. Chem. Soc.* **1973**, *95*, 4483–4486.
(14) Solomon, J. J.; Meot-ner, M.; Field, F. H. *J. Am. Chem. Soc.* **1974**, *96*, 3727–3732.
(15) Goren, A.; Munson, B. *J. Phys. Chem.* **1976**, *80*, 2848–2854.
(16) Rosenstock, H. M.; Draxl, K.; Steiner, B. W.; Herron, J. T. *J. Phys. Chem. Ref. Data* **1977**, *6*, Suppl. No. 1.
(17) Tsang, C. W.; Harrison, A. G. *J. Am. Chem. Soc.* **1976**, *98*, 1301–1308.
(18) Meot-ner, M.; Field, F. H. *J. Am. Chem. Soc.* **1973**, *95*, 7207–7211.
(19) Hatch, F.; Munson, B. *Anal. Chem.* **1977**, *49*, 731–733.

RECEIVED for review September 5, 1984. Accepted November 19, 1984. Supported by Grant 5R01 GM 25269 from the National Institute of General Medicine.

Methane Enhanced Negative Ion Mass Spectra of Hexachlorocyclopentadiene Derivatives

Elizabeth A. Stemmler and Ronald A. Hites*

School of Public and Environmental Affairs and Department of Chemistry, Indiana University, Bloomington, Indiana 47405

The methane, electron capture, negative ion mass spectra of 24 bridged polycyclic chlorinated pesticides are presented. The effects of ion source pressure and temperature upon the spectra are discussed. These spectra differ from spectra which have previously appeared in the literature, although they were obtained under similar conditions of pressure and temperature. The spectra presented here consist of molecular ions, $[M + H - Cl]^-$ ions and various fragment ions, while the previously reported spectra were dominated by low mass ions such as Cl^- and by $[M + Cl]^-$ adduct ions. In order to better understand why similar operating conditions result in different modes of ionization (electron capture vs. adduct ion formation), the spectrum of α-chlordane was examined with different concentrations of chloride ion and varying amounts of sample molecules present in the ion source. Results of this study indicate that the $[M + Cl]^-/M^-$ ratio increases with increasing sample concentration and added chloride ion. The spectra reported here should be observed when working with the small size samples normally encountered when using capillary column GCMS.

The polychlorinated, bicyclic compounds shown in Figure 1 are derivatives of hexachlorocyclopentadiene (1). Many of these compounds were introduced in the 1940s as insecticides. It was later discovered that some of these compounds (or their degradation products) were carcinogenic, and thus, with the exception of the endosulfans (18–20) and Pentac (23), their use has been banned or severely restricted (*1*). Although their use has been curtailed, these compounds are environmentally persistent and have been found in fish (*2*) and in sediment (*3*). The electron impact (*4*) and positive chemical ionization (*5*) spectra of these compounds have been reported.

The derivatives of hexachlorocyclopentadiene, like many environmental contaminants, contain atoms or functionalities which stabilize a negative charge. Thus, the detection and identification of these compounds should be facilitated by the formation of negative ions. Negative ions may be generated (a) by electron capture (electron capture negative ion mass spectrometry, ECNIMS) using a nonreactive reagent gas such as methane or argon (*6*) or (b) by ion/molecule reactions (negative chemical ionization mass spectrometry, NCIMS) using a reactive reagent gas (*7–9*). Advantages of ECNIMS over electron impact and positive chemical ionization include selective ionization in the presence of complex matrices (*10*) and greater sensitivity (*6*).

Dougherty et al. reported the methane negative ion (MNI) mass spectra of ten of these chlorinated bicyclic insecticides (*11*). The mass spectra were dominated by $[M + Cl]^-$ and other adduct ions in the high mass region. At low mass, ions such as Cl^-, HCl_2^-, and H_2OCl^- were the most intense peaks in the spectra of six compounds. In our laboratory, using the same reagent gas and similar temperature and pressure conditions, we observed spectra which differed from the spectra reported by Dougherty et al. (*11*). Our results are in agreement with the spectra of chlordane (*12–14*) and nonachlor (*12*) which have recently appeared in the literature. These spectra are dominated by molecular ions and fragment ions resulting from electron capturing processes. Adduct ions are not observed under our conditions.

This paper will present the MNI mass spectra of the hexachlorocyclopentadiene derivatives given in Figure 1. Interpretively useful features of these spectra and the effects of pressure and temperature will be discussed. The questions of why different modes of ionization (electron capture vs. ion/molecule reactions) are observed under similar conditions of pressure and temperature and how the sample and chloride ion concentrations effect the $[M + Cl]^-/M^-$ ratio will be addressed.

EXPERIMENTAL SECTION

All studies were carried out on a Hewlett-Packard 5985B GC/MS system equipped for EI and CI operation. Samples were introduced via a 30 m × 0.25 mm DB-5 fused silica column (J&W Scientific, Rancho Cordova, CA) with helium as the carrier gas. Methane reagent gas was introduced through a modified transfer line (*15*) at a flow rate sufficient to achieve the desired source pressure. During the experiments reported here the source pressure was monitored by measuring the voltage reading from a thermocouple gauge tube which was located on the side of the ion source. The opening where the direct insertion probe entered the source was plugged; this avoided variations in source conductance, and thus, the flow of methane necessary to achieve a given pressure. We have since installed a capacitance manometer in our system. Pressure measurements of 1 torr, measured by the thermocouple gauge, correspond to a pressure of 0.25 torr, measured with the capacitance manometer. Pressures reported in this paper are the thermocouple gauge measurements converted to the corresponding capacitance manometer pressures. The ion source temperature was varied between 250 °C and 100 °C and was monitored by a thermocouple located in the ion source block. Electron energy was typically 230 eV; electron emission current was kept at 300 μA. The mass axis was calibrated with the m/z 281 and 400 ions of perfluorokerosene-L (PCR Research Chemicals, Inc., Gainesville, FL), the m/z 123 ion of nitrobenzene (Aldrich), and the m/z 633 ion of perfluorotributylamine. After the system was tuned, a standard of 1 ng/μL of chlordene (8) and α-chlordane (15) was run to check instrument performance.

With the exception of Pentac (23) (Chemical Services, Inc., Westchester, PA), all compounds used in this study were obtained from the EPA Health Effects Research Laboratory, Office of Research and Development, Research Triangle Park, NC. The isotopically labeled compounds were also obtained from this laboratory. These compounds were synthesized from hexachlorocyclopentadiene which contained 92.9% ^{37}Cl (*16*). Octachlorofulvalene (24) was synthesized by partial dechlorination of Pentac (23) with triisopropyphophite (Aldrich) according to Mark (*17*). Dark blue crystals were obtained with the correct melting point. The methane-d_4 was obtained from KOR Isotopes, Cambridge, MA. All standards were made up in hexane at a concentration of about 10 ng/μL, and 1-μL injections were used. Samples were injected in the splitless mode (0.7 min load).

Methylene chloride–methane spectra were obtained by introducing methylene chloride (EM Science) such that it accounted for about 20% of the total ion source pressure as measured with the thermocouple gauge. At this concentration, the chloride ion

0003-2700/85/0357-0684$01.50/0 © 1985 American Chemical Society

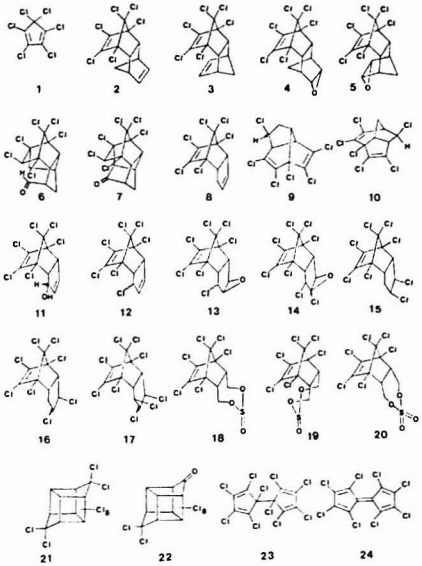


Figure 1. Derivatives of hexachlorocyclopentadiene: (1) hexachlorocyclopentadiene, (2) aldrin, (3) isodrin, (4) dieldrin, (5) endrin, (6) endrin aldehyde, (7) endrin ketone, (8) chlordene, (9) α-chlordene, (10) γ-chlordene, (11) 1-hydroxychlordene, (12) heptachlor, (13) heptachlor epoxide, (14) oxychlordane, (15) α-chlordane, (16) γ-chlordane, (17) *trans*-nonachlor, (18) endosulfan I, (19) endosulfan II, (20) endosulfan cyclic sulfate, (21) mirex, (22) kepone, (23) pentac, (24) octachlorofulvalene.

current was not depleted when compounds entered the ion source. The ion source temperature was 200 °C, and the ion source pressure was about 1 torr. The CH_2Cl_2/CH_4 plasma showed ions at m/e 35, 71, and 119 (Cl^-, HCl_2^-, and $CH_2Cl_3^-$) in a ratio of 100:1.5:5.8.

Direct insertion probe spectra were obtained by using submicrogram amounts of Pentac (23) and octachlorofulvalene (24) or several microgram quantities of α-chlordane (15). Ion source temperature was 200 °C and the probe held at 100 °C for 5 min and programmed up to 250 °C at 10 °C/min.

RESULTS AND DISCUSSION

The tabulated spectra of the 24 chlorinated bicyclic compounds, obtained at ion source temperatures of 250 °C and 100 °C, are shown in Tables I and II, respectively. Ion intensities were normalized to the base peak in the spectra; only the mass and intensity of the lightest ion in each ion cluster are reported. In the following discussion, the effects of pressure and temperature upon the spectra will be reported. This will be followed by an examination of fragmentation patterns and their relationship to molecular structure. Features of these spectra which are interpretively useful and indicative of a particular group of compounds will be emphasized.

Pressure. The effect of ion source pressure on sensitivity and on ion abundance was studied in the range of 0.1–0.8 torr at an ion source temperature of 100 °C using α-chlordane (15). Increasing the ion source pressure resulted in enhanced sensitivity, which has been attributed to an increase in collisional stabilization and/or a decrease in electron energy (*18*). Typically, maximum sensitivity was realized at a pressure of approximately 0.35 torr. The intensity of individual ions

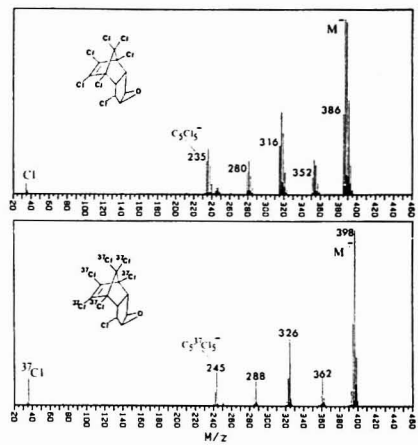


Figure 2. Methane enhanced negative ion mass spectra of heptachlor epoxide and [^{37}Cl]heptachlor epoxide. Ion source temperature was 100 °C.

relative to the total ion current varied by less than a factor of 5 over the range of 0.1–0.8 torr. While the ion source pressure has a large effect upon sensitivity, the appearance of the spectrum does not change very much with pressure.

Temperature. The ion source temperature has a significant effect upon ion intensities, as has been noted by many investigators (*19–22*). The chlorinated bicyclic compounds show an enhancement in molecular ion formation at low ion source temperatures. The relative intensity of fragment ions increases with increasing ion source temperature (see Tables I and II). These effects were observed when the ion source pressure was kept constant and when the reagent gas flow was held constant. Spectra obtained at different temperatures can differ dramatically, thus source temperature is an important parameter which must be carefully controlled. In our laboratory, it was concluded that the greatest structural information was usually obtained when spectra were run at an ion source temperature of 100 °C.

Molecular Ions. At 100 °C, molecular ions are observed for all compounds except mirex (21), kepone (22), and pentac (23). The molecular ion is the most intense peak for endrin (5), endrin aldehyde (6), γ-chlordene (10), heptachlor epoxide (13), oxychlordane (14), α- and γ-chlordane (15, 16), *trans*-nonachlor (17), and endosulfan I and II (18, 19). No $[M - H]^-$ ions are observed for any of the compounds.

C_5Cl_5 and C_5Cl_4O Ions. To further understand the formation of the ion at m/z 235 and other fragment ions, the spectra of isotopically labeled heptachlor epoxide and *trans*-nonachlor were measured (see Figures 2 and 3). These compounds were synthesized from 92.9% [^{37}Cl]hexachlorocyclopentadiene (*16*) yielding structures in which the hexachlorocyclopentadiene moiety contains chlorine-37 while remaining portion of the molecule contains chlorines of normal isotopic distribution.

A fragment ion at m/z 235 (C_5Cl_5) is observed for all compounds containing a hexachlorocyclopentadiene moiety. Spectra of the isotopically labeled compounds show that the C_5Cl_5 ion is shifted from m/z 235 to 245, and thus it contains five chlorine-37 atoms. The measured intensities are m/z 241 (7%), 243 (39%), 245 (100%) (theoretical 6:38:100). These results indicate that this ion may result from a retro-Diels–

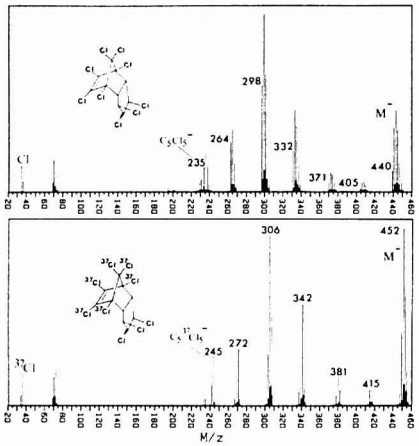
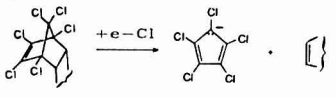
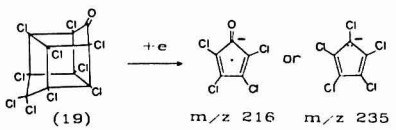


Figure 3. Methane enhanced negative ion mass spectra of *trans*-nonachlor and [^{37}Cl]-*trans*-nonachlor. Ion source temperature was 250 °C.

Scheme I



Scheme II

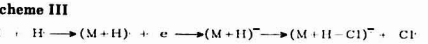


Alder reaction preceded by or followed by chlorine loss (see Scheme I) or from another type of ring opening reaction (see below) producing an aromatic anion containing [$4n + 2$] electrons. This m/z 235 ion is not observed for α- and γ-chlordene (**8** and **9**), which do not contain the hexachlorocyclopentadiene moiety. Pentac (**23**), for which loss of a chlorine would be more facile than cleavage of a carbon–carbon bond (see below) does not exhibit the m/z 235 ion either. The endosulfans (**18–20**) and endrin aldehyde and ketone (**6, 7**) appear to yield this ion; however, it is confused by overlapping ion clusters, requiring high resolution data for accurate assignments.

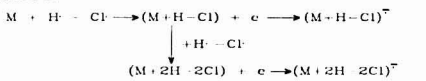
Another fragment ion of this type is observed in the spectrum of Kepone (**22**) and appears at m/z 216 (C_5Cl_4O). This ion may result from a retrocycloaddition reaction where the negative charge is retained on the carbonyl-containing five membered ring (see Scheme II). This reaction would also give the m/z 235 ion observed in the spectra of Kepone (**22**) and mirex (**21**).

[M + H − Cl]⁻ Ions. For many of the chlorinated bicyclic compounds, the first fragment ion appears 34 mass units lower than the molecular ion. Exceptions to this type of behavior include Pentac (**23**), which shows a loss of 35 from the molecular ion, endosulfan cyclic sulfate (**20**) and endosulfan II

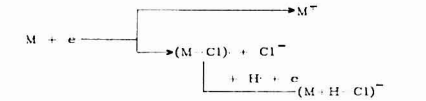
Scheme III



Scheme IV



Scheme V



(**19**) (at 250 °C), both of which show losses of 36. A number of compounds, such as heptachlor (**12**), oxychlordane (**14**), α-chlordane (**15**), and *trans*-nonachlor (**17**) showed weak [M − 34] ions. Multiple losses of 34 are also observed.

The loss of 34 mass units is accounted for by the loss of a chlorine radical and the addition of a hydrogen radical. A number of mechanisms exist which rationalize this loss. The most reasonable mechanisms involve reactions between sample molecules and hydrogen radicals, which are generated upon electron bombardment of the methane reagent gas. Reports of reactions between molecules and various alkyl and hydrogen radicals have appeared in the literature (*23–26*). These reactions are thought to occur rapidly prior to ionization and are characterized by: (a) a dependence upon emission current (with increasing emission currents, the intensity of ions resulting from molecules which have undergone radical reactions increases relative to molecular ions) and (b) reversion to simpler spectra lacking the radical additions when using a nitrogen plasma (*25*). Use of fully deuterated methane showed that the added species resulted from the methane plasma (*23*). In addition to our observations, examples of a loss of 34 mass units have been observed for the methyl derivative of a hydroxy polychlorinated dibenzofuran (*27*) and octachlorodibenzofuran (*28*).

In our experiments, we have observed that [M − 34]⁻ ions increase relative to the molecular ion as the emission current increases. Experiments using argon or nitrogen as the reagent gas also show the [M − 34]⁻ ions; however, the positive chemical ionization spectrum of the reagent gas shows ions at m/z 18 and 41 for argon (H_2O^+ and ArH^+) and m/z 18, 29, and 30 (H_2O^+, N_2H^+, and $N_2H_2^+$) for nitrogen. Experiments using fully deuterated methane show ions of similar intensity resulting from losses of both 34 and 33 (M + H − Cl and M + D − Cl). These results indicate that sources of hydrogen are present even in the absence of the hydrocarbon reagent gas.

Three general mechanisms which account for this behavior are shown in Schemes III–V. In Scheme III, addition of a hydrogen radical could be followed by electron capture and chloride loss. Scheme IV shows an addition–elimination reaction which could occur prior to ionization by electron capture. A series of addition–elimination reactions occurring prior to electron capture could account for the multiple losses of 34. A third possibility is shown in Scheme V where dissociative capture yields a [M − Cl] radical which can interact with a hydrogen radical and then undergo electron capture. An ion–radical reaction is also possible (*24*).

If ionization proceeded via Scheme III, some evidence for $(M + H)^-$ or $(M - Cl)^-$ ions should be observed. No evidence for $(M + H)^-$ ions has been observed and $(M - Cl)^-$ ions appear at low abundance in only a limited number of cases. Scheme V is also possible; however, multiple losses of 34 would ne-

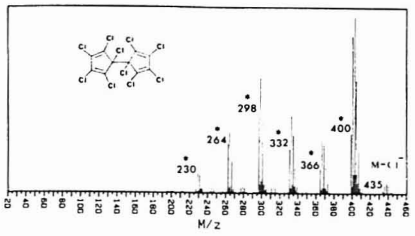


Figure 4. Methane enhanced negative ion mass spectrum of pentac. Ion source temperature was 250 °C. Asterisk indicates ions of the $C_{10}Cl_{8-x}H_x$ series.

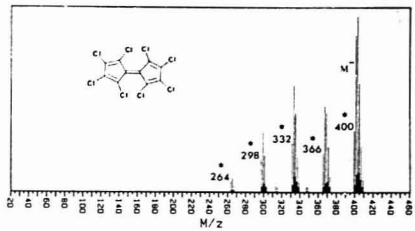
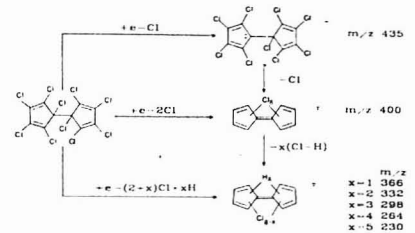


Figure 5. Methane enhanced negative ion mass spectra of octachlorofulvalene. Ion source temperature was 200 °C. Asterisk indicates ions of the $C_{10}Cl_{8-x}H_x$ series.

Scheme VI



cessitate a series of dissociative capture reactions followed by radical attack. This scheme also suggests that the abundance of chloride ion and radical addition products should be comparable, which is often not the case. The addition–elimination type mechanism (Scheme IV) accounts for the M^- ions, the $[M + H - Cl]^-$ ions, and the ion series differing by 34 mass units.

$C_{10}Cl_{8-x}H_x$ Ion Series. A number of compounds show an ion series differing by 34 mass units. A good illustration of this behavior is the spectrum of Pentac (**23**) (see Figure 4) which shows a series of ions beginning at m/z 230 ($C_{10}Cl_3H_5$) (addition of five hydrogens and loss of seven chlorines) and ending with m/z 400 ($C_{10}Cl_8$). The ions at m/z 264 ($C_{10}Cl_4H_4$), 298 ($C_{10}Cl_5H_3$), 332 ($C_{10}Cl_6H_2$), and 366 ($C_{10}Cl_7H$) fall in between. This series of ions results from the addition of up to five hydrogen atoms. In addition, other compounds with ten carbon skeletons yield the same series of ions. These are chlordene (**8**), 1-hydroxychlordene (**11**), heptachlor (**12**), α- and γ-chlordane (**15**, **16**), *trans*-nonachlor (**17**), mirex (**21**), and Pentac (**23**). A number of oxygenated ten-carbon compounds also show this ion series at m/z values 16 mass units higher: 1-hydroxychlordene (**11**), heptachlor epoxide (**13**), oxychlordane (**14**), and Kepone (**22**).

The first ions appearing in the spectrum of Pentac (**23**) result from the loss of one and two chlorine atoms to yield ions at m/z 435 and m/z 400. Loss of one chlorine would leave one of the five-membered rings with $[4n + 2]$ electron—a favorable aromatic Huckel system (see m/z 435, Scheme VI). Loss of a second chlorine yields the most intense ion in the spectrum. This ion has the formula $C_{10}Cl_8$ and is the first ion in a series of ions which have the general formula $C_{10}Cl_{8-x}H_x$. The remaining ions result from the loss of one to five 34 mass units from m/z 400 (see m/z 366, 332, ..., 230, Scheme VI).

The ion at m/z 400 may be the radical anion of octachlorofulvalene (**24**). This compound is electron deficient and forms charge-transfer complexes with aromatic π donors (*29*). The methane enhanced negative ion mass spectra of octachlorofulvalene is shown in Figure 5. This compound yields the ion series $C_{10}Cl_{8-x}H_x$ ($x = 0$ to 4) supporting the assignment

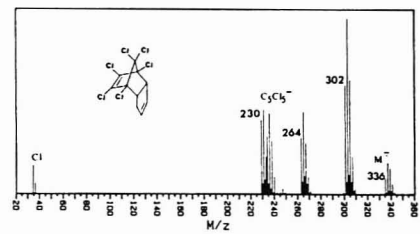
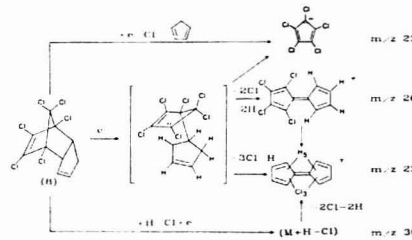


Figure 6. Methane enhanced negative ion mass spectra of chlordene. Ion source temperature was 100 °C. Asterisk indicates ions of the $C_{10}Cl_{8-x}H_x$ series.

Scheme VII



of ion structures made in Scheme VI. The electron accepting ability of octachlorofulvalene is of interest with regard to losses of m/z 34. Previous radical additions were observed for compounds which form charge-transfer complexes (*24*). The ability to form charge-transfer complexes was used to explain the rapidity of the radical reactions and, thus, the ability of radical reactions to complete with ionization.

The other ten carbon compounds which exhibit this series of ions can be classified as methanoindene (chlordene-like) or cage (mirex-like) structures. Because both structural types show the same ion series as Pentac (**23**) and octachlorofulvalene (**24**), these ions may be structurally similar, and the fragmentation of the methanoindene and cage compounds may be explained in the following manner:

Methanoindene compounds, such as chlordene (**8**) (see Figure 6), may capture an electron and form the ring-opened intermediate shown in Scheme VII. The intermediate is generated when a carbon–carbon bond is broken and an allyl anion and an allyl radical are generated. The loss of one chlorine and two hydrogens yields the $C_{10}Cl_4H_4$ ion at m/z 264. The ion at 34 mass units lower (m/z 230) may result from a parallel reaction where the $(M + H - Cl)$ species captures

Table I. Methane Enhanced Negative Ion Mass Spectra of Hexachlorocyclopentadiene Derivatives, Source Temperature 250 °C

	1 C5Cl6		2 C12C16H8		3 C12C16H8		4 C12C16H8O		5 C12C16H8O		6 C12C16H8O		7 C12C16H8O		8 C10C16H6		9 C10C16H6		10 C10C16H6		11 C10C16H6O	
	m/e	INT	m/e	INT	m/e	INT	m/e	INT	m/e	INT	m/e	INT	m/e	INT	m/e	INT	m/e	INT	m/e	INT	m/e	INT
M	270	--	362	--	362	--	378	4.6	378	10	378	0.8	378	2.7	336	--	336	--	336	--	352	--
M-Cl+H			328	5.0	328	46	344	33	344	33	344	9.2	344	9.8							318	2.8
M-Cl	235	61											343	12								
M-Cl-H													342	3.7								
M-2Cl+2H																						
M-2Cl+H	201	2.4																	266	6.3		
M-2Cl																	265	18	265	12		
M-2Cl-H																	264	7.1				
M-2Cl-2H															264	52					280	65
M-3Cl+H															232	50						
M-3Cl																						
M-3Cl-H															230	12	230	30	230	11	246	41
M-3Cl-2H																					245	62
M-3Cl-3H																					244	7.4
M-4Cl+2H																						
M-4Cl+H																						
M-4Cl																	196	9.3			212	31
M-4Cl-H																						
M-4Cl-2H																	194	5.9				
M-4Cl-3H																						
M-5Cl+3H																						
M-5Cl+2H																						
M-5Cl+H																						
M-5Cl																						
M-5Cl-H																						*
M-6Cl+4H																						
M-6Cl+2H																						
M-6Cl																						
M-7Cl+5H																						
M-7Cl+3H																						
M-7Cl+H																						
M-8Cl+6H																						
M-8Cl+4H																						
m/e 235		61		50		60		67		35	235	1.2				31		--		--		14
HCl2										5.3		1.0		2.4								10
C12										7.4				7.4								
Cl		26		100		100		17		35		8.3		12		18		100		100		23
Others			208	4.6	208	5.9	208	2.7	236	44	236	16	236	14							196	19
			227	4.6	227	37	227	2.1	270	60	*268	8.0	*270	16							230	28
			*256	2.8	*255	2.0	246	4.0	306	35	*272	100	*272	62							264	76
			*258	5.5	*258	9.4	*272	3.2			*304	14	*306	60								
							*274	7.2			*306	40	*308	100								

* Lowest mass and most intense ion in a complex cluster.

Table II. Methane Enhanced Negative Ion Mass Spectra of Hexachlorocyclopentadiene Derivatives, Source Temperature 100 °C

	1 C5Cl6		2 C12C16H8		3 C12C16H8		4 C12C16H8O		5 C12C16H8O		6 C12C16H8O		7 C12C16H8O		8 C10C16H6		9 C10C16H6		10 C10C16H6		11 C10C16H6O	
	m/e	INT	m/e	INT	m/e	INT	m/e	INT	m/e	INT	m/e	INT	m/e	INT	m/e	INT	m/e	INT	m/e	INT	m/e	INT
M	370	--	362	1.2	362	26	378	46	378	53	378	53	378	27	336	10	336	4	336	51	352	17
M-Cl+H			328	63	328	65	344	63	344	51	344	21	344	67	302	62	302	63	302	40	318	6
M-Cl	235	61											343	35								
M-Cl-H											342	1.9	342	4.1							316	2
M-2Cl+2H			294	2.6	294	2.2	310	9.4														
M-2Cl+H	201	2.4																				
M-2Cl																	266	9.6	266	4.3		
M-2Cl-H																	265	11	265	5.3	281	21
M-2Cl-2H															264	35					280	75
M-3Cl+H																						
M-3Cl																						
M-3Cl-H															230	45	230	5			246	7.0
M-3Cl-2H																					245	16
M-3Cl-3H																						
M-4Cl+2H																					212	5.2
M-4Cl+H																						
M-4Cl																						
M-4Cl-H																						
M-4Cl-2H																						
M-4Cl-3H																						
M-5Cl+3H																						
M-5Cl+2H																						
M-5Cl+H																						
M-5Cl																						
M-5Cl-H																						
M-6Cl+4H																						
M-6Cl+2H																						
M-6Cl																						
M-7Cl+5H																						
M-7Cl+3H																						
M-7Cl+H																						
M-8Cl+6H																						
M-8Cl+4H																						
m/e 235		61		26		5.0		10		5.2						33		--				2.9
HCl2														4.8								2.1
C12														12								
Cl		26		17		35		5.1		19		1.1		33		27		60		14		2.9
Others									*308	1.3	*270	18	*270	2.5							264	2.8
									*312	8.7	*272	14	*274	6.9								
											*306	6.4	*306	20								
											*308	9.1	*310	61								

* Lowest mass and most intense ion in a complex cluster.

12 C10C17H		13 C10C17H5O		14 C10C18H4O		15 C10C18H6		16 C10C18H6		17 C10C19H5		18 C9C16H6SO3		19 C9C16H6SO3		20 C9C16H6SO4		21 C10C112		22 C10C1100		23 C10C110	
m/e	INT	m/e	INT	m/e	INT	m/e	INT	m/e	INT	m/e	INT	m/e	INT	m/e	INT	m/e	INT	m/e	INT	m/e	INT	m/e	INT
370	--	386		420	2.9	406	2.9	406	33	440	11	404	9.8	404	42	420	0.6	540	--	486	--	470	--
								372	12	406	0.6	370	6.7										
						371	1.1	371	0.6	405	2.2											435	1.6
														368	24	384	50						
		316	41					338	3.7	372	1.0												
								337	1.4	371	4.9	335	2.0										
								336	0.6			334	6.1	334	40	350	29			416	16	400	34
298	39	314	1.6	348	16											349	4.5						
																348	4.7						
264	78	280	63	314	64													435	8.7	381	31	366	14
		279	3	313	24											314	3.0						
				312	1.8	298	9.1	298	35	332	24												
230	13	246	48	280	43															348	14	332	25
		245	11	279	18													400	35			330	2.8
		244	10	278	11	264	79	264	76	298	60												
				277	6.9																		
196	3.2	212	18	246	30	232	11	232	12	262	1.2									314	12	298	45
		211	2.4	245	3.0													366	1.3			296	2.8
		210	8.4	244	7.2	230	7.7	230	8.0	264	27							365	35				
																						294	1.6
				212	14															280	14	264	28
				210	2.5	196	1.1	196	1.2	230	5.5							332	6.5			262	3.2
																		330	2.8			260	
																				246	18	230	11
										196	2.0							298	12			228	1.9
																		296	1.2				
																						196	1.3
	7		63		26		24		13		14							264	3.5				
	3.2		11		2.5		10		4.1		20								2.9		17		
					0.9		3.7				5.7								1.8				
	20		100		7.0		19		4.7		17		36		8.7		3.2		1.8		5.9		6.3
																			24				
				*226	1.0	*337	4.3	*337	1.4			99	6.9	99	6.8	80	5.5			216	78		
				*281	20	*341	6.5	*340	5.1			*232	6.5	*232	30	97	100						
												*237	27	*236	24	185	15						
												*239	16	*239	12	*268	2.1						
												*242	100	*242	100	*270	2.5						
												*268	18	*268	34								
												*270	24	*270	46								

12 C10C17H5		13 C10C17H5O		14 C10C18H4O		15 C10C18H6		16 C10C18H6		17 C10C19H5		18 C9C16H6SO3		19 C9C16H6SO3		20 C9C16H6SO4		21 C10C112		22 C10C1100		23 C10C110	
m/e	INT	m/e	INT	m/e	INT	m/e	INT	m/e	INT	m/e	INT	m/e	INT	m/e	INT	m/e	INT	m/e	INT	m/e	INT	m/e	INT
370	17	388	100	420	36	406	34	406	34	440	26	404	54	404	54	420	35	540	--	486	--	470	--
		352	11			372	3.1	372	17	406	1.4	370	22	370	23								
336	1.3													368	3.0	*384	56					435	1.3
								338	6.9	372	1.3	336	4.8	336	4.9								
						337	1.6			371	1.4												
		*316	26			336	1.1							334	1.4					416	13	400	36
*298	42			*348	21																		
																						366	7.2
264	78	280	12	314	28													435	19	381	47		
				313	8.0																		
						298	1.0	298	1.0	332	0.8												
																				348	17	332	17
230	14																			347	6		
																		400	33	346	6	330	1.4
						264	8.9	264	2.2	298	5.1											328	1.7
																						298	19
																		366	35				
						230	1.6			264	2.4												
																		332	10			264	6.2
	30		12		6.6		4.4		1.0		1.7		1.0		0.6				1.6		8.9		
	3.0						2.0				1.2								1.0				
	20		1.0		1.0		2.8				2.0		1.8		0.5				2.4		17		2.0
		*241	4.5	*277	1.6							306	1.2	*240	1.2	*350	4.8			216	17		
		*248	3.9	*282	5.9									*242	1.4	*352	7.8				0.2		
														*304	1.5								
														*308	3.0								

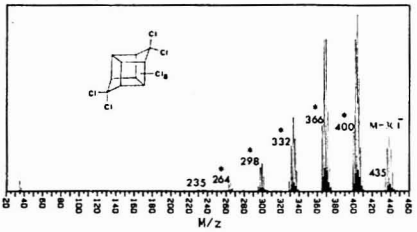
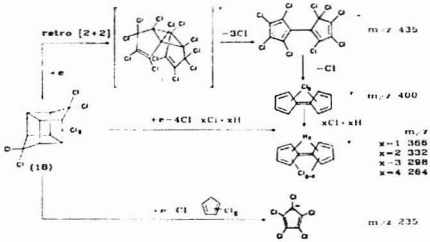


Figure 7. Methane enhanced negative ion mass spectra of mirex. Ion source temperature was 250 °C. Asterisk indicates ions of the $C_{10}Cl_{8-x}H_x$ series.

Scheme VIII



an electron and loses a chlorine and two hydrogens via a similar intermediate.

The cage compounds, such as mirex (18) (see Figure 7), may open by a retro [2 + 2] cycloaddition to form an intermediate (see Scheme VIII) which may undergo cleavage of a carbon–carbon bond and a loss of three chlorines to yield an ion at m/z 435, as seen with Pentac. Loss of one more chlorine yields the $C_{10}Cl_8$ ion at m/z 400, which is followed by the remaining $C_{10}Cl_{8-x}H_x$ ions of this series, differing by 34 mass units. Many oxygenated methanoindene compounds and kepone also show ions which have the general formula $C_{10}Cl_{8-x}H_xO$ at m/z 280, 314, 348, 382, and 416.

$[M + Cl]^-$ Ions. Significant differences were observed between the spectra reported here and those which appeared in the literature (*11*). The spectra differ in two respects: (a) many of the previously published spectra were dominated by low mass even electron negative ions such as Cl^-, H_2OCl^-, Cl_2^-, and HCl_2^- and (b) in the molecular ion region, the most prevalent ions previously reported resulted from adduction of the molecule with ionic species such as Cl^-, H_2OCl^-, OH^-, HCl_2^-, ClO^-, and Cl_3^-. Molecular ion intensities ranged from 0 to 39% of the intensity of the $[M + Cl]^-$ ion. Dimers, which were temperature and pressure dependent, were also reported. Little fragmentation was observed, except displacement of chlorine by oxygen at $(M - 19)^-$.

In contrast, the spectra observed in our laboratory showed only low abundance ions corresponding to Cl^-, Cl_2^-, and HCl_2^-. In the molecular ion region, molecular ions and the fragment ions described above dominate. The only adduct ions observed resulted from association with chloride ion and were observed for only a few compounds. In the concentration range normally used (up to about 10 ng injected), adduct ions were of low intensity (~1% relative to M^-) if observed at all. With our ion source modification (see Experimental Section), oxygen in the ion source was reduced, and $(M - 19)^-$ ions were not observed.

Our spectra and the previously published spectra were obtained under similar conditions of pressure and temperature and with the same reagent gas. There were, however, two major differences: (a) The previous spectra were obtained on an AEI MS-902 double focusing mass spectrometer equipped with an SRIC chemical ionization source, while our spectra were obtained on an HP 5985B quadrupole instrument. (b) We used capillary column gas chromatography to introduce, typically, up to 10 ng of sample while the direct introduction probe was used in the previous study to introduce microgram quantities of sample (*11*, *30*).

Scheme IX

1) $M + e \longrightarrow [M]^{\cdot -} \longrightarrow M^-$

2) $M + e \longrightarrow (M-Cl)\cdot + Cl^-$

3) $M + Cl^- \longrightarrow (M+Cl)^-$

4) $M + M^- \longrightarrow M_2^- \longrightarrow (M+Cl)^- + (M-Cl)\cdot$

Table III. Adduct Ion Ratios and Molecular Anion Sensitivity of α-Chlordane Using Methane and Methane–Methylene Chloride

	methane		methane–methylene chloride	
	10 ng	500 ng	10 ng	500 ng
$[M + Cl]^-/M^-$	0.0072 (±0.0003[a])	0.075 (±0.012)	0.93 (±0.04)	1.14 (±0.02)
M^-	100[b]	650	1	48

[a] One standard deviation. [b] Integrated area of m/z 410, normalized to 100, for 10 ng with methane.

The disparity between these spectra is disturbing when considering gas-enhanced negative ion mass spectrometry as an analytical tool for identification purposes. In an effort to explain these spectral differences, we undertook a study to determine factors which enhanced the formation of adduct ions in our system. Scheme IX shows a series of reactions which may be occurring in the ion source. Reactions 1 and 2 show electron capture. Depending upon the molecule, the energy of the electron, and the collisional frequency with neutral molecules, molecular anion formation or dissociation to yield a chloride ion and an (M – Cl) radical may occur. Adduct ions may be generated via interaction of sample molecules with this chloride ion (reaction 3) or by abstraction of chlorine from another sample molecule by the molecular anion (reaction 4).

Factors which may influence the ratio of molecular ion to chloride adduct ion include the concentration of chloride ion, the concentration of electrons and their energy distribution, the concentration of sample molecules, and the rate of electron capture vs. the rate of chloride attachment. We chose to study variations in the ratio of adduct ions to molecular ion by varying the concentrations of chloride ion and sample molecules. α-Chlordane was selected for study because this compound contains sp^3 hybridized sites which should facilitate chloride attachment, assuming the chloride ion interacts at a carbon center in α-chlordane, as has been reported (*8*).

As mentioned above, adduct ions were not normally observed under our operating conditions. Initially, we felt that this was due to the lower amount of chloride ion generated under our operating conditions. It was suggested that the addition of methylene chloride would increase the abundance of adduct ion with a parallel increase in sensitivity (*31*). Thus, spectra were measured in the presence and absence of methylene chloride, under conditions which are reported to favor adduct ion formation (*8*), and comparisons were made regarding the $[M + Cl]^-/M^-$ ratio and sensitivity.

The results of this study, carried out in the range of 10–500 ng injected, are tabulated in Table III. In the absence of

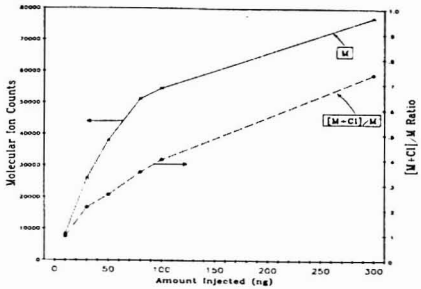


Figure 8. Molecular ion and $[M + Cl]^-/M^-$ ratio vs. amount injected for α-chlordane.

added methylene chloride, the $[M + Cl]^-/M^-$ ratio is less than 0.1 and increases as the amount injected increases (see below). In the presence of added methylene chloride, the $[M + Cl]^-/M^-$ ratio is at least an order of magnitude larger compared with methane alone; however, this $[M + Cl]^-/M^-$ ratio is not as high as that observed by Dougherty ($[M + Cl]^-/M^- = 8$) (*11*), suggesting that the high $[M + Cl]^-/M^-$ ratios observed by Dougherty may not be attributed solely to high chloride ion concentration. Molecular ion sensitivities were at least an order of magnitude higher using methane compared with methane–methylene chloride. This study indicates that the $[M + Cl]^-/M^-$ ratio increases with an added source of chloride ion and that no analytical advantage is realized by working with methylene chloride instead of methane.

Another study was undertaken where sample concentration was varied. Figure 8 shows a plot of the amount of α-chlordane injected vs. molecular ion abundance and $[M + Cl]^-/M^-$ ratio using methane as the reagent gas. As the amount of compound injected increased, the molecular ion exhibited a nonlinear response. This behavior has been noted in prior work (*6*, *7*, *32*) and is attributed to saturation of the electron population. The onset of this nonlinear region and the $[M + Cl]^-/M^-$ ratio varies with ion source conditions. The amount of adduct ion generated tracked this nonlinear behavior in molecular anion current. When low sample concentrations are used, adduct ions were not observed, either because of the low concentration of sample molecules or chloride anion or because the rate of electron capture is rapid relative to the chloride attachment process. However, with increasing sample concentrations, the $[M + Cl]^-$ ion begins carrying a larger percentage of the ion current. This may occur because the percentage of sample available for ionization via the competing process of chloride attachment increases when electron capture processes are limited. Alternatively, higher sample concentrations may result in an increase in intermolecular chloride transfer resulting in ionization via reaction 4 in Scheme IX.

Introduction of a larger quantity of α-chlordane (15) was accomplished by using the direct introduction probe. In this case, spectra were obtained which resembled Dougherty's spectra (see Figure 9) in terms of the $[M + Cl]^-/M^-$ ratio, although additions of oxygen, ClO, HCl_2, or Cl_3 were not observed.

Our results indicate that both an increase in sample concentration and chloride ion concentration result in an increase in the $[M + Cl]^-/M^-$ ratio. These observations suggest that the difference between our spectra and those of Dougherty may be due to differences in sample concentration and/or differences in the amount of chloride ion present in the ion source. The previous spectra (*11*) were obtained by using the direct introduction probe technique which resulted in the introduction of larger amounts of sample than are normally encountered using capillary column gas chromatography. With small sample sizes, we observe electron capture processes dominating over chloride attachment. The ions attributed to electron capture processes approach a limiting value with larger sample sizes, and the $[M + Cl]^-/M^-$ ratio increases. The amount of molecular ion relative to chloride ion and other fragment ions depends, in part, upon the electron population and energy distribution. If larger sample concentrations are used, or if ion source conditions favor chloride ion formation vs. molecular ion formation, then adduct ion formation may dominate the spectra. Under normal capillary column GC/MS conditions, they will not.

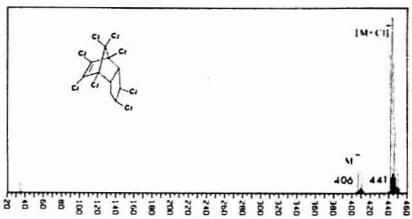


Figure 9. Methane enhanced negative ion mass spectra of α-chlordane. Direct insertion probe. Ion source temperature was 200 °C.

ACKNOWLEDGMENT

We thank Bruce D. McVeety and William J. Simonsick, Jr., for helpful discussions.

Registry No. 1, 77-47-4; 2, 309-00-2; 3, 465-73-6; 4, 60-57-1; 5, 72-20-8; 6, 7421-93-4; 7, 53494-70-5; 8, 3734-48-3; 9, 56534-02-2; 10, 56641-38-4; 11, 2597-11-7; 12, 76-44-8; 13, 1024-57-3; 14, 27304-13-8; 15, 5103-71-9; 16, 5566-34-7; 17, 39765-80-5; 18, 959-98-8; 19, 33213-65-9; 20, 1031-07-8; 21, 2385-85-5; 22, 143-50-0; 23, 2227-17-0; 24, 6298-65-3.

LITERATURE CITED

(1) Bailey, R. A.; Clark, H. M.; Ferris, J. P.; Krause, S.; Strong, R. L. "Chemistry of the Environment"; Academic Press: New York, 1978; p 168.
(2) Clark, J. R.; DeVault, D.; Bowden, R. J.; Weishaar, J. A. *J. Great Lakes Res.* **1984**, *10*, 38.
(3) Frank, R.; Thomas, R. L.; Holdrinet, M.; Kemp, A. L. W.; Braun, H. E. *J. Great Lakes Res.* **1979**, *5*, 18.
(4) Damico, J. N.; Barron, R. P.; Ruth, J. M. *Org. Mass Spectrom.* **1968**, *1*, 331.
(5) Biros, F. J.; Dougherty, R. C.; Dalton, J. *Org. Mass Spectrom.* **1972**, *6*, 1161.
(6) Hunt, D. F.; Crow, F. W. *Anal. Chem.* **1978**, *50*, 1781.
(7) Hunt, D. F.; Stafford, G. C.; Crow, F. W.; Russell, J. W. *Anal. Chem.* **1976**, *48*, 2098.
(8) Tannenbaum, H. P.; Roberts, J. D.; Dougherty, R. C. *Anal. Chem.* **1975**, *47*, 49.
(9) Smit, A. L. C.; Field, F. H. *J. Am. Chem. Soc.* **1977**, *99*, 6471.
(10) Dougherty, R. C. *Biomed. Mass Spectrom.* **1981**, *8*, 283.
(11) Dougherty, R. C.; Dalton, J.; Biros, F. J. *Org. Mass Spectrom.* **1972**, *6*, 1171.
(12) Jansson, B.; Wideqvist, U. *Int. J. Environ. Anal. Chem.* **1983**, *13*, 309.
(13) Dixon, D. J. *Appl. Mass Spectrom. Trace Anal.* **1982**, 139.
(14) Ribick, M. A.; Dubay, G. R.; Petty, J. D.; Stalling, D. L.; Schmitt, C. J. *Environ. Sci. Technol.* **1982**, *16*, 310.
(15) Jensen, T. E.; Kaminsky, R.; McVeety, B. D.; Wozniak, T. J.; Hites, R. A. *Anal. Chem.* **1982**, *54*, 2388.
(16) Chien, D. H. T.; Heys, J. R. *J. Agric. Food Chem.* **1982**, *30*, 396.
(17) Mark, V. *Org. Synth.* **1966**, *46*, 93.
(18) Gregor, I. K.; Guilhaus, M. *Int. J. Mass Spectrom. Ion Phys.* **1984**, *56*, 167.
(19) Miwa, B. J.; Garland, W. A.; Blumenthal, P. *Anal. Chem.* **1981**, *53*, 793.
(20) Stan, H. J.; Kellner, G. *Biomed. Mass Spectrom.* **1982**, *9*, 483.
(21) Greaves, J.; Bekesi, J. G.; Roboz, J. *Biomed. Mass Spectrom.* **1982**, *9*, 406.
(22) Crow, F. W.; Bjorseth, A.; Knapp, K. T.; Bennett, R. *Anal. Chem.* **1981**, *53*, 619.
(23) McEwen, C. N.; Rudat, M. A. *J. Am. Chem. Soc.* **1979**, *101*, 6470.
(24) McEwen, C. N.; Rudat, M. A. *J. Am. Chem. Soc.* **1981**, *103*, 4343.

(25) Henis, N. B. H.; Busch, K. L.; Bursey, M. M. *Inorg. Chim. Acta* **1981**, *53*, L31.
(26) Stöckl, D.; Budziklewicz, H. *Org. Mass Spectrom.* **1982**, *17*, 376.
(27) Deinzer, M.; Griffin, D.; Miller, T.; Lamberton, J.; Freeman, P.; Jonas, V. *Biomed. Mass Spectrom.* **1982**, *9*, 85.
(28) Rappe, C.; Buser, H. R.; Stalling, D. L.; Smith, L. M.; Dougherty, R. C. *Nature (London)* **1981**, *292*, 524.
(29) West, R. *Pure Appl. Chem.* **1971**, *28*, 379.
(30) Dougherty, R. C.; Bergner, A.; Levonowich, P.; Roberts, J. D. *Adv. Mass Spectrom. Biochem. Med.* **1976**, *1*, 181.
(31) Dougherty, R. C., personal communication, Florida State University, 1983.
(32) Hass, J. R.; Friesen, M. D.; Busch, K. L.; Bursey, M. M. "American Society for Mass Spectrometry, 26th Annual Conference on Mass Spectrometry and Allied Topics, St. Louis, MO, (1978) Abstracts, p. 390.

RECEIVED for review September 17, 1984. Accepted November 13, 1984. The work was supported by the U.S. Department of Energy (Grant No. 80EV-10449) and the U.S. Environmental Protection Agency (Grant No. R808865).

Combination of Chemical Reduction and Tandem Mass Spectrometry for the Characterization of Sulfur-Containing Fuel Constituents

Karl V. Wood*

Engine/Fuels Laboratory, Chemistry Building, Purdue University, West Lafayette, Indiana 47907

R. Graham Cooks, James A. Laugal, and Robert A. Benkeser

Department of Chemistry, Purdue University, West Lafayette, Indiana 47907

Tandem mass spectrometry has been combined with a calcium/mixed amines reduction system to characterize an SRC-II middle distillate fraction for sulfur-containing polynuclear aromatic hydrocarbons. Parent scans, which characterize a complex mixture for all components which fragment to common structural moieties, were used to identify alkylbenzothiophenes and dibenzothiophenes as well as alkylbenzothiophene sulfones.

A chemical reduction scheme has been applied to a middle distillate of an SRC-II coal-derived liquid in order to facilitate characterization of sulfur-containing constituents by tandem mass spectrometry (MS/MS) (*1–4*). The identification of sulfur-containing polynuclear aromatic hydrocarbons (PNAs) in coal and liquids derived from coal (*5–7*) is of particular interest because of the environmental effect these constituents have after combustion (*8*). However, these compounds have proven difficult to identfy because of their low relative concentration and characteristic mass overlap with hydrocarbon components (*9*). The approach used here is an alternative to the rather complex separation schemes which have been used to address these problems by concentrating sulfur-containing PNAs prior to GC/MS (*6, 7, 9*).

EXPERIMENTAL SECTION

A Finnigan (Model 4500) triple quadrupole mass spectrometer was used to characterize the reduction products (*10, 11*). This system consists of three coaxially arranged quadrupole rod assemblies. The first and third quadrupoles are conventional mass analyzers and the second quadrupole is used as a focusing collision cell. Samples were admitted into the mass spectrometer with the direct insertion probe. Negative ion chemical ionization (NICI) was employed with isobutane as the reagent gas (0.4 torr). Argon was used as the collision gas at a gauge pressure of 2.0 mtorr. The collision energy was set at 20 eV.

The chemical reduction utilizes calcium metal (10–12 g) in a mixed amine solvent system (*12*) consisting of ethylenediamine and methylamine or *n*-butylamine. The calcium-mixed amine reducing system seems superior to the lithium–ethylenediamine system in the reduction of polynuclear organic sulfur compounds. The lithium–ethylenediamine system has been reported to reduce dibenzothiophene to a plethora of products (*13*). The reduction of SRC-II middle distillate which follows is typical of the general procedure.

A 500-mL dry round bottom flask was fitted with a single Hershberg stirrer and an ethylene glycol cooled (−26 °C) Friedrichs condenser. The system was flushed with methylamine vapor and the flask then filled with 75 mL of condensed methylamine gas. Calcium metal shot (12.0 g), white sand (24 g), SRC-II middle distillate (3.3 g), and 75 mL of dry ethylenediamine were also added. The brown mixture was stirred for 24 h, after which time the methylamine was allowed to evaporate. Technical diethyl ether (100 mL) was added to the flask immersed in ice, and hydrolysis of the gray product was effected with a solution of NH_4Cl (27 g in 100 mL of water). The aqueous layer was separated, made acidic with concentrated HCl, and then extracted several times with diethyl ether. The ether extracts of the base-soluble layer were combined and dried over anhydrous sodium sulfate. The original ether layer (base insoluble fraction) was washed with aqueous HCl followed by aqueous $NaHCO_3$ and then also dried over anhydrous sodium sulfate. The solvent volume of both fractions was reduced by means of a vacuum jacketed distillation column to yield a brownish base-insoluble liquid fraction (1.6 g) and a brownish base-soluble liquid fraction (2.0 g) (*14*).

The middle distillate SRC-II sample was obtained from Charles E. Schmidt of the Pittsburgh Energy Technology Center. The sodium salts of benzenesulfinate and *p*-toluenesulfinate, as well as the other reagents, were obtained commercially and used without further purification.

RESULTS AND DISCUSSION

Calcium has been shown to be an effective metal in reducing aromatic substrates (*12*). In the case of aromatic heterocycles containing a thiophene moiety, the thiophene ring is opened by calcium through reductive cleavage of the carbon–sulfur bond (*14*). For example, carbon–sulfur bond cleavage in benzothiophene yields *o*-ethylthiophenol. In basic media, the reduced benzothiophene exists as a thiophenolate anion which resists further reduction. The unsaturated substituent present

0003-2700/85/0357-0692$01.50/0 © 1985 American Chemical Society

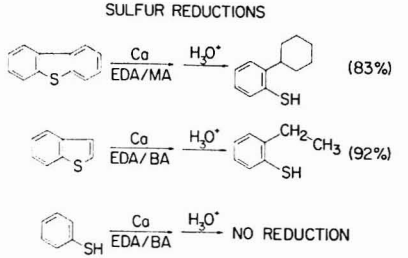


Figure 1. Major reduction products of dibenzothiophene, benzothiophene, and thiophenol. (Ca is calcium, EDA is ethylenediamine, MA is methylamine, and BA is *n*-butylamine.)

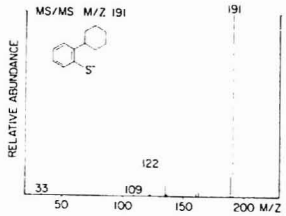


Figure 2. Negative ion chemical ionization daughter spectrum of the conjugate anion, *m/z* 191, of *o*-cyclohexylthiophenol, the reduction product of dibenzothiophene: argon collision gas pressure, 2.0 mtorr; collision energy, 20 eV.

after carbon–sulfur bond cleavage is reduced rapidly to yield the alkylated thiophenol. Figure 1 shows the principal reduction products and reaction yields for benzothiophene, dibenzothiophene, and thiophenol.

Figure 2 is the NICI daughter spectrum of the conjugate anion, *m/z* 191, of the reduction product of dibenzothiophene. Of particular interest is the ion at *m/z* 122, which corresponds to the negative thiatropylium radical anion, $C_7H_6S^{-\cdot}$. This ion is important because it is also the principal fragment ion in the daughter spectrum of the reduction product of benzothiophene. Therefore, it might be possible to characterize the reduction products of both alkylbenzothiophenes and dibenzothiophenes by a parent scan of *m/z* 122. This scan characterizes a complex mixture for all components which, upon collision-induced dissociation, fragment to a common structural moiety, in this case the negative thiatropylium radical anion, $C_7H_6S^{-\cdot}$. Figure 3 is a NICI parent scan of *m/z* 122, which gives evidence for the reduction products of C_0–C_4 alkylbenzothiophenes (*m/z* 137, 151, 165, 179, and 193) and dibenzothiophene (*m/z* 191) in the reduced middle distillate fraction of a SRC-II coal-derived liquid. This confirms the value of parent spectra, combined with the calcium/mixed amine reduction system, in characterizing thiophene derivatives in coal liquids. Individual components suggested by the parent spectrum were confirmed by daughter spectra. Figure 4 is the comparison of the NICI daughter spectrum of *m/z* 137 from the reduced middle distillate fraction of a SRC-II coal-derived liquid with the NICI daughter spectrum of the $(M - H)^-$ ion (*m/z* 137) of *o*-ethylthiophenol. The similarity of the two spectra confirms the presence of the reduced benzothiophene in the reduced SRC-II coal-derived liquid sample.

Under chemical reduction conditions similar to those used in the benzothiophene study (*15*), sulfones are reduced to the ring-opened sulfinic acids. These species can be identified

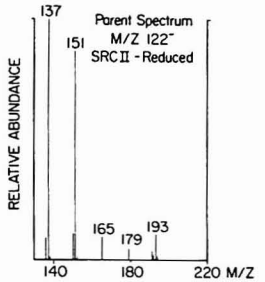


Figure 3. Negative ion chemical ionization parent scan of *m/z* 122 of the reduced SRC-II middle distillate: argon collision gas pressure, 2.0 mtorr; collision energy, 20 eV.

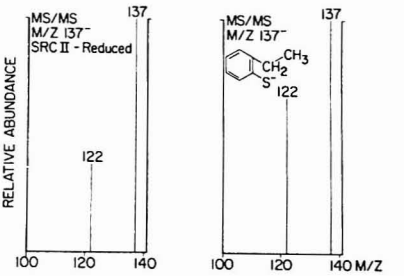


Figure 4. Comparison of the negative ion chemical ionization daughter spectrum of *m/z* 137 of the reduced SRC-II middle distillate with the negative ion chemical ionization daughter spectrum of the conjugate anion, *m/z* 137, of *o*-ethylthiophenol: argon collision gas pressure, 2.0 mtorr; collision energy, 20 eV.

Table I. Daughter Spectra of $(M - H)^-$ Derived from Two Sulfinate Salts and the First Three Members of the Benzothiophene Sulfones from Reduced SRC-II[a]

$(M - H)^-$ ion	sample	relative abundance		
		$(M - H)^-$	loss of SO_2	SO_2^-
141^-	sodium benzenesulfinate	80	100	35
155^-	sodium *p*-toluenesulfinate	100	85	38
169^-	reduced SRC-II	100	15	33
183^-	reduced SRC-II	100	15	45
197^-	reduced SRC-II	100	15	45

[a] Ion intensities are given in percent relative abundance. All major ions are included. Collision energy was 20 eV; argon collision gas pressure was ca. 2 mtorr.

by major fragment ions in the NICI daughter spectra of the corresponding $(M - H)^-$ ions due to loss of SO_2 and formation of SO_2^-. For example, benzenesulfinate and *p*-toluenesulfinate show these ions as the only significant fragments (see Table I). These results indicate that a NICI parent scan of *m/z* 64 (which could be S_2^- in addition to SO_2^-) could provide information on the presence of sulfones in the original sample. Figure 5 is a NICI parent scan of 64^- from the reduced coal-derived liquid. A prominent series can be seen at *m/z* 169, 183, ... indicating the presence of alkylbenzothiophene sulfones, as confirmed by the daughter spectra (Table I). A second, much weaker series *m/z* 121, 135, ... is also present in Figure 5, indicating the possible presence of alkylthiophene

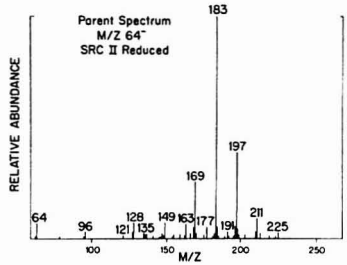


Figure 5. Negative ion chemical ionization parent scan of m/z 64 of the reduced SRC-II middle distillate: argon collision gas pressure, 2.0 mtorr; collision energy, 20 eV.

sulfones. The SRC-II middle distillate sample had been stored in screw-top vials on a laboratory shelf for 2 years, suggesting that air oxidation may be the reason for the presence of the sulfones.

The NICI parent scans of both m/z 64 and 122 provide useful information for characterizing a complex SRC-II coal-derived liquid for sulfur-containing constituents. At present, additional parent scans are being investigated for the identification of other series of sulfur-containing PNAs. Furthermore, the chemical reduction scheme has been used on a heavy distillate as well as four different coal samples with varying amounts of total sulfur and organic sulfur. The heavy distillate shows dibenzothiophene and its homologues; these and other results of these analyses will be presented in a subsequent publication.

Registry No. $C_7H_6S^-$, 94203-57-3; dibenzothiophene, 132-65-0; benzothiophene, 95-15-8; thiophenol, 108-98-5; *o*-cyclohexylthiophenol conjugate anion, 94203-55-1; *o*-ethylthiophenol conjugate anion, 94203-56-2; *o*-ethylthiophenol, 4500-58-7.

LITERATURE CITED

(1) McLafferty, F. W. *Science* **1981**, *214*, 280.
(2) Cooks, R. G.; Busch, K. L. *J. Chem. Educ.* **1982**, *59*, 926.
(3) Yost, R. A.; Fetterolf, D. *Mass Spectrom. Rev.* **1983**, *2*, 1-45.
(4) Hunt, D. F.; Shabanowitz, J. *Anal. Chem.* **1982**, *54*, 574.
(5) Czogalla, C. D.; Broberg, F. *Sulfur Rep.* **1983**, *3*.
(6) Lee, M. L.; Willey, C.; Castle, R. N.; White, C. M. In "Polynuclear Aromatic Hydrocarbons: Chemistry and Biological Effects"; Bjorseth, A., Dennis, A. J., Eds.; Battelle Press: Columbus, OH, 1980; pp 59-73.
(7) Willey, C.; Iwao, M.; Castle, R. N.; Lee, M. L. *Anal. Chem.* **1981**, *53*, 400-407.
(8) Markuszewski, R.; Miller, L. J.; Straszheim, W. E.; Fan, C. W.; Wheelock, T. D.; Greer, R. T. In "New Aproaches in Coal Chemistry"; Blaustein, B. D., Bockrath, B. C., Friedman S., Eds.; American Chemical Society: Washington, DC, 1981; ACS Symposium Series 169, pp 401-415.
(9) Kong, R. C.; Lee, M. L.; Iwao, M.; Tominaga, Y.; Pratap, R.; Thompson, R. D.; Castle, R. N. *Fuel* **1984**, *63*, 702-708.
(10) Yost, R. A.; Enke, C. G. *Anal. Chem.* **1979**, *51*, 1251A.
(11) Slayback, J. R. B.; Story, M. S. *Ind. Res./Dev.* **1981** (Feb), 129.
(12) Benkeser, R. A.; Belmonte, F. G.; Kang, J. *J. Org. Chem.* **1983**, *48*, 2796.
(13) Reggel, L.; Zahn, C.; Wender, I.; Raymond, R. *Bull.—U.S., Bur. Mines* **1985**, *No. 615*, 37.
(14) Laugal, J. A. Ph.D. dissertation, Purdue University, 1984.
(15) Truce, W. E.; Tate, D. P.; Burdge, D. N. *J. Am. Chem. Soc.* **1960**, *82*, 2872-2876.

RECEIVED for review October 15, 1984. Accepted November 19, 1984. This work was supported by the Department of Energy under Contracts DE-FG22-82-DC50803 (K.V.W. and R.G.C) and DE-AC02-81-ER10989 (R.A.B.).

Identifying Alkylbenzene Isomers with Chemical Ionization–Proton Exchange Mass Spectrometry

Steven B. Hawthorne* and David J. Miller

University of North Dakota Energy Research Center, Box 8213, University Station, Grand Forks, North Dakota 58202

Chemical ionization–proton exchange mass spectrometry (CIPE) allows the number of unsubstituted aromatic carbons in alkylbenzene isomers to be determined. Only the aromatic hydrogens undergo exchange with deuterium when deuterated water, methanol, or ethanol is used as the reagent gas. Chemical ionization with deuterated methanol gives an acceptable mass spectral background and allows the determination of the number of unsubstituted positions on the benzene ring yielding structural information often unavailable from conventional electron impact spectra. Structural isomers such as propyl-, methylethyl-, and trimethylbenzene can easily be identified. The comparison of CIPE spectra from standard compounds, which are often unavailable, is not required to determine the number of unsubstituted aromatic carbons in alkylbenzene isomers. The method also allows ortho and para to be distinguished from meta disubstituted alkylbenzenes. Deuteriomethanol chemical ionization is used to characterize alkylbenzenes in a complex and relatively well studied sample, diesel exhaust.

Alkylbenzene isomers are major species in samples of industrial and environmental interest including coal-derived liquids, petroleum products, and urban air. Unfortunately, the ability of conventional gas chromatography/mass spectrometry with electron impact ionization (EI) to differentiate among alkylbenzene isomers of the same molecular weight is limited. Electron impact mass spectra of these species are often indistinguishable, and appropriate standards which would allow identifications based on a comparison of chromatographic retention indexes and standard mass spectra are generally unavailable for larger molecular weight isomers (alkylbenzene isomers containing four or more alkyl carbon atoms). Some alkylbenzene isomers can be identified with the use of methane and isobutane chemical ionization (CI) and a study of the resultant fragmentation patterns (*1–6*), but such methods depend upon the availability of appropriate standards.

Chemical ionization with deuterated reagents can be used to determine the number of protons bonded to heteroatoms in several classes of compounds including aromatic and aliphatic alcohols, carboxylic acids, amines, amides, and mercaptans (*7–10*). Deuterium exchange with aromatic protons has also been reported under certain conditions with D_2O and CH_3CH_2OD reagent gases (*11–13*). Although the proton exchange mechanism is not well understood, ionization of the benzene ring by addition of H^+ or D^+ appears to be necessary

0003-2700/85/0357-0694$01.50/0 © 1985 American Chemical Society

for proton exchange to occur. The species can then undergo up to n proton exchanges where n equals the number of unsubstituted positions on the benzene ring, i.e., n equals the number of aromatic protons. For example, a disubstituted benzene undergoing ionization and maximum proton exchange with ROD reagent gas will show an (M + 6) mass peak.

In the present study, the phenomenon of aromatic proton exchange on alkylbenzenes is exploited in order to develop methodology which allows the number of alkyl-substituted positions on a benzene ring to be determined. The use of reagent gases D_2O, CH_3OD, and CH_3CH_2OD was investigated in order to determine their ability to exchange deuterium with aromatic hydrogens and to provide an acceptably low background of mass spectral peaks. This method allows rapid and routine changeover to and from electron impact mode and works well with complex samples. The method is applied to the characterization of alkylbenzene isomers in diesel exhaust.

EXPERIMENTAL SECTION

A Hewlett-Packard Model 5985B gas chromatograph/mass spectrometer equipped with a dual electron impact/chemical ionization source was used to obtain all of the mass spectra reported. Deuteriomethanol (KOR Isotopes, Cambridge, MA), deuterioethanol (Aldrich Chemical Co., Milwaukee, WI), and D_2O (Stohler Isotope Chemicals, Waltham, MA) were all ≥99% isotopically pure and used as received. The reagents were introduced directly into the source through $^1/_{16}$ in. o.d. stainless steel tubing running through the heated transfer block collinear with the chromatographic column. Source pressure and ionizing voltage were optimized for each reagent gas by introducing m-diisopropylbenzene at a constant rate into the source through the direct insertion probe and maximizing the intensity of the (M + 6) ion that is formed from the addition of D^+ and the exchange of all four aromatic hydrogens for deuterium. The source temperature was also optimized for each reagent by varying it from 100 to 200 °C and observing the effect on chemical ionization induced proton exchange on 150-ng samples of m-diisopropylbenzene injected into the chromatographic column.

All gas chromatographic separations were performed with a Hewlett-Packard Model 5840 gas chromatograph (GC/MS) or a Model 5730 (FID) equipped with a 60 m × 0.32 mm i.d., SE-54 fused-silica capillary column (J and W Scientific, Rancho Cordova, CA). Electron impact spectra were collected at 70 eV and a source temperature of 200 °C.

Samples of diesel exhaust were collected from the exhaust stream of a diesel tractor into 100-mg Tenax-GC traps by using a personal air sampling pump (Du Pont Model P4000) calibrated to draw 100 mL/min. The collected species were thermally desorbed at 220 °C for 10 min and swept with helium directly into the chromatographic column for cryogenic trapping at −50 °C. The column was then heated to 0 °C and the sample species were eluted at a temperature programming rate of 8 °C/min. Detailed sample collection and analysis methods have been reported elsewhere (*14*).

RESULTS AND DISCUSSION

Maximum intensity of the (M + 6) ion for m-diisopropylbenzene with each reagent gas occurred at a source pressure of approximately 0.2 torr. This pressure of reagent gas was used for all following experiments. Source temperature had only a small effect on the extent of proton exchange with each reagent gas when varied from 100 to 200 °C. Since one of the goals of this method was to allow rapid conversion from standard EI conditions to chemical ionization–proton exchange (CIPE) conditions, the standard EI source temperature of 200 °C was used for all further work. Electron voltage was also optimized and was approximately 50 eV for each reagent gas. Under the described conditions, routine changeover from EI to CIPE conditions and back can easily be accomplished in less than 5 min.

Even though chemical ionization of m-diisopropylbenzene readily occurs when D_2O is used as the reagent gas, very little proton exchange was observed at any of the conditions described above. Since proton exchange with D_2O remained minimal when other alkylbenzene isomers (e.g., 1,3,5-triethylbenzene and n-hexylbenzene) were used as sample species, further work was limited to CH_3OD and CH_3CH_2OD reagent gases.

Table I. Relative Abundance of Reagent Ion Clusters Formed from CH_3OD and CH_3CH_2OD

cluster	mass	rel intens, %
$CH_3OD_2^+$	35	29
$(CH_3OD)_2D^+ - D_2O$	48	28
$(CH_3OD)_2D^+$	68	100
$(CH_3OD)_3D^+ - D_2O$	81	19
$(CH_3OD)_3D^+$	101	18
$(CH_3OD)_4D^+ - D_2O$	114	0.2
$CH_3CH_2OD_2^+$	49	9.1
$(CH_3CH_2OD)_2D^+ - D_2O$	76	6.2
$(CH_3CH_2OD)_2D^+$	96	100
$(CH_3CH_2OD)_3D^+ - D_2O$	123	9.3
$(CH_3CH_2OD)_3D^+$	143	46
$(CH_3CH_2OD)_4D^+ - D_2O$	170	0.2

Both CH_3OD and CH_3CH_2OD reagent gases were successful at producing mass spectra showing ionization and complete proton exchange with the test species m-diisopropylbenzene, 1,3,5-triethylbenzene, and n-hexylbenzene. However, CH_3CH_2OD is less desirable as a reagent gas because it produces significant background ions in the mass region of interest. Mass and relative intensity data for reagent ion clusters generated from CH_3OD and CH_3CH_2OD are shown in Table I. The ion clusters are in the general form of $(ROD)_nD^+$ and $(ROD)_nD^+$ minus D_2O. When a mass range of 10–400 is scanned, both reagent gases give a similar background total ion current, and a similar distribution of reagent ion clusters. But, because of its higher molecular weight, CH_3CH_2OD produces a high background current at masses as high as m/z 143 (and its ^{13}C isotope peak at m/z 144), making the analysis of low concentrations of C_2, C_3, and C_4 alkylbenzene isomers very difficult. In contrast, CH_3OD produces no significant background ions above m/z 101 (and its ^{13}C isotope m/z 102). Since the identification of alkylbenzene isomers using CIPE does not depend upon fragmentation patterns, the lower mass regions do not have to be monitored, and all alkylbenzene isomers containing two or more alkyl carbon atoms can be analyzed without interference from reagent ion background when CH_3OD is used for the reagent gas.

As shown in Figure 1, data from chemical ionization–proton exchange mass spectrometry can be used to determine the number of unsubstituted aromatic carbons in alkylbenzene isomers. Mass spectra generated with CH_3OD reagent gas of the eight isomers of C_3 alkylbenzenes show that trimethyl, methylethyl, and propyl isomers can easily be identified. CIPE mass spectra for several alkylbenzene isomers are given in Table II. The number of unsubstituted positions on the benzene ring (X) can be determined by the formula $X = M_2 - M_1 - 2$ where M_1 is the molecular weight of the alkylbenzene isomer, M_2 is the mass representing maximum exchange of the aromatic protons, and the number 2 is subtracted to account for the D^+ added to the alkylbenzene isomer during the chemical ionization step. For example, the number of unsubstituted positions on a trimethylbenzene would be $X = 125 - 120 - 2 = 3$ (Table II).

All of the standard alkylbenzene compounds that have been studied give reproducible CIPE mass spectra which can easily be predicted based on the number of aromatic hydrogens available for exchange with deuterium from the reagent gas. The predictability of the spectra given in Table II demonstrates that standard compounds do not necessarily need to be available and analyzed in order to allow classification of

Table II. CIPE Mass Spectra of Alkylbenzene Isomers with CH_3OD Reagent Gas

compound	mol wt	% rel abundance[a]						
		M	(M + 2)	(M + 3)	(M + 4)	(M + 5)	(M + 6)	(M + 7)
o-xylene	106	25	14	21	30	49	100	
m-xylene		27	28	40	57	100	39	
p-xylene		27	12	18	26	44	100	
ethylbenzene		35	40	56	71	100	54	34
propylbenzene	120	23	13	20	30	49	67	100
isopropylbenzene		18	13	21	30	49	67	100
o-ethyltoluene		17	16	23	32	52	100	
m-ethyltoluene		24	55	68	83	100	35	
p-ethyltoluene		8	14	20	28	49	100	
1,2,3-trimethylbenzene		29	62	77	99	100		
1,2,4-trimethylbenzene		29	48	66	86	100		
1,3,5-trimethylbenzene		18	100	72	39	15		
o-diethylbenzene	134	19	26	35	46	70	100	
m-diethylbenzene		26	54	67	81	100	36	
p-diethylbenzene		25	7	11	18	43	100	
1,2,3,4-tetramethylbenzene		25	92	100	96			
1,2,3,5-tetramethylbenzene		12	100	58	19			
1,2,4,5-tetramethylbenzene		22	41	57	100			
1-methyl-4-isopropylbenzene		23	26	38	56	91	100	
pentamethylbenzene	148	9	100	38				
n-pentylbenzene		21	11	19	29	44	69	100
n-hexylbenzene	162	23	12	19	28	42	66	100
m-diisopropylbenzene		21	90	100	97	81	30	
p-diisopropylbenzene		24	66	84	89	93	100	
1,3,5-triethylbenzene		8	100	57	19	4		
hexamethylbenzene		6	100					

[a] All CIPE mass spectra were generated as described in the text from approximately 150-ng samples injected into the chromatographic column of the GC/MS. Ion abundances are not correct for the contribution of the ^{13}C isotope.

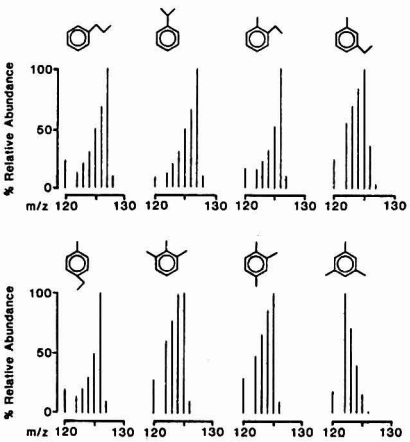


Figure 1. Chemical ionization–proton exchange mass spectra of C_3 alkylbenzene isomers with CH_3OD reagent gas.

sample species based on their CIPE spectra. This is particularly important for the analysis of complex hydrocarbon samples where appropriate standard compounds and sufficient time for the generation of standard spectra are often unavailable.

The relative intensity of the CIPE mass spectral peaks also yields information concerning the position of alkyl substituents on the benzene ring. All of the ortho- and para-disubstituted alkylbenzenes that have been studied (Table II) show the greatest spectral intensity at the mass representing exchange of all aromatic protons (i.e., the (M + 6) peak). In contrast, all of the meta-disubstituted alkylbenzenes show an intensity of about 30% to 40% at the (M + 6) peak. This general trend continues with more highly substituted benzenes (e.g., compare 1,2,3- to 1,3,5-trimethylbenzene, and 1,2,3,4- to 1,2,3,5-tetramethylbenzene), and may, in part, be a result of reduced exchange at sterically hindered aromatic carbons. However, the directive influences of the attached alkyl groups (*11*, *12*) may also determine the rate of proton exchange at any one position. For example, both 1,2,4-trimethylbenzene and 1,2,4,5-tetramethylbenzene have sterically hindered positions but do not show reduced proton exchange. Such exceptions make the assignment of some positional isomers difficult, unless CIPE spectra of standard compounds are available. At present, ortho- and para-disubstituted benzenes can be distinguished from meta isomers without the use of standard compounds. The results in Table II demonstrate that, when appropriate standards are available, CIPE spectra can also be used to identify some other positional isomers (e.g., the three tetramethylbenzenes).

The use of the CIPE technique to identify alkylbenzene isomers in a diesel exhaust sample is shown in Figures 2 and 3 and Table III. Initial classification of alkylbenzene isomers by molecular weight was based on a study of the M and (M + 2) masses generated by the CIPE experiment and confirmed by EI analysis. Major proportions of the exhaust sample consisted of alkanes (as identified by GC/MS with EI ionization, Figure 2), and many of the components were poorly resolved even with high-resolution capillary gas chromatography. Even so, the simple and highly characteristic nature of alkylbenzene CIPE spectra made it possible to assign the number of unsubstituted aromatic carbons for over 75 isomers of C_3 to C_7 alkylbenzenes (Figure 3 and Table III). Since this method does not depend upon the study of fragmentation patterns, identifications could be made even in the presence of overlapping spectra resulting from poorly resolved species.

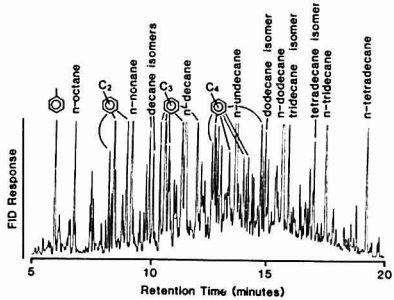


Figure 2. Gas chromatographic separation of organic species found in diesel exhaust. Diesel exhaust samples were collected into Tenax traps and analyzed as described in the text.

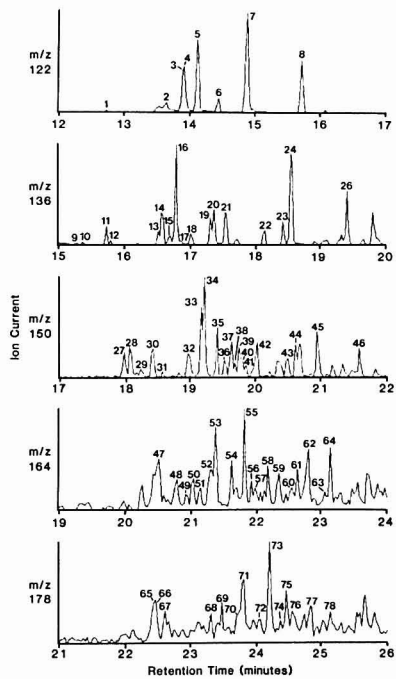


Figure 3. Selected ion chromatograms of alkylbenzene isomers in diesel exhaust analyzed by chemical ionization–proton exchange mass spectrometry. Each selected ion chromatogram was reconstructed from the total ion chromatogram generated with a scan range of m/z 104 to 400. The mass displayed in each chromatogram is the $(M + 2)(M + D^+)$ ion of the alkylbenzene species. Peak numbers refer to Table III.

The CIPE spectra of the C_3 and C_4 alkylbenzenes were also used to distinguish between meta- and ortho- or para-disubstituted isomers (Table III). Since few higher molecular weight disubstituted alkylbenzene standards were available, the determination of meta vs. ortho or para isomers is not reported for alkylbenzenes containing more than four alkyl carbons.

Table III. Chemical Ionization–Proton Exchange Determination of Aromatic Substitution for Alkylbenzene Isomers Found in Diesel Exhaust

m/z (Figure 3)	no. of aromatic hydrocarbons	possible alkyl substituents[a]	peak no. (Figure 3)
122	5	Pr	1, 2
	4	Me-Et	3 (m), 4 (o-p), 6 (o-p)
	3	$(Me)_3$	5, 7, 8
136	5	Bu	9, 10, 15
	4	Me-Pr or $(Et)_2$	11 (m), 12 (o-p), 13 (m), 14 (m), 17 (o-p), 18 (o-p)
	3	$(Me)_2$-Et	16, 19, 20, 21, 22
	2	$(Me)_4$	23, 24, 26
150	5	Pe	30, 31, 32
	4	Me-Bu or Et-Pr	27, 28, 29, 35, 36
	3	Me-$(Et)_2$ or $(Me)_2$-Pr	37, 38, 40, 41, 42, 43
	2	$(Me)_3$-Et	33, 34, 39, 44, 45, 46
	1	$(Me)_5$	ND[b]
164	5	Hx	58
	4	Me-Pe, Et-Bu, or $(Pr)_2$	51, 52, 54, 56
	3	$(Me)_2$-Bu, Me-Et-Pr, or $(Et)_3$	47, 48, 49, 50, 55, 57, 59, 60, 61, 63, 64
	2	$(Me)_3$-Pr, $(Me)_2$-$(Et)_2$	ND
	1	$(Me)_4$-Et	53, 62
178	5	Hp	70
	4	Me-Hx, Et-Pe, or Pr-Bu	73, 74, 75, 76, 77
	3	$(Me)_2$-Pe, Me-Et-Bu, $Me(Pr)_2$, or $(Et)_2$-Pr	71, 72
	2	$(Me)_3$-Bu, $(Me)_2$-Et-Pr, or Me-$(Et)_3$	65, 67, 68, 69, 78
	1	$(Me)_4$-Pr or $(Me)_3$-$(Et)_2$	66

[a] Key: Me, methyl; Et, ethyl; Pr, propyl; Bu, butyl; Pe, pentyl; Hx, hexyl; and Hp, heptyl. None of these designations implies whether the alkyl substituent is normal or branched. [b] ND, not detected.

The analysis of the complex hydrocarbon mixture found in diesel exhaust demonstrates the ability of CIPE mass spectrometrty to provide structural information about alkylbenzene isomers that is generally unavailable from EI spectra. The number of unsubstituted aromatic carbons can easily be determined without standard spectra or the study of fragmentation patterns, making CIPE ideal for the analysis of highly complex samples. A study of the relative intensities of a particular specie's CIPE spectra also allows identification of some positional isomers and is particularly useful for distinguishing ortho- and para- from meta-disubstituted alkylbenzenes. A greater understanding of the mechanism of proton exchange is needed before the potential of CIPE mass spectra to determine positional isomers can be fully exploited.

Registry No. CH_3OD, 1455-13-6; H_2, 1333-74-0; D_2, 7782-39-0; *o*-xylene, 95-47-6; *m*-xylene, 108-38-3; *p*-xylene, 106-42-3; ethylbenzene, 100-41-4; propylbenzene, 103-65-1; isopropylbenzene, 98-82-8; *o*-ethyltoluene, 611-14-3; *m*-ethyltoluene, 620-14-4; *p*-ethyltoluene, 622-96-8; 1,2,3-trimethylbenzene, 526-73-8; 1,2,4-trimethylbenzene, 95-63-6; 1,3,5-trimethylbenzene, 108-67-8; *o*-diethylbenzene, 135-01-3; *m*-diethylbenzene, 141-93-5; *p*-diethylbenzene, 105-05-5; 1,2,3,4-tetramethylbenzene, 488-23-3;

1,2,3,5-tetramethylbenzene, 527-53-7; 1,2,4,5-tetramethylbenzene, 95-93-2; 1-methyl-4-isopropylbenzene, 99-87-6; pentamethylbenzene, 700-12-9; *n*-pentylbenzene, 538-68-1; *n*-hexylbenzene, 1077-16-3; *m*-diisopropylbenzene, 99-62-7; *p*-diisopropylbenzene, 100-18-5; 1,3,5-triethylbenzene, 102-25-0; hexamethylbenzene, 87-85-4; butylbenzene, 104-51-8; dimethylethylbenzene, 29224-55-3; butylmethylbenzene, 27458-20-4; ethylpropylbenzene, 82162-13-8; diethylmethylbenzene, 25550-13-4; dimethylpropylbenzene, 82161-99-7; ethyltrimethylbenzene, 41903-41-7; methylpentylbenzene, 1320-01-0; butylethylbenzene, 82169-27-5; dipropylbenzene, 31621-49-5; ethylmethylpropylbenzene, 94278-81-6; ethyltetramethylbenzene, 94278-82-7; heptylbenzene, 1078-71-3; hexylmethylbenzene, 27133-94-4; ethylpentylbenzene, 94278-83-8; butylpropylbenzene, 94278-84-9; dimethylpentylbenzene, 94278-85-0; butylethylmethylbenzene, 94278-86-1; dipropylmethylbenzene, 42300-93-6; diethylpropylbenzene, 94278-87-2; butyltrimethylbenzene, 94278-88-3; dimethylethylpropylbenzene, 94278-89-4; methyltriethylbenzene, 41903-42-8; propyltetramethylbenzene, 94278-90-7; diethyltrimethylbenzene, 67143-86-6; *n*-octane, 111-65-9; *n*-decane, 124-18-5; *n*-undecane, 1120-21-4; *n*-dodecane, 112-40-3; *n*-tridecane, 629-50-5; *n*-tetradecane, 629-59-4; methylpropylbenzene, 28729-54-6; butyldimethylbenzene, 82161-98-6; nonane, 111-84-2.

LITERATURE CITED

(1) Daishima, S.; Iida, Y. *Shitsuryo Bunseki* **1983**, *31*, 73.
(2) Munson, M. S. B.; Field, F. H. *J. Am. Chem. Soc.* **1967**, *89*, 1047.
(3) Harrison, A. G.; Lin, P. H.; Leung, H. W. *Adv. Mass Spectrom.* **1978**, *7B*, 1394.
(4) Daishima, S.; Iida, Y. *Shitsuryo Bunseki* **1982**, *30*, 249.
(5) Daishima, S.; Iida, Y. *Shitsuryo Bunseki* **1982**, *30*, 61.
(6) Iseda, K. *Nagoya Kogyo Gijutsu Shikensho Hokoku* **1982**, *31*, 306.
(7) Buchanan, M. V. *Anal. Chem.* **1982**, *54*, 570.
(8) Lin, Y. Y.; Smith, L. L. *Biomed. Mass Spectrom.* **1979**, *6*, 15.
(9) Hunt, D. F.; McEwen, C. N.; Upham, R. A. *Anal. Chem.* **1972**, *44*, 1292.
(10) Buchanan, M. V. *Anal. Chem.* **1984**, *56*, 546.
(11) Hunt, D. F.; Sethi, S. K. *J. Am. Chem. Soc.* **1980**, *102*, 6953.
(12) Freiser, B. S.; Woodin, R. L.; Beauchamp, J. L. *J. Am. Chem. Soc.* **1975**, *97*, 6893.
(13) Martinsen, D. P.; Buttrill, S. E., Jr. *Org. Mass. Spectrum.* **1976**, *11*, 762.
(14) Hawthorne, S. B.; Sievers, R. E. *Environ. Sci. Technol.* **1984**, *18*, 483.

RECEIVED for review October 9, 1984. Accepted November 16, 1984. This work was performed under Cooperative Agreement No. DE-FC21-83FE60181 for the U.S. Department of Energy, Office of Fossil Energy.

Laser Mass Spectra of Simple Aliphatic and Aromatic Amino Acids

Cass D. Parker and David M. Hercules*

Department of Chemistry, University of Pittsburgh, Pittsburgh, Pennsylvania 15260

Mass spectra of amino acids have been studied using the LAMMA laser microprobe. Quasi-molecular ions, $(M + H)^+$ and $(M - H)^-$, are produced in high yields. The major neutral fragment loss from $(M + H)^+$ corresponds to HCOOH. Loss of other acids is related to the amino group position. For alkyl amino acids, acid loss plus formation of imino ions (m/z 30) are the only significant fragments at threshold power densities. Fragmentation is limited in the negative ion spectra; $(M - H)^-$ and CN^- are the only ions observed at low power densities. Fragmentation in both the positive and negative ion spectra is influenced by substituents on the alkyl or aryl chains; the electron density of an aryl group has a significant effect. In α–β fission, the phenylalanine quasi-molecular ion gives the α-fragment, but no α-fragment is observed for tryptophan. Significant thermal decomposition of amino acids does not occur in laser mass spectrometry; spectra are comparable to chemical ionization using reagent gases having high proton affinities.

The use of mass spectrometry to study nonvolatile organic compounds has been expanded in recent years, particularly for biomolecules which require derivatization for conventional chemical ionization (CI) or electron impact (EI) methods. Introduction of fast-heating direct insertion probes (*1*) and new ionization sources such as field desorption (FD) (*2*), secondary ion mass spectrometry (SIMS) (*3*), fast atom bombardment mass spectrometry (FAB) (*4*), plasma desorption mass spectrometry (PDMS) (*5*), and laser mass spectrometry (LMS) (*6*) make derivatization no longer necessity for many compounds.

Mass spectra of the amino acids have been reported with several ionization sources: electron impact (EI) (*7*), FD (*8*), CI (*9*), SIMS (*3*), FAB (*10*), and LMS (*11*). Mass spectra of the amino acids obtained by these techniques show similarities; for example, all show quasi-molecular $(M + H)^+$ ions (except EI which shows M^+) and peaks corresponding to loss of formic acid from the quasi-molecular ion. Negative ion spectra have been reported by SIMS and low energy electron impact (LEEI) (*12*). SIMS reported detection of $(M - H)^-$ quasi-molecular ions, while LEEI reported $(M - H)^-$, with fragmentation arising from $M^{-\cdot}$; losses included NH_2, H_2O, CO_2H, and the alkyl chain.

We report here results obtained for amino acids using laser mass spectrometry (LMS). The positive-ion spectra resemble those obtained by using other techniques. Of particular interest is the similarity to CI mass spectra obtained by using reagent gases having relatively high proton affinities. This attests to the "softness" of LMS as a technique for obtaining spectra of organic compounds. Fragmentation is not extensive at threshold power densities, particularly in negative-ion LMS.

EXPERIMENTAL SECTION

Laser mass spectra were obtained with commercially available instrumentation: the Leybold-Heraeus LAMMA-500 and LAMMA-1000 laser microprobes. Mass spectra of DOPA, phenylalanine methyl ester hydrochloride, and tryptophan were obtained only on the LAMMA-1000; other samples were run on both instruments; fragmentation patterns did not differ significantly. The LAMMA-500 is described in detail elsewhere (*13*). The major difference between the two instruments is that the laser beam

0003-2700/85/0357-0698$01.50/0 © 1985 American Chemical Society

Table I. Positive Ion Laser Mass Spectra of Amino Acids, Intensities Releative to Base Peak (100%)

compound	$(M + H)^+$	$(M + H - NH_3)^+/(M + H - H_2O)^+$	$(M + H - CO_2H_2)^+$	m/z 30	other
glycine (75)	100		89 (m/z 30)		
alanine (89)	100		92		
β-alanine (89)	100	3/7	5	58[a]	
valine (117)	100		23	36	
leucine (131)	100		43	12	
isoleucine (131)	64		100	5	
proline (115)	40		100		
3-aminobutyric acid (103)	100		11		85 (m/z 44)[a]
4-aminobutyric acid (103)	95	0/13		100[b]	11 (m/z 44)[a]
6-aminocapric acid (131)	100	13/25	3	63	
histidine (156)	100		99	19	
3-methylhistidine (170)	100		80	12	
phenylalanine (165)	100		100		22[c]
tyrosine (181)	75	8/0	45	20	100[d]
tryptophan (204)	7	22/0	17		100[d]
tryptophan (204)[j]	21	41/0	9		100[d]
DOPA (197)	100	47/0	51		93[d]
phenylalanine methyl ester (179)[j]	100		11[f]		11[e]
proline methyl ester (129)	100		54[f]		
glycine ethyl ester (103)	100		48[g] (m/z 30)		
N,N-dimethylglycine	6	−/11[i]	100		4[h]

[a] $(M + H - H_3CCO_2H)^+$. [b] $(M + H - H_3CCH_2CO_2H)^+$. [c] α fragment at m/z 74, H_2N^+=CHCOOH. [d] $(M + H - H_2NCH_2CO_2H)^+$. [e] α fragment at m/z 88, H_2N=CHCOOCH$_3$. [f] $(M + H - HCO_2CH_3)^+$. [g] $(M + H - HCO_2CH_2CH_3)^+$. [h] $(M + H - HCO_2CH_3)^+$. [i] $(M + H - H_3COH)^+$. [j] LAMMA-1000 data numbers in parentheses for all compounds are formula weights.

irradiates the sample by transmission in the LAMMA-500 and by front-surface in the LAMMA-1000.

The output of a frequency quadrupled Q-switched Nd-YAG laser, 265 nm, 15 ns pulse width, is focused on the sample through a microscope objective. Spectra obtained from the LAMMA-500 used a 32× objective. In the LAMMA-500 changes in laser spot size had little effect on the spectra. The laser energy was varied with a set of neutral density filters to give the lowest power density needed to obtain a mass spectrum, ~10^8 W/cm^2. Ions formed were accelerated to 3 kV into the drift tube of a time of flight mass spectrometer having first-order correction for ion kinetic energy spread. The output from a 17-stage electron multiplier was coupled to a Biomation transient recorder after appropriate amplification. The transient recorder acted as a storage buffer for selected mass ranges. The timing sequence was triggered by the laser pulse. Data were transferred directly to a strip chart recorder or to a HP-1000 computer system for data processing. The mass scale of the TOF is linear with time. Calibration of the positive and negative ion mass scales were done daily. This involved calculation of the TOF time constant, k ($m - kt^{1/2}$), using mass markers for both positive and negative ion spectra. The compound selected as a mass marker was tris(ethylenediamine)cobalt(III) iodide, Co(en)$_3$I$_3$. This complex gives a characteristic pattern due to ion/molecule reaction products of the form $(Co_nI_{n-1})^+$ and $(Co_nCNI_{n-2})^+$ in its positive ion spectra, and $(Co_nI_{n+1})^-$, $(Co_nI_{n+1}CN)^-$, and $(Co_nI_{1n+1})^-$ in its negative ion spectra. The ion/molecule reactions yield ions up to m/z 1300. The cobalt–amine complex does not have the inherent matrix problems associated with CsI, which yields a scale accurate only to m/z ±2 with changing thickness or laser power.

All amino acids were obtained from Sigma Chemical Co. and were run without further purification. Powdered samples were dissolved or suspended in methanol or ethanol and evaporated onto polymer coated Cu SEM grids. Suspension or dissolution had little effect on the spectra. A major effect can be correlated with crystal size in the LAMMA-500. Very small crystals gave the most consistent and reproducible spectra. Water was not used as a solvent due to sodium and/or potassium contamination which leads to extensive cationization.

RESULTS AND DISCUSSION

Table I shows the results obtained for the positive ion LMS of the aliphatic and aromatic amino acids studied. Figure 1 shows the positive ion LMS of leucine, which is typical of the

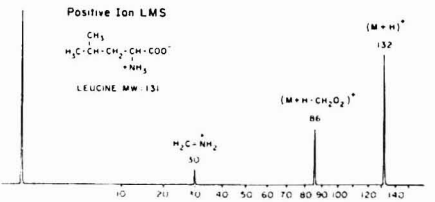
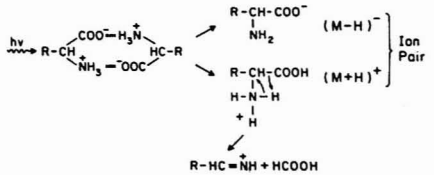


Figure 1. Positive ion LMS of leucine, single trace.

Scheme I. Ion Formation in LMS of Amino Acids



alkyl-substituted amino acids. The major ions observed for leucine are the quasi-molecular ion $(M + H)^+$ at m/z 132, and the fragment ions $(M + H - CO_2H_2)^+$, m/z 86, and H_2C=NH_2^+, m/z 30. The aromatic acids exhibit additional fragment ions in their positive-ion LMS; e.g., α–β fission results in either an ion at m/z 74 H_2N^+=CHCOOH or an aryl moiety corresponding to $(M + H - H_2CNH_2COOH)^+$. The LMS of substituted amino acids, e.g., hydroxy, sulfhydryl, guanidino, etc., will be discussed in a separate communication (*14*).

As seen in Table I, the quasi-molecular ion $(M + H)^+$ is an intense peak in the spectra of most amino acids. The $(M + H)^+$ ion results from intermolecular proton transfer between the amino and acid groups of neighboring amino acids (*14*), as shown in Scheme I. Proton transfer is the major mechanism for $(M + H)^+$ and $(M - H)^-$ ion production, not only at threshold power densities but even at power levels up to 100

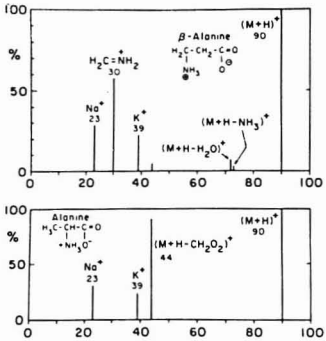


Figure 2. Positive ion LMS of β-alanine and alanine.

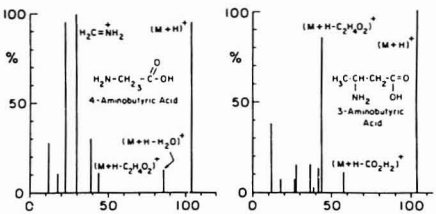


Figure 3. Positive ion LMS of 4-aminobutyric acid and 3-aminobutyric acid.

times threshold. The proton transfer reaction in LMS places the charge on the amino group rather than on the carboxyl function; the net reaction is transfer of a proton from an ammonium group to a carboxylate. Fragmentation of the quasi-molecular ion $(M + H)^+$ will be determined by the location of the charged ammonium group in the molecule. Evidence that protonation of the amino group is a reasonable view for LMS will be presented below.

Neutral Acid Loss. The major neutral loss from $(M + H)^+$ in the LMS of most simple amino acids is determined by the position of the amino group on the alkyl chain. For α-amino acids this corresponds to loss of formic acid (HCOOH) from the quasi-molecular ion $(M + H)^+$. However, due to positional amine group dependence, formic acid loss is not observed for 4-aminobutyric acid, ornithine, lysine, and arginine; also, it is weak in the spectra of β-alanine and 3-aminobutyric acid.

The relationship between neutral acid loss and amino group position is seen clearly by comparison of data for alanine, β-alanine, 3-aminobutyric acid, and 4-aminobutyric acid. Figures 2 and 3 show the positive ion LMS of these compounds. One can see that as the position of the amino group moves away from the carboxyl group (α → γ) the major acid loss fragment accordingly moves from formic through acetic to propionic acid. It is clear that this positional dependence of the amino group is valuable for differentiating between positional amino acid isomers. As Figures 2 and 3 show, alanine can be distinguished readily from β-alanine, as can 3-aminobutyric acid from 4-aminobutyric acid.

Comparing 3-amino- and 4-aminobutyric acids, we find that acid loss α to the amino group is not the only neutral acid loss seen. Acid loss occurs to a lesser extent β to the amino group. In 3-aminobutyric acid this corresponds to the loss of formic acid; for 4-aminobutyric acid it is loss of acetic acid. Acid loss

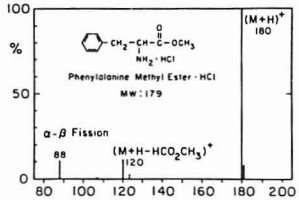
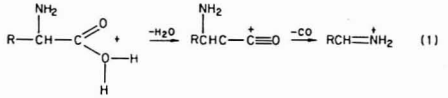


Figure 4. Positive ion LMS of phenylalanine methyl ester HCl.

β to the amino group has not been reported previously. The mechanism by which this loss occurs is not currently understood; the losses are seen even near threshold.

As an aid to understanding the intramolecular hydrogen transfer mechanism in amino acids, we have studied the LMS of amino acid esters in addition to the position dependence of amino group fragmentation. The major fragment ions observed in LMS of several amino acid alkyl esters correspond to loss of alkyl formate from the quasi-molecular $(M + H)^+$ ion. An example is shown in Figure 4 for the LMS of phenylalanine methyl ester. The major neutral fragment loss is methyl formate at m/z 120. Leclercq et al. obtained similar results by CI for amino acid esters (*15*).

Several mechanisms have been proposed for loss of the carboxyl function in amino acids. Meot-Ner and Field (*16*) proposed direct loss of formic acid from a doubly cyclic intermediate, based on their temperature dependence studies using butane CI. Tsang and Harrison (*17*) presented convincing arguments for a concerted two-step process, in CH_4-CI, equivalent to the loss of formic acid from $(M + H)^+$, as outlined in eq 1. (This will be referred to as the T–H mechanism.) The T–H mechanism considers that protonation occurs initially on the carboxyl group with subsequent rapid loss of water and CO



Also, a simple bond breaking mechanism has been assumed for SIMS spectra of amino acids (*3*) in which the acid loss peak arises by loss of CO_2H from the parent molecule (i.e., M − 45). This is comparable to fragmentation of $M^{+\cdot}$ in conventional EI spectra. This mechanism seems to be unlikely, however, given the similarities between SIMS and CI spectra; losses from $(M + H)^+$ are clearly documented in CI.

Most of the results we have obtained for LMS of amino acids are consistent either with the T–H mechanism or with loss of a molecular acid (formic acid for α-amino acids) in a single step. However, several differences are observed which are more consistent with direct loss of a molecular acid in LMS, although they do not allow for a clear-cut distinction between the two possibilities. The important observations are changes in the amino acid spectra as a function of amine group position and the extent of water loss from $(M + H)^+$ observed for LMS vs. CI.

In LMS, the initial proton transfer occurs between amino acid pairs as shown in Scheme I (*14*). In this process a proton is transferred from a protonated amino group on one molecule to a carboxylate group on another. When the two acids involved separate, the charge on $(M + H)^+$ will be on the amino group; the carboxyl group will be neutral. For the T–H mechanism to operate, proton transfer would be required from the protonated amino group to either the carbonyl or hydroxyl group prior to water elimination (e.g., the first step in eq 1).

Table II. Comparison of Relative Intensities[a] of $(M + H)^+$ and Its Fragment Ions

acid	$(M + H)^+$		$(M + H - H_2O)^+$		$(M + H - H_2CO_2)^+$		$(M + H - RHCO_2)^+$		$(M + H - NH_3)^+$	
	LMS	CI[b]	LMH	CI[b]	LMS	CI[b]	LMS	CI[b]	LMS	CI[b]
alanine	52	23	0	0	48	77	c	c	0	0
β-alanine	58	28	4	17	3	0	33	55	2	0
3-aminobutyric	51	22	0	7	6	0	43	71	0	0
4-aminobutyric	43	17	6	55	5	0	46	0	0	28
6-aminohexanoic	49	41	11	49	2	0	34	0	4	10

[a] The intensity of each peak is calculated as the fraction of the ion current associated with the $(M + H)^+$ peak and the four fragment ion peaks. The currents due to other peaks in the spectrum (all weak) are not included in the calculation. [b] Calculated from the data of ref 17 for CH_4-CI. [c] $(M + H - H_2CO_2)^+$ and $(M + H - RHCO_2)^+$ are equivalent in this molecule.

Such a proton transfer is energetically unfavorable and would require ions of high internal energy, which is inconsistent with the limited fragmentation observed in LMS. A protonated amino group represents the lowest energy state in a molecule containing both amino and carboxylate functions. Longevaille et al. (*18*) have shown for molecules containing both OH and NH_2 groups that protonation of the amino group represents the most stable state of an ion, even though the OH group has a comparable cross section for initial protonation in CI. Therefore, it is reasonable that the protonated amino group in an amino acid will determine the decomposition sequence of the ion.

Deuterium labeling studies have shown that one proton in the acid fragment lost comes from the protonated amino group; a similar situation is observed for the loss of alkyl formates from amino acid esters. The proton affinity of a carbonyl group is higher than that for a hydroxyl group (*18*), so if transfer of an ammonium proton within $(M + H)^+$ occurs, protonation of the carbonyl part of the carboxyl group is more likely than the ether oxygen. Thus, the ability of an ester to protonate the ether oxygen in a thermally equilibrated molecule would be poor, and for esters the first step of the T–H mechanism seems to be improbable. However, loss of methyl formate is a significant process in the LMS of methyl esters.

Tsang and Harrison calculated that the α-aminoacylium ion is unstable by 6 kcal/mol which is the driving force for the second step in eq 1 and explains the absence of peaks corresponding to $(M + H - 18)^+$ in the CH_4-CI spectra of amino acids. Therefore as one separates the amino and carboxyl groups on the aliphatic chain, water loss from the quasi-molecular ion should assume increasing importance, because stability of the resulting carbonium ion no longer is influenced by the NH_2 group. This is consistent with the results reported (*17*) for CH_4-CI of 4-aminobutyric acid (4ABA) and 6-aminohexanoic acid (6AHA), as shown in Table II. Note that the peak corresponding to $(M + H - H_2O)^+$ in CH_4-CI is more intense for these two acids than for the other three listed. Also, the other three acids show significant loss of a molecular acid in CH_4-CI but no such loss is observed for 4ABA and 6AHA. These results for CH_4-CI are consistent with the T–H mechanism. On the other hand, if loss of a molecular acid α to the protonated amino group is the mechanism, no significant water loss peak should be observed for any acid; the only major peak in the spectrum should correspond to loss of the molecular acid, RCOOH (where R = H for α-amino acids, R = CH_3 for β-amino acids, etc.).

Table II also shows a comparison of LMS and CH_4-CI (*17*) for alanine (Ala), β-alanine (β-Ala), 3-aminobutyric acid (3-ABA), 4-ABA, and 6-AHA. The data are presented as the fraction of ion current observed for the $(M + H)^+$ peak and its immediate fragment ions: $(M + H - H_2O)^+$, $(M + H - NH_3)^+$, $(M + H - H_2CO_2)^+$, and $(M + H - RHCO_2)^+$. Several very interesting comparisons can be made. First, in the case of LMS, the $(M + H)^+$ ion is significantly more intense than that for CH_4-CI. This is a clear indication that the ions in LMS have low internal energy. Second, no amino acid shows an intense water loss peak in LMS (see Table I), but in CH_4-CI water loss is significant for β-Ala and is a major pathway for 4-ABA and 6-AHA. Third, loss of $RHCO_2$ is very significant in the LMS of 4-ABA and 6-AHA but is not observed in their CH_4-CI spectra. Fourth, loss of NH_3 is not significant for any aliphatic amino acid in LMS but is significant in the CI of 4-ABA and 6-AHA. Thus, for the set of five amino acids listed in Table II, clear differences are observed between the LMS and the CH_4-CI spectra.

It is difficult to explain the differences enumerated above between CH_4-CI and LMS if the T–H mechanism is common to both techniques. On the other hand, loss of a molecular acid from $(M + H)^+$ as a major pathway in LMS is totally consistent with the experimental results. This pathway explains why major peaks at m/z 30 are observed for both 4-ABA and 6-AHA but not for the other amino acids. Also, it explains why no significant water loss is observed for these two compounds, while this loss is significant in CH_4-CI. The proposed mechanism is also consistent with lack of ammonia loss in LMS, since proton equilibrium is established in the initial proton transfer event. In addition to explaining the differing results between CH_4-CI and LMS for the amino acids, loss of the molecular acid is equally consistent with the results observed for all α-amino acids. Therefore, we propose that direct loss of a molecular acid from the quasi-molecular ion, $(M + H)^+$, is the major pathway responsible for the loss of RCOOH for the LMS of the amino acids.

The above considerations do not invalidate the T–H mechanism for CH_4-CI; these results are totally consistent with this mechanism. It is also clear that although the four-center intermediate proposed for loss of molecular formic acid shown in Scheme I may be aesthetically pleasing, it corresponds to a 1,3-H transfer and is symmetry forbidden. Although such transfers are known in mass spectrometry (*19*), they have high activation energy and must be viewed as unlikely for the low internal energy ions encountered in LMS. The double cyclic intermediate of Meot-Ner and Field represents a possibility that avoids the symmetry forbiddeness and merits further consideration. One must also consider the possibility that in the laser experiment the initial loss could occur from an electronically excited state of the carboxyl group which also would relax the symmetry forbiddeness of the four-center intermediate.

Loss of Water. The intensity of the water loss peak in LMS is small compared to CI using a heatable probe (*9*, *16*). In CI loss of water results in a peak having an intensity 40 to 100% of the base peak, depending on the reagent gas. For example, in aspartic acid the water loss peak is 50% of the quasi-molecular ion in CI, while it is only 3% in LMS (*20*). Others have concluded (*9*, *18*) that lactam formation occurs prior to vaporization and ionization in CI, consistent with a thermal reaction. We have observed that water loss from the amine terminus amino acids β-Ala, 4-ABA, and 6-AHA is small, as shown in Table II. If the intensity of the water loss

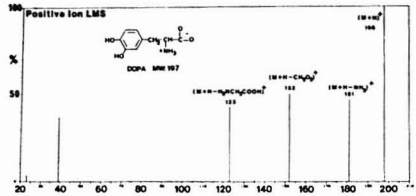


Figure 5. Positive ion LMS of DOPA (dihydroxyphenylalanine).

peak can be equated with thermal decomposition, we can conclude that thermal decomposition does not contribute significantly to ion production at threshold in LMS.

It is particularly interesting to compare water loss for 3-ABA and 4-ABA. No peak corresponding to water loss is observed for 3-ABA, but a peak amounting to 6% of the base peak, $(M + H)^+$, is observed for 4-ABA. If water loss is due to a thermal reaction, one would expect a correlation between lactam stability and the presence of a water loss peak. Water loss for 4-ABA will give rise to a lactam having a five-membered ring

$$H_2NCH_2CH_2CH_2COOH \xrightarrow{-H_2O} H_2NCH_2CH_2CH_2C{=}O \qquad (2)$$

while 3-ABA would require a four-membered ring, which clearly would be less stable. The water loss for 6-AHA is the most significant for all of the amino acids reported in Table II. The relative intensity of this peak depended strongly on the power density used in the laser experiment, more significantly than for the other peaks except for ammonia loss. The water loss peak for 6-AHA increased above 11% (as calculated in Table II) using moderate power densities. This behavior is consistent with formation of a seven-membered cyclic lactam for 6-AHA as indicated for 4-ABA in eq 2 above. Such behavior is consistent for "thermal" reactions observed for other systems in LMS.

Loss of Ammonia. Loss of ammonia from the quasi-molecular ion $(M + H)^+$ is highly selective for LMS of the aliphatic and aromatic amino acids. Only β-alanine, 6-AHA, tyrosine, DOPA, and tryptophan show fragment ions corresponding to NH_3 loss. The aromatic amino acids show NH_3 loss only if the aryl ring is electron releasing. For example, Figure 5 shows the LMS of DOPA (3,4-Dihydroxyphenylalanine); the ammonia loss peak corresponds to 50% of the base peak.

Fales et al. proposed that ammonia loss (*9*) in aromatic systems occurs through an $Ar_1\theta$-3 participation reaction of the *p*-hydroxyphenyl ring (*21*). They predicted that the order of decreasing intensity of ammonia loss from $(M + H)^+$ would be tryptophan > tyrosine > histidine, and phenylalanine, based on the electron releasing character of the aromatic rings. Although DOPA was not included in their results, addition of DOPA to the correlation would result in the following amended order: DOPA > tryptophan > tyrosine > histidine > phenylalanine.

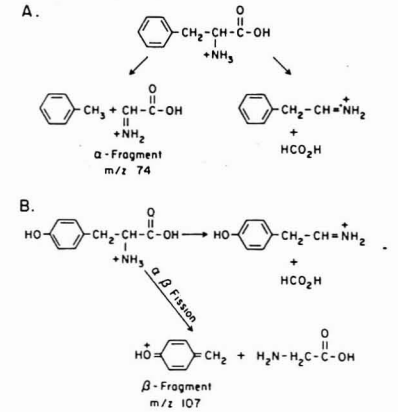
Generally, our results support $Ar_1\theta$-3 participation as the mechanism of ammonia loss in LMS of the aromatic amino acids. Table III shows a comparison of CH_4CI, H_2CI, and LMS for the aromatic amino acids. All three techniques follow the order predicted. If loss of ammonia is based solely on $Ar_1\theta$-3 participation of a substituted aromatic ring, one would expect that tyrosine would be the last acid in the predicted order to show a significant ion due to ammonia loss. This result is observed in LMS along with a notable overall decrease in intensity for the ammonia loss peak, compared to the chemical ionization methods.

Table III. Relative Intensities of $(M + H - NH_3)^+$ Peaks[a]

	CH_4-CI (*10*)	H_2-CI (*17*)	LMS
β-alanine	4		3
histidine	4		0
phenylalanine	2	2	0
tyrosine	55	17	2
tryptophan	100	100	22
DOPA			51

[a] Measured relative to base peak at 100.

Scheme II. Effect of Electron Releasing Group on the Fragmentation of Aromatic Amino Acids: (A) Phenylalanine, (B) Tyrosine



α–β Fission. The aromatic amino acids show loss of formic acid to a lesser extent as the electron releasing nature of the aromatic ring system increases. The electron releasing effect of the aromatic ring introduces the competing fragmentation pathway of α–β fission, which leads to one of two ions at threshold: m/z 74, $H_2N^+{=}CHCOOH$, the α fragment, or $(M + H - H_2NCH_2COOH)^+$, $ArCH_2^+$, the β fragment, as outlined in Scheme II. For example, comparison of phenylalanine and tyrosine indicates that the former gives predominantly the α fragment with charge retention on the iminium group. Tyrosine, however, gives primarily the β fragment (m/z 107) with charge migration to the phenolic hydroxyl group. The data of Table I show that for tryptophan, competition between α–β fission and formic acid loss favors α–β fission to an even greater extent, i.e., $(M + H - CO_2H_2)^+$ is only 17% of the α–β fission peak, which is the base peak.

α–β fission for the aromatic amino acids was first reported by Biemann (*22*). Fales et al. (*9*) compared CH_4-CI results for amino acids with EI data (*7*, *22*). Our LMS results for these aromatic amino acids clearly follow the electron releasing nature of the aromatic ring system, i.e., decreasing iminium and ester type ions with increasing electron density. The β fragment is intense in the LMS of DOPA, tryptophan, and tyrosine which is also the case in the other mass spectral techniques. However, only CI and LMS show a very weak or nonexistent β fragment for phenylalanine, 9% and 0%, respectively. The much lower intensity in CH_4-CI and LMS of phenylalanine reflects the lower internal energy of the molecule in these ionization processes.

Negative Ions. The negative ion LMS of aliphatic and aromatic acids show mostly quasi-molecular $(M - H)^-$ ions at

Table IV. Relative Intensities of Negative Ion LMS of Aliphatic and Aromatic Amino Acids[a]

	(M − H)⁻	(M − H − NH₃)⁻ [b]	m/z 74	(M − H − RH)⁻ (m/z 72)	other
glycine	100				
alanine	100				
β-alanine	100	4 (71)			
valine	100			26	
leucine	100			2	
proline	100			15	
3-amino-butyric	100	1		5	
4-amino-butyric	100				7[c] (71)
histidine	100	3 (138)			43 (65)[d]
3-methyl-histidine	100			72	68 (65)[d] 5[e]
phenyl-alanine	100	9 (147)		35	
tyrosine	100	2 (163)	7	24	
trypto-phan	100	2 (186)	10	26	
DOPA	100	33 (179)	8	40	

[a] Mass value of ions are given in parentheses. [b] α Fragment (HN=CHCOO)⁻ of α–β fission. [c] (M − H − H_3CNH_2)⁻. [d] Decomposition of imidazole ring, $C_3N_2H^-$, $^-C{\equiv}CNHC{\equiv}N$. [e] (M − H − CH_2)⁻.

threshold energy; for example, see Figure 6 for the negative ion LMS of tryptophan. Fragmentation is very limited. Formation of cluster ions occurs as the laser power is increased above threshold. In order to see fragmentation in negative ion LMS, especially for the aromatic amino acids, sufficient laser power must be used to obtain some fragmentation without inducing severe cluster–ion formation or extensive ion/molecule reactions.

Table IV reports the ions observed in the negative ion LMS of the aliphatic and aromatic amino acids. It is clear that fragmentation is limited and that negative ion LMS gives complementary information for molecular weight determination, i.e., a combination of $(M - H)^-$ and $(M + H)^+$ peaks. The fragment ion in negative LMS common to most amino acids is loss of the alkyl group, i.e., $(M - H - RH)^-$ at m/z 72, corresponding to $HN{=}CHCOO^-$. Loss of ammonia is seen in the negative ion LMS of several amino acids. Tryptophan and DOPA show extensive fragmentation due to their "highly substituted" aromatic ring systems.

Loss of ammonia from the quasi-molecular ion $(M - H)^-$ depends on the nature of the amino acid R group. If R is a simple alkyl group, ammonia loss is not observed. The exception is for terminus amino acids; β-alanine shows ammonia loss resulting in an ion at m/z 71. 4-Aminobutyric acid does not lose ammonia; however, it does lose methylamine (7%), similarly giving an ion at m/z 71.

Voigt and Schmidt reported negative ion results using LEEI (*12*) corresponding to loss of NH_2 and/or loss of H_2O for the aliphatic amino acids. The loss of NH_2 from $M^{-\cdot}$ is very intense in the LEEI spectra. As our data indicate, the loss of NH_3 in LMS is very limited or nonexistent for the aliphatic

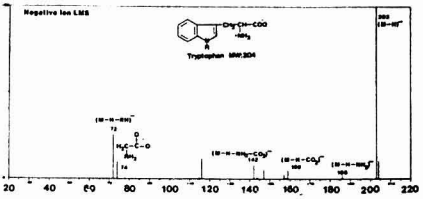


Figure 6. Negative ion LMS of tryptophan.

amino acids. Loss of water is not observed in the LMS of any amino acid studied.

Loss of RH from the aliphatic amino acids shows no pattern related to R group size. The relative intensities are scattered. The aromatic amino acids lose both ammonia and RH from the quasi-molecular ion $(M - H)^-$. Negative ion LMS of aromatic amino acids having smaller ring electron densities show higher intensities for ammonia loss, except for methylhistidine and DOPA. An $Ar_1\beta$-3 participation reaction is not reasonable for negative ion LMS. The aromatic dienone resulting from an $Ar_1\beta$-3 reaction cannot be resonance stabilized as a negative ion. The alternative is a pyrolytic E_i elimination between the amine group and the benzylic hydrogens α to it. The electron density would affect the lability of these hydrogens. Competition between E_i elimination of ammonia and loss of RH would predict a marked decrease in intensity of the ammonia loss peak at some point as the electron density increases. The absence of an electron releasing function accounts for the absence of ammonia loss for the alkylamino acids.

The α–β fission fragment observed at m/z 74 ($H_2NCH_2C{-}OO^-$) for tyrosine, tryptophan, and DOPA points to competition that decreases the intensity of the ammonia loss peak for these aromatic amino acids; DOPA is somewhat of an anomaly. Detection of m/z 74 in the negative ion LMS of tryptophan, tyrosine, and DOPA is additional evidence for the α–β fission argument presented in the positive ion LMS of aromatic amino acids.

The aromatic amino acids show losses in negative-ion LMS which do not correspond to the other amino acids. Many of these additional losses are related to the structure of the specific amino acid; thus generalization is difficult. The two imidazole amino acids studied, histidine and 3-methylhistidine, show an ion at m/z 65. This ion has a probable formula of C_3N_2H which does not correspond to any obvious structure related to the imidazole ring without invoking ring opening. A possible structure could be $^-C{\equiv}CNHC{\equiv}N$. However, without exact mass measurements, it is not possible to attempt an assignment.

Table V shows the additional fragment ions that are found in the negative ion LMS of the high electron density aromatic amino acids. Most of these constitute small percentages of the base peak. The fragment ion intensities follow the trend developed previously; increasing electron density results in increased fragment ion intensity.

Table V. Additional Fragment Ions from Aromatic Amino Acids[a]

	$(M - H - CO_2H_2CNH_2)^-$	$(M - H - CO_2 - C_2H_3NH_2)^-$	$(M - H - CO_2 - NH_3)^-$	$(M - H - CO_2H_2)^-$	$(M - H - CO_2)^-$
tyrosine (181)	1 (106)	4 (93)	4 (119)	2 (134)	
tryptophan (204)		12 (116)	8 (142)	2 (157)	5 (159)
DOPA (197)	34 (122)	17 (109)	61 (135)	17 (150)	

[a] Relative intensity to base peak, 100%. [b] m/z values are given in parentheses.

ACKNOWLEDGMENT

We wish to thank F. W. McLafferty for useful comments and suggestions. Preparation of this manuscript was done partly while D.M.H. was a guest at the University of Münster, West Germany. Thanks are due to the von Humboldt Foundation and to A. Benninghoven for their hospitality and support.

Registry No. DOPA, 59-92-7; glycine, 56-40-6; L-alanine, 56-41-7; β-alanine, 107-95-9; L-valine, 72-18-4; L-leucine, 61-90-5; L-isoleucine, 73-32-5; L-proline, 147-85-3; 3-aminobutyric acid, 541-48-0; 4-aminobutyric acid, 56-12-2; 6-aminocapric acid, 15623-17-3; L-histidine, 71-00-1; 3-methylhistidine, 368-16-1; L-phenylalanine, 63-91-2; L-tyrosine, 60-18-4; L-tryptophan, 73-22-3; L-phenylalanine methyl ester, 2577-90-4; L-proline methyl ester, 2577-48-2; glycine ethyl ester, 459-73-4; *N,N*-dimethylglycine, 1118-68-9; phenylalanine methyl ester hydrochloride, 7524-50-7.

LITERATURE CITED

(1) Cotter, R. J. *Anal. Chem.* **1980**, *52*, 1589A.
(2) Beckey, H. D. *Int. J. Mass Spectrom. Ion Phys.* **1969**, *2*, 500-503.
(3) Benninghoven, A.; Jaspers, D.; Sichtermann, W. *Appl. Phys.* **1976**, *11*, 35-39.
(4) Barber, M.; Bordoli, R. S.; Sedgwick, R. D.; Tyler, A. N. *J. Chem. Soc., Chem. Commun.* **1981**, 325-327.
(5) Macfarlane, R. D.; Torgerson, D. F. *Science* **1976**, *191*, 920-925.
(6) Conzemius, R. J.; Capellen, J. M. *Int. J. Mass Spectrom. Ion Phys.* **1980**, *34*, 197-271.
(7) Junk, G.; Svec, H. *J. Am. Chem. Soc.* **1963**, *85*, 839-845.
(8) Winkler, H. V.; Beckey, H. D. *Org. Mass Spectrom.* **1972**, *6*, 655-660.
(9) Milne, G. W. A.; Axenrod, T.; Fales, H. M. *J. Am. Chem. Soc.* **1970**, *92*, 5170-5175.
(10) Surman, D. J.; Vickerman, J. C. *J. Chem. Res.* **1981**, 170-171.
(11) Schiller, C.; Kupka, K.-D.; Hillenkamp, F. *Fresenius' Z. Anal. Chem.* **1981**, *308*, 304-308.
(12) Voigt, D.; Schmidt, J. *Biomed. Mass Spectrom.* **1978**, *5*, 44-46.
(13) Denoyer, E.; Van Grieken, R.; Adams, F. *D. F. S. Natusch Anal. Chem.* **1982**, *54*, 26-41A.
(14) Parker, C. D.; Hercules, D. M., submitted to *Anal. Chem.*
(15) Leclercq, P. A.; Desiderio, D. M., *Org. Mass Spectrom.* **1973**, *17*, 515.
(16) Meot-Ner, M.; Field, F. H. *J. Am. Chem. Soc.* **1973**, *95*, 7207-7211.
(17) Tsang, C. W.; Harrison, A. G. *J. Am. Chem. Soc.* **1976**, *98*, 1301-1308.
(18) Longevialle, P.; Girard, J. P.; Rossi, J. C.; Tichy, M. *Org. Mass Spectrom.* **1979**, *14*, 414-415.
(19) McLafferty, F. W.; Barbalas, M. P.; Turecek, F. *J. Am. Chem. Soc.* **1983**, *105*, 1-3.
(20) Parker, C. D., unpublished studies of dicarboxylic acids, University of Pittsburgh, 1983.
(21) Baird, R.; Winstein, S. *J. Am. Chem. Soc.* **1963**, *85*, 567-578.
(22) Biemann, K.; Siebl, J.; Gapp, F. *Biochem. Biophys. Res. Commun.* **1959**, *1*, 307.

RECEIVED for review May 10, 1984. Accepted November 15, 1984. This work was supported in past by the Office of Naval Research.

Comparison of Canonical Variates Analysis with Target Rotation and Least-Squares Regression as Applied to Pyrolysis Mass Spectra of Simple Biochemical Mixtures

Lloyd V. Vallis and Halliday J. MacFie*

Agricultural Research Council, Meat Research Institute, Langford, Bristol BS18 7DY, United Kingdom

Colin S. Gutteridge

Cadbury Schweppes PLC, Group Research, Lord Zuckerman Research Centre, The University, Whiteknights, Reading, Berks, United Kingdom

The estimation of the number, identity, and proportions of biochemical compounds present in mixtures is often carried out by target transformation. We have previously shown this to be equivalent to projection in a principal component space. In this paper we derive an analogous method, based on canonical variates analysis, that uses the replicate information from the samples. The superior performance of this approach is demonstrated by using pyrolysis mass spectra of mixtures of glycogen, dextran, and bovine serum albumin.

The estimation of constituents in mixtures from mixture spectra of various kinds is an important problem in analytical chemistry. A range of statistical techniques have been used for extracting information from the mixture spectra, including regression analysis, generalized spectral subtraction, principal components analysis, (sometimes called principal factor analysis), and canonical variates analysis (discriminant analysis). Principal components analysis (PCA) is the method most commonly used. It appears in the work of Lawton and Sylvestre (*1*) on the deconvolution of mixture spectra and in target transformation (*2*, *3*), which has been shown to be equivalent to projection on to principal component vectors (*4*), and in the graphical rotation method of Windig et al. (*5*).

When replicate mixture spectra are available it may be possible to obtain improved results by using a method which maximizes differences between mixtures in relation to differences within mixtures (*6*). These authors combine principal components analysis, discriminant analysis, and graphical rotation to interpret sets of pyrolysis mass spectra from biological materials. The technique they call discriminant analysis is often called canonical variates analysis (CVA) in statistical texts (*7*–*10*). In this paper we describe the CVA analogue of projection onto PCA vectors (target transformation). A comprehensive set of pyrolysis mass spectra data from mixtures of three biological compounds is analyzed by both methods. Some results from ordinary least-squares regression analysis are also included for comparison.

THEORY

Mixture Model. A basic assumption in the analysis is that the constituent spectra combine linearly to produce a mixture spectrum (Beer's law). Expressed mathematically

$$\mathbf{y} = X\mathbf{b} + \mathbf{e} \quad (1)$$

where $\mathbf{y}$ is a $p \times 1$ vector of observable spectral values, X is

0003-2700/85/0357-0704$01.50/0 © 1985 American Chemical Society

a $p \times k$ matrix with known constituent spectra as its columns, $\mathbf{b}$ is a $k \times 1$ vector of unknown proportions, and $\mathbf{e}$ is a $p \times 1$ vector of random errors with mean 0. The elements of $\mathbf{y}$, X, and $\mathbf{b}$ are nonnegative, and the elements of $\mathbf{b}$ sum to 1.

The observed spectra may contain purely relative intensities, so that only the shape of a spectrum is significant. Then it is usual to normalize the spectra in some way, e.g., by scaling so that the sum of the intensities in a spectrum is a constant.

Additional constraints may be imposed on X or $\mathbf{b}$ in special cases. For example the constituent spectra $\mathbf{x}_j$, $j = 1$ to k, may be assumed to have shapes defined by known shape functions with few unknown parameters (*11*). In the case of a set of mixtures $\mathbf{y}_j$, $j = 1$ to n, there may be a parametric model relating the unknown proportions $\mathbf{b}_j$ to some known experimental variables such as time or initial proportions (*12*).

We consider the case of a set of related mixtures of a few constituents in which there is no mathematical model relating the constituents proportions with an "external variable" such as time. It is assumed that reference spectra for a number of likely constituents are available. The aim of the data analysis is to find the number, identity, and proportions of constituents in the set of mixtures.

CVA (1) Data of Full Rank. This is the ordinary CVA described in textbooks. By full rank data we mean that the within-mixtures sample covariance matrix has an inverse. This implies that

$$(n - g) \geq p \tag{2}$$

where n p-dimensional observations (spectra) have been obtained from g mixtures. Rarely, collinearity of observations may cause singularity of the sample covariance matrix (no inverse exists) even when condition (2) is satisfied.

We now proceed to show how CVA of mixture data may be used in conjunction with reference spectra of likely constituents to determine the number, identity, and proportions of constituents in a set of mixtures.

CVA (2) Data of Less Than Full Rank. In the context of CVA, data of less than full rank is such that the within-groups (e.g., within-mixtures) sample covariance matrix is singular. This implies that

$$(n - g) < p \tag{3}$$

or that at least one linear relationship among the components of the data vector holds for every data unit. In the rest of this paper we assume that singularity is due solely to condition (*3*). The problem may be avoided by preliminary data reduction to reduce p so that $(n - g) \geq p$.

Several methods of data reduction are available. The one which we use here is principal components analysis (PCA). The basic idea is that most of the variation in the data can be retained in a relatively small number of principal components which are then subjected to CVA. The canonical variates from the reduced data are used in the same way as canonical variates from data of full rank in the mixture analysis.

The principal components are obtained from the total covariance matrix. When $p > (n - 1)$ a worthwhile saving in computer memory may be made by extracting principal components by a principal coordinates analysis (*13*) of the $n \times n$ association matrix. The question arises as to how many PC's to use in the subsequent CVA. The maximum number one can use is $(n - g)$. Clearly one wants to avoid using very small PC's which could receive spuriously large weights in the CVA due to rounding errors. Windig et al. (*6*), working with correlation matrices of 100 variables, discard the principal components corresponding to latent roots less than one. Hoogerbrugge et al. (*14*) state, without explanation, that the number of PC's retained have to be less than a quarter of the number of spectra in the data set. They routinely use selection of PC's which account for more than 1% of the total variance. We have also found this selection rule satisfactory to date for mixture analysis, but it is unlikely to be satisfactory as a general rule.

Estimating the Number of Constituents. This estimation is based on examination of the latent roots λ_j obtained as solutions to the equations

$$Bl_j = \lambda_j W l_j, \quad j = 1, \ldots, t \tag{4}$$

in which B and W are symmetric $p \times p$ matrices of sums of squares and products (SSP matrices) for variation between mixture spectra and between replicate spectra within mixtures, respectively, and $t = \min(p, g - 1)$ is the maximum number of nonzero λ_j. Here l_j is the latent vector associated with λ_j.

Variation in the proportions of k constituents in the mixtures should produce $k - 1$ major roots and a set of minor roots which are separated from the major roots by a distinct change of magnitude. This implies that the mixture means lie close to a $(k - 1)$-dimensional hyperplane. The residual distances from the hyperplane are due to experimental errors and also to deviations from the mixture model. This examination can be aided by plotting the roots against their ranks.

One can also carry out a formal χ^2 significance test on the equality of remaining roots after excluding the $k - 1$ larger roots (*15*, *16*). However, the use of the χ^2 tests assumes large samples, which rarely occurs in practice.

Identifying Constituents. If a $(k - 1)$-dimensional subspace (hyperplane) has been found for the mixture set, one can test for the presence of a potential constituent by looking at the position of the canonical variate transformation of its spectrum. Potential constituents can be tested independently in this way. Two criteria should be satisfied.

(1) Canonical variate residuals of constituents should be comparable with those of the mixtures. Canonical variate residuals are simply the canonical variate scores on all but the first $k - 1$ canonical axes.

Suppose $\mathbf{c}_2$ is the $t - k + 1$ dimensional vector of canonical variate residuals for a potential constituent, where $t = \min(p, g - 1)$ is the full dimensionality of the canonical space, and the g columns of the matrix Z_2 are corresponding canonical residuals for the mixture means. Residual mean squares can be defined for the mixtures and a constituent respectively as

$$s_M^2 = \text{trace}\,(Z_2 Z_2')/((t - k + 1)(g - k)) \tag{5}$$

$$= \sum_{i=k}^{t} \sum_{j=1}^{g} z_{ij}^2/((t - k + 1)(g - k)) \tag{6}$$

and

$$s_C^2 = \text{trace}\,(\mathbf{c}_2 \mathbf{c}_2)/(t - k + 1) \tag{7}$$

$$\sum_{i=k}^{t} c_{ij}^2/(t - k + 1) \tag{8}$$

Then the ratio

$$F = s_C^2/s_M^2 \tag{9}$$

may be used in an approximate F test with $(t - k + 1)$ and $(t - k + 1)(g - k)$ degrees of freedom to judge a potential constituent. The foregoing method is analogous to the use of residuals in the SIMCA method (*17*) for classifying test objects.

(2) The canonical variate transformations of constituent spectra should form a region enclosing the mixtures in the mixture subspace. This can be checked graphically if the mixtures consist of only a few constituents. Alternatively, the distance of a test spectrum from the mixtures mean can be compared with that of its nearest neighbors. These distances are computed using only the first $k - 1$ canonical variate axes.

Table I. Latent Roots from Principal Components and Canonical Variates Analysis of 63 Mixtures of GLY, DEX, and BSA

method	data analyzed	no. of variables	latent roots (as % of total) 1	2	3	4	5	6	7	8	remainder
PCA	mean spectra	104	62.1	17.4	10.3	1.7	1.4	1.1	0.8	0.7	4.5
PCA	replicate spectra (ungrouped)	104	44.0	27.9	9.0	3.2	2.5	1.7	1.5	1.1	9.1
CVA	first 8 PC's of ungrouped replicate spectra	8	79.2	17.5	0.8	0.7	0.6	0.5	0.4	0.3	0.0
CVA	replicate spectra	104	71.5	9.2	3.7	2.3	1.8	1.4	1.1	1.0	8.0

This implies that the full canonical variate test vector should form a reasonably small angle with the mixture hyperplane. Note that the vectors are measured from an origin taken at the mixtures mean. At present we do not have an objective criterion for the angle but suggest that a test vector forming an angle of cosine less than 0.9 with the mixture hyperplane is a strong candidate for rejection. In practice both the squared distance S_c^2 and the cos criteria would be examined.

Estimating Proportions. Once the constituents in the set of mixtures are identified, the proportions may be estimated from the canonical variate transformation of eq 1, using only the first $k - 1$ canonical variates, contained in the $k \times (k - 1)$ matrix L_1. That is

$$L_1'\mathbf{y} = L_1'(X\mathbf{b} + \mathbf{e}) \tag{10}$$

and by obvious substitutions

$$\mathbf{z}_1 = C_1\mathbf{b} + \mathbf{h}_1 \tag{11}$$

where the subscript 1 in (10) and (11) means that the subscripted matrix or vector is the partition corresponding to the first $k - 1$ canonical variates. Thus C_1 is a $(k - 1) \times k$ matrix. We can augment eq 11 with the constraint that $b_1 + ... + b_k = 1$, which can be written in matrix form as

$$\mathbf{1}'\mathbf{b} = 1 \tag{12}$$

Hence

$$\begin{pmatrix} \mathbf{z}_1 \\ 1 \end{pmatrix} = \begin{pmatrix} C_1 \\ \mathbf{1}' \end{pmatrix} \mathbf{b} + \begin{pmatrix} \mathbf{h}_1 \\ 0 \end{pmatrix} \tag{13}$$

and thus the estimates of the proportion are

$$\hat{\mathbf{b}} = \begin{pmatrix} C_1 \\ \mathbf{1}' \end{pmatrix}^{-1} \begin{pmatrix} \mathbf{z}_1 \\ 1 \end{pmatrix} \tag{14}$$

$$= A\begin{pmatrix} \mathbf{Z}_1 \\ 1 \end{pmatrix} \tag{15}$$

where A is the inverse matrix in eq 14. A covariance matrix (conditional on A) for $\hat{b}$ is

$$\text{cov}(\hat{\mathbf{b}}) = A \text{ cov}\begin{pmatrix} \mathbf{Z}_1 \\ 1 \end{pmatrix} A' \tag{16}$$

$$= (1/r)A\begin{pmatrix} I & 0 \\ 0 & 0 \end{pmatrix} A' \tag{17}$$

where I is a $k - 1$ dimensional identity matrix and r is the number of replications taken on the mixture.

In the Appendix we show that (17) is equivalent to using eq 14 to estimate **b** for individual replicates and computing a pooled sample covariance matrix from the replicate estimates.

EXPERIMENTAL SECTION

Materials. The mixture constituents were the polyhexoses glycogen (GLY) and dextran (DEX) and a protein, bovine serum albumin (BSA) all of which were obtained from the Sigma Chemical Co. Concentrated suspensions of each compound in water were prepared prior to mixing at the correct concentration. Sixty-three mixtures were prepared by using proportions of constituents as illustrated in Figure 1. The mixtures were pipetted onto clean Curie-point wires and the water was evaporated to leave a constant sample size of 50 μg.

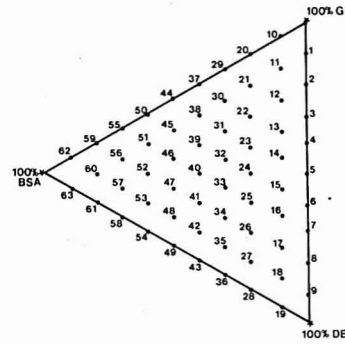


Figure 1. Mixture triangle showing the proportions of constituents in 63 experimental mixtures. The proportions vary in steps of 10%.

Pyrolysis Mass Spectrometry. Spectra were obtained with a Curie-point pyrolysis mass spectrometer (Pyromass 8-80, VG Gas Analysis, Ltd., Middlewich, U.K.). This instrument is similar in concept to that designed by Meuzelaar et al. (*18*), except that it utilizes a magnetic mass analyzer. A full description of the Pyromass 8-80 can be found in Shute et al. (*19*). The key conditions used in this study were as follows: pyrolysis, 510 °C for 2 s; electron energy, 16 eV; scan time, 1.3 s/cycle; number of scans, 33; mass range, m/z 12–300. Mass spectra of three analyses of each pure constituent and mixture were recorded and the mass intensity data over the range m/z 51–154 were used for the statistical analyses.

RESULTS AND DISCUSSION

Since there are three replicates of the 63 mixtures and 104 variables, the within-mixtures dispersion matrix will be nonsingular unless some variables are collinear. The latter is found not to be the case, and therefore a CVA is possible. However we present results from combined PC-CVA for comparison.

Estimates of the Number of Constituents. As explained before, the number of constituents with varying concentrations in the mixtures is one more than the number of major latent roots. Therefore the two major latent roots in Table I from CVA of 104 mass intensities indicate the presence of three constituents. In the case of CVA of the first eight principal components, accounting for 90.9% of total variance, the presence of three constituents is shown even more clearly. By contrast, the three major latent roots from PCA of the mean spectra indicate the presence of a fourth constituent or failure of the mixture model equation (*1*). Van de Meent et al. (*20*) have suggested that an extra component could occur because of chemical interaction between two or more constituents. This would be indicated by systematic change of the extra component values with changing concentrations of one or more constituents. No such systematic variation was observed and we conclude that the third PC is spurious and caused by giving equal weight to variables that are not associated with large

Table II. Statistics for the Presence of Constituents in Mixtures of GLY, DEX, and BSA

mixture analysis method	constituent	residual mean squares: constituents	residual mean squares: mixtures	F ratio	F prob	cosine of angle[b] between test vector and mixture plane
CVA	GLY	8.53	10.800	0.79	P>0.10	0.948
	DEX	14.46		1.34	P=0.04	0.942
	BSA	46.59		4.31	P<0.01	0.948
		(d.f. = 60)	(d.f. = 3600)			
PC-CVA[a]	GLY	4.902	1.169	4.19	P<0.01	0.959
	DEX	2.685		2.30	P=0.03	0.977
	BSA	1.959		1.68	P>0.10	0.966
		(d.f. = 6)	(d.f. = 372)			
PCA	GLY	0.2254	0.07028	3.21	P<0.01	0.766
	DEX	0.0865		1.23	P>0.10	0.922
	BSA	0.1143		1.63	P<0.01	0.970
		(d.f. = 60)	(d.f. = 3600)			

[a] CVA done on the 8 PC's with variance >1% of the total variance. [b] The angles refer to CV axes in the CVA and PC-CVA methods. In the PCA method the angles referred to PC axes and original axes are identical.

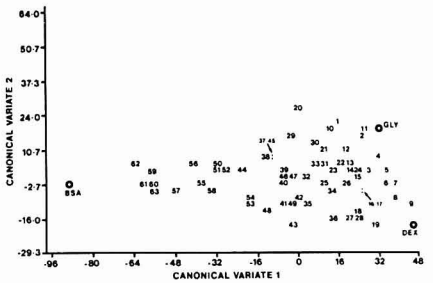


Figure 2. Plot of the first two dimensions of canonical variate means of the Py-MS data from 63 mixtures and the constituents (GLY, DEX, BSA). The canonical variate transformation was derived from CVA of the mixture spectra, and the reference spectra of the constituents were superimposed afterward.

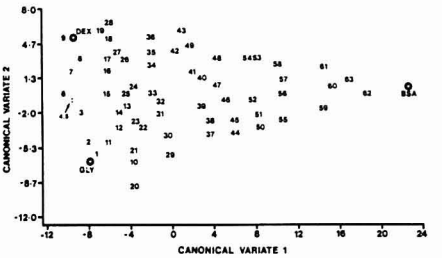


Figure 3. Plot of the first two dimensions of the canonical variate means of the Py-MS data from 63 mixtures with the constituent spectra (GLY, DEX, BSA) superimposed. The canonical variate transformation was derived from CVA of the first eight principal components of the mixtures.

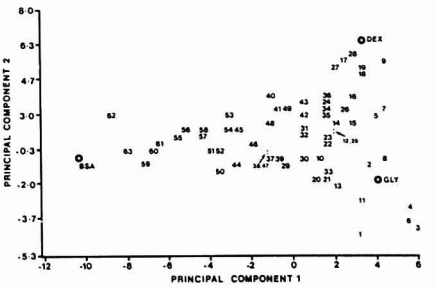


Figure 4. Plot of the first two principal components of the PyMS data from 63 mixtures with the constituent spectra (GLY, DEX, BSA) superimposed. The PCA was done on the mixture mean spectra averaged over replicates.

between sample variation. This is a graphic example of the power of the CVA technique.

Identification of the Constituents. The transformations of the three constituent and 63 mixture spectra on to the CVA space are shown in Figure 2. The idealized equilateral triangle of Figure 1 has been recovered as a triangle elongated in the BSA direction, reflecting the close similarity of GLY and DEX spectra relative to BSA. The positions of GLY and DEX pure spectra appear correct and the cosines in Table II reflect this. The occurrence of a significant F ratio for DEX may be attributed to the large number of degrees of freedom used for this test. If the degrees of freedom are based on the underlying dimensionality of the data rather than the number of mass intensities measured on a spectra, as is done for the PC-CVA, the F ratio is nonsignificant. The cosine of the BSA test vector is satisfactorily high, and its projection is outside the mixtures but the F test shows a significant deviation from the plane, even using the reduced degrees of freedom. Clearly the F test is very sensitive to deviations from the mixture plane and should be regarded with some circumspection.

The PC-CVA solution, shown in Figure 3, is similar to the CVA solution in the sense that cosines (Table II) are satisfactory, but now the F test for GLY is significant, even at the reduced degrees of freedom. This result also occurs in the PCA method but, in contrast, the cosine for GLY is also unacceptably small. This must be at least partly due to the projection of GLY falling inside the mixture region (Figure 4).

Estimates of the Proportions of Constituents. Statistics for estimates of composition of the experimental mixtures are given in Table III. There is only a small amount of bias (average deviations) in the estimates by the CVA method, but the root mean square (RMS) deviations are fairly large. Figure 5 illustrates these results for the CVA method. Note that in Figure 5 a group of points with the same true proportion of a given constituent are not replicates but means of mixtures which have varying amounts of the other constituents. The standard errors (SE's) of the estimates by the CVA method

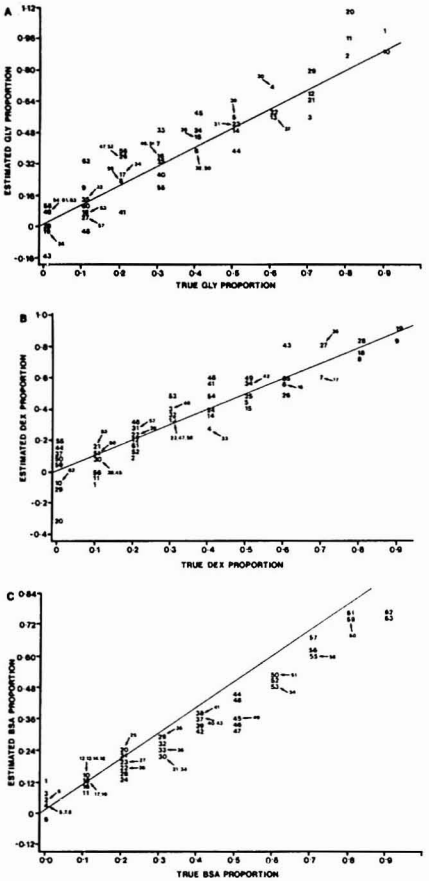


Figure 5. Estimates of proportions of GLY, DEX, and BSA obtained by the CVA method plotted against the true proportions.

indicate good agreement between replicates (Table III).

With three-constituent mixtures the deviations of estimated composition from known composition can be shown in a single graph, as shown in Figure 6 for the CVA method. This shows again the under-estimation of the BSA proportion shown clearly in Figure 5c. It also shows outstanding errors in the estimated proportions of GLY and DEX for mixture number 20.

The underestimation of the BSA may also be due to a "response effect" of the pyrolysis mass spectrometer. Equal weights of BSA, DEX, or GLY may yield different total ion currents, although DEX and GLY would be expected to behave similarly. The calculation of "response factors" (i.e., the ratio between total ion current and weight in mixtures) could be used to correct for this underestimation, but methods for doing this are not yet available for Py-MS data.

The directions of increasing concentration are given by the perpendiculars from the constituent point to the opposite side of the triangle (*4*). These directions are shown schematically

Table III. Summary Statistics for Estimates of Composition of 63 Mixtures from Py-MS Data

mixture analysis method	constituent	deviation of estimates from true proportions, % av	% RMS	std errors of estimates
CVA	GLY	3.2	9.6	1.6
	DEX	0.3	10.0	1.5
	BSA	−3.5	7.2	0.5
PCA-CVA[a]	GLY	−1.0	9.1	5.0
	DEX	5.7	11.3	4.9
	BSA	−4.7	5.9	1.8
PCA	GLY	13.1	26.2	
	DEX	−5.0	21.8	
	BSA	−8.0	10.1	
regression	GLY	7.0	14.5	3.6[b]
	DEX	−0.5	12.5	3.7[b]
	BSA	−6.5	8.8	1.9[b]

[a] CVA done on the 8 PC's with variance >1% of the total variance. [b] Average over 63 mixtures.

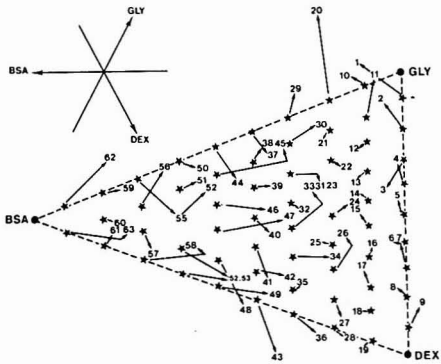


Figure 6. Known and estimated composition of 63 mixtures of GLY, DEX, and BSA. The estimates are obtained by the CVA method. Positions of mixture numbers denote estimated composition and positions of star symbols denote known composition. The known and estimated composition of each mixture are connected by an arrowed line. Coincident points are marked by ":". The directions of increasing concentrations are represented in the top left.

in Figure 6. Note that vectors from the centroid to the pure constituent points are *not* necessarily the concentration directions (cf. Figure 2).

The results in Table III for the PC-CVA method show a shift in bias from GLY to DEX and a small increase in the amount of bias when compared with the CVA results. The RMS deviations are very similar to those for the CVA method. The corresponding SE's of the estimates are about three times as large, but are still acceptable.

The average and RMS deviations by the PCA and regression methods (Table III) are large, confirming the poor performance of these methods in contrast to the CVA method. The PCA method, which is the one we mainly wanted to compare with CVA, gave poor results.

CONCLUSION

With this set of data, the CVA method is shown to be much superior to the PCA method of mixture analysis (target transformation). This is due to the fact that the CVA method makes optimum use of the within-mixtures information, while

the PCA method ignores it completely. A necessary requirement for application of the CVA method is replication of the mixture spectra. When the number of dimensions in the spectra exceeds the degrees of freedom of the within-mixtures SSP matrix, the CVA method can be applied to the principal components of the total SSP matrix. The number of principal components used must not exceed the degrees of freedom of the within-mixtures SSP matrix. We have found the arbitrary rule of using only the principal components accounting for at least 1% of the total variance satisfactory for mixture analysis.

The CVA analogue of the principal components target transformation method is a useful addition to the range of techniques available for statistical analysis of high dimensional spectra from mixtures.

APPENDIX

To show that the covariance matrix of $\hat{\mathbf{b}}$ obtained from the replicate estimates is equivalent to eq 17, we note that the jth replicate estimate of the composition of mixture i is

$$\hat{\mathbf{b}}_{ij} = A\mathbf{z}^*_{ij} \quad \text{with A as defined previously}$$

and

$$\mathbf{z}^*_{ij} = \begin{pmatrix} \mathbf{Z}_{1,ij} \\ 1 \end{pmatrix} \text{with } \mathbf{z}_{1,ij}$$

the vector of the first $k-1$ canonical variate scores of the jth replicate of the ith mixture. Then a pooled sample covariance matrix of the estimates, for a given A, is

$$\begin{aligned} \text{cov}\,(\hat{\mathbf{b}}_{ij}) &= \sum_{ij}(\hat{\mathbf{b}}_{ij} - \hat{\mathbf{b}}_{i\cdot})(\hat{\mathbf{b}}_{ij} - \hat{\mathbf{b}}_{i\cdot})'/(n-g) \\ &= \sum_{ij}[A(\mathbf{z}^*_{ij} - \mathbf{z}^*_{i\cdot})(\mathbf{z}^*_{ij} - \mathbf{z}^*_{i\cdot})'A']/(n-g) \\ &= A\sum_{ij}[(\mathbf{z}^*_{ij} - \mathbf{z}^*_{i\cdot})(\mathbf{z}^*_{ij} - \mathbf{z}^*_{i\cdot})']A'/(n-g) \\ &= A\begin{pmatrix} I_{k-1} & 0 \\ 0 & 0 \end{pmatrix}A' \end{aligned}$$

where I_{k-1} denotes the $k-1$ dimensional identity matrix. Hence, when $\hat{\mathbf{b}}_{i\cdot}$ is based on r_i replicates

$$\text{cov}\,(b_{i\cdot}) = (1/r_i)A\begin{pmatrix} I_{k-1} & 0 \\ 0 & 0 \end{pmatrix}A'$$

This is entirely equivalent to eq 17.

LITERATURE CITED

(1) Lawton, W. H.; Sylvestre, E. A. *Technometrics* **1971**, *13*, 617.
(2) Weiner, P. H.; Malinowski, E. R.; Levinstone, A. R. *J. Phys. Chem.* **1970**, *74*, 4537.
(3) Malinowski, E. R.; Howery, D. G. "Factor Analysis in Chemistry"; Wiley: New York, 1980.
(4) Vallis, L.; MacFie, H. J. H.; Gutteridge, C. S. *J. Anal. Appl. Pyrol.* **1983**, *5*, 333.
(5) Windig, W.; Kistemaker, P. G.; Haverkamp, J. *J. Anal. Appl. Pyrol.* **1982**, *3*, 199.
(6) Windig, W.; Haverkamp, J.; Kistemaker, P. G. *Anal. Chem.* **1983**, *55*, 81.
(7) Chatfield, C.; Collin, A. J. "Introduction to Multivariate Analysis"; Chapman and Hall: London, 1980; p 153.
(8) Maxwell, A. E. "Multivariate Analysis in Behavioural Research"; Chapman and Hall: London, 1977; p 96.
(9) Lachenbruch, P. A. "Discriminant Analysis"; Hafner Press: New York, 1975; p 66.
(10) Rao, C. R. "Advanced Statistical Method in Biometric Research"; Wiley: New York, 1952; Section 9c.
(11) Pitha, J.; Jones, R. N. *Can. J. Chem.* **1967**, *45*, 2347.
(12) Sylvestre, E. A.; Lawton, W. H.; Maggio, M. S. *Technometrics* **1974**, *16*, 353.
(13) Gower, J. C. *Biometrika* **1966**, *53*, 325.
(14) Hoogerbrugge, R.; Willig, S. J.; Kistemaker, P. G. *Anal. Chem.* **1983**, *55*, 1710.
(15) Bartlett, M. S. *J.R. Statist. Soc., B* **1947**, *9*, 176.
(16) Rao, C. R. "Linear Statistical Inference and Its Applications", 2nd ed.; Wiley: New York, 1973; Section 8c.6.
(17) Wold, S.; Sjojstrom, In "Chemometrics, Theory and Practice"; Kowalski, B. R., Ed.; American Chemical Society: Washington, DC, 1977; Am. Chem. Soc. Symp. Ser. No. 52.
(18) Meuzelaar, H. L. C.; Kistemaker, P. G.; Eshuis, W.; Boerboom, H. J. H. "Advances in Mass Spectrometry"; Heyden: London, 1978; Vol. 7, p 1452.
(19) Shute, L. A.; Gutteridge, C. S.; Norris, J. R.; Berkeley, R. C. W. *J. Gen. Microbiol.* **1984**, *130*, 343.
(20) van de Meent, D.; de Leeuw, J. W.; Schenck, P. A.; Windig, W.; Haverkamp, J. *J. Anal. Appl. Pyrol.* **1982**, *4*, 133.

RECEIVED for review September 27, 1984. Accepted December 3, 1984.

Carbon-13 Nuclear Magnetic Resonance Spectrometric and Gas Chromatography/Mass Spectrometric Characterization of Lipids in Corn Suspension Cells

Dennis James Ashworth,* Douglas Owen Adams, Benjamin Yunwen Giang, Michael Tung-hai Cheng, and Rino Yul Lee

Western Research Center, Stauffer Chemical Company, 1200 South 47th Street, Richmond, California 94804

Carbon-13 NMR spectrometry has been applied in conjunction with gas chromatography/mass spectrometry to the characterization of lipid distribution and structure in suspension cells of corn (*Zea mays* var. Black Mexican Sweet). Growth of the cells in the presence of sodium [1-^{13}C]acetate or [2-^{13}C]-acetate followed by NMR analysis of the extracted lipids displayed an initial incorporation of acetate into oleate (18:1). After 24 h, NMR analysis suggested that >90% of the labeled oleate had been converted to linoleate (18:2). Integration of the enriched carbonyl resonances of the neutral and polar lipid's fatty acids showed an even distribution of the label between the two lipid groups. ^{31}P NMR spectrometry showed the polar lipids to be primarily represented by phosphatidylcholine. GC/MS analysis of the derivitized fatty acids suggested that the oleate/linolenate ratios may be characteristic of the respective netural and polar lipids.

In the course of investigating the effects of various herbicides on fatty acid biosynthesis in suspension cells of corn, a necessary prerequisite was the characterization of the lipid components prior to herbicide treatment (*1*). In plant cells, the various polar and neutral lipids are generally composed of C_{16} (palmitic, 16:0; palmitoleic, 16:1) and C_{18} (stearic, 18:0; oleic, 18:1; linoleic, 18:2 linolenic, 18:3) saturated and unsaturated fatty acids esterified to the 1 and 2 positions of a glycerol backbone. Modifications to the 3 position of glycerol by the addition of monoalkyl phosphates, sugars, or additional acyl groups then generates the three major classes of lipids (*2*).

The biosynthesis of C_{16} and C_{18} fatty acids consists of the acyl carrier protein (ACP) mediated head to tail linkage of consecutive acetate units to generate palmitoyl-ACP (*3–6*). Further elongation of this substrate by the transfer of a two-carbon unit from malonyl-ACP yields stearoyl-ACP which undergoes an initial unsaturation to generate oleayl-ACP (*7*). Further details as to the transitional events which lead from the fatty acid-ACP complex through free acids and/or coenzyme A esters to neutral and phospholipid formation are less clear (*8*). Likewise, the specific metabolic steps leading to the more highly unsaturated linoleic (18:2) and linolenic (18:3) fatty acids have yet to be firmly established (*9–12*).

Carbon-13 nuclear magnetic resonance (NMR) spectrometry has emerged as an extremely powerful tool for structural analysis of biomolecules and the observation of metabolic processes (*13–18*). In the studies reported here, the metabolism of carbon-13 labeled acetate to various saturated and unsaturated fatty acids in suspension cells of nonphotosynthetic corn has been monitored by NMR spectrometry. In addition, gas chromatographic/mass spectrometric (GC/MS) characterization of the lipid derived fatty acid methyl esters has been performed to aid in the analysis of the distribution of the fatty acids and the characterization of the structure of the intact lipids.

Table I. Growth Inhibition of Nonphotosynthetic Corn Suspension Cells (*Zea mays* var. Black Mexican Sweet) by Sodium, Potassium, and Ammonium Acetate[a]

concn, mM	sodium acetate	potassium acetate	ammonium acetate
0	100.0	100.0	100.0
0.5	99.1	86.6	91.3
1.0	100.0	92.1	102.9
2.5	93.3	87.5	95.3
5.0	83.7	67.9	62.1
7.5	49.0	46.6	44.6
10.0	30.0	32.7	32.1

[a] Cultures were grown 14 days at the indicated acetate concentration (in triplicate) and the final packed cell volumes determined. Results (average) are expressed as percentage of control packed cell volume.

MATERIALS AND METHODS

Suspension cells of corn (*Zea mays* var. Black Mexican Sweet) were used in all experiments and were cultured in a modified (2 mg/L 2,4-D and 132 mg/L L-asparagine) Linsmaier and Skoog medium (*19*). The nonphotosynthetic cells were transferred weekly under aseptic conditions with 15 mL of 7 day old cells being transferred into 25 mL of fresh medium. One milliliter of 7 day old culture contained approximately 150 mg of fresh weight of cells. All culture flasks were maintained at 27 °C under conditions of 16 h of light and 8 h of dark on a rotary shaker at 125 rpm. A preliminary experiment was conducted to establish the maximum concentration of acetate which could be used in the metabolism study without inhibiting cell growth and to evaluate the effect of various acetate cations (Na^+, K^+, and NH_4^+) on growth. Flasks containing 10 mL of fresh medium were inoculated with 2 mL of 7 day old suspension cells. To each respective culture (in triplicate) was then added sodium, potasium, or ammonium acetate to give the concentrations shown in Table I. The cells were grown 14 days at 27 °C and the final packed cell volumes were determined by pouring the contents of each culture flask into a graduated 15-mL centrifuge tube and centrifuging at 550*g* for 2 min. The starting packed cell volume of each flask prior to acetate addition was approximately 0.8 mL.

Preparation of corn suspension cells prior to NMR analysis was initiated by transferring 15 mL of 7 day old cells into 25 mL of fresh medium. The cells were given 3 days to stabilize in the new culture medium at which time sodium [1-^{13}C]acetate or [2-^{13}C]-acetate was added to a final concentration of 2.0 mM (except where indicated). The cells were then harvested after a specific time following acetate addition. One flask of cells was used for each time point. Cells were collected by vacuum (aspirator) filtration on to Whatman No. 1 filter circles (9 cm) for 1 min with concurrent distilled water washing to remove any extracellular acetate or medium. The fresh weight of the cells was then determined. A typical 40-mL culture contained 3.4 g fresh weight of cells at 2 h. The isolated cells were extracted according to Bligh and Dyer (*20*) to separate water and chloroform soluble metabolites. Following concentration of the chloroform (lipid) fraction,

0003-2700/85/0357-0710$01.50/0 © 1985 American Chemical Society

the residue was dissolved in 0.6 mL of $CDCl_3$ for NMR analysis. Carbon-13 labeled sodium [1-^{13}C]acetate (99%) and sodium [2-^{13}C]acetate (99%) were purchased from MSD Isotopes and were used without further purification.

Fractionation of the lipids into polar and neutral classes was performed by dissolving the chloroform residue (approximately 25 mg) from the Bligh and Dyer extraction in 10 mL of diethyl ether. One gram of activated silicic acid was added and the suspension was allowed to stir at 5 °C for 30 min. After centrifugation the resulting ether layer was collected and the silica was washed two additional times with 10 mL of ether followed by centrifugation and ether collection. Concentration of the combined ether extract yielded the separated carbon-13 enriched neutral lipids for NMR and GC/MS analysis. The phospholipids were recovered by washing the silica with 3–10 mL portions of methanol followed by centrifugation, methanol collection, and concentration (*21*). Base hydrolysis of isolated lipids and subsequent fatty acid esterification was performed in 10 mL of 2 N NaOH for 2 h at 100 °C. The cooled solution was acidified with 2 N HCl and the free fatty acids were extracted with 2–10 mL portions of diethyl ether. Concentration and addition of ethereal diazomethane to the residue generated the corresponding methyl esters. Acid catalyzed transesterification of the lipids was performed by the addition of 10 mL of methanol, containing 0.1 mL of trifluoromethanesulfonic acid, to the lipid residue. Refluxing at 65 °C for 2 h followed by concentration of the solution yielded the methyl esters.

Carbon-13 NMR spectrometry was performed on a Varian XL-200 NMR spectrometer operating at 50.1 MHz. All spectra were obtained at 28 °C employing an 11 kHz spectral width (1.45 s acquisition time) and 8.8 μs pulse width (50° pulse angle) with continuous broad-band ^{1}H decoupling for 32K data points. Spectra were acquired for 38K transients and resonance chemical shifts are relative to deuteriochloroform (77.0 ppm). Phosphorus-31 NMR spectra were recorded on the same instrument at 81.0 MHz utilizing the same spectral width, pulse width, and data points as in the carbon-13 NMR experiments. Phosphorus-31 chemical shifts are relative to 85% H_3PO_4 (0.0 ppm).

GC/MS analysis was performed on a Finnigan-MAT Model 4021 gas chromatograph/mass spectrometer system equipped with a Model 9600 gas chromatograph. Fatty acid esters were separated on both a 1.8 m 10% OV-101 packed column and a 30 m × 0.25 mm (i.d.) DB 1701 fused silica capillary column with injection port temperatures of 210 °C and helium carrier gas. Both column oven temperatures were programmed from 40 °C to 200 °C at 30 °C/min and then from 200 °C to 250 °C at 4 °C min. Samples were dissolved in dichloromethane to a concentration of 0.5–2.0 μg/μL and 1.0 μL was inejected (50:1 split). The electron impact mass spectra were obtained at 70 eV electron energy and 250 μA emission current.

RESULTS

Initial experiments were performed to obtain the natural abundance carbon-13 NMR spectra of the total extracted corn cell lipids. Extraction of the lipids prior to acetate treatment and extraction following 2.0 mM sodium [1-^{13}C]acetate and 2.0 mM [2-^{13}C]acetate treatment for 7 h produced the three respective spectra shown in Figure 1. The natural abundance carbon-13 spectrum (Figure 1A) allowed observation of all extracted lipid carbons. However, because of the large number of resonances present, with considerable overlapping of resonances in many cases, the assignment of specific resonances to particular fatty acids was difficult. This difficulty was reduced, as was an increase in sensitivity gained, when the suspension cells were treated with 2.0 mM sodium [2-^{13}C]-acetate (Figure 1B) or sodium [1-^{13}C]acetate (Figure 1C) for 7 h prior to lipid extraction. A comparison of the resonance chemical shifts observed in Figure 1 parts B and C to thhe carbon chemical shifts obtained from the appropriate authentic reference compounds (Table II), allowed the tentative identification of oleic and linoleic acids as constituents of the isolated lipids since the route of fatty acid biosynthesis from 1- or 2-labeled acetate results in fatty acids with alternate carbons labeled (*22*). All remaining resonances in spectra A,

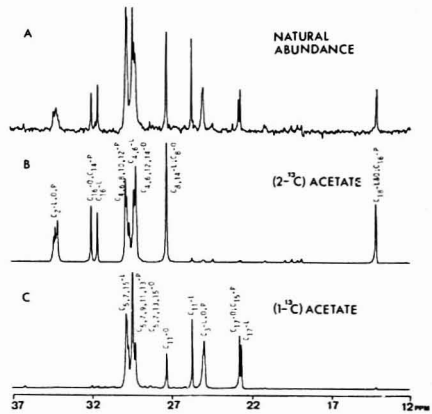


Figure 1. Carbon-13 NMR spectra of isolated corn cell lipids following culture growth for 7 h in (A) normal medium, (B) medium and 2.0 mM sodium [2-^{13}C]acetate, and (C) medium and 2.0 mM sodium [1-^{13}C]acetate. Resonance assignments correspond to major labeled fatty acids present: P, palmitate; O, oleate; L, linoleate.

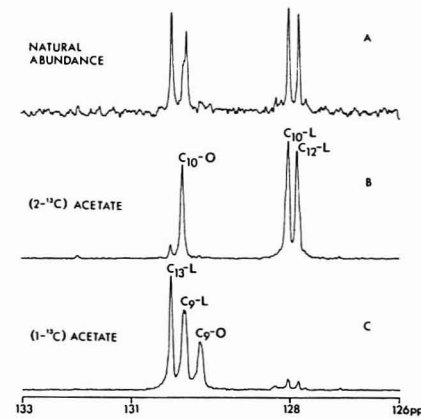


Figure 2. Olefinic region expansion of extracted lipids carbon-13 NMR spectra obtained from nonphotosynthetic corn suspensions cells grown for 7 h in (A) normal medium, (B) 2.0 mM sodium [2-^{13}C]acetate, and (C) 2.0 mM sodium [1-^{13}C]acetate: O, oleate; L, linoleate.

B, and C could not be unambiguously assigned to specific fatty acids due to the lack of unique carbon chemical shifts for the remaining aliphatic carbons of palmitic, palmitoleic (*22*), stearic (*23*), oleic, linoleic, and linolenic acids.

Further characterization of the carbon-13 enriched lipid components was obtained by examination of the olefinic regions of the respective spectra (Figure 2). All spectra (Figure 2A–C) lack resonances assignable to linolenic acid (130.1, 127.7, 128.2, 128.1, 127.0, and 131.8 ppm) with the 131.8 and 127.0 ppm resonances being the most distinct resonances absent in the spectra. However, spectra in Figure 2 parts B and C do allow the identification of oleic and linoleic acids as major enriched lipid components due to each respective fatty acid's unique olefinic carbons chemical shifts. These results

Table II. Carbon-13 Chemical Shifts of Pertinent Fatty Acids and Lipids[a]

Compound	Position	C-1	C-2	C-3	C-4	C-5	C-6	C-7	C-8	C-9	C-10	C-11	C-12	C-13	C-14	C-15	C-16	C-17	C-18	CH_2O (glyc$_1$)	CHO (glyc$_2$)	CH_2OP (glyc$_3$)	CH_2OP (chol$_1$)	CH_2N (chol$_2$)	$N(CH_3)_3$ (chol$_3$)	P (chol$_4$)	Ref.
Palmitic Acid		180.69	34.14	24.68	29.10	29.29	29.48	29.65	29.73	29.73	29.73	29.73	29.7[illegible]	29.42	31.97	22.71	14.06										(22,35)
1,2-dipalmitoyl-phosphatidylcholine	1	173.51	34.13	24.88	29.18	29.35	29.35	29.56	29.71	29.71	29.71	29.71	29.71	29.35	31.90	22.67	14.09			62.97	70.46	63.31	59.29	66.27	54.30	-.36	(36)
	2	173.15	34.30	24.96	29.15	29.35	29.35	29.56	29.71	29.71	29.71	29.71	29.71	29.35	31.90	22.67	14.09				7.7Hz	3.4Hz	3.7Hz	6.7Hz			
Oleic Acid		180.63	34.09	24.62	29.03	29.15	29.03	29.66	27.12	129.61	129.90	27.19	29.7[illegible]	29.33	29.54	29.33	31.91	22.68	14.04								(23,37,38)
1,2-dioleoyl-phosphatidylcholine	1	173.65	34.08	24.84	29.18	29.28	29.28	29.73	27.19	129.59	129.90	27.19	29.7[illegible]	29.28	29.50	29.28	31.86	22.64	14.06	62.96	70.36	63.47	59.31	66.16	54.20	-.38	
	2	173.35	34.24	24.95	29.12	29.28	29.28	29.73	27.19	129.59	129.90	27.19	29.7[illegible]	29.28	29.50	29.28	31.86	22.64	14.06		7.2Hz	4.8Hz	5.0Hz	6.9Hz			
Linoleic Acid		180.58	34.07	24.59	28.89	29.10	29.02	29.54	27.13	129.87	128.00	25.58	127.84	130.06	27.15	29.31	31.49	22.53	13.99								(23,37,38)
1,2-dilinoleoyl-phosphatidylcholine	1	173.49	34.08	24.84	29.13	29.26	29.17	29.64	27.16	129.93	128.02	25.59	127.83	130.18	27.18	29.30	31.48	22.54	14.05	62.96	70.44	63.34	59.28	66.29	54.32	-.40	
	2	173.14	34.27	24.92	29.09	29.24	29.17	29.64	27.16	129.93	128.02	25.59	127.85	130.18	27.18	29.30	31.48	22.54	14.05		7.8Hz	5.3Hz	5.1Hz	6.7Hz			
Linolenic Acid		180.57	34.05	24.57	28.96	29.08	29.00	29.50	27.12	130.10	127.69	25.55	128.18	28.14	25.46	127.05	131.81	20.48	14.19								(37)
Tripalmitoyl-glycerol(Tripalmitin)	1 + 3	173.24	34.04	24.86	29.11	29.27	29.35	29.47	29.69	29.69	29.69	29.69	29.69	29.35	31.92	22.68	14.10										
	2	172.83	34.21	24.90	29.09	29.27	29.35	29.47	29.69	29.69	29.69	29.69	29.69	29.35	31.92	22.68	14.10										
1-palmitoyl-2-linoleoyl-phosphatidylcholine	1	173.52	34.12	24.88	29.16	29.32	29.32	29.65	29.69	29.69	29.69	29.69	29.69	29.32	31.90	22.67	14.10			62.98	70.55	63.31	59.26	66.39	54.45	-.40	(24,34)
	2	173.13	34.30	24.93	29.09	29.24	29.24	29.65	27.18	129.95	128.04	25.61	127.85	130.20	27.18	29.34	31.49	22.55	14.06		8.1Hz	5.5Hz	4.7Hz	6.4Hz			
1-oleoyl-2-palmitoyl-phosphatidylcholine	1	173.51	34.10	24.86	29.13	29.31	29.31	29.71	27.18	129.67	129.98	27.21	29.71	29.31	29.52	29.31	31.89	22.67	14.11	62.96	70.49	63.40	59.24	66.37	54.46	-.39	
	2	173.19	34.32	24.96	29.13	29.35	29.35	29.54	29.71	29.71	29.71	29.71	29.71	29.35	31.89	22.67	14.11				7.4Hz	4.8Hz	4.3Hz	6.9Hz			

[a] All compounds were purchased from Sigma Chemical Co. and spectra were obtained from approximately 10 mg/0.6 mL $CDCl_3$ solutions. All chemical shifts are relative to internal deuteriochloroform at 77.0 ppm. Phosphorus-31 chemical shifts are relative to external 85% H_3PO_4 at 0.0 ppm. Two and three bond carbon-phosphorus coupling constants are shown below glycerol and choline carbon chemical shifts.

Table III. Distribution of Methyl Esters of Fatty Acids Obtained by Hydrolysis/Methylation of Extracted Corn Suspension Cells Lipids Followed by GC/MS Analysis

sample	lipid source	hydrolysis method	% by wt of fatty acid esters					calcd original wt of sample, mg
			$C_{16:0}$	$C_{18:0}$	$C_{18:1}$	$C_{18:2}$	$C_{18:3}$	
A	neutral	base	19.0	0.9	12.0	64.4	3.7	6.0
B	polar	base	22.4	1.0	5.8	53.3	17.5	5.8
C	polar	acid	18.9	0.8	3.3	54.7	22.3	6.4
D	neutral	acid	24.9	0.9	10.4	60.4	3.2	7.3
E	mixture	base	21.2	0.5	14.5	60.4	3.4	15.2
F	mixture	acid	19.4	0.5	7.5	60.2	12.4	30.9

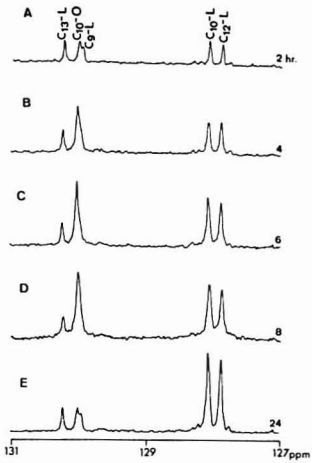


Figure 3. Carbon-13 NMR spectra of [2-^{13}C]acetate incorporation into unsaturated fatty acids of corn suspension cells. Cultures were grown under identical conditions for the indicated length of time followed by extraction of the lipids from the cells. All samples were dissolved in 0.6 mL of $CDCl_3$ and ^{13}C spectra were acquired under identical conditions. Spectra are displayed in the absolute intensity mode: O, oleate; L, linoleate.

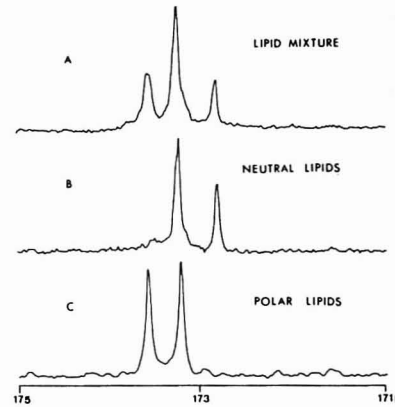
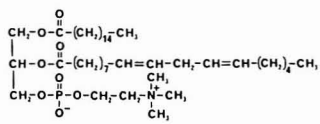


Figure 4. Carbonyl region expansion of ^{13}C NMR spectra of (A) lipid mixture obtained from extracted corn suspension cells, (B) separated neutral lipids, and (C) polar lipids obtained from lipid mixture. Cells were grown 8 h in the presence of 2.0 mM sodium [1-^{13}C]acetate prior to lipid extraction.

therefore supported the identification of oleate and linoleate obtained from analysis of the aliphatic region (Figure 1).

The identification of palmititic acid as a major lipid component of these plant cells was accomplished due to methyl palmitate's early, well-resolved gas chromatographic retention time. However, in the course of standardizing hydrolysis and methylation conditions for GC/MS identification of the lipid derived esters, an authentic sample of 1-palmitoyl-2-linoleoyl-L-glycero-3-phosphorylcholine was used. Upon acid



1-palmitoyl-2-linoleoyl-L-glycero-3-phosphorylcholine

catalyzed methanolysis in dilute trifluoromethanesulfonic acid, only methyl palmitate was observed in the GC/MS analysis of the sample. Yet when 2 N aqueous sodium hydroxide was used for lipid hydrolysis followed by ethereal diazomethane esterification, both methyl palmitate and methyl linoleate were observed by GC/MS. This result suggested that under the acidic conditions employed for lipid methanolysis, only fatty acids esterified to the 1 and 3 positions of glycerol were being cleaved possibly due to steric hinderance of the methanol approach to the 2-acyl linkage (aqueous 2 N HCl did cleave the 2-acyl linkage). This same terminal position specificity was also observed when 1-oleoyl-2-palmitoyl-L-glycero-3-phosphorylcholine was treated with dilute methanolic trifluoromethanesulfonic acid. This observation was used to further characterize the lipid structures.

Carbon-13 NMR analysis of the time course of [2-^{13}C]-acetate incorporation into lipids is shown in Figure 3. Observed in the olefinic expansion (Figure 3A) are essentially the natural abundance signals of linoleate and one additional resonance corresponding to the C_{10} of oleate. The appearance of the C_{10} resonance of oleate after just 2 h suggests some carbon-13 enrichment from acetate already at this position since the C_9 of oleate would also be observable just upfield of the C_9 of linoleate at 129.6 ppm if the oleate C_{10} was not already enriched. Because treatment of the cells with [2-^{13}C]acetate enriches only the even-numbered carbons of oleate and linoleate, after 4 h (Figure 3B) the C_{10} position of oleate becomes further enriched. The C_9 of linoleate, not enriched by [2-^{13}C]acetate, is now masked by the oleate C_{10} while the C_{10} and C_{12} of linoleate are still at natural abundance intensity. After 6 h (Figure 3C), all even-numbered olefinic carbons were further enriched until a maximum was reached at 8 h (Figure 3D) at which time no extracellular [2-^{13}C]acetate remained in the medium (depleted at approximately 7 h). After 24 h however, it can be observed that all labeled oleate had been depleted, yet the incorporation of label into linoleate had continued. These observations suggest a flow of carbon from acetate, through oleate to linoleate. The same results were observed by the repeat of the experiment using [1-^{13}C]acetate.

Further characterization of the lipids was accomplished by separating the mixture into polar and lipid fractions. While carbon-13 NMR analysis of the olefinic and aliphatic regions of the separated components only displayed, in the neutral fraction, an approximate 15% increase in oleate relative to linoleate, an examination of the enriched ester carbonyl regions did reveal distinctive carbonyl carbon chemical shifts for the respective polar and neutral fractions and for the specific 1- and 2-acyl chains (Figure 4). This observation is consistent with the chemical shifts reported in Table II and has been explained by steric interactions with the glycerol carbons and adjacent acyl chains (23-26). The distinct carbonyl chemical shifts observed in the separated polar and neutral lipids (Figure 4B, C) suggest that integration of the most upfield (neutral lipid 2-acyl carbonyl) and most downfield (polar lipid 2-acyl carbonyl) carbonyl resonances of the total extracted lipid mixture (Figure 4A) could qualitatively allow the cellular polar/neutral lipid ratio to be determined.

Phosphorus-31 NMR analysis of the separated polar lipids qualitatively showed phosphatidylcholine to be the major phophorus-containing component with resonances corre-

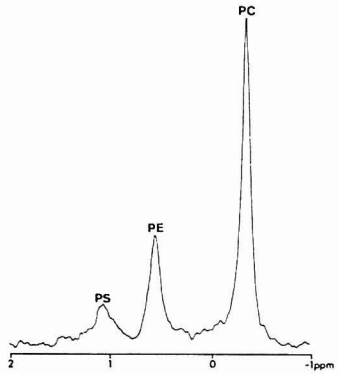


Figure 5. Phosphorus-31 NMR spectrum of extracted polar lipids from corn suspension cells. Resonance assignments are based on comparisons of chemical shifts to authentic reference compounds: phosphatidylcholine (PC), -0.4 ppm; phosphatidylinositol, -0.1 ppm (broad); phosphatidylethanolamine (PE), 0.5 ppm; phosphatidylserine (PS), 0.9 ppm (broad); and phosphatidylglycerol, 1.8 ppm. Chemical shifts are relative to external 85% H_3PO_4 (0.0 ppm).

sponding to phosphatidylethanolamine and phosphatidylserine also present (Figure 5). The ratio of these resonances did not change throughout the time course (2–24 h) experiments.

Characterization of the total (carbon-13 labeled and unlabeled) fatty acid pools was achieved by hydrolysis and methylation of the lipids to the corresponding fatty acid methyl esters (FAMES) followed by GC/MS analysis. The distribution of FAMES obtained by base hydrolysis of the separated neutral and polar lipid fractions is shown in Table III, samples A and B. A considerable difference can be observed between the oleate and linolenate distributions. The neutral lipids contain approximately two times the oleate yet only one-fourth the linolenate as compared to the polar lipid sample. This difference was also observed upon acid catalyzed methanolysis of the neutral and polar lipid fractions (Table III, samples C and D). In this case three times more oleate and one-seventh the linolenate were found in the neutral lipids as compared to the polar. Because of the selective 1-acyl transesterification with trifluoromethanesulfonic acid methanolysis, a comparison of the later oleate and linolenate ratios (Table III, samples C and D) to the former (samples A and B) oleate and linolenate ratios suggest a fairly uniform distribution of the observed fatty acids among the 1, 2, and 3 positions of the triacylglycerols and the 1 and 2 positions of the remaining lipids. Clearly linoleate appears to occupy approximately half of all lipid fatty acid positions in the separated polar lipids (Table III, sample B) and nearly two-thirds of the fatty acid positions in the neutral lipids (Table III, sample A). This was observed whether the free FAMES were generated by acid catalyzed methanolysis or base hydrolysis. Therefore the linoleate as well as the other observed fatty acids appear to be evenly distributed. A comparison of the fatty acid distributions when a mixture of polar and neutral lipids were hydrolyzed in base to the distribution when hydrolysis/methanolysis was catalyzed by acid (selective 1- and 3-acyl hydrolysis) showed a preferential 1-and/or 3-position esterification of linoleate to the glycerol backbone and a preferential 2-position enrichment with oleate (Table III, samples E and F). This result is substantiated by a comparison of samples A and B and samples C and D in Table III. Finally, a comparison of the distribution of fatty acids obtained from the cultured cells following 1 h of acetate treatment to the fatty acid distribution obtained from a culture grown 24 h in 2.0 mM acetate showed that acetate feeding did not alter the fatty acid distributions.

DISCUSSION

The results presented here describe the use of NMR spectrometry for the observation of in vivo synthesis of fatty acids from acetate in extracts of corn suspension cells and the structural features of specific fatty acids and intact lipids which can be obtained by the use of NMR spectrometry in conjunction with gas chromatography/mass spectrometry. The results obtained from the observation of [1-^{13}C]acetate and [2-^{13}C]acetate incorporation into fatty acids as a function of time (Figure 3) suggest a flow of the labeled carbons into oleate by way of palmitate and stearate, and finally into linoleate (*27*). GC/MS analysis of the total labeled and unlabeled fatty acid pool showed significant (approximately 10% of total) linolenate to be present in the cells. However, incorporation of carbon-13 labeled acetate into linolenate was not observed (*28*) and continued culture growth up to 72 h likewise did not show detectable conversion of the labeled oleate or linoleate to linolenate. Whether linolenate is derived from desaturation of linoleic acid (*11*), linoleoylphosphatidylcholine (*29*), linoleoylmonogalactosyldiglyceride (*12*), or from elongation of dodecatrienoic acid (*10*) is yet to be firmly established. Nevertheless, the results obtained here fail to show the conversion of carbon-13 labeled linoleate to linolenate after 24 h of growth in 2 mM sodium acetate.

The rapid increase in oleate labeling followed by its subsequent near disappearance and the concurrent increase in linoleate labeling has been observed by using other methods of analysis (*11, 12, 27, 30, 31*). The result suggests a relatively small rapidly turning-over pool of oleate since >90% of the labeled oleate observed following 8 h of cell growth in 2 mM [2-^{13}C]acetate had disappeared by 24 h. GC/MS analysis (Table III) also sugests a relatively small pool of oleate. The results obseved here also suggest that desaturation of oleate to linoleate as well as elongation of palmitate to oleate, via stearate, occurs while the respective fatty acids are esterified (*32*). This conclusion is based on carbon-13 NMR analysis which failed to show the presence of any detectable free labeled fatty acids or carboxylates in the spectra of the isolated lipids.

While NMR analysis enabled observation of the flow of labeled acetate into lipids and identification of the unsaturated fatty acid esters, mass spectrometric analysis allowed identification of unresolved (in the NMR spectra) fatty acids and the determination of the individual fatty acid pool sizes. The results show linoleate to be the most abundant fatty acid present in the polar and neutral lipids occupying over half the acyl sites in the isolated lipids. Palmitate was found to be the next most abundent fatty acid occupying approximately 20% of the remaining polar and neutral lipid acyl positions. Interestingly, the presence of palmitoleate (16:1) was not observed. This is consistent with other findings suggesting localization of palmitoleate in photosynthetic tissue (*2, 11, 27, 31, 33*). Stearate was found to be present in low (approximately 1% of total) yet constant abundance and was evenly distributed between polar and neutral lipid fractions. Perhaps most interesting were the reciprocal distributions of oleate and linolenate between the polar and neutral lipids. When oleate comprised a relatively high percent (10–12%) of the total lipid in the separated neutral lipids, linolenate was found to be relatively low (approximately 3%). Conversely, when linolenate was relatively high (17–22%) in the polar lipids, oleate was found to be low (3–5%). The uniform distribution of palmitate, stearate, and linoleate observed in both polar and neutral lipid fractions suggest that the high

oleate-low linolenate in neutral, high linolenate-low oleate in polar lipids may be characteristic of the lipid structures in nonphotosynthetic corn suspension cells.

CONCLUSIONS

The picture that emerges from the work on corn suspension cells presented here is one of neutral and polar lipids composed of palmitic, stearic, oleic, linoleic, and linolenic acids. Growth of the cells in [1-^{13}C]acetate and [2-^{13}C]acetate quickly enriches palmitate and oleate. The labeled oleate is then converted into linoleate with little (<10%) of the labeled oleate remaining. No conversion of labeled linoleate to linolenate was observed. From observation of the C_1 labeled fatty acid esters obtained by growth of the cells in the presence of [1-^{13}C]-acetate, the distribution of the carbon-13 label between neutral and polar lipids was found to be nearly equal. The polar lipids were primarily represented by phosphatidylcholine with lesser amounts of phosphatidylethanolamine and phosphatidylserine also observed. From GC/MS analysis of the total and separated neutral and polar lipids, the relative oleate/linolenate ratios appear to be characterisitc of the respective neutral and polar lipids. The results presented here have provided the necessary characterization of the nonphotosynthetic corn lipid structure and biosynthesis to allow a greater understanding of the effects of various herbicides on lipid biosynthesis and structure. NMR spectrometry in conjunction with gas chromatography/mass spectrometry offers an attractive alternative to the traditional carbon-14 incorporation/thin-layer chromatographic regime normally employed in lipid analysis.

Registry No. 16:0, 57-10-3; 18:0, 57-11-4; 18:1, 112-80-1; 18:2, 60-33-3; 18:3, 463-40-1; 1,2-(16:0)PC, 2644-64-6; 1,2-(18:1)PC, 4235-95-4; 1,2-(18:2)PC, 6542-05-8; 1-(16:0)-2-(18:2)PC, 6931-84-6; 1-(18:1)-2-(16:0)PC, 17118-56-8; tripalmitin, 555-44-2; sodium acetate, 127-09-3; potassium acetate, 127-08-2; ammonium acetate, 631-61-8.

LITERATURE CITED

(1) Enzra, G.; Gressel, J.; Flowers, H. M. *Pestic. Biochem. Physiol.* **1983**, *19*, 255–234.
(2) Harwood, J. L. In "The Biochemistry of Plants. A Comprehensive Treatise"; Stumpf, P. K., Ed.; Academic Press: New York, 1980; Vol. 4, pp 1–48.
(3) Jacobson, B. S.; Jaworski, J. G.; Stumpf, P. K. *Plant Physiol.* **1974**, *54*, 484–486.
(4) Jaworski, J. G.; Goldschmidt, E. E.; Stumpf, P. K. *Arch. Biochem. Biophys.* **1974**, *163*, 769–776.
(5) Ohlrogge, J. B.; Kuhn, D. N.; Stumpf, P. K. *Proc. Natl. Acad. Sci. USA* **1979**, *76*, 1194–1198.
(6) Shine, W. E.; Manch, M.; Stumpf, P. K. *Arch. Biochem. Biophys.* **1976**, *172*, 110–116.
(7) Stumpf, P. K. In "MTP International review of Science, Biochemistry of Lipids II"; Goodwin, T. W., Ed.; Butterworth: London, 1977; Vol. 14, pp 215–238.
(8) Gurr, M. I. In "MTP International Review of Science, Biochemistry of Lipids"; Goodwin, T. W., Ed.; Butterworth: London, 1974; Vol. 4, pp 181–235.
(9) Harris, R. V.; James, A. T. *Biochim. Biophys. Acta* **1964**, *106*, 456–464.
(10) Jacobson, B. S.; Kannangara, C. G.; Stumpf, P. K. *Biochim. Biophys. Res. Commun.* **1973**, *52*, 1190–1198.
(11) Cherif, A.; Dubacq, J. P.; Mache, R.; Oursel, A.; Tremolieres, A. *Phytochemistry* **1975**, *14*, 703–706.
(12) Ohnishi, J.; Yamada, M. *Plant Cell Physiol.* **1980**, *21*, 1607–1618.
(13) Ashworth, D. J.; Mettler, I. J. *Biochemistry* **1984**, *23*, 2252–2257.
(14) Parks, J. S.; Cistola, D. P.; Small, D. M.; Hamilton, J. A. *J. Biol. Chem.* **1983**, *258*, 9262–9269.
(15) Metcalf, J. C.; Birdsall, N. J. M.; Feeney, J.; Lee, A. G.; Levine, Y. K.; Partington, P. *Nature (London)* **1971**, *233*, 199–201.
(16) Fusion, M. M.; Prestegard, J. H. *J. Am. Chem. Soc.* **1983**, *105*, 168–176.
(17) Chan, S. I.; Feigenson, G. W.; Seiter, C. H. A. *Nature (London)* **1971**, *231*, 110–112.
(18) Colnago, L. A.; Seidl, P. R. *J. Agric. Food. Chem.* **1983**, *31*, 461–463.
(19) Linsmaier, E. M.; Skoog, F. *Physiol. Plant.* **1965**, *18*, 100–127.
(20) Bligh, E. G.; Dyer, W. J. *J. Biochem. Physiol.* **1959**, *37*, 911–917.
(21) Tang, W. J.; Castelfranco, P. A. *Plant Physiol.* **1968**, *43*, 1232–1238.
(22) Burlingame, A. L.; Balogh, B.; Welch, J.; Lewis, S.; Wilson, D. *J. Chem. Soc., Chem. Commun.* **1972**, 318–319.
(23) Batchelor, J. G.; Cushley, R. J.; Prestegard, J. H. *J. Org. Chem.* **1974**, *39*, 1698–1705.
(24) Santaren, J. F.; Rico, M.; Guilleme, J.; Ribera, A. *Org. Magn. Reson.* **1982**, *18*, 98–103.
(25) Lacey, C. J.; Loew, L. M. *J Org. Chem.* **1983**, *48*, 5214–5221.
(26) Assmann, G.; Highet, R. Jj.; Sokoloski, E. A.; Brewer, H. B. *Proc. Natl. Acad. Sci. USA* **1974**, *71*, 3701–3705.
(27) Williams, J. P.; Watson, G. R.; Leung, P. K. *Plant Physiol.* **1976**, *57*, 179–184.
(28) Siebertz, H. P.; Heinz, E. *Z. Natureforsch., C* **1977**, *32C*, 193–205.
(29) Stymne, S.; Appelquist, L. A. *Plant Sci. Lett.* **1980**, *17*, 287–294.
(30) MacCarthy, J. J.; Stumpf, P. K. *Planta* **1980**, *147*, 384–388.
(31) Roughan, P. G.; Mudd, J. B.; McManus, T. T.; Slack, C. R. *Biochem. J.* **1979**, *184*, 571–574.
(32) Murphy, D. J.; Mukherjee, K. D.; Woodrow, I. E. *Eur. J. Biochem.* **1984**, *139*, 373–379.
(33) Appelquist, L. A.; Stumpf, P. K.; von Wettstein, D. *Plant Physiol.* **1968**, *43*, 163–187.
(34) Santaren, J. F.; Rico, M.; Ribera, A. *Org. Magn. Reson.* **1983**, *21*, 238–242.
(35) Couperus, P. A.; Clague, A. D. H.; van Dongen, J. P. C. M. *Org. Magn. Reson.* **1978**, *11*, 590–597.
(36) Schmidt, C. F.; Barenholz, Y.; Huang, C.; Thompson, T. E. *Biochemistry* **1977**, *16*, 3948–3954.
(37) Wenkert, E.; Bockwalter, B. L.; Burfitt, I. R.; Gasic, M. J.; Gottlieb, H. E.; Hagaman, E. W.; Schell, F. M.; Wovkulich, P. M. In "Topics In Carbon-13 NMR Spectroscopy"; Levy, G. C., Ed.; Wiley: New York, 1976; Vol. 2, pp 82–87.
(38) Rutar, V.; Burgar, M.; Blinc, R.; Ehrenberg, L. *J. Magn. Reson.* **1977**, *27*, 83–90.

RECEIVED for review August 20, 1984. Accepted November 19, 1984.

Application of Auger Electron Spectrometry to Trace Analysis: Determination of Less Than 10 ppm Sulfur in Copper

Siegfried Hofmann* and Roland Frech[1]

Max-Planck-Institut für Metallforschung, Institut für Werkstoffwissenschaften, Seestrasse 92, D-7000 Stuttgart 1, West Germany

The use of AES to determine bulk concentration at the parts-per-million level is demonstrated for 4 ppm sulfur in single crystalline copper. The method consists of several cycles combining AES measurements of the segregation kinetics of sulfur on a Cu (110) surface at 1082 K and subsequent sputter cleaning. From the different time dependencies of the increase of the surface enrichment of sulfur, the specific sulfur depletion for each cycle is obtained. This allows an extrapolation to the original bulk concentration. Advantages and limitations of the method are discussed.

It is generally agreed that the detection limit of Auger electron spectroscopy (AES) is of the order of 0.1 at.%, that is, in the mg/g range (*1-3*). However, this value is obtained for a sample volume which is approximately given by the product of the primary electron beam diameter (d) and the Auger electron escape depth (λ): This restriction means that for a bulk metallic sample and typical parameters $d = 10\ \mu m$, $\lambda = 1$ nm only about 10^{-13} cm^3 or 10^{10} atoms contribute to the analyzed volume. Thus, the above-mentioned detection limit corresponds to 10^7 atoms or $\simeq 10^{-14}$ g (*4*). That means, traces of elements in a bulk sample should be detectable only if it is possible to enrich these elements in a surface layer (*5*). A mechanism which leads to an effective surface enrichment is thermally activated surface segregation (*5-12*). For favorable solute/solvent combinations surface enrichment factors of up to 10^7 are obtained (*6-8*). The potential of segregation enhancement to allow AES measurement of bulk composition has been shown for tin in copper single crystals (*5, 6*) and was applied to determine sulfur in polycrystalline nickel (*7*). In the sulfur–copper system, a direct comparison with microtitration results is possible to test the validity of the AES measurements.

The aim of this paper is to demonstrate the capabilities and limitations of the application of surface segregation kinetics (as detected by AES) to trace analysis for the case of sulfur in copper single crystals. Under certain conditions (discussed below) the method can also be used to analyze polycrystalline material.

In thermodynamic equilibrium the surface composition of a solid solution system generally differs from the bulk composition. The tendency to the surface enrichment of one component depends mainly on atomic size and electronic bonding parameters, a measure of which is the segregation enthalpy, ΔH (*10*). Assuming a diluted binary system ($X_b \ll 1$), and neglecting the segregation entropy (generally $\Delta S/R < 1$), the solute segregation for the most simple case of maximum coverage of one monolayer is described by the Langmuir–McLean equation (*8-11*)

$$\frac{X_s}{1 - X_s} = X_b \exp\left(-\frac{\Delta H}{RT}\right) \tag{1}$$

where X_s and X_b are the segregant mole fractions at the surface and in the bulk, respectively. (Note that ΔH must be negative for $X_s > X_b$ to occur.) By use of ΔH and T an enrichment factor $\beta(T) = X_s/X_b$ can be defined using eq 1. Values of $\beta(T)$ for a number of solute/solvent systems can be found in ref 8.

Assuming $X_s = 10^{-3}$ in the surface layer as the detection limit for AES, $\beta(T) > 1000$ is a prerequisite for bulk analysis in the parts-per-million range. As a rule, β is high for elements with low solubility in the respective matrix and vice versa. For example, β (1000 K) is about 2×10^7 for S in Cu (*12*), 5×10^4 for P in Cu (*12*), 2×10^3 for Sn in Cu (*8*), 2×10^2 for Au in Ni, and 70 for Cu in Ni (*8*).

Application of eq 1 to the determination of X_s requires the establishment of a thermodynamic equilibrium and careful quantification of the AES signal intensities. These conditions are less stringent if one uses the technique described below which combines the kinetics of surface segregation and sputter removal of the surface layer.

It has been shown that the initial kinetics of surface segregation, i.e., the increase of the surface concentration X_S with time, is described by (*6, 9, 13*)

$$X_s = X_b\left[1 + \frac{2}{d}\left(\frac{Dt}{\pi}\right)^{1/2}\right] \tag{2}$$

where d is the thickness of a monatomic layer, D is the bulk diffusivity, and t is the annealing time at a constant temperature. Equation 2 is generally valid for small X_s. However, for high enrichment factors (high ΔH) and low solute content, it is valid up to a considerable fraction of the equilibrium X_s defined by eq 1 (*6, 13*). The starting condition for eq 2 is a homogeneous concentration distribution from the surface into the bulk. A sputter-cleaned surface approximates this condition fairly well, despite the possibility of distortions by preferential sputtering. A further prerequisite (as also for eq 1) is a negligible influence of other species on the segregation of the solute being considered. Within the framework of Guttman's ternary segregation theory (*14*), this means no attractive interaction between the additional impurities and the solute. Deviations in the segregation kinetics from eq 2 according to this effect have been treated by Tyson (*15*).

EXPERIMENTAL SECTION

Single crystal rods of high-purity copper (99.9998% Fa. Preussag-Metall, Goslar) with a diameter of 11 mm were grown by the Bridgeman technique in high-purity graphite molds. Thin plates of 0.3 mm thickness and with known orientations (checked by Laue X-ray diffraction) were cut out by spark erosion. Surface contaminants were removed by etching in concentrated HNO_3. The samples were then electropolished in 80% H_3PO_4 at an anode potential of 1.2 V to obtain a smooth surface. Subsequently, they were cleaned sequentially in an ultrasonic bath with acetone, ethylene, and distilled water and dried in hot air. The samples were mounted in the AES test chamber on a copper plate, which was indirectly heated by a tungsten filament. Temperatures up to 1250 K (measured with Pt/PtRh thermocouple) could be achieved. After several heating cycles and Ar^+ bombardment, the surface contaminants (mainly C and O) were removed leaving only S as the segregation species. Chemical analyses by microtitration have shown the residual sulfur content between 4 and

[1] Present address: IBM Deutschland, D-7030 Böblingen, West Germany.

0003-2700/85/0357-0716$01.50/0 © 1985 American Chemical Society

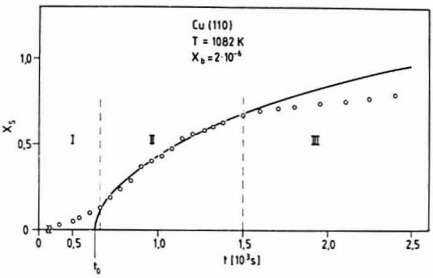


Figure 1. Dependence of the surface coverage X_s of S at a Cu (110) surface on the annealing time t at T = 1082 K, $X_b = 2 \times 10^{-6}$. t_0 denotes the starting point of the idealized segregation kinetics (eq 2, region II) as shown by the full drawn line.

6 ppm and phosphorus below 1 ppm.

Sputter cleaning of the surface was done by Ar^+ ion bombardment at 1 keV and 7×10^{-3} Pa Ar in the test chamber, with a current density (not determined) of the order of a few $\mu A/cm^2$. Typical duration time of the sputtering run after each anneal was 10 min, resulting in an estimated sputter depth of about 5 to 10 nm and a clean copper surface where the Auger signal of S was well below the detection limit. The sputter removal of sulfur could be followed with time and shows an exponential decay typical for monolayer enrichment. Presumably there is preferential sputtering of sulfur as well as sputtering enhanced migration of S. Both effects are restricted to the altered layer of atomic mixing (about 1 nm for 1 keV Ar^+ ions (*3*)) and are favorable for effective sputter cleaning. No evidence was found for possible distortions from lateral diffusion of S from the unsputtered areas, as could be checked by a reproducibility test of the segregation kinetics with variations of the diameter of the sputtered area. The segregation kinetics were obtained as a function of the annealing time at constant sample temperature by measuring simultaneously the increase of the sulfur AES signal (at 152 eV) and the decrease of the Cu (60 eV) signal. The Auger spectrometer (TFA, Phys. El. Ind.) was operated at 3 keV primary energy, 25-μA beam current, 100-μm beam diameter, and 4-V modulation voltage. Spectra were recorded in the derivative mode ($dN(E)/dE$), taking the peak to peak height as the intensity of the respective element signal.

RESULTS AND DISCUSSION

Starting with a sputter cleaned (110) surface at room temperature, a typical run for a sample heated to 1082 K is shown in Figure 1. The Auger peak to peak height (APPH) of the S (152 eV) signal is directly proportional to the mole fraction X_s of sulfur in the first monolayer. (A quantification of X_s was performed by comparison of AES with LEED results (*12*).) Different spectra can be compared by normalization with the APPH ratio of S (152 eV) and Cu (60 eV) as described by ref 5 for Sn on Cu. X_s is plotted as a function of the annealing time. This dependence can be divided into three regions (I, II, III, Figure 1). Region I, which shows an increasing slope, is determined by two effects: At first, the heating of the sample surface is delayed by the heat flow from the heater to the sample until thermal equilibrium is established. The second effect is presumably due to defect agglomerates which are induced by Ar^+ ion bombardment prior to annealing. These induced defects act as additional sinks for sulfur atoms and therefore cause a further delay of their arrival at the surface.

In region II, X_s is still far below the equilibrium surface concentration (defined by eq 1), and the segregation kinetics follow the diffusion law for transport to an ideal sink as described by eq 2, i.e., a square root law with time (*6*, *13*). However, we have to account for a certain time lag, t_0, as

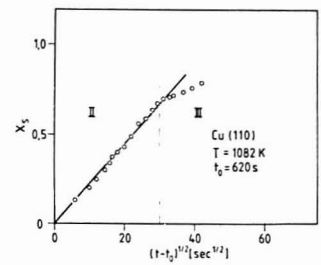


Figure 2. Data from Figure 1: X_s plotted as a function of $(t - t_0)^{1/2}$. The slope in region II yields the bulk diffusivity after eq 3a.

discussed for region I. Because the bulk concentration X_b is far below the measurement limit, under these conditions eq 2 is replaced by

$$X_s = \frac{2X_b}{d}\left[\frac{D(t - t_0)}{\pi}\right]^{1/2} \tag{3}$$

where t_0 defines the starting time for the ideal segregation kinetics. The parabolic dependence shown in Figure 1 can be linearized by plotting X_s against $(t - t_0)^{1/2}$ after eq 3 as shown in Figure 2. The fit defines t_0. The slope of the curve in region II determines the product $X_b D^{1/2}$

$$\frac{X_s}{(t - t_0)^{1/2}} = \frac{2}{d\pi^{1/2}}(X_b D^{1/2}) \tag{3a}$$

In region III (Figures 1 and 2) the approximation of the surface as an ideal sink is not valid (*6*, *9*), since the surface concentration of sulfur approaches its equilibrium value for the given temperature and X_b (eq 1) (*6*).

In the following analysis only region II is considered. From eq 3 and 3a it is obvious that the determination of X_b requires the knowledge of X_s and the diffusivity D (the thickness of a monolayer in Cu is d = 0.256 nm). However, it is possible to measure different runs at the same temperature but with different X_b. Since D stays constant, a quantitative measure of X_s will be sufficient to get X_b without knowing the value of D. The technique of decreasing X_b by combined segregation and sputtering has been described earlier (*16*) and is used here in subsequent steps: After having reached the equilibrium surface concentration, the sample is brought to room temperature and the segregated sulfur is removed by Ar^+ ion bombardment with a constant spot diameter. The same run at the same sample temperature can now be repeated and so on.

The bulk content of sulfur will be diminished by the same amount after each run, if the sputtered area and the segregated amount of sulfur are kept constant. If ΔX_b denotes the constant sulfur depletion per run, and X_b^0 the bulk content before the first run, then the bulk content after n runs is X_b^n

$$X_b^n = X_b^0 - n \cdot \Delta X_b \tag{4}$$

with n = 1, 2, 3, ..., designating the number of the respective annealing/sputtering cycle. After each run at 1082 K, i.e., when region III is attained, the sample is further annealed at a temperature of about 1190 K to enhance attainment of equilibrium segregation. At this temperature, $X_s \simeq 0.8$ is obtained. (According to eq 1 with ΔH = −140 kJ/mol (*15*), X_s should only vary between 0.85 and 0.74 for X_b between 4 and 2 ppm, respectively.) The removal of this sulfur layer in a well-defined spot given by the diameter of the Ar^+ ion beam, b, corresponds to a certain amount of sulfur. The diameter b can be measured by moving the sample with a

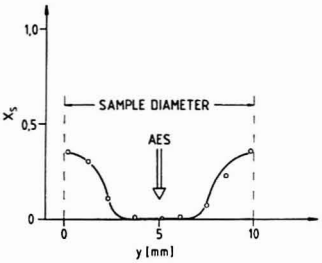


Figure 3. Lateral distribution of the surface coverage of S on a Cu surface after segregation and sputtering with 1-kV Ar ions.

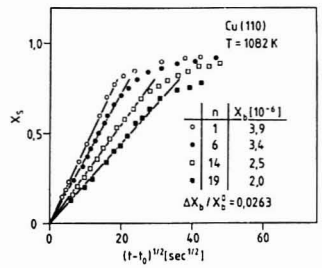


Figure 4. Subsequent runs of segregation and sputtering showing the change in slope of the sulfur surface coverage X_s as a function of $(t - t_0)^{1/2}$. The ratio $\Delta X_b/X_b^0$ is determined after eq 7b.

micrometer drive in front of the analyzer electron beam after sputtering as shown in Figure 3. A diameter of $b = 5.6$ (±0.3) mm is obtained. Note that b is large as compared to the sample thickness (0.3 mm).

The total number of S atoms removed (n_S) can be calculated by: $n_S = X_S \cdot n_{Cu}(110) \cdot A$, where $X_S = 0.8$, $n_{Cu}(110) = 1.08 \times 10^{19}$ m^{-2}, the areal density of Cu atoms at the (110) surface, and $A = 24.6 \times 10^{-6}$ m^2, the area of the sputtered spot. This yields $n_s = 2.12 \times 10^{14}$ and has to be compared to the total number of Cu atoms in the sample: $n_{Cu} = \rho V N_A / M$. With ρ the density (8.96 g/cm^3) $N_A = 6.02 \times 10^{23}$ (Avogadro's number), M the atomic weight (63.54), and $V = 2.36 \times 10^{-8}$ m^3 we obtain $n_{Cu} = 2.0 \times 10^{21}$. Thus, with respect to the bulk, the fractional depletion of sulfur is

$$\Delta X_b = n_S / n_{Cu} = 1.05 \times 10^{-7} \quad (5)$$

Any two cycles at the same temperature allow the determination of X_b^0 after eq 4 when $\Delta X_b/X_b^n$ is known. If m and k denote the numbers of the cycles, according to eq 3a the ratio of the slopes, $q_{(m,k)}$, is given by

$$q_{(m,k)} = \frac{X_b^m D_m^{1/2}/d}{X_b^k D_k^{1/2}/d} = \frac{X_b^m}{X_b^k} \quad (6)$$

since $D_m = D_k$. As seen from eq 3a and 6, $q(m,k)$ can be directly taken from plots $X_s = f(t - t_0)$ as shown in Figure 4. Inserting eq 4 in eq 6 gives

$$q_{(m,k)} = \frac{1 - m(\Delta X_b/X_b^0)}{1 - k(\Delta X_b/X_b^0)} \quad (7a)$$

and for $\Delta X_b/X_b^0$

$$\frac{\Delta X_b}{X_b^0} = \frac{1 - q(m,k)}{m - kq(m,k)} \quad (7b)$$

Table I. Compilation of the Results from Figure 4 and Equation 3a at T = 1082 K[a]

n	$10^{12} X_b^n D^{1/2}$, m/s$^{1/2}$	$10^6 X_b^n$	$10^{12} D$, m^2/s
0		4.0	
1	11.4	3.9	8.48
6	9.82	3.4	8.34
14	6.98	2.5	7.79
19	5.69	2.0	8.10

[a] The bulk atomic fraction of sulfur, X_b^n, after n segregation/sputtering cycles is calculated with eq 5 and 7b, and the bulk diffusion constant D (1082 K) of S in Cu from the slopes $X_b^n D^{1/2}$ in Figure 4.

Figure 4 shows some typical results for X_s plotted as a function of $(t - t_0)^{1/2}$ after eq 3 for subsequent experimental runs. The slope (eq 3a) defines $X_b^n D^{1/2}$. Applying eq 7b, $\Delta X_b/X_b^0 = 0.0263$ is obtained from which $X_b^0 = 4.0$ ppm can be calculated with the result of eq 5. Knowing X_b^n, the bulk diffusivity D can be calculated with eq 3a. A compilation of the data is given in Table I. The mean value of D is: D (1082 K) = 8.2 (±0.3) × 10^{-12} m^2 s^{-1} for the concentrations 2×10^{-6} to 4×10^{-6} of S in Cu. At the end of the measurements (19th run), the sample was chemically analyzed by microtitration which gave a value of 2.6 ppm (with an estimated standard deviation of 0.4 ppm in good agreement with AES analysis (2.0 ppm)). A slightly higher value for the chemical analysis is expected, since in the AES runs the amount of sulfur on the total surface (outside the sputtered area) remains fairly constant and gives no contribution to the segregation measurements but contributes to chemical analysis.

$D(T)$ for different temperatures was determined by the procedures described above. In this way, the bulk diffusion constant of sulfur in copper, $D = D_0 \exp(-Q/RT)$ with $D_0 = (3 \pm 2) \times 10^{-4}$ m^2/s and $Q = 158 \pm 5$ kJ/mol is obtained (*12*). This value is independent of surface orientation and is also valid for polycrystalline materials. As discussed above, a knowledge of $D(T)$ enables the determination of X_b with eq 3 with only one segregation experiment, i.e., without knowing the sputtered area.

The described analysis technique can also be applied to polycrystalline materials. However, in this case complications may arise because grain boundaries act as high diffusivity paths and as additional sources of sulfur. At increased temperature, S will be released from the grain boundaries to the surface at a higher rate than by bulk diffusion. Therefore, the initial increase of the S signal is faster until the grain boundaries contain no excess sulfur. After that, the surface segregation kinetics (via bulk diffusion) are the same as those for single crystals. Compared to Figure 1, this means that region II is attained at increased t_0 (and correspondingly higher X_s), above which eq 3 is valid. Therefore, in the case of very fine grained material (e.g., mean grain diameter below 10 μm), the grain boundary contribution becomes prevalent and region I may extend to region III, leaving no region II for evaluation. Thus, the analysis via surface segregation kinetics is restricted to polycrystalline material with larger grains and is best suited for single crystals.

The precision of the segregation/sputtering method for determining the bulk content of S in Cu mainly depends on that of the AES measurements. The slope of a curve given by several points (cf. Figure 4) is used for the evaluation which considerably decreases the relative error, resulting in a precision of at least 2×10^{-8} (20 ppb or 0.5% at 4 ppm S content). On the other hand, the accuracy of the method depends mainly on the systematic errors in the determination of the surface coverage by quantitative AES and on the sputtered area. In our case, both quantities have been carefully mea-

sured; the AES results were supported by LEED measurements on the Cu (110) surface (12). Therefore, the estimated accuracy is about ±10%. In general, the systematic error for quantification of the surface coverage by the decrease in the matrix signal (5) is higher and depends mainly on the knowledge of the mean escape depth of the Auger electrons, which may be wrong by ±30% (17).

With conventional trace analysis techniques, e.g., acid digestion in combination with microtitrimetric or spectrophotometric determination of sulfur in metals, a detection limit of 0.2 ppm, an accuracy of typical ±10% at 2 ppm and ≤±10% precision can be achieved with about 0.5 g of a sample consumed (18). As compared to these figures, the segregation/sputtering and AES method shows comparable accuracy, better precision, lower detection limit, and negligible sample consumption (<10 μg).

CONCLUSIONS

The use of AES in combination with surface segregation and ion sputtering has been demonstrated for the bulk analysis of 2 to 4 ppm S in Cu. The advantages of this direct instrumental analysis method are that it is relatively fast, with good accuracy and high precision in the range of 20 ppb. A negligible amount of the sample is consumed.

Its general applicability is limited by the following requirements:

(a) The element to be analyzed must be in the matrix in solid solution (not in a second phase)

(b) The element must have a sufficiently high negative segregation enthalpy so that the enrichment factor at the measurement temperature is larger than $1/X_b$.

(c) Evaporation from the surface must be negligible, as well as surface diffusion from outside the sputtered area.

(d) No distortions due to other constituents should occur. This means that no third element prevents surface segregation (e.g., by site competition) or complicates the segregation kinetics by direct interaction. Interaction with structural defects (e.g., grain and phase boundaries) should be negligible. These conditions are generally met for high purity materials in a single crystalline or large grain polycrystalline state.

ACKNOWLEDGMENT

We thank G. P. Shewmon for helpful discussions and A. Meyer for the microtitration analyses.

Registry No. S, 7704-34-9; Cu, 7440-50-8.

LITERATURE CITED

(1) Chang, C. C. In "Characterization of Solid Surfaces"; Kane, P. F., Larabee, G. B., Eds.; Plenum Press: New York, 1974; pp 509-575.
(2) Evans, D. A. *Anal. Chem.* **1975**, *47*, 818A.
(3) Briggs, D., Seah, M. P., Eds. "Practical Surface Analysis by AES and XPS"; Wiley: Chichester, 1983.
(4) Holloway, P. H. *Surf. Sci.* **1977**, *66*, 479.
(5) Hofmann, S.; Erlewein, J. *Mikrochim. Acta* **1979**, *I*, 65.
(6) Hofmann, S.; Erlewein, J. *Surf. Sci.* **1978**, *77*, 591.
(7) Winkler, A.; Rendulic, K. D. *Mikrochim. Acta, Suppl.* **1981**, *9*, 321.
(8) Seah, M. P. *Catal. J.* **1979**, *57*, 450.
(9) Lea, C.; Seah, M. P. *Philos. Mag.* **1977**, *35*, 213.
(10) Wynblatt, P.; Ku, R. C. *Surf. Sci.* **1977**, *65*, 511.
(11) Abraham, F. F.; Brundle, C. R. *J. Vac. Sci. Technol.* **1981**, *18*, 506.
(12) Hofmann, S., Frech, R., submitted for publication in *Surf. Sci.*
(13) Hofmann, S.; Erlewein, J. *Scr. Metall.* **1976**, *10*, 857.
(14) Guttmann, M. *Surf. Sci.* **1975**, *53*, 213.
(15) Tyson, W. R. *Acta Metall.* **1977**, *26*, 1471.
(16) Hofmann, S. *Mater. Sci. Eng.* **1980**, *42*, 55.
(17) Seah, M. P.; Dench, W. *SIA, Surf. Interface Anal.* **1979**, *1*, 2.
(18) Watson, A., Grallath, E., Kaiser, G., Tölg, G. *Anal. Chim. Acta* **1978**, *100*, 413.

RECEIVED for review August 21, 1984. Accepted November 12, 1984.

Two-Column Method for Preconcentration of Trace Metals in Natural Waters on Acrylate Resin

Chi-Chung Wan, Solomon Chiang, and Alfio Corsini*

Department of Chemistry, McMaster University, Hamilton, Ontario, Canada L8S 4M1

Conditions for the direct preconcentration on XAD-7 columns were determined for several trace metal ions in aqueous solutions of low and high salinity. Low breakthrough volumes in the presence of humic materials necessitated their prior removal at low pH by means of a precolumn of XAD-7. The two-column procedure was applied to the determination of trace metals in seawater and lake water. The final effluent for measurement by graphite-furnace atomic absorption spectrometry is readily matrix matched and permits use of the standard calibration curve procedure for the majority of trace metals determined. This results in a reduction of sample consumption and analysis time.

Graphite-furnace atomic absorption spectrometry (GFAAS) and inductively coupled plasma atomic emission spectrometry (ICPAES) are two important techniques for the measurement of trace metal-ion concentrations in natural waters. The direct determination of trace concentrations in natural waters by these techniques is limited, however, because of low concentrations and/or matrix interference problems (although it should be noted that matrix modifiers (e.g., ref 1) are useful in direct GFAAS measurements). It is customary, therefore, to employ preconcentration methods (2-4) as adjuncts to GFAAS and ICPAES.

Chelate solvent extraction and Chelex 100 ion exchange are two important methods of preconcentration but each suffers limitations. For example, the former seldom provides enrichment factors greater than 20, unless a back-extraction step is included (5); and the latter requires relatively large volumes of eluent to strip the column quantitatively (5, 6). Improved enrichment factors have been reported with "ligand-immobilized" chelate ion-exchange columns (7-10) but ligand bleeding may be a disadvantage. The low capacity of these materials is not a disadvantage provided their use is restricted to solutions of very low metal-ion concentrations. Also, each method may lead to different analytical results for water samples containing natural complexing agents such as humic substances, halides, and carbonates (11-16). The portion of

0003-2700/85/0357-0719$01.50/0 © 1985 American Chemical Society

the bound metal-ion content displaced from the natural ligands is dependent on the preconcentration method and the relative labilities and stabilities of all complexes involved. Hence, natural ligands pose a serious matrix problem to total (soluble) metal-ion determinations and this difficulty may not necessarily be fully compensated by the method of standard additions (*5*, *17*).

An ideal method for the preconcentration of trace metals from natural waters should have the following characteristics: it should simultaneously allow isolation of the analyte from the matrix and yield an appropriate enrichment factor; it should be a simple process, requiring the introduction of few reagents in order to minimize contamination, hence producing a low sample blank and a correspondingly lower detection limit; and it should produce a final solution that is readily matrix matched with solutions of the analytical calibration method.

Our previous work has shown that metal ions at low concentration in the presence of acetate and inorganic species such as NH_4Cl, NH_4Br, NH_4NO_3, and NH_4SCN are retained directly by SM-7 (XAD-7) resin (*18*). There was an indication, however, that with SM-7 natural ligands in a lake water sample prevented quantitative recovery of metal-ion spikes (*18*). This observation and the work of others on the adsorption of organic compounds on XAD resins (e.g., ref 19–22) prompted attempts in our laboratory to remove organic ligands, particularly humic materials, by passing the water sample through a precolumn of XAD-7 at pH 1–2, before preconcentration of the trace metals on the analytical column at pH 8. This two-column approach is described in the present study and results obtained on its application to the determination of several trace elements in freshwater and seawater samples by GFAAS are reported.

EXPERIMENTAL SECTION

Apparatus. Metal-ion determinations were made with a Perkin-Elmer 373 atomic absorption spectrophotometer equipped with a HGA 2200 graphite-furnace atomizer. Sample injections of 5, 10, or 20 μL were made manually with Eppendorf micropipets. Humic substances were measured with a GCA McPherson double-beam spectrophotometer, Model EU-700, at a wavelength of 250 nm. Activities of $^{64}Cu(II)$ were detected with a NaI well-counter in conjunction with a Canberra Model 30 multichannel analzyer. The γ-radiation from the 0.51-MeV positron annihilation reaction was measured. Typical counting times were 100 s. All glass and plastic laboratory ware was cleaned by washing with detergent solution, soaking in 2 M HNO_3, and rinsing thoroughly with distilled deionized water (DDW). A horizontal laminar-flow work station (bench-top model, Canadian Cabinets, Ottawa, Ontario) was used to provide a clean-air working environment for the preparation of solutions and columns and for the loading and stripping of columns.

Reagents. All chemicals were reagent grade or better (e.g., Baker InstraAnalyzed grade for HNO_3 and NH_3). DDW was used throughout this work. Solutions of metal ions were prepared by dilution of 1000-ppm standard solutions (Fisher Scientific). Soil humic material (Aldrich Chemical Co., Milwaukee, WI) was used as a model for marine humics. A primary stock solution of 10 g/L was prepared by dissolution of the humic material in aqueous ammonia (pH 11). Secondary stock solutions at lower pH values were prepared by adjustment of the pH of aliquots of the primary solution with dilute HNO_3. Undissolved or precipitated residue was filtered before dilution to a concentration of ~1 g/L. Working solutions were prepared by dilution of the secondary stock solutions followed by pH measurement.

Seawater Reference Material, NASS-1, was obtained from the National Research Council of Canada, Ottawa, Ontario. It had been acidified to pH 1.6 to preserve the integrity of the trace metal content. Coastal seawater samples (Sandy Cove, Nova Scotia) were obtained from the Atlantic Regional Laboratory, National Research Council of Canada, Halifax, Nova Scotia. These samples had been passed through a white-sand filter and preserved at pH 1.7. Lake Ontario samples were supplied by Canada Centre for Inland Waters, Burlington, Ontario. The samples were centrifuged to remove suspended particulates and acidified to pH 1.7.

Column Preparation. Either Bio-Beads SM-7 (Bio-Rad) or Amberlite XAD-7 (Rohm and Haas) was used in the columns. Both resins, supplied as 20–50 mesh, were ground and sieved to 80–100 mesh. SM-7 is an upgraded form of XAD-7. It was further purified by successive washings under suction with 5% HNO_3, 2–3% NH_3, DDW, and methanol. The XAD-7 was washed successively with methanol, diethyl ether, and acetone to remove organic contaminants and then treated exactly as the SM-7. The borosilicate columns were as described before (*18*); both 10- and 20-cm columns were used. The columns were slurry-packed to bed heights of 3, 6, or 15 cm with resin in DDW. Respectively, these heights required about 0.5, 1.0, and 2.5 g of dry resin. Newly packed columns were washed with about 200 mL of 1% (v/v) HNO_3 to remove metal contaminants and then with dilute aqueous ammonia and DDW until the effluent pH was 8–9. The columns were backwashed with DDW to achieve uniform packing. Prior to percolation of a sample or test solution, the column was conditioned with about 50 mL of pH 8 buffer (NH_3/NH_4Cl) which had been previously passed through a Chelex 100 column. Retained metal ions were eluted with 1% HNO_3. After completion of an experiment, the column was rinsed with dilute ammonia and DDW and stored for the next experiment.

Chelex-100 columns (1 × 6 cm bed height, 200–400 mesh resin) were also prepared and operated as described by others (*5*, *23*). The columns were conditioned with 50 mL of pH 5.4 buffer prior to percolation of samples or test solutions.

Breakthrough Curves. A breakthrough curve is a graphical representation of the ratio of effluent and influent concentrations vs. effluent volume. The effect of various experimental parameters on the breakthrough volume is a direct measure of the effectiveness of the column for preconcentration. In this study, the effect on breakthrough volume of the following parameters was determined: particle size; metal-ion concentration; alkali metal and alkaline-earth salts; and humic substances.

Two-Column Procedure. Because of the low breakthrough volumes of metal ions in the presence of humic material, it was necessary to remove the humics by percolation of the preacidified sample through a precolumn of XAD-7 at pH 1.6–1.7. The effluent containing the trace metals was then buffered to pH 8 and passed through the XAD-7 analytical column to preconcentrate the trace metals. Both columns contained about 0.50 g of 80–100 mesh XAD-7 resin (1 × 3 cm bed). Test solutions and samples were percolated through both columns at a flow rate of 1 mL/min. Elution of the retained metal ions was effected with 5.00 mL of 1% HNO_3.

The two-column procedure was tested with synthetic samples (100-mL aliquots) prior to its application to lake water samples. The samples contained NH_4Cl (0.01 M), humic substances at 10 ppm, and up to 20 μg/L each of Cr(III), Fe(III), Ni(II), Mn(II), Cd(II), Co(II), Cu(II), and Pb(II). The solutions were allowed to equilibrate for 48 h before analysis. The Lake Ontario samples were from nearshore (station 41) and offshore (station 302) locations. For these samples, 200-mL aliquots were taken. Direct GFAAS was used when permitted by metal-ion concentrations. The samples were also percolated through Chelex-100 columns (flow rate, 1 mL/min). The retained metal ions were eluted with 25.0 mL of 14% HNO_3. Methods of calibration included both standard calibration curves and standard additions. Standard spikes were added to the acidified samples before passage through the XAD-7 precolumn.

The Seawater Reference Material, NASS-1, was used to test the two-column method for natural waters of high salinity. The procedures for this and other seawater samples was the same as that for the lake water samples except that 10 mL of 0.010 M NH_4NO_3 was used to rinse the column of entrained salts prior to elution. Calibration was by standard calibration curves and standard additions. Standard additions was not applied to NASS-1, owing to restrictions of its availability and cost. Blank controls were as previously specified (*18*).

RESULTS AND DISCUSSION

XAD-7 (SM-7) resin is a cross-linked polymer of methyl methacrylate and its structure and characteristics have been documented (*24*, *25*). Although its use for the retention and

separation of organic solutes is well-known (e.g., ref 22 and 24), its application to the preconcentration of metal ions at trace levels has only recently been described (*18*).

A reasonable mechanism to explain the retention of metal ions on the resin is ion exchange involving free carboxylic acid sites that would arise if methylation of the ester was incomplete. Supporting evidence for this mechanism involves the strong pH dependence of metal-ion retention and elution (*18*) and data derived from potentiometric titration of resin previously washed with either dilute HNO_3 or aqueous ammonia. When 10.0 g of the acid-washed resin (80–100 mesh) in 100 mL of standard HNO_3 (~0.03 M) was titrated with standard NaOH (~0.1 M), the end point was displaced by 3.1 mL from the end point for the titration blank. The consumption of titrant occurred over the pH range 4–7, indicative of a weak acid. Titration of the ammonia-washed resin in 100 mL of HNO_3 gave an end point that was little displaced (<0.05 mL of NaOH) from that of the blank, presumably because the resin was in the ammonium salt form prior to placement in the HNO_3 solution; furthermore, the titration curve displayed a prolonged buffer region in the range pH 4–7, which is readily accounted for by conversion of the ammonium salt to free weak acid after immersion in the HNO_3. From the observed volume displacement, the amount of carboxylic acid impurity was calculated to be about 30 μmol/g of 80–100 mesh (dry) resin. The capacity of this resin for Cu(II) is also about 30 μmol/g. If these numbers are not coincidence, they suggest that the impurity sites are too distant for a 1:2 stoichiometric interaction in the resin and that an anion is required for charge balance of the exchanged divalent cation.

The effectiveness of XAD-7 columns for the direct preconcentration of trace levels of metal ions is dependent on a number of factors, which are discussed below.

pH and Flow Rate. The effect of pH on the retention of metal ions on a column of XAD-7 was demonstrated earlier (*18*). Typically, at a 1.0 mL/min flow rate, maximum retention for divalent ions occurs in the pH range 7–9 and for Fe(III) and Cr(III), in the pH range 4–6. The pH dependence for column operation corresponds well with the pH dependency of distribution ratios determined by the batch equilibrium method (*26*).

At pH 8, retention of Fe(III) and Cr(III) is about 80–85%. This is sufficient to permit passage of a single aliquot of sample (at pH 8) for the simultaneous preconcentration of +2 and +3 ions for samples in short supply (although as explained below, Cr(III) is best handled separately). Column passage at pH values close to 4 should be avoided for Cr(III) and Fe(III) since retention decreases abruptly below this value (*18*) and slight errors in pH adjustment lead to low breakthrough volumes.

Variation of flow rate over the range 0.8–5.6 mL/min has little effect on percent retention, provided that the pH is within the optimal range for the particular metal ion. For all analytical work involving test and sample solutions (vide infra), a flow rate of 1.0 mL/min was used.

Particle Size. The effect of particle size on the column retention of metal ions was determined by measurement of breakthrough volumes for solutions of increasing concentration of Cu(II), selected as a model ion. A significantly higher breakthrough volume is attained for resin of smaller particle size. No breakthrough was observed on either a 20–50 or 80–100 mesh resin column (1 × 6 cm) after percolation of 2.7 L of a solution containing 5 μg/L of Cu(II). Percolation was terminated at this point. For a 10 mg/L solution, breakthrough was observed at about 180 and 450 mL, respectively, although the occurrence of hydrolysis at this high concentration invalidates quantitative utility of the data. For practical purposes, the XAD-7 procedure is intended for the

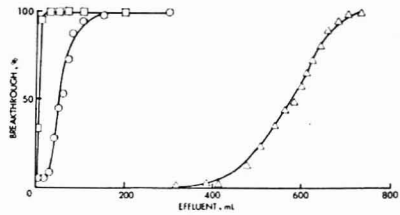


Figure 1. Breakthrough curves for solutions of 10 mg/L each of Cu(II) (△), Na^+ (□), and Ca(II) (○) on a 1 × 6 cm XAD-7 column (80–100 mesh): flow rate, 1 mL/min; pH 7.0.

preconcentration of microgram per liter levels of metals. At these levels, a very large volume of solution would be required to reach breakthrough. In practice, sample availability and time restrictions almost always limit the volume of sample to less than 500 mL, usually 100–200 mL. Therefore, a 1 × 3 cm column (~0.50 g) of 80–100 mesh XAD-7 is adequate for the preconcentration of trace metals since in many natural waters the total concentration of trace metals is about 10 μg/L (~10^{-7} mol/L, assuming an average atomic weight of 100). A 1 × 3 cm column provides a good safety margin in terms of capacity and yields a higher preconcentration factor.

Salts. Batch equilibrium studies showed that as the ionic strength increases, the uptake of Cu(II) drops to a lower level. For example, at 0.75 M NH_4Cl (or NH_4NO_3) plus 0.01 M ammonium acetate, the capacity of 20–50 mesh resin is reduced to 1.7 μmol/g of resin from 5.6 in the absence of chloride or nitrate salts. Therefore, it was necessary to study the effect of ionic strength on the breakthrough volume in anticipation of the preconcentration of trace metal ions from seawater. Solutions of NaCl adjusted to ionic strengths 0.01, 0.02, 0.5, and 0.8 at pH 8 were spiked with 1 μg/L of ^{64}Cu and the breakthrough volume for each solution was determined on a 3-cm column of 80–100 mesh XAD-7, at a flow rate of 1 mL/min. No breakthrough could be detected at any ionic strength after passage of up to 1 L of solution. Furthermore, when natural seawater from which humic materials were removed was spiked to 1 μg/l with ^{64}Cu(II), no breakthrough of Cu(II) and presumably of other trace metals in the seawater could be detected after passage of at least 1 L. Therefore, the salts do not seriously affect the capacity of the 3-cm column for preconcentration of trace metals in seawater.

It is desirable that alkali-metal and alkaline-earth salts not be preconcentrated to a large degree with the trace metals because a high concentration of these salts in the acid effluent would be detrimental to GFAAS measurement of the trace metals. Figure 1 shows that the breakthrough volumes for Na^+ and Ca(II) are very low compared to that of Cu(II). Ten milliliters of 0.01 M NH_3/NH_4NO_3 (pH 8) was found adequate to rinse the NaCl and $CaCl_2$ from the XAD-7 column without removing trace heavy metals after passage of seawater samples. This rinsing procedure was subsequently used after preconcentration of seawater samples and prior to elution of the trace metals with the 1% HNO_3.

Humic Substances. The preponderance of dissolved organic ligand in natural waters is humic substances (humic and fulvic acids). The binding of metal ions with humic material is well-known and its presence has a strong effect on the retention of metal ions on XAD-7 resin, as is illustrated in Figure 2. With increasing concentration of humic material, the percent retention is decreased further than shown. In correspondence with Figure 2, Figure 3 illustrates that the percent breakthrough for metal ions is negligible in the absence of humics but in their presence, it is high for all three test ions, i.e., Fe(III), Cu(II), and Mn(II). There is no question

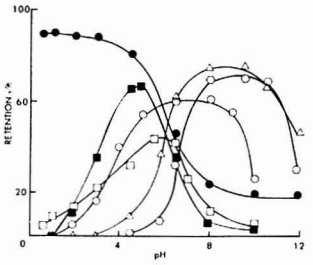


Figure 2. Retention of humic substances (●, 10 mg/L) and of metal ions (■, Fe(III); □, Cr(III); ○, Cu(II); △, Pb(II); and ◇, Cd(II)) in the presence of humic substances as a function of pH: 1 × 6 cm XAD-7 column (20–50 mesh); metal-ion concentration, 20 μg/L; flow rate, 1 mL/min; sample volume, 100 mL.

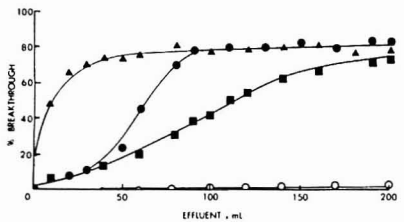


Figure 3. Breakthrough curves for Fe(III) (○), Cu(II) (○), and Mn(II) (◇) in the absence of humic materials and for Fe(III) (▲), Cu(II) (●), and Mn(II) (■) in the presence of 10 mg/L of humic materials: 1 × 6 cm XAD-7 column (20–50 mesh); flow rate, 1 mL/min; metal-ion concentration, 5 μg/L each; pH 6.3 for Fe(III); pH 8.0 for Cu(II) and Mn(II).

that the major effect of the humics on breakthrough volume is at least in part related to thermodynamic factors since in separate batch equilibrium experiments the distribution ratio for Cu(II) was found to be 21 in the presence of humic material vs. 319 in its absence (for 20–50 mesh resin). Similar observations were made for Cd(II), Co(II), and Mn(II). Therefore, the stability of the ion–resin complex is not high enough to cause complete displacement of the metal ions from their humate complexes and the breakthrough volume is thus substantially lowered. It is also clear that the lability of the metal humate complexes relative to residence time in the column (3 min/mL) is too low to cause complete displacement of the metal from the humate complex to the resin. Therefore, for total metal determination, the metal humates must first be dissociated and the humic ligands removed from the solution, otherwise a considerable fraction of metal ions will not be retained by the column. The metal humates are readily dissociated in acid solution (pH <2) and as shown in Figure 2, the liberated humic material is adsorbed on XAD-7 at low pH. Since the metal ions pass through at low pH, the effluent can be raised to pH 8 and passed through a second XAD-7 column to preconcentrate the trace metal ions. The effectiveness of this two-column procedure was tested with synthetic solutions containing humic material (10 mg/L) and several trace elements, each present at 20 μg/L. When humic materials were removed by the precolumn, quantitative recovery was obtained, except for Cr(III). When the precolumn was not used, recovery for all elements was well below 100%.

Elution of Retained Metal Ions. Of various eluting agents tried, 1% HNO_3 was found to be the most satisfactory (*18*); the metal ions are quantitatively eluted and blank values are lower than those obtained when Chelex 100 columns are stripped with 14% HNO_3 (e.g., 0.20 ± 0.07 vs. 1.0 ± 0.2 μg/L for Fe(III); 0.02 ± 0.01 vs. 0.16 ± 0.08 for Cr(III); and 0.004 ± 0.001 vs. 0.02 ± 0.01 for Cd(II)).

The effect of bed height (3, 6, and 15 cm) on elution volume was determined. Since the volume of eluent decreases with decreasing bed height, a shorter column gives a greater preconcentration factor. A 1 × 3 cm bed of 80–100 mesh resin has adequate capacity and allows superior column packing and retained metal ions can be eluted by 5 mL of 1% HNO_3. For a 200-mL sample volume, this represents a preconcentration factor of 40. No attempt was made to reduce the particle size and bed height further since for sizes above 100 mesh, the flow rates are too low to be practical and for elution volumes less than 5 mL, volumetric errors become significant.

Table I. Analysis of Seawater Reference Material, NASS-1 by Two-Column Method[a]

element	two-column result, μg/L	ref value, μg/L
Fe	0.233 ± 0.016	0.192 ± 0.036
Cu	0.108 ± 0.018	0.099 ± 0.010
Ni	0.245 ± 0.044	0.257 ± 0.027
Mn	0.025 ± 0.004	0.022 ± 0.007
Pb	0.043 ± 0.005	0.039 ± 0.006
Co	0.007 ± 0.001	0.004 ± 0.001
Cd	0.025 ± 0.003	0.029 ± 0.004
Cr	0.077 ± 0.008	0.184 ± 0.016

[a] Standard calibration curve used. The precision measure for the two-column method is one standard deviation; for the reference values, 1.96 standard deviations.

Table II. Analysis of Coastal Seawater

	Chelex-100[a]	XAD-7 two-column[a]	
element	SAM, μg/L	SAM, μg/L	calib curve, μg/L
Fe	3.96 ± 0.08	4.20 ± 0.23	3.49 ± 0.16
Cu	1.10 ± 0.10	1.18 ± 0.06	1.14 ± 0.06
Ni	0.43 ± 0.04	0.37 ± 0.04	0.42 ± 0.04
Mn	0.95 ± 0.04	0.78 ± 0.08	0.83 ± 0.08
Pb	0.34 ± 0.08	0.36 ± 0.02	0.35 ± 0.07
Co	<0.2	0.01 ± 0.005	0.011 ± 0.003
Cd	0.038 ± 0.006	0.048 ± 0.007	0.044 ± 0.004
Cr	0.52 ± 0.02	0.45 ± 0.06	0.15 ± 0.02

[a] Preconcentration factor 40 for XAD-7 vs. 8 for Chelex-100 method.

Analysis of Natural Waters. The two-column procedure was used for the preconcentration of trace metals in the Reference Seawater Material, NASS-1, in a nearshore seawater (Sandy Cove, Nova Scotia) and in Lake Ontario water samples. Because the effluent collected from the analytical column is relatively free of organic ligands and inorganic salts and is essentially a solution of the trace metals in 1% HNO_3, a standard calibration rather than standard additions method could be used to obtain the concentrations of trace metals; i.e., only calibration of the instrument rather than calibration of the overall chemical procedure is required. For several samples, however, the standard addition method (SAM) was used as a means of verification.

Results for the analyses of NASS-1 and the nearshore seawater sample are given in Tables I and II, respectively. Aliquots were preconcentrated 40-fold and analyzed in triplicate. Generally, the results for NASS-1 and the coastal seawater are in satisfactory agreement with the reference values (which represent pooled results from several analytical procedures) or the alternate verification procedures.

Results for the analysis of the synthetic freshwater test solution by the two-column calibration curve procedure also agreed well with the nominal values of the trace metals taken and are not presented here. Data for the Lake Ontario sample

Table III. Analysis of Lake Ontario Water, Station 302

element	direct analysis, μg/L	Chelex-100 calib curve, μg/L	XAD-7 two column SAM, μg/L	XAD-7 two column calib curve, μg/L
Cd	<0.1	0.031 ± 0.002	0.047 ± 0.010	0.038 ± 0.004
Mn	0.89 ± 0.08	0.72 ± 0.04	0.80 ± 0.02	0.125 ± 0.011
Cr	1.13 ± 0.19	0.31 ± 0.07	1.00 ± 0.12	0.50 ± 0.12
Cu	1.81 ± 0.19	2.17 ± 0.41	1.41 ± 0.22	1.95 ± 0.07
Ni	<3	1.38 ± 0.11	1.71 ± 0.06	1.47 ± 0.26
Fe	5.14 ± 0.31	5.53 ± 0.72	5.60 ± 0.48	4.94 ± 0.55
Co	<1	<0.1	0.085 ± 0.018	0.093 ± 0.017
Pb	<1	0.41 ± 0.04	0.78 ± 0.09	0.64 ± 0.18

from station 302 are presented in Table III. The concentrations of some elements are high enough for measurement by GFAAS without preconcentration; these results are included for comparison. The standard calibration method was used for all three techniques; in addition, the SAM method was applied to the XAD-7 two-column procedure. The results represent triplicate determinations. Good agreement exists among the three techniques for all the elements, except for Cr and Mn. The Lake Ontario sample from station 41 was analyzed in identical fashion and the level of agreement among the three methods was essentially the same as that obtained for the station 302 sample.

With regard to Cr(III), the XAD-7 standard calibration procedure consistently gives low results, whether the sample is seawater or freshwater. It is noteworthy that low results for Cr(III) are also returned by the Chelex-100 standard calibration method. The low results are because of the kinetically controlled low breakthrough volume for Cr(III) which leads to partial loss of the ion before the total sample is passed through the second column. Therefore, for Cr(III) the method of standard additions, which compensates for this loss, must be used.

The results for Mn(II) in lake water are particularly interesting. Whereas the two-column calibration curve procedure yields quantitative return of Mn(II) in the seawater samples, it yields low results for the two Lake Ontario samples (see example in Table III). By comparison, when the two-column method is combined with SAM calibration, the result is in reasonable agreement with both the direct and Chelex-100 (calibration curve) procedures. This observation is a strong indication that in the Lake Ontario samples, Mn exists in two or more forms all of which are retained on Chelex-100 but not all on XAD-7. In fact, Mn in a spiked Lake Ontario water broke through the XAD-7 analytical column at a very low volume. No breakthrough was observed on Chelex-100 during passage of the 200-mL aliquot. For the XAD-7 SAM procedure, the satisfactory result shows that the Mn(II) spike must equilibrate rapidly with the other form(s) in the sample. Since the samples were taken from oxic regions of Lake Ontario, Mn in higher oxidation states is suspected but efforts to identify species such as Mn_2O_3 or MnO_2 (27) have not been successful to date. Although identification of the species is lacking, it appears that comparison of the two-column calibration curve procedure to either the two-column SAM procedure or the Chelex procedure can be a useful way to obtain an indication of Mn speciation and perhaps other elements. (Cr is an obvious element to consider but the situation would be complicated by the early breakthrough of Cr(III).)

XAD-7 (SM-7) is a useful resin for the preconcentration of several trace metals in natural waters. The two-column XAD-7 procedure is simple and reliable and can be combined with the standard calibration curve procedure for subsequent GFAAS measurement. The use of the calibration curve procedure reduces considerably both the amount of sample and time required for analysis. The standard additions method is required for Cr and, in nonmarine samples, Mn. For these elements, no advantages of economy exist. Furthermore, since humic materials are largely removed by the precolumn, the concern with regard to complete equilibration of standard addition spikes or, alternatively, of quantitative separation of the trace element by a resin material (17), is greatly decreased. The precision, expressed as a relative standard deviation, averages 10% over all elements, concentrations, and samples.

ACKNOWLEDGMENT

We are indebted to the Canada Centre for Inland Waters and the Atlantic Regional Laboratory, National Research Council of Canada, for the generous supply of water samples and to D. Burgess for helpful advice and assistance in the radioisotope work. We are also grateful to the reviewers for several constructive suggestions.

Registry No. XAD-7, 37380-43-1; Fe, 7439-89-6; Cu, 7440-50-8; Ni, 7440-02-0; Mn, 7439-96-5; Pb, 7439-92-1; Co, 7440-48-4; Cd, 7440-43-9; Cr, 7440-47-3; water, 7732-18-5.

LITERATURE CITED

(1) Guevremont, R. *Anal. Chem.* **1980**, *52*, 1574.
(2) Leyden, D. E.; Wegscheider, W. *Anal. Chem.* **1981**, *53*, 1059A.
(3) Bachmann, K. *CRC Crit. Rev. Anal. Chem.* **1981**, *12*, 1.
(4) van Grieken, R. *Anal. Chim. Acta* **1982**, *143*, 3.
(5) Sturgeon, R. E.; Berman, S. S.; Desaulniers, A.; Russell, D. S. *Talanta* **1980**, *27*, 85.
(6) Pakalno, P.; Batley, G. E.; Cameron, A. J. *Anal. Chim. Acta* **1978**, *99*, 333.
(7) Sturgeon, R. E.; Berman, S. S.; Willie, S. N.; Desaulnier, A. *Anal. Chem.* **1981**, *53*, 2337.
(8) Sturgeon, R. E.; Berman, S. S.; Willie, S. N. *Talanta* **1982**, *29*, 167.
(9) Phillips, R. J.; Fritz, T. S. *Anal. Chem.* **1978**, *50*, 1504.
(10) Sugawara, K. F.; Westall, H. H.; Schucker, G. D. *Anal. Chem.* **1974**, *46*, 489.
(11) Riley, J. P.; Skirrow, G. "Chemical Oceanography", 2nd ed.; Academic Press: New York, 1975; Vol. 1–3.
(12) Batley, G. E.; Florence, T. M. *Mar. Chem.* **1976**, *4*, 347.
(13) Ruzic, I. *Anal. Chim. Acta* **1982**, *140*, 99.
(14) Schnitzer, M.; Khan, S. U. "Humic Substances in the Environment"; Marcel Dekker: New York, 1972.
(15) Stumm, W.; Morgan, J. "Aquatic Chemistry"; Wiley Interscience: New York, 1970.
(16) Stumm, W.; Bilinski, H. "Advances on Water Pollution Research"; Jenkins, S. H.; Ed.; Pergamon Press: New York, 1972.
(17) Corsini, A.; Wan, C. C.; Chiang, S. *Talanta* **1982**, *29*, 857.
(18) Corsini, A.; Chiang, S.; DiFruscia, R. *Anal. Chem.* **1982**, *54*, 1433.
(19) MacCarthy, P.; Peterson, M. J.; Malcoln, R. L.; Thurman, E. M. *Anal. Chem.* **1979**, *51*, 2041.
(20) Curtis, M. A.; Witt, A. F.; Schram, S. B.; Rogers, L. B. *Anal. Chem.* **1981**, *53*, 1195.
(21) Pietrzyk, D. J.; Kroeff, E. P.; Rotsch, T. D. *Anal. Chem.* **1978**, *50*, 497.
(22) Aiken, G. R.; Thurman, E. M.; Malcom, R. L.; Walton, H. F. *Anal. Chem.* **1979**, *51*, 1799.
(23) Kingston, H. M.; Barnes, I. L.; Brady, T. J.; Rain, T. C. *Anal. Chem.* **1978**, *50*, 2064.
(24) Pietrzyk, D. J.; Chu, C. C. *Anal. Chem.* **1977**, *49*, 757.
(25) "Technical Bulletin on Amberlite XAD Resins"; Rohm and Haas Co.: Philadelphia, PA, 1972.
(26) Chiang, S. Ph.D. Thesis, McMaster University, Hamilton, Ontario, Canada, 1983.
(27) Burns, N. M.; Nriagu, J. O. *J. Fish Res. Board Can.* **1976**, *33*, 463.

RECEIVED for review August 29, 1984. Accepted November 13, 1984. This research was supported by the National Research Council of Canada and by the Natural Science and Engineering Research Council of Canada.

Preconcentration of Cadmium from Highly Acidic Saline Solutions and Direct Determination of Bismuth, Cadmium, Mercury, Antimony, Tin, and Thallium in Highly Acidic Aqueous Solutions with Electrically Vaporized Thin Gold Film Atomic Emission Spectrometry

Stephen W. Brewer

Chemistry Department, Eastern Michigan University, Ypsilanti, Michigan 48197

Richard D. Sacks*

Department of Chemistry, University of Michigan, Ann Arbor, Michigan 48109

Corrosion-resistant Au thin films are routinely produced for analysis of highly acidic solutions by electrically vaporized thin film atomic emission spectrometry. Direct determination of Bi, Cd, Hg, Sb, Sn, and Tl from 2 M HCl is possible, with detection limits ranging from 0.085 to 6.5 mg/L, useful concentration ranges of about 2 decades, and relative errors of +5.7% to −26%. Simple batch separation/preconcentration of Cd(II) with a microbead strong base anion exchange resin allows determination of Cd in complex acidic solutions near the 10 ng/mL (10 ppb) concentration level with relative errors of around 8%. The method is not expensive; materials cost for a single cadmium determination is about $12, including preparation of the analytical curve. Materials cost for preparation of the analytical curve plus five cadmium determinations is about $20.00.

The determination of traces of toxic heavy metals in very acidic or saline aqueous solutions has long been of interest (*1-3*). Seawater, other brines, acid mine waters, and plating bath liquors are among these solution types. Seawater, ~0.5 M in NaCl, contains trace levels of a number of toxic heavy metals (*1*). The presence of high concentrations of group 1 and 2 salts can make determination of trace heavy metals difficult. Concomitant effects among trace metals have been reported in determinations by atomic absorption spectrometry with electrothermal atomization, a widely used method (*4, 5*).

Recent work (*6-12*) on electrically vaporized thin metal films as alternative vaporization and excitation sources for atomic emission spectrometry has shown their utility in analyses of refractory powder samples and ground solids such as coal, flour, dried spinach, and river sediments. In these investigations, using ~350 μg Ag thin films, Goldberg and Sacks (*12*) found that aqueous solutions could be used as standards. They noted, however, that aqueous standards containing more than 500 ng of the element of interest were difficult to vaporize completely, because thick salt crusts formed when the solution droplets dried. Samples of more than 100 μg of particles suspended in 2-propanol were also not easy to vaporize. Goldberg and Sacks (*12*) also found that slightly acidic (~0.1 M HCl) aqueous solutions eroded Ag films badly.

A number of the problems in determinations of trace heavy metals in acidic aqueous solutions of high salt content have been addressed in the present investigation. First, acid-resistant Au films have been developed. Second, optimum analysis wavelengths and radiation integration time intervals (*12*) have been selected for determination of Bi, Cd, Hg, Sb, Sn, and Tl. Third, direct sequential determinations of four metals, Bi, Cd, Hg, and Tl, dissolved together at widely varying (0.35–35 mg/L) concentrations in 2 M HCl have been performed, showing no significant interelement effects, and showing promise for future simultaneous determinations of these elements.

Table I. Conditions for Short and Long Discharges

support gas	long (*12*) 60% Ar/40% O_2	short (*9*) 60% Ar/40% O_2
pressure	atmospheric	atmospheric
capacitance, μF	30	22.5
charging voltage, kV	8.0	4.0
inductance, μH	1200	residual
ringing frequency, kHz	0.830	15.5
energy, J	960	180
peak current, kA	1.0	7.9

EXPERIMENTAL SECTION

Discharge Circuit. The discharge circuit, chamber, film holding cassette, and gas flow conditions used to vaporize thin films have been described in detail (*9, 10, 12*). Two types of discharge, called "short" and "long" were investigated for their analytical utility. Table I shows conditions and characteristics of each discharge type.

Thin Film Production. Thin Ag films on polypropylene substrates were prepared with the apparatus described by Clark and Sacks (*9*). Thin Au films were prepared with the same vacuum system and substrate holder. A tungsten boat, coated with Al_2O_3, was used for melting and evaporating gold. A special brass die was constructed to put sample-holding dimples into plastic substrate strips before they were coated with Au.

Optical and Electrical Monitoring. Goldberg and Sacks (*12*) have described optical and electrical monitoring techniques and apparatus. In earlier work with Ag films, photographic detection was used. In later work with Au films, photoelectric detection, with 80 μm entrance and exit slits, was used. As in Goldberg and Sacks' work (*12*) the discharge chamber was placed 68 cm from the entrance slit, without ancillary optics.

Experimental Procedure. Thin films of Ag were prepared according to Clark and Sacks' procedure (*9*). Thin films of Au were prepared on the same plastic substrate material. Chunks of Au weighing from 1 to 2 g were cut from a solid bar, then hammered flat and thin enough to cut with scissors. The thin foil was cleaned in concentrated HCl, washed with distilled water, and dried in air. Then 0.2500 ± 0.0007 g batches were weighed, mass control being important (*7*). For each evaporation, 0.25 g was placed in the alumina-coated tungsten crucible. The substrate material was cleaned in an ultrasonic bath with 75% 2-propanol/25% H_2O (v/v), and cut into 7.3 × 1.6 cm strips. Two cylindrical dimples, each centered 2.44 cm from an end of the strip, each 0.85 cm in diameter and 0.16 cm deep, were pounded into

0003-2700/85/0357-0724$01.50/0 © 1985 American Chemical Society

Table II. Characteristics of Thin Films Deposited on Polypropylene Substrates

	Ag (*12*)	Au
substrate dimensions, cm	7.3 × 1.6 × 0.05	7.3 × 1.6 × 0.5
film dimensions, cm	7.3 × 1.6	7.3 × 1.6
vaporized surface area, cm^2	7.9	7.9
film thickness, Å	400	230
cylindrical dimple dimensions, cm	none	2 dimples, each 0.85 diameter by 0.16 deep, centered 2.44 cm from ends
film mass vaporized, μg	350	350
resistance, Ω	5.0–10.0	16.0–40.0

each strip with a brass die and rubber mallet. The strips were cleaned again and attached to the substrate holder with transparent tape, with dimples concave downward toward the crucible. Strips of Al foil were placed on top of the plastic strips and secured to the metal holder to conduct heat away from the plastic and prevent its melting. The evaporation chamber was evacuated to a nominal 2×10^{-5} torr. The crucible was heated to white heat in ~5 s with a 250-A current and held at white heat until all the Au was observed to evaporate, a process that took ~10 s. The evaporation chamber was brought up to atmospheric pressure, and the plastic strips, coated with thin Au films, were removed. Films with resistances between 15 and 40 Ω gave good results. Film and substrate properties are summarized in Table II.

Standard solutions for direct determinations were prepared by dissolving reagent-grade metal salts in demineralized water–HCl solutions, usually 2 M HCl. Drops of 5 to 200 μL were placed in dimples of Au films and dried with a heat lamp. Because of the volatility of $SbCl_3$, Sb(III) solutions were air-dried.

A strong base anion exchange resin was used for isolation and preconcentration of cadmium. Two methods were tried for isolation and preconcentration. In the first method, 20-mg batches of resin were placed in plastic vials and equilibrated with 20-mL samples of solutions of Cd(II) in 2 M HCl or 1.5 M HCl–0.5 M NaCl for 1 h with stirring. Then 10-mL aliquots of the suspension were placed in conical centrifuge tubes and spun for ~10 min at ~2100 rpm. The supernate was drawn off, and the resin beads were resuspended in demineralized water. Aliquots of 50 μL were placed on Ag films in 10 roughly equal drops and dried under a heat lamp. The resin beads, of 9 ± 2 μm diameter, were left on the film surface.

In the second method, 50-mg batches of the anion exchanger were equilibrated with 50-mL samples of Cd(II) and other metals in 2 M HCl, in 2 M HCl–0.5 M NaCl, or 2 M HCl–0.43 M HNO_3 for 1 h with stirring. Twenty milliliters of the suspension was filtered through a polycarbonate filter of 47 mm diameter and 1 μm pore size. The center of the filter, containing the resin, was cut out and put into a conical centrifuge tube. One milliliter of demineralized water was added to the tube to remove the metal from the resin. The tube was placed in a sonic bath for 5 min to break the resin away from the filter. To ensure equilibration, the tube was stirred on a vortex mixer for 1 min. The tube was centrifuged at ~2100 rpm for ~10 min, and one 50-μL drop of supernate was placed in each dimple of an Au film. Five films were prepared from each solution. Solutions from HCl–HNO_3 mixtures were air-dried to minimize erosion of the Au film; solutions from HCl or HCl–NaCl mixtures were dried with a heat lamp.

Five films were vaporized for the blank and for each different metal concentration. Intensities were recorded photoelectrically with a 1P28 photomultiplier tube and the gated integrator described in ref 12. The integration interval extended over the entire discharge.

Materials and Reagents. Silver films were made from high-purity (99.999%) 100-mesh Ag needles. No purity figures were available for the surplus Au used to make films, but photographic spectra showed Ag, with a few weak lines, to be the major impurity. Some weak Cu lines were visible and may have come from Cu connections in the holder or from the Au. Aminex A-28 strong base anion exchanger, in acetate form, with a bead diameter of 9 ± 2 μm, was bought from Bio-Rad Laboratories, Richmond, CA. National Bureau of Standards SRM 1643a, Trace Elements in Water, was the standard used. Polycarbonate membrane filters were supplied by Nuclepore Corp., Pleasanton, CA. Tungsten evaporation boats, catalog number S35B-A0-W, were bought from R. D. Mathis Co., Long Beach, CA.

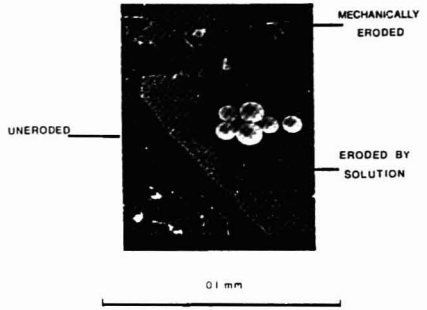


Figure 1. Secondary electron image (SEI) taken with scanning electron microscope (SEM) of area on Ag thin film eroded by ~pH 1 suspension of resin beads. Egg-shaped objects are resin beads.

RESULTS AND DISCUSSION

Acid Resistant Films. A disadvantage of using either Ag or Al films is that they are easily eroded by even slightly acidic solutions. In Figure 1, a secondary electron image (SEI) obtained with a scanning electron microscope (SEM) shows a portion of an Ag film eroded by an aqueous solution of ~pH 1. The egg-shaped objects within the eroded area are resin beads. Erosion of the film increases its electrical resistance, makes the discharge harder to initiate, and may cause poorer sampling of the surface by the plasma. Au films are not eroded by 2 M HCl alone, nor by 0.5 M HNO_3 alone. If droplets containing both nitrates and chlorides in acidic solution are put on the films, however, they must be air-dried rather than lamp-dried, as hot acidic solutions of nitrates and chlorides will dissolve thin layers of Au. Despite the high cost of Au, thin films of it are inexpensive to make. Presently, each Au film costs 5¢ or less for raw materials. Corrosion resistance and low cost are desirable features of Au films.

Optimum Analysis Wavelengths and Time Gates. Until the present work, no systematic study had been made of optimum analysis wavelengths in electrically vaporized thin film spectrometry. For each of six elements, Bi, Cd, Hg, Sb, Sn, and Tl, at least four spectral lines were examined for sensitivity and linearity. For each element at least one neutral atom resonance line was studied, and one neutral atom nonresonance line. Ion lines, resonance and nonresonance, were studied whenever possible because earlier work had shown the plasmas generated to be highly ionized (*10*, *11*). Each spectral line was studied under two discharge conditions, short and long (see Table I), with radiation from each discharge being integrated over the duration of the discharge. Concentrations of each metal ranged from 2 to 800 mg/L in 10-μL samples, corresponding to metal masses ranging from 0.02 to 8 μg. Fifty four analytical curves were generated.

Six wavelengths, shown in Table III, were selected for analysis. Long discharges were found to give the lowest detection limits and best linearity, with the exception of thallium, for which a short discharge gave as good results as a long

Table III. Optimum Analysis Lines for Long Discharges

element	no of lines studied	wavelength of best line, nm	line type[a]	detection limit[b] in 10 μL sample, ng	detection limit[b] in 10 μL sample, mg/L	log–log slope	useful concn range,[c] mg/L
Bi	4	306.772	atom, res	11	1.1	0.89	1.1–40.0
Cd	4	226.502	ion, res	0.85	0.085	1.05	0.085–8.0
Hg	4	253.652	atom, res	7.5	0.75	0.70	0.75–100
Sb	4	217.589	atom, res	32.	3.2	0.73	3.2–800
Sn	7	283.999	atom, nonres	20.0	2.0	0.77	2.0–400
Tl	4	377.572	atom, res	65	6.5	0.79	6.5–800

[a] Key: atom, neutral atom; ion, singly charged positive ion; res, resonance line; nonres, nonresonance line. [b] Concentration that will produce a net signal intensity >3 times the standard deviation of blank intensity. [c] Concentration range over which a log–log plot is without curvature; above top concentration value slope changes sharply to lower value.

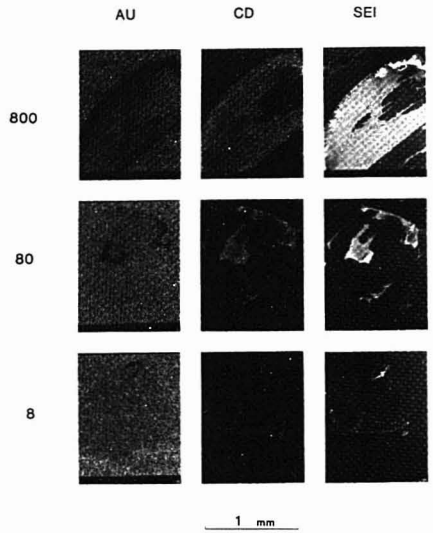


Figure 2. Au Mα, Cd Lα, and SEI photographs taken with SEM of 5-μL droplets of 800, 80, and 8 mg/L Cd(II) in 2 M HCl deposited on Au thin films and lamp-dried.

discharge. For Bi, Tl, Hg, and Sb, neutral atom resonance lines gave the best results. A neutral atom nonresonance line was best for Sn, and an ion resonance line for Cd. In most cases, log–log plots of relative intensity showed downward curvature above metal concentrations of 40 mg/L, corresponding to total metal masses of 0.40 μg in 10-μL samples. Detection limits ranged from a low of 0.85 ng of Cd to 65 ng of Tl. log–log slopes ranged from a sublinear 0.70 for Hg, to nearly linear values of 0.89 and 1.05 for Bi and Cd, respectively. Relative standard deviations of net relative intensities ranged from about 10% to about 50% near the detection limit. It is probable that detection limits could be improved by simultaneous recording of background and signal radiation with a multichannel device. Time-gating of discharge radiation integrations improved neither linearity nor detection limits.

Goldberg and Sacks (*12*) had concluded that sampling of aqueous solution residues by the discharge is incomplete above sample sizes of about 0.50 μg. They noted that no enhancement of detection limits is possible with time-gating of radiation when residues this large are present. They ascribed the difficulty of sampling these residues to the formation of thick salt ridges formed on drying aqueous solutions. Duchane

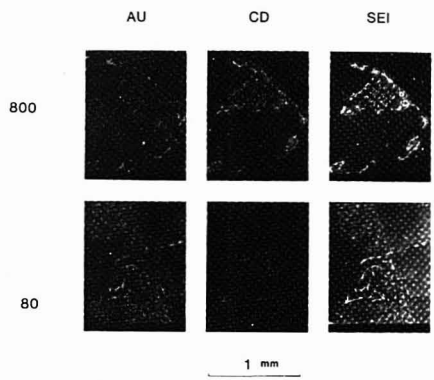


Figure 3. Au Mα, Cd Lα, and SEI photographs taken with SEM of residues left, after long discharges, from 5-μL droplets of 800 and 80 mg/L Cd(II) in 2 M HCl deposited on Au thin films and lamp-dried.

and Sacks (*7, 8*) had also observed these ridges. Figures 2 and 3 support these observations.

Figure 2 shows photomicrographs of deposits of $CdCl_2$ from 5-μL droplets dried on Au film surfaces. The photographs were taken with an SEM having an energy dispersive X-ray spectrometer. In Figure 2, columns are labeled Au for Au Mα X-ray maps, Cd for Cd Lα X-ray maps, and SEI for secondary electron images. Rows are labeled 800 for residues from 800 mg/L Cd solution (as $CdCl_2$ in 2 M HCl), 80 for residues from 80 mg/L Cd solution, and 8 for residues from 8 mg/L Cd solution. In the first row, labeled 800, a thick ridge of $CdCl_2$ is visible in the SEI. The $CdCl_2$ deposit is also visible in the Cd Lα X-ray map. In the Au Mα X-ray map, Au Mα intensity is diminished in regions where the $CdCl_2$ crust is thickest, owing to absorption of Au Mα radiation by cadmium and chlorine. Similar effects are seen in the second row of images, labeled 80, but they are less pronounced than those in the first row, because the salt mass is 10-fold lower. In the third row, labeled 8, the ridge effect almost disappears.

The photographs in Figure 3 show solution residues left on Au surfaces after sampling by long discharges. Row and column symbols are almost the same as those in Figure 2. Only the 8 mg/L row has been left out, because no traces of 8 mg/L droplet residues could be seen with the SEM after sampling by the discharge. The presence of $CdCl_2$ residues and Au film after discharge suggests incomplete vaporization of analyte material and may account for the downward curvature seen in most working curves beyond 0.40 μg of metal.

Direct Determination of Bi, Cd, Hg, and Tl. Direct determination of Bi, Cd, Hg, and Tl mixed together in 2 M

Table IV. Direct Determination of Bi, Cd, Hg, and Tl from 2 M HCl Solutions[a]

element	concn taken,[b] mg/L	concn found,[c] mg/L	% rel error
Bi	3.5	3.9 ± 0.9	+11
Cd	0.35	0.26 ± 0.04	−26
Hg	3.5	3.7 ± 0.8	+5.7
Tl	35.0	28.2 ± 7.6	−19.4

[a] Solutions studied each contained all four elements. [b] Sample size was 100 μL. [c] Plus or minus values are estimates of standard deviation based on five determinations.

Table V. Direct Determination of Cd from NBS SRM 1643a

Major Constituents (Noncertified)

element	concn, μg/g	mass on film,[a] μg
Ca	27	11.0
Na	8	3
K	2	0.8

Recovery of Cd[a]

	Cd concn, ng/g	Cd mass, ng
taken[b]	10 ± 1	4.1 ± 0.4
found[c]	5.9 ± 3.7	2.4 ± 1.5
rel error, %	−41%	−41%

[a] 400-μL sample. [b] Plus or minus values reported by NBS. [c] Plus or minus values are estimates of standard deviation based on five determinations.

HCl showed no apparent interelement effects. Relative errors in recovery of these elements were the same as would be expected if the elements were determined unmixed by the method used. Solutions for analytical curves were made up to contain 8 to 40 mg/L Tl(III), 0.8 to 4.0 mg/L Bi(III) and Hg(II), and 0.08 to 0.4 mg/L Cd(II). A solution 35 mg/L in Tl(III), 3.5 mg/L in Bi(III) and Hg(II), and 0.35 mg/L in Cd(II) was used for recovery study. Results are summarized in Table IV. Relative errors in recovery ranged from +5.7% for Hg to −26% for Cd(II). These errors were about the same as could be expected if the Tl, Hg, Bi, and Cd were not mixed, but isolated in 2 M HCl. It should also be noted that Cd was determined in a solution with a 100-fold excess of Tl and 10-fold excesses of Bi and Hg. Relative errors could possibly be reduced if line and background intensities were measured simultaneously.

Direct determination of Cd in a still more complex matrix, with great excesses of group 1 and 2 salts, near the detection limit for Cd, is just possible. NBS SRM 1643a, Trace Elements in Water, was chosen as the more complex matrix. Table V shows masses of major group 1 and 2 constituents in SRM 1643a present on the film surface prior to discharge. The concentration of Cd found showed −41% relative error from the certified value. The relatively large masses of Ca and Na salts on the film may have impaired the accuracy of the determination through formation of crusts. Two other difficulties may be considered. First, droplets of 200 μL are not as easily applied and dried as 50-μL droplets. Second, the concentration of Cd in NBS 1643a was very near the detection limit for this set of experimental conditions. Separation and preconcentration of Cd have overcome these problems.

Separation/Preconcentration of Cd from Brine and Complex Mixtures. More accurate results were seen when Cd in brine and complex mixtures was determined after a separation/preconcentration step. Aminex A-28 was chosen for batch separation of Cd(II) from highly acidic, high chloride



Figure 4. SEI taken with SEM of resin suspension deposited on Ag thin film after attempt to separate suspension from 0.5 M NaCl solution. Cubic crystals are NaCl. Spheres are resin beads. Erosion of Ag thin film is visible.

content, aqueous solutions for two reasons. First, similar resins have high distribution coefficients for Cd(II) and other heavy metals in 2 M HCl, so that small batches of resin could remove significant amounts of anionic chloro complexes of Cd(II) from solution, leaving group 1 and 2 metals behind. Second, the beads' size offered the possibility of easy direct vaporization in a discharge. Early experiments with Ag films, involving direct application of suspended beads to the films, and photographic detection yielded mixed results. Preconcentration of Cd with single batch extractions from 2 M HCl and from 1.5 M HCl–0.5 M NaCl was efficient, giving D_G values of 1400 and 1560, respectively. D_G values, where

$$D_G = \frac{\mu g \text{ of Cd}}{g \text{ of resin}} \Big/ \frac{\mu g \text{ of Cd}}{mL \text{ of soln}} \quad (1)$$

were measured for batch extractions with atomic absorption. When separation of Cd from NaCl solutions was tried, some NaCl was carried with the resin beads onto the film surfaces, as the SEI in Figure 4 shows. The spheres in Figure 4 are resin beads, and the cubic crystals are NaCl. Although their small diameters suggested easy vaporization (*12*), resin beads were not completely vaporized in long or short discharges. Figure 5 shows SEI's of beads left on Ag films after short and long discharges. Beads left after short discharges appear to be undisturbed, and those left after long discharges appear to be charred. NaCl crystals were not much vaporized by either type of discharge.

Separation of Cd(II) from saline solutions was improved when the resin beads, after equilibration with solution, were filtered and equilibrated with distilled water. A significant fraction of the Cd(II) was released from the resin so that the water, with relatively few beads and little NaCl, could be applied to films and dried. Table VI shows the analytical results of separation and preconcentration of Cd(II) by the latter procedure, from solutions of 0.5 M NaCl–2 M HCl, 2M HCl, and 0.43 M HNO_3–2 M HCl (SRM 1643a with added

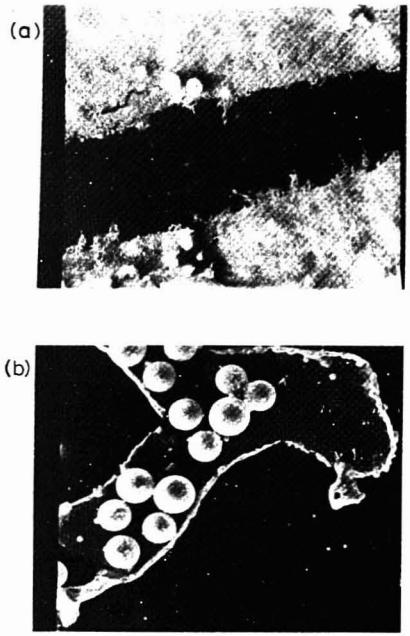


Figure 5. SEI's taken with SEM of resin suspensions deposited on Ag thin films and subjected to (a) long and (b) short discharges. Note charred appearance of beads after long discharge, and undisturbed appearance of beads after short discharge.

Table VI. Determination of Cd after Separation/Preconcentration

solution	concn taken, ng/mL (ppb)	concn found,[c] ng/mL (ppb)	% rel error
0.5 M NaCl–2 M HCl[a]	11.5	15.8 ± 4.6	+37.4
2 M HCl[a]	11.5	12.4 ± 1.3	+7.8
NBS 1643a (0.43 M HNO_3–2 M HCl)	8.4 ± 0.8[b]	7.8 ± 2.3	−7.7

[a] Solution also contains 115 ng/mL Bi and Hg and 1150 ng/mL Tl. [b] Corrected for density and dilution with HCl. Plus or minus values reported by NBS. [c] Plus or minus values are estimates of standard deviation based on five determinations.

HCl). With the preconcentration step, 50-μL drops could be used, and very little excess salt was loaded onto the film. An attempt was made to determine Cd directly from 0.5 M NaCl–2 M HCl without preconcentration, but large crystal residues of NaCl (~1.5 mg of NaCl per 50-μL drop) prevented efficient vaporization of the analyte. In Figure 6, SEI photomicrographs of residues taken directly from 0.5 M NaCl–2.0 M HCl solutions and of residues left after preconcentration from these solutions are shown to emphasize this point. Large crystals of NaCl are visible before (a) and after (b) vaporization of the film when no preconcentration was done. When preconcentration was done, separation was not quite complete,

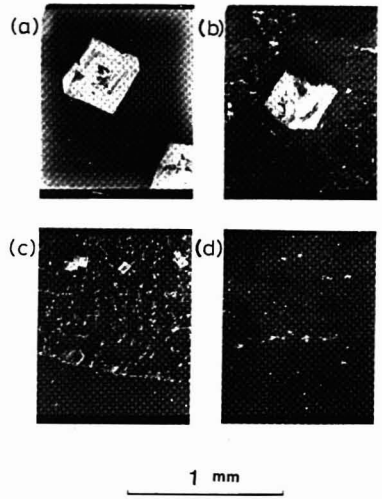


Figure 6. SEI's taken with SEM of Au thin films with no separation/preconcentration (a) before discharge and (b) after long discharge and with separation/preconcentration (c) before discharge and (d) after long discharge.

as Figure 6c shows that some resin beads and some NaCl were transferred to the film surface. Little evidence of residues of such beads and crystals after preconcentration and discharge is visible in Figure 6d. The small number of crystals and beads were not difficult to vaporize but may have impaired the accuracy of Cd determination from 0.5 M NaCl–2 M HCl, relative error being about +37.4%. More accurate results, as Table VI shows, were obtained from application of preconcentration to 2 M HCl and to SRM 1643a, with relative errors in Cd determination of +7.8% and −7.7%, respectively.

Goldberg and Sacks (*12*) pointed out some advantages enjoyed by the application of electrically vaporized thin film spectrometry to analysis of solid powders. The method appears to be applicable to determination of heavy metals in complex aqueous solutions as well. It should be stressed that the method is inexpensive even when Au films are used. A single determination of Cd in solution reported here, including preparation of the analytical curve, for example, costs about $12.00 for film materials, support gas, and resin. The Au films cost only about $2.00 of that total. Materials cost for preparation of the analytical curve plus five cadmium determinations is about $20.00. Simultaneous multielement determinations at minimum materials cost are a definite prospect and may offer improved measurement statistics.

ACKNOWLEDGMENT

Photomicrographs were taken by L. Marcotty, W. Wagner, and B. Winter of the Electron Microbeam Analysis Laboratory at the University of Michigan, Ann Arbor, MI.

Registry No. Bi, 7440-69-9; Hg, 7439-97-6; Sb, 7440-36-0; Sn, 7440-31-5; Tl, 7440-28-0; Cd, 7440-43-9; Au, 7440-57-5.

LITERATURE CITED

(1) Brooks, R. R. *Analyst (London)* **1960**, *85*, 745–748.
(2) Leyden, D. E.; Patterson, T. A.; Alberts, J. J. *Anal. Chem.* **1975**, *47*, 733–735.
(3) Buchanan, A. S.; Hannaker, P. *Anal. Chem.* **1984**, *56*, 1379–1382.
(4) Syty, A *CRC Crit. Rev. Anal. Chem.* **1974**, *4*, 155–228.

(5) Cruz, R.; VanLoon, J. C. *Anal. Chim. Acta* **1974**, *72*, 231-243.
(6) Duchane, D. V.; Sacks, R. D. *Anal. Chem.* **1978**, *50*, 1752-1757.
(7) Sacks, R. D.; Duchane, D. V. *Anal. Chem.* **1978**, *50*, 1757-1765.
(8) Duchane, D. V.; Sacks, R. D. *Anal. Chem.* **1978**, *50*, 1765-1769.
(9) Clark, E. M.; Sacks, R. D. *Spectrochim. Acta, Part B* **1980**, *35B*, 471-488.
(10) Suh, S. Y.; Collins, R. J.; Sacks, R. D. *Appl. Spectrosc.* **1981**, *35*, 42-52.
(11) Suh, S. Y.; Sacks, R. D. *Spectrochim. Acta, Part B* **1981**, *36B*, 1081-1096.
(12) Goldberg, J.; Sacks, R. *Anal. Chem.* **1982**, *54*, 2179-2186.

RECEIVED for review October 2, 1984. Accepted November 26, 1984. This work was supported by the National Science Foundation through Grant No. CHE 78-25542 and by the Graduate School of Eastern Michigan University through the Research and Sabbatical Leaves Program.

Performance Studies under Flow Conditions of Silica-Immobilized 8-Quinolinol and Its Application as a Preconcentration Tool in Flow Injection/Atomic Absorption Determinations

Monte A. Marshall[1] and Horacio A. Mottola*

Department of Chemistry, Oklahoma State University, Stillwater, Oklahoma 74078

The use of silica-immobilized 8-quinolinol prepared by an improved synthetic route has been evaluated as a preconcentration material for trace metal ions in flow systems. Breakthrough capacities were evaluated under different flow, temperature, and geometric characteristics of the preconcentrating column. Mass transfer limitations under flow conditions explain the dependence of breakthrough capacities on these variables. The capabilities of this material for on-line preconcentration of copper(II) using flow injection analysis (FIA) for sample processing and atomic absorption spectrometry (AAS) for detection have also been evaluated. The relatively high capacities of these simply and reproducibly prepared materials as well as the absence of swelling complications afforded by the inorganic silica framework allow for their effective use in FIA/AAS by implementation of rather simple manifolds. Results obtained for the determination of ng/mL levels of copper(II) in some EPA water samples agreed very well with reported values.

Bonded silicas, widely used in liquid chromatographic separations, have recently shown recognized potential for sample preconcentration or matrix isolation. The so-called "extraction columns", employing bonded silicas, have become popular for sample preparation prior to chromatographic separations, virtually replacing the more laborious liquid-liquid extraction procedures. In fact, bonded-phase sample preparation has been identified as a growing technological trend (*1*) and has received prevalent attention for the selective preconcentration of trace metal ions (*2-7*). The immobilization of reagents on silica supports offers some distinct advantages over immobilization on organic polymer supports. First, the silica is readily modified by a variety of silylating agents allowing for a myriad of functional groups to be immobilized. Second, since the bound group is at the surface of the support, high exchange rates are generally observed (*2, 4*) whereas some highly cross-linked organic polymer matrices may require hours for equilibration (*8*). Third, silica offers excellent swelling resistance with changes in solvent composition having little effect on the support at pH <9 (*9*). Therefore, silica surfaces are excellent choices for the immobilization of analytical reagents.

Silica-immobilized 8-quinolinol, SHQ, has proven to be a particularly useful material for sample preparation, matrix isolation, and preconcentration of trace metal ions (*4-7*). The selectivity of SHQ for transition-metal ions over the alkali and alkaline-earth metal ions makes it useful for samples containing large quantities of the latter (e.g., seawater, natural waters, etc.).

Most procedures utilizing SHQ for preconcentration and matrix isolation have involved manual, off-line, operation in which a relatively large volume of sample is passed through a column containing SHQ after which an aqueous acid solution is used to elute the isolated metal ion into a relatively small volume. The eluted metal is then determined, commonly by atomic absorption spectrometry AAS. Procedures such as the one just described become burdensome and time-consuming, in practice, and are subject to human errors due to the required manipulations. In recent years, however, automated sample processing techniques have been developed which reduce the number of manual manipulations of the sample. Flow injection analysis, FIA, is one of those techniques which is a very useful sample introduction approach in atomic spectrometry (*10-12*). Little effort has been directed, however, toward the incorporation of on-line preconcentration/matrix isolation into the FIA/AAS instrumental system. Olsen et al. (*13*) have utilized Chelex-100, an iminodiacetate chelating resin, for the on-line preconcentration of some heavy metal ions in seawater prior to AAS determination. A complex manifold involving backwashing is required, however, in order to overcome the serious swelling problems encountered with Chelex-100. Malamas and co-workers have also investigated on-line preconcentration/matrix isolation using SHQ (*14*). The SHQ used in their work, however, exhibited very low breakthrough capacity and the support was a relatively expensive controlled pore glass. The effect of different experimental parameters (e.g., flow rate, temperature, column di-

[1]Present address: Monsanto Co., Corporate Research Center, 800 N. Lindbergh Blvd., St. Louis, MO 63167.

0003-2700/85/0357-0729$01.50/0 © 1985 American Chemical Society

mensions) when SHQ is used under flow conditions, apparently, has not been studied in detail.

The work described here involved a critical study of the use of SHQ prepared using silica gel and an improved synthetic route employing (aminophenyl)trimethoxysilane (*15*, *16*) under a variety of experimental conditions which influence breakthrough capacities. The implementation of a preconcentration column containing SHQ in on-line FIA/AAS utilizing a very simple manifold and low cost support is also described.

EXPERIMENTAL SECTION

Reagents and Solutions. All reagents were of analytical grade and used as received unless otherwise indicated. Deionized/distilled water was used for all aqueous solution preparation and as carrier solution in FIA/AAS determinations. Copper standards were prepared from a 993 μg/mL standard stock solution (Aldrich Chemical Co., Milwaukee, WI). Water pollution quality control check samples were obtained from the U.S. Environmental Protection Agency Monitoring and Support Laboratory (Cincinnati, OH) and were prepared as directed.

The SHQ was prepared by the new diazo coupling procedure described previously (*15*). The silica support was silica gel suitable for column chromatography (Baker Chemical Co., Phillipsburg, NJ) which had been sieved in order to obtain a particle size range of 150–250 μm (60–100 mesh). This silica gel was acid washed with 0.10 M HCl and dried in an oven at 120 °C for at least 12 h before use.

Apparatus. A Perkin-Elmer 290B atomic absorption spectrophotometer (Norwalk, CT) with an air/acetylene flame and a Hewlett-Packard HP-7128A recorder (Palo Alto, CA) were used for copper determinations in the FIA/AAS experiments. The FIA setup consisted of a Gilson Minipuls 2 peristaltic pump (Gilson Medical Electronics, Inc., Middleton, WI), a sliding rotary valve for sample injection (intercalation) constructed from Plexiglas and Teflon (*17*) (the original design was modified by adding a clamp and ferrules to the injection valve ports so that somewhat higher pressures could be tolerated), connecting tubes of Teflon (0.5 mm i.d. and 1.5 mm o.d.), and all connections made with low pressure tube and fittings ($^1/_4$ in. × 28 TPI, Alltech Associates South, Inc., Houston, TX). The Minipuls 2 pump was also used to propel solutions in capacity studies under flow conditions. A Brinkman IC-2 water circulator (Westbury, NY) was used for thermostating the column, reagents, and connecting tubing when performing temperature studies.

A Beckman DB-GT spectrophotometer (Fullerton, CA) was used for all colorimetric determinations.

Column Preparation. Columns were prepared by placing a small dimethylchlorosilane-treated glass wool plug at one end of a silanized glass column and aspirating a water-slurry of SHQ into the column until filled. Another small silanized glass wool plug was then inserted into the other end. Two column dimensions were investigated: column 1 was 1.43 mm i.d. × 100 mm long and column 2 was 2.60 mm i.d. × 30 mm long. The resulting total volumes were both about 160 μL and both columns contained 0.065 g of SHQ.

Procedure for Extraction Studies. Typically, 20.00 mL of 100 μg/mL metal ion solution was added to a 100-mL volumetric flask and diluted to the mark with 0.125 M buffer solution. Solutions used for dilution included: sodium chloride (pH 1–3), sodium formate (pH 3–4), sodium acetate (pH 4–6), sodium phosphate (pH 6–8), and sodium borate (pH 8–9). Usually 0.20 g of SHQ was equilibrated with 10.00 mL of a standard metal ion solution for 1 h after which the solid was removed by filtration and the metal ion concentration in the filtrate was determined. In all cases, care was taken to ensure that the bound 8-quinolinol was present in excess. Actual excesses ranged from 8- to 14-fold. Copper(II) was determined by AAS, iron(III) by the 1,10-phenanthroline/reducing agent method, cobalt by the thiocyanate method, nickel by the dimethylglyoxime/oxidizing agent method, and calcium by the purpurate (murexide) method. All of the colorimetric procedures can be found in a single reference (*18*).

Procedure for Breakthrough Studies. The manifold for breakthrough studies is shown in Figure 1. All breakthrough studies were performed with Cu(II) as the metal ion probe at pH 5.00. First, with the column removed, the Cu(II) solution was

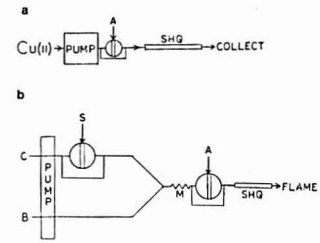


Figure 1. Flow manifolds for (a) breakthrough studies and (b) FIA/preconcentration/AAS: A, eluting acid (1.0 M HCl + 1.0 M HNO_3); C, carrier (distilled/deionized water); B, buffer (0.10 M $NH_4C_2H_3O_2$ + HCl, pH 5.0); S, sample; M, delay mixing coil, SHQ, silica-immobilized 8-quinolinol column (0.065 g).

pumped through the system in order to fill all the tubing up to the column. Then, the column was placed in the system and pumping was resumed at a specified flow rate and temperature. Fractions were collected in 2-mL vials at 1.00-mL intervals. In some cases, on-line monitoring of the effluent with the column exit connected directly to the nebulizer of the AAS, was performed. The breakthrough capacity was calculated from the volume of solution required to give 1.0% of the maximum signal.

Procedure for FIA/Preconcentration/AAS Determination. The manifold for these studies is shown in Figure 1b. Distilled/deionized water was used as a carrier at a flow rate of 4.0 mL/min into which an acidified sample could be intercalated. This sample/carrier was then merged with a buffer (0.10 M ammonium acetate + HCl, pH 5.00) at a flow rate of 0.5 mL/min to give an overall flow rate of 4.5 mL/min through the delay-mixing coil where neutralization of acidified samples occurred. The buffered sample then passed onto an SHQ column where some of the metal ions present in the sample were extracted. The volume injected was commonly 10.0 mL. Therefore, the preconcentration step consumed about 2.2 min neglecting dispersion. In the interest of ensuring complete passage of the sample (since some dispersion actually occurs), 4 min was allowed for the preconcentration part of the cycle. During this preconcentration step, the second injection valve [A] was in the "fill" position. After preconcentration, the metal ions were eluted from the SHQ column by injecting (intercalating) a 1.0-mL plug of 1.0 M HCl/1.0 M HNO_3 through the acid injection valve [A]. The eluted metal ions then passed into the flame of the AAS and the resulting transient signal was recorded.

In some cases, the preconcentrating SHQ column, the acid injection valve, and the delay-mixing coil were removed and samples containing the Cu(II) were injected (intercalated) into a water carrier and passed directly into the flame. This was done in order to make comparison of FIA/AAS and FIA/Preconcentration/AAS.

RESULTS AND DISCUSSION

Extraction Studies. A thorough understanding of the extraction behavior of different metal ions that might be present in a given sample is necessary when SHQ is used for preconcentration and/or matrix isolation of metal ions in water samples. Extraction–pH profiles for metal ions give insight into the selectivity of SHQ and aid in the choice of practical operating pH. Figure 2 shows extraction–pH profiles for Cu(II), Fe(III), Ni(II), Co(II), and Ca(II) chosen to illustrate the point of transition metal ion selectivity of the SHQ material. The figure makes apparent such selectivity over alkaline-earth metal ions [i.e., Ca(II)] and suggests the use of SHQ for preconcentration and matrix isolation for aqueous samples containing large amounts of alkali and alkaline-earth metal ions. Selectivity between individual transition-metal ions is not so good, however, and stringent pH control and gradient elution are required for chromatographic separation of these species on SHQ (*19*). Kinetic differences can also

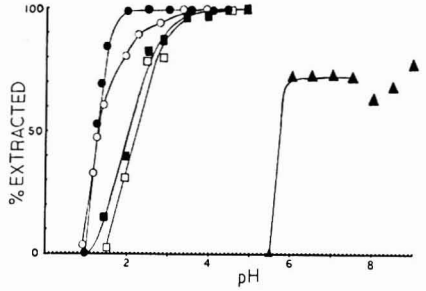


Figure 2. Extraction behavior of SHQ as a function of pH: Cu^{2+} (●), Fe^{3+} (○), Ni^{2+} (■), Co^{2+} (□), Ca^{2+} (▲).

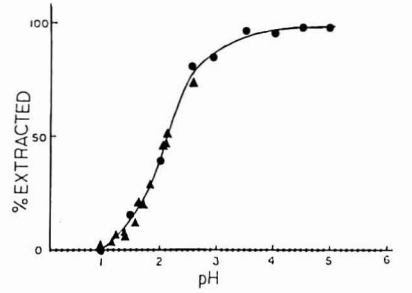


Figure 3. Extraction behavior of Ni^{2+} as a function of pH for diazo-coupled SHQ prepared from (aminophenyl)trimethoxysilane (●) and conventionally diazo-coupled SHQ (▲).

affect selectivity under the dynamic conditions prevailing in chromatographic separations (*19*).

The data in Figure 2 also indicate quantitative extraction of transition-metal ions under fairly acidic conditions. Figure 3 shows extraction–pH profiles for Ni(II) using as extraction reagents: (1) diazo-coupled SHQ using (aminophenyl)trimethoxisilane and (2) diazo-coupled SHQ by conventional procedures. Both of the diazo-coupled materials give similar extraction curves which indicates the structural similarities of the immobilized groups in both cases. These immobilized materials are, in essence, 5-phenylazo derivatives of 8-quinolinol and the extraction at low pH may be due, in part, to the acid-strengthening effect that occurs when 8-quinolinol is diazo-coupled to silica (*15*). 5-Phenylazo-8-quinolol which is the closest free solution analogue of the immobilized material, has been shown to be considerably more acidic than 8-quinolinol itself (*20*). These extraction studies indicate that a pH of 5 for preconcentration of transition-metal ions is effective since these ions will combine with the immobilized ligand at such a pH while alkali and alkaline-earth metal ions will be excluded from chelation.

Breakthrough Studies. The total amount of counterions extracted per unit mass of solid chelating material is commonly called the apparent capacity (*21*). It is usually measured under batch conditions in which an excess of a known metal ion is allowed to equilibrate with the solid chelating ion exchanger at a fixed pH and the apparent capacity is then determined by the amount of metal ion extracted. In dynamic column operation, however, the breakthrough capacity, which is defined as the amount of metal ion that can be extracted per unit mass of solid under the existing operating conditions

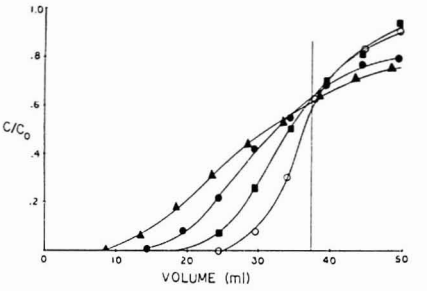


Figure 4. Breakthrough curves as a function of flow rate, column 1: temperature, 25 °C; C/Co, influent concentration/effluent concentration. Flow rates are 2.0 mL/min (▲), 1.0 mL/min (●), 0.5 mL/min (■), 0.25 mL/min (○). Test solution is 20.0 μg/mL Cu(II), pH 5.0. The vertical line at 37 mL represents the apparent batch capacity. (See text.)

prior to being detected in the column effluent, is more useful quantity. The breakthrough capacity depends on a variety of factors; factors which cause an increase in the rate of ion exchange result in an increase in the breakthrough capacity (*21*). Essentially all applications of SHQ involve its use under flowing conditions. Efficient column utilization, therefore, requires that breakthrough capacities be as large as possible allowing the use of a small quantity of solid SHQ. Factors which directly affect breakthrough capacities and have been studied in this work, are flow rate, temperature, and column dimensions. Other factors which can affect breakthrough capacities include initial total capacity, particle size, concentration of counterion, and preference of the ion exchanger for the counterions from the feed solution.

The initial total capacity of the SHQ used in these studies was considerably larger than the capacity of similar materials used in preconcentration studies which have been reported previously (*4–7*, *14*, *19*). This is a result of optimization of the synthetic route (*15*) and the pore size/surface area of the support (*16*). The apparent batch capacity for the SHQ used in most of this work was 185 μmol/g using copper(II) as probe at pH 5. In some cases a capacity as high as 230 μmol/g was used.

Small particle sizes also, in general, increase the breakthrough capacity (*21*). The resulting increase in pressure drop across the column, however, precludes the use of very small particles. This is particularly true for use of SHQ in FIA/AAS where the aspiration rate of the nebulizer (4.4 mL/min in this work) dictates the minimum flow rate through the column. A relatively large particle size range (150–250 μm) was chosen for this work as it provided adequate permeability when using a low-pressure peristaltic pump at flow rates near the nebulizer aspiration rate.

A large breakthrough capacity is also favored by a low counterion concentration (*21*). In these studies, the counterion concentration was kept constant at a value significantly higher than concentrations expected to be encountered in practice. The copper(II) concentration used in all breakthrough studies was 20 μg/mL, and the breakthrough capacities reported here are, then, on the conservative side since at lower Cu(II) concentrations larger breakthrough capacities may be obtained.

Copper(II) was chosen as metal ion probe because it is easily detected via AAS and has a large formation constant with SHQ. Copper(II) has also been widely used in previous studies under batch conditions (*15*, *16*, *19*, *22–25*) which facilitates comparison to previous work in some of the studies reported here.

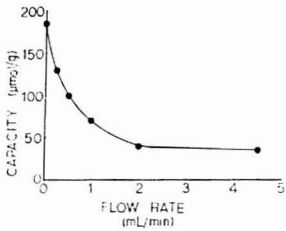


Figure 5. Capacity as a function of flow rate.

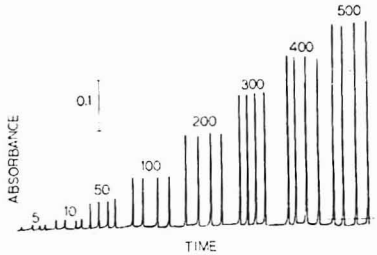


Figure 6. Signal profiles for standard solutions of copper(II). Numbers above signals are in units of ng/mL. (Time is not to scale since the recorder was off during the preconcentration cycle.) The crossbar on the 500 ng/mL signals represents the steady state signal that would be obtained without preconcentration.

A series of breakthrough curves, or isoplanes, for column 1 at various flow rates are shown in Figure 4. As expected, breakthrough occurs earlier at high flow rates and as the flow rate decreases the breakthrough capacity increases. The curves cross roughly at a volume corresponding to the apparent batch capacity, also as expected. This is the volume at which breakthrough would occur at infinitely low flow rate. Figure 5 shows breakthrough capacities as a function of flow rate. An approximate exponential decay in capacity is observed as the flow rate increases. At a flow rate of 4.5 mL/min (near the aspiration rate of the nebulizer), for example, the breakthrough capacity is 37 μmol/g (apparent batch capacity, 185 μmol/g); therefore the breakthrough capacity is about 20% of the apparent capacity. It appears that only the most accessible complexation sites are available for reaction since the residence time of a given cross section of the solution in the column is less than 2 s.

All the foregoing observations indicate that beneficial conditions are those which increase the rate of exchange. Increasing the temperature, then, should also result in higher breakthrough capacities (*21*). We have investigated the effect of temperature on the breakthrough curves (isoplanes) of SHQ at constant flow rate and column dimensions. The rate of ion exchange is indeed facilitated at higher temperatures and the breakthrough capacities are somewhat larger. An increase in breakthrough capacity of 30%, in fact, is observed upon increasing the temperature from 25 °C to 45 °C. There are probably two contributing factors to the increase in ion exchange rate. The first is the increase in complexation rate and the second is the increase of diffusion coefficients with temperature. One, or both factors may contribute to the observed increase in breakthrough capacity, depending on the particular system and experimental conditions. It has been pointed out that diffusion processes are normally rate limiting for conventional ion exchangers but that rate control by the complexation reaction can occur with chelating groups that form sluggishly reacting complexes (*21*). The effect of temperature on breakthrough capacities, however, is much smaller than the flow rate effect for the case of Cu(II). Therefore, for practical purposes, use of the columns at room temperature is preferable for the sake of simplicity in experimental design.

As column dimensions change (at constant volume, type of exchanger, and mass of solid) a shift in the isoplanes is also expected (*21*). In general, long, narrow columns give larger breakthrough capacities than short, wide columns. A convenient manner in which to express the dimensional characteristics of a column is to calculate the aspect ratio which is simply the ratio of length to inside diameter of the column. Therefore, columns with large aspect ratios are expected to yield larger breakthrough capacities than those with smaller aspect ratios. The effect of column dimension on the isoplanes for the two columns studied at two different flow rates has been investigated. The columns had aspect ratios of 67.9 and 11.6, respectively. Within the limitations of the dimensions studied, at low flow rates (0.25 mL/min) very little difference was observed in the breakthrough capacities of the two columns. As expected, however, as the flow rate increased to 1.0 mL/min, the column with the larger aspect ratio (column 1) was observed to yield a slightly larger breakthrough capacity (approximately 15% greater) and, therefore, in the FIA/AAS studies described later, the preconcentration column used had dimensions similar to that of column 1.

The effect of column dimensions on breakthrough capacities can be interpreted as a diffusional effect. At small aspect ratios and relatively high flow rates, radial diffusion within the column does not occur quickly enough to utilize as many of the available complexation sites within the column. At lower flow rates or larger aspect ratios, more of the complexation sites are accessible and a concomitant increase in the breakthrough capacity is observed.

FIA/Preconcentration/AAS Studies. Incorporation of an on-line preconcentration/matrix isolation system into an FIA/AAS unit (Figure 1b) was implemented to illustrate the lowering of detection limits, good reproducibility, and minimal sample manipulation affordable by such implementation. When combining FIA with AAS, flow rates are restricted to values greater than the normal aspiration rate of the nebulizer which may result in large pressure drops when using packed columns. In fact, commercially available supports (particle sizes in the 74 to 250 μm range) contain too many small particles which result in an unacceptable upper flow rate of about 2.0 mL/min. Separation of a 150–250 μm fraction by sieving resulted in a useful support affording flow rates above the normal aspiration rate, in this case (4.5 mL/min). As already mentioned, at this flow rate the breakthrough capacity is about 37 μmol/g, indicating that for 0.065 g of SHQ (the amount usually employed in these studies) about 1.5 L of a 100 ng/mL Cu(II) solution could be passed through the column prior to breakthrough, assuming a 1:1 complex (*15*, *19*). Operation after breakthrough is not possible because quantitative extraction would not be achieved.

A series of Cu(II) standard solutions were processed using the FIA/preconcentration/AAS described and the resulting signal profiles are shown in Figure 6. For comparison, the steady-state signal for 500 ng/mL copper solution is also shown. A considerable enrichment factor can be observed; it amounts to approximately 35-fold when using 10-mL sample volumes. Larger enrichment factors may be obtained by increasing the sample volume. A limit to enrichment, however, is the presence of analyte in the carrier or reagent(s). The blank signal, in these cases becomes larger with larger sample volumes.

Three different sample introduction situations were studied and a summary of their characteristics is presented in Table

Table I. Performance of Various Sample Introduction Techniques for AAS[a]

parameter	conventional AAS	FIA/ AAS[b]	FIA/preconcentration/ AAS
sample size (mL)	> 1.0	0.18	10
corr coeff, of working curve	0.9999	0.9999	0.9986
slope of working curve (cm mL μg^{-1})	0.727	0.439	26.1
sensitivity (AU mL μg^{-1})	0.022[c]	0.013	0.792
y intercept (cm)	−0.018	0.010	0.412
limit of detection (μg/mL)[d]	0.18	0.19	0.0015
analytical throughput (h^{-1})	100	200	15

[a] Metal copper; wavelength, 324.7 nm. [b] No preconcentration; carrier, water; flow rate, 4.5 mL/min. [c] Perkin-Elmer 290B Manual reports 0.029 AU mL μg^{-1} for conventional AAS. [d] Estimated from the standard deviation of the y intercept of the working curve (Si) and defined as the concentration corresponding to 3Si.

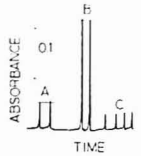


Figure 7. Signal profiles for real samples: A, EPA sample 1; B, EPA sample 2; C, tap water. (Time is not to scale. Crossbars indicate expected signal assuming that the EPA-reported value is the true value.)

I. The intercept of the FIA/preconcentration/AAS working curve is somewhat larger than for the other approaches as a result of a larger blank signal due to the presence of copper in the carrier and reagents. Sensitivity and limit of detection, however, are improved dramatically. The sacrifice is in sample throughout because of the time required for preconcentration. Smaller sample sizes and high analytical throughout can be achieved using FIA/AAS without preconcentration but with sensitivities and limits of detection comparable to conventional AAS. It should be mentioned that the use of a peristaltic pump rather than aspiration alone reduces the signal dependence on viscosity changes. These, as well as other advantages of FIA/AAS have been pointed out in a recent review (*12*).

The presence of up to 0.10 M Na^+ in the sample had no effect on the signal obtained and Na^+ was readily observed in the flame during the preconcentration cycle. Also, no carry-over of Cu(II) was observed indicating efficient elution by 1.0 M HCl + 1.0 M HNO_3. The column can be used for at least 6 months without any noticeable deterioration in performance.

The system and conditions described were applied to the determination of copper ion in some EPA quality control water samples and in tap water. Typical signal profiles for these determinations are shown in Figure 7. The bars above the signals of the EPA samples indicate the peak height that should be expected if the value reported by EPA were the true value. The agreement is very good as can be seen from the results presented in Table II.

Another interesting aspect of FIA/preconcentration/AAS lies in the dispersion occurring in the system. Dispersion in systems such as the one described in this paper is due, primarily, to dispersion between the column and the flame. Therefore, the volume of the tubing upstream from the column is of little consequence (*14*). It is of interest also to note that an acidic solution (second injection valve) is being intercalated into a buffer. This solution, however, is relatively concentrated

Table II. Results of Copper Determinations in Water Samples

sample[a]	Cu concn ng/mL determined	reported
EPA-1	51 ± 4.6	50
EPA-2	252 ± 2.6	250
EPA-3	38 ± 3.0	40
EPA-4	8.9 ± 1.6	8.3
Tap[b]	26 ± 2.0	NA[c]

[a] Other elements known to be present (concentration in ng/mL in parentheses): EPA-1, Al (450), As (60), Be (250), Cd (13), Cr (80), Co (80), Fe (80), Pb (120), Mn (75), Hg (3.5), Ni (80), Se (30), V (250), Zn (80); EPA-2, Al (700), As (200), Be (750), Cd (50), Cr (150), Co (500), Fe (600), Pb (250), Mn (350), Hg (7.5), Ni (250), Se (40), V (750), Zn (200); EPA-3, Al (350), As (40), Be (150), Cd (10), Cr (60), Co (70), Fe (50), Pb (80), Mn (55), Hg (3.0), Ni (70), Se (20), V (200), Zn (60); EPA-4, Al (106), As (27), Be (29), Cd (9.1), Cr (7.1), Co (43), Fe (22), Pb (43), Mn (13), Hg (0.7), Ni (17), Se (11), V (130), Zn (10); tap water, unknown. [b] Stillwater, OK. [c] Not available.

(1.0 M HCl + 1.0 M HNO_3) whereas the buffer is more dilute (0.10 M acetate), the flow rate is high, and the connecting tubing short between the acid injection valve and the flame. The overall result is that only the extremities of the acid plug are neutralized and dispersion is minimized, thereby allowing for a high local concentration of acid in the center of the plug for efficient elution of the preconcentrated metal(s).

The possibility of coupling on-line FIA/preconcentration with multielement detection techniques (e.g., inductively coupled plasma spectroscopy) is of interest in providing higher sensitivities and lower limits of detection when materials as the one described here are used for preconcentration in combination with the selectivity and convenience of a single multielement determination.

Registry No. H_2O, 7732-18-5; Cu, 7440-50-8; Fe, 7439-89-6; Ni, 7440-02-0; Co, 7440-48-4; Ca, 7440-70-2; 8-quinolinol, 148-24-3.

LITERATURE CITED

(1) Yago, L. S. *Am. Lab.* (*Fairfield, Conn.*) **1984**, *16* (1), 4–6.
(2) Leyden, D. E.; Luttrell, G. H. *Anal. Chem.* **1975**, *47*, 1612-1617.
(3) Leyden, D. E.; Luttrell, G. H.; Sloan, A. E.; DeAngelis, N. J. *Anal. Chim. Acta* **1976**, *84*, 97–108.
(4) Sugawara, K. F.; Weetall, H. H.; Schucker, G. D. *Anal. Chem.* **1974**, *46*, 489–492.
(5) Guedes da Mota, M. M.; Romer, F. G.; Griepink, B. *Fresenius' Z. Anal. Chem.* **1977**, *287*, 19–22.
(6) Moorhead, E. D.; Davis, P. H. *Anal. Chem.* **1974**, *46*, 1879–1880.
(7) Sturgeon, R. E.; Berman, S. S.; Willie, S. N.; Desaulniers, J. A. H. *Anal. Chem.* **1981**, *53*, 2337–2340.
(8) Vernon, F.; Eccles, H. *Anal. Chim. Acta* **1973**, *63*, 403–414.
(9) Iler, R. K. "The Chemistry of Silica"; Wiley: New York, 1979; p 47.
(10) Browner, R. F.; Boorn, A. W. *Anal. Chem.* **1984**, *56*, 787A–798A.
(11) Browner, R. F.; Boorn, A. W. *Anal. Chem.* **1984**, *56*, 875A–888A.
(12) Tyson, J. F. *Anal. Proc.* **1983**, *20*, 488–491.
(13) Olsen, S.; Pessenda, L. C. R.; Ruzicka, J.; Hansen, E. H. *Analyst* (*London*) **1983**, *108*, 905–917.
(14) Malamas, F.; Bengtsson, M.; Johansson, G. *Anal. Chim. Acta* **1984**, *160*, 1–10.
(15) Marshall, M. A.; Mottola, H. A. *Anal. Chem.* **1983**, *55*, 2089–2093.
(16) Marshall, M. A.; Mottola, H. A. *Anal. Chim. Acta* **1984**, *158*, 369–373.
(17) Hansen, E. H.; Ruzicka, J. *J. Chem. Educ.* **1979**, *56*, 677–680.
(18) Sandell, E. B. "Colorimetric Determination of Traces of Metals", 3rd ed.; Interscience: New York, 1959.
(19) Jezorek, J. R.; Freiser, H. *Anal. Chem.* **1979**, *51*, 366–373.
(20) Takamoto, S.; Fernando, Q.; Freiser, H. *Anal. Chem.* **1965**, *37*, 1249–1251.
(21) Helfferich, F. "Ion Exchange"; McGraw-Hill: New York, 1962.
(22) Hill, J. M. *J. Chromatogr.* **1973**, *76*, 455–458.
(23) Fulcher, C.; Crowell, M. A.; Bayliss, R.; Holland, K. B.; Jezorek, J. R. *Anal. Chim. Acta* **1981**, *129*, 29–47.
(24) Jezorek, J. R.; Fulcher, C.; Crowell, M. A.; Bayliss, R.; Greenwood, B.; Lyon, J. *Anal. Chim. Acta* **1981**, *131*, 223–231.
(25) Shahwan, G. J.; Jezorek, J. R. *J. Chromatogr.* **1983**, *256*, 39–48.

RECEIVED for review August 6, 1984. Accepted November 19, 1984. Support from the National Science Foundation [Grant CHE-8312494] made the reported work possible.

Automated Iodometric Method for Determination of Trace Chlorate Ion Using Flow Injection Analysis

Kevin G. Miller, Gilbert E. Pacey,* and Gilbert Gordon

Department of Chemistry, Miami University, Oxford, Ohio 45056

This paper describes two approaches for the determination of chlorate ion at levels of 1×10^{-5} M and 1×10^{-6} M, respectively. Both methods utilize the reaction of chlorate ion with iodide ion to produce iodine. By use of the condition described in the rate law $-d[ClO_3^-]/dt = k[ClO_3^-][I^-]^{1.5}[H^+]^2$, high acid concentration will accelerate the reaction. However, at high acid concentrations the oxidation of I^- by O_2 is extremely fast. Therefore, these methods were developed by using flow injection analysis which excludes air from the flow stream. The first method can detect 1×10^{-5} M ClO_3^-. The second method employed a stopped-flow condition which can detect 1×10^{-6} M ClO_3^-. Both methods exhibit excellent relative standard deviation and accuracy in the determination of unknown ClO_3^-.

Methods of chemical analysis of solutions containing chlorine-containing oxidizing agents appear to be well-defined in the chemical literature (*1–8*). Late in 1979, the *Federal Register* (*9*) published restrictions which should be placed on residual oxidants such as chlorine dioxide, chlorite ion, and chlorate ion which result from the chlorine dioxide treatment of water to be used as drinking water. In the 1979 update of "Drinking Water and Health", the National Academy of Science estimated acceptable exposure values of 0.38 mg/L for chlorine dioxide and 0.21 mg/L for chlorite ion. The *Federal Register* also reports "... EPA feels that whenever chlorine dioxide is used *residual oxidants* should be monitored and kept below 0.5 mg/L. EPA will consider establishing an MCL for chlorine dioxide, chlorite or chlorate or the *aggregate* as *total oxidant* for inclusion in the Revised Regulations after further studies have been fully evaluated ...".

Some modifications of these limits are being considered. It would appear that dosage and residual levels of chlorine dioxide in drinking water are likely to be set at 1 mg/L, as is common in European water treatment plants (*10, 11*). The EPA appears to be revising the recommendation of chlorine dioxide dosage to 1 mg/L because of unresolved questions regarding health effects (*12*). The National Research Council's Safe Drinking Water Committee has recommended 7-day no-adverse-response levels (SNARLs) of 0.125 mg/L for each of the following species: chlorate, chlorite, chlorine dioxide, and chloramine (*12*). Without a question, quantitative discrimination among oxidized chlorine species at low concentrations is an important requisite for assessing disinfection alternatives.

In the context of this paper it should be noted that in early 1980 *none* of the analytical techniques in the literature for the analysis of chlorine-containing oxidizing agents was capable of routinely determining chlorate ion concentrations at the sub-milligram-per-liter level. The purpose of this paper is to describe the underlying chemical reactions and interactions of the oxychlorine species and to present improved methodology which provides for the analysis of chlorate ion in drinking water at levels greater than 0.1 mg/L.

Reference 1 describes in detail seven manual methods for chlorine ($HOCl + OCl^- + Cl_2$) residual analysis. In general, these methods describe procedures for the determination of the total oxidizing power of the solution and can be readily modified for the determination of aggregate chlorine-containing species including chlorite ion, chlorine dioxide, and chlorate ion along with other species such as Cl_2O (the anhydride of hypochlorous acid) and the like.

The methods described include two iodometric methods, phenylarsine oxide amperometric titration, *N,N*-diethyl-*p*-diphenyldiamine (DPD)–ferrous ion titration, DPD colorimetric, leuco crystal violet, and syringaldazine. Details of these methods are given in the "state-of-the-art" compilation by Symons (*13*) and the "comparison of methods" by Bender (*14*). The relative usefulness of each method along with descriptions of known interferences such as turbidity, organic matter, ionic materials, solids, color, buffering capacity, and the nature of the sample and the time between collection of the sample and the actual analysis are described in the original references (*1*). It must be emphasized, however, that each of these manual methods is based on the total oxidizing capacity of the solution being analyzed and is readily subject to interferences from the presence of other potential oxidizing agents and/or intermediates from concomitant chemical reactions (*16*). Under ideal conditions some of the methods are accurate to better than ±1% relative error—especially in the absence of common interferences, whereas other methods are almost semiquantitative in nature with many common species interfering with both the precision and accuracy of the measurements. Typical of the species most difficult to analyze is chlorate ion at levels below 5 mg/L where the published manual methods prior to 1982 gave results no more reliable than ±25–50%.

Clearly there is a need for improved and automated methods to determine the oxy-chlorinated species, chlorate ion, chlorite ion, hypochlorous acid/chlorine, and chlorine dioxide. These methods must be capable of routine precise determination of low levels (below 0.5 mg/L) of the oxychlorinated species without significant interference. In this paper we demonstrate that automation for chlorate ion using flow injection analysis (FIA) (*15*) will not only improve precision and throughput but increase selectivity and sensitivity.

Improved analytical techniques and/or methodology require a detailed understanding of the potential reactions and interactions of the species under investigation as well as the chemistry of various intermediates associated with the analyses under consideration (*16*). For example, the detailed analysis of solutions containing chlorine or hypochlorous acid along with chlorite ion at pH 2, 7, and 10 are indeed quite different in that the reaction between residual chlorine (Cl_2 and/or HOCl) with chlorite ion varies markedly as a function of pH—being very rapid at pH 2 and almost negligible at pH 10. Likewise, the self-disproportionation of chlorine dioxide is almost instantaneous at pH 12 whereas it is infinitesimally slow at pH 4. Without a detailed understanding of reactions and interactions such as these, the validity of the methods themselves may be suspect and the reported analyses might be in considerable error owing to various side reactions and interactions.

Several details with respect to the reactions and interactions of hydrogen ion or chlorine and/or hypochlorous acid with

0003-2700/85/0357-0734$01.50/0 © 1985 American Chemical Society

chlorite ion have been reported by Emmenegger and Gordon (*17*), Kieffer and Gordon (*18*), and most recently by Tang and Gordon (*19–21*). Detailed studies of the decomposition of chlorine dioxide have been carried out by Emerich (*22*). Clearly, the knowledge about these interactions discovered in this research laboratory permits us to develop improved and selective methods for oxychlorinated compounds.

The Ikeda-Tang revised iodometric method (*20*) is reported to be capable of accurately measuring chlorate ion concentrations below 100 mg/L and as low as 0.3 mg/L.

The iodometric method has been used widely to measure oxychlorine species such as hypochlorite and/or hypochlorous acid and chlorite ion accurately and precisely (*4*). However, the reaction of chlorate ion with iodide ion is slow under mildly acidic conditions

$$ClO_3^- + 6I^- + 6H^+ \rightarrow 3I_2 + Cl^- + 3H_2O \qquad (1)$$

According to Bray (*23*) the rate of reaction 1 is proportional to the chlorate ion concentration and the square of the hydrogen ion concentration and is a linear function of the concentrations of chloride and iodide ions. The report by Hadjiioannou and co-workers (*24*) suggests that the reaction obeys the following rate law:

$$-d[ClO_3^-]/dt = k[ClO_3^-][I^-]^{1.5}[H^+]^2 \qquad (2)$$

where k is (35 ± 1.0) $M^{-3.5}$ s^{-1} at 30 °C and ionic strength 1.0 M. The rate law given in eq 2 is the system on which the development of these methods is based.

Thus, normally the quantitative iodometric determination of chlorate ion is possible only in the presence of a large excess of hydrochloric acid.

Unfortunately, under these conditions iodide ion is readily oxidized by air

$$4I^- + 4H^+ + O_2 \rightarrow 2I_2 + 2H_2O \qquad (3)$$

The removal of air from the sample solution by using sodium carbonate is effective to prevent air oxidation of iodide ion (*20*). Ditz (*25*) and Rupp (*26*) have suggested using bromide ion in the presence of 7.5 M hydrochloric acid to reduce chlorate ion. The bromine produced thereby is determinated iodometrically. However, these modified iodometric methods are primarily applicable to the determination of chlorate ion in the relatively high concentration range (above 0.02 N).

For the determination of chlorate ion in concentrations such as in the millimolar and submillimolar range, additional modifications of the iodometric method are necessary in order to avoid the air oxidation of iodide ion (*8*, *19*, *27*, *28*).

A recent study (*28*) has suggested that hexane is an effective shielding agent to prevent the air oxidation of iodide ion and that the interference from air oxidation can be minimized when chlorate ion is reduced with iodide ion in 6 M hydrochloric acid followed by neutralization to approximately 3 M with either 50% (w/w) sodium hydroxide or solid sodium phosphate (Na_2HPO_4).

The revised Ikeda-Tang (*20*) method gives indications that flow injection analysis (FIA) could be successfully used to improve the iodometric method for the determination of chlorate ion. The two major problems that must be overcome are the rate of the reaction and the air oxidation of iodide ion. The rate of reaction is significantly increased in the presence of 12 M hydrochloric acid. As mentioned earlier the rate of air oxidation of iodide ion in the presence of excess hydrochloric acid is very fast. Thus, the use of 12 M hydrochloric acid in an open environment of a laboratory is not practical. However, in FIA the solutions are contained inside tubing and the enclosed reagents are effectively isolated from the oxidants that are present in the atmosphere.

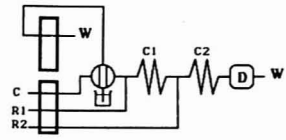


Figure 1. Diagram of the FIA automated system: C, carrier stream (triply distilled water); R1, reagent 1 (12 M HCl); R2, reagent 2 (0.3 M KI); C1, reaction coil 1 (100 cm); C2, reaction coil 2 (100 cm); D, detector (370 nm); W, waste. All pumping rates were 0.32 mL/min. Injection volume was 30 μL.

This paper describes a method for the determination of chlorate ion by iodometry using the FIA technique to automate and significantly improve the method.

EXPERIMENTAL SECTION

The potassium iodide, sodium chlorate, and hydrochloric acid (Fisher Scientific Co.) used were all reagent grade and were used without further purification. Deionized doubly distilled water was used for all solutions which were degassed with prepurified nitrogen, except for the HCl which was degassed by ultrasonication. The prepurified nitrogen was passed through a scrubber containing 0.1 M chromium(II) in 1 M sulfuric acid to remove any residual oxygen.

The FIA system used was a Tecator 5020 analyzer with a Tecator Chemifold II (Figure 1) which was utilized in each of the two modes used to carry out the determination. The first mode was a standard FIA system for higher concentrations of chlorate ion. The second mode was a modified stopped-flow system for lower concentrations of chlorate ion. In traditional stopped-flow measurements, the sample is injected into the system, mixed with the reagent(s), and allowed to flow into the flow cell. Once in the cell, the flow is stopped and an increase in absorbance is observed. When we tried a traditional stopped-flow system, any time the flow was stopped an increase in absorbance was observed whether a sample was present or not. It appears that at the higher reagent concentrations used, the photooxidation of iodide ion to iodine is significant. Thus, the method was modified by stopping the sample before it entered the flow cell. After sufficient time had passed the flow was restarted and the sample carried into the flow cell and detected.

The detector used as an Isco V^4 variable wavelength HPLC detector (Isco, Inc.) set at 370 nm with a 0.5-cm flow cell. The 370 nm corresponds to the isosbestic point of I_2 and I_3^- which was determined by plotting the absorbance vs. wavelength for six solutions with various percentages of I^- and I_2.

RESULTS AND DISCUSSION

Initial experiments with increased HCl acid concentrations demonstrated improved sensitivity. Thus, 12 M hydrochloric acid was used as reagent one (R1) in our system (Figure 1). Reagent two (R2) was 0.3 M iodide solution which was used to form I_3^- and maintain constant I^- ion concentration.

By incorporation of the method into the closed FIA system, the problem of air oxidation of iodide ion at elevated concentration of acid is eliminated. There were two FIA systems used to determine chlorate ion: standard FIA and modified stopped-flow FIA. In the standard FIA system, the sample was mixed with the reagents as it flowed through the tubing to the detector. With this method it is possible to determine chlorate ion concentrations as low as 1.0×10^{-5} M with good reproducibility (Table I). A typical calibration curve is linear and is described by the equation $y = [((0.0256\ AU)/(1.0 \times 10^{-5}\ M))[ClO_3^-] - 0.0004\ AU]$, where AU is absorbance units, with a correlation coefficient of 0.9995. This method offers five significant improvements over the batch method. First, it is faster, ~0.5 min/sample by FIA compared to 20 min/sample for the batch method. Second, it is simpler, since FIA eliminates the need for any air exclusion step such as a hexane layer used in the batch method (*20*). Third, since the iodine

Table I. Absorbance Values and Precision of Standard Solutions Using Standard FIA

concn, M	rel abs[a]	RSD, %
blank	0.004 ± 0.000	0
1.0×10^{-5}	0.024 ± 0.000	0
2.4×10^{-5}	0.059 ± 0.002	3.4
4.8×10^{-5}	0.118 ± 0.002	1.7
7.2×10^{-5}	0.185 ± 0.001	0.5
1.0×10^{-4}	0.257 ± 0.001	0.4

[a] The uncertainty corresponds to the standard deviation from the average of five injections.

Table II. Accuracy of the Determination of Unknown Chlorate Ion Samples

actual concn, M	experimentally determined ClO_3^- concn,[a] M	% error
1.6×10^{-5}	1.6×10^{-5}	0
9.2×10^{-6}	9.3×10^{-5}	1.1
4.8×10^{-5}	4.8×10^{-5}	0

[a] The reported concentrations are the average of five injections.

formed is detected optically, the titration step of the batch method is eliminated in the FIA method. Fourth, the detection limit in the FIA method is improved by an order of magnitude over the batch method. Fifth, the blank is relatively small and very reproducible (±2%).

Unknown chlorate ion samples between 1×10^{-4} and 1×10^{-5} M were determined by using the standard FIA system. The results are shown in Table II. The reproducibility observed for the unknowns was similar to that of the standards. The accuracy of the method is excellent and the problems of air oxidation are minimized.

For lower concentrations of chlorate ion (<0.8 mg/L) a modified stopped-flow FIA method was developed. In this method the sample is injected into the carrier stream and pumped along the tube until it has been mixed with the two reagents. The pumps are then shut off *before* the sample enters the flow cell to allow the reaction to proceed until sufficient iodine is formed to allow detection. It is necessary to stop the sample before the detector due to photochemical reactions which were promoted by the spectrophotometer source. After the optimum time interval the pumps are restarted and the sample is carried into the flow cell where it is measured by optical detection. By varying the amount of time that the pumps are stopped, it is possible to determine an optimum time that offers a good compromise between sensitivity and high sample throughput. For the method reported here, 40 s appears to be the optimal stop time. Longer stop times do not increase peak heights significantly and also reduced sampling rate. This method allows determination of chlorate ion concentrations from 1.0×10^{-5} to 1.0×10^{-6} M (0.83–0.083 mg/L) with good reproducibility as shown in Table III. The calibration curve from weighed standards resulted in a straight line calibration curve corresponding to the equation $y = [((0.0498\ AU)/(1.0 \times 10^{-5}\ M))[ClO_3^-] + 0.0143\ AU]$, where AU is absorbance units, with a correlation coefficient is 0.9999.

The detection limit (2σ) of this method is 2 orders of magnitude better than the detection limit of the batch method. While slower than the standard FIA method, a sampling rate of ~1 min/sample is possible. Unknown chlorate ion samples between 1×10^{-5} and 1×10^{-6} M were measured by using the modified stopped-flow FIA system. The results of these unknowns are shown in Table IV. As can be seen the accuracy of this method is extremely good. The reproducibility observed for the unknowns was similar to the standards.

Table III. Absorbance Values and Precision of Standard Solutions Using Modified Stopped-flow FIA

concn,[a] M	rel abs[b]	RSD, %
blank	0.0146 ± 0.0004	2.7
1.0×10^{-6}	0.0192 ± 0.0003	1.7
2.4×10^{-6}	0.0258 ± 0.0004	1.6
4.8×10^{-6}	0.0386 ± 0.0008	2.1
7.2×10^{-6}	0.0504 ± 0.0009	1.8
1.0×10^{-5}	0.0640 ± 0.0016	2.5

[a] 1×10^{-6} M = 0.083 mg of ClO_3^-/L. [b] The uncertainty corresponds to the standard deviation from the average of five injections.

Table IV. Accuracy of the Determination of Unknown Chlorate Ion Samples Using Modified Stopped-Flow FIA

actual concn, M	experimentally determined ClO_3^- concn, M	% error
2.6×10^{-6}	2.4×10^{-6}	7.7
3.2×10^{-6}	3.2×10^{-6}	0
4.0×10^{-6}	3.7×10^{-6}	7.5
6.0×10^{-6}	6.0×10^{-6}	0
7.0×10^{-6}	7.0×10^{-6}	0

[a] The reported concentrations were the average of five injections.

Any potential interference from chlorine dioxide and chlorite ion can be eliminated by exploiting kinetic discrimination. Under mildly acidic conditions chlorate ion reacts slowly with iodide ion, and therefore, the chlorine dioxide and chlorite ion can be determined first. Then chlorate ion can be determined by this method. With the regulatory agencies setting stricter limits on residual chlorine containing oxidants when chlorine dioxide is used to disinfect drinking water, a method which is capable of determining chlorate in the submillimolar concentration range is crucial. Our adaptation of the modified Ikeda-Tang method to flow injection analysis allows rapid determination of chlorate ion at both high and/or low concentrations. In addition, detection limits are improved by an order of magnitude in standard FIA and by 2 orders of magnitude in modified stopped flow. Since the iodine formed is directly measured photometrically no titration is needed, thus simplifying the procedure. Finally, samples with concentrations higher than 1.0×10^{-5} M can be run at a rate of ~2 samples/min. For samples with concentrations $<1.0 \times 10^{-5}$ M but $>1.0 \times 10^{-6}$ M, the sampling rate is of the order of ~1 sample/min.

Registry No. ClO_3^-, 14866-68-3.

LITERATURE CITED

(1) "Standard Methods for the Examination of Water and Wastewater", 14th ed.; American Public Health Association: New York, 1975.
(2) White, G. C. "Handbook of Chlorination"; Van Nostrand-Reinhold: New York, 1972; pp 228–277.
(3) Vogel, A. I. "Textbook of Quantitative Inorganic Analysis", 4th ed.; Longman: New York, 1978.
(4) Kolthoff, I. M.; Belcher, R. "Volumetric Analysis"; Wiley: New York, 1957; Vol. 3.
(5) Gordon, G.; Kieffer, R. G.; Rosenblatt, D. H. "The Chemistry of Chlorine Dioxide, Progress in Inorganic Chemistry"; Lippard, S. J., Ed.; Wiley: New York, 1972; Vol. 15.
(6) Wojtowicz, J. A. "Kirk-Othmer: Encyclopedia of Chemical Technology", 3rd ed.; Wiley: New York, 1979; Vol. 5.
(7) Noack, M. G.; Doerr, R. L. "Kirk-Othmer: Encyclopedia of Chemical Technology", 3rd ed.; Wiley: New York, 1979; Vol. 5.
(8) Miltner, R. J. In Proceedings AWWA Water Quality Technology Conf., Dec 6–7, 1976, San Diego, CA; AWWA: Denver, CO, 1977; Paper No. 2A-5.
(9) *Fed. Regist.* (Rules and Regulations), **1979**, *44* (231), 68637.
(10) Miller, G. W.; et al. An Assessment of Ozone and Chlorine Dioxide Technologies for Treatment of Municipal Water Supplies; EPA Rept. EPA-600/2-78-147; Munic. Envir. Res. Lab., USEPA: Cincinnati, OH, 1978.

(11) Sontheimer, H. "European Experience with Problems of Drinking Water Quality. Safe Drinking Water: Current and Future Water Problems"; Russell, C. S., Ed.; Resources for the Future: Washington, DC, 1978.
(12) "Drinking Water and Health"; National Research Council, National Academy Press: Washington, DC, (1980 and 1982; Vol. 3 and 4).
(13) Symons, J. M. Second Conference on Water "Chlorination: Environmental Impact and Health Effects", Gatlinburg, TN, 1977.
(14) Bender, D. F. Environmental Monitoring Series, EPA-600/4-78-019, 1978.
(15) Ruzicka, J.; Hansen, E. "Flow Injection Analysis"; Wiley: New York, 1981.
(16) Gordon, G. Proceedings of the American Water Works Association, The 1982 Water Quality Technology Conference 1982, 1, 175-189.
(17) Emmenegger, F.; Gordon, G. Inorg. Chem. 1967, 6, 633.
(18) Kieffer, R. G.; Gordon, G. Inorg. Chem. 1968, 7, 235.
(19) Tang, T.-F.; Gordon, G. Anal. Chem. 1980, 52, 1430.
(20) Ikeda, Y.; Tang, T. F.; Gordon, G. Anal. Chem. 1984, 56, 71.
(21) Tang, Tsung-fei; Gordon, Gilbert Environ. Sci. Technol. 1984, 18, 212.
(22) Emerich, Dwight E. Ph.D. Thesis, Miami University, 1981.
(23) Bray, W. C. J. Phys. Chem. 1903, 7, 92.
(24) Nikolelis, D. P.; Karayannis, M. I.; Hadjiioannou, T. P. Anal. Chim. Acta 1977, 94, 415.
(25) Ditz, H. Chem-Ztg. 1901, 25, 727.
(26) Rupp, E. Z. Anal. Chem. 1917, 56, 580.
(27) Aelta, E. M.; Roberts, P. V.; Hernadez, M. J.—Am. Water Works Assoc. 1984, 76, 64-70.
(28) Tang, T. F. M.S. Thesis, Miami University Oxford, OH, 1980.
(29) Long, G. L.; Winefordner, J. D. Anal. Chem. 1983, 55, 712A-724A.

RECEIVED for review October 1, 1984. Accepted December 3, 1984.

Determination of Nitrate by a Flow System with a Chemiluminescent NO_x Analyzer

Kunio Yoshizumi* and Kazuyuki Aoki

Tokyo Metropolitan Research Institute for Environmental Protection, 2-7-1 Yuraku-cho, Chiyoda-ku, Tokyo 100, Japan

Toshikazu Matsuoka

Department of Applied Science, Tokyo Denki University, 2-2 Kandanishiki-cho, Chiyoda-ku, Tokyo 101, Japan

Shukuji Asakura

Department of Safety Engineering, Yokohama National University, 156 Tokiwadai, Hodogaya-ku, Yokohama 240, Japan

A high sensitivity analytical method to determine nitrate in a solution by use of a NO_x chemiluminescent analyzer was developed through a modification of Cox's original batch reactor methods. A flow sample injection system was used and the acidic reducing solution in the reaction vessel was heated at 100 °C. The detection limit was improved to be 1 ng of NO_3^-/mL for a 5-mL solution sample. Nitric oxide recovery in an acidic solvent was observed to be 100% over the ranges of 55–68 wt % of sulfuric acid and 40–95 wt % of phosphoric acid solutions. The reactive species in the concentrated acidic solution was estimated to be HNO_3 and not NO_3^- or NO_2^+. Atmospheric particulate nitrate and gaseous nitric acid were measured at 1-h intervals with Teflon and polyamide filters using the analytical method studied. It was shown that the apparent total nitrate formation rate was 4.5%/h in a downtown neighborhood in Tokyo in summer.

Particulate nitrate and gaseous nitric acid in ambient air have been of recent concern as atmospheric photochemical reaction products. Moreover, the behavior of these species in the atmosphere is important to understand the fate of NO_x emitted from combustion processes such as internal combustion engines, boilers, incinerators, and so on (*1–7*).

Nitrate collected on a filter has been mostly sensitively analyzed by ion chromatography (*8, 9*) and the Cd-NEDA (Cd reduction/*N*-(1-naphthyl)ethylenediamine) method (*10, 11*). Thermal decomposition of nitrate to nitric oxide was also studied to determine nitrate by Moskowitz (*12*) and Spicer et al. (*13*). Recently, Cox developed highly sensitive analytical methods for nitrate and nitrite in a solution in which they were reduced to nitric oxide and measured by a NO_x chemiluminescent analyzer (*14*). The preparation of a sample is much simplier in his methods compared to other methods (*8–11*) because suspended material and color do not interfere.

In this study, we modified Cox's methods (*14*) to eliminate the influence of impurity in reagents on the detection and to analyze rapidly a large number of samples such as atmospheric nitrates collected on filters. The optimum operating conditions were also investigated. Further, the analytical method was applied to the measurements of atmospheric particulate nitrate and gaseous nitric acid in a short time interval in downtown Tokyo.

EXPERIMENTAL SECTION

Apparatus. A schematic diagram of the analytical system is shown in Figure 1 which is different from Cox's original batch reactor without external heating (*14*). Teflon tubing was used for all gas lines with glassware. High-purity nitrogen gas was used as a carrier at a flow rate of 200 mL/min. The reaction vessel was electrically heated to keep the reducing solution at appropriate temperature. Usually, a 0.5-mL sample was supplied to the reaction vessel by an injector. Nitric oxide produced in the reduction reaction in the vessel was measured with a Beckman Model 952 NO_x chemiluminescent analyzer. The nitric oxide mode of the analyzer was used. Acidic mist was removed by a cold trap consisting of an impinger in an ice water bath. The signal from the NO_x analyzer was processed with a strip chart recorder and an electronic integrator.

Reagents. Quantitative evaluation of samples was obtained by comparison with standards on the basis of peak area. Anhydrous potassium nitrate and sodium nitrite (Wako Pure Chemical) were used to prepare standard solutions of the respective anions. Known concentration of nitric oxide gas (Takachiho Chemical) was also used to calibrate the analytical system. Solutions of reagent grade 4% ferrous ammonium sulfate and 2%

0003-2700/85/0357-0737$01.50/0 © 1985 American Chemical Society

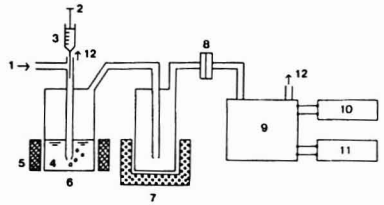


Figure 1. Schematic diagram of analytical system: 1, high-purity nitrogen carrier gas; 2, injector; 3, solution sample; 4, reducing solution; 5, electric heater; 6, reaction vessel; 7, cold trap; 8, Teflon filter; 9, NO_x chemiluminescent analyzer; 10, strip chart recorder; 11, electronic integrator; 12, vent.

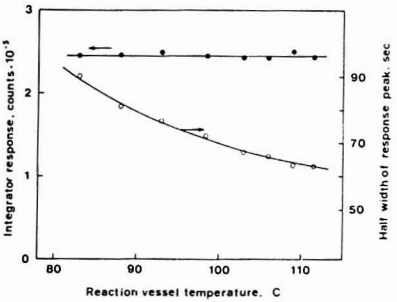


Figure 2. Effect of reaction vessel temperature on response of the analytical system: ●, integrator response; O, half width of response peak on a recorder.

ammonium molybdate in water were prepared for nitrate determination following Cox's original methods (*14*). High-purity water obtained by passing distilled water through an ion exchange column was used. Sulfuric acid or phosphorus acid (Wako Pure Chemical) was added to an equal volume mixture of these solutions to provide the proper reducing conditions as mentioned later whereas 57.6 wt % of sulfuric acid was used as a solvent in Cox's original method.

Air Sampling. The collection of nitrate and nitric acid in the atmosphere was done by pumping ambient air at 20 L/min through a Teflon filter (Sumitomo FP080) and a polyamide filter (Sartorius SM119) with 47 mm diameter in series. The Teflon filter collected particulate nitrate and the polyamide filter collected gaseous nitric acid. Sampling was made in 1-h intervals on the roof of the Tokyo Metropolitan Research Institute for Environmental Protection in the summer of 1982. Extraction of nitrate ion from a filter was done by shaking it with 10 mL of high-purity water for 1 h. As for the Teflon filter, 0.5 mL of ethanol was impregnated before the addition of water. Extracted sample solutions were analyzed under the optimum conditions mentioned later.

RESULTS AND DISCUSSION

Modification of Cox's Original Methods. The effect of the reaction vessel temperature on the analytical response is shown in Figure 2. The reducing solution was electrically heated to accelerate the reduction reaction of nitrate to nitric oxide. In this case, sulfuric acid in the reducing solution was set to be 60 wt %. The nitric oxide recovery was found to be 100% over all the temperature range. With the increase of the temperature, the half width of the response peak which closely related to the reduction rate in the vessel was observed to be smaller, which means that more rapid response was obtained. However, the evaporation of the solution also became too rapid. Therefore, the optimum vessel temperature

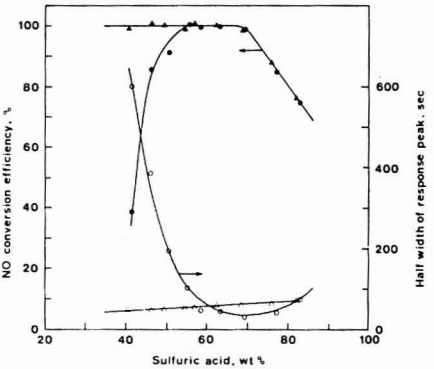


Figure 3. Effect of sulfuric acid concentration in reducing solution on analytical response; ●, conversion efficiency of supplied nitrate to nitric oxide; O, half width of nitrate response peak; ▲, conversion efficiency of supplied nitrite to nitric oxide; Δ, half width of nitrite response peak.

was concluded to be 100 °C in this experiment.

Further, various amounts of nitrate solution, nitrite solution, and niric oxide gas were injected into the reaction vessel to calibrate the analytical system. The consistency among their responses was observed as a good linear calibration curve between 1 and 1000 ng of NO_3^-/mL through an origin with a high correlation coefficient, 0.9997. In this study, after the base line response caused by impurity in the reducing solution was well minimized, a solution sample was injected into the flow reaction vessel shown in Figure 1. Therefore, the influence of the impurity on the response could be eliminated completely. The detection limit for nitrate was 1 ng of NO_3^-/mL for a 5-mL solution sample which is more sensitive by a factor of about 5 and 100 when compared with Cox's original batch basis methods (*14*) and ion chromatography by Mulik et al. (*9*), respectively. Moreover, a sample could be supplied by an injector to our flow system without changing reducing solution on every sample injection. It resulted in more rapid operation in the analysis. The measurement time per sample was reduced to about 3 min. It is an additional advantage for aerosol analysis that this method is free from the interference of ethanol in the concentration of 5%. This feature is useful to extract aerosol components on a non-hydrophilic Teflon filter into a water solution.

Effect of Acid Concentration on Nitrate Conversion to Nitric Oxide. Figure 3 shows the effect of sulfuric acid concentration in the reducing solution on the conversion efficiencies of nitrate and nitrite to nitric oxide. It was found that supplied nitrate was converted to nitric oxide by 100% over the range of 55–68 wt % of sulfuric acid concentration. The reduction rates shown by the half width of the response peak were retarded in the range of sulfuric acid concentration less than 55 wt %. High and low sulfuric acid concentrations seemed to disturb the reduction of nitrate to nitric oxide. Bayliss et al. (*15*) studied the distribution of nitrate species which consisted of nitrate ion (NO_3^-), nitric acid (HNO_3), and nitronium ion (NO_2^+) in concentrated sulfuric acid solutions by spectrophotometry. Their results suggest that a reactive species in the reduction is nitric acid (HNO_3) which was observed to be a dominant species in the corresponding sulfuric acid concentration range (*15*) although nitronium ion is a reactive species on aromatics nitration (*16*). On the other hand, the reduction efficiency of nitrite was observed to be 100% except in the range of more than 68 wt % of sulfuric

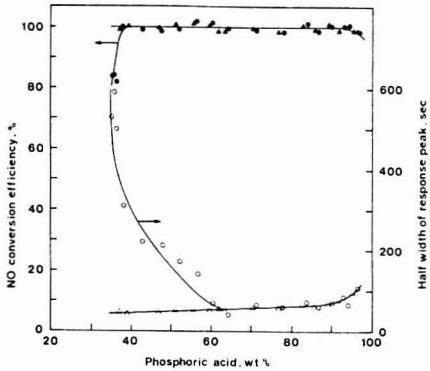


Figure 4. Effect of phosphoric acid concentration in reducing solution on analytical response: ●, conversion efficiency of supplied nitrate to nitric oxide; O, half width of nitrate response peak; ▲, conversion efficiency of supplied nitrite to nitric oxide; △, half width of nitrite response peak.

acid concentration. The reduction rate is rapid enough over almost all the concentration range with a slightly retarded trend for concentrations of more than 68 wt %.

Figure 4 shows the reduction efficiencies of nitrate and nitrite to nitric oxide by using phosphoric acid as a solvent. A comparison of Figure 3 and Figure 4 indicates that the reactivity characteristics in the sulfuric acid and phosphoric acid systems are qualitatively similar. One hundred percent of nitric oxide recovery in phosphoric acid solution was observed over the wider range of 40–95 wt %. The reduction rate became slower in the ranges of less than 63 wt % and more than 90 wt % of phosphoric acid concentration. These results could be explained by the fact that nitronium ion exists over a more narrow range in phosphoric acid due to lower hydrogen ion activity in phosphoric acid than in sulfuric acid (*17*). Therefore, nitric acid which is considered to be reactive in the reduction as mentioned before exists over a wider range in the phosphoric acid concentration.

In summary, we obtained a wider reactive range on the reduction of nitrate by using phosphoric acid as a solvent in comparison with sulfuric acid. As for a routine analysis, phosphoric acid solvent can be concluded to be more useful because a greater number of sample injections could be done with 100% of nitric oxide recovery. Especially, 90 wt % of phosphoric acid is recommended as a solvent for the start condition of a routine analysis.

Ambient Nitrate Measurements. The results of the application of the analytical method to the measurements of particulate nitrate and gaseous nitric acid in ambient air are shown in Figure 5 on the short time average basis with other related gaseous and meterological data which were obtained through a continuous air quality monitoring system by the Tokyo Metropolitan Government. The separation of nitrate and nitrite in the particulate was not made because the nitrite amount could be considered negligibly small as shown by Spicer (*1*). On the first day, August 24, 1982, about 3 m/s of south wind (typical seasonal wind in the neighborhood of Tokyo in summer) blew continuously through all the daytime. The values of pollutants as a whole represented low pollution levels.

However, on the second day, August 25, 1982, about 1 m/s of weak north wind blow until about 11:00 JST and then shifted to 2–3 m/s of south wind. The particulate nitrate and gaseous nitric acid formation seemed to be based on photo-

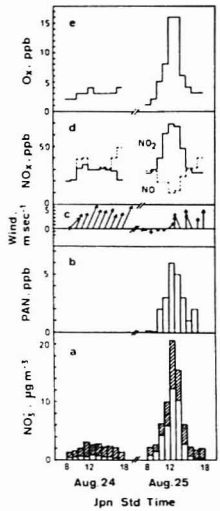


Figure 5. Diurnal pattern of nitrogenous compounds in ambient air in downtown Tokyo in summer: a, particulate nitrate (hatched) and gaseous nitric acid (nonhatched); b, PAN by gas chromatography (courtesy of Masataka Sofuku of the Tokyo Metropolitan Research Institute for Environmental Protection); c, wind speed and direction (The ordinate shows the magnitude of a wind speed. The direction of a arrow shows the direction of wind).; d, nitrogen dioxide (solid line) and nitric oxide (dashed line) by Saltzman method; e, oxidant by KI method (c–e, courtesy of Air Quality Monitoring Section of the Tokyo Metropolitan Government).

chemical reactions because PAN (peroxyacetylnitrate) and oxidant concentrations behaved similarily with them. Moreover, NO_2 values were observed to be inversely correlated with NO values. This is considered to be due to the consumption of NO by O_3 to form NO_2 according to $NO + O_3 = NO_2 + O_2$. Thus, the measured oxidant concentration became low because O_3 was simultaneously consumed.

Nitrogenous species balance in the field, which have not been completely evaluated so far because of lack of measurement of particulate nitrate (*18*) or gaseous nitric acid (*9*), could be examined for the results given in Figure 5 by consideration of the following nitrogenous gas–nitrate distribution factor as a modification of the gas–particle distribution factor by Grosjean and Friedlander (*20*):

$$Fn = \frac{\text{PAN} + \text{particulate } NO_3^- + \text{gaseous } NO_3^-}{NO + NO_2 + \text{PAN} + \text{particulate } NO_3^- + \text{gaseous } NO_3^-}$$

In this case, terms of PAN and gaseous NO_3^- (which refers to gaseous nitric acid) are added because they are also nitrogenous species converted from NO_x in the atmosphere. The distribution factors on our ambient measurements were found to be 1.71%, which is similar to an average value of 1.34% through the first day, during 9:00–10:00 JST and 15.1% during 12:00–13:00 JST on the second day. It is considered that under these meterological conditions, air pollutants were blown to Tokyo Bay until about 11:00 JST and then carried back to our sampling site which is located nearby without the significant addition of pollutants because sources in the bay were negligible. Thus, the apparent total nitrate formation rate is evaluated to be 4.5 %/h as an upper limit from the gradient

of Fn between 9:00–10:00 and 12:00–13:00 ignoring NO_x removal rate in the neighborhood of downtown Tokyo in summer. This is considered to be comparable to nitrate formation rates evaluated in the plume chemistry by Meagher et al. (*4*), Richars et al. (*5*), and Forrest et al. (*6*).

In this case, the volatility of NH_4NO_3 (*21–23*) and the reaction of sulfuric acid with nitrate (*24*), which have been discussed as artifact nitrate terms, might result in the decrease of particulate nitrate measurement on a Teflon filter and the increase of nitric acid measurement on a polyamide filter. However, shorter time interval sampling would suppress the artifact effects to the greater extent because it would decrease the contact time of sampled nitrate with ambient sulfuric acid and increase the possibility of keeping the equilibrium with respect to NH_4NO_3 through the sampling time. The 1-h interval sampling in this study is thought to help avoid artifact production although 2 h to 1 days inverval samplings have been made so far in the low volume filer sampling (*25–28*).

Registry No. NO_3^-, 14797-55-8.

LITERATURE CITED

(1) Spicer, C. W. *Atmos. Environ.* **1977**, *11*, 1089–1097.
(2) Orel, A. E.; Seinfeld, J. H. *Environ. Sci. Technol.* **1977**, *11*, 1000–1007.
(3) Appel, B. E.; Kothny, E. L.; Hoffer, E. M.; Hidy, G. M.; Wesolowski, J. J. *Environ. Sci. Technol.* **1978**, *12*, 418–425.
(4) Meagher, J. F.; Stockburger, L., III; Bonanno, R. J.; Bailey, E. M.; Luria, M. *Atmos. Environ.* **1981**, *15*, 749–762.
(5) Richards, L. W.; Andersen, J. A.; Blumenthal, D. L.; Brandt, A. A. *Atmos. Environ.* **1981**, *15*, 2111–2134.
(6) Forrest, J.; Garber, R.; Newman, L. *Atmos. Environ.* **1981**, *15*, 2273–2282.
(7) Spicer, C. W.; Howes, J. E., Jr.; Bishop, T. A.; Arnold, L. H.; Stevens, R. K. *Atmos. Environ.* **1982**, *16*, 1487–1500.
(8) Small, H.; Stevens, T. S.; Bauman, W. C. *Anal. Chem.* **1975**, *47*, 1801–1809.
(9) Mulik, J.; Puckett, D.; Williams, D.; Sawicki, W. E. *Anal. Lett.* **1976**, *9*, 653–663.
(10) Morris, A. W.; Riley, J. P. *Anal. Chim. Acta* **1963**, *29*, 272–283.
(11) Sandberg, J. S.; Levaggi, D. A.; Demandel, R. E.; Siu, W. J. *Air Pollut. Control Assoc.* **1976**, *26*, 559–564.
(12) Moskowitz, A. H. "Particle Size Distribution of Nitrate Aerosols in the Los Angeles Air Basin"; EPA/600/3-77/053, 1977.
(13) Spicer, C. W.; Schumaker, P. M.; Kouyoumjian, J. A.; Joseph, D. W. "Sampling Methodology for Atmospheric Particulate Nitrates"; EPA/600/2-78/367, 1978.
(14) Cox, R. D. *Anal. Chem.* **1980**, *52*, 332–335.
(15) Bayliss, N. S.; Watts, D. W. *Aust. J. Chem.* **1963**, *16*, 943–946.
(16) Ingold, C. K.; Millen, D. J.; Poole, H. G. *J. Chem. Soc.* **1959**, 2576–2587.
(17) Bayliss, N. S.; Watts, D. W. *Aust. J. Chem.* **1956**, *9*, 319–329.
(18) Spicer, C. W. Reaction of NOx in Smog Chambers and Urban Atmospheres, Formation and Fate of Atmospheric Nitrates, Workshop Proceedings; Barnes, H. M., Ed.; EPA-600/9-81-025, 1981.
(19) Spicer, C. W.; Joseph, D. W.; Ward, G. F. "Studies of NOx reactions and O_3 Transport in Southern California-Fall, 1976"; PB 83-200 360, 1983.
(20) Grosjean, D.; Friedlander, S. K. *J. Air Pollut. Control Assoc.* **1975**, *25*, 1038–1044.
(21) Kadowaki, S. *Atmos. Environ.* **1977**, *11*, 671–675.
(22) Stelson, A. W.; Friedlander, S. K.; Seinfeld, J. H. *Atmos. Environ.* **1979**, *13*, 369–371.
(23) Yoshizumi, K.; Okita, T. *J. Air Pollut. Control Assoc.* **1983**, *33*, 224–226.
(24) Harker, A. B.; Richards, L. W.; Clark, W. E. *Atmos. Environ.* **1977**, *11*, 87–91.
(25) Okita, T.; Morimoto, S.; Izawa, M. *Atmos. Environ.* **1976**, *10*, 1085–1089.
(26) Forrest, J.; Tanner, R. L.; Spandau, D.; D'Ottavio, T.; Newman, L. *Atmos. Environ.* **1980**, *14*, 137–144.
(27) Grennfelt, P. *Atmos. Environ.* **1980**, *14*, 311–316.
(28) Cadle, S. H.; Countess, R. J.; Kelly, N. A. *Atmos. Environ.* **1982**, *16*, 2501–2506.

RECEIVED for review September 26, 1984. Accepted November 19, 1984.

Estimation of Acidity in Rainfall by Electrical Conductivity

Robert A. Stairs* and Jaleh Semmler[1]

Department of Chemistry, Trent University, Peterborough, Ontario, Canada K9J 7B8

Measurement of electrical conductivity of a sample of rain, or other natural freshwater, and of the same sample after passage through a bed of ion exchange resin in H^+ form, allows the calculation of acidity (or alkalinity) and salinity. Results for 64 samples of rain, compared with those based on titration, are as follows: for acidity $C(\kappa) = -0.0070 + 1.0809C(t)$, ±0.0135, from −0.05 (alkaline) to 0.160 mequiv L^{-1}; for salinity, $C(\kappa) = 0.0017 + 0.9996C(t)$, ±0.0191, from zero to 0.330 mequiv L^{-1}. The method is suitable for automation.

The method described here was conceived in the context of an acid precipitation study. It is, however, adaptable with caution to the proximate analysis of freshwaters generally. The principle is simple. All ions contribute to the conductivity of a solution in direct proportion to their concentrations in equivalents per unit volume and their equivalent conductances. A solution containing a single ionic solute, such as hydrochloric acid, requires only a single conductance measurement for analysis. Two solutes, for instance HCl plus NaCl, require two measurements. The second measurement is performed after the solution has been allowed to pass through a column of a strongly acidic, cation exchange resin, which will replace the sodium ions with hydrogen ions.

The two conductances should conform to eq 1a,b where κ_1

$$\kappa_1 = \Lambda_a C_a + \Lambda_s C_s \quad (1a)$$

$$\kappa_2 = \Lambda_a C_a + \Lambda_a C_s \quad (1b)$$

and κ_2 are the measured conductances, Λ_a and Λ_s the equivalent conductances of HCl and NaCl, and C_a and C_s the corresponding concentrations. The values of Λ_a and Λ_s should be appropriate to the conditions (temperature and concentration). If the solutions are sufficiently dilute, as rainwater may be expected to be, the limiting values $\Lambda°$ may be used without serious error. They are obtained from the single-ion values $\lambda°_i$, representative examples of which are listed in Table I (*1*). If correction is necessary, a brief iteration may be used, with Λ a suitable function of the ionic strength.

Rainwater usually contains appreciable amounts of an assortment of ions: Ca^{2+}, Mg^{2+}, NH_4^+, K^+, Na^+, SO_4^{2-}, NO_3^-, Cl^-, and H^+ or HCO_3^- (not both), as well as CO_2. The value of $\lambda°$ for H^+ is uniquely large. Those for the other cations cluster around 0.062 (±0.011) S cm^{-2} $mequiv^{-1}$, and the anions (except OH^- and HCO_3^-) are similarly clustered, around 0.076 (±0.005). This leads to the expectation that treatment of

[1] Present address: Department of Chemistry, University of Waterloo, Waterloo, Ontario, Canada N2L 3G1.

0003-2700/85/0357-0740$01.50/0 © 1985 American Chemical Society

Table I. Ions Present in "Representative Rain":[a] Concentrations and Limiting Equivalent Conductances

ion	C_i, equiv L^{-1}	$\lambda°_i$,[b] S cm^{-2} $equiv^{-1}$	ion	C_i, equiv L^{-1}	$\lambda°_i$,[b] S cm^{-2} $equiv^{-1}$
H^+	0.067 ± 0.005	0.3499	OH^-		0.1976
Na^+	0.004 ± 0.001	0.0502	SO_4^{2-}	0.067 ± 0.005	0.0800
K^+	0.001 ± 0.001	0.0735	NO_3^-	0.030 ± 0.003	0.0714
NH_4^+	0.023 ± 0.002	0.0734	Cl^-	0.005 ± 0.001	0.0764
Ca^{2+}	0.010 ± 0.001	0.0595	HCO_3^-		0.0445
Mg^{2+}	0.003 ± 0.001	0.0531			
"mean cation"[c]		0.0663 ± 0.0030	"mean anion"[c]		0.0774 ± 0.0062

[a] Eastern Ontario, 1981. From the Acid Precipitation in Ontario Survey (3). [b] Conventional values (1) divided by 1000. Temperature 25 °C. [c] "Mean cation" and "mean anion" values of $\lambda°$ are means weighted according to the relative concentrations of the individual ions.

rainwater in the manner described above for NaCl–HCl solutions should yield conductances that could be used to obtain estimates of the acidity C_a and the salinity C_s (defined as the total concentration of all neutral salts, in equiv L^{-1}) through equations (1a,b) with suitable mean values of Λ_a and Λ_s. The value of Λ_s is calculated from $\lambda°$ for H^+, combined with a "mean anion" value obtained by weighting the individual $\lambda°$ values according to their expected relative concentrations. Λ_a is similarly obtained from the "mean cation" and "mean anion" values. The large value of $\lambda°$ for H^+ ensures that Λ_a and Λ_s will differ by much more than their uncertainties.

Rainfall in the Peterborough area is usually slightly acidic (Table I). Occasionally, however, it is alkaline. The method described above would yield, in these cases, a false indication of acidity. The required equations are then different. Assume a salinity C_s as before, and an alkalinity C_b due to bicarbonate. Treatment with the acid resin will convert the salt to acid as before, and the bicarbonate will be converted to CO_2, which does not contribute to the conductance. The equations are now

$$\kappa_1 = \Lambda_s C_s + \Lambda_b C_b \quad (2a)$$

$$\kappa_2 = \Lambda_a C_s \quad (2b)$$

where the new constant Λ_b is the sum of $\lambda°$ for HCO_3^- and the "mean cation" value, as above.

In the laboratory, the choice of which pair of equations to use is easily made on the basis of a single pH measurement, but the intention is to use this method as the basis of an automatic device. It should record rain acidity (or alkalinity) and salinity, and either transmit the data in real time to a readout device or store the data for later retrieval. The choice may be made on the basis of a third conductance, measured after passage of a separate sample over a strongly basic anion exchange resin in bicarbonate form. In an acidic sample, acid will be removed as CO_2 and salt converted to bicarbonate. In an alkaline sample, both salts and bicarbonate appear as bicarbonate. The resulting conductances will be

(acidic case) $$\kappa_3 = \Lambda_b C_s \quad (3a)$$

(basic case) $$\kappa_3 = \Lambda_b(C_s + C_b) \quad (3b)$$

where Λ_b is as defined above. Discrimination is then accomplished through the function defined by

$$q = \frac{\kappa_3 \Lambda_a}{\kappa_2 \Lambda_b} \quad (4)$$

From eq 1b and 3a, appropriate to the acidic case, it is seen that

$$q = \frac{C_s}{C_a + C_s} < 1 \quad (5a)$$

but from eq 2b and 3b, for the basic case

$$q = \frac{C_s + C_b}{C_s} > 1 \quad (5b)$$

Table II. Model Calculations: Effect of CO_2, with C_s = 0.0200 mequiv L^{-1} and C_{CO_2} = 0.0300 mmol L^{-1}

assumed C_s, mequiv L^{-1}	calculated $\hat{C}_a$, mequiv L^{-1}	calculated $\hat{C}_s$, mequiv L^{-1}
0.1000	0.1002	0.0198
0.0800	0.0802	0.0198
0.0600	0.0603	0.0197
0.0400	0.0404	0.0196
0.0200	0.0208	0.0192
0	0.0045	0.0155

Both in the laboratory and in an automatic device in the field, then, the method involves measurement of three conductances: untreated, acid treated, and base treated by resins. The first and second are the basis of calculation of either acidity and salinity or alkalinity and salinity, as determined by the second and third, through the function q. At present this is being done in the laboratory digitally, using an HP-41CV programmable calculator. For the field device, both analogue and digital approaches are being explored.

The effect of the omnipresent carbon dioxide was explored in a model calculation. First the specific conductances were calculated, using eq 1a and 1b with the addition of terms for the contribution of that fraction, α, of the CO_2 which has ionized

$$\kappa_1 = \Lambda_a C_a + \Lambda_s C_s + \alpha \Lambda_{CO_2} C_{CO_2} \quad (6a)$$

$$\kappa_2 = \Lambda_a(C_a + C_s) + \alpha' \Lambda_{CO_2} C_{CO_2} \quad (6b)$$

where

$$\alpha = \frac{-(K_1 + C_a) - ((K_1 + C_a)^2 + 4K_1 C_{CO_2})^{1/2}}{2C_{CO_2}}$$

α' is similar, but with C_a replaced by $C_a + C_s$, and K_1 is the first dissociation constant for aqueous CO_2.

Then the reverse calculation was performed by use of the unmodified eq 1a and 1b. The results of a typical calculation are summarized in Table II, which compares the assumed and recalculated values of C_s and C_a, for a series of solutions with C_{CO_2} = 0.03 mmol L^{-1}, C_s = 0.02 mequiv L^{-1}, and several values of C_a. The effect is small except very close to zero acidity. A similar calculation for alkaline samples produced a similar result. Acids less weak than CO_2, however, can cause more serious error.

EXPERIMENTAL SECTION

Rain was collected in plastic garbage bags supported in laundry baskets, at two locations on the roof of the laboratory building and one in the fenced enclosure of the Trent University weather station.

Titration was carried out with 0.01 M sodium hydroxide on 500-mL samples (when possible) using an Orion Mod.701A pH meter with 91-01 glass and Ag/AgCl reference electrodes. The end points were located by using a simplified Gran plot (2): antilog_{10} (4 − pH) and antilog_{10} (pH − 10) were plotted against

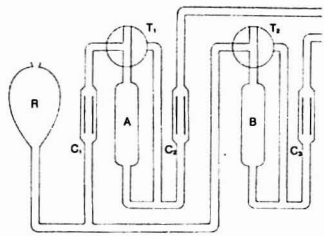


Figure 1. Conductance apparatus (schematic).

volume of NaOH added. The first function yielded a falling straight line that was extrapolated to intersect the volume axis at v_1. The second function yielded a rising straight line that was extrapolated backward to intersect the axis at v_2. A second sample, of similar size, was first treated by passage through a bed of strongly acid cation exchanger and then similarly titrated, yielding the volumes v_3 and v_4.

On interpretation of the results, two cases were distinguished:

(a) Acidic samples (initial pH <5.6) gave a value of v_1 clearly nonzero. This value was taken as a measure of the concentration (in equivalents per liter) of total strong acids ($HNO_3 + H_2SO_4$). Since the resin treatment converts salts of strong acids to the free acids, v_3 represents acids and salts. The differences $v_2 - v_1$ and $v_4 - v_3$ were averaged (unless they were very different) and taken to represent the concentration of dissolved CO_2. (Though this was not of particular concern, it was noted that it remained relatively constant in all samples, at 0.025 ± 0.005 mmol L^{-1}.)

(b) Alkaline samples (initial pH >5.6) gave no straight line portion in the graph of antilog (4 − pH) vs. volume. The value of v_1 was taken to be zero. Carbon dioxide was measured by v_2. The first end point in the second titration, v_3, was taken as representing salts of strong acids, and $v_4 - v_2 - v_3$ as the carbon dioxide arising from bicarbonate originally present, i.e., the bicarbonate alkalinity. (Rain samples, being exposed to atmospheric CO_2, can have no carbonate or hydroxide alkalinity.) Multiplication of these volumes by C_b/v_s, where C_b is the concentration of the titrant NaOH in millimoles per liter and v_s the sample volume, yields acidity (or alkalinity) and salinity in milliequivalents per liter and carbon dioxide concentration in millimoles per liter (because it was only titrated to bicarbonate at the second end point). It is not possible to express the acidity or salinity in moles, owing to the mixed valences of the ionic species present.

The conductance measurements were carried out by using small flow-through cells with bright platinum electrodes, using a bridge assembled from a Leeds and Northrup students' potentiometer and a decade resistance box, with a square-wave oscillator at ca. 1 kHz as source and an oscilloscope as null-point detector. The measurements were done at 25.0 °C. The experimental arrangement is shown schematically in Figure 1.

The rain sample, about 200 mL, was poured into the reservoir R. From there, portions of it passed slowly (at about 5 mL min^{-1}) through the two paths: (a) through the cell C_1, the acid resin column A, the cell C_2 and to waste, and (b) through the basic resin column B, the cell C_3, and to waste. The conductances κ_1, κ_2, and κ_3 were measured repeatedly during the slow passage of solution, and the results averaged.

Calibration was effected by turning the two taps T_1 and T_2, so that the resin columns were bypassed, and passing 0.0100 M KCl solution through all the cells.

Chemicals used were analytical reagent grade. Resins used were Dowex-50W(H^+) (strongly acidic) and Rexyn 201 (OH) (strongly basic). Water was purified by reverse osmosis, and polished by means of the Gelman "Water I".

RESULTS

Rainfall Analyses. During the period of 28 May 1982 to 8 September 1983, 64 samples of rain have been analyzed using both methods.

The pH titration method using Gran's plot, or a version of it, is becoming standard in acid precipitation analysis, so the results from this method were taken as "true". Portions of the same samples were also analyzed as described above, i.e., by conductance before and after treatment with strongly acidic resin. Minor rearrangement of equations (1) yields

$$\kappa_2 = \Lambda_a(C_a + C_s)$$
$$\kappa_2 - \kappa_1 = (\Lambda_a - \Lambda_s)C_s \qquad (7)$$

Accordingly κ_2 was plotted against $C_a + C_s$ (from the titration results) and $\kappa_2 - \kappa_1$ vs. C_s. The slopes yielded estimates of the effective values Λ_a and Λ_s, which were compared with values calculated for "representative rain". The composition of this "rain" is shown in Table I, and represents analyses during 1981 of rain from four sites surrounding Peterborough within 200 km, roughly averaged (3). Table III shows the predicted and empirical values of Λ_a and Λ_s, with the predicted value of Λ_b. Too few examples of alkaline rain were encountered, and too few determinations of κ_3 have been made, to allow a reliable estimate of Λ_b to be made from the data.

The same data were fitted to eq 8, where $C(\kappa)$ is the concentration of acid or salt calculated from the conductance data and $C(t)$ is the corresponding concentration obtained by titration. Table IV shows the values of a and b obtained from the fit of 64 points. The "predicted" values of Λ_a, Λ_b, and Λ_s were used. The standard error of estimate (defined in a note in the table) and the standard errors of the constants are also shown, with the ranges of acidity (alkalinity) and salinity covered by the measurements. No obvious bias was noted within the precision of the measurements.

$$C(\kappa) = a + bC(t) \qquad (8)$$

The precision, as measured by the standard error of estimate, was not particularly good, being in the case of each parameter about 15% of a typical value. As the basis for the design of a low-cost, automatic device, it should nevertheless provide a means both of monitoring rainfall in one locality for acidity and of creating a network of data-collecting stations that need not be visited after every rainfall. The present need is not for highly precise local data, but for a finer array of points at which time-resolved data are obtained. With such an array, it should be possible to make more reliable analyses of the growth and movement of storms that carry unusual acid loads.

Table III. Predicted and Empirical Values of Mean Equivalent Conductances[a]

	predicted	empirical
Λ_a	0.427 ± 0.003	0.456 ± 0.030
Λ_s	0.144 ± 0.007	0.150 ± 0.030
Λ_b	0.111 ± 0.006	(0.14 ± 0.07)

[a] Units are S cm^{-2} $mequiv^{-1}$.

Table IV. Correlation of Conductance and Titration Results[a]

	acidity[b]	salinity
a	−0.0070 ± 0.0025	0.0017 ± 0.0040
b	1.0809 ± 0.0380	0.9996 ± 0.0361
s[c]	0.0135	0.0191
range	−0.0500 to 0.1600	0.0050 to 0.3300

[a] Fit of eq 8 for acidity and for salinity for 64 rain samples. All concentrations in mequiv L^{-1}. [b] Negative acidity = alkalinity (bicarbonate). [c] Standard error of estimate, $s = [\sum_i (C_i(K) - \hat{C}_i(K))^2/(n-2)]^{1/2}$.

ACKNOWLEDGMENT

The assistance of Luna Ho, Jeffrey Hudson, Ligia Sanchez and Lorie Windrem is acknowledged. The manuscript was typed by Dorothy Sharpe.

Registry No. Water, 7732-18-5.

LITERATURE CITED

(1) Parsons, R. "Handbook of Electrochemical Constants"; Butterworth: London, and Academic Press: New York, 1959; p 85.
(2) "Acid Precipitation in Ontario Study", ARB-11-82 ARSP; Air Resources Branch, Ontario Ministry of the Environment: Toronto, 1982.
(3) Galloway, J. N.; Crosby, B. J., Jr.; Likens, G. E. *Limnol. Oceanogr.* **1979**, *24* (6), 1161–1165.

RECEIVED for review September 4, 1984. Accepted November 19, 1984. This research was supported by the Air Resources Branch of the Ontario Ministry of the Environment.

Hydration of Nitric Acid and Its Collection in the Atmosphere by Diffusion Denuders

Delbert J. Eatough,* Vernon F. White, and Lee D. Hansen

Thermochemical Institute and Department of Chemistry, Brigham Young University, Provo, Utah 84602

Norman L. Eatough

Department of Chemistry, California State Polytechnical University, San Luis Obispo, California 93407

Elizabeth C. Ellis

Southern California Edison, Rosemead, California 91770

The collection and determination of gas-phase nitric acid by use of denuder tubes are dependent either on the direct measurement of nitric acid collected in a denuder or on the analysis of total inorganic nitrate with and without prior removal of gas-phase nitrate by a denuder. In both cases, the amount of nitric acid predicted to be collected by the denuder is dependent on the diffusion coefficient used to describe the collection of nitric acid by the denuder. It has been assumed in past studies that the species present in the atmosphere and collected by the denuder is $HNO_3(g)$. Both field and laboratory studies with tungstic acid and nylon denuders show that the species present and collected is actually $HNO_3 \cdot x H_2O(g)$, where the value of x is dependent on the atmospheric water concentration. Thus, the diffusion coefficient is also dependent on the atmospheric water concentration. Gas-phase ammonia is also shown to exist as the monohydrate at atmospheric water concentrations. In addition, the collection efficiency of tungstic acid diffusion denuders for hydrated nitric acid is affected by the atmospheric water concentration. Both the hydration of nitric acid and the apparent hydration of the denuder surface must be taken into account if a tungstic acid denuder is used to collect gas phase nitric acid.

The determination of gas-phase nitric acid in the atmosphere is important to the understanding of the contribution of NO_x emissions to rain or fog chemistry and to visibility. It is known from the results of both laboratory and ambient studies that the collection of gas-phase nitric acid is complicated by shifts in the equilibria of volatile nitrate compounds as well as by the release of $HNO_3(g)$ from aerosols acidified during sampling. Shifts in the particulate nitrate–$HNO_3(g)$ equilibrium can occur if either the concentrations of gas-phase nitric acid, ammonia, and/or water are altered or the temperature or pressure of the airstream is changed during sampling. The equilibrium between $HNO_3(g)$ and $NH_4NO_3(s)$ can result in ambient concentrations of $HNO_3(g)$ of several parts per billion (*1*). Removal of either $NH_3(g)$ or $HNO_3(g)$ by a denuder results in volatilization of both $NH_3(g)$ and $HNO_3(g)$ from $NH_4NO_3(s)$ until equilibrium is again achieved. In addition, the collection of aerosols on a filter can result in particle–particle interactions which lead to the release of HNO_3 from aerosols during sampling by reactions such as

$$NaNO_3(s) + H_2SO_4(l) = NaHSO_4(s) + HNO_3(g) \quad (1)$$

Two techniques have been used to monitor gas-phase nitric acid in the atmosphere on a real-time basis. These are the specific detection of $HNO_3(g)$ using Fourier transform infrared spectrometry (*2*, *3*) and the measurement of $HNO_3(g)$ by difference as NO(g) using chemiluminescence after reduction of $NO_2(g)$ and $HNO_3(g)$ with and without removal of $HNO_3(g)$ (*2*, *4*). The chemiluminescent technique requires removal of particulate matter from the airstream prior to the measurement of $HNO_3(g)$ and the IR method requires heating and/or reduction of the pressure of the sampled airstream containing both gases and particles in the measurement chamber. Thus, each of these previously deployed real-time measurement schemes has the problem of artifact formation of $HNO_3(g)$ during the measurement.

There are two general approaches which have been used to sample gas-phase nitric acid in filter sampling trains. Both methods allow for the collection of total inorganic gaseous and aerosol nitrate. However, both techniques have sampling artifact problems caused by the separation of gaseous and aerosol nitrate during sampling.

The first approach measures gas-phase nitric acid by first removing particulate matter on a filter which has been shown not to collect $HNO_3(g)$ and then collecting nitric acid gas on a suitable stack of scrubbing filters. Filters such as Teflon membrane (*5*) or acid washed quartz (*6*) do not collect gas-phase nitric acid or nitrogen oxides. Nylon (*7*, *8*) or NaCl impregnated filters (*9*) are effective for the collection of nitric acid without interference from the absorption of nitrogen oxides. However, Forrest et al. (*6*, *9*) have shown that loss of $HNO_3(g)$ from particles can occur due to reactions similar to that in eq 1 and, in addition, they have demonstrated that volatilization of $NH_4NO_3(s)$ can occur during high volume sampling. Both of these effects are also present during low volume collection of nitrate (*10*, *11*). Similar loss of $HNO_3(g)$ from $NH_4NO_3(s)$ has been demonstrated in laboratory ex-

0003-2700/85/0357-0743$01.50/0 © 1985 American Chemical Society

periments (*12*) by passing clean air through filters containing NH_4NO_3(s). Appel et al. (*12*) have also shown that absorption of HNO_3(g) can occur on collected particulate matter exposed to HNO_3(g) in the laboratory.

The second approach to the collection of gas-phase nitric acid and aerosol inorganic nitrate uses a denuder to scrub nitric acid from the gas phase prior to sampling of the particulate matter. The particulate nitrate is collected with a filter pack system containing a filter to collect aerosols and a backup filter to remove any HNO_3(g) evolved from the collected aerosols. The HNO_3(g) concentration is determined either by analysis of the filters following the denuder tube for total inorganic nitrate and comparison with the total inorganic nitrate collected on a filter pack which is not preceded by a denuder (the denuder difference experiment) or analysis of the denuder tube for nitrate. The denuder tube methods are dependent on the displacement of the equilibrium between aerosol nitrate compounds and gas-phase nitric acid being slow compared to the sample travel time through the denuder. It has been shown that the expected diffusion coefficient, 0.12 cm^2/s, can be obtained for collection of HNO_3(g) in dry laboratory air using either nylon (*13*) or tungstic acid (*14*) denuders. However, in experiments in the field, the expected deposition pattern in a diffusion denuder is often not obtained (*13, 14*). This has been attributed to collection of HNO_3 from aerosol due to shifts in aerosol gas equilibria during the passage of the sampled air stream through the denuder (*13*), to possible association reactions of HNO_3(g) in the atmosphere (*14*), and to the collection of NO_x (*15*) or possibly other nitrogen compounds (*14*) by the denuder. Data obtained to date disagree on the importance of the collection of NO_x by a tungstic acid denuder (*14, 15*). Shaw et al. (*7*) have reported data which suggest that sampling with denuders does not result in volatilization of particulate nitrate during flow through the denuder. However, this conclusion is based on comparison of total collected gaseous and particulate nitrate under several different sampling configurations and not on analysis of the collection profile of HNO_3(g) in the denuder. Their data do show loss of particulate nitrate from the filter during sampling.

Experiments with denuder tube collection of nitrate from laboratory generated ammonium nitrate aerosols have been reported by the groups at Brookhaven (*6*) and at the University of Washington (*16*). In these studies, nitrate loss from aerosols during passage through a denuder was measured as the difference in either total nitrate or total number and size distribution of particles entering and exiting the denuder. Actual deposition of nitrate in the denuder was not measured. These results may be misleading because, since the loss of HNO_3(g) from the aerosol involves a surface reaction, the high ratio of total to surface nitrate in laboratory generated aerosols would be expected to result in loss of only a small percentage of the total aerosol nitrate during passage through the denuder. The nitrate in ambient aerosols would be expected to be mainly at the surface of the particulate matter and hence a much larger percentage of the total aerosol nitrate could be lost to the denuder.

We report here the results of field and laboratory experiments with both tungstic acid and nylon denuders which indicate that there is no volatilization of nitric acid from aerosols during sampling of a gas–aerosol mixture. Furthermore, the data indicate that the species sampled as gas-phase nitric acid is $HNO_3 \cdot xH_2O$. This observation reconciles the discrepancies in the literature with respect to the collection of gas-phase nitric acid by denuders since the interpretation of denuder data is dependent on the diffusion coefficient assumed. The diffusion coefficient for the hydrated species which exists in the atmosphere is lower than that for HNO_3(g), the species previously assumed to be present. The data also indicate that the collection efficiency of the tungstic acid denuder for the hydrated gas-phase nitric acid (and hence the apparent diffusion coefficient) is decreased with increasing atmospheric water concentration.

EXPERIMENTAL SECTION

Tungstic Acid Denuder Tube Preparation. Tungstic acid denuder tubes were prepared as short sections which could be individually analyzed for nitrate. Three foot lengths of heavy wall glass tubing with an inside diameter of 0.56 ± 0.01 cm were used to make the denuder sections. The inside of the glass tube was coated with a thin film of a 0.5 M NaOH, 0.05 M Na_2WO_4 solution in 50/50 v/v H_2O–isopropyl alcohol solution. The coating was air-dried while rolling the tubes on a horizontal roller to maintain an even, thin coating. After drying, the sodium tungstate was converted to tungstic acid by passing HCl(g) through the tube. After being washed with water to remove NaCl, the tubes were fired at 500 °C in a furnace for about 8 h. The resulting tubes were cut into 15-cm sections and six sections were combined to form the denuder. The final tubes were clear with a slight yellow tint. Break-through capacity for the prepared tubes was not directly measured, but the sampling of gas-phase nitric acid concentrations over the range of 0.1–16 μmol of HNO_3/m^3 was investigated. The data obtained at the higher concentrations indicate that the capacity of the 15 cm sections is at least 600 nmol/section compared to about 10 nmol/section reported by Braman et al. (*14*) for 35 cm × 6 mm o.d. (4 mm i.d. (*17*)) tubes prepared by vacuum deposition of tungstic oxide from a tungsten wire.

Determination of NO_3^- and NH_4^+ in Tungstic Acid Denuders. A major goal of this research was the determination of the deposition pattern of nitrate in tungstic acid denuders. It is possible that adsorption of NO_x, PAN, or similar compounds (*14, 15*) may interfere with the determination of nitrate by the method of Braman et al. (*14*). Therefore, an analysis procedure was developed for the direct determination of nitrate. Recovery of collected HNO_3(g) and NH_3(g) from the denuder was determined by addition of standard samples of 50 to 200 nmol of each gas to 15 cm denuder tube sections. The nitrate was found to be strongly complexed to the tungstic acid surface and could not be quantitatively removed with H_2O or aqueous HCl but was extractable with hot aqueous base. Lithium hydroxide was used as the base to allow for the ion chromatographic determination of NH_4^+. The nitrate and ammonia were quantitatively extracted with three successive 3-mL portions of 1.0 mM LiOH at 90 °C. Nitrate and ammonium ions in the extract solution were determined by ion chromatography using 3.0 mM $NaHCO_3$–2.4 mM Na_2CO_3 and 5.0 mM HNO_3 eluents, respectively. A small amount of tungstate ion was removed during the extraction. Since tungstate has an elution time longer than that for sulfate, it did not interfere with the determination of nitrate. The tubes could be regenerated two or three times by washing with HCl solution and heating at 500 °C for 8 h, but repeated extraction and regeneration results in loss of activity. The freshly prepared denuder tubes gave blank values of 3–5 nmol/section for both nitrate and ammonia. This is 20 times higher than the blank values of about 0.05–0.15 reported by Braman et al. (*14*) for tubes prepared by vacuum deposition of WO_3 in glass tubes. However, the capacity of the tungstic acid denuders prepared by us for collection of nitric acid (>0.6 μmol/15 cm section) was correspondingly larger.

Nylon Denuder Tube Preparation. Nylon reversibly adsorbs HNO_3(g) (*2*), presumably by protonation of the amide groups in the nylon. The nitrate can be recovered by aqueous extraction and analyzed by ion chromatography. Diffusion-denuder tubes were made by placing rolled tubes of nylon-membrane sheets (Membrana) inside Teflon carrier tubes. The inside diameter of the Teflon tube was 0.70 cm. Six 10-cm nylon tubes were used in each denuder. Nitric acid collected in the denuder was extracted with water and determined by ion chromatography. Nitrate blanks, 2.6 ± 0.5 nmol/section, were found to be comparable to those for the tungstic acid denuder.

Laboratory Studies. The collection of both HNO_3(g) and NH_3(g) by the tungstic acid denuder and of HNO_3(g) by the nylon denuder in the absence of particles was determined. The HNO_3(g) was generated by passing N_2 over fuming HNO_3 ($HNO_3 \cdot 0.5H_2O$) and into a dry N_2 stream or by passing N_2 over 70% aqueous

Table I. Configuration of the Sampling Systems for the Collection of HNO_3(g)

sampler	sample flow rate, L/min	material collected: gas phase	material collected: particles
1.a. tungstic acid denuder + quartz filter + nylon filter + oxalic acid filter	1.5	$HNO_3 + NH_3$	total nitrate and ammonia after denuder
1.b. same as 1.a.			
1.c. quartz filter + nylon filter + oxalic acid filter	10.0		total nitrate and ammonia in particles and gas phase
1.d. quartz filter + nylon filter + oxalic acid filter	20.0		total nitrate and ammonia in particles and gas phase
2. nylon denuder + quartz filter + nylon filter	2.0	HNO_3	total nitrate after denuder

HNO_3 and into cleaned laboratory air. Water in the dry N_2 stream was removed with a liquid N_2 cryogenic trap. The NH_3(g) was generated by passing N_2 over concentrated NH_4OH and into cleaned laboratory air. Particles in the gas stream were removed with an acid washed quartz filter and the resulting gas was pulled through the denuder at a flow rate of 1.5 or 2.0 L/min. After the denuder, HNO_3 was collected with a nylon filter or (in some experiments with 70% aqueous HNO_3) an aqueous bubbler. An oxalic acid coated filter collected NH_3. The collected nitric acid or ammonia was determined by ion chromatography as described above.

Field Experiments. Field evaluation of the collection of gas-phase nitric acid by the tungstic acid and nylon denuders and of NH_3(g) by the tungstic acid denuder was conducted by sampling in the Los Angeles area. Samples from the Los Angeles Basin were collected over a 4-day period in August 1983 at the City of Hope Hospital in Duarte. Table I shows the five sampling configurations used. Samples were collected during both the daytime and nighttime over both 4- and 8-h sampling periods. The collected samples were analyzed for nitrate and ammonia by using the techniques described under the preparation of the two denuder systems.

RESULTS AND DISCUSSION

Diffusion Coefficient of HNO_3(g) and NH_3(g) in Air. The diffusion coefficient of a gas collected in a diffusion denuder can be calculated by using the Gormley–Kennedy (*18*) equation and data on the fractional penetration of gases through the denuder. This approach has been used by Durham and Spiller (*13*) and Braman et al. (*14*) to give the diffusion coefficient at 1 bar and 25 °C, $D_0 = 0.106 \pm 0.006$ and 0.121 ± 0.006 cm^2/s, respectively, for the diffusion of HNO_3 in a dry gas stream. These results compare well with the values of 0.122 cm^2/s calculated by Braman et al. (*14*) using the method of Wilke and Lee (*19*) and 0.113 cm^2/s calculated by Durham and Spiller (*13*) from Gilliland's correlation equation for diffusing polar molecules (*20*).

Any NO_2 present in the nitric acid samples used to generate HNO_3(g) in the laboratory studies could interfere with the determination of D_0 for nitric acid if NO_2 is absorbed by the tungstic acid denuder (*15*) since the NO_2 will be converted to HNO_2 and HNO_3. The presence of NO_2 can be identified from the ion chromatographic detection of NO_2^-. Data obtained in aqueous bubblers without a denuder indicated that the amount of NO_2 in the HNO_3 generated from the 70% aqueous HNO_3 was 3 mol % of the HNO_3. In the presence of a tungstic acid denuder at an HNO_3 concentration of 16 μmol/m^3, 32% of this NO_2 was deposited in the denuder with the deposition pattern being linear. These results are comparable to those obtained in recent studies by Hegg (*15*). In all laboratory experiments where the HNO_3 after the denuder was collected on a nylon filter, the concentrations of NO_2^- in the extract solutions from the tungstic acid denuder sections varied from not detectable to 3% of the nitrate concentration. In all cases where deposition of NO_2 was detected, the deposition pattern in the tungstic acid denuder was linear. At these low concentrations, the presence of NO_2 did not affect the laboratory data. These results do, however, suggest that at higher concentrations NO_2 may be a significant interferent.

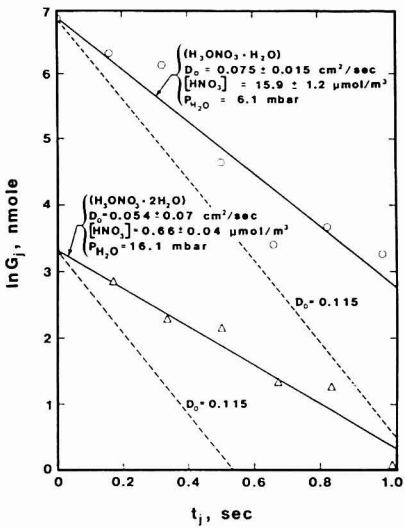


Figure 1. ln G_j vs. t_j for the collection of HNO_3(g) by a tungstic acid denuder at two different concentrations of atmospheric water. The indicated D_0 values are calculated from a weighted least-squares fit of the data to eq 2. The dashed lines are the slopes expected for $D_0 = 0.115$ cm^2/s (*13*, *14*).

We have evaluated our data for the collection of gas-phase nitric acid in both the tungstic acid and nylon denuders using the Gormley–Kennedy (*18*) equation as formulated by Durham and Spiller (*13*)

$$G_j = 0.819T_i[e^{(3.657D_i dt_v/r^2)} - 1]e^{(-3.657D_i t_j/r^2)}, \quad j > 1 \qquad (2)$$

where G_j is the amount deposited in the jth section of the denuder, T_i is the total amount that entered the denuder, D_i is the gas diffusion coefficient at the experimental conditions, dt_v is the axial displacement time for transport through equal length sections of the denuder, t_j is the axial displacement time for travel of the gas from the inlet through section j, and r is the radius of the cyclindrical denuder. Examples of our results with the tungstic acid denuder are illustrated in Figure 1 for generation of gaseous nitric acid from 60% HNO_3(aq) into air with either 6 or 16 mbar of H_2O. As shown in both Figures 1 and 2, the measured diffusion coefficient of nitric acid is dependent on the atmospheric water

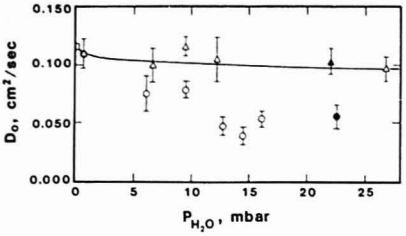


Figure 2. Experimentally determined values for D_0 for $HNO_3(g)$ as a function of atmospheric water concentration for both laboratory (○, this study tungstic acid denuder; △, this study nylon denuder; and □, Braman (*14*) and Durham (*13*)) and field (this study, (●) tungstic acid or (▲) nylon denuder) data. The solid line is calculated from literature thermodynamic values for the interaction of H_2O with nitric acid; see text.

concentration. The calculated D_i values are corrected to 1 bar and 25 °C to obtain a D_0 value. The observed decrease (in Figure 2) in the calculated D_0 value for nitric acid with increasing $H_2O(g)$ concentration is due to the hydration of $HNO_3(g)$ in the case of the nylon denuder (△ in Figure 2), and a combination of hydration of nitric acid and decreased adsorption efficiency of the denuder surface in the case of the tungstic acid denuder (○ in Figure 2).

Gas-phase nitric acid will reversibly bind water molecules to form $HNO_3 \cdot xH_2O$, where the value of x is dependent on the atmospheric water concentration (*21*, *22*). Equilibrium constants for formation of the hydrated species of the gas-phase nitrate ion where $x = 2$, 3, or 4 have been reported over the temperature range of 40–230 °C (*21*). We have extrapolated these data to 25 °C to obtain equilibrium constants for the formation of the hydrated $HNO_3(g)$ species with $x = 2$, 3, or 4 and to estimate values for the equilibrium constants for formation of the hydrated species with $x = 1$. It can be expected that the equilibrium constants measured by mass spectrometry for hydration of the NO_3^- ion in the gas phase would overpredict hydration of the HNO_3 molecule in the gas phase. If we assume that the equilibrium constant for the reaction

$$H_3O^+ + NO_3^-(x-1)H_2O^- = HNO_3 \cdot xH_2O \qquad (3)$$

is independent of the value of x, then the equilibrium constants for the hydration of gas-phase HNO_3 can be calculated from the equilibrium constants obtained from mass spectral data if a value for the equilibrium constant for reaction 4 can be estimated from

$$HNO_3(g) + H_2O(g) = HNO_3 \cdot H_2O(g) \qquad (4)$$

literature data. We have estimated the $\Delta G°$ value for reaction 4 to be −13.5 kJ/mol from literature data (*23*) for the free energy of formation of gas-phase HNO_3 and H_2O, and liquid-phase nitric acid hydrates, assuming that the free energy of vaporization of the hydrates are similar to that for $HNO_3(l)$ and $H_2O(l)$. The calculated dependence of D_0 on atmospheric water concentration using this $\Delta G°$ value is shown in Figure 2. These calculations predict values of x between 0.8 and 1.2 when P_{H_2O} varies from 5 to 30 mbar. The average value for D_0 obtained from the laboratory data in this range of P_{H_2O} is 0.103 cm^2/s. The average value of D_0 obtained from the field data at ≈22 mbar of H_2O is 0.104 ± 0.011. The laboratory and field measured D_0 values for collection of nitric acid by the nylon denuders is in good agreement with that calculated from the equilibrium constants reported by Lee et al. (*21*) as described.

The D_0 values calculated from the laboratory data obtained with the tungstic acid denuder are significantly lower than those calculated from the data obtained with the nylon denuder or the results predicted from the mass spectral studies of nitric acid hydration. Furthermore, there is a steady increase in the discrepancy in the data obtained with the tungstic acid denuder up to about 15 mbar of H_2O. This implies a steady decrease in the collection efficiency of the tungstic acid denuder over this concentration range of H_2O. Such a change could occur, for example, by alteration of the tungstic acid surface by hydration.

In the laboratory diffusion denuder experiments, the total nitric acid passing through the denuder was determined by collection of the gas in the denuder and on nylon filters after the denuder. The percent of nitric acid captured by the denuder for all the experiments with nylon denuders was 93 ± 3%. For the tungstic acid denuder experiments with atmospheric water concentrations above 5 mbar, the average percent of the nitric acid captured in the denuder was 92 ± 4%. The ratio of the total calculated from least-squares fit of the denuder data to eq 2 to the experimentally determined total nitric acid was 1.01 ± 0.09 and 1.15 ± 0.02 for the same comparison. Thus, it appears that while the total collection efficiency of the tungstic acid denuder is not significantly affected by the reduced efficiency for collection of nitric acid, the concentration of nitric acid calculated from eq 2 is high.

The diffusion coefficient of NH_3 was determined at atmospheric H_2O concentrations of 7 and 14 mbar to be 0.154 ± 0.019 cm^2/s. This value is substantially lower than the D_0 values of 0.236 (*24*) and 0.247 (22) cm^2/s determined in dry air. These results indicate that the gas-phase ammonia molecule is also hydrated in the presence of atmospheric water. We were unable to find published data on the interaction between ammonia and water in the gas phase. The D_0 value for ammonia determined by us in the presence of water is equal to the D_0 value expected if ammonia exists as a monohydrate. This would be consistent with the expected strong interaction of a water molecule with the lone electron pair of the ammonia molecule.

Field Studies. Passage of an aerosol–gas mixture through the denuder will result in the removal of gases which sorb to the denuder wall. As a result, the concentration of the gas will decrease exponentially during travel through the denuder according to eq 2. If the system sampled has gases in equilibrium with the aerosol, then the removal of the gas-phase component will result in a loss of material from the aerosol to the gas phase. Thus, the equilibrium position for a mixture of $HNO_3(g)$, $NH_3(g)$, and $NH_4NO_3(s)$ after continued passage through a denuder would result in disappearance of the aerosol phase and excess deposition in later denuder sections. If the rate of attainment of equilibria between aerosols and the gas phase is slow enough that significant volatilization does not occur during the time the aerosols are in the denuder, then the deposition pattern in the denuder will follow eq 2. Rapid attainment of equilibria would result in a positive deviation of the experimental results from that predicted by eq 2, especially for the last denuder sections.

Typical results obtained in this study in the Los Angeles atmosphere for the collection of $HNO_3(g)$ by both the tungstic acid and nylon denuders and $NH_3(g)$ by the tungstic acid denuder are shown in Figure 3. The data are linear as predicted by eq 2. The uncertainties in the experimental values for collected ammonia (6 nmol) and nitric acid (2.5 and 0.5 nmol for tungstic acid and nylon, respectively) as determined from scatter in the blank values are shown as the error bars on each data point. Table II gives all the results obtained in the field studies. The calculated D_0 values are in agreement with that expected for a monohydrate of ammonia and for the nitric acid hydrate species present at the measured atmospheric water concentration of 22 mbar H_2O (see Figure 2).

These results suggest that either no significant volatilization of aerosol occurs during passage of the mixture through the denuder or that no potentially volatile nitrate was present in the aerosol. The D_0 values calculated from the field data for the collection of nitric acid by the tungstic acid denuder (● in Figure 2) are lower than those obtained with the nylon denuder (▲ in Figure 2), indicating that the hydration effects on the tungstic denuder seen in the laboratory studies are also reflected in the field data. However, the difference in calculated total nitric acid obtained between the Nylon denuders and the tungstic acid denuder was greater than the 15% positive error expected for the tungstic acid denuder based on the laboratory data. Furthermore, the concentration of nitric acid calculated for the tungstic acid denuder data from eq 2 was higher (by as much as a factor of 2) than the value calculated by dividing the total collected by the denuder by 0.92 to estimate total nitric acid gas entering the denuder.

A second possible artifact which could be present in the field data is the adsorption of NO_x by the tungstic acid denuder (*15*).

Table II. Experimental Results from the 1983 Los Angeles Basin Field Experiments[a]

sampling date	sampling time, PDT	T, °C	P_{H_2O}, mbar	D_0 (HNO_3), cm^2/s	gas phase [HNO_3], nmol/m^3 calcd[b]	gas phase [HNO_3], nmol/m^3 exptl[c]	gas phase + aerosol [NO_3^-], nmol/m^3 den[d]	gas phase + aerosol [NO_3^-], nmol/m^3 FP[e]	D_0 (NH_3), cm^2/s	gas phase [NH_3], nmol/m^3
1 Aug	11–15	33	22.1 ± 0.6	0.047 ± 0.008	160 (95)[f]	160	276	249	0.121 ± 0.021	192
	15–19	33	21.9 ± 0.4	0.062 ± 0.012	220 (115)[f]	214	317	212	0.132 ± 0.015	200
	11–19[g]	33	22.0 ± 0.5	0.117 ± 0.009	58	48				
1–2 Aug	20–01	25	22.0 ± 0.3	0.065 ± 0.014	280 (216)[f]	146	304	181	0.111 ± 0.044	165
2 Aug	10–14	33	21.9 ± 0.7	0.055 ± 0.012	185 (104)[f]	160	721	555		
	10–18[g]	33	21.3 ± 0.9	0.087 ± 0.020	220	131				
	14–18	34	20.6 ± 1.0	0.042 ± 0.010	315 (164)[f]	232	481	486	0.188 ± 0.032	2500
2–3 Aug	22–02[g]	24	23.0 ± 0.9	0.105 ± 0.050	78	74				
	22–06	24	23.2 ± 0.7	0.070 ± 0.028	70 (40)[f]	58	89	68	0.136 ± 0.007	373
3 Aug	07–10	27	22.8 ± 0.4	0.049 ± 0.025	296 (158)[f]	163	238	127		
	10–14	31	21.9 ± 0.8	0.056 ± 0.025	325	167	290	228	0.104 ± 0.017	2600
	10–14[g]	31	21.9 ± 0.8	0.104 ± 0.011	69	60				
	14–18[g]	34	19.7 ± 2.4	0.107 ± 0.018	92	91				

[a] The uncertainties in the D_0 values here and throughout the paper are the standard deviation of the mean calculated from the weighted linear regression analysis of the denuder data. [b] Calculated from weighted least-squares fit of the data to eq 2. [c] Experimentally determined assuming 92% of the total nitric acid was collected by the denuder. [d] Total nitrate collected by the denuder sampling configurations 1.a. and 1.b. in Table I. [e] Total nitrate collected by the filter pack sampling configurations 1.c. and 1.d. in Table I. [f] Calculated from least-squares fit of the data to eq 2 after corrected for NO_2(g), see text. [g] Data obtained with a nylon denuder.

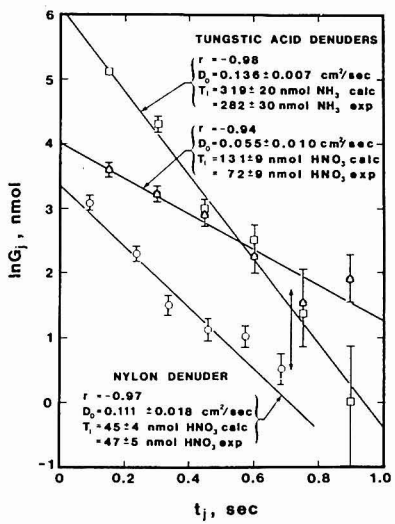


Figure 3. ln G_j vs. t_j for the collection of HNO_3(g), △, and NH_3(g), □, by a tungstic acid denuder and for the collection of HNO_3(g), ○, by a nylon denuder sampling the Los Angeles atmosphere. The indicated D_0 and T_i values are calculated from eq 2.

The concentrations of NO_x and NO_2 were monitored during the field sampling; the concentration of NO was negligibly small and the concentration of NO_2 varied from 45 to 80 ppb, averaging about 65 ppb. Our data reported in this study and the data obtained by Hegg (*15*) indicate that at these concentrations of NO_x, at least 10% of the NO_x passing through a tungstic acid denuder would be sorbed by the denuder. It was not possible to detect the possible adsorption of NO_2(g) by analysis for NO_2^- since the samples were extracted in the field and stored for several weeks before analysis. Under these conditions, NO_2^- is oxidized to NO_3^- before the analytical determination. Total nitrate during the periods when nitric acid was collected by the tungstic acid denuder was determined with a denuder followed by a filter pack and by a filter pack only. Higher total nitrate concentrations were measured with a denuder followed by the filter pack (Table II). This result indicates that a gas-phase species which was not collected by the filter pack was collected by the denuder and determined as nitrate. Uncertainties of 10 to 20% in the individual numbers make estimation of the amount of artifact nitrate present in the tungstic acid denuder for any single run difficult. The average calculated for all the runs gave 36% of the nitrate collected by the tungstic acid denuder as originating from a gas other than nitric acid. It was assumed this artifact nitrate was uniformly deposited in the denuder and the data were corrected for this artifact and fit to eq 2 to obtain the results given in parentheses in Table II. The corrected data are in better agreement with the nylon denuder data. In addition, the difference between the calculated and experimental nitric acid resulting from this correction was 14 ± 12 nmol/m^3 compared to 58 ± 58 nmol/m^3 before the correction. The diffusion coefficient calculated from the tungstic acid denuder data using this correction varied from 0.05 to 0.10 cm^2/s (not shown in Table II) and averaged 0.076 ± 0.020 cm^2/s.

The data from the filter packs placed after the denuder (see Table I) show that volatile nitrate was present in the aerosol in sufficient quantity that any appreciable volatilization of HNO_3 during passage through the denuder would have been detected. For example, the concentration of nitrate and ammonia present in the aerosols associated with the nylon denuder data given in Figure 3 were 140 and 340 nmol/m^3, respectively. Of the nitrate present in the aerosol phase, 20% was collected on the quartz filter and 80% was collected on the nylon filter after the quartz filter. The double ended arrow, ↔, in Figure 3 indicates the displacement that would have been expected in the last nitrate data point if 5% of the aerosol nitrate had been collected by that section of the nylon denuder.

The results of these experiments are in agreement with the laboratory studies of Forrest et al. (*6*) and Larson and Taylor (*16*).

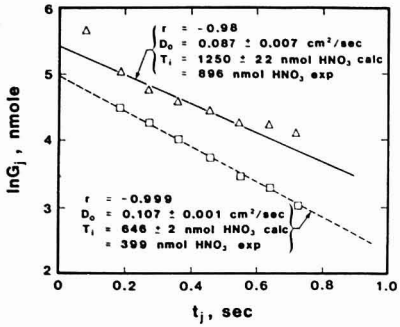


Figure 4. ln G_j vs. t_j for the collection of $HNO_3(g)$ by a nylon denuder sampling the Los Angeles atmosphere. Data are from Durham and Spiller (*13*). The □ data are corrected assuming a D_0 value of 0.115 and loss of aerosol $HNO_3(g)$ in the denuder (see text). The indicated D_0 and T_i values are calculated from eq 2.

These investigators have studied the collection of $HNO_3(g)$ by denuders from laboratory generated NH_4NO_3 aerosols and have concluded that the volatilization of $HNO_3(g)$ from the aerosols during sampling through the denuder is not significant. The results of Durham and Spiller (*13*) using nylon denuders are also in agreement with these results if the effect of the formation of a hydrated gas-phase $HNO_3 \cdot xH_2O$ species is taken into consideration. The data reported by Durham and Spiller (*13*) are plotted in Figure 4. The triangles in Figure 4 are the experimental data. Weighted linear regression analysis of the data for $j > 1$ gives $r = -0.98$, $D_0 = 0.087 \pm 0.007$, and $T_i = 1250 \pm 22$ nmol. The value of D_0 is consistent with that expected for hydrated $HNO_3(g)$ in the Los Angeles basin and with the results obtained in this study. Durham and Spiller (*13*) assumed that the data should give a D_0 value of the unhydrated $HNO_3(g)$ molecule (0.115 cm^2/s) and corrected the data to give a slope consistent with this D_0 value by assuming $HNO_3(g)$ from aerosols was collected in the denuder. The data obtained by making this correction to the data of Durham and Spiller (*13*) are shown as the squares, □, at the data points and dashed linear regression line. This treatment of the data predicts that about half of the nitrate in the denuder originated from aerosol nitrate. However, there is no significant improvement in the fit to the data by this correction; and furthermore, the resulting calculated T_i value is not in agreement with that measured in the experiment, assuming 92% of the total gas-phase nitric acid would be collected by the denuder.

The report by Braman et al. (*14*) on the use of the tungstic acid denuder for the collection of $HNO_3(g)$ also suggested that gas-phase nitric acid may be hydrated, D_0 values of 0.05 cm^2/s being reported by them. They were, however, unable to quantitatively interpret their results. The D_0 value of 0.05 cm^2/s reported by Braman et al. for collection of $HNO_3(g)$ in the atmosphere (*14*) is consistent with our observed alteration of the tungstic acid surface in the presence of atmospheric water.

The formation of a nitric acid hydrate in the gas phase will significantly affect the equilibrium between aerosol $NH_4NO_3(g)$, $HNO_3(g)$, and $NH_3(g)$. The first calculations on the expected equilibria (*25*) assumed a dry aerosol and unhydrated gas-phase species. Early experiments reported that the product of gas-phase HNO_3 and NH_3 in the atmosphere was comparable to that predicted by the calculations of Stelson et al. (*25*). Since then reports have appeared describing the predicted effect of aerosol moisture on the gas–aerosol equilibrium position (*1*, *26*). The formation of a hydrated or liquid aerosol of ammonium nitrate will shift the equilibrium from the gas phase toward the aerosol. The formation of hydrated gas-phase nitric acid and ammonia will shift the predicted equilibrium from the aerosol toward the gas phase. The chemistry occurring in the atmospheric NH_3–HNO_3–H_2O system is obviously complex and not yet well characterized. The early observations of agreement between the prediction of Stelson et al. (*25*) and experimental observations would appear to be fortuitous.

The results of this study show that use of a nylon denuder tube system for the separation of gas and aerosol nitrate species in field sampling is viable. If near quantitative removal of $HNO_3(g)$ by the denuder is desired, the denuder system must be designed to remove a gas with a D_0 value of about 0.09 cm^2/s.

ACKNOWLEDGMENT

Appreciation is expressed to James Cheney, U.S. Environmental Protection Agency, for assistance in the sampling program, and to Fern Mortensen, John R. Bennett, and Miriam S. Brutsch for technical assistance.

LITERATURE CITED

(1) Bassett, M.; Seinfield, J. H. *Atmos. Environ.* **1983**, *17*, 2237–2252.
(2) Spicer, C. W.; Howes, J. E., Jr.; Bishop, T. A.; Arnold, L. H.; Stevens, R. K. *Atmos. Environ.* **1982**, *16*, 1487–1500.
(3) Tuazon, E. C.; Winer, A. M.; Graham, R. A.; Pitts, J. N., Jr. *Adv. Environ. Sci. Technol.* **1980**, *10*, 259–300.
(4) Kelly, T. J.; Stedman, D. H.; Kok, G. L. *Geophys. Res. Lett.* **1978**, *6*, 375–378.
(5) Appel, B. R.; Wall, S. M.; Tokiwa, Y.; Haik, M. *Atmos. Environ.* **1979**, *13*, 319–325.
(6) Forrest, J.; Spandau, D. J.; Tanner, R. L.; Newman, L. *Atmos. Environ.* **1982**, *16*, 1473–1485.
(7) Shaw, R. W., Jr.; Stevens, R. K.; Bowermaster, J. *Atmos. Environ.* **1982**, *16*, 845–853.
(8) Grosjean, D. *Anal. Lett.* **1982**, *15*, 785–796.
(9) Forrest, J.; Tanner, R. L.; Spandau, D.; D'Ottavio, T.; Newman, L. *Atmos. Environ.* **1980**, *14*, 137–144.
(10) Eatough, D. J.; Ellis, E. C. *Aerosol Sci. Technol.* **1983**, *2*, 177.
(11) Farber, R. J.; Huang, A. A.; Bregman, L. D.; Mahoney, R. L.; Eatough, D. J.; Hansen, L. D.; Blumenthal, D. L.; Keifer, W. S.; Allard, D. W. *Sci. Total Environ.* **1982**, *23*, 345–360.
(12) Appel, B. R.; Wall, S. M.; Tokiwa, Y.; Haik, M. *Atmos. Environ.* **1980**, *14*, 549–554.
(13) Durham, J. L.; Spiller, L. L. "Measurement of Gaseous, Volatile, and Non-volatile Inorganic Nitrate in Riverside, California"; Proceedings of the Division of Environmental Chemistry, 184th National Meeting of the American Chemical Society, Kansas City, 1982.
(14) Braman, R. S.; Shelley, T. J.; McClenney, W. A. *Anal. Chem.* **1982**, *54*, 358–364.
(15) Hegg, D., unpublished results on the collection of NO_2 by tungstic acid denuders, University of Washington, 1983.
(16) Larson, T. V.; Taylor, G. S. *Atmos. Environ.* **1983**, *17*, 2489–2495.
(17) Gailey, P. C.; McClenny, W. A.; Braman, R. S.; Shelly, T. J. *Atmos. Environ.* **1983**, *17*, 1517–1519.
(18) Gormley, P. G.; Kennedy, M. *Proc. R. Ir. Acad. Sci., Sect. A* **1949**, *52*, 163–169.
(19) Wilke, C. R.; Lee, C. Y. *Ind. Eng. Chem.* **1955**, *47*, 1253–1257.
(20) Foust, A. S.; Wenzel, L. A.; Clump, C. W.; Maus, L.; Anderson, L. B. "Principles of Unit Operations"; Wiley: New York, 1964; p 107.
(21) Lee, N.; Keesee, R. G.; Castleman, A. W., Jr. *J. Chem. Phys.* **1980**, *72*, 1089–1094.
(22) Kay, B. D.; Hermann, V.; Castleman, A. W., Jr. *Chem. Phys. Lett.* **1981**, *80*, 469–474.
(23) Wyman, D. D.; et al. *J. Phys. Chem. Ref. Data* **1982**, *11*, Supplement No. 2.
(24) Fuller, E. N.; Schettler, P. D.; Giddings, J. C. *Ind. Eng. Chem.* **1966**, *58*, 19–27.
(25) Stelson, A. W.; Friedlander, S. K.; Seinfeld, J. H. *Atmos. Environ.* **1979**, *13*, 369–371.
(26) Stelson, A. W.; Seinfeld, J. H. *Atmos. Environ.* **1982**, *16*, 993–1000.

RECEIVED for review May 23, 1984. Resubmitted and accepted December 6, 1984. This work (Contribution No. 345, Thermochemical Institute) was supported by Southern California Edison Co.

Solution Studies of Systems with Polynuclear Complex Formation: Copper(II) and Cadmium(II) D-Gluconate Systems

Kjell Blomqvist and Ebbe R. Still*

Department of Chemistry, Åbo Akademi, SF-20500 Åbo 50, Finland

Gluconate (HG = D-gluconic acid) is widely used as an efficient masking reagent for cations in strongly alkaline solutions. The complex formation with Cu^{2+} and Cd^{2+} has been studied by means of combined pH and pM measurements (25 °C, 0.5 mol/L KNO_3). Dimeric species of the composition $M_2H_{-4}G_2^{2-}$ seem to form in solutions containing an excess of the ligand. The evaluated stability constants are presented. A diagram is given which compares the masking ability of EDTA, tartrate, citrate, and gluconate for cupric ions.

Naturally occurring hydroxycarboxylic acids belong to the oldest complex-forming agents applied by mankind. Important members of this class of reagents are citric and tartaric acids, as well as the sugar acids. An example of the last group is D-gluconic acid, which is extensively used as a masking reagent for cations in alkaline solutions. Numerous practical and industrial applications have been reported for such systems (*1*).

When comparing the complexing ability of the mentioned hydroxycarboxylic acids, we note that citrate and tartrate carry a larger negative charge than gluconate because there are more carboxyl groups present in the ligand. The stability of the "normal" 1:1 metal:ligand complexes will therefore follow the order: citrate > tartrate > gluconate.

Investigations of metal–gluconate systems (*1*) indicate that two or more hydroxyl groups of the anion may ionize at high pH values (ionization of the hydroxyl group in α-position to the carboxyl group is a well-known phenomenon, the following dissociable protons may come from the ligand and/or from coordinated water molecules). This property makes the reagent a powerful chelating agent in alkaline solutions. The gluconate anion contains a greater number of hydroxyl groups than tartrate and citrate. Consequently, in ternary metal–OH–hydroxycarboxylate systems gluconate may be a better sequestering agent than citrate (and even tartrate) for cations with a strong polarizing power in order to dissociate protons.

We have an interest in the formation of basic metal hydroxycarboxylate complexes (*2–4*). Our main concern is the alkaline pH region where an ionization of the ligands occurs. The deprotonated alcoholic group has bridge-bonding ability (like the OH^- ion in metal hydrolysis reactions) and we may expect to find polymeric species present in solution. The formation of such species has, however, to a large extent been overlooked in the literature and most of the investigators explain their experimental data in terms of only mononuclear complexes (*5*).

We wanted to reinvestigate the cupric– and cadmium–gluconate systems in order to compare the complex-forming ability of a monohydroxycarboxylate (citrate) and a polyhydroxycarboxylate ligand. The study was carried out with the aid of combined pH and pM (=$-\log [M^{2+}]$) measurements as an ion-selective electrode is available for both cations. The theory for the evaluation of the data has been outlined previously (*2*, *4*).

Dimeric complex species have been proposed earlier in the cupric and cadmium gluconate systems (*1*). Of other metal–OH–gluconate systems we note that dimeric species seem to be formed by manganese(II) (polarography, ESR, and magnetic susceptibilty) (*6*), and by lead(II) (emf work with a lead amalgam electrode) (*7*). The species proposed in the latter study were $PbH_{-3}G^{2-}$ ($Pb(OH)_3G^{2-}$), $Pb_2H_{-5}G^{2-}$, and $Pg_2H_{-4}G_2^{2-}$, where HG denotes D-gluconic acid.

EXPERIMENTAL SECTION

All chemicals were of reagent grade and were used as received. The experiments were carried out at 25 ± 0.1 °C in solutions of ionic strength 0.5 mol L^{-1} KNO_3.

The potentiometric measurements were carried out with two Orion Model 801 pH/mV meters. A Radiometer metal-ion selective Selectrode was used for the pCu and pCd measurements. The linearity of the electrode response was tested by using various metal buffers and was found to be good. The $E_M°$ value of the Selectrode was measured in the metal ion solution before the addition of the ligand and was checked after the titration. A glass electrode was used for the pH measurements and the hydrogen ion concentration was calculated from the pH readings using the relationship $-\log [H^+] = pH - 0.14$.

All the calculations were performed with the aid of a programmable pocket calculator of the type HP-41 CV.

RESULTS

Gluconic acid forms weak complexes with potassium ions and the protonation constant was determined in the same ionic medium. The result is given in Table II.

The data required to analyze the equilibria in a system containing polynuclear species must involve variables measured over a wide concentration range. We have chosen to use combined pH and pM measurements as variables, since in emf work the response signal is a logarithmic function of the variable and it is possible to cover several decades of the concentration range.

The evaluation of the stability constants follows the theory outlined earlier (*2*, *4*, *8*). A short presentation of the methodology and theory is given below (all charges of the species are omitted):

Solutions containing the metal ion (M) and the ligand (L) are mixed in an appropriate ratio and the acidic solution is gradually neutralized with potassium hydroxide. The used C_M:C_L ratio (C denotes total concentration) depends on which kind of complex species are predominantly formed (mononuclear, dinuclear, monoligand, diligand, etc.). From the measured pH and pM values the constants can be calculated provided the stoichiometry of the complexes is known. The amount of base consumed at the neutralization could be used in the evaluation procedure, but usually this variable is used only for checking (and refining) the results.

The stability constants of a mononuclear monoligand complex can thus relatively simply be determined by performing a series of combined pH and pM measurements on a well pM-buffered solution, i.e., a solution containing the ligand in excess. Let us further assume that not more than two protons or hydroxide ions can be taken up by the complex ML, thus forming MHL, MH_2L, $MH_{-1}L$ (MOHL), and $MH_{-2}L$ ($M(OH)_2L$). The pM value of the solution will be governed by the conditional constant (*8*)

$$K'^{M_pL_q}_{(ML)'} = [(ML)']/([M][L']) = K^{M_pL_q}_{ML}\alpha_{ML(H,OH)}/\alpha_{L(H)} \quad (1)$$

0003-2700/85/0357-0749$01.50/0 © 1985 American Chemical Society

where

$$[(ML)'] = \sum_{i=-2}^{2} [MH_iL] = [MH_{-2}L] + [MH_{-1}L] + [ML] + [MHL] + [MH_2L] \quad (2)$$

$$[L'] = \sum_{i=0}^{t} [H_iL] = [L] + [HL] + [H_2L] + ... + [H_tL] \quad (3)$$

$\alpha_{L(H)}$ and $\alpha_{ML(H,OH)}$ denote distribution or side-reaction coefficients and have their usual definitions (*9*)

$$\alpha_{L(H)} = [L']/[L] = 1 + [H]K_{HL}^{H} + [H]^2K_{H_2L}^{2H} + ... \quad (4)$$

$$\alpha_{ML(H,OH)} = [(ML)']/[ML] \quad (5)$$

Substitution of the mass balance equations into eq 1 yields (*8*)

$$\log K_{ML} + \log \alpha_{ML(H,OH)} = pM + \log \alpha_{L(H)} + \log \{(C_M - [M'])/(C_L - C_M + [M'])\} \quad (6)$$

[M'] is the concentration of uncomplexed metal ion. If [M'] differs from [M], it is mostly a question of metal hydrolysis.

The left-hand side of eq 6 contains the unknown constants of the chelates, whereas all the terms on the right-hand side are calculable. The pM value of the solution can be measured at different pH values and log $\alpha_{L(H)}$ can be calculated from the known protonation constants of the ligand. A plot of log K_{ML} + log $\alpha_{ML(H,OH)}$ = log $K_{(ML)'}^{ML}$ as a function of pH will show the chelates formed in solution. The plot will indicate the species formed and will provide good estimates of the unknown stability constants. The values of the constants can then be refined by nonlinear regression analysis with the conditional constant as error variable (*8*).

Let us now assume that a condensation reaction will give predominating dimeric species in solution. The dimers have a 2:2 stoichiometry of the composition $M_2H_iL_2$, i.e., a stepwise protonation or deprotonation of the dimer is allowed. The free metal ion concentration of the solution will be determined by the conditional constant (*2*)

$$K_{(M_2L_2)'}^{2M,2L'} = \frac{[(M_2L_2)']}{[M]^2[L']^2} = K_{M_2L_2}^{2M,2L}\alpha_{M_2L_2(H,OH)}/(\alpha_{L(H)})^2 \quad (7)$$

Insertion of the mass balance equations yields

$$\log K_{M_2L_2} + \log \alpha_{M_2L_2} = 2pM + 2 \log \alpha_L + \log (C_M - [M'])/\{2(C_L - C_M + [M'])^2\} \quad (8)$$

The equation shows that dilution experiments can be used to test the existence of dimeric (or higher polymeric) species in solution. In most cases $[M'] \ll C_M$ and a dilution by a factor of 10 will diminish the pM value by 0.5 units (at constant pH value and for fixed C_M:C_L ratio). On the other hand, if a monomer predominates, the pM value will remain constant on dilution (see eq 6).

This means that a wrong assumption of the degree of polymerization of the chelate will give an "apparent" constant depending on the total concentration of the reactants. A comparison of eq 6 and 8 (with the assumptions given above and at a fixed pH value) yields for the reaction

$$2\ ML \rightarrow M_2L_2 \quad (9)$$

the following relationship between the constant for the dimer and the "apparent" constant K_{ML}^{app} obtained when assuming monomers in solution:

$$K_{M_2L_2} = (K_{ML}^{app})^2/(2C_M) \quad (10)$$

This means that K_{ML}^{app} will be proportional to $C_M^{1/2}$.

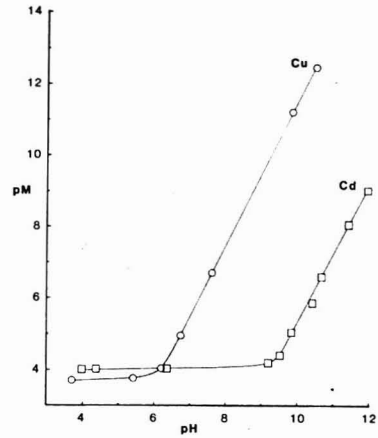


Figure 1. The figure shows recorded pM values vs. pH for solutions with a C_M:C_G ratio of 1:3, C_{Cd} = 0.1 mmol/L, and C_{Cu} = 0.2 mmol/L, respectively.

Table I. Dilution Experiments Probing the Dimeric Nature of the Formed Complexes

A. Calculated Values of $K_{CdH_{-2}G}^{app}$ as a Function of C_{Cd}

C_{Cd}	C_G	log $K_{CdH_{-2}G}^{app}$
3×10^{-4}	9×10^{-4}	−14.62
2×10^{-4}	6×10^{-4}	−14.70
1×10^{-4}	3×10^{-4}	−14.76

B. Experiment at Constant pH Values[a]

pH	log C_{Cu}	emf reading	$dpCu/dpC_{Cu}$
10.544	−4.000	−66.1	
10.544	−4.405	−59.3	−0.61
10.543	−4.812	−51.7	−0.63

[a] The potential (in mV) is recorded vs. calomel.

Combined pH and pM measurements have been used in the study of the copper(II)– and cadmium(II)–gluconate complexes. The solutions were mixed in a C_M:C_G ratio of 1:3 in order to avoid the formation of 2:1 metal:gluconate complexes. The results of two experiments are given in Figure 1 as a plot of pM vs. pH. The M:G ratio in the chelates is 1:1 and the slopes of the plots are +2 at alkaline pH values. Consequently, the composition of the chelates is $(MH_{-2}G)_n^{n-}$ in this pH region.

Diluton experiments can be used to determine the value of n. Experiments have been carried out with C_M values of 0.1, 0.2, 0.3, and 0.5 mmol/L and C_M:C_G = 1:3 (and 1:2). The results show that the "apparent" constant K_{ML}^{app} goes with the square root of C_M or that the spacing (*2*), dpM/dpC_M, is ca. −1/2.

Table IA shows three of the titrations performed in the cadmium–gluconate system indicating that K_{ML}^{app} is proportional to $C_{Cd}^{1/2}$. Table IB gives emf readings obtained in a dilution experiment at pH 10.54 in the cupric gluconate system. The calculated spacing (−0.62) slightly exceeds the theoretical value for a dimer (−0.50), but the performed titrations are in accordance with predominating dimeric species and not higher polymerized ones.

Table II. Stability Constants of Complexes $M_pH_qG_r$ Formed in Metal D-Gluconate Solutions (25 °C, 0.5 mol/L KNO_3)

p	q	r	reaction	log β_{pqr} ($\pm 3\sigma$)
0	1	1	$H^+ + G^- \rightleftarrows HG$	3.56 ± 0.03
2	−4	2	$2Cu^{2+} + 2G^- \rightleftarrows Cu_2H_{-4}G_2^{2-} + 4H^+$	−13.7 ± 0.1
2	−4	2	$2Cd^{2+} + 2G^- \rightleftarrows Cd_2H_{-4}G_2^{2-} + 4H^+$	−25.9 ± 0.1

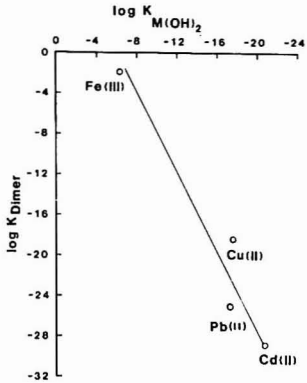


Figure 2. The ionization constant of basic metal–gluconate formation as a function of cation hydrolysis reaction. The definitions of the reaction equilibria are given in the text.

Consequently, dimeric species of the composition $M_2H_{-4}G_2^{2-}$ predominate in alkaline solutions. The obtained stability constants are presented in Table II.

Intermediate species of the type $M_2H_{-i}G_2^{(i-2)-}$ (i = 1, 2, 3) are not observed in the experiments of this study. The reason for this may be due to the dilute solutions used in the experiments (there is a solubility problem at higher metal ion concentrations, especially in the cadmium gluconate system).

DISCUSSION

The polarizing power of the cation is operative in the ionization process of metal hydroxycarboxylate complexes. In Figure 2 we compare the constants of the reactions

$$M^{n+}(+ 2H_2O) \rightleftarrows M(OH)_2^{(n-2)+} + 2H^+ \quad K_{M(OH)_2}$$

and

$$2MG^{(n-1)+} \rightleftarrows M_2H_{-4}G_2^{(2n-6)+} + 4H^+ \quad K_{dimer}$$

[Estimates (*10*) of the hydrolysis constants and literature values (*5*, *7*) for the $MG^{(n-1)+}$ complexes have been used (log $K_{CuG} \simeq 2.4$, log $K_{CdG} \simeq 1.5$). The value for the ferric complex (*5*) is based on an assumption of dimeric species and not mononuclear ones predominating in solution and on eq 10.]

The figure shows that to a first approximation the two ionization constants are linearly dependent of each other (as illustrated by a straight line with a slope of −2).

We may also compare the formation of basic citrate and gluconate complexes in reactions not involving the ionization of protons. Such a comparison is made in Table III (estimates of the appropriate hydrolysis constants of the cation are taken from literature values (*10*)). It is found that the stability of the citrate and gluconate complexes as defined by the reactions given in the table is of the same order of magnitude (for lead(II) the corresponding values amounted to 11.8 and 12.1, respectively). The high value of the gluconate complexes is surprising and may indicate a rather special stereochemical structure in the complex species.

Table III Stability of Basic Citrate and Gluconate Complexes According to the Reactions Given Below[a]

reaction	log K Cu(II)	log K Cd(II)
$2MOH^+ + 2Ci^{3-} \rightleftarrows M_2H_{-2}Ci_2^{4-} (+ 2H_2O)$	21.2	15.4
$2M(OH)_2 + 2G^- \rightleftarrows M_2H_{-4}G_2^{2-} (+ 4H_2O)$	21.6	15.6

[a] Values as far as possible valid at 25 °C, μ = 0.5. [b] H_3Ci = citric acid.

Table IV. Formation Constants for Copper(II) and Proton Interactions with EDTA, Citrate, and D(+)-Tartrate Used in the Calculation of Figure 3

p	q	r	interaction	log β_{pqr}
0	1	1	protonation of EDTA	10.23
0	2	1		16.41
0	3	1		19.07
0	4	1		21.08
1	0	1	Cu(II)–EDTA	18.86
1	−1	1		7.4
0	1	1	protonation of citrate	5.65
0	2	1		9.95
0	3	1		12.74
2	−1	2	Cu(II)–citrate	10.82
2	−2	2		5.80
0	1	1	protonation of tartrate	3.72
0	2	1		6.36
2	−2	2	Cu(II)–tartrate	0.1
2	−3	2		−7.0
2	−4	2		−17.3

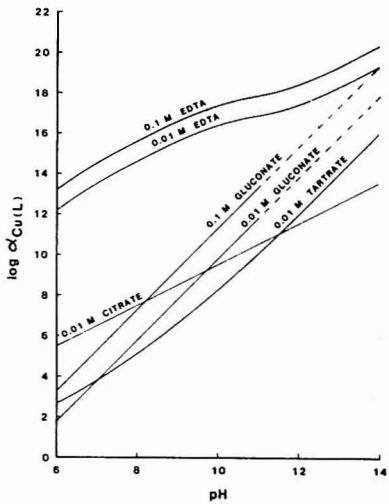


Figure 3. log $\alpha_{Cu(L)}$ as a function of pH in the presence of the complexing agents citrate, D(+)-tartrate, gluconate, and EDTA (L denotes the ligand). The plots are made for $C_{Cu}:C_L$ = 1:10.

The stability of the reactions given in Table II clearly shows the good masking effect of citrate, and especially gluconate, toward cation hydrolysis reactions. The usefulness of an organic reagent for various masking purposes can be expressed by means of α-coefficients (*9*). In Figure 3 the α-coefficients

for cupric ions and the complexing agents EDTA, citrate, D(+)-tartrate, and gluconate are presented (C_{Cu}:C_L = 1:10). The formation of dimeric species is accounted for (the formation constants used in the calculations are given in Table IV).

The figure shows the ability of gluconate to mask copper(II) efficiently in alkaline solutions, whereas citrate is a poorer masking agent. At neutral pH values citrate forms stronger complexes with copper(II) due to its higher negative charge.

EDTA is able to mask copper more efficiently than the mentioned hydroxycarboxylate ligands in neutral and weakly alkaline solutions. A comparison of the Cu-EDTA and Cu-gluconate log α curves for the two total concentrations shows the greater dilution effect occurring in systems containing dimeric species.

Registry No. Cu^{2+}, 15158-11-9; EDTA, 60-00-4; tartaric acid, 87-69-4; citric acid, 77-92-9; gluconic acid, 526-95-4.

LITERATURE CITED

(1) Sawyer, D. T. *Chem. Rev.* **1964**, *64*, 633.
(2) Still, E. R.; Wikberg, P. *Inorg. Chim. Acta* **1980**, *46*, 147.
(3) Grenthe, I.; Wikberg, P.; Still, E. R. *Inorg. Chim. Acta* **1984**, *91*, 25.
(4) Blomqvist, K.; Still, E. R. *Inorg. Chem.*, in press.
(5) Sillén, L. G.; Martell, A. E. "Stability Constants of Metal Ion Complexes"; The Chemical Society: London, 1964 and 1972; Special Publications Nos. 17 and 25.
(6) Bodini, M. E.; Willis, L. A.; Riechel, T. L.; Sawyer, D. T. *Inorg. Chem.* **1976**, *15*, 1538.
(7) Coccioli, F.; Vicedomini, M. *J. Inorg. Nucl. Chem.* **1978**, *40*, 2103, 2106.
(8) Still, E. R. *Anal. Chim. Acta* **1980**, *116*, 77.
(9) Ringbom, A. "Complexation in Analytical Chemistry"; Wiley-Interscience, New York, 1963.
(10) Baes, C. F., Jr.; Mesmer, R. E. "The Hydrolysis of Cations"; Wiley-Interscience: New York, 1976.

RECEIVED for review September 10, 1984. Accepted November 27, 1984. This work is part of a program financially supported by the Academy of Finland.

High-Sensitivity Spectroelectrochemistry Based on Electrochemical Modulation of an Absorbing Analyte

Chwu-Ching Jan, Barry K. Lavine,[1] and Richard L. McCreery*

Department of Chemistry, The Ohio State University, 140 West 18th Avenue, Columbus, Ohio 43210

When a laser beam passes parallel to an electrode surface, the light diffracted by the electrode samples the solution within less than 10 μm of the surface. If an absorber is generated electrochemically, the diffracted light is attenuated rapidly (<50 ms) and the attenuation is related to absorber concentration by Beer's law. A modulated potential was used to generate and remove absorber, leading to a modulated diffraction intensity which is linearly related to concentration. The effects of frequency, diffraction angle, and phase shift were examined and conditions for linearity of signal with concentration were determined. The detection limit for trianisylamine in acetonitrile was 2×10^{-8} M, with the selectivity inherent to a spectroelectrochemical method. Finally, a small amplitude ac potential was superimposed on a dc ramp, resulting in an output similar to that from ac voltammetry, but detected optically. The detection limits of the new method are compared to those for alternative spectroelectrochemical techniques.

Electroanalytical techniques based on amperometry and voltammetry can be extraordinarily sensitive, as evidenced by the picomole detection limits for amperometric detectors in liquid chromatography (*1*, *2*) or the 10^{-8}–10^{-10} M levels measurable by anodic stripping voltammetry (*3*) and pulse polarographic methods (*4*). Electroanalytical techniques can be miniaturized for use in vivo (*5*, *6*) and are relatively fast and inexpensive. When a spectroscopic probe is combined with electrochemistry, a more selective analytical determination may be made. An analyte is detected on the basis of both its spectroscopic properties and its electroactivity, and potential interfering Faradaic or non-Faradaic processes can usually be rejected because they are invisible to the spectroscopic probe. For example, transmission or reflection spectroelectrochemistry can be used to monitor electrogenerated absorbers, and the optical response is generally insensitive to processes which might interfere with conventional amperometric methods, such as charging current, surface Faradaic reactions, and any Faradaic processes which do not involve an absorber (*7*–*10*). The result is a more specific analytical probe for events associated with charge transfer.

In the majority of spectroelectrochemical techniques (*7*), the optical path length is determined by the diffusion layer thickness and is therefore quite short, usually less than 0.1 mm. Absorbances are generally less than 0.01, and sensitivity and detection limits are several orders of magnitude poorer than amperometric methods. Spectroelectrochemical techniques have been very useful for kinetic and thermodynamic studies, but their application to analysis has been inhibited by poor sensitivity. Several approaches have been used to improve sensitivity, some of which are based on parallel geometry (*11*, *12*), where the optical beam passes parallel to the electrode surface rather than normal to it. Thin-layer cells have been constructed with path lengths of ca. 1 cm (*13*, *14*), with one design (*15*) employing fiber optics to couple the cell to a commercial spectrophotometer. We have reported a different approach based on parallel geometry, in which optical diffraction is employed to limit the optical measurement to a region within a few micrometers of the electrode surface (*16*, *17*). In effect, the electrode is used to fill or empty the region sampled by the spectroscopic beam on a time scale of 100 ms or less. Although the sampled region can be filled rapidly, it may have a path length which is much longer than the diffusion layer, resulting in significant sensitivity improvement over normal incidence reflection or transmission techniques. The most important advantage of the diffraction method in the present context is the ability to repeatedly fill and empty the sampled region of the solution electrochemically, thereby modulating the concentration of absorber. In effect, the op-

[1] Present address: Department of Chemistry, Pennsylvania State University, University Park, PA 16802.

0003-2700/85/0357-0752$01.50/0 © 1985 American Chemical Society

tical probe monitors the near surface concentration of the redox system which can be rapidly modulated by the electrode potential. On combination of this modulation with phase sensitive detection, high analytical sensitivity may be achieved. In this report, the modulation technique is described and its performance for quantitatively measuring concentrations of dilute species in solution is evaluated.

THEORY

It has been shown both theoretically and experimentally (*16, 17*) that light diffracted by an electrode is sensitive to the presence of absorbing species near the electrode surface. A beam passing parallel to a planar surface is attenuated by the local absorber concentration, then a diffraction pattern is formed on a target placed downstream from the electrode. Light diffracted at angles of more than 1° is rapidly (<200 ms) attenuated when an absorber is generated at the electrode, and the attenuation is quantitatively related to absorber concentration. The rate of attenuation is a complex function of diffraction angle, concentration, and diffusion coefficients, but larger diffraction angles always result in more rapid attenuation. After 0.02–1 s, the attenuation of diffracted light by electrogenerated absorber reaches a constant value which is simply related to the absorber concentration by Beer's law

$$A = \log (I_0/I_t) = \epsilon b C_a \qquad (1)$$

where A is absorbance, I_0 is the diffracted light intensity at a particular angle before absorber is generated, I_t is the diffracted intensity after its limiting value is reached, ϵ is the molar absorptivity of the electrogenerated absorber (assuming a colorless precursor), C_a is the concentration of the electrogenerated absorber in the region sampled by the diffracted light, and b is the electrode length along the optical axis. A reasonable analogy for this process is an imaginary "cell" with a short (<10 μm) dimension normal to the electrode, which can be filled or emptied electrochemically. The diffracted light monitors the absorbance in this "cell", and is related to concentration in a simple Beer's law fashion. The limiting absorbance occurs when the conversion of colorless precursor to absorber has been completed in the "cell". At this point, $C_a = \gamma C_p^b$, where $\gamma = (D_p/D_a)^{1/2}$ and C_p^b is the bulk precursor concentration (*18*). D_p was assumed to equal D_a in this discussion.

Using the theory described previously (*16, 17*), one predicts that the absorbance reaches 95% of its limiting value when $(Dt)^{1/2} = 3.5 \times 10^{-4}$ cm, or at 12 ms for $D = 1.0 \times 10^{-5}$ cm^2/s. Modulation of the potential to alternately form and remove absorber should modulate the diffracted intensity. If the period of the modulation is long compared to 10 ms, the intensity of the diffracted light will be a square wave whose amplitude is dictated by Beer's law. Rearrangement of eq 1 for the case of small absorbances yields eq 2, provided $2.303\epsilon b C_a \ll 1$. For the case of a large potential modulation to the diffusion limits, eq 3 shows that the magnitude of the diffusion limited intensity modulation, ΔI_{diff}, is linear with the absorber concentration which is in turn linear with bulk precursor concentration. The assumption of small absorbances is important not only for mathematical convenience. As shown previously (*17*), high absorbances (>0.3) yield absorbance/time transients which have a peak at short times and will not produce a simple square wave when modulated. In this case, the relationship between the modulated intensity and concentration will be monotonic, but nonlinear. Given eq 3, it is possible to use a phase-sensitive detector to monitor the modulated intensity, and the demodulated output of the detector will be linearly related to the bulk concentration of the species producing the absorber at the electrode.

$$I_t = I_0(1 - 2.303\epsilon b C_a) \qquad (2)$$

$$\Delta I_{diff} = I_0 - I_t = 2.303 I_0 \epsilon b C_a = 2.303 I_0 \epsilon B \gamma C_p^b \qquad (3)$$

The discussion so far as well as previous reports (*16, 17*) on diffractive spectroelectrochemistry have considered the diffusion limited case where the initial and final potentials are far from the formal potential. Consider an alternative experiment, where the square wave potential modulation amplitude is small, on the order of 10 mV instead of the several hundred millivolts considered above. If the dc potential is scanned while the small ac modulation is superimposed, the resulting ac intensity will be a function of potential, with a maximum value at the half-wave potential. The experiment is similar to ac polarography and has been reported for the case of external reflection geometry (*19*). The advantages of optical detection of voltammetric response have been discussed and lie principally in the absence of charging or background current and in the specificity for absorbing species.

The theoretical response of diffracted light to an ac voltammetric wave form may be derived if it is assumed that the diffracted light monitors the surface concentration of absorber. Consider an experiment in which a square wave potential modulation of magnitude ΔE is superimposed on a slowly varying average potential of E_{dc}. Assume that the optical response is an ideal square wave, that E_{dc} is scanned slowly relative to the modulation period, and that the reduced form is the absorber. Finally, assume that the charge transfer reaction is reversible, so the surface concentrations may be calculated from the Nernst equation. Given these assumptions, the concentration of absorber in the idealized "cell" may be calculated from eq 4 (*18*)

$$C_a = \gamma C_p^b/(1 + \gamma\theta) \qquad (4)$$

where

$$\theta = \exp\left[\frac{nF}{RT}(E - E^{\circ\prime})\right]$$

By use of eq 1 and 4, a derivation very similar to that for ac polarography (*20*) yields an expression for the ac intensity

$$\Delta I = 2.303 I_0 \epsilon b C_p^b \gamma \frac{nF\,\Delta E}{4RT\cosh^2(a/2)} \qquad (5)$$

where

$$a = \frac{nF}{RT}(E_{dc} - E_{1/2})$$

ΔE = potential modulation amplitude

$$E_{dc} = \text{dc potential}, E = E_{dc} \pm \frac{\Delta E}{2}$$

Equation 5 was derived assuming small ΔE. As with ac polarography, the largest ΔI occurs at $E_{dc} = E_{1/2}$, and the full width at half maximum is $90.58/n$ mV for small ΔE. ΔI_{peak} is given by eq 6 for small ΔE. When ΔE becomes larger than

$$\frac{\Delta I_{peak}}{\Delta I_{diff}} = \frac{nF}{RT}\Delta E \qquad (6)$$

about $10/n$ mV, eq 5 and 6 become inaccurate, but the curve shape is easily calculated by substituting the two potentials of the square wave into eq 4 and 2 and taking the intensity difference. Table I shows ΔI_{peak} and peak widths for a range of ΔE values, with the only assumption being validity of the Nernst equation for determining the absorber concentration in the region sampled by the diffracted light. It should be reiterated that this treatment assumes ideal square wave response, i.e., a rise time of the change in diffracted intensity which is negligible compared to the modulation period. The experimental results shown below demonstrate that both the diffusion limited and small amplitude responses are somewhat lower than an ideal square wave.

Table I. Peak Amplitudes and Widths for Small Amplitude ac Modulation with dc Scan[a]

ΔE, mV	$\Delta I_{peak}/\Delta I_{diff}$ (theor)	nW, mV (theor)	$\Delta I_{peak}/\Delta I_{diff}$ (exptl)	nW, mV (exptl)
0.01	9.73×10^{-5}	90.58		
1	9.73×10^{-3}	90.58		
5	0.0486	90.66	0.0346	
10	0.0970	90.8	0.0889	95
20	0.192	92.0	0.185	91
30	0.284	93.6	0.272	94
40	0.371	96.0	0.356	96
50	0.451	99	0.445	100
60	0.525	102.8	0.514	100
70	0.592	107.0	0.588	105
80	0.652	112	0.642	110
90	0.704	117	0.687	120
100	0.750	123	0.722	120
200	0.960	204		
500	0.9999	500		

[a] ΔE, potential modulation amplitude; ΔI_{peak}, maximum ac intensity of diffracted light for potential modulation of ΔE; ΔI_{diff}, diffusion limited modulated intensity; W, full width at half maximum; n, number of electrons. Experimental conditions were those in Figure 8.

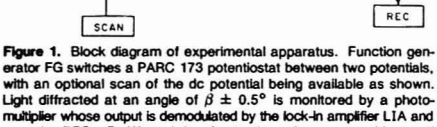


Figure 1. Block diagram of experimental apparatus. Function generator FG switches a PARC 173 potentiostat between two potentials, with an optional scan of the dc potential being available as shown. Light diffracted at an angle of $\beta \pm 0.5°$ is monitored by a photomultiplier whose output is demodulated by the lock-in amplifier LIA and recorder REC. R, W, and A refer to the reference, working, and auxiliary electrodes, ref is the reference wave form for the LIA. Laser is a 5-mW He-Ne operating at 632.8 nm.

EXPERIMENTAL SECTION

A block diagram of the experimental apparatus is shown in Figure 1. With the exception of electrode preparation, the cell and alignment procedure were the same as used previously (*17*). To increase the level of light reaching the photomultiplier (PMT), a 17 mm high by 1 mm wide vertical slit was used to select the portion of the diffraction pattern entering the PMT. Given the 1 m focal length of the lens, the slit accepted a 1° segment of the diffracted light, and the angles cited here are at the center of the accepted range (β in Figure 1).

The electrode polishing procedure was modified somewhat to produce higher quality surfaces. A 1-in. cube of stainless steel was cut down the center and holes were made to allow the two pieces to be bolted together. With the block screwed together, one face was polished on a wheel with 600 grit sandpaper. A strip of platinum with dimensions 0.15 mm × 5 mm × 30 mm was inserted between the block halves, with the 0.15 mm × 5 mm edge protruding slightly from the sanded face. The assembly was sanded again, then polished with a series of abrasives, inspecting the results with a microscope between steps. The series was as follows: 15-μm, 6-μm, and 1-μm diamond compounds, followed by 0.3-μm and 0.05-μm alumina polishing abrasives. During the course of experiments, further polishing was unnecessary for several months, although the electrode was occasionally cleaned in warm concentrated sulfuric acid. A nylon clamp held two glass microscope slides against the platinum electrode to form the cell shown in Figure 1. The electrode was aligned relative to the beam in the same way as described previously (*17*). The electrode length along the optical axis was calibrated by filling the thin-layer cell with known concentrations of potassium ferricyanide. This path length was 0.168 mm, a value which agreed to within 1.2% with that determined from the limiting absorbance of the diffraction experiments.

A PARC 173 potentiostat was used to control the potential, using resistance compensation tuned as recommended by the manufacturer. Since nearly all of the ohmic potential losses occurred in the thin-layer portion of the cell, no special efforts were taken in positioning the reference and auxiliary electrodes. A function generator switched the potential between the two values set on the potentiostat and also provided the reference wave form for a PARC 186A lock-in amplifier. In most cases the demodulated signal was recorded on a strip chart recorder, but in some cases the intensity vs. time signal was recorded with a Tektronix 7854 digital oscilloscope interfaced to an Apple II$^+$ microcomputer. For all measurements, the PMT gain was adjusted to produce a 2.00-V dc signal when no absorber was present in solution. The lock-in amplifier gain increased at frequencies below 100 Hz, being about 20% high at 5 Hz. Calibration curves were constructed from known square wave inputs at 5, 10 and 20 Hz to correct for this error. In experiments where a potential scan was used, a Bioanalytical system CV-1B voltammetry instrument was employed, by using the x-axis output to drive an external input on the PARC 173.

Tris(4-methoxyphenyl)amine (TAA) was obtained from Robert Walters at the University of Illinois, Chicago Circle. TAA is oxidized to a stable cation radical with an $E°$ of 0.52 V vs. SCE in acetonitrile containing tetraethylammonium perchlorate (*21*). The molar absorptivity of the cation radical was measured by absorbance measurements after bulk coulometry in a 3-cm-path length cell, and the diffusion coefficient was measured by both chronoamperometry and chronoabsorptometry. ϵ is 11 000 M^{-1} cm^{-1} at 633 nm and D is 1.30×10^{-5} cm^2/s, both in agreement with previous measurements (*16*, *22*, *23*). Although the compound was not used here, an error in the previously reported (*17*) tris-(4-bromophenyl)amine cation radical molar absorptivity was discovered. The correct value, determined by external reflection chronoabsorptometry and thin-layer spectroelectrochemistry, is 11 300 M^{-1} cm^{-1} at 633 nm.

RESULTS

The rise time of the diffraction signal at 2.6° for a potential step to the diffusion limit for TAA oxidation is shown in Figure 2. The diffracted intensity is significantly higher for the short electrodes used here compared to previous work, and higher diffraction angles could be monitored. The rise time to 95% of the limiting absorbance is 16 ms, slower than the 10 ms predicted from theory, but much faster than was observed previously (*16*, *17*). The absorbance measured with light diffracted at 2.6° reaches a constant value after 20 ms, and this value is maintained for at least 10 min.

Wave forms for the applied potential, signal, and background of a diffusion limited square wave potential modulation are shown in Figure 3 for a 5-Hz modulation frequency. The signal was obtained from a solution of 2.14×10^{-4} M TAA in 0.1 M TEAP, with an electrode length of 0.168 mm. Background runs were carried out with the same conditions, the only change being the absence of TAA. The theoretical peak to peak signal calculated from eq 3 and expressed in terms of the PMT output is 0.182 V. The observed signals taken from Figure 3 are 0.187, 0.183, and 0.184 V at 5, 10, and 20 Hz, respectively.

When the lock-in amplifier was used to demodulate signals similar to those in Figure 3, the results shown in Figure 4 are obtained. As predicted from eq 3, the demodulated signal was linear in bulk absorber concentration. Since the modulated intensity signal is not a perfect square wave, however, the proportionality between the lock-in amplifier output and concentration depends on several variables, including modulation frequency, the reference phase, and diffraction angle. Figure 5 shows the dependence of signal magnitude on the

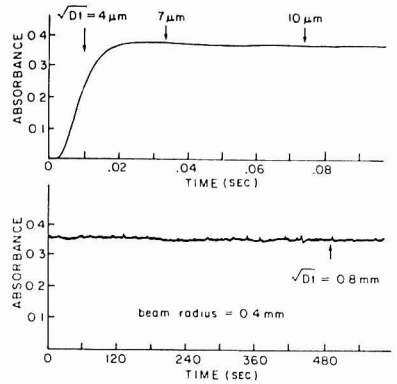


Figure 2. Response of diffracted light to a single potential step resulting in diffusion limited generation of $TAA^{+\cdot}$. Absorbance is defined as the common log of diffracted intensity at $\beta = 2.6°$ before the potential step divided by the time-dependent diffracted intensity. $(Dt)^{1/2}$ values indicate approximate diffusion layer thickness. Theoretical limiting absorbance is 0.37; TAA concentration is 2.0 mM. Noise in lower curve is caused by low frequency variations in laser intensity.

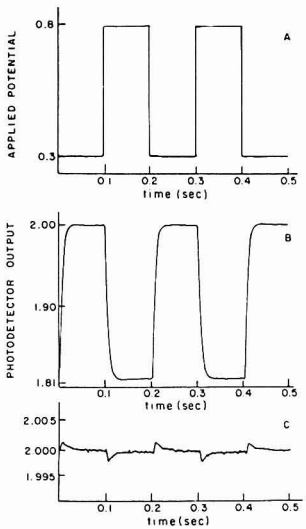


Figure 3. Applied potential and response wave forms for diffusion limited generation and removal of $TAA^{+\cdot}$. Trace A is applied potential, trace B is photodetector output in volts for light diffracted at 2.6° for a solution containing 2.14×10^{-4} M TAA and 0.1 M TEAP. Curve C is photodetector output for a solution containing only 0.1 M TEAP. The background signal magnitude was not dependent on TEAP concentration.

diffraction angle, defined for the center of the slit preceding the PMT relative to the undiffracted beam. Curve *a* was obtained with the phase angle on the lock-in amplifier (ϕ) set for maximum signal, curve *b* was for $\phi = 0$. An ideal square wave of amplitude equal to that predicted from eq 3 would have produced a signal of 102 mV. The observed signal is

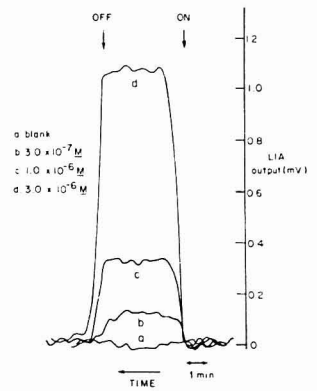


Figure 4. LIA output for solutions of TAA in TEAP/acetonitrile. Modulation frequency was 10 Hz. Signal lagged reference by 20°, and LIA time constant was 10 s. Letters on curves indicate bulk TAA concentrations, as shown. At point marked "on", cell was connected to potentiostat, at "off", it was disconnected.

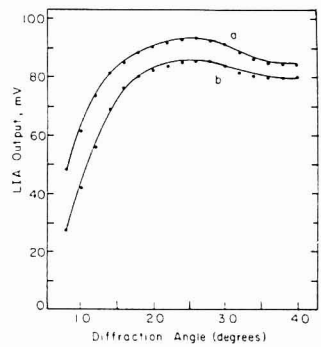


Figure 5. Demodulated signal magnitude vs. diffraction angle β: 5 Hz modulation frequency, TAA concentration = 2.40×10^{-4} M. Theoretical signal from eq 3 is 102 mV. Curve b is for a LIA phase shift of 0°, curve a is for the optimum phase shift at a given diffraction angle. Photometric gain was increased at higher diffraction angles to maintain initial photodetector output at 2.00 V.

always lower than this square wave value because of the finite rise time of the change in diffracted intensity. Plots of signal magnitude vs. phase shift (ϕ) are shown in Figure 6 for three different frequencies, with phase shift being defined as negative when the signal lags the reference wave form. As would be predicted for a finite rise time of the change in diffracted intensity, the phase angle of maximum response shifts more negative with increasing frequency. Figure 7 is a plot of signal vs. frequency for phase angles of zero and the value for maximum signal (ϕ_{max}). At 100 Hz, ϕ_{max} was −140°, and the maximum signal was about 18% of its value at 5 Hz.

The background response shown in Figure 3 differed from the absorbance signal in both time course and phase relationships and could effectively be eliminated by choice of phase angle. At values of −15°, −20°, and −40° for 5, 10, and 20 Hz, respectively, the lock-in output for the background signal crossed zero. These values are fortuitously close to those for the maximum absorbance signal, as shown in Figure 6.

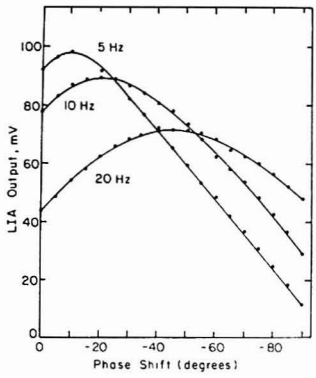


Figure 6. Demodulated output vs. LIA phase shift at various modulation frequencies. Theoretical signal is 110 mV for the TAA concentration of 2.59×10^{-4} M.

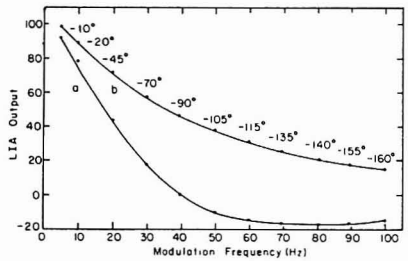


Figure 7. Effect of frequency on LIA output for a phase shift of 0° (curve a) and phase shifts equal to the optimum for each frequency (curve b), diffraction angle 2.6°.

Because of this convenient elimination of background, the phase angles for zero background were used to construct calibration curves. The LIA response was linear with concentration over at least the range from 3×10^{-7} to 1×10^{-4} M for TAA. Slopes of log/log plots of response vs. concentration are of 1.011 ($r = 0.9997$), 0.996 ($r = 0.9996$), and 1.007 ($r = 0.9990$) at 5, 10, and 20 Hz, respectively, for phase angles of −15°, −20°, and −40°.

The detection limit for the conditions of Figure 4 was approximately 1×10^{-7} M, but this value could be improved by changing experimental conditions. Since the background signal could be effectively eliminated by proper selection of phase, the detection limit was determined by noise rather than background. The diffracted intensity at 2.6° is fairly weak, requiring high photometric gain and accompanying noise. A lower diffraction angle results in higher intensity at the cost of a slower rise time of changes in the diffracted intensity and poorer linearity. In addition, a higher modulation frequency yielded less noise and improved signal/noise ratio. At a 1.4° diffraction angle, 30 Hz modulation frequency, and −94° phase shift, the signal decreased by about 40% compared to Figure 4, but the noise decreased more. By use of these conditions, the ratio of the signal for a 4.3×10^{-8} M TAA solution to the standard deviation of the background was 6.0. Defining the detection limit as the concentration where the ratio of signal to background standard deviation is 2, the detection limit for TAA is less than 2×10^{-8} M.

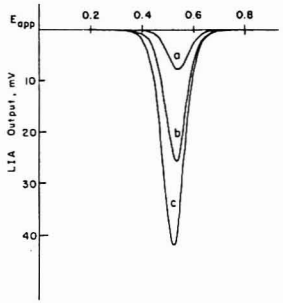


Figure 8. LIA output vs. dc potential for small amplitude square wave ac potential superimposed on a slow dc scan (2 mV/s) 10 Hz modulation: phase shift, −20°; time constant, 0.3 s; TAA concentration, 2.57×10^{-4} M; curve a, $\Delta E = 10$ mV; b, $\Delta E = 30$ mV; c, $\Delta E = 50$ mV. Reverse scans were superimposed on forward scans within the pen width. Peaks occur at +0.52 V vs. SCE.

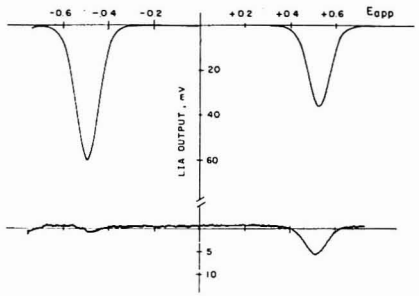


Figure 9. Small amplitude ($\Delta E = 70$ mV, modulation frequency = 10 Hz) scanning experiment for mixture of TAA and benzoquinone: upper curve, LIA phase shift = −20°; lower curve, phase shift = −109°. Peak at +0.52 V is due to 1.57×10^{-4} M TAA; peak at −0.50 V is 2.57×10^{-3} M benzoquinone.

All results described so far were obtained with a large amplitude (500 mV) potential modulation centered approximately at $E°$. The results of a small amplitude experiment with potential scanning are shown in Figure 8 for three different modulation amplitudes. The modulation frequency was 10 Hz and the phase of the lock-in amplifier was set at that for minimum background (−20°). The 2 mV/s scan rate was slow relative to the modulation period and the time constant of the lock-in amplifier (0.3 s). Table I includes the peak output of the lock-in amplifier for modulation amplitudes from 5 to 100 mV. The peak outputs for scanning experiments are reported relative to the experimental diffusion limited values obtained with large ΔE. Both experimental responses are about 20% lower than ideal square wave response at −20° for a 10 Hz modulation frequency. The detection limit for a scanning experiment at 10 Hz was 2×10^{-7} M for a 60 mV modulation amplitude.

A background interference was encountered when a high concentration of a nonabsorbing electroactive species was present. Benzoquinone is reduced to its anion radical at −0.5 V in acetonitrile, but both oxidized and reduced forms do not absorb at 633 nm. Figure 9 shows a scanning experiment for a mixture of TAA with a 16-fold excess of benzoquinone. The peak at −0.5 V is due to the quinone and is probably due to thermal or concentration induced refractive index gradients.

Table II. Comparison of Spectroelectrochemical Techniques

technique	$(\epsilon C)_{min}$[a]	$(\epsilon C)_{min}$,[b] cm^{-1}	conditions[c]
optically transparent electrode (7)	$0.886A_{min}(Dt)^{-1/2}$	0.18	
optically transparent thin-layer electrode (7)	Ab^{-1}	0.1	b = 0.02 cm
internal reflection spectroelectrochemistry (23)	$A_{min}(N_{eff}\delta\gamma^{1/2})^{-1}$	0.02	$A_{min} = 1 \times 10^{-5}$, N = 10, δ = 4000 Å
fiber optic thin-layer cell (15)	$A_{min}b^{-1}$	0.002	b = 1.0 cm
long path thin-layer cell (13)	$A_{min}b^{-1}$	0.0012	b = 1.62 cm
multiple specular reflection (24)	$[A_{min}T(\cos\alpha)/4L](\pi/Dt)^{1/2}$	1.5×10^{-4} calcd[d] 0.028 exptl[d]	
sinusoidally modulated ac reflectance (19)	$[0.87\omega^{1/2}(\cos\theta)\ RT/D^{1/2}\Delta EnF]\Delta R_{min}$	0.025	$\Delta R_{min} = 1 \times 10^{-5}$, ω = 100 Hz, ΔE = 20 mV, $E = E_{1/2}$, θ = 45°
glancing incidence reflection (25)	$(A_{min} \sin\beta/4)(\pi/Dt)^{1/2}$	0.0015	β = 1°
parallel absorption (12)	$A_{min}b^{-1}$	0.0044	b = 0.45 cm
diffraction with signal averaging (17)	$A_{min}b^{-1}$	0.002 (calcd) 0.013 (exptl)	exptl A_{min} = 0.015 b = 1.1 cm
modulated diffraction (this work)	$\Delta I_{min}(2.3I_0b\gamma)^{-1}$	2.2×10^{-4} (exptl)[e]	

[a] Minimum value for ϵC derived from equations for absorbance given in original references. [b] Calculated value for conditions listed, unless indicated as an experimental value. Reported experimental values were always higher than calculated values. [c] A_{min}, minimum measurable absorbance; D, diffusion coefficient of reactant. For the purposes of comparison, A_{min} = 0.002, $D = 1.0 \times 10^{-5}$ cm^2/s, and t = 10 s unless stated otherwise. [d] Calculated value for T = 100 μm, L = 4 cm, α = 45°, t = 10 s, A_{min} = 0.002. Observed value was lowest reported. [e] Corresponds to minimum measurable $\Delta I/I$ of 8×10^{-6}.

These effects have a different phase relationship than the absorbance signal, since they are transient effects. Figure 9 also shows a scan carried out at a phase angle which minimizes the quinone signal. While the TAA signal is decreased, the quinone peak is virtually eliminated.

DISCUSSION

The rapid response to a constant absorbance shown in Figure 2 demonstrates that diffracted light is effectively sampling a region very close to the electrode. $(Dt)^{1/2}$ at 20 ms is 4 μm, implying that the diffracted light at 2.6° is sampling a less than 4 μm thick portion of the diffusion layer adjacent to and driven by the electrode. The faster response of absorbance over previous work (17) is a consequence of the higher diffraction angle allowed by the shorter electrode. The 168-μm optical path length is being achieved after only 4 μm worth of diffusion, since the diffusion direction is across rather than parallel to the beam. In addition, the diffraction experiment is theoretically applicable to cases where both reactant and product absorb, with only the change in molar absorptivity being important to the response.

For a modulation experiment producing an ideal square wave, the lock-in amplifier output would be predicted to be half of the peak to peak signal calculated from eq 2 or 3. Furthermore, an ideal diffracted intensity vs. time wave form would track the applied potential and the phase shift would be zero. Since the rise time of the attenuation of the diffracted light is finite, the change in diffracted intensity always lags the applied potential and the demodulated signal is slightly smaller than that predicted from eq 2 or 3. Notice that phase shifts ϕ will be in the range of 0° to −50° or −180° to −230° depending upon whether Ox or Red is the absorber but are always reported as the lower range here. The signal magnitudes and phase shifts depend on several experimental variables in predictable fashions, as shown in Figures 5–7. First, larger diffraction angles increase the signal because the rise time of the change in diffracted intensity is faster at higher angles. In effect, the larger angles sample regions closer to the electrode and the electrode process can more rapidly generate and remove absorber. Second, higher modulation frequencies decrease the signal and increase the magnitude of the phase shift. For a fixed rise time of the attenuation of the diffracted light determined by the diffraction angle, an increase in frequency will produce a more distorted square wave, lower demodulation signal, and larger phase shift. As shown in Figure 6, the phase of maximum signal shifts more negative at higher frequencies. The net result of these effects is a demodulated signal which is 10–30% lower than that predicted from eq 3. As noted in the results section, the LIA response was linear with concentration over the range from 3×10^{-7} to 1×10^{-4} M TAA. Higher concentrations could certainly be determined, although some nonlinearity is likely because the shape of the wave form will change when the absorbance exceeds about 0.3. Given such high absorbance values, a modulation technique is probably unnecessary and single step experiments would be a simpler approach.

The TAA detection limit of 2×10^{-8} M corresponds to an absorbance of 4×10^{-6} in a 0.0168-cm cell. Electrochemical modulation of the absorber permits such low absorbances to be measured, and the combination of small absorbance and relatively long path length results in low detection limits. An attempt to improve the detection limits by increasing the electrode length b did result in an increased signal, but also more noise. Larger b leads to lower diffracted intensity and increased solution noise, and detection limits were comparable for b = 0.05 cm and 0.0168 cm.

The origin of the background signals shown in Figure 3 is not clear, but they are likely to result from refractive index gradients generated by ion motion during double layer charging. The transient charging current would cause temporary concentration gradients near the electrode, and the resulting refractive index gradients would affect the diffraction pattern. If a Faradaic process involving nonabsorbers occurs, these gradients would be larger and would lead to the signal observed in Figure 9. It is important to note that absorber generation leads to a constant attenuation of diffracted light (Figure 2), while a refractive index gradient is a transient phenomenon associated with current flow. Therefore the two effects have different phase relationships, and the background can be decreased relative to the absorbance signal with proper

choice of phase. Thus an absorber should be distinguishable from a nonabsorber even if they have the same redox potential, but care must be taken when determining an absorbing redox system in the presence of a large concentration of a nonabsorbing electroactive species.

The experiments in Figures 8 and 9 and eq 5 and 6 are very similar to the corresponding expressions for ac polarography, and the two methods have the same peak width. The two techniques are conceptually similar, in that their potential dependence is derived from the fraction of a redox system in one redox state at the electrode surface. An important difference is that ac voltammetry measures the **flux** of redox material reaching or leaving the surface, while the spectroelectrochemical method measures the **concentration** at or near the surface. In addition, the spectroelectrochemical method possesses the added selectivity of a spectroscopic absorption measurement of redox activity over more common monitoring of current.

A direct comparison of the present method with other spectroelectrochemical techniques is not straightforward due to differences in time scale and instrumental variables. In several cases, techniques were designed for examining reaction mechanisms, and analytical sensitivity was not optimized. With these caveats in mind, Table II compares several techniques with respect to their ability to measure the minimum product of molar absorptivity and bulk concentration, $(\epsilon C^b)_{min}$. This quantity provides the most relevant comparison of detection limits since it is composed of variables related only to the analyte and not the instrument or technique. The spectroelectrochemical techniques listed vary significantly in both their optical path lengths and their minimum measurable absorbance, A_{min}. With comparable A_{min}, those techniques with long path lengths will have better detection limits. Furthermore, those methods which are amenable to signal averaging will improve detection limits by decreasing A_{min}. The low detection limits of the modulated diffraction technique presented here result from both relatively long path length and signal to noise enhancement provided by potential modulation.

Registry No. TAA, 13050-56-1.

LITERATURE CITED

(1) Roston, D. A.; Shoup, R. E.; Kissinger, P. T. *Anal. Chem.* **1982**, *54*, 1417A.
(2) Caudill, W. L.; Howell, J. O.; Wightman, R. M. *Anal. Chem.* **1982**, *54*, 2532.
(3) Vydra, F.; Stulik, K.; Julakova, E. "Electrochemical Stripping Analysis"; Halsted Press: New York, 1977.
(4) Flato, J. D. *Anal. Chem.* **1972**, *44*, 75A.
(5) Adams, R. N. *Anal. Chem.* **1976**, *48*, 1126A.
(6) Wightman, R. M. *Anal. Chem.* **1981**, *53*, 1125A.
(7) Heineman, W. R.; Hawkridge, F. M.; Blount, H. N. In "Electroanalytical Chemistry"; Bard, A. J., Ed.; Marcel Dekker: New York, 1984; Vol. 13, pp 1-113.
(8) McCreery, R. L. In "Physical Methods in Chemistry"; Rossiter, B., Ed.; Wiley: New York, in press.
(9) Robinson, R. S.; McCurdy, C. W.; McCreery, R. L. *Anal. Chem.* **1982**, *54*, 2356.
(10) Bancroft, E. E.; Sidwell, J. S; Blount, H. N. *Anal. Chem.* **1981**, *53*, 1390.
(11) Tyson, J. F.; West, T. S. *Talanta* **1980**, *27*, 335.
(12) Pruiksma, R.; McCreery, R. L. *Anal. Chem.* **1981**, *53*, 202.
(13) Zak, J.; Porter, M. D.; Kuwana, T. K. *Anal. Chem.* **1983**, *55*, 2219.
(14) Porter, M. D.; Kuwana, T. *Anal. Chem.* **1984**, *56*, 529.
(15) Brewster, J. D.; Anderson, J. L. *Anal. Chem.* **1982**, *54*, 2560.
(16) Rossi, P.; McCurdy, C. W.; McCreery, R. L. *J. Am. Chem. Soc.* **1981**, *103*, 2524.
(17) Rossi, P.; McCreery, R. L. *J. Electroanal. Chem.* **1983**, *151*, 47.
(18) Bard, A. J.; Faulkner, L. R. "Electrochemical Methods"; Wiley: New York, 1980; p 161.
(19) Hinman, A. S.; McAleer, J. F.; Pons, S. *J. Electroanal. Chem.* **1983**, *154*, 45.
(20) Bard, A. J.; Faulkner, L. R. "Electrochemical Methods"; Wiley: New York, 1980; pp 331-332.
(21) Nelson, R. F.; Adams, R. N. *J. Am. Chem. Soc.* **1968**, *90*, 3925.
(22) Winograd, N.; Kuwana, T. *J. Am. Chem. Soc.* **1971**, *93*, 4343.
(23) Winograd, N.; Kuwana, T. *Anal. Chem.* **1971**, *43*, 252.
(24) Baumgartner, C. E.; Marks, G. T.; Aikens, D. A.; Richtol, H. H. *Anal. Chem.* **1980**, *52*, 267.
(25) Skully, J. P.; McCreery, R. L. *Anal. Chem.* **1980**, *52*, 1885.

RECEIVED for review July 27, 1984. Accepted December 3, 1984. Major support for this work was provided by the chemical analysis division of the National Science Foundation, with additional support from the Technicon Instrument Corporation.

Pulsed Infrared Laser Thermal Lens Spectrophotometry of Flowing Gas Samples

Scott L. Nickolaisen and Stephen E. Bialkowski*

Department of Chemistry and Biochemistry, Utah State University, Logan, Utah 84322

The behavior of the pulsed infrared laser thermal lens signal is studied for flowing gas samples. Possible sources of decreased TLS signal are discussed including flow rate and cell temperature. The TLS signal is found to be independent of the flow rate at all flow rates studied. It is calculated that absorbances as low as 2.5×10^{-7} in argon and 1×10^{-7} in liquid carbon disulfide should be detectable. The possibilities of using this technique as a chromatography detector for ultratrace amounts of analyte are also discussed.

The use of laser analytical techniques has produced interesting results both in terms of sensitivity and in the selectivity of the specific technique (*1*). This progress has for the most part been due to the high spectral brightness and good optical characteristics of the laser source (*2*). There are effectively two major classes of laser analytical techniques for spectrophotometric analysis. The first class relies on the luminescent relaxation mechanism. Among this class is laser-induced breakdown spectroscopy (*3*), single and multiphoton laser excited fluorescence (*4*), and light scattering spectroscopies. The second class derives the analytical signal from dark relaxation pathways of the laser excited analyte (*5*). The latter category includes photoacoustic (*6*), photothermal lensing (*7*) and deflection (*8*), and interferometry (*9*). Absorption spectrophotometry utilizing laser light sources may also be placed in this category.

0003-2700/85/0357-0758$01.50/0 © 1985 American Chemical Society

Perhaps the most well-known of the laser analytical techniques in the latter category, which derives the signal from an optical source, is thermal lens spectrophotometry (TLS). There are two means by which sample excitation can be performed in TLS. The most common method is to use a chopped continuous wave (CW) laser. This method may be used in either the single or dual laser configuration (*7, 10–14*). The second means by which the sample can be excited is through the use of a pulsed laser. In this case, the excitation laser cannot be used as a probe and the use of a pulsed laser necessitates a dual laser configuration. This method of sample excitation results in signals which are in general quite different than those obtained with CW excitation (*7, 13*). With the exception of the works by Imasaka et al. (*15, 16*) and ourselves (*17–19*), pulsed laser TLS has not been exploited for analytical purposes. It has, however, found widespread use for solutions to problems of a physical chemistry nature (*20–24*).

It is well-known that there is a need for development of better detectors for chromatography and the use of laser analytical techniques has not been overlooked (*25, 26*). However, there have been relatively few studies of the use of TLS for flowing sample analysis (*27–30*). The latter two studies demonstrated the utility of CW laser TLS for flowing sample detection. However, the sensitivity of the technique was found to decrease with increasing flow rate, thus limitations on the applicability of CW laser TLS were discovered.

In this paper we report on the use of pulsed infrared laser TLS for flowing sample analysis. Unlike the CW laser technique, there is no degradation of sensitivity at moderate flow rates. The advantages to the use of pulsed infrared laser sample excitation are as follows: first, the rise time of the analytical signal is much shorter than the time scales for probe laser power fluctuation or gas dynamic effects such as turbulence, mass transfer, and thermal diffusion (*5, 7, 14–21, 24, 27, 28, 29, 31, 32*); second the infrared source allows a wide variety of analytes to be excited, not just those with visible transitions; and third, the high pulse energy of the TEA-CO_2 laser allows for multiphoton excitation of the analyte, thereby increasing the temperature rise in the sample while narrowing the spatial distribution of this profile (*33*). The latter effects will result in a greater signal and may even overcome the limitation of infrared excitation, over that of visible–ultraviolet, due to the lower transition energy. The present work specifically addresses the utility of the pulsed infrared laser TLS technique for flowing gas analysis, but there is no reason why this technique could not be used for liquid phase analytes as well.

THEORY

The theories for both CW laser and pulsed laser excited TLS have been described by a number of authors and have been summarized by Fang and Swofford (*7*). Of importance to this study are the temporal characteristics of the pulsed laser TLS signal and the differences between the pulsed and CW excitation source. One of the ways by which thermooptical methods of analysis can be compared is by the theoretical enhancement factors (*7, 10*). The ratio of the pulsed laser enhancement factor to that of the CW laser is (*15*)

$$\frac{3^{3/2}E_p}{P_{cw}\omega_0^2}K \tag{1}$$

where E_p is the pulsed laser energy, K is the thermal diffusivity, P_{cw} is the CW laser power, and ω_0 is the $1/e$ electric field radius of the excitation laser. This equation is for typical optics with matched probe excitation beam radii in the sample. Typical values for the thermal diffusivity are 1.0×10^{-7} m^2/s for liquid benzene and 1.9×10^{-5} m^2/s for argon gas at standard conditions. In these experiments ω_0^2 is about 1.5 $\times 10^{-7}$ m^2, although smaller beam waist radii may be obtained with visible lasers (*2*). For equivalent average energies, the enhancement factor ratio is close to unity for liquid-phase samples but very much greater than one for gas-phase samples. Thus, the pulsed laser technique is clearly preferable for gas-phase analysis.

Another point to consider is that of the rise time of the signal. When a CW laser is used as an excitation source, the temperature change resulting in the TLS signal increases slowly in time as energy is put into the sample. Carter and Harris (*34*) have shown that for the aberrant lens model, the temporal response of the signal is

$$\frac{I(0) - I(t)}{I(0)} = \frac{0.58\Theta_{cw}}{(1 + t/t_c)} \tag{2}$$

where $I(t)$ is the transmitted intensity at time t, $I(0)$ is the transmitted intensity prior to turning the excitation source on, the parameter Θ_{cw} is a dimensionless collection of variables which is related to the strength of the thermal lens, and t_c is the thermal response time constant, $t_c = \omega^2/4K$. The signal, defined above is not given in the form usually used for CW excited TLS, but rather in that form used for pulsed laser TLS. After a time equal to the thermal time constant, the signal has reached 50% of the maximum value; to reach 90% of this value requires that $t = 9t_c$.

In contrast, the temporal behavior of the pulsed laser TLS signal, assuming neglectable contributions due to mass diffusion (*31*) and acoustic effects (*32*), is for $t_r < t_c$ (*17*)

$$\frac{I(0) - I(t)}{I(0)} = \Theta_p(1 - e^{-t/t_r}) \tag{3}$$

where, again, Θ_p is a parameter proportional to the strength of the thermal lens and t_r is the first-order time constant for excited state relaxation. This expression was derived assuming a parabolic lens (*33, 34*), a laser pulse which is much shorter than the excited state relaxation time, and a pseudo-first-order relaxation mechanism. The signal reaches 90% of its maximum value in $2.303t_r$.

Values of t_r range from about 1 μs for gas-phase analytes at standard conditions down to picoseconds or even femtoseconds in solution phase. For example, the relaxation time constant for dichlorodifluoromethane in argon at standard conditions and excited with a CO_2 laser is $t_r = 0.15$ μs (*35*). This is actually slow relative to the other vibrational relaxation times compared in the latter reference. The thermal response time constant for the same system with $\omega_0^2 = 1.5 \times 10^{-7}$ m^2 is $t_c = 2.0$ ms. Thus the time required for the CW laser excited TLS signal to attain 90% of the maximum value is over 5 orders of magnitude longer than that for pulsed laser excitation.

The rise time of the pulsed laser TLS signal will be ultimately limited by the acousic transit time (*24, 32*). This is the time required for the pressure disturbance created by the increased temperature to dissipate from the excited region, $t_a = \omega_0/c$, where c is the sound velocity. The sound velocity for argon is $c = 321$ m/s (*36*) and the acoustic transit time is $t_a = 1.2$ μs. The sound velocity of benzene is 1395 m/s and the acoustic transition time will be correspondingly shorter in liquid phase.

EXPERIMENTAL SECTION

The TLS optical apparatus used in this study has been previously described (*17*) and will only be outlined here. A pulsed CO_2 laser was employed as the excitation source, and a CW He–Ne laser was used as the probe laser. The pump laser was a TEA-CO_2 laser constructed in this laboratory. The rate of pulsing was 3.75 Hz, and the laser was operated on the P32 line of the 10.6-μm transition at 933 cm^{-1}. Transverse mode control was accomplished with the use of an intercavity iris. Each pulse lasted about 150

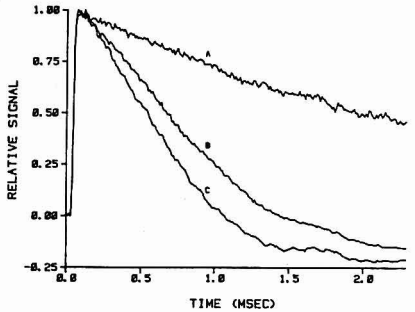


Figure 1. Time-resolved TLS signal for 0.1% chlorodifluoromethane in argon at flow rates of (A) no flow, (B) 60 mL/min, and (C) 150 mL/min.

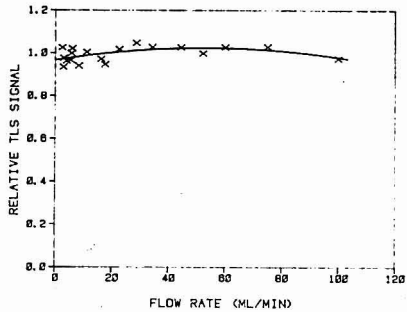


Figure 2. Relative TLS signal as a function of flow rate for 9.9 ppm dichlorodifluoromethane in argon at atmospheric pressure.

ns with a 3-μs "tail". The laser energy per pulse was less than 100 mJ, thus each pulsed delivered approximately 600 kW of power. The probe laser was a 5-mW Uniphase Model 1105P He-Ne laser which operated at the wavelength of 632.8 nm. The CO_2 laser was passed through a germanium flat where approximately half of the beam was transmitted. The transmitted portion of the beam was mixed at the Ge flat with the He–Ne laser so that the two beams were collinear. That portion of the CO_2 beam reflected at the Ge flat was used to monitor the energy of the CO_2 laser by means of a Laser Precision Model RjP-735 energy monitor.

The flowing cell was constructed in this laboratory from stainless steel. It had the dimensions of 0.7 cm i.d. by 5.5 cm length. It was mounted with NaCl windows which were sealed to the cell using O-rings. The inlet and outlet ports were placed as close to the ends of the cell as possible to reduce any dead volume within the cell. The CO_2 and He–Ne lasers were focused through the center of the cell using a 30-cm focal length BaF_2 lens and a 25-cm focal length fused silica lens, respectively. The positioning of these lenses was such that the He–Ne beam focus was about 15 cm past the cell. The detector used was an EG&G SCD-040-A PIN photodiode with a pinhole size of 0.06 mm radius. The detector was placed about 1 m from the sample cell. The detector signal was amplified by an ac coupled LM741C differentiating amplifier. The diode signal was recorded with a Physical Data Model 522A, 20 MHz, 8 bit transient digitizer. The CO_2 monitor was connected to an ADAC Corp. Model 1012, 16 channel, 12 bit, programmable gain A/D converter. Both the A/D converter and transient digitizer were interfaced with a DEC LSI 11/2 microprocessor. Data acquisition was accomplished by means of a computer program which corrected the photodiode signal for variations in the energy of the CO_2 laser. For each data point taken, the signal from 100 pulses was averaged and recorded.

The gas sample used for the study of flow rate and temperature dependence was a Matheson gas cylinder analyzed to 9.9 ppm dichlorodifluoromethane (FC-12) in argon. The gas cylinder was connected to the cell input port, and a bubble meter by which the flow rate was measured was connected to the output port. The gas flow rate was controlled with a needle valve connected to the cylinder regulator. The temperature of the cell was adjusted by use of a heating cord wrapped around the flow cell. For the GC runs a 1.22 m × 5 mm i.d. 20% Carbowax 20 M on Chromosorb-P 80/100 mesh column in a Gow-Mac Series 550 gas chromatograph was used with argon as the carrier gas. Signals for the GC runs were collected with the A/D converter and CO_2 laser energy fluctuation were not accounted for.

RESULTS AND DISCUSSION

Typical pulsed laser TLS signals detected by the PIN diode-pinhole detector without preamplification are illustrated in Figure 1. These signals were obtained for 100 averages of a 0.1% by volume mixture of chlorodifluoromethane in the flow cell. The high concentration of chlorodifluoromethane was required to obtain a signal of 50 mV, which is the minimum input range of the transient digitizer. The rapid rise time of the signal is apparent. In fact, the rise time of the data illustrated in Figure 1 is limited by the sampling interval of 5 μs. Thus; the probe laser intensity change occurred on a time scale less than 5 μs. This figure also illustrates the effect of sample flow on the TLS signal. While the signal maxima are the same, the signal decay rate increases with flow rate.

The gas flow rate dependent TLS signal for the dichlorodifluoromethane/argon mixture at 100 kPa is illustrated in Figure 2. The flow rate ranges from about 3 mL/min to 100 mL/min corresponding to a maximum linear flow of 4.3 cm/s through the 3.8 mm cross section of the flow cell. As can be seen, the signal is found to be essentially constant over the range studied. This observation is in sharp contrast to previous studies of the flow rate dependent CW laser TLS signal. Dovichi and Harris (*27*, *28*) found that with a sample residence time in a liquid flow cell of 3.04 s, the CW laser TLS signal was diminished by a factor of 43%. The calculated minimum residence time in these experiments is 26 ms. No signal decrease was observed. This significant difference is due to the nature of the TLS signals. In these experiments, the data are obtained over a short (100 μs) time.

The short signal rise times, and thus the data acquisition time, have several important implications in chromatographic and flowing sample applications. The first implication is that the signal does not decrease as rapidly with flow rate as does the CW TLS signal. We would not expect to observe a signal decrease unless the gas dynamic mass transfer time scale was on the order of that of the rise time of this signal. This will occur at about $t_r = \omega_0/V$, where V is the linear flow rate of the sample. Since the rise time of the signal in these experiments is limited by the acoustic transit time, as discussed above, the linear velocity may have to be on the order of the sound velocity for signal degradation to occur.

The second implication of the rapid signal acquisition time is that the sample rate can be higher than that of the CW laser TLS case. In this case however, it is not the rise time of the signal that limits the sample rate, but rather the decay time. The decay time constant for pulsed laser TLS signals is shorter than that for the CW case since the signal decreases proportional to $(1 + 2t/t_c)^{-2}$. So in the time required for the CW laser signal to decay to 1/2 the maximum value, the pulsed laser signal has decayed to 1/9, 1/4 to 1/49, etc. The time required for the signal to decay to 1% of the maximum in these experiments is 44 ms. In essence, the time required to obtain a CW laser signal is that of the characteristic rise time. If, for example, the analyte composition was to change abruptly, it would take $9t_c$ for the CW laser signal to respond. For analytes that elute off of a chromatography column in time less than t_c, the signal would be that of the convolution of the

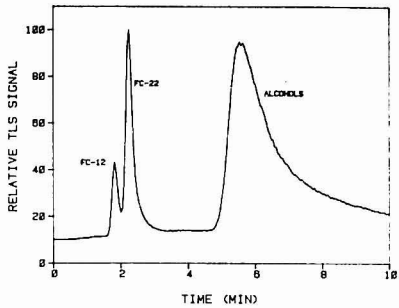


Figure 3. Demonstration of the use of pulsed laser TLS for packed column GC. The three peaks are due to chlorotrifluoromethane, dichlorodifluoromethane, and ethanol, respectively. Response due to benzene solvent was not observed at the excitation wavelength used.

thermal Green's function (7) with that of the temperature source due to the transient analyte. This would serve to diminish the maximum signal as well as lower the effective resolution of the separation process. For the pulse laser case, if the analyte elutes in a time less than the repetition rate of the laser, then there is a chance that no signal will result. The signal decay time limits this rate to about 22 Hz, and any analyte which elutes in less than 44 ms could be missed.

Figure 3 illustrates the response of the pulsed TLS apparatus to a GC separated mixture of halocarbons and alcohols in benzene solvent. In this case a packed column was used so that the resolution is not as high as could be obtained with modern capillary columns. The data were collected as a function of time in such a manner as to sum each consecutive 10 data into one datum. The effective time constant is thus ten times the repetition rate. However, due to the large pulse to pulse energy variations of the CO_2 laser used in these experiments, this was necessary to obtain acceptable S/N. It is apparent from this figure that there is no problem with using the low repetition rates for packed column GC analyte detection.

The data in Figure 2 indicate that the TLS signal obtained at the lower flow rates might be less than that for a high one. In investigating this we found that the signal obtained just after the CO_2 laser was turned on was in fact greater than that obtained after the sample had been irradiated for several minutes. Further, the recovery time was found to be about 5 min. With even the slowest flow rate of 3 mL/min, the time required to replace the contents of the flow cell is less than 1 min. We subsequently rule out the possibility of a chemical transformation taking place as a result of laser irradiation which diminishes the signal. It is more likely that the temperature of the cell is increasing due to the buildup of heat from the repetitively pulsed sample. With the faster flow rates, the rate of cooling of the flow cell is sufficient to overcome the heating rate and thus the signal does not diminish in time.

The effect of temperature of the TLS signal for gas samples can be determined rather easily. The parameter, Θ_p, in eq 3 is (17)

$$\Theta_p = \frac{8\alpha E_p l}{\pi\omega_0^4 \rho C_p}\left(\frac{dn}{dT}\right)_p \qquad (4)$$

Here α is the exponential absorption coefficient, l is the length of the sample cell, n_0 is the refractive index of the gas, ρ is the molar density and C_p is the heat capacity. Since C_p and α do not vary significantly over a small temperature range, the main temperature-dependent parameters are ρ and $(dn/dT)_p$. Bailey et al. (20) have shown that the temperature dependence of $(dn/dT)_p \propto 1/T^2$, and that of ρ is $1/T$. Overall, the TLS signal should decrease as $1/T$. We have confirmed this effect by measuring the signal at a flow rate of 67 mL/min while varying the flow cell temperature from 30 °C to 110 °C. The implication of this effect in the use of pulsed laser TLS in GC effluent detection is that since the sample cell will generally be operated at elevated temperature, the signal can be expected to decrease over that at room temperature.

The third implication of the fast rise time of the pulsed laser TLS signal is that the effects of turbulence and other mass transport effects will be minimized. If the rise time of the signal is faster than the characteristic mass transport effect time, then these effects will not be manifested in the signal. One effect that may be important in gas-phase analytes is that of mass diffusion. The characteristic time constant for mass diffusion is $t_p = \omega_0^2/4D$, D being the mass diffusion coefficient. This is not an important consideration at pressures above 5 kPa. The turbulence time scales are much more difficult to estimate but are probably about that of the flow rate limited mass transport through the laser beam diameter in the cell. Thus, if the flow rate is fast enough that the signal diminishes over that of static conditions, turbulence could be expected to decrease the precision of the measurement (28, 29). The standard deviations of the TLS signals obtained over the range of flow rates demonstrated no significant variation with flow rate. In these experiments, the major contribution to fluctuations in the TLS signal was not that of the turbulence in the flow cell, as found by Dovichi and Harris (28, 29), but rather was due to the pulse to pulse laser energy and mode changes. The relative precision due to these effects can be seen in Figure 2 at the lower flow rates.

The relative precision of the data in Figure 2 is 4% and that of each point, an average of 100, ranged from 1.4% to 5%. The precision of the measurements obtained in these experiments may be expressed as the sum of those relative deviations due to pump laser mode variations, intensity changes in both the pump and probe lasers, alignment errors from vibrations and laser pointing noise, intrinsic gas dynamic variances, and instrumental errors as a result of digitization of the signals, instrumental noise, and interferences. Signal variations as a function of pump laser energy fluctuations were compensated for in the data reduction. Instrumental noise and interference were less than the least significant bit of the transient digitizer (<0.4%). The major instrumental variance was due to the quantization error in the transient digitizer, 1.5% for a 1/4 full scale signal. Large relative errors due to gas dynamic effects may be ruled out since the precision of measurements do not vary with flow rate.

Major factors controlling the signal precision appear to be a result of pulse to pulse TEA-CO_2 laser mode variations and pointing error, and short-term intensity variations in the probe laser intensity. The long-term variation of optical setup is 0.4%. This relative variation was determined by monitoring the probe laser with the PIN photodiode through the pinhole. Thus, probe laser pointing noise, long-term intensity variance, and optical table vibrations should all affect this test signal. The short-term probe laser intensity variations are more important to consider since the ac coupled preamplifier was used. The relative standard deviation of these high frequency probe laser intensity fluctuations was found to be 4% when the preamplifier was used. The sum of these relative errors does not account for the signal variance since signal averaging would result in a precision improvement.

Errors due to the mode variations of the pump laser are difficult to determine. The TLS signal should be sensitive to these mode variations since they affect the energy distri-

bution at the focus and the beam divergence and subsequently the focus location and may result in effective pointing noise (7). We have examined the data distribution by plotting the signal data as a function of CO_2 laser energy (19). The correlation between these two parameters is much lower than that predicted from the variances due to the sources discussed above. We believe that this low correlation is due to the CO_2 laser mode variance, and this variance is the main contribution to the signal variance.

Finally, it is useful to compare the short time TLS signals that we have obtained in the gas phase to those that would be expected to be observed in solution. In these experiments we have shown that the flow of gas does not significantly degrade the TLS signal up to flow rates of 100 mL/min. Thus, the minimum amount of dichlorodifluoromethane that should be detectable is 1 ppbv, found in ref 17. This detection limit corresponds to an absorbance of 2.5×10^{-7} in the 7 cm path length cell used in that study. The enhancement factors for liquids and gases are not significantly different. In fact, the ratio of enhancement factors of CS_2 to Ar is only 0.6 (15, 16). CS_2 is a suitable solvent for infrared TLS using a CO_2 laser since there are no major absorptions near the laser wavelength. The minimum detectable absorbance in flowing CS_2 solutions could be as low as 4×10^{-7}.

CONCLUSION

The technique described here promises to be a very useful analytical tool. Quantitative measurements on a static cell have produced detection limits of 1 ppbv FC-12 (17) and the results of these experiments indicate that comparable detection limits should be possible for a flowing sample. This technique will work for any analyte which has a significant absorption coefficient within operating wavelength range of the infrared pump laser. This includes a number of environmentally important pollutants such as ammonia and many substituted ethylenes, ethanes, and freons (34). The pulsed laser configuration decreases the problem of signal dependence on flow rate because of the fast signal rise time. This technique may offer great sensitivity as an LC detector as well. Modifications in cell design and construction would be necessary for LC; specifically, windows other than sodium chloride would be used when working with a liquid carrier phase. However, although the sensitivity of this technique is very good, the precision is not. There is still much work to be performed in order to understand the source of the poor precision and to correct for the presumably detectable factors resulting in the signal variances.

LITERATURE CITED

(1) Harris, T. D. *Anal. Chem.* **1982**, *54*, 741A–750A.
(2) Demtröder, W. "Laser Spectroscopy"; Springer-Verlag: New York, 1982.
(3) Cremers, D. A.; Radziemski, L. J. *Anal. Chem.* **1983**, *55*, 1245–1256.
(4) Birge, R. R. In "Ultrasensitive Laser Spectroscopy"; Kliger, D. S., Ed.; Academic Press: New York, 1983; pp 109–174.
(5) Hu, C.; Whinnery, J. R. *Appl. Opt.* **1973**, *12*, 72–79.
(6) Tam, A. C. In ref 4, pp 2–108.
(7) Fang, H. L.; Swofford, R. L. In ref 4, pp 176–233.
(8) Jackson, W. B.; Amer, N. M.; Boccara, A. C.; Fournier, D. *Appl. Opt.* **1981**, *20*, 1333–1343.
(9) Friedrich, D. M. In ref 4, pp 311–342.
(10) Dovichi, N. J.; Harris, J. M. *Anal. Chem.* **1979**, *51*, 728–731.
(11) Carter, C. A.; Harris, J. M. *Anal. Chem.* **1983**, *55*, 1256–1261.
(12) Swofford, R. L.; Morrell, J. A. *J. Appl. Phys.* **1978**, *49*, 3667–3674.
(13) Kliger, D. S. *Acc. Chem. Res.* **1980**, *13*, 129–134.
(14) Perry, J. W.; Ryabov, E. A.; Zewail, A. H. *Laser Chem.* **1982**, *1*, 9–15.
(15) Mori, K.; Imasaka, T.; Ishibashi, N. *Anal. Chem.* **1982**, *54*, 2034–2038.
(16) Mori, K.; Imasaka, T.; Ishibashi, N. *Anal. Chem.* **1983**, *55*, 1075–1079.
(17) Long, G. R.; Bialkowski, S. E. *Anal. Chem.* **1984**, *56*, 2806–2811.
(18) Long, G. R.; Bialkowski, S. E. *Anal. Chem.*, in press.
(19) Long, G. R.; Bialkowski, S. E., manuscript in preparation.
(20) Bailey, R. T.; Cruickshank, F. R.; Pugh, D.; Johnstone, W. *J. Chem. Soc., Faraday Trans. 2* **1981**, *77*, 1387–1397.
(21) Trevor, P. L.; Rothem, T.; Barker, J. R. *Chem. Phys.* **1982**, *68*, 341–349.
(22) Vaida, V.; Turner, R. E.; Casey, J. L.; Colson, S. O. *Chem. Phys. Lett.* **1978**, *54*, 25–29.
(23) Gupta, M. C.; Hong, S. D.; Gupta, A.; Moacanin, J. *Appl. Phys. Lett.* **1980**, *37*, 505–507.
(24) Siebert, D. R.; Grabiner, F. R.; Flynn, G. W. *J. Chem. Phys.* **1974**, *60*, 1564–1574.
(25) Yeung, E. S. In "Lasers in Chemical Analysis"; Helftje, G. M., Travis, J. C., Lytle, F. E., Eds.; Humana: NJ, 1981; pp 273–290.
(26) Brown, J. C.; Hayes, J. M.; Warren, J. A.; Small, G. J. In "Lasers in Chemical Analysis"; Helftje, G. M., Travis, J. C., Lytle, F. E., Eds.; Humana: NJ, 1981; pp 237–261.
(27) Buffett, C. E.; Morris, M. D. *Anal. Chem.* **1982**, *54*, 1824–1825.
(28) Dovichi, N. J.; Harris, J. M. *Anal. Chem.* **1981**, *53*, 689–692.
(29) Leach, R. A.; Harris, J. M. *J. Chromatogr.* **1981**, *218*, 15–19.
(30) Sepaniak, M. J.; Vargo, J. D.; Kettler, C. N.; Maskarinec, M. P. *Anal. Chem.* **1984**, *56*, 1252–1257.
(31) Bialkowski, S. E. *Chem. Phys. Lett.* **1984**, *104*, 448–454.
(32) Barker, J. R.; Rothem, T. *Chem. Phys.* **1982**, *68*, 331–339.
(33) Twarowski, A. J.; Kliger, D. S. *Chem. Phys.* **1977**, *20*, 253–258.
(34) Carter, C. A.; Harris, J. M. *Appl. Opt.* **1984**, *23*, 476–481.
(35) Xing-Xiao, M.; Zhu-De, X. *Chem. Phys. Lett.* **1983**, *96*, 563–565.
(36) Berry, R. S.; Rice, S. A.; Ross, J. "Physical Chemistry"; Wiley: New York, 1980; pp 1080–1089.

RECEIVED for review October 22, 1984. Accepted December 14, 1984. This research was supported in part by BRSG S07 RR07093-17 awarded by the Biomedical Research Support Grant Program, Division of Research Resources, National Institutes of Health. Much of the equipment was obtained through a grant from Research Corporation.

ADDENDUM

Analysis of Polynuclear Aromatic Mixtures by Liquid Chromatography/Mass Spectrometry

Kenneth J. Krost (*Anal. Chem.* 1985, *57*, 763–765).

The following material was inadvertently omitted from the publication:

EXPERIMENTAL SECTION

Materials. The chromatogrphic columns used were obtained from E. I. du Pont de Nemours, Inc., Wilmington, DE (Zorbax ODS, C_{18} octadecylsilane, bonded to SIL silica particles, 4.6 mm i.d. × 25 cm length), and Varian Instrument Corp., Walnut Creek, CA (Micropak, MCH-10, octadecylsilane bonded to 10-μm silica particles, 4.0 mm i.d. × 30.0 cm length).

The reverse-phase solvents, water and methanol, were obtained from Burdick and Jackson, Muskegan MI, HPLC grade. The following compounds were obtained from Aldrich Chemical Co. Inc., Milwaukee, WI: benzo[a]pyrene, 99+%;

The equipment used was a Finnigan 3200 mass analyzer combined with the standard Kaplon belt-driven interface. Data were acquired using a Finnigan/Incos 2300 data system. The high-performance liquid chromatograph used was a Varian Model 5000 combined with a Varian Vista 401 dedicated computer/terminal. Electron ionization spectra were taken with a standard Finnigan CI source at pressures of 5×10^{-6} torr.

RESULTS AND DISCUSSION

Eluent Flow and Composition. A schematic of the system used in this study is shown in Figure 1. A split ratio of 1:5 between the analyzer and waste solvent was generally maintained. A wide variance in flow, composition, and pressure was used for the eluents. Of particular importance was the flow-pressure curve for water and hexane (Figure 2). Clearly, when water was used in reverse-phase separations, severe flow and compositional restrictions occurred. However, at the other extreme, the system accommodated hexane with no significant rise in analyzer pressure.

Analysis of Polynuclear Aromatic Mixtures by Liquid Chromatography/Mass Spectrometry

Kenneth J. Krost

U.S. Environmental Protection Agency, Environmental Monitoring Systems Laboratory, Research Triangle Park, North Carolina 27711

The use of high-performance liquid chromatography combined with mass spectrometry is discussed for the analysis of polynuclear aromatic hydrocarbons. Parameters were determined as a function of eluent composition and flow. Precision and sensitivity were evaluated, along with the effect of the aforementioned parameters on overall performance.

High-performance liquid chromatography (HPLC) has proven to be an invaluable analytical tool in the separation of organic compounds. A basic incompatibility however exists with mass spectrometry. Up to 1000 cm^3/min of vapor can be generated from the eluent solvent during normal operation. Under these conditions, maintaining the low-mass analyzer pressure necessary for electron ionization mass spectrometry is all but impossible.

Three general approaches have been taken to circumvent this incompatibility. First is direct liquid injection, which involves vaporizing the eluent with the analyte (*1*, *2*). The vapor is then directed as an aerosol to the ion source, serving as both an analyte carrier and a reagent gas for chemical ionization. Pressures of 10^{-3} torr are observed in the ionization chamber. Furthermore, solvent flow is limited to 10–15 μL/min. When conventional mass spectrometry is used, informational content is limited to chemical ionization spectra.

Scott described a second general technique used in HPLC/MS analysis, in which the analyte was deposited onto a moving wire (*3*, *4*). This was followed sequentially by solvent evaporation and thermal desorption. Unfortunately, the capacity of the transport wire was restricted to around 1% of a standard HPLC column flow (1.0 cm^3/min), with a concurrent loss in instrument sensitivity.

A third popular technique involves analyte deposition onto a moving belt, followed by thermal eluent stripping (*5–9*). This technique suffers from the previously discussed incompatibility. Necessity dictates the use of a sample splitter, with a loss in sensitivity of up to 95%.

A fourth popular technique is that described by Vestal (*10*). This technique involves thermospraying effluents directly into the ion source and pumping away excess vapor. A conventional electron beam is used to provide gas-phase reagent ions for chemical ionization of solute molecules.

SAMPLE VOLATILIZATION

Conditions necessary for sample volatilization were established by using a standard test mixture of anthracene (12.4 ng/μL), pyrene (13.2 ng/μL), chrysene (10.2 ng/μL), and benzo[*a*]pyrene (10.2 ng/μL). A sample loop of 10 μL was used for injection. During eluent stripping, one attempts to preserve the analyte while removing excess eluent. Figure 3 depicts this situation. Analyte losses, incurred during eluent stripping, accounts for a significantly lowered molar response for pyrene and anthracene. The recoveries of benzo[*a*]pyrene and chrysene, however, vary from essentially zero at temperatures of 100 °C to semiquantitative at temperatures of 200 °C. In the lowered response observed for pyrene and anthracene, one is dealing with a loss in sensitivity due to prevolatilization prior to the ionization source. In the case

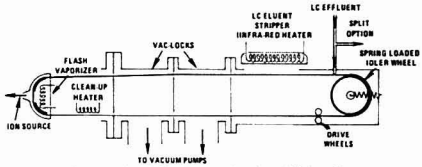


Figure 1. Schematic of Finnigan belt-driven LC interface.

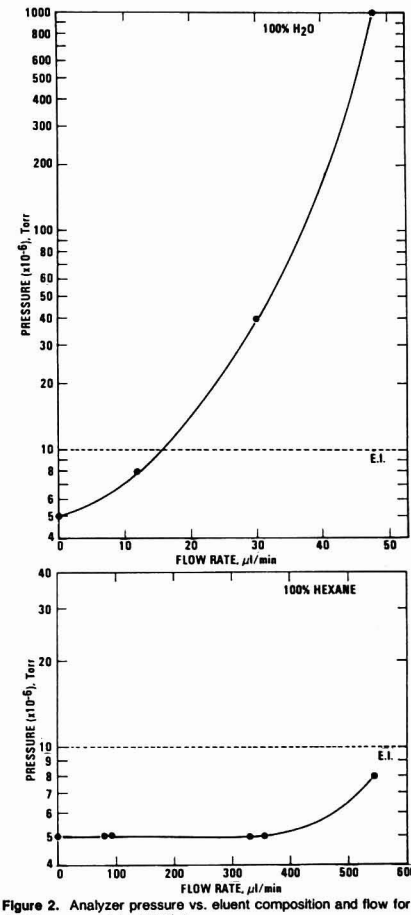


Figure 2. Analyzer pressure vs. eluent composition and flow for (a) 100% water and (b) 100% hexane.

This article not subject to U.S. Copyright. Published 1985 by the American Chemical Society

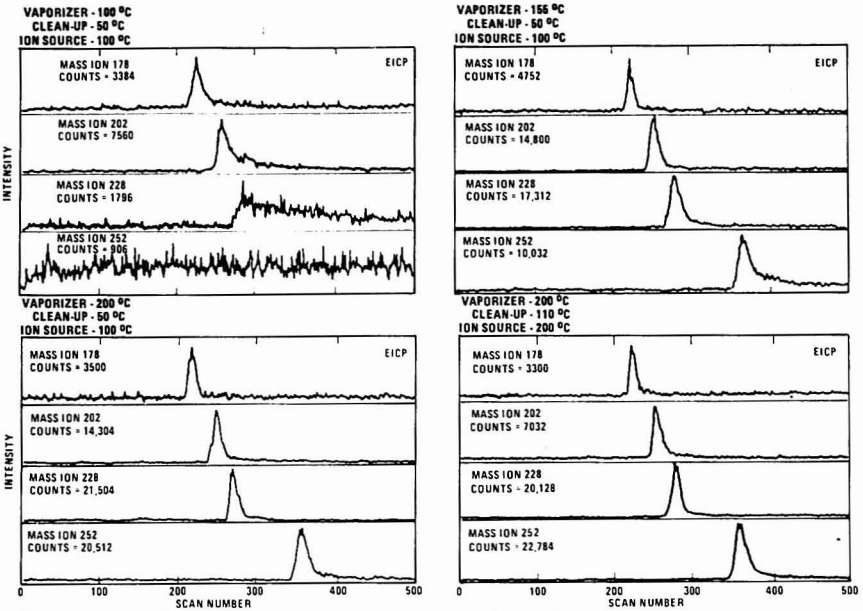


Figure 3. Ion intensity as a function of volatilization temperature: (a) vaporizer 100 °C, cleanup 50 °C, ion source 100 °C; (b) vaporizer 155 °C, cleanup 50 °C, ion source 100 °C; (c) vaporizer 200 °C, cleanup 50 °C, ion source 100 °C; (d) vaporizer 200 °C, cleanup 110 °C, ion source 200 °C.

Table I. Precision Measurements of Standard Mixture

	ANTHRACENE(178)	PYRENE(202)	CHRYSENE(228)	B(a)P(252)
UNCORRECTED RAW DATA				
NUMBER OF READINGS	12	12	12	12
CONC. IN STD. ABSOLUTE AMOUNT	22ng	24ng	18ng	18ng
PEAK AREA AVERAGE COUNTS	4763	10,972	20,073	20,006
RANGE OF PEAK AREA	6400-3888	13,136-8736	29,248-14,416	24,544-14,768
ERROR AT 1.0 SD, percent	16.4	13.0	19.0	16.0
ABSOLUTE ERROR AT 2.0 SD	22±7ng	24±6ng	18±7ng	18±6ng
STANDARD DEVIATION	-3.52ng	-3.12ng	-3.42ng	-2.88ng
CORRECTED RAW DATA				
ERROR AT 1.0 SD, percent	12.4	10.2		9.1
ABSOLUTE ERROR AT 2.0 SD	22±5ng	24±5ng		18±3ng

of chrysene and benzo[*a*]pyrene losses at reduced temperatures are probably caused by lack of volitilization. The necessity of choosing volatilization temperatures appropriate for the compounds under consideration is apparent.

PRECISION AND SENSITIVITY

Table I summarizes the precision and sensitivity for 12 determinations of the compounds in the standard polynuclear aromatic mixture.

In the corrected data, the use of an internal standard (chrysene) was used to normalize the response of the three other compounds. In the uncorrected data, no internal standard was used to normalize the response of the three compounds under evaluation. This experiment was designed

to evaluate the effect of an internal standard to compensate for instrumental variations.

The variation for benzo[a]pyrene was somewhat less than either the corrected or uncorrected values of other compounds. This phenomenon probably reflects the fact that less sample loss occurred during solvent stripping. It evidences the need for accurate control of LC interface setting. The use of internal standards will not adequately compensate for day-to-day variation in stripper and volatilization temperatures.

CONCLUSIONS

PNA sensitivity is, to an extent, a direct function of compound volatility. Losses incurred during eluent stripping appear to be a significant factor in the case of lower molecular weight compound sensitivity. Volatilization temperatures are critical for the recovery of high molecular weight compounds. The lower limit of detectability for polynuclear aromatics in the ion-selective mode is approximately 10 ng.

The precision observed on corrected raw data appears somewhat better at higher PNA molecular weights. This again probably reflects losses during solvent stripping and prevolatilization.

LITERATURE CITED

(1) Tal'rose, V. L.; Karpov, G. V.; Gordoershii, I. G.; Skurat, V. E. *Russ. J. Phys. Chem.* **1968**, *42*, 1658.
(2) Tal'rose, V. L.; Grishin, V. D.; Skurat, V. E.; Tantsyrev, G. D. "Recent Developments in Mass Spectrometry"; Ogta, K., Hagakawa, T., Eds.; University Park Press: Baltimore, MD, 1970.
(3) Scott, R. P. W.; Scott, G. C.; Munroe, M.; Hess, J. *J. Chromatogr.* **1974**, *99*, 395.
(4) Scott, R. P. W. *J. Chromatogr. Libr.* **1977**, *11*.
(5) McFadden, W. H.; Schwartz, H. L.; Evans, S. *J. Chromatogr.* **1978**, *122*, 389.
(6) McFadden, W. H.; Bradford, D. C.; Games, E. E.; Gower, J. L. *Am. Lab (Fairfield, Conn.)* **1977**, *9*, 55.
(7) Dark, W. A.; McFadden, W. H.; Bradford, D. C. *J. Chromatogr. Sci.* **1977**, *15*, 454.
(8) Dark, W. A.; McFadden, W. H. *J. Chromatogr. Sci.* **1978**, *16*, 289.
(9) McFadden, W. H.; Bradfor, D. C.; Eglinton, G.; Hagibrahim, S.; Dark, W. A.; Nicolaides, N., 26th Annual Conference of Mass Spectrometry and Allied Topics; May 1978, St. Louis, MO.

RECEIVED for review October 5, 1984. Accepted December 3, 1984. This article has not been subjected to Agency review and does not necessarily reflect the views of the Agency. Mention of trade names or commercial products does not constitute endorsement or recommendation for use.

CORRESPONDENCE

Ionization and Mass Analysis of Nonvolatile Compounds by Particle Bombardment Tandem-Quadrupole Fourier Transform Mass Spectrometry

Sir: Recent advances in the development of new ionization techniques have now made it possible to generate $(M + H)^+$, $(M - H)^-$, and $(M + \text{cation})^+$ ions as well as structurally significant fragment ions from many polar biological molecules having molecular weights up to as high as 13000 (*1–3*). Techniques such as fast atom bombardment (FAB) or liquid secondary ion mass spectrometry (L-SIMS) in which sample ions are ejected from a liquid matrix such as glycerol under bombardment with kilovolt atoms or ions, respectively, are presently in widespread use on both commercial quadrupole and magnetic sector instruments.

Unfortunately, advances in the design of instrumentation for mass analysis and structural characterization of the ejected ions have not kept pace with developments in new ionization methodology. Large magnetic sector instruments operating at full accelerating potential provide molecular weight information up to 12000 for samples in the 0.05–5 nmol range. Ion current in the mass range greater than 3000 daltons is usually too weak, however, to allow determination of molecular structure from fragmentation patterns. Collision-activated dissociation provides a mechanism for enhancing the structural information obtained in particle bombardment experiments, but kinetic energy released during the fragmentation process limits the resolution achieved by using tandem four sector instruments on samples at the 50 pmol level to ca. 2000. Considerably higher resolution can be achieved if the quantity of sample is increased by a factor of 10–100. Above mass 2500–3000, the combination of weak sample ion current and low ion transmission at unit resolution following the collision cell severely restricts the analytical utility of tandem sector instruments. Presently available tandem quadrupole instruments provide structurally rich collision-activated dissociation (CAD) spectra at unit resolution (*4*, *5*), but inefficient ion transmission above mass 1000 makes these instruments unsuitable for trace level analysis of high molecular weight biological materials.

Fourier transform mass spectrometry (FT-MS) offers an attractive alternative to the above instrumental methods (*6–10*). It can provide a mass range in excess of 10000 daltons in principle and can function as an ion storage device to accumulate ions produced in low abundance. Mass analysis is accomplished in Fourier transform mass spectrometry without destruction of the ions, and mixture components can be separated by using the double resonance technique. Consecutive collision-activated dissociation (*11*, *12*) and photodissociation (*13–16*) experiments can be performed on the same ion population. Long ion storage times and ultrahigh mass resolution have been demonstrated, but only when the pressure in the analyzer cell is below 10^{-8} torr. Glycerol and other liquid matrices employed in the particle bombardment ionization methods all have vapor pressures in excess of 10^{-6} torr and are therefore difficult to use in conjunction with Fourier transform mass spectrometry.

One way to overcome the problem associated with high gas flow during the ionization step is to use a differentially pumped, two compartment cell within a conventional Fourier transform mass spectrometer. An instrument containing such a cell has recently become available from Nicolet Instruments. Another approach utilizes a tandem-quadrupole Fourier transform mass spectrometer (QFT-MS) in which sample introduction and ionization are carried out in a differentially pumped quadrupole ion source and only the ions of interest

0003-2700/85/0357-0765$01.50/0 © 1985 American Chemical Society

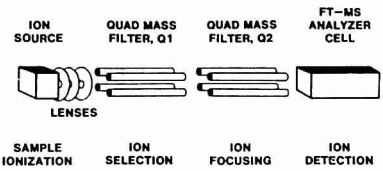


Figure 1. The tandem-quadrupole Fourier transform mass spectrometer.

are then transferred to the ion cyclotron resonance cell for mass analysis. Two of the present authors demonstrated the feasibility of injecting ions from a quadrupole ion source through the intense fringing fields of a superconducting magnet (*17*) and recently showed that daughter ions produced by collision-activated dissociation could be detected at a mass resolution of 140 000 (*18*, *19*). Here we report initial results obtained with a cesium bombardment ion source (*20*) on a second quadrupole Fourier transform mass spectrometer constructed at the University of Virginia.

EXPERIMENTAL SECTION

Tandem-Quadrupole Fourier Transform Mass Spectrometer. This instrument, shown schematically in Figure 1, consists of a standard Model 4500 ion source, lens system, and quadrupole mass filter from the Finnigan-MAT Corp., San Jose, CA, a second set of 86.25 cm long, quadrupole rods termed the guiding quadrupole, an 8.75 × 2.8 × 2.8 cm ion cyclotron resonance cell, and a 7-T superconducting magnet with a 15 cm diameter bore from Oxford Instruments, Oxford, England. The guiding quadrupole and the cyclotron resonance cell are separated by 0.95 cm. Ions enter the ion cyclotron resonance cell through a 90% transmission, 1.75 cm by 1.75 cm, nickel screen which serves as both the ion entrance aperture and one of two trapping plates. The system is currently pumped with Varian VHS4, HS2, and VHS4 oil diffusion pumps placed at the ion source, quadrupole 1, and the entrance to the guiding quadrupole, respectively. The first two pumps have water-cooled baffles and operate with estimated pumping speeds of 500 and 175 L s^{-1}, respectively. The third pump contains a liquid nitrogen baffle and has an estimated pumping speed of 550 L s^{-1}. At present no effort is made to decelerate the ions as they enter the ion cyclotron resonance cell. We assume that the ions observed in the experiments described here become stabilized as a result of collisions with residual gas molecules in the ion cyclotron resonance cell. The electronics and data system to operate the Fourier transform mass spectrometer were obtained from Ionspec, Irvine, CA. Ionization of nonvolatile samples was accomplished by using glycerol as the liquid matrix and a cesium ion gun from Antek, Inc., Palo Alto, CA (*20*). The Antek gun was mounted directly on the Finnigan Model 4500 ion source.

Operation of the Tandem-Quadrupole Fourier Transform Mass Spectrometer in Conjunction with a Particle Bombardment Ion Source. Samples were prepared by adding 1 μL of a 1 nmol μL^{-1} solution of peptide in 5% acetic acid to 1 μL of glycerol on a stainless steel probe. The resulting mixture was then subjected to particle bombardment using 4–6 keV cesium ions. Quadrupoles 1 and 2 were operated in the rf only mode. For Met-Arg-Phe-Ala, mol wt 523; Leu-Trp-Met-Arg-Phe-Ala, mol wt 822; angiotensin, mol wt 1295; and renin tetradecapaptide, mol wt 1757; the rf power on Q1 and Q2 was set so as to transmit only those ions above mass 280. The ion cyclotron resonance cell was operated with a trapping potential of 1.5–2.0 V. Mass spectra were produced by using the computer to apply a sequence of pulses to the cell while the sample was being continually bombarded with particles from the cesium ion gun. The first, quench pulse, is applied to the trapping plates to clear the cell of all charged particles. After a delay time set between 100 and 4000 ms, an rf pulse containing a range of frequencies is applied to the two opposite transmitter plates to accelerate the ions trapped in the cell and to cause them to move coherently at their cyclotron frequency. Ion image currents induced on the other two opposite side plates, receiver plates, are then detected, amplified, and digitized. The resulting time-averaged signal is then Fourier transformed to produce the desired mass spectrum.

RESULTS AND DISCUSSION

Figure 2A shows the mass spectrum obtained from 1 nmol

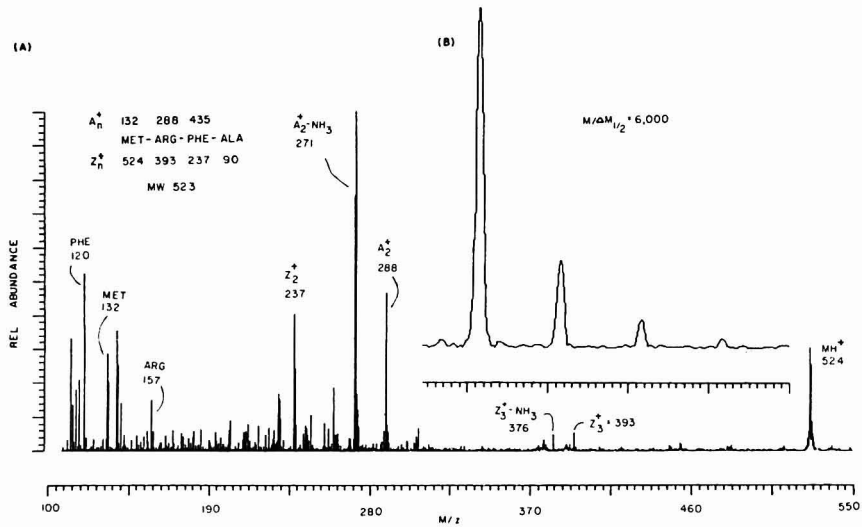


Figure 2. (a) Mass spectrum of Met-Arg-Phe-Ala, mol wt 523, obtained by bombarding the sample in glycerol with 4–6 keV cesium ions. Data over the mass range, 100–550, were obtained by using an rf excitation pulse having a bandwidth of 1 MHz. (b) Narrow band mass spectrum recorded over the mass range, 520–530, by using an rf excitation pulse of 10 kHz.

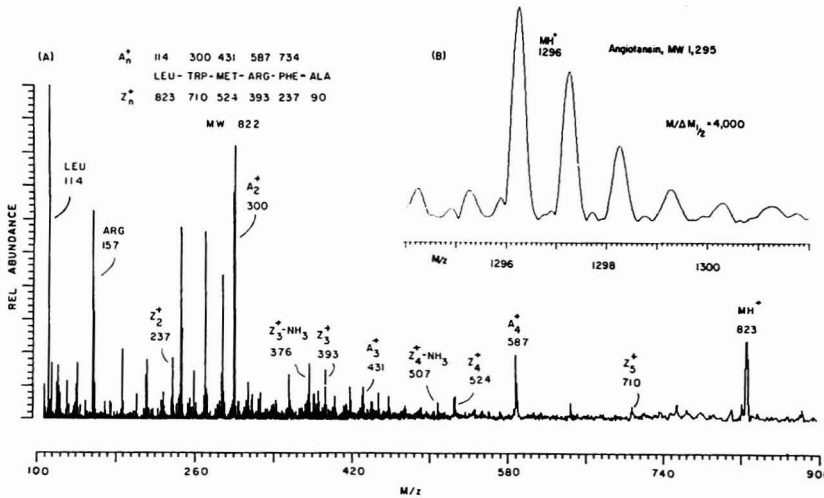


Figure 3. (a) Mass spectrum of the hexapeptide, Leu-Trp-Met-Arg-Phe-Ala, mol wt 822, obtained by bombarding the sample in glycerol with 4–6 keV cesium ions. Data over the mass range, 100–900, were recorded by using an rf excitation pulse having a bandwidth of 1 MHz. (b) Narrow band mass spectrum of angiotensin, mol wt 1295, recorded over the mass range, 1295–1305, by using an rf excitation pulse of 10 kHz.

of Met-Arg-Phe-Ala, mol wt 523, dissolved in 1 μL of glycerol using the combination of cesium ion bombardment and the newly constructed tandem-quadrupole Fourier transform mass spectrometer. The spectrum of the hexapeptide, Leu-Trp-Met-Arg-Phe-Ala, mol wt 822, appears in Figure 3A. To acquire these two sets of data, quadrupoles 1 and 2 were operated in the rf only mode and were set so as to reject all ions below mass 280. Ions above mass 280 were allowed to accumulate in the cell for 500–2000 ms. No effort was made to decelerate the ions as they entered the cell so only a small fraction, less than 0.1%, of the transmitted ions is actually stored in the present experiments. These presumably fall into stable orbits after undergoing stabilizing collisions with residual gas molecules in the cell. This stored ion population was irradiated with rf having a bandwidth of 1 MHz. Image currents so produced were then detected, amplified, digitized, and Fourier transformed. Fifty such scans were summed together to generate the spectrum in Figure 2A. Ten scans were accumulated for the spectrum in Figure 3A.

Figure 2B shows the spectrum of Met-Arg-Phe-Ala recorded in the narrow band mode using a frequency bandwidth of 10 kHz. Again, ions above mass 280 were allowed to accumulate in the cell for 3000 ms and then mass analyzed. Fifty scans, taken over the mass range, 520–530, were then summed together to produce the data shown. Transient lifetime was measured at 52 ms. Isotope peaks corresponding to the presence of one, two, and three carbon-13 atoms appear in this spectrum at close to the expected theoretical abundance. The resolution at m/z 524 is 6000.

Figure 3B shows the mass spectrum of angiotensin, Asp-Arg-Val-Tyr-Ile-His-Pro-Phe-His-Leu, recorded in the narrow band mode by using a frequency bandwidth of 10 kHz. Ions were allowed to accumulate in the cell for 1000 ms and then mass analyzed. Twenty scans were summed together to produce the spectrum shown. Resolution at the MH^+ ion, m/z 1296, is 4000. A spectrum of renin tetradecapeptide, mol wt 1757, recorded in the narrow band mode showed an MH^+ ion having a signal to noise of 5/1.

Without dc/rf voltage on the rods, the efficiency of ion transmission through the quadrupole filters is greater than 90% and only ions above m/z 280 enter the ion cyclotron resonance cell. Conventional FAB or L-SIMS spectra are usually dominated by glycerol MH^+ and its solvated oligomers plus low mass fragment ions produced from both glycerol and the sample under the particle bombardment ionization conditions. If allowed to enter the ion cyclotron resonance cell, these ions would quickly exceed the capacity of the cell and seriously impair the capability of the instrument to detect weak signals due to sample MH^+ ions. Quadrupole filters 1 and 2 thus provide a convenient mechanism for extending the dynamic range of the ion cyclotron resonance cell. In its final configuration the tandem quadrupole Fourier transform instrument will operate with a low mass cutoff that can be set anywhere below mass 2000.

Although only ions of mass greater than m/z 280 enter the ion cyclotron resonance cell in the present experiments, Figure 2A clearly shows a substantial number of signals at masses lower than this cutoff. In the absence of evidence to the contrary, we assume that these ions, and some of the higher mass fragments as well, result from decomposition of vibrationally excited MH^+ ions having lifetimes greater then ca. 1 ms, the time required to traverse the two quadrupoles, and less than 3000 ms, the maximum time the ions spent in the cell prior to mass analysis.

Fragmentation observed in Figures 2A and 3A is consistent with that expected from conventional fast atom bombardment, liquid secondary ion mass spectrometry, or low energy collision-activation dissociation experiments. Ions of type A_n^+ and $\bar{A}_n^+$, corresponding to the general formula, $H-(NHCHRCO)_n^+$ and $H(NHCHRCO)_nNHCHR^+$, respectively, define the sequence of amino acids from the amino terminus. Ions of type Z_n^+, corresponding to the general formula $^+H-(NH_2CHRCO)_nOH$, define the sequence of amino acids from the carboxyl terminus of the peptide. Ions indicating the presence of individual amino acids in the peptide are of the type, $H_2NCHRCO^+$ or H_2NCHR^+.

As was indicated earlier, transient times exceeding 100 ms and resolution in excess of 100 000 at m/z 1000 can easily be achieved if the pressure in the ion cyclotron resonance cell is kept below 10^{-8} torr. In the present experiments the cell pressure could only be maintained at 2×10^{-7} torr, with or without sample in the ion source, because the system is still under construction and is now operating with temporary pumps of marginal capacity on the cell. In its final configuration the pumping system on the tandem-quadrupole Fourier transform instrument will maintain the cell pressure at 10^{-9} or below.

Initial results presented in this and four earlier papers (*16–19*) provide us with considerable encouragement in our effort to develop a new approach to biopolymer sequencing using the tandem-quadrupole Fourier transform mass spectrometer. Previous work demonstrated that ions produced in a quadrupole ion source could be transmitted with high efficiency through the fringing fields of a superconducting magnet using rf only quadrupoles and then stored in an ion cyclotron resonance cell (*17–19*). Here we have shown that the tandem-quadrupole Fourier transform instrument can also be employed for mass analysis of ions produced by cesium ion bombardment of nonvolatile sample dissolved in a volatile liquid matrix. Laser photodissociation of peptide MH^+ ions in an ion cyclotron resonance cell has recently been found to proceed with high efficiency and yield excellent sequence information (*16*). Thus it now seems reasonable to assume that large oligopeptides produced by either chemical or enzymatic cleavage of proteins can be completely sequenced at the low picomole level by using a pulsed cesium ion gun to minimize sample consumption during the ionization process, rf only quadrupoles to transmit selectively only the high mass ions of interest, an ion cyclotron resonance cell operated at low pressure to accumulate and store MH^+ ion produced in low abundance, laser photodissociation to generate fragment ions characteristic of the amino acid sequence, and Fourier transform mass spectrometry to produce a mass spectrum of the daughter ions at high resolution. This same approach should also work well for the characterization of oligonucleotides, oligosaccharides, and glycoproteins.

ACKNOWLEDGMENT

The authors are indebted to Jon Amy, Michael Story, and Robert Finnigan of Finnigan-MAT Corp. for their many contributions to the development of the tandem-quadrupole Fourier transform mass spectrometer.

Registry No. Met-Arg-Phe-Ala, 67368-29-0; Leu-Trp-Met-Arg-Phe-Ala, 53214-98-5; angiotensin, 484-42-4; renin tetradecapeptide, 64315-16-8; cesium ion, 18459-37-5.

LITERATURE CITED

(1) Hunt, D. F. *Int. J. Mass Spectrom. Ion Phys.* **1982**, *45*, 111–123.
(2) Busch, K. L.; Cooks, R. G. *Science* **1982**, *218*, 247–254.
(3) Rinehart, K. L., Jr. *Science* **1982**, *218*, 254–260.
(4) Hunt, D. F.; Bone, W. M.; Shabanowitz, J.; Rhodes, G.; Ballard, J. M. *Anal Chem.* **1981**, *53*, 1704–1706.
(5) Fitton, J. E.; Hunt, D. F.; Marasco, J.; Shabanowitz, J.; Winston, S.; Dell, A. *FEBS Lett.* **1984**, *169*, 25–29.
(6) Comisarow, M. B.; Marshall, A. G. *Chem. Phys. Lett.* **1974**, *25*, 282–283.
(7) McIver, Jr., R. T. *Am. Lab. (Fairfield, Conn.)* **1980**, *12* (11), 18–24.
(8) Wilkins, C. L.; Gross, M. L. *Anal. Chem.* **1981**, *53*, 1661A–1676A.
(9) Bowers, W. D.; Hunter, R. L.; McIver, R. T., Jr. *Ind. Res./Dev.* **1983**, *25* (11), 124–128.
(10) Carlin, T. J.; Frieser, B. S. *Anal. Chem.* **1983**, *55*, 955–958.
(11) McIver, R. T., Jr.; Bowers, W. D. In "Tandem Mass Spectrometry"; McLafferty, F. W., Ed.; Wiley: New York, 1983; pp 287–301.
(12) Cody, R. B.; Burnier, R. C.; Cassady, C. J.; Freiser, B. S. *Anal. Chem.* **1982**, *54*, 2225–2228.
(13) Dunbar, R. C. In "Gas Phase Ion Chemistry"; Bowers, M. T., Ed.; Academic Press: New York, 1979; pp 181–220.
(14) Thorne, L. R.; Wright, C. A.; Beauchamp, J. L. In "Ion Cyclotron Resonance II"; Hartmann, H., Wanczek, K. P., Eds.; Springer-Verlag: Berlin, 1982; pp 43–97.
(15) Jasinski, J. M.; Rosenfeld, R. N.; Meyer, F. K.; Brauman, J. L. *J. Am. Chem. Soc.* **1982**, *104*, 652–658.
(16) Bowers, W. D.; Delbert, S. S.; Hunter, R. L.; McIver, R. T., Jr. *J. Am. Chem. Soc.*, in press.
(17) McIver, Jr., R. T.; Hunter, R. L.; Story, M. S.; Syka, J.; Labunsky, M.; Presented at the 31st Annual Conference on Mass Spectrometry and Allied Topics, Boston, MA, 1983.
(18) McIver, R. T., Jr.; Hunter, R. L.; Bowers, W. D. Presented at the "32nd Annual Conference on Mass Spectrometry and Allied Topics", San Antonio, TX, 1984.
(19) McIver, R. T., Jr.; Hunter, R. L.; Bowers, W. D. *Int. J. Mass Spectrom. Ion Phys.*, in press.
(20) Abreth, W.; Straub, K. M.; Burlingame, A. L. *Anal. Chem.* **1982**, *54*, 2029–2034.

Donald F. Hunt*
Jeffrey Shabanowitz

Department of Chemistry
University of Virginia
Charlottesville, Virginia 22901

Robert T. McIver, Jr.*
Richard L. Hunter

Department of Chemistry
University of California
Irvine, California 92717

John E. P. Syka

Finnigan-MAT Corp.
355 River Oaks Parkway
San Jose, California 95134

RECEIVED for review September 4, 1984. Accepted November 28, 1984. This research was supported by grants awarded to D.F.H. from the NIH (AM26533 and a Fogarty Senior International Fellowship) and to R.T.M. from the National Science Foundation and by a gift to D.F.H. from the Monsanto Co.

Hollow Fiber Postcolumn Reactor for Liquid Chromatography

Sir: A great deal of attention has been focused on postcolumn derivatization for enhanced detection of species eluting from liquid chromatography columns. Frei and Scholten (*1*) have reviewed many of the theoretical and technical aspects of reaction detectors, including the problems associated with their use, while Takata and Muto (*2*) first discussed reaction detectors for uses such as enhanced electrochemical detection. Hollow fiber membranes have been reported for postcolumn reaction in both unpacked and packed hollow fiber suppressors for ion chromatography (*3, 4*).

The requirements for good postcolumn derivatization can be reduced to three key components: (a) reagent introduction, (b) delay or reaction/mixing loops, and (c) proper detection devices. Both (b) and (c) are essentially fixed by the reaction time/temperature and chemistry chosen. Part a, the reactor itself, allows more flexibility. For example, with reagent mixing, techniques such as air segmentation, pumping reagent into a mixing device, and packed beds of reagent granules have all been used. Unfortunately, each of these methods has its drawbacks. Air segmentation and mixing devices require an additional pump and lead to band spreading and dilution,

0003-2700/85/0357-0768$01.50/0 © 1985 American Chemical Society

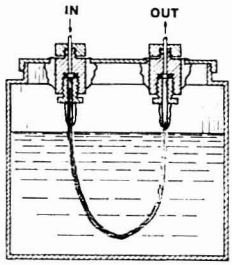


Figure 1. Schematic of a typical hollow fiber membrane postcolumn reactor.

reducing the sensitivity gained through derivatization. Packed beds of reagent require a sparingly soluble reagent, usually deplete rapidly, and also cause band spreading, particularly as the reagent depletes.

We have developed new reactor devices which eliminate or control the problems associated with other reactor designs. These devices are easily adapted to conventional liquid chromatography equipment and are applicable to a wide variety of reagent and reactor systems (*5*, *6*).

EXPERIMENTAL SECTION

Apparatus. With the exception of the hollow fiber devices, commercially available liquid chromatography equipment was used in all cases. Chromatographic conditions will be presented in the Results and Discussion section for each system. A typical hollow fiber reactor, shown in Figure 1, was composed of a loop of five, 325 μm i.d. sulfonated polyethylene hollow fibers 8 in. long. After being attached to suitable connecting fittings, this loop was suspended in a container of the appropriate reagent. Typical ion exchange capacity was 1 mequiv/g on a dry weight basis. Eluent flow was through the fibers. Means for preparing the fibers and devices are found elsewhere (*3*, *4*). For experiments with fluorescamine (4-phenylspiro[furan-2-(3*H*),1′(3′*H*)-phthalan]-3,3′-dione), hollow fibers of 60% poly(dimethylsilane), 40% α-methylstyrene copolymer were used (SR-a/751-7010 from Bio-Rad Laboratories).

Reagents. HPLC grade solvents and 0.45 μm filtered water were used for reagent solution and mobile phase preparation. Chemicals used were ACS reagent grade or better and were obtained from commercial sources (except for samples of the nitrophenols which were obtained from Dow Chemical USA, Midland, MI).

RESULTS AND DISCUSSION

Enhanced Detection of Nitrophenols. Rarely is the best pH for a particular separation also the optimum for detection. A case in point is that of substituted nitrophenols such as 2,4-dinitro-6-*sec*-butylphenol (2,4-DNP) and its related sulfonated compounds 3-nitro-4-hydroxy-5-*sec*-butylbenzenesulfonic acid (4-OH) and 2-hydroxy-3-nitro-5-*sec*-butylbenzenesulfonic acid (2-OH). An aqueous solution containing trace amounts of these three compounds and large amounts of other UV absorbing organics can be separated by conventional HPLC on a Partisil ODS-2 column using a mobile phase adjusted to pH 7.0. However, a large tailing peak eluting with the sample solvent front reduces the detection limit when 280 nm is used as the detection wavelength. By inserting the hollow fiber postcolumn reactor shown in Figure 1 between the column and the detector and filling the reactor with 2 N ammonium hydroxide, resulting in permeation of ammonia through the fiber wall into the eluent, the pH of the eluent is raised to 10 and 410-nm detection of the ionized phenols is possible. This reduces the interferences from other organics seen at 280 nm and resuls in enhanced detection of the nitrophenols.

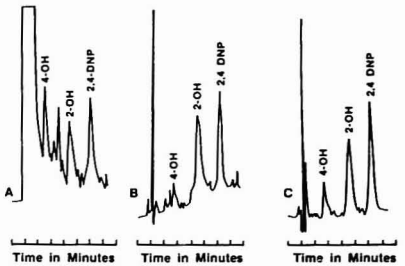


Figure 2. Comparison of nitrophenols with (A) 280 nm detection, no postcolumn reactor, and eluent pH of 6.0; (B) 410 nm detection, 0.1 N NaOH pumped into tee postcolumn, and pH of 10 at detection; and (C) 410 nm detection, hollow fiber reactor, and pH 10 at detection.

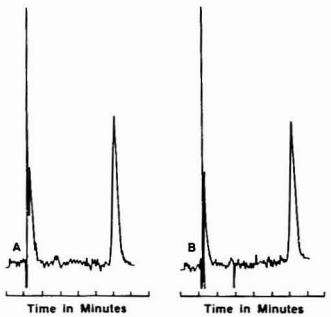


Figure 3. Comparison of band spreading with (B) and without (A) the hollow fiber reactor.

Figure 2 illustrates the results obtained for three experiments: (A) detection at 280 nm with no pH change; (B) detection at 410 nm with 0.1 N NaOH pumped into a mixing tee at 10% of the eluent flow rate; and (C) detection at 410 nm using the holow fiber reactor to adjust the eluent to pH 10. Chromatographic conditions were as follows: column, Partisil SAX 10/25; eluent, 12% methanol/water with 0.08 M sodium perchlorate and 0.104 M ammonium acetate adjusted to pH 6.0 with glacial acetic acid; flow rate, 2.0 mL/min; injection size, 100 μL. The sample used in these experiments was a synthetic aqueous waste stream with high levels of organics spiked to 1 ppm with each of the nitrophenols. Note in particular the improved base line stability and enhanced sensitivity to 4-OH when the hollow fiber reactor is used.

The chromatograms in Figure 3 illustrate the excellent flow characteristics of the hollow fiber reactor. The 2,4-dinitro-6-*sec*-butylphenol chromatography is shown with and without the hollow fiber reactor in line. The detection wavelength was 280 nm and no pH change was performed so that the peak area would remain unchanged and only the peak broadening due to fiber flow dynamics would be measured. The calculated number of theoretical plates was found to be 2000 in the absence of the hollow fibers (A) and 1940 with the hollow fibers in line (B) indicating less than a 5% loss of resolution due to the reactor. Chromatographic conditions were given in Figure 2. Applications of this device in the determination of nitrophenols in wastewater allowed detection in the 25 to 100 ppb level with excellent linearity over 2 orders of magnitude and precision of 6% or better (95% confidence level) at the 1 ppm level with a fixed wavelength detector.

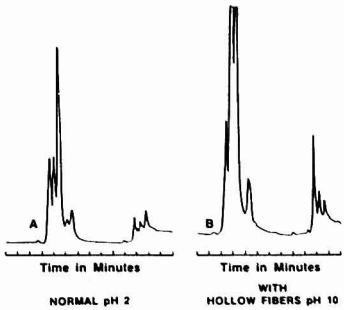


Figure 4. Effect of changing pH with a postcolumn reactor on the fluorescence detection of phenols.

Enhanced Fluorescent Detection of Phenols. The fluorescence of some phenols is known to be pH dependent (7), usually increasing in intensity with increasing pH at a given pair of excitation/detection wavelengths. Unfortunately most HPLC columns are limited to a maximum pH of about 8 due to their silica base material. A hollow fiber reactor similar to that in Figure 1 was used to increase the pH of the eluent from a phenol separation. Figure 4 shows the effect of changing the eluent pH from 2.0 (A) to 10.0 (B) on the detection of a mixture of hydroxycarboxybenzenes. Fluorescence excitation was at 320 nm with detection at 440 nm. Chromatographic conditions were as follows: eluent, gradient starting at 0.2 M phosphoric acid in water and proceeding to 0.2 M phosphoric acid in 20% acetonitrile/water; injection size, 10 μL; flow rate, 1.0 mL/min; column, Zorbax ODS. Note the selective increase in the sensitivity for some compounds without a concomitant loss of resolution.

Fluorescent Detection of Amines. Detection of primary amines by reaction with fluorescamine to form fluorescent products is a well-established technique (8). This system was chosen to show the efficiency of the hollow fiber postcolumn reactor when used in a chemical reaction mode. The reaction proceeds rapidly with 2 mg/mL of fluorescamine in acetonitrile solution outside the membrane. Figure 5 is a comparison of two 10-μL injections of 1 mg/mL benzylamine onto a Waters micro-C18 column. The mobile phase was 30% acetonitrile/water 0.01 M in ammonium acetate with a flow rate of 2.0 mL/min. The letter A denotes the point at which an injection was made prior to the addition of reagent to the fiber system while letter B is the point at which reagent was added to the reactor. A second injection of amine was made at point C. The rapid reaction of fluorescamine and primary amines makes this application ideally suited for postcolumn reaction since a delay or reaction coil is not required. Also of interest is the rapid equilibration of the hollow fiber unit upon addition of the reagent. No major base line disruption is observed and base line noise is not significantly increased.

Reaction of Ninhydrin with Amino Acids. A much slower reaction, ninhydrin color formation with amino acids, was also studied and satisfactory performance achieved with the hollow fiber postcolumn reactor. A 90 °C delay/reaction coil was used prior to the detector. The delay coil provided a 3-min delay at a flow rate of 0.52 mL/min and was approximately 2 m in length. Two-hundred microliter injections of 50 ppm glycine were made to simulate the elution of amino acids from a chromatography column. The eluent was 0.02 M citric acid in water adjusted to pH 4.0 with NaOH. The device illustrated in Figure 1 was used as the reactor with 10% ninhydrin in water on the outside of the fibers. Only 75%

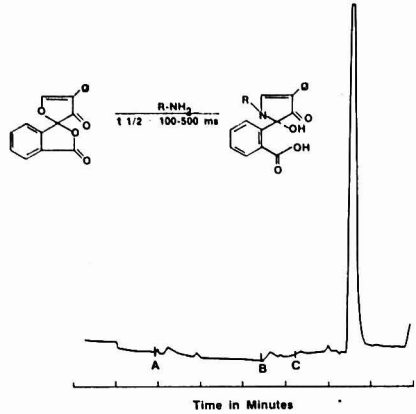


Figure 5. Effect of fluorescamine addition on detection of benzylamine.

reaction of the amino acid with ninhydrin was observed under these conditions; however, with the use of either internal standards or with alternating injections of standards, the excellent reproducibility and stability of this system allowed the detection of amino acid with good precision. Detection limit of glycine using this system is in the parts-per-million range and illustrates the use of the hollow fiber reactor in a case where complete reaction is not necessary for useful detection enhancement. (Simulated chromatograms are not shown.)

Selection and Use of Hollow Fibers. There are several considerations in making and applying a hollow fiber reactor to a particular system. The type of membrane material should be chosen for maximum reagent flux with minimum sample loss and be compatible with the solvent and mobile phase used. Since, however, most peaks eluting from chromatography columns are relatively dilute, it is possible to use membranes with virtually no permeation selectivity of the reagent over that of the sample material. This is principally due to the first-order nature of membrane permeation which results in roughly similar percentages of material permeating when in contact with the membrane (assuming approximately the same molecular weights). This allows the use of high concentrations of reagent on the outside of the membrane to permeate only a small percentage through the membrane but resulting in a high concentration in the eluent. Correspondingly, only a small percentage of the sample permeates into the reagent chamber during its passage through the fibers.

A primary consideration and problem in preparing these units is connection of the fibers into the LC system. Due to the wide variety of fittings available, there is no universally acceptable configuration. Units used in this laboratory have generally had the fibers potted into a fitting with a 1/4-28 male thread, using an appropriate adapter to $^1/_{16}$ in. narrow bore tubing. Potting materials of choice have been silicone rubber, fluorosilicone rubber, and epoxy—selected depending upon the solvent resistance required.

In multiple fiber units, to minimize band spreading, there must be equal flow through all fibers of the unit. This requires the fibers to be the same length, uniform in inner diameter, and have no flaws which restrict flow. To promote equal flow, it is desirable to keep a minimum pressure drop of 2–5 psi across the unit; this can be controlled by the number of fibers, length of the fibers, and fiber size. Note that these parameters will also affect the residence time of the sample in the unit

and also the flux of the reagent into the eluent flow stream.

Band spreading due to unequal fiber lengths or diameters in multifiber units can be minimized by adjusting the size of the hollow fiber unit so that it has a total volume inside the fibers which is smaller than the volume of the peaks eluted. In this case only moderate end effects on the sample peaks will be observed in most systems.

Reagent Addition. Several parameters should be considered for reagents in postcolumn reactions. The flux rate through a membrane is dependent upon the concentration gradient across the membrane. Thus as the reagent is depleted from the reservoir, the flux into the eluent will decrease. The effect this has on a particular analysis will depend on the system being studied. For example, if a large reservoir is used or a high reagent concentration is used to permeate excess reagent into the eluent, little effect will be seen on the analysis. Clearly the point should be determined for a given system where reagent depletion begins to affect the analysis and regeneration of the reagent performed prior to that time. Alternatively, a slow flow of fresh reagent may be used to replenish the reservoir by flowing around the fiber bundle. Attention should also be given to the choice of solvent used for the reagent as it may have either a benificial or detrimental effect in the flux of reagent through the membrane.

Other Potential Uses for Hollow Fiber Reactors. This new technique of passive reagent addition or pH change is also applicable to electrochemical, turbidimetric, and conductometric detection as well as to vibrational and electronic wavelength detection. These devices may be used both following chromatography and in flow injection analysis applications. The use of two or more reactors and multiple detectors may be desirable with particularly difficult sample matrices.

Registry No. 2,4-DNP, 88-85-7; 4-OH, 93037-41-3; 2-OH, 94042-50-9; benzylamine, 100-46-9; glycine, 56-40-6.

LITERATURE CITED

(1) Frei, R. W.; Scholten, A. H. M. T. *J. Chromatogr. Sci.* **1979**, *17*, 152-160.
(2) Takata, Y.; Muto, G. *Anal. Chem.* **1973**, *45*, 1864-1868.
(3) Stevens, T. S.; Davis, J. C.; Small, H. *Anal. Chem.* **1981**, *53*, 1488-1492.
(4) Stevens, T. S.; Jewett, G. L.; Bredeweg, R. A. *Anal. Chem.* **1982**, *54*, 1206-1208.
(5) Davis, J. C. United States Patent 4 448 691, 1984.
(6) Peterson, D. P.; Davis, J. C. United States Patent 4 451 374, 1984.
(7) Schulman, S. G. *Rev. Anal. Chem.* **1971**, *1*, 85-111.
(8) Udenfriend, S.; Stein, S.; Bohlen, S.; Dairman, P.; Leimgurber, W.; Weigele, M. *Science* **1972**, *178*, 871-872.

[1] Present address: Surface Science Laboratories, Standard Oil (Ohio), Cleveland, OH 44128.
[2] Present address: PPG Research Center, Barberton, OH 44203.

James C. Davis*[1]
Dennis P. Peterson[2]

Dow Chemical USA
Midland, Michigan 48640

RECEIVED for review January 27, 1983. Resubmitted October 15, 1984. Accepted November 15, 1984.

Adding Forward Searching Capabilities to a Reverse Search Algorithm for Unknown Mass Spectra

Sir: Mass spectrometry, especially with direct coupling to the gas chromatograph (GC/MS), is the most widely used tool for the identification of unknown organic molecules. The modern GC/MS can produce dozens or hundreds of unknown electron-ionization mass spectra per hour, for which many computer matching systems have been proposed (*1-13*). Of these, it is well-known that forward searching algorithms are substantially superior for unknown mass spectra of pure compounds (*1-3*) and that reverse searching (*4-6*) is advantageous for spectra of mixtures. We describe here a combination of forward and reverse searching that shows substantially improved performance for spectra of both pure compounds and mixtures without prior knowledge of purity.

Reverse searching, which is considered necessary even for capillary column GC/MS (*1, 2, 14*), gives matching credit only for peaks of the reference spectrum that are in the unknown, not vice versa. Because of this, matching an unknown spectrum of pure dioctyl phthalate retrieves those of octenes (Table I), a logical impurity, as the fragmentation of C_8H_{16} in the phthalate is the source of many peaks in its spectrum similar to those from octenes (Figure 1). This causes the reliability value (the probability that the degree of match found indicates the correct answer) predicted by the probability based matching (PBM) system (*4, 6, 8, 12, 13, 15-17*) to be misleadingly high (32%) for 3-octene; 14 of the top 20 matches are C_nH_{2n} compounds. However, these would be rated poor matches by forward searching, which would also require the presence of phthalate peaks. The scheme described here for combining reverse and forward searching capabilities is based on the automatic subtraction of matching reference spectra (*8*).

EXPERIMENTAL SECTION

Calculations were carried out with a Hewlett-Packard HP-1000 computer, matching against a library of 76 663 different mass spectra of 67 128 different compounds from the Wiley/NBS data base (*13, 18*) (spectra of isotopically labeled compounds were omitted). A total of 392 different compounds, each of which was represented in the file by more than one different spectrum, were selected at random from the file. The spectrum of highest "quality index" (*19*) of each compound was used to make the "pure spectrum" file of unknowns. Groups of three of these spectra, ordered by increasing molecular weight, were combined in 60:30:10 (total ions) proportion for the file of 130 unknown mixture spectra. Reference spectra used as unknowns were omitted from the PBM results.

The PBM program used ("system a") includes several modifications of the original (*4, 6*), such as ranking of retrieved spectra by reliability values (*15*), abundance based flagging of spurious peaks (*15-17*), and quadratic scaling to minimize experimental abundance variations (*16, 17*). Class I matches are the same compound or a stereoisomer; class IV matches represent compounds that are sufficiently similar structurally to make difficult their differentiation by mass spectrometry (*6, 15*). For retrieved spectra the maximum "% contamination" (%C) and minimum "% component" values allowed are 80% (75% for Table I) and 10%, respectively, restricting the retrieval of minor mixture components.

In forward searching modification "b" the predicted reliability value is adjusted to reflect the magnitude of the %C value; the adjustment is based on PBM results using the 392 unknowns (*17*). For the final system "c", each reference spectrum which matches with a predicted reliability value >10% is subtracted from the

0003-2700/85/0357-0771$01.50/0 © 1985 American Chemical Society

Table I. PBM Matching (Class IV) of Mass Spectra of Pure Bis(2-ethylhexyl) Phthalate and Its 3:1 Mixture with 3-Octene

		pure			mixture		
serial no.	compound	*a*	*b*	*c*	*a*	*b*	*c*
56290	bis(2-ethylhexyl) phthalate[d]	47[e]	50	61	56	22	45
78723	diisooctyl phthalate	42	37	50	35	20	37
67538	2-methyl-1-butene	34	<10	6	43	24	54
2942	(*Z*)-3-octene	32	14	13	(47	27	97)[f]
1545	3,4-dimethyl-1-pentene	31	<10	8	<10	<10	<10
78728	bis(2-ethylhexyl) phthalate	29	44	77	40	24	55
	all octenes[g]	25	14	9	55	24	83
	(no. of octenes retrieved)	(2)	(1)	(2)	(13)	(10)	(12)
	all C_nH_{2n} compounds	24	14	9	49	23	64
	(no. of C_nH_{2n} compounds)	(14)	(1)	(3)	(18)	(16)	(17)

[a] Results using the previous reverse search system (*14*). [b] With forward search, using the % contamination value to correct the reliability value, assuming that the unknown is the spectrum of a pure compound. [c] With forward search contribution using multiple subtraction, but with no knowledge of the purity of the unknown. [d] The unknown spectrum itself was not in the reference file used. [e] Reliability value, %. [f] The spectrum used as the 25% component of the unknown. [g] Average results for all retrieved reference spectra of C_8H_{16} olefins; the number retrieved is shown on the next line in parentheses.

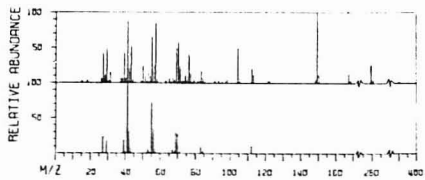


Figure 1. PBM matching of the upper mass spectrum, that of pure bis(2-ethylhexyl) phthalate, incorrectly predicted (Table I) the presence of (*Z*)-3-octene (bottom) with 32% reliability, an example based on a user complaint.

unknown, and the resulting residual mass spectra are matched (procedure b) against each of the other best-matching reference spectra, for each saving the highest reliability value. References 15–17 give complete details.

RESULTS AND DISCUSSION

Unknown Mass Spectra of Pure Compounds. The PBM results include a "percent contamination (%C)" value based on the relative proportion of the unknown peaks used in matching. Because important peaks such as m/z 149 of the bis(2-ethylhexyl) phthalate spectrum were not used in retrieving the C_nH_{2n} compounds (Table I), all of these matches show high (>67%) %C values. By use of the 392 "unknown" spectra of pure compounds, an excellent correlation was found between the %C value and the difference between the predicted and actual reliability (ΔRL) of the match; a high %C value gave a large positive ΔRL value, on average, while a low %C value gave a large negative ΔRL value. Thus, this "procedure b" can be applied if the user determines that the unknown spectrum represents a component of relatively high purity, such as that of a narrow GC peak. As illustrated by the pure unknown (procedure b of Table I), for incorrect answers this greatly reduces the predicted reliability values and thus the number retrieved. Not surprisingly, when used with mixture spectra (Table I, mixture b), the incorrect assumption of purity leads to poor reliability values for all answers.

Plotting the actual matching reliability (proportion of all answers which are correct) found at different values of recall

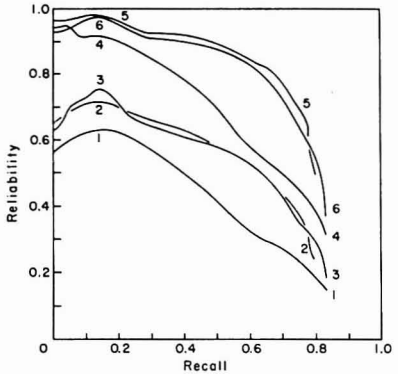


Figure 2. The reliability (proportion correct) of answers from PBM matching of 392 unknown spectra of pure compounds as a function of recall (proportion of correct answers retrieved): (1) class I matches of reverse search a; (2, 3) of forward searches b and c (see footnotes *a*–*c*, Table I); (4) class IV matches of reverse search *a*; (5, 6) of forward searches *b* and *c*.

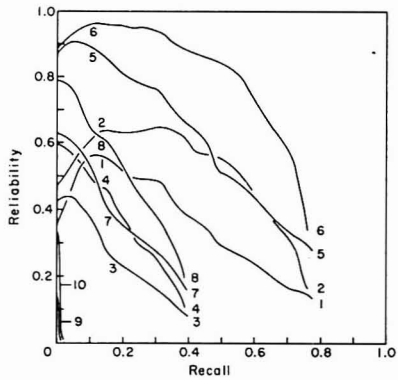


Figure 3. Recall/reliability plots (legend, Figure 2) of PBM matches of 130 unknown spectra of 60:30:10 mixtures: (1, 2) class I matches of 60% components, reverse and forward searches (a and c); (3, 4) same, 30% components; (5, 6) class IV matches of 60% components, reverse and forward searches (a and c); (7, 8) same, 30% components; (9, 10) same, 10% components.

(proportion of correct answers retrieved) provides a quantitative evaluation of the performance of a retrieval system (*20*). Such data from the 392 pure unknowns (Figure 2, lines 2 vs. 1 and 5 vs. 4) show that the inclusion of forward-searching capabilities has indeed produced a very substantial improvement.

Unknown Spectra without Purity Designation. In most cases a purity assessment by the user is inconvenient and could even be inaccurate. To obviate this, a previous method (*8*) to extract component "pure" spectra from unknown mixture spectra was used. In this procedure c each of the best-matching reference spectra are subtracted from that of the unknown, and the resulting residual mass spectra are matched against all best-matching reference spectra. For each reference the highest reliability value should represent the "most purified" similar spectrum that can be extracted from the unknown. Although this procedure is unnecessary for unknown spectra of pure compounds, for these fortunately the retrieval performance (Figure 2, lines 3 vs. 2 and 6 vs. 5) is almost as high as with the purity designated. In the

pure phthalate example (Table I, pure c) the reliability values of the incorrect answers are low, while the phthalate values have actually improved (highest 77%).

Unknown Mass Spectra of Mixtures. For the phthalate example it is conceivable that this modified algorithm is less sensitive to the data causing the original retrieval of the octenes. To see if their data can be recognized when actually present, to the spectrum of the phthalate was added that of the best matching octene. The results from this mixture spectrum (Table I, mixture c) are striking; where the pure phthalate spectrum gave two octene spectra of average reliability 9%, with 25% 3-octene present 12 octenes were retrieved of average reliability 83%. This value was only 55% with the original algorithm (Table I, mixture a); thus the subtraction procedure not only gives improved discrimination against incorrect similar spectra but also gives better recognition of mixture components. This is also shown dramatically by the recall/reliability plot of results from the 110 mixture "unknowns" (Figure 3, lines 1 vs. 2, 3 vs. 4, 5 vs. 6, 7 vs. 8), with the performance for the 60% and 100% components now nearly equal.

For the PBM algorithm incorporating weighted file ordering (*12*) on a commercial GC/MS system, these additions should increase the average search time per unknown by ~20%; "real-time" identifications will still be possible during a 40-min GC/MS run for ~100 components. The addition of forward search capabilities has reduced the number of class IV wrong answers for unknown mass spectra of both pure compounds and mixtures by approximately half (Figures 2 and 3).

ACKNOWLEDGMENT

We thank B. L. Atwater (Fell), D. R. Bartholomew, R. G. Dromey, I. K. Mun, and J. W. Serum for stimulating discussions.

LITERATURE CITED

(1) Pesyna, G. M.; McLafferty, F. W. "Determination of Organic Structures by Physical Methods"; Nachod, F. C., Zuckerman, J. J.; Randall, E. W.; Eds.; Academic Press: New York, 1976; Vol 6, pp 91-155.
(2) Chapman, J. R. "Computers in Mass Spectrometry"; Academic Press: London, 1978; Chapters 5-7.
(3) Hertz, H. S.; Hites, R. A.; Biemann, K. *Anal. Chem.* **1971**, *43*, 681.
(4) McLafferty, F. W.; Hertel, R. H.; Villwock, R. D. *Org. Mass Spectrom.* **1974**, *9*, 690.
(5) Abramson, F. P. *Anal. Chem.* **1975**, *47*, 45.
(6) Pesyna, G. M.; Venkataraghavan, R.; Dayringer, H. E.; McLafferty, F. W. *Anal. Chem.* **1976**, *48*, 1362.
(7) Dromey, R. G. *Anal. Chem* **1979**, *51*, 229.
(8) Atwater (Fell), B. L.; Venkataraghavan, R.; McLafferty, F. W. *Anal. Chem.* **1979**, *51*, 1945.
(9) Domokos, L.; Henneberg, D.; Weimann, B. *Anal. Chim. Acta* **1983**, *150*, 37.
(10) Cleij, P.; van't Klooster, H. A.; van Houwelingen, J. C. *Anal. Chim. Acta* **1983**, *150*, 23.
(11) Shackelford, W. M.; Cline, D. M.; Faas, L.; Kurth, G. *Anal. Chim. Acta* **1983**, *146*, 15.
(12) Mun, I. K.; Bartholomew, D. R.; Stauffer, D. B.; McLafferty, F. W. *Anal. Chem.* **1981**, *53*, 1938.
(13) McLafferty, F. W.; Stauffer, D. B. *Int. J. Mass Spectrom. Ion Proc.* **1984**, *58*, 139.
(14) Davis, J. M.; Giddings, J. C. *Anal. Chem.* **1983**, *55*, 418.
(15) Atwater (Fell), B. L.; Stauffer, D. B.; Peterson, D. W.; McLafferty, F. W. *Anal. Chem.*, in press.
(16) Stauffer, D. B. PhD Thesis, Cornell University, 1984.
(17) Stauffer, D. B.; Ellis, R. D.; Peterson, D. W.; McLafferty, F. W. submitted for publication in *Anal. Chem.*
(18) Electronic Data Division, Wiley, New York.
(19) Speck, D. D.; Venkataraghavan, R.; McLafferty, F. W. *Org. Mass Spectrom.* **1978**, *13*, 209.
(20) McLafferty, F. W. *Anal. Chem.* **1977**, *49*, 1441.

Douglas B. Stauffer
Fred W. McLafferty*

Chemistry Department
Cornell University
Ithaca, New York 14853

Robert D. Ellis
David W. Peterson

Scientific Instrument Division
Hewlett-Packard
1501 California Avenue
Palo Alto, California 94304

RECEIVED for review July 9, 1984. Resubmitted November 26, 1984. Accepted December 3, 1984. This research was supported under the Industry/University Cooperative Research Projects Program of the National Science Foundation, Grant CHE-8303340.

Trace Element Determination in Flames by Laser Enhanced Ionization Spectrometry

Sir: Laser-enhanced ionization (LEI) or optogalvanic spectroscopy (OGS) in flames has been developed during the last few years, particularly by a group at the National Bureau of Standards (NBS) in Washington as a technique for trace element analysis in water solutions (*1-5*). Substantial theoretical and experimental work in this field has demonstrated the applicability and potential of the method for this purpose (*6-8*). In particular, extremely low detection limits have been achieved—in many cases in the sub-part-per-billion (sub-ppb) region.

The basic principle for laser-enhanced ionization is that atoms in a flame are excited by laser irradiation to higher energy levels, from which they are more easily ionized by collisions with the flame molecules. This process causes a charge increase, which is monitored by applying an electric field over the region of interaction and measuring the corresponding current increase.

This work reports on detection limits for one-step laser-enhanced ionization in flames for a number of elements, using a pulsed excimer laser system for excitation. Detection limits in the part-per-billion to part-per-trillion region are obtained for 13 elements. These limits compare favorably with those reported previously in the literature, using a similar method of analysis, and they are in some cases the lowest values reported for any direct method of analysis, without any preceding sample preparation. Although the method can in principle detect only one element at a time, we want to stress that a considerable number of elements can be detected with high sensitivity with the same experimental setup without changing the dye of the laser system. This fact might be of great importance for practical applications of the method.

EXPERIMENTAL TECHNIQUE

The experimental setup for laser-enhanced ionization in flames, used in the present work, is shown in Figure 1. Since this setup has been described in more detail elsewhere (*8*), only its basic features are described here.

The laser light is generated by an excimer pumped dye laser (Lambda Physik EMG 102 and EMG 2002), yielding 10-ns pulses at 20 mJ (in Rhodamine 6G), frequency doubled using a KDP crystal (efficiency ~1%), and directed into the flame about 1 cm above the burner. The repetition rate for the laser is normally 10-30 Hz. The burner is a conventional air/acetylene single-slot

0003-2700/85/0357-0773$01.50/0 © 1985 American Chemical Society

Table I. Data for Transitions Used in LEI

	LEI (this work)							LEI (NBS)					
element	λ, nm	E_1–E_2, cm^{-1}	E_{ION},[a] cm^{-1}	E_X,[b] cm^{-1}	A_{ik},[c] 10^8/s	rel int[d]	det lim (1-step), ng/mL	λ, nm	E_1–E_2, cm^{-1}	A_{ik},[c] 10^8/s	rel int[d]	det lim (1-step), ng/mL	det lim (2-step), ng/mL
Bi	302.46	15437–48489	58 790	22 751	0.88	2400	30	306.8	0–32588	2.07	36 000	2	
Co	304.4	0–32842	63 430	2254	0.19	3100	4	252.1	0–39649		4300	10	
								591.68	39649–56546				0.08
Cr	301.49	7927–41086	54 570	19 675		1400	24	298.6	8308–41782		2100	2	
								301.8	8095–41225		2800	2	
Fe	302.06	0–33096	63 700	2492		2800	0.08	302.06	0–33096		2800	2	
								298.4	0–33507	0.28	1400	4	
Ga	294.36	826–34787	48 388	20 360	1.4	9500	0.04	287.4	0–34782	1.2	5000	0.07	
In	303.94	0–32892	46 670	19 114		8000	0.02	303.94	0–32892		8000	0.006	
								451.1	2213–24373	1.0	18 000	100	
								501.8	24373–44294				0.6
Mg	285.21	0–35051	61 671	8431	5.3	60000	0.003	285.21	0–35051	4.95	60 000	0.1	
Mn	292.56	18532–52703	59 970	26 904		190	2	279.5	0–35770		6200	0.3	
								403.1	0–24802		27 000	30	
								602.2	24802–41404		290		5
Na	285.28	0–35043	41 449	28 663	0.006		0.001	285.28	0–35043	0.006		0.05	
								589.0	0–16973	0.62	20 000	6	
								568.8	16973–34549	0.12			0.04
Ni	301.2	3410–36601	61 579	8213	1.5	3700	1	300.2	205–33501		4000	2	
								576.76	33501–50834				0.08
Pb	287.33	10650–45443	59 820	20 416	0.37	2800	2	280.2	10650–46329	1.6	10 000	0.6	
								283.3	0–35287	0.58	9500	3	
								600.19	35287–51944		8		0.09
Sn	286.33	0–34914	59 232	10 596	0.54	10000	15	283.99	3428–38629	1.7	14 000	2	
								283.99	3428–38629	1.7	14 000	8	
								597.03	38629–55374	0.096			0.3
Tl	291.82	7793–42049	49 267	27 038	0.42	2800	0.015	291.8	7793–42049	0.42	2800	0.09	

[a] E_{ION}, ionization limit. [b] E_X, excess of energy above the ionization limit for a photoionization process. [c] A_{ik}, transition probability (*11*). [d] Rel int, relative line intensity (*12*).

Table II. A Comparison of Detection Limits (ng/mL) for Various Trace Element Analysis Techniques[a]

element	LEI (this work) (1-step exc.)	LEI (NBS) (1-step)	LEI (NBS) (2-step)	AAS (in flame)	AAS (flameless)	LIF	ICP
Bi	30	2	0.08	50	0.4	3	50
Co	4	10	0.08	2	0.2	1000	2
Cr	24	2		2	0.2	1	0.9
Fe	0.08	2		4	1	30	0.2
Ga	0.04	0.07		50	0.1	0.9	14
In	0.02	0.006	0.6	30	0.04	0.2	30
Mg	0.003	0.1		0.1	0.004	0.2	0.7
Mn	2	0.3	5	0.8	0.02	0.4	0.1
Na	0.001	0.05	0.04	0.8		0.1	0.2
Ni	1	2	0.08	5	0.9	2	4
Pb	2	0.6	0.09	10	0.2	10	10
Sn	15	2	0.3	100	0.3	25	30
Tl	0.015	0.09		20	1	4	200

[a] AAS, atomic absorption spectroscopy; LIF, laser induced fluorescence; ICP, inductively coupled plasma; detection limits for AAS and ICP from ref 13 and for LIF from ref 14.

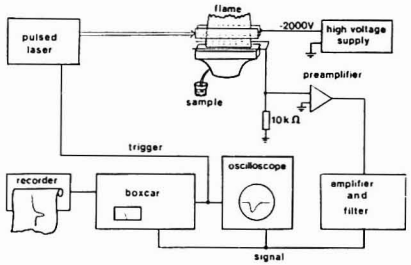


Figure 1. Block diagram of the experimental arrangement for laser enhanced ionization spectroscopy in flames by one-step laser excitation.

burner, of the type used in atomic absorption spectrometry (AAS), and the sample, in the form of a water solution, is aspirated into the flame via a nebulizer as in AAS. A potential of ~2000 V is applied between a pair of plates, located outside the flames, and a pair of stainless steel rods placed slightly above the grounded burner. The signal is collected on the rods, amplified by a video preamplifier, and averaged in a boxcar integrator. In order to reduce electrical interference, the plates, the rods, and the amplifier are all shielded by a copper enclosure.

RESULTS

With the experimental setup described above we have determined detection limits for 13 elements in water solution, and the results are collected in the tables below. All the measurements were performed with one-step laser excitation, using frequency-doubled light from the dye Rhodamine 6G with wavelengths ranging from 285 nm to 305 nm. For some elements, however, the laser transition used was not the optimal one with respect to the ion production but was the best available in this wavelength region. These elements are included in this investigation in order to demonstrate the above-mentioned ability of detecting a considerable number of elements with high sensitivity using frequency-doubled light from one single dye.

In the tables we have compared our results with the corresponding results obtained at NBS using LEI (*1–5*), as well as with the results found in the literature for other trace element analysis methods (atomic absorption spectroscopy, AAS; laser induced fluorescence, LIF; and inductively coupled plasma, ICP). A typical measurement was performed with a repetition rate of the laser of 10 Hz and a total time constant of the boxcar of 3 s. The detection limit is defined as the lowest concentration, which yields a signal clearly distinguable from that of the blank. This was done by comparing the signal for a given concentration with the uncertainty in the blank level due to noise, drift, etc. when sampled for 1 min. This uncertainty represents two standard deviations in a number of such measurements.

DISCUSSION AND CONCLUSIONS

As can be seen from Table I, our LEI detection limits compare favorably with those reported by NBS, and we shall briefly comment on this comparison here. Obviously, a more direct comparison can be performed only in cases where the same wavelength region has been used by the two groups, i.e., for Cr, Fe, In, Mg, Na, Ni, and Tl.

For Fe, Mg, Na, and Tl the detection limits presented here are significantly lower than those reported by NBS, while for Cr and In we have not been able to reach the limits of NBS.

A possible explanation for our noticeably low detection limits for Fe and Mg might be that, in addition to the collisional ionization, photoionization can take place from the excited state. In the present work we are using an excimer laser system (Lambda Physik), which generates very short, intense pulses (~10 ns, ~200 kW), while the Fe and Mg data of NBS are obtained with a flash-lamp pumped laser system (Chromatix) with longer, less intense pulses (~1 μs, ~1 kW). The high laser intensity increases the probability for photoionization, particularly when the laser photon energy is close to the ionization energy of the laser-excited state (*9*). The excess energy (i.e., the energy exceeding the ionization limit) when two photons are absorbed (see Figure 2) is included in Table I.

When this excess energy is small, the photoionization process may compete with, or even dominate over, the collisional ionization process. We believe this to be the most reasonable explanation for our extremely low detection limits for Fe and Mg.

For Na our detection limit refers to a hypothetical solution without any sodium impurity. This limit is obtained by comparing the sodium signal (for a known concentration) with the noise level of the blank solution *off* the sodium resonance, while the corresponding NBS value is obtained by comparing with the noise level *on* resonance.

The detection limit obtained for Cr in our work is more difficult to explain when compared with the corresponding NBS value. It is interesting to note, however, that our previously reported results, obtained with a Chromatix laser, gave comparable sensitivities for Cr and Fe, in agreement with the results reported by NBS (*6*).

For the remaining elements, Bi, Co, Ga, Mn, Pb, and Sn, we have worked in a different and in most cases less optimal, wavelength region than that used by the NBS group. In some

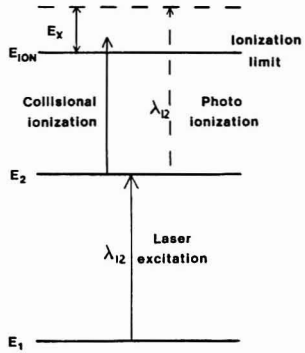


Figure 2. Excitation and ionization scheme for one-step laser enhanced ionization in flames. E_1 and E_2 denote the lower and upper laser level, respectively, while E_{ION} represents the ionization limit. E_x is the excess energy above the ionization limit when a second photon is absorbed in a photoionization process.

of these cases (Co, Ga, and Pb) we still get comparable detection limits, while in other cases our limits are considerably higher, either due to unfavorable oscillator strength of available lines in our experiment or to high energy of the lower level of the laser transition (see Table I).

In comparing the detection limits of LEI, for the elements studied here, with those of other standard methods of analysis, such as AAS in flame, flameless AAS, LIF, and ICP (see Table II), we find that, when an optimal wavelength is used, one-step LEI has detection limits which are quite comparable with those of flameless AAS and usually superior to those of the other methods. In addition, LEI has in comparison with flameless AAS, the advantage of having the flame as an atomizer. Furthermore, it can be noted that even with rather unfavorable excitation lines, for instance, LEI can compete with AAS in flames.

These observations, supporting those obtained earlier by the NBS group, demonstrate the power of the LEI method as a tool for trace-element analysis. The high sensitivity of the method has the consequence that preconcentration, frequently used in other methods, is here usually superfluous. Furthermore, we have shown elsewhere that LEI in flame can be conveniently combined with high pressure liquid chromatography (HPLC) (*10*).

The work reported here is the first in a series of works we intend to perform in order to investigate the applicability of the LEI method for trace-element analysis under various experimental conditions. Besides using different dyes, which make other elements available for investigation as well as more optimal lines available for some of the elements studied here, our results can be improved particularly in the following two ways. (a) The use of two-step laser excitation (*5*, *8*) can increase the rate of ionization considerably and reduce the detection limits accordingly. In the case of Mg, for instance, we have found that the signal can be enhanced at least 2 orders of magnitude by using a second laser-excitation step. In addition, a second excitation makes it possible to reduce optical interferences substantially, which could be of great importance for investigating real samples. (b) For elements with low degrees of atomization in an ordinary air/acetylene flame, the number of free atoms in the flame, and consequently the LEI signal, can be considerably improved by means of a higher flame temperature, e.g., by using an N_2O/acetylene flame. It should be noted, however, that "improvements" of this kind may lead to a substantial increase in complexity of the analysis, and any of them should be used only when there is a definite need for it.

ACKNOWLEDGMENT

The authors wish to thank Thomas Berglind for stimulating discussions.

Registry No. Bi, 7440-69-9; Co, 7440-48-4; Cr, 7440-47-3; Fe, 7439-89-6; Ga, 7440-55-3; In, 7440-74-6; Mg, 7439-95-4; Mn, 7439-96-5; Na, 7440-23-5; Ni, 7440-02-0; Pb, 7439-92-1; Sn, 7440-31-5; Tl, 7440-28-0; H_2O, 7732-18-5.

LITERATURE CITED

(1) Green, R. B.; Keller, R. A.; Schenck, P. K.; Travis, J. C.; Luther, G. C. *J. Am. Chem. Soc.* **1976**, *98*, 8517.
(2) Turk, G. C.; Travis, J. C.; DeVoe, J. R. *Anal. Chem.* **1979**, *51*, 1890.
(3) Turk, G. C.; Travis, J. C.; DeVoe, J. R.; O'Haver, T. C. *Anal. Chem.* **1978**, *50*, 817.
(4) Travis, J. C.; Turk, G. C.; Green, R. *Anal. Chem.* **1982**, *54*, 1006A.
(5) Turk, G. C.; Mallard, W. G.; Schenck, P. K.; Smyth, K. C. *Anal. Chem.* **1979**, *51*, 2408.
(6) Berglind, T.; Rubinsztein, H.; Rosén, A. Institute of Physics, Chalmers University of Technology, GIPR-216, 1980, unpublished results.
(7) Travis, J. C.; Schenck, P. K.; Turk, G. C.; Mallard, W. G. *Anal. Chem.* **1979**, *51*, 1516.
(8) Axner, O.; Berglind, T.; Heully, J. L.; Lindgren, I.; Rubinsztein-Dunlop, H. *J. Appl. Phys.* **1984**, *55*, 3215.
(9) Curran, F. M.; Lin, K. C.; Lerol, G. E.; Hund, P. M.; Crouch, S. R. *Anal. Chem.* **1983**, *55*, 2382.
(10) Berglind, T.; Nilsson, S.; Rubinsztein-Dunlop, H., submitted for publication in *Anal. Chem.*
(11) Reader, J.; Corliss, C. H.; Wiese, W. L.; Martin, G. A. *Natl. Stand. Ref. Data Ser. (U.S., Natl. Bur. Stand.) NSRDS-NBS 68.*
(12) Striganov, A. R.; Sventitskii, N. S. *NBS Monograph (U.S.)* **1968**, *no. 145.*
(13) Weeks, S. J.; Haraguchi, H.; Winefordner, J. D. *Anal. Chem.* **1978**, *50*, 360.
(14) Fassel, V. A. *Science* **1978**, *202*, 183.

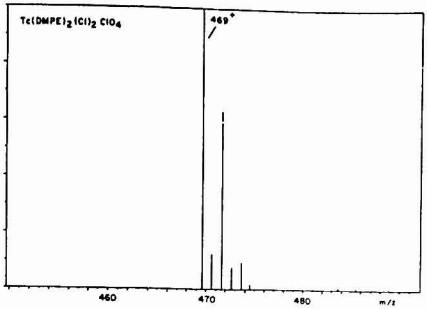
Ove Axner
Ingvar Lindgren
Ingemar Magnusson
Halina Rubinsztein-Dunlop*
Department of Physics
Chalmers University of Technology/University of Gothenburg
S-412 96 Göteborg, Sweden

RECEIVED for review November 30, 1983. Resubmitted July 23, 1984. Accepted November 5, 1984. This work has been supported by the Swedish Natural Science Research Council.

Differentiation of Cationic from Neutral Transition-Metal Complexes Using Wires as Field Desorption Emitters

Sir: Numerous types of emitters have been described for field desorption (FD) mass spectrometry (*1*). Carbonaceous microneedles (*2–4*) or microneedles formed from metal carbonyls (*5*), silicone whiskers (*6*), and cathodically reduced

0003-2700/85/0357-0776$01.50/0 © 1985 American Chemical Society



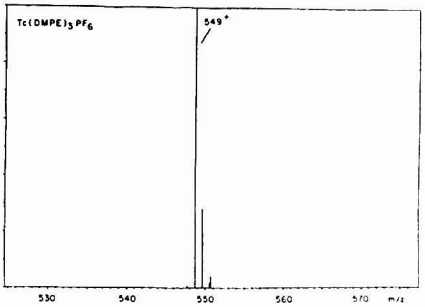
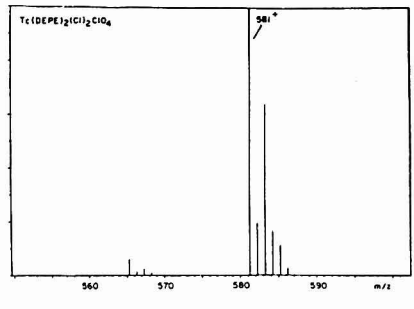


Figure 1. Portions of the field desorption mass spectra of (a) Tc(DMPE)$_2$(Cl)$_2$ClO$_4$ and (b) Tc(DMPE)$_3$PF$_6$ obtained from an unactivated wire: DMPE, bis(1,2-dimethylphosphino)ethane; DEPE, bis(1,2-diethylphosphino)ethane.



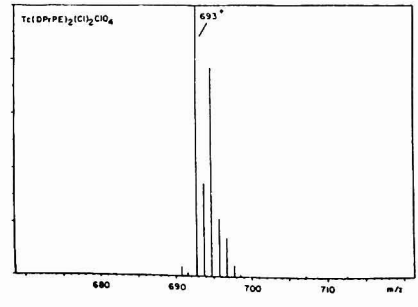


Figure 2. Portions of the field desorption mass spectra of (a) Tc(DEPE)$_2$(Cl)$_2$ClO$_4$ and (b) Tc(DPrPE)$_2$(Cl)$_2$ClO$_4$ obtained from an unactivated wire: DPrPE, bis(1,2-dipropylphosphino)ethane. The two chlorine isotope pattern is observed for both cations.

metal dendrites (*7–9*) have been used. All preparation procedures involve emitter "activation" which yields microneedles or dendrites attached to the wire. These procedures are time and labor intensive but are necessary to enhance local field strengths and affect field desorption.

Rollgen and Giessmann suggested the use of unactivated tungsten wires as FD emitters for compounds with low appearance potentials (*10*). They reported ion emission for organic salts from unactivated 10-μm wires. This paper reports similar observations for FD mass spectra of cationic technetium complexes. Comparisons are made with cobalt and carbon emitters. The method has the added advantage of differentiating cationic from neutral transition metal complexes, as neutral complexes fail to yield ions from these unactivated wires. This distinction is often less evident from fast atom bombardment mass spectra (*11*, *12*).

EXPERIMENTAL SECTION

All spectra were obtained on a VG-ZAB-2F mass spectrometer. By use of the VG-2035 data system, mass spectra were recorded at 20-s exponential scans over a 1500 dalton range. Calibration was afforded using Ethaquad in the FAB mode (*13*).

Both 10- and 25-μm tungsten wire were spot-welded onto standard Vacuum Generators or Vacumetric field desorption beads. The sample was transferred to the wire via a syringe. Desorption from the 10-μm wire was noted at ca. 18–20 mA. The best anode temperature of 25-μm wire emitters was ca. 120 mA and was established by using the desorption chemical ionization controller. Preparation, loading, and signal intensity favored the thicker wire so subsequent spectra were recorded from 25-μm unactivated wires. The field anode was held at a positive potential of 8 kV while the counterelectrode was at a negative potential of 4 kV.

RESULTS AND DISCUSSION

Intense and long-lived (ca. 5 min) ion emission was noted for each cationic transition-metal complex examined. Figure 1 shows a portion of the field desorption mass spectra of Tc(DMPE)$_2$(Cl)$_2$ClO$_4$ (top) and of Tc(DMPE)$_3$PF$_6$ (bottom). These spectra were not averaged as is often necessary for weak or fluctuating FD signals (*14*) and represent standard FAB mass spectral scanning conditions. The absence of fragmentation contrasts with their FAB mass spectra (*12*) where significant fragmentation was observed. Their intensity and lack of fragmentation are due to the efficient desorption of the preformed cation under even low field strength conditions and the absence of field-enhanced fragmentation often observed using high field strength emitters. The unactivated wire affords desorption with minimal or no fragmentation. An increase in emitter current did not significantly enhance fragmentation.

Figure 2 shows other examples, Tc(DEPE)$_2$(Cl)$_2$ClO$_4$ (top) and Tc(DPrPE)$_2$(Cl)$_2$ClO$_4$ (bottom). As for Tc(DMPE)$_2$(Cl)$_2$ClO$_4$, both contain an isotope pattern which is consistent with the presence of two chlorines. Both also exhibit ion intensities which are similar to those obtained from activated or high field strength emitters.

Attempts to ionize neutral transition-metal complexes such as Cr(ACAC)$_3$, VO(ACAC)$_2$, or structurally similar neutral technetium metal complexes from unactivated 10- or 25-μm

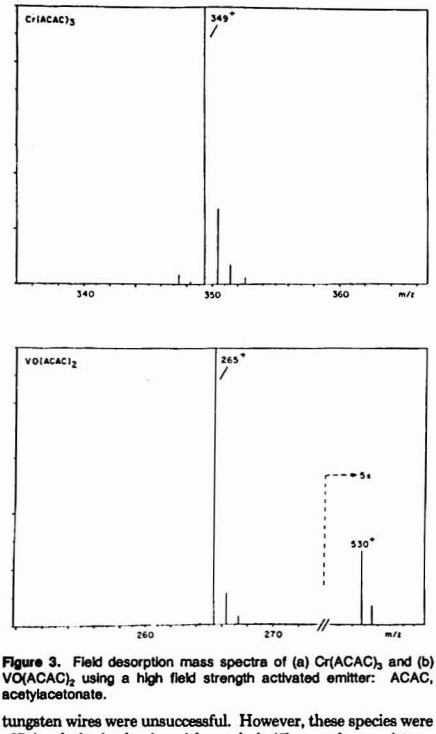


Figure 3. Field desorption mass spectra of (a) $Cr(ACAC)_3$ and (b) $VO(ACAC)_2$ using a high field strength activated emitter: ACAC, acetylacetonate.

tungsten wires were unsuccessful. However, these species were efficiently ionized using either cobalt (*7*) or carbon emitters. Figure 3 shows portions of the FD mass spectra of $Cr(ACAC)_3$ (top) and $VO(ACAC)_2$ (bottom) using carbon emitters. Both yield an intense molecular ion, $Cr(ACAC)_3^+$ at m/z 349 and $VO(ACAC)_2^+$ at m/z 265. Some dimer is also seen for $VO(ACAC)_2$ at m/z 530.

The use of unactivated tungsten wires as field desorption emitters provides a rapid differentiation of cationic from neutral transition-metal complexes. It affords intense signals due to the intact cation with no fragmentation. The method avoids emitter activation and allows wires to be used for subsequent analyses.

Registry No. $Tc(DMPE)_2(Cl)_2ClO_4$, 94481-35-3; $Tc(DMPE)_3PF_6$, 89378-28-9; $Tc(DEPE)_2(Cl)_2ClO_4$, 94481-37-5; $Tc(DPrPE)_2(Cl)_2ClO_4$, 94481-39-7; $Cr(ACAC)_3$, 21679-31-2; $VO(ACAC)_2$, 3153-26-2; W, 7440-33-7; C, 7440-44-0.

LITERATURE CITED

(1) Beckey, H. D. "Principles of Field Ionization and Field Desorption Mass Spectrometry"; Pergamon Press: New York, 1977.
(2) Beckey, H. D.; Hilt, E.; Schulten, H.-R. *J. Phys. E: Sci. Instrum.* **1973**, *6*, 1043-1044.
(3) Linden, H. B.; Hilt, E.; Beckey, H. D. *J. Phys. E: Sci. Instrum.* **1978**, *11*, 1033-1036.
(4) Beckey, H. D.; Schulten, H.-R. *Angew. Chem., Int. Ed. Engl.* **1975**, *6*, 403-413.
(5) Lehmann, W. D.; Fischer, R. *Anal. Chem.* **1981**, *53*, 743-747.
(6) Matsuo, T.; Matsuda, H.; Katakuse, I. *Anal. Chem.* **1979**, *51*, 69-72.
(7) Bursey, M. M.; Rechsteiner, C. E.; Sammons, M. C.; Hinton, D. M.; Colpitts, T. S.; Tvaronas, K. M. *J. Phys. E.: Sci. Instrum.* **1976**, *9*, 145-147.
(8) Semrav, G.; Heitbaum, J. *Anal. Chem.* **1979**, *51*, 1998-2000.
(9) Goldenfeld, I. V.; Veith, H. J. *Int. J. Mass Spectrom. Ion. Phys.* **1981**, *40*, 361-363.
(10) Röllgen, F. W.; Giessmann, U.; Heinen, H. J.; Reddy, S. J. *Int. J. Mass Spectrom. Ion Phys.* **1977**, *24*, 235-238.
(11) Cerny, R. L.; Sullivan, B. P.; Bursey, M. M.; Meyer, T. J. *Anal. Chem.* **1983**, *55*, 1954-1958.
(12) Unger, S. E. *Anal. Chem.* **1984**, *56*, 363-368.
(13) DeStefano, A. J.; Keough, T. *Anal. Chem.* **1984**, *56*, 1846-1849.
(14) Snelling, C. R., Jr.; Cook, J. C.; Millberg, R. M.; Herniing, M. E.; Rinehart, K. L., Jr. *Anal. Chem.* **1984**, *56*, 1474-1481.

Steve E. Unger
The Squibb Institute for Medical Research
P.O. Box 4000
Princeton, New Jersey 08540

RECEIVED for review October 22, 1984. Accepted December 3, 1984.

AIDS FOR ANALYTICAL CHEMISTS

Modified Interface for Pyrolysis Gas Chromatography with Capillary Columns

Robert S. Whiton and Stephen L. Morgan*
Department of Chemistry, University of South Carolina, Columbia, South Carolina 29208

In analytical pyrolysis gas chromatography (PGC), the sample is thermally fragmented by a rapid temperature rise either in a heated chamber attached to the injection port or in the injection port of the GC. The volatile fragments are swept by carrier gas into the chromatographic column where they are separated and passed to a detector. Analytical pyrolysis is routinely used to fingerprint polymeric materials or to obtain structural information from nonvolatile or thermally labile compounds.

To achieve an efficient chromatographic separation, the sample must be transferred to the column as a narrow plug. If the volume of the injection port is too large, the sample may be transferred to the column as an excessively wide band. This problem has been well recognized in the field of pyrolysis GC (*1*, *2*). In capillary GC, the injection port volume problem is compounded by the small internal volume of the column and the low carrier gas flow. Chromatographic bands can be narrowed by cold trapping of pyrolysates on the column or in a precolumn cold trap (*3*), but subambient cooling is required. The normal capillary GC injection mode, split injection, uses a rapid carrier flow (50–100 mL/min) through the injection port to sweep the sample rapidly into the column. Only a small portion of carrier flow (1 mL/min) enters the column and the remainder is vented to atmosphere. Because only 1–2% of the sample enters the column, sensitivity is lowered. This lack of sensitivity may be compensated for by

0003-2700/85/0357-0778$01.50/0 © 1985 American Chemical Society

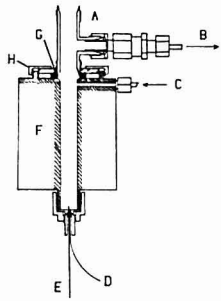


Figure 1. Diagram of modified capillary inlet for pyrolysis GC: (A) bored through tee fitting; (B) purge flow outlet; (C) carrier gas inlet; (D) split flow capillary; (E) capillary column; (F) injection port block; (G) cored septum; (H) retaining ring.

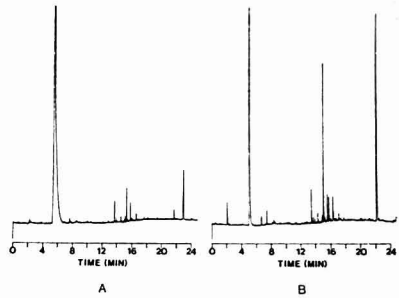


Figure 2. Pyrograms of 0.5 μg of polystyrene on a cross-linked dimethylsilicone capillary column: (A) CDS interface with 23:1 split ratio and 0.73 mL/min column flow; (B) modified capillary interface with 19:1 split ratio and 0.82 mL/min column flow. Column oven temperature was held at 40 °C for 5 min, then programmed at 15 °C/min to 220 °C.

larger sample loadings on the pyrolysis probe, but undesirable secondary reactions may occur (*4*, *5*). Larger sample size may also lead to the formation of temperature gradients within the sample, which may adversely effect the reproducibility of the pyrolysis process (*6*). Sensitivity can be increased by using lower split flows, but smaller pyrolysis interface volumes are required to avoid chromatographic band broadening. This paper presents a simple reduced dead volume system to permit pyrolysis in the injection port of a gas chromatograph.

EXPERIMENTAL SECTION

Chemicals. Polystyrene was obtained from Waters Associates (Milford, MA). Phenylalanine was obtained from Sigma Chemical Co. (St. Louis, MO). Both samples were used without further purification.

Chromatographic Instrument and Conditions. The gas chromatograph employed in this study was a Model 5880A Level 4 (Hewlett-Packard, Avondale, PA) equipped for single capillary column operation with flame ionization detection. Separations were performed on a 12.5 m × 0.2 mm fused silica column coated with cross-linked dimethylsilicone (Hewlett-Packard, Avondale, PA) or on a 23 m × 0.2 mm fused silica column coated with cross-linked OV-1701. Helium was employed as the carrier gas in all experiments and carbon dioxide was used as a coolant for cryogenic oven programming.

Pyrolysis Equipment. The pyrolysis unit employed was a Model 120 Pyroprobe (Chemical Data Systems, Oxford, PA) with a platinum filament. All samples were pyrolyzed at 800 °C for 1 s with a heating rate of approximately 75 °C/ms.

Two different interfacing techniques were employed. The commercial CDS pyrolysis GC interface consists of a heated box containing a metal tube with a glass liner, into which the pyrolysis probe is inserted. The interface box is usually mounted for horizontal probe insertion on a Hewlett-Packard gas chromatograph. In this work, the commercial pyroprobe interface was connected to the GC injection port via a $^1/_8$ in. stainless steel tube silver soldered to the insert weldment of the injection port. The fused silica capillary column was threaded through the injection port into the interface. This pyroprobe interface configuration is identical with that employed in our previous work (*3*, *7*, *8*).

A diagram of the modified pyrolysis interface is shown in Figure 1. The body of the interface was a bored through stainless steel $^1/_4$ in Swagelok tee fitting (Swagelok, part no. SS-400-3-BT) held to the top of the GC injection port by the retaining ring of the injection port weldment assembly. The junction between the interface tee and the injection port was sealed by a septum with a 7-mm hole cut out of the center. The pyrolysis probe was inserted into the GC injection port through the tee fitting and sealed with a $^1/_4$ in. Vespel ferrule and the knurled ring supplied with the pyroprobe. Carrier gas entered the interface through the injection port split vent. Approximately 80–100 mL/min of gas was diverted upward and exited through the side arm of the tee fitting, which was connected to the septum purge line of the gas chromatograph. This flow swept away septum bleed products which would otherwise have created a severe background problem. The rest of the carrier gas was channeled downward past the pyrolysis ribbon to the column and split vent. The end of the fused silica column projected about 0.5 cm into the injection port, approximately even with the end of the pyrolysis ribbon. The split flow exited through a piece of fused silica capillary tubing passed through the same single hole graphite ferrule as the column. The inlet of the split flow capillary was approximately flush with the bottom of the injection port. The exit of the split flow capillary was connected to the standard GC split flow line. Column pressure and split flow were controlled in the normal fashion.

RESULTS AND DISCUSSION

Recent attempts in this laboratory to improve the sensitivity of PGC for biologically important materials have shown the need for a pyrolysis interface with a dead volume smaller than that of the existing system. Additional needs included improved control and monitoring of the interface temperature and elimination of cold spots in the pyrolysis interface–GC injection port connection.

A simple and inexpensive solution to the interface problem involves mounting the pyrolysis probe directly in the injection port of the GC. This modification places the sample close to the head of the column and reduces band broadening, allowing smaller split ratios to be employed. There are no cold spots in the system to caused condensation, and the temperature can be accurately and precisely controlled. The simple geometry of the system permits it to be easily cleaned, and the injection port can be converted into the normal capillary injection configuration in a few minutes. We have employed these injection port modifications on a Hewlett-Packard Model 5992A GC-MS and accurately reproduced pyrograms previously obtained on the HP-5880. It should be noted that the modified interface described here employs the normal metal GC injection port. Pyrolysates which are readily sorbed or degraded may require a glass-lined system. The vertical positioning of the probe rules out the use of the coil filament probe with a quartz sample boat. Furthermore, care must be taken to ensure that the sample adheres firmly to the ribbon in the vertical position.

Pyrograms of polystyrene utilizing each interface system, but with otherwise similar flow conditions and recorder attenuation, are shown in Figure 2. Pyrogram 2A was obtained with the commercial interface mounted as described above. Obvious broadening occurs for the peak eluting at about 5 min, which is not cold trapped effectively at the initial column

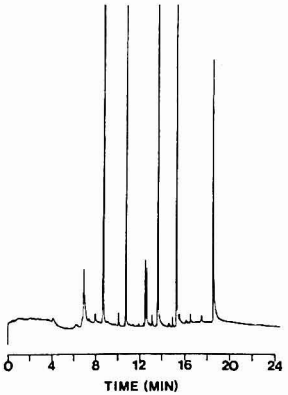


Figure 3. Pyrogram of 10 nmol of phenylalanine on a cross-linked OV-1701 capillary column with zero sample split ratio and 0.59 mL/min column flow. Column oven temperature was held at 0 °C for 2 min, then ramped at 15 °C/min to 220 °C.

temperature. This peak also tails due to slow transfer into the column. Such peak broadening and tailing may make it difficult to separate early eluting components of more complex pyrograms and may also make the accurate determination of peak areas difficult. Pyrogram 2B was obtained by using the modified interface system. The early eluting peak is narrower and more symmetric because of the reduced mixing volume of the interface.

Later eluting components of the pyrograms are cold trapped on the column and therefore exhibit narrow and symmetric peaks in both pyrograms. In Figure 2A with the commercial interface, the peak eluting at about 23 min is diminished in height and area (in comparison to the peak in pyrogram 2B), indicating that the less volatile components are being condensed at cold spots in the system. Heating the interface–GC injection port transfer line often eliminates such a problem. The modified interface, with the probe inserted in the GC injection port itself, does not suffer from the problem of cold spots as long as the injection port is kept at an adequately high temperature. As a final note, repeated pyrolysis of polystyrene on both systems indicated that peak heights and areas are much more reproducible using the modified interface (2% relative standard deviation) in comparison to the externally mounted interface (7–9% relative standard deviation).

Figure 3 illustrates a pyrogram of phenylalanine obtained using the modified interface with zero split flow and cyrogenic oven temperature programming. These experimental conditions provide maximum sensitivity for all pyrolysates in addition to enhanced resolution for the early eluting components. This combination of experimental techniques may permit structural elucidation by analytical pyrolysis on samples in the nanogram to microgram range.

ACKNOWLEDGMENT

The authors thank Matt Przybyciel for preparation of the OV-1701 column.

Registry No. Polystyrene, 9003-53-6; phenylalanine, 63-91-2.

LITERATURE CITED

(1) Levy, R. L. In "Chromatographic Reviews"; Lederer, M., Ed.; Elsevier: Amsterdam, 1966; Vol. 8, pp 48–89.
(2) Berezkin, V. G. *CRC Crit. Rev. Anal. Chem.* **1981**, *11*, 1–18.
(3) Jacques, C. A.; Morgan, S. L. *J. Chromatogr. Sci.* **1980**, *18*, 679–683.
(4) Simon, W.; Giacobbo, H. *Angew. Chem., Int. Ed. Engl.* **1965**, *4*, 938–943.
(5) Levy, R. L. *J. Gas Chromatogr.* **1967**, *5*, 107–113.
(6) Irwin, W. J. "Analytical Pyrolysis, A Comprehensive Guide"; Marcel Dekker: New York, 1982; p 50.
(7) Morgan, S. L.; Jacques, C. A. *Anal. Chem.* **1982**, *54*, 741–747.
(8) Hudson, J. R.; Morgan, S. L.; Fox, A. *Anal. Biochem.* **1982**, *120*, 59–65.

RECEIVED for review September 10, 1984. Accepted November 5, 1984. This work was supported in part by NIH Grant No. 27135. The donation of a gas chromatographic instrument by Hewlett-Packard (Palo Alto, CA) is gratefully acknowledged.

Anion Contamination of Environmental Water Samples Introduced by Filter Media

P. C. Jay

Environmental Research Branch, Atomic Energy of Canada Limited, Chalk River Nuclear Laboratories, Chalk River, Ontario, Canada K0J 1J0

During measurement of the anion content of surface water and groundwater, contamination can occur from leachable anions present in membrane-type filter media used in the process of filtering samples. Cation contamination of environmental water samples, due to filtration, is well established in the literature. Robertson (*1*) has shown that many types of filter materials contain significant levels of metallic impurities that can contaminate solutions during the filtration process. Apart from Cl^-, he did not report on other anion impurities in these materials. Kosta (*2*) in an otherwise extensive review of contamination as a limiting parameter, reports only that major contaminants such as chloride and sodium may exceed the 1 $\mu g/cm^2$ level in filters based on cellulose esters (Millipore). Other workers (*3*, *4*) have shown Cl^-, Br^-, NO_3^-, and SO_4^{2-} contamination from specific filters but there is no report that surveys the leachable anion content of those membrane-type filters commonly used in water analyses. The work reported here shows that filters from several manufacturers contain considerable amounts of leachable anions and that if such filters are used without careful prewashing, inaccurate data will result.

EXPERIMENTAL SECTION

An ion chromatograph with eluent suppression [ICES] coupled to a Hewlett-Packard HP3390A reporting integrator was used to determine the anion content of leachates obtained from deionized distilled water (DDW) washes of several types of membrane filters. The ICES system was an extensively modified Dionex 10 ion chromatograph with a hollow-fiber suppressor (*5*). A 0.003 M $NaHCO_3$/0.0024 M Na_2CO_3 eluent and a 0.050 M H_2SO_4 regenerant was used throughout this work. With a 100 μL sample

0003-2700/85/0357-0780$01.50/0 Published 1985 by the American Chemical Society

Table I. Leachable Anion Content of Membrane Filters[a]

filter type	F^-	Cl^-	PO_4^{3-}	NO_3^-	SO_4^{2-}
Millipore SSWP 3 μm, 47 mm	1.0	11.2	1.0	21.7	8.7
Millipore RAWP 1.2 μm, 47 mm	4.6	8.8	<0.2	31.0	5.4
Millipore HAWP 0.45 μm, 47 mm	1.0	7.7	<0.2	3.6	<0.5
Millipore VCWP 100 μm, 47 mm	2.1	7.8	1.8	25.5	4.5
Millipore GSWP 0.22 μm, 47 mm	2.0	8.2	2.8	26.5	5.4
Millipore SCWP, 8 μm, 47 mm	1.0	9.1	1.2	20.8	6.8
Gelman GA-8 0.2 μm, 47 mm	9.8	88.0	<0.2	1.0	24.1
Gelman GA-6 0.45 μm, 47 mm	5.8	42.0	<0.2	59.7	22.6
Gelman GA-3 1.2 μm, 47 mm	1.2	5.9	2.9	3.5	20.8
Gelman GA-1 5.0 μm, 47 mm	1.4	8.9	<0.2	24.8	24.9
Gelman Tuffryn HT-100 0.1 μm, 25 mm	<0.02	10.3	<0.2	<0.2	2.9
Gelman Tuffryn Glass Fibre A-E 47 mm	37.0	16.2	<0.2	0.8	5.0
Gelman Tuffryn GN-6 0.45 μm, 47 mm	4.17	3.80	936.0	3.40	1.8
Whatman GF/F microfibre 1.6 μm, 47 mm	12.6	142.0	<0.2	1.2	1.3
Nucleopore Membra-fil 0.45 μm, 25 mm	0.1	1.4	<0.2	6.2	5.9
Nuclepore Polycarbonate 0.4 μm, 25 mm	<0.02	1.8	<0.2	<0.2	<0.5
0.2 μm, 25 mm	<0.02	1.1	<0.2	<0.2	<0.5
0.1 μm, 25 mm	<0.02	1.2	<0.2	<0.2	<0.5
DDW	<0.02	<0.08	<0.2	<0.2	<0.5

[a] All values are given as μg of anion per single filter disk leached by 10 mL of deionized water.

Table II. Anion Content of Water Samples from a Dystrophic Lake on CRNL Property (Perch Lake) after Filtration through Unwashed Membrane Filters

type of filter	anion content, μg/mL				
	F^-	Cl^-	PO_4^{3-}	NO_3^-	SO_4^{2-}
Gelman GA-8 0.2 μm, 47 mm	4.32	32.17	<0.2	0.50	11.76
GA-6 0.45 μm, 47 mm	0.54	9.04	<0.2	6.84	6.06
GA-1 5.0 μm, 47 mm	0.23	6.41	<0.2	9.43	8.07
Millipore GSWP 0.22 μm, 47 mm	0.13	5.03	0.48	1.04	9.04
RAWP 1.2 μm, 47 mm	0.12	5.10	<0.2	1.09	7.97
VCWP 100 μm, 47 mm	0.18	5.26	<0.2	2.41	6.91
unfiltered lakewater	0.05	4.60	<0.2	<0.2	5.70

injection loop, the detection limits (in μg/mL) were as follows: F^-, 0.02; Cl^-, 0.08; NO_2^-, 0.1; PO_4^{3-}, 0.2; Br^-, 0.4; NO_3^-, 0.2; SO_4^{2-}, 0.5.

Sample chromatograms processed by the integrator were calibrated by comparison with a chromatogram representing 1 μg/mL of each of F^-, Cl^-, and NO_2^- and 10 μg/mL of each of PO_4^{3-}, Br^-, NO_3^-, and SO_4^{2-}.

Several filter-washing techniques were used to assess the relative efficiency of contaminant removal. In all cases the DDW used for washing was obtained from a Corning "Megapure" system with a LD2A demineralizer and a 3508A ultrahigh purity cartridge. Blank determinations of this DDW by ICES showed no detectable anion concentrations. Filters were held in a standard 47 mm Whatman filter holder No. 1960 004 made of borosilicate glass with a sintered glass frit filter support that had been previously washed with liter quantities of DDW until blank determinations showed no detectable anions in the wash water.

The six types of Millipore filters tested (SSWP, RAWP, HAWP, VCWP, GSWP, and SCWP) are porous membranes composed of pure cellulose esters in pore sizes ranging from 0.45 to 100 μm. Three types of Gelman unsupported membrane filters were tested: Type GA metricel (cellulose triacetate) with pore sizes ranging from 0.2 to 5 μm, Type HT Tuffryn (high temperature aromatic polymer) 0.1 μm pore size, and type GN metricel (mixed esters of cellulose) 0.45 μm pore size. A Gelman Type A-E glass fiber media without binder was also tested. The two types of Nucleopore filters tested were Membra-fil and Polycarbonate. Membra-fil, 0.45 μm pore size, is a cast membrane of mixed esters of cellulose or of pure nitrocellulose. Polycarbonate is an extremely thin porous film with straight through capillary pores. Pore sizes were 0.1 μm, 0.2 μm, and 0.4 μm. The other glass fiber filter tested was a Whatman GF/F microfiber.

In those cases where washing was done on the filter holder, the unwashed disks were taken directly from their packages, using prewashed stainless forceps, and placed directly into the holder.

A filter washing bath constructed of borosilicate glass with an inner Teflon container to hold the filter disks (Figure 1) was designed for use in the bulk washing of filters. Nylon monofilament line was threaded through holes in the Teflon holder so that individual disks would be separated from each other, thus permitting free circulation of the wash waters around them. A four-gallon carboy filled with DDW was connected to the bottom opening of the filter bath and DDW was gravity fed to the bath at a rate of approximately 1 L/h for 4 h. Slots equally spaced around the bottom circumference of the Teflon holder dispersed the water evenly throughout the bath.

RESULTS AND DISCUSSION

Table I presents the water-leachable F^-, Cl^-, PO_4^{3-}, NO_3^-, and SO_4^{2-} content of 10 mL of DDW from a series of wash waters filtered through 18 common membrane and glass fiber filter disks that had not been prewashed.

Although all filters contain leachable anion concentrations sufficient to cause contamination of environmental water samples, there were large differences between different groups of filters with the polycarbonate group showing the lowest leachable anion content. All Millipore filters showed unacceptable levels of leachable anions with some values as high as 31 μg of NO_3^- per disk and 8.7 μg of SO_4^{2-} per disk. Compared with most Millipore filters, Gelman filters showed approximately five times more SO_4^{2-} per disk, GA-8 and GA-6 yielded high Cl^- concentrations and GN-6 was extremely high in PO_4^{3-} (936 μg per disk). The nitrite and bromide content of all the filters examined were below detection limits, i.e., 0.1 and 0.4, respectively. It is evident from these results (Table

Table III. Leachable Anion Content of Filter Disks after 4 L of DDW (20 mL/min) was flushed through in Filter Wash (5 mL Then Flushed through Filter Disks and Analyzed for Anion Content)

filter type	leachable anion/disk after washing
Millipore SSWP 3 μm, HAWP 1.2 μm, GSWP 0.22 μm, SCWP 8 μm, RAWP 1.2 μm	F^-, Cl^-, NO_2^-, PO_4^{3-}, Br^-, NO_3^-, SO_4^{2-} below detection limits
Gelman GA-8 0.2 μm, GA-6 0.45 μm, GA-3 1.2 μm, GA-1 5.0 μm, Tuffryn HT-100 0.1 μm, Glass Fibre A-E, GN-6 0.45 μm	same as above
Whatman GF/F microfiber 1.6 μm	same as above
Nuclepore Membra-fil 0.45 μm	same as above
Polycarbonate 0.4 μm, 0.2 μm, and 0.1 μm	same as above
Millipore VCWP 100 μm	0.17 μg Cl^-; below detection limits for F^-, NO_2^-, PO_4^{3-}, Br^-, NO_3^- and SO_4^{2-}

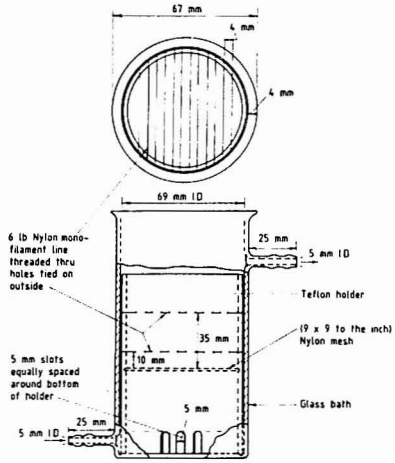


Figure 1. Bath used for washing membrane-type filters.

I) that all the listed filters require prewashing to avoid sample contamination.

To demonstrate that error is introduced by unwashed filter media when an environmental water sample is passed through them, a sample of known anion content from a dystrophic lake on CRNL property (Perch Lake) was used to wash six types of membrane filters. Ten-milliliter washes were made, and the anion content of the wash waters was analyzed. Table II shows the results obtained. In all cases the filter media produced inaccurate results with leachable anions being added to the known unfiltered lakewater concentrations.

"In situ" washing, i.e., flushing DDW through the filters while they were held in a standard 47 mm holder, was unsuccessful in removing all impurities. This is probably due to the fact that the 47 mm glass disk holder exposes only about 10 cm^2 of total filter area leaving 8 cm^2 held between the ground glass rims allowing diffusion to cause slow leach out from the unexposed portion. Presoaking filters in 100 mL of DDW in beakers for 24 h gave approximately the same results as "in situ" washing, i.e., detectable leachable anions still remained on the filter disks.

Table III presents the anion content of the 18 types of filters tested after they had been washed in the specially designed filter bath (Figure 1) with 4 L of DDW at a flow rate of 1 L/h. After being washed, the filter disks were removed from the bath and placed in glass filter holders and 5 mL of DDW was flushed through them. These 5-mL wash samples were than analyzed for anion content. In all filters the leachable anion concentrations were below detection limits except for VCWP which showed a trace of Cl^-.

Membrane-type filter media used in analyses of environmental samples containing low concentrations of anions introduce contamination risks sufficient to require that the filter disks be carefully prewashed. This prewashing and indeed the filtration process itself is time consuming and often inconvenient for routine analysis of large numbers of samples. When this is the case an on-column filtration procedure has been used in our laboratories (*6*). This filtration procedure consists of a 4 × 30 mm anion concentrator precolumn (Dionex P/N 030986) installed immediately before the separator column on the ICES. This precolumn worked extremely well as a filter and as many as 4100 surface and groundwater samples were routinely analyzed in the laboratory before it required replacement. Any samples that contained a large concentration of particulates were centrifuged before injection into the ICES.

ACKNOWLEDGMENT

The author thanks J. M. Judd for helpful discussions throughout the course of this work.

Registry No. NO_2^-, 14797-65-0; PO_4^{3-}, 14265-44-2; NO_3^-, 14797-55-8; SO_4^{2-}, 14808-79-8; H_2O, 7732-18-5; F^-, 16984-48-8; Cl^-, 16887-00-6; Br^-, 24959-67-9; Millipore SSWP, 94293-99-9; Millipore RAWP, 94293-97-7; Millipore HAWP, 66419-15-6; Millipore VCWP, 94294-00-5; Millipore GSWP, 94293-96-6; Millipore SCWP, 94293-98-8; Gelman GA-8, 9012-09-3; Tuffryn HT-100, 94483-18-8; Nucleopore Membra-fil, 94294-01-6.

LITERATURE CITED

(1) Robertson, D. E. "Ultrapurity"; Zief, M., Speights, R., Eds.; Marcel Dekker: New York, 1972; pp 220–221.
(2) Kosta, L. *Talanta* **1982**, *29* (11B), 985–992.
(3) Butler, F. E.; Jungers, R. H.; Porter, L. F.; Filey, A. E.; Toth, F. J. "Ion Chromatographic Analysis of Environmental Pollutants"; Sawicki, E., Mulik, J. D., Wittgenstein, E.; Eds.; Ann Arbor Science: Ann Arbor, MI, 1978; pp 65–67.
(4) Dams, R.; Rahn, K. A.; Winchester, J. W. *Environ. Sci. Technol.* **1972**, *56*, 441–448.
(5) Judd, J. M.; Jay, P. C. Report No. AECL 8411, Chalk River Nuclear Laboratories, 1984.
(6) Jay, P. C.; Judd, J. M. *Int. J. Environ. Anal. Chem.*, in press.

RECEIVED for review September 18, 1984. Accepted November 13, 1984.

Corrosion Resistant Coating for Laboratory Equipment

Larry P. Morgenthaler* and Armand F. Lange, Jr.

Quality Assurance Laboratory, University of Nevada at Las Vegas, 4505 Maryland Parkway, Las Vegas, Nevada 89154

It is sometimes desired to render the surface of an active metal such as aluminum impervious to the effects of dilute acid or base solutions.

Such a situation recently arose in our laboratory when we wished to use a high-pressure gas drying tube as a container for dilute nitric or hydrochloric acid. While the body of the vessel was made of inert plastic, the end caps were made of aluminum or one of its alloys. The end caps were also threaded to accept gas fittings, and any protective material that might be used to protect the end caps from the acid would have to protect the thread cuts as well. At the same time, the protective material could not prevent the proper seating of the O-ring pressure seals.

In this particular application there was no mechanical stress applied to the coating, and it only needed to operate at or near room temperature. The coating had to be free flowing during application so that it would readily fill in voids and conform to complex shapes. On drying, the coating had to be chemically inert and noncontaminating and could not chip, crack, or flake.

A number of coating materials were considered but were eliminated by failure to meet one or more of the criteria

0003-2700/85/0357-0782$01.50/0 © 1985 American Chemical Society

previously mentioned or by lack of assurance that the coating material would be able to stand up to extended acid exposure. If the material were to eventually degrade, the coating should be easily removable prior to recoating.

The final decision was to coat the aluminum surfaces with a thin film of polyethylene. There is, to our knowledge, no commercial product available to produce this coating, but one can be easily prepared in the laboratory. Low molecular weight branched polyethylenes are soluble in some organic solvents such as toluene or xylene at slightly elevated temperatures, usually just below the boiling points of those solvents. Parafilm M (a product and registered trademark of American Can Co.) is a commonly available laboratory film of proprietary composition. It may be speculated that Parafilm M is a composite of waxes, plasticizers, and polyethylene. While this speculation may be incorrect, the solubility properties are very similar to those of a low molecular weight polyethylene but the setting properties are more waxlike. The flexibility and elasticity suggest a plasticized polymer. The important property, however, is that the Parafilm M is soluble, and that on evaporation of the solvent, an adhesive film is produced that retains the properties of the original Parafilm M. (In the following discussion Parafilm M will be referred to as a "polymer" although that may be technically incorrect.)

The polymer solution is prepared by heating, with continuous stirring, small pieces of Parafilm M with approximately 10 times their weight of toluene. When the solvent becomes sufficiently hot, but below its boiling point, the polymer dissolves to form a clear solution.

The surface to be protected is coated with the hot solution by flowing it on with a brush or cotton swab. The solution must be applied while it is hot as the polymer precipitates on cooling.

The solvent is allowed to evaporate at room temperature or with the assistance of an infrared heat lamp and leaves behind a uniform coating of the polymer on the material to be protected. The wet polymer solution is subject to abrasion, and care should be taken to allow it to dry completely before handling.

The thickness of the coating can be controlled by varying the polymer concentration in the solvent, 10% by weight appears to be the highest workable concentration. The thickness can also be increased by applying repeated coatings, allowing each to dry completely before applying the next.

The effectiveness of the coating was tested by covering the flat surface of a disposable aluminum roasting pan with the polymer. A number of test solutions (approximately 0.5 mL of each) were placed on the coated surface and covered with petri dishes to prevent evaporation. The solutions used were as follows: 1:1, water:hydrochloric acid; 1:1, water:nitric acid; 1:1:1, water:nitric acid:30% hydrogen peroxide; 1:1, water:sulfuric acid; 1 M sodium hydroxide; 0.005 M mercuric chloride.

After 96 h there was no indication of attack on the metal by any of the test solutions.

While this film acts as a hydrophobic barrier to solutions, it may permit the diffusion of gases or covalent compounds through the polymer. The coating is intended only as protection against attack by dilute aqueous electrolytes.

The polymer coating may be hardened by the addition of 1% to 5% of conventional polyethylene (CPE) to the hot solvent. The resulting film appears to gain mechanical strength and hardness, but is less adherent to the protected surface.

The Parafilm M coating is inert, noncontaminating, and flexible and has not been found to crack or peel from the protected surface. It is easily prepared with common laboratory solvents. While it cannot tolerate mechanical abrasion or thermal stress, it can help to solve some simple corrosion problems encountered in the laboratory.

Registry No. Polyethylene (homopolymer), 9002-88-4; aluminum, 7429-90-5.

RECEIVED for review September 24, 1984. Accepted November 5, 1984. Although the research described in this article has been funded wholly or in part by the United States Environmental Protection Agency through Cooperative Agreement CR 809-706-0103 to the University of Nevada, Las Vegas, it has not been subjected to Agency review and therefore does not necessarily reflect the views of the Agency and no official endorsement should be inferred. Mention of trade names or commercial products does not constitute endorsement or recommendation for use.

Two-Phase Titration of Poly(oxyethylene) Nonionic Surfactants with Tetrakis(4-fluorophenyl)borate

Masahiro Tsubouchi,* Nakamichi Yamasaki, and Kazumichi Yanagisawa

Laboratory of Chemistry, Kochi Medical School, Nankoku, Kochi 781-51, Japan

Anionic and poly(oxyethylene) nonionic surfactants are widely used in both industrial and domestic detergents. It is known that the nonionic surfactant can form spirals which can trap metal ions such as potassium (*1*) and barium (*2*). The reaction between anions and the complex cation formed by the nonionic surfactant and the metal ions has been made the basis for spectrophotometric methods (*1*, *3*, *4*) and precipitation titration (*5*) for determination of the nonionic surfactant. However, it is generally difficult to determine total nonionic surfactants in the presence of anionic surfactants because the metal ion complexes of the nonionic surfactants form ion pairs with the anionic surfactants present.

Two-phase titration is one of the most frequently used methods for the determination of ionic surfactants. This paper presents a simple method for the determination of nonionic surfactant in the presence of an anionic surfactant by two-phase titration.

EXPERIMENTAL SECTION

Apparatus. A 25-mL buret was used.

Materials. The nonionic surfactants used were Triton X-100, Triton X-405 (Rohm & Haas Co.), poly(ethylene glycol) mono-*p*-isooctylphenyl ether (Wako Pure Chemical Ind.), poly(oxyethylene) lauryl alcohol ether, and poly(oxyethylene) sorbitan monopalmitate (Nakarai Chemicals Ltd.). The number-average degree of polymerization of the oxyethylene chain of the surfactants used is 8–12, except for Triton X-405 (for which it is 40). The nonionic surfactants were dried at 80 °C and dissolved in water. The titrant was prepared by dissolving sodium tetrakis-

0003-2700/85/0357-0783$01.50/0 © 1985 American Chemical Society

Table I. Effect of Concentration of Titrant

[titrant], M	[Triton X-100], mg	mean titer,[a] mL	std dev, mL
1×10^{-3}	1	1.84	0.04
1×10^{-3}	3	5.51	0.05
5×10^{-4}	0.3	1.10	0.04
5×10^{-4}	1	3.67	0.06
5×10^{-4}	2	7.34	0.07
5×10^{-4}	3	11.01	0.07
2×10^{-4}	0.3	2.75	0.06
2×10^{-4}	1	9.20	0.08

[a] Results of 10 sample solutions.

(4-fluorophenyl)borate ($C_{24}H_{16}F_4BNa$, Dojindo Laboratories, Kumamoto, Japan, purity is more than 98%) in water. Victoria Blue B (color index 44045, $C_{33}H_{32}N_3Cl$) was dissolved in ethanol to make a 0.04% solution; it was used as an indicator.

Procedure. To 10 mL of a surfactant solution (nonionics, 0.3–3 mg/10 mL; anionics, less than 5×10^{-4} M) in a 300-mL Erlenmeyer flask, were added 5 mL of 6 M potassium hydroxide solution, 1 to 2 drops of the indicator, and 5 mL of 1,2-dichloroethane. The mixture was titrated with the titrant (5×10^{-4} M) with vigorous shaking after each addition, until a color change from red (λ_{max} 505 nm) to blue (λ_{max} 615 nm) took place in the organic phase.

One milligram of nonionic surfactant requires ca. 3.6 mL of 5×10^{-4} M titrant, irrespective of the anionic surfactant present.

RESULTS AND DISCUSSION

It is reported that a 12-unit ethylene oxide polymer combines with one barium regardless of the kind of alkyl or alkylaryl groups in the nonionic surfactant (2). The nonionic surfactant can also trap potassium ions in its spirals and be extracted into dichloroethane from 1 to 2 M potassium hydroxide, as an ion pair with tetrakis(4-fluorophenyl)borate, but any anionic surfactant in the mixture is not extracted.

The aqueous phase remains colorless throughout the titration, due to the insolubility of the Victoria Blue B in alkaline water. An indicator–tetrakis(4-fluorophenyl)borate ion pair is formed at the end point, but the indicator does not react with anionic surfactants in the presence of alkaline water (more than 0.2 M of potassium hydroxide). The best color change and most constant titer were obtained at a concentration of potassium hydroxide from 1 to 2 M in the aqueous layer at the end point.

The results of titration of Triton X-100 are shown in Table I. With a 2×10^{-4} M titrant, a blank titration is necessary because the color change at the end point is not sharp. There is a slight tendency to decrease the sharpness of the end point with increasing amounts of nonionic surfactant because of its lather. The volume of titrant required is proportional to the amount of nonionic surfactant present in the sample solution, indicating that the nonionic surfactant is stoichiometrically extracted. The volumes 5×10^{-4} M titrant needed for 2 mg of nonionic surfactant were found to be as follows: Triton X-100, 7.3–7.4 mL; Triton X-405, 6.7–6.8 mL; poly(ethylene glycol) mono-*p*-isooctylphenyl ether, 7.4–7.5 mL; poly(oxyethylene)sorbitan monopalmitate, 7.1–7.2 mL; poly(oxyethylene) lauryl alcohol ether, 6.8–6.9 mL. The volumes vary with the products and type of surfactant, but it seems that in general the volume needed for the same weight of nonionic surfactant is almost constant, about 3.6 mL of 5×10^{-4} M titrant/mg of nonionic surfactant. It is reasonable to consider that the hydrophile–lipophile balance values of the surfactants used are similar, making the method usable for a range of surfactants.

Table II. Titration of 1 mg of Poly(ethylene glycol) with 5×10^{-4} M Titrant

$HO(CH_2CH_2O)_nH$ mean mol wt	mL of titer	*n*-[PEG]/[titrant][a]
200	1.3	31.5
400	4.8	9.0
600	5.1	8.6
1000	5.1	8.7
2000	4.8	9.5
3000	4.7	9.5
7500	4.7	9.7
20000	4.6	10.0

[a] [PEG]/[titrant]: combination ratio of poly(ethylene glycol) to titrant.

Chloroform cannot be used as the organic solvent, since it does not give a sharp end point. If sodium tetraphenylborate is used as the titrant, potassium hydroxide gives precipitates and the use of sodium hydroxide in place of potassium hydroxide does not give a sharp end point.

The following species do not interfere at the 10^{-3} M level: Na^+, NH_4^+, Al^{3+}, Cl^-, NO_3^-, SO_4^{2-}, and triethanolamine. Anionic surfactants (5×10^{-4} M) such as dodecyl sulfate, dodecyl benzenesulfonate, and bis(2-ethylhexyl)sulfosuccinate do not disturb the titration, but separation of the two layers is poor when the concentration of these anionic surfactants is more than 1×10^{-3} M, causing positive errors. Cationic surfactants disturb the titration.

The results of the titration of poly(ethylene glycol) appear in Table II. It is seen that a 9–10 unit ethylene oxide polymer combines with one tetrakis(4-fluorophenyl)borate. The number-average degree of polymerization of commercial nonionic surfactants is mainly 8–13.

A commercial detergent was diluted with water, and the anionic surfactant was first titrated with a solution of cationic surfactant (tetradecyldimethylbenzylammonium chloride) (6). A second aliquot of sample solution was diluted with water to reduce the concentration of anionic surfactant to 5×10^{-4} M or less, and the nonionic surfactant was then determined by the procedure. The result found was 0.37 M anionic surfactant and 0.12 g/mL of nonionic surfactant in the detergent. A recovery test was done by adding 1.0 mg of Triton X-100 to the 1500-fold diluted detergent, and 1.03 mg was found.

Registry No. Victoria Blue B, 2580-56-5; Triton X-100, 9002-93-1; poly(ethylene glycol)mono-*p*-isooctylphenyl ether, 51651-58-2; poly(oxyethylene) lauryl alcohol ether, 9002-92-0; poly(oxyethylene) sorbitan monopalmitate, 9005-66-7; sodium tetrakis(4-fluorophenyl)borate, 25776-12-9.

LITERATURE CITED

(1) Toei, K.; Motomizu, S.; Umano, T. *Talanta* **1982**, *29*, 103–106.
(2) Uno, T.; Miyajima, K. *Chem. Pharm. Bull.* **1963**, *11*, 80–82.
(3) Anderson, N. H.; Girling, J. *Analyst (London)* **1982**, *107*, 836–838.
(4) Murai, S. *Bunseki Kagaku* **1984**, *33*, T18–T21.
(5) Uno, T.; Miyajima, K. *Chem. Pharm. Bull.* **1963**, *11*, 75–80.
(6) Tsubouchi, M.; Yamasaki, N.; Matsuoka, K. *J. Am. Oil Chem. Soc.* **1974**, *56*, 921–923.

RECEIVED for review September 10, 1984. Accepted November 7, 1984.

AUTHOR INDEX

Adams, D. O., 710
Allen, T. W., 666
Amin, T. A., 648
Aoki, K., 737
Apfel, M. A., 651
Asakura, S., 737
Ashworth, D. J., 710
Axner, O., 773

Baldwin, R. P., 591
Benkeser, R. A., 692
Bialkowski, S. E., 758
Blomqvist, K., 749
Brewer, S. W., 724
Brooks, J. J., 640

Cassidy, R. M., 615
Cheng, M. T.-h., 710
Chess, E. K., 633
Chiang, S., 719
Clerc, J. T., 578
Coetzee, J. F., 581
Cooks, R. G., 692
Corsini, A., 719
Crawford, R. J., 659

Davis, J. C., 768
Dowling, S. D., 602
Dreyer, R. N., 675
Dütsch, S., 578

Eatough, D. J., 743
Eatough, N. L., 743
Elchuk, S., 615
Ellis, E. C., 743
Ellis, R. D., 771

Fenn, J. B., 675
Finkelmann, H., 651
Frech, R., 716

Galvez, J., 585
Giang, B. Y., 710
Gilpin, R. K., 596
Gordon, G., 734
Grimsrud, E. P., 659
Gustafson, F. J., 621
Gutteridge, C. S., 704

Halbert, M. K., 591
Hale, M. D., 640
Hansen, L. D., 743
Hawthorne, S. B., 694
Hellgeth, J. W., 610
Hercules, D. M., 698
Hileman, F. D., 640
Hites, R. A., 684
Hofmann, S., 716
Hoshino, H., 625
Howard, W. A., 606
Hsu, T.-B., 606
Hunt, D. F., 765
Hunter, R. L., 765
Hurtubise, R. J., 666
Hussam, A., 581

Jan, C.-C., 752
Janini, G. M., 651
Jay, P. C., 780
Jenny, H.-B., 578
Johnson, C. C., 610

Knighton, W. B., 659
Krost, K. J., 763

Lange, A. F., Jr., 782
Later, D. W., 633
Laub, R. J., 651
Laugal, J. A., 692
Lavine, B. K., 752
Lee, R. Y., 710
Lindgren, I., 773
Lucke, R. B., 633
Lühmann, B.-H., 651

MacFie, H. J., 704
Magnusson, I., 773
Markell, C. G., 621
Marshall, M. A., 729
Matsuoka, T., 737
Mazer, T., 640
McCreery, R. L., 752
McGuire, J. M., 680
McIver, R. T., Jr., 765
McLafferty, F. W., 771
Miller, D. J., 694
Miller, K. G., 734
Morgan, S. L., 778
Morgenthaler, L. P., 782
Mottola, H. A., 729
Munson, B., 680

Narang, R. S., 648
Nelson, D. A., 606
Nickolaisen, S. L., 758
Noble, R. W., 640

Olson, K. L., 672

Pacey, G. E., 734
Parker, C. D., 698
Périsset, P. M. J., 578
Peterson, D. P., 768
Peterson, D. W., 771
Pretsch, E., 578
Price, A., 651

Roberts, W. L., 651
Rogers, L. B., 606, 628
Rubinsztein-Dunlop, H., 773

Sacks, R. D., 724
Schlatter, K. J., 578
Seitz, W. R., 602
Semmler, J., 740
Shabanowitz, J., 765
Shaw, T. J., 651
Shell, T. L., 640
Silver, H. F., 666
Simon, W., 578
Simpson, S. M., 621
Smith, C. A., 651
Stairs, R. A., 740
Stauffer, D. B., 771
Stemmler, E. A., 684
Still, E. R., 749
Suffolk, B. R., 596
Syka, J. E. P., 765

Taylor, L. T., 610
Tsubouchi, M., 783

Unger, S. E., 776

Vallis, L. V., 704
Van Hare, D. R., 628
Vargo, J. D., 672

Wan, C.-C., 719
Warden, S. W., 659
Weimer, W. C., 633
White, V. F., 743
Whitehouse, C. M., 675
Whiton, R. S., 778
Wolff, G., 578
Wood, K. V., 692
Wright, C. W., 633

Yamasaki, N., 783
Yamashita, M., 675
Yanagisawa, K., 783
Yoshizumi, K., 737
Yotsuyanagi, T., 625

Future Articles

Computer-Based Numerical Integration for the Calculation of Retention Times in Gradient High-Performance Liquid Chromatography
Sterling A. Tomellini, Richard A. Hartwick, and Hugh B. Woodruff

Potassium Hydroxide Eluent for Nonsuppressed Anion Chromatography of Cyanide, Sulfide, Arsenite, and Other Weak Acids
Tetsuo Okada and Tooru Kuwamoto

Interface of a Microbore High-Performance Liquid Chromatograph with a Diffuse Reflectance Fourier Transform Infrared Spectrometer
Christine M. Conroy, Peter R. Griffiths, and Kiyokatsu Jinno

Background Detection and Correction in Multicomponent Analysis
D. W. Osten and B. R. Kowalski

Rapid and Precise Method for the Measurement of Vapor/Liquid Equilibria by Headspace Gas Chromatography
Abul Hussam and Peter W. Carr

Moderate-Power Helium Plasma as an Element-Selective Detector for Gas Chromatography of Dioxins and Other Halogenated Compounds
David L. Haas and Joseph A. Caruso

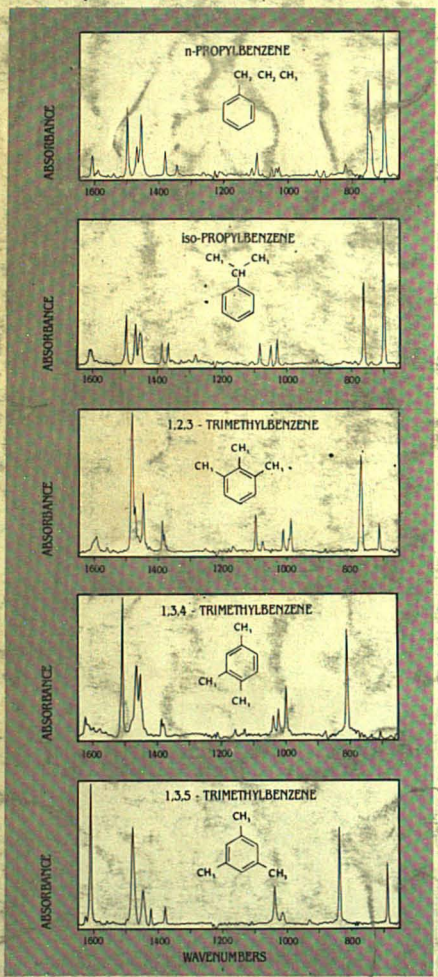
Angular Distribution X-ray Photoelectron Spectroscopy Studies on Compacted Lead Ion Selective Membrane Powders
Vaneica Young and Paul C. McCaslin

Distribution of Electrochemical Activity on Graphite–Epoxy Surfaces
Royce C. Engstrom, Michael Weber, and Jane Werth

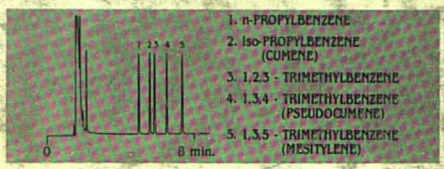
Isomer-Specific Analysis By Cryolect GC/IR

Sidney Bourne

The Cryolect™ is a new approach to GC/IR, trapping the GC effluent in a solid argon matrix. The Cryolect stores up to five hours of chromatographic effluent with five-second peak resolution, and offers sub-nanogram sensitivity for most compounds.



Each spectrum obtained from 10 ng, 4 cm⁻¹ resoution, 32 sec measurment time.



Cryolect chromatogram of C_3 substituted benzenes 10 ng each.

Cryolect GC/IR and GC/MS are two powerful techniques for the characterization of complex organic mixtures. They are comparable in sensitivity, and have complementary strengths. GC/MS is strong in providing the molecular weight of the compound, and in characterizing a homologous series of compounds; Cryolect GC/IR is strong in providing the functional groups and skeletal structure of compounds, and in differentiating isomers.[1]

The five IR spectra of the fingerprint regions of the C-3 substituted benzenes illustrate the Cryolect's power. Each of the five spectra is unique and can be unambiguously identified from spectral libraries. The position of the band in each spectrum between 750 and 850 wavenumbers, which is due to the out-of-plane aromatic deformation, allows a spectroscopist to assign each spectrum to its correct structure. On the other hand, the mass spectra of four of these five compounds are indistinguishable.

Summary

The Cryolect provides the analyst with an extremely sensitive complement to GC/MS.

Reference

1. P.R. Griffiths, J.S. De Haseth, and L.V. Azarraga. *Anal. Chem.*, **55**, 1361A (1983).

This is the third in a series of short technical notes on the Cryolect, a new and more sensitive approach to GC/FT-IR. These notes will appear each month on the back cover of **Analytical Chemistry**. *For expanded versions of these notes, contact Mattson.*

6333 Odana Rd.
Madison, Wisconsin 53719
U.S.A.
(608) 273-2370
Telex: 262006

Silbury Business Centre
356 Silbury Boulevard
Central Milton Keynes MK9 2LR
England
Tel. (0908) 679961
Telex: 825264 Silbus G

Mattson Instruments, Inc.

CIRCLE 137 ON READER SERVICE CARD